Petrogenesis and contrasting eruption styles of peralkaline silicic magmas from Terceira and São Miguel, Azores

Adam John Jeffery

Vol. I Thesis

Thesis submitted for the degree of Doctor of Philosophy in Earth Sciences

October 2016

Keele University

PREFACE

This thesis represents an original contribution to science, and has been divided into two separate volumes. The first volume comprises the main body of the thesis, including an introductory chapter, a literature review and context chapter, and a chapter detailing the various methods and analytical techniques used. This is followed by two main body chapters, in which the scientific results of two individual case studies are provided and discussed. This culminates in a synthesis chapter, where the implications of this work are considered in both a regional and a global context. Finally, the primary conclusions and research implications are detailed in a conclusions chapter. The second volume of this work comprises various appendices, providing in full the datasets employed throughout the study, including: a list of sampling locations, a list of samples, mineral chemical data, whole rock and glass chemical data, tests of data quality, and results of thermobarometry.

ABSTRACT

The petrogenetic processes through which peralkaline silicic magmas are generated in oceanic island environments, as well as the controls on their eruptive behaviour, are not well understood. This study utilises two such systems, Pico Alto and Furnas, Azores, to elucidate the petrogenesis, storage conditions, and eruption of peralkaline silicic magmas, and employs a variety of complementary approaches, including petrographic analysis, whole rock and mineral chemistry, thermobarometry, and petrogenetic modelling. For both of the investigated systems, shallow-crustal, volatile-undersaturated fractional crystallisation of mantle-derived parental melts is the dominant mechanism of magmatic differentiation. Magma mixing and mingling processes are also shown to play a key role, with abundant evidence for mixing of trachytic magmas with either trachytic or mafic magmas. Furthermore, mingling between trachytic magmas and syenitic crystal mushes is recorded as enclaves in syenitic ejecta which represent the near-complete, *in-situ* crystallisation of trachytic magmas in a thermal boundary layer at the margins of a magma reservoir. Phase assemblages of the syenitic ejecta range from miaskitic to agpaitic, and include rare zirconosilicates such as eudialyite and dalyite. The observed compositional variability of dalyite is demonstrably linked to the compositional evolution of residual melt, coupled with a nucleation delay introduced by variable pore sizes. At both volcanic centres, peralkaline silicic magmas accumulate in shallow crustal reservoirs and develop vertical compositional zonation. These reservoirs inhibit the ascent and eruption of less evolved compositions, and generate a compositional Daly gap. Contrasting eruptive behaviour observed both within and between the volcanic centres of this study is shown to be linked primarily to the degree of pre-eruptive magma volatile undersaturation and, at Furnas, interaction with external water. The presented models provide new insights into peralkaline magmatic systems, and may be applicable to similar peralkaline silicic systems, both within the Azores archipelago, and at similar oceanic island settings worldwide.

ACKNOWLEDGEMENTS

There are a number of people who must be acknowledged for their contribution to this study, whether academic, analytical, emotional, or financial.

First and foremost, I am entirely indebted to my Ph.D supervisor and advisor Dr Ralf Gertisser, not only for the extraordinary opportunity to undertake this project, but also for his invaluable support, endless patience, and good humour. It is clear that without his guidance, I would not be where I am today. I must also gratefully acknowledge my second supervisor Dr Brian O'Driscoll for his support and unerring advice throughout this process. I also acknowledge the co-authors of the journal articles which have been produced from this thesis, who I name in no particular order: Adriano Pimentel, Steve Self, José Pacheco, Andreas Kronz, Rob Jackson, and Sean Whitley. I am grateful to Martin Menzies and Ralf Halama for kindly accepting to review this work as external and internal examiners, respectively.

I wish to gratefully acknowledge the postgraduate cohort of which I was a small part. Their moral support and camaraderie proved vital throughout the process and so I name them in no particular order here: Liam Bullock, Lizzie Harling, Luke Hepworth, Amy Gough, Steve Rogers, Rosie Smithells, Amir Levy, John Weatherill, Tom Randles, Helen Doherty, Jamie Hansen, and Michael Kelly. I gratefully acknowledge Katie Preece for her greatly appreciated support in the acquisition of XRF analyses. I am also grateful to the support staff; to Pete Greatbatch and David Wilde for the production of myriad thin sections and invaluable assistance in the preparation of samples for FTIR analysis, to Richard Burgess for his assistance in all things computational and mechanical, and to Dave Emley, Ian Wilshaw, and Andy Lawrence for support throughout.

I acknowledge the Mineralogical Society of Great Britain and Ireland, the Keele University Postgraduate Association, and the International Association of Sedimentologists for providing funding for this research. I thank Andy Tindle and Bertrand Lézé for their analytical support in the production of electron microprobe and X-ray fluorescence data, respectively. I am also grateful to Matthew Kershaw and Jill Clarke for assistance with FTIR analyses.

I offer my sincere thanks to my family and extended family. Without their support and assistance, it is clear that this project would not have been possible, and I owe them much. Finally, but by no means least, I offer my special thanks to my fiancé Kelly, for her patience, her assistance during fieldwork, and her understanding throughout this sometimes difficult process.

CONTENTS

VOLUME I. THESIS

LIST OF FIGURES

LIST OF TABLES

LIST OF EQUATIONS

GENERAL ABBREVIATIONS

Ab	Albite
Ap	Apatite
Aeg	Aegirine
Aen	Aenigmatite
Amp	Amphibole
An	Anorthite
apfu	Atoms per formula unit
BSE	Back scattered electron
Ca-Ts	Ca-Tschermak
CCI	Caldeira-Castelinho Ignimbrite Formation
Cpx	Clinopyroxene
Dal	Dalyite
Di	Diopside
DRE	Dense rock equivalent
EAFZ	East Azores Fracture Zone
EAR	East African Rift
EDS	Energy dispersive spectroscopy
ED-XRF	Energy dispersive x-ray fluorescence
EMPA	Electron microprobe analysis
En	Enstatite
Eud	Eudialyte
eV	Electron volt
FMQ	Fayalite-magnetite-quartz buffer
fO_2	Oxygen fugacity
Fe-Ts	Ferri-Tschermak
Fs	Ferrosilite
Fsp	Feldspar
FTIR	Fourier transform infrared spectroscopy
GVI	Grota do Vale Ignimbrite Formation
Hd	Hedenbergite
Hem	Haematite
HFSE	High field strength element
HREE	Heavy rare earth element
ICP-AES	Inductively coupled plasma atomic emission spectroscopy
ICP-MS	Inductively coupled plasma mass spectrometry
Ign-i	Ignimbrite-I Formation
Ilm	Ilmenite
Jd	Jadeite
K_{alk}	Alkalinity modulus
LAI	Lajes-Angra Ignimbrite Formation
LET	Least evolved trachyte
LFG	Lower Furnas Group
LILE	Large ion lithophile element

LMI	Linhares-Matela Ignimbrite Formation
LREE	Light rare earth element
LTG	Lower Terceira Group
MAR	Mid-Atlantic Ridge
MET	Most evolved trachyte
MFG	Middle Furnas Group
MORB	Mid-ocean ridge basalt
MPa	Megapascal
Mt	Magnetite
OIB	Ocean island basalt
Or	Orthoclase
P	Pressure
PAVC	Pico Alto Volcanic Complex
PI	Peralkalinity index
PIF	Povoação Ignimbrite Formation
PNI	Pedras Negras Ignimbrite Formation
ppl	Plane polarised light
PSR	Peralkaline silicic rocks
Pyr	Pyrophanite
Qtz	Quartz
REE	Rare earth element
RFC	Rayleigh fractionation
rl	Reflected light
Sdl	Sodalite
SEE	Standard error of estimate
SEM	Scanning electron microscope
T	Temperature
TAS	Total alkalis vs. silica
Ti-Aeg	Ti-aegirine
Ti-Ts	Ti-Tschermak
UFG	Upper Furnas Group
Usp	Ulvöspinel
UTG	Upper Terceira Group
VFI	Vila Nova-Fanal Ignimbrite Formation
WAFZ	West Azores Fracture Zone
WD-XRF	Wavelength dispersive x-ray fluorescence
Wo	Wollastonite
xpl	Cross polarised light
XRF	X-ray fluoresence

CHAPTER 1: INTRODUCTION

1.1 Chapter outline

This chapter provides a brief outline of this study, including an introduction to the topics addressed in this work and a general background on the geology of the study area. The rationale of the project is then discussed in detail, and the specific aims and objectives outlined. Finally, the structure of the thesis is provided, detailing the contents of each chapter.

1.2 General introduction

The processes through which silicic magmas are generated, transported, stored, and erupted have been the subject of study since the earliest petrological investigations, and their elucidation facilitates a greater understanding of the petrographical, chemical, temporal, and spatial diversity of igneous rocks. Advances during the late 20th and the early 21st century have highlighted the complex interplay of processes such as fractional crystallisation, magma mixing or mingling, and crustal assimilation that operate in silicic magmatic systems, and have provided a wealth of robust physical and geochemical models which can be applied to magmatic systems of variable scales and chemical compositions (e.g. Hildreth 1981; Sisson and Bacon 1999; Bachmann and Bergantz 2004; Hildreth 2004; Pistone *et al.*, 2015). Although peralkaline silicic rocks are volumetrically less significant than their subalkaline counterparts, their petrogenesis and eruption is often considered to be more complex (Macdonald, 2012). The application of magma system models derived from large-volume metaluminous rhyolitic systems (generally from subduction zone or continental geodynamic environments) to low-volume, peralkaline, oceanic island systems is compounded by the significant physio-chemical contrasts between the two. For example, peralkaline silicate melts have been shown to exhibit low viscosities when compared to metaluminous or peraluminous melts; such an observation has profound implications for the processes of magma evolution in such systems, and almost certainly plays a role in the eruptive behaviour of such magmas.

As such, this study addresses the petrogenesis and eruption of peralkaline silicic magmas in an oceanic island setting, utilising two case studies from the Azores archipelago: the Pico Alto volcanic complex on Terceira island, and Furnas volcano on São Miguel island. This involves a detailed petrographical and geochemical study targeting various peralkaline silicic lithologies that represent the range of compositions and eruptive styles observed in the Azores. This comprises a detailed petrological investigation into the pre-eruptive magma system of the ignimbrites of Terceira, and a

comparative study of the caldera-forming and post-caldera magma systems of Furnas volcano, São Miguel. Together, these case studies are then placed into the global context of peralkaline silicic magmatism, drawing upon examples of peralkaline silicic centres worldwide. Finally, the contrasting eruption styles of peralkaline silicic magmas are considered, aiming to place constraints upon the primary controls of the contrasting eruptive behaviour of peralkaline silicic magmas.

1.3 Background and rationale

The Azores archipelago comprises nine, widely spread volcanic islands which lie in the central north Atlantic Ocean (Lat. 37°N to 40°N, Long. 25°W to 32°W), 1,300 km west of the Portuguese mainland (Figure 1.1). The islands represent the subarial portions of a large submarine plateau (the Azores Plateau), which straddles the Mid-Atlantic Ridge (MAR). Whilst the two westernmost islands (Corvo and Flores) lie to the west of the MAR, the remaining seven islands lie to the east, either close to, or on, a hyper-slow spreading centre named the Terceira Rift. The volcanic activity of the region is widely acknowledged to result from the complex interaction between the MAR and a melting anomaly often referred to as the Azores Mantle Plume, though the precise nature of the anomaly remains a matter of some debate (e.g. Schilling, 1991; Widom & Shirey, 1996; Courtillot *et al.*, 2003; Beier *et al.*, 2012 and references therein; Métrich *et al.*, 2014). Like many oceanic island volcanic systems associated with mantle plumes, the Azorean islands have erupted magmas belonging to an alkaline trend with Na/K > 1, and a bimodal compositional distribution which indicates the presence of a Daly gap (White *et al.*, 1979; Zanon, 2015b). Mafic magmas (typically basalt to hawaiite) are generally the most common, being erupted as thin lava flows and associated scoriaceous pyroclastic material, from fissure zones comprising multiple fractures, generally exhibiting a WNW-ESE trend (e.g. Zanon, 2015b). In contrast, silicic magmas (typically trachytic in composition) are predominantly erupted from vents within central volcanoes during Plinian to sub-Plinian events, and exhibit a wide range of eruption styles, including pumice falls and pyroclasic density currents during sub-Plinian to Plinian events (e.g. Self, 1971; Duncan *et al.*, 1999; Pimentel *et al.*, 2015), as well as lava domes and coulées during effusive activity (e.g. Self,1976). Furthermore, silicic magmas are frequently peralkaline, ranging from comendite and comenditic trachyte to pantellerite and pantelleritic trachyte.

As such, the Azores exhibit a number of petrological problems: 1) How do the silicic magmas form?, 2) how and when do they become peralkaline?, and 3) what

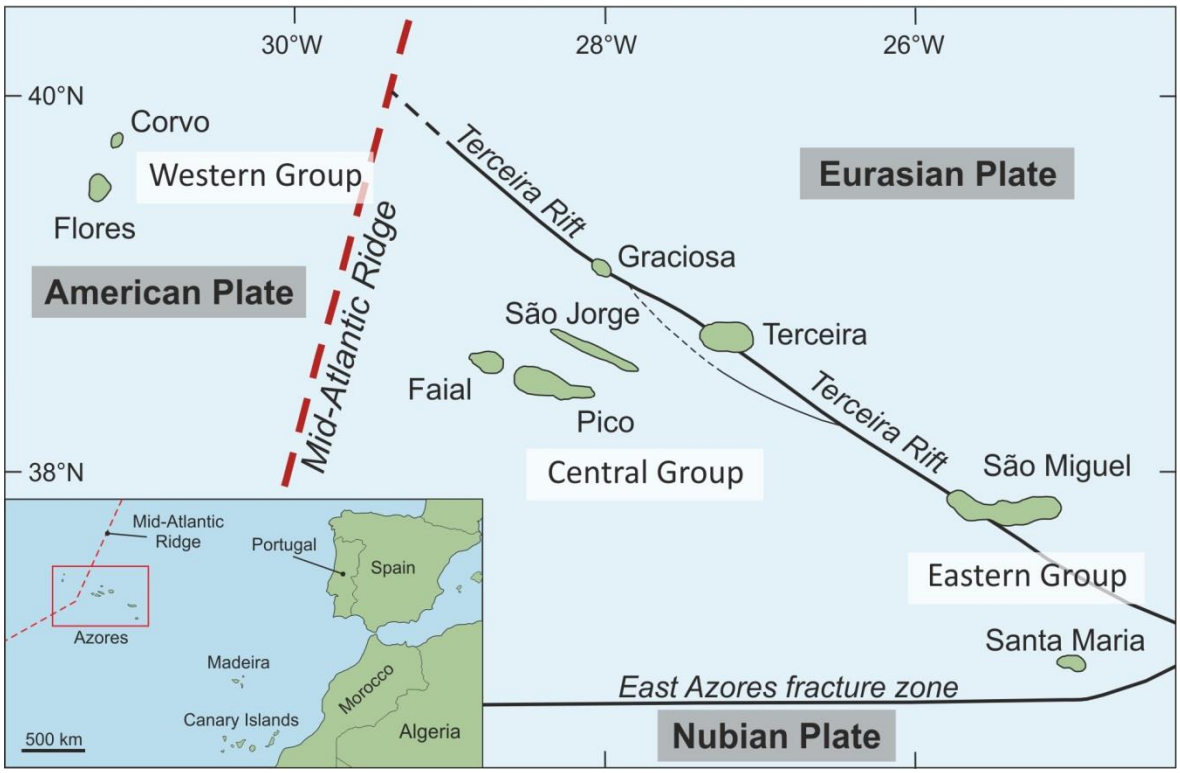

FIGURE 1.1: Generalised map showing the tectonic arrangement of the Azores archipelago. Tectonic plates are shown in grey boxes, island groupings in white. Inset: Location map showing the position of the Azores archipelago within the North Atlantic Ocean.

controls their eruptive diversity? To address these fundamental research questions, this study utilises two case studies; the Pico Alto volcanic complex (and by extension, Guilherme Moniz volcanic centre), Terceira island, and Furnas volcano, São Miguel island. On Terceira, focus is given to the major ignimbrite-forming phases of the island's volcanic history. Although the deposits of pyroclastic density currents are not uncommon on Atlantic island volcanoes, on Terceira they constitute a significant proportion of the islands volcanic stratigraphy, with at least seven ignimbrite-forming eruptions of peralkaline silicic magma in the last 90 ka. With the exception of a small number of thin pumice fall deposits at the base of two of the ignimbrite formations, evidence is lacking for the presence of sustained Plinian eruption columns, suggesting that these eruptions essentially 'boiled-over'. During the ~ 20 to 23 ka between the most recent ignimbrite-forming phase and the present, the eruptive behaviour of Pico Alto has been dominated by effusive activity.

In contrast, Furnas volcano on São Miguel exhibits a volcanic history in which peralkaline silicic magmas have been erupted in a variety of styles. At least two caldera-forming events led to the production of ignimbrites similar to those of Terceira. The most recent activity of the volcano has been limited to sub-Plinian eruptions which generated substantial pumice fall deposits and rare pyroclastic surges. A number of these eruptions appear to have been terminated with the extrusion of a lava dome of similar composition to the earlier erupted material.

A detailed petrological study of both locations will allow the reconstruction of the prevailing petrogenetic processes and P-T-fO_2-*X* conditions of the underlying magma reservoirs, and will represent a valuable contribution to the understanding of the petrogenesis of peralkaline silicic magmas, not only within the regional context of the Azores, but also in the larger, global context of peralkaline silicic magmatism, in which the Azores are, at least to some extent, somewhat underrepresented. Furthermore, the post-caldera sub-Plinian eruptions provide the opportunity to evaluate the temporal evolution of a peralkaline silicic magma reservoir over a geologically short period of ~ 5 ka.

The quantification of the pre-eruptive P-T-fO_2-*X* conditions of both systems will also facilitate a discussion on the most likely controls of diverse eruptive styles exhibited by Pico Alto and Furnas. Eruptive behaviour is generally accepted to be controlled by the complex interplay of various processes, including magma ascent rates, composition, rheology, supply, and initial pre-eruptive volatile contents (e.g. Jaupart and Allègre, 1991; Woods and Koyaguchi, 1994; Barclay *et al.*, 1996; Dingwell *et al.*, 1998; Andújar and Scaillet, 2012 and references therein), as well as additional external factors such as the syn-eruptive widening of the vent, (e.g. Wilson *et al.*, 1980) and interaction of ascending magmas with external water (Self and Sparks, 1978; Kokelaar, 1986). Many of these variables can be investigated directly if the pre-eruptive P-T-fO_2-*X* conditions are known, allowing constraints to be placed upon the origins of diverse eruptive behaviour of peralkaline silicic magmas.

Finally, the results of this study have clear implications for ongoing risk management in the Azores. The most recent ignimbrite-forming episode on Terceira (~ 20 to 23 ka) produced an ignimbrite which, despite it's relatively low volume (at least 0.3 km^3 DRE, Self, 1976), covered most of the island (Gertisser *et al.*, 2010), including the modern location of the island's only airport. A greater understanding of the processes which might lead to a recurrence of ignimbrite-forming volcanism on Terceira is clearly of great importance. Similarly, the caldera-forming episodes of Furnas volcano might be expected to yield ignimbrites of up to ~ 2 km^3 DRE, based upon the largest such event. Even the comparatively low volume (generally < 0.3 km^3 DRE) post-caldera eruptions of Furnas have been demonstrated to be capable of covering nearby towns in as much as 16 m of tephra fall, inevitably leading to structural failure of buildings as far away as the regional capital of Ponta Delgada (~ 30 km from Furnas).

1.4 Aims and objectives

As discussed above, the ultimate aims of this study are to investigate the petrogenetic process operating within two peralkaline silicic magmatic systems, constrain the P-T-fO_2 conditions under which the erupted magmas are stored and evolve, and to elucidate the primary controls upon the eruptive behaviour of such magma compositions, facilitating a discussion on the origins of diverse eruptive behaviour observed both within and between individual volcanic centres. As such, this study is divided into four principal aims, detailed below:

Aim 1: To place quantitative constraints upon the petrogenesis and pre-eruptive magma storage conditions of ignimbrite-forming eruptions from Terceira.

Objective 1.1: Utilise petrogenetic models to evaluate the generation and differentiation of peralkaline silicic magmas on Terceira.

Objective 1.2: Apply thermobarometric models to place constraints upon the P-T-fO_2 conditions of the pre-eruptive magma system.

Objective 1.3: Produce a schematic model for the Terceiran magma plumbing system, accounting for observed petrographical and geochemical features.

Aim 2: To investigate the petrogenesis and pre-eruptive magma storage conditions of the caldera-forming and the post-caldera eruptions of Furnas volcano, São Miguel.

Objective 2.1: Generate petrogenetic models to determine the origin of the peralkaline silicic magmas of Furnas volcano.

Objective 2.2: Investigate the pre-eruptive P-T-fO_2 conditions of the peralkaline silicic magmas through the application of thermobarometry.

Objective 2.3: Produce a schematic model for the Furnas magma plumbing system, accounting for observed petrographical and geochemical features.

Objective 2.4: Provide a critical comparison of the caldera-forming and post-caldera magma systems of Furnas.

Aim 3: To compare critically the magma plumbing systems of Terceira and Furnas with other peralkaline silicic centres, both within the Azores archipelago, and worldwide.

Objective 3.1: Compile available data for the P-T-fO_2-*X* conditions and volatile contents of peralkaline silicic systems.

Aim 4: To provide insight into the factors controlling the contrasting eruptive behaviour of peralkaline silicic magmas.

Objective 4.1: Investigate the roles of magma composition, volatile content, storage depth, and viscosity in the determination of eruptive style.

1.5 Thesis outline

This thesis is built around two complimentary studies into separate peralkaline silicic centres which constitute Chapters 4 and 5. Chapters 1, 2, and 3 are intended to introduce the study and provide background material relevant to the subject matter and the methods employed throughout this thesis. The results of chapters 4 and 5 are combined and expanded upon in chapter 6, which places this study into a global context and discusses the most promising targets for future investigation. Finally, chapter 7 provides a summary of the main conclusions of this work. The entire dataset used by this study, as well as validation of analytical data quality, is given in a number of appendices. The contents of chapter 4, and to a lesser extent chapter 6, are either in press or being prepared for submission for publication (Jeffery *et al.*, 2016a, 2016b). Similarly, a significant proportion of the contents of chapter 5 have been accepted for publication (Jeffery *et al.*, 2016c), and the remainder is currently in preparation (Jeffery *et al.*, 2016d).

Chapter 1 – Introduction

This chapter provides an introduction to the contents of this thesis, including a general introduction to the subject matter of this thesis, a brief outline of the study area and its geology, as well as the justification for, and the precise aims and objectives of, this research project. Additionally, an outline of the thesis structure is provided, including a summary of each of the presented chapters.

Chapter 2 – Literature review and context

The second chapter of this thesis provides a full literature review for this study. The tectonic setting of the Azores archipelago is discussed, providing relevant background for the following chapters. This is followed by a broad review of magma genesis in oceanic island volcanic settings, and a specific review relating to the petrogenesis and eruption of Azorean magmas. Additionally, a review of peralkaline silicic magmas is presented,

covering the origins, occurrence, and geochemical characteristics of such magmas. Location-specific literature reviews are provided in Chapters 4 and 5.

Chapter 3 – Methodologies

This chapter discusses the various analytical techniques employed by this study, including WD-XRF, ED-XRF, ICP-AES, ICP-MS, EMPA, SEM, and FTIR. Tests of data quality for each method are given in Appendix E. Additionally a full account of each of the applied thermobarometrical and petrogenetic models is given, including equilibrium testing procedure and selected partition coefficients.

Chapter 4 – The peralkaline ignimbrite-forming magmas of Terceira

The fourth chapter of this thesis represents a petrological study of the pre-eruptive magma system of the ignimbrite-forming eruptions of Terceira. The greater part of this chapter is in preparation for submission to the *Journal of Petrology*, in a manuscript entitled "Petrogenesis of the peralkaline ignimbrites of Terceira, Azores" (Jeffery *et al.*, 2016b). This manuscript was produced in collaboration with R. Gertisser, B. O'Driscoll, A. Pimentel, J. M. Pacheco, and S. Self. My contribution to the data collection and writing was 75 % and 80 %, respectively. Additionally, a small portion of this chapter comprises a study into the compositional variability of dalyite, a rare potassium zirconosilicate that was identified in the lithologies of this study. The results of this study have been accepted for publication in a research article in *Mineralogical Magazine*, entitled "On the compositional variability of dalyite, $K_2ZrSi_6O_{15}$: a new occurrence from Terceira island", and are, at the time of writing, in press (Jeffery *et al.*, 2016a). This article was produced in collaboration with R. Gertisser, R. A. Jackson, B. O'Driscoll, and A. Kronz. My contribution to the data collection and the writing of the manuscript was 80 % and 80 %, respectively.

Chapter 5 – Constraints upon the magma system of Furnas volcano, São Miguel

This chapter details the results of a petrological investigation into the pre-eruptive magma system of both the caldera-forming and the post-caldera phases of Furnas volcano. The larger part of this chapter deals with the temporal evolution of the post-caldera magma system at Furnas, and has been accepted for publication in *Contributions to Mineralogy and Petrology* as a research article entitled “Temporal evolution of a post-caldera, mildly peralkaline magmatic system: Furnas volcano, São Miguel, Azores” (Jeffery *et al.*, 2016c). This article was produced in collaboration with R. Gertisser, B. O’Driscoll, J. M. Pacheco, A. Pimentel, S. Whitley, and S. Self. My contribution to the data collection and the writing of the manuscript was 75 % and 80 %, respectively. The remainder of the chapter, which deals with the older, caldera-forming deposits of Furnas, is currently being prepared as a manuscript intended for submission to the *Journal of Volcanology and Geothermal Research (*Jeffery *et al.*, 2016d). In this instance, my contribution to data collection and manuscript preparation was 80 % and 80 %, respectively.

Chapter 6 – The magma systems of Terceira Island and Furnas volcano, São Miguel: implications for the evolution and contrasting eruption styles of peralkaline magmas

This chapter represents a synthesis of chapters 4 and 5, drawing together the results of both case studies and discussing them in the larger context of peralkaline silicic magmatism. The pre-eruptive magma systems of both case studies are compared directly with peralkaline magma systems from similar and contrasting geodynamic environments, facilitating a broader discussion on the petrogenetic processes operating in peralkaline magma systems. Furthermore, this discussion is then applied to the topic of eruptive behaviour, linking the processes of magma evolution and the conditions of magma storage to the contrasting eruption styles observed. Finally, the implications of this study are utilised to highlight potentially promising areas of further research.

Chapter 7 – Summary and conclusions

The final chapter of this thesis provides a concise summary of the results of the research presented, and the implications for peralkaline magma systems.

CHAPTER 2: LITERATURE REVIEW AND CONTEXT

2.1 Chapter outline

This chapter is intended to provide a review of the fundamental literature relating to the topics covered by this thesis, upon which the following chapters will build. This begins with a discussion of the complex geodynamic setting of the Azores archipelago, providing a structural context for the following chapters. This is followed by a review of magma genesis in oceanic island volcanic settings and, more specifically, in the Azores archipelago. Finally, a brief review is provided of peralkaline rocks, including their geochemical characteristics, the petrogenetic processes from which they are derived, and their global occurrences and tectonic associations. A review of more specific topics, such as the volcanic structure and stratigraphy of each of the two islands of this study, is included in the corresponding chapter.

2.2 The geodynamic setting of the Azores archipelago

The Azores archipelago comprises nine islands located in the central North Atlantic Ocean (see Section 1.3). The islands themselves are divided geographically into the western, central, and eastern groups (Figure 1.1), and represent the subaerial expression of the Azores Plateau, a bathymetric and gravity anomaly denoting a morphologically complex area (~ 5.8×10^6 km^2) of thickened oceanic crust that formed between 20 and 7 Ma (e.g. Kaula, 1970; Krause and Watkins, 1970; Luis *et al.*, 1994; Gente *et al.*, 2003; Luis and Miranda, 2008; Marques *et al.*, 2013). The plateau is broadly triangular in shape, bounded by three major tectonic features; the Mid-Atlantic Ridge in the west, the East Azores Fracture Zone (EAFZ) to the south and the Terceira Rift to the north-east (Krause and Watkins, 1970; Ridley *et al.*, 1974; Madeira and Ribeiro, 1990) (Figure 2.1). Together these structures mark a tectonic triple junction between the North-American, Eurasian and Nubian plates (Vogt and Jung, 2004; Silveira *et al.*, 2006; Marques *et al.*, 2013). The Mid-Atlantic Ridge runs approximately N-S between the western and central island groups, bisecting the Azores Plateau asymmetrically. As it passes through the Azores region, its median valley becomes significantly less defined (Krause, 1966), dying out from the north at around 39°30'N, and from the south at around 37°30'N (Searle, 1980). Within this diffuse region, the trend of the Mid-Atlantic ridge is significantly altered from N-S to NE-SW by a high density of transform faults (Madeira and Ribeiro, 1990).

The EAFZ is a seismically–active transform fault system that represents the westernmost expression of the Alpide Tectonic Zone, extending eastward from the Strait of Gibraltar to the MAR and marking the boundary between the Eurasian and Nubian plates (Ridley *et al.*, 1974; Silveira *et al.*, 2006). It is believed to continue to the Sohm Abyssal Plain as the seismically-inactive West Azores fracture zone (WAFZ), offset to the North by the MAR (Tolstoy, 1951).

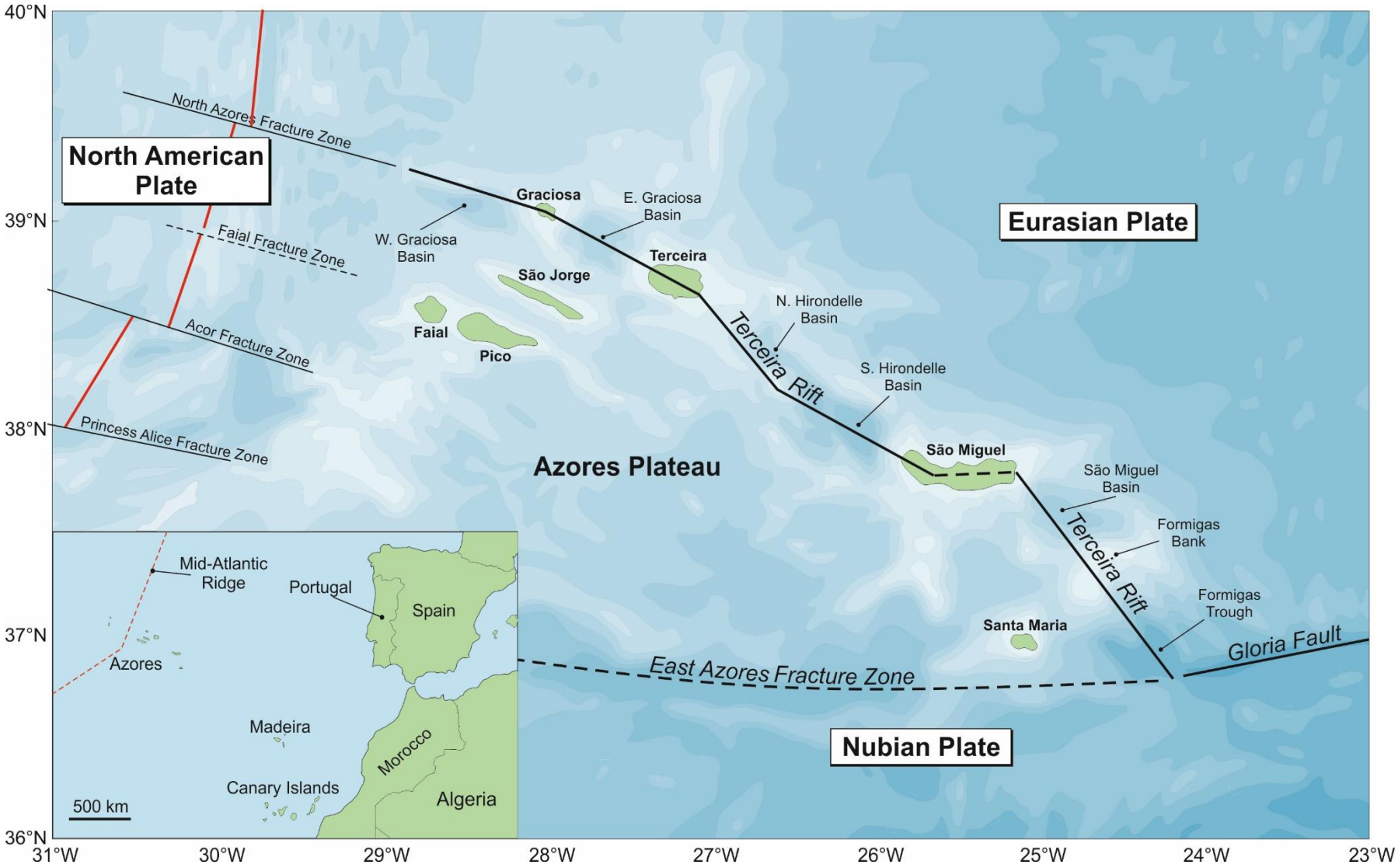
40°N
39°N
38°N
37°N
36°N
31°W
30°W
29°W
28°W
27°W
26°W
25°W
24°W
23°W
North American Plate
Eurasian Plate
Nubian Plate
Azores Plateau
North Azores Fracture Zone
Faial Fracture Zone
Acor Fracture Zone
Princess Alice Fracture Zone
East Azores Fracture Zone
Gloria Fault
Graciosa
E. Graciosa Basin
W. Graciosa Basin
São Jorge
Terceira
Faial
Pico
N. Hirondelle Basin
S. Hirondelle Basin
Terceira Rift
São Miguel
São Miguel Basin
Formigas Bank
Formigas Trough
Santa Maria
Mid-Atlantic Ridge
Portugal
Spain
Azores
Madeira
Canary Islands
Morocco
Algeria
500 km

◄ **FIGURE 2.1:** A map of the major tectonic features and plate boundaries of the Azores plateau, constructed after Searle (1980); Freire Luis *et al.* (1994); Vogt and Jung (2004). Bathymetry shown with contour intervals of 500 m. Inset: Location map showing the position of the Azores archipelago.

The Terceira Rift is defined by a series of basins and volcanic massifs, such as the islands of São Miguel, Terceira and Graciosa (Ridley *et al.*, 1974; Vogt and Jung, 2004), as well as the João de Castro seamount, a volcanically active seamount that became subaerial between the islands of Terceira and São Miguel in 1638 and 1720, but was rapidly eroded (Nunes *et al.*, 2003; Vogt and Jung, 2004). The Terceira Rift extends roughly SE from the Mid-Atlantic Ridge for 550 km before terminating at the Gloria Fault, defining a trend that runs obliquely to the EAFZ. The rift most likely originated as a 'leaky' transform fault, a term introduced by Menard and Atwater (1968), which formed in response to a change in the direction of crustal spreading (Krause and Watkins, 1970). Vogt and Jung (2004) proposed that, with a spreading rate of 2 to 4 mm/a, the Terceira Rift represents the slowest spreading-centre in the world, and considered it to mark the boundary between the Nubian and Eurasian plates; however, Marques *et al.* (2013) utilised GPS data to contest this hypothesis.

The Azores plateau is a morphologically complex area of elevated oceanic crust, asymmetric to the MAR and with a maximum altitude of 2,300 m above the surrounding -3,000 m sea floor (Ribeiro, 2002; Freire Luis and Neves, 2006). Its complexity is considered the result of interaction between tectonic and magmatic activity (Ribeiro, 2002). It exhibits a roughly triangular shape, defined by the MAR, EAFZ and TR, and has a surface area of approximately 400,000 km^2 (Lourenço *et al.*, 1998). Vogt and Jung (2004) utilised detailed aeromagnetic studies to suggest the presence of a separate Azores microplate between 10 – 3.85 Ma, taking on the movement of the Eurasian plate post-2.45 Ma. The GPS dataset provided by Marques *et al.* (2013) does not support this, instead suggesting that Nubia-Eurasia plate motion is accommodated by a 140 km-wide diffuse zone of extension, bounded to the north by the Terceira Rift.

2.3 Magma genesis in the Azores

2.3.1 The origin of oceanic island basalts (OIBs)

Oceanic island basalts (OIBs) are a group of geochemically-distinctive rocks that are found in both oceanic and continental settings, but are typically associated with oceanic islands and seamounts (e.g. Fitton, 2007; White, 2010). Due to their frequent occurrence in oceanic intraplate settings, their study has been instrumental in the understanding of mantle heterogeneity, melt generation and magma evolution (Hofmann, 2003). In such settings, where contamination with continental crust can be ruled out, their compositions can be related directly to their mantle source (Greenough *et al.*, 2005). As a group, they exhibit substantial geochemical variability (e.g. Gast *et al.*,1964; Dupré *et al.*, 1982; White, 1985; Allègre *et al.*, 1987; Weaver, 1991; Hanan and Graham, 1996; Hauri, 1996), which has required the distinction of mantle geochemical end-members, such as EM1, EM2, HIMU and FOZO, to account for their petrogenesis (e.g. Zindler and Hart, 1986; Hart, 1988). Despite this, OIBs can be distinguished readily from N-MORBs due to their distinctive isotope geochemistry and typically less depleted nature. For example, Fitton *et al.* (1997) presented the ΔNb parameter, which quantifies the deviation from a reference line in Nb/Y versus Zr/Y space, and utilised it to highlight the distinctive compositions of Icelandic basalts compared to N-MORBs (Figure 2.2). The geochemical and isotopic contrast between OIBs and N-MORBs is considered to reflect mantle heterogeneity, with N-MORBs originating within a source that has been progressively depleted by melt extraction (traditionally attributed to the upper mantle), and OIBs instead arising from a less depleted source region (generally considered to be the lower mantle) (e.g. Hofmann, 1997).

Various petrogenetic models have been proposed to reconcile the disparity between OIBs and N-MORBs with the structure of the mantle. The chain-like arrangement

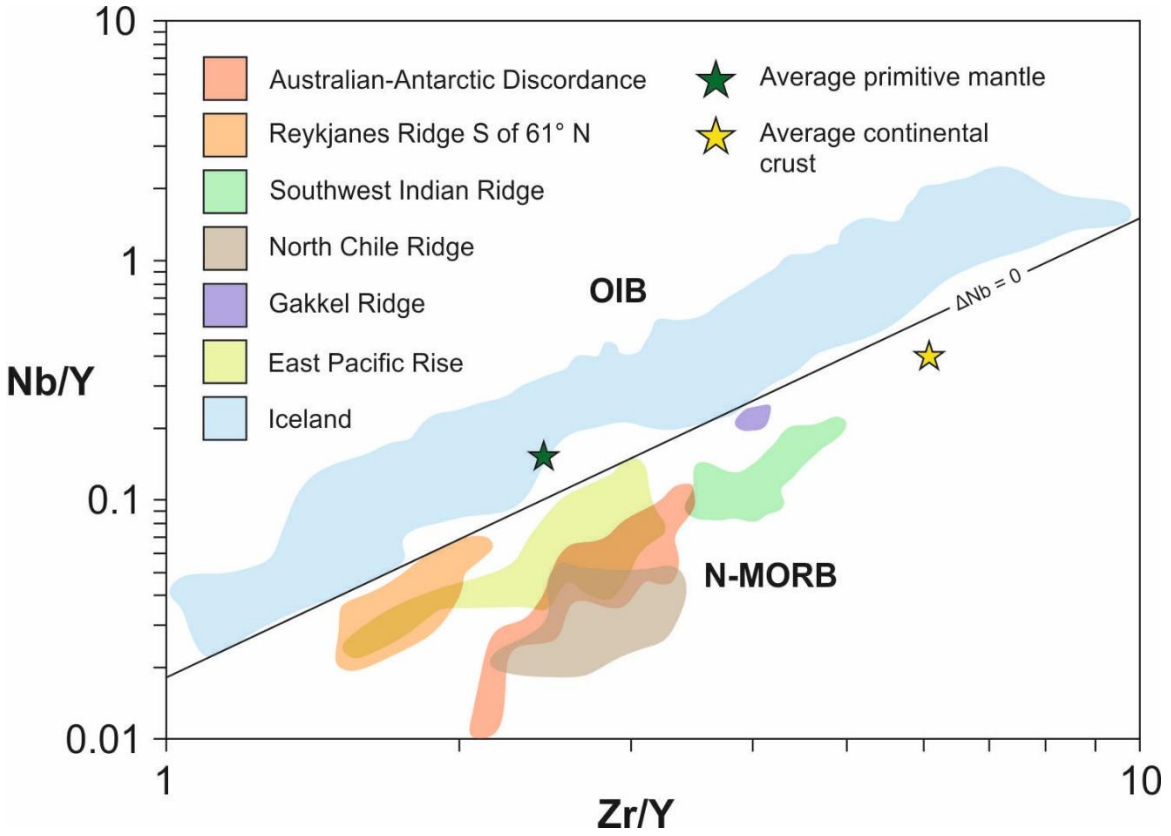

FIGURE 2.2 Discrimination diagram highlighting the variation in ΔNb between OIB and N-MORB compositions, utilising basalts from various oceanic ridge segments and the Icelandic neovolcanic zones. After Fitton *et al.* (1997)

of oceanic islands and seamounts led to the mantle plume hypothesis of Morgan (1971), which suggested that OIBs originate from upwelling plumes of recycled oceanic crust stored in the lower mantle (including subducted oceanic crust), whereas N-MORBs represented the upper mantle. Although adapted forms of the original plume model are frequently applied (e.g. Courtillot *et al.*, 2003; Ritsema and Allen, 2003; White, 2010), some authors largely reject it's application on the basis of numerous alternative interpretations of those datasets that are considered to form the core body of evidence in favour of mantle plumes (e.g. Anderson and Natland, 2005 and references therein; Foulger, 2012; Anderson, 2013). For example, the geochronologically-progressive volcanism of islands and seamounts, often cited as evidence for the plume theory, may also be used in support of alternative models such as sequential volcanic loading, propagating fractures, and membrane stresses (Clague and Dalrymple, 1987, 1989;

Koppers *et al.*, 2001). Furthermore, the application of the plume model typically involves the assumption of mantle homogeneity, which is contradicted by numerous studies which advocate mantle heterogeneity (e.g. Sleep, 1984; Hofmann and Jochum, 1996; Korenaga and Kelemen, 2000; Salters and Dick, 2002; Hofmann, 2003; Anderson, 2006).

2.3.2 Petrogenesis of Azorean magmas

The Azores plateau is widely believed to represent a region of interaction between the Mid-Atlantic Ridge (MAR) and a melting anomaly (e.g. Schilling, 1991). Since the initial recognition of plume-like characteristics in the Azores (e.g. Morgan, 1971; Schilling, 1975; White *et al.*, 1975), a large number of studies have contributed petrological and geochemical evidence that links the Azores source region to other proposed hot spots associated with mantle plumes. For example, Schilling (1975) noted that basalts from the Azores plateau portion of the MAR showed LREE enrichment relative to typical MAR basalts. Soon afterwards, the Azores plateau basalts were shown to have more radiogenic $^{87}Sr/^{86}Sr$ ratios and elevated concentrations of large-ion-lithophile elements (LILES), compared to those typical of basalts from more 'normal' MAR sections (White *et al.*, 1976). Schmincke (1973) applied whole-rock major element data to highlight the deviation of the Azores (as well as other Atlantic Ocean islands) from the hypothesis of McBirney and Gass (1967), which stated that the Niggli quartz number (i.e. the degree of silica over/undersaturation) of mantle-derived magmas and their derivatives should decrease with increasing distance from the MAR, resulting in silica-oversaturated magmas in the vicinity of the MAR, becoming silica-undersaturated towards the continents. Further isotopic studies highlighted low Nd and high Pb isotopic ratios in the Azorean tholeiites (e.g. Dupré and Allègre, 1980; Ito *et al.*, 1987). Widom and Shirey (1996) provided Os isotope data for various alkali basalts and trachybasalts from six of the nine Azorean islands, concluding that their unusually radiogenic signature was indicative of a mantle plume and could potentially result from a contribution from the lower mantle or the D"

layer. Further studies have added to this database of major, trace and isotopic dataset (e.g. Widom *et al.*, 1997; Turner *et al.*, 1997; Moreira *et al.*, 1999; Bourdon *et al.*, 2005; Madureira *et al.*, 2005; Jean-Baptiste *et al.*, 2009; Beier et al, 2008, 2010; Prytulak and Elliot, 2009; Beier *et al.*, 2012, 2013), building a substantial body of geochemical evidence to support the Azores plume model. Further support exists in the form of geophysical studies that revealed the presence of magnetic, tomographic, and gravimetric anomalies beneath the Azores archipelago (e.g. Searle, 1980; Freire Luis *et al.*, 1994; Goslin *et al.*, 1998; Cannat *et al.*, 1999; Escartín *et al.*, 2001; Silveira *et al.*, 2006), alongside geoid topography (e.g. Bowin *et al.*, 1984; Cazenave et al., 1992) and ridge-axis elevation (e.g. Anderson *et al.*, 1973; Le Douaran and Francheteau, 1981; Thibaud *et al.*, 1998).

However, since it's recognition, the nature and depth of the melting anomaly remains a subject of debate. Alternative or complimentary models of the derivation of enriched magmas in the Azores include the inclusion of additional mantle components, such as fragments of continental lithosphere, either remaining from the opening of the Atlantic (e.g. Bonatti, 1971) or delaminated and advected (e.g. McKenzie and O'Nions, 1983, 1995). Alternatively, subducted oceanic crust may represent an additional mantle component (e.g. Kurz *et al.*, 1982). Widom *et al.* (1997) showed that the source of São Miguel magmas has a similar trace element signature to hydrous metasomatised peridotite, and suggested the recycling of subcontinental lithospheric mantle that had been subjected to two distinctive metasomatism events.

In the scheme of Courtillot *et al.* (2003), where 49 catalogued hotspots were categorised according to properties such as buoyancy flux, rare gas isotopic ratios and shear velocities, the Azores do not classify as a 'primary' plume (i.e. a plume originating from the D" layer). Instead, the Azores plume was considered to be an upper mantle feature, ultimately derived from a passive response to lithospheric break-up. Whilst this would entirely contradict such studies as Widom and Shirey (1996), Courtillot *et al.* (2003) note that, in the case of the Azores, not all of the criteria are well constrained, and so their conclusions may be subject to change with further study. Beier *et al.* (2012) calculated

potential mantle temperatures that were relatively low (1,400 to 1,490 °C), even in the suspected region of the plumes centre. They postulate that this may indicate a high volatile content in the mantle source, which prompts partial melting and thus contributes an additional component to the melting anomaly. They conclude that magmatism in the Azores is therefore the result of both a thermal anomaly and volatile-induced melting.

As such, there is no clear consensus on the origin or nature of the Azores melting anomaly, with many contradictory or absent datasets; however, the current state of research does at least appear to suggest that the traditional model of a deep mantle upwelling is not valid for the Azores archipelago.

2.3.3 Volcanic activity of the Azores archipelago

The volcanic activity of the nine islands of the Azores is likely to extend as far back as the Oligocene-Miocene (Zanon, 2015b) (Figure 2.3). The majority of the erupted magmas of the Azores archipelago have been mafic in composition, typically ranging from basalt or alkali basalt to hawaiite (Zanon, 2015b). These have predominantly been erupted effusively, forming thin lava flows (e.g. Booth *et al.*, 1978; Zanon *et al.*, 2013), although a smaller number of cinder cones, hornitos, and spatter ramparts are also present. A number of hydromagmatic eruptions have also occurred (e.g. the São Roque tuff cone (Zanon *et al.,* 2009); the Capelas tuff cone (Solgevik *et al.,* 2007; Mattsson, 2010), and the Serreta Ridge (Gaspar *et al.*, 2003)). More evolved, silicic magmas have been erupted primarily via Plinian or sub-Plinian activity from the central vents of the various volcanic complexes (e.g. Self, 1976; Guest *et al.*, 1999; Gertisser *et al.*, 2010; Pimentel *et al.*, 2015). Silicic magmas have also been erupted effusively, forming lava domes and coulées (e.g. Booth *et al.*, 1978; Self, 1974, 1976; Pimentel, 2006).

The large number of published geochemical datasets (Self and Gunn, 1976; White *et al.*, 1979; Widom and Shirey, 1996; Widom *et al.*, 1997; Moreira *et al.*, 1999; Claude-Ivanaj *et al.*, 2001; Snyder *et al.*, 2004, 2007; Madureira *et al.*, 2005; França *et al.*, 2006;

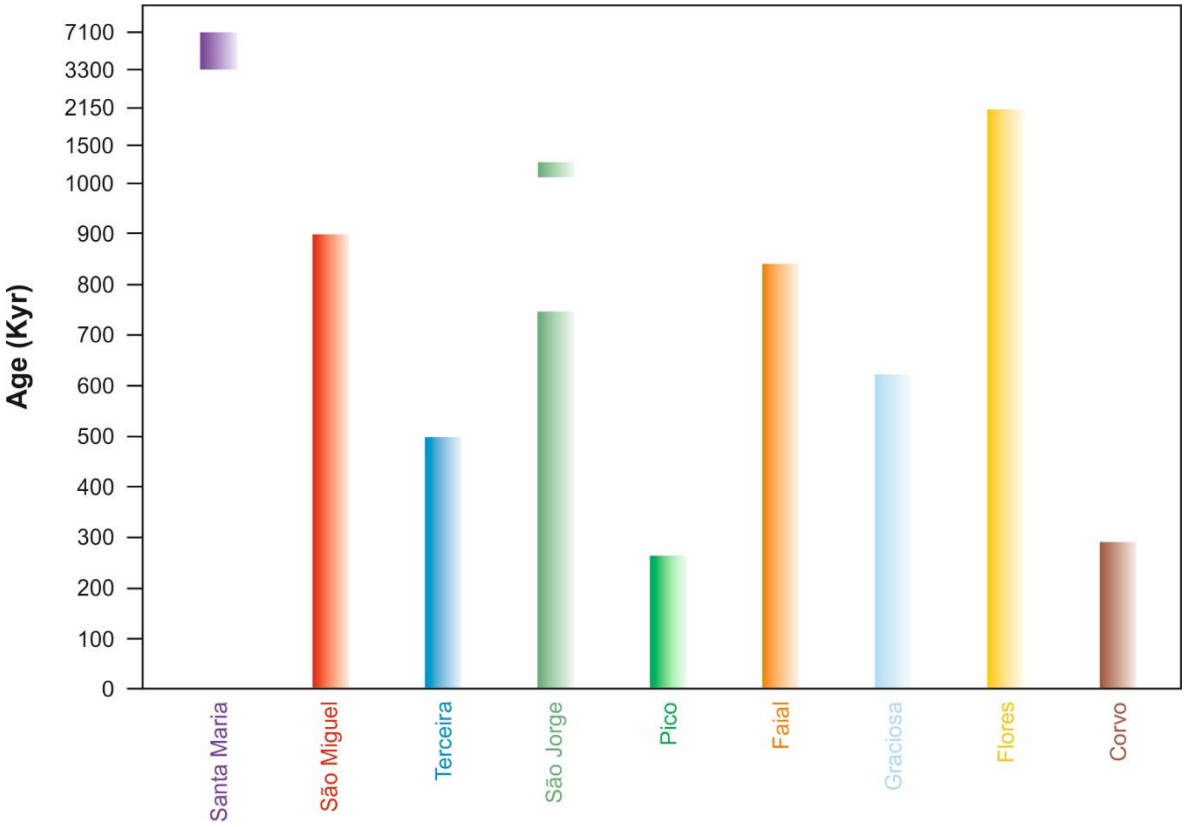

FIGURE 2.3: Relative ages of volcanic activity across the Azores archipelago. Data from Abdel-Monem *et al.* (1975), Self (1976), Féraud *et al.* (1980), Gandino *et al.* (1985), Serralheiro *et al.* (1989), Johnson *et al.* (1998), Nunes (1999), Calvert *et al.* (2006), Hildenbrand *et al.* (2008). Figure after Zanon (2015b)

Beier *et al.*, 2006, 2007, 2008, 2012, 2013; Elliott *et al.*, 2007; Pfänder *et al.*, 2007; Millet *et al.*, 2009; Prytulak and Elliott, 2009; Madureira *et al.*, 2011, Genske *et al.*, 2012; Larrea *et al.*, 2013; Zanon *et al.*, 2013) allowed Zanon (2015b) to discuss at length the petrology of the erupted Azorean magmas. When considered as a whole, the Azorean suite ranges from 40 to ~ 68 wt. % SiO_2 (Figure 2.4), forming an alkaline magma series from basalt or alkali basalt to trachyte, with some basanites on Santa Maria. Alkali contents lie between 1.7 and 13.5 wt. %, and Na/K ratios exceed unity. White *et al.* (1979) first noted that the erupted magmas of the Azores were bimodal in composition, with a relative lack of intermediate magmas highlighting the presence of a 'Daly gap'. Mafic products have been generally erupted from fissural zones, and range from sub-aphyric to highly porphyritic with abundant olivine xenocrysts (e.g. Larrea *et al.*, 2013; Zanon *et al.*, 2013; Zanon and Frezzotti, 2013). Glomerocrysts of varying composition, including gabbroic, dunitic, and dioritic, are found in mafic lavas across the archipelago (Zanon, 2015b).

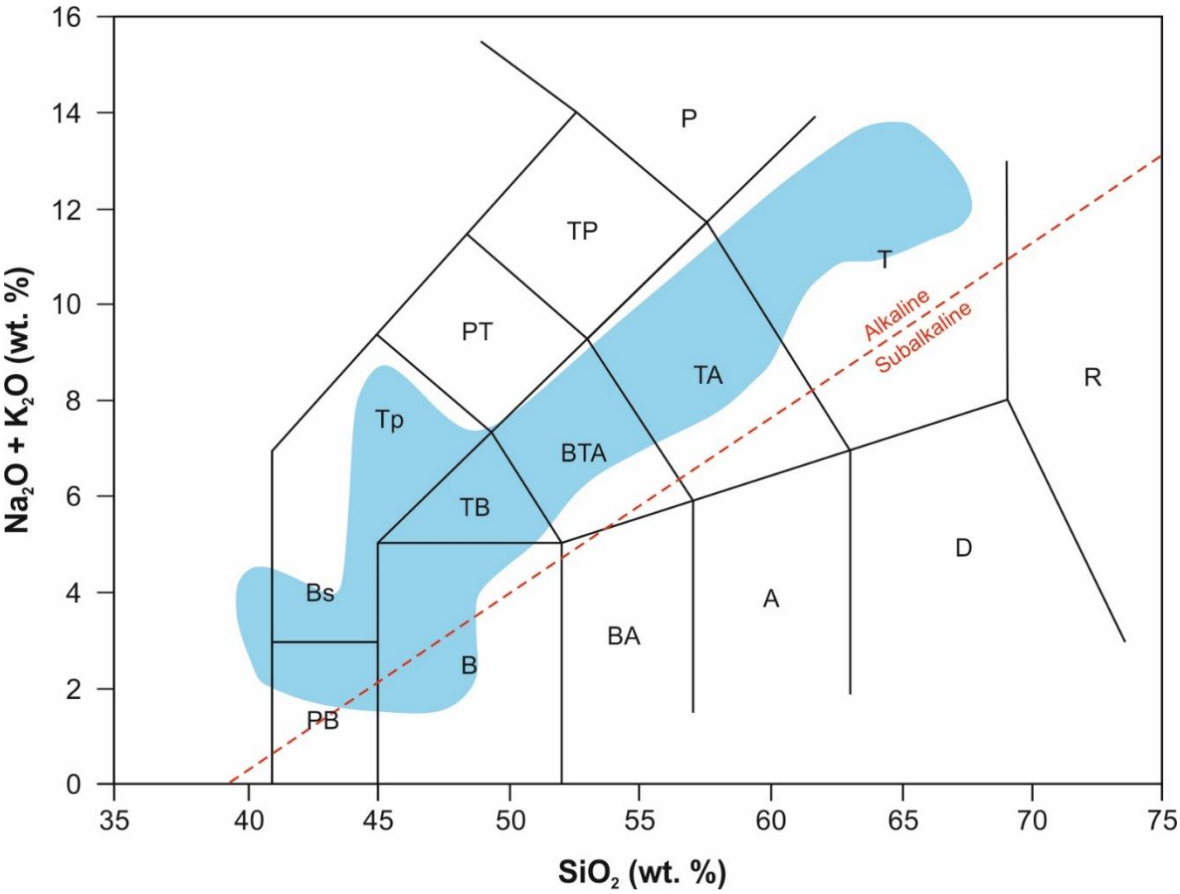

FIGURE 2.4: Total alkali vs. silica classification of the volcanic products of the Azores archipelago (blue field). Abbreviations used: PB = picrobasalt, B=basalt, BA = basaltic andesite, A = andesite, D = dacite, R = rhyolite, Bs = basanite, TB = trachybasalts, BTA = basaltic trachyandesite, Ta = trachyandesite, T = trachyte, Tp = tephrite, PT = phonotephrite, TP = tephriphonolite, P = phonolite. Figure after Zanon (2015b)

Intermediate magmas (mugearites or basaltic trachyandesites, and benmoreites or trachyandesites) are infrequent in occurrence, but have been described in some detail on São Miguel (Beier *et al.*, 2006), Faial (Zanon *et al.*, 2013), Corvo (Larrea *et al.*, 2013), Graciosa (Zanon, 2015b), and Terceira (Mungall, 1993). Mugearitic compositions are often highly porphyritic (~ 30 vol. %), but benmoreitic compositions are frequently close to aphyric. Mineral assemblages of each are generally dominated by plagioclase, with subsidiary clinopyroxene and olivine (Zanon, 2015b). In contrast to the mafic magmas, the trachytic magmas are generally sub-aphyric to aphyric, with phase assemblages which are invariably dominated by alkali feldspar, with lesser plagioclase, clinopyroxene, Fe-Ti oxides, biotite, olivine, and rare kaersutite. Accessory phases include quartz, apatite, aenigmatite, eudialyte, and astrophyllite.

Zanon (2015b) noted compositional variation of the mafic magmas of each island at MgO contents in excess of 5 wt. %. For example, the mafic magmas of São Miguel are generally more potassic than those of other islands, and also have higher P_2O_5 concentrations. The mafic magmas of Santa Maria are generally lower in SiO_2 than on other islands, lying between ~ 42 and ~ 43 wt. %. In contrast, those of Pico cluster around 47 wt. %. Furthermore, the magmas of Pico and Faial are generally more sodic than those of other islands. This variability likely reflects variation in the degree and depth of partial melting, as well as the role of crystal accumulation.

2.4 The evolution and chemistry of peralkaline rocks

2.4.1 Characteristics of peralkaline rocks

The condition of peralkalinity is defined as a molecular excess of (Na_2O + K_2O) over Al_2O_3, and is quantified by the peralkalinity index (P.I. = mol. (Na_2O + K_2O)/Al_2O_3), where values in excess of unity indicate peralkalinity. Additional indicators of peralkalinity include normative acmite (ac), elevated FeO_t contents, extreme enrichment of the halogens (Cl and F, which have been reported to have reached values in excess of 1 wt. %), the presence of key index minerals, such as Na-pyroxene, Na-amphibole and aenigmatite, and extreme enrichment of the rare earth elements (REE), high field strength elements (HFSE) and large ion lithophile elements (LILE) (Macdonald, 2012). Peralkaline rocks exist over a large range in silica contents, encompassing comendites (high Al_2O_3, low FeO_t peralkaline rhyolite) and pantellerites (low Al_2O_3, high FeO_t peralkaline rhyolite) and their trachytic equivalents (see Macdonald, 1974a), granites (e.g. Harris and Rickard, 1987), nepheline syenites (e.g. Marks *et al.*, 2008; Andersen *et al.*, 2010) and most of the lamproites (e.g. Bergman, 1987; Mitchell and Bergman, 1991). The lamproites are a group of rare rocks of peralkaline, ultrapotassic composition, that do not fall within the scope of this study. As such, this review focuses instead upon the peralkaline silicic rocks (i.e. comendites, pantellerites, comenditic trachytes, pantelleritic trachytes; Macdonald, 1974a), and their intrusive equivalents (granites and syenites).

In the peralkaline silicic rocks (PSRs), defined here as rocks of broadly felsic composition with a PI in excess of unity, mineral assemblages typically include alkali-feldspar, clinopyroxene, Fe-rich olivine, sodic- and sodic-calcic-amphiboles (generally riebeckite, arfvedsonite or katophorite, Leake *et al.*, 1997), aenigmatite, biotite, Ti-magnetite, ilmenite, apatite and quartz or feldspathoid-group minerals (e.g. Carmichael, 1962; Sutherland, 1974). Alkali-feldspar is typically the most abundant phase, with both anorthoclase and sanidine reported (e.g. Ablay *et al.*, 1998; Peccerillo *et al.*, 2003; Avanzinelli *et al.*, 2004; Ren *et al.*, 2006). Clinopyroxene generally exhibits a

compositional range from hedenbergite, through aegirine-augite and aegirine, with or without a compositional gap between the Ca and Na end-members (e.g. Aoki, 1964; Ferguson, 1978; Marks *et al.*, 2004; Halama *et al.*, 2005). Carmichael (1962) first noted an antipathetic relationship between the mineral aenigmatite and both olivine and ilmenite. This relationship was expanded upon by Nicholls and Carmichael (1969), who highlighted a 'no-oxide' field in T-fO_2 space where depending upon the peralkalinity of the magma, aenigmatite would crystallise in place of Fe-Ti oxides.

Prior to the 1990s, PSRs were generally considered to have very low water contents, particularly when compared to metaluminous silicic rocks (e.g. Nicholls and Carmichael, 1969; Bailey and Macdonald, 1987). This was largely based upon the high Cl content of PSRs, which was considered to rule out the exsolution of water, but also because experimental phase equilibrium studies produced superior results with low water contents than with high water contents (e.g. Morey and Hesselgesser, 1952; Bailey, 1974; Scaillet and Macdonald, 2001). This hypothesis was challenged by melt inclusion studies, which suggested that numerous PSRs had elevated pre-eruptive water contents, often greater than 1.4 wt. % and up to 5 wt. % in some cases (e.g. Harris, 1986; Lowenstern and Mahood, 1991; Wilding *et al.*, 1993; Barclay *et al.*, 1996; Troll and Schmincke, 2002; Gioncada and Landi, 2010; Neave *et al.*, 2012). This view is now widely accepted.

The unusual, and often extreme, compositions of peralkaline silicic melts have significant implications for their rheological behaviour, which can in turn exert great control on pre-, syn- and post-eruptive processes. Fluorine has long been known to play a significant role in lowering melt viscosities by substituting for bridging oxygens (e.g. Wyllie and Tuttle, 1961; Manning, 1981; Dingwell *et al.*, 1985; Lange, 1994; Whittington *et al.*, 2001; Giordano *et al.*, 2004), and therefore acts as a major control on viscosity in F-enriched, peralkaline melts. Increasing water contents also leads to a decrease in viscosity, an effect that is magnified in felsic melts (Giordano and Dingwell, 2003). Additional volatiles such as CO_2, S, Br, I and Cl are broadly considered to be of less importance for viscosity determination (e.g. Dingwell and Hess, 1998; Zimova and Webb,

2006). As a result of fluorine and water enrichment, as well as the abundance of alkalis, peralkaline melts are known to exhibit lower viscosities than their metaluminous counterparts, which themselves have lower viscosities than peraluminous melts (e.g. Bottinga and Weill, 1972; Shaw, 1972).

More recent studies have noted significant differences and non-linear behaviour in the rheology of both dry and H_2O-bearing peralkaline and metaluminous melts, which are thought to reflect differences in their structural configuration (Giordano *et al.*, 2006). As a result, studies aimed at the production of a model for the prediction of melt viscosities (e.g. Hui and Zhang, 2007; Giordano *et al.*, 2008) have not yet succeeded in accurately predicting the viscosity of peralkaline melts, despite incorporation of temperature, water content and anhydrous composition (Di Genova *et al.*, 2013). The latter authors conducted an experimental study upon the viscosity of pantelleritic melt compositions at variable temperatures and water contents. Their comparison of experimental data with available viscosity models allowed them to propose a new model that can determine the viscosity of pantelleritic (highly peralkaline) melts, based upon water content and temperature, with an accuracy of 0.25 log units. Although they noted that further work is required to extend the compositional range of peralkaline melts to which the model might be applied, this represents a significant step in the modelling of peralkaline melts.

2.4.2 The origin of silicic peralkaline melts

Following the initial discovery of peralkaline silicic igneous rocks on Pantelleria Island by Foerstner (1881), multitudinous studies have aimed to elucidate and quantify the processes of magma petrogenesis and evolution that lead to the formation and eruption of these unusual magmas (e.g. Washington, 1913a, 1913b; 1914; Bowen, 1937; Zeis, 1960; Roux and Varet, 1975; Harris, 1983; Mahood, 1984; Mungall and Martin, 1995; Bohrson and Reid, 1997; Scaillet and Macdonald, 2001; White *et al.*, 2009; Markl *et al.*, 2010; Macdonald, 2012). Although there is no real consensus on the petrogenetic conditions

that lead to the generation of peralkaline silicic melts, multiple models have been proposed: 1) evolution via fractional crystallisation of a mantle-derived alkali basalt parent magma (e.g. Barberi *et al.*, 1975; Civetta *et al.*, 1998; Peccerillo *et al.*, 2007), possibly including some assimilation of the crust (e.g. Peccerillo *et al.*, 2003), 2) partial melting of either shallow level alkali gabbros, or lower crustal mafic lithologies, followed by fractional crystallisation (e.g. Trua *et al.*, 1999), 3) partial melting of continental crust due to fluxing of alkali-bearing volatiles (e.g. Black *et al.*, 1997), 4) volatile transfer between silicate melts and a separate vapour phase (e.g. Ewart *et al.*, 1968; Bailey and Macdonald, 1975), 5) high pressure partial melting of hydrous mantle lithologies and direct extraction of the resulting silicic magmas (e.g. Self and Gunn, 1976).

Of these models, the latter is the least favoured due to incompatibility with experimental data (e.g. Mysen *et al.*, 1974), and the first is perhaps the most frequently applied (e.g. Weaver, 1977; Novak and Mahood, 1986; Macdonald *et al.*, 1995, 2008; Civetta *et al.*, 1998; Peccerillo *et al.*, 2003; Sumner and Wolff, 2003; Avanzinelli *et al.*, 2004; Lowenstern *et al.*, 2006; White *et al.*, 2006, 2009; Flude *et al.*, 2008; Parker and White, 2008; Marshall *et al.*, 2009). Barberi *et al.* (1975) utilised major and trace element and Sr-isotope systematics to illustrate a genetic link between the mildly alkaline basalts and pantellerites of the Boina Centre, Afar Rift, Ethiopia, invoking shallow-crustal fractional crystallisation as the only required evolutionary process. Peccerillo *et al.* (2007) applied similar methods to the mafic to peralkaline silicic rocks of the northern sector of the main Ethiopian rift, and highlighted not only the prevalence of shallow-crustal fractional crystallisation, but also the need for minor interaction with crustal lithologies. The basalt-comendite and basalt-pantellerite suites of Terceira Island, Azores were investigated by Mungall and Martin (1995), who, on the basis of major and trace element modelling, concluded that the evolution of both suites was controlled by fractional crystallisation.

Although widely adopted, this petrogenetic model is not universal and multiple studies highlight the need for additional or alternative processes to fully account for the

generation of peralkaline silicic magmas. For example, Bohrson and Reid (1997, 1998) demonstrated that the peralkaline silicic magmas erupted on Socorro Island, Mexico, originated in a two stage process, beginning with the derivation of trachytic magmas via partial melting of alkali gabbros, followed by fractional crystallisation towards peralkaline trachytes and rhyolites. A similar conclusion was reached previously by Mahood *et al.* (1990) for the pantellerites of Pantelleria, Italy. The peralkaline rhyolites of the Greater Olkaria volcanic complex, Kenya, have been shown to have no genetic relationship with their associated basalts, and are potentially the result of partial melting of both amphibolite grade Proterozoic crust and Miocene-Holocene volcaniclastic crust in response to fluxing of alkali-bearing volatiles (Davies and Macdonald, 1987; Macdonald *et al.*, 1987; Black *et al.*, 1997).

2.4.3 Tectonic associations and global occurrences

Peralkaline rocks occur in a wide variety of tectonic environments. Here, emphasis is given only to the peralkaline silicic rocks, excluding, for example, peralkaline mafic and ultramafic rocks such as lamproites. Relating to the subdivision of tectonic regimes, the classification scheme of Macdonald (1974b) is adopted, applying three following broad tectonic categories: 1) continental rifting and epeirogenic uplift environments 2) complex tectonic environments, and 3) oceanic environments.

The first category is the most volumetrically significant and is estimated to account for more than 90 vol. % of peralkaline silicic rocks (Macdonald, 1974b), despite being generally limited to the system of rift valleys and grabens that extend from western Europe, through the Mediterranean and into northern and eastern Africa, and constitute the intercontinental rift belt of Illies (1969). Of the various sections that comprise this belt, the East African Rift system (EAR) is arguably the most significant, due to both the volume and compositional range of peralkaline silicic magmas erupted there. As such, the volcanoes of the East African Rift system (e.g. Emuruangogolak, Menengai, Longonot,

Nasaken and Silali) have been the subject of numerous studies aimed at investigating the origin and evolution of peralkaline silicic magmas (e.g. Sceal and Weaver, 1971; Weaver *et al.*, 1972; Barberi *et al.*, 1974; Leat *et al.*, 1984; Davies and Macdonald, 1987; Macdonald *et al.*, 1987, 1995; Smith *et al.*, 1995; Trua *et al.*, 1999; Peccerillo *et al.*, 2003; Scaillet and Macdonald, 2003; Rogers *et al.*, 2004; Ren *et al.*, 2006). Further examples of PSRs within the intercontinental rift system include; the peralkaline granites of northern Corsica (e.g. Quin, 1962; Bonin *et al.*, 1978), the comendites and pantellerites of Pantelleria island (the type locality for pantellerites) (e.g. Washington, 1913a, 1913b, 1914; Mahood and Baker, 1986; Civetta *et al.*, 1998), various peralkaline intrusive lithologies found within the alkaline province of central Europe and France (e.g. Brousse and Varet, 1966; Wimmenauer, 1974; Bernth *et al.*, 2002) and the peralkaline granitic dykes of the Oslofjord province (e.g. Nystuen, 1975; Rasmussen *et al.*, 1988; Neumann *et al.*, 1992).

Also included within this group, though not part of the intercontinental rift belt, are the Gardar Igneous Province and the British Tertiary Province. The Gardar igneous province comprises a series of well-exposed, alkaline intrusive and extrusive rocks (including the notable Ilímaussaq intrusion), which are exposed in south-west Greenland and frequently attributed to a failed rift (e.g. Upton, 1974; Upton *et al.*, 2003; Marks *et al.*, 2003). Among these lithologies are peralkaline granitoids and comenditic rhyolites (Upton, 1974). The British Tertiary Province also includes pantelleritic granites in such localities as Ailsa Craig, Holy Island and Rockall Island, despite the dominance of calc-alkaline lithologies (e.g. Sabine, 1960; Thompson, 1969; Macdonald, 1974b; Ferguson, 1978).

The second major tectonic division of peralkaline silicic rocks (complex tectonic environments) includes a variety of rocks and locations that cannot be easily classified. The rocks included within this category are typically associated, either directly or indirectly, with an orogenic event and are often subordinate to calc-alkaline rocks. Macdonald (1974b) provided multiple examples of such PSRs, including a series of post-orogenic Caledonian dykes on the Shetland islands (e.g. Phemister *et al.*, 1950), the

Basin-and-Range province of the western USA (e.g. Noble and Parker, 1974), the Circum-Japan Sea alkaline province (e.g. Aoki, 1959), Sardinia (e.g. Araña *et al.*, 1974), as well as the arfvedsonite-aenigmatite microgranites of Ailsa Craig (e.g. Howie and Walsh, 1981; Morra *et al.*, 1994).

The third category comprises oceanic island tectonic settings. Many instances of peralkaline rocks within the stratigraphy of oceanic islands have been reported. For example, the stratigraphy of Socorro island in the eastern Pacific Ocean is dominated by PSRs, which account for up to 80 % of the surface of the island and include pantellerites (e.g. Bryan, 1966; Bohrson *et al.*, 1996; Bohrson and Reid, 1997). Iceland, whilst dominated by the mafic rocks of the Tertiary flood basalts, also exhibits intermediate and felsic lithologies that constitute around 10 % of the exposed volcanic rocks (e.g. Carmichael, 1964; Thorarinsson, 1967). Of these, a small proportion is known to be peralkaline, either pantelleritic (e.g. Lysuskard, Sigurdsson, 1970) or comenditic (e.g. Hrafnitinnusker, Ljosufjoll and Midhyrna, Bailey and Macdonald, 1970; Thórsmörk, Jørgensen, 1980; Torfajökull, Macdonald *et al.*, 1989). The island of Gran Canaria, Canary islands, has also produced PSRs ranging from comendite to pantellerite, and represents (alongside the Azores) a distinctive example of an oceanic island setting where PSRs have been predominantly erupted explosively to form ignimbrites, rather than the more common effusive eruptions and resulting lava flows and domes (e.g. Araña *et al.*, 1973; Macdonald, 1974b; Schmincke, 1974; McDougall and Schmincke, 1976). Additional reported examples include isla San Benedicto, eastern Pacific Ocean (e.g. Richards, 1966), Reunion island, western Indian Ocean (e.g. Upton and Wadsworth, 1972), Pitcairn island, south Pacific Ocean (e.g. Carter, 1967) and Kerguelen, southern Indian Ocean (e.g. Nougier, 1970).

Baker (1974) provided a substantial review of PSRs in oceanic island settings and suggested two further subdivisions; 1) PSRs originating from islands near to the crestal zone of oceanic rises, and 2) PSRs originating from islands that rise above large submarine plateaus. This was undertaken on the basis of lithological associations. They

suggested that the former category (which includes such examples as Bouvet island, south Atlantic Ocean (e.g. Broch, 1946; Baker, 1967), Ascension island, south Atlantic Ocean (e.g. Daly, 1925; Atkins *et al.*, 1964; Harris, 1983) and Easter island, south Pacific Ocean (e.g. Baker *et al.*, 1974) typically includes a relatively linear suite of rocks that ranges from transitional or mildly alkaline basalt, hawaiite, mugearite, and comendites/comenditic trachytes. The second subdivision includes the Azores (e.g. Machado, 1967), Gran Canaria (e.g. Araña *et al.*, 1973) and Kerguelen (e.g. Nougier, 1970), and differs from the first in that the included locations are believed to display multiple evolutionary trends, with the standard trend towards PSRs as well as a trend towards silica-undersaturated phonolitic compositions (Macdonald, 1974b). The observation was also made that the locations of the second group are commonly associated with either granitic and syenitic intrusive complexes, or syenitic ejecta within the extrusive rocks, though it is also noted that Ascension island deviates from this trend. Macdonald (1974b) suggested that the variations observed between different tectonic subgroups of oceanic islands could indicate alternative petrogenetic mechanisms.

CHAPTER 3: METHODOLOGIES

3.1 Chapter outline

This chapter provides a full account of each of the methodologies applied in Chapters 4 and 5. This includes detailed descriptions of sample preparation and analysis procedure for a number of quantitative analytical methods (including wavelength dispersive X-ray fluorescence (WD-XRF), inductively coupled plasma atomic emission spectroscopy (ICP-AES), inductively coupled plasma mass spectrometry (ICP-MS), electron microprobe analysis (EMPA), scanning electron microscopy (SEM), and Fourier transform infrared spectroscopy (FTIR)). Additionally, thermobarometrical models utilised to derive estimates of pre-eruptive P-T-fO_2-H_2O_{melt} conditions are listed in full, and the applied equilibrium testing strategies given for each model. Various petrogenetic modelling procedures are also given, including mass balance, trace element, and thermodynamic models. Finally, a methodology for solid state modelling, applied only to the investigation of dalyite compositional variation (Chapter 4), is provided.

3.2 Whole-rock geochemistry

Whole rock major and trace element analyses were undertaken using an Applied Research Laboratories 8420+ dual goniometer wavelength dispersive X-ray fluorescence (XRF) spectrometer, and inductively coupled plasma mass spectrometry (ICP-MS), using an Agilent 7500s quadrupole mass spectrometer at The Open University, U.K.. Additional major and trace element analyses were produced using a Bruker AXS S4 Pioneer XRF spectrometer at the University of East Anglia, U.K, and at Bureau Veritas Mineral Laboratories, Canada, using inductively coupled plasma atomic emission spectroscopy (ICP-AES) for major element analysis and ICP-MS for trace element analysis. Further analyses of selected trace elements were produced using a Niton Xl3t energy dispersive XRF (ED-XRF) spectrometer at Keele University, U.K. All data derived from facilities at the Open University were produced by R. Gertisser, whilst data generated via ED-XRF were produced by S. Whitley. All remaining whole rock data were produced by the author.

For XRF analyses, samples were cleaned using distilled water and weathered surfaces were removed, before crushing using a jaw-crusher and an agate mill. Fused glass discs for major element analysis were prepared using 0.7 g of rock powder mixed with 3.5 g of lithium metaborate. Trace element concentrations were determined using PVC bound pressed powder pellets. Loss on ignition (LOI) was reported as weight difference after ignition at 1,000 °C for two hours. For major elements, the instrument was calibrated using the following international standards: BCR-2, DTS-1, DTS-2, G2, GXR-1, GXR-2, GXR-3, BHVO-2, BCS-368, BCS-376, AC-E, BE-N, BX-N, GS-N, UB-N, LKSD-3, MRG-1, STSD-1, SARM-2. For trace elements, the Geoquant calibration of Bruker was applied. Data quality was evaluated using the following secondary standards: WS-E, OUG94, GSP-2, W2a, AC-E, BHVO-1, QLO-1, DNC-1, W-2, AGV-2, BCR-2, SDO-1, Mess-2, STSD-2. The mean deviation from the accepted standard values was < 10 %, and reproducibility was < 3 % for major elements and < 10 % for trace elements.

Samples analysed via ICP-MS at the Open University, U.K., were prepared using a standard HF-HNO_3 digestion procedure (e.g. Eggins *et al.*, 1997). The instrument was calibrated using up to six international standards (BCR1, BIR1, AC, RGM1, BHVO1-2, AGV1), using recommended element concentrations. Instrumental drift was monitored by and corrected using an internal standard solution containing Be, In, Rh, Tm, Re and Bi, which was introduced on-line during analysis. Residual drift in individual elements was corrected externally using replicate determinations of a representative sample after every 10 unknowns. Samples analysed via ICP-AES and ICP-MS at Bureau Veritas Mineral Laboratories, Canada, were cleaned to remove altered surfaces, and crushed in an agate mill prior to drying at 60 °C, mixing with a $LiBO_2/Li_2B_4O_7$ flux and dilute nitric acid digestion. LOI was reported as weight difference after ignition for two hours at 1,000 °C. The instrument was calibrated using up to twelve international standards (AGV-1, BCR-2, BHVO-1, BHVO-2, BIR-1, RGM-1, WS-E, JB2, JB3, SO-18, DS9, OREAS45EA). Standard analyses for ICP-AES and ICP-MS indicate accuracy of < 5 % for major elements and < 7 % for trace elements, whilst reproducibility was < 1 %.

For samples analysed by XRF at Keele University, U.K., a minimum of five clasts were analysed for each eruptive unit. Clasts were analysed individually where possible. Samples had any visibly weathered surfaces removed prior to soaking in distilled water for at least 24 hours and crushing in an agate mill. Elemental determinations were performed on PVC bound pressed powder pellets, using 8 g of rock powder. Reproducibility was found to be in the order of 0.5% for Zr, and <2.5% for Nb, Rb, and Sr. The data were calibrated with a calibration curve comprising up to 37 igneous standards, and up to 27 secondary standards comprising various igneous rocks from Furnas, and also from nearby Terceira Island. Calculated 2 sigma errors were found to be < 4 % relative for Zr and Nb, and < 2 % relative for Rb.

3.3 Electron microprobe analysis

Major element compositions of mineral phases and glass (both melt inclusions and groundmass glass) were analysed using a JEOL JXA 8900 RL electron microprobe at the University of Göttingen, Germany, a CAMECA SX 100 electron microprobe at The Open University, U.K., and a CAMECA SX 100 electron microprobe at the University of Manchester, U.K. All data derived from the University of Göttingen were produced by the author. Data from the Open University were generated by R. Gertisser, and data from the University of Manchester were produced by B. O'Driscoll.

3.3.1 Mineral phases

For mineral phases, peak counting times per element were 10 to 30 seconds using a 5 to 10 µm defocused beam, an acceleration voltage of 20 kV and a beam current of 20–27 nA. The following natural minerals and synthetic materials (denoted as formulae) were used as primary standards: olivine, albite, sanidine, TiO_2, haematite, anorthite, wollastonite, Cr_2O_3, rhodonite, celsian, $ZrSiO_4$ and $HfSiO_4$. Mineral phase and volcanic glass standards (VG-568, KN-18 and KE-12) were routinely analysed as secondary standards.

3.3.2 Groundmass glass

Major element and volatiles (Cl, F, S) in groundmass glass were analysed using peak counting times ranging from 90 to 120 seconds for volatiles and 10 to 30 seconds for major elements, with a 10 to 20 µm defocussed beam, an acceleration voltage of 15 to 20 kV, and a beam current of 10 to 15 nA. To minimise Na-loss, Na was always analysed first, with a peak count time of 10 seconds. Detection limits for Cl, and F were ~ 60, and 220 ppm, respectively. Detection limits for S were ~ 300 ppm and ~ 80 ppm at the

University of Göttingen and the Open University, respectively. Volcanic glass standards (BCR-2G, VG-2, KN-18 and KE-12) were routinely analysed as secondary standards.

3.3.3 Melt inclusions

Grain mounts for melt inclusions analyses were prepared by gently crushing pumice clasts and sieving to different size fractions. Alkali feldspar phenocrysts were then hand picked from the 0.5 to 1 mm fraction, using a binocular microscope. Alkali feldspar crystals were inspected for melt inclusions individually, using immersion oil with a similar refractive index to feldspars. Those determined suitable were mounted into a block of EpoThin low viscosity epoxy resin. The blocks were then hand polished until the melt inclusion was exposed on the surface, using silicon carbide pads (grit sizes 1200 and 600 µm) lubricated with water, and a TexMet C polish pad lubricated with a solution of 0.3 µm Alumina Micropolish and ROS-2 polishing oil. Fe-Ti oxide phases were also collected from the sieved samples, using a hand magnet to separate them from the remaining material. Unlike alkali feldspar crystals, > 50 crystals were sprinkled onto a bleb of epoxy resin on a glass slide. When set, this slide was then machine polished, and checked for exposed melt inclusions.

Major element and volatiles (Cl, F, S) in melt inclusions were analysed using peak counting times ranging from 90 to 120 seconds for volatiles and 10 to 30 seconds for major elements, using a 10 to 20 µm defocussed beam, an acceleration voltage of 15 to 20 kV, and a beam current of 10 to 15 nA. As for groundmass glass analyses, Na-loss was minimised by analysing Na first, with a peak count time of 10 seconds. Volcanic glass standards (BCR-2G, VG-2, KN-18 and KE-12) were routinely analysed as secondary standards.

3.4 Scanning electron microscope analysis

Backscatter electron images, semi-quantitative analyses and element maps were produced using a Hitachi TM-3000 scanning electron microscope (SEM) equipped with a Bruker Quantax 70 energy dispersive system (EDS) at Keele University, U.K. Element maps were produced using a minimum analysis time of 300 seconds. All images and analyses were produced by the author.

3.5 Fourier transform infrared spectroscopy

3.5.1 Sample preparation

A number of feldspar-hosted melt inclusions that had previously been analysed via EMPA were selected for FTIR analysis. Resin mounts were lightly polished to remove the residual carbon coating, and then attached, polished side down, to a glass slide using Lakeside 70C cement. The unpolished side was then carefully hand polished using the same procedure outlined above for EMPA melt inclusion analyses, until the melt inclusion was exposed on both surfaces. The crystal was subsequently removed from the glass slide by submerging it in a methanol bath, which dissolved the Lakeside 70C cement. For mounting, a thin slit, ~ 350 µm thick, was cut into the middle of a glass cover slip, and the double polished crystals were glued into place across the opening to allow analysis without contamination.

3.5.2 Analytical methods

The water content of alkali feldspar hosted melt inclusions was determined using spectra collected with a Thermo Nicolet Nexus FTIR spectrometer coupled with a Continuµm IR microscope at the Open University, U.K. Operation conditions included standard EverGlo mid-infrared source optics, a Ge-on-KBr beamsplitter, and a liquid nitrogen-cooled MCT-A* detector (11,700 – 750 cm^{-1}). In all of the analyses, CO_2 was below the detection limit (~ 100 ppm, cf. Gertisser *et al.*, 2012). The concentration of dissolved water was determined using the height of the total water (H_2O + OH^-) peak at 3,550 cm^{-1} and the Beer-Lambert law:

$$H_2O\ (wt.\%) = 100 \times \left(\frac{MA}{\rho d \varepsilon}\right) \tag{3.1}$$

where *M* is the molecular weight of H_2O (18.02) *A* is the height of the absorption peak, ρ is the sample density (g L^{-1}), *d* is the thickness of the sample (cm), and ε is the molar absorption coefficient (l $mol^{-1}cm^{-1}$). The thickness of each sample (± 3 μm) was determined using a Mitutoyo Digimatic Indicator. The density of the trachytic glass at 298 K and 0.1 MPa was estimated to be 2510 g L^{-1}, assuming a nonlinear temperature dependence of melt volume (e.g. Gottsmann and Dingwell, 2002). Due to the variability of the molar absorption coefficient as a function of ((Si/Al)/total cations) (Mandeville *et al.*, 2002), the following approach given by Seaman *et al.* (2009) was used:

$$\varepsilon = 54.2 \times \left(\frac{Si + Al}{total\ cations}\right) + 28.7 \tag{3.2}$$

The application of this approach led to a calculated molar absorption coefficient of 73.

3.6 Thermobarometry

3.6.1 Alkali feldspar thermometry

Pre-eruptive magmatic temperatures were estimated using the alkali feldspar-melt thermometer of Putirka (2008). To minimize the error introduced by mineral-liquid disequilibrium, the Kd_{Ab-Or} equilibrium test proposed by Mollo *et al.* (2015) was applied, allowing a single suitable liquid composition to be selected for each case. Input pressure values were set at 100 MPa, and it was observed that a variation of 0.1 GPa led to a change in temperature of only 0.1 ºC, suggesting that the thermometer is not significantly influenced by variations in pressure. The standard error of estimate (SEE) associated with the thermometer is ± 23 ºC.

3.6.2 Alkali feldspar hygrometry

In addition to pre-eruptive temperatures, magmatic H_2O contents were also estimated, using the hygrometer of Mollo *et al.* (2015). Temperature estimates derived from alkali feldspar-melt thermometry were used as primary inputs, alongside feldspar and potential equilibrium liquid compositions. The SEE associated with these results is ± 0.53 wt. %.

3.6.3 Clinopyroxene Thermobarometry

Estimates of pre-eruptive P-T conditions were attempted using three clinopyroxene-melt thermobarometrical models. The first utilises jadeite-diopside/hedenbergite exchange equilibria to produce estimates of both P and T for hydrous melts (Putirka *et al.*, 1996, 2003). This model (referred to here as model P03) has a SEE of ± 33 °C and ± 170 MPa and has been applied successfully to a number of studies aimed at reconstructing pre-eruptive intensive parameters of magma plumbing systems (e.g. Schwarz *et al.*, 2004; Longpré *et al.*, 2008; Stroncik *et al.*, 2009; Hildner *et al.*, 2011; Barker *et al.*, 2012; Dahren *et al.*, 2012; Jeffery *et al.*, 2013). The second model that has been applied (P08-33)

represents a recalibration of P03, and therefore is also based upon jadeite-diopside/hedenbergite exchange equilibria. This model calculates T estimates with an SEE that is improved by around 10 to 20 °C relative to P03 (Putirka, 2008, equation 33). The third applied model yields estimates of crystallisation pressures in hydrous melts and is based upon the partitioning of Al between melt and clinopyroxene (Putirka, 2008, equation 32c). This model is referred to here as P08-32c and has a SEE of ± 150 MPa.

To provide an independent test of P-T estimates derived from clinopyroxene-melt thermobarometrical models, two additional models were applied which are based upon clinopyroxene composition only (Putirka, 2008, equations 32d and 32b). These models (P08-32d and P08-32b) are based upon the thermometer and barometer of Nimis & Taylor, (2000) and Nimis, (1995), respectively, but have been recalibrated for hydrous systems. As such, both models require an estimate of melt H_2O content to achieve SEEs of ± 87 °C and ± 260 MPa, respectively.

3.6.4 Two oxide Thermometry

Where both ilmenite and Ti-magnetite were present, temperature and oxygen fugacity (fO_2) estimates were calculated using the ILMAT program of Lepage (2003), applying the model of Andersen *et al.* (1993), and utilising the calculation scheme of Stormer (1983) to determine values for X_{hem}, X_{ilm}, X_{mag}, X_{ulv}. The application of alternative calculation schemes was shown to lead to variation of no more that 5 % in the calculated results. Equilibrium between mineral pairs was evaluated using the Mn-Mg partitioning test of Bacon and Hirschmann (1988).

3.7 Petrogenetic modelling

3.7.1 Mass balance models

Least squares mass balance calculations after Bryan *et al.* (1969) were performed using the IgPet software package. Models were typically run using multiple steps to simulate evolution from a basaltic parental magma to an evolved trachytic daughter. Model results were considered acceptable if $\sum r^2 = < 1$.

3.7.2 Trace element models

Trace element modelling was undertaken using the Rayleigh fractionation law equation:

$$C_l = C_O F^{(\bar{D}-1)} \tag{3.3}$$

and the batch melting law equation:

$$\frac{C_l}{C_O} = \frac{1}{\bar{D}(1-F)+F} \tag{3.4}$$

where C_l is the concentration of the element in the liquid, C_O is the concentration of the element in initial melt or rock, $\bar{D}$ is the bulk partition coefficient for the element and F is the fraction of melt either remaining after fractionation or produced during melting. A bulk partition coefficient for each trace element was calculated using the following equation:

$$\bar{D} = \sum X_A \, KD^A \tag{3.5}$$

where X_A is the fraction of mineral A in the rock, and KD^A is the partition coefficient for the element in mineral A. Partition coefficient values were taken from literature values found in the GERM KD database (Nielsen 2006).

3.7.3 Thermodynamic models

Magmatic differentiation processes were modelled thermodynamically using the MELTS algorithms (Ghiorso & Sack 1995; Asimow & Ghiorso 1998; Gualda *et al.* 2012), which, for a given bulk rock composition, temperature, pressure, and oxygen fugacity, compute phase equilibria relations by minimisation of Gibbs energy. To model RFC processes, the first step of the model determines the liquidus phase for the given conditions and subtracts it from the liquid, yielding a new liquid composition. The temperature is then lowered incrementally, calculating a new equilibrium assemblage at each temperature step. The Rhyolite-MELTS calibration (Gualda *et al.* 2012) was used to calculate various fractional crystallisation models over three starting water contents (0.5, 1.5, and 2.5 wt. %), four isobaric pressures (50, 150, 250, and 500 MPa) and redox conditions ranging from FMQ +2 to FMQ -2. Additional models were generated for polybaric conditions, assuming a pressure change from 500 to 150 MPa at varying points during magma evolution. Due to the capability of differentiation trends in peralkaline magmas to decrease the SiO_2 content of residual liquids (e.g. Scaillet & Macdonald, 2001), the MgO content and calculated peralkalinity index were used as primary differentiation indices.

3.8 Solid state modelling

Solid state modelling calculations were carried out to investigate the substitution of a number of potential substituting cations (Ti, Hf, Fe, Ba and Mg) into the dalyite crystal structure. This was undertaken by R. A. Jackson, using the GULP code (Gale, 1997). This code uses effective interatomic potentials to model the interactions between atoms, and has been widely used to calculate the structure and properties of inorganic materials. The Buckingham potential, supplemented by an electrostatic term, is used:

$$V(r) = A \exp(-r/\rho) - Cr^{-6} + q_1q_2/r \qquad (3.6)$$

In this equation, the parameters A, ρ, and C are fitted to structures and properties of related materials; here they have been transferred from studies on zircon (Akhtar & Waseem, 2001; Finch and Hanchar, 2003). The charges of the interacting ions are q_1 and q_2. The experimental and calculated lattice parameters for dalyite are given in Table 3.1 below, using the experimental structure from Fleet (1965) for comparison.

Table 3.1 Comparison of experimental and calculated lattice parameters for dalyite

Lattice parameter	Experimental	Calculated	% difference
a/Å	7.371	7.211	-2.17
b/Å	7.730	7.679	-0.66
c/Å	6.912	6.787	-1.80
β/degrees	106.23	104.82	-1.33

It is seen that the lattice parameters agree to within a few percent, which gives confidence in using this transferred potential. The calculations reported here have been used to obtain the energies involved when various ions are substituted into the dalyite lattice. The calculation of substitutional and solution energies for dopant ions in materials has been widely described elsewhere; see, for example, a recent study of Nd, Gd and Yb ions in BaF_2 (Mujaji *et al.*, 2014). However, a brief summary will be given here. In the case of the

substitution of Ti^{4+} into the dalyite lattice, the following reaction (solution scheme) is considered, assuming substitution at the Zr^{4+} site:

$$TiO_2 + Zr_{Zr} \rightarrow Ti_{Zr} + ZrO_2 \quad (3.7)$$

The energy of this reaction (the solution energy), E_{sol}, is then calculated, as follows:

$$E_{sol} = [E_{latt}(ZrO_2) + E(Ti_{Zr})] - E_{latt}(TiO_2) \quad (3.8)$$

In this case no charge compensation is needed, but considering substitution at the K^+ site, the following scheme was assumed (with charge compensation by K^+ vacancies):

$$TiO_2 + 4K_K \rightarrow Ti_K^{\bullet\bullet\bullet} + 3V_K' + 2K_2O \quad (3.9)$$

The solution energy for this reaction is:

$$E_{sol} = [E(Ti_K^{\bullet\bullet\bullet}) + 3E(V_K') + 2E_{latt}(K_2O)] - E_{latt}(TiO_2) \quad (3.10)$$

In each case, a similar procedure is adopted, and a single solution scheme is assumed. More complex solution schemes, such as coupled substitutions, cannot be ruled out. Note that in the above expressions, Kröger-Vink notation has been used (Kröger & Vink, 1956).

CHAPTER 4: PETROGENESIS OF THE PERALKALINE IGNIMBRITES OF TERCEIRA

4.1 Chapter outline

This chapter presents the results of a detailed petrological study of the peralkaline ignimbrites and associated syenitic ejecta of the Pico Alto volcanic complex, Terceira, Azores. The study utilises petrographic analysis, major and trace element geochemistry, mineral chemistry, thermobarometry, and petrogenetic modelling, aiming to place constraints upon the origin and evolution of the variably evolved trachytic magmas of Pico Alto. Based upon the discussed data, a conceptual model for the underlying magmatic system is provided, accounting for the observed petrographic and geochemical features of the eruptive deposits. Additionally, a sub-study is provided, in which the compositional variability of the rare zirconosilicate dalyite ($K_2ZrSi_6O_{15}$) is evaluated based upon available published analyses and twelve new analyses provided by this study.

The dataset employed in this chapter includes mineral chemical data produced by R. Gertisser and B. O'Driscoll, in addition to the author. Furthermore, molecular modelling applied to the compositional variability of dalyite was undertaken by R. Jackson. The results of the dalyite-based sub-study have been published as a research article in Mineralogical Magazine (Jeffery *et al.*, 2016a). The results of this study relating to the pre-eruptive magma system of Pico Alto and the petrogenesis of the ignimbrites have been prepared for submission to the Journal of Petrology (Jeffery *et al.*, 2016b).

4.2 Introduction

Terceira, one of the nine islands of the Azores archipelago, exhibits a number of petrological problems which are typical of oceanic island silicic centres. For example, in addition to the alkali basalts that are typical of oceanic islands, a significant proportion (86 vol. %; Self, 1976) of recently (< 23 ka) erupted material is felsic and peralkaline, extending to pantelleritic compositions. Furthermore, in addition to abundant silicic lava flows and domes, the volcanic stratigraphy of Terceira includes at least seven ignimbrite formations, some of which exhibit variably welded units, basal pumice falls and dilute pyroclastic density currents (surges) (Gertisser *et al.*, 2010), attesting to a history of spasmodic explosive eruptions of silicic magmas (Self, 1974, 1976; Gertisser *et al.*, 2010). Although ignimbrite forming eruptions have occurred on other Azorean islands, including Faial (Pacheco, 2001), São Miguel (Duncan *et al.*, 1999), and Graciosa (Gaspar, 1996), they represent a relatively minor component of each island's eruptive history. Such phenomena have also been reported at similar locations worldwide, such as Pantelleria (e.g. Foerstner, 1881), Gran Canaria (e.g. Araña *et al.*, 1973), Ascension (e.g. Daly, 1925), and Socorro (e.g. Bryan, 1966). The origins of the eruptive diversity observed on Terceira are likely to be influenced not only by pre-eruptive volatile content, but also by factors including magma supply, ascent rates, and rheology (e.g. Barclay *et al.*, 1996; Dingwell *et al.*, 1998; Andújar and Scaillet, 2012), as well as physical factors such as vent geometry (e.g. Wilson *et al.*, 1980) and interaction with external water (e.g. Self and Sparks, 1978).

Studies of peralkaline magmatic systems have highlighted their complexity, revealing the interplay of petrogenetic processes such as fractional crystallisation, crustal assimilation, magma mixing, and remobilisation and/or partial melting of cumulate material (e.g. Roux and Varet, 1975; Harris, 1983; Mahood, 1984; Mungall and Martin, 1995; Bohrson and Reid, 1997; Scaillet and Macdonald, 2001; Macdonald *et al.*, 2008; White *et al.*, 2009; Markl *et al.*, 2010). Considering the further complexity introduced by P-T-fO_2

and compositional variability, each such system is, to some extent, unique (Macdonald, 2012). However, peralkaline complexes are, in some respects, unified by the occurrence of key petrological phenomena such as compositional zonation of the pre-eruptive magma reservoir, and the generation of crystal-poor to aphyric eruptive material (e.g. Civetta *et al.*, 1984; Mahood and Hildreth, 1986; Macdonald *et al.*, 1994; Troll and Schmincke, 2002; Peccerillo *et al.*, 2003; Sumner and Wolff, 2003; Rogers *et al.*, 2004; Macdonald, 2012). Mungall and Martin (1995) showed that the most recently extruded (< 23 ka) peralkaline silicic magmas on Terceira could be generated via extended fractional crystallisation of an alkali basaltic parental composition. However, the relationship of this magmatic regime to the older (~ 20 to ~ 86 ka; Gertisser *et al.*, 2010), spasmodic, ignimbrite-forming eruptions is unclear, as are the factors controlling the contrasting eruption styles of broadly similar magma compositions.

In this chapter, whole-rock major and trace element geochemistry, melt inclusion and groundmass glass major and volatile element analyses, mineral chemistry, thermobarometry, and petrogenetic modelling is applied to the ignimbrites of Terceira and a suite of associated syenite ejecta, aiming to (1) elucidate the petrogenesis of the peralkaline, ignimbrite-forming silicic magmas of Terceira, (2) constrain the pre-eruptive conditions of magma storage, and (3) place the ignimbrites within the context of the identified magma series of Mungall and Martin (1995) as well as the magmatic suite of the island.

During the course of this study, the rare mineral dalyite ($K_2ZrSi_6O_{15}$) was identified as an accessory phase within the syenitic ejecta described in this chapter. Dalyite is a rare potassium zirconium silicate, with the empirical formula $K_2ZrSi_6O_{15}$. It was first identified in peralkaline granitic ejecta found within the pyroclastic sequences of Green Mountain and Middleton Peak, Ascension Island (Van Tassel, 1952). Since its discovery, it has been identified as an accessory phase in a variety of rocks, including peralkaline granites and syenites, late-stage pegmatites, charoitites, lamproites, lamprophyres, fenites and carbonatites (e.g. Furnes *et al.*, 1982; Robins *et al.*, 1983; Harris & Rickard, 1987;

Linthout *et al.*, 1988; Konev *et al.*, 1996). Having been established as a general indicator of peralkaline conditions, silica-oversaturation, and high chemical potential of K_2O (μK_2O) (e.g. Marks *et al.*, 2011), the presence and composition of dalyite may provide important insights into the evolution of these magmatic systems.

The discovery of dalyite in the mildly peralkaline rocks of Terceira provided the opportunity not only to report its first known occurrence on Terceira, but also to investigate the minerals compositional variability by combining 29 published quantitative analyses with a further 12 high quality quantitative chemical analyses produced as part of this study. Using these analyses, alongside whole rock major element analyses of the host syenites, the geochemical variability of dalyite is discussed in the context of previously published compositions from both similar and contrasting rock types. The findings of this investigation can be found in Jeffery *et al.* (2016a), and are integrated into this chapter. To provide context for this, suitable literature pertaining to the minerals occurrence and composition is also reviewed in this chapter.

4.3 Geological background

4.3.1 Geological history of Terceira

Terceira belongs to the central group of the Azores and is the third largest island in the archipelago, with a surface area of approximately 382 km^2 and a population of 58,000. The geological study of Terceira Island began as early as the sixteenth century, with the work of Gaspar Frutuoso, a Portuguese historian and humanist who described the rocks of Terceira, as well as most of the other Azorean islands. Further investigation of Terceira occurred in the late 19th century, when Charles Darwin visited the island in 1876 and compared the rocks of Terceira with those of Ascension Island. Fouqué (1883) discussed the petrology of the trachytes of the island (see Zbyszewski, 1966). The first geochemical analysis of Azorean rocks came in the early 20th century with the study of Esenwein (1929). More recent descriptions of the geology of Terceira can be found in Friedlander (1929); Agostinho (1931), Berthois (1953), Machado (1955), and Zbyszewski (1971).

4.3.1.1 Structure of the island

Terceira island comprises four central volcanoes; Santa Bárbara, Pico Alto, Guilherme Moniz and Cinco Picos, of which the latter two are considered extinct (Self, 1974, 1976; Gertisser *et al.*, 2010) (Figure 4.1). Cinco Picos in the south-east of the island is the oldest of the four central volcanoes, with K/Ar and $^{40}Ar/^{39}Ar$ ages of 370 ka to 388 ka (Feraud *et al.*, 1980; Calvert *et al.*, 2006), though the total range of reported ages extends up to 3.5 Ma (White *et al.*, 1976; Ferreira and Azevedo, 1995). Morphologically, it comprises a heavily eroded, 7 × 9 km caldera, the largest caldera in the Azores (e.g. Machado, 1955). The caldera collapse event was preceded by highly explosive volcanic activity and is considered to be younger than 370 ka (e.g. Machado, 1955; Calvert *et al.*, 2006). The pre- and post-caldera products of Cinco Picos span a compositional range

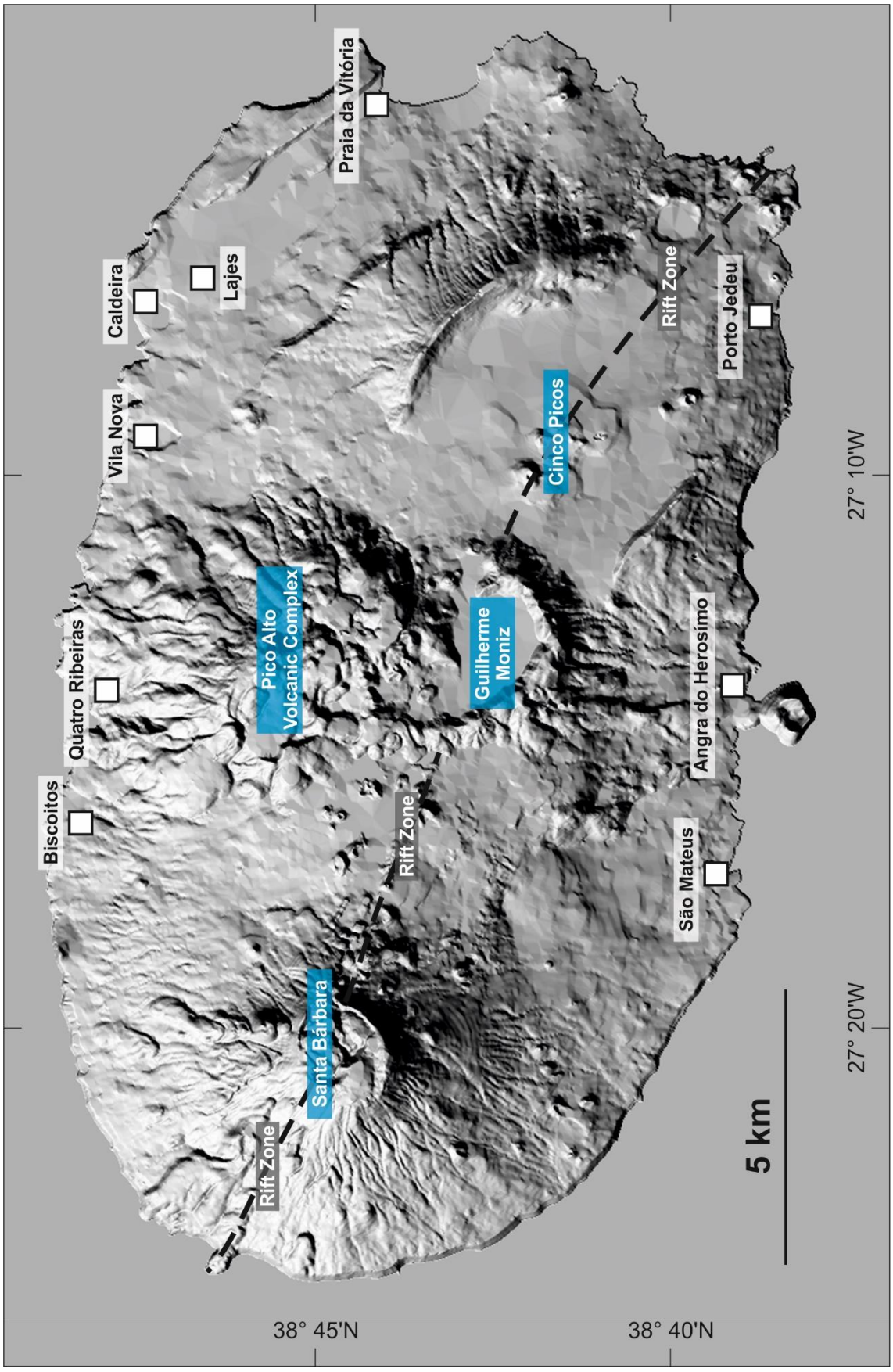
Praia da Vitória
Caldeira
Lajes
Vila Nova
Quatro Ribeiras
Biscoitos
Pico Alto Volcanic Complex
Guilherme Moniz
Cinco Picos
Rift Zone
Rift Zone
Rift Zone
Rift Zone
Porto Jedeu
Angra do Heroísmo
São Mateus
Santa Bárbara
5 km
27° 10'W
27° 20'W
38° 45'N
38° 40'N

◄ **FIGURE 4.1:** A digital relief map of Terceira island, showing selected towns and villages (white squares), the rift zone that runs approximately NW-SE through the island (dashed line) and the four volcanic centres (Cinco Picos, Guilherme Moniz, the Pico Alto Volcanic Complex and Santa Bárbara). After Gertisser *et al.*, (2010)

from basalts erupted from cinder cones and vents, to trachyte lava flows and pyroclastic lithologies (Self, 1974; Calvert *et al.*, 2006). However, no post-caldera trachytic vents occur within the caldera itself, instead being limited to the south-eastern flanks of the volcano.

Guilherme Moniz volcano is located slightly south of the centre of the island and, like Cinco Picos, comprises an 8 × 2 km caldera, with basaltic rocks in its floor and peralkaline trachytic rocks exposed in the caldera walls (e.g. Agostinho, 1931). The volcano is $^{40}Ar/^{39}Ar$ dated at around 270 ka, whilst the caldera-collapse event is constrained to no more than 111 ka (Calvert *et al.*, 2006). The caldera itself may have formed incrementally, each collapse event related to a significant eruption of trachytic ignimbrite (Calvert *et al.*, 2006). The southern portion of the caldera overlies the western flank of Cinco Picos, confirming its stratigraphical position. To the north, the caldera of Guilherme Moniz is itself overlain by the deposits of the Pico Alto Volcanic Complex (PAVC). Due to the spatial association of Guilherme Moniz and the PAVC, the possibility that some of the ignimbrite formations originated from Guilherme Moniz cannot be ruled out. As such, the two are considered together for the purposes of this study, and are referred to throughout this thesis simply as Pico Alto or the PAVC.

The PAVC was named by Lloyd and Collis (1981) and is considered by Calvert *et al.* (2006) to represent the younger part of Guilherme Moniz volcano. The area lacks the clear morphological structure of the other central Terceiran volcanoes, and is described as “a chaotic assemblage of trachytic domes and coulées” by Self (1974). Unlike Guilherme Moniz and Cinco Picos, the PAVC comprises exclusively peralkaline trachytic rocks, with no exposed mafic lithologies (Self and Gunn, 1976). Estimations of the age of the PAVC suggest that it formed after the Lajes Ignimbrite (Self, 1974; Lloyd and Collis, 1981), suggesting that it is younger than ~ 20 ka. Radiocarbon ages acquired from various PAVC

lithologies by Calvert *et al.* (2006) exhibit a total range of around 8,700 to 1,000 ^{14}C y. B.P.

Santa Bárbara is the youngest of the four Terceiran volcanoes, considered to have become subaerial within the past 100,000 years (e.g. Calvert *et al.*, 2006). It takes the distinctive form of a 1,000 m-high, truncated stratovolcano, believed to have lost it's summit during a caldera-forming eruption around 15 ka (Mungall and Martin, 1995). Compositionally, this landform is made up of post-caldera, peralkaline silicic lavas and pumice falls, which overlie mafic rocks including hawaiites and mugearites (Self, 1974). The modern summit region notably comprises a nested caldera, and it is suggested by Self (1974) that Santa Bárbara grew as a basaltic stratovolcano before entering a period of explosive silicic volcanism that led to caldera formation, as did Guilherme Moniz and Cinco Picos before it.

The island is bisected from NW-SE by a 2 km-wide Rift Zone that cross-cuts Santa Bárbara, Guilherme Moniz and Cinco Picos. The rift is defined by various scoria cones, spatter rings, lava flows and collapse pits (Mungall and Martin, 1995). It is considered to be volcanically active along its entire length, even where it traverses the extinct volcanic centres, Guilherme Moniz and Cinco Picos, and contributed young basalts to the caldera floor of Cinco Picos. Self and Gunn (1976) noted that the north-western section of the rift zone has been the most active during the last 50,000 years; prior to this the majority of rift zone activity occurred along its central and south-eastern sections. The Rift Zone is considered to represent the surface expression of the Terceira Rift and therefore the ultimate control on both mafic and felsic volcanism on Terceira (Self, 1974, 1976; Gertisser *et al.*, 2010).

4.3.1.2 Geochemistry of Terceira

The volcanic products of Terceira range from alkali basalt, through hawaiite, mugearite, and benmoreite, to comendite and pantellerite, and their trachytic equivalents (Figure 4.2)

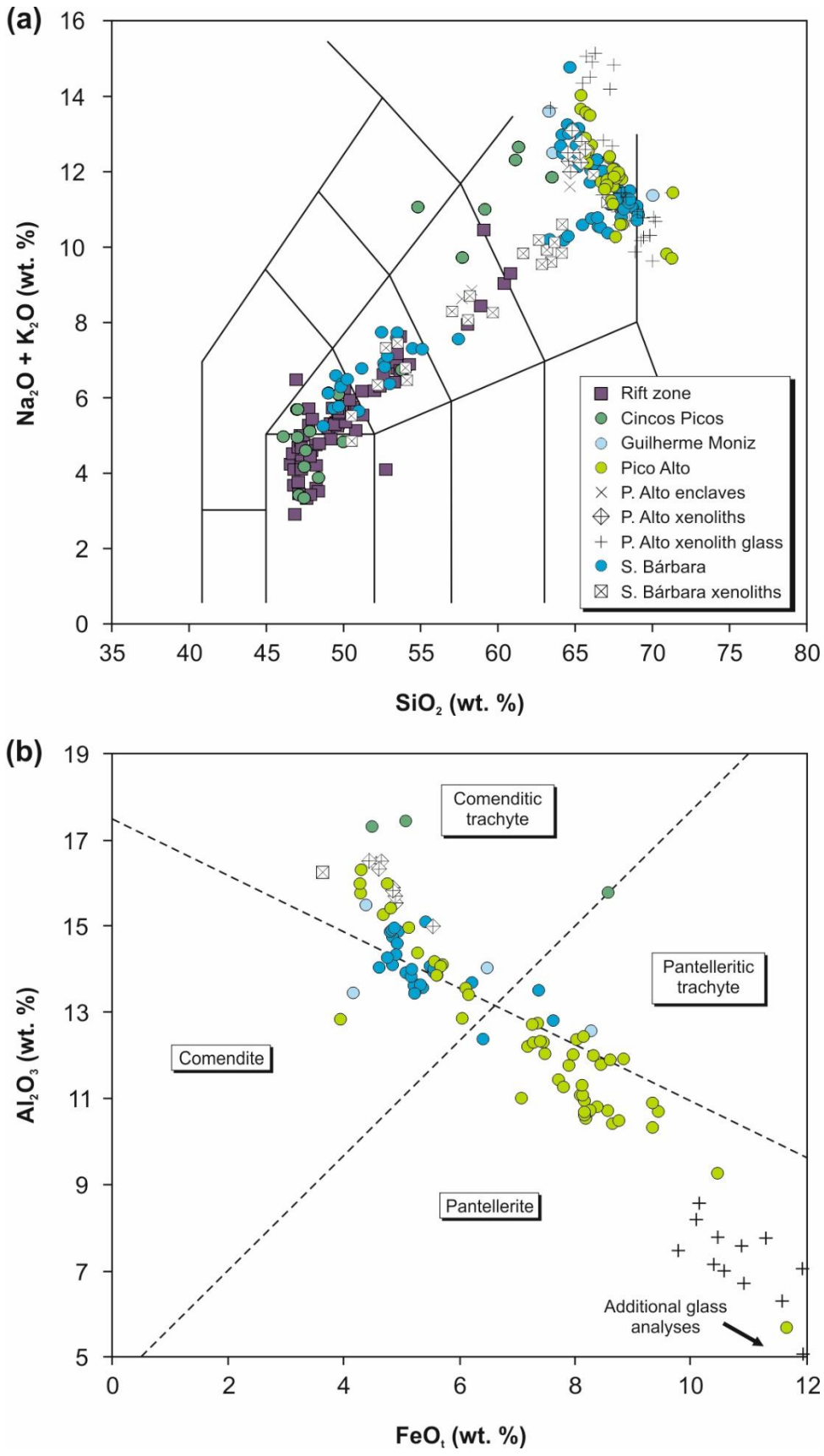

FIGURE 4.2: Major element compositions of the Terceira suite plotted into **a)** the total alkali-silica (TAS) classification scheme of Le Bas *et al.* (1986), and **b)** the FeO_t vs. Al_2O_3 classification scheme for peralkaline rocks of Macdonald (1974a). All data collected from Self (1974), Mungall (1993), and Madureira *et al.* (2011)

(Self and Gunn, 1976). Overall, a bimodal distribution of the data is observed, with a dearth of intermediate compositions that is typical of oceanic islands and indicates the presence of a Daly gap (e.g. Daly, 1925; Chayes, 1963). This compositional bimodality is seen in at least two of the four eruptive centres, namely Cinco Picos and Santa Bárbara. In contrast, the eruptive products of the rift zone and the PAVC are characterised by almost exclusively mafic and felsic products, respectively (Figure 4.2a). A suite of medium to coarse grained monzodioritic to monzonitic ejecta from Santa Bárbara appear to partially bridge the Daly gap (Mungall, 1993), and led Mungall and Martin (1995) to suggest that on Terceira, as well as other similar ocean island volcanoes, the compositional gap reflects the inability of intermediate magmas to erupt rather than a genuine scarcity of such compositions (e.g. Marsh, 1981; Walker, 1989; Petford *et al.*, 1994).

Compositional variation diagrams plotted against MgO reveal relatively well defined trends (Figure 4.3). Silica initially shows a uniform concentration of ~ 47 wt. %, until ~ 4 wt. % MgO, at which point it increase steadily to 65 to 72 wt. % silica. TiO_2 and FeO_t both exhibit a downward kink at ~ 6 wt. % MgO. A similar trend is observed for P_2O_5, though with a greater degree of scatter. The alkalis Na_2O and K_2O exhibit gently curved profiles. Interstitial glass analyses from syenitic enclaves from the PAVC (Mungall, 1993) indicate late stage (< 1 wt. % MgO) enrichment in Na_2O, reaching concentrations of up to ~ 12.5 wt. %. In contrast, CaO behaves compatibly, with a gently curved, concave-downwards trend. Al_2O_3 contents increase slowly until ~ 1 wt. % MgO, at which point concentrations fall from ~ 18 to ~ 5 wt. %. MnO shows uniform concentrations of ~ 0.2 wt. % until, at ~ 1 wt. % MgO, concentrations increase rapidly to ~ 0.8 wt. %. Peralkalinity indices increase slowly until ~1 wt. % MgO, when they increase rapidly to values of up to 5. Trace elements such as Zr, Nb, Rb, and Y all exhibit strongly incompatible behaviour, whilst Sr becomes strongly compatible at ~ 4 wt. % MgO (Figure 4.4). The trend for Ba is similar to that of Sr, but with far greater scatter.

Self and Gunn (1976) identified two distinct basaltic magma series on Terceira; a

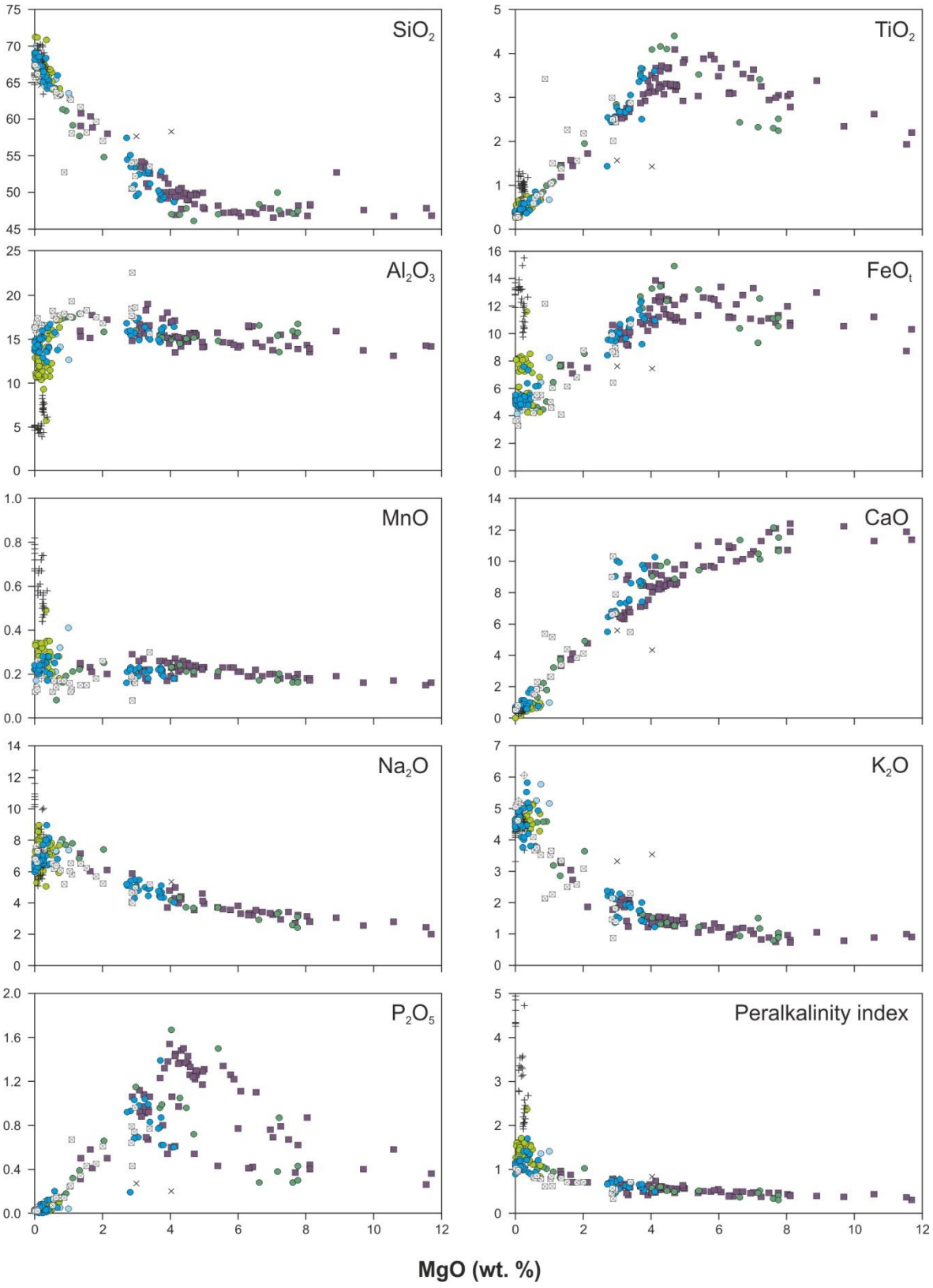

FIGURE 4.3: Major element compositions plotted against MgO for the Terceira suite. Symbols are as given in Figure 4.2. All data collected from Self (1974), Mungall (1993), and Madureira *et al.* (2011)

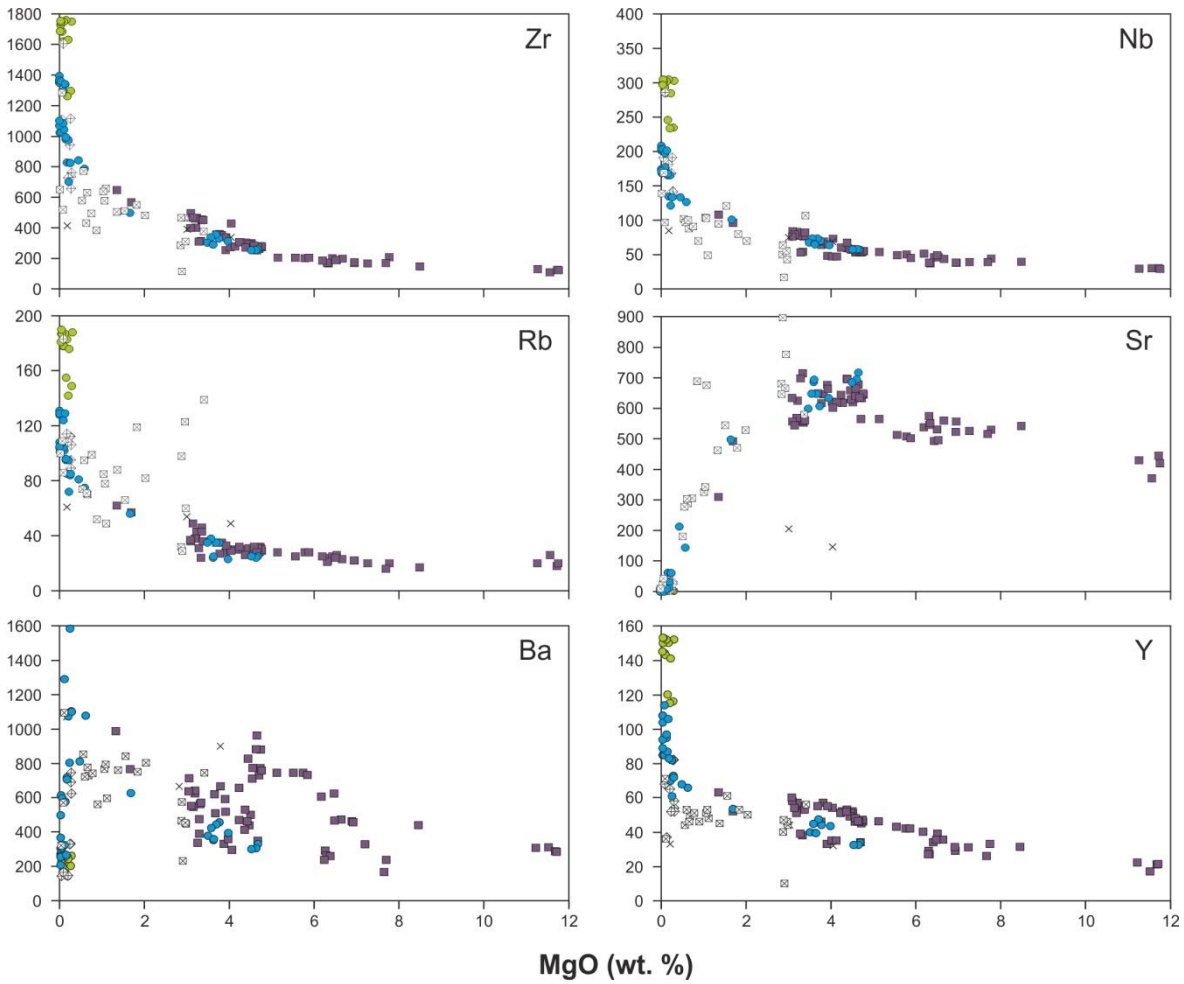

FIGURE 4.4: Trace element compositions plotted against MgO for the Terceira suite. Symbols are given in Figure 4.2. All data collected from Mungall (1993) and Madureira *et al.* (2011)

silica-undersaturated trend associated primarily with the oldest volcanic centre, Cinco Picos, and a silica-saturated to -oversaturated trend associated with the younger volcanic centres and rift zone. The latter series was further divided by Mungall and Martin (1995), who identified two discrete trends within the silica-saturated to –oversaturated series, terming them the on-rift and off-rift basalts, and associating them with the PAVC and Santa Bárbara, respectively. The same authors suggested that, together with fO_2 variations linked to the thermal disassociation of water, these two magma series contributed to the contrasting compositions observed at the two centres (pantelleritic vs. comenditic).

4.3.1.3 Ignimbrite stratigraphy

On Terceira, ignimbrites represent a significant proportion of the exposed stratigraphy (Figure 4.5). The stratigraphy of the island is divided into the Upper Terceira Group (UTG) and the Lower Terceira Group (LTG), each comprising various trachytic, rhyolitic and phonolitic lava flows, pumice falls and ignimbrites (Self, 1976; Gertisser *et al.*, 2010). The base of the UTG is marked by a prominent and extensive ignimbrite, namely the Lajes-Angra Ignimbrite Formation (LAI) (Self, 1974, 1976). At least 116 separate eruptions of Santa Bárbara and Pico Alto, alongside Rift Zone activity, contribute ignimbrites, pumice falls and lava flows to the UTG, overlying the LAI (Self, 1974).

The LAI comprises two distinct members; the Angra Ignimbrite (exposed in the southern coastal cliffs) and the Lajes Ignimbrite (exposed in both the northern and southern coastal cliffs), and ranges in thickness from 1 to 25 m (Self, 1971; Gertisser *et al.*, 2010). Radiocarbon studies undertaken by Self (1974) provided an age of 23,000 ± 350 B.P. for the Angra Member, and 18,600 ± 700 B.P. and 19,700 ± 300 B.P. for the Lajes Member. This formed the basis of the original argument that the Angra Member constituted an older event relative to the Lajes Member. However, Gertisser *et al.* (2010) note that the two members cannot be found in the same outcrop and provided nine new radiocarbon dates, limiting the overall age range of both members to 20,110 ± 470 – 23,150 ± 730 B.P. This removes the original time gap between members and allows them be considered contemporaneous (Figure 4.6).

Self (1971) studied the Lajes Member in detail, describing ‘an unsorted, mostly non-welded deposit of trachytic composition’. Juvenile clasts reach sizes of 1 m in diameter (Self, 1971, 1976), and range from highly vesicular pumice to dense vitrophyric clasts (Gertisser *et al.*, 2010). Self (1971, 1976) described fine-grained, alkali-feldspar-rich deposits with thicknesses less than 1 m that drape the landscape at elevations in excess of 300 m above sea level, suggesting that the pyroclastic density currents responsible for deposition of the LAI covered all but the highest topography. Exposures can be found in

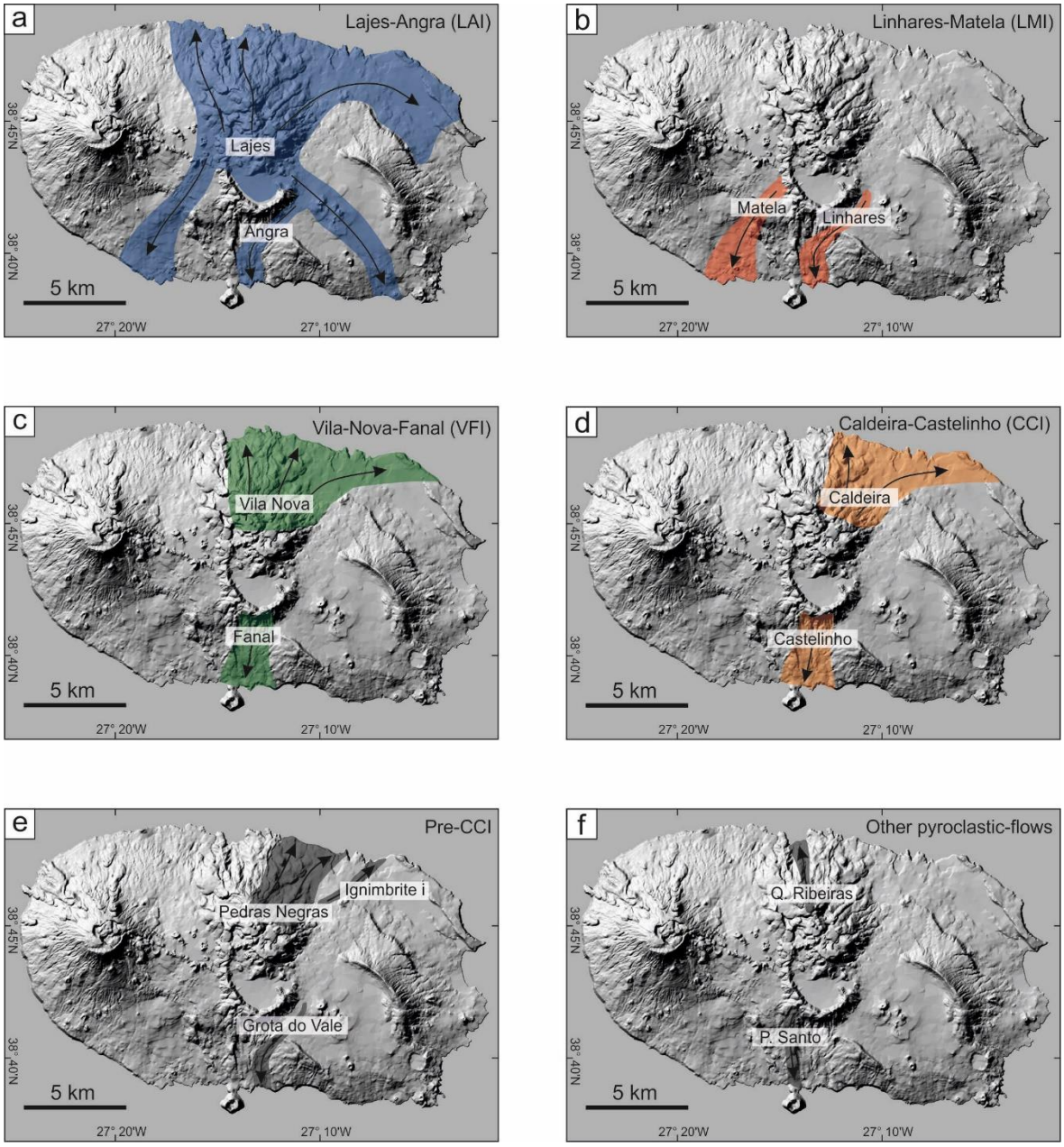

FIGURE 4.5: Map showing the spatial distribution and estimated flow paths of the various ignimbrites and pyroclastic units on Terceira, after Gertisser *et al.*, (2010). (a) Lajes-Angra Ignimbrite (LAI); (b) Linhares-Matela Ignimbrite (LMI); (c) Vila Nova-Fanal Ignimbrite (VFI); (d) Caldeira-Castelinho Ignimbrite (CCI); (e) ignimbrites that pre-date the CCI (Pedras Negras Ignimbrite Formation, Grota do Vale Ignimbrite Formation, Ignimbrite-I Formation); (f) other pyroclastic deposits (Quatro Ribeiras pyroclastic flow, Posto Santo spatter flow)

the northern coastal cliffs, from Biscoitos in the west to Lajes in the east (Self, 1971). Two additional outcrops are located in the southern coastal cliffs near Porto Judeu and São Mateus, and, despite being notably thinner (2-4 m) than the northern examples, exhibit the same general features, including a well-developed welded base (Gertisser *et al.*, 2010).

Gertisser *et al.* (2010) noted the presence of two distinctive layers in the Lajes

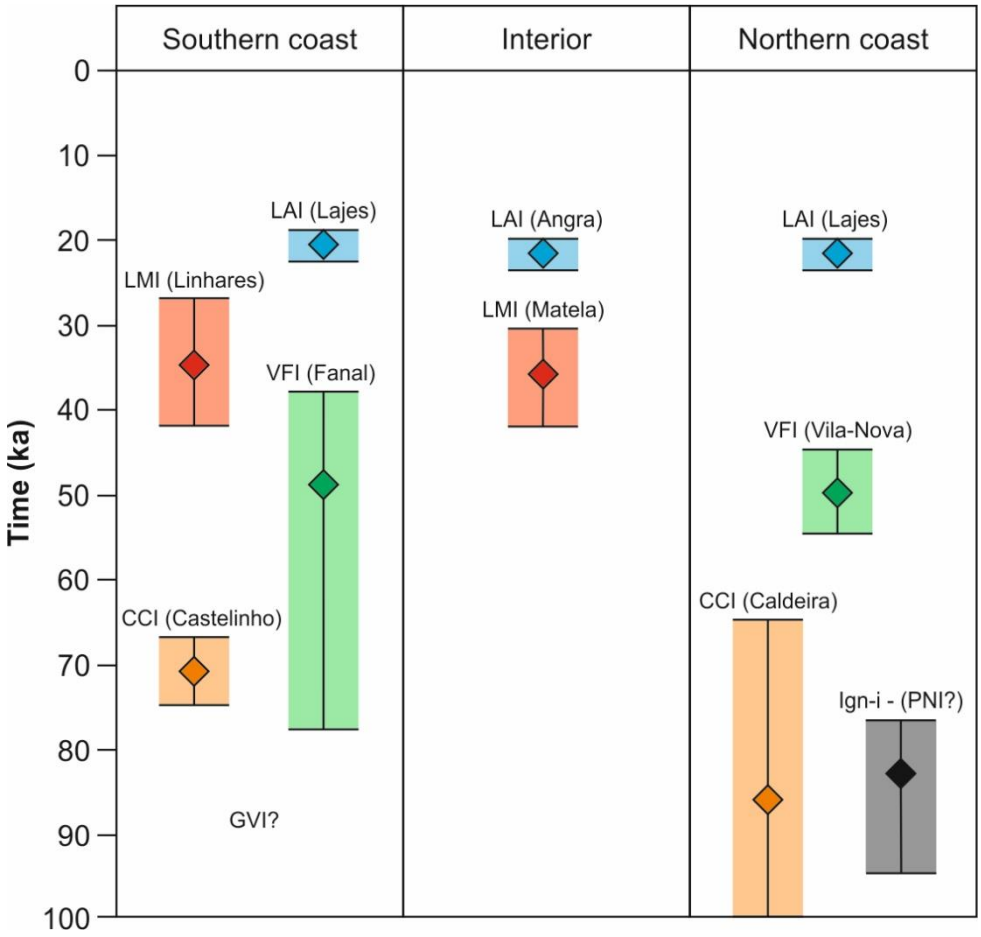

FIGURE 4.6: A schematic representation of the ignimbrite stratigraphy of Terceira Island, after Gertisser *et al.*, (2010). Abbreviations used: LAI = Lajes-Angra Ignimbite Formation, LMI = Linhares-Matela Ignimbrite Formation, VFI = Vila Nova-Fanal Ignimbrite Formation, CCI = Caldeira-Castelinho Ignimbrite Formation, PNI = Pedras Negras Ignimbrite Formation, Ign-i = Ignimbrite-i Formation, GVI = Grota do Vale Ignimbrite Formation

Member, marked by pumice concentrations at the top of each layer. These were interpreted as individual flow units and show minor variations in textural characteristics. The lower unit is typically more welded and contains a population of surface-derived, basaltic, lithic clasts. The upper unit is generally thicker than the lower unit, often exhibiting a welded base whose thickness varies with the overall thickness of the unit. Rarely, syenitic cognate xenoliths can be found. The Angra Member exhibits broadly similar characteristics to the Lajes Member, including a lower flow unit that is welded and depleted in the coarsest clast sizes relative to the upper flow unit, which is unwelded (Gertisser *et al.*, 2010). It is restricted topographically to a small area north of Angra do

Heroísmo, and is exposed in the coastal cliffs to the east of the town, reaching thicknesses of 20 m.

Self (1974) determined a total volume for the LAI of 0.33 km^3 dense-rock equivalent (DRE) on land, but acknowledged that the presence of ignimbrite exposures at sea level suggests that the original pyroclastic flows entered the sea, rendering the actual totals far larger than predicted. However, Gertisser *et al.* (2010) cited the small volume of the calderas on Terceira, alongside evidence for their gradual formation via numerous eruptive phases, to suggest that individual eruptions are unlikely to have generated more than 1-2 km^3 of magma.

Stratigraphically below the LAI, interstratified pumice falls, lava flows and at least six ignimbrite formations combine to form the Lower Terceira Group (LTG) (Gertisser *et al.*, 2010). These include the Linhares-Matela Ignimbrite Formation (LMI), the Vila Nova-Fanal Ignimbrite Formation (VFI), the Calderia-Castelinho Ignimbrite Formation (CCI), the Pedras Negras Ignimbrite Formation (PNI), the Grota do Vale Ignimbrite Formation (GVI) and the Ignimbrite-i Formation (Self, 1974, 1976; Gertisser *et al.*, 2010). Gertisser *et al.*, (2010) defined and described two additional pyroclastic units that lie stratigraphically within the LTG; the Posto Santo spatter-flow deposit, and the Quatro Ribeiras pyroclastic flow deposit.

The LMI is the uppermost ignimbrite formation in the LTG, comprising the Linhares and Matela Members. The Linhares Member outcrops in a quarry to the north of Angra, and is separated from the overlying LAI by a lava flow and approximately 10 m of pyroclastic fall deposits (Gertisser *et al.*, 2010). It is dark grey and non-welded in outcrop, restricted to the south of the island and contains pumice clasts of up to 1 m in size. The Matela Member is found in a single outcrop, near the Matela lava dome in the islands interior. Self (1974) described a thin, dark ignimbrite exposed in the no longer accessible cliffs of Angra harbour, which Gertisser *et al.* (2010) suggested may have been an additional outcrop of the LMI, based upon it's description and stratigraphical position. The location of these outcrops appears to restrict the LMI to the south of the island.

The LMI differs from other ignimbrite formations in that it bears plagioclase alongside large phenocrysts of alkali-feldspar. Clinopyroxene and oxides are present as a microphenocryst population (Self, 1974; Gertisser *et al.*, 2010). Groundmass glass shows slight flattening and in places a poorly developed eutaxitic texture. Gertisser *et al.* (2010) provided radiocarbon dates ranging from 34.7 ± 7.5 ka to 37.3 ± 5 ka (Figure 4.6).

The VFI is made up of multiple pyroclastic flow units and associated fall units, and is divided into two members; the Vila-Nova Member, seen in the northern coasts, and the Fanal Member, seen in the southern coasts (Self, 1974; Gertisser *et al.*, 2010). Stratigraphically, they underlie the LMI. Self (1974) describes them as 'light grey, non-welded and pumice-rich' and notes a maximum thickness of around 20 m, though this thickness has been altered by erosion (Gertisser *et al.*, 2010). Although widely distributed to the north of Pico Alto, deposits are limited in the south, and are found only in the area surrounding Angra. Self (1974) and Gertisser *et al.* (2010) described up to eight unwelded flow units, defined by pumice rich layers (corresponding to layer 2b using the standard ignimbrite succession of Sparks *et al.*, 1973). Some are as thin as 50 cm and their number varies from exposure to exposure based upon localised flow conditions (Self, 1974). The mineralogy is similar to the overlying ignimbrites, with large alkali-feldspar phenocrysts, clinopyroxene and oxides. Gertisser *et al.* (2010) provided $^{40}Ar/^{39}Ar$ dates of 50 ± 10 ka and 58 ± 20 ka (Figure 4.6).

The CCI also comprises two members; the Caldeira Member in the north and the Castelinho Member in the south, both of which are stratigraphically below the VFI. Self, (1974) describes the CCI as "…grey, essentially non-welded ignimbrites, up to 25 m thick…". In places the beginnings of welding can be seen, attributed to vapour phase crystallisation (Smith, 1960). Of all the ignimbrites on Terceira, it is the only one to exhibit a well-developed basal-surge layer, featuring cross bedding of both fine- and coarse-grained pumice beds (Self, 1974; Gertisser *et al.*, 2010). The CCI's crystal content is similar to that of the overlying ignimbrite formations, comprising alkali-feldspar, clinopyroxene and magnetite. However, it can be easily distinguished by the relative

abundance of syenitic cognate xenoliths, which can reach sizes of 25 cm in diameter (Gertisser *et al.*, 2010). Self (1974) noted the presence of a thick unit of brecciated ignimbrite material and lithic blocks, overlying the basal surge layer. Gertisser *et al.* (2010) interpreted this feature as a debris flow, comprising blocks of proximal juvenile material from an earlier stage of the same eruption. An additional ignimbrite unit occurs stratigraphically beneath the debris flow and above the base of the CCI. This unit was named the Porto do Pipas Ignimbrite by Self, (1974), and comprises a single flow unit of unwelded, pumice-rich ignimbrite. The only known exposure is in the Angra Harbour cliffs, (no longer accessible), where it was observed to be ~ 4 m thick, but heavily eroded (Gertisser *et al.*, 2010). Gertisser *et al.* (2010) obtained two $^{40}Ar/^{39}Ar$ ages of 71 ± 4 ka and 83 ± 18 ka from anorthoclase crystals, showing that the CCI is considerably older than the overlying VFI (Figure 4.6).

The PNI is exposed exclusively on the northern coast, found as dark-weathering, heavily-eroded remnants between Quatro Ribeiras to the west and Vila Nova to the east. Gertisser *et al.* (2010) describe it as "…a dark-weathering ignimbrite…" with "…fairly crystal-poor, dark and relatively dense pumiceous clasts of similar composition to the other ignimbrites…". The base is marked by a yellowish welded layer that exhibits basaltic lithic clasts derived from an underlying lava flow. The Ignimbrite-i Formation is found in only a single small outcrop at the base of a cliff section west of Caldeira, where it is welded with large, crystal-rich fiamme. Stratigraphically, both the PNI and Ign-i underlie the CCI, though the relationship between the two remains ambiguous due to the scattered nature of their outcrops (Gertisser *et al.*, 2010). Their position at the base of the ignimbrite stratigraphy is supported by an $^{40}Ar/^{39}Ar$ age of 89 ± 9 ka acquired from Ign-i (Gertisser *et al.*, 2010) (Figure 4.6).

The GVI is found in only one exposure, near to the mouth of the Grota do Vale stream on the south coast. Stratigraphically, it is the lowest ignimbrite on the south coast, and does not correlate with either of the lowest ignimbrites from the north coast (PNI and Ign-i). It is heavily altered and comprises two flow units with small fiamme and a well-

developed eutaxitic texture. The exposure is only 1.5 m thick, but the top is eroded, so the original thickness is unknown. A notable feature of the GVI is the presence of biotite in the juvenile clasts, a mineral that is not found in any of the other Terceira ignimbrites. Gertisser *et al.* (2010) also define two further pyroclastic density current deposits on the island; the Posto Santo spatter flow and the Quatro Ribeiras pyroclastic flow. The former is similar in composition to the other, previously described pyroclastic lithologies and comprises a poorly sorted unit, with abundant spatter clasts, which overlies nearby lava flows related to Guilherme Moniz. The latter is also of similar composition to the other pyroclastic units of Terceira and comprises a clast-supported pyroclastic flow deposit that lies, stratigraphically, between the LAI and VFI (Gertisser *et al.,* 2010).

4.3.2 The occurrence of dalyite

Due to the occurrence of the rare mineral dalyite in the investigated Terceira rocks, a brief account of the mineral, its origins, and its composition, is given here. Following the initial discovery of dalyite (Van Tassel, 1952), it was next identified in peralkaline syenitic ejecta from Fogo volcano, São Miguel, Azores (Cann, 1967; Widom *et al.*, 1993); where it was observed as an entirely intercumulus phase and therefore inferred by Ridolfi *et al.* (2003) to be the last mineral to crystallise (alongside quartz). Lazebnik & Makhotko (1982) identified dalyite in the Murun Complex, Siberia, Russia, also providing additional quantitative analyses. Furnes *et al.* (1982) and Robins *et al.* (1983) noted the presence of dalyite within a highly potassic lamprophyric dyke in Sunnfjord, Norway. Raade & Mladeck (1983) reported dalyite within a peralkaline granite pluton at Gjerdingen, Norway, where it was typically found in close contact with janhaugite $Na_3Mn_3Ti_2Si_4O_{15}(OH,F,O)_3$. Harris and Rickard (1987) recorded the occurrence of dalyite, alongside eudialyte, in a peralkaline granitic dyke that cross-cuts the nepheline syenites of the Straumsvola Complex, Antarctica. In 1988, an enstatite-sanidine-phlogopite lamproite in south-eastern Spain was reported to contain the mineral's first known occurrence in an extrusive rock (Venturelli *et*

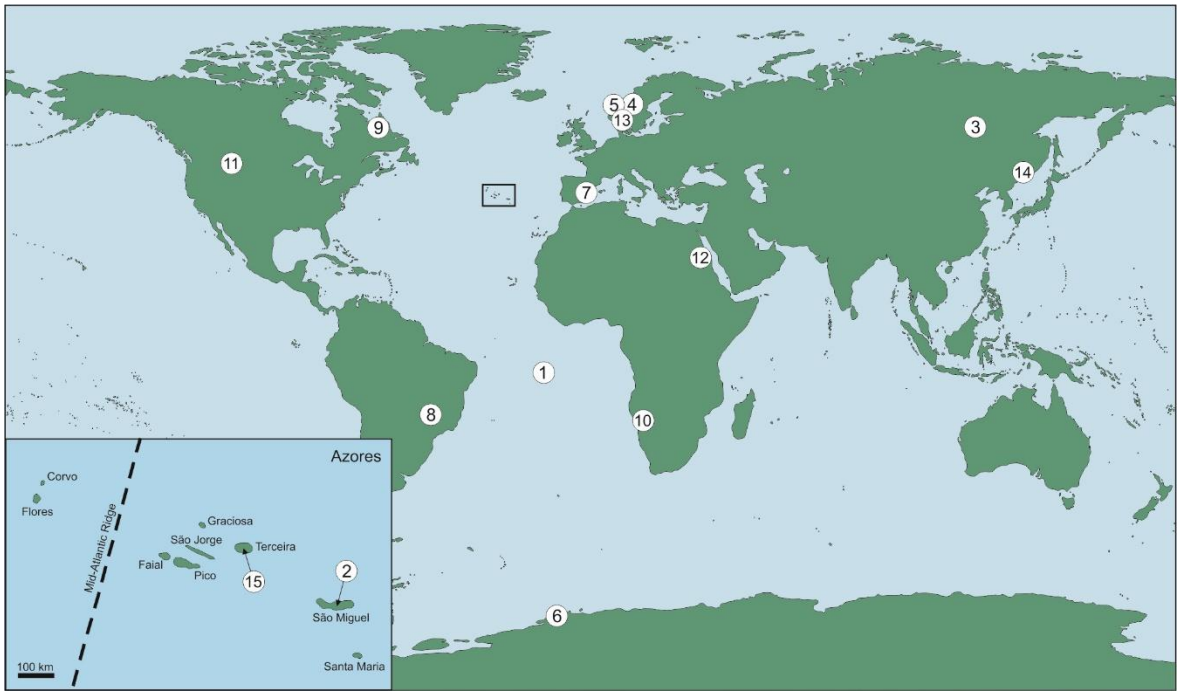

FIGURE 4.7: Reported occurrences of dalyite worldwide. 1) Ascension Island, South Atlantic Ocean (Van Tassel, 1952); 2) Fogo volcano, São Miguel, Azores (Cann, 1967); 3) the Murun Complex, Siberia, Russia (Lazebnik and Makhotko, 1982; Dolivo-Dobrovol'skiy and Yevdokimov, 1991; Konev *et al.*, 1996; Reguir, 2001); 4) Gjerdingen, Norway (Raade and Mladeck, 1983); 5) Sunnfjord, Norway (Robins *et al.*, 1983); 6) the Straumsvola Complex, Dronning Maud Land, Antarctica (Harris and Rickard, 1987); 7) Cancarix, South Eastern Spain (Venturelli *et al.*, 1984; Linthout *et al.*, 1988); 8) the Serra Negra and Salitre Complex, Brazil (Mariano and Francis, 1989; Mariano and Marchetto, 1991); 9) the Strange Lake Complex, Canada (Birkett *et al.*, 1992; Salvi and Williams-Jones, 1995); 10) the Brandberg Complex, Namibia (Schmitt *et al.*, 2000); 11) Gordon Butte, Montana, USA (Chakhmouradian and Mitchell, 2002); 12) the Zargat Na'am ring complex, Egypt (Saleh, 2006); 13) Langesundfjord, Norway (Andersen *et al.*, 2010); 14) the Shibanovsky Massif, Russia (Stepnova *et al.,* 2013); 15) Terceira Island, Azores (this study)

al., 1984; Linthout *et al.*, 1988). Soon afterwards, dalyite was observed within fenites from the Serra Negra and Salitre – carbonatite alkaline igneous complex, Brazil (Mariano & Francis, 1989; Mariano & Marchetto, 1991; Brod, 1999). Dalyite was later identified in the Strange Lake peralkaline granite complex, Canada, and noted to have nucleated heterogeneously onto older zircon crystals (Birkett *et al.*, 1992; Salvi & Williams-Jones, 1995). Subsequent reported occurrences include the Amis peralkaline granite intrusion of the Brandberg Complex, Namibia (Schmitt *et al.*, 2000), the various lithologies of the Murun Complex, Siberia, Russia (e.g. Dolivo-Dobrovol'skiy & Yevdokimov, 1991; Konev *et al.*, 1996; Reguir, 2001), the Gordon Butte pegmatites, Montana, USA (Chakhmouradian and Mitchell, 2002), peralkaline granite dykes to the north of the Zargat Na'am ring complex, Egypt (Saleh, 2006), more unusually, a nepheline-bearing pegmatite,

Langesundfjord, Norway (Andersen *et al.*, 2010) and the alkali syenites and metasomatites of the Shibanovsky Massif, Russia (Stepnova *et al.*, 2013) (Figure 4.7).

Van Tassel (1952) provided the first description of the physical properties, chemical composition, unit cell and x-ray powder diffraction data of dalyite. It is a triclinic, colourless mineral of moderate positive relief, exhibiting up to second order interference colours. The unit cell was defined as $K_2ZrSi_6O_{15}$, though the potential substitutions of Na for K, and Hf for Zr, were suggested. The chemical similarity between dalyite and wadeite ($K_2ZrSi_3O_9$) was also noted.

The crystal structure of dalyite was determined by Fleet (1965), who defined it as a phyllosilicate comprising four-, six- and eight-membered rings of SiO_4 tetrahedra. These sheets are linked by regular ZrO_6 octahedra and irregular $(K,Na)O_8$ polyhedra. Robins *et al.* (1983) provided 10 quantitative chemical analyses of dalyite from Sunnfjord, Norway and presented evidence for the substitution of Zr with Ti, and K with Fe, suggesting the more accurate empirical formula $(K,Na,Fe)_2(Zr,Ti)Si_6O_{15}$. They also highlighted the compositional similarity between dalyite and darapiosite ($KNa_2LiMnZnZrSi_{12}O_{30}$), sogdianite ($(K,Na)_2Li_2(Li,Fe,Al,Ti)_2Zr_2(Si_2O_5)_6$), and zektzerite ($LiNaZrSi_6O_{15}$). Further chemical analyses of dalyite were reported by Harris *et al.* (1982), Lazebnik and Makhotko (1982), Harris and Rickard (1987), Linthout *et al.* (1988), Birkett *et al.* (1992), Konev *et al.* (1996), Reguir (2001), Chakhmouradian and Mitchell (2002), and Ridolfi *et al.* (2003).

4.4 Field descriptions and sampling

Detailed investigation and sampling of the seven ignimbrite formations of Terceira (i.e. the Lajes-Angra Ignimbrite Formation (LAI), the Linhares-Matela Ignimbrite Formation (LMI), the Vila Nova-Fanal Ignimbrite Formation (VFI), the Caldeira-Castelinho Ignimbrite Formation (CCI), the Pedras Negras Ignimbrite Formation (PNI), the Ignimbrite-i Formation (Ign-i), and the Grota do Vale Ignimbrite Formation (GVI), as defined by Gertisser *et al.*, 2010) was undertaken during two fieldwork sessions in November 2011 and April 2013. During the course of fieldwork, a total of 26 locations were defined along the north and south coastlines, and 113 samples were collected for further analysis, including juvenile pumice clasts, lithic clasts, ash, and syenitic ejecta. All locations are shown in Figure 4.8. A full list of samples is given in Appendix B.

4.4.1 The Lajes-Angra Ignimbrite Formation

The LAI is the youngest of the seven ignimbrite formations on Terceira, and can be found at various localities on both north and south coasts. It was observed at locations 18 to 20, 22 to 24, 26 to 38, 40, 42, 43 and 52 (Figures 4.8, 4.9), but due to the nature of the outcrops, and the stratigraphic position of the LAI, it is not readily accessible at locations 18 to 20, 28 and 52. Substantial facies variations are present, including welded units, regionally- and locally-developed flow units with well-developed inverse grading of pumice clasts, massive, pumice-rich units, deposit thickness variations and transitions from dense, dark pumice to vesicular, light pumice clasts.

At location 23, the Lajes Member of the LAI is found at the top of the cliff section, where it exhibits a light coloured weathered surface and two clearly defined flow units (Figure 4.9a). The lower unit is dominated by light grey ash with occasional light grey pumice clasts up to ~ 3 cm in size. The upper unit is characterised by an abundance of black pumice clasts, which reach sizes of ~ 40 cm. The base of the LAI is here marked by a distinctive anorthoclase-rich, ashy layer which is approximately 1 cm in thickness.

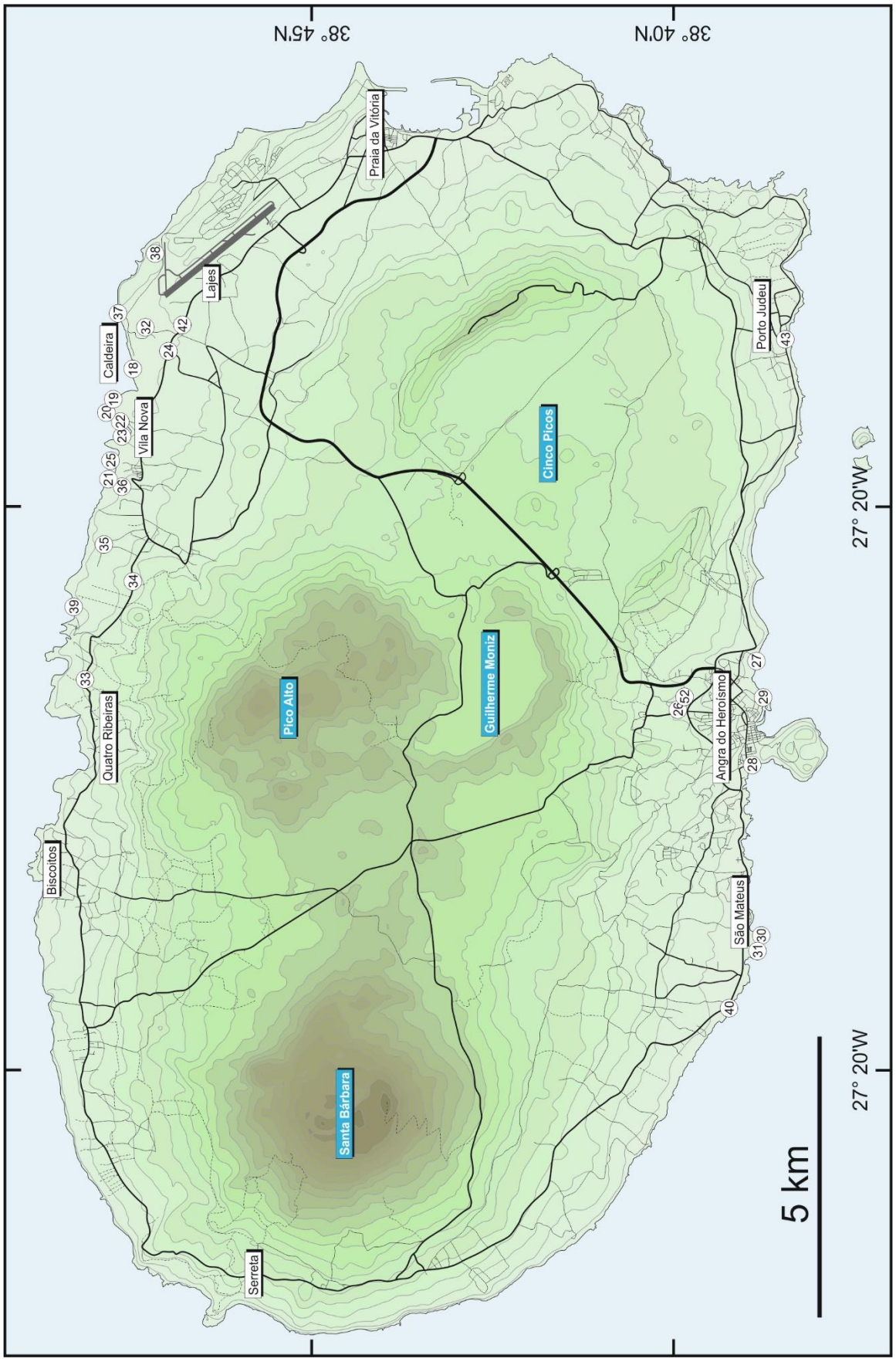
38° 45'N
38° 40'N
27° 20'W
27° 20'W
5 km
Praia da Vitória
Lajes
Caldeira
Vila Nova
Porto Judeu
Cinco Picos
Pico Alto
Guilherme Moniz
Santa Bárbara
Quatro Ribeiras
Biscoitos
Angra do Heroísmo
São Mateus
Serreta

◄ **FIGURE 4.8:** A summary map of Terceira, showing the sampling localities of the study in relation to major settlements and infrastructure. Contours taken from GeoMapApp©

FIGURE 4.9: Representative field photographs of the LAI. **a)** Lajes ignimbrite overlying undifferentiated fall deposits at the top of the Vila Nova bay section. Scale = 30 cm **b)** Roadside outcrop of the Lajes ignimbrite on the coastal road to Quatro Ribeiras. Scale = 30 cm **c)** The Lajes ignimbrite ramping over pre-existing topography (dipping to the south). Base is partially welded. Scale highlighted **d)** Coastal outcrop of the Lajes ignimbrite near São Mateus, exhibiting highly welded base **e)** Lajes ignimbrite exposed ~ 20 m west of Location 30. Characteristic black pumice clasts are abundant, but welded base is not seen. Scale highlighted

At location 34, on the coastal road to Quatro Ribeiras (Figure 4.9b), the Lajes ignimbrite is exposed in a number of roadside outcrops, and includes abundant,

FIGURE 4.9 continued: f) The Lajes ignimbrite and underlying undifferentiated fall deposits exposed near the coast to the west of Vila Nova bay. Scale = 30 cm **g)** Partially welded outcrop of the Lajes ignimbrite on the road to Caldeira. Scale = 30 cm **h)** Outcrop of the Lajes ignimbrite near the Agualva stream, bearing substantial black pumice clasts (highlighted scale = 30 cm) **i)** Lajes ignimbrite with characteristic black pumice clasts, east of Caldeira. Scale = 30 cm **j)** The base of the Lajes ignimbrite exposed in Porto Judeu. Scale = 20 cm

characteristic black pumice clasts containing large anorthoclase crystals. At location 24, the Lajes ignimbrite is seen dipping to the south, overlying various undifferentiated fall deposits (Figure 4.9c). The lower portion of the outcrop is partially welded and comprises black ash and black, glassy pumice clasts, up to 15 cm in length, bearing large anorthoclase crystals. The thin-crystal-dominated layer observed at location 23 is also

FIGURE 4.9 continued: k) Outcrop of the Lajes ignimbrite to the north of the U.S. airbase, showing characteristic black pumices and two flow units. Scale = 50 cm **l)** Small outcrop of the Lajes ignimbrite at São Bartolomeo on the south coast. Scale = 30 cm **m)** Small roadside outcrop of the Lajes ignimbrite to the east of Caldeira. Scale = 30 cm **n)** The Angra Member of the LAI, exposed on the northern margins of Angra (highlighted scale = 30 cm) **o)** Highly pumiceous outcrop of the Angra ignimbrite below the fort, on the eastern margins of Angra. Hammer for scale (30 cm)

present at the base of this location. The upper portion of the outcrop is light in colour, and contains light coloured, vesicular pumice clasts up to ~ 30 cm in size. Location 30 is situated on the south coast, near São Mateus, and comprises the Lajes ignimbrite overlying pre-LAI lithologies. The lowermost layer is strongly welded, with small (< 6 cm) glassy fiamme (Figure 4.9d). The overlying unit is unwelded and dominated by black, vitreous plumice clasts containing large anorthoclase crystals. Lithic clasts are abundant

compared with other locations, and are variable in lithology, including lavas of various colour and vesicularity. At location 31, ~ 20 m west along the beach, the upper portion of the same outcrop is found, comprising abundant dark pumice clasts up to ~ 30 cm (Figure 4.9e).

At location 36, a 2 m thick outcrop of the Lajes ignimbrite is seen overlying various fall deposits (Figure 4.9f). The contact between the two is marked by a thin (~ 1 cm) crystal-rich layer, as seen elsewhere. Pumice clasts reach ~ 10 cm in size and are predominantly light grey and vesicular, though black pumice clasts bearing large anorthoclase (~ 2 mm) crystals are also present. At location 32, a small outcrop of the Lajes ignimbrite is present at the side of the road to Caldeira, exhibiting flattened pumice clasts and abundant lithics (Figure 4.9g). To the west of Caldeira, near the Agualva stream, a substantial thickness of the Lajes ignimbrite is present (location 35, Figure 4.9h). A variety of lithic clasts are abundant and, alongside black, anorthoclase-bearing pumice clasts, reach sizes of up to ~ 50 cm. Additionally, small clasts of medium grained syenite are present. To the east of Caldeira, a distinctive, black-weathering outcrop of the Lajes ignimbrite is present (Figure 4.9i), with similarly abundant lithic clasts, alongside light grey and black, vitreous pumice clasts and rare, medium grained syenite nodules.

On the south coast, in Porto Judeu, another outcrop of the Lajes ignimbrite is present at the port (Figure 4.9j), with abundant pumice clasts up to ~ 10 cm in size. At location 38, to the north of the airport, a distinctive black outcrop of the Lajes ignimbrite is seen, reaching a thickness of ~ 2 m, overlying a number of fall deposits and soils (Figure 4.9k). As seen elsewhere, the base of the LAI is marked by a thin (~ 1 cm) anorthoclase-dominated unit. Two individual flow units may be present, distinguished by coarsening-upward, black, vitreous pumice clasts. At location 40, near São Bartolomeo, a small outcrop of the Lajes ignimbrite can be found, distinguished by the presence of black, vitreous pumice clasts (Figure 4.9l). A similarly small outcrop of the Lajes ignimbrite was found at location 42, at the roadside, to the south east of Caldeira (Figure 4.9m). Here,

characteristicly large, black pumice clasts are present, in addition to abundant light pumice clasts.

The Angra Member of the LAI was identified at two locations in the south of the island. At location 26, to the north of Angra, a substantial thickness (~ 5 m) of the Angra ignimbrite is present, characterised by light pumice clasts up to 20 cm in size, in a light ashy matrix. The outcrop exhibits no clearly defined stratification or grading (Figure 4.9n). On the south coast, beneath the fort in Angra, another outcrop of the Angra ignimbrite was identified (Figure 4.9o). As observed at location 26, it comprises abundant light coloured pumice clasts up to ~ 15 cm in size, set in a light coloured ashy matrix. Unilke location 26 however, the lower portion of the outcrop exhibits a welded basal layer.

4.4.2 The Linhares-Matela Ignimbrite Formation

The LMI was identified and sampled in two locations by R. Gertisser in 2006 (see Gertisser *et al.*, 2010). The first location is an active (at the time of writing) quarry to the north of Angra (UTM: 481746E, 4280372N). Here, the Linhares Member was identified and described as a dark-grey, non-welded ignimbrite, separated from the overlying LAI by ~ 10 m of fall deposits and a lava flow. The second location, where the highly weathered Matela Member was identified, is in the central portion of the island, near the Matela lava dome (UTM: 478376E, 4282746N).

4.4.3 The Vila Nova-Fanal Ignimbrite Formation

The VFI was identified at three locations (locations 23, 25 and 28). At location 23a, at Porto da Vila Nova, the Vila Nova Member is exposed in the cliff, reaching ~ 14 m in thickness. It overlies a series of ash and fine lapilli falls which overlie the CCI (Figure 4.10a). Here, it comprises a light grey, pumice rich ignimbrite which exhibits at least four flow units, each defined by coarsening upward pumice clasts.

FIGURE 4.10: Field photographs of the VFI **a)** Base of the Vila Nova ignimbrite exposed in Porto da Vila Nova. Highlighted scale = 32 cm **b)** Upper outcrop of Vila Nova ignimbrite with five flow units defined by distinctive coarsening upward pumice clasts. Scale = 50 cm **c)** Pumice fall deposit at the base of the VFI. Pick for scale (32 cm) **d-e)** Poorly sorted, unstratified, outcrop of the Vila Nova ignimbrite showing highly vesicular, light grey pumice clasts. Pick for scale (32 cm)

Lithic clasts and obsidian chips are uncommon and range in size from 0.5 to 7 cm and 0.5 to 1 cm, respectively. Pumice clasts are dark to light grey, porphyritic and reach sizes of ~ 40 cm in the lowest flow unit, compared to ~ 20 cm in overlying flow units.

Location 23b, on the footpath up the western cliffs of Porto da Vila Nova, offers the opportunity to access the upper portion of the Vila Nova outcrop (Figure 4.10b). At least 5

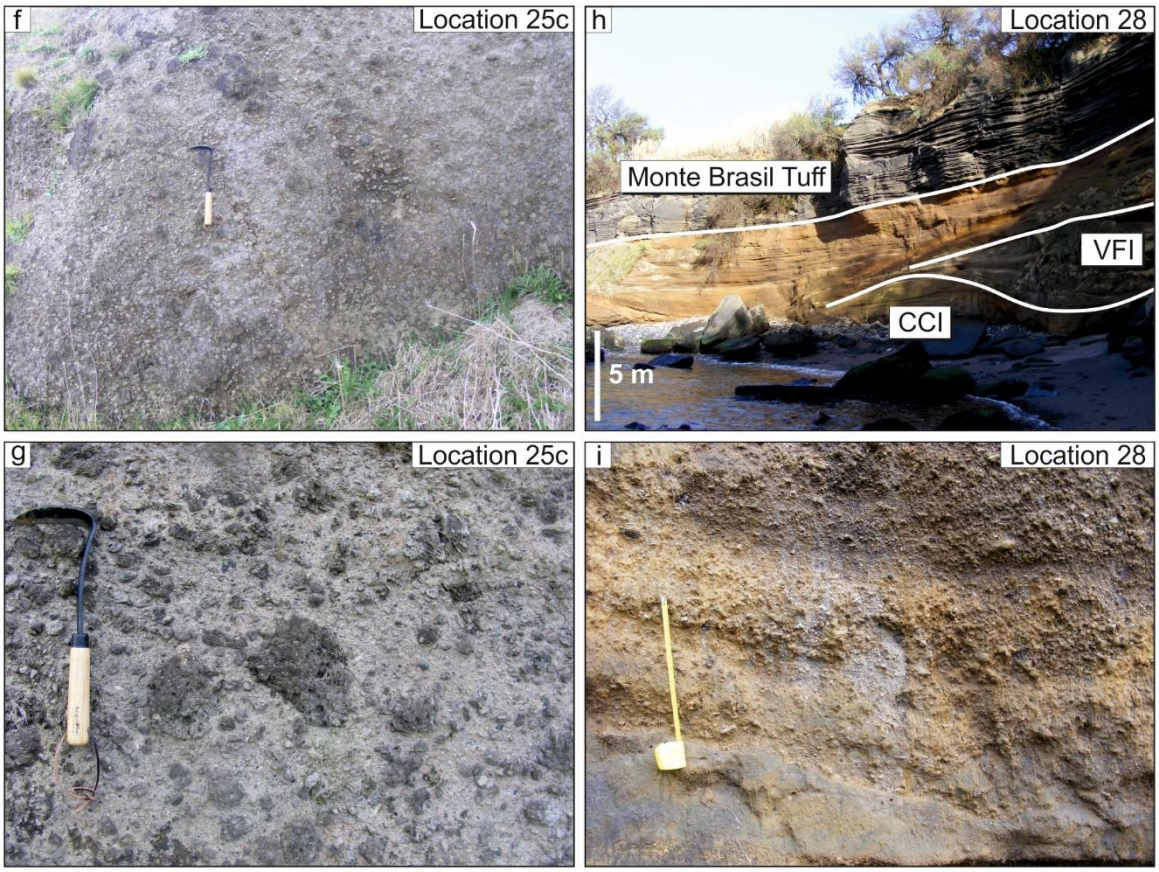

FIGURE 4.10 CONTINUED: f-g) Unstratified exposure of the Vila Nova ignimbrite exhibiting dense, dark grey, porphyritic pumice clasts. Pick for scale (30 cm) **h)** Digitised outcrop photograph of the Fanal Member of the VFI overlying the CCI in Baía do Fanal and showing substantial thickness variation **i)** Photograph of the Fanal ignimbrite showing slight stratification. Scale = 30 cm

flow units are present, again defined by coarsening upward pumice clasts, though they are somewhat thinner than those seen at the base of the VFI, at location 23a (~ 0.5 to 0.6 m compared to 2 to 4 m). Lithologically, these units are extremely similar to the described flow units at location 23a. Juvenile pumice clasts were sampled from the 3 accessible flow units observed at location 23a (samples T025 to T032, T108, T109), and also from the 5 flow units seen at location 23b (samples T103 to T107).

Approximately 600 m to the west of Porto da Vila Nova, the Vila Nova ignimbrite is exposed at the top of the coastal cliffs (location 25). At location 25a, the base of the VFI is marked by a well sorted pumice fall deposit, up to 40 cm in thickness (Figure 4.10c). Pumice clasts are light in colour and vesicular. Lithics are rare, but some small (< 1 cm)

obsidian chips are present. This is overlain by associated ash and fine lapilli fall units, ~ 50 cm thick. At location 23b, around 50 m west of 23a, a ~ 3 m thick unit of pumiceous, poorly sorted ignimbrite is present (Figure 4.10d), overlain by a well sorted pumice fall deposit, ~ 30 cm in thickness. The ignimbrite is rich in light grey, vesicular pumice clasts, up to 30 cm in size, which generally coarsen upwards. Approximately 30 m south west of location 23b, a similar unit of pumice rich ignimbrite is present (Figure 4.10f, g). Although it's maximum thickness is only ~ 1.25 m, and it is underlain by a thin (~ 3 cm) grey ash and two fining upward pumice lapilli fall units, it likely corresponds to the base of the VFI. Samples of ash and juvenile pumice clasts were collected from the pumice falls, the ignimbrite and a number of pre-VFI units (samples T039 to T048, T072, T094 to T096). The Fanal Member of the VFI is exposed in Baía do Fanal, in Angra do Heroísmo (location 28). Here, it ranges from 2 to 6 m in thickness and overlies the CCI (Figure 4.10h). Its base is marked by a pumice lapilli fall deposit, ~ 10 cm in thickness and made up of light, vesicular pumice clasts (0.5 to 3 cm) and uncommon lithic clasts (< 1 cm). This is overlain by a finer grained pumice lapilli fall which is somewhat thicker (~ 25 cm) and generally fines upwards. The main body of the ignimbrite is very pumice rich, with abundant light, vesicular pumice clasts (0.5 to 5 cm) and rare lithics. Some stratification can be observed, defined by coarsening upward pumice clasts (Figure 4.10i), allowing the recognition of ~ 3 flow units. Juvenile pumice clasts were collected from the basal fall deposit and the lowermost ignimbrite flow unit (samples T056, T057, T112, T113).

4.4.4 The Caldeira-Castelinho Ignimbrite Formation

The CCI was identified at 7 locations (locations 18, 19, 20, 23, 25, 28 and 39) (Figure 4.11). At location 18, ~ 800 m west of Caldeira, the Caldeira Member of the CCI can be seen overlying the ignimbrite-i Formation and capped by various tuffs, lavas and the LAI. It approaches 10 m in thickness and is made up of 3 poorly sorted flow units, each characterised by well defined

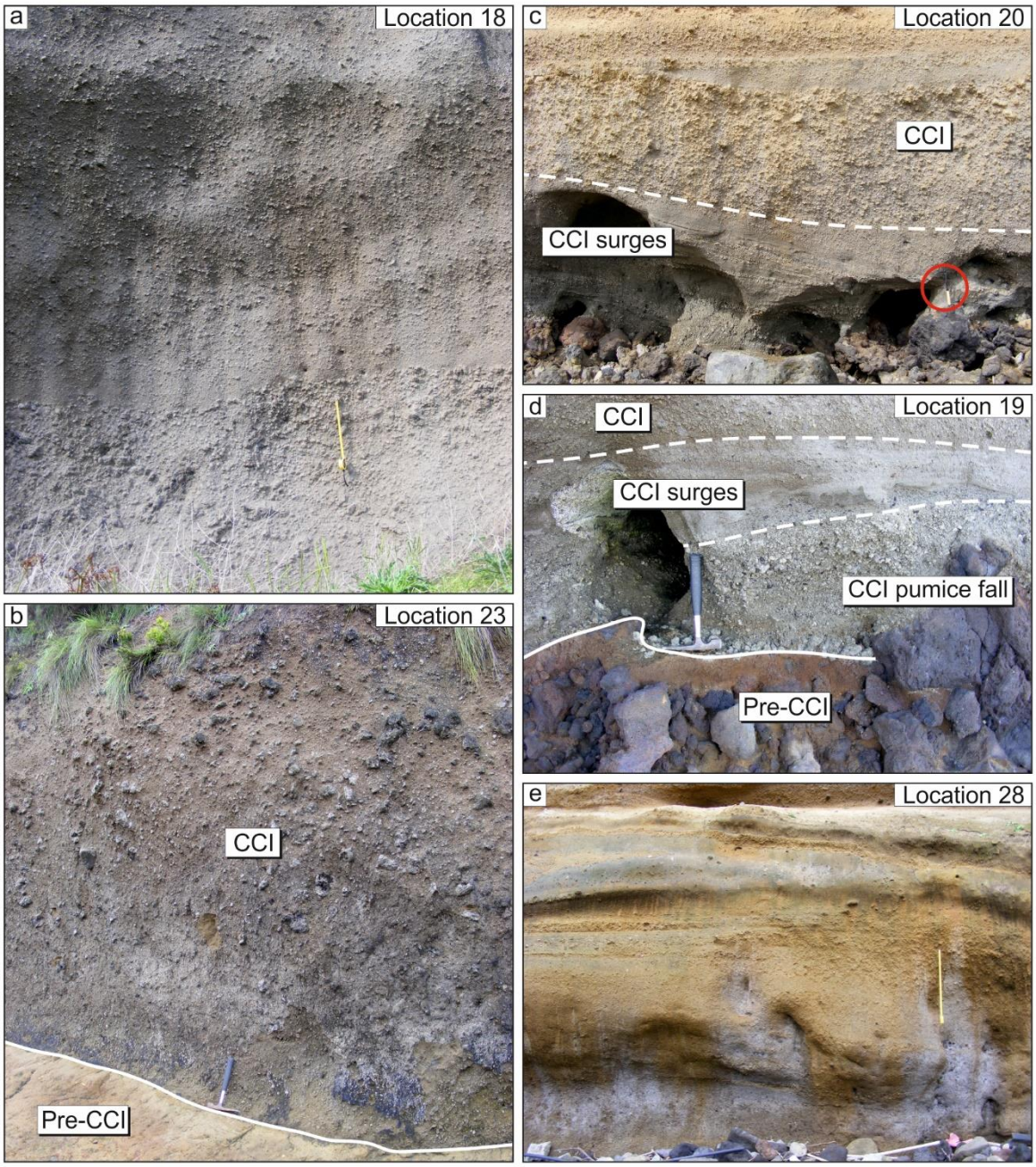

FIGURE 4.11: Field photographs of the CCI **a)** Caldeira Member of CCI showing two flow boundaries marked by pumice grading patterns. Scale = 30 cm **b)** Digitised photograph of the Caldeira Member of CCI with pronounced, coarse, dark grey pumice clasts, overlying altered yellow ashes. Hammer for scale (30 cm) **c)** Digitised image of the fine grained, cross bedded surge deposits underlying the main body of the CCI. Highlighted scale = 32 cm **d)** Digitised photograph highlighting the pumice fall deposit and underlying rubbly lava flow at the base of the CCI. These are overlain by fine grained surges and ignimbrite. Hammer for scale (30 cm)**e)** Pumice rich exposure of the Castelinho Member of the CCI. Scale = 50 cm

coarsening upward pumice clasts (Figure 4.11a). Juvenile clasts are typically light grey and highly vesicular, though denser glassy clasts are also present. All pumice clasts are porphyritic, with alkali feldspar phenocrysts up to 5 mm in size. Dark to light grey lithic

clasts and small (< 1 cm) obsidian chips are also abundant. Juvenile pumice clasts were sampled from the lower and middle flow units (samples T002 to T004, T076 to T078).

At location 23, at Porto da Vila Nova, the stratigraphic relationship between the CCI and the overlying VFI can be seen. Here, the Caldeira Member of the CCI is found near sea level, overlying a distinctive, nodule bearing unit of orange tuff, at least 1.1 m in thickness (Figure 4.11b). The overlying CCI is ~ 6.5 m thick and unstratified, with porphyritic pumices, both dark and light, up to 30 cm in diameter. Dark grey lithics represent a relatively small component (< 10 %). Rarely, small syenitic nodules can be seen. It is overlain by a ~ 10 cm thick soil, various fall deposits and a substantial thickness of the VFI.

At location 20, at Ponta das Escaleiras, the Caldeira ignimbrite is present at the base of the cliffs. It is divided into two flow units, defined by coarsening upward pumice clasts. At the base of the outcrop, a distinctive surge unit of cross bedded ash and fine lapilli (< 1 cm) is exposed (Figure 4.11c). If the unit is traced to the east (location 19), a thin (~ 30 cm) pumice rich fall deposit can be seen, between the surges and an underlying a'a lava flow (Figure 4.11d). This pumice fall deposit is unusual in that it is not seen at any other CCI outcrops. Juvenile pumice clasts, syenite nodules and obsidian chips were sampled from both locations, including the basal pumice fall deposit, the surges and both of the two overlying ignimbrite flow units (samples T005 to T011, T064 to T070). The Castelinho Member of the CCI is exposed in Baía do Fanal, in Angra do Heroísmo (location 28, Figure 4.11e). At the base of the cliff, a ~ 2.5 m thick exposure can be seen, overlain by various fall deposits, and the VFI. The deposit comprises a partially stratified, pumice rich ignimbrite, with small pumice lapilli (up to 3 cm) forming thin bands rarely more than 1 clast thick, of which some are laterally continuous, and others pinch out. Lithic clasts are uncommon, but reach sizes of up to 15 cm. Juvenile pumice clasts were collected from the upper and lower outcrop (samples T054, T055, T111).

At location 25, the uppermost Caldeira ignimbrite is exposed at the top of the cliff (location 23a), overlain by a soil, ~ 20 cm thick, and the VFI. Vesicular, pale pumice clasts are abundant and range from ~ 0.5 to 6 cm in size. Fine to coarse grained syenitic nodules are particularly common here, ranging from < 5 to ~ 25 cm. Samples of juvenile pumice and syenite nodules were collected (samples T038, T073).

An additional outcrop of the CCI can be found in the cliffs east of Ponta do Misterio. At the base of the cliff, an extremely poorly sorted, polymict debris flow deposit is exposed. The presence of coarse grained syenite nodules, up to 40 cm in size, suggests that this deposit forms part of the CCI, and likely relates to the CCI debris flow unit described by Gertisser *et al.*, (2010). Syenite was collected from this location (sample T092).

4.4.5 The Pedras Negras Ignimbrite Formation

The PNI was identified and sampled at location 21, at the base of the coastal cliffs to the north of Vila Nova (Figure 4.12). It overlies yellow ashes, and is itself overlain by ~ 30 to 50 cm thick ashes, followed by the CCI. This outcrop is black, ~ 3 m thick and unwelded. Juvenile pumice clasts are black and dense, with large alkali feldspar phenocrysts, up to 1 cm in size. The outcrop coarsens upwards, becoming more lithic rich and bearing pumice clasts up to ~ 30 cm in size. Pumice clasts from the upper, coarse region were sampled (samples T012, T093).

4.4.6 Grota do Vale Ignimbrite Formation

The GVI was identified at location 27, at the base of the coastal cliffs on the south coast, ~ 1.5 km east of Angra harbour (Figure 4.8). The somewhat unusual presence of biotite, as noted by Gertisser *et al.* (2010), facilitated its identification. At location 27a, the ignimbrite overlies a rubbly, a'a lava flow, and has an erosive upper surface with an overlying lava

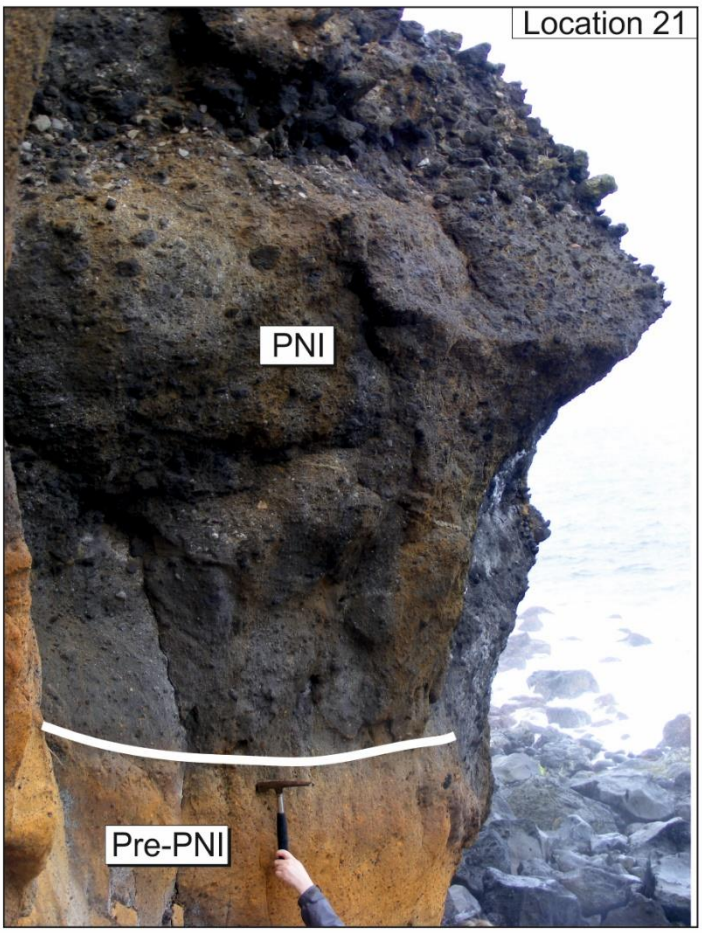

FIGURE 4.12: Digitised field photograph showing the base of the PNI and underlying orange tuffs. Hammer for scale (30 cm)

flow. The outcrop exhibits a pronounced lower welded layer, with dark, glassy, and sometimes porphyritic, fiamme, up to ~ 20 cm in size (Figure 4.13). The upper region of the unit is unwelded and altered, though biotite bearing juvenile clasts can still be identified. Approximately 500 m to the east, an additional exposure of the GVI was identified (Location 27b). Here, it is extremely altered, though the presence of two bounding lava flows and biotite bearing juvenile clasts confirm its relation to location 27a. This exposure is ~ 2.5 m thick and, though less defined, appears to exhibit deformed juvenile clasts and fiamme in the lower ~ 0.75 m section. Some stratification can be seen in the upper 1.75 m region, and small (< 3 cm) lithics are common, though examples up to 20 cm in size can be found. Samples were collected from both locations (samples T050 to T053, T063).

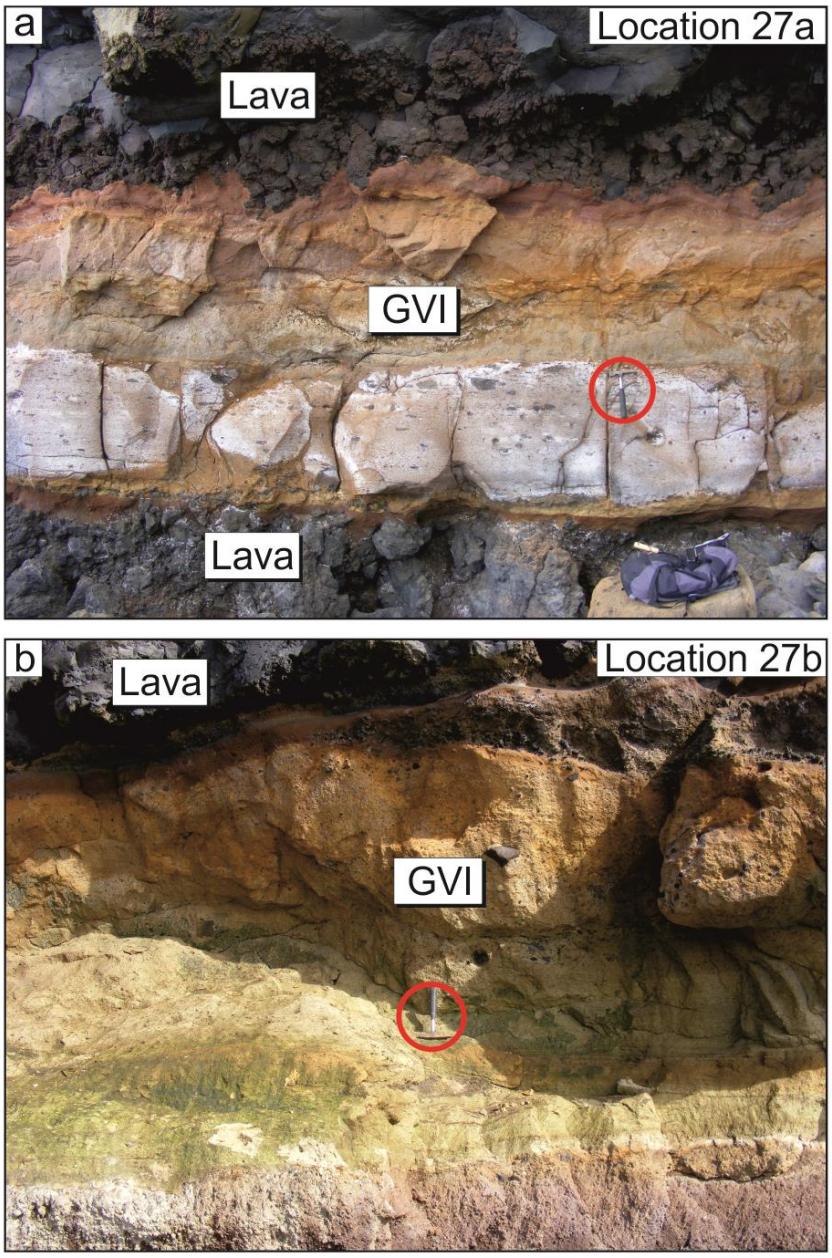

FIGURE 4.13: Field photographs of the GVI **a)** Thin ignimbrite exposure with distinctive lower welded basal layer and dark fiamme. Upper and lower margins bound by rubbly lava flows. Highlighted scale = 30 cm **b)** Outcrop of heavily altered, biotite bearing ignimbrite, also bound by an upper and lower rubbly lava flow. Highlighted scale = 30 cm

4.4.7 The Ignimbrite-i Formation

The only known outcrop of Ign-i is found at location 18, on the north eastern coastline, where it exists as a small exposure at the base of the cliffs, directly beneath the CCI (Figure 4.14). The outcrop is dense and welded, with dark, crystal rich fiamme, and a

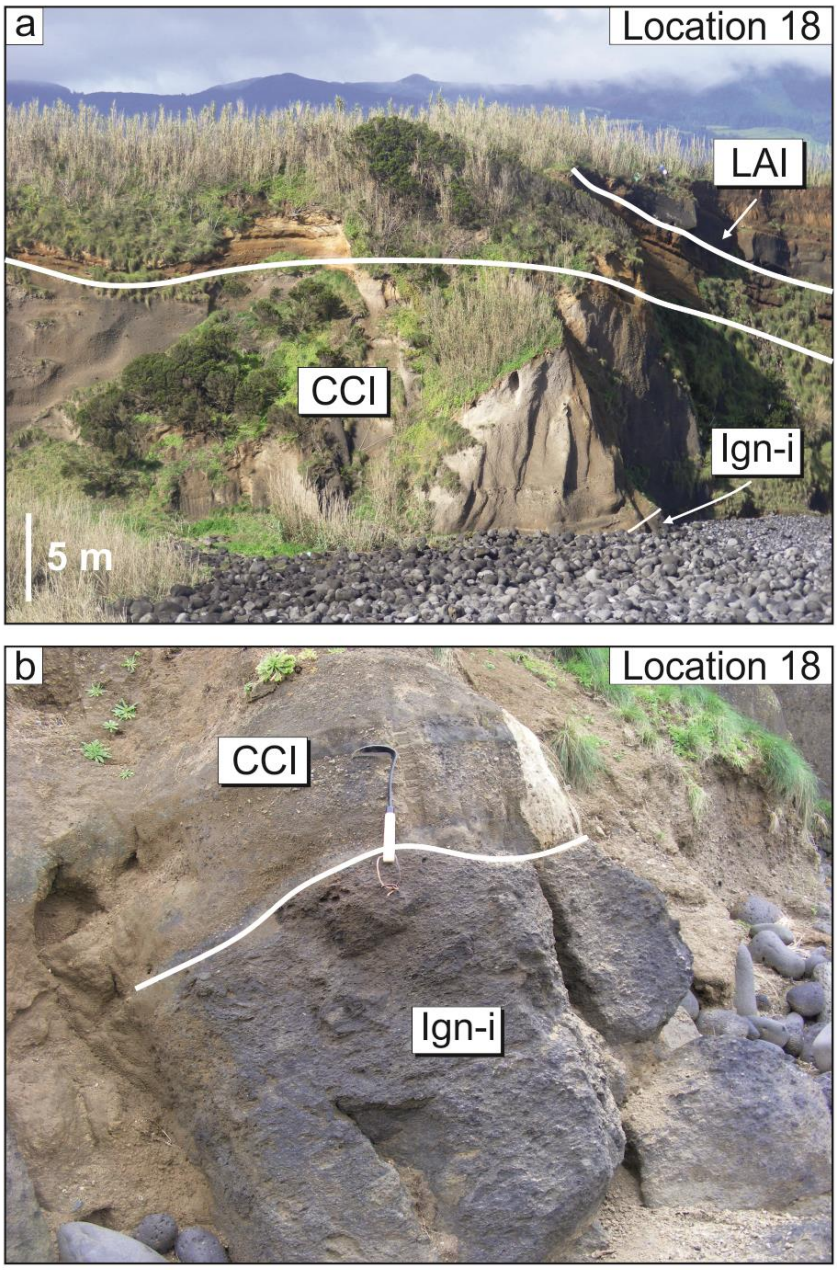

FIGURE 4.14: Field photographs of Ign-i **a)** Digitised photograph showing the relationship between Ign-i and the overlying, younger ignimbrite formations **b)** Digitised photograph highlighting the boundary between Ign-i and the overlying CCI. Pick for scale (32 cm)

heavily eroded upper boundary. The heavily eroded remnant is ~ 1 m thick and was sampled (sample T001, T075).

4.5 Results

4.5.1 Petrography

The mineral assemblages of the ignimbrites of Terceira include alkali feldspar, clinopyroxene, and Ti-magnetite ± ilmenite and olivine (Self 1974; Gertisser *et al.*, 2010). The GVI is a notable exception to this, in that it also contains biotite, a mineral that is not observed in any of the other ignimbrite formations (Gertisser *et al.*, 2010). Syenite ejecta from the CCI exhibit more complex mineral assemblages, including alkali feldspar, clinopyroxene, amphibole, aenigmatite, Ti-magnetite, ilmenite, quartz, olivine, biotite, apatite, dalyite, and eudialyte (Jeffery *et al.*, 2016a). Furthermore, a number of syenite nodules also contain enclaves characterised by mineral assemblages similar to that of the host syenite. Here, a detailed account of the petrography of the ignimbrites, syenite ejecta, and enclaves is given.

4.5.1.1 Ignimbrites

Juvenile pumice clasts sampled from the ignimbrites of Terceira exhibit similar mineral assemblages, characterised by the presence of alkali feldspar, clinopyroxene, and Ti-magnetite, and olivine ± ilmenite (Self, 1974; Gertisser *et al.*, 2010). The GVI is a notable exception to this, in that it also contains biotite, a mineral that is not observed in any of the other ignimbrite formations (Gertisser *et al.*, 2010). Additionally, the LMI is distinguished by the occurrence of plagioclase in addition to alkali feldspar.

In all of the ignimbrites, alkali feldspar is the dominant phase, reaching up to ~ 15 modal % of the juvenile material (Gertisser *et al.*, 2010). Alkali feldspar phenocrysts are generally unzoned, tabular, and up to ~ 4 mm in length (Figure 4.15a). However, crystal fragments and heavily resorbed and embayed examples are also common, the latter being prolific in the LMI (Figure 4.15b). Clinopyroxene may be found as large, euhedral phenocrysts (up to ~ 3 mm) (Figure 4.15c), or more commonly as relatively euhedral microphenocrysts up to 200 µm in length (Figure 4.15d). Clinopyroxene frequently

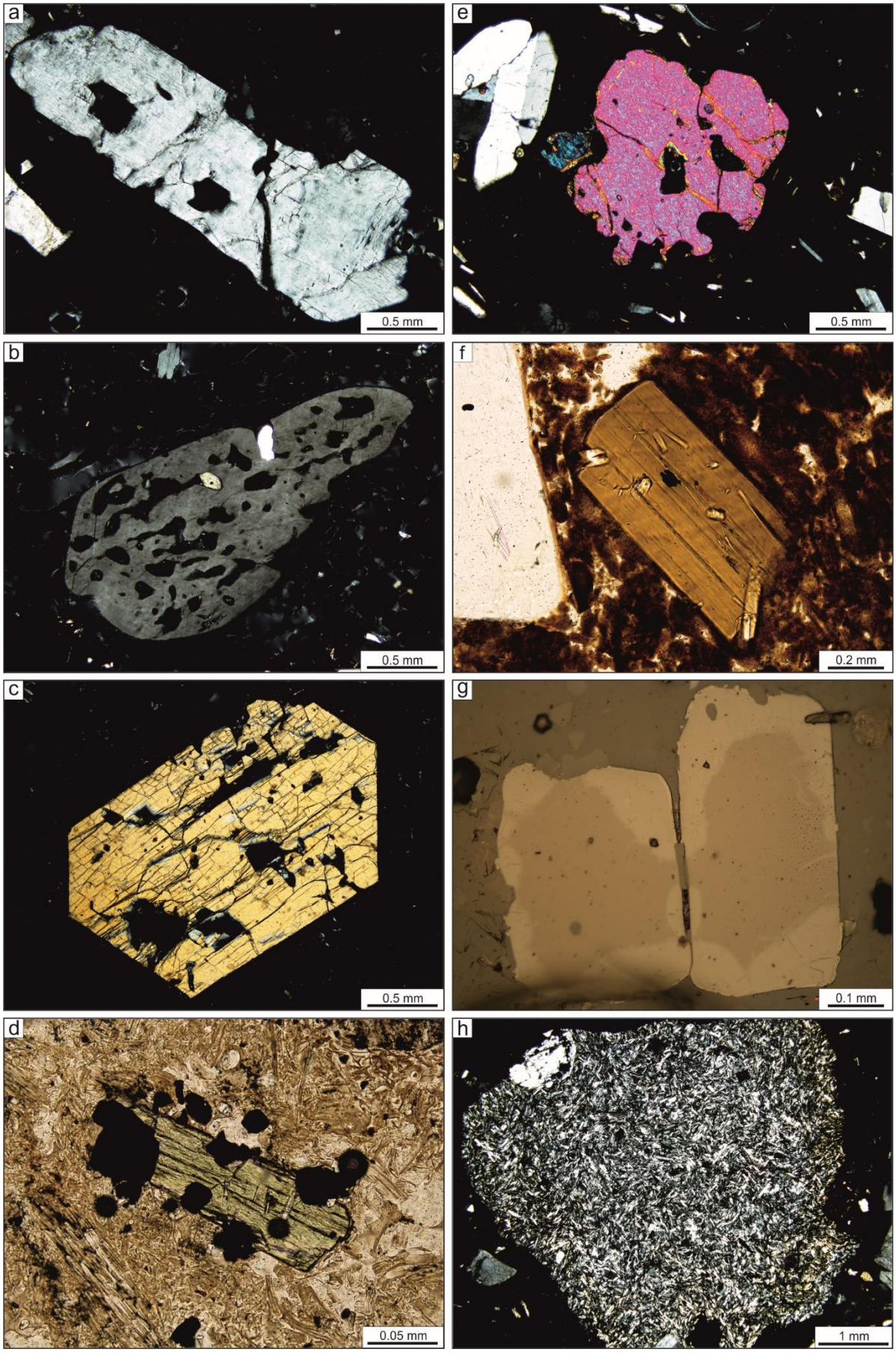
a
0.5 mm
e
0.5 mm
b
0.5 mm
f
0.2 mm
c
0.5 mm
g
0.1 mm
d
0.05 mm
h
1 mm

◄ **FIGURE 4.15:** Representative photomicrographs of the Terceira ignimbrite formations **a)** Large alkali feldspar phenocryst set in vesicular glass (xpl) **b)** Large, highly resorbed alkali feldspar phenocryst showing pronounced embayment structures (xpl) **c)** Large, euhedral clinopyroxene phenocryst (xpl) **d)** Small phenocryst of green clinopyroxene with abundant Fe-Ti oxide inclusions (ppl) **e)** Highly resorbed and partially embayed olivine phenocryst with smaller phenocrysts and microphenocrysts of alkali feldspar and clinopyroxene, set in vesicular glass (xpl) **f)** Small, euhedral biotite phenocryst with a number of small, acicular apatite inclusions (ppl) **g)** Two zoned Ti-magnetite grains (rl) **h)** Medium grained syenitic fragment, comprising predominantly alkali feldspar, set in vesicular glass. A phenocrystic alkali feldspar is visable at the upper left margin (xpl)

displays a spatial association with Fe-Ti oxides, which are often partially or entirely included within clinopyroxene crystals. Olivine is generally found as equant phenocrysts that do not exceed 2 mm and are frequently resorbed and embayed (Figure 4.15e). Where present, biotite is present as small, euhedral phenocrysts that generally do not exceed ~ 1 mm, and often contain small inclusions of apatite (Figure 4.15f). Fe-Ti oxides exhibit equant, subhedral forms that rarely exceed 1 mm in size. Some examples display optically visible zonation patterns, with prominent, irregular cores, and rims of highly variable thickness (Figure 4.15 g). Apatite is present in trace amounts throughout, and is generally restricted to small, acicular inclusions within other phases.

In addition to phenocryst phases, juvenile pumice clasts also rarely contain porphyritic syenite clasts, which may reach sizes of up to ~ 6 mm (Figure 4.15h). These clasts have a sharp but irregular contact with the surrounding glass, and exhibit a phase assemblage that is dominated by a relatively coarse alkali feldspar groundmass and rare alkali feldspar phenocrysts.

4.5.1.2 Syenites

The syenitic ejecta of the CCI exhibit a variety of macroscopic textures, including inter- and intra-nodule grain size variations (Figure 4.16a), schlieren structures (Figure 4.16b), and fine grained enclaves of darker material, with rounded, lobate forms and chilled margins (Figure 4.16c). Individual nodules can exhibit relatively high porosity, containing up to ~ 10 vol. % unfilled intercumulus void space in the freshest samples. Schlieren may anastomose or bifurcate, and are characterised by an abundance of clinopyroxene, amphibole, and aenigmatite, which may be either intercumulus or phenocrystic (up to ~ 1

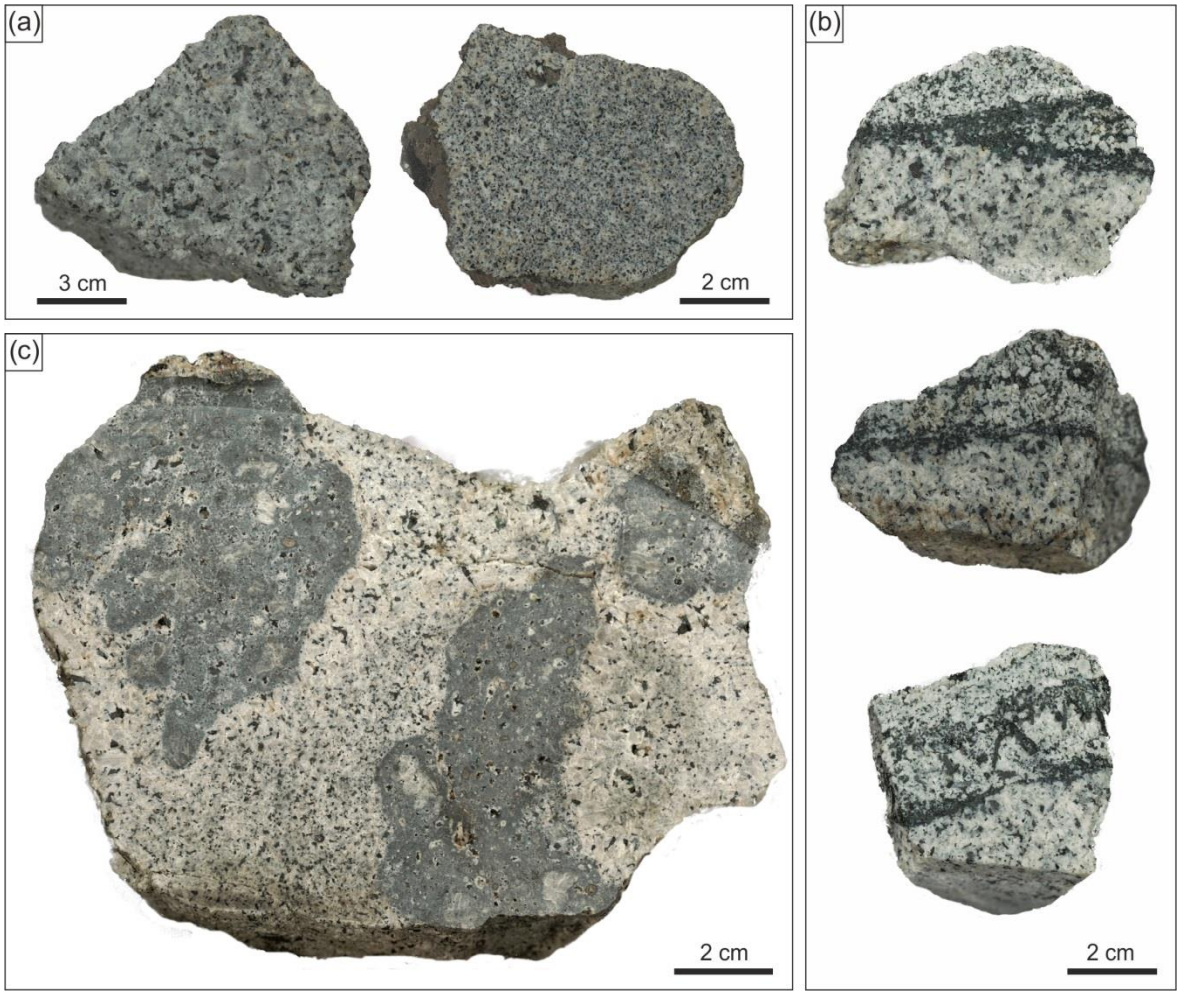

FIGURE 4.16: Representative photographs for the CCI syenites **a)** Examples of coarse and medium grained syenitic nodules **b)** Examples of schlieren within individual syenite clasts. Schlieren are dominated by dark clinopyroxene, amphibole, and aenigmatite, and may anastomose or bifurcate **c)** A large, coarse grained syenitic block with numerous darker enclaves, which exhibit rounded, 'finger-like' margins and chilled margins

cm). These features typically form a boundary between two different variaties of syenite, which can be distinguished on the basis of contrasting modal mineralogy and/or grainsize (Figure 4.16b).

The nodules are characterised by more complex mineral assemblages than those of the various Terceiran ignimbrite formations, comprising alkali feldspar, clinopyroxene, amphibole, aenigmatite, Ti-magnetite, ilmenite, quartz, olivine, apatite, dalyite, eudialyte, and biotite, in approximate order of decreasing abundance (Jeffery *et al.*, 2016a). Alkali feldspar is the most abundant phase, constituting ~ 75 vol. % of each nodule, and forming a cumulus network, regardless of grain size. Individual crystals range from large, tabular

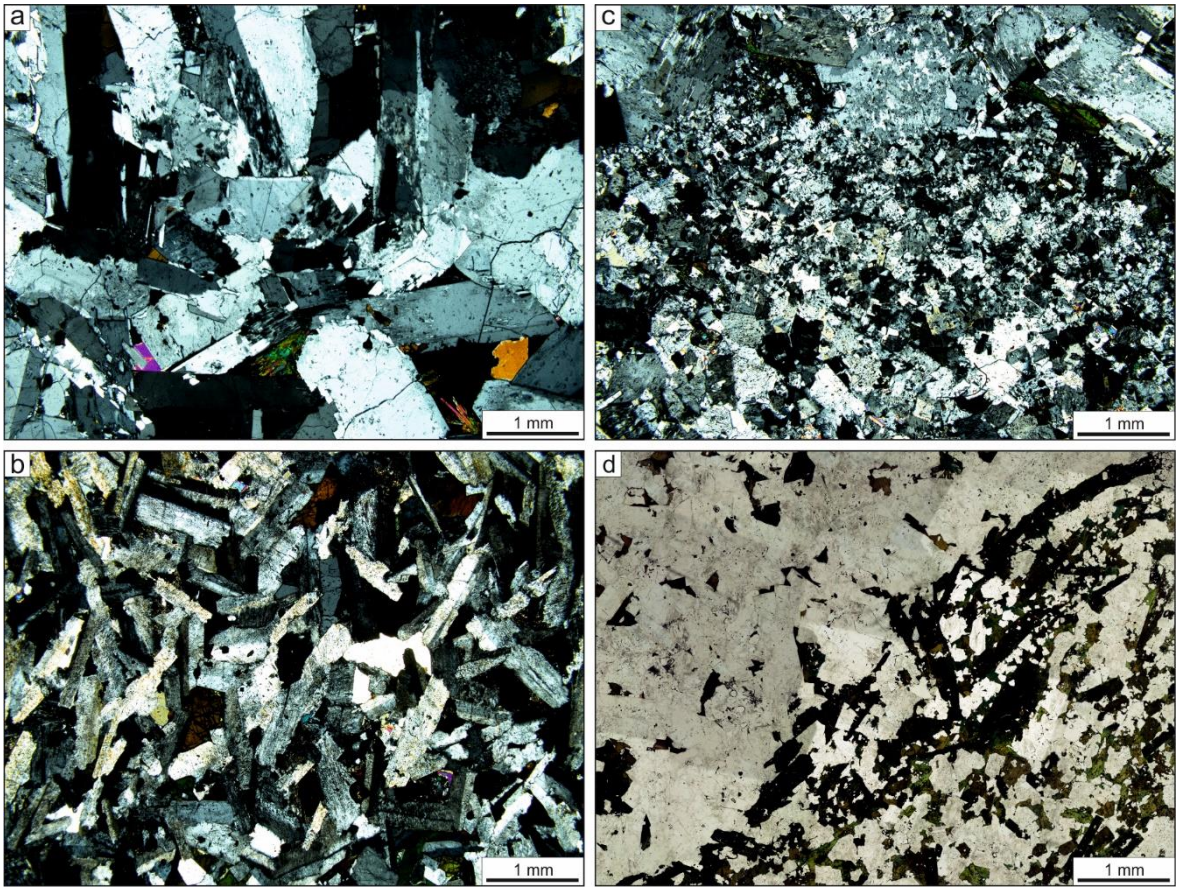

FIGURE 4.17: Representative photomicrographs for the large scale textural variation within the CCI syenite nodules **a)** Coarse grained syenite with large tabular alkali feldspars and intercumulus clinopyroxene (xpl) **b)** Medium grained syenite dominated by alkali feldspar lathes (xpl) **c)** Granophyric patch comprising intergrown alakali feldspar and quartz surrounded by coarse syenite (upper margin) (xpl) **d)** Schlieren structure defined by an abundance of clinopyroxene, amphibole, and aenigmatite (ppl)

crystals (up to ~ 10 mm, Figure 4.17a) to smaller lathes (up to ~ 2 mm, Figure 4.17b), and from fresh and unaltered, to heavily altered and perthitic. Feldspar is also present as small, irregular crystals which, together with quartz, form granophyric patches (Figure 4.17c).

Clinopyroxene, amphibole, and aenigmatite represent the dominant intercumulus phases, with a cumulative volume of up to ~ 10 vol. %. All three phases are concentrated in schlieren, where their abundance may reach as high as ~ 50 vol. % (Figure 4.17d), but are also present in subordinate quantities throughout the syenite. Within schlieren structures, clinopyroxene is present as patches of acicular crystals that partially pseudomorph large aenigmatite crystals, of which only ragged relict crystals remain (Figure 4.18a). This relationship between clinopyroxene and aenigmatite is not limited to

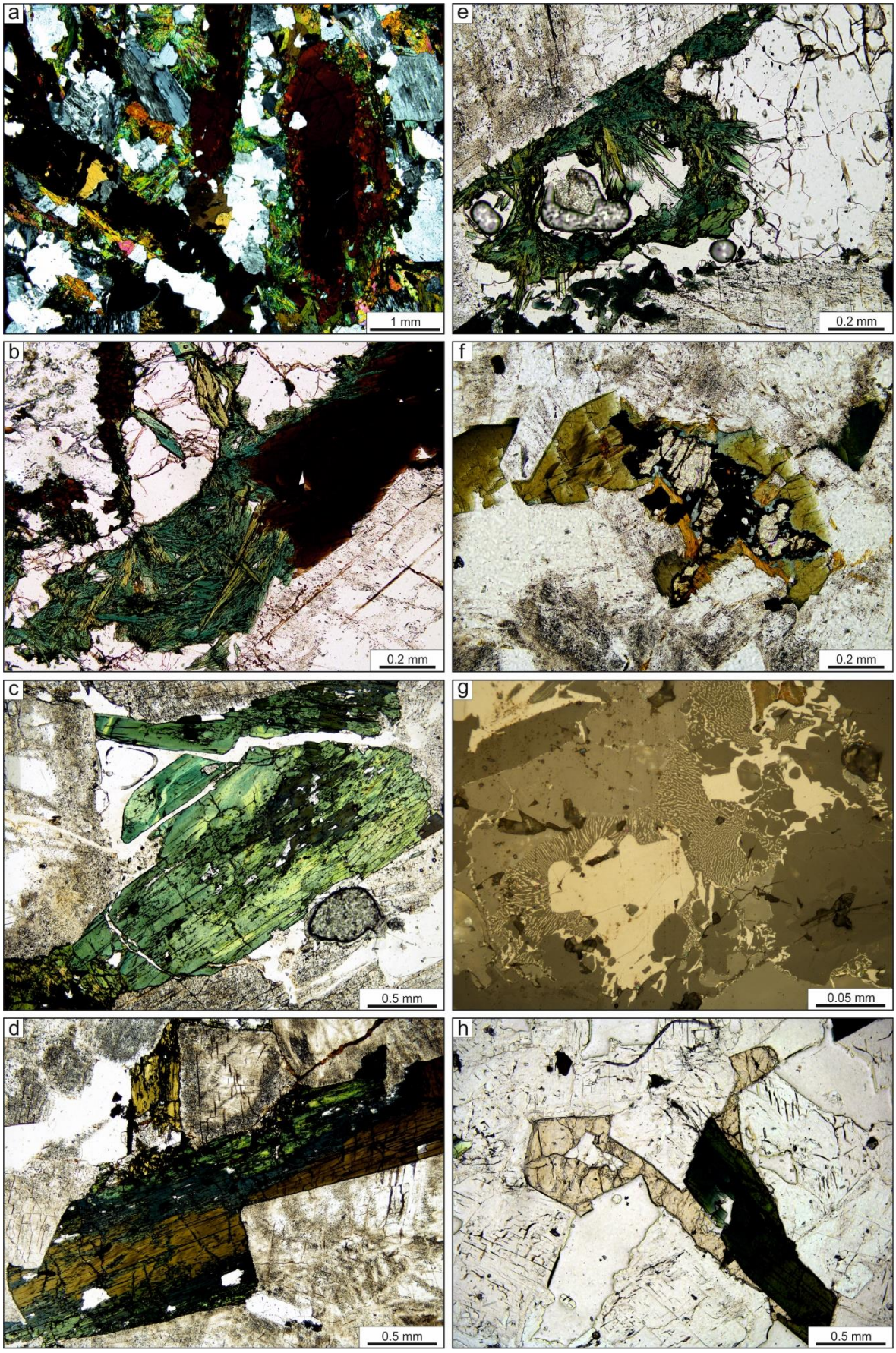
a
1 mm
e
0.2 mm
b
0.2 mm
f
0.2 mm
c
0.5 mm
g
0.05 mm
d
0.5 mm
h
0.5 mm

◄ **FIGURE 4.18:** Representative photomicrographs of mineral textures within the CCI syenites **a)** Abundant amphibole, acicular clinopyroxene, and large ragged aenigmatite within a schieren structure (ppl) **b)** Patch of acicular clinopyroxenes replacing a large, ragged aenigmatite crystal (ppl) **c)** Large clinopyroxene crystal exhibiting subtle, irregular zoning patterns (ppl) **d)** Large zoned crystal, showing a gradual transition from brown to blue amphibole, with green clinopyroxene at the margins (ppl) **e)** Acicular needles of clinopyroxene projecting outwards into a pore space partially filled with quartz (ppl) **f)** Typical breakdown structure associated with olivine, showing relict olivine cores, and numerous breakdown products including amphibole, Fe-Ti oxides, and phyllosilicates (ppl) **g)** Increased magnification of olivine breakdown texture, showing symplectites of Fe-Ti oxides (rl) **h)** Anhedral eudialyte crystal (brown) and associated clinopyroxene (green to extinct) partially filling an intercumulus cavity (ppl)

schlieren structures and may be found throughout the syenite ejecta (Figure 4.18b). Excluding the previously described schlieren structures, clinopyroxene exists as intercumulus crystals that can reach sizes of up to ~ 3 mm, and often exhibit irregular or patchy zonation (Figure 4.18c). Furthermore, clinopyroxenes frequently show a spatial association with amphiboles, appearing to have nucleated heterogeneously on, or to have replaced, pre-existing amphibole crystals (Figure 4.18c, d). Similarly, amphiboles reach sizes of ~ 4 mm and are frequently zoned, with a brownish amphibole generally making up the central portion of a given crystal, and a blue amphibole located at the crystal margins (Figure 4.18d). The margins between individual zones are almost exclusively irregular and gradational.

Quartz is also limited to intercumulus pore spaces, where it occurs as aggregates of rounded crystals up to ~ 1 mm in size. Together with phases such as acicular clinopyroxene (Figure 4.18e), eudialyte, or dalyite (see below), quartz aggregates may either partially or entirely fill the pore. Fe-Ti oxides are present as small (< 100 μm) equant crystals that are frequently included within other phases and do not account for more than 1 vol. % of the rock. More rarely, examples reach sizes of up to ~ 400 μm and may represent an intercumulus phase rather than an inclusion.

Olivine is uncommon in the syenites, and, when present, exists as anhedral relict crystals which exhibit a complex reaction texture (Figure 4.18f). Breakdown rims are typically characterised by an inner rim of bluish phyllosilicates and an outer rim of orange phyllosilicates. Additional breakdown products include brown amphiboles and Fe-Ti oxides, which may exhibit a symplectitic texture (Figure 4.18f, g). Apatite is present in

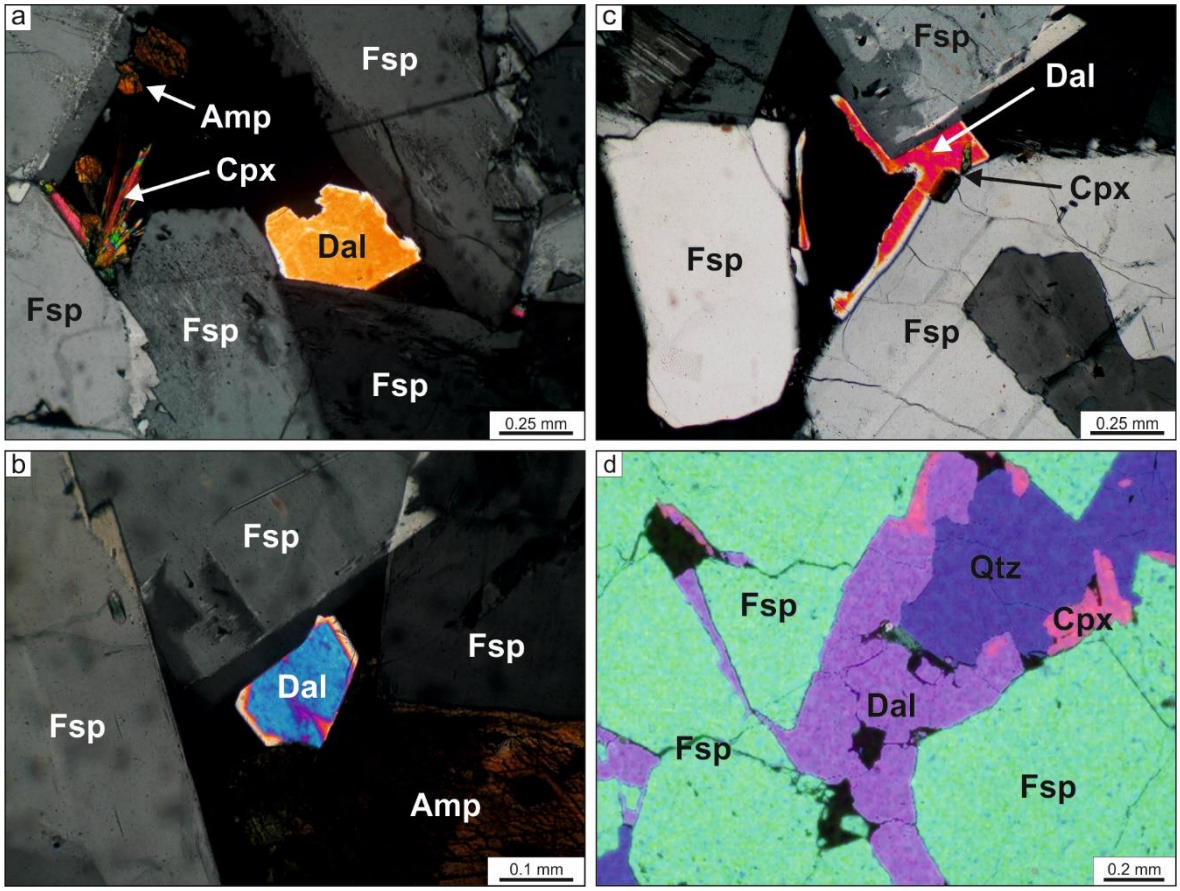

FIGURE 4.19: Representative photomicrographs of dalyite in the CCI syenite ejecta **a)** A large dalyite crystal which partially infills an interstitial void between larger alkali-feldspar crystals. Also visible are small amphibole crystals and stellate clinopyroxene (xpl) **b)** An anhedral dalyite crystal which partially fills an interstitial void between large alkali-feldspars and a large amphibole crystal (xpl) **c)** An anhedral dalyite crystal forming an incomplete rim around the edges of an interstitial cavity. A small clinopyroxene crystal appears to have been included within the dalyite. A resorbed, optically distinctive feldspar core is visible within the large feldspar to the lower right of the image (xpl) **d)** An element map highlighting a large, anhedral dalyite crystal filling an interstitial space, together with intergrown quartz and small amounts of clinopyroxene. Colours used: Red = Fe, Purple = Zr, Blue = Si, Green = Al. Abbreviations used: Qtz = quartz, Fsp = alkali-feldspar, Amp = amphibole, Cpx = Clinopyroxene, Dal = dalyite

trace amounts, and is limited to small (< 100 µm) acicular crystal inclusions within other phases. Eudialyte is found as irregular crystals (generally < 1 mm) which partially or entirely fill intercumulus spaces (Fig 4.18h), and are frequently associated spatially with clinopyroxene. Examples of irregular patchy or oscillatory zoning are common. Dalyite is typically present as small (< 0.5 mm) sub- to anhedral crystals (Fig. 4.19a-c), though can reach sizes of 1 to 1.5 mm (Fig. 4.19d). It is almost exclusively anhedral and confined to the interstices, either filling or partially filling void spaces. It is often associated spatially with quartz, and in some cases can be found as inclusions within larger interstitial quartz

crystals. Biotite is uncommon and, where present, exists as small inclusions within alkali-feldspars.

4.5.1.3 Enclaves

Dark enclaves found within individual syenite ejecta are coarsely porphyritic, with phenocrysts up to ~ 8 mm in length set in a fine grained microcrystalline groundmass (4.20a, b). Mineral assemblages are similar to those of the host syenite, with alkali feldspar, amphibole, clinopyroxene, Fe-Ti oxides, olivine, plagioclase, apatite, eudialyte, dalyite, and aenigmatite, in approximate order of abundance. As in all of the rocks in this study, alkali feldspar is the dominant phase, occurring as large phenocrysts and as small (< 200 μm), anhedral groundmass crystals. Phenocrystic alkali feldspar is characterised by relatively inclusion poor, rounded crystal cores, mantled by inclusion-rich rims of variable thickness (~ 50 to 750 μm) (Figure 4.20c, d). In contrast to the interior (core-rim) boundary, which is frequently sharp, the exterior boundary between rim and groundmass is frequently diffuse and poorly defined. Phenocryst cores often exhibit patchy or, more rarely, oscillatory zoning patterns.

Amphibole is present both as a minor population of microphenocrysts that typically do not exceed ~ 500 μm in length, and as an abundant groundmass phase (Figure 4.20b). Clinopyroxene is also present in abundance in the groundmass, but also exists as phenocrysts and microphenocrysts (~ 250 to 1000 μm) which frequently exhibit thin (< 50 μm) reaction rims and resorption textures. Larger examples may also show concentric, oscillatory zoning patterns (Figure 4.20e). Fe-Ti oxides are restricted to equant microphenocrysts (< 150 μm) that are often included within other phases, and small groundmass crystals that do not exceed 25 μm. More rarely, glomerocrystic clusters of Fe-Ti oxides are present, mantled by a variety of unidentified phyllosilicates. Olivine is found exclusively as ragged phenocrysts up to ~ 3 mm in size, and surrounded by a distinctive double rim of fine grained, pseudomorphing breakdown products (Figure 4.20f).

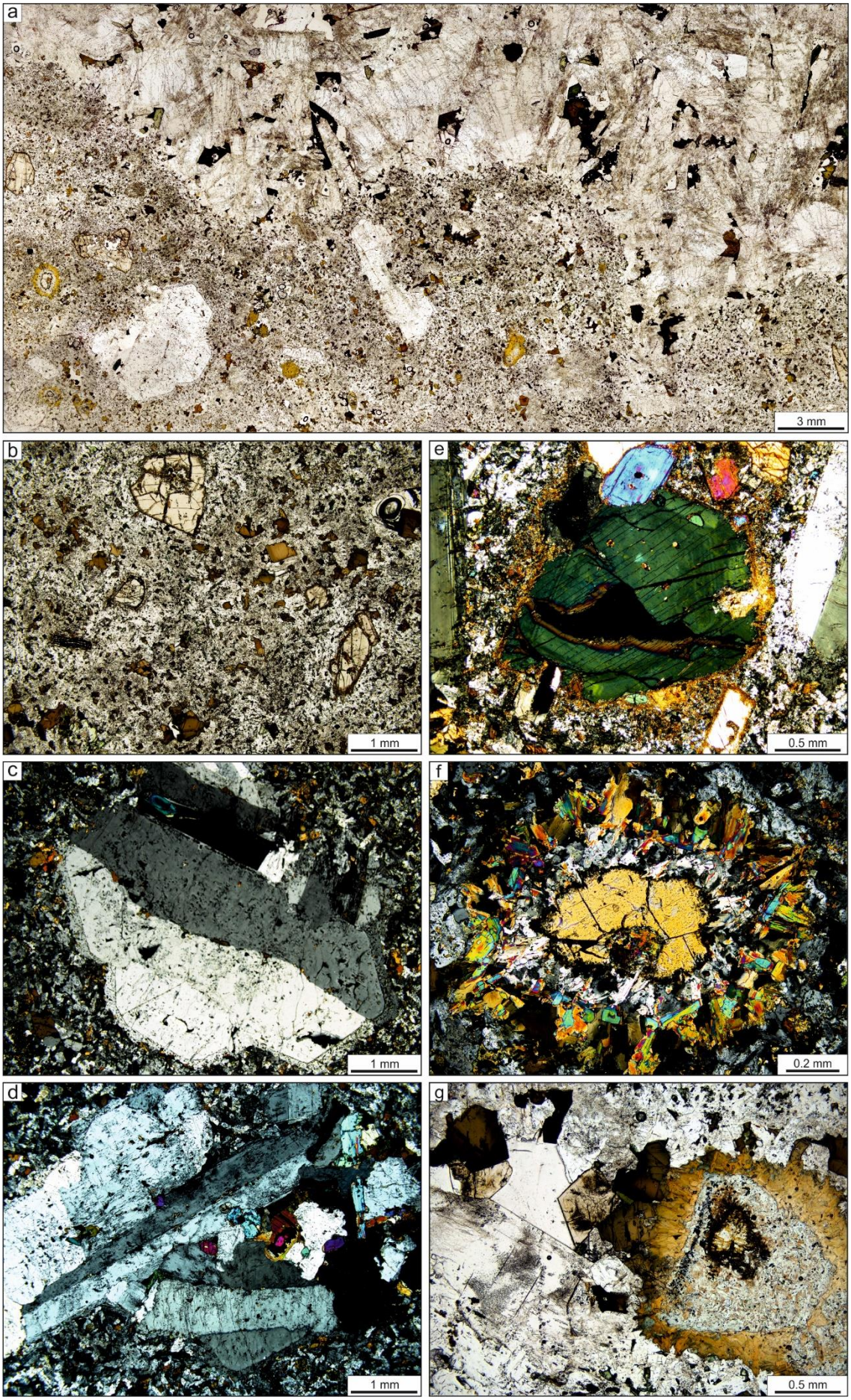
a
3 mm
b
1 mm
e
0.5 mm
c
1 mm
f
0.2 mm
d
1 mm
g
0.5 mm

◄ **FIGURE 4.20:** Representative photomicrographs of the CCI syenite enclaves **a)** Low magnification photomicrograph showing the lobate nature of the contact between enclave and host syenite (ppl) **b)** Fine grained alkali feldspar- and amphibole-dominated groundmass , with phenocrystic clinopyroxene (ppl) **c)** Large and somewhat rounded alkali feldspar phenocryst with characteristic inclusion-rich rim (xpl) **d)** Large glomerocryst comprising alkali feldspar, clinopyroxene, and highly reacted olivine (xpl) **e)** Large clinopyroxene phenocryst showing subtle oscillatory zoning towards it's margins (xpl) **f)** Highly reacted olivine phenocryst, with a relict olivine core surrounded by a characteristic double rim of unidentified phyllosilicates (xpl) **g)** Highly reacted olivine phenocryst showing relict core and double breakdown rim (right side of image). Also, a small cavity, partially infilled by amphibole and two eudialyte crystals (left side of image) (ppl)

In each instance the outer rim comprises predominantly orange and green phyllosilicates, whereas the inner rim is made up of unidentified silicate and Fe-Ti oxide phases. In some instances, the original olivine crystal has been entirely replaced. Apatite is limited to small (< 100 µm), acicular crystals found in the groundmass and as inclusions within other mineral phases. Eudialyte and dalyite are both present in trace amounts, and are limited to miarolitic cavities, where they range from anhedral to euhedral, and reach sizes of up to ~ 500 µm (Figure 4.20 g). Unlike the host syenites, in the enclaves aenigmatite is rare and restricted to miarolitic cavities, where it is predominantly found as small, irregular patches within clusters of acicular clinopyroxene. Plagioclase is rare, and can be found as crystals up to ~ 8 mm in size.

4.5.2 Mineral chemistry

4.5.2.1 Feldspars

Representative feldspar analyses from each of the ignimbrites of Terceira are provided in Table 4.1. The entire dataset is given in Appendix C and is plotted into the anorthite-albite-orthoclase ternary classification scheme in Figure 4.21. Feldspar compositions show little variation from one ignimbrite to another, and generally lie in a linear trend that extends through the anorthoclase field. Notable exceptions include the VFI, where the trend is slightly extended into the oligoclase field, and the LMI, where a small number of analyses indicate more calcic compositions that lie in the oligoclase, andesine, and labradorite fields (Figure 4.21). The calcic compositions in the LMI correlate with those

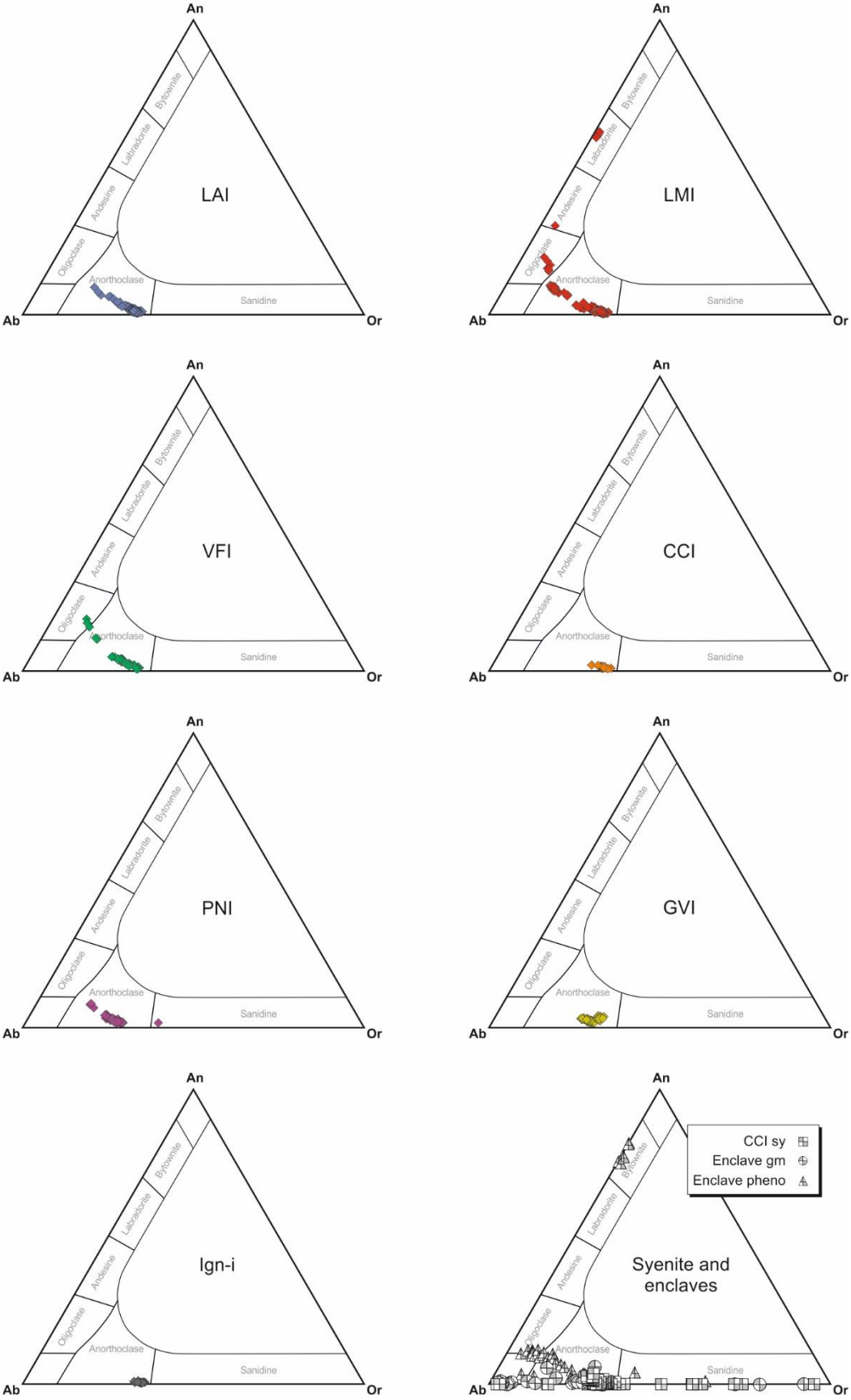

FIGURE 4.21: Feldspar compositions for the lithologies of Terceira plotted into the ternary An-Ab-Or system. Abbreviations used: sy = syenite, gm = groundmass, pheno = phenocryst

Table 4.1: Representative feldspar analyses from the lithologies of Terceira

Unit	**LAI**		**LMI**		**VFI**		**CCI**		**PNI**		**GVI**		**Ign-i**	
Sample	TER1-1	TER3-2	TER5-2	TER5-2	TER2-2	TER11-2B	TER2-2	TER2-1	T012	T012	TER13-1	TER19-1	TER10-2	T001
No.	25/1	9/1	19/1	28/1	58/1	24/1	78/1	94/1	Fsp04	Fsp34	100/1	Fsp03	Fsp09	Fsp9
SiO_2	64.09	67.67	52.79	67.40	63.11	67.10	66.79	67.62	65.09	66.76	65.91	66.27	64.23	66.80
TiO_2	0.07	0.04	0.10	0.11	0.07	0.01	0.03	0.04			0.77			
Al_2O_3	20.74	19.42	28.95	18.49	21.94	18.77	18.76	18.49	20.69	19.25	15.57	19.25	21.17	18.85
BaO	0.87	0.09	0.00	0.06	0.52	0.02	0.18	0.03	0.33	0.11		0.10	1.25	0.01
FeO	0.39	0.38	0.68	0.59	0.24	0.35	0.26	0.30	0.27	0.29	4.21	0.35	0.29	0.25
SrO	0.05	0.02	0.15	0.02	0.16	0.06	0.01	0.00	0.00	0.00		0.00	0.00	0.01
MgO	0.01	0.00	0.11	0.02	0.01	0.00	0.00	0.00			0.47			
CaO	1.87	0.24	12.79	0.16	3.68	0.09	0.37	0.15	1.75	0.38	0.85	0.37	2.22	0.09
Na_2O	8.53	7.84	4.13	7.97	8.45	7.75	8.03	7.79	8.82	8.31	7.19	7.90	9.25	7.65
K_2O	2.87	5.60	0.20	5.41	1.73	5.90	5.16	5.87	2.79	4.98	4.94	5.15	1.80	6.16
Total	99.49	101.31	99.92	100.23	99.91	100.05	99.58	100.29	99.74	100.08	99.90	99.40	100.21	99.83
Si	2.884	2.982	2.405	3.003	2.823	2.997	2.992	3.010	2.904	2.976	3.000	2.974	2.869	2.992
Ti	0.002	0.001	0.003	0.004	0.002	0.000	0.001	0.001			0.026			
Al	1.100	1.009	1.555	0.971	1.157	0.988	0.990	0.970	1.088	1.011	0.835	1.018	1.114	0.995
Ba	0.015	0.002	0.000	0.001	0.009	0.000	0.003	0.000	0.006	0.002		0.002	0.022	0.000
Fe	0.015	0.014	0.026	0.022	0.009	0.013	0.010	0.011	0.010	0.011	0.160	0.013	0.011	0.009
Sr	0.001	0.000	0.004	0.000	0.004	0.002	0.000	0.000	0.000	0.000		0.000	0.000	0.000
Mg	0.001	0.000	0.008	0.001	0.000	0.000	0.000	0.000			0.032			
Ca	0.090	0.011	0.625	0.008	0.176	0.004	0.018	0.007	0.084	0.018	0.041	0.018	0.106	0.004
Na	0.744	0.670	0.365	0.689	0.733	0.671	0.698	0.672	0.763	0.718	0.635	0.687	0.801	0.664
K	0.165	0.315	0.011	0.308	0.099	0.336	0.295	0.334	0.159	0.283	0.287	0.295	0.103	0.352
Sum	5.018	5.004	5.002	5.006	5.012	5.012	5.008	5.006	5.013	5.019	5.016	5.008	5.026	5.018
Ab	74.45	67.23	36.46	68.59	72.74	66.32	69.05	66.36	75.89	70.46	65.92	68.73	79.32	65.08
An	9.03	1.14	62.40	0.77	17.48	0.43	1.75	0.70	8.32	1.76	4.28	1.78	10.52	0.43
Or	16.51	31.62	1.14	30.64	9.78	33.26	29.20	32.93	15.79	27.78	29.80	29.48	10.16	34.48

Table 4.1 continued

Unit	**CCI sy**		**CCI enc (pheno)**		**CCI enc (groundmass)**	
Sample	TER30-6	TER30-6	T073A8	Spec 1	Spec 1	Spec 1
No.	Fsp16	Fsp16	Pheno2	Pheno5	Fspar 1	Fspar 2
SiO_2	67.89	67.22	47.11	66.01	65.51	66.23
TiO_2						
Al_2O_3	19.05	18.17	31.45	19.72	19.36	19.19
BaO	0.02	0.02	bdl	0.25	0.18	0.14
FeO	0.33	1.25	0.54	0.10	0.82	0.35
SrO	bdl	0.09	0.11	0.07	bdl	bdl
MgO						
CaO	0.02	bdl	15.32	0.63	0.24	0.17
Na_2O	7.92	5.76	2.75	10.37	8.75	8.57
K_2O	5.71	8.89	0.15	2.19	4.36	4.85
Total	100.94	101.40	97.43	99.35	99.22	99.50
Si	2.999	3.006	2.223	2.946	2.952	2.971
Ti						
Al	0.992	0.957	1.749	1.038	1.028	1.015
Ba	0.000	0.000		0.004	0.003	0.002
Fe	0.012	0.047	0.021	0.004	0.031	0.013
Sr		0.002	0.003	0.002		
Mg						
Ca	0.001		0.775	0.030	0.012	0.008
Na	0.678	0.499	0.251	0.897	0.764	0.745
K	0.322	0.507	0.009	0.125	0.251	0.277
Sum	5.005	5.019	5.032	5.046	5.041	5.033
Ab	67.8	49.6	24.3	85.3	74.4	72.3
An	0.1	0.0	74.8	2.9	1.1	0.8
Or	32.1	50.4	0.9	11.9	24.4	26.9

feldspars which exhibit the previously described resorbed textures that are common in the LMI feldspar population.

The three youngest ignimbrites (LAI, LMI, VFI) exhibit the most pronounced linear trends and the largest compositional ranges. The older ignimbrite formations (CCI, PNI, GVI, Ign-i) appear to have feldspar populations that are slightly more restricted when compared to their younger counterparts. The total compositional range of the Terceira ignimbrites is $Or_{1\text{-}36}$, $Ab_{36\text{-}81}$, $An_{0\text{-}62}$.

Minor substituting elements such as BaO, FeO, and SrO are present in small amounts and are often below detection, reaching maximum values of 1.25, 0.74, and 0.19 wt. %, respectively. SrO shows a positive correlation with An, reaching concentrations around 0.19 wt. % at An contents of ~ 20 wt. %. A small number of analyses from the LMI deviate substantially from this trend, with SrO values that lie between 0.11 and 0.16 wt. %,

despite their highly calcic compositions (~ 61 wt. % An). BaO also exhibits a positive correlation with An, though this is limited to An contents between 0 and ~ 5 wt. %. Above 5 wt. % the trend is lost in data scatter. Below ~ 20 wt. % An, FeO contents show no obvious relationship with An. However, FeO concentrations reach their highest (up to 0.5 wt. % higher than sodic feldspar analyses) in the calcic analyses described from the LMI.

Feldspars within the syenite nodules exhibit a similar range to the ignimbrites (Or_{17-40}, Ab_{60-83}, An_{0-4}), though the inclusion of perthitic feldspars extends this range towards the albite and orthoclase end members. Concentrations of BaO and SrO are less than observed in the ignimbrites (up to 0.27 and 0.09 wt. %, respectively). Groundmass feldspars in the syenite hosted enclaves show a linear trend between anorthoclase and albite, with a compositional range of (Or_{2-35}, Ab_{65-97}, An_{0-6}), and BaO and SrO contents of up to 0.38 and 0.05 wt. %, respectively. In contrast, analyses of the large enclave feldspar crystals reveal a bimodal population, with the majority of analyses being classified as anorthoclase or sanidine (Or_{4-63}, Ab_{36-89}, An_{0-12}), and a smaller number of analyses indicating the presence of labradorite and bytownite (Or_{0-1}, Ab_{18-38}, An_{62-82}). The latter population contains SrO concentrations that are somewhat higher than those of the alkali feldspars (0.15 compared with 0.09 wt. %).

4.5.2.2 Pyroxenes

Clinopyroxene compositions for the Terceira ignimbrites are plotted in the Wo-En-Fs system in Figure 4.22. Representative quantitative analyses are given in Table 4.2, and the full dataset can be found in Appendix C. For the purposes of classification, the 10 component scheme of Marks *et al.* (2008) was utilised, where, alongside the quadrilateral components diopside (Di), hedenbergite (Hd), enstatite (En), and ferrosilite (Fs), the additional components aegirine (Aeg), Ti-aegirine (Ti-Aeg), jadeite (Jd), Ti-Tschermak (Ti-Ts), Ca-Tschermak (Ca-Ts), and ferri-Tschermak (Fe-Ts) are considered. Application of the Q+J diagram of Morimoto *et al.* (1988) indicates that all of the ignimbrite analyses can

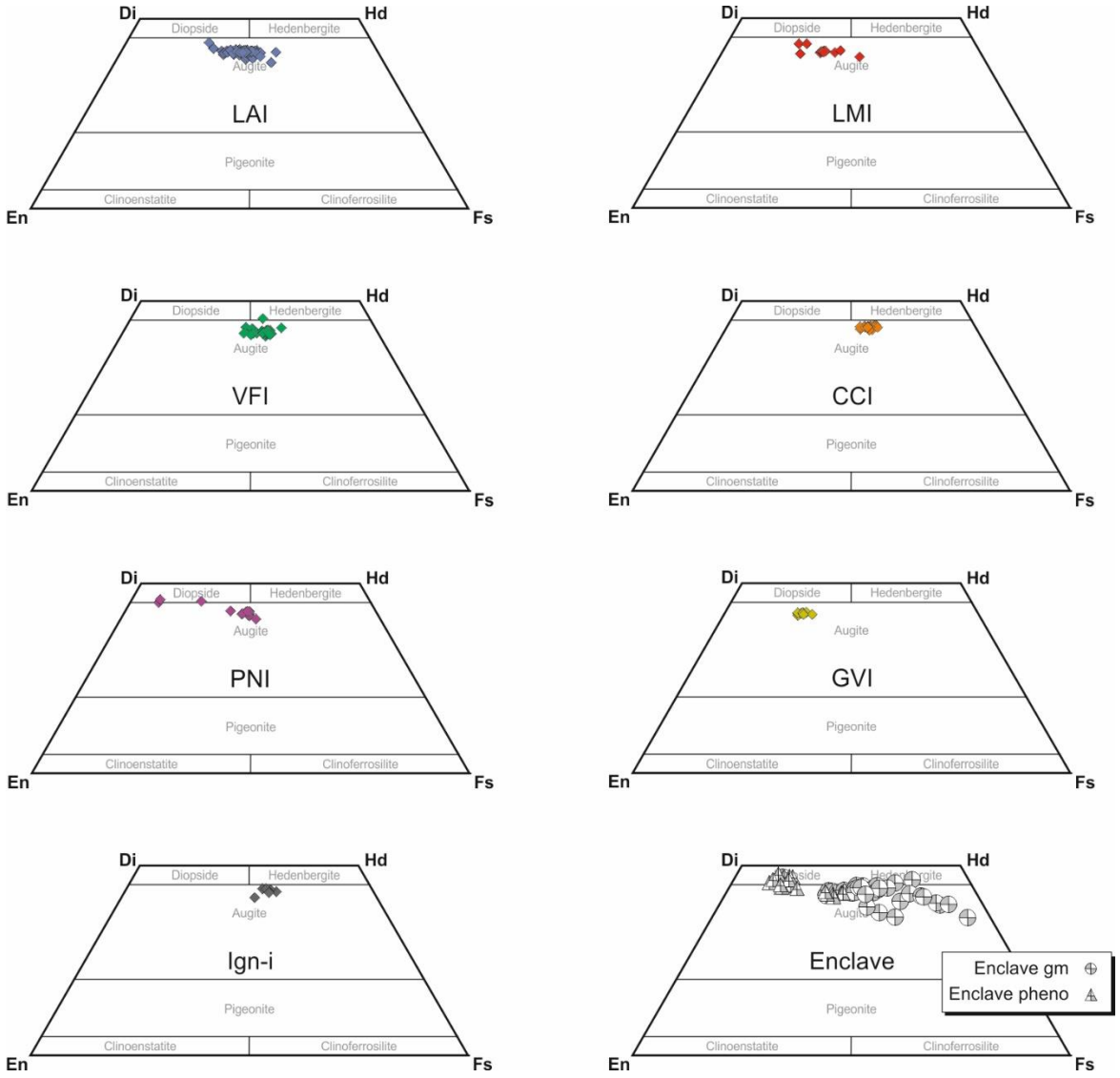

FIGURE 4.22: Clinopyroxene compositions of the lithologies of Terceira plotted into the quadrilateral, threecomponent (wollastonite-enstatite-ferrosilite) scheme of Morimoto *et al.* (1988). Abbreviations used: gm = groundmass, pheno = phenocryst

be classified adequately using the quadrilateral components (Figure 4.23). When the analyses are plotted in the quadrilateral, three component (Wo-En-Fs) scheme of Morimoto *et al.* (1988), the Terceira analyses exhibit a linear trend through the augite field, characterised by variable Mg and Fe contents at relatively constant Ca contents. A small number of analyses cross the upper boundary of the augite field into either diopside or hedenbergite (Figure 4.22). In the 10 component system, Di and Hd are the dominant components (up to 72 and 49 mol. %, respectively). Minor components such as Ti-Ts, Ca-

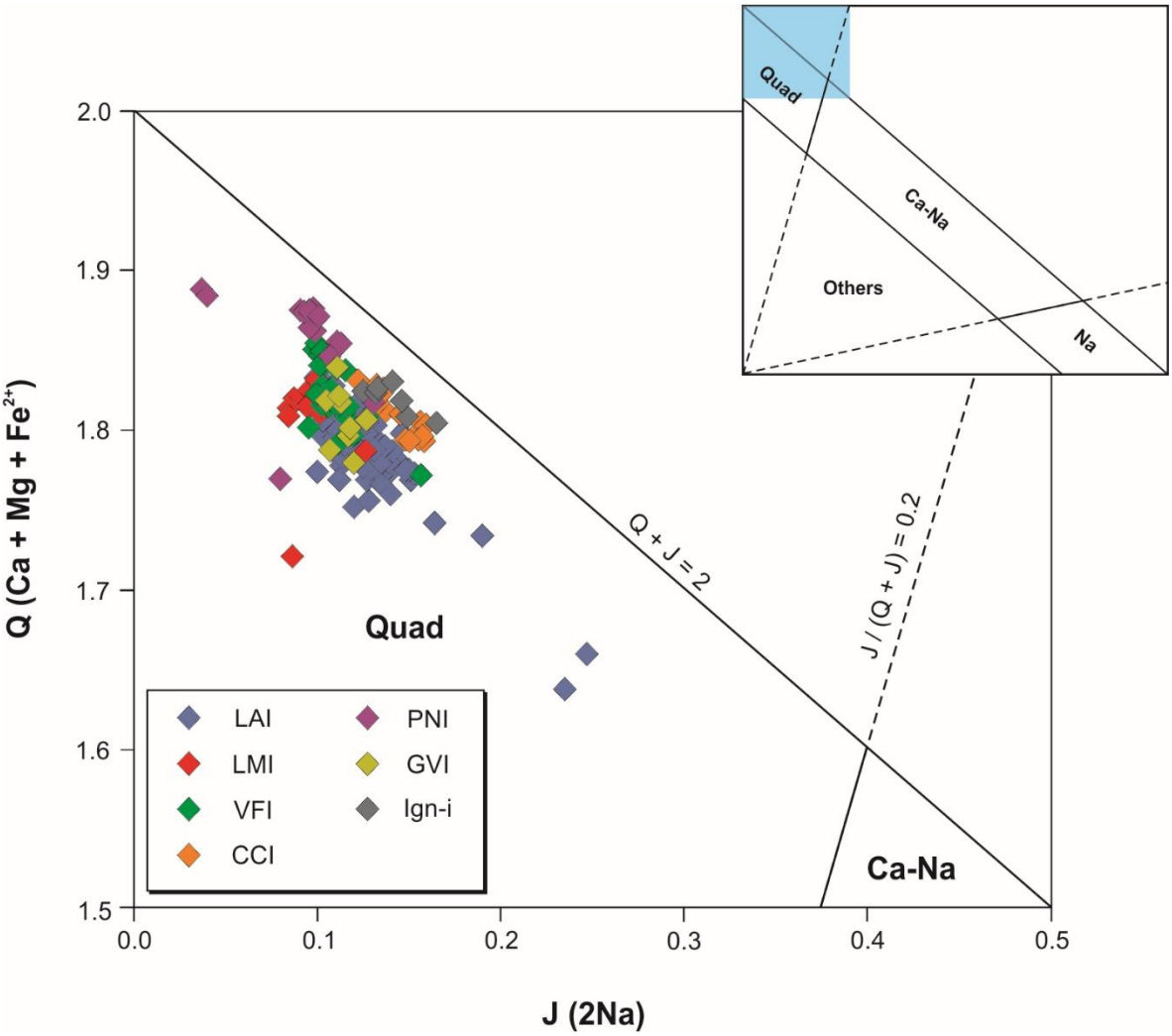

FIGURE 4.23: Q + J clinopyroxene classification diagram showing analyses from the Terceira ignimbrites, after Morimoto *et al.* (1988)

Ts, and Fe-Ts do not exceed 10 mol. %. Aegirine concentrations range from 0 to 12 mol. %, whilst Jd contents do not exceed 2 mol. %. A single exception to this exists in the LAI, where one analysis contains 11 mol. % Jd. The analyses are best defined using Di, Hd, and Aeg, which exhibit ranges of Di_{33-72}, Hd_{9-49}, and Aeg_{0-12} (Figure 4.24). In Di-Hd-Aeg space, most of the Terceira ignimbrites exhibit a trend of progressive enrichment in Hd, with little to no increase in the aegirine component.

In contrast, the syenite clinopyroxene is dominated by aegirine-augite to aegirine, with a total compositional range of Qd_{0-96}, Aeg_{4-99}, Jd_{0-7}. Groundmass clinopyroxene from the enclaves also reveal a trend from standard quadrilateral clinopyroxene to aegirine-augite, with a total compositional range of Qd_{43-97}, Aeg_{3-57}, Jd_{0-9}. The enclave phenocrysts

Table 4.2: Representative clinopyroxene analyses from the lithologies of Terceira

Unit		**LAI**			**LMI**			**VFI**		**CCI**	
Sample	TER1-1	TER4-1	TER10-3	TER5-2	TER5-2	TER5-2	TER2-2	TM-2(1)	TM-1(1)	TM-2(2)	TM-2(2)
No.	19/1	121/1	38/1	120/1	112/1	113/1	142/1	Px05	Px02	Px06	Px12
SiO_2	48.71	50.41	50.06	45.78	50.83	50.34	50.51	48.69	49.62	51.01	50.83
TiO_2	1.57	0.41	0.31	3.50	0.49	0.66	0.84	0.40	0.41	0.36	0.33
Al_2O_3	2.72	0.48	0.29	5.94	0.80	0.81	1.14	0.43	0.36	0.43	0.35
Cr_2O_3	0.02	0.00	0.01	0.09	0.03	0.02	0.01	0.00	0.00	0.02	0.00
FeO	10.88	17.21	19.20	10.41	12.95	17.74	15.59	16.87	19.18	16.86	18.08
MnO	0.58	1.54	1.46	0.25	1.01	1.34	1.05	1.15	1.26	1.23	1.37
MgO	12.66	9.97	7.57	12.86	12.44	9.50	10.39	8.19	6.90	8.63	8.00
CaO	20.99	18.99	19.00	20.48	20.15	19.02	19.93	21.74	19.70	20.14	19.60
Na_2O	0.68	0.94	1.25	0.59	0.69	0.84	0.79	0.62	0.85	0.89	0.81
K_2O	0.01	0.01	0.00	0.02	0.01	0.00	0.01	0.00	0.01	0.00	0.00
Total	98.81	99.96	99.15	99.91	99.38	100.28	100.26	98.09	98.29	99.56	99.37
Si	1.849	1.938	1.963	1.716	1.931	1.937	1.928	1.923	1.975	1.979	1.988
Ti	0.045	0.012	0.009	0.099	0.014	0.019	0.024	0.012	0.012	0.011	0.010
Al	0.121	0.022	0.013	0.262	0.036	0.037	0.051	0.020	0.017	0.019	0.016
Cr	0.001	0.000	0.000	0.003	0.001	0.001	0.000	0.000	0.000	0.001	0.000
Fe^{2+}	0.204	0.406	0.493	0.178	0.286	0.457	0.394	0.399	0.563	0.480	0.542
Fe^{3+}	0.141	0.148	0.137	0.148	0.125	0.114	0.104	0.158	0.075	0.067	0.049
Mn	0.019	0.050	0.048	0.008	0.032	0.044	0.034	0.039	0.043	0.040	0.045
Mg	0.716	0.571	0.443	0.719	0.704	0.545	0.591	0.482	0.409	0.499	0.466
Ca	0.854	0.783	0.798	0.823	0.820	0.784	0.815	0.920	0.840	0.837	0.821
Na	0.050	0.070	0.095	0.043	0.051	0.063	0.058	0.047	0.065	0.067	0.061
K	0.000	0.000	0.000	0.001	0.000	0.000	0.000	0.000	0.001	0.000	0.000
Sum	4.000	4.000	4.000	4.000	4.000	4.000	4.000	4.000	4.000	4.000	4.000
Aeg	5	7	9	4	5	6	6	5	7	7	5
Fe-Ts	5	4	2	5	4	3	2	6	0	0	0
Jd	0	0	0	0	0	0	0	0	0	0	0
Ti-Aeg	0	0	0	0	0	0	0	0	0	0	1
Ti-Ts	4	1	1	10	1	2	2	1	1	1	1
Al-Ts	0	0	0	0	0	0	0	0	0	0	0
Di	58	41	35	54	53	39	45	45	33	41	36
Hd	18	33	42	14	24	35	32	41	49	42	45
En	7	8	5	9	9	8	7	2	4	5	5
Fs	2	7	6	2	4	7	5	2	6	5	7

Table 4.2 continued:

Unit	**CCI**		**PNI**			**GVI**			**Ign-i**	
Sample	TM-1(2)	PNI-12	PNI-13	PNI-18	TER13-1	TER13-1	TER13-1	IGI-4	IGI-10	IGI-2
No.	Px08	12/1	13/1	18/1	64/1	67/1	102/1	37/1	43/1	35/1
SiO_2	51.42	52.64	52.72	52.14	51.03	52.90	53.60	51.52	51.44	52.04
TiO_2	0.34	0.71	0.48	0.47	0.43	0.44	0.44	0.89	0.26	0.36
Al_2O_3	0.34	3.31	0.77	0.53	0.54	0.58	0.50	1.05	0.35	0.33
Cr_2O_3	0.03	0.70	0.04	0.00	0.00	0.00	0.00	0.02	0.00	0.00
FeO	18.46	3.93	13.53	15.49	10.45	10.78	11.13	17.06	18.06	19.10
MnO	1.22	0.07	1.01	1.17	1.19	1.21	1.24	1.24	1.38	1.35
MgO	7.48	16.74	11.37	9.88	14.38	14.09	13.82	9.37	7.92	7.34
CaO	20.16	22.32	20.34	19.95	20.27	20.25	19.99	19.19	19.71	19.61
Na_2O	1.04	0.29	0.64	0.68	0.74	0.79	0.78	0.85	0.99	1.11
K_2O	0.00	0.00	0.00	0.00	0.00	0.00	0.00	0.00	0.00	0.00
Total	100.49	100.70	100.89	100.31	99.03	101.03	101.51	101.18	100.11	101.23
Si	1.990	1.907	1.986	1.996	1.920	1.956	1.977	1.964	1.995	2.003
Ti	0.010	0.019	0.013	0.014	0.012	0.012	0.012	0.025	0.008	0.010
Al	0.015	0.141	0.034	0.024	0.024	0.025	0.022	0.047	0.016	0.015
Cr	0.001	0.020	0.001	0.000	0.000	0.000	0.000	0.001	0.000	0.000
Fe^{2+}	0.536	0.113	0.415	0.489	0.163	0.239	0.289	0.508	0.531	0.574
Fe^{3+}	0.062	0.006	0.012	0.007	0.166	0.095	0.055	0.036	0.054	0.041
Mn	0.040	0.002	0.032	0.038	0.038	0.038	0.039	0.040	0.045	0.044
Mg	0.432	0.904	0.639	0.564	0.806	0.776	0.760	0.533	0.458	0.421
Ca	0.836	0.866	0.821	0.818	0.817	0.802	0.790	0.784	0.819	0.809
Na	0.078	0.020	0.047	0.050	0.054	0.057	0.056	0.063	0.074	0.082
K	0.000	0.000	0.000	0.000	0.000	0.000	0.000	0.000	0.000	0.000
Sum	4.000	4.000	4.000	4.000	4.000	4.000	4.000	4.000	4.000	4.000
Aeg	6	1	1	1	5	6	5	4	5	4
Fe-Ts	0	0	0	0	6	2	0	0	0	0
Jd	1	1	2	2	0	0	0	1	1	2
Ti-Aeg	1	0	1	2	0	0	0	2	1	2
Ti-Ts	0	2	1	0	1	1	1	2	0	0
Al-Ts	0	3	0	0	0	0	0	0	0	0
Di	36	73	48	42	60	57	54	38	36	33
Hd	48	9	34	39	15	20	23	39	45	48
En	4	9	8	7	10	10	11	8	5	4
Fs	5	1	5	6	3	4	5	8	6	7

Table 4.2 continued

Unit		**CCI sy**			**CCI enc (pheno)**			**CCI enc (groundmass)**	
Sample	TER30-1	TER30-1	TER30-1	Spec 1	Spec 1	Spec 1	Spec 1	Spec 1	Spec 1
No.	Px1	Px2	Px3	Pheno4	Pheno5	Pheno6	Cpx 8	Cpx 9	Cpx 10
SiO_2	52.75	52.33	52.03	47.02	48.45	45.88	50.54	50.50	50.81
TiO_2	1.99	2.20	3.36	1.64	1.60	2.57	0.40	0.39	0.33
Al_2O_3	0.34	0.30	0.25	3.46	4.31	6.59	0.56	0.46	0.58
Cr_2O_3	bdl	bdl	0.01	0.11	0.16	0.02	0.01	0.02	bdl
FeO	27.40	26.94	26.09	16.10	6.20	7.34	15.33	18.16	18.38
MnO	0.70	0.83	0.71	0.74	0.09	0.11	1.06	1.13	1.11
MgO	0.13	0.15	0.09	8.47	14.53	13.32	9.09	7.03	6.84
CaO	1.79	0.89	1.76	17.13	22.27	21.52	20.49	20.24	19.61
Na_2O	12.47	13.14	12.64	2.49	0.35	0.44	1.17	1.28	1.42
K_2O	bdl	0.03	bdl	0.53	0.03	0.03	0.06	0.05	0.10
Total	97.57	96.81	96.94	97.69	97.99	97.83	98.72	99.26	99.20
Si	2.020	2.008	2.005	1.826	1.822	1.737	1.961	1.977	1.990
Ti	0.057	0.063	0.097	0.048	0.045	0.073	0.012	0.012	0.010
Al	0.015	0.013	0.011	0.158	0.191	0.294	0.026	0.021	0.027
Cr			0.000	0.004	0.005	0.001	0.000	0.001	
Fe^{2+}	0.122	0.041	0.113	0.220	0.099	0.114	0.377	0.493	0.515
Fe^{3+}	0.756	0.823	0.728	0.303	0.096	0.119	0.120	0.101	0.087
Mn	0.023	0.027	0.023	0.024	0.003	0.004	0.035	0.037	0.037
Mg	0.007	0.008	0.005	0.491	0.815	0.752	0.526	0.410	0.399
Ca	0.073	0.037	0.073	0.713	0.897	0.873	0.852	0.849	0.823
Na	0.926	0.977	0.944	0.187	0.025	0.033	0.088	0.097	0.108
K		0.002		0.026	0.001	0.001	0.003	0.003	0.005
Sum	4.000	4.000	4.000	4.000	4.000	4.000	4.000	4.000	4.000
Aeg	76	82	73	19	3	3	9	10	9
Fe-Ts	0	0	0	6	4	4	2	0	0
Jd	4	2	2	0	0	0	0	0	2
Ti-Aeg	12	13	20	0	0	0	0	0	0
Ti-Ts	0	0.0	0	5	5	7	1	1	0
Al-Ts	0	0	0	0	1	3	0	0	0
Di	0	0	0	41	71	63	46	36	34
Hd		1	4	20	9	10	36	47	47
En	0	0	0	4	5	6	3	2	3
Fs	1	0	0	2	1	1	3	3	4

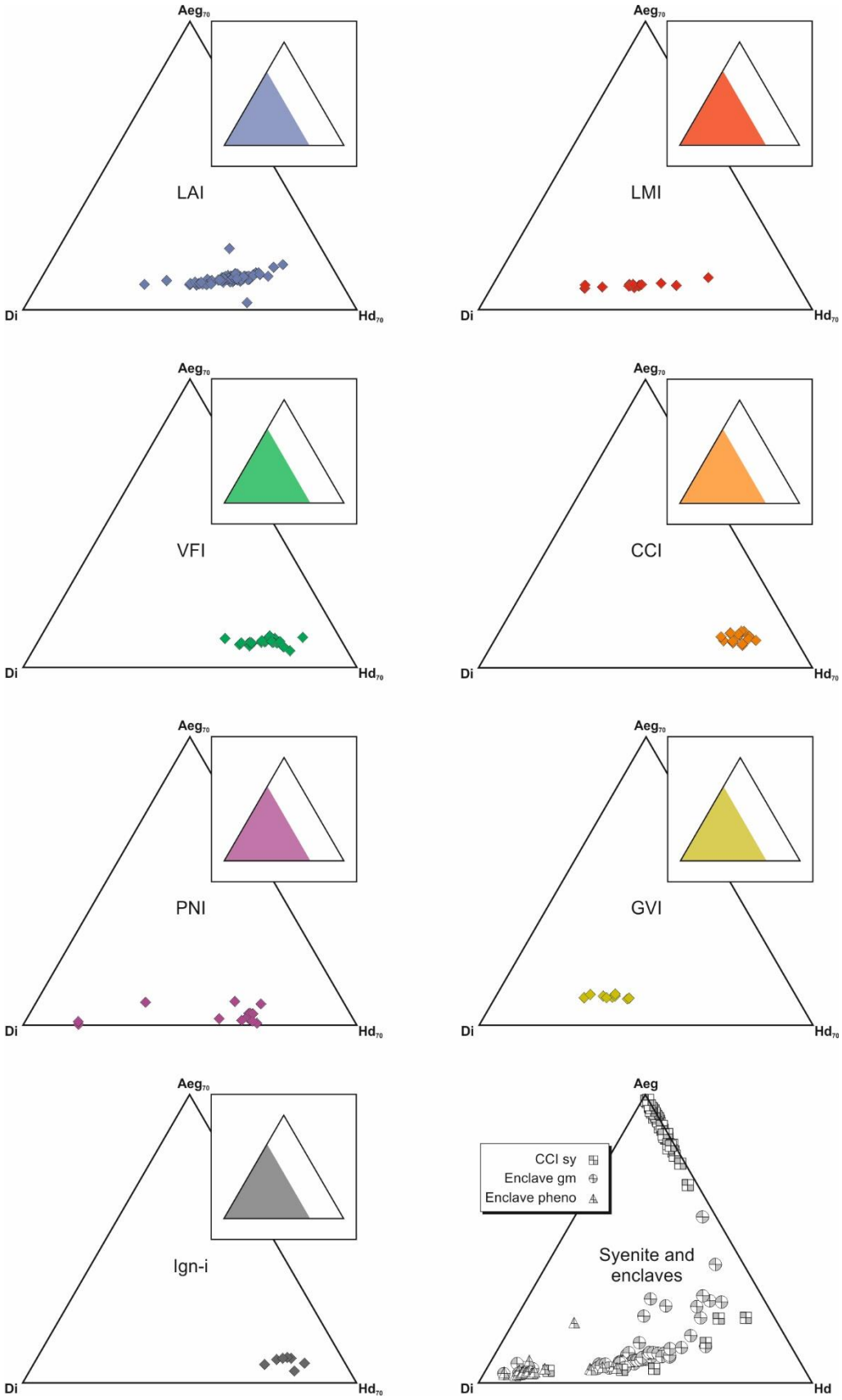

FIGURE 4.24: Diopside-hedenbergite-aegirine ternary diagrams illustrating clinopyroxene compositional trends from the lithologies of Terceira. Abbreviations used: sy =syenite, gm = groundmass, pheno = phenocryst

exhibit a bimodal distribution of quadrilateral compositions; one comparable to the ignimbrite clinopyroxene (Wo_{42-43}, En_{31-35}, Fs_{22-26}), and another which is more Mg-rich (Wo_{44-48}, En_{40-46}, Fs_{8-15}). In the ternary Di-Hed-Aeg system (calculated using the 10 component scheme of Marks *et al.*, 2008), all of the analyses define a single trend in which hedenbergite content increases with little change in aegirine content until ~ Hed_{55}, at which point aegirine increases rapidly.

4.5.2.3 Olivine

The olivine phenocrysts within the ignimbrites exhibit a compositional range of Fa_{59-82}. A single forsteritic olivine was identified in the Ign-i Formation, with a contrasting composition of Fo_{75}, Fa_{25}. EDS spectra produced at Keele University, U.K. indicate that large olivine crystals in the syenite-hosted enclaves are forsteritic in composition.

4.5.2.4 Fe-Ti Oxides

Representative analyses of Fe-Ti oxides are given in Table 4.3. Ti-magnetite is the most common Fe-Ti oxide present in the ignimbrites and exhibits a compositional range of Mt_{5-53}, Usp_{45-94}, Sp_{1-6}, with Al_2O_3 and MgO contents of up to 3.0 and 2.1 wt. %, respectively (Figure 4.25). Manganese contents are generally high, ranging from 1.3 to 2.4 wt. %. Ti-magnetite in the syenite ejecta shows a smaller compositional range of Mt_{32-57}, Usp_{35-68}, Sp_0, and significantly lower Al_2O_3 and MgO contents below 0.2 wt. %. However, MnO concentrations are similarly high, reaching 2.45 wt. %. Ilmenite is less common in the ignimbrites than Ti-magnetite, and exhibits a restricted compositional range of Ilm_{90-92}, Hem_{3-5}, Pyr_5. Aluminium contents are exclusively below 0.1 wt. % and MgO concentrations do not exceed 1.8 wt. %. The Mn component is comparable to that of Ti-magnetite, with MnO contents up to 2.3 wt. %. Ilmenite in the syenite ejecta also show a restricted range (Ilm_{90-94}, Hem_{1-4}, Pyr_{5-7}), low Al_2O_3 and MgO (< 0.1 and < 0.25 wt. %, respectively), and high MnO (up to 3.6 wt. %).

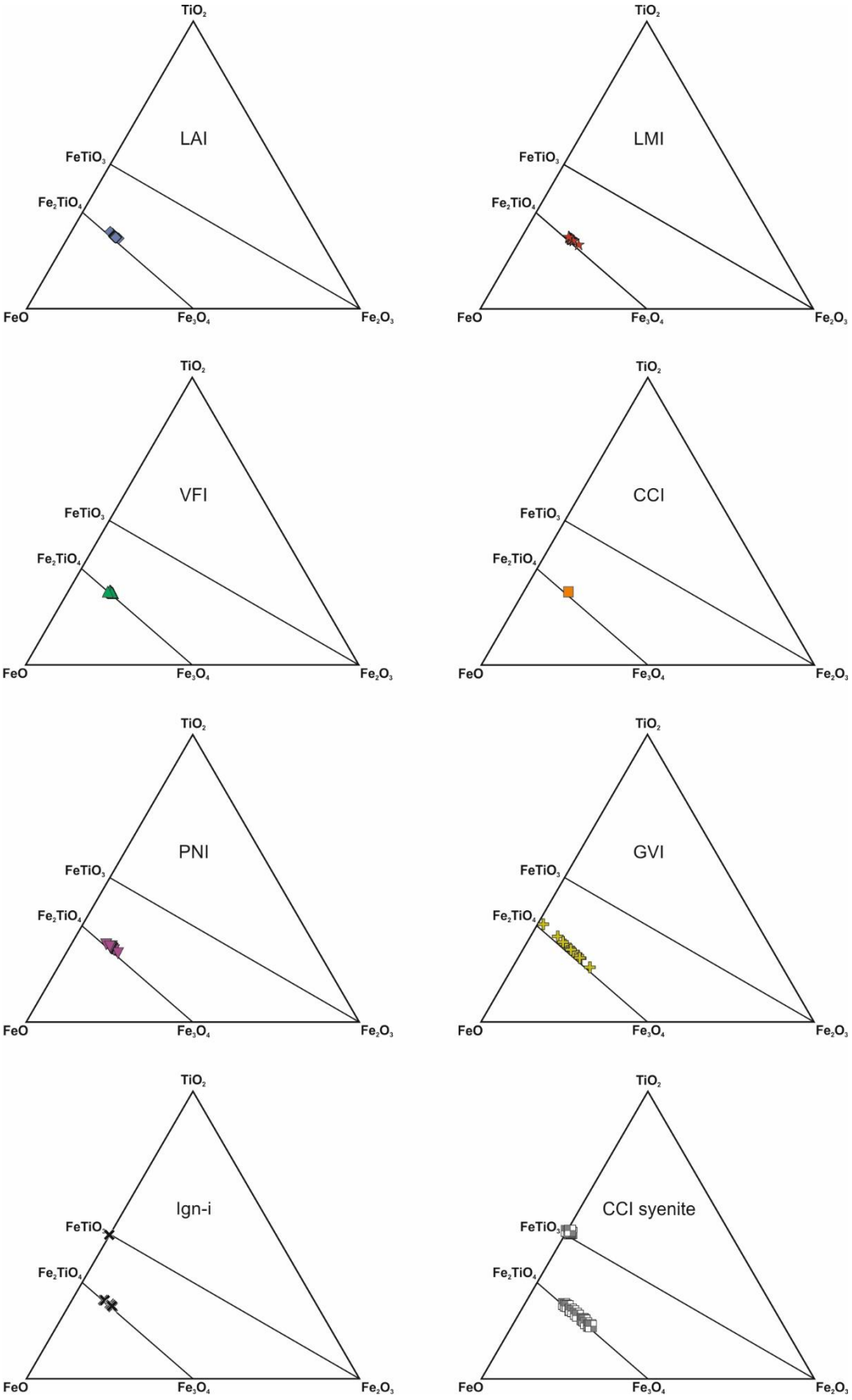

FIGURE 4.25: TiO_2-FeO-Fe_2O_3 ternary diagrams showing Fe-Ti oxide compositions for the lithologies of Terceira

Table 4.3: Representative Fe-Ti oxide analyses from the ignimbrites and syenite ejecta of Terceira

Unit			**LAI**			**LMI**		**VFI**		**CCI**		**PNI**	
Sample	TER1-1	TER1-1	TER3-2	TER4-1	TER5-2	TER5-2	TER2-2	TER2-2	TER2-1	T012	T012	T012
No.	51 / 1 .	53 / 1 .	63 / 1 .	154 / 1 .	168 / 1 .	169 / 1 .	199 / 1 .	200 / 1 .	204 / 1 .	23 / 1 .	24 / 1 .	25 / 1 .
Mineral	Ti-mag	Ti-mag	Ilmenite	Ilmenite	Ti-mag	Ti-mag	Ti-mag	Ti-mag	Ti-mag	Ti-mag	Ti-mag	Ti-mag
TiO_2	22.38	22.37	51.10	51.10	22.32	21.53	23.14	22.97	22.91	22.83	22.58	22.54
Al_2O_3	0.61	0.62	0.07	0.04	0.73	0.72	0.60	0.62	0.51	0.82	0.95	0.84
Cr_2O_3	bdl	0.03	0.02	0.01	0.03	0.01	0.02	0.01	0.02	bdl	bdl	bdl
FeO	71.90	72.25	45.00	45.55	71.84	72.38	71.00	71.06	71.08	69.90	68.78	68.68
MnO	1.81	1.81	2.30	2.32	1.53	1.63	1.62	1.64	1.77	1.58	1.72	1.67
MgO	1.14	1.10	1.68	1.59	0.93	0.87	0.80	0.81	0.73	0.88	0.67	0.73
Total	97.85	98.19	100.17	100.61	97.37	97.14	97.17	97.11	97.02	96.01	94.70	94.45
Ti	0.624	0.622	0.954	0.950	0.626	0.605	0.652	0.647	0.647	0.650	0.652	0.653
Al	0.027	0.027	0.002	0.001	0.032	0.032	0.026	0.027	0.023	0.037	0.043	0.038
Cr		0.001	0.000	0.000	0.001	0.000	0.001	0.000	0.001			
Fe^{2+}	1.504	1.504	0.843	0.843	1.526	1.505	1.556	1.550	1.550	1.550	1.558	1.557
Fe^{3+}	0.725	0.729	0.091	0.099	0.715	0.757	0.669	0.678	0.683	0.663	0.652	0.656
Mn	0.057	0.057	0.048	0.049	0.048	0.052	0.051	0.052	0.056	0.051	0.056	0.054
Mg	0.063	0.061	0.062	0.059	0.052	0.048	0.045	0.045	0.041	0.050	0.038	0.042
Sum	3.000	3.000	2.000	2.000	3.000	3.000	3.000	3.000	3.000	3.000	3.000	3.000
Usp	62.4	62.2			62.6	60.5	65.2	64.7	64.7	65.0	65.3	65.3
Mt	36.3	36.5			35.8	37.9	33.5	33.9	34.1	33.2	32.6	32.8
Sp	1.3	1.4			1.6	1.6	1.3	1.4	1.1	1.8	2.1	1.9
Ilm			91.1	90.6								
Hem			4.3	4.7								
Pyr			4.6	4.6								

Table 4.3 continued

Unit		**GVI**			**Ign-i**				**CCI Sy**			
Sample	TER13-1	TER13-1	TER13-1	T001	T001	T001	TER30-3	TER30-3	TER30-3	TER30-3	TER30-3	TER30-6
No.	78 / 1 .	79 / 1 .	91 / 1 .	54 / 1 .	55 / 1 .	62 / 1 .	MAG 1	MAG 2	MAG 8	ILM 3	ILM 4	ILM 5
Mineral	Ti-mag	Ti-mag	Ti-mag	Ti-mag	Ti-mag	Mph	Ti-mag	Ti-mag	Ti-mag	Ilmenite	Ilmenite	Ilmenite
TiO_2	23.98	21.02	15.60	23.05	23.58	22.89	16.68	16.71	15.00	51.13	50.19	50.32
Al_2O_3	0.69	0.72	0.81	0.36	0.29	0.33	0.13	0.15	0.09	bdl	0.01	bdl
Cr_2O_3	0.01	0.01	0.01	bdl	0.01	bdl	0.01	0.01	0.01	bdl	bdl	bdl
FeO	66.23	68.51	74.62	70.46	70.38	70.55	74.92	74.28	76.64	45.62	45.11	45.85
MnO	1.76	1.76	1.81	1.83	1.88	1.81	2.23	2.06	2.26	2.66	2.81	2.86
MgO	1.82	1.73	1.23	0.45	0.42	0.52	0.10	0.04	0.04	0.21	0.15	0.11
Total	94.49	93.74	94.08	96.14	96.56	96.11	94.06	93.25	94.04	99.62	98.27	99.14
Ti	0.690	0.608	0.448	0.659	0.672	0.654	0.486	0.492	0.437	0.971	0.967	0.961
Al	0.031	0.033	0.036	0.016	0.013	0.015	0.006	0.007	0.004		0.000	
Cr	0.000	0.000	0.000		0.000		0.000	0.000	0.000			
Fe^{2+}	1.529	1.451	1.320	1.575	1.588	1.567	1.407	1.421	1.360	0.907	0.900	0.895
Fe^{3+}	0.589	0.752	1.066	0.666	0.643	0.676	1.021	1.009	1.122	0.057	0.066	0.079
Mn	0.057	0.057	0.059	0.059	0.060	0.058	0.073	0.068	0.074	0.057	0.061	0.062
Mg	0.104	0.099	0.070	0.025	0.024	0.029	0.006	0.002	0.003	0.008	0.006	0.004
Sum	3.000	3.000	3.000	3.000	3.000	3.000	3.000	3.000	3.000	2.000	2.000	2.000
Usp	69.0	60.8	44.9	65.9	67.2	65.4	48.6	49.2	43.7			
Mt	29.5	37.6	53.3	33.3	32.1	33.8	51.1	50.5	56.1			
Sp	1.5	1.6	1.8	0.8	0.6	0.7	0.3	0.3	0.2			
Ilm										91.9	91.1	90.5
Hem										2.7	3.1	3.7
Pyr										5.4	5.7	5.8

4.5.2.5 Biotite

Biotite phenocrysts found in the GVI are characterised by high TiO_2 contents (5.7 to 6.0 wt. %), variable SiO_2 (36.6 to 39.3 wt. %), Na_2O contents of up to 1.2 wt. %, and Fe/Fe+Mg ratios of ~ 0.35 (Figure 4.26). Occupation of the hydroxyl sites is characterised by variably high F contents (0.630 to 0.881 apfu) and low Cl contents (< 0.015 apfu).

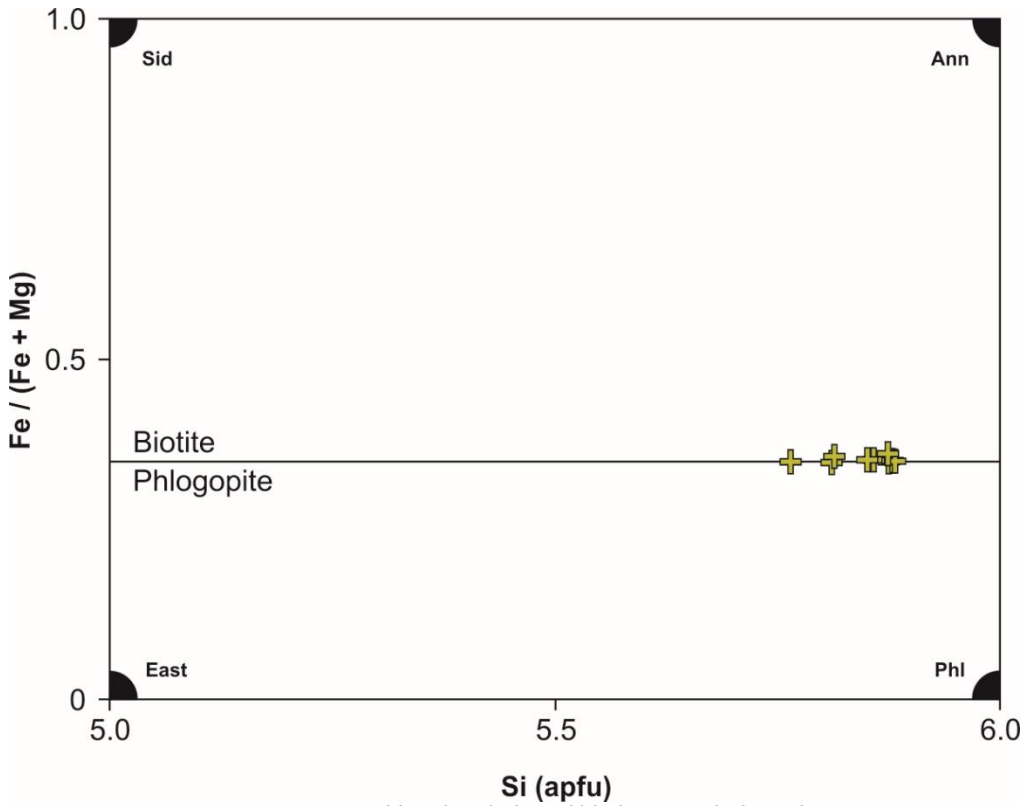

FIGURE 4.26: Compositional variation of biotite crystals from the GVI

4.5.2.6 Amphibole

Following the nomenclature of Leake *et al.* (1997), the amphiboles from the syenite ejecta belong to the sodic-calcic and the sodic group (Figure 4.27), and are classified as katophorite to ferrorichterite, and ferroeckermannite and arfvedsonite, respectively. Fluorine concentrations range from 0.714 to 1.055 apfu, whereas Cl contents are exclusively < 0.015 apfu. Individual crystals are often zoned, with Na-Ca-amphibole in the core, and Na-amphibole rims. Amphiboles in the groundmass of syenite-hosted enclaves range from calcic to sodic-calcic, and can be classified as ferroedenite, and katophorite

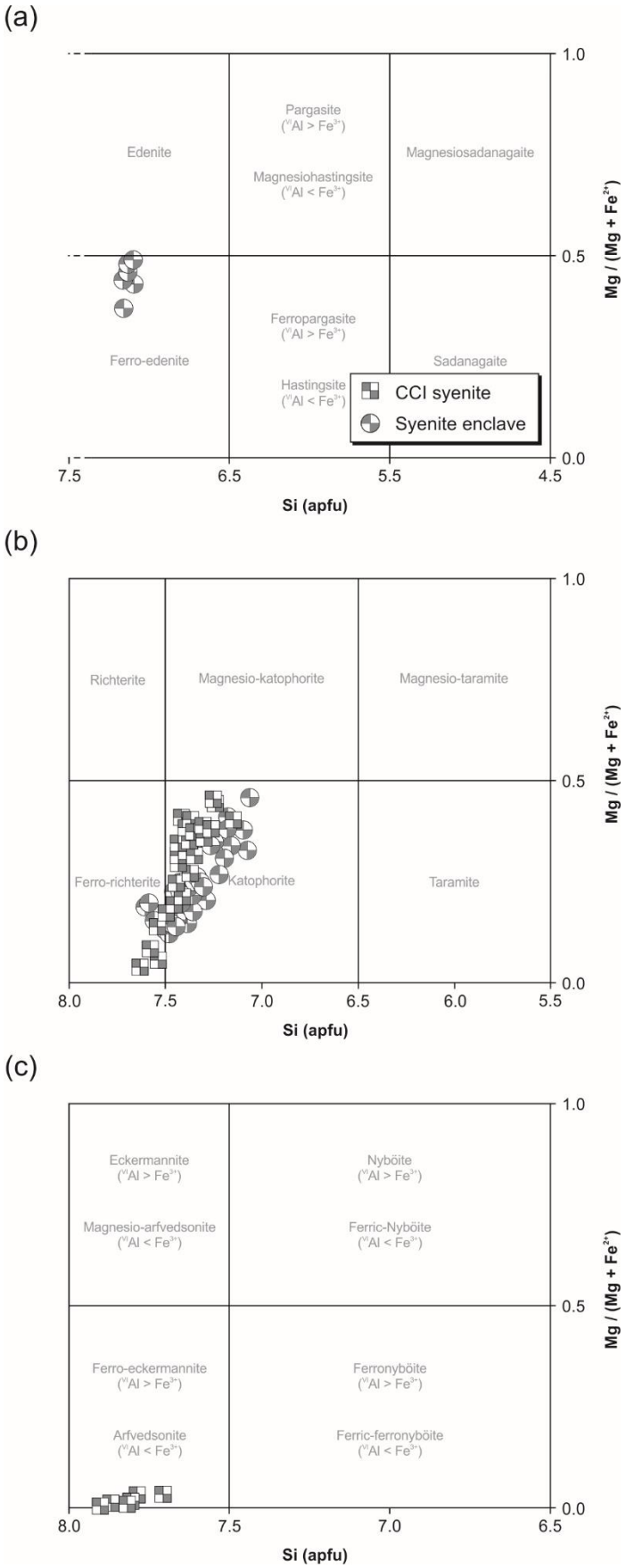

FIGURE 4.27: Amphibole compositions from the CCI syenite and syenite-hosted enclaves classified using the **a)** Ca amphibole scheme, **b)** Na-Ca amphibole scheme, and **c)** Na-amphibole scheme of Leake *et al.* (1997)

and ferrorichterite, respectively (Figure 4.27). Occupation of the hydroxyl site is characterised by a greater range than amphiboles from the syenites, with F ranging from 0.093 to 1.247 apfu, and Cl not exceeding 0.015 apfu.

4.5.2.7 Aenigmatite

The aenigmatite found within the CCI syenite ejecta exhibits a very restricted compositional range, close to the ideal chemical formula for aenigmatite (Figure 4.28, Table 4.4). TiO_2 contents cluster around 8 to 9 wt. %, whilst Na_2O values lie between 6.5 and 7.5 wt. %. Al_2O_3 contents do not exceed 1.2 wt. %.

4.5.2.8 Dalyite

Chemical analyses of the CCI syenite dalyite (samples TER 30-1 and TER 30-7) are reported in Table 4.5. The data reveal that the CCI syenite dalyite does not deviate substantially from the empirical formula, with Na being the most significant substituting element (~ 0.10 to 0.20 apfu), substituting for K. The combined totals of atomic Na and K are close to the ideal total of 2 cations, and Fe contents are often below the detection limit (0.038 wt. %, average error = 0.052 wt. %), highlighting limited incorporation of Fe in the dalyite structure. The low contents of Ti and Hf (up to 0.030 and 0.013 apfu, respectively), indicate that replacement of Zr with Ti and Hf is limited. These analyses suggest that the CCI dalyite corresponds to the more precise formula $(K_{1.79\text{-}1.87}Na_{0.12\text{-}0.19})(Zr_{0.90\text{-}0.96}\ Ti_{0.004\text{-}0.030}Hf_{0.010\text{-}0.013})(Si_{6.01\text{-}6.06}O_{15})$. Calculated alkalinity moduli (Khomyakov, 1995) values range from 21.90 to 22.39. In addition to Na, Fe Ti and Hf, the data suggest that trace amounts of Al, Ba, Mg, and Mn may be present, though these are all very close to the detection limit. This is supported by their occurrence in trace amounts in various literature analyses (Table 4.6).

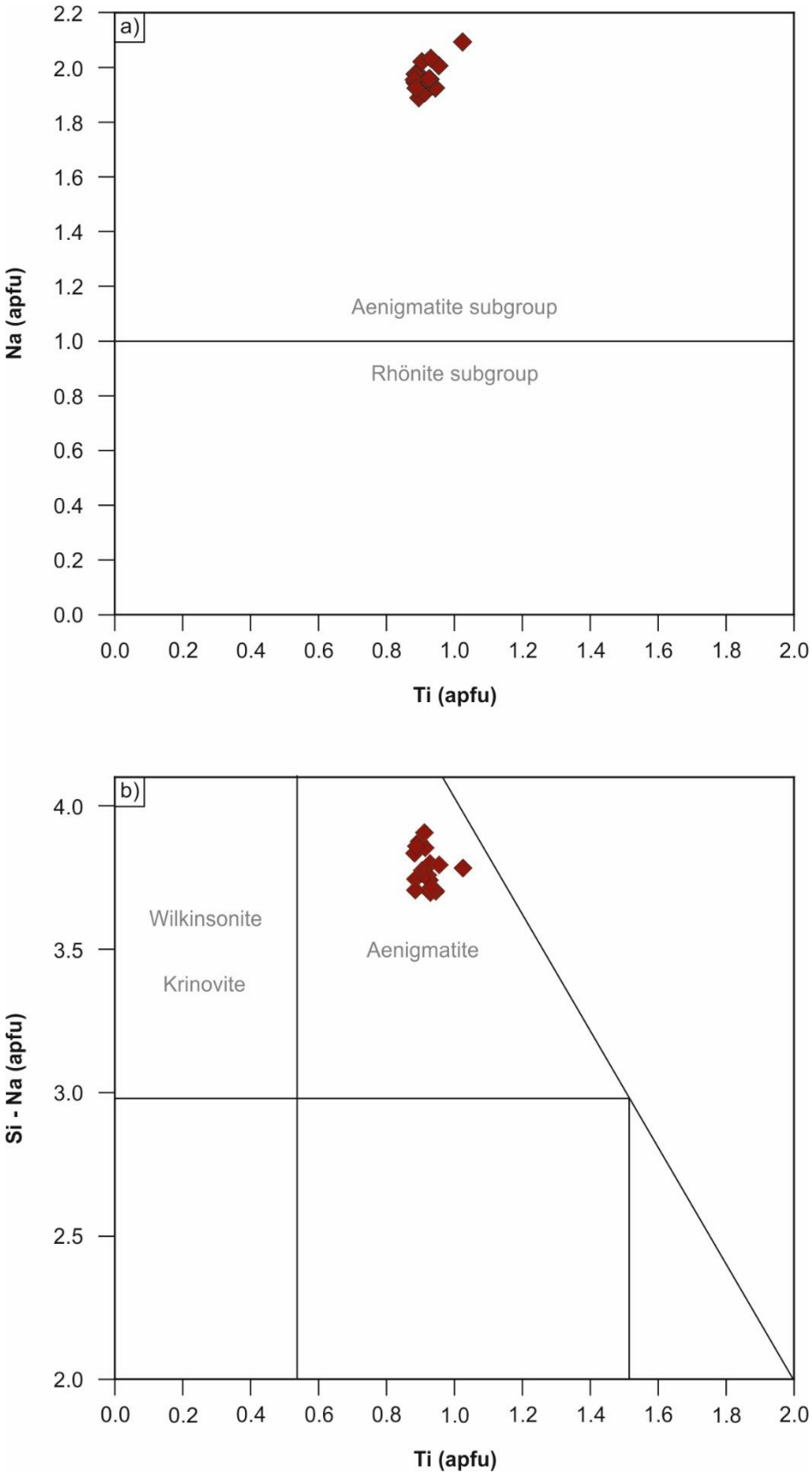

FIGURE 4.28: Aenigmatite compositions from the CCI syenite ejecta. Classification schemes from Kunzmann (1999) **a)** Aenigmatite compositions plotted into the projection to the base of the aenigmatite- and rhönite-subgroup polyhedra **b)** Aenigmatite compositions plotted into the projection onto the side of the aenigmatite-subgroup polyhedra

Table 4.4: Electron microprobe analyses of aenigmatite from the CCI syenite ejecta

Sample	**TER30-3**	**TER30-3**	**TER30-3**	**TER30-6**	**TER30-6**	**TER30-6**	**TER30-6**	**TER30-6**	**TER30-6**	**TER30-6**	**TER30-7B**	**TER30-7B**	**TER30-7B**	**TER30-7B**	**TER30-7B**	**TER30-7B**
Analysis	Aenig01	Aenig02	Aenig03	Aenig04	Aenig05	Aenig06	Aenig07	Aenig08	Aenig09	Aenig10	Aenig_1	Aenig_2	Aenig_3	Aenig_4	Aenig_5	Aenig_6
SiO_2	41.19	40.52	41.53	40.46	40.43	40.22	40.87	40.51	40.49	40.78	40.43	38.82	40.55	39.56	39.84	39.92
TiO_2	8.55	8.37	8.58	8.32	8.68	8.37	8.28	8.54	8.70	8.32	8.85	8.66	9.40	8.64	8.61	8.60
Al_2O_3	0.50	0.87	0.38	0.97	0.90	1.18	0.73	0.99	0.69	0.83	0.40	0.76	bdl	0.76	0.68	0.35
FeO	41.73	42.13	41.64	41.15	41.72	42.31	41.49	41.23	41.70	41.54	40.79	41.33	38.28	41.75	41.44	41.23
MnO	1.66	1.53	1.74	2.04	1.37	1.46	1.45	1.48	1.53	1.41	1.62	1.51	2.90	1.53	1.62	1.69
MgO	0.21	0.19	0.24	0.18	0.38	0.28	0.33	0.29	0.26	0.31	0.23	0.35	0.08	0.37	0.32	0.16
CaO	0.31	0.42	0.24	0.74	0.78	0.81	0.64	0.71	0.60	0.71	0.22	0.68	bdl	0.53	0.54	0.17
Na_2O	7.41	6.85	7.15	7.21	7.11	7.14	7.12	6.92	7.07	7.00	7.21	6.85	7.45	7.06	7.06	7.28
K_2O	0.01	bdl	0.01	0.01	0.02	bdl	bdl	0.02	bdl	bdl	bdl	bdl	bdl	bdl	bdl	bdl
Total	101.56	100.93	101.52	101.08	101.41	101.80	100.91	100.70	101.04	100.90	99.75	98.96	98.65	100.21	100.11	99.39
Si	5.794	5.764	5.861	5.718	5.700	5.649	5.788	5.759	5.740	5.782	5.798	5.625	5.874	5.653	5.698	5.747
Ti	0.905	0.896	0.911	0.884	0.921	0.884	0.882	0.913	0.928	0.887	0.954	0.945	1.024	0.929	0.926	0.931
Al	0.083	0.145	0.062	0.162	0.149	0.196	0.121	0.166	0.116	0.139	0.068	0.129		0.129	0.114	0.060
Fe^{2+}	4.366	4.590	4.561	4.254	4.362	4.289	4.419	4.502	4.453	4.477	4.460	4.353	4.340	4.324	4.359	4.346
Fe^{3+}	0.543	0.421	0.353	0.610	0.557	0.681	0.495	0.400	0.491	0.448	0.432	0.656	0.297	0.666	0.597	0.617
Mn	0.198	0.184	0.208	0.244	0.164	0.174	0.174	0.178	0.184	0.169	0.197	0.185	0.355	0.185	0.196	0.206
Mg	0.043	0.040	0.050	0.039	0.081	0.058	0.069	0.062	0.054	0.065	0.050	0.076	0.016	0.078	0.068	0.034
Ca	0.047	0.065	0.036	0.111	0.118	0.122	0.096	0.108	0.091	0.108	0.034	0.105		0.081	0.083	0.026
Na	2.021	1.889	1.956	1.976	1.944	1.944	1.955	1.907	1.943	1.924	2.006	1.925	2.093	1.957	1.959	2.033
K	0.001		0.002	0.001	0.004			0.003								
Sum	14.000	14.000	14.000	14.000	14.000	14.000	14.000	14.000	14.000	14.000	14.000	14.000	14.000	14.000	14.000	14.000

bdl = below detection limit

Table 4.5: Electron microprobe analyses of dalyite from the CCI syenite ejecta

Sample	**TER 30-1**	**TER 30-1**	**TER 30-1**	**TER 30-1**	**TER 30-1**	**TER 30-7**	**TER 30-7**	**TER 30-7**	**TER 30-7**	**TER 30-7**	**TER 30-7**	**TER 30-7**
Group	1	1	1	1	1	1	1	1	1	1	1	1
Suggested origin	Magmatic	Magmatic	Magmatic	Magmatic	Magmatic	Magmatic	Magmatic	Magmatic	Magmatic	Magmatic	Magmatic	Magmatic
SiO_2	62.9	62.6	62.4	62.2	62.4	62.9	63.0	62.4	62.6	62.6	63.0	63.0
TiO_2	0.10	0.23	0.19	0.13	0.11	0.17	0.10	0.12	0.41	0.09	0.06	0.27
Al_2O_3	bdl	bdl	0.03	0.03	bdl	bdl	0.04	0.04	0.05	0.03	bdl	bdl
Cr_2O_3	bdl	bdl	bdl	bdl	bdl	bdl	bdl	bdl	bdl	bdl	bdl	bdl
FeO	bdl	0.06	bdl	0.06	0.09	bdl	0.07	0.07	0.11	0.05	0.06	bdl
MnO	bdl	0.03	bdl	bdl	bdl	bdl	bdl	0.04	bdl	bdl	bdl	bdl
MgO	bdl	bdl	bdl	bdl	bdl	bdl	bdl	bdl	0.03	bdl	bdl	bdl
CaO	bdl	bdl	bdl	bdl	bdl	bdl	bdl	bdl	bdl	bdl	bdl	bdl
Na_2O	0.99	0.95	0.99	1.00	0.90	0.90	0.67	0.71	0.67	0.72	0.66	0.66
K_2O	14.6	15.0	14.9	14.8	14.7	14.8	15.0	15.0	15.0	15.2	15.3	15.1
ZrO_2	20.0	20.5	19.8	20.4	20.4	20.4	19.7	20.3	19.1	20.0	20.6	20.2
HfO_2	0.46	0.40	0.38	0.40	0.39	0.45	0.39	0.39	0.42	0.42	0.48	0.38
BaO	0.06	0.06	0.08	bdl	bdl	0.05	0.08	bdl	bdl	bdl	bdl	bdl
Total	**99.08**	**99.78**	**98.81**	**98.89**	**98.98**	**99.72**	**98.99**	**99.05**	**98.33**	**99.01**	**100.17**	**99.57**
Si	6.05	6.01	6.03	6.01	6.02	6.03	6.06	6.02	6.05	6.04	6.02	6.04
Ti	0.007	0.016	0.013	0.009	0.008	0.012	0.008	0.009	0.030	0.006	0.004	0.019
Al	bdl	bdl	0.004	0.003	bdl	bdl	0.005	0.004	0.006	0.004	bdl	bdl
Cr	bdl	bdl	bdl	bdl	bdl	bdl	bdl	bdl	bdl	bdl	bdl	bdl
Fe	bdl	0.005	bdl	0.004	0.007	bdl	0.005	0.006	0.009	0.004	0.005	bdl
Mn	bdl	0.002	bdl	bdl	bdl	bdl	bdl	0.004	bdl	bdl	bdl	bdl
Mg	bdl	bdl	bdl	bdl	bdl	bdl	bdl	bdl	0.004	bdl	bdl	bdl
Ca	bdl	bdl	bdl	bdl	bdl	bdl	bdl	bdl	bdl	bdl	bdl	bdl
Na	0.18	0.18	0.18	0.19	0.17	0.17	0.13	0.13	0.13	0.13	0.12	0.12
K	1.79	1.84	1.83	1.82	1.81	1.81	1.84	1.85	1.85	1.87	1.87	1.85
Zr	0.94	0.96	0.93	0.96	0.96	0.95	0.92	0.96	0.90	0.94	0.96	0.94
Hf	0.013	0.011	0.010	0.011	0.011	0.012	0.011	0.011	0.011	0.012	0.013	0.010
Ba	0.002	0.002	0.003	bdl	bdl	0.002	0.003	bdl	bdl	bdl	bdl	bdl
Sum	**8.982**	**9.026**	**9.000**	**9.007**	**8.986**	**8.986**	**8.982**	**8.994**	**8.990**	**9.006**	**8.992**	**8.979**
K_{alk}	21.98	22.34	22.39	22.32	22.06	21.99	21.90	22.03	21.98	22.27	22.13	21.94

bdl = below detection limit

Table 4.6: Electron microprobe data for dalyite taken from the literature

Location	**Ascension**	**Ascension**	**Straumsvola**	**Strange Lake**	**Gordon Butte**	**Agua de Pau**	**Agua de Pau**	**Agua de Pau**	**Agua de Pau**
Group	1	1	1	1	1	1	1	1	1
Host rock	Granite ejecta	Granite ejecta	Granite dyke	Granite	Alkaline pegmatite	Syenitic ejecta	Syenitic ejecta	Syenitic ejecta	Syenitic ejecta
Suggested origin	Magmatic	Magmatic	Magmatic	Magmatic	Magmatic	Magmatic	Magmatic	Magmatic	Magmatic
No.	1†	2*	3	4	5	6	7	8	9
SiO_2	61.85	63.25	62.07	62.55	60.35	62.23	61.35	61.35	61.36
TiO_2	-	0.12	0.13	0.08	1.78	0.08	0.11	0.14	0.15
Al_2O_3	-	-	-	bdl	bdl	-	-	-	-
FeO	0.33	0.03	bdl	0.06	0.18	-	-	-	-
MnO	-	bdl	bdl	-	bdl	-	-	-	-
MgO	-	-	-	-	bdl	-	-	-	-
CaO	-	bdl	bdl	bdl	bdl	-	-	-	-
Na_2O	1.75	0.79	bdl	bdl	0.02	0.69	0.37	0.44	0.49
K_2O	14.60	14.63	15.71	15.08	15.34	13.80	14.56	14.60	14.72
ZrO_2	21.70	20.43	20.63	20.38	18.21	23.72	23.57	23.27	23.49
HfO_2	-	-	-	0.81	-	-	-	-	-
BaO	-	-	-	-	bdl	-	-	-	-
P_2O_5	-	-	-	-	-	-	-	-	-
La_2O_3	-	bdl	bdl	0.04	-	-	-	-	-
Ce_2O_3	-	bdl	bdl	0.06	bdl	-	-	-	-
Nb_2O_5	-	bdl	bdl	-	1.65	-	-	-	-
Total	**100.23**	**99.25**	**98.54**	**98.96**	**97.53**	**100.52**	**99.96**	**99.80**	**100.21**
Si	5.94	6.05	6.03	6.04	5.92	5.94	5.92	5.92	5.91
Ti	-	0.01	0.01	0.01	0.13	0.01	0.01	0.01	0.01
Al	-	-	-	bdl	bdl	-	-	-	-
Fe	0.03	0.00	bdl	0.01	0.02	-	-	-	-
Mn	-	bdl	bdl	-	bdl	-	-	-	-
Mg	-	-	-	-	bdl	-	-	-	-
Ca	-	bdl	bdl	bdl	bdl	-	-	-	-
Na	0.33	0.15	bdl	bdl	0.00	0.13	0.07	0.08	0.09
K	1.79	1.79	1.95	1.86	1.92	1.68	1.79	1.80	1.81
Zr	1.02	0.95	0.98	0.96	0.87	1.10	1.11	1.10	1.10
Hf	-	-	-	0.02	-	-	-	-	-
Ba	-	-	-	-	bdl	-	-	-	-
P	-	-	-	-	-	-	-	-	-
La	-	bdl	bdl	0.00	-	-	-	-	-
Ce	-	bdl	bdl	0.00	bdl	-	-	-	-
Nb	-	bdl	bdl	-	0.07	-	-	-	-
Sum	**9.11**	**8.95**	**8.97**	**8.90**	**8.93**	**8.86**	**8.90**	**8.91**	**8.92**
K_{alk}	23.27	21.68	21.74	20.90	21.50	20.43	20.90	21.10	21.30

Analysis 1 from Ascension Island, (Van Tassel, 1952), analyses 2-3 from the Murun complex, Russia (Lazebnik and Makhotko, 1982),analysis 4 from Ascension Island, (Harris and Rickard, 1987), analyses 5-14 from Sunnfjord, Norway (Robins *et al.*, 1983), analysis 15 from Straumsvola, Antarctica (Harris and Rickard, 1987), analyses 16-21 from Cancarix, Spain (Linthout *et al.*, 1988), analysis 22 from the Strange Lake complex, Canada (Birkett *et al.*, 1992), analyses 23-24 from the Murun complex, Russia (Konev *et al.*, 1996), analysis 25 from Gordon Butte, USA (Chakhmouradian and Mitchell, 2002), analyses 26-29 from Fogo, São Miguel Island (Ridolfi *et al.*, 2003). Abbreviations and symbols used: n.d. = not determined; † Analysis includes 0.64 wt. % H_2O; * Average of three analyses

Table 4.6 continued

Location	**Murun**	**Murun**	**Murun**	**Murun**	**Murun**	**Murun**	**Sunnfjord**	**Sunnfjord**	**Sunnfjord**	**Sunnfjord**	**Sunnfjord**
Group	2	2	2	2	2	2	2	2	2	2	2
Host rock			Charoitite	Charoitite	Charoitite	Charoitite	Syenite dyke	Syenite dyke	Syenite dyke	Syenite dyke	Syenite dyke
Suggested	Magmatic or	Magmatic or	Magmatic or	Magmatic or	Magmatic or	Magmatic or	Magmatic	Magmatic	Magmatic	Magmatic	Magmatic
No.	10	11	12	13	14	15	16	17	18	19	20
SiO_2	63.62	60.82	63.44	62.35	61.83	62.25	63.39	61.86	64.94	64.12	64.22
TiO_2	1.87	0.69	2.92	5.86	0.69	1.56	0.64	1.22	1.59	0.83	0.88
Al_2O_3	0.03	bdl	bdl	0.02	bdl	bdl	0.03	0.01	bdl	0.15	0.06
FeO	bdl	bdl	0.01	0.07	bdl	bdl	0.22	0.30	0.26	0.31	0.19
MnO	-	-	-	-	bdl	bdl	0.05	bdl	0.06	bdl	bdl
MgO	-	-	-	-	bdl	bdl	bdl	0.08	bdl	bdl	0.05
CaO	0.02	0.03	bdl	bdl	bdl	bdl	0.04	bdl	0.03	bdl	bdl
Na_2O	0.11	0.03	bdl	0.10	bdl	bdl	0.04	bdl	0.09	bdl	bdl
K_2O	14.99	15.41	16.75	16.68	15.15	15.65	15.93	16.64	14.08	15.80	16.36
ZrO_2	21.50	22.16	16.68	14.84	20.60	19.13	19.49	18.83	19.13	20.17	19.68
HfO_2	-	-	-	-	bdl	bdl	-	-	-	-	-
BaO	bdl	bdl	bdl	bdl	bdl	bdl	0.08	0.03	0.11	0.04	0.03
P_2O_5	-	-	-	-	bdl	bdl	0.10	0.12	bdl	bdl	bdl
La_2O_3	-	-	-	-	bdl	bdl	-	-	-	-	-
Ce_2O_3	-	-	-	-	bdl	bdl	-	-	-	-	-
Nb_2O_5	-	-	-	-	bdl	0.60	-	-	-	-	-
Total	**102.14**	**99.14**	**99.79**	**99.92**	**98.27**	**99.19**	**100.01**	**99.09**	**100.29**	**101.42**	**101.47**
Si	5.94	5.92	6.01	5.89	6.00	5.98	6.04	5.98	6.08	6.02	6.03
Ti	0.13	0.05	0.21	0.42	0.05	0.11	0.05	0.09	0.11	0.06	0.06
Al	0.00	bdl	bdl	0.00	bdl	bdl	0.00	0.00	bdl	0.02	0.01
Fe	bdl	bdl	0.00	0.01	bdl	bdl	0.02	0.02	0.02	0.02	0.01
Mn	-	-	-	-	bdl	bdl	0.00	bdl	0.00	bdl	bdl
Mg	-	-	-	-	bdl	bdl	bdl	0.01	bdl	bdl	0.01
Ca	0.00	0.00	bdl	-	bdl	bdl	0.00	bdl	0.00	bdl	bdl
Na	0.02	0.01	bdl	0.02	bdl	bdl	0.01	bdl	0.02	bdl	bdl
K	1.78	1.91	2.03	2.01	1.88	1.92	1.94	2.05	1.68	1.89	1.96
Zr	0.98	1.05	0.77	0.68	0.98	0.90	0.91	0.89	0.87	0.92	0.90
Hf	-	-	-	-	bdl	bdl	-	-	-	-	-
Ba	bdl	bdl	bdl	bdl	bdl	bdl	0.00	0.00	0.00	0.00	0.00
P	-	-	-	-	bdl	bdl	0.01	0.01	bdl	bdl	bdl
La	-	-	-	-	bdl	bdl	-	-	-	-	-
Ce	-	-	-	-	bdl	bdl	-	-	-	-	-
Nb	-	-	-	-	bdl	0.03	-	-	-	-	-
Sum	**8.85**	**8.94**	**9.02**	**9.03**	**8.91**	**8.93**	**8.97**	**9.05**	**8.79**	**8.94**	**8.98**
K_{alk}	20.34	21.48	22.51	22.48	21.07	21.47	21.71	22.65	19.34	21.16	21.80

Table 4.6 continued

Location	**Sunnfjord**	**Sunnfjord**	**Sunnfjord**	**Sunnfjord**	**Sunnfjord**	**Cancarix**	**Cancarix**	**Cancarix**	**Cancarix**	**Cancarix**	**Cancarix**
Group	2	**2**	**2**	**2**	**2**	**2**	**2**	**2**	**2**	**2**	**2**
Host rock	Syenite dyke	Syenite dyke	Syenite dyke	Syenite dyke	Syenite dyke	Lamproite	Lamproite	Lamproite	Lamproite	Lamproite	Lamproite
Suggested origin	Magmatic	Magmatic	Magmatic	Magmatic	Magmatic	Magmatic	Magmatic	Magmatic	Magmatic	Magmatic	Magmatic
No.	21	22	23	24	25	26	27	28	29	30	31
SiO_2	62.75	62.25	62.53	62.58	62.04	62.60	62.45	62.65	62.95	62.65	63.00
TiO_2	1.08	1.54	1.21	1.61	1.71	1.25	1.10	1.10	0.75	1.15	0.85
Al_2O_3	0.01	0.13	0.12	0.07	0.03	0.10	0.10	0.10	0.05	0.05	0.05
FeO	0.60	0.31	0.19	0.15	0.28	0.18	0.18	0.18	0.18	0.09	0.18
MnO	0.04	0.05	bdl	bdl	0.03	bdl	-	-	-	-	-
MgO	0.65	0.10	0.08	0.02	0.06	bdl	bdl	-	0.05	bdl	0.05
CaO	0.04	0.04	0.06	bdl	0.02	bdl	-	-	-	-	-
Na_2O	bdl	0.19	bdl	bdl	0.07	0.15	0.15	0.15	0.10	0.15	0.15
K_2O	15.79	15.33	15.98	16.17	13.93	15.75	16.10	16.10	15.95	16.25	16.10
ZrO_2	18.29	19.22	18.46	20.23	20.16	19.10	19.20	19.35	19.40	19.60	19.70
HfO_2	-	-	-	-	-	-	-	-	-	-	-
BaO	bdl	0.19	0.21	0.20	0.22	0.45	0.30	0.40	0.15	0.25	0.35
P_2O_5	0.04	0.10	bdl	bdl	bdl	-	-	-	-	-	-
La_2O_3	-	-	-	-	-	-	-	-	-	-	-
Ce_2O_3	-	-	-	-	-	-	-	-	-	-	-
Nb_2O_5	-	-	-	-	-	-	-	-	-	-	-
Total	**99.29**	**99.45**	**98.84**	**101.03**	**98.55**	**99.58**	**99.58**	**100.03**	**99.58**	**100.19**	**100.43**
Si	6.01	5.97	6.02	5.94	5.97	6.00	6.00	6.00	6.02	5.99	6.00
Ti	0.08	0.11	0.09	0.11	0.12	0.09	0.08	0.08	0.05	0.09	0.06
Al	0.00	0.01	0.01	0.01	0.00	0.01	0.01	0.01	0.01	0.01	0.01
Fe	0.05	0.02	0.02	0.01	0.02	0.02	0.02	0.02	0.02	0.02	0.02
Mn	0.00	0.00	bdl	bdl	0.00	bdl	-	-	-	-	-
Mg	0.09	0.01	0.01	0.00	0.01	bdl	bdl	-	0.01	bdl	0.01
Ca	0.00	0.00	0.01	bdl	0.00	bdl	-	-	-	-	-
Na	bdl	0.04	bdl	bdl	0.01	0.03	0.03	0.03	0.02	0.03	0.03
K	1.93	1.87	1.96	1.96	1.71	1.93	1.97	1.97	1.95	1.99	1.96
Zr	0.85	0.90	0.87	0.94	0.95	0.90	0.90	0.91	0.91	0.91	0.91
Hf	-	-	-	-	-	-	-	-	-	-	-
Ba	bdl	0.01	0.01	0.01	0.01	0.02	0.01	0.02	0.01	0.01	0.01
P	0.00	0.01	0.00	bdl	bdl	-	-	-	-	-	-
La	-	-	-	-	-	-	-	-	-	-	-
Ce	-	-	-	-	-	-	-	-	-	-	-
Nb	-	-	-	-	-	-	-	-	-	-	-
Sum	**9.02**	**8.96**	**9.00**	**8.98**	**8.82**	**8.99**	**9.02**	**9.01**	**8.99**	**9.02**	**9.01**
K_{alk}	21.42	21.29	21.78	21.80	19.55	21.83	22.20	22.17	21.89	22.28	22.06

4.5.3 Whole-rock geochemistry

4.5.3.1 Major element geochemistry

The whole rock major element data of this study is presented in Appendix D. Whole rock major element compositions of the ignimbrite formations are classified as trachyte (Figure 4.29, Table 4.7, 4.8) and exhibit little variation, with SiO_2 contents clustering around 63 wt. %, Al_2O_3 contents of ~ 15 wt. %, total alkali contents of ~ 12 wt. %, and uniformly low MgO (< 0.5 wt. %) (cf. Gertisser *et al.*, 2010). The analyses are almost exclusively peralkaline, with calculated peralkalinity indices (mol. ($Na_2O + K_2O$ / Al_2O_3 > 1)) that range from 0.98 to 1.43. Syenite ejecta have similar bulk rock compositions to the ignimbrites, with calculated peralkalinity indices between 1.08 and 1.14 (Jeffery *et al.*, 2016a). Enclaves within syenitic ejecta exhibit slightly different bulk rock chemistry, with lower SiO_2 and total alkali contents of 61 to 62 wt. % and ~ 11 wt. %, respectively. Additionally, the enclaves lie on the boundary between metaluminous and peralkaline compositions, with peralkalinity indices of 0.97 to 1.01. On the basis of the Al_2O_3 versus FeO_t classification scheme of Macdonald (1974a), all of the peralkaline samples of this study are comenditic trachyte, with the exception of a basal pumice fall within the VFI, and a single anorthoclase-hosted melt inclusion from the CCI, which are classified as pantelleritic trachyte and pantellerite, respectively (Figure 4.29c).

In Figure 4.30, the major element compositions of this study, alongside available literature data, are plotted against MgO. For the purpose of clarity, and due to the association of the ignimbrite formations with the Pico Alto volcanic complex and Guilherme Moniz, compositions from Santa Bárbara and Cinco Picos are not shown. Despite the removal of these compositions, the overall trend still adheres to the description given in Section 4.3.1.2, with silica values that increase steadily from ~ 47 wt. to ~ 72 wt. % when MgO falls to ~ 4 wt. %. The total alkali content ranges from ~ 3 wt. % in the most mafic compositions, to ~ 15 wt. % in the most extreme, felsic compositions. The data for Al_2O_3, TiO_2, and FeO_t exhibit strongly curved profiles, with the former

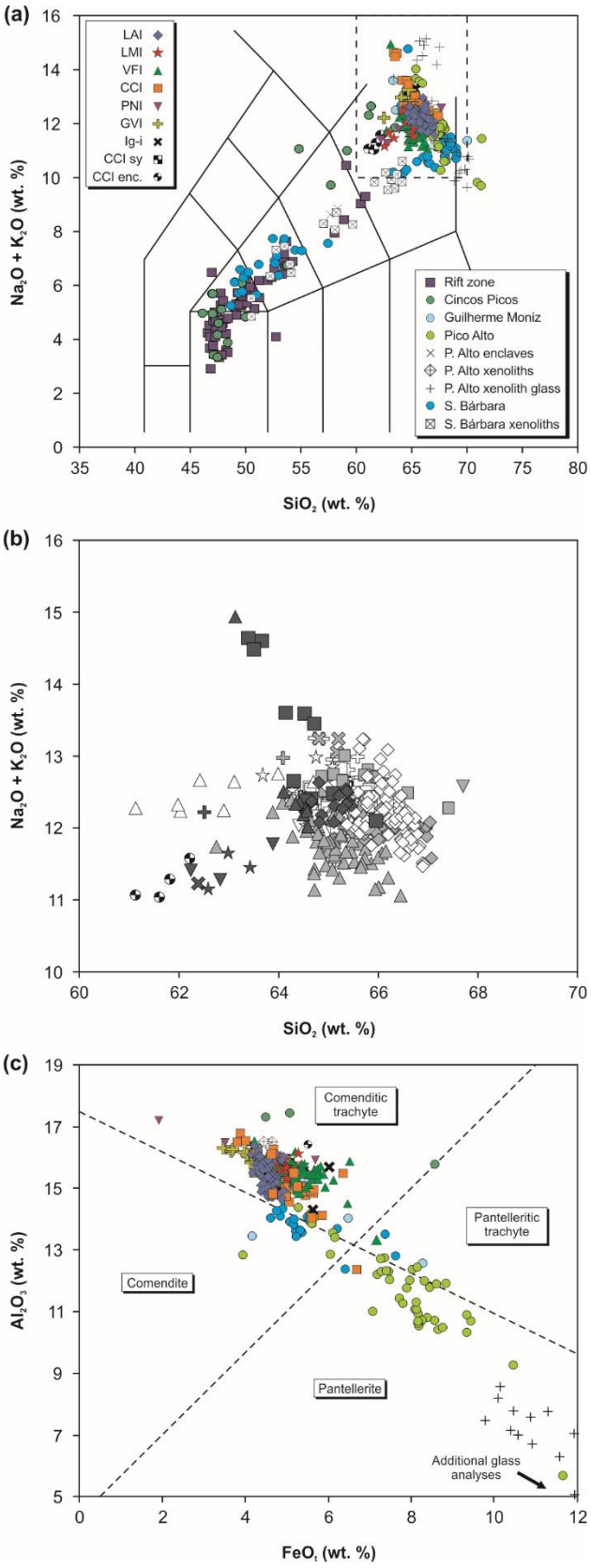

FIGURE 4.29: Major element compositions of the ignimbrites of Terceira compared with available literature data **a)** Total alkali-silica (TAS) classification of the ignimbrites and associated lithologies **b)** Enlarged portion of the TAS classification scheme showing only the ignimbrites, syenites, and enclaves. For the ignimbrites, whole rock analyses are shown in dark grey, melt inclusions in light grey, and groundmass glass in white **c)** FeO_t vs. Al_2O_3 classification scheme for peralkaline rocks of Macdonald (1974a). All data collected from Self (1974), Mungall (1993), and Madureira *et al.* (2011). Abbreviations used: sy = syenite, enc = enclave

Table 4.7: Major and trace element compositions of Terceira, analysed by XRF

Sample no.	**T034**	**T035**	**T036**	**T037**	**T013**	**T025**	**T026**	**T028**	**T029**	**T031**	**T005**	**T024**	**T002**	**T003**	**T010**	**T011**
Unit	LAI	LAI	LAI	LAI	VFI	VFI	VFI	VFI	VFI	VFI	CCI	CCI	CCI	CCI	CCI	CCI
Notes	Ign	Ign	Ign	Ign	Fall	Ign	Ign	Ign	Ign	Ign	Fall	Surge	Ign	Ign	Ign	Ign
SiO_2	64.46	62.78	64.81	62.30	60.78	61.99	63.23	62.21	61.93	61.95	61.39	62.06	61.76	62.61	63.29	62.11
TiO_2	0.61	0.59	0.59	0.67	0.46	0.57	0.57	0.57	0.56	0.61	0.46	0.45	0.58	0.62	0.61	0.47
Al_2O_3	15.29	15.91	15.36	16.02	13.32	14.84	15.51	15.28	14.94	15.28	14.79	14.82	15.04	15.49	16.10	14.04
Fe_2O_3	5.10	5.04	5.04	4.81	7.93	5.86	5.73	5.82	5.83	5.75	5.16	5.16	5.82	5.72	5.12	6.20
MnO	0.21	0.21	0.20	0.19	0.28	0.22	0.22	0.23	0.22	0.22	0.21	0.21	0.22	0.21	0.19	0.25
MgO	0.36	0.35	0.34	0.41	0.17	0.30	0.31	0.33	0.32	0.37	0.37	0.35	0.34	0.40	0.48	0.24
CaO	0.68	0.65	0.66	0.79	0.47	0.90	0.95	0.92	0.90	1.06	0.63	0.61	0.94	1.11	0.99	0.55
Na_2O	7.37	6.90	7.52	6.72	6.03	6.92	7.29	7.09	6.91	7.03	6.95	7.45	6.91	7.22	7.43	6.81
K_2O	5.02	4.80	5.05	4.77	4.04	4.78	4.82	4.76	4.75	4.72	4.92	4.91	4.73	4.74	4.94	4.70
P_2O_5	0.09	0.09	0.08	0.11	0.04	0.08	0.09	0.09	0.09	0.10	0.05	0.05	0.10	0.10	0.08	0.04
LOI	0.76	2.54	0.12	3.20	6.39	3.16	0.76	2.34	3.17	2.86	5.00	4.04	3.21	1.29	0.29	4.46
Total	99.95	99.86	99.77	99.99	99.91	99.62	99.48	99.64	99.62	99.95	99.93	100.11	99.65	99.51	99.52	99.87
P.I.	1.15	1.04	1.16	1.01	1.07	1.12	1.11	1.10	1.11	1.09	1.13	1.19	1.10	1.10	1.09	1.16
Sc	bdl	bdl	bdl	bdl	bdl	bdl	bdl	bdl	bdl	bdl	bdl	bdl	bdl	bdl	bdl	bdl
V	bdl	bdl	bdl	bdl	bdl	bdl	bdl	bdl	bdl	bdl	bdl	bdl	bdl	bdl	bdl	bdl
Cr	bdl	bdl	bdl	bdl	bdl	bdl	bdl	bdl	bdl	bdl	bdl	bdl	bdl	bdl	bdl	bdl
Ni	bdl	bdl	bdl	bdl	bdl	bdl	bdl	bdl	bdl	bdl	bdl	bdl	bdl	bdl	bdl	bdl
Cu	bdl	bdl	bdl	bdl	bdl	bdl	bdl	bdl	bdl	bdl	bdl	bdl	bdl	bdl	bdl	bdl
Zn	156	205	154	133	315	163	155	157	160	151	179	184	158	149	144	241
As	10	11	bdl	bdl	26	11	bdl	bdl	bdl	bdl	11	12	bdl	bdl	bdl	17
Rb	102	93	102	73	192	100	93	94	99	89	133	135	94	89	94	174
Sr	bdl	12	bdl	16	bdl	20	26	23	22	36	bdl	bdl	24	36	18	bdl
Y	58	55	57	45	131	62	57	58	61	56	78	78	59	55	56	108
Zr	686	664	693	491	2258	772	706	701	762	678	1043	1073	714	666	674	1550
Nb	118	113	118	88	354	129	119	118	127	115	176	180	121	113	121	255
Mo	bdl	bdl	bdl	bdl	17	bdl	bdl	bdl	bdl	bdl	11	11	bdl	bdl	bdl	14
Ba	243	309	239	524	bdl	502	746	605	531	714	bdl	bdl	596	799	315	bdl
La	87	90	83	71	239	106	90	100	97	96	137	140	98	86	90	194
Ce	139	139	133	121	340	166	158	158	166	161	191	193	163	155	142	261
Pb	bdl	bdl	bdl	bdl	26	bdl	bdl	bdl	bdl	bdl	bdl	bdl	bdl	bdl	bdl	bdl
Th	13	12	14	10	40	15	13	13	14	13	18	19	13	13	13	26
U	bdl	bdl	bdl	bdl	11	bdl	bdl	bdl	bdl	bdl	bdl	bdl	bdl	bdl	bdl	bdl

Table 4.8: Major element compositions of Terceiran lithologies analysed via ICP-MS

Sample no.	**T001**	**TO73SY**	**T073EA**	**T073EB**	**T073A1**	**T073A3**
Unit	Ign-i	Syenite	Sy-enc	Sy-enc	Sy-enc	Sy-enc
Notes	Ign	Ejecta	Enclave	Enclave	Enclave	Enclave
SiO_2	61.31	64.23	60.13	61.4	60.91	60.56
TiO_2	0.99	0.48	1.03	0.85	0.89	0.97
Al_2O_3	15.40	15.92	16.00	16.19	16.05	16.18
Fe_2O_3	6.56	4.68	6.5	6.03	6.18	6.18
MnO	0.21	0.19	0.22	0.22	0.22	0.2
MgO	1.26	0.24	1.54	1.07	1.43	1.53
CaO	1.98	0.58	2.51	1.94	2.2	2.29
Na_2O	7.01	7.32	6.77	7.18	6.99	6.94
K_2O	4.03	5.03	4.12	4.25	4.13	3.91
P_2O_5	0.18	0.05	0.19	0.15	0.15	0.16
LOI	0.70	1	0.6	0.4	0.5	0.7
Total	98.97	99.25	98.96	99.08	99.03	99.00
P.I.	1.03	1.10	0.97	1.01	0.99	0.97

displaying a steep downturn from ~ 18 to ~ 5 wt. % at MgO contents of ~ 1 wt. %. The latter two have similar, though less steep downturns, which both occur at MgO values of ~ 4 wt. %. In particular, FeO_t also displays a late stage enrichment trend at MgO values below 0.5 wt. %, where FeO_t values increase from ~ 4 wt. % to values as high as ~ 8 wt. % within the rocks of Pico Alto, and up to 16 wt. % in the interstitial glass analyses of Mungall, (1993). Peralkalinity indices increase slowly until ~1 wt. % MgO, when they increase rapidly to values of up to 5.

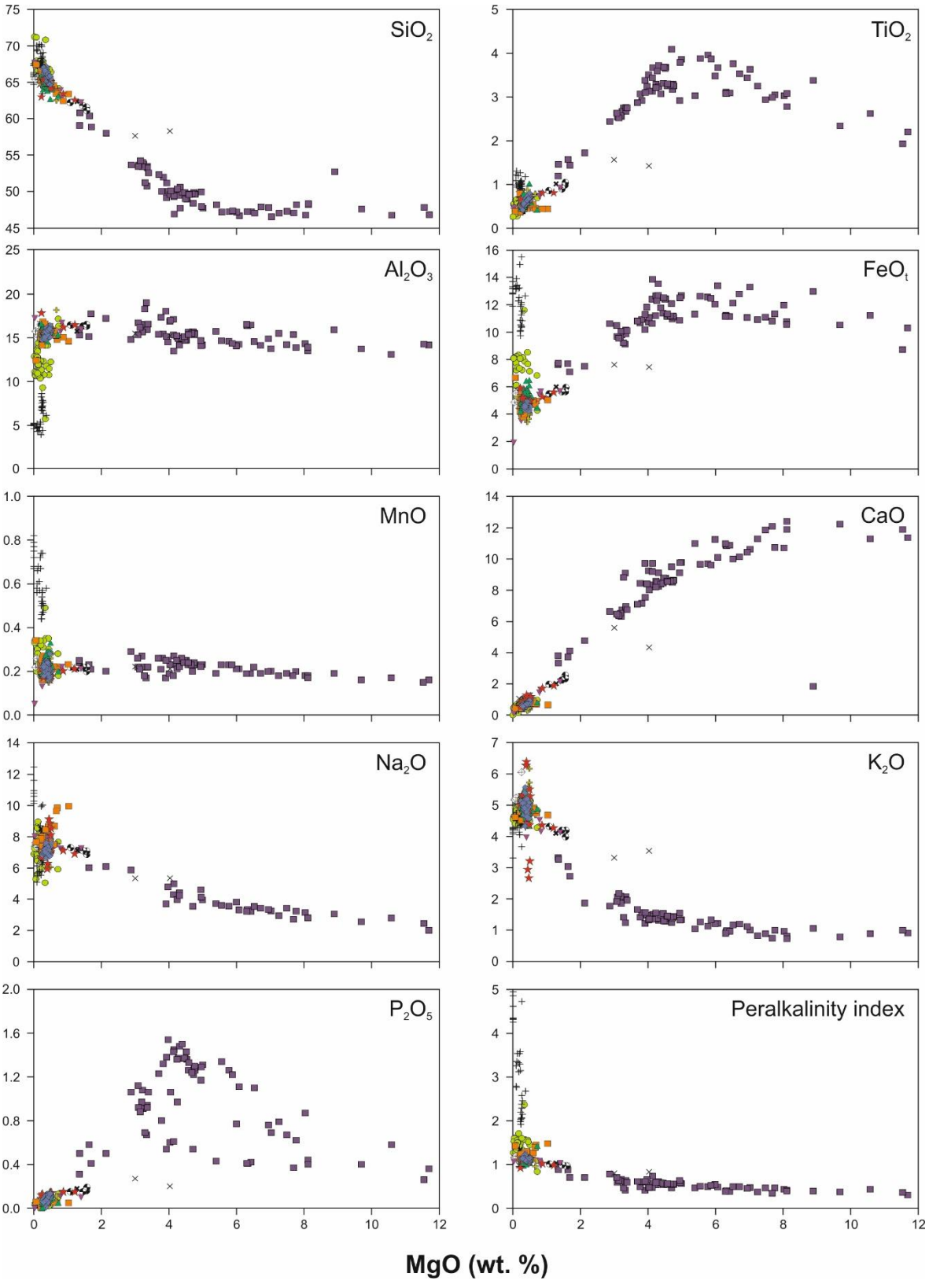

FIGURE 4.30: Major element compositions of the Terceira ignimbrites, syenites, enclaves, and the Terceira suite, plotted against MgO. Symbols are as given in Figure 4.29. All data collected from Self (1974), Mungall (1993), and Madureira *et al.* (2011)**.** All analyses measured in wt. %

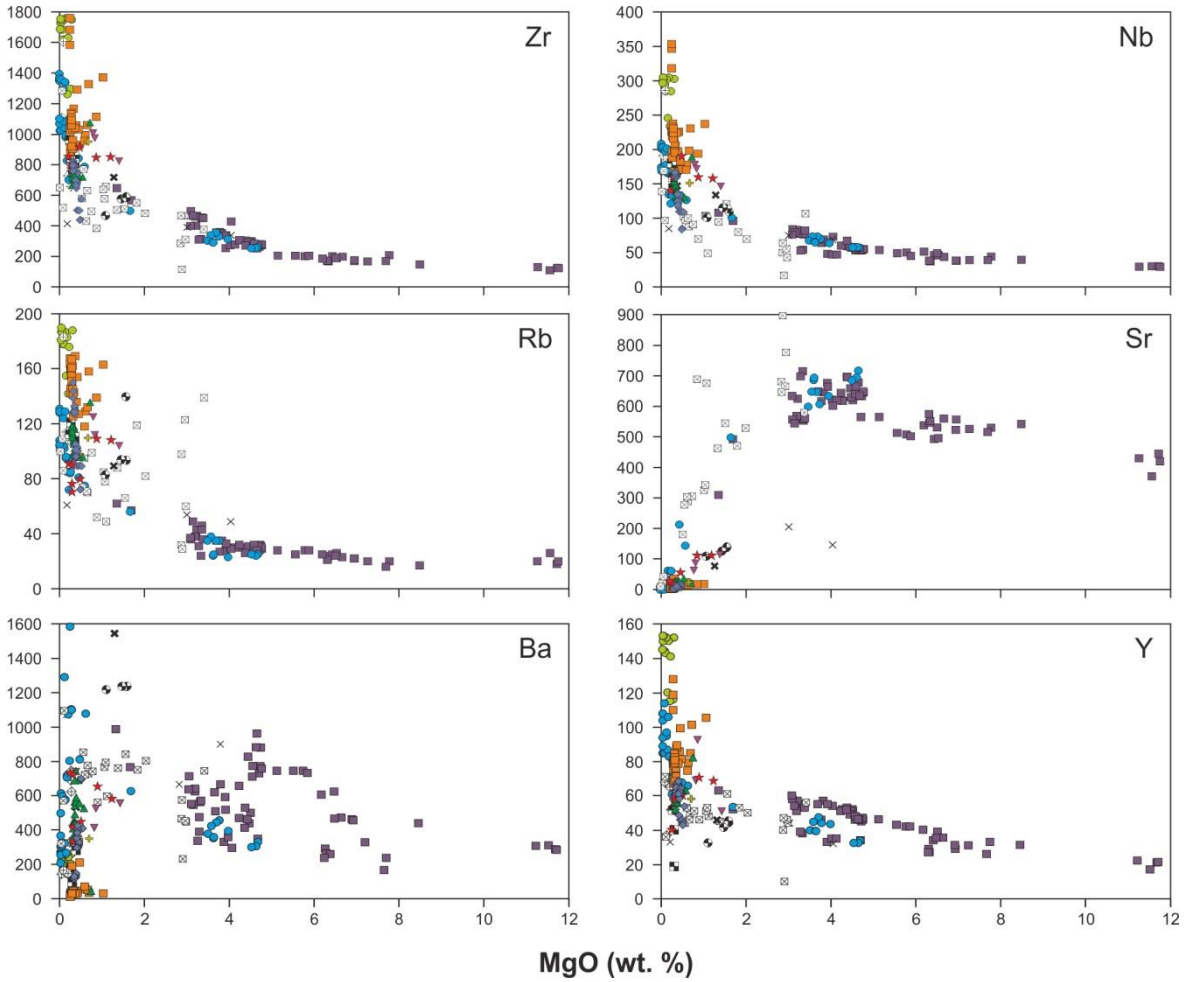

FIGURE 4.31: Trace element compositions of the Terceira ignimbrites, syenites, enclaves, and the Terceira suite, plotted against MgO. Symbols are given in Figure 4.29. All data collected from Mungall (1993) and Madureira *et al.* (2011). Trace element concentrations given in ppm

4.5.3.2 Trace element geochemistry

Trace element data for the seven ignimbrite formations, syenite ejecta, and syenite-hosted enclaves is given in Appendix D. Selected trace elements are plotted against MgO in Figure 4.31. Overall, trace elements such as Zr, Nb, Rb, and Y show an incompatible trend in the mafic and intermediate compositions (> 1 wt. % MgO), which steepens at trachytic compositions (< 1 wt. % MgO). In contrast, Sr concentrations increase from ~ 500 to ~ 700 ppm in the mafic and intermediate portion of the trend, whilst the felsic portion of the trend is generally restricted to values below ~ 150 ppm. Unlike Sr, Ba shows

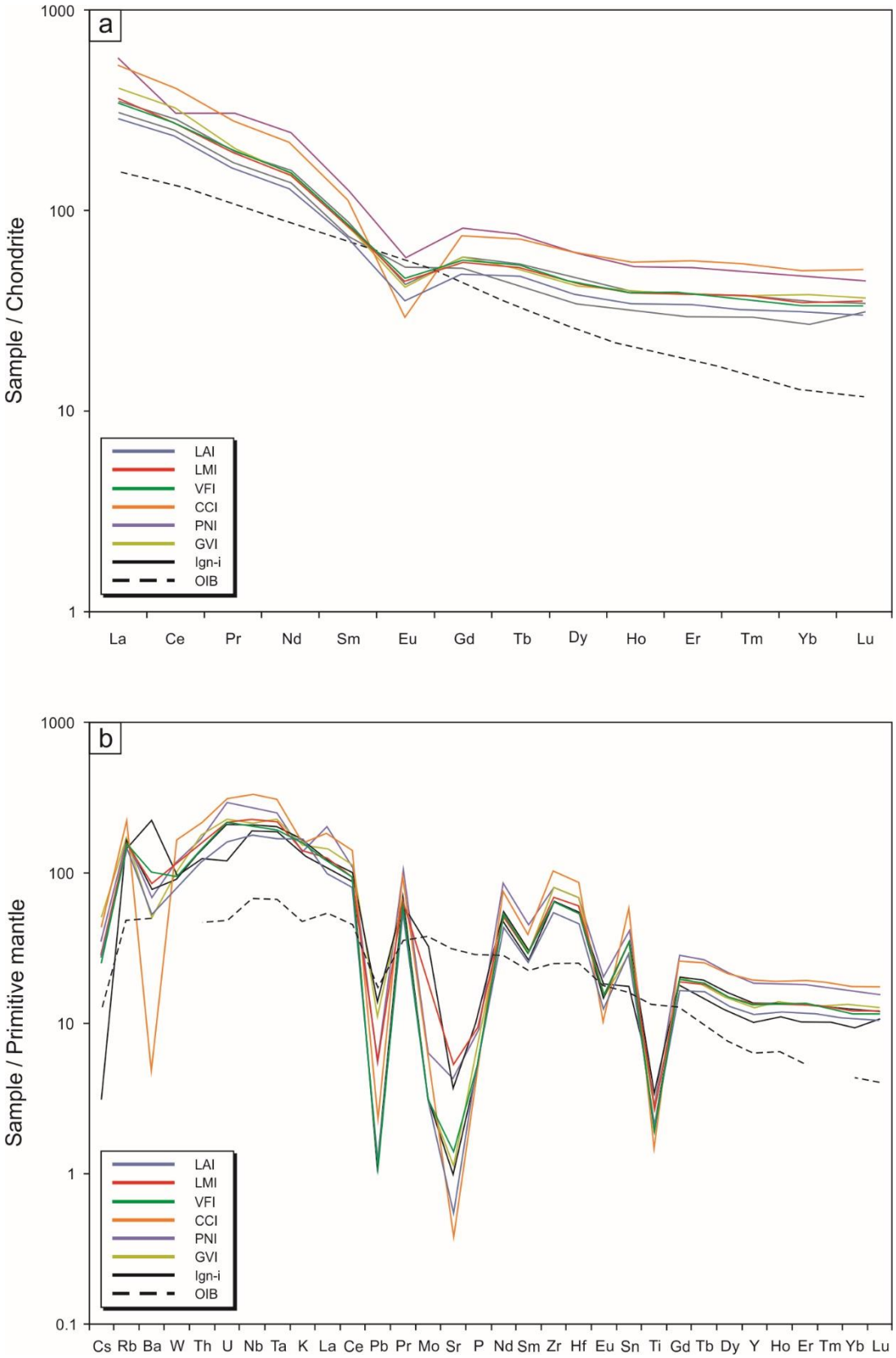

FIGURE 4.32: Trace element variation diagrams for the ignimbrites of Terceira **a)** chondrite-normalised REE diagram displaying each of the ignimbrite formations relative to a standard OIB composition (Sun and McDonough, 1989) **b)** primitive mantle-normalised multi element diagram showing each of the ignimbrites alongside a standard OIB composition (Sun and McDonough, 1989)

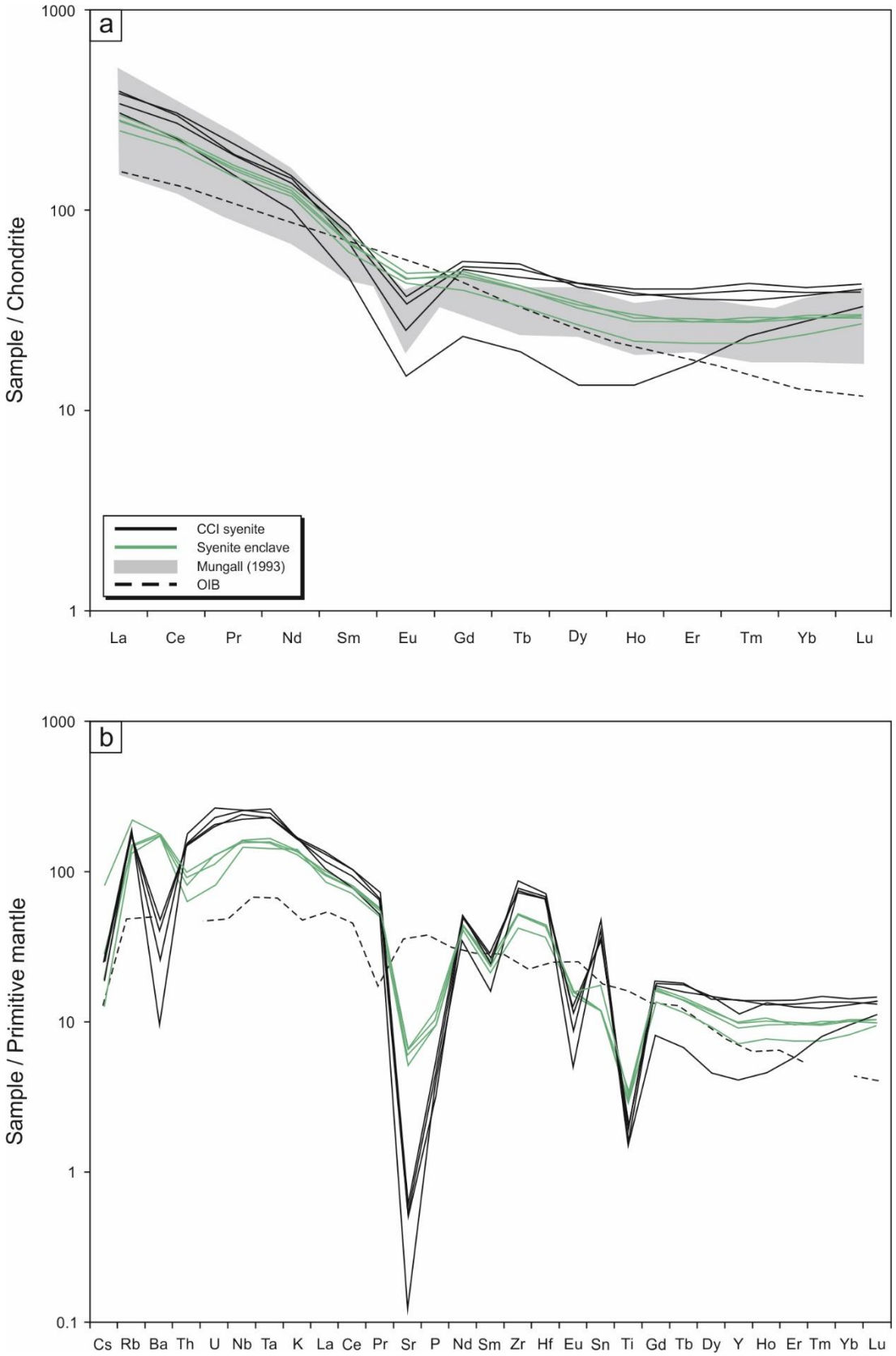

FIGURE 4.33: Trace element variation diagrams for the syenites and enclaves of Terceira **a)** chondrite-normalised REE diagram displaying syenite and enclave data relative to a standard OIB composition (Sun and McDonough, 1989). Grey field indicates data of Mungall (1993) **b)** primitive mantle-normalised multi element diagram showing syenite and enclave data alongside a standard OIB composition (Sun and McDonough, 1989)

Table 4.9: Trace element compositions of various Terceiran lithologies, analysed by ICP-MS

Sample no.	**TER10-3**	**TER5-2**	**TER11-2B**	**TER35-2**	**TER56-1**	**TER10-2**	**T001**	**TER13-1**	**TER30-1**	**TER35-1**	**TER30-6**	**TO73SY**	**T073EA**	**T073EB**	**T073A1**	**T073A3**
Unit	LAI	LMI	VFI	CCI	PNI	Ign-i	Ign-i	GVI	Syenite	Syenite	Syenite	Syenite	Sy-enc	Sy-enc	Sy-enc	Sy-enc
Notes	Ign	Ign	Ign	Ign	Ign	Ign	Ign	Ign	Ejecta	Ejecta	Ejecta	Ejecta	Enclave	Enclave	Enclave	Enclave
Ba	371	586	701	33	472	534	1545.00	348.00	345	67	282	181	1236	1216	1235	1234
Be	5	5	5	7	6	5	6.00	4.00	4	6	4	4	3	3	3	2
Co	0.3	3	0.8	0.8	3	0.5	5.60	0.90	1.1	1	1.5	0.8	5.7	3.1	4.9	6.3
Cs	0.8	0.9	0.8	1.4	1.1	0.9	0.10	1.60	0.6	0.8	0.8	0.8	0.9	0.4	0.6	2.6
Ga	31.4	29.3	30.3	33.4	30.2	29.6	32.20	30.40	33	36.1	32.5	34.1	28.4	27.4	27	28.3
Hf	14.3	18.5	16.9	26.9	20.7	16.8	16.80	20.50	21	20.4	21.2	22	13.8	11.3	13.1	13.7
Nb	127.7	160.6	147.2	237	185.8	146.9	133.60	151.40	169.6	159.5	183.5	180	111.3	101	115.1	113.8
Rb	94.9	100.9	97.3	145	105.3	98.5	89.50	109.60	110.6	120.9	107.2	112.2	93.4	82.9	93.8	139.6
Sn	5	6	6	10	7	6	3.00	5.00	6	7	6	8	2	2	2	3
Sr	11.3	111.3	29.6	7.8	89.1	20.6	77.10	23.60	12.9	2.6	11.5	10.6	139.9	109.1	125.6	136.9
Ta	6.9	8.9	7.9	12.7	10.1	8.1	7.70	9.10	9.4	9.4	10.8	9.9	6.5	5.8	6.7	6.4
Th	10	13.4	12.3	18.2	14.5	12.1	10.40	15.20	12.6	12.9	13.2	15	7	5.4	7.7	8.5
U	3.4	4.5	4.5	6.5	6.1	4.3	2.50	4.70	4.1	4.3	4.8	5.5	2.7	1.7	2.3	2.7
V	<8	14	<8	<8	11	<8	58.00	<8	<8	<8	<8	<8	48	21	31	43
W	1.6	2.3	1.9	3.3	2.3	1.8	1.90	2.00	<0.5	0.8	<0.5	0.6	2.5	1	1	1.3
Zr	610.1	773.2	719.1	1149.6	882.7	721.8	716.90	904.30	812.6	832.3	863.2	961.8	583.9	467.3	576.5	590.7
Y	52.6	61.9	60.5	87.6	84.2	61.2	45.90	58.10	63.4	18.7	62.8	51.4	44.3	32.5	41.5	45.3
La	67.8	86.1	81.9	124.7	137.6	83.4	73.80	97.10	89.7	72.2	80.2	91.8	70.5	59.1	66.7	65.7
Ce	143.7	167.6	168.6	250.7	186.5	175	153.70	199.00	185.6	139.2	167.7	180.8	141.2	125.9	136.6	137.3
Pr	15.49	18.71	18.76	26.77	29.38	18.97	16.71	19.87	20.14	14.22	17.86	18.04	15.86	13.89	15.46	15.03
Nd	59.8	70.7	72.5	102.1	114.1	74.7	64.50	71.90	68.6	46.9	64.7	67.7	60.6	54.9	58.9	57.2
Sm	11.19	12.96	13.06	17.33	19.54	13.53	11.46	12.81	12.8	7.12	11.81	10.74	11.45	9.46	10.73	10.48
Eu	2.06	2.58	2.66	1.69	3.36	2.49	3.03	2.44	2.09	0.85	1.94	1.44	2.8	2.52	2.62	2.65
Gd	9.87	11.4	11.63	15.42	16.85	12.1	10.61	12.19	11.17	4.78	10.73	10.31	10.14	8.16	9.88	9.57
Tb	1.76	1.96	1.98	2.69	2.83	2.04	1.59	1.90	1.98	0.73	1.89	1.71	1.57	1.24	1.51	1.5
Dy	9.71	10.95	11.07	15.7	15.67	11.6	8.76	10.73	10.37	3.39	10.91	10.85	8.84	6.78	8.25	8.56
Ho	1.95	2.21	2.23	3.13	2.99	2.23	1.80	2.25	2.11	0.75	2.27	2.17	1.63	1.25	1.57	1.7
Er	5.6	6.36	6.46	9.32	8.61	6.36	4.88	6.40	6.24	2.79	6.7	5.93	4.74	3.57	4.59	4.57
Tm	0.82	0.96	0.92	1.38	1.26	0.96	0.75	0.95	1	0.59	1.09	0.9	0.71	0.55	0.7	0.74
Yb	5.31	5.97	5.72	8.59	7.95	6.01	4.60	6.47	6.56	4.72	6.95	6.35	5.06	4.06	4.89	4.92
Lu	0.77	0.9	0.85	1.3	1.14	0.88	0.79	0.94	0.98	0.83	1.07	1.01	0.76	0.69	0.75	0.73
Mo	0.2	1.3	0.2	0.4	0.4	0.2	2.00	0.20	0.3	0.2	0.3					
Cu	0.5	3.3	0.9	2	2.8	0.7	4.70	4.70	1.3	0.5	0.8					
Pb	0.2	1.0	0.2	0.4	1.0	0.2	2.5	2.0	2.9	0.9	1.6					
Zn	12	49	12	13	42	12	61	34	21	7	18					
Ni	bdl	3.0	0.2	0.2	2.6	0.1	5.5	0.2	bdl	bdl	bdl	bdl	bdl	bdl	bdl	bdl
As	bdl	bdl	bdl	bdl	bdl	bdl	0.7	bdl	bdl	bdl	bdl					
Cd	bdl	0.1	bdl	bdl	bdl	bdl	bdl	0.2	0.1	bdl	bdl					
Sb	bdl	bdl	bdl	bdl	bdl	bdl	bdl	bdl	bdl	bdl	bdl					
Bi	bdl	bdl	bdl	bdl	bdl	bdl	bdl	bdl	bdl	bdl	bdl					
Ag	bdl	bdl	bdl	bdl	bdl	bdl	bdl	bdl	bdl	bdl	bdl					
Au	0.7	bdl	bdl	1.3	0.5	0.6	1.6	0.6	bdl	bdl	bdl					
Hg	bdl	bdl	bdl	bdl	bdl	bdl	bdl	bdl	bdl	bdl	bdl					
Tl	bdl	bdl	bdl	bdl	bdl	bdl	bdl	bdl	bdl	bdl	bdl					
Se	bdl	bdl	bdl	bdl	bdl	bdl	bdl	bdl	bdl	bdl	bdl					

no clear trend. Instead, considerable scatter is observed throughout the suite, with mafic and intermediate compositions ranging from ~ 200 to 1000 ppm, and felsic compositions ranging from < 20 to ~ 1550 ppm.

Chondrite-normalised (Sun and McDonough, 1989) REE patterns are shown in Figure 4.32 and 4.33 and indicate a relatively uniform enrichment of the LREEs relative to the HREEs, with a total range of La_N/Yb_N ratios between 8.3 and 12.4. All of the samples exhibit variable negative Eu anomalies, with Eu/Eu* (where Eu* = (Sm + Gd) / 2) values of 0.31 to 0.83 in the ignimbrites, 0.41 to 0.52 in the syenites, and 0.76 to 0.86 in the enclaves. A single syenite sample deviates notably from the other samples, with a significant depletion of MREEs.

Primitive mantle-normalised (Sun and McDonough, 1989) multi-element diagrams are given in Figure 4.32 and 4.33. The ignimbrites are characterised by pronounced depletions in Ba, Sr, Eu, P, and Ti. A notable exception to this observation is the Ignimbrite-i Formation, which exhibits a slight enrichment in Ba relative to other ignimbrites. Syenitic ejecta and enclaves display a similar geochemical profile to the ignimbrites, with the same troughs for Ba, Sr, Eu, P, and Ti. However, in the syenites, these troughs are deeper than in the ignimbrites, and in the enclaves, they are shallower. As observed for the Ignimbrite-i Formation, the enclaves do not exhibit the same trough for Ba, and instead indicate a slight enrichment.

4.5.4 Melt inclusions

Melt inclusion analyses indicate similar compositions to groundmass glass and whole rock analyses. All of the analyses are classified as trachyte, with SiO_2 between ~ 60 and ~ 67 wt. %, Al_2O_3 between 12 and 17 wt. %, total alkali contents of ~ 12 wt. %, and MgO contents below 0.5 wt. % (Table 4.10). The majority of samples are peralkaline (P. I. = 0.99 to 1.43). FTIR analyses of selected melt inclusions indicate water contents that range from 2.5 to 4.2 wt. %, with an average of 3.5 wt. % (Table 4.11). In contrast, CO_2 was not

Table 4.10: Representative melt inclusion data for the ignimbrites of Terceira

Sample	Unit	Identifier	SiO_2	TiO_2	Al_2O_3	FeO_t	MnO	MgO	CaO	Na_2O	K_2O	P_2O_5	Total	Peralkalinity	Cl	F	S
T038IIb	LAI	MI01	63.93	0.66	14.68	4.59	0.20	0.37	0.62	6.56	4.97	0.09	96.67	1.10	2795	2022	151
T0382	LAI	MI01	63.23	0.69	15.51	4.10	0.20	0.44	0.77	6.63	4.94	0.13	96.64	1.05	1511	857	171
T0383	LAI	MI19	64.76	0.54	14.95	4.39	0.24	0.41	0.67	7.18	4.52	0.05	97.71	1.12	2096	1469	155
T0383	LAI	MI20	64.24	0.56	15.12	4.29	0.22	0.35	0.61	7.38	4.20	0.06	97.04	1.10	2279	1986	193
T0383	LAI	MI21	65.43	0.40	14.59	4.29	0.22	0.29	0.54	6.85	4.94	0.05	97.59	1.14	2556	1505	135
VFI_3	VFI	02_B	61.56	0.50	14.92	5.11	0.24	0.35	0.80	5.95	5.01	0.08	94.52	1.02	3124	2388	273
VFI_3	VFI	02_C	62.37	0.67	13.87	6.17	0.28	0.38	0.99	6.35	4.47	0.08	95.63	1.10	4881	2252	220
VFI_4	VFI	09_A	62.21	0.48	15.09	4.84	0.22	0.32	0.83	6.22	4.89	0.08	95.19	1.03	2436	1461	173
VFI_2	VFI	01_C	61.36	0.52	14.84	4.85	0.18	0.31	0.73	6.43	4.77	0.05	94.04	1.06	2791	1352	208
VFI_2	VFI	01_D	63.70	0.54	14.43	5.23	0.23	0.36	0.75	6.35	4.53	0.11	96.22	1.06	3653	1752	291
CCI I	CCI	MI5b	61.53	0.42	14.89	4.50	0.20	0.27	0.63	7.26	4.79	0.03	94.52	1.15	3515	2042	207
CCI I	CCI	MI6	63.55	0.41	14.98	4.46	0.24	0.24	0.45	7.44	4.88	0.05	96.70	1.17	4207	2203	141
TM-1(2)	CCI	MI04	64.22	0.61	15.51	4.58	0.20	0.29	0.77	7.33	4.80	0.04	98.34	1.11	3893	1774	710
TM-2(2)	CCI	MI05	64.92	0.80	14.95	5.64	0.21	0.24	0.71	8.01	4.51	0.01	100.00	1.21	6850	2613	1046
TM-2(2)	CCI	MI06	64.99	0.78	14.91	5.22	0.21	0.21	0.59	7.84	4.76	0.04	99.55	1.21	5817	3142	1258
TM-1(5)	PNI	MI01	66.99	0.46	16.99	1.90	0.05	0.03	0.09	7.94	4.51	0.00	98.95	1.06	3619	2965	50
T012I	PNI	MI04	65.47	0.37	16.30	3.48	0.13	0.24	0.54	7.34	5.15	0.06	99.09	1.08	913	1222	216
TM-1(6)	Ign-i	MI03	61.69	0.89	13.59	5.35	0.18	0.20	0.64	8.07	4.53	0.05	95.19	1.34	6398	4751	129
TM-2(6)	Ign-i	MI01	66.12	0.75	15.65	4.50	0.17	0.25	0.74	8.47	4.77	0.04	101.46	1.22	6959	2611	155
TM-2(6)	Ign-i	MI03	65.93	0.76	15.14	4.83	0.19	0.21	0.65	8.61	4.78	0.03	101.12	1.28	6567	3658	174
AM-2(5)	GVI	MI01	65.04	0.89	16.08	4.76	0.16	0.45	0.87	8.35	4.81	0.08	101.48	1.18	3673	2150	257

Table 4.11: Melt inclusion FTIR data for the ignimbrites of Terceira

Sample	Unit	Analysis no.	Peak height (cm^{-1})	Density (kg/m^3)	Thickness (cm)	Molar absorptivity (cm^{-1})	H_2O (wt. %)
TER11-2	VFI	1	0.764	2510	0.00300	73	2.50
TER11-2	VFI	2	0.775	2510	0.00300	73	2.54
TER10-2-2	Ign-i	1	1.495	2510	0.00510	73	2.88
TER10-2-2	Ign-i	1	1.461	2510	0.00510	73	2.82
TER10-2-2	Ign-i	1	1.499	2510	0.00510	73	2.89
TER10-2-1	CCI	1	2.245	2510	0.00530	73	4.16
TER10-2-1	CCI	2	2.190	2510	0.00530	73	4.06
TER10-2-1	CCI	3	2.174	2510	0.00530	73	4.03
TER10-2-1	CCI	1	2.162	2510	0.00530	73	4.01
TER10-2-1	CCI	2	2.093	2510	0.00530	73	3.88
TER10-2-1	CCI	1	1.915	2510	0.00530	73	3.55
TER10-2-1	CCI	2	1.922	2510	0.00530	73	3.57
CCI MI06	CCI	1	1.914	2510	0.00453	73	4.16
CCI MI07	CCI	1	1.599	2510	0.00453	73	3.47
CCI MI05	CCI	1	1.703	2510	0.00456	73	3.67
CCI MI05	CCI	2	1.63	2510	0.00456	73	3.51
CCI MI05	CCI	3	1.793	2510	0.00456	73	3.87

detected in any of the inclusions, and was therefore considered to be below the detection limit of FTIR spectroscopy (~ 100 ppm). Melt inclusions from the LAI and VFI indicate relatively uniform pre-eruptive concentrations of Cl and F (average = 2,400 ppm and 1,500 ppm, respectively). Melt inclusions from the CCI record higher average volatile contents of ~ 3,700 ppm Cl and ~ 1,800 ppm F. Available melt inclusion analyses for the older ignimbrites suggest that the GVI and PNI are comparable to the CCI, whilst the Ignimbrite-i Formation exhibits the greatest degree of halogen enrichment, with ~ 6,640 ppm Cl and 3,670 ppm F. Sulphur concentrations do not exceed 600 ppm, and are frequently below the detection limit (~ 300 ppm).

4.5.5 Groundmass glass

Due to the generally low crystal contents of the pumices in the ignimbrite formations, major element compositions of groundmass glass are similar to whole rock compositions, and are classified as trachyte. Silica contents show a range of ~ 61 to ~ 68 wt. %, with Al_2O_3 contents of ~ 15 wt. %, total alkali contents of ~ 12 wt. % and MgO contents that rarely exceed 0.5 wt. %. All of the analyses are peralkaline, with peralkalinity indices between 1.05 and 1.26, and are classified as comenditic trachyte. Groundmass glass analyses record similarly low S contents to the melt inclusions (< 350 ppm). Average Cl and F concentrations are typically very similar to those of the melt inclusions (2,220 and 1,600 ppm, respectively).

4.5.6 Solid state modelling

Calculated solution energies (E_{sol}) for a number of potential substitutions within dalyite are presented in Table 4.12. In each instance, the lowest E_{sol} value is considered to highlight the most likely substitution. Model results for Ti indicate Ti↔Si substitution as the most energetically favourable (E_{sol} = - 0.98 eV), though Ti↔Zr substitution is also likely (E_{sol} = - 0.25 eV). Modelling of Hf is more conclusive, with Hf↔Zr substitution representing the most likely scenario (E_{sol} = - 0.31 eV). The incorporation of the R^{2+} cations Fe^{2+}, Mg^{2+} and Ba^{2+} was also modelled, but charge balancing necessitates the presence of site vacancies, in this case assumed to be a single O vacancy. Results indicate that, in the case of Fe^{2+} and Mg^{2+} the lowest energy scenario is replacement of K. Nevertheless, the calculated E_{sol} values of 8.86 eV and 9.61 eV, respectively, highlight the overall difficulty of their inclusion within the dalyite structure. Modelling of Ba yields a similar result, though the calculated E_{sol} value of 4.94 eV for Ba↔K substitution is noticeably lower than other R^{2+} cations.

Table 4.12: Results of molecular modelling for various solution schemes for dalyite substitution

Substitution	Solution scheme	E_{sol} (eV)
Ti → Zr	$TiO_2 + Zr_{Zr} \rightarrow Ti_{Zr} + ZrO_2$	-0.25
Ti → Si	$TiO_2 + Si_{Si} \rightarrow Ti_{Si} + SiO_2$	-0.98
Ti → K	$TiO_2 + 4K_K \rightarrow Ti_K^{\bullet\bullet\bullet} + 3V_K' + 2K_2O$	30.64
Hf → Zr	$HfO_2 + Zr_{Zr} \rightarrow Hf_{Zr} + ZrO_2$	-0.31
Hf → Si	$HfO_2 + Si_{Si} \rightarrow Hf_{Si} + SiO_2$	2.67
Hf → K	$HfO_2 + 4K_K \rightarrow Hf_K^{\bullet\bullet\bullet} + 3V_K' + 2K_2O$	29.09
Fe^{2+} → Zr	$FeO + Zr_{Zr} \rightarrow Fe_{Zr}'' + V_O^{\bullet\bullet} + ZrO_2$	12.52
Fe^{2+} → Si	$FeO + Si_{Si} \rightarrow Fe_{Si}'' + V_O^{\bullet\bullet} + SiO_2$	13.69
Fe^{2+} → K	$FeO + K_K \rightarrow Fe_K^{\bullet} + V_K' + K_2O$	8.86
Mg^{2+} → Zr	$MgO + Zr_{Zr} \rightarrow Mg_{Zr}'' + V_O^{\bullet\bullet} + ZrO_2$	12.97
Mg^{2+} → Si	$MgO + Si_{Si} \rightarrow Mg_{Si}''+ V_O^{\bullet\bullet} + SiO_2$	14.07
Mg^{2+} → K	$MgO + K_K \rightarrow Mg_K^{\bullet} + V_K' + K_2O$	9.61
Ba^{2+} → Zr	$BaO + Zr_{Zr} \rightarrow Ba_{Zr}'' + V_O^{\bullet\bullet} + ZrO_2$	12.54
Ba^{2+} → Si	$BaO + Si_{Si} \rightarrow Ba_{Si}''+ V_O^{\bullet\bullet} + SiO_2$	16.58
Ba^{2+} → K	$BaO + K_K \rightarrow Ba_K^{\bullet} + V_K' + K_2O$	4.94

4.6 Discussion

In this section, the combined dataset presented above is used to provide insights into the pre-eruptive magmatic systems which fed the ignimbrite-forming eruptions of Terceira. First, the pre-eruptive P-T-fO_2 conditions of the ignimbrite-forming magmas are explored, followed by a detailed examination of the roles of various petrogenetic processes in their origins. Second, the latest stages in the evolution of the trachytes are discussed based upon the textural variation of the syenite ejecta. Additionally, the compositional variability of dalyite is discussed, both within the local context of Pico Alto, and within the global context of dalyite occurrences. Third, a conceptual model is presented, considering the variability of magma rheology and chemical zonation, aiming to account for the petrological features observed in each the ignimbrites. Finally, the ignimbrites are considered within the context of the magmatic suite of Terceira, and compared with the effusive eruptions of the Pico Alto Volcanic Complex.

4.6.1 Pre-eruptive P-T-fO_2 conditions

4.6.1.1 Temperature estimates

Estimates of pre-eruptive temperatures of the ignimbrite-forming trachytes were determined via two-oxide (Andersen *et al.*, 1993) and alkali feldspar-melt equilibria (Putirka, 2008; Mollo *et al.*, 2015). Due to the relative scarcity of ilmenite, estimates derived from two-oxide models were calculated for the LAI and the CCI syenite ejecta. Conversely, the abundance of alkali feldspar facilitated the calculation of temperature estimates for all of the ignimbrite formations and the syenite ejecta.

Two-oxide temperature estimates for the LAI range from 773 to 873 ºC (average = 830 ºC, *n* = 590), whilst estimates for the syenite ejecta lie between 616 and 769 ºC (average = 687 ºC, *n* = 20) (Figure 4.34a). These values should be considered representative of the final pre-eruptive magmatic temperatures and/or syn-eruptive

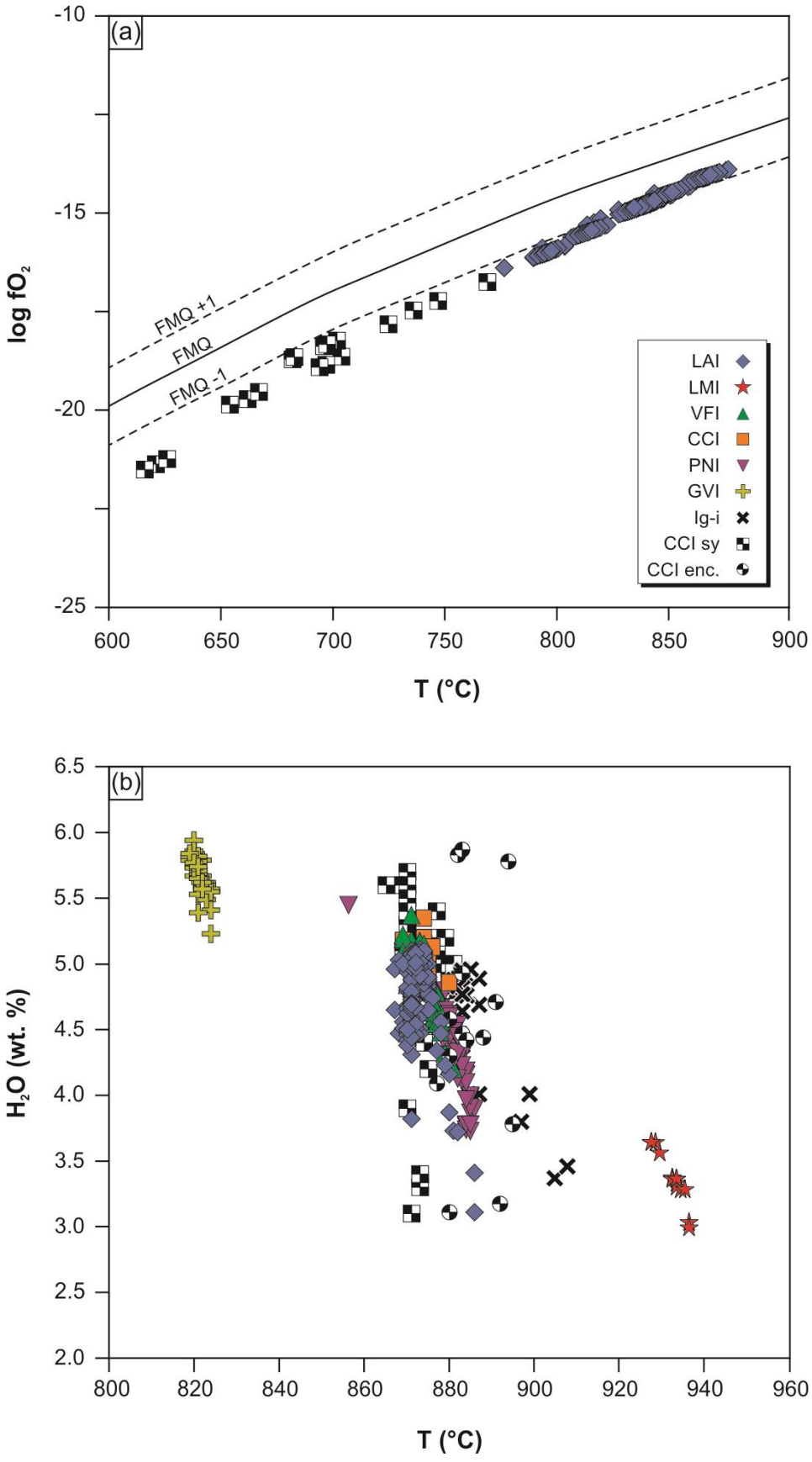

FIGURE 4.34: Summarised results of thermobarometry applied to the lithologies of Terceira **a)** T-fO_2 estimates derived from two-oxide models **b)** T-H_2O_{melt} estimates derived from alkali feldspar-melt thermometry and hygrometry

conditions along the plumbing system, due to the rapid re-equilibration timescales of coexisting Fe-Ti oxides (e.g. Gardner *et al.* 1995; Venezky and Rutherford 1999; Pimentel *et al.*, 2015). The alkali feldspar-melt temperatures for the LAI, VFI, CCI, PNI, and Ign-i lie between 857 to 907 ºC (average = 879 ºC, *n* = 324) (Figure 4.34b). Notably, the results of the LMI and the GVI deviate from this, with contrasting temperature ranges of 927 to 936 ºC (average = 932, *n* = 14) and 819 to 824 (average = 821, *n* = 42), respectively. Temperature estimates for the CCI syenites are hotter than those predicted via two-oxide models, with a range of 864 to 880 ºC (average = 873, *n* = 31). Alkali feldspar-based temperature estimates for the syenite-hosted enclaves range from 737 to 984 °C (average = 877, *n* = 17).

4.6.1.2 Oxygen fugacity

The pre-eruptive redox conditions of the magma system were evaluated via two-oxide models. As above, estimates could only be determined for the LAI and the CCI syenites. Ti-magnetite and ilmenite pairs in the LAI indicate redox conditions close to 1 log unit below FMQ (Figure 4.34a). The CCI syenites yield similar results, extending from 1 to 2 log units below FMQ.

4.6.1.3 Constraints upon pressure

The depth of the magma storage system can be estimated quantitatively via the H_2O solubility model of Di Matteo *et al.* (2004). If the maximum water content determined via FTIR of melt inclusions (4.2 wt. %) is applied, and water saturated conditions assumed, then the minimum pressure associated with the ignimbrite-forming eruptions is ~ 80 MPa. This value is increased to ~ 135 MPa if the maximum estimate of water content derived from alkali feldspar hygrometry is applied (6.0 wt. %). Assuming a crustal density of 2,800 kg/m^3, this equates to depths of between 2.2 and 3.7 km. These depths are consistent

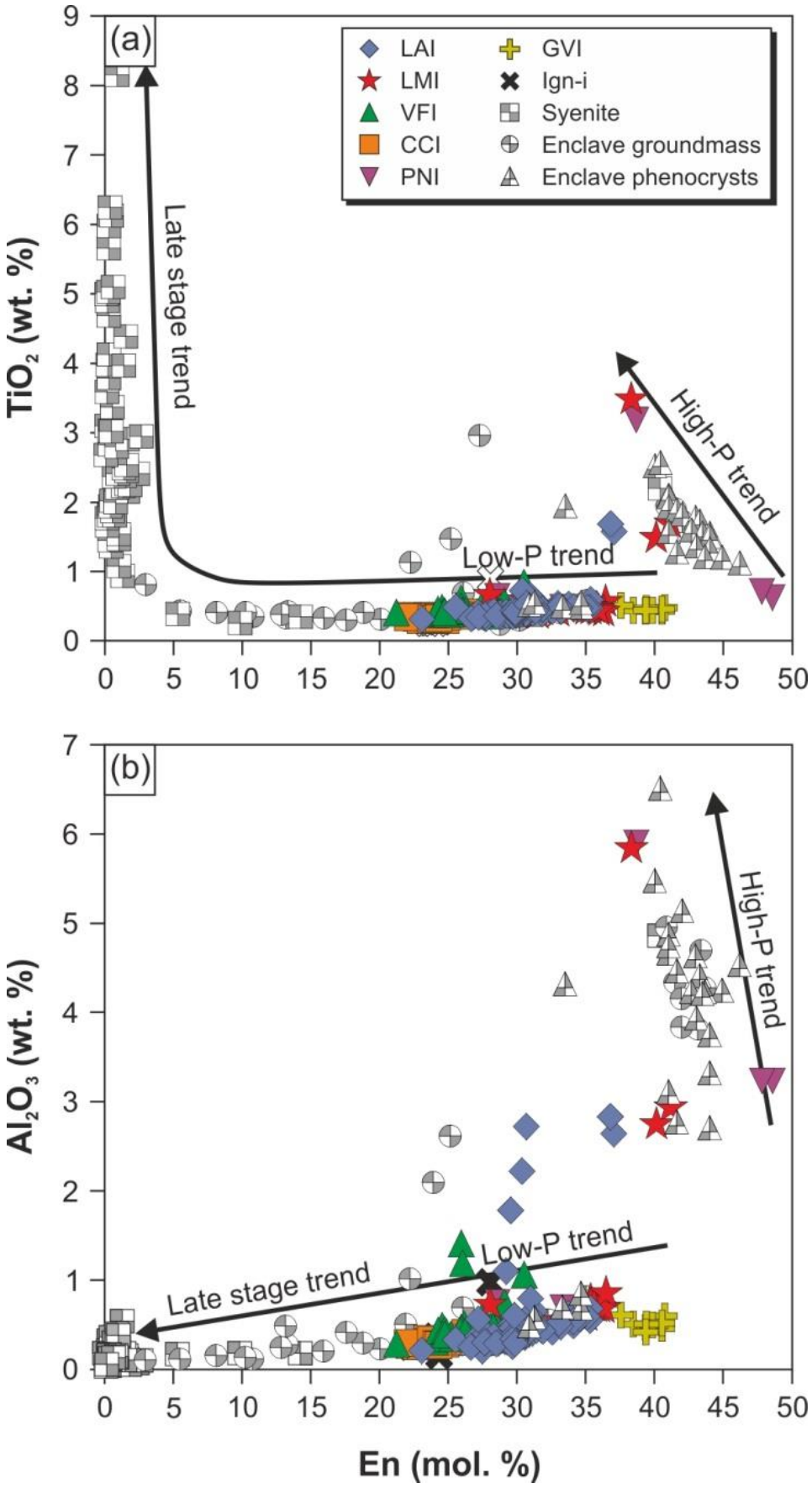

FIGURE 4.35: Variations in TiO_2 and Al_2O_3 content of Terceira clinopyroxenes, related to pressure of crystallisation

with the occurrence of aenigmatite in the syenite ejecta, as this phase is only stable at pressure in excess of 100 MPa (Di Carlo *et al.*, 2010).

The crustal depths at which the Terceira ignimbrite-forming magma evolved can also be investigated using the clinopyroxene population. The rocks of this study all contain clinopyroxene, ranging compositionally from diopside, augite, and aegirine-augite in the enclaves to augite in the ignimbrites, and finally to aegirine-augite and aegirine in the syenites. Due to the Na-rich nature of the syenite clinopyroxene population, they were considered unsuitable for thermobarometry. Furthermore, clinopyroxene compositional and Fe-Mg exchange tests for equilibrium between crystals and melts (Putirka, 2008) indicate a lack of equilibrium within the suite, precluding the application of clinopyroxene-based thermobarometrical models to any of the rocks of this study. However, insights may still be gained from clinopyroxene chemistry. The TiO_2 and Al_2O_3 contents of clinopyroxene throughout the suite show substantial variations (~ 0.2 to 8.2 and ~ 0.1 to 6.6 wt. %, respectively), and, if considered alongside En content, allow the distinction of two chemical trends (Figure 4.35). The first trend is marked by a rapid increase in both TiO_2 and Al_2O_3 over a relatively small decrease in En content, and comprises predominantly diopside phenocrysts from the enclaves, with a lesser contribution from the ignimbrites and the syenites. In contrast, the second trend is marked by consistently low TiO_2 and Al_2O_3 contents (< 0.5 wt. %) at En contents between 20 and 40 mol. %, and primarily consists of augite phenocrysts from the ignimbrites, with a small number of enclave phenocrysts. The groundmass clinopyroxene of the enclaves, and the aegirine from the syenites appear to continue this trend to extremely low En contents (< 5 mol. %), where Al_2O_3 remains low, but TiO_2 rapidly increases to ~ 8 wt. %. The Al_2O_3 content of clinopyroxene is widely recognised to be positively correlated with crystallisation pressure (e.g. Thompson, 1974; Beier *et al.*, 2006). It is therefore suggested that the two trends observed for Terceira are related primarily to a change in the depth of crystallisation that occurred at ~ En_{40}, and which allows the qualitative construction of a framework for the

magma plumbing system. The first trend (high TiO_2 and Al_2O_3) is considered to reflect an initial period of crystallisation under high pressure conditions, whereas the second trend (low TiO_2 and Al_2O_3) indicates lower pressure, shallow crustal conditions (cf. Beier *et al.*, 2006). The continuation of this trend and the eventual enrichment of TiO_2 in clinopyroxene, as defined by the enclave groundmass and the syenites, are likely to reflect the late stage processes associated with near-complete solidification of trachytic melt under low pressure conditions. These observations can be accounted for by a two-stage differentiation history, in which primitive, mantle-derived melts stall in the lower crust and differentiate to broadly hawaiitic compositions, before ascending to a shallow crustal magma storage zone, where continued differentiation leads to the erupted peralkaline silicic magmas. Similar, multi-stage models have been invoked at other Azorean volcanoes (Sete Cidades, São Miguel, Beier *et al.*, 2006; Caldeira, Faial, Zanon *et al.*, 2013; Zanon and Frezzotti, 2013; Furnas, São Miguel, Jeffery *et al.*, 2016c), and other North Atlantic oceanic islands (e.g. La Palma, Klügel *et al.*, 2000; Madeira, Schwarz *et al.*, 2004).

The distribution of the dataset between these two trends shows that the majority of clinopyroxenes from the ignimbrites, the syenites, and the groundmass of the enclaves adhere to the low pressure trend. The majority of high pressure clinopyroxenes are found as phenocrysts in the enclaves, where low pressure phenocrysts are also present. It is therefore suggested that the enclaves provide direct evidence not only for the mingling /mixing of trachyte and syenitic mush under low pressure conditions (see above), but also for the mingling/mixing of trachytes stored in shallow crustal reservoirs with ascending mafic magmas from the high pressure storage region. In fact, the enclaves are likely to represent hybridised magmas with multiple populations of crystals. The presence of heavily reacted, forsteritic olivine further substantiates this.

4.6.2 The origin of the ignimbrite-forming trachytes

The petrogenetic processes that generate peralkaline silicic magmas in oceanic island settings include: (1) where no compositional gap (Daly Gap) exists between mafic and felsic compositions, extended fractional crystallisation of a mantle-derived alkali basalt parent magma (e.g. Barberi *et al.*, 1975; Civetta *et al.*, 1998; Peccerillo *et al.*, 2007), possibly including some assimilation of the crust (e.g. Peccerillo *et al.*, 2003), and (2) where a Daly Gap is present, partial melting of alkali gabbro cumulates, producing peralkaline silicic magmas directly (e.g. Avanzinelli *et al.*, 2004), which may evolve further via fractional crystallisation (e.g. Trua *et al.*, 1999). To investigate the petrogenetic processes that give rise to the ignimbrite-forming trachytes of Terceira, a number of petrogenetic models are applied: 1) Major element mass balance models, 2) Thermodynamic models, and 3) Trace element Rayleigh fractionation and batch melting models.

4.6.2.1 Fractional crystallisation

The prominent role of fractional crystallisation in the generation of evolved magmas in peralkaline silicic systems is well established (e.g. Barberi *et al.*, 1975; Peccerillo *et al.*, 2003; Macdonald *et al.*, 2008, 2015; Macdonald, 2012), and was demonstrated quantitatively for a series of young (predominantly < 23 ka) lavas from Terceira by Mungall and Martin (1995). However, in terms of their eruptive character and their temporal occurrence (~ 22 to ~ 86 ka; Gertisser *et al.*, 2010), the ignimbrites of Terceira may represent a volcanologically and petrologically distinctive system, and should be considered separately. Thus, to validate the role of fractional crystallisation, a number of petrogenetic models are applied. To act as a starting point for each model, a variety of potential compositions are available (Self and Gunn, 1976). Mungall and Martin (1995) recognised three distinctive basaltic compositions, which they termed the on-rift, off-rift, and primitive basalts. Of these, the latter corresponds to the silica-undersaturated series

of Self and Gunn (1976), whilst the on- and off-rift basalts form the silica-oversaturated trend, and were linked to Pico Alto and Santa Bárbara, respectively (Mungall and Martin, 1995). Gertisser *et al.* (2010) attributed the Terceiran ignimbrites primarily to the Pico Alto volcanic complex and possibly Guilherme Moniz. For this reason, the on-rift basalts are considered to be the most suitable starting composition for mass balance and trace element models. However, to evaluate the potential effects of varying parental compositions, on-rift, off-rift, and primitive basalts were all applied as potential parental compositions for thermodynamic (Rhyolite-MELTs) modelling.

To evaluate simple fractional crystallisation processes, two major element mass balance models for the liquid line of descent of the Terceira magmas were run, each comprising five compositional steps: 1) alkali basalt to hawaiite, 2) hawaiite to mugearite, 3) mugearite to benmoreite, 4) benmoreite to least evolved trachyte (LET), and 5) LET to most evolved trachyte (MET). Whole rock and mineral chemical data for alkali basaltic, hawaiitic, mugearitic, benmoreitic, and pantelleritic rocks were taken from Mungall (1993), whilst mineral chemical data for comenditic trachytic compositions were taken from the ignimbrites of this study (Table 4.13). Two on-rift basalts (samples 89-13 and 89-19 of Mungall, 1993) were selected as suitable parent compositions on the basis of Mg# (58 and 53, respectively; mol. $Mg/(Mg+Fe^{2+})\cdot 100$) and Zr content (168 and 188 ppm, respectively). However, these compositions are not indicative of primary melt, and so the determined degrees of fractionation should be considered to be minima.

Both major element mass balance models are in broad agreement that the LET compositions can be reliably reproduced (average $\sum r^2 = 0.178$) by 84 to 85 % fractionation of an assemblage of plagioclase (46 to 50 %), clinopyroxene (26 %), olivine (10 to 11 %), Ti-magnetite (4 to 7 %), ilmenite (4 %), and apatite (2 to 3 %) (Table 4.14). The MET compositions can be produced by a further 14 to 19 % fractionation (87 % total from

Table 4.13: Mineral compositions used for major element mass balance modelling

Composition	**Basalt**						**Hawaiite**					
Mineral	Pl	Ol	Cpx	Ti-mag	Ilm	Ap	Pl	Ol	Cpx	Ti-mag	Ilm	Ap
SiO_2	51.31	39.20	51.16				54.14	37.28	49.20			
TiO_2		0.04	1.09	21.50	48.80			0.06	2.40	21.50	48.80	
Al_2O_3	28.73	0.02	2.32	1.48	0.04		26.50	0.03	4.35	1.48	0.04	
Fe_2O_3												
FeO	0.70	18.94	6.07	68.53	45.37		0.73	30.02	8.40	68.53	45.37	
MnO		0.28	0.16	0.66	0.67			0.46	0.20	0.66	0.67	
MgO	0.17	41.58	16.71	1.74	1.73		0.11	33.38	13.79	1.74	1.73	
CaO	13.60	0.31	18.61	0.02	0.19	55.70	10.75	0.36	21.57	0.02	0.19	55.70
Na_2O	3.63	0.05	0.31				5.00	0.03	0.45			
K_2O	0.19						0.34					
P_2O_5						41.82						41.82
H_2O						0.59						0.59

Composition	**Mugearite**						**Benmoreite**					
Mineral	Pl	Ol	Cpx	Ti-mag	Ilm	Ap	Pl	Ol	Cpx	Ti-mag	Ilm	Ap
SiO_2	55.57	35.83	47.20				58.33	36.82	50.72			
TiO_2		0.05	2.33	16.50	35.80			0.02	1.13	16.50	35.80	
Al_2O_3	25.62	0.02	4.36	2.57	1.74		23.81	0.01	2.69	2.57	1.74	
Fe_2O_3												
FeO	0.64	35.66	9.53	73.42	51.29		0.71	32.66	8.41	73.42	51.29	
MnO		0.93	0.26	0.81	0.56			0.78	0.31	0.81	0.56	
MgO	0.08	28.41	13.27	1.77	3.00		0.07	30.56	13.96	1.77	3.00	
CaO	9.73	0.23	19.58	0.09	0.00	55.70	6.96	0.22	20.88	0.09	0.00	55.70
Na_2O	5.66	0.02	0.56				6.94	0.00	0.52			
K_2O	0.41						0.77					
P_2O_5						41.82						41.82
H_2O						0.59						0.59

Composition	**LET and MET**						**Pantellerites**					
Mineral	K-spar	Ol	Cpx	Ti-mag	Ilm	Ap	K-spar	Ol	Cpx	Ti-mag	Ilm	Ap
SiO_2	66.18	33.10	50.52				67.02	30.09	49.97			
TiO_2	0.06	0.04	0.39	22.56	51.10			0.04	0.51	22.56	50.40	
Al_2O_3	18.75	0.03	1.86	0.60	0.07		18.77	0.01	0.50	0.60	0.02	
Fe_2O_3												
FeO	0.49	50.39	15.94	71.77	45.00		0.34	56.85	16.81	71.77	45.78	
MnO		3.48	1.33	1.78	2.30			4.04	1.17	1.78	2.19	
MgO	0.01	14.28	10.05	1.12	1.68		0.00	7.93	9.15	1.12	0.19	
CaO	0.29	0.26	19.89			55.70	0.20	0.47	20.25		0.00	55.70
Na_2O	7.82		0.87				7.68	0.00	0.64			
K_2O	5.47		0.00				6.24					
P_2O_5						41.82						41.82
H_2O						0.59						0.59

Table 4.14: Results of major element mass balance modelling from parental basalt to pantellerite

Step 1: Alkali basalt to hawaiite

	Liquid Composition			Fractionating Phases		Liquid Composition			Fractionating Phases	
Sample	Basalt		Hawaiite			Sample	Basalt	Hawaiite		
	89-13		90-139				89-19	89-25		
	Obs	Calc	Obs				Obs	Calc	Obs		
SiO_2	47.85	48.12	50.43	Ol	10.4	SiO_2	47.07	47.34	49.94	Ol	10.4
TiO_2	3.44	3.45	3.22	Cpx	32.2	TiO_2	3.76	3.77	3.17	Cpx	33.7
Al_2O_3	14.85	14.85	15.18	Fsp	46.5	Al_2O_3	14.51	14.52	15.66	Fsp	37.7
FeO_t	11.07	11.09	11.21	Mt	6.8	FeO_t	12.13	12.14	10.96	Mt	11.7
MnO	0.20	0.21	0.25	Ilm	3.6	MnO	0.22	0.22	0.23	Ilm	4.1
MgO	6.95	6.93	4.23	Ap	0.6	MgO	6.53	6.51	4.72	Ap	2.5
CaO	10.44	10.39	8.20			CaO	10.00	9.96	8.50		
Na_2O	3.34	3.22	4.39			Na_2O	3.53	3.38	4.22		
K_2O	1.10	0.88	1.54			K_2O	1.15	0.98	1.38		
P_2O_5	0.76	0.85	1.35			P_2O_5	1.09	1.18	1.22		
$\sum r^2$	0.085					$\sum r^2$	0.076				
F	0.544					F	0.690				

Step 2: Hawaiite to mugearite

	Liquid Composition			Fractionating Phases		Liquid Composition			Fractionating Phases	
Sample	Hawaiite		Mugearite			Sample	Hawaiite	Mugearite		
	90-139		89-58				89-25	89-48		
	Obs	Calc	Obs				Obs	Calc	Obs		
SiO_2	50.43	50.51	53.69	Ol	11.2	SiO_2	49.94	50.11	54.04	Ol	13.4
TiO_2	3.22	3.22	2.54	Cpx	34.3	TiO_2	3.17	3.18	2.55	Cpx	17.8
Al_2O_3	15.18	15.33	16.68	Fsp	30.2	Al_2O_3	15.66	15.63	15.61	Fsp	54.4
FeO_t	11.21	11.21	9.68	Mt	11.9	FeO_t	10.96	10.97	10.06	Mt	6.0
MnO	0.25	0.22	0.22	Ilm	4.8	MnO	0.23	0.23	0.27	Ilm	4.7
MgO	4.23	4.22	3.09	Ap	7.5	MgO	4.72	4.71	3.21	Ap	3.6
CaO	8.20	8.18	6.46			CaO	8.50	8.49	6.31		
Na_2O	4.39	4.08	4.67			Na_2O	4.22	4.19	5.02		
K_2O	1.54	1.66	2.05			K_2O	1.38	1.21	1.85		
P_2O_5	1.35	1.38	0.92			P_2O_5	1.22	1.27	1.08		
$\sum r^2$	0.118					$\sum r^2$	0.038				
F	0.801					F	0.615				

Table 4.14 continued

Step 3: Mugearite to benmoreite

	Liquid Composition			Fractionating Phases		Liquid Composition			Fractionating Phases	
Sample	Mugearite		Benmoreite			Sample	Mugearite		Benmoreite		
	89-58		89-30				89-48		89-30		
	Obs	Calc	Obs				Obs	Calc	Obs		
SiO_2	53.69	53.67	58.91	Ol	10.7	SiO_2	54.04	53.86	58.91	Ol	12.1
TiO_2	2.54	2.54	1.44	Cpx	21.3	TiO_2	2.55	2.54	1.44	Cpx	33.5
Al_2O_3	16.68	16.55	17.69	Fsp	48.2	Al_2O_3	15.61	15.77	17.69	Fsp	24.8
FeO_t	9.68	9.69	7.10	Mt	5.7	FeO_t	10.06	10.04	7.10	Mt	17.7
MnO	0.22	0.23	0.21	Ilm	9.3	MnO	0.27	0.22	0.21	Ilm	3.8
MgO	3.09	3.10	1.69	Ap	4.9	MgO	3.21	3.21	1.69	Ap	8.2
CaO	6.46	6.47	4.12			CaO	6.31	6.31	4.12		
Na_2O	4.67	4.88	5.72			Na_2O	5.02	4.83	5.72		
K_2O	2.05	1.96	2.72			K_2O	1.85	2.17	2.72		
P_2O_5	0.92	0.91	0.40			P_2O_5	1.08	1.05	0.40		
$\sum r^2$	0.053					$\sum r^2$	0.151				
F	0.698					F	0.792				

Step 4: Benmoreite to LET

	Liquid Composition			Fractionating Phases		Liquid Composition			Fractionating Phases	
Sample	Benmoreite		LET			Sample	Benmoreite		LET		
	89-30		TER 4-1				89-30		TER 21-1		
	Obs	Calc	Obs				Obs	Calc	Obs		
SiO_2	58.91	58.47	65.40	Ol	6.1	SiO_2	58.91	58.24	65.46	Ol	10.5
TiO_2	1.44	1.43	0.63	Cpx	6.5	TiO_2	1.44	1.41	0.62	Cpx	0.3
Al_2O_3	17.69	17.40	15.36	Fsp	77.6	Al_2O_3	17.69	17.84	15.42	Fsp	78.3
FeO_t	7.10	7.10	4.75	Mt	6.1	FeO_t	7.10	7.07	4.70	Mt	8.7
MnO	0.21	0.17	0.21	Ilm	2.7	MnO	0.21	0.18	0.22	Ilm	1.1
MgO	1.69	1.76	0.42	Ap	1.0	MgO	1.69	1.75	0.41	Ap	1.0
CaO	4.12	4.22	0.76			CaO	4.12	4.20	0.76		
Na_2O	5.72	6.40	7.31			Na_2O	5.72	5.95	7.25		
K_2O	2.72	2.77	5.07			K_2O	2.72	3.14	5.06		
P_2O_5	0.40	0.26	0.10			P_2O_5	0.40	0.23	0.10		
$\sum r^2$	0.557					$\sum r^2$					
F	0.485					F					

Table 4.14 continued

Step 5: LET to MET

Liquid Composition				Fractionating Phases		Liquid Composition				Fractionating Phases	
Sample	LET		MET			Sample	LET		MET		
	TER 4-1		TER 55-1				TER 21-1		TER 10-1		
	Obs	Calc	Obs				Obs	Calc	Obs		
SiO_2	65.40	65.15	64.65	Ol	4.7	SiO_2	65.46	64.79	64.31	Ol	3.6
TiO_2	0.63	0.49	0.54	Cpx	2.0	TiO_2	0.62	0.45	0.52	Cpx	0.0
Al_2O_3	15.36	15.67	15.87	Fsp	89.1	Al_2O_3	15.42	15.88	16.26	Fsp	92.3
FeO_t	4.75	4.79	4.88	Mt	3.1	FeO_t	4.70	4.73	4.67	Mt	3.0
MnO	0.21	0.20	0.21	Ilm	0.0	MnO	0.22	0.18	0.18	Ilm	0.0
MgO	0.42	0.36	0.45	Ap	1.1	MgO	0.41	0.44	0.47	Ap	1.1
CaO	0.76	0.84	0.92			CaO	0.76	0.85	0.86		
Na_2O	7.31	7.60	7.51			Na_2O	7.25	7.77	7.65		
K_2O	5.07	4.90	4.90			K_2O	5.06	4.97	5.00		
P_2O_5	0.10	-0.01	0.07			P_2O_5	0.10	-0.05	0.07		
$\sum r^2$	0.190					$\sum r^2$	0.467				
F	0.861					F	0.806				

Step 6: MET to pantellerite

Liquid Composition				Fractionating Phases		Liquid Composition				Fractionating Phases	
Sample	MET		Pantellerite			Sample	MET		Pantellerite		
	TER 55-1		90-159				TER 10-1				
	Obs	Calc	Obs				Obs	Calc	Obs		
SiO_2	64.65	64.84	67.34	Ol	1.8	SiO_2	64.31	64.61	67.49	Ol	2.1
TiO_2	0.54	0.57	0.56	Cpx	3.0	TiO_2	0.52	0.56	0.55	Cpx	2.6
Al_2O_3	15.87	15.51	10.74	Fsp	92.4	Al_2O_3	16.26	16.00	10.80	Fsp	92.6
FeO_t	4.88	4.89	8.18	Mt	2.4	FeO_t	4.67	4.67	8.36	Mt	2.4
MnO	0.21	0.21	0.34	Ilm	0.0	MnO	0.18	0.2	0.34	Ilm	0.0
MgO	0.45	0.41	0.3	Ap	0.3	MgO	0.47	0.38	0.17	Ap	0.3
CaO	0.92	0.91	0.72			CaO	0.86	0.84	0.63		
Na_2O	7.51	7.16	7.31			Na_2O	7.65	7.11	7.13		
K_2O	4.90	5.40	4.46			K_2O	5.00	5.50	4.49		
P_2O_5	0.07	0.10	0.04			P_2O_5	0.07	0.11	0.04		
$\sum r^2$	0.411					$\sum r^2$	0.58				
F	0.277					F	0.208				

FIGURE 4.36: Summary figure showing the predicted fractionating assemblages, assuming fractional crystallisation of the On-rift basalt, with variable initial H_2O contents, and under variable pressure and redox conditions. Models marked with a cross failed to run to completion. Filled squares represent phases which crystallised as part of the predicted fractionated assemblage

parent) of an assemblage that is dominated by alkali feldspar (89 to 92 %), olivine (4 to 5 %), clinopyroxene (0 to 2 %), Ti-magnetite (3 %), and apatite (1 %) (average $\sum r^2 = 0.329$). In contrast to the formulations of Mungall and Martin (1995), the inclusion of amphibole at any stage of the models leads invariably to failure.

To investigate the role of fractional crystallisation under variable P-T-fO_2 conditions, a total of 180 isobaric fractional crystallisation models and a small number of polybaric models were produced using the Rhyolite-MELTs program, for variable crustal pressure values (50, 150, 250, 500 MPa), initial water contents (0.5, 1.5, 2.5 wt. %), and redox conditions (FMQ -2 to FMQ +2). Polybaric models were run with a change in

FIGURE 4.37: Summary figure showing the predicted fractionating assemblages, assuming fractional crystallisation of the Off-rift basalt, with variable initial H_2O contents, and under variable pressure and redox conditions. Models marked with a cross failed to run to completion. Filled squares represent phases which crystallised as part of the predicted fractionated assemblage

pressure from 500 MPa to 150 MPa at either 1,100 or 1,000 °C, which corresponds to hawaiitic or benmoreitic compositions. The on-rift, off-rift, and primitive basaltic compositions described above were used as parental melt compositions. Each model was evaluated based upon its capability to reproduce the major element compositions of the ignimbrite formations, and the Terceiran liquid line of descent.

Regardless of the set conditions of the model, all three parental compositions include feldspar and clinopyroxene in their predicted fractionating assemblages (Figures 4.36, 4.37, 4.38). The primitive basalt also invariably includes olivine, which is generally favoured by lower oxygen fugacities with increasing depth in the on- and off-rift basalt

FIGURE 4.38: Summary figure showing the predicted fractionating assemblages, assuming fractional crystallisation of the primitive basalt, with variable initial H_2O contents, and under variable pressure and redox conditions. Filled squares represent phases which crystallised as part of the predicted fractionated assemblage

models. Apatite is ubiquitous, save for primitive basalt models, where it is not predicted at the most oxidising conditions, and does not occur at all for the 250 MPa model. Similarly, Ti magnetite occurs in nearly all of the models. Ilmenite is common throughout, but becomes slightly less so in the primitive basalt models at higher initial water contents. Quartz is predicted to fractionate from both on- and off-rift basalt models at redox conditions of FMQ or above. In contrast, quartz appears rarely in the primitive basalt models. Amphiboles are not predicted to fractionate in any of the models, save one; the on-rift basalt model at 250 MPa, 1.5 wt. % initial water, FMQ +1. The crystallisation of biotite is favoured by higher initial water contents, higher pressures, and higher oxygen

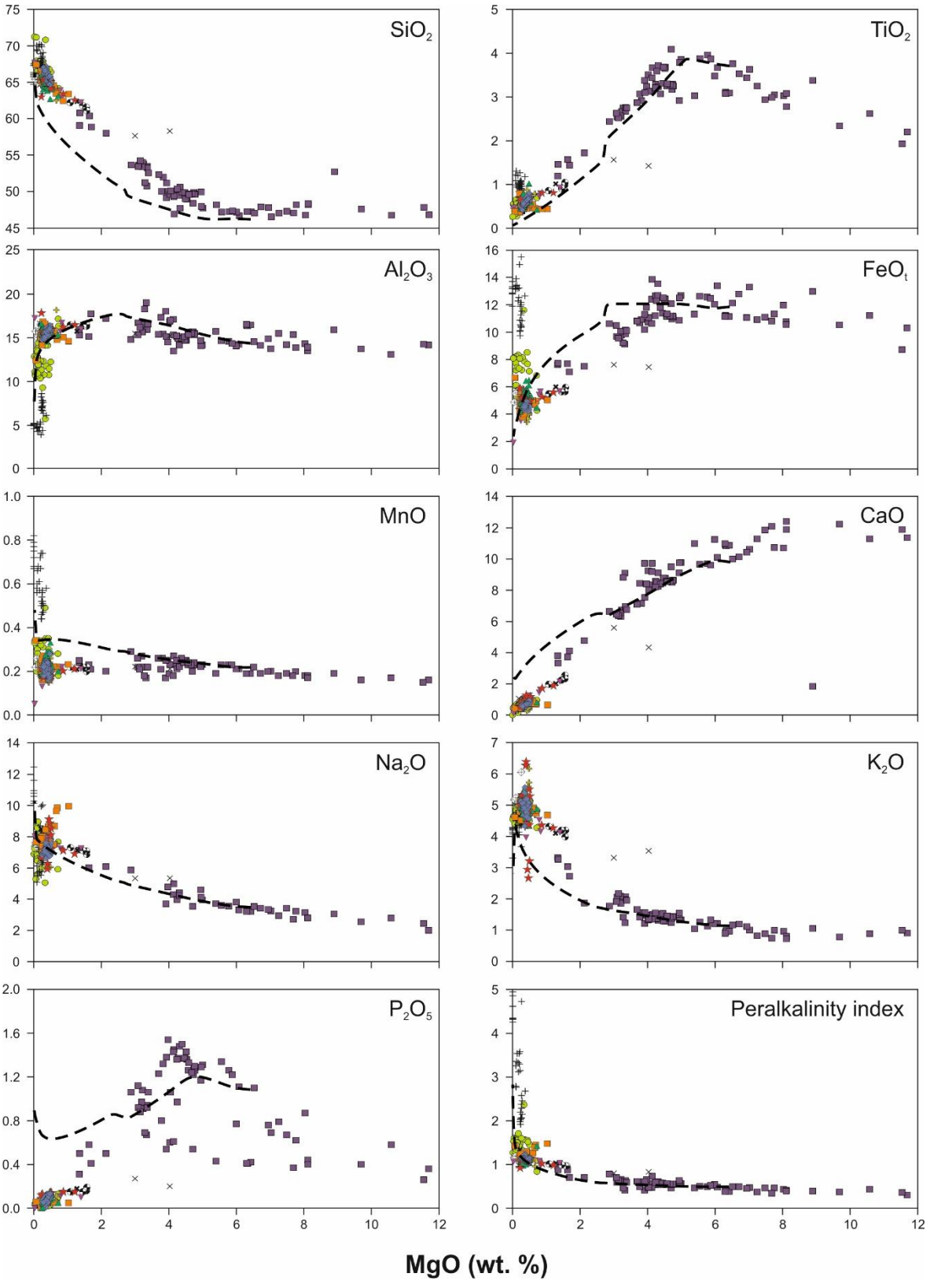

FIGURE 4.39: Rholite-MELTs modelled liquid line of descent assuming polybaric conditions (see text), plotted with available data for Pico Alto, Guilherme Moniz, and the Rift zone.

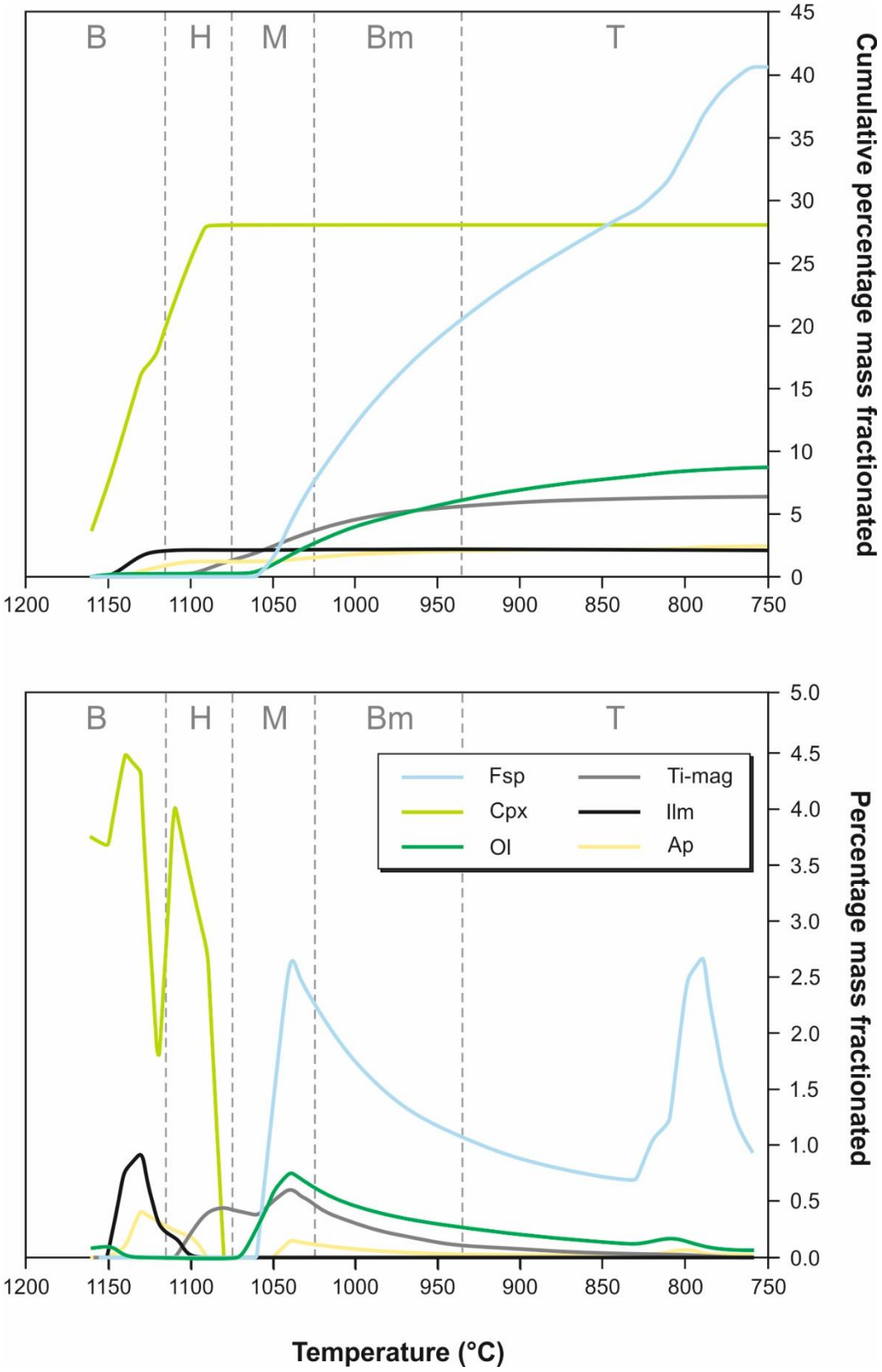

FIGURE 4.40: Summary of fractionation history of the most applicable Rhyolite-MELTs model (polybaric, 500 to 150 MPa, FMQ -1, 1.5 wt. % initial water content. Abbreviations used: Fsp = feldspar, Cpx = clinopyroxene, Ol = olivine, Ti-mag = Ti-magnetite, Ilm = ilmenite, Ap = apatite, B = basalt, H = hawaiite, M = mugearite, Bm = benmoreite, T = trachyte

fugacities. The increase in the stability of biotite in response to increasing depth is particularly pronounced in the primitive basalt models (Figure 4.37).

In addition to supporting fractional crystallisation as the dominant mechanism of differentiation within the Terceira suite, the models also provide further validation of the pre-eruptive P-T-fO_2 conditions determined above. For example, isobaric models run at 500 MPa invariably fail to achieve the SiO_2 and total alkali contents that are observed in the ignimbrites, suggesting that a significant proportion of the liquid line of descent is representative of shallow crustal conditions. This is consistent with Mungall and Martin (1995), who suggested that the on-rift basalts evolved to more silicic compositions at relatively shallow depths. Altering the redox conditions to > FMQ leads to the development of peralkalinity at higher MgO values than observed on Terceira. Similarly, the highest and lowest initial water contents lead to the development of peralkalinity at lower or higher MgO contents, respectively, most likely due to the strong control of water content upon the onset of feldspar crystallisation.

Overall, the results of modelling indicate that the major element compositions of the Terceiran ignimbrites can be reproduced by a polybaric model in which the melt differentiates at 500 MPa until it has reached a hawaiitic composition (~ 1,100 °C), at which point the pressure is reduced to 150 MPa. Relatively reducing conditions (FMQ -1) and a hydrous parental basalt composition (1.5 wt. % H_2O) lead to the best results. For this model, olivine is the liquidus phase, and exhibits two crystallisation intervals (1180 to 1150 ºC and 1060 °C onwards). This is followed by clinopyroxene (1160 to 1090 ºC), ilmenite (1140 ºC onwards), apatite (1140 to 1100 ºC and 1040 °C onwards), Ti-magnetite (1100 ºC onwards), and feldspar (1050 ºC onwards) (Figure 4.40). The total fractionation at 850 °C is 74 %, of a mineral assemblage dominated by clinopyroxene (38 %), feldspar (37 %), olivine (11 %), Ti-magnetite (8 %), apatite (3 %), and ilmenite (3%)

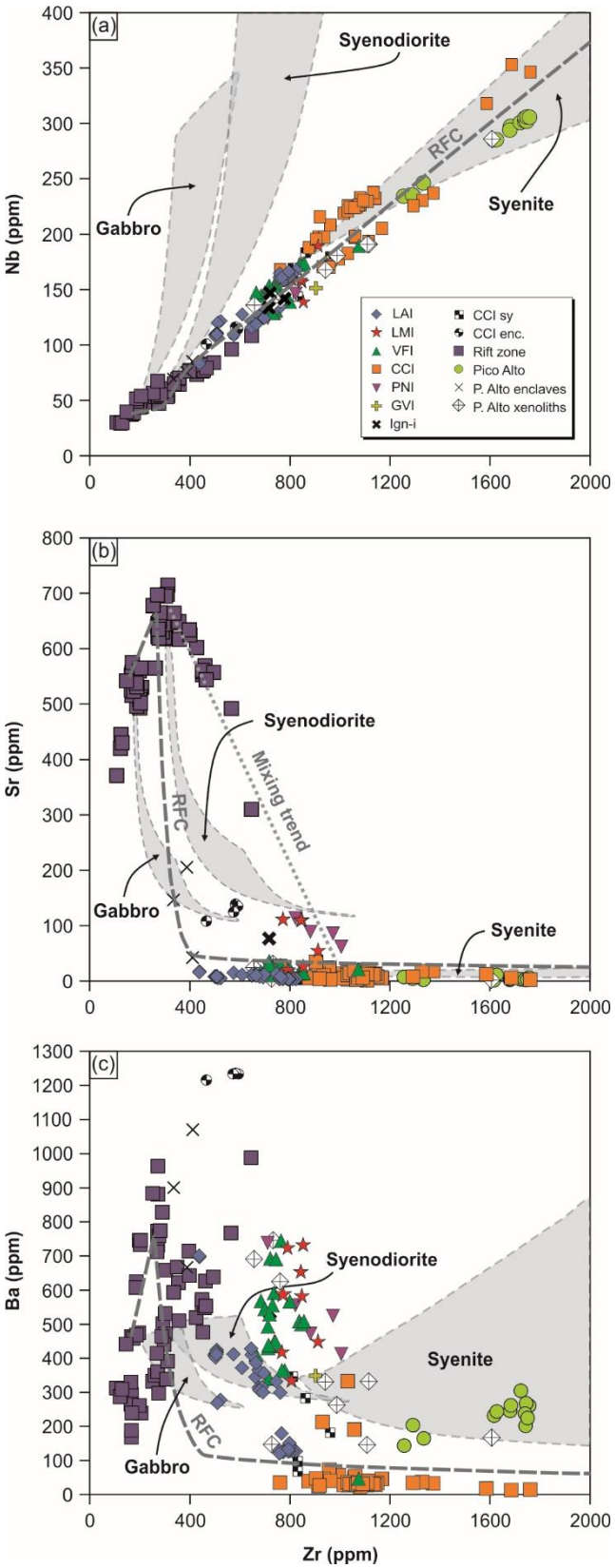

FIGURE 4.41: Results of trace element Rayleigh fractionation and batch melting modelling for the lithologies of Terceira. Grey fields indicate range of compositions generated by varying degrees of partial melting of gabbro, syenodiorite, or syenite, assuming variable mineral assemblages

Table 4.15: Partition coefficients selected for trace element modelling

Rayleigh fractionation - Step 1 and batch melting							
	Plag	**Cpx**	**Ol**	**Mt**	**Ilm**	**Ap**	**K Fsp**
Nb		0.100	0.010	0.900	2.000		
Cr		5.300	2.800	153.000	25.850	9.000	
Y		2.390	0.003	0.004	0.024		
Zr		0.120	0.060	0.700	0.290		
Sr		0.512	0.020		0.740	1.200	
Ba		0.040	0.030			0.050	
Rb		0.130	0.040	0.110			
Ni		2.500	34.000	48.000	3.800		

Rayleigh fractionation - Step 2							
	Plag	**Cpx**	**Ol**	**Mt**	**Ilm**	**Ap**	**K Fsp**
Nb	0.010		0.010	0.900			
Cr	0.340		2.800	153.000		9.000	
Y	0.023		0.003	0.004			
Zr	0.010		0.060	0.700			
Sr	10.000		0.020			1.200	
Ba	5.900		0.030			0.050	
Rb	0.050		0.010	0.110			

Rayleigh fractionation - Step 3							
	Plag	**Cpx**	**Ol**	**Mt**	**Ilm**	**Ap**	**K Fsp**
Nb			0.010	0.900			0.004
Cr			2.800	153.000		9.000	
Y			0.003	0.004			0.017
Zr			0.060	0.700			0.003
Sr			0.020			1.200	2.300
Ba			0.030			0.050	3.409
Rb			0.010	0.110			0.320

To further investigate the role of fractional crystallisation, and to evaluate the applicability of partial melting of various crustal lithologies as a petrogenetic process, closed system Rayleigh fractional crystallisation (RFC) and batch melting models of selected trace elements were produced (Figure 4.41). Experimental and natural partition coefficients selected from the GERM KD database (Nielsen 2006) are given in Table 4.15 (Paster *et al.*, 1974; McCallum and Charette 1978; Larsen 1979; Shimizu 1980; Villemant *et al.*, 1981; Watson and Green 1981; Luhr *et al.*, 1984; Lemarchand *et al.*, 1987; Mahood and Stimac 1990; McKenzie and O'Nions 1991; Nielsen, 1992; Nielsen *et al.*, 1992; Ewart

and Griffin 1994; Horn *et al.*, 1994; Esperança *et al.*, 1997; Wood and Trigila 2001; Adam and Green 2006; Klemme *et al.*, 2006). The final fractionation trend comprises three stages, each calculated using phase assemblages and proportions predicted by the most suitable Rhyolite-MELTs model (see above): 1) Clinopyroxene + Olivine + Ilmenite + Ti-magnetite + Apatite, 2) Plagioclase + Olivine + Ti-magnetite + Apatite, 3) Alkali feldspar + Olivine + Ti-magnetite + Apatite. RFC models for incompatible elements such as Zr and Nb provide a good fit to the trend observed for Terceira and indicate that the compositional range of the ignimbrites can be accounted for by between ~ 65 and 90 % fractionation of an alkali basalt parent. The RFC models for compatible elements such as Sr, Ba, Cr, and Ni are less well defined due to the substantial scatter observed in the Terceira suite, particularly within the broadly intermediate portion of the suite. However, modelled trends adhere closely to the generally low concentrations of Sr, Cr, and Ni observed in the suite. The model fit to Ba data is poor due to the substantial scatter in the dataset, with the majority of the dataset plotting above the RFC trend. Overall, these models are in agreement with incompatible element models, suggesting that the compositions observed in the ignimbrites can be produced by between ~ 65 and ~ 90 % fractional crystallisation. In contrast, batch melting models calculated for hypothetical gabbroic, syenodioritic, and syenitic lithologies of variable phase assemblages are almost exclusively incompatible with the trends observed in the Terceira suite (Figure 4.41). For example, partial melting of either gabbroic or syenodioritic rock compositions yield trends that deviate significantly from the Terceira suite (e.g. Zr vs. Nb; Figure 4.41a), and generally fail to achieve the high concentrations of incompatible elements and extremely low concentrations of compatible elements (e.g. Sr, Ba; Figure 4.41b, c). Partial melting of a syenitic crustal lithology provides a better fit, but requires degrees of melting in excess of 50 % and notably cannot generate the least evolved trachytic compositions of the ignimbrites (~ 400 to 800 ppm Zr).

In summary, the results presented here suggest that the ignimbrites of Terceira can be accounted for by extended fractional crystallisation of a basaltic parental magma. Although the role of partial melting of crustal lithologies cannot be ruled out entirely, model results indicate that any contribution from such processes is small and probably limited to syenitic rocks. Various petrogenetic models are in broad agreement that the entire compositional range exhibited by the ignimbrites of Terceira can be accounted for by between ~ 65 and ~ 90 % fractionation.

4.6.2.2 In-situ crystallisation

Syenite bulk rock major element compositions are similar to the trachytes (Figure 4.29), and the depletion of compatible trace elements such as Sr, Ba, and P (attributed here to fractional crystallisation; Figure 4.41c, d) are also present, and may be even more extreme. If the syenites represented cumulate material derived from the fractional crystallisation of trachytic magmas, then they should exhibit compositions that are uniformly less evolved than the ignimbrite-forming trachytes. Additionally, the syenites exhibit negative Eu anomalies which are comparable to the trachytes (Figure 4.33, 4.32). The Terceira trachytes exhibit a negative correlation between Eu/Eu* and differentiation indices such as Zr and Nb, suggesting that any accumulation of plagioclase would buffer, or even counteract the continued development of a negative anomaly. Based upon their petrographical and geochemical characteristics, it is therefore suggested that the syenitic ejecta do not represent fragments of cumulate from which the trachytes are derived, and instead provide direct evidence for the role of *in-situ* crystallisation of trachytic magma, most likely in the thermal boundary layer at the edge of a magma reservoir (cf. Tait *et al.*, 1989b; Turbeville, 1993; Widom *et al.*, 1993).

4.6.2.3 Magma mixing and remobilisation of crystal mush

The rocks of Terceira provide abundant evidence for the role of open system processes such as magma mixing and magma interaction with partially or totally solidified crystal mushes. Mungall (1993) reports trachytic lava flows containing mafic enclaves, as well as disaggregated and partially melted syenitic xenoliths in basaltic lava, providing evidence for physical interaction of mafic and felsic magmas. The same author cites reverse zonation of phenocryst phases to infer the mixing of intermediate magmas shortly before eruption. The syenite-hosted enclaves of this study provide direct evidence for the mingling/mixing of variably evolved felsic magmas. If the syenite ejecta are considered to represent randomly sampled portions of a crystal mush derived from *in-situ* crystallisation in a thermal boundary zone, then it is suggested that the syenite-hosted enclaves must indicate the injection of a LET into another trachytic reservoir, passing through the marginal crystal mush. Although it cannot be ruled out that the syenites may instead represent significantly older, crustal lithologies, the prevalence of fresh, unaltered textures and the, in some cases extreme, friability of individual nodules does not support this interpretation. Furthermore, the intruding mafic trachyte contains a mixed phase assemblage, in which a basaltic assemblage of diopside, forsterite, and bytownite is juxtaposed against a more felsic assemblage of oligoclase, anorthoclase and augite, implying that the basaltic assemblage is antecrystic. In fact, the trachytic assemblage may also, to some extent, be antecrystic. The observed sieve-textures at the rims of the largest anorthoclase crystals may have originated from the mingling of ascending hawaiites and trachytes stored in the shallow crust, and the subsequent reheating of the latter, implying that they represent the true phenocryst assemblage of the trachyte. Alternatively, these textures may indicate disequilibrium between relatively mafic trachyte and large anorthoclase crystals originating from the surrounding syenitic mush, introduced during trachyte-syenite interaction and subsequent disaggregation of the latter. Some evidence exists for the remobilisation and disaggregation of syenitic mush in the form of

glomerocrystic fragments comprising large, cumulus (and often perthitic) alkali feldspar and intercumulus aegirine-augite or Na-amphibole, two phases that are not observed in any lithology other than the syenites. The presence of such glomerocrysts as well as individual crystals which do not exhibit a perthitic texture suggests that both processes occur.

Further evidence for mingling/mixing may be seen in the calculated RFC models, where a number of lithologies deviate from the modelled trend (Figure 4.41). In particular, the syenite-hosted enclaves, intermediates (mugearites and benmoreites), and a number of the ignimbrite-forming trachytes exhibit Sr concentrations which form a mixing trend in which the ignimbrite-forming trachytes of the LMI, PNI and Ign-i are mixed with hawaiitic compositions (Figure 4.41b). This is consistent with the observed petrographical features for mixing in these lithologies (abundant resorbed crystals), mineral chemistry (rare forsteritic olivine and plagioclase), and also, to some extent, thermometric evidence (higher temperatures predicted for the LMI; Figure 4.34b). This mixing trend is also present for other compatible elements such as Ba, Cr, and Ni, but is less distinct due to the observed scatter. In particular, Ba shows a potential (but highly scattered) mixing trend between hawaiites and trachytes, although lithologies such as the syenite-hosted enclaves reach concentrations in excess of both the maximum concentration predicted by closed system RFC (~ 800 ppm), and the proposed mixing trend, reaching values as high as ~ 1250 ppm. The enrichment of Ba is a feature that is typical of peralkaline systems and is frequently attributed to the resorption of alkali feldspars (e.g. Macdonald *et al.*, 2008; Macdonald, 2012). The presence of feldspars with resorption textures throughout the ignimbrites provides evidence for this process in the ignimbrite-forming trachytes of Terceira.

4.6.3 Volatiles and degassing

Pre-eruptive water contents estimated via alkali feldspar-melt hygrometry exhibit a negative correlation with temperature estimates (Figure 4.34b). Furthermore, the Cl and F contents of melt inclusions, and to a lesser extent groundmass glass, both exhibit a positive correlation with peralkalinity indices (Figure 4.42). The greater volatile concentrations are generally restricted to those ignimbrite formations which are, on the basis of trace element geochemistry and peralkalinity indices, the most differentiated. As such, the volatile concentrations of the ignimbrite-forming magmas of Terceira are likely to have been controlled primarily by fractionation, and are indicative of volatile-undersaturated conditions.

As observed at many peralkaline silicic centres (e.g. Macdonald, 2012), the halogen concentrations of the ignimbrite-forming trachytes of Terceira are sufficient to warrant their further consideration. Chlorine is often emitted as hydrogen chloride (HCl) during volcanic eruptions, and has been shown to have significant environmental impacts (e.g. Symonds *et al.*, 1992, 1994; Millard *et al.*, 2006; Rose *et al.*, 2006; Pyle and Mather, 2009). Similarly, fluorine, emitted as HF, has been shown to have severe implications for

Table 4.16: Melt inclusion and groundmass glass halogen data for the ignimbrites of Terceira

Unit	**Analysis**	**Cl**				***n***	**F**				***n***
		Min	Average	Max	Stdev (2σ)		Min	Average	Max	Stdev (2σ)	
LAI	Melt inclusion	1511	2212	2795	719	30	857	1452	2022	523	30
	Groundmass glass	1500	2244	4200	894	42	300	1714	3120	1456	36
LMI	Melt inclusion										
	Groundmass glass	1540	1960	2336	623	9	306	784	1290	582	9
VFI	Melt inclusion	2015	2679	4881	833	63	633	1575	2388	713	63
	Groundmass glass	220	1460	2830	2604	6	560	800	1000	445	3
CCI	Melt inclusion	1662	3552	6850	3249	16	624	1760	3142	1482	13
	Groundmass glass	1160	2678	3720	2175	13	190	1728	3960	2049	13
PNI	Melt inclusion	913	2266	3619	n/a	2	1222	2094	2965	n/a	2
	Groundmass glass	341	1455	2264	1274	10	249	725	1420	952	8
GVI	Melt inclusion	n/a	3673	n/a	n/a	1	n/a	2150	n/a	n/a	1
	Groundmass glass	227	2223	3371	703	9	1700	2031	2608	531	9
Ign-i	Melt inclusion	6398	6641	6959	576	3	2611	3673	4751	2140	3
	Groundmass glass										

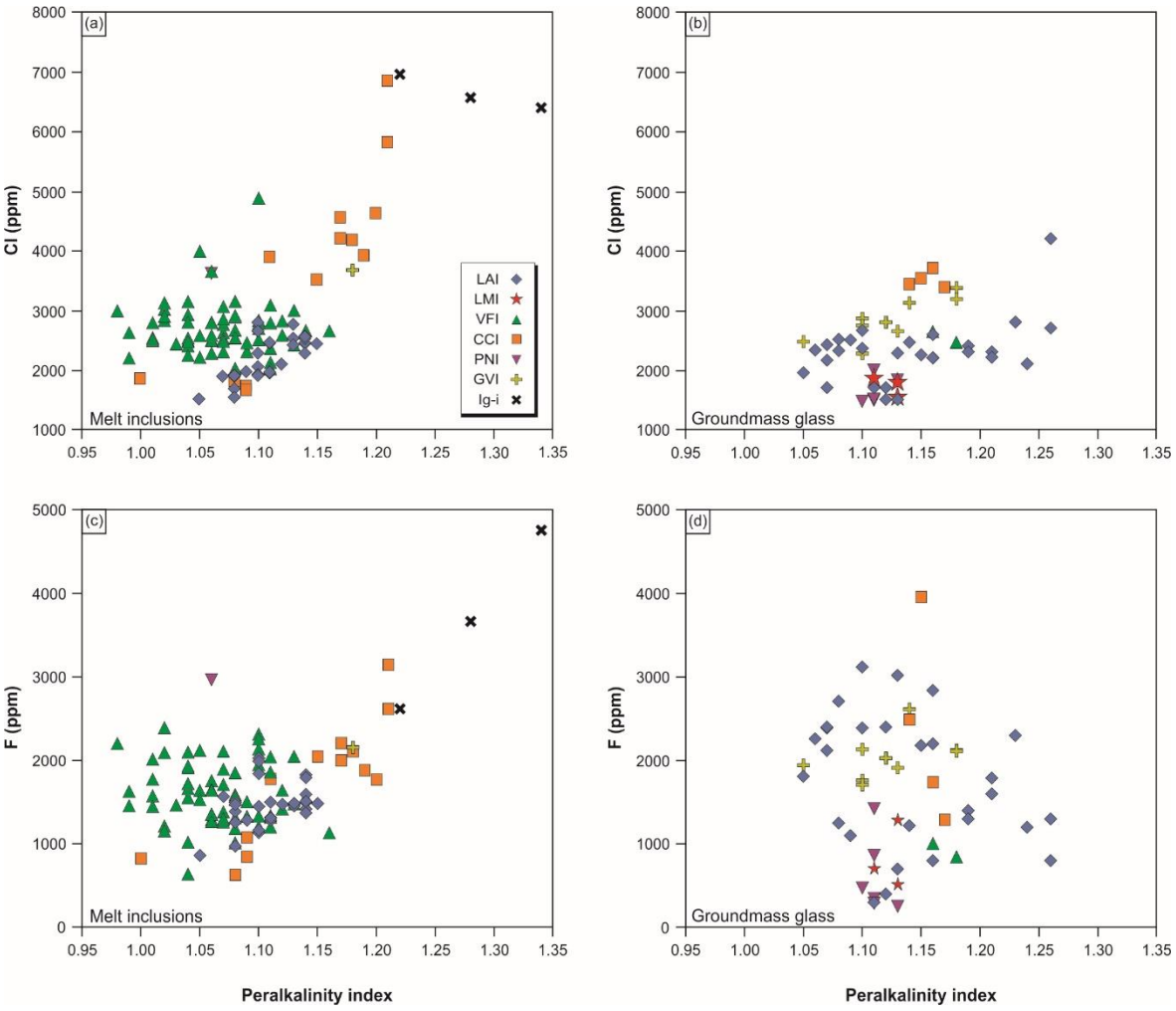

FIGURE 4.42: Variations in halogen concentration of melt inclusions and groundmass glass plotted against peralkalinity indices

agriculture (e.g. Cronin *et al.* 2003). The comparison of volatile concentrations recorded by melt inclusions and groundmass glass allows some constraints to be placed upon the degassing behaviour of the halogens (Table 4.16). For example, the average Cl and F contents of groundmass glass from the LAI and CCI lie within the calculated 2-sigma standard deviations of melt inclusion concentrations from the respective formations, suggesting that neither element was degassed during eruption (cf. Urabe, 1985; Shinohara, 1991; Lowenstern, 1994; Neave *et al.*, 2012). In contrast, both Cl and F concentrations of the VFI groundmass glass lie below the 2-sigma limits of the melt inclusions (by 400 and 62 ppm, respectively), suggesting that they have been degassed to a limited extent. Available data for the older ignimbrite formations is less conclusive, but

highlights variable behaviour. For example, the average Cl concentration of PNI melt inclusions is 2,266 ppm, whilst that of the groundmass glass is only 1,455 ppm. Similarly, average F contents of the melt inclusions are 2,094, whilst average groundmass glass contents are only 725, suggesting that they may have degassed.

4.6.4 Near solidus processes

The syenitic ejecta found within the CCI have been shown to represent bulk solidification of trachytic magmas similar to those erupted in each of the ignimbrite-forming phases of Pico Alto. As such, their phase assemblages and textures provide insights into the final stages of evolution of the silica-oversaturated, peralkaline silicic magmas of Terceira. Here, the observed textural relationships between various phases within the syenites, as well as the occurrence of the rare zirconosilicate mineral dalyite, are considered in terms of their implications for this low temperature, magmatic to hydrothermal transition period.

4.6.4.1 Syenite phase assemblages and reactions

There are a variety of textures within the syenitic ejecta which may provide insights into varying T-fO_2-X conditions during the final stages of crystallisation. For example, the occurrence of phases such as Na-clinopyroxene, Na-amphibole, and aenigmatite, within the syenite ejecta and not in the erupted trachytes indicates that the trachytes were stored at temperatures sufficiently high to preclude the crystallisation of these phases. This study recognises three distinct evolutionary phases in the development of the syenites: (1) an initial magmatic phase in which crystallisation is dominated by alkali feldspar, as observed in the trachytes, (2) a late stage magmatic phase in which continued cooling and differentiation has driven residual melts to high peralkalinity (e.g. PI > 1.4), leading to the crystallisation of aenigmatite, aegirine-augite/aegirine, and Na-amphibole of varying composition, and (3) a transitional phase between late-stage magmatic and hydrothermal,

in which quartz, and rare zirconsiliciate phases such as dalyite and eudialyte form within intercumulus void spaces.

The first of these phases is considered to be represented by the alkali feldspar cumulus network exhibited ubiquitously by the syenite ejecta. The second phase is envisaged to occur when the peralkalinity of the residual liquid reaches values in excess of ~ 1.25, allowing the crystallisation of aenigmatite (cf. Di Carlo *et al.*, 2010; Macdonald *et al.*, 2011). The crystallisation of aenigmatite is controlled by T-P-fO_2-$aSiO_2$ conditions, and so its occurrence cannot be used to directly determine any one of these variables, and the pressure conditions under which it is stable are poorly understood (e.g. Scaillet and Macdonald, 2001; Di Carlo *et al.*, 2010). However, its occurrence is broadly consistent with the low temperatures (Marsh, 1975) and relatively reducing conditions (Kunzmann, 1999) estimated for the Pico Alto magma plumbing system. The crystallisation of amphibole and clinopyroxene during this phase is considered to begin with Na-Ca amphiboles and aegirine augite. As the peralkalinity of the residual melt increases, the Na content of the amphiboles increases (Di Carlo *et al.*, 2010), yielding the zoning observed patterns from Na-Ca group to Na-group amphiboles. This may also apply to the patchy zonation observed in Na-clinopyroxenes (Larsen, 1976; Nyonfang and Nono, 2003). The crystallisation of these phases is likely to reduce the oxygen fugacity further, as suggested by two-oxide estimates which extend to around two log units below FMQ.

The third and final evolutionary stage is considered to lead to the crystallisation of quartz, dalyite, eudialyte, Na-amphibole, and acicular, Ti-rich aegirine within the remaining intercumulus void spaces. This stage may be associated with an increase in oxygen fugacity, which stabilises aegirine and destabilises aenigmatite, resulting in the breakdown of aenigmatite to radial clusters of acicular, Ti-rich aegirine. This is consistent with proposed fO_2 evolutionary paths proposed for agpaitic nepheline syenites from the Ilímaussaq Intrusion, South Greenland, where a pronounced increase in fO_2 has been proposed during the final stages of crystallisation (< 750 ˚C; Markl *et al.*, 2001). Based upon the T-fO_2 evolution diagram of Schönenberger *et al.* (2006), an increase of more

than 3 log units (reaching values in excess of FMQ +1) is required to inititate the observed breakdown of aenigmatite. Numerous examples of aegirine with relict, Na-amphibole cores imply that this replacement reaction may also extend to the amphiboles. Furthermore, rare olivines with distinctive Fe-Ti oxide-rich breakdown rims likely reflect an increase in oxygen fugacity, leading to oxidation of Fe^{2+}. The final residual silicate melt is envisaged to be extremely peralkaline, and enriched in HFSE and REE, and is likely to be represented by thin films of intercumulus glass analysed by Mungall (1993). This melt is considered to be sufficiently extreme to allow crystallisation of dalyite and eudialyte, as well as aegirine.

4.6.4.2 Dalyite compositional variation

To facilitate a wider discussion of the compositional variability of dalyite, all available analyses are divided into two groups: 1) those found within peralkaline syenitic or granitic rocks and 2) those found within other lithologies, including lamproites, lamprophyres and charoitites. As such, the dalyite analyses from Terceira, São Miguel, Ascension, Straumsvola, Strange Lake and Gordon Butte are included in group 1, whereas analyses from Sunnfjord, Murun and Cancarix occupy group 2. All analyses were tested for quality using the following criteria: a) analysis total = 100 wt. % ± 1.5, b) total cations = < 9.05 apfu, c) cation total for the tetrahedral site = 6 apfu ± 0.05, d) cation total for the octahedral site = 1 apfu ± 0.05. Only those analyses which passed all four criteria were applied to the following discussion, reducing the size of dataset from 43 to 25 analyses.

The overall average calculated K_{alk} for the combined dataset is 21.94, with minimum and maximum values of 20.90 and 22.51, respectively. This shows essentially no variation between groups 1 and 2, with average values of 21.98 and 21.91, respectively. Figure 4.43a shows the available dalyite analyses in K–Na space. The data typically lie within 0.05 apfu of the one-to-one line, indicating the role of one-to-one K↔Na substitution within the polyhedral sites. Group 1 analyses are characterised by a relative

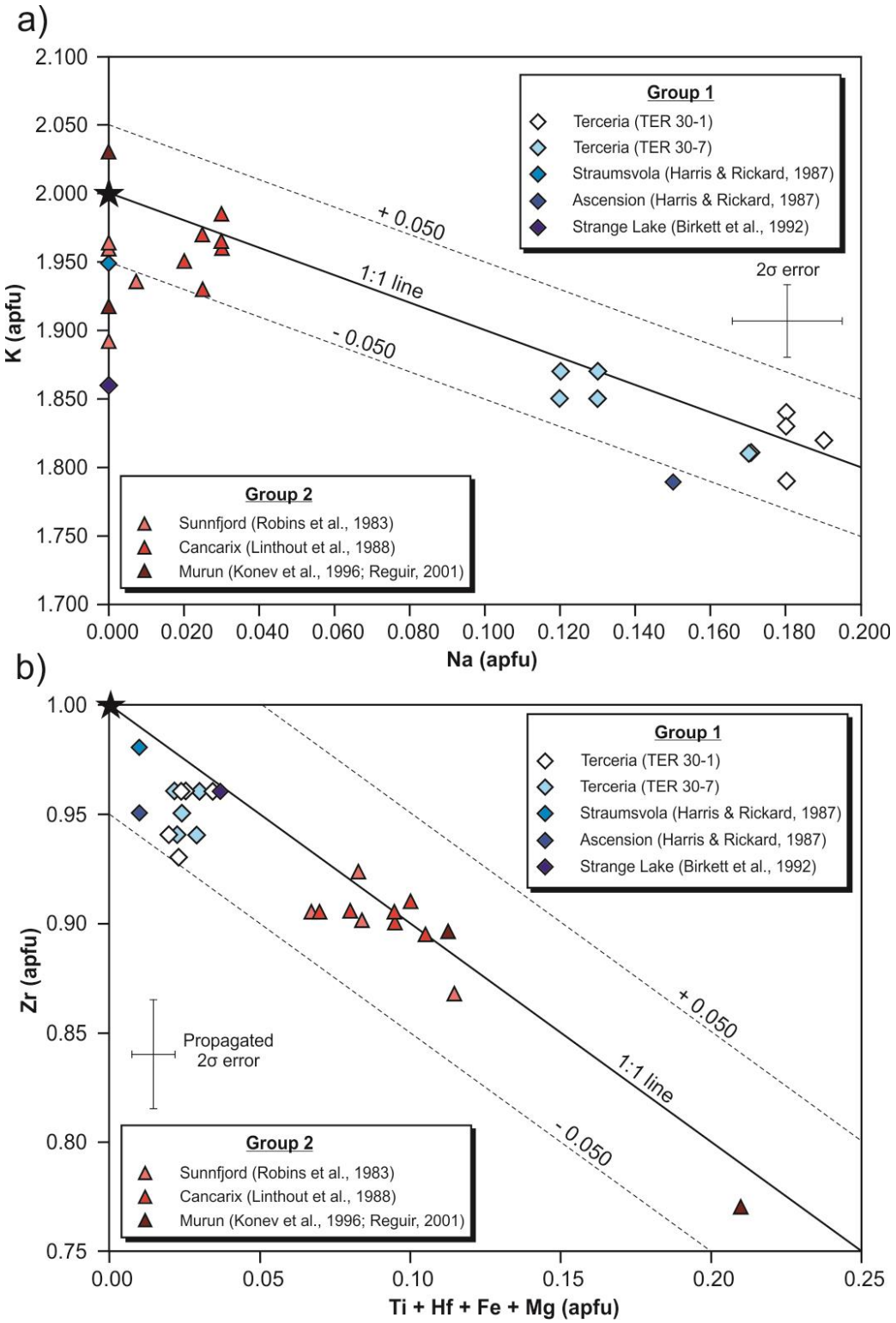

FIGURE 4.43: Geochemical variation diagrams highlighting the variable degree of substitution within the dataset. The ideal composition of dalyite is highlighted with a black star symbol. The maximum error is applicable to the new data for Terceira (TER 30-1 and TER 30-7) only and is calculated as described in the text. Group 1 dalyite is denoted by diamonds, group 2 by triangles. Only analyses that passed all of the filtering criteria described in the text are shown **a)** Bivariate plot showing the degree of K↔Na substitution in the dataset. **b)** Bivariate plot showing the degree of substitution in the octahedral site. Data for Hf, Mg and Fe is presented where analyses permit

abundance of Na (0.12 to 0.19 apfu) and a corresponding paucity of K (1.79 to 1.87 apfu), though two analyses from Straumsvola and Strange Lake (analyses 3 & 4, Table 4.6) exhibit Na concentrations below the detection limit, alongside a slight deficiency in K. This discrepancy in older dalyite analyses may indicate Na loss during analysis, as suggested by Birkett *et al.* (1992). The dalyite from Strange Lake may also have been subject to alteration, as it is described as being frequently rimmed by elpidite or vlasovite.

In contrast to group 1, group 2 analyses are closer to the ideal dalyite formula, with significantly lower concentrations of Na (< 0.015 to 0.03 apfu). The relatively sodic nature of group 1 and potassic nature of group 2 dalyite correlates with the relatively sodic nature of the group 1 rocks and the generally potassic nature of group 2 rocks. For example, reported whole rock Na_2O/K_2O ratios of group 1 typically lie between 1 and 1.5 (Harris and Rickard, 1987; Ridolfi *et al.*, 2003). In contrast, group 2 whole rock Na_2O/K_2O is likely to be significantly lower, given their often highly potassic nature, as is the case for the Cancarix dalyite (Na_2O/K_2O = 0.1, Linthout *et al.*, 1988; Salvioli-Mariani & Venturelli, 1996). Harris & Rickard (1987) made a similar observation, noting that the dalyite analyses from Sunnfjord (analyses 16 to 25, Table 4.6) exhibit lower Na contents than dalyite from Ascension Island (analysis 2, Table 4.6), which they attributed to the higher Na_2O/K_2O ratio of the latter. However, they also noted that Straumsvola dalyite (analysis 3, Table 4.6) has essentially no Na, despite a highly comparable Na_2O/K_2O ratio to that of group 1 samples (1.35).

Another potential control that must be considered is the crystallisation mechanism of each example, which must also play a role in the composition of dalyite. For example, the dalyite-bearing, ultrapotassic Sunnfjord dyke is reported to be heavily hydrothermally-altered (Furnes *et al.*, 1982), suggesting that any dalyite present may be metasomatic in origin, or a magmatic composition that has been altered by metasomatism. It can be seen in Table 4.6 that those analyses which may have been influenced by metasomatism (e.g. Sunnfjord, Murun) frequently exhibit Na contents below detection. However, although the Straumsvola analysis (itself an average of three analyses) contains no significant Na, the

peralkaline granite host rock is described as being very fresh (Harris & Rickard, 1987), and so the reported Na-poor dalyite cannot be attributed entirely to the effects of crystallisation mechanism or alteration.

The degree of substitution within the octahedral sites is highlighted in Figure 4.43b. Ti and Hf are considered as the most suitable substitutes, though the R^{2+} cations Mg, Mn and Fe are also considered (where data is available), due to the similarity of their ionic radii with Zr. The data plot within 0.05 apfu of the one-to-one line, indicating one-to-one cation exchange. In the case of Fe, Mn and Mg, this would introduce a charge imbalance which can be mitigated by a single oxygen vacancy. Although solid-state modelling suggests that R^{2+}↔K substitution should be energetically favourable, the calculated E_{sol} values are still too large (8.86 eV & 9.61 eV), and the difference in ionic radii too great, to fully justify the placement of R^{2+} cations in the polyhedral sites. The substitutions of Hf↔Zr and Ti↔Zr are both supported by solid-state modelling (E_{sol} = -0.31 eV & -0.25 eV, respectively, though in the latter case, the modelling also indicates the potential of Ti↔Si substitution (E_{sol} = -0.98 eV). However, there is no evidence within the dataset to support such a substitution.

Group 1 analyses remain close to the ideal dalyite formula, with 0.91 to 0.98 apfu Zr. Group 2 analyses exhibit a greater degree of substitution, generally clustering between 0.85 and 0.94 apfu Zr, with 0.05 to 0.12 apfu Ti. It is notable that one of the two analyses from the charoitites of the Murun Complex is enriched in the davanite component ($K_2TiSi_6O_{15}$), with 0.21 apfu Ti. This may relate to the unusual nature of their charoititic host rock, which is typically considered to be metasomatic rather than magmatic in origin (e.g. Reguir, 2001 and references therein). This alternative origin may explain the apparent geochemical deviation from the rest of the dataset.

The dataset indicates the presence of small amounts of Ba within Group 2 dalyite. On the basis of solid-state modelling and ionic radii, it is suggested that the most likely mechanism for its inclusion within the dalyite structure is Ba↔K. The resulting charge imbalance could be mitigated by a single vacancy in the polyhedral site, in which case the

Ba content may be used as a proxy for the polyhedral vacancies in each analysis (up to 0.02 apfu). This may, in part, account for analyses in which the structural total is less than the ideal 9 apfu. Alternatively, structural deficits may result from the presence of Li. Significant concentrations of Li have been reported in peralkaline rocks and Li-enrichment can occur via metasomatic processes (e.g. Borley, 1963; Hawthorne *et al.*, 1996; Brenan *et al.*, 1998; Hawthorne *et al.*, 2001; Marks *et al.*, 2008). Although the mechanisms of Li-substitution in dalyite are unclear, its inclusion may contribute to the frequently low structural totals observed within the dataset.

The key geochemical parameters required to stabilise dalyite are high μK_2O and high $aSiO_2$ (Marks *et al.*, 2011). For example, an insufficiently high silica activity will lead to the crystallisation of wadeite ($K_2ZrSi_3O_9$) in place of dalyite (Marks *et al.*, 2011). Dalyite is therefore limited to silica-saturated to –oversaturated lithologies, although its occurrence in a nepheline-bearing pegmatite from Langesundfjord, Norway (Andersen *et al.*, 2010) appears to contradict this. The additional requirement of high μK_2O is likely due to high K_2O contents in the melts, achieved either by slowly increasing K_2O via fractional crystallisation and/or crustal assimilation of potassic rocks in the group 1 samples, or by producing melts with initially high K_2O values via the more unusual processes suggested to produce ultrapotassic rocks, such as partial melting of metasomatised mantle lithologies, (e.g. Mitchell & Bergman, 1991).

The geochemical variations observed between the groups of this study are likely to represent major element variations in the melts themselves. For example, the group 2 dalyites generally show elevated Ti and Fe contents relative to the group 1 dalyites, which may relate to the relatively Ti- and Fe-rich whole rock compositions of lamproites and lamprophyres, particularly when compared to the low Ti contents of group 1 whole rock analyses (< 0.7 wt. %). Additionally, group 2 analyses exhibit significantly lower degrees of Na substituting for K, which might be expected given the K_2O-rich nature of their whole rock analyses.

4.6.4.3 Dalyite crystallisation on Terceira

Dalyite is generally considered to be a late-stage, magmatic mineral phase (e.g. Harris & Rickard, 1987; Ridolfi *et al.*, 2003) that may be altered, either during later magmatic or sub-solidus stages, to minerals such as elpidite, $Na_2ZrSi_6O_{15}\cdot 3(H_2O)$ (Cann, 1967), catapleiite, $Na_2Zr(Si_3O_9)\cdot 2H_2O$ (Birkett *et al.*, 1992; Chakhmouradian & Mitchell, 2002) and intergrown quartz and zircon (Cann, 1967). Key features of the Terceira dalyite, notably the dominantly anhedral crystal forms, its restricted occurrence in interstitial pore spaces and its lack of inclusion within other mineral phases, all point towards late-stage, post-cumulus, magmatic crystallisation, though extension of the crystallisation interval into the sub-solidus deuteric stage cannot be ruled out. Evidence for the alteration of primary dalyite compositions is lacking. Its textural association and occasional intergrowth with quartz suggests that the crystallisation of these two phases was largely contemporaneous. This conclusion is in agreement with that of Ridolfi *et al.* (2003), who studied similar parageneses in syenite nodules erupted by Fogo volcano, São Miguel, Azores.

The dalyite analyses from Terceira display two clusters in Na-K space (Fig. 4.42a), with one cluster of more sodic compositions (0.17 to 0.19 Na apfu), and another cluster of more potassic compositions (0.12 to 0.13 Na apfu). The difference between these clusters cannot be entirely accounted for by the calculated two-sigma errors of ±0.015 apfu, and is considered to represent bimodality in the dataset. Both clusters lie within 0.05 apfu of the one-to-one line and, as such, the trend of the data likely highlights the role of varying degrees of one-to-one Na↔K substitution within the Terceira samples. The presence of two subgroups may imply that two separate populations of dalyite are present, either derived from multiple processes that each led to the crystallisation of compositionally distinct dalyite, or a single process that is capable of producing a heterogeneous dalyite population. No visible correlation exists between dalyite composition and textural features such as crystal form or size, or the degree to which they infill pores. Instead, the two

clusters of dalyite analyses can be related to the two separate samples in which dalyite was analysed (TER-30-1 and TER 30-7), with the most sodic dalyite analyses being from TER 30-1. The compositional variations may therefore reflect random sampling of a syenitic mush in which geochemical heterogeneity is sufficiently large in scale that it yields 'inter-nodule' variations in dalyite composition, whilst 'intra-nodule' variations are more limited. Such heterogeneity may be primary (i.e. derived from original compositional variations in the melt, perhaps originating from multiple magma batches that contributed to a single crystal mush body), or secondary, originating from the variable degree of fluid-feldspar reaction (albitisation; e.g. Lee and Parsons, 1997) in the crystal mush during deuteric alteration. The late stage albitisation of the rock would lead to a bulk rock increase in Na and an enrichment of K in the albitizing fluids. The prevalence of coarse patchy perthitic feldspars in the Terceira syenites provides evidence for the prominent role of albitisation in their late stage evolution. Evidence for primary bulk compositions being the underlying control upon dalyite composition exists in the bimodality of the dataset, with the most sodic dalyites found in the most sodic whole rock analysis.

However, a single analysis from sample TER 30-7 falls within the cluster of TER 30-1 analyses (Fig. 4.42a, Table 4.5), indicating that a simple relationship between dalyite chemistry and bulk rock composition cannot entirely account for the observed variation. As such, alternative processes that might influence the degree of Na↔K substitution are explored. One example that is considered here is the role of variable pore size in the compositional evolution of interstitial melts. Because heterogeneous nucleation is energetically favourable compared to homogenous nucleation, the dominant process that drives the compositional evolution of a melt within a pore under closed system conditions is the crystallisation of surrounding cumulus phases, as components that are incompatible in the pore wall minerals become enriched in the residual melt. In the Terceira syenite nodules, alkali-feldspar is the most abundant phase, and surrounds the majority of pore spaces, suggesting that the post-cumulus, heterogeneous nucleation of feldspar onto pore walls will exert the strongest influence upon interstitial melt compositions. Due to its albite-

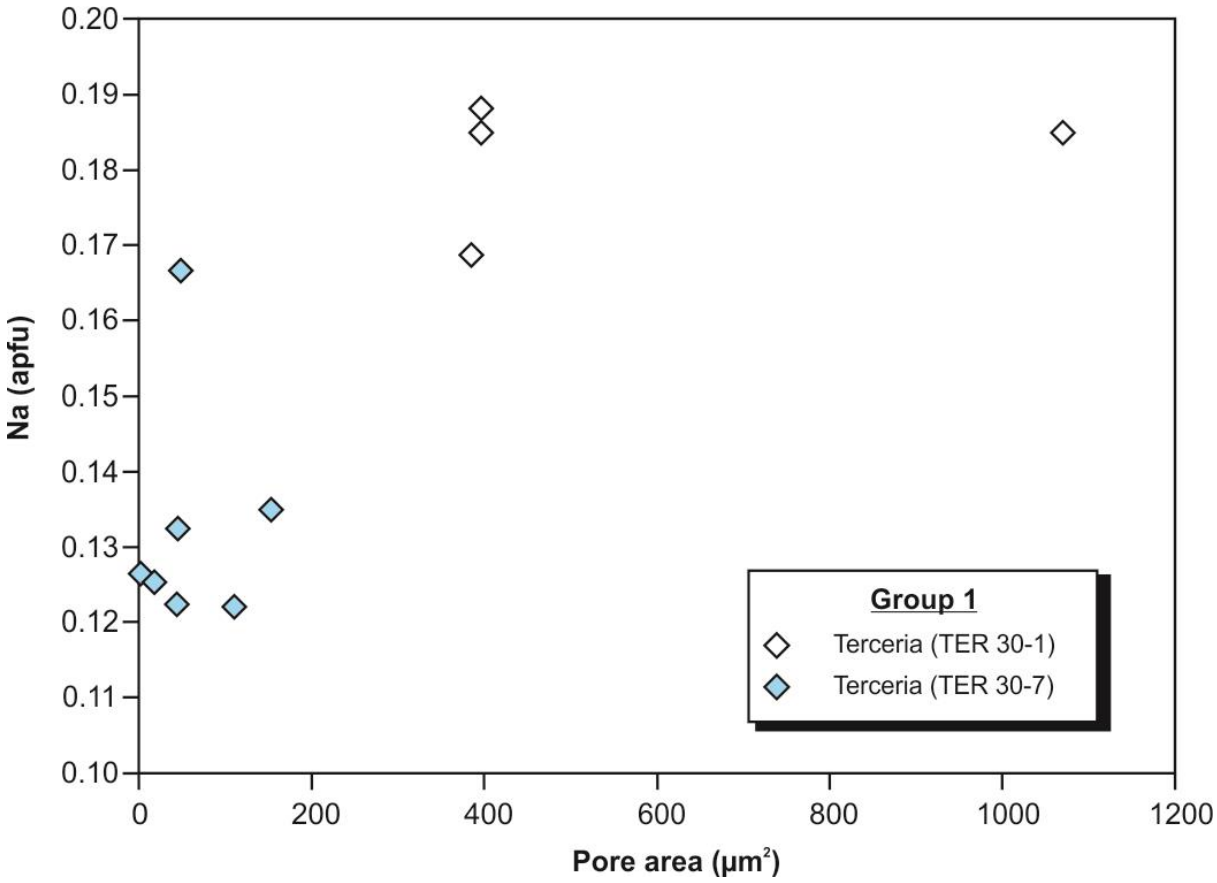

FIGURE 4.44: Bivariate plot of measured pore area against the Na content of dalyite within the pore

rich composition (~ Ab_{64}, average Na/K = 1.67), this effect is likely to promote the development of depressed Na/K ratios in the liquid as evolution continues. Petrographic evidence for this process exists in the form of optically distinguishable rims on many of the pore-wall feldspars (e.g. Fig. 4.19a). During the sub-solidus deuteric stage, albitisation also contributes to the depression of liquid Na/K ratios via the replacement of alkali feldspar with near end member albite. Thus, it is suggested that during the late stage magmatic and sub-solidus deuteric evolution of the syenite, the majority of liquid-filled pores were evolving towards more potassic compositions.

It is proposed that the observed variation in Terceira dalyite composition could be related to the timing of crystallisation relative to the evolution of the interstitial melt. The thermodynamics of crystallisation in pore spaces has been shown to be fundamentally different compared to a free fluid (Bigg, 1953; Melia and Moffitt, 1964; Putnis *et al.*, 1995; Scherer, 1999). In particular, a fluid confined to a pore space can achieve greater degrees

of supersaturation prior to the onset of crystallisation compared with an unconfined fluid, thus introducing a nucleation delay that is more substantial in smaller pores (e.g. Putnis and Mauthe, 2001; Holness *et al.*, 2007; Holness and Sawyer, 2008). As such, the dalyite crystals that grew in smaller pores would have nucleated later than those in larger pores, and would record more evolved compositions. Holness and Sawyer (2008) also cited the prevalence of single-grain pseudomorphs in small pores and poly-mineralic aggregate pseudomorphs in larger pores as petrographic evidence for the relative ease of nucleation in larger pores. This feature can also be observed in the CCI syenite, where larger pores are frequently filled with aggregates of late-crystallising phases such as quartz, clinopyroxene, dalyite, and eudialyte (Figure 4.19d), whilst small pores generally contain only a single crystal of one of these phases (Figure 4.19b).

Considering the previously described evolutionary trend of relative K-enrichment during both late stage magmatic and sub-solidus stages, dalyite in smaller pores should therefore have more potassic (and therefore less sodic) compositions. To test this hypothesis, dalyite-bearing pore spaces were digitised and measured using ImageJ to determine the two-dimensional area. This was then plotted against the Na content of the dalyite crystal within them (Figure 4.44), yielding a positive correlation that suggests that the size of a pore exerts, at least to some extent, a control over the composition of the dalyite crystallising within it.

A single data point in Figure 4.44 appears to deviate from the broadly linear trend observed in the rest of the data (pore area = 1.07 mm^2, Na content = 0.18). Unlike other reported dalyites, this dalyite crystal is found in a pore that is bounded by a large clinopyroxene crystal, in addition to alkali-feldspar. It is therefore suggested that this deviation in pore size vs. Na content space may highlight the influence of other minerals in the evolution of interstitial melts. Given the relatively high Na contents and negligible K contents of the Terceira clinopyroxene (Na/K = 6 to 2584), the pore wall crystallisation of clinopyroxene would greatly accelerate the described evolutionary trend of K-enrichment in interstitial melt, leading to dalyite compositions that appear unusually K-rich when

compared with the suggested feldspar-controlled trend (Figure 4.44). The pore wall crystallisation of amphibole would also produce this effect but to a lesser degree (Na/K = 5.7 to 8.9).

In summary, it is suggested that the dalyite from Terceira is predominantly late-stage magmatic in origin, and the observed compositional variability is influenced by the K-enrichment (and relative Na-depletion) trend of late stage interstitial melt resulting from pore wall crystallisation of sodic alkali feldspar. Any continued crystallisation during a sub-solidus deuteric stage is considered to have been subject to a similar K-enrichment trend, driven by albitisation of alkali feldspar. Variation in Na content is likely to have been controlled, at least in part, by the larger nucleation delay that is introduced in smaller pores compared to larger ones, with early-forming dalyite having more sodic compositions, and late-forming dalyite having less sodic (and therefore more potassic) compositions.

4.6.5 The magma plumbing system

4.6.5.1 The implications of viscosity for differentaition

Viscosity is of first order importance for both the evolution and eruption of magmas, and is controlled by magma temperature, composition, and the abundance of volatile components (H_2O, CO_2, S, F, Cl) (Shaw, 1972; Dingwell *et al.*, 1996; Dingwell and Hess, 1998). To estimate the pre-eruptive viscosity of the ignimbrite-forming trachytes, the model of Giordano *et al.* (2006) was used, as this model has been calibrated for a wide range of magma compositions and has been shown by recent experimental work to be able to reproduce magma viscosity to within < 0.2 log units (Vona *et al.*, 2011). The minimum and maximum temperature and H_2O_{melt} estimates, and the average composition of each ignimbrite were applied as input variables. The total range of crystal free viscosity estimates range from $10^{3.1}$ to $10^{4.0}$ Pa s. These values were converted into magma viscosities using the method of Dingwell *et al.* (1993):

$$\eta_{magma} = \eta_{melt}(1 + 0.75((f/f_m)/(1-f/f_m)))^2 \quad (4.1)$$

where η_{magma} and η_{melt} are the viscosities of magma and melt, respectively, f is the volume fraction of crystals, and f_m is the concentration of crystal required to achieve an 'infinite' viscosity. The latter value was set to 0.6, following Andújar and Scaillet (2012), whilst the volume fraction of crystals was set to values between 0 and 0.2, in accordance with petrographic observations (cf. Self, 1971; Gertisser *et al.*, 2010). Results exhibit a total range of viscosities extending from $10^{3.1}$ (aphyric, high water) to $10^{4.3}$ Pa s (20 % crystallinity, low water), and indicate that the pre-eruptive viscosities of the ignimbrite-forming trachytes were relatively low, extending to values more than 1 order of magnitude less than is typical for metaluminous silicic melts (~ $10^{4.5}$ Pa s, Scaillet *et al.,* 1998). This observation has significant implications not only for eruptive behaviour (cf. Andújar and Scaillet, 2012), but also for the dominant mechanism of differentiation within the trachytes. Due to the difficulties of two-phase flow in relatively cool, high viscosity magmas, the generation of crystal poor silicic magmas is frequently attributed to the extraction of interstitial melt from a crystal mush via processes such as compaction, hindered settling, micro-settling, and gas-driven filter pressing (Sisson and Bacon 1999; Bachmann and Bergantz 2004; Hildreth 2004; Pistone *et al.*, 2015). However, the application of such models to peralkaline systems is hindered by the reduced viscosities associated with peralkalinity, which may allow efficient fractionation via crystal settling (Macdonald, 2012; Marks and Markl, 2015 and references therein), and the apparent absence of erupted crystal-rich magmas typically termed monotonous intermediates (Hildreth, 1981). As such, the efficiency of two-phase flow in the pre-eruptive magma system of the Terceira ignimbrites was evaluated via the calculation of Stokes' settling velocities for alkali feldspar crystals, supplemented by the hindered settling equation, which allows the estimation of settling rates in polydispersed suspensions (Bachmann and Bergantz, 2004):

$$U_{hs} = U_{Stokes} \times f(c) \quad (4.2)$$

where U_{hs} is the hindered settling velocity, U_{Stokes} is Stokes settling velocity, and f(c) is a correction factor calculated as:

$$f(c) = \frac{(1 - c)^2}{(1 + c^{1/3})^{\left[\frac{5c}{3(1-c)}\right]}} \quad (4.3)$$

where c is equal to the crystal fraction. Crystal sizes were set to 2 mm, in accordance with petrographic observations. Melt densities were set to 2250 kg/m^3, based upon the typical densities predicted by Rhyolite-MELTs. Results indicate that the alkali feldspars in the highest viscosity trachytes are capable of settling at rates of between 1.99 (unhindered) and 0.39 m a^{-1} (hindered settling, 40 % crystallinity), whilst those of the lowest viscosity trachytes reach rates of between 19.00 (unhindered) and 3.78 m a^{-1} (hindered settling, 40 % crystallinity). These estimates suggest that, unlike typical rhyolites (where calculated settling rates are unlikely to exceed ~ 0.67 m a^{-1}, assuming unhindered settling and melt viscosity of $10^{4.5}$ Pa s), the peralkaline ignimbrite-forming trachytic magmas of Terceira may still be able to differentiate efficiently via fractional crystallisation and crystal settling, as suggested at Furnas.

4.6.5.2 Zoned magma bodies

Despite their major element homogeneity, the ignimbrites of Terceira exhibit substantial internal trace element variations (e.g. ~ 900 to ~ 1,350 ppm Zr in the CCI; Gertisser *et al.*, 2010). A minor basal pumice fall of the VFI exhibits an even more extreme compositional variation when compared to the overlying ignimbrite flow units (~ 2,250 ppm Zr compared to ~ 700 ppm, respectively). On the basis of the trace element RFC models presented in this study, this reflects up to ~ 15 % fractionation. These phenomena are typically

considered to originate from the eruption of a zoned magma body (e.g. Hildreth, 1981), assuming that the zoning patterns have not been altered by syn-eruptive conduit processes. It is therefore suggested that the pre-eruptive magma reservoir from which the ignimbrite-forming eruptions were fed was often zoned gradationally, with the most evolved and most volatile rich trachyte overlying progressively less evolved trachytes. A similar trace element profile may be observed in the CCI, where juvenile pumice clasts from the basal pumice fall and surge deposits exhibit incompatible element enrichment compared to the overlying ignimbrite (e.g. ~ 1,000 vs. ~ 650 ppm Zr). However, in this instance a number of analyses from the ignimbrite at various locations record incompatible enrichments that are even greater than the basal deposits, suggesting a more complex situation, such as the tapping of multiple magma bodies (e.g. Cooper *et al.* 2012; Zanon *et al.* 2013; Pimentel *et al.*, 2015). The preservation of this zonation until eruption indicates that convection is not sufficient to enable the reservoirs to homogenise. One exception to this observation is the LMI, where available data indicate a more restricted range of incompatible trace elements (~ 760 to ~ 910 ppm Zr). The LMI exhibits abundant evidence for having been mixed with a hotter, less differentiated magma prior to eruption (e.g. presence of resorbed antecrysts, high pre-eruptive temperatures, mixing trend with hawaiitic compositions). The rather limited chemical zonation of the LMI may therefore reflect a homogenisation event, in which an influx of hotter magma initiated large scale convection within the reservoir, and possibly triggered an eruption shortly afterwards.

4.6.5.3 A model for the magma system

Based upon the topics discussed above, this section presents a conceptual model for the magma plumbing system from which the ignimbrite-forming episodes of Terceira were fed (Figure 4.45). Based upon the results of thermodynamic modelling and water solubility, the presence of a magma storage zone at shallow crustal depths (~ 2.2 to 3.7 km is

inferred, assuming a crustal density of 2,800 km/m^3). This is consistent with the low concentrations of S and CO_2 in melt inclusions. At least the upper portion of this zone is considered to be exclusively trachytic in composition, based upon the entirely trachytic compositions of alkali feldspar-hosted melt inclusions. The most applicable Rhyolite-MELTs model included a polybaric regime in which basaltic magmas undergo an initial fractionation period towards hawaiitic compositions at high pressures (~ 500 MPa), equivalent to the lower crust (~ 14 km). It is therefore suggested that ascending mantle-derived basalts are likely to stall in the lower crust and differentiate to hawaiitic compositions via fractional crystallisation of a clinopyroxene-dominated assemblage, before ascending further and stalling in the lower portion of the shallow crustal zone. Based upon the mixed crystal populations found in syenite-hosted trachytic enclaves, the hawaiites are inferred to be introduced to the dominantly trachytic magmas of the shallow crustal system in a mixing zone in the lower regions of the shallow system. Here, they are envisaged to mingle and mix with large volumes of trachytes, generating hybridised trachytes represented by the syenite-hosted enclaves, with multiple phase assemblages: (1) anorthoclase, (2) diopside + forsterite + bytownite, and (3) oligoclase + augite. Based upon the overwhelming abundance of anorthoclase in the ignimbrite-forming trachytes, the first assemblage is considered to be representative of the trachytes and is therefore the true phenocryst assemblage of the upper system. The second assemblage is the phenocryst assemblage of the ascending hawaiites introduced during mixing. This is consistent with the high Al_2O_3 and TiO_2 contents of the diopside phenocrysts, which indicate high pressure crystallisation (Figure 4.35). Due to the adherence of augite phenocrysts to the low-pressure trend, the third assemblage is incompatible with the ascending hawaiites, and must therefore be attributed to the shallow magma storage zone. However, oligoclase is rare in the ignimbrites and is frequently heavily resorbed. Furthermore, the augite population of the ignimbrites is not in equilibrium with the host trachyte, and Rhyolite-MELTs and mass balance models predict little to no clinopyroxene crystallisation at trachytic compositions. Furthermore, the more sodic clinopyroxene found

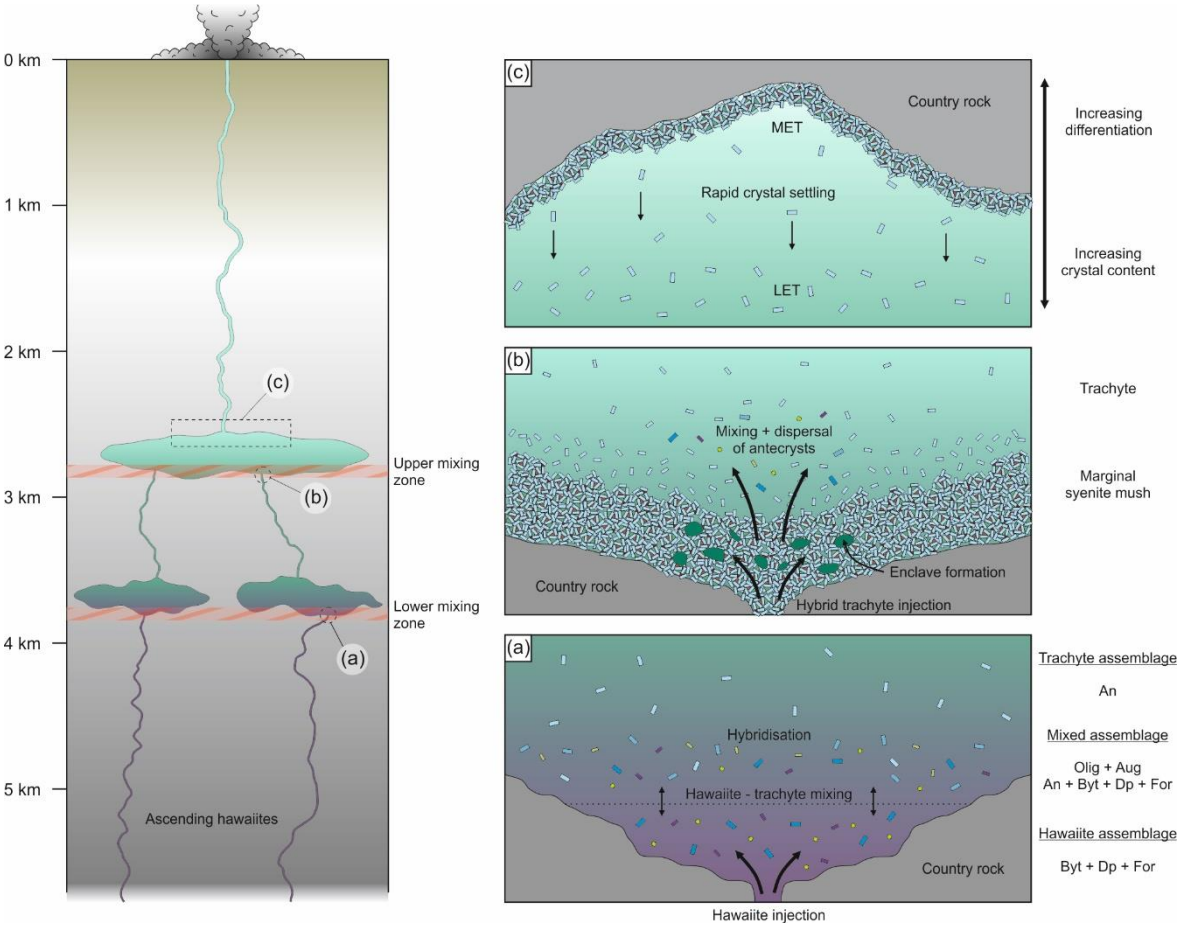

FIGURE 4.44: Conceptual model for the magma plumbing system of the Pico Alto Volcanic Complex, comprising a prominent magma storage zone in the shallow crust. Abbreviations used: Byt = bytownite, Dp = diopside, For = forsterite, An = anorthoclase, Olig = oligoclase, Aug = augite (a) Ascending hawaiites (phase assemblage = Byt + Dp + For) are mixed with trachytes (phase assemblage = An), forming hybridised intermediate to silicic magmas (phase assemblage = Olig + Aug + An + Byt + Dp + For) (b) Injection of hybridised trachyte into peralkaline trachyte in the uppermost portion of the shallow crustal storage zone, passing through a marginal syenitic crystal mush and forming enclaves therein. Replenishment initiates further mixing and introduces antecrysts to the eruptible portion of the reservoir (c) Efficient crystal settling in the uppermost eruptible cap of peralkaline trachyte generates crystal poor magma and chemical zoning

in the syenitic ejecta and the groundmass of the syenite-hosted enclaves clearly indicates its formation at temperatures lower than those of the trachytes (< 800 °C). The oligoclase and augite observed in the enclave magmas are therefore considered to represent an assemblage derived from the benmoreitic to LET hybrid magmas resulting from the mixing of relatively small proportions of hawaiite with trachyte. The hybridised trachytes may then ascend further, out of the lower mixing zone and into the upper regions of the shallow magma storage zone, where the most differentiated magmas are inferred to be present. Based upon their mineral assemblages and calculated viscosities, differentiation of these

trachytic magmas is likely to be controlled by the crystallisation and rapid fractionation (via crystal-settling) of anorthoclase, driving the melt towards MET compositions. Compositional zonation of these magma bodies is likely to result, as the lower density, more evolved liquids migrate upwards to form a lens of low viscosity, hydrous, crystal-poor MET. Additional processes which may play a role in the construction of a zoned magma body include the ascent of bubbles through volatile saturated magma which may lead to upward migration of alkalis, halogens, and other fluid mobile elements (Hildreth and Wilson, 2007) and the generation of low density, hydrous melts via sidewall crystallisation (e.g. Huppert *et al.*, 1986). The preservation of this zonation until eruption suggests that the reservoir is unable to homogenise via efficient convection. This may be linked to the development of a system of multiple, individually convecting layers (Huppert and Sparks, 1984), or alternatively a strong density contrast associated with the range of water contents indicated by the water contents of alkali feldspar-hosted melt inclusions and alkali feldspar hygrometry (~ 2 wt. %) (cf. Hildreth and Wilson, 2007).

Due to the dominance of trachytic compositions at this uppermost level, individual magma reservoirs are likely to be surrounded by a marginal syenitic crystal mush developing via *in-situ* crystallisation in the thermal boundary zone. This mush may then be sampled during eruption, providing the syenite ejecta observed in the CCI and, to some extent, in the LAI. The presence of hybridised trachytic enclaves within these syenitic ejecta is considered to record the injection of hybridised trachyte into an upper trachytic reservoir, through the marginal mush zone. The abundance of miarolitic cavities in both enclave and host syenite provide evidence for the shallow depth of this magma storage zone. The subsequent mixing of these hybrids with the overlying trachytes may contribute to the development of zonation of the magma body, and likely accounts for the occurrence of anorthoclase, resorbed oligoclase, augite, and more rarely, calcic plagioclase, diopside, and forsterite (e.g. LMI and PNI) in the ignimbrites. Furthermore, the replenishment of the uppermost reservoir with hybridised mafic trachyte may act as a trigger for eruption. The

calculated rates of crystal settling imply that the antecrystic population introduced during mixing would settle rapidly, implying relatively rapid eruption following replenishment.

4.6.6 The ignimbrites in the context of the magmatic suite of Terceira

When considered in the context of the Terceira suite, the ignimbrites, syenites, and enclaves lie close to the end (< 2 wt. % MgO) of a single liquid line of descent which characterises the volcanic products of the island (Figure 4.30, 4.31). Mungall and Martin (1995) further subdivided this trend, noting the presence of a more oxidising Santa Bárbara trend at low MgO contents (< 1 wt. %). For the purpose of clarity, and due to the association of the ignimbrites with the Pico Alto volcanic complex (and therefore the Rift zone, Mungall and Martin, 1995), the rocks of Santa Bárbara, and Cinco Picos are not shown. The mafic to intermediate region of this trend comprises the various lava flows and adventive cones associated with the Rift zone (Self 1974, 1976; Mungall and Martin, 1995; Madureira *et al.*, 2011), whilst the felsic region is made up of the syenite enclaves, the ignimbrites (including bulk rock, groundmass glass, and melt inclusions) and the syenites (Mungall, 1993; Gertisser *et al.*, 2010; Tomlinson *et al.*, 2014; this study), the lava flows of Pico Alto, and the residual glass in syenite ejecta (Mungall and Martin, 1995), listed in order of increasing differentiation and peralkalinity. The addition of a sixth step to major element mass balance models discussed above, in which a MET composition is utilised as a parental composition and a pantellerite is used as a daughter, indicates that the pantellerites which are typical of the Pico Alto Volcanic Complex can be generated via 72 to 79 % fractionation (93 to 97 % total from basaltic parent) of an assemblage comprising predominantly alkali feldspar (92 %), clinopyroxene (3 %), olivine (2 %), Ti-magnetite (2 %), and apatite (< 1%) (average $\sum r^2$ = 0.496). The ignimbrite-forming magmas are therefore likely to have evolved to pantelleritic compositions, had they been stored for long enough to allow continued fractionation.

In the overall trend, Al_2O_3 contents show little variation until ~ 1 wt. % MgO, indicating only a minor role of plagioclase feldspar (Figure 4.30). This point corresponds broadly to benmoreitic compositions, and is in agreement with the results of Rhyolite-Melts modelling. At MgO contents of < 1 wt. %, Al_2O_3 rapidly declines from ~ 16 to ~ 5 wt. %, indicating significant fractionation of initially plagioclase and then alkali feldspar. A similar, kinked trend is observed in FeO_t and TiO_2, where concentrations show little change until ~ 4 wt. % MgO, when they decline from ~ 12 to ~ 4 wt. %, and ~ 3.5 to < 1 wt. %, respectively. As is common in peralkaline systems, a late-stage (< 1 wt. % MgO) FeO_t enrichment stage is present, leading to concentrations of up to ~ 15 wt. % in the most evolved trachytic liquids. The peralkalinity index of the system shows a gradual increase, becoming peralkaline close to the benmoreite-trachyte boundary, followed by a rapid increase during the final stages.

A compositional gap is observed in the suite at ~ 1.5 to 3.0 wt. % MgO, which likely corresponds to the described Daly gap of Terceira (Self and Gunn, 1976). Although Mungall and Martin (1995) used monzonitic xenoliths to bridge this gap, no such xenoliths are reported from Pico Alto. However, the benmoreitic lavas of Mungall (1993) and the syenite-hosted enclaves of this study begin to narrow this gap. At Pico Alto, this gap may reflect a genuine scarcity of intermediate compositions due to prevalent magma hybridisation in the shallow magma storage zone (ascending mafic magmas with trachytes, and hybridised trachytes with more evolved trachytes). The presence of overlying lower density trachytic magma is also likely to inhibit the ascent of hawaiite-trachyte hybrids from the lower mixing zone, instead mixing them into the more evolved trachytes.

4.7 Conclusions

The ignimbrite-forming comenditic trachytes of Terceira can be generated by extended fractional crystallisation of hydrous (1.5 wt. %), mantle-derived basaltic parental magmas at redox conditions around 1 log unit below the fayalite-magnetite-quartz buffer. Pre-eruptive water contents measured in melt inclusions and estimated via alkali feldspar hygrometry extend from 2.5 to 6.0 wt. % and, based upon solubility modelling, indicate the presence of a prominent magma storage reservoir at shallow crustal depths (~ 3 to 4 km) in which silicic magmas are stored. This is supported by low S and CO_2 contents of melt inclusions. Volatile contents of melt inclusions and groundmass glass indicate volatile-undersaturated conditions prior to eruption, with volatile concentrations being controlled primarily by fractionation. Comparison of melt inclusion and groundmass glass halogen concentrations suggest that both Cl and F were not generally degassed during eruption, though this may not be the case for all of the ignimbrite-forming trachytes. Syenitic ejecta of similar bulk rock composition to the trachytes provide evidence for the *in-situ* crystallisation of trachytic magmas in a thermal boundary layer in the upper crustal reservoir. The abundance of miarolitic cavities in these rocks also indicates shallow crustal conditions.

The results of thermodynamic modelling, as well as the minor presence of Al_2O_3- and TiO_2-rich clinopyroxenes, provides evidence for an initial high pressure fractionation step in the lower crust (~ 14 km), in which basalts differentiate via fractional crystallisation to hawaiitic compositions. Trachytic enclaves within syenite ejecta contain mixed crystal populations, indicating a two-stage mixing process in which ascending hawaiites are mixed with trachytic magmas in the base of the shallow crustal storage zone, to create a hybridised trachyte, which then ascends further and is mixed with more evolved trachytes, passing first through a syenitic crystal mush at the margin of a magma reservoir. Calculated magma viscosities for the ignimbrite-forming trachytes extend to values more than 1 order of magnitude lower than is typical for metaluminous silicic magmas.

Estimated crystal settling rates suggest that fractional crystallisation is likely to remain a viable process of magmatic differentiation in the trachytic magmas stored in the shallow crust, and likely contributes to the substantial trace element compositional zonation observed in the ignimbrites. Major element mass balance modelling indicates that the most evolved, pantelleritic compositions of Terceira can be generated by continued fractionation of alkali feldspar from the ignimbrite-forming comenditic trachytes.

The newly-described occurrence of the rare potassium zirconosilicate mineral dalyite ($K_2ZrSi_6O_{15}$) allows the minerals compositional variability to be assessed. Comparison of available quantitative analyses produced during this study and published analyses indicates the substitution of Na for K is generally more significant in peralkaline granites and syenites than in highly potassic rock types such as lamproites. The degree of substitution of Ti for Zr is shown to be greater in highly potassic rocks than in peralkaline granites and syenites, possibly reflecting the greater Ti-contents of the former. Furthermore, the incorporation of small amounts of Ba occurs in dalyite found in the highly potassic lithologies, most likely via Ba↔Zr substitution. The incorporation of Fe into dalyite is minimal in peralkaline granites and syenites, but becomes more significant in highly potassic lithologies. Mineral chemical data and solid state modelling suggest that this is most easily achieved via Fe^{2+}↔Zr substitution, though high E_{sol} values and charge balancing requirements must hinder this relationship. Finally, the dalyite found within the syenite ejecta of Pico Alto shows variation in the degree of Na↔K substitution that does not relate obviously to texture, and cannot be entirely attributed to ‘inter-nodule’ diversity. This feature is instead linked to relative K-enrichment induced by the effects of pore wall crystallisation (during a late-stage magmatic phase) and albitisation (during a sub-solidus, deuteric phase), coupled with the variation in nucleation delay that is introduced by variable pore sizes.

CHAPTER 5: THE MAGMATIC SYSTEM OF FURNAS VOLCANO, SÃO MIGUEL

5.1 Chapter overview

This chapter provides a detailed petrological study of Furnas volcano, targeting the young (< 5 ka) post-caldera activity, and an older, caldera forming eruption. The study incorporates petrographical analysis, major and trace element geochemistry, mineral chemistry, thermobarometry, and petrogenetic modelling, aiming to place constraints upon the origin and evolution of the trachytic magmas of Furnas volcano throughout its history. Through the application of this dataset, a conceptual model is proposed for the magmatic plumbing system of the volcano, accounting for the observed petroglogical features of the eruptive products, and allowing a discussion on the range of eruption styles at Furnas. Furthermore, using the geochemical variations observed in the deposits of the most recent eruptions of Furnas, a model is presented to characterise the temporal, physical, and chemical evolution of the magma system over a relatively short geological timescale of less than 5,000 years.

A small amount of the chemical data used in this study was collected by R. Gertisser. The portions of this chapter relating to the petrogenesis and temporal evolution of the Upper Furnas Group have been accepted for publication as an original research article in Contributions to Mineralogy and Petrology (Jeffery *et al.*, 2016c). The remaining material, relating primarily to the Povoação Ignimbrite Formation and the contrasting eruptive behaviour of Furnas, has been prepared for submission to the Journal of Volcanology and Geothermal Research (Jeffery *et al.*, 2016d).

5.2 Introduction

With an eruptive history dominated by variably explosive activity, Furnas volcano is one of the most active and dangerous volcanoes in the Azores archipelago, and represents an example of an oceanic island volcanic centre that exhibits many of the petrogenetic problems associated with peralkaline magmatic systems, including: 1) a volumetric abundance of felsic products with a peralkaline affinity, 2) an apparent Daly Gap, and 3) a spatial concentration of felsic products within the volcano's caldera complex, with mafic products on the flanks (Booth *et al.*, 1978; Moore 1991a, 1991b). Recent (< 5 ka), post-caldera activity has been dominated by low volume (< 0.1 km^3 DRE), sub-Plinian magmatic/phreatomagmatic eruptions of trachytic magma, whereas suggested caldera-forming eruptions led to the formation of comparatively large ignimbrites (Guest *et al.*, 1999). For example, the Povoação Ignimbrite Formation (PIF), attributed to the first of at least two caldera-forming events, is estimated to have had a minimum eruptive volume of ~ 2 km^3 DRE, and is likely to represent the largest eruption of Furnas (Schmincke and Weibel, 1972; Booth *et al.*, 1978; Moore, 1990; Duncan *et al.*, 1999). The current caldera complex is occupied by ~ 1,500 inhabitants, with several hundred more in the vicinity, and the hazard assessment of Cole *et al.* (1999) demonstrated that even the relatively small post-caldera eruptions could blanket nearby towns in up to 16 m of tephra, prompting roof collapses as far away as Ponta Delgada. As such, the potential hazards associated with a caldera-forming eruption of the same scale as that of the PIF, which reaches up to 40 m in thickness (Duncan *et al.*, 1999), are evident, and a greater understanding of the processes of magma genesis and evolution operating in the underlying magma system, and their effect upon eruption style, is of clear benefit to the future risk assessment.

Guest *et al.* (1999) suggested that, like neighbouring volcanoes Sete Cidades and Fogo (Agua de Pau), the felsic magmas of Furnas were largely generated via fractional crystallisation (cf. Storey *et al.,* 1989; Moore, 1991a; Widom *et al.*, 1992), and that the observed geographical distribution of mafic and felsic eruption products could result from

the presence of established trachytic magma reservoirs that intercept ascending mafic magmas (cf. Wolff, 1987). However, the evolution of peralkaline trachyte has not been quantitatively demonstrated at Furnas, and constraints upon the plumbing system are currently limited to geophysical studies (e.g. Machado, 1972; Camacho *et al.*, 1997; Montesinos *et al.*, 1999), which broadly point towards a magma reservoir at shallow depths in the crust (~ 5 km).

In this chapter, detailed petrography, mineral chemistry, thermobarometry, whole rock major and trace element geochemistry, as well as petrogenetic modelling, is applied to 9 of the 10 recent post-caldera eruptions that together constitute the UFG, and the older PIF. With this dataset, this study aims to: 1) investigate the petrogenesis and differentiation of mildly peralkaline silicic magmas at Furnas volcano and generation of the Daly Gap, 2) place constraints upon the P-T-fO_2 conditions of the magma plumbing system beneath Furnas, 3) evaluate the compositional evolution of a periodically-tapped, metaluminous to mildly peralkaline magma plumbing system over a period of ~ 5,000 years (Guest *et al.*, 1999), and 4) compare the pre-eruptive magma systems of both caldera-forming and post-caldera activity at Furnas and evaluate the positions of the caldera-forming PIF eruption and the younger, sub-Plinian eruptions of the Upper Furnas Group (UFG) in the context of the temporal evolution of magma plumbing system of Furnas volcano. A greater understanding of the pre-eruptive plumbing system of Furnas has implications for the ongoing risk management of this highly active and hazardous volcano (e.g. Jones *et al.*, 1999; Chester *et al.*, 2002), as well as for the processes that generate mildly peralkaline silicic magmas in such settings (e.g. Macdonald, 2012), and the re-establishment and temporal evolution of post-caldera magmatic systems (e.g. Bachmann *et al.*, 2012).

5.3 Geological background

5.3.1 Structure of the island

With a surface area of 759 km^2 and a population of approximately 150,000, the isle of São Miguel is the largest in the archipelago. The island comprises four central volcanoes; one basaltic shield volcano (Povoação/Nordeste volcanic complex) and three dominantly trachytic stratovolcanoes (Sete Cidades, Fogo (also known as Agua de Pau) and Furnas) (Figure 5.1) (e.g. Booth *et al.*, 1978; Cole *et al.*, 1999; Guest *et al.*, 1999). Moore (1990) chose to divide the island into six distinct zones, one for each of the central volcanoes, and two regions of predominantly mafic cinder cones and lava flows that lie between Sete Cidades and Fogo (the Waist Zone, e.g. Booth *et al.*, 1978) and, between Fogo and Furnas (the Achada das Furnas complex, e.g. Guest *et al.*, 1999). These zones have been retained in the most recent contributions to the structure and stratigraphy of São Miguel, though the Waist Zone and the Achada das Furnas Complex have been renamed the Picos and Congro fissural volcanic systems, respectively (Gaspar *et al.*, 2015).

The Povoação/Nordeste volcanic complex (zone 6 of Moore, 1990) is a heavily-eroded shield volcano, occupying at least 180 km^2 at the eastern end of the island (e.g. Moore, 1990). Compositionally, the volcano comprises dominantly (> 90 %) mafic rocks and represents the oldest volcanic activity on the island (~ 1 to 4 Ma) (Abdel-Monem *et al.*, 1975; Fernandez, 1980). The southern section of the shield is truncated by the Povoação caldera, which was subsequently partially in-filled with five intra-caldera eruptions of ankaramitic, mugearitic and trachytic lavas, which were then covered by the eruption products of neighbouring Furnas volcano (Moore, 1990). The caldera is believed to have formed before 100,000 B.P., based upon its highly eroded form and the absence of fumaroles (Moore, 1990). The limited trachytic rocks found on Nordeste are concentrated on its southern flank and in the vicinity of the Povoação caldera.

Sete Cidades volcano forms the western section of the island (zone 1 of Moore, 1990) and comprises a 5 km-diameter circular caldera, with walls up to 550 m high, an

incomplete ring of six intra-caldera cratered trachytic cones and two intra-caldera lakes (Lagoas Verde and Azul) (e.g. Booth *et al.*, 1978; Queiroz, 1998). The volcano became subaerial around 210 ka, and is characterised by trachytic eruption products (~ 73 vol. %) with subsidiary mafic lithologies (hawaiite, mugearite, basalt, ankaramite and basanite; ~ 27 vol. %; Moore, 1991a). Moore (1990) estimated a subaerial volume of ~ 70 km^3, that formed at an average rate of 0.2×10^{-3} to 0.3×10^{-3} km^3/y. Prior to caldera formation (~ 22 ka; Moore, 1990), trachytic vents appear to have been generally concentrated towards the summit, whereas the more mafic lithologies were typically erupted on the flanks (Moore, 1991a). Post-caldera activity has been broadly similar, with at least six cone-forming eruptions of trachytic material within the caldera, and various eruptions of mafic and silicic lithologies from radial flank fissures and the Terceira Rift (Moore, 1990). The most recent activity of the volcano includes three submarine eruptions (presumed to be basaltic) off the western coastline in 1638, 1682 and 1811, and one terrestrial eruption in 1713 (Booth *et al.*, 1978).

Fogo volcano corresponds to zone 3 of Moore (1990) and occupies a central position on the island (e.g. Wallenstein, 1999). The volcano became subaerial around 200 ka and comprises a caldera complex, made up of a prominent inner caldera (~ 15.2 ka) with a lake (Lagoa do Fogo) and an older, outer caldera (46 to 26.5 ka) preserved on the northern, western and eastern flanks (Moore, 1991a). Compositionally, Fogo is more silicic than Sete Cidades, and is dominated by, often peralkaline trachytic rocks (~ 94 vol. %), with minor mafic lithologies (ankaramite, basanite, basalt, hawaiite and mugearite; Moore, 1991a). Moore (1990) provides an estimate of 80 km^3 for the volcano's subaerial volume, which has increased at an average rate of 0.2×10^{-3} km^3.

In the west an 18 km long region of lava flows, cinder cones and fissure vents runs approximately E-W between Sete Cidades and Fogo, and is known as the Picos Fissure system (e.g. Booth *et al.*, 1978; Moore, 1990; Guest *et al.*, 1999). This feature corresponds to zone 2 of Moore (1990) and is generally considered to be the surface

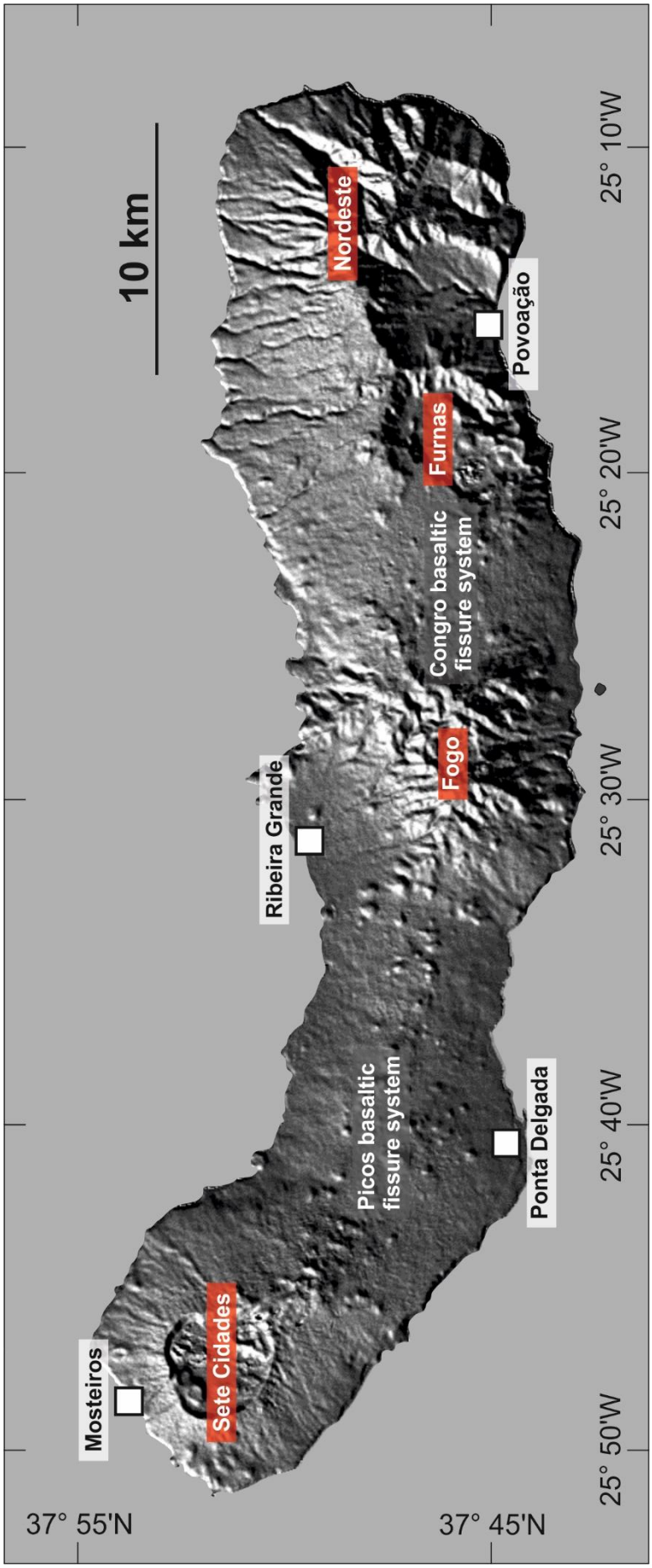
10 km
Nordeste
Povoação
Furnas
Congro basaltic fissure system
Fogo
Ribeira Grande
Picos basaltic fissure system
Ponta Delgada
Sete Cidades
Mosteiros
25° 10'W
25° 20'W
25° 30'W
25° 40'W
25° 50'W
37° 55'N
37° 45'N

◄ **FIGURE 5.1:** A digital relief map of São Miguel island, showing selected towns and villages (white squares), the four central volcanoes (Sete Cidades, Fogo, Furnas and Nordeste), alongside the two rift structures (the Waist Zone and Achada das Furnas). Map generated using GeoMapApp©.

expression of the Terceira Rift (e.g. Haase and Beier, 2003; Widom and Farquhar, 2003). Eruption products are almost entirely limited to basanite and ankaramite, with only four known trachytic lavas (Moore,1990). Many of these erupted mafic lavas contain mafic and ultramafic xenoliths (e.g. Moore, 1991a).

An additional rift structure, named the Congro Fissure system, stretches 5 km from Fogo to Furnas and is characterized by numerous cinder cones and lava flows that span a similar compositional range to that of the Picos Fissure system (zone 2) (e.g. Moore, 1990; Guest *et al.*, 1999). The most recent activity in the area occurred around 3.8 ka and included explosive and dome-forming eruptions of trachyte, as well as an ankaramitic lava flow (Moore, 1990).

5.3.2 Furnas volcano: an overview

Of the three active volcanoes on São Miguel, Furnas is the easternmost (zone 5 of Moore, 1990), and is located between Fogo to the west and the Nordeste shield to the east (Guest *et al.*, 1999, 2015). It is also the youngest, having become subaerial around 100 ka (Moore, 1990; Cole *et al.*, 1999). Since then it has grown at an estimated average rate of 0.6×10^{-3} km^3/y, to attain a subaerial volume of around 60 km^3 (Moore, 1990; Moore, 1991a). Unlike Sete Cidades and Fogo, Furnas volcano has no well-developed volcanic edifice, instead comprising an 8 × 5 km diameter caldera complex that adjoins to the older Povoação caldera to the east, and is divided into an outer and inner caldera (Figure 5.2) (e.g. Booth *et al.*, 1978; Guest *et al.*, 1999). Moore, (1990, 1991a) attributed caldera formation to a single eruption event that occurred around 12 ka, whilst Guest *et al.* (1999) considered two separate caldera-forming eruptions, with one dated at around 30 ka leading to formation of the outer caldera, and another at 12 ka generating the inner caldera (cf. Sibrant *et al.*, 2015). Moore (1990) highlighted the proximity of Nordeste to

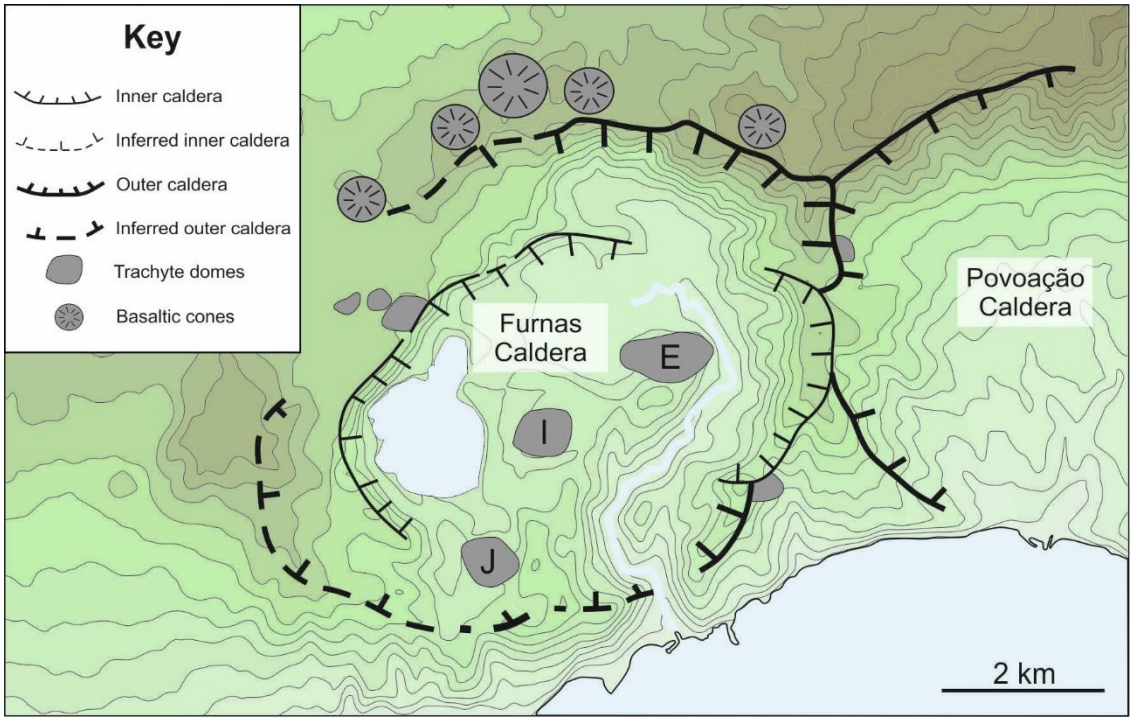

FIGURE 5.2: A schematic map of the nested caldera of Furnas volcano and the neighbouring Povoação caldera. The lava domes associated with the Furnas E, I and J are labelled. After Guest *et al.* (1999) and Cole *et al.* (1999)

Furnas, as well as the presence of a syenitic xenolith (K-Ar dated at 0.973 ± 0.029 Ma) in a Furnas trachytic pumice deposit, to postulate a connection between the two magma systems at depth.

The eruption products of Furnas are not dissimilar to those of Sete Cidades and Fogo, with trachytic pyroclastics and lavas accounting for 89 vol. %, and the remaining 11 vol. % made up of ankaramite, basanite, basalt, hawaiite and mugearite (Moore, 1991a). The apparent presence of a Daly Gap, observable in the previously described products of Sete Cidades and Fogo, can also be seen in the Furnas products, with comparatively rare intermediate lithologies. Mafic vents are limited spatially to the flanks of the volcano, and trachytic vents are generally restricted to the caldera complex itself.

5.3.3 Furnas volcano: volcanic history and stratigraphy

Furnas is considered one of the most active and dangerous volcanoes in the entire Azores archipelago, having erupted at least 10 times in the last 5000 years, and has

exhibited both effusive and caldera-forming, explosive activity during its subaerial existence (Cole *et al.*, 1999; Guest *et al.*, 1999). Approximately 3,000 people inhabit Furnas caldera, with several thousand more in the immediate vicinity. A stratigraphical study by Guest *et al.* (1999) revealed that more than 90% of eruption products relating to Furnas are pyroclastic in origin, suggesting a volcanic history dominated by explosive activity.

The deposits of Furnas overlie those of Nordeste volcano and, as a result, often contain lithic clasts derived from the older Nordeste eruption products (Fernandez, 1980; Moore, 1990). Guest *et al.* (1999) chose to divide the stratigraphy into three groups; the Upper (UFG), Middle (MFG) and Lower (LFG) Furnas Groups. The LFG and MFG comprise numerous trachytic pyroclastic units, with minor trachytic domes and basaltic cones (Figure 5.3) (Moore, 1990). The boundary between the two groups is marked by the Povoação Ignimbrite formation (PIF), a voluminous, partially welded ignimbrite that fills much of the Povoação caldera and is believed to represent the first caldera-forming eruption of Furnas volcano (Schmincke and Weibel, 1972; Booth *et al.*, 1978; Duncan *et al.*, 1999). Although Moore (1990) dated this ignimbrite at ~ 12 ka, Guest *et al.* (1999) suggest that this date relates instead to a younger welded ignimbrite, most likely generated during the second caldera-forming event. They used radiocarbon dates from soils directly beneath the PIF to produce the age bracket of 30 to 35 ka. As such, in the stratigraphy of Furnas, the age of the PIF is generally given as ~ 30 ka (e.g. Cole *et al.*, 1999; Duncan *et al.*, 1999; Guest *et al.*, 1999).

The UFG is made up of at least ten intra-caldera, sub-plinian eruptions of trachytic pumice, named Furnas A to J (or Furnas 1630) in order of decreasing age (Booth *et al.*, 1978). Three of these eruptions are known to have also produced lava domes in their final

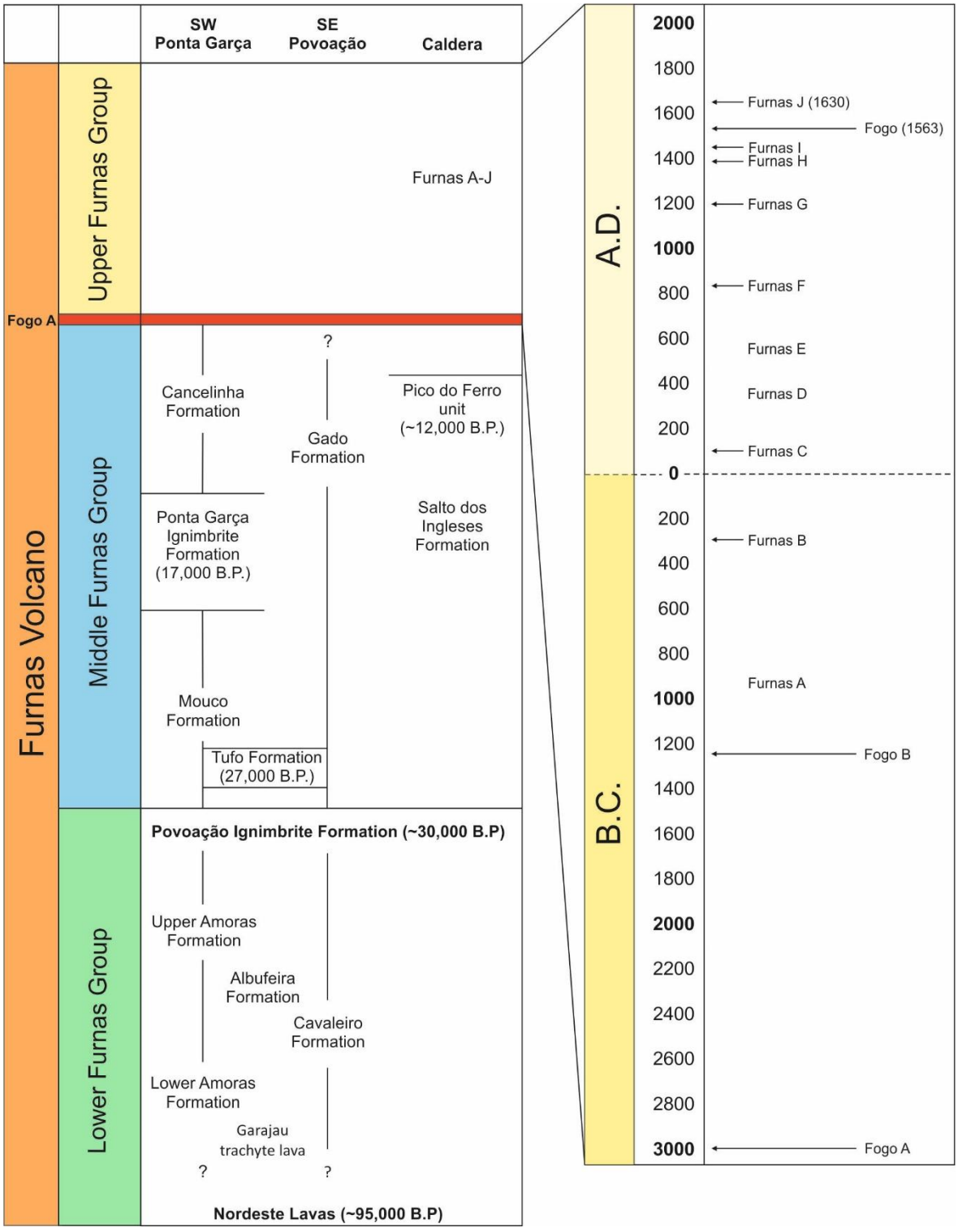

FIGURE 5.3: The summarised stratigraphy of Furnas volcano, including the Lower, Middle and Upper Furnas Groups of Guest *et al.*, (1999). The divisions are marked by the Povoação Ignimbrite formation and the Fogo A deposit from nearby Fogo volcano, respectively. Deposits of the Upper Furnas Group with associated uncalibrated ^{14}C dates are shown with arrows, alongside two further deposits of Fogo (Fogo B and Fogo 15683. After Guest *et al.* (1999) and Cole *et al.* (1999).

stages (Furnas E, I and J) (Cole *et al.*, 1999).The dominant lithology of the UFG is inter-bedded lapilli and ash beds, which are typical of Furnas volcano, and are inferred to be the result of complex transitions between magmatic and phreatomagmatic activity during eruption (Guest *et al.*, 1999). The boundary between the MFG and UFG is marked by a deposit from nearby Fogo volcano, named Fogo A (Walker and Croasdale, 1971). Radiocarbon ages for Fogo A range from 4.5 to 5.4 ka (Moore and Rubin, 1991; Pensa *et al.*, 2015), but its age is generally reported as 5 ka (Guest *et al.*, 1999). Although the deposit is not genetically related to Furnas, it is well-known and easily identified, and was therefore chosen to mark the base of the UFG. Further deposits from Fogo are also commonly presented within the stratigraphy of the UFG to act as reference points (e.g. Cole *et al.*, 1999).

Of the ten eruptions in the UFG, at least two are believed to have occurred since the islands settlement in the 15th century (Furnas H, I and J). Limited historical accounts of the Furnas I eruption include a sighting of vapour rising from the caldera and luminescence, taken as an indication of lava dome extrusion (Guest *et al.*, 1999). The accounts of the Furnas J eruption in 1630, in conjunction with detailed study of the deposits, allowed the development of a comprehensive eruption narrative, given by Cole *et al.* (1995). This includes initial earthquakes, transitions between magmatic and phreatomagmatic behaviour and extrusion of a trachytic lava dome.

5.4 Field descriptions and sampling

During the course of two fieldwork sessions (November 2011 and April 2013), a total of 94 samples of juvenile pumice, lithic clasts, ash, syenitic ejecta, lava, and scoria were collected from 25 locations within the caldera and on the volcano's flanks. Primary targets were the various volcaniclastic deposits of the Upper Furnas Group (UFG) and the Povoação Ignimbrite Formation (PIF). All locations are shown in Figure 5.4 and a full list of samples if given in Appendix B.

5.4.1 The Upper Furnas Group

Seven of the ten Upper Furnas Group eruptions were sampled from a total of thirteen locations (Figure 5.4). Samples of Furnas A and B were provided by Dr R. Gertisser, whilst Furnas D was not sampled due to poor exposure and lack of juvenile material (Booth *et al.*, 1978). Furnas C was sampled at location 8, a prominent roadside outcrop to the north of the caldera (Figure 5.4, 5.5, 5.6a). Here, it crops out as a > 3 m thick exposure of alternating, thinly bedded (typically < 10 cm) ash and pumice lapilli fall out deposits, overlain by a thin (~ 5 cm) palaeosol (Figure 5.6b). Juvenile clasts are highly vesicular white pumice lapilli, with very low crystal content. Interbedded ash layers are grey in colour, and range from well sorted ash to poorly sorted ash to lapilli. Samples of juvenile material were collected from the upper (samples S010, S016, S065) and lower (samples S011, S066) sections of the outcrop.

Furnas E was also identified at location 8, overlying the Furnas C deposits and underlying the distinctive deposits of the Fogo 1563 eruption of nearby Fogo volcano (Walker and Croasdale, 1971) (Figure 5.6b). Here, it is ~ 0.5 m thick, with grey ash containing fine lapilli lenses, grading into a slightly weathered, coarse white pumice fall. Its base is marked by the thin palaeosol that marks the top of Furnas C, and its top is marked by another thin weathering horizon and palaeosol. Juvenile pumice clasts are highly vesicular and more crystal rich than those of Furnas C. Grey ash and juvenile pumice

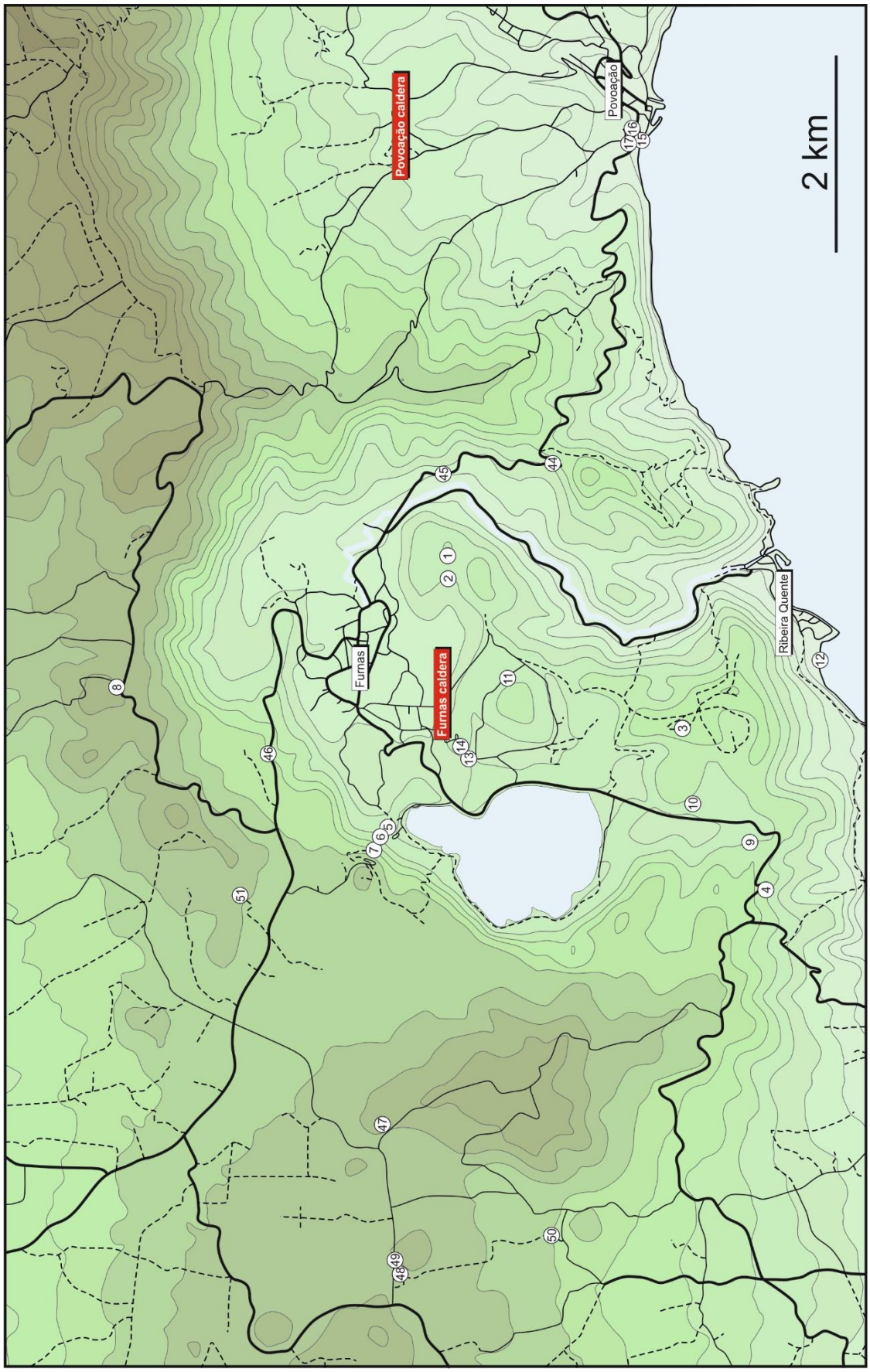
Povoação caldera
Furnas caldera
Furnas
Povoação
Ribeira Quente
2 km

◄ **FIGURE 5.4:** Map of Furnas caldera and the surrounding area, showing sampling locations. Roads are marked with solid lines, tracks with dashed lines. Generated using GeoMapApp©

clasts were sampled from outcrop (samples S012, S064).

Furnas F was sampled at location 13, a roadcut in the Furnas I tuff ring, north-west of the Furnas I lava dome (Figure 5.4). The deposit comprises at least 3.5 m of various grey ash beds and lithic-rich lapilli falls, overlain by a single massive, poorly sorted, lithic-rich unit of at least 3.5 m thickness (Figure 5.5, 5.6c). The deposit is particularly rich in lithic clasts throughout, and pumice clasts range from white and highly vesicular, to grey, dense clasts, all with relatively abundant alkali-feldspar phenocrysts. Ashes and juvenile pumice clasts were sampled throughout the section (samples S041 to S046, S057 to S060).

Furnas G was sampled from locations 5 and 6, both of which lie close to the southern end of the footpath from Pico do Ferro to the northern rim of Furnas lake (Figure 5.4, 5.5). The deposit is ~ 1.5 m thick and comprises well stratified, fine grained lapilli (< 5 cm) and ash beds, with three distinctive coarser lapilli beds (Figure 5.6d). Juvenile pumice clasts are light grey and extremely crystal poor. Lithic clasts are common, though not to the extent of Furnas F. Juvenile pumice clasts were collected from each of the three coarser units (samples S006 to S008).

Furnas H was identified at locations 1 and 2, near the summit of Pico Marconas (Figure 5.4, 5.5). The deposit is made up of a single, unstratified, coarse pumice fall deposit, up to ~ 3 m in thickness (Figure 5.6e). At location 1, it is separated from an overlying grey ash by a thin, poorly developed palaeosol. Pumice clasts are light, highly vesicular, crystal poor and coarser than previous UFG eruptions. Although generally massive, at location 2 the uppermost outcrop becomes significantly coarser (> 15 cm), and the lowermost outcrop is slightly finer grained and more lithic rich. Samples of juvenile pumice clasts were collected from both locations (samples S001, S002, S092).

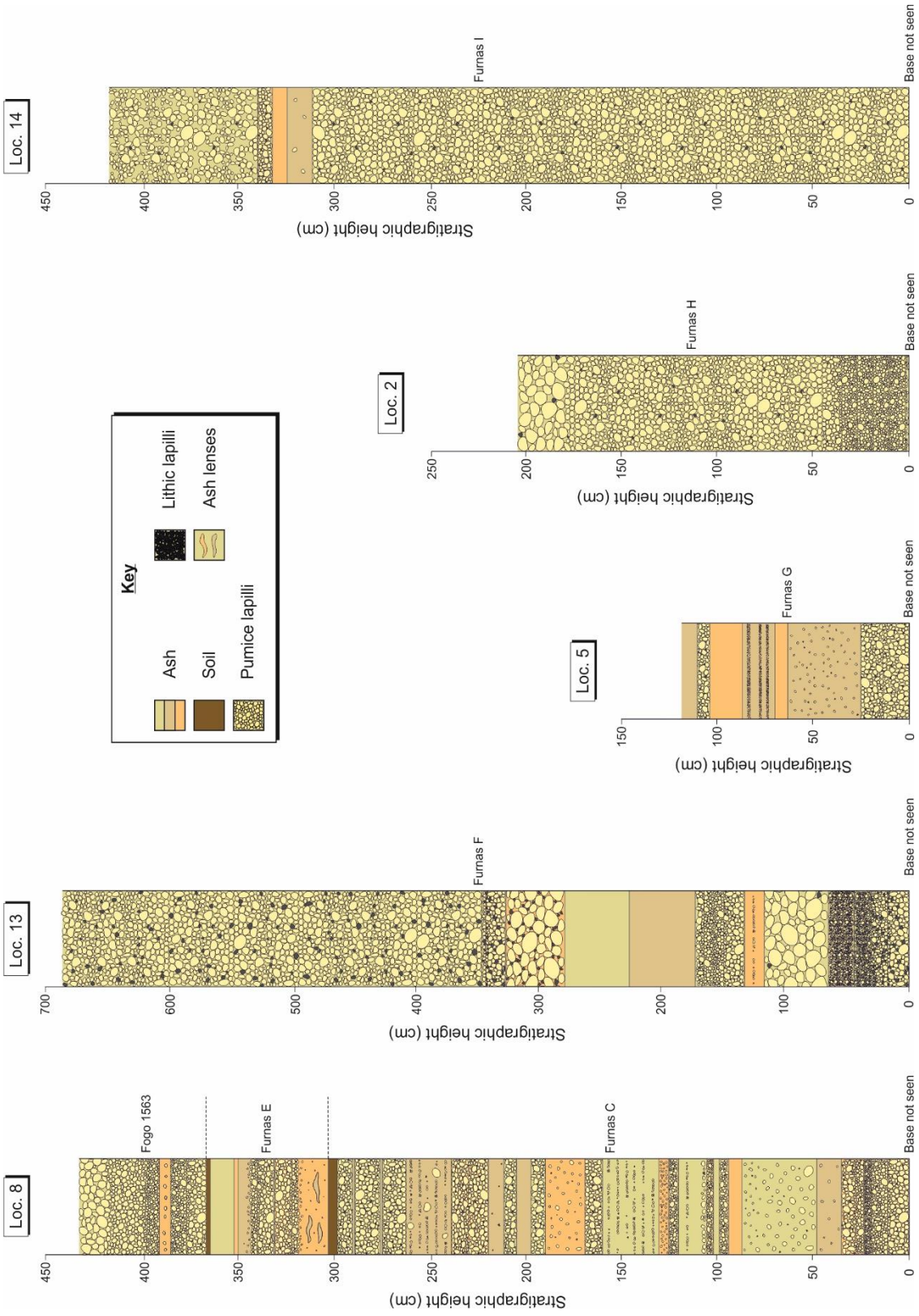
Loc. 14
Furnas I
Base not seen
Stratigraphic height (cm)
Loc. 2
Furnas H
Base not seen
Stratigraphic height (cm)
Loc. 5
Furnas G
Base not seen
Stratigraphic height (cm)
Key
Ash
Soil
Pumice lapilli
Lithic lapilli
Ash lenses
Loc. 13
Furnas F
Base not seen
Stratigraphic height (cm)
Loc. 8
Fogo 1563
Furnas E
Furnas C
Base not seen
Stratigraphic height (cm)

◄ **FIGURE 5.5:** Summarised stratigraphic logs of the Furnas C, E, F, G, H, and I outcrops

Furnas I was sampled at location 14, in a roadcut of the Furnas I tuff ring (Figure 5.4, 5.5). The lower ~ 3 m of the ~ 4.5 m outcrop is made up of unstratified, coarse lapilli fall (Figure 5.6f). This unit is made up of coarse white pumice that is less vesicular than Furnas H pumice and has a relatively high crystal content. Lithic clasts are rare and generally small (< 2 cm) when present. This unit is overlain by two thin (~ 10 cm) ashy units, the first dark grey, the second light grey, followed by an ~ 10 cm thick lithic-rich fall deposit. The upper ~ 1 m of deposit is similar to the lowermost unit, with abundant coarse white pumice clasts and rare lithics. Unlike the lowermost unit however, this unit is less pumice rich and contains a greater proportion of light grey ash. Sample of ash and juvenile pumice were collected (samples S036 to S040, S061). The lava dome associated with the Furnas I eruption was sampled at location 11 (Figure 5.4), at a roadside outcrop on the north western margin of the dome.

The deposits of the Furnas J eruption of the UFG was identified and sampled at locations 3, 4, 9, 10 and 12 (Figure 5.4, 5.5, 5.7). The nomenclature of Cole *et al.* (1995), in which the deposit is divided into at least 6 lapilli layers (L1 to Lf) and 5 ash layers (A1 to A5), is utilised here for the description of the Furnas J deposits. At location 3, a pumice quarry ~ 0.5 km to the east of the Furnas J dome, the uppermost deposit of the eruption (Lf) was identified (Figure 5.8a). This consists of a well sorted, coarse pumice fall deposit of > 8 m thickness. Some large lenses of extremely coarse pumice (> 30 cm) can be seen. Juvenile pumice clasts are white and highly vesicular, with a low crystal content and occasional banding. This is underlain by a substantial ash layer which corresponds to unit A5 of Cole *et al.* (1995). Juvenile pumice clasts were collected from the lower portion of Lf and a prominent lapilli bed in the uppermost A5 layer (samples S003, S004, S074 to S076).

At location 4 (Figure 5.8b), the lowest lapilli unit of the Furnas J eruption (L1) is present in a small roadside outcrop, ~ 1.5 km south west from the Furnas J dome.

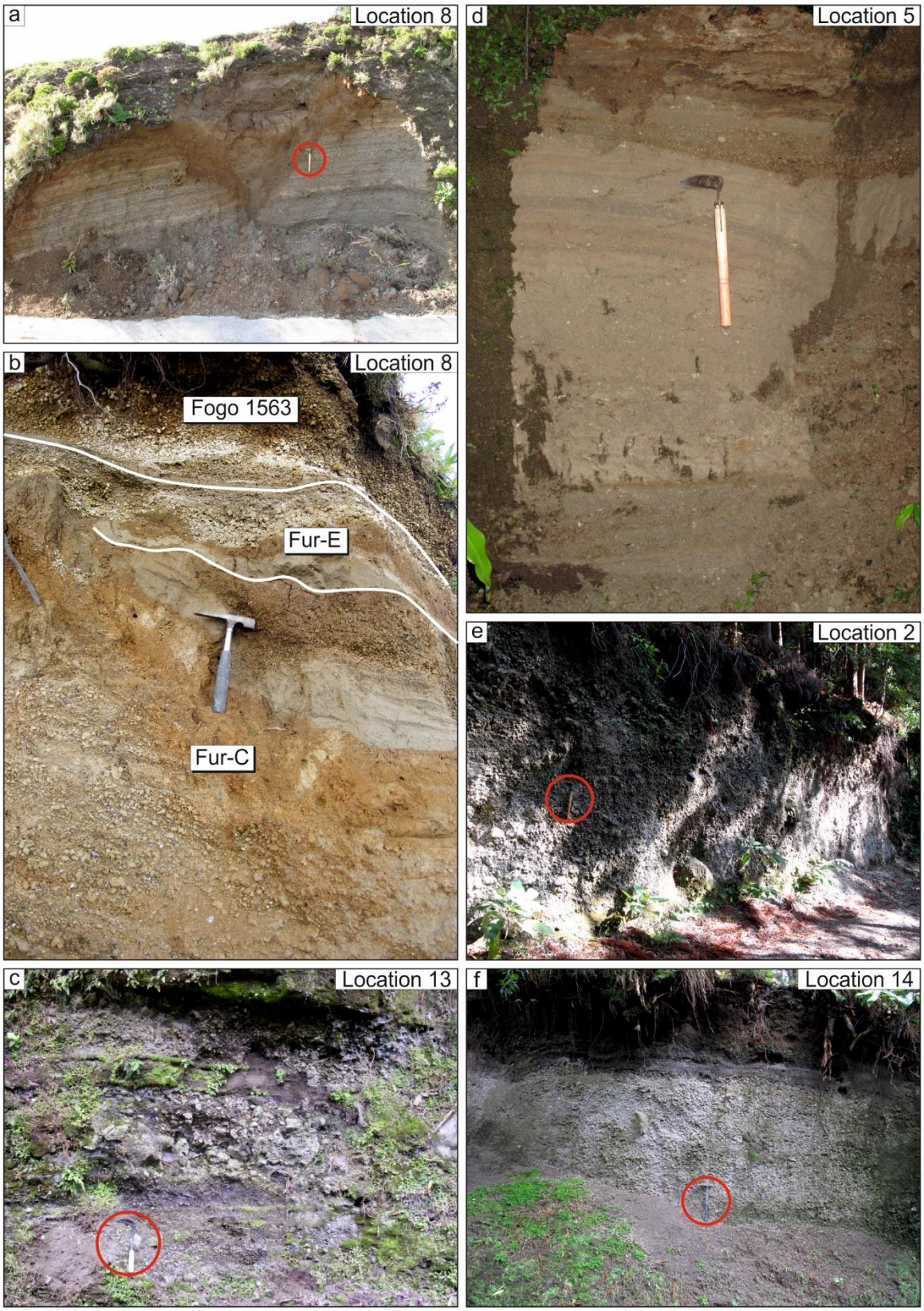

FIGURE 5.6: Field photographs of UFG outcrops **a)** Stratified lapilli and ash of Furnas C. Highlighted = 35 cm **b)** Upper Furnas C and overlying Furnas E and Fogo 1563 deposits. Hammer for scale (30 cm) **c)** Ash and lapilli fall deposits associated with Furnas F. Highlighted scale =32 cm. **d)** Fine grained, stratified lapilli and ash beds of Furnas G. Pick for scale (35 cm) **e)** Massive pumice fall deposit of Furnas H. Highlighted scale = 35 cm **f)** Unstratified pumice fall and overlying ashy units of Furnas I. Highlighted scale = 35 cm

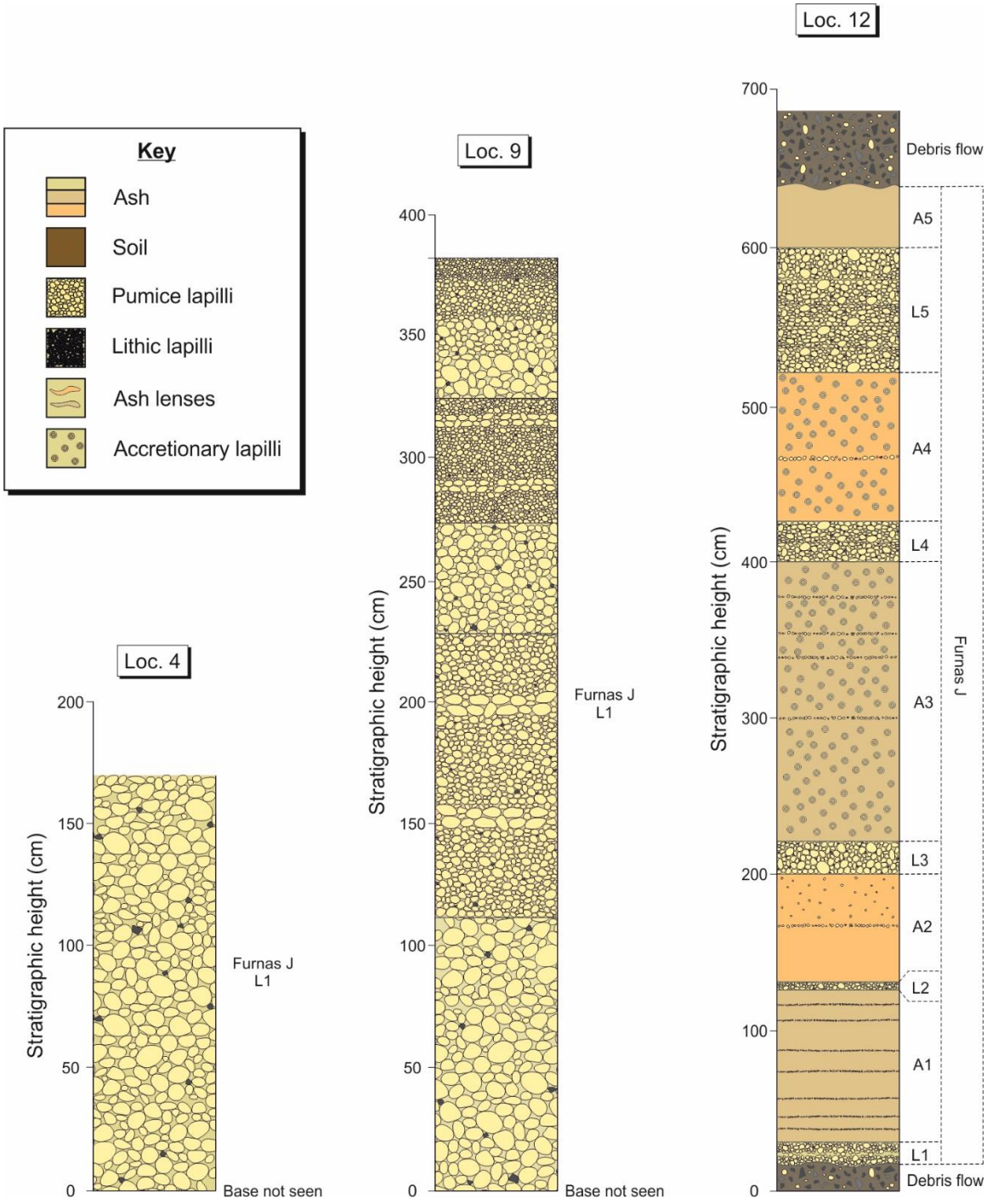

FIGURE 5.7: Stratigraphic logs of Furnas J deposits

The deposit is made up of very coarse, highly vesicular white pumice with a low crystal content. Juvenile pumice clasts were collected (samples S005, S094). A more proximal outcrop of L1 was identified at location 9 (Figure 5.8c), ~ 8 km south west of the dome. Here, it reaches a thickness in excess of 5 m and whilst similar to location 4, exhibits some stratification (Figure 5.7). The lowermost outcrop comprises ~ 1.1 m of very coarse

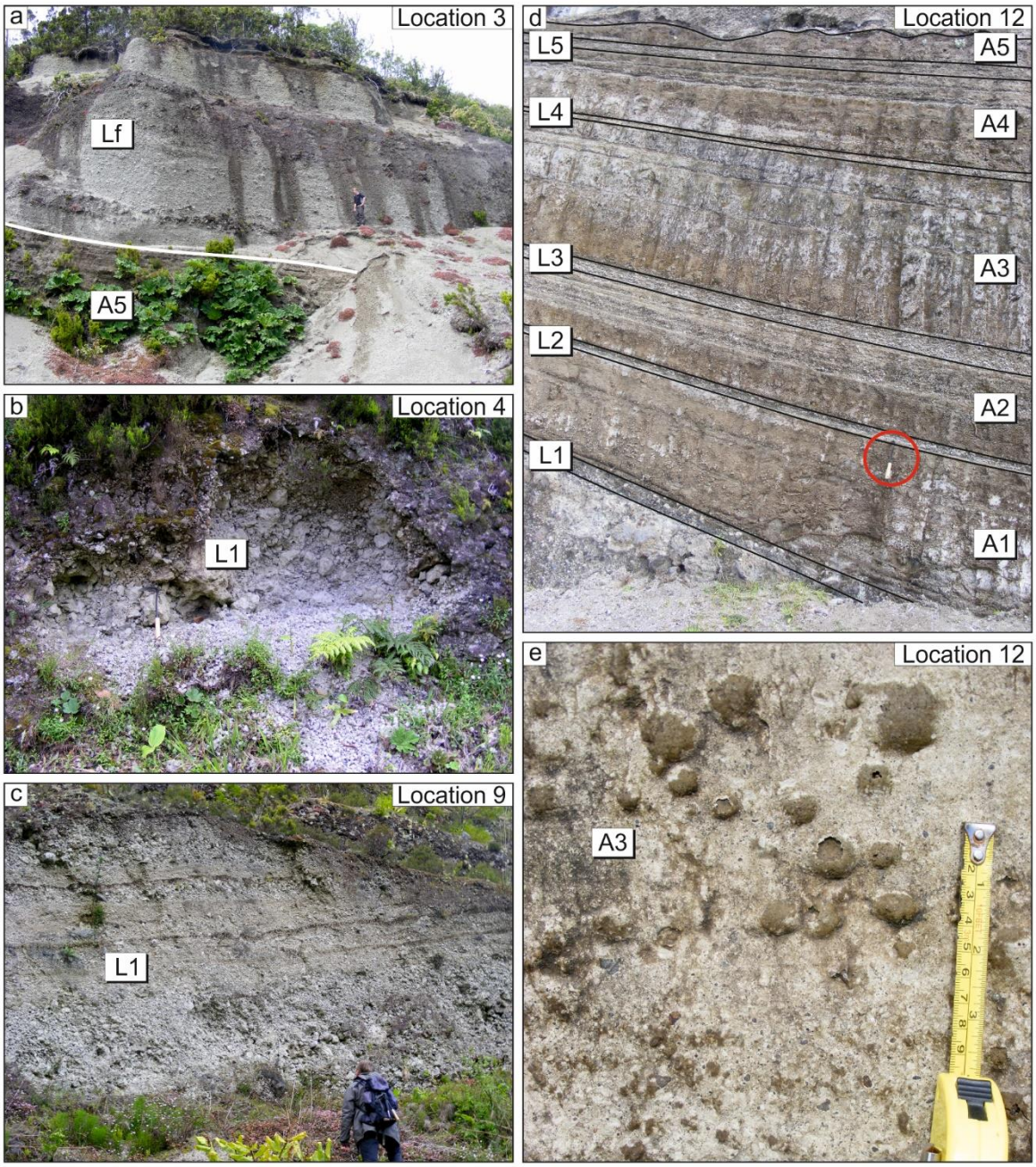

FIGURE 5.8: Field photographs of Furnas J deposits **a)** Uppermost, massive, fall deposit of coarse white pumice (Lf), overlying poorly stratified ash layer (A5). Stratigraphy highlighted. Person for scale **b)** Lowermost fallout layer of Furnas J (L1), made up of very coarse white pumice. Pick for scale (32 cm) **c)** Proximal outcrop of L1 showing stratification. Person for scale **d)** Distal deposit, with most units present. Stratigraphy is digitised. Highlighted scale = 32 cm **e)** Large accretionary lapilli within unit A3. Scale = 10 cm

(10 to 30 cm) angular, crystal-poor white pumice fall, with similarly coarse, angular, blue-grey lithic clasts. This unit grades into overlying units of alternating medium and coarse grained pumice fall, which cumulatively reach ~ 2 m in thickness. The uppermost unit in the outcrop is also dominated by coarse, white pumice, similar to the lowermost unit, and

exhibits normal grading. Samples of juvenile pumice and lithic clasts were collected from the lowermost, accessible units.

The more distal fallout deposits of Furnas J were sampled at location 12, on the beach of Ribeira Quente, ~ 2 km south east of the dome (Figure 5.4, 5.8d). This location corresponds to location 57 of Cole *et al.* (1995), and exhibits the majority of the Furnas J sequence (Figure 5.7). The base of the deposit is marked by a prominent debris flow with poorly sorted clasts of white, grey and glassy black pumice, as well as various lavas and rare syenitic lithologies. Lapilli layers L1 to L5 are present as thin (< 30 cm) units intercalated with ash layers A1 to A5, which thicken substantially to the west. Many of the ash units contain accretionary lapilli up to 3 cm in size (Figure 5.8e). Samples of juvenile pumice lapilli were collected from each lapilli layer, a number of thin lapilli layers within the ash units, and syenitic nodules (samples S024 to S034, S080 to S088). The lava dome associated with the final stages of the Furnas J eruption was sampled at location 10 (Figure 5.4), on its south western flank (sample S021) and on the top of the dome (sample S022).

5.4.2 The Povoação Ignimbrite Formation

At three locations in and around the town of Povoação, the Povoação Ignimbrite Formation was identified and sampled (locations 15 to 17) (Figure 5.4). The base of the formation was observed at location 17b, on a trail from the western road out of Povoação down to the beach. Here, a pumice fall deposit of ~ 50 cm thickness underlies the welded base of the Povoação ignimbrite, with well sorted white pumices up to 5 cm in size (Figure 5.9a; 5.10). Juvenile pumice clasts were sampled from this initial pumice fall (sample S052). At location 15, on the beach of Povoação, the welded base of the Povoação ignimbrite was found. This densely welded outcrop contains dark, glassy fiamme up to 30 cm in long axis (Figure 5.9, 5.10). This juvenile glassy material was sampled (sample S047, S048).

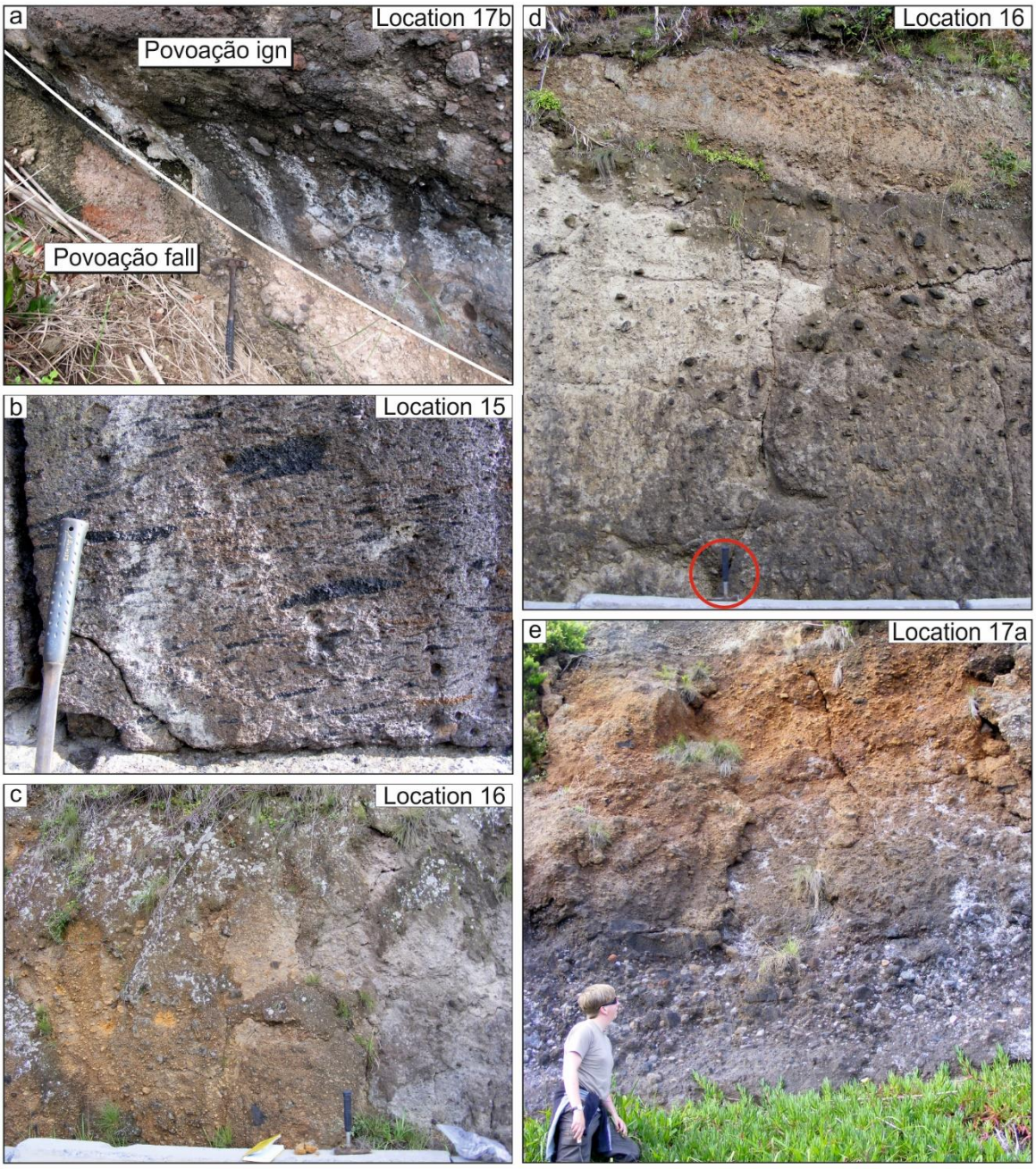

FIGURE 5.9 Field photographs of the Povoação Ignimbrite Formation **a)** Base of the Povoação ignimbrite with underlying pumice fall deposit. Hammer for scale (35 cm) **b)** Strongly welded base of the Povoação ignimbrite with distinctive glassy fiamme. Hammer for scale (35 cm) **c)** Roadside outcrop of partially welded Povoação ignimbrite with orange weathering (outcrop no longer accessible). Hammer for scale (30 cm) **d)** Partially welded, unaltered Povoação ignimbrite with distinctive dark grey pumice clasts (outcrop no longer accessible). Highlighted scale = 30 cm **e)** Coarse grained, lithic rich base of Povoação ignimbrite, overlain by pumice rich, unwelded ignimbrite

The partially or unwelded portions of the Povoação ignimbrite were located at locations 16 and 17a, around 130 m east of location 17b. Location 16 presents ~ 5 m of slightly welded pumiceous ignimbrite with abundant dense, crystal rich, grey pumice clasts up to ~ 20 cm in size (Figure 5.9c, d, 5.10). The lower outcrop comprises a ~ 4 m thick unit of

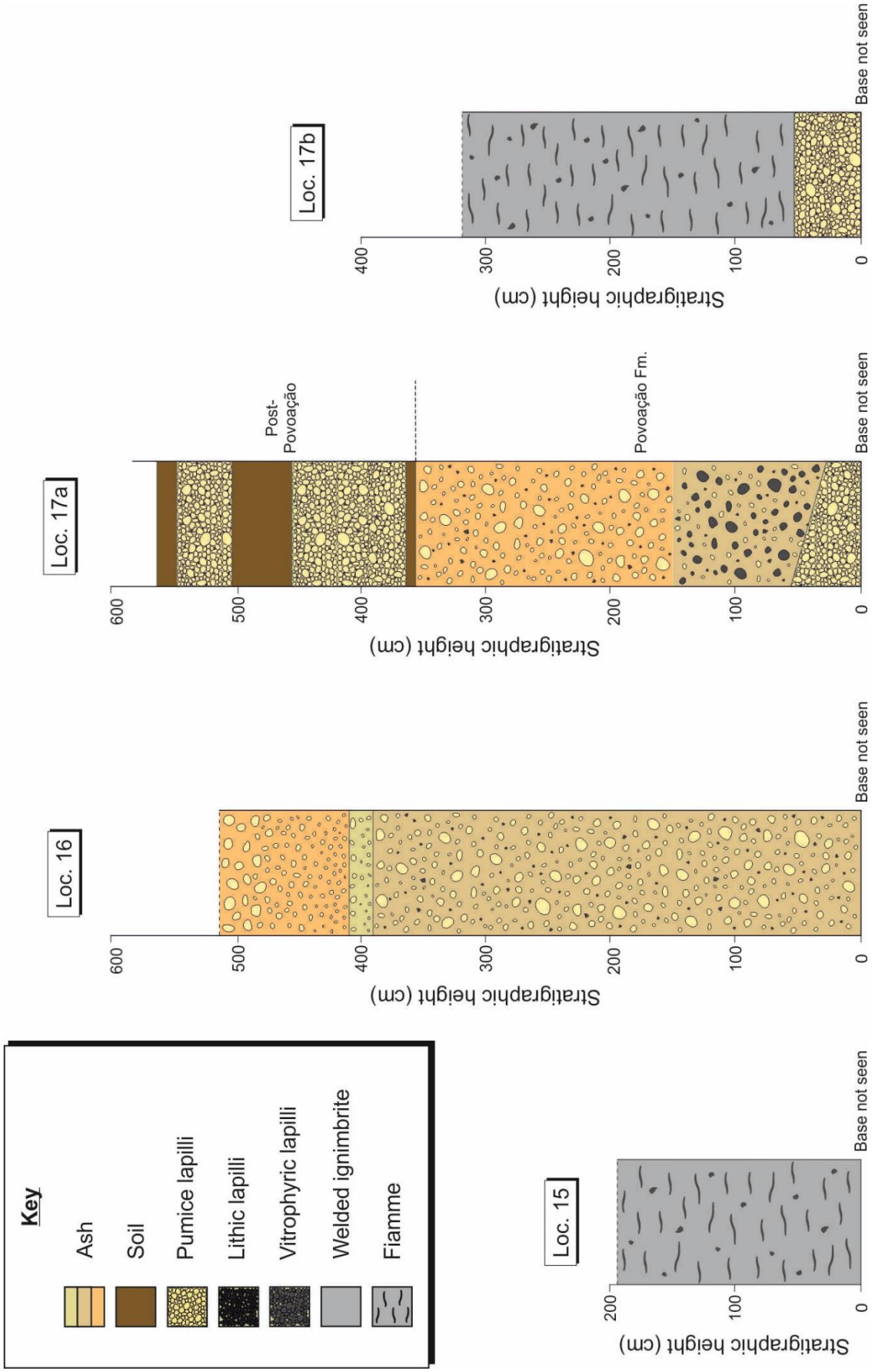
Key
Ash
Soil
Pumice lapilli
Lithic lapilli
Vitrophyric lapilli
Welded ignimbrite
Fiamme
Loc. 15
Base not seen
0
100
200
Stratigraphic height (cm)
Loc. 16
Base not seen
0
100
200
300
400
500
600
Stratigraphic height (cm)
Loc. 17a
Post-Povoação
Povoação Fm.
Base not seen
0
100
200
300
400
500
600
Stratigraphic height (cm)
Loc. 17b
Base not seen
0
100
200
300
400
Stratigraphic height (cm)

◄ **FIGURE 5.10:** Summarised stratigraphic logs of the Povoação Ignimbrite Formation. Location numbers are given in Figure 5.4

unstratified, coarse pumice rich (5 to 20 cm) ignimbrite, overlain by a thin (~ 40cm), reversely graded unit of finer grained (3 to 10 cm), and a thicker (~ 1 m) unit, also pumiceous and exhibiting reverse grading. Juvenile pumice clasts were collected from the lower unit (sample S049, S050).

5.5 Results

5.5.1 Petrography

5.5.1.1 Upper Furnas Group pumice falls

The fall deposits of the UFG are dominated by non-welded, highly vesicular, crystal poor to aphyric pumice clasts. The dominant mineralogy shows little variation throughout the deposits, comprising alkali feldspar, clinopyroxene, biotite, Fe-Ti oxides, and apatite, in approximate order of abundance. The majority of samples are entirely glassy, though some examples were found in which minor groundmass microlites are apparent. Additionally, a small number of pumice clasts from layer Lf of Furnas J (Figure 5.7) exhibit pronounced banding, notably higher crystal contents, more abundant groundmass microlites (Figure 5.11a), and rare inclusions of dense, crystalline material, of similar mineralogy to the pumice, which range in size from ~ 0.5 to 6 mm (Figure 5.11b).

Alkali feldspar is by far the most abundant phase, and exists as phenocrysts (up to ~ 2 mm), microphenocrystic fragments, and, more rarely, groundmass microlites. Phenocrysts are commonly tabular and euhedral (Figure 5.11c), but rare examples are rounded, with pronounced embayment structures (Figure 5.11d). Small crystal fragments with irregular, fractured forms are also present (Figure 5.11e), which may also be heavily resorbed (Figure 5.11f). Such examples are particularly common in the banded pumices of Furnas J described above. Where groundmass microlites are present, they are almost exclusively acicular, and do not exceed 100 μm in length (Figure 5.11a).

Clinopyroxene is common in the UFG fall deposits, and exists as relatively well formed, green microphenocrysts, typically less than 0.5 mm in length. Inclusions of acicular apatite are frequently observed (Figure 5.11g), and Fe-Ti oxide inclusions are ubiquitous (Figure 5.11h). In some instances, Fe-Ti oxides are only partially included in the host clinopyroxene, and have clearly impinged upon the growth of their host. More rarely,

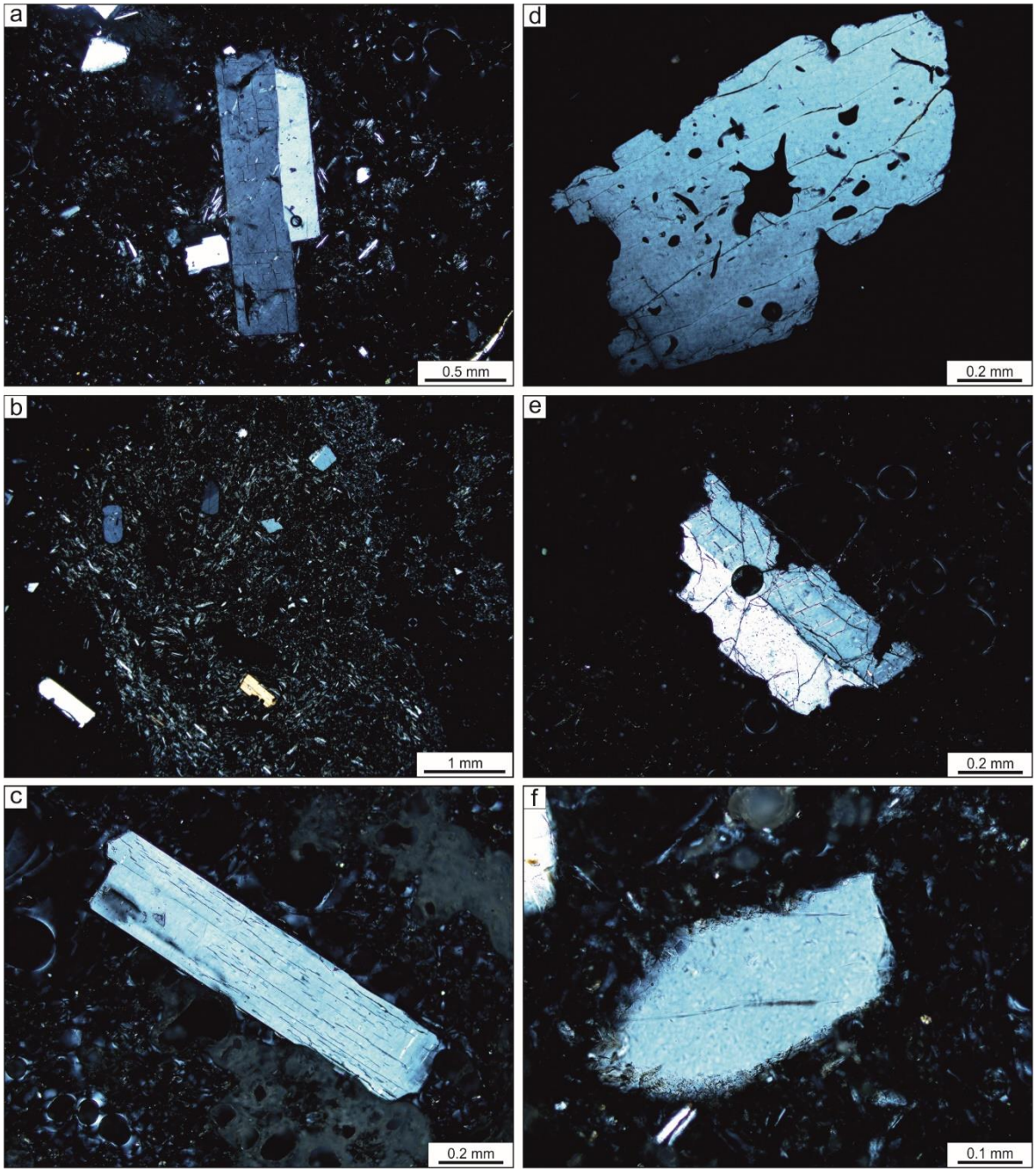

FIGURE 5.11: Representative photomicrographs of the UFG pumice falls **a)** Large alkali feldspar crystal surrounded by microphenocrystic fragments and groundmass microlites of the same mineral (xpl)l **b)** Small xenolithic clast of broadly trachytic composition, with dominant alkali feldspar and minor clinopyroxene (xpl) **c)** Large euhedral alkali feldspar phenocrysts (xpl) **d)** Large alkali feldspar showing highly resorbed and embayed edges (xpl) **e)** Large, irregular alkali feldspar fragment (xpl) **f)** Small, preserved, heavily resorbed alkali feldspar microphenocryst (xpl)

small (< 50 μm) clinopyroxene crystals are seen with more irregular crystal forms, either heavily fractured, or rounded and resorbed. Such examples are very rare, but are somewhat more abundant in the banded pumices of Furnas J.

Biotite is somewhat less common than clinopyroxene, and occurs as small (<0.5

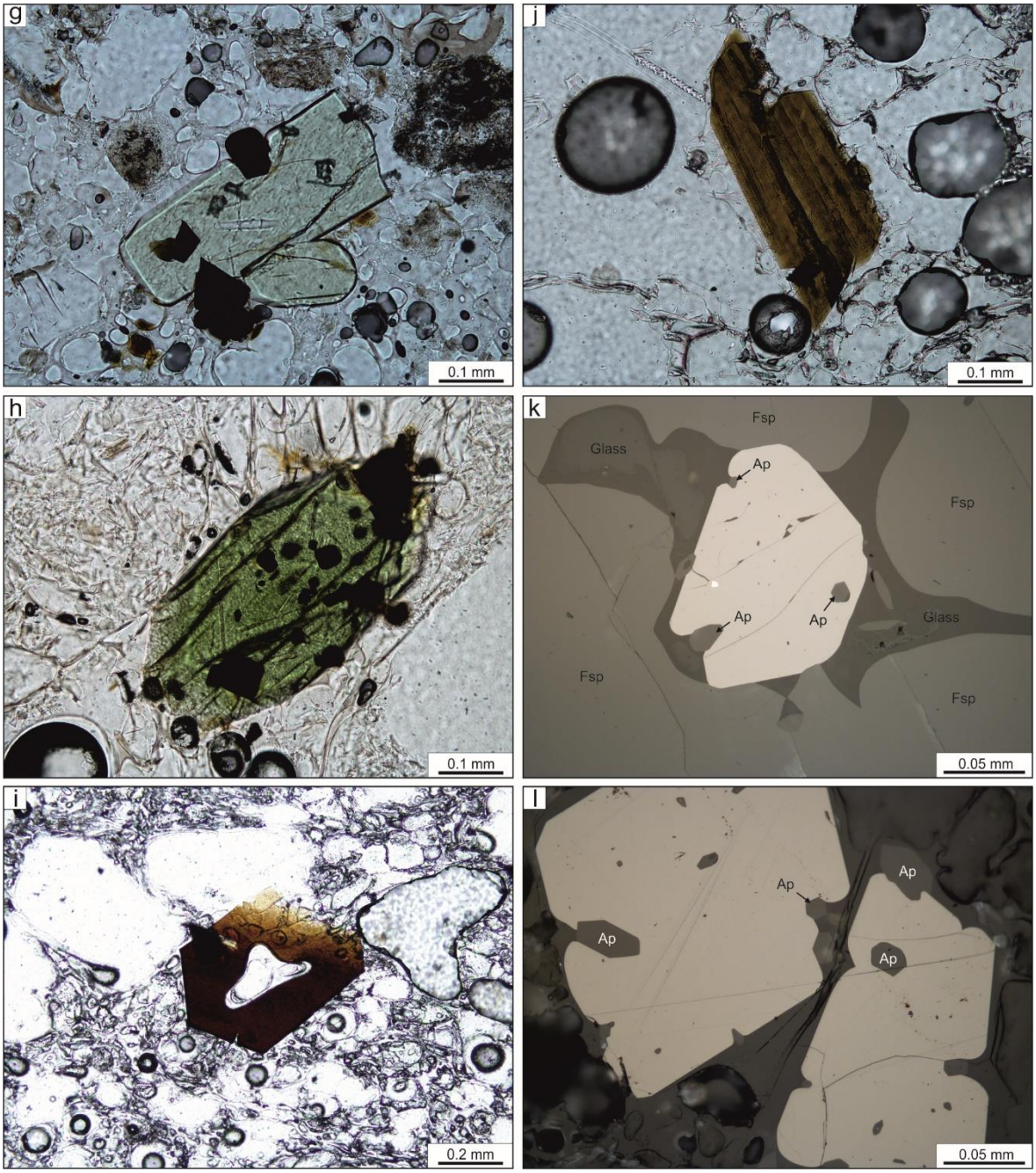

FIGURE 5.11 CONTINUED: g) Pale green clinopyroxene with associated oxides which partilally impinge upon clinopyroxene growth. Also, needle-like inclusions of apatite (ppl) **h)** Strongly green, well formed clinopyroxene crystal with a number of oxide and apatite inclusions (ppl) **i)** Euhedral crystal of biotite viewed down the c-axis, with evidence for partial resorption (ppl) **j)** Small subhedral biotite crystal, more typical of the UFG pumice falls (ppl) **k)** Fe-Ti oxide inclusion, surrounded by glass, found within the resorbed feldspar shown in Figure 8.xb. Apatite is also present, either included within the oxide or impinging upon its growth (rl) **l)** Two Fe-Ti oxide grains with numerous apatite inclusions and apparent embayment structures where apatite has inhibited crystal growth (rl). Abbreviations used: Fsp = alkali feldspar, Ap = apatite

mm) microphenocrysts (Figure 5.11i, j). Crystal forms are dominantly euhedral to subhedral and rarely show limited evidence for resorption. Fe-Ti oxides are generally very small (< 0.5 mm), subhedral, and frequently associated spatially with clinopyroxenes.

More rarely, they may be found as inclusions within feldspars. They are ubiquitously associated with small, acicular apatite crystals, which may be partially or fully included within the Fe-Ti oxide host (Figure 5.11k, l).

5.5.1.2 Upper Furnas Group lava domes

Samples collected from the UFG lava domes reveal mineral assemblages that are broadly similar to the UFG pumice falls, including phenocrysts and microphenocrysts of alkali feldspar, clinopyroxene, Fe-Ti oxides, biotite, and apatite, in approximate order of abundance. However, due to several key mineralogical and textural differences, the two domes are treated separately.

The lava dome associated with Furnas J is dominated by alkali feldspar, which can be found as phenocrysts up to ~ 5 mm in size, and also as relatively coarse, acicular microlites in the groundmass (up to ~ 0.4 mm) (Figure 5.12a). Phenocrystic feldspars range from euhedral to subhedral, with rounded edges and uncommon embayments providing evidence for partial resorption. Feldspar groundmass microlites frequently exhibit a well defined trachytic texture, which is also taken up by proximal phenocrysts. Rarely, feldspars are observed as distinctive glomerocrysts that reach sizes of up to ~ 2 mm, and comprise a number of partially resorbed feldspar phenocrysts that meet at irregular and often lobate boundaries.

Clinopyroxene is found throughout the dome as phenocrysts (up to ~ 1 mm) and groundmass microlites (up to ~ 0.1 mm). As observed in the UFG pumice falls, it is characteristically green and ubiquitously associated with smaller Fe-Ti oxide crystals which are partially or totally included within the larger clinopyroxene crystal (Figure 5.12b). Phenocrystic and microphenocrystic clinopyroxenes display brown alteration rims that also extend along any fractures the cut through the crystal. In addition to Fe-Ti- oxides, small apatite needles are also frequently observed as inclusions.

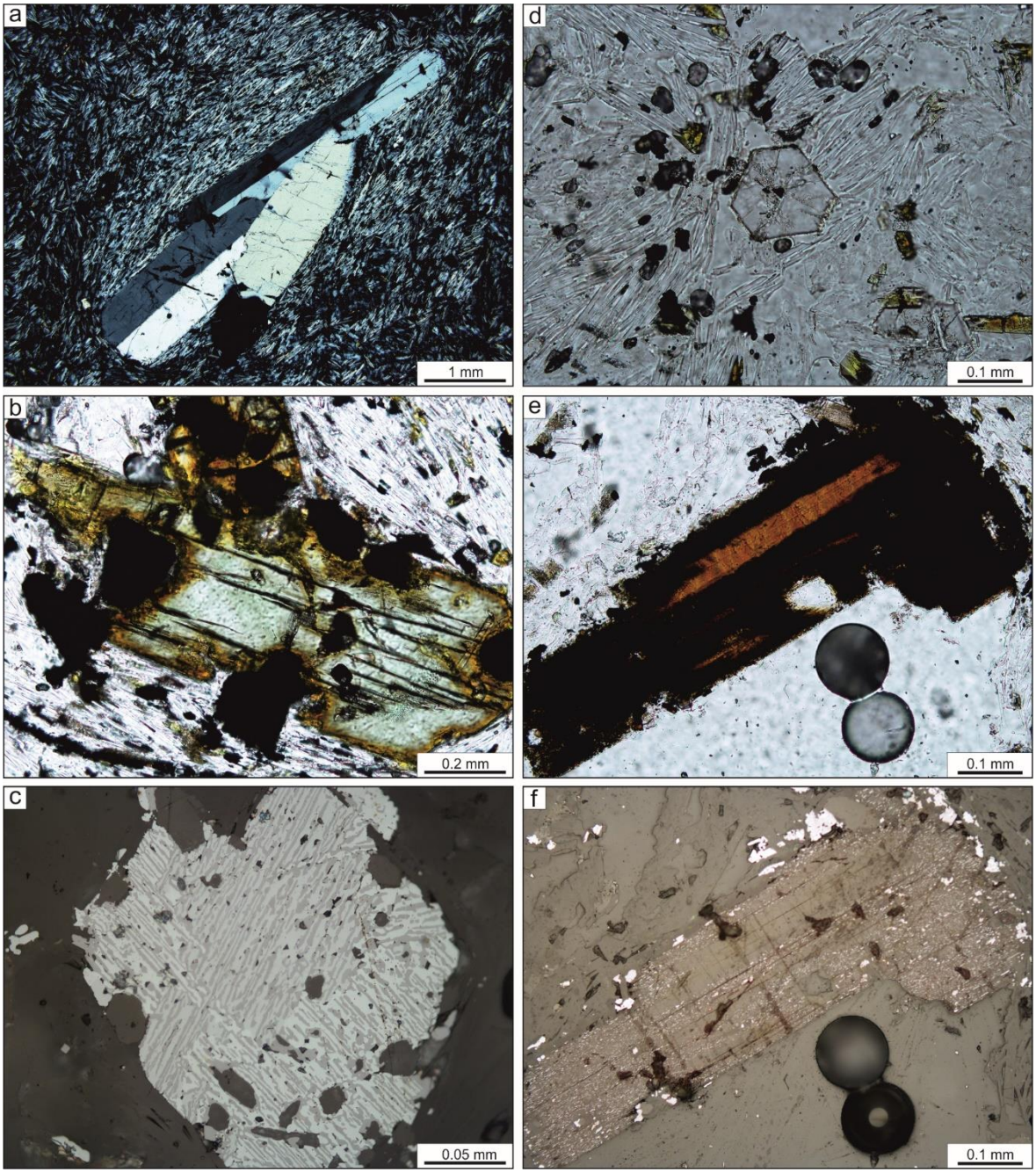

FIGURE 5.12: Representative photomicrographs of the Furnas J lava dome **a)** Large, slightly rounded alkali feldspar phenocrysts set in a groundmass of aligned feldspar microlites (xpl) **b)** Green clinopyroxene microphenocryst showing brown alteration rim and characteristic spatial association with Fe-Ti oxides (ppl) **c)** Ragged Fe-Ti oxide crystal with numerous apatite and inclusions and slightly irregular exsolution texture (rl) **d)** Small, euhedral sodalite microphenocryst surrounded by acicular groundmass feldspars and clinopyroxenes (ppl) **e)** Highly altered biotite phenocryst (ppl), with **f)** distinctive Fe-Ti oxide-bearing alteration rim (rl)

Fe-Ti oxides are found as uncommon microphenocrysts (generally between 0.25 and 0.5 mm in size) and abundant groundmass crystals (< 50 μm). Microphenocrysts frequently exhibit exsolution lamellae (Figure 5.12c), which range from relatively ordered

to entirely irregular. Such features are rare in the groundmass oxides. Like the UFG pumice falls, inclusions and partial inclusions of apatite are abundant.

In contrast to the UFG pumice falls, the Furnas J dome also contains sodalite, which can be found as well formed, equant microphenocrysts that are typically no larger than ~ 0.2 mm in size (Figure 5.12d). Inclusions of feldspar and clinopyroxene are extremely common, and feldspar microlites frequently impinge upon the sodalite crystal faces. In some cases, sodalite appears rounded and partially embayed, indicating resorption.

Biotite is uncommon and is generally found as microphenocrysts, less than 0.2 mm in length. Examples are frequently well formed and often aligned with the trachytic texture in the groundmass. Rare examples of larger, phenocrystic biotite, up to 0.75 mm in length, are present in some samples (Figure 5.12e). Unlike microphenocrystic biotite, these examples are ubiquitously ragged and exhibit prominent reaction rims, which contain abundant small Fe-Ti oxides, and also run along some fractures and cleavage planes (Figure 5.12f).

The Furnas I lava dome is similar to the Furnas J dome, with alkali feldspar phenocrysts surrounded by a coarse, alkali feldspar-based groundmass (Figure 5.13a), as well as uncommon alkali feldspar glomerocrysts that show irregular and lobate interior grain boundaries (Figure 5.13b). Green clinopyroxene is found as rounded phenocrysts (up to ~ 1 mm) in length, and as small microlites in the groundmass (Figure 5.13c). Fe-Ti oxides are present as frequently exsolved microphenocrysts that are associated with the clinopyroxene phenocrysts, and as groundmass crystals. Biotite was rarely observed in the Furnas I dome, as small subhedral microphenocrysts (< 0.2 mm), or rare, ragged phenocrysts with an Fe-Ti oxide-rich reaction rim (Figure 5.13d, e). Sodalite microphenocrysts are generally small (< 0.2 mm) and euhedral, with abundant inclusions

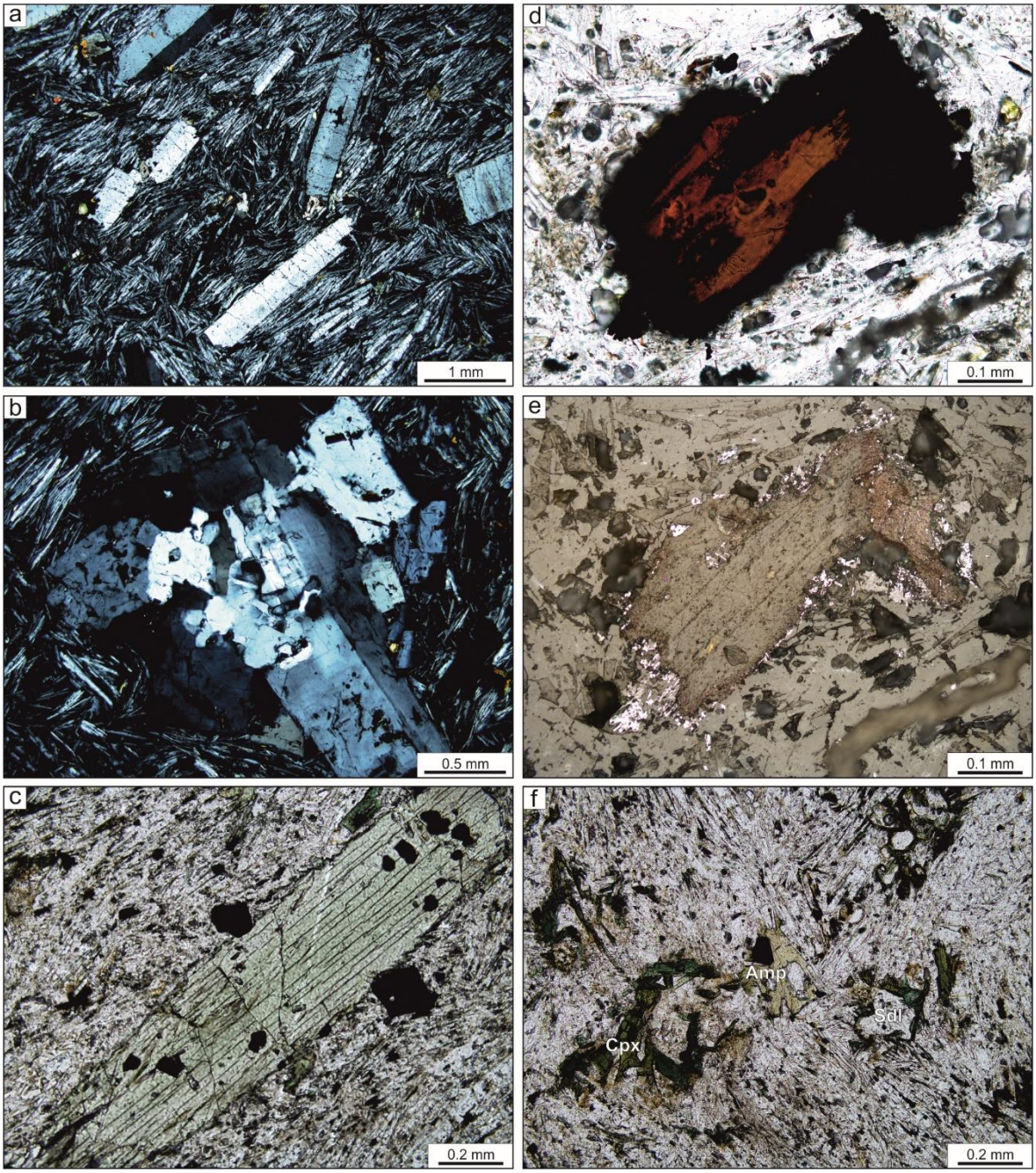

FIGURE 5.13: Representative photomicrographs of the Furnas I lava dome **a)** Elongate and partially aligned alkali feldspar phenocrysts surrounded by a coarse, alkali feldspar dominated groundmass (xpl) **b)** Alkali feldspar glomerocryst showing irregular and lobate interior grain boundaries (xpl) **c)** Green clinopyroxene phenocrysts with numerous included and spatially associated Fe-Ti oxide crystals (ppl) **d)** Heavily resorbed and reacted red-brown amphibole showing (ppl) **e)** a prominent reaction rim with numerous small, bleb-like Fe-Ti oxides (rl) **f)** Irregular green clinopyroxene, green amphibole and sodalite in an alkali feldspar dominated groundmass (ppl). Abbreviations used: Amp = amphibole, Cpx = clinopyroxene, Sdl = sodalite

of feldspar and clinopyroxene. Unlike the Furnas J dome, the Furnas I dome also contains a green amphibole, found only as anhedral, interstitial crystals in the groundmass (Figure 5.13f).

5.5.1.3 Furnas syenite ejecta

At Ribeira Quente (location 12), a number of coarse to medium grained syenitic clasts were sampled from the pyroclastic flow units associated with the Furnas J eruption (Figure 5.4, 5.5) (Cole *et al.*, 1995). Individual specimens rarely exceed ~ 10 cm in size, and, in some instances, contain enclaves of darker, finer-grained rock. Boundaries between enclave material and host syenite range from sharp and well defined to irregular and diffuse and, in some samples, both boundary types can be observed (Figure 5.14). Mineral assemblages of both syenite and enclaves are dominated by alkali feldspar, with subsidiary clinopyroxene, amphibole, Ti-magnetite, ilmenite, biotite, pyrrhotite, and rare zircon.

Within the syenite, alkali feldspars account for more than 90 % of the phase assemblage, and form a cumulus framework of euhedral to subhedral, tabular crystals up to 5 mm in length (Figure 5.15a). Perthitic textures are ubiquitous. Clinopyroxene is present in two distinctive forms: 1) predominantly anhedral, intercumulus crystals which reach up to ~ 2 mm in length and are often zoned (Figure 5.15a), and 2) radial clusters of fine grained, acicular crystals which are either in close association with large, ragged amphibole crystals (Figure 5.15b), or project inwards from the margin of void spaces (Figure 5.15c). Amphiboles are similar to clinopyroxene, being restricted to intercumulus, anhedral crystals which do not exceed 2 mm, are frequently ragged and in close spatial association with acicular clinopyroxene, and are often zoned (Figure 5.15b). Biotite is uncommon and found only as relatively small (< 1 mm) and ragged crystals, which are frequently included within larger feldspars (Figure 5.15d). Ilmenite and Ti magnetite are limited to small (< 0.5 mm), irregular crystals which are often associated spatially, or included within clinopyroxene and pyrrhotite (Figure 5.15e). The latter forms small, irregular patches within intercumulus spaces, and often exhibits concentric growth zoning (Figure 5.15e).

Syenite-hosted enclaves are finer grained than their host, comprising

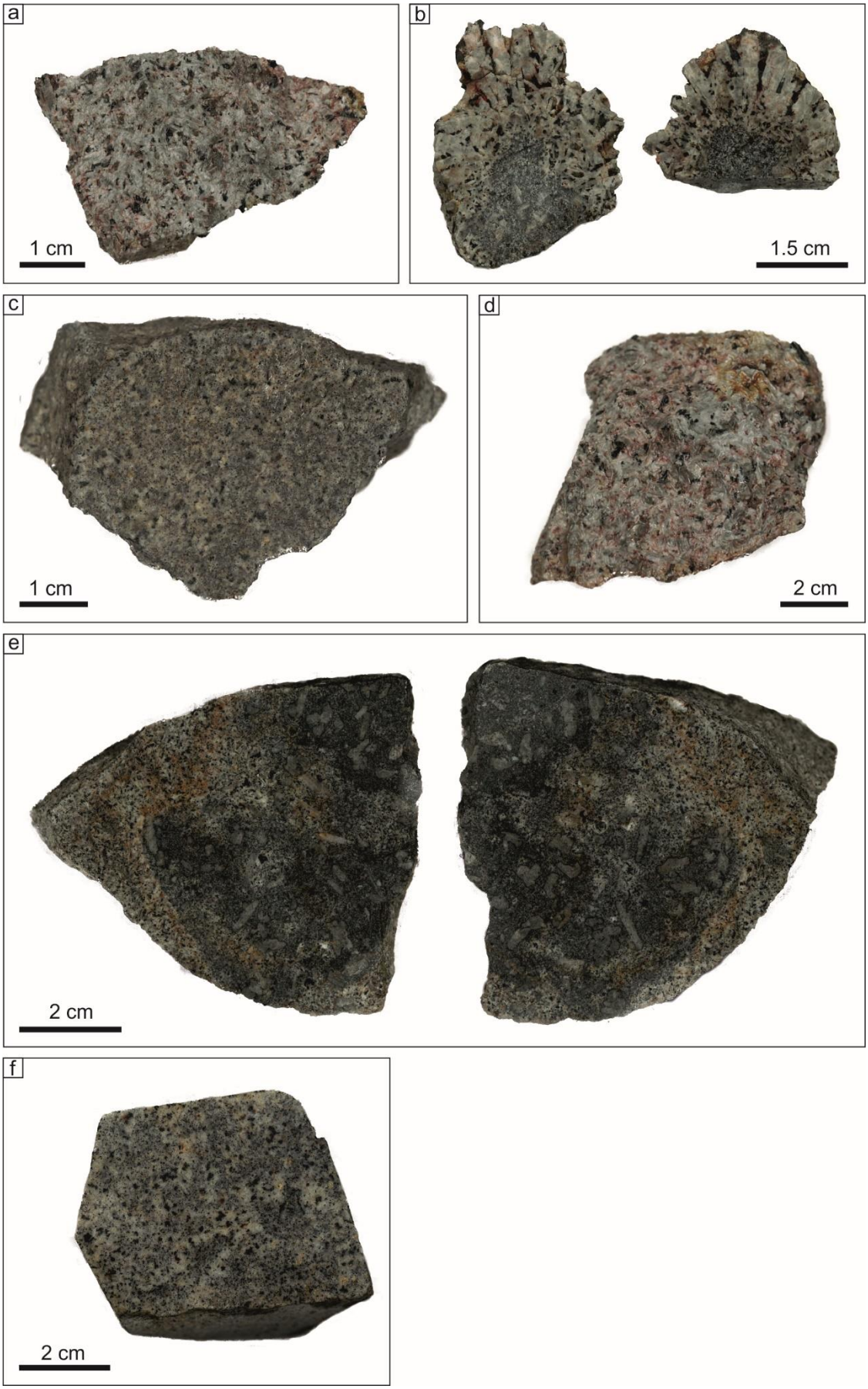

FIGURE 5.14: Representative hand specimen photographs of the Furnas J syenite ejecta and syenite-hosted trachyte enclaves

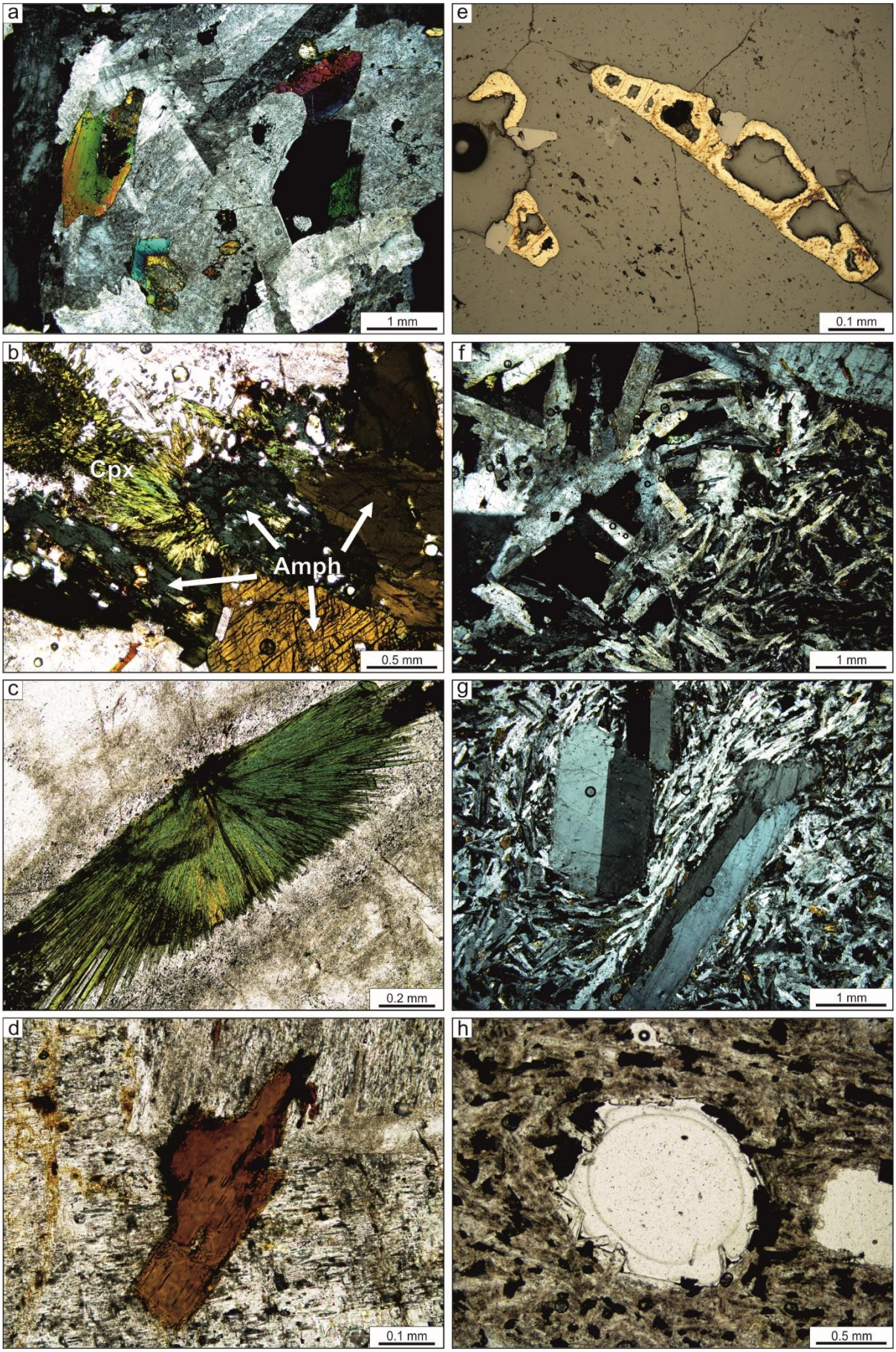
a
1 mm
e
0.1 mm
b
Cpx
Amph
0.5 mm
f
1 mm
c
0.2 mm
g
1 mm
d
0.1 mm
h
0.5 mm

◄ **FIGURE 5.15:** Representative photomicrographs of the Furnas J syenite ejecta and syenite-hosted enclaves **a)** Coarse grained syenite with cumulus, perthitic alkali feldspars and intercumulus, zoned clinopyroxene (xpl) **b)** Large ragged amphiboles and associated acicular clinopyroxene. A strongly zoned amphibole is visible in the centre-right (ppl) **c)** Radial aggregate of acicular clinopyroxene filling an interstitial void space (ppl) **d)** Small ragged biotite crystal included within larger perthitic feldspars (ppl) **e)** Concentric pyrrhotite growth patterns and associated Fe-Ti oxides partially filling an intercumulus void space (rl) **f)** Contact zone between coarse grained syenite and medium grained enclave (xpl) **g)** Alkali feldspar phenocrysts set within the finer grained groundmass of the enclaves. Numerous amphiboles and clinopyroxenes are visible in the groundmass, which exhibits a trachytic texture (xpl) **h)** Miarolitic cavity within an enclave, showing late stage growth of alkali feldspar and amphibole at its margins (ppl)

predominantly a medium grained groundmass of alkali feldspar laths up to ~ 1 mm in length (Figure 5.15f). Large, tabular, euhedral phenocrysts of alkali feldspar are also common, reaching sizes up to~ 10 mm (Figure 5.15g). Groundmass feldspars often exhibit a trachytic texture, which is deflected by the phenocrysts (Figure 5.15g). Additional groundmass phases include green clinopyroxenes, abundant brown amphiboles, and Fe-Ti oxides. Miarolitic cavities are common, and generally contain late stage growths of alkali feldspar and amphibole at their margins (Figure 5.15h).

5.5.1.4 Povoação pumice fall

The Povoação pumice fall comprises extremely crystal poor vesicular pumices, and exhibits a broadly similar mineral assemblage to the UFG pumice falls, with alkali feldspar, green clinopyroxene, Fe-Ti oxides, and apatite, in approximate order of abundance. These are set in microlite-free, highly vesicular glass. Like other Furnas lithologies, alkali feldspar is the dominant mineral phase, and can be found as microphenocrysts (generally < 0.25 mm) and, more rarely, as phenocrysts (up to 1 mm in size). Regardless of size, all alkali feldspar crystals are highly fractured crystal remnants with anhedral forms and frequent evidence of partial resorption (Figure 5.16a). Clinopyroxene can be found as subhedral to anhedral microphenocrysts (< 0.25 mm) and occasional phenocrysts (up to 0.75 mm in size). Where found, it is frequently associated with Fe-Ti oxides and acicular apatite, both of which are found as abundant inclusions in the majority of clinopyroxene crystals (Figure 5.16b). Fe-Ti oxides are unexsolved and generally host a number of inclusions, which are predominantly apatite or melt (now glass), or more unusually,

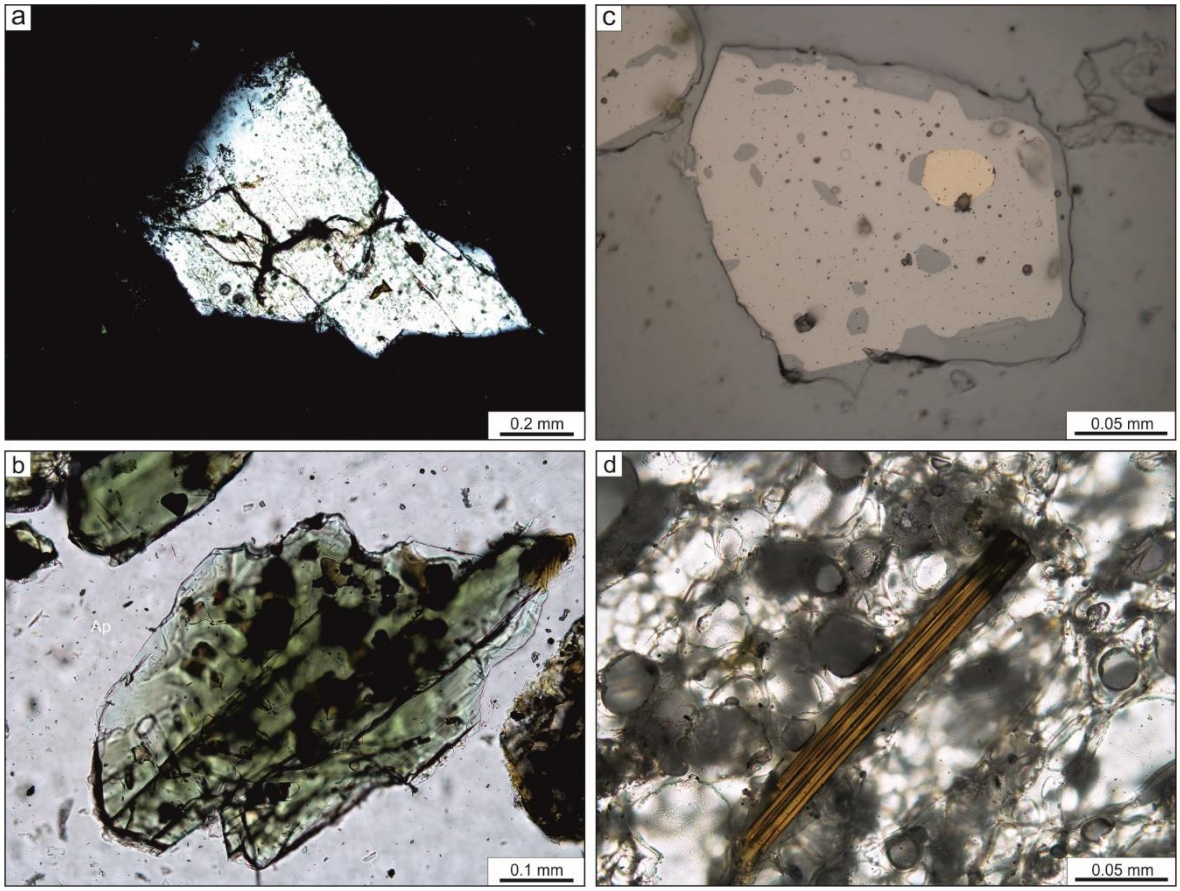

FIGURE 5.16: Representative photomicrographs of the Povoação pumice fall **a)** Irregular, fragmented alkali feldspar phenocrysts (xpl) **b)** Anhedral green clinopyroxene phenocrysts with abundant inclusions of equant Fe-Ti oxides, acicular apatite, and brown melt inclusions (ppl) **c)** Small Fe-Ti oxide crystal with a number of apatite and melt inclusions, as well as a prominent sulphide grain (rl) **d)** Small, euhedral bitotie crystal surrounded by highly vesicular glass (ppl)

sulphide (Figure 5.16c). Biotite is uncommon, and found as small (< 0.25 mm), euhedral microphenocrysts (Figure 5.16d).

5.5.1.5 Povoação ignimbrite

The Povoação ignimbrite contains pumice clasts that range from vesicular and crystal poor, to dense vitrophyre, with a mineral assemblage comprising alkali feldspar, green clinopyroxene, biotite, Fe-Ti oxides, and apatite, in approximate order of abundance.

As in previously described Furnas lithologies, alkali feldspar represents the most abundant phase, and is present in a number of forms, including large, euhedral phenocrysts (up to ~ 4mm in length) (Figure 5.17a), small, partially resorbed microphenocrystic crystal fragments (< ~ 0.5 mm) (Figure 5.17b), and large

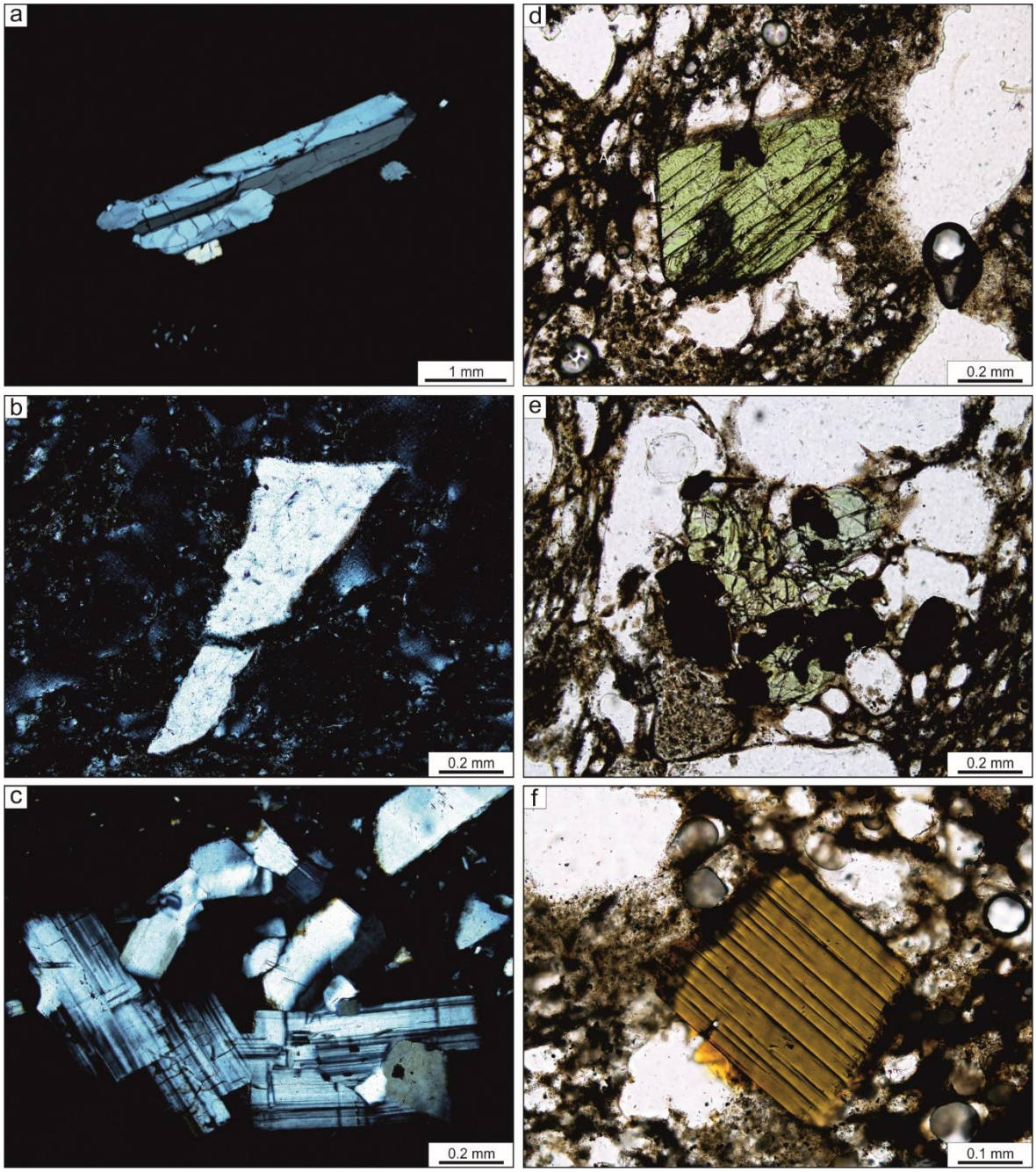

FIGURE 5.17: Representative photomicrographs of the Povoação ignimbrite **a)** A large euhedral phenocryst of alkali feldspar surrounded by vesicular glass(xpl) **b)** An example of an anhedral microphenocryst of alkali feldspar, with partially resorbed crystal margins (xpl) **c)** Glomerocrystic crystal cluster comprising both euhedral and anhedral alkali feldspar crystals (xpl) **d)** Relatively well formed, green clinopyroxene microphenocryst with a number of Fe-Ti oxide inclusions (ppl) **e)** A glomerocrystic cluster of relatively euhedral Fe-Ti oxides and green clinopyroxene (ppl) **f)** a euhedral microphenocryst of biotite surrounded by vesicular glass (ppl)

glomerocrysts (up to ~ 2 mm in size) comprising multiple, euhedral feldspars, often displaying irregular internal grain boundaries (Figure 5.17c).

Green clinopyroxene can be found as microphenocrysts (generally < 0.5 mm) that range from euhedral to subhedral and usually contain included or partially included Fe-Ti

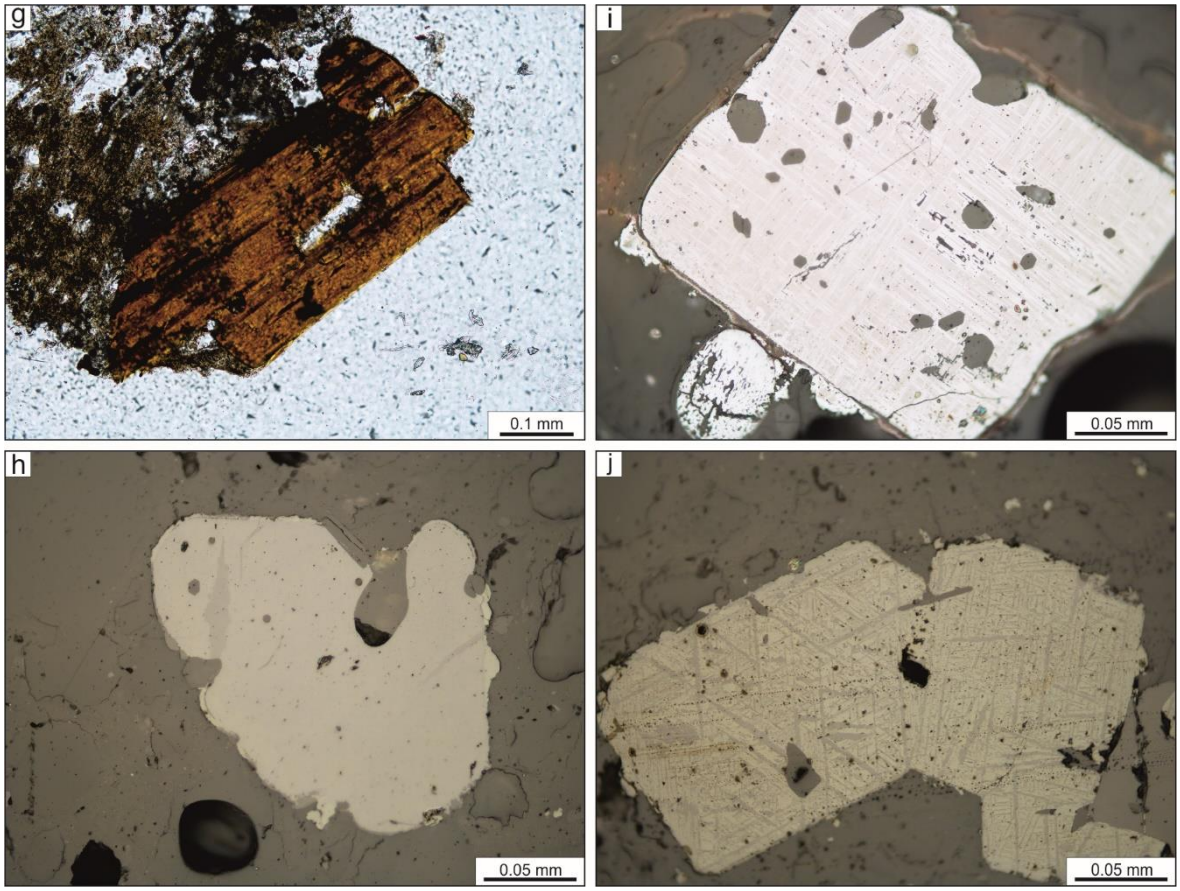

FIGURE 5.17 CONTINUED: g) Large, ragged phenocryst of biotite with evidence of resorption (ppl) **h)** Embayed Fe-Ti oxide crystal small apatite inclusions and partial inclusions (rl) **i)** Subhedral Fe-Ti oxide with numerous inclusions of both apatite and melt (now glass), and regular exsolution lamellae (rl) **j)** Multiple euhedral Fe-Ti oxides with pronounced, regular exsolution lamellae (rl)

oxides (Figure 5.17d). Alternatively, clinopyroxene can be found as glomerocrystic clusters of anhedral clinopyroxene and Fe-Ti oxides (Figure 5.17e). Biotite is also present as microphenocrysts (< 0.5mm) which are typically euhedral (Figure 5.17f), but may show some evidence of partial resorption (Figure 5.17g), and occasionally contains small inclusions of acicular apatite. Fe-Ti oxides are restricted to small (< 0.5 mm) microphenocrysts that range from relatively euhedral to anhedral with pronounced embayment structures (Figure 5.17h). Inclusions of apatite and melt (now glass) are common but not ubiquitous (Figure 5.17i). As described in the UFG, some Fe-Ti oxides exhibit a regular exsolution texture, as seen in Figures 5.17i and 5.17j. However, this feature is not universal, and numerous examples exhibit no evidence for exsolution.

5.5.2 Mineral chemistry

5.5.2.1 Feldspars

Feldspar phenocrysts compositions for the UFG and PIF are presented in Figure 5.18. Representative quantitative analyses are given in Table 5.1, and the full dataset can be found in Appendix C. The majority of UFG analyses lie upon the anorthoclase-sanidine boundary, with compositions that lie within Or_{23-48}, Ab_{48-69}, An_{0-7}. A notable exception to this exists in Furnas H, where a single feldspar analysis shows a significantly less potassic composition (Or_{16}, Ab_{65}, An_{19}), plotting in the uppermost anorthoclase field. Feldspar phenocrysts analyses from the lava domes of Furnas J and Furnas I exhibit a similar range to their respective pumice falls, though they extend to slightly more sodic compositions. Substituting elements such as BaO, SrO and FeO are frequently below the detection limit, and reach maximum concentrations of 0.19, 0.07, and 0.74 wt. %, respectively. The less potassic crystal from Furnas H has similar Fe and Sr contents, but exhibits a significantly larger Ba content of 0.92 wt. %.

The PIF feldspars are more generally potassic than those of the UFG, plotting almost entirely within the sanidine field, and exhibiting a compositional range of Or_{36-56}, Ab_{40-63}, An_{2-7}. The feldspars within the Povoação fall are slightly more potassic than those of the Povoação ignimbrite, though a single analysis is significantly more calcic (Or_{5}, Ab_{55}, An_{40}), plotting as andesine. Similarly, the Povoação ignimbrite exhibits three analyses which are less potassic (Or_{21-31}, Ab_{40-64}, An_{12-15}), and are classified as anorthoclase. Maximum concentrations of BaO, SrO, and FeO in the Povoação ignimbrite feldspars are comparable with the UFG feldspars, with maximum values of 0.36, 0.09, and 0.68 wt. % respectively. However, the Povoação fall feldspars display higher contents of both BaO and SrO (1.58 and 0.36 wt. %, respectively).

Feldspar compositions from the Furnas J syenite ejecta are broadly similar to those of the UFG and PIF, straddling the boundary between the anorthoclase and sanidine fields (Figure 5.19). With the exception of a small number of analyses which plot

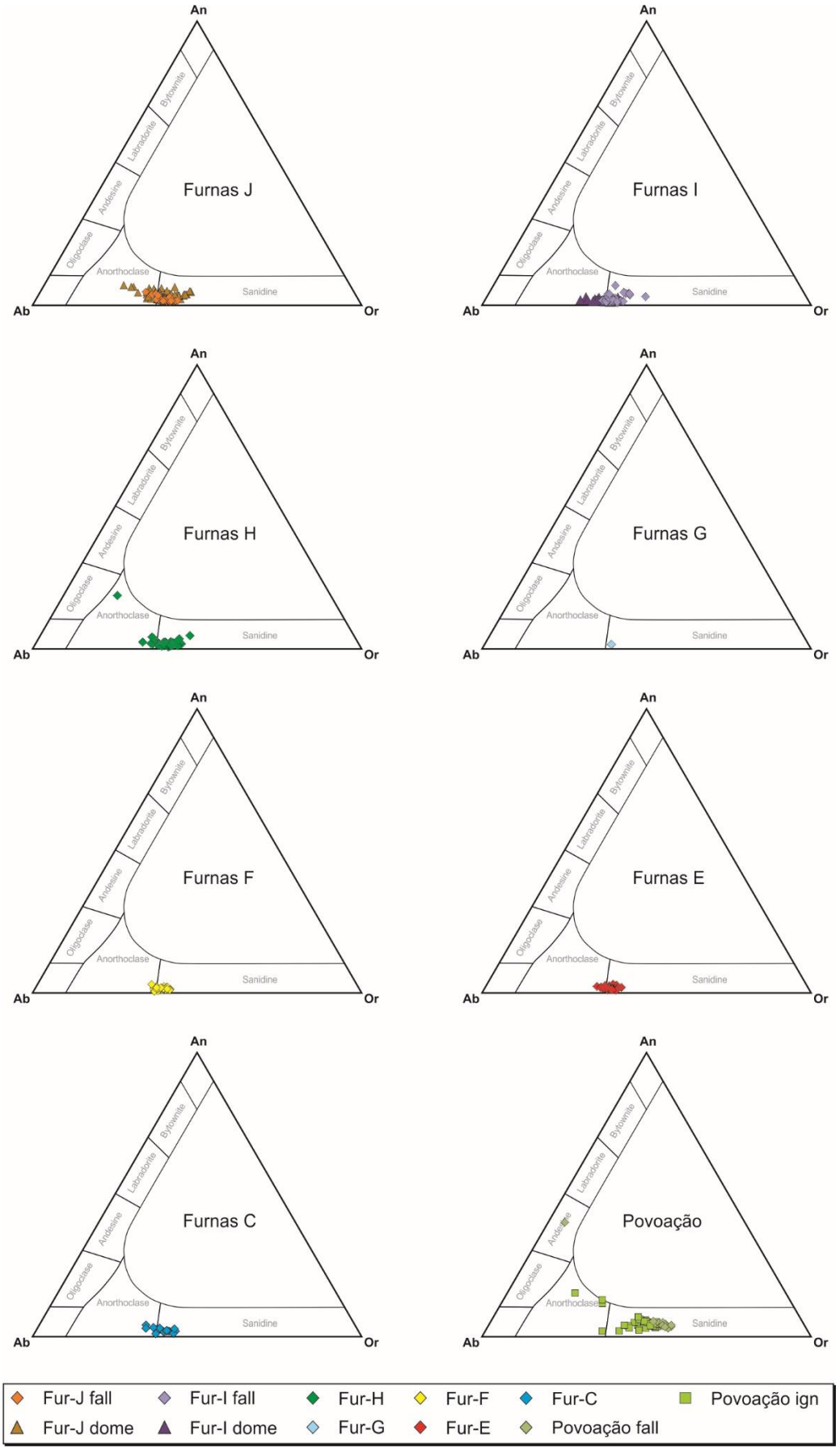

FIGURE 5.18: Feldspar compositions for the UFG and PIF, plotted into the ternary An-Ab-Or system

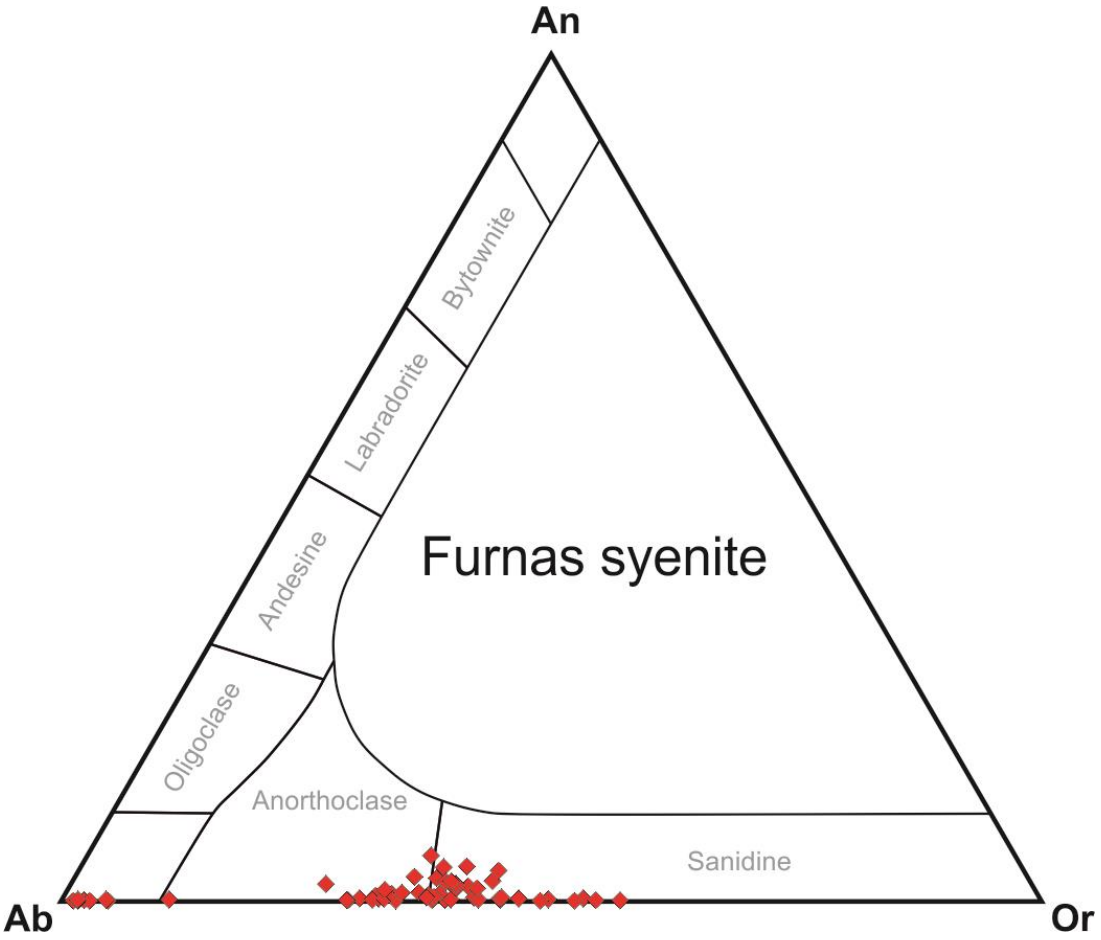

FIGURE 5.19: Feldspar compositions for the Furnas J syenite ejecta, plotted into the ternary An-Ab-Or system

near pure end member albite compositions, the population can be defined by the range Or_{26-57}, Ab_{43-72}, An_{0-5} (Table 5.2). The albitic analyses are indicative of albitisation of the syenite during deuteric alteration, as shown by the abundance of patchy perthitic textures in the alkali feldspars. Barium and strontium concentrations are lower than both the UFG and the PIF, and do not exceed 0.07 and 0.03 wt. %, respectively. The analysed FeO contents are more comparable to the UFG and the PIF, being almost entirely restricted to < 0.6 wt. %.

Table 5.1 Representative feldspar compositions for the UFG and PIF

Unit	**Fur-J**		**Fur-J dome**		**Fur-I**		**Fur-I dome**		**Fur-H**	
Sample	S018	S018	SM7-1	SM7-1	S038	S038	SM5-1	SM5-1	S003	S003
No.	Fsp9	Fsp36	29/1	KFsp11	Fsp10	Fsp28	13/1	KFsp22	Fsp34	Fsp9
SiO_2	64.84	66.19	63.94	66.67	65.55	64.83	66.29	66.95	61.69	64.40
TiO_2			0.15				0.10			
Al_2O_3	19.57	19.00	19.50	19.40	19.11	18.98	18.72	19.36	22.97	19.73
BaO	0.01	0.03	0.02	0.00	0.00	0.02	0.00	0.00	0.92	0.03
FeO	0.34	0.25	0.64	0.30	0.28	0.49	0.70	0.25	0.22	0.20
SrO	0.00	0.00	0.00	0.00	0.00	0.00	0.03	0.01	0.07	0.00
MgO			0.01				0.00			
CaO	1.02	0.38	1.41	0.45	0.56	0.67	0.42	0.27	3.86	1.03
Na_2O	7.29	6.19	7.72	6.53	7.13	5.61	8.00	6.57	7.28	5.83
K_2O	5.59	7.34	4.87	7.15	6.56	8.50	5.06	7.13	2.75	8.02
Total	98.66	99.38	98.25	100.50	99.20	99.10	99.32	100.54	99.76	99.25
Si	2.942	2.987	2.919	2.975	2.966	2.960	2.982	2.983	2.780	2.932
Ti			0.005				0.003			
Al	1.047	1.011	1.049	1.020	1.019	1.021	0.993	1.017	1.220	1.059
Ba	0.000	0.001	0.000	0.000	0.000	0.000	0.000	0.000	0.016	0.001
Fe	0.013	0.009	0.025	0.011	0.011	0.019	0.026	0.009	0.008	0.008
Sr	0.000	0.000	0.000	0.000	0.000	0.000	0.001	0.000	0.002	0.000
Mg			0.001				0.000			
Ca	0.049	0.018	0.069	0.022	0.027	0.033	0.020	0.013	0.186	0.050
Na	0.641	0.542	0.683	0.565	0.625	0.497	0.697	0.568	0.636	0.515
K	0.324	0.423	0.284	0.407	0.379	0.495	0.291	0.405	0.158	0.466
Sum	5.017	4.990	5.035	5.001	5.027	5.025	5.012	4.995	5.007	5.029
Ab	63.2	55.1	66.0	56.9	60.6	48.5	69.2	57.6	64.9	49.9
An	4.9	1.9	6.7	2.2	2.6	3.2	2.0	1.3	19.0	4.9
Or	31.9	43.0	27.4	41.0	36.7	48.3	28.8	41.1	16.1	45.2

Table 5.1 continued

Unit	**Fur-G**	**Fur-F**		**Fur-E**		**Fur-C**		**Povo fall**		**Povo ign**	
Sample	MI01Fsp	S042	S042	S012	S012	S016	S016	EPF	EPF	SM10-1	SM-10
No.		Fsp40	Fsp35	Fsp36	Fsp24	MI01_fsp	Fsp8	MI05Fsp	Fsp6	43 / 1	KFsp37
SiO_2	67.05	66.88	66.19	66.29	65.94	66.06	65.15	57.14	65.19	63.04	66.37
TiO_2										0.06	
Al_2O_3	19.38	19.42	19.16	19.32	19.31	20.07	19.55	26.74	19.58	21.61	19.76
BaO	0.02	0.00	0.00	0.02	0.01	0.00	0.00	0.15	0.13	0.04	0.11
FeO	0.26	0.29	0.26	0.29	0.24	0.23	0.24	0.43	0.30	0.41	0.22
SrO	0.00	0.00	0.00	0.00	0.00	0.01	0.00	0.36	0.09	0.02	0.03
MgO										0.00	
CaO	0.36	0.41	0.26	0.52	0.44	0.61	0.39	8.31	0.73	3.30	0.78
Na_2O	6.93	7.07	6.71	7.63	6.63	7.42	6.47	6.20	4.61	7.54	5.15
K_2O	6.72	6.44	7.28	6.16	7.39	5.81	7.52	0.89	9.58	3.68	9.05
Total	100.71	100.51	99.86	100.22	99.97	100.22	99.32	100.22	100.22	99.70	101.47
Si	2.980	2.977	2.977	2.965	2.966	2.947	2.952	2.573	2.951	2.834	2.958
Ti										0.002	
Al	1.015	1.019	1.015	1.018	1.024	1.055	1.044	1.419	1.045	1.145	1.038
Ba	0.000	0.000	0.000	0.000	0.000	0.000	0.000	0.003	0.002	0.001	0.002
Fe	0.010	0.011	0.010	0.011	0.009	0.009	0.009	0.016	0.012	0.015	0.008
Sr	0.000	0.000	0.000	0.000	0.000	0.000	0.000	0.009	0.002	0.001	0.001
Mg										0.000	
Ca	0.017	0.019	0.013	0.025	0.021	0.029	0.019	0.401	0.036	0.159	0.037
Na	0.597	0.610	0.585	0.662	0.578	0.642	0.568	0.541	0.405	0.657	0.445
K	0.381	0.366	0.418	0.351	0.424	0.331	0.435	0.051	0.553	0.211	0.515
Sum	5.001	5.002	5.017	5.032	5.023	5.012	5.027	5.014	5.005	5.025	5.003
Ab	60.0	61.3	57.6	63.7	56.5	64.1	55.6	54.5	40.7	64.0	44.6
An	1.7	1.9	1.3	2.4	2.1	2.9	1.9	40.4	3.6	15.5	3.7
Or	38.3	36.7	41.1	33.9	41.4	33.0	42.5	5.1	55.7	20.5	51.6

Table 5.2 Representative feldspar analyses for the Furnas J syenite

Unit					**Furnas J syenite**					
Sample	FurJSyC	FurJSyC	FurJSyC	FurJSyC	Fur-J	Fur-J	FurJSyC	FurJSyC	FurJSyC	FurJSyC
No.	Fsp16	Fsp24	Fsp25	Fsp28	MI05Fsp	MI02Fsp	Fsp11	Fsp10	Fsp9	Fsp12
SiO_2	68.89	67.49	67.01	67.15	66.20	66.75	66.12	66.26	65.95	65.65
Al_2O_3	19.48	19.69	19.16	19.33	19.22	19.36	19.62	19.84	19.71	20.14
BaO	0.00	0.01	0.00	0.01	0.02	0.00	0.01	0.04	0.02	0.07
FeO	0.20	0.21	0.26	0.24	0.36	0.28	0.21	0.19	0.20	0.21
SrO	0.00	0.00	0.00	0.00	0.01	0.00	0.00	0.00	0.00	0.00
CaO	0.00	0.02	0.10	0.28	0.41	0.56	0.77	0.85	0.85	1.14
Na_2O	11.49	11.23	7.18	7.95	6.80	7.01	6.39	6.96	6.60	7.00
K_2O	0.92	0.85	6.71	5.93	6.94	6.55	7.79	6.67	7.00	6.29
Total	100.98	99.50	100.42	100.89	99.96	100.51	100.90	100.81	100.34	100.50
Si	2.993	2.976	2.987	2.977	2.973	2.974	2.954	2.950	2.952	2.932
Al	0.998	1.023	1.007	1.010	1.017	1.017	1.033	1.041	1.040	1.060
Ba	0.000	0.000	0.000	0.000	0.000	0.000	0.000	0.001	0.000	0.001
Fe	0.007	0.008	0.010	0.009	0.013	0.011	0.008	0.007	0.008	0.008
Sr	0.000	0.000	0.000	0.000	0.000	0.000	0.000	0.000	0.000	0.000
Ca	0.000	0.001	0.005	0.013	0.020	0.027	0.037	0.040	0.041	0.054
Na	0.968	0.960	0.621	0.683	0.592	0.606	0.553	0.601	0.573	0.606
K	0.051	0.048	0.382	0.335	0.398	0.372	0.444	0.379	0.400	0.358
Sum	5.017	5.016	5.010	5.028	5.013	5.006	5.029	5.019	5.014	5.020
Ab	95.0	95.1	61.6	66.2	58.7	60.3	53.5	58.9	56.5	59.5
An	0.00	0.11	0.5	1.3	2.0	2.6	3.6	4.0	4.1	5.3
Or	5.0	4.8	37.9	32.5	39.4	37.1	42.9	37.1	39.4	35.2

5.5.2.2 Pyroxenes

Clinopyroxene compositions for the UFG and PIF are plotted in the Wo-En-Fs system in Figure 5.20. Representative quantitative analyses are given in Table 5.3, and the full dataset can be found in Appendix C. For classification, the 10 component scheme of Marks *et al.* (2008) was applied, where, alongside the quadrilateral components diopside (Di), hedenbergite (Hd), enstatite (En), and ferrosilite (Fs), the additional components aegirine (Aeg), Ti-aegirine (Ti-Aeg), jadeite (Jd), Ti-Tschermak (Ti-Ts), Ca-Tschermak (Ca-Ts), and ferri-Tschermak (Fe-Ts) are considered. Application of the Q+J diagram of Morimoto *et al.* (1988) indicates that the majority of UFG and PIF analyses can be classified adequately using the quadrilateral components (Figure 5.21). When plotted in the quadrilateral, three component (Wo-En-Fs) scheme of Morimoto *et al.* (1988), both UFG and PIF pyroxenes are seen to approximate the diopside-augite boundary (Figure 5.20). Analyses derived from the Furnas J and Furnas I lava domes do not show any significant compositional variation compared of their corresponding pumice falls. Minor components such as Ti-Ts, Ca-Ts, and Fe-Ts are generally < 10 mol. %, as are En and Fs. The analyses are best defined using Di, Hd, and Aeg, which exhibit ranges of Di_{45-70}, Hd_{12-37}, and Aeg_{2-18} (Figure 5.22). In Di-Hd-Aeg space, some Furnas samples exhibit a trend of enrichment in Hd, with little to no increase in the aegirine component (e.g. Furnas G). Other units show more homogenous compositions (e.g. Furnas H), though some comparatively Di-rich outliers are present. The Povoação ignimbrite shows similar clinopyroxene compositions to the Povoação pumice fall, though both are somewhat richer in Di than the UFG. The Furnas J lava dome has a larger range than the Furnas J pumice fall, extending to more Di-rich compositions. Similarly, the Furnas I lava dome clinopyroxenes show a somewhat greater range than the Furnas I pumice fall, though this range extends to more Aeg-rich compositions. Two outliers within this unit have compositions of Di_{33}, Hd_{37}, Aeg_{26}, and Di_{12}, Hd_{7}, Aeg_{58}, and may represent a continuation

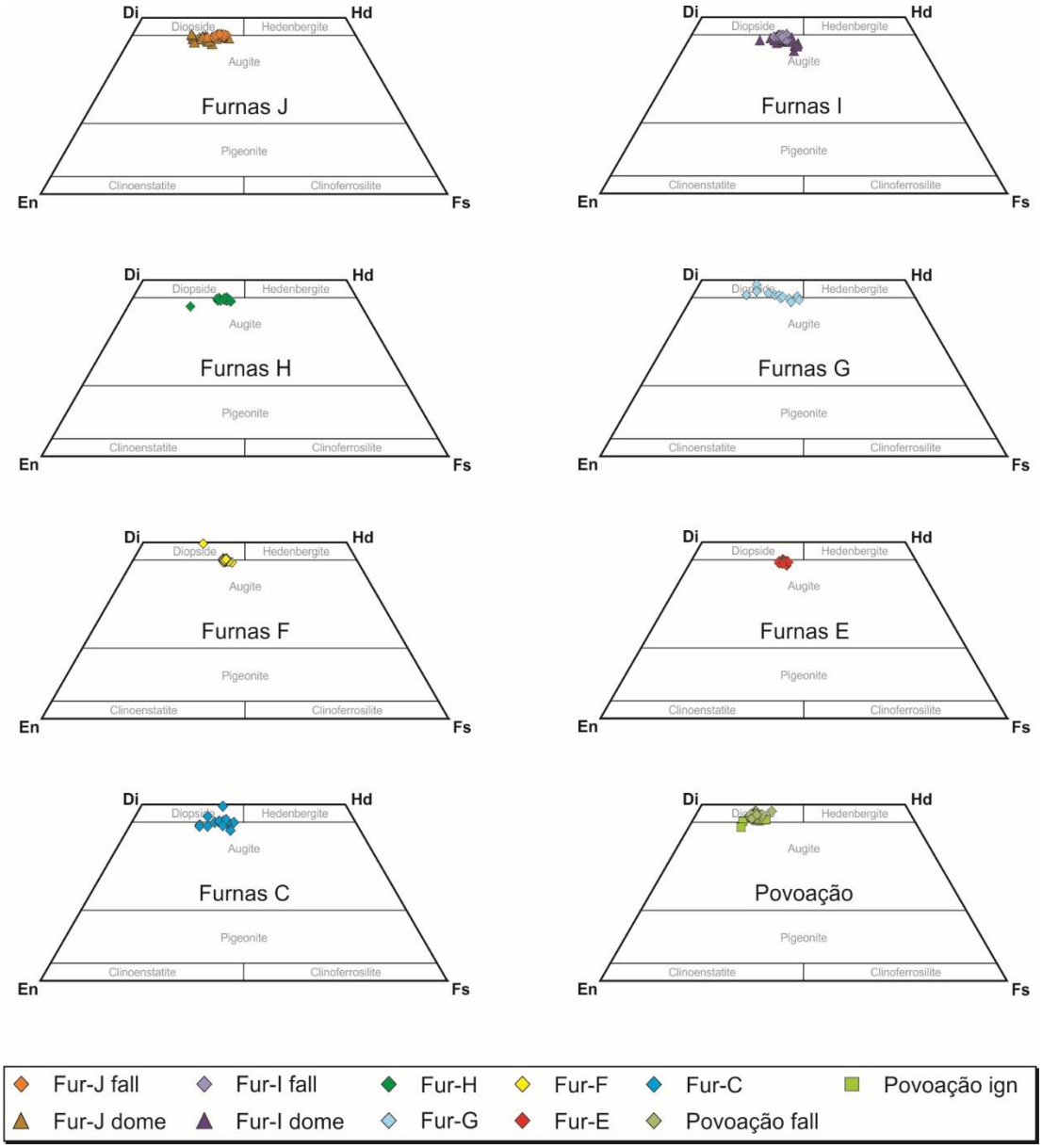

FIGURE 5.20: Clinopyroxene compositions of the UFG and PIF plotted into the quadrilateral, three component (wollastonite-enstatite-ferrosilite) scheme of Morimoto *et al.* (1988)

of the described trend, where Aeg enrichment begins after initial Hd enrichment. These analyses plot within the Ca-Na field of Figure 5.21, and, when plotted in the Quad-Jd-Aeg classification scheme of Morimoto *et al.* (1988), lie within the aegirine-augite field, rendering them the most compositionally evolved compositions in the UFG or PIF.

A number of clinopyroxene analyses yield high Al_2O_3 and TiO_2 contents (up to 8.9 and 3.9 wt. %, respectively. Figure 5.23 shows that both Al_2O_3 and TiO_2 contents correlate negatively with Hd content, with Al_2O_3 reaching relatively constant values around 1 wt. %

Table 5.3 Representative clinopyroxene analyses for the UFG and PIF

Unit	**Fur-J**		**Fur-J dome**		**Fur-I**		**Fur-I dome**		**Fur-H**		**Fur-G**
Sample	FM-11	FM-11	SM7-1	SM 7-1	FM-1 2	FM-1 2	SM 5-1	SM5-1	FM-1 3	FM-2 3	FM-2 4
No.	Px01	Px07	73 / 20	Clino05	Px04	Px03	Clino10	71 / 1	Px10	Px09	Px06
SiO_2	52.85	52.43	51.10	52.31	52.65	51.69	52.63	49.67	52.05	52.35	50.57
TiO_2	0.48	0.42	0.81	0.42	0.45	0.77	0.53	0.65	0.47	0.52	1.13
Al_2O_3	0.93	0.61	1.89	0.86	0.93	1.32	1.14	0.73	2.49	0.99	2.77
Cr_2O_3	0.00	0.00	0.02	0.00	0.01	0.00	0.00	0.00	0.01	0.00	0.01
FeO	10.56	12.73	8.23	12.89	10.92	12.67	9.80	18.31	8.95	13.06	7.54
MnO	1.17	1.65	0.70	1.58	1.37	1.66	0.93	1.70	0.54	1.64	0.36
MgO	12.78	10.92	13.84	10.65	11.91	10.87	13.44	5.92	14.64	10.57	14.13
CaO	21.46	21.60	21.50	20.48	21.02	20.20	21.25	16.90	20.69	20.61	22.10
Na_2O	0.64	0.87	0.66	1.23	0.84	1.27	0.63	3.43	0.38	1.22	0.58
K_2O	0.01	0.00	0.00	0.00	0.01	0.00	0.00	0.00	0.00	0.00	0.01
Total	100.88	101.23	98.75	100.42	100.12	100.45	100.34	97.30	100.22	100.97	99.20
Si	1.968	1.967	1.921	1.975	1.981	1.948	1.961	1.961	1.928	1.967	1.887
Ti	0.014	0.012	0.023	0.012	0.013	0.022	0.015	0.019	0.013	0.015	0.032
Al	0.041	0.027	0.084	0.038	0.041	0.059	0.050	0.034	0.109	0.044	0.122
Cr	0.000	0.000	0.001	0.000	0.000	0.000	0.000	0.000	0.000	0.000	0.000
Fe^{2+}	0.286	0.321	0.183	0.329	0.311	0.306	0.261	0.336	0.240	0.329	0.153
Fe^{3+}	0.043	0.078	0.075	0.078	0.032	0.094	0.044	0.269	0.037	0.081	0.082
Mn	0.037	0.052	0.022	0.051	0.044	0.053	0.029	0.057	0.017	0.052	0.011
Mg	0.709	0.611	0.776	0.599	0.668	0.611	0.746	0.348	0.808	0.592	0.786
Ca	0.856	0.868	0.866	0.828	0.847	0.816	0.848	0.715	0.821	0.830	0.884
Na	0.046	0.063	0.048	0.090	0.061	0.092	0.045	0.262	0.027	0.089	0.042
K	0.001	0.000	0.000	0.000	0.001	0.000	0.000	0.000	0.000	0.000	0.000
Sum	4.000	4.000	4.000	4.000	4.000	4.000	4.000	4.000	4.000	4.000	4.000
Aeg	4	6	5	8	3	9	4	26	3	8	4
Fe-Ts	0	1	1	0	0	0	0	0	0	0	2
Jd	0	0	0	1	2	0	0	0	0	1	0
Ti-Aeg	0	0	0	0	1	0	0	0	0	0	0
Ti-Ts	1	1	2	1	1	2	1	2	1	1	3
Ca-Ts	0	0	1	0	0	1	1	0	4	0	1
Di	58	53	66	50	55	50	59	33	58	49	69
Hd	26	32	17	32	29	29	23	37	19	32	14
En	7	4	6	5	6	6	8	1	11	5	5
Fs	3	3	2	3	3	3	3	1	4	3	1

Table 5.3 continued

Unit	**Fur-G**	**Fur-F**		**Fur-E**		**Fur-C**		**Povo fall**		**Povo ign**	
Sample	FM-1 4	FM-1 5	FM-1 5	AM-1 3	AM-2 3	FM-1 6	FM-2 6	AM-1 4	AM-1 4	SM 10-1	SM10-1
No.	Px07	Px11	Px06	Px08	Px02	Px08	Px06	Px03	Px02	Clino12	105 / 1
SiO_2	52.27	44.14	51.77	52.73	51.61	51.61	51.77	52.38	49.32	49.04	51.46
TiO_2	0.36	3.85	0.53	0.36	0.47	0.59	0.68	0.83	1.48	1.79	0.52
Al_2O_3	0.76	8.88	1.08	0.65	1.03	1.04	1.13	1.81	3.41	4.95	1.36
Cr_2O_3	0.00	0.03	0.00	0.00	0.00	0.01	0.00	0.00	0.00	0.34	0.00
FeO	14.39	8.50	13.01	11.84	12.45	9.81	13.61	7.72	10.33	7.36	9.63
MnO	1.60	0.10	1.67	1.51	1.66	0.98	1.79	0.64	0.61	0.14	1.13
MgO	9.65	11.53	10.45	11.71	10.69	13.42	10.68	14.02	11.43	14.57	12.44
CaO	21.08	22.39	20.71	21.74	20.01	21.34	19.88	22.90	22.64	20.50	21.96
Na_2O	1.03	0.47	1.31	0.74	1.16	0.69	1.28	0.63	0.89	0.44	0.85
K_2O	0.03	0.01	0.00	0.00	0.01	0.01	0.02	0.00	0.00	0.01	0.00
Total	101.17	99.90	100.53	101.28	99.09	99.49	100.83	100.93	100.12	99.14	99.34
Si	1.976	1.653	1.953	1.969	1.973	1.938	1.949	1.926	1.850	1.828	1.939
Ti	0.010	0.108	0.015	0.010	0.014	0.017	0.019	0.023	0.042	0.050	0.015
Al	0.034	0.392	0.048	0.029	0.046	0.046	0.050	0.079	0.151	0.217	0.060
Cr	0.000	0.001	0.000	0.000	0.000	0.000	0.000	0.000	0.000	0.010	0.000
Fe^{2+}	0.384	0.147	0.298	0.303	0.331	0.213	0.322	0.169	0.194	0.181	0.208
Fe^{3+}	0.070	0.119	0.113	0.067	0.067	0.095	0.107	0.068	0.131	0.049	0.095
Mn	0.051	0.003	0.053	0.048	0.054	0.031	0.057	0.020	0.020	0.004	0.036
Mg	0.544	0.644	0.588	0.652	0.609	0.751	0.600	0.768	0.639	0.810	0.698
Ca	0.854	0.898	0.837	0.870	0.820	0.859	0.802	0.902	0.910	0.819	0.886
Na	0.075	0.034	0.096	0.054	0.086	0.050	0.093	0.045	0.065	0.032	0.062
K	0.001	0.001	0.000	0.000	0.000	0.000	0.001	0.000	0.000	0.000	0.000
Sum	4.000	4.000	4.000	4.000	4.000	4.000	4.000	4.000	4.000	4.000	4.000
Aeg	7	3	10	5	7	5	9	4	7	3	6
Fe-Ts	0	4	1	1	0	2	1	1	3	1	2
Jd	0	0	0	0	2	0	0	0	0	0	0
Ti-Aeg	0	0	0	0	0	0	0	0	0	0	0
Ti-Ts	1	11	2	1	1	2	2	2	4	5	1
Ca-Ts	0	5	0	0	0	0	0	0	0	5	0
Di	47	58	51	56	49	62	48	70	64	59	64
Hd	37	14	31	30	31	20	30	17	21	13	22
En	4	4	4	5	6	7	6	4	1	12	3
Fs	3	1	2	3	4	2	4	1	0	3	1

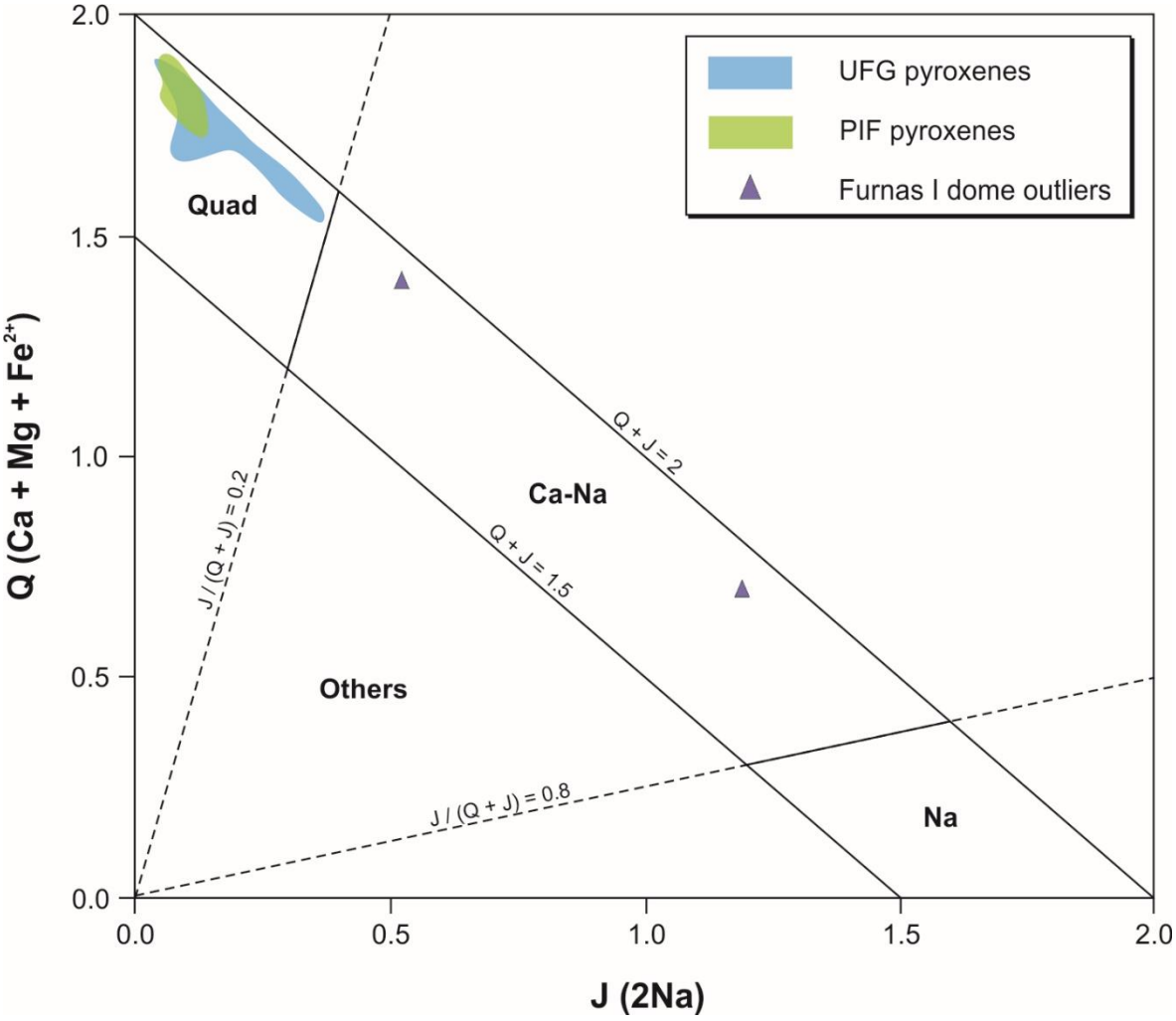

FIGURE 5.21: Q + J clinopyroxene classification diagram showing analyses from the UFG and PIF, after Morimoto *et al.* (1988)

at ~ Hd_{25}, and TiO_2 plateauing at around 0.5 wt. % at ~ Hd_{20}.

The clinopyroxene analyses from the Furnas J syenite ejecta reveal a stark contrast with those of both the UFG and the PIF, with a compositional range from diopside, through aegirine-augite, to aegirine (Qd_{0-93}, Jd_{0-8}, Aeg_{6-96}) (Figure 5.24, 5.25). The minor components Ti-Ts, Ca-Ts, and Fe-Ts are present only in small quantities (< 2 mol. %), whilst the jadeite, enstatite, and ferrosilite components do not exceed 8, 4, and 4 mol. %, respectively). The Ti-aegirine component is generally present in small concentrations (~ 6 mol. %), but extends to values as high as 34 mol. % in a small number of examples. Titanium contents range from 0.2 to 6 wt. %, and show a uniform concentration of ~ 0.5 wt. % until the diopside component is reduced to ~ 10 mol. %, at

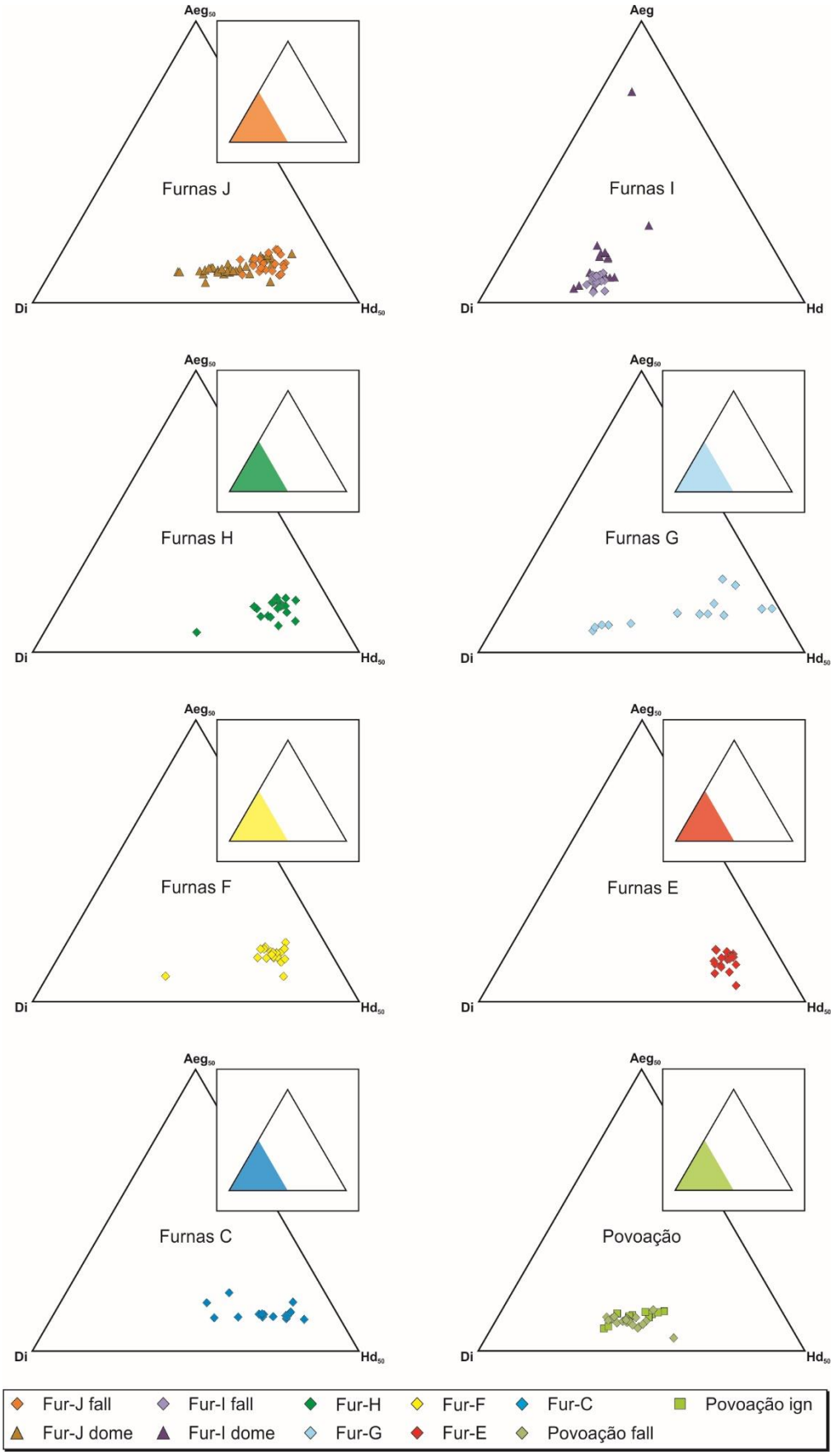

FIGURE 5.22: Diopside-hedenbergite-aegirine ternary diagrams illustrating clinopyroxene compositional trends from the UFG and PIF

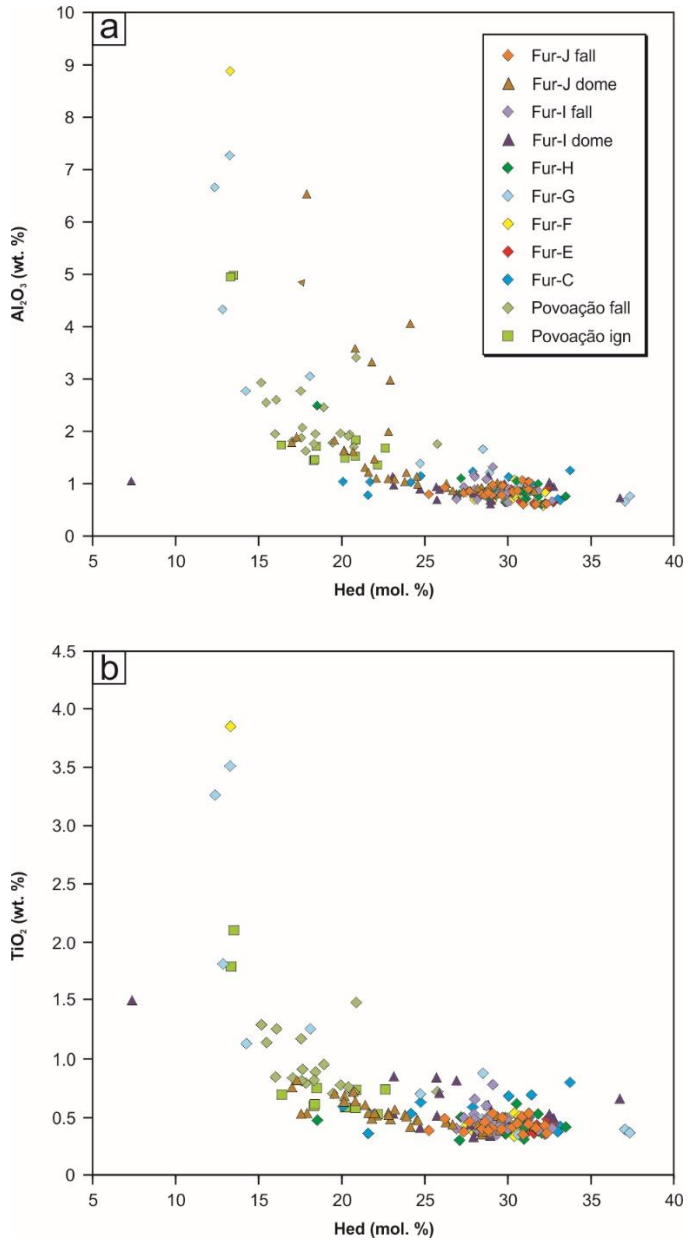

FIGURE 5.23: Evolution of clinopyroxene Al_2O_3 and TiO_2 contents in the UFG and PIF

which point a negative correlation between TiO_2 and diopside is observed. Aluminium contents exhibit a smaller range of 0.3 to 1.5 wt. % and do not correlate with other compositional variables. Manganese is also present in small amounts (0.5 to 3.3 t. %), and shows an initially negative correlation with diopside, until ~ Di_{25}, when manganese concentrations decrease with diopside. In Di-Hed-Aeg space, the data reveal a poorly defined trend of initial enrichment in hedenbergite, followed by aegirine enrichment (Figure 5.22). An apparent compositional gap is observable, separating low-Na aegirine-

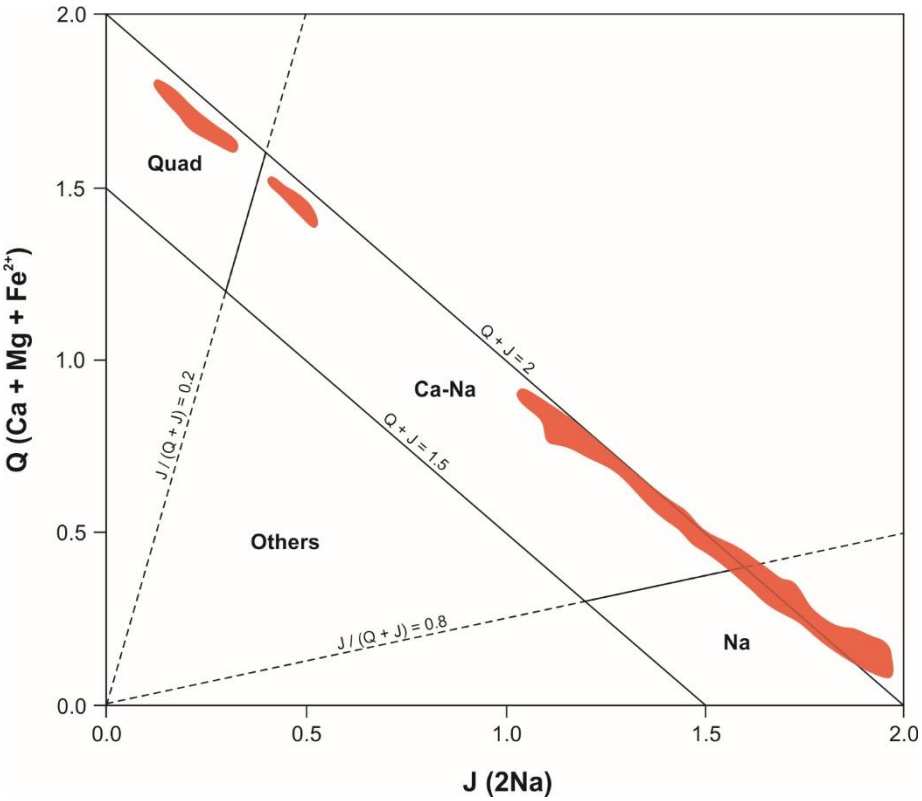

FIGURE 5.24: Q + J clinopyroxene classification diagram showing analyses from the Furnas J syenite ejecta, after Morimoto *et al.* (1988)

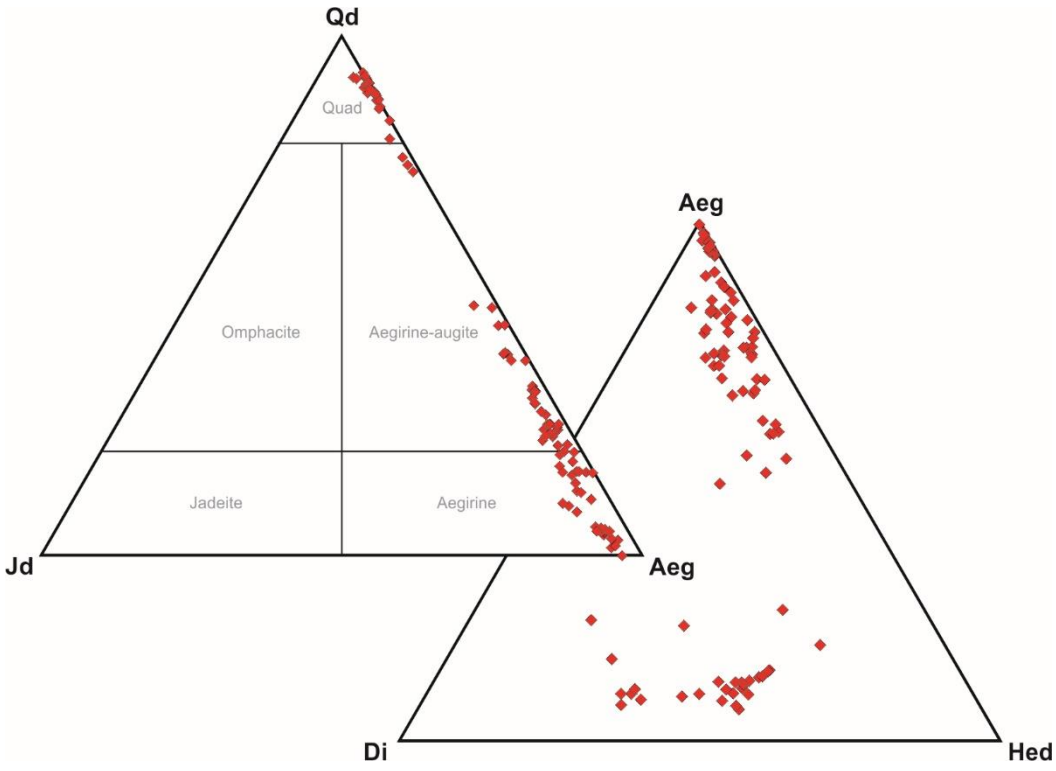

FIGURE 5.25: Clinopyroxene compositions for the Furnas J syenites plotted into the Qd-Jd-Aeg and Aeg-Di-Hed ternary systems

augite from high-Na aegirine-augite and aegirine, and can also be seen in the Q + J and Qd-Jd-Aeg classification schemes of Morimoto *et al.* (1988).

5.5.2.3 Biotite

Biotite analyses from the UFG and PIF are Mg-rich, characterised by relatively constant Fe / (Fe + Mg) ratios (~ 0.41 and ~ 0.37 respectively), and variable Si contents (5.44 to 5.71 and 5.21 to 5.57 apfu, respectively) (Figure 5.26). Representative analyses are given in Table 5.4, and the entire dataset can be found in Appendix C. Both UFG and PIF analyses exhibit high Ti contents (0.56 to 0.93 and 0.73 to 0.99 apfu, respectively), and a negative correlation is observed between Ti and the sum of the octahedrally-coordinated

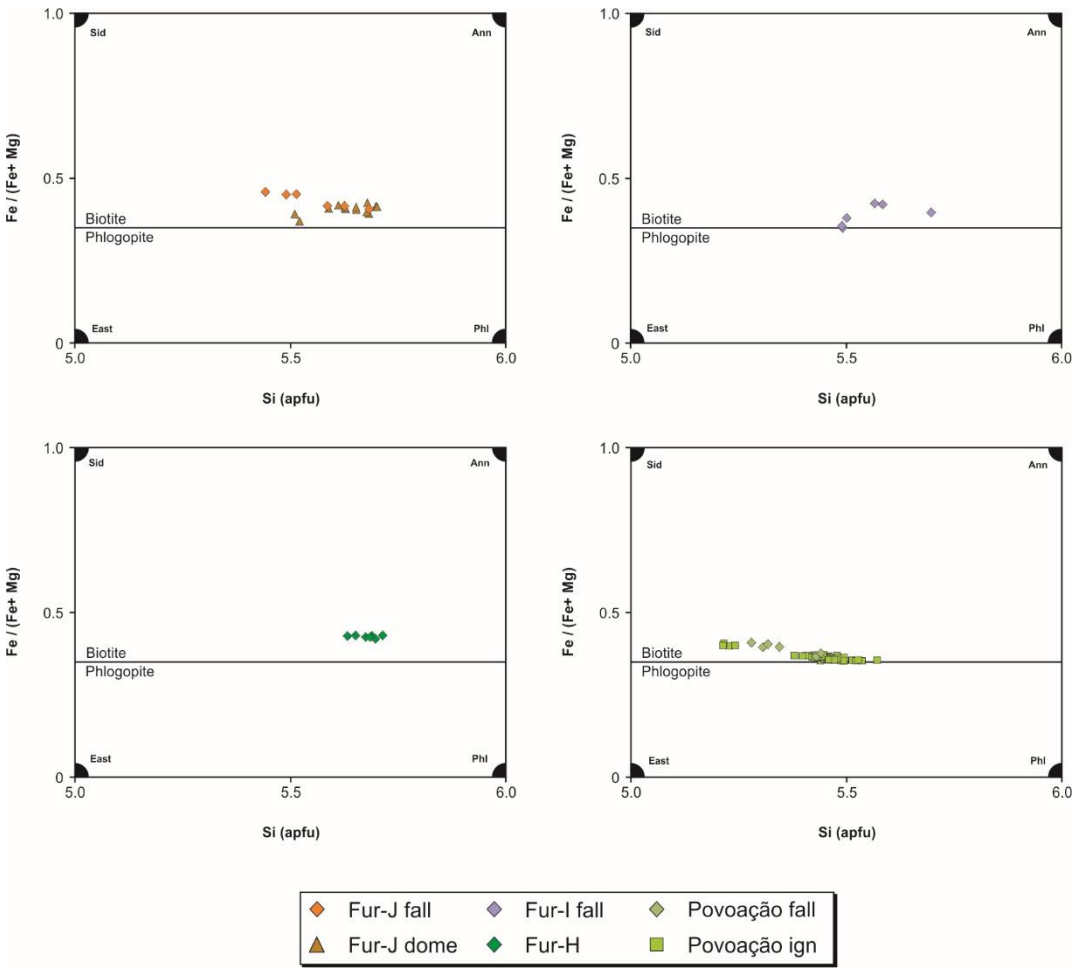

FIGURE 5.26: Compositional variation of biotite from the UFG and PIF. Abbreviations: Sid = siderophyllite, East = eastonite, Ann = annite, Phl = phlogopite

Table 5.4 Representative biotite analyses for the UFG and PIF

Unit	**Furnas J**		**Furnas J dome**		**Furnas I**		**Furnas H**		**Povo fall**		**Povo ign**	
No.	Bio1	Bio3	7-1a	7-1b	Bio2	Bio6	Bio06	Bio02	Bio01	Bio3	68 / 1	170 / 3
SiO_2	37.52	35.86	37.37	37.52	36.83	37.08	36.81	37.88	36.23	34.24	36.83	34.19
TiO_2	5.43	8.12	5.13	5.29	4.99	8.36	5.52	5.09	7.31	8.27	6.69	8.58
Al_2O_3	12.09	12.95	11.95	12.18	11.70	13.26	12.05	12.13	13.63	14.00	13.28	14.09
FeO	16.35	17.13	17.33	16.84	15.84	13.18	17.20	17.38	14.18	15.07	13.39	14.92
MnO	0.58	0.53	0.58	0.62	0.57	0.23	0.59	0.65	0.24	0.25	0.33	0.37
MgO	13.40	11.38	13.28	13.71	13.64	13.84	12.86	13.39	13.65	12.24	13.65	12.24
CaO	0.00	0.00	0.05	0.00	0.00	0.00	0.01	0.02	0.00	0.00	0.04	0.02
Na_2O	0.90	0.98	1.03	0.90	0.78	0.86	0.91	0.87	0.77	0.70	0.83	0.78
K_2O	8.87	8.55	8.32	8.62	8.72	8.90	8.79	8.66	9.55	8.24	8.55	7.74
BaO			0.02	0.04							0.10	3.17
ZnO			0.07	0.07							0.07	0.02
Total	95.14	95.50	95.11	95.78	93.06	95.70	94.74	96.07	95.56	93.01	93.75	96.10
H_2O*	3.30	3.52	2.32	3.16	3.08	3.70	3.32	3.26	3.74	3.68	3.51	3.73
F	1.37	0.90	3.40	1.71	1.66	0.72	1.23	1.51	0.54	0.42	0.93	0.41
Cl	0.04	0.03	0.05	0.04	0.03	0.02	0.05	0.04	0.03	0.03	0.07	0.02
Si	5.683	5.442	5.679	5.654	5.697	5.492	5.632	5.696	5.429	5.280	5.572	5.216
Ti	0.619	0.927	0.587	0.600	0.580	0.931	0.635	0.576	0.824	0.959	0.761	0.985
Al^{IV}	2.158	2.316	2.140	2.163	2.133	2.315	2.173	2.150	2.408	2.545	2.368	2.533
Al^{VI}	0.000	0.000	0.000	0.000	0.000	0.000	0.000	0.000	0.000	0.000	0.000	0.000
Fe	2.071	2.174	2.202	2.122	2.049	1.633	2.201	2.186	1.777	1.943	1.695	1.903
Mn	0.074	0.068	0.075	0.078	0.074	0.028	0.077	0.083	0.030	0.033	0.043	0.048
Mg	3.025	2.574	3.007	3.079	3.145	3.056	2.933	3.002	3.049	2.814	3.078	2.783
Ca	0.000	0.000	0.007	0.000	0.000	0.000	0.002	0.003	0.000	0.000	0.006	0.003
Na	0.265	0.289	0.302	0.263	0.233	0.246	0.269	0.255	0.225	0.210	0.244	0.230
K	1.714	1.655	1.612	1.656	1.720	1.681	1.715	1.661	1.825	1.621	1.649	1.506
Ba			0.001	0.002							0.006	0.189
Zn			0.008	0.008							0.008	0.002
Sum	15.609	15.446	15.621	15.625	15.633	15.383	15.638	15.611	15.568	15.404	15.429	15.400
OH*	3.335	3.560	2.353	3.172	3.180	3.656	3.392	3.272	3.736	3.785	3.541	3.799
F	0.656	0.433	1.633	0.816	0.812	0.338	0.595	0.718	0.255	0.206	0.443	0.195
Cl	0.009	0.007	0.014	0.011	0.008	0.006	0.013	0.010	0.008	0.008	0.017	0.006

*OH calculated after Tindle & Webb (1990)

cations Fe and Mg (Figure 5.27a). When Ti is plotted against Al, a positive correlation that approximates the proportion 1:2 is observed (Figure 5.27b), suggesting that Ti may be accommodated in the octahedral sites via the coupled substitution of $Mg^{2+} + 2Si^{4+} \leftrightarrow Ti^{4+} + 2Al^{3+}$, proposed by Wagner *et al.* (1987). Alternatively, this may be achieved via the generation of vacancies in the *X* site ($Mg^{2+} + 2\ K^{+} \leftrightarrow Ti^{4+} + 2\ \square$) (cf. Deer *et al.*, 1992; Marks *et al.*, 2008). If Na is considered as a substitute for K, the analyses indicate that the

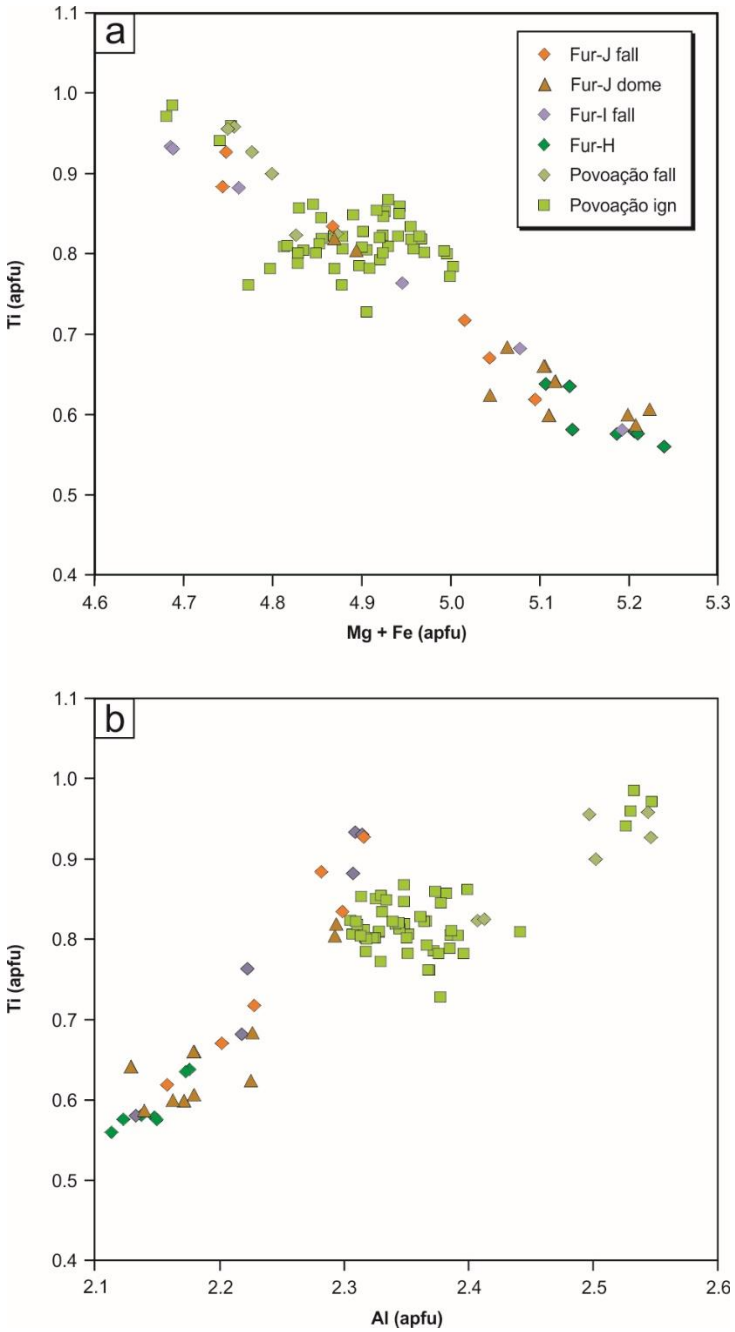

FIGURE 5.27: Compositional trends observed in biotite. **a)** Negative correlation between M site cations and Ti suggest octahedral coordination of Ti **b)** Positive correlation between Al and Ti highlighting the role of the coupled substitution $Mg^{2+} + 2Si^{4+} \leftrightarrow Ti^{4+} + 2Al^{3+}$

maximum value for *X* site vacancies is ~ 0.29 apfu, constituting ~ 15 % site vacancy. In addition to low Si contents, Al values are also low and 8 – (Al + Si) deficits range from 0.06 to 0.26, indicating the presence of tetrahedrally-coordinated Ti^{4+} or Fe^{3+} (e.g. Mann *et al.*, 2006). Occupation of the hydroxyl sites is characterised by variably high F contents (0.32 to 1.63 apfu) and low Cl contents (< 0.02 apfu). The UFG analyses exhibit

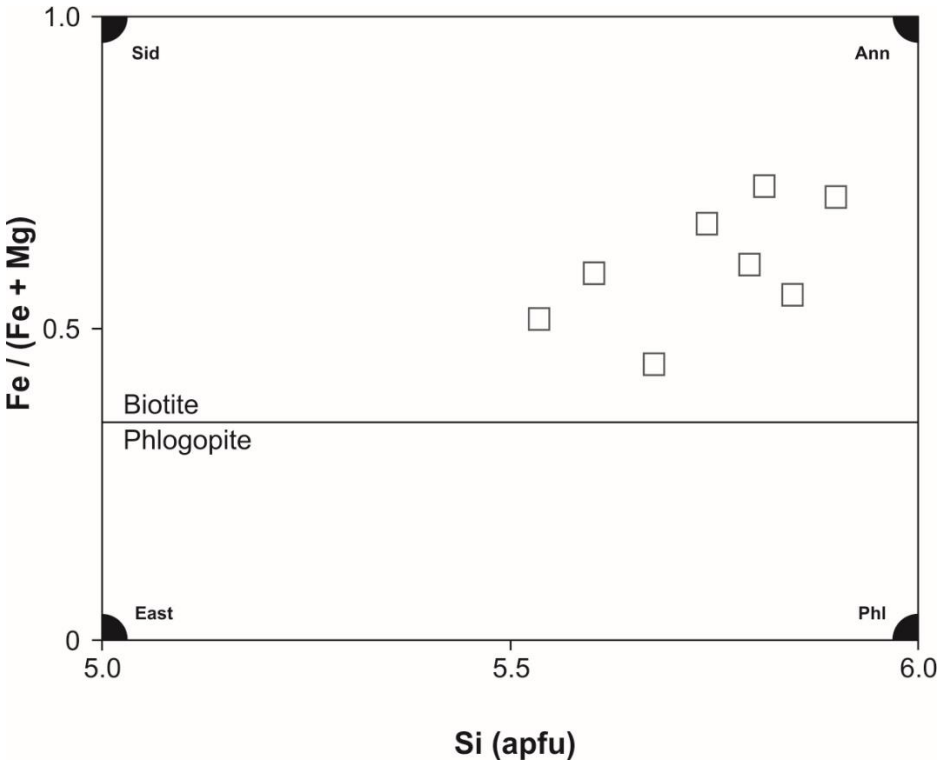

FIGURE 5.28: Compositional variation of biotite from the Furnas J syenite ejecta. Abbreviations: Sid = siderophyllite, East = eastonite, Ann = annite, Phl = phologopite

significantly greater concentrations of F than the PIF analyses, which are limited to 0.44 apfu. A small number of PIF analyses also show a significant Ba content of up to 0.19 apfu. Biotite from the Furnas J syenite ejecta are very similar to those found in the pumice falls and lava domes, with variable Si contents (5.54 to 5.90 apfu), and high Ti (0.42 to 0.84 apfu) (Figure 5.28). Similarly, the hydroxyl sites are dominated by F (0.75 to 1.12 apfu), with little Cl (< 0.02 apfu). However, Fe / (Fe + Mg) ratios extend to larger values (0.44 to 0.72).

5.5.2.4 Amphibole

Quantitative analyses of amphibole from the Furnas I lava dome and Furnas J syenites are presented in Figure 5.29 and Table 5.5. Following the nomenclature of Leake *et al.* (1997), all of the analyses are Na-Ca amphiboles of magnesio-katophoritic to richteritic composition. The analyses indicate relatively Al-poor compositions, with 8 – (Al + Si) values between ~ 0.02 and ~ 0.08 apfu, indicating the presence of tetrahedrally-

Table 5.5 Amphibole analyses from the Furnas I lava dome and Furnas J syenite ejecta

Unit			**Furnas I dome**					**Furnas J syenite**		
Sample	SM 5-1	SM 5-1	SM 5-1	SM 5-1	SM 5-1	S035	S035	S035	S035	S035
No.	Bio06	Bio07	Bio08	Bio09	Bio10	Amph CZ1a	Amph CZ2a	Amph CZ2b	Amph CZ2c	Amph CZ2d
SiO_2	50.63	50.20	50.45	49.78	50.34	45.18	46.65	46.38	45.36	46.83
TiO_2	1.55	1.33	1.06	1.37	1.42	2.41	1.68	2.42	2.38	2.32
Al_2O_3	3.09	2.69	2.43	3.08	2.46	4.47	3.42	3.24	3.37	3.66
Cr_2O_3	0.02	bdl	bdl	0.02	0.01					
FeO	12.61	16.07	16.99	14.03	16.47	27.39	27.47	32.08	32.42	28.44
MnO	1.16	1.58	1.67	1.32	1.63	1.93	2.21	1.73	1.88	1.92
MgO	14.82	12.41	11.49	13.61	11.81	3.56	3.84	0.514	0.6487	3.1
CaO	7.59	6.96	6.47	7.38	6.54	5.32	5.08	0.9615	1.51	1.45
Na_2O	5.20	5.41	5.74	5.33	5.70	6.07	6.21	8.58	7.97	8.42
K_2O	1.24	1.33	1.36	1.32	1.30	1.58	1.55	1.57	1.66	1.63
NiO	bdl	bdl	bdl	0.04	bdl					
Total	97.92	97.98	97.66	97.28	97.69	97.91	98.11	97.48	97.20	97.77
F						1.21	1.34	0.94	0.89	1.47
Cl	0.01	0.01	bdl	0.01	bdl	0.01	bdl	bdl	0.01	bdl
Structural formula on the basis of 23 oxygens										
Si	7.389	7.446	7.550	7.385	7.515	7.153	7.350	7.436	7.299	7.342
Ti	0.170	0.148	0.119	0.153	0.160	0.287	0.199	0.292	0.288	0.274
Al^{IV}	0.531	0.470	0.429	0.539	0.433	0.834	0.635	0.564	0.639	0.658
Al^{VI}	0.000	0.000	0.000	0.000	0.000	0.000	0.000	0.049	0.000	0.018
Cr	0.003			0.002	0.001	0.000				
Fe^{2+}	1.267	1.671	1.895	1.487	1.830	3.329	3.276	3.689	3.523	3.009
Fe^{3+}	0.272	0.322	0.232	0.254	0.226	0.298	0.344	0.612	0.840	0.720
Mn	0.144	0.198	0.212	0.166	0.206	0.259	0.295	0.235	0.256	0.255
Mg	3.224	2.744	2.563	3.010	2.628	0.840	0.902	0.123	0.156	0.725
Ca	1.187	1.106	1.037	1.173	1.046	0.902	0.858	0.165	0.260	0.244
Na	1.471	1.556	1.666	1.533	1.650	1.863	1.897	2.667	2.486	2.559
K	0.231	0.252	0.260	0.250	0.248	0.319	0.312	0.321	0.341	0.326
Ni				0.004						
Sum	15.889	15.914	15.963	15.956	15.944	16.085	16.066	16.154	16.088	16.129
F						0.606	0.668	0.477	0.454	0.729
Cl	0.003	0.003		0.002		0.002			0.001	
OH*	1.997	1.997	2.000	1.998	2.000	1.392	1.330	1.523	1.545	1.271

*OH calculated after Tindle & Webb (1990)

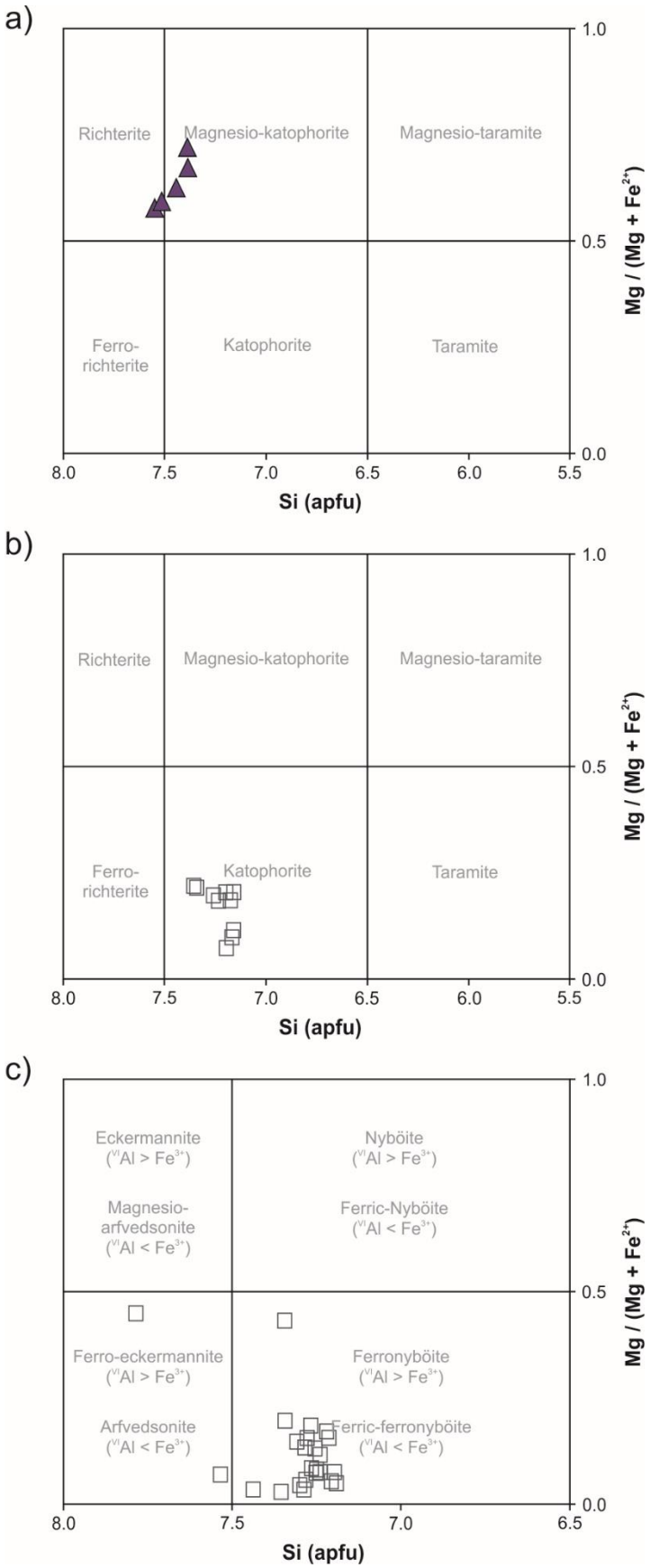

FIGURE 5.29: Amphibole analyses from the UFG plotted into the Na-Ca and Na amphibole classification schemes (Leake *et al.*,1997) **a)** Furnas I lava dome Na-Ca amphibole analyses **b)** Furnas J syenite Na-Ca amphibole analyses **c)** Furnas J syenite Na amphibole analyses

coordinated Fe^{3+} (Hogarth *et al.*, 1987)or Ti^{4+} (Oberti *et al.*, 1992). Both Fe^{3+} and K remain relatively constant (~ 0.26 and ~ 0.25 apfu, respectively), whilst Fe^{2+} and Mg exhibit somewhat larger ranges (1.27 to 1.90 and 2.62 to 3.22 apfu, respectively). A one-to-one correlation between Na and Ca indicates a simple substitution of the two, with the analyses becoming more Fe^{2+}-rich and less Mg-rich with increasing Na contents. Chlorine concentrations are negligible, and do no not exceed 0.01 wt. %. The presence of F in the hydroxyl site was not quantified but cannot be ruled out.

Amphiboles in the Furnas J syenites exhibit a larger compositional range, which includes Na-Ca amphiboles of kataphoritic composition, and Na amphiboles of ferric-ferronyböitic and arfvedsonitic composition. Fluorine concentrations in the hydroxyl site range from 0.45 to 1.21 apfu, and show no significant variation between Na-Ca and Na groups. Chlorine contents are extremely low (< 0.006 apfu).

5.5.2.5 Fe-Ti oxides

Quantitative analyses of both ilmenite and Ti-magnetite for the UFG and PIF are presented in TiO_2-FeO-Fe_2O_3 ternary diagrams in Figure 5.30. Representative quantitative analyses are given in Table 5.6, and the full dataset can be found in Appendix C. Ti-magnetite shows a compositional range of Mag_{35-68}, Usp_{22-63}, Sp_{1-10} in the UFG, which is somewhat smaller than that of the PIF (Mag_{26-71}, Usp_{23-73}, Sp_{1-9}). The UFG Ti-magnetite has an average Al_2O_3 content of 0.9 wt. %, lower than the PIF (1.9 wt. %), but both UFG and PIF have similar ranges (~ 0.3 to 4.6 wt. %). MgO and MnO contents reach 2.7 and 2.0 wt. %, respectively, and show significant difference between the UFG and the PIF.

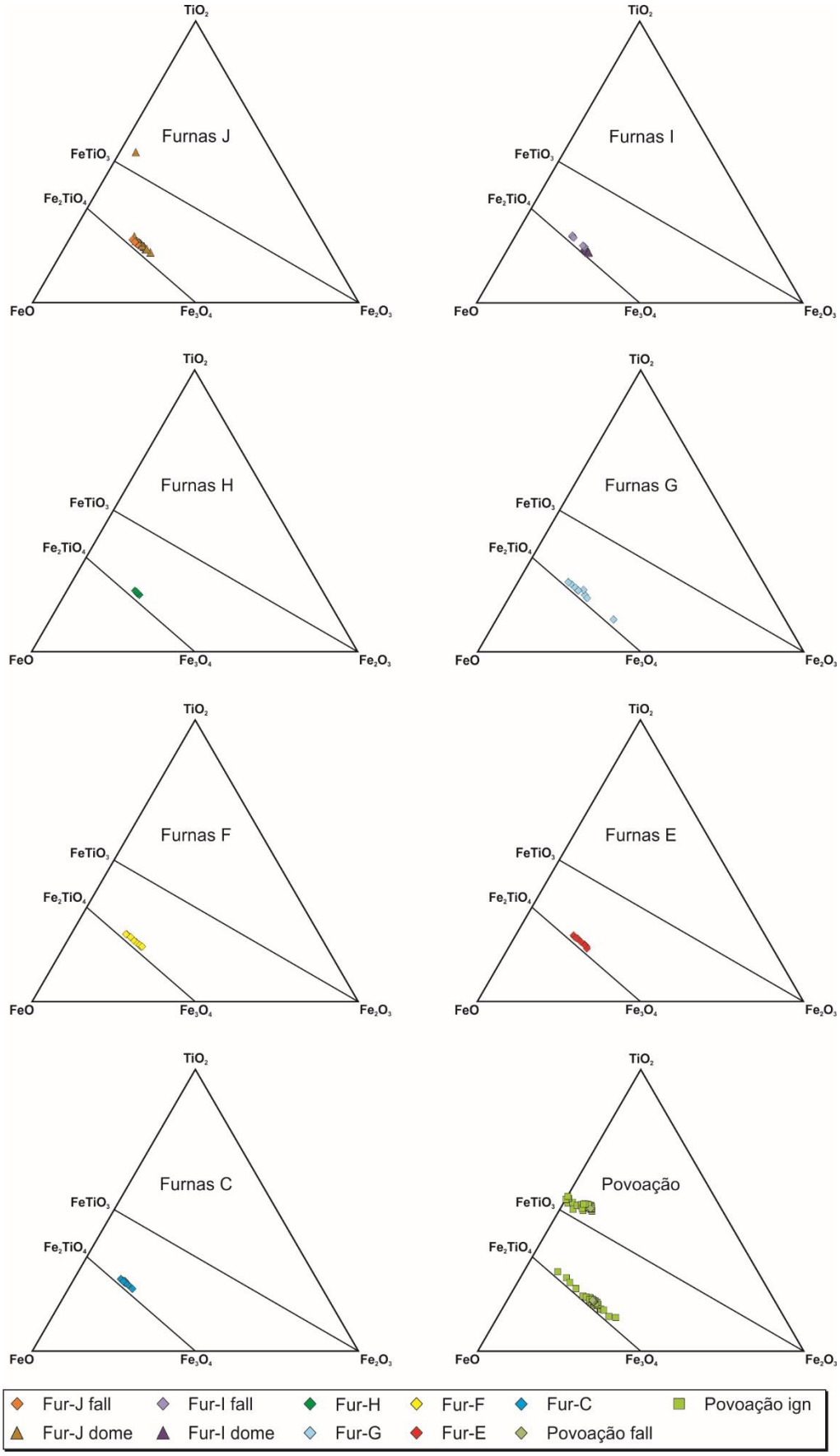

FIGURE 5.30: TiO_2-FeO-Fe_2O_3 ternary diagrams showing Fe-Ti oxide compositions for the UFG and PIF

Table 5.6 Representative Fe-Ti oxide analyses for the UFG and PIF

Unit		**Furnas J**		**Furnas J dome**		**Furnas I**		**Furnas I dome**		**Furnas H**		**Furnas G**	
Sample	FM-1(1)	FM-1(1)	SM 7-1	SM7-1	SM 7-1	FM-1(2)	FM-1(2)	SM5-1	SM 5-1	FM-1(3)	FM-2(1)	FM-1(4)	FM-1(4)
No.	Ox1	Ox4	Oxide02	120 / 1	Oxide02	Ox1	Ox2	110 / 1	Oxide18	Ox4	Ox1	Ox7	Ox8
Mineral	Ti-mag	Ti-mag	Ilm	Ti-mag	Ti-mag	Ti-mag	Ti-mag	Ti-mag	Ti-mag	Ti-mag	Ti-mag	Ti-mag	Ti-mag
TiO_2	17.21	18.43	48.97	15.66	19.42	16.10	19.91	14.33	15.94	16.37	17.96	7.88	21.41
Al_2O_3	0.97	1.31	0.03	0.73	0.45	0.87	0.95	0.52	0.28	0.80	0.97	4.63	1.26
Cr_2O_3	0.00	0.00	0.00	0.00	0.00	0.00	0.00	0.00	0.00	0.00	0.00	0.10	0.00
FeO	74.08	71.59	42.26	73.44	70.79	74.89	71.07	76.48	76.09	75.29	74.27	77.18	70.68
MnO	2.60	2.17	3.93	3.03	3.44	2.73	2.55	3.00	3.30	2.76	2.63	2.02	2.31
MgO	1.34	1.83	3.31	1.90	2.29	1.29	1.39	0.53	0.28	1.08	1.41	2.80	1.36
NiO	0.00	0.00				0.01	0.01			0.00	0.00	0.02	0.00
V_2O_3	0.01	0.01				0.00	0.01			0.01	0.02	0.28	0.01
SiO_2	0.03	0.06				0.08	0.06			0.06	0.07	0.06	0.08
ZnO	0.26	0.22				0.24	0.26			0.25	0.26	0.38	0.26
Total	96.50	95.62	98.50	94.76	96.39	96.20	96.21	94.86	95.89	96.61	97.59	95.34	97.37
Ti	0.483	0.519	0.915	0.445	0.543	0.453	0.561	0.411	0.454	0.459	0.498	0.216	0.597
Al	0.042	0.058	0.001	0.033	0.020	0.038	0.042	0.024	0.013	0.035	0.042	0.199	0.055
Cr	0.000	0.000	0.000	0.000	0.000	0.000	0.000	0.000	0.000	0.000	0.000	0.003	0.000
Fe^{2+}	1.320	1.344	0.710	1.241	1.308	1.290	1.397	1.284	1.332	1.308	1.334	0.993	1.445
Fe^{3+}	0.990	0.899	0.168	1.078	0.894	1.051	0.831	1.155	1.079	1.041	0.956	1.355	0.745
Mn	0.082	0.069	0.083	0.097	0.108	0.086	0.081	0.097	0.106	0.087	0.082	0.062	0.073
Mg	0.074	0.102	0.123	0.107	0.127	0.072	0.078	0.030	0.016	0.060	0.077	0.152	0.075
Ni	0.000	0.000				0.000	0.000			0.000	0.000	0.000	0.000
V	0.000	0.000				0.000	0.000			0.000	0.001	0.008	0.000
Si	0.001	0.002				0.003	0.002			0.002	0.003	0.002	0.003
Zn	0.007	0.006				0.007	0.007			0.007	0.007	0.010	0.007
Sum	3.000	3.000	2.000	3.000	3.000	3.000	3.000	3.000	3.000	3.000	3.000	3.000	3.000
Usp	48	52		44	54	45	56	41	45	46	50	22	60
Mt	50	45		54	45	53	42	58	54	52	48	68	37
Sp	2	3		2	1	2	2	1	1	2	2	10	3
Ilm			85										
Hem			8										
Pyr			8										

Usp = Ulvöspinel; Mt = Magnetite; Sp = Spinel; Ilm = Ilmenite; Hem = Hematite; Pyr = Pyrophanite

Table 5.6 continued

Unit	Furnas F		Furnas E		Furnas C		Povo fall				Povo ign		
Sample	FM-2(5)	FM-1(5)	AM-2(3)	AM-2(3)	FM-1(6)	FM-1(6)	AM-2(4)	AM-2(4)	AM-2(4)	AM-2(2)	SM10-1	AZ02-6	AM-2(2)
No.	Ox1	Ox8	Ox7	Ox6	Ox1	Ox5	Ox1	Ox6	Ox3	Ox2	Oxide46	49 / 1	Ox1
Mineral	Ti-mag	Ti-mag	Ti-mag	Ti-mag	Ti-mag	Ti-mag	Ti-mag	Ti-mag	Ilm	Ti-mag	Ti-mag	Ilm	Ilm
TiO_2	15.91	20.72	15.29	20.23	18.73	22.79	13.58	14.11	44.99	8.42	24.51	41.84	52.27
Al_2O_3	0.85	0.93	0.57	0.93	0.92	0.93	2.12	2.28	0.24	2.52	0.49	0.20	0.16
Cr_2O_3	0.00	0.00	0.00	0.00	0.00	0.00	0.00	0.01	0.00	0.00	0.00	0.00	0.00
FeO	76.16	72.16	76.64	72.73	74.12	71.08	75.83	76.14	46.49	78.70	63.95	45.53	38.43
MnO	2.82	2.64	2.92	2.81	2.56	2.58	1.34	1.26	1.47	2.17	2.60	2.71	1.94
MgO	1.33	1.21	0.54	1.37	1.20	1.22	2.61	2.73	3.93	2.66	1.05	2.54	3.17
NiO	0.00	0.00	0.01	0.00	0.00	0.00	0.01	0.00	0.00	0.01			0.00
V_2O_3	0.01	0.01	0.00	0.00	0.00	0.02	0.28	0.26	0.14	0.14			0.09
SiO_2	0.06	0.07	0.10	0.08	0.08	0.03	0.03	0.06	0.01	0.04			0.01
ZnO	0.27	0.25	0.28	0.27	0.28	0.23	0.20	0.13	0.05	0.28			0.02
Total	97.41	97.99	96.34	98.42	97.88	98.88	96.00	96.98	97.32	94.93	92.60	92.81	96.09
Ti	0.441	0.575	0.432	0.558	0.519	0.628	0.376	0.386	0.843	0.234	0.725	0.830	1.007
Al	0.037	0.040	0.025	0.040	0.040	0.040	0.092	0.098	0.007	0.110	0.023	0.006	0.005
Cr	0.000	0.000	0.000	0.000	0.000	0.000	0.000	0.000	0.000	0.000	0.000	0.000	0.000
Fe^{2+}	1.275	1.422	1.305	1.391	1.369	1.476	1.186	1.198	0.666	1.013	1.577	0.669	0.823
Fe^{3+}	1.076	0.804	1.103	0.839	0.916	0.702	1.147	1.118	0.303	1.416	0.527	0.335	0.000
Mn	0.088	0.082	0.093	0.087	0.080	0.080	0.042	0.039	0.031	0.068	0.087	0.061	0.042
Mg	0.073	0.067	0.030	0.075	0.066	0.067	0.143	0.148	0.146	0.146	0.062	0.100	0.121
Ni	0.000	0.000	0.000	0.000	0.000	0.000	0.000	0.000	0.000	0.000			0.000
V	0.000	0.000	0.000	0.000	0.000	0.000	0.008	0.008	0.003	0.004			0.002
Si	0.002	0.003	0.004	0.003	0.003	0.001	0.001	0.002	0.000	0.001			0.000
Zn	0.007	0.007	0.008	0.007	0.007	0.006	0.005	0.003	0.001	0.008			0.000
Sum	3.000	3.000	3.000	3.000	3.000	3.000	3.000	3.000	2.000	3.000	3.000	2.000	2.000
Usp	44	58	43	56	52	63	38	39		23	73		
Mt	54	40	55	42	46	35	58	56		71	26		
Sp	2	2	1	2	2	2	5	5		5	1		
Ilm									82			78	96
Hem									15			16	0
Pyr									3			6	4

Usp = Ulvöspinel; Mt = Magnetite; Sp = Spinel; Ilm = Ilmenite; Hem = Hematite; Pyr = Pyrophanite

5.5.3 Whole-rock geochemistry

5.5.3.1 Major element geochemistry

Major element data and calculated normative mineralogies for the UFG are presented in Table 5.7. The full dataset can be found in Appendix D. All CIPW normative mineralogies were calculated using the method of Kelsey (1965) and the USGS excel calculation sheet of Jacob B. Lowenstern. The Fe_2O_3/FeO ratio was estimated following the method of Kress & Carmichael (1991), assuming a temperature of 900 °C, a pressure of 100 MPa, and redox conditions at the QFM buffer reaction curve.

The analyses for Furnas A and B have noticeably lower SiO_2 and Na_2O values, in addition to elevated LOI values. The calculated peralkalinity indices are also significantly lower than other UFG eruptions (0.73 and 0.82, respectfully, compared with ~ 1.06). These apparent deviations from the norm are considered to be the unavoidable result of sample alteration and lead to the erroneous occurrence of quartz, corundum, anorthite and hypersthene in the CIPW norm, at the expense of acmite and Na-metasilicate. For these reasons, neither of these two analyses is considered in the context of the following discussion.

The UFG samples exhibit little major element variation, with SiO_2 values that cluster around 63 wt. %, low MgO contents (< 0.5 wt. %), and high total alkali abundances (~ 13 wt. %). Using the Total-Alkali vs. Silica diagram of Le Bas *et al.* (1986), the UFG samples plot uniformly within the trachyte field (Figure 5.31). The UFG pumice falls are mildly peralkaline, with peralkalinity indices that range from 1.02 to 1.13. The UFG lava domes range from metaluminous to mildly peralkaline, with a range of 0.95 to 1.05. All of the samples are silica undersaturated, with a range in normative nepheline of 0.15 to 6.10 wt. % normative nepheline), which correlates positively with peralkalinity index. All analyses include normative orthoclase, albite, diopside, olivine, ilmenite, and apatite. The majority of samples also include Na-metasilicate in the norm (up to 1.85 wt. %), which is

Table 5.7 Whole rock major element and CIPW normative data for the Upper Furnas Group

Unit	**Furnas A**	**Furnas B**	**Furnas C**	**Furnas C**	**Furnas C**	**Furnas E**	**Furnas F**	**Furnas G**	**Furnas H**	**Furnas I**
Sample	FUR-2	FUR-3	SM1-2	SM3-1	SM1-1	SM1-3	SM4-1	S008	SM2-1	SM4-2
Position	*Fall*	*Fall*	*Lower fall*	*Lower fall*	*Upper fall*	*Fall*	*Fall*	*Fall*	*Fall*	*Fall*
SiO_2	57.69	58.25	61.24	60.78	61.04	61.04	63.11	61.13	61.59	61.95
TiO_2	0.71	0.69	0.41	0.41	0.44	0.47	0.51	0.41	0.44	0.47
Al_2O_3	19.51	18.39	16.87	17.10	17.43	17.50	17.57	16.89	16.90	17.18
Fe_2O_3	0.72	0.62	1.06	1.00	1.02	1.00	0.94	0.96	0.99	0.96
FeO	2.45	2.01	3.13	2.97	3.02	2.92	2.81	2.81	2.81	2.75
MnO	0.11	0.10	0.29	0.27	0.27	0.27	0.25	0.27	0.27	0.26
MgO	0.41	0.39	0.31	0.30	0.34	0.37	0.39	0.25	0.33	0.37
CaO	0.98	0.92	0.75	0.72	0.76	0.72	0.83	0.71	0.70	0.75
Na_2O	5.31	5.63	7.51	7.44	7.47	7.71	7.04	7.42	7.98	7.74
K_2O	5.10	5.30	5.32	5.13	5.30	5.39	5.87	5.40	5.46	5.64
P_2O_5	0.18	0.22	0.06	0.05	0.06	0.06	0.07	0.05	0.06	0.07
LOI	6.35	6.86	2.31	3.10	2.49	2.00	0.54	2.92	2.29	1.89
Total	99.52	99.37	99.26	99.27	99.64	99.46	99.93	99.22	99.82	100.02
P.I.	0.73	0.82	1.07	1.04	1.03	1.06	1.02	1.07	1.13	1.10
Quartz	4.01	2.46								
Corundum	4.19	2.42								
Orthoclase	32.32	33.88	32.42	31.50	32.24	32.66	34.90	33.14	33.09	33.95
Albite	48.24	51.47	52.35	53.41	51.74	50.35	52.81	52.84	51.42	50.80
Anorthite	3.98	3.39								
Nepheline			3.58	4.52	5.51	6.10	2.83	3.33	3.54	3.94
Diopside			3.02	2.94	3.01	2.81	3.17	2.91	2.76	2.92
Hypersthene	4.25	3.45								
Olivine			3.83	3.61	3.58	3.59	2.93	3.29	3.41	3.24
Magnetite	1.12	0.97			0.12		0.52			
Ilmenite	1.45	1.41	0.80	0.81	0.86	0.91	0.97	0.81	0.86	0.91
Apatite	0.44	0.54	0.14	0.13	0.15	0.15	0.16	0.12	0.14	0.16
Acmite			3.16	3.01	2.79	2.97	1.70	2.88	2.94	2.83
Leucite										
K-Metasilicate										
Na-Metasilicate			0.70	0.06		0.47		0.68	1.85	1.27

Fe_2O_3/FeO ratio calculated following Kress & Carmichael (1991); P.I. = peralkalinity index

Table 5.7 continued

Unit	**Furnas I**	**Furnas I**	**Furnas I**	**Furnas I**	**Furnas J**	**Furnas J**	**Furnas J**	**Furnas J**	**Furnas J**	**Furnas J**
Sample	S037	S038	SM5-1	S023	AZ02-4	SM6-1	SM8-1	SM7-1	SM7-2	S022
Position	*Lower fall*	*Upper fall*	*Dome*	*Dome*	*Fall*	*Fall*	*Flow*	*Dome*	*Dome*	*Dome*
SiO_2	61.26	61.35	63.42	62.69	61.00	61.50	61.40	62.64	62.88	62.52
TiO_2	0.47	0.47	0.46	0.55	0.47	0.48	0.48	0.57	0.57	0.56
Al_2O_3	17.01	17.04	17.55	17.71	17.04	17.02	17.03	17.58	17.88	17.64
Fe_2O_3	0.90	0.91	0.93	0.86	0.96	0.96	0.94	0.90	0.94	0.87
FeO	2.57	2.59	2.73	2.56	2.73	2.72	2.72	2.74	2.91	2.52
MnO	0.25	0.25	0.24	0.22	0.25	0.25	0.24	0.24	0.20	0.22
MgO	0.31	0.31	0.34	0.39	0.36	0.38	0.37	0.47	0.46	0.38
CaO	0.71	0.70	0.76	0.82	0.76	0.79	0.78	0.88	0.90	0.87
Na_2O	7.63	7.64	7.39	7.00	7.78	7.83	7.47	6.61	6.44	7.29
K_2O	5.60	5.59	5.78	5.95	5.56	5.59	5.59	5.97	5.95	5.96
P_2O_5	0.07	0.07	0.07	0.08	0.06	0.07	0.07	0.09	0.09	0.09
LOI	2.77	2.29	0.49	0.54	1.92	2.15	2.51	0.96	0.75	0.21
Total	99.55	99.21	100.15	99.37	98.90	99.73	99.59	99.65	99.97	99.13
P.I.	1.09	1.09	1.05	1.01	1.10	1.11	1.08	0.99	0.95	1.05
Quartz										
Corundum										
Orthoclase	34.19	34.08	34.27	35.58	33.91	33.83	34.06	35.75	35.45	35.61
Albite	51.26	51.39	52.64	52.44	49.86	50.34	51.20	54.10	54.66	49.94
Anorthite								0.66	2.31	
Nepheline	3.75	3.75	3.05	3.37	4.64	4.05	3.75	1.41	0.15	4.46
Diopside	2.76	2.71	2.88	3.10	3.02	3.09	3.06	2.70	1.37	3.26
Hypersthene										
Olivine	2.98	3.03	3.09	2.45	3.20	3.15	3.16	2.75	3.39	2.60
Magnetite				0.70				1.32	1.37	
Ilmenite	0.92	0.92	0.89	1.06	0.93	0.94	0.93	1.10	1.08	1.08
Apatite	0.17	0.17	0.16	0.19	0.15	0.17	0.16	0.22	0.22	0.21
Acmite	2.69	2.72	2.70	1.13	2.86	2.85	2.80			2.54
Leucite										
K-Metasilicate										
Na-Metasilicate	1.27	1.23	0.32		1.44	1.59	0.88			0.30

Fe_2O_3/FeO ratio calculated following Kress & Carmichael (1991); P.I. = peralkalinity index

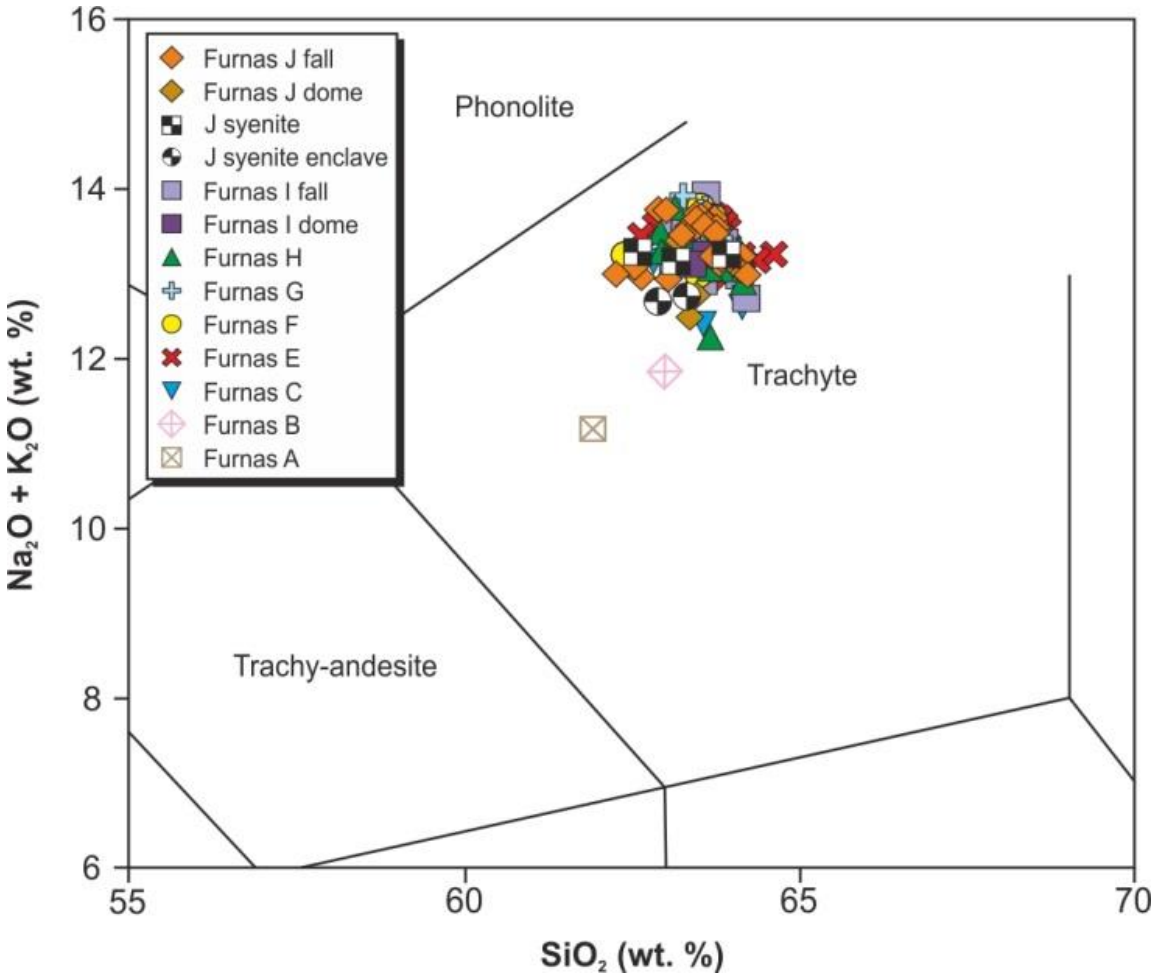

FIGURE 5.31: UFG lithologies plotted into the Total Alkali-Silica diagram of Le Bas *et al.* (1986)

replaced by magnetite in a small number of analyses. All of the analyses include up to 3.16 wt. % normative acmite, with the exception of two analyses from the Furnas J lava dome, where it is replaced by up to 2.31 wt. % anorthite.

The lithologies of the PIF are similar to those of the UFG, being characterised by relatively uniform major element compositions, with SiO_2 values that cluster around 63 wt. %, MgO concentrations that generally do not exceed ~ 0.5 wt. %, and high total alkali contents (~ 13 wt. %) (Table 5.8). All of the PIF whole rock, groundmass glass, and melt inclusion analyses plot uniformly within the trachyte field of the Total Alkali-Silica classification scheme of Le Bas *et al.* (1986) (Figure 5.32). The samples are

Table 5.8: Whole rock major element analyses and CIPW normative mineralogies for the PIF

	AZ02-6 Povoacao Ign	SM9-1 Povoacao Ign	SM10-1 Povoacao Ign	S049 Povoacao Ign	S051 Povoacao Ign	S052 Povoacao Fall	S052B Povoacao Fall
SiO_2	62.59	61.82	62.70	61.92	61.73	58.95	60.24
TiO_2	0.74	0.73	0.72	0.73	0.74	0.53	0.55
Al_2O_3	18.13	17.86	18.19	18.02	18.02	17.57	17.14
Fe_2O_3	0.68	0.66	0.66	0.67	0.67	0.56	0.61
FeO	2.17	2.09	2.08	2.12	2.12	1.76	1.93
MnO	0.13	0.14	0.14	0.13	0.15	0.17	0.18
MgO	0.50	0.49	0.48	0.57	0.47	0.45	0.55
CaO	1.28	1.31	1.31	1.31	1.23	0.80	0.96
Na_2O	6.16	6.25	6.36	6.14	5.99	6.64	6.81
K_2O	6.53	6.60	6.65	6.26	6.50	5.64	5.78
P_2O_5	0.11	0.11	0.10	0.12	0.09	0.04	0.05
LOI	0.43	1.49	0.61	1.50	2.30	6.45	4.70
Total	99.45	99.55	100.00	99.49	100.01	99.56	99.50
PI	0.95	0.98	0.97	0.94	0.94	0.97	1.02
Orthoclase	39.00	39.80	39.51	37.75	39.31	35.80	36.03
Albite	49.83	47.88	48.28	51.00	49.63	52.24	50.72
Anorthite	2.56	1.19	1.47	3.18	3.16	1.59	
Nepheline	1.51	3.30	3.18	1.09	1.21	4.39	4.51
Diopside	2.66	4.00	3.76	2.23	2.11	2.03	3.97
Hypersthene							
Olivine	1.78	1.21	1.24	2.05	1.93	1.91	1.85
Magnetite	1.00	0.98	0.96	0.99	0.99	0.87	0.17
Ilmenite	1.42	1.41	1.38	1.42	1.44	1.08	1.10
Apatite	0.25	0.25	0.23	0.28	0.21	0.10	0.12
Acmite							1.53

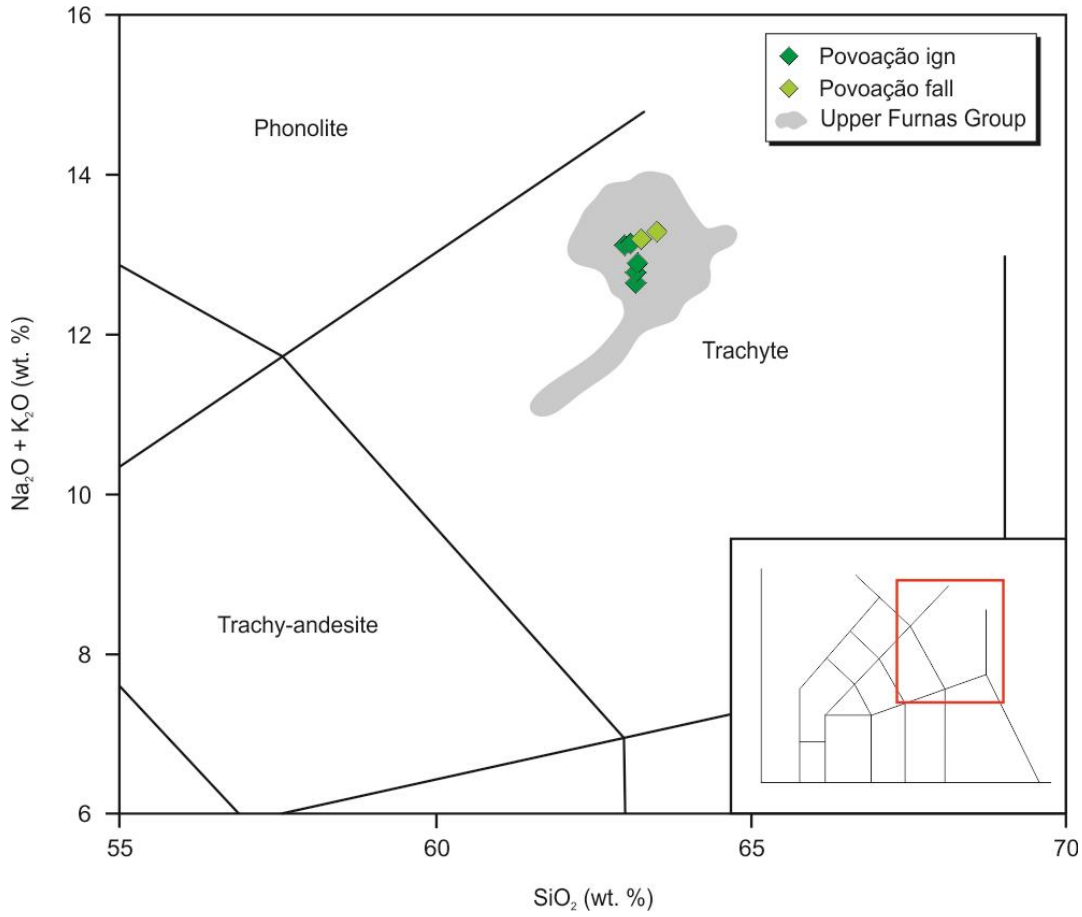

FIGURE 5.32: PIF lithologies plotted into the Total Alkali-Silica diagram of Le Bas *et al.* (1986)

metaluminous to mildly peralkaline, with a total range of peralkalinity indices (defined as molar (Na+K)/Al) of 0.93 to 1.03. Normative mineral assemblages indicate that all of the samples are silica undersaturated, with up to 7.4 wt. % normative nepheline. Most analyses also include in their normative mineral assemblages: orthoclase, albite, anorthoclase, diopside, olivine, magnetite, ilmenite, and apatite. Samples which are peralkaline also include Na-metasilicate.

5.5.3.2 Trace element geochemistry

Trace element analyses for the UFG are presented in Table 5.9, 5.10. Chondrite-normalised REE patterns shown in Figure 5.33a, and compared with a standard OIB Sun and McDonough (1989), reveal a relatively uniform enrichment in LREEs relative to HREEs, with La_N/Yb_N ratios

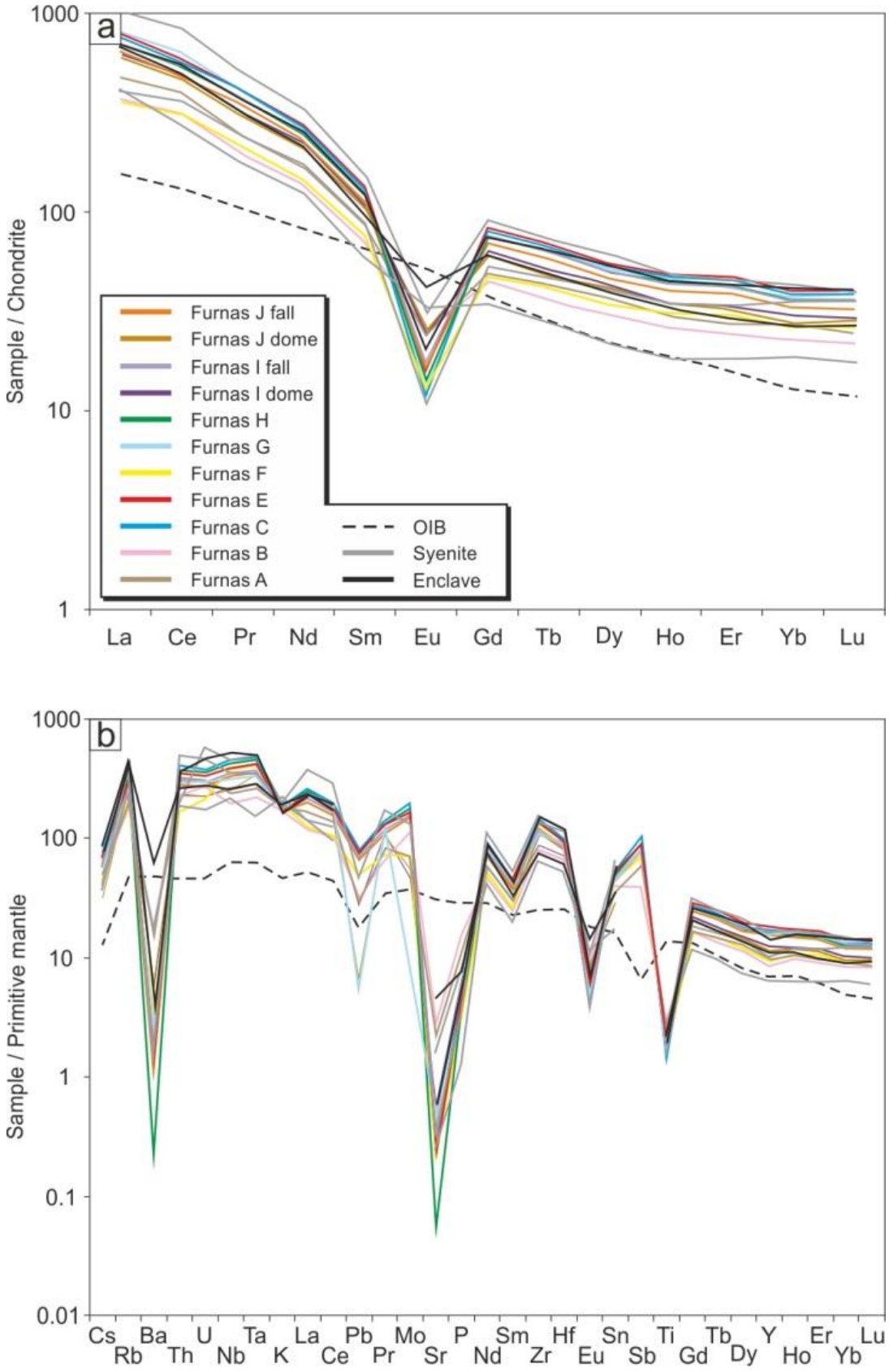

FIGURE 5.33: Trace element variation diagrams for the UFG **a)** chondrite-normalised REE diagram displaying each of the UFG lithologies relative to a standard OIB composition (Sun and McDonough, 1989) **b)** primitive mantle-normalised multi element diagram showing each of the UFG units alongside a standard OIB composition (Sun and McDonough, 1989)

Table 5.9: Trace element abundances of the UFG, quantified via XRF

Unit	**Furnas A**	**Furnas B**	**Furnas C**	**Furnas C**	**Furnas C**	**Furnas E**	**Furnas F**	**Furnas G**	**Furnas H**	**Furnas I**
Sample	FUR-2	FUR-3	SM1-2	SM3-1	SM1-1	SM1-3	SM4-1	S008	SM2-1	SM4-2
Position	*Fall*	*Fall*	*Lower fall*	*Lower fall*	*Upper fall*	*Fall*	*Fall*	*Fall*	*Fall*	*Fall*
Rb	149	144	230	225	226	228	212	221	238	212
Sr	46	51	6	5	10	4	8	bdl	2	4
Y	49	40	76	75	76	79	69	66	79	68
Zr	1254	1010	1443	1461	1460	1498	1253	1424	1494	1288
Nb	193	177	289	292	293	302	255	256	303	261
Ba	103	115	21	17	20	11	33	bdl	5	11
Pb	15	11	15	15	16	13	14	21	16	13
Th	31	24	30	29	29	32	24	29	30	26
U	8	6	8	7	9	8	7	bdl	8	6
Sc	2	1	2	1	2	3	3	bdl	3	3
V	11	17	bdl	1	5	3	6	bdl	bdl	bdl
Cr	5	5	4	4	6	5	5	bdl	2	5
Co	2	bdl	1	bdl	bdl	1	bdl		1	bdl
Ni	4	3	4	4	4	4	3	bdl	3	2
Cu	5	5	3	4	5	5	4	bdl	3	2
Zn	103	90	189	194	190	190	186	175	188	170
Ga	31	31	32	33	32	33	31		33	30
Mo	13	25	12	13	11	14	4	12	13	11
As	12	12	10	8	7	8	7	13	8	4
S	305	488	52	50	51	49	26		59	48

bdl = below detection limit

Table 5.9 continued

Unit	Furnas I	Furnas I	Furnas I	Furnas I	Furnas J	Furnas J	Furnas J	Furnas J	Furnas J	Furnas J
Sample	S037	S038	SM5-1	S023	AZ02-4	SM6-1	SM8-1	SM7-1	SM7-2	S022
Position	*Lower fall*	*Upper fall*	*Dome*	*Dome*	*Fall*	*Fall*	*Flow*	*Dome*	*Dome*	*Dome*
Rb	205	206	223	173	211	209	204	180	161	161
Sr	bdl	bdl	4	10	3	5	4	8	11	11
Y	61	62	67	52	68	68	66	63	70	70
Zr	1275	1296	1248	1021	1267	1258	1230	961	991	991
Nb	233	235	253	187	259	257	251	197	199	199
Ba	bdl	bdl	17	bdl	9	5	bdl	30	44	44
Pb	20	bdl	13	bdl	12	15	11	8	8	8
Th	26	26	26	22	28	26	25	20	18	18
U	bdl	bdl	8	bdl	7	6	4	5	7	7
Sc	bdl	bdl	2	bdl	bdl	2	2	bdl	1	1
V	bdl	bdl	3	bdl	2	bdl	6	2	2	2
Cr	bdl	bdl	6	bdl	3	6	4	5	3	3
Co			bdl		bdl	1	bdl	2	bdl	bdl
Ni	bdl	bdl	5	bdl	2	1	5	4	3	3
Cu	bdl	bdl	4	bdl	4	4	4	6	2	2
Zn	161	162	139	126	170	169	164	143	327	327
Ga			32		30	30	28	29	29	29
Mo	11	11	1	bdl	11	10	11	5	3	3
As	14	11	4	10	10	8	5	3	2	2
S			18		61	53	77	29	23	23

bdl = below detection limit

Table 5.10 Trace element abundances of the UFG, analysed via ICP-MS

Unit	Fur A	Fur B	Fur C	Fur E	Fur F	Fur G	Fur H	Fur I	Fur I	Fur J	Fur J
Sample	FUR-2	FUR-3	SM1-2	SM1-3	SM4-1	S008	SM2-1	SM4-2	S023	SM6-1	S022
Position	Fall	Fall	Lower Fall	Fall	Fall	Fall	Fall	Fall	Dome	Fall	Dome
Li			26.3	27.6	21.9		25.5	25.6		23.2	
Sc			3	3	2		2	2		2	
Ti			2615	2938	3136		2514	2954		2966	
V	11	9	1	2	1	bdl	bdl	bdl	bdl	1	bdl
Cr			2.8	1.0	0.7		bdl	bdl		1.3	
Co	1.5	1.0	1.2	bdl	bdl	0.6	bdl	bdl	bdl	bdl	bdl
Ni	1.1	0.9	2.0	0.6	bdl	bdl	bdl	bdl	bdl	0.7	bdl
Cu	2.2	2.3	3.9	3.2	2.8	0.9	2.6	2.7	0.6	4.4	bdl
Zn	45	37	178	182	167	9	173	171	105	163	37
Rb	135.0	132.8	229.3	223.1	135.6	209.4	214.3	215.3	167.9	202.0	155.9
Sr	46.1	50.2	5.9	3.8	4.5	7.6	1.1	4.5	11.8	4.2	9.2
Y	43.9	35.5	78.0	81.1	42.7	68.3	74.9	73.5	56.6	67.1	52.0
Zr	1196.0	956.2	1621.0	1678.0	1409.0	1359.0	1544.0	1500.0	986.7	1391.0	898.6
Nb	170.1	157.7	314.2	327.8	277.2	254.4	301.7	294.1	190.4	275.0	179.2
Mo	4.5	7.9	12.3	11.8	4.5	0.5	11.3	11.0	2.9	10.5	3.5
Sn	6	7	9	9	8	7	9	8	5	8	5
Sb	bdl	bdl	0.5	bdl	bdl	bdl	bdl	bdl	bdl	bdl	bdl
Cs	1.6	1.6	2.3	2.3	1.4	1.9	2.2	2.2	1.4	2.0	1.0
Ba	102	120	11	8	23	15	2	12	39	6	42
La	112.1	89.6	179.3	185.4	86.0	187.1	170.8	167.9	147.8	154.7	145.8
Ce	244.5	196.2	349.9	360.4	188.6	384.2	334.0	332.7	303.3	302.6	293.8
Pr	22.88	19.20	38.27	39.34	20.71	37.86	36.14	35.89	30.39	33.31	29.33
Nd	78.1	65.0	121.6	127.4	69.1	120.7	116.4	116.6	104.7	108.3	96.5
Sm	13.09	10.85	19.64	20.58	11.56	19.20	18.79	18.73	16.19	17.49	16.01
Eu	1.38	1.48	0.69	0.92	0.76	0.74	0.82	1.01	1.41	0.95	1.47
Gd	10.06	9.33	16.36	17.11	9.82	15.76	15.61	15.60	13.01	14.45	12.41
Tb	1.60	1.38	2.50	2.62	1.58	2.35	2.40	2.38	1.92	2.21	1.80
Dy	9.32	7.77	13.44	14.14	8.76	13.36	12.93	12.73	11.13	11.85	10.62
Ho	1.71	1.51	2.64	2.78	1.76	2.66	2.55	2.50	1.95	2.32	1.97
Er	4.59	4.07	7.45	7.78	5.05	6.93	7.16	6.99	5.58	6.51	5.34
Yb	4.59	3.92	6.53	6.82	4.53	6.37	6.27	6.12	5.16	5.69	4.71
Lu	0.63	0.57	0.97	1.01	0.68	0.98	0.93	0.91	0.74	0.84	0.73
Hf	28.3	21.6	30.6	31.8	26.7	30.1	29.5	28.4	21.7	26.6	20.3
Ta	10.9	10.3	19.4	20.1	16.9	16.0	18.7	18.0	12.0	17.2	13.9
Pb	5.3	5.9	14.5	14.9	9.1	0.9	13.6	13.5	5.1	12.7	1.2
Th	27.7	22.3	34.0	34.8	14.2	28.6	31.9	30.6	20.3	27.8	19.1
U	6.5	6.6	7.8	8.2	4.5	7.4	7.4	7.2	4.8	6.6	4.7
Be	7	2				6			9		7
Ga	29.7	28.4				30.7			27.0		25.8
W	3.7	2.7				4.6			1.8		2.2
As	5.0	7.2				bdl			1.7		2.0
Cd	bdl	bdl				bdl			1		bdl
Bi	bdl	bdl				bdl			bdl		bdl
Ag	bdl	bdl				bdl			bdl		bdl
Au	2.2	0.9				1.3			0.9		bdl
Hg	bdl	bdl				bdl			bdl		bdl
Tl	bdl	bdl				bdl			bdl		bdl
Se	bdl	0.7				bdl			bdl		bdl
Tm	0.68	0.62				1.09			0.79		0.74

bdl = below detection limit

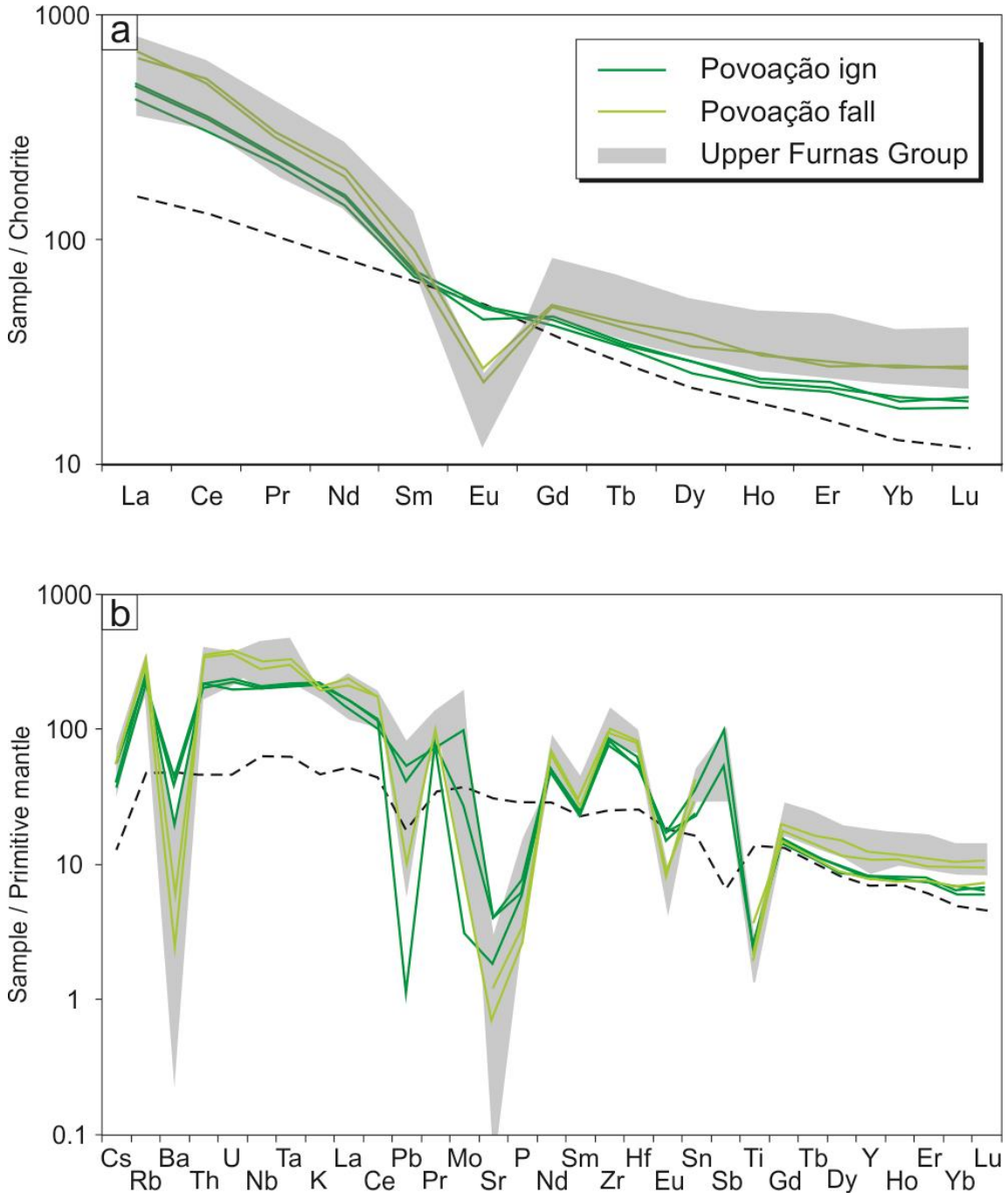

FIGURE 5.34: Trace element variation diagrams for the PIF. The compositional range of the UFG is shown as a grey field **a)** chondrite-normalised REE diagram displaying each of the Povoação ignimbrite and pumice fall relative to a standard OIB composition (Sun and McDonough, 1989) **b)** primitive mantle-normalised multi element diagram showing each of the PIF units alongside a standard OIB composition (Sun and McDonough, 1989)

between 19 and 31. They also display a pronounced, negative Eu anomaly, with Eu/Eu* (where Eu* = (Sm + Gd) / 2) values between 0.04 and 0.15. This anomaly is somewhat smaller in the lava domes, and in the first two eruptions of the UFG (Furnas A and B),

Table 5.11 Trace element compositions of the PIF, determined via ICP-MS

	SM10-1 Povoacao Ign	S049 Povoacao Ign	S051 Povoacao ign	S052 Povoacao Fall	S052B Povoacao Fall
Li	13.0				
Sc	2				
V	14	31	26	bdl	11
Cr	0.6				bdl
Co	0.7	2.4	0.6	0.7	88.5
Ni	0.4	3.8	0.3	1.2	bdl
Cu	3.4	11.0	0.7	2.3	
Zn	88	33	5	16	
Rb	142.8	146.4	158.3	192.8	208.4
Sr	85.0	84.5	39.1	15.1	25.6
Y	36.7	36.6	37.9	50.2	49.1
Zr	890.6	867.2	976.5	1099.0	1101.9
Nb	144.6	143.1	146.6	205.7	219.1
Mo	6.3	1.7	0.2	0.5	
Sn	4	6	4	5	7
Sb	0.3	0.5	bdl	bdl	
Cs	1.2	1.8	1.3	1.8	1.9
Ba	311	261	136	18	41
La	98.1	112.1	114.8	151.3	160.6
Ce	184.4	209.7	211.3	313.6	300.4
Pr	20.29	21.84	22.11	28.19	26.73
Nd	65.7	72.5	72.0	95.9	88.5
Sm	10.36	11.04	10.97	13.62	11.70
Eu	2.86	2.89	2.54	1.54	1.34
Gd	8.49	8.93	9.26	10.51	10.27
Tb	1.23	1.27	1.28	1.60	1.52
Dy	6.43	7.21	7.20	9.58	8.50
Ho	1.24	1.30	1.35	1.73	1.76
Er	3.46	3.60	3.83	4.72	4.53
Yb	3.00	3.36	3.23	4.60	4.64
Lu	0.45	0.48	0.50	0.69	0.68
Hf	15.8	17.0	19.5	25.5	24.7
Ta	8.6	8.6	8.9	12.8	13.2
Pb	9.9	7.6	0.2	1.9	
Th	17.9	17.3	18.7	29.7	29.1
U	4.1	4.6	4.9	7.9	7.8
Be		5	3	10	5
Ga		25.5	26.7	26.5	28.3
W		2.6	2.8	3.9	191.5
As				bdl	
Cd				0.1	
Bi				bdl	
Ag				bdl	
Au				1.7	
Hg				bdl	
Tl		bdl	bdl	bdl	
Se		bdl	bdl	bdl	
Tm				0.73	0.70

though the effects of post depositional alteration cannot be ruled out in the latter. Figure 5.33b presents a multi- element diagram, showing UFG data and a standard OIB, normalised against the primitive mantle composition of Sun and McDonough (1989). Notable troughs occur for Ba, Sr, Eu, Ti, and, in some cases, Pb. In particular, Sr and Ba reach concentrations which are lower than primitive mantle concentrations.

Trace element analyses for the PIF are given in Table 5.11, 5.12. Chondrite-normalised REE patterns are similar to those of the UFG, and indicate enrichment of LREEs relative to HREEs, with La_N/Yb_N ratios of ~ 33.5 (Figure 5.34a). The basal pumice fall exhibits a negative Eu anomaly, with Eu/Eu* values of ~ 0.37. In contrast, the ignimbrite displays only a slight negative anomaly (Eu/Eu* = 0.75 to 0.9). Primitive mantle-normalised multi element patterns highlight variable, but significant troughs for Ba, Sr, Pb, and Ti (Figure 5.34b).

Table 5.12 Trace element concentrations of the PIF, determined via XRF

	AZ02-6	SM9-1	SM10-1
	Povoacao Ign	Povoacao Ign	Povoacao Ign
Rb	150	151	149
Sr	85	88	86
Y	36	36	35
Zr	810	860	841
Nb	133	140	138
Ba	297	287	308
Pb	18	10	10
Th	16	18	16
U	4	4	4
Sc	bdl	2	2
V	12	11	12
Cr	5	9	5
Co	2	bdl	2
Ni	5	2	2
Cu	13	5	4
Zn	95	87	88
Ga	23	24	24
Mo	6	6	7
As	9	1	1
S	100	53	72

5.5.4 Groundmass glass

Groundmass glass from pumice clasts were analysed for the various units of the UFG and PIF. The 'Y'-shaped triple junctions between three or more vesicles were targeted to ensure the largest possible analysis area. Due to the previously described crystal-poor nature of the pumice clasts, groundmass glass compositions are similar to whole-rock compositions.

Representative analyses of the UFG are presented in Table 5.13, whilst the entire dataset is reported in Appendix D. The analyses are relatively homogeneous and plot in the trachyte field of the total alkali-silica scheme of Le Bas *et al.* (1986) (Figure 5.35), with between 60.5 and 65 wt. % SiO_2, and 12.9 to 13.9 wt. % total alkali content. CaO and MgO contents are uniformly low; < 0.9 and < 0.4 wt. %, respectively. All of the analyses are mildly peralkaline, with calculated peralkalinity indices that range from 1.03 to 1.14. Halogen contents show little variation, with ~ 3200 ppm Cl, and ~ 2000 ppm F. Sulphur concentrations are exclusively below the detection limit (≤ 300 ppm). Calculated normative mineralogies comprise albite (~ 53 wt. %), orthoclase (~ 33 wt. %), nepheline (~ 2.7 wt. %), diopside (~ 3 wt. %), olivine (~ 3 wt. %), ilmenite (~ 1 wt. %), apatite (~ 0.1 wt. %), acmite (~ 2.5 wt. %), and Na-metasilicate (~ 1.2 wt. %). All analyses are silica undersaturated (1.3 to 3.9 wt. % normative nepheline).

All available analyses from the PIF are given in Table 5.14. The groundmass glass of the PIF is similar to that of the UFG, with 62.7 to 64.7 wt. % silica, total alkali abundances between 12.4 and 13.6 wt. %, and low CaO and MgO contents (< 1.2 and < 0.4 wt. %, respectively). Peralkalinity indices range from 0.94 to 1.03, indicating metaluminous and mildly peralkaline compositions. When plotted into the total alkali-silica diagram, both ignimbrite and fall deposits plot in the trachyte field, close to the UFG analyses (Figure 5.35). As in the UFG, sulphur concentrations are very low, in this case exclusively below detection (< 160 ppm). Halogen abundances are somewhat lower than in UFG analyses, with ~ 1700 ppm Cl, and ~ 750 ppm F. Calculated normative

Table 5.13 Representative groundmass glass analyses from the UFG

Unit	**Fur J**	**Fur J**	**Fur I**	**Fur I**	**Fur H**	**Fur H**	**Fur G**	**Fur G**	**Fur F**	**Fur F**	**Fur E**	**Fur E**	**Fur C**	**Fur C**
Sample	S005	S005	S036	S036	S002	S002	S008	S008	S042	S042	S012b	S012b	S010	S010
Number	GG14	GG03	GG01	GG04	GG02	GG04	GG07	GG06	GG06	GG01	GG06	GG10	GG08	GG10
SiO_2	62.99	62.93	63.57	62.91	64.29	63.99	63.29	62.92	61.72	61.79	63.55	63.42	63.44	63.41
TiO_2	0.50	0.46	0.47	0.47	0.49	0.46	0.40	0.41	0.42	0.40	0.41	0.46	0.40	0.40
Al_2O_3	17.22	17.23	17.48	17.17	17.85	17.31	17.37	17.28	16.92	16.72	17.46	16.94	17.60	17.30
Fe_2O_3	0.87	0.87	0.86	0.88	0.90	0.86	0.98	0.95	0.84	0.93	0.83	0.94	0.93	0.95
FeO	2.50	2.48	2.56	2.52	2.65	2.51	2.83	2.64	2.45	2.63	2.37	2.67	2.73	2.71
MnO	0.29	0.28	0.23	0.29	0.29	0.26	0.23	0.31	0.30	0.30	0.23	0.28	0.25	0.32
MgO	0.31	0.32	0.34	0.33	0.35	0.35	0.32	0.28	0.30	0.31	0.27	0.30	0.26	0.26
CaO	0.71	0.74	0.69	0.72	0.87	0.74	0.71	0.73	0.70	0.75	0.79	0.72	0.70	0.77
Na_2O	7.55	7.62	7.26	7.74	7.28	7.30	7.78	8.43	7.40	7.90	8.14	8.13	7.69	7.99
K_2O	5.77	5.95	5.61	5.61	5.91	5.97	5.58	5.41	5.36	5.51	5.29	5.36	5.44	5.62
P_2O_5	0.08	0.03	0.08	0.06	0.09	0.06	0.01	0.08	0.06	0.03	0.08	0.08	0.01	0.03
Total	98.79	98.92	99.16	98.71	100.98	99.82	99.51	99.44	96.48	97.26	99.42	99.30	99.45	99.75
P.I.	1.08	1.10	1.03	1.10	1.03	1.07	1.08	1.14	1.06	1.13	1.09	1.13	1.05	1.11
Cl	3070	3100	3650	2820	2900	2720	3520	3460	3460	3400	2180	2890	2800	3330
F	1750	2020	2250	1590	1510	1420	2090	2170	2550	2750	1210	1920	1750	1950
S	bdl	bdl	bdl	bdl	bdl	bdl	bdl	170	bdl	bdl	bdl	bdl	bdl	bdl
Quartz														
Corundum														
Orthoclase	34.52	35.55	33.43	33.58	34.59	35.34	33.14	32.15	32.83	33.48	31.44	31.90	32.33	33.29
Albite	52.89	50.93	55.49	53.33	52.79	53.30	52.89	52.52	54.97	52.05	55.60	55.23	54.48	52.50
Anorthite														
Nepheline	2.30	2.80	2.00	2.44	3.00	1.41	3.07	3.56	2.33	2.62	2.76	1.34	3.30	2.89
Diopside	2.68	3.05	2.54	2.80	3.23	2.88	3.03	2.75	2.80	3.17	2.95	2.66	2.98	3.15
Hypersthene														
Olivine	2.85	2.73	2.97	2.92	2.80	2.83	3.21	3.08	2.93	3.06	2.50	3.10	3.00	2.99
Magnetite			0.03		0.12									
Ilmenite	0.97	0.89	0.90	0.90	0.92	0.88	0.77	0.79	0.84	0.78	0.79	0.88	0.77	0.76
Apatite	0.18	0.08	0.19	0.15	0.21	0.13	0.02	0.18	0.14	0.06	0.19	0.20	0.02	0.07
Acmite	2.55	2.54	2.45	2.58	2.35	2.49	2.85	2.76	2.52	2.77	2.42	2.74	2.71	2.76
Leucite														
K-Metasilicate														
Na-Metasilicate	1.08	1.44		1.30		0.73	1.01	2.21	0.64	2.03	1.36	1.97	0.42	1.59

Fe_2O_3/FeO ratio calculated following Kress & Carmichael (1991); P.I. = peralkalinity index. bdl = below detection limit. Volatiles given in ppm

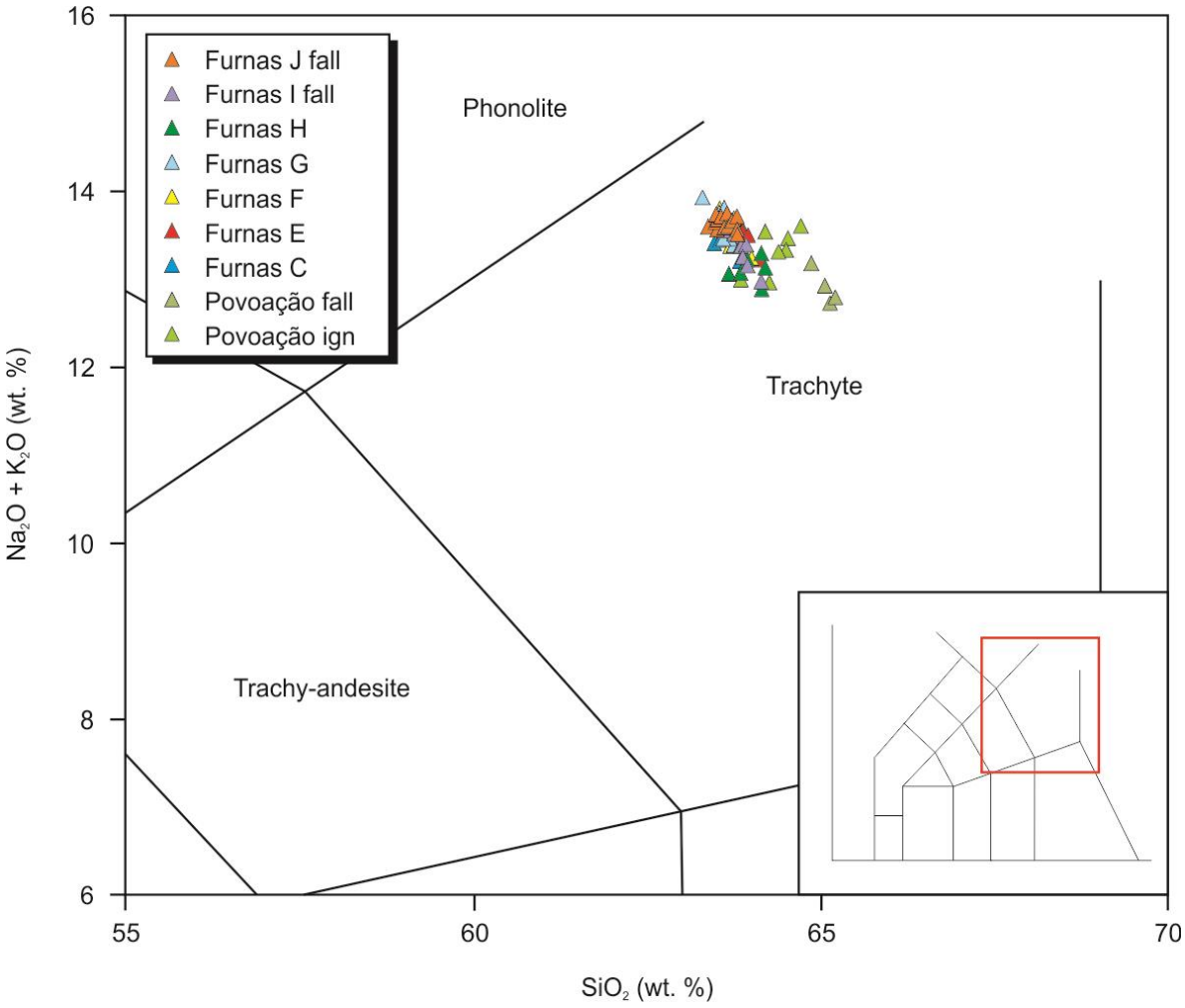

FIGURE 5.35: Groundmass glass analyses for the UFG and PIF, plotted into the total alkali-silica diagram of Le Bas *et al.* (1986)

mineralogies are more varied than the UFG, but are typified by the presence of abundant orthoclase (~ 40 wt. %), albite (~ 54 wt. %), and small amounts of ilmenite (~ 1 wt. %). Additional phase that are predicted for some analyses include: anorthite (~ 1.5 wt. %), nepheline (~ 1.4 wt. %), diopside (~ 2.6 wt. %), hypersthene (~ 1.4 wt. %), olivine (~ 0.9 wt. %), magnetite (0.8 wt. %), apatite (~ 0.1 wt. %), acmite (~ 0.8 wt. %), Na-metasilicate (0.13 wt. %), and corundum (0.06 wt. %). All but two of the analyses are silica undersaturated, with up to 2.4 wt. % normative nepheline. The remaining two analyses instead yield small amounts of quartz in their normative mineralogies (~ 0.34 wt. %). However, this is considered to be the result of the selected Fe_2O_3/FeO ratio, as the conversion of even 0.3 wt. % Fe_2O_3 to FeO (and thus a shift towards slightly more reducing conditions) prior to calculation can mitigate this effect entirely.

Table 5.14 Quantitative analyses of groundmass glass from the PIF

Unit	**Povo fall**	**Povo fall**	**Povo fall**	**Povo fall**	**Povo ign**	**Povo ign**	**Povo ign**	**Povo ign**	**Povo ign**	**Povo ign**	**Povo ign**
Sample	S052	S052	S052	S052	SM 10-1	SM 10-1	SM 10-1	SM 10-1	SM 10-1	SM 10-1	SM 10-1
Number	GG01	GG02	GG03	GG06	GG01	GG04	GG05	GG06	GG07	GG09	GG10
SiO_2	63.52	63.87	63.94	62.74	64.19	63.59	63.45	63.85	64.45	64.64	64.70
TiO_2	0.45	0.44	0.43	0.44	0.56	0.77	0.53	0.65	0.58	0.57	0.53
Al_2O_3	17.74	17.54	17.49	17.22	18.10	18.77	18.19	18.17	18.55	18.38	18.66
Fe_2O_3	0.55	0.59	0.60	0.60	0.58	0.55	0.55	0.49	0.55	0.55	0.46
FeO	1.65	1.72	1.77	1.75	1.69	1.64	1.62	1.43	1.63	1.62	1.37
MnO	0.18	0.19	0.20	0.19	0.15	0.11	0.08	0.10	0.09	0.10	0.03
MgO	0.24	0.24	0.22	0.21	0.26	0.27	0.28	0.23	0.33	0.29	0.11
CaO	0.79	0.89	0.83	0.83	0.87	0.88	0.74	0.71	1.13	0.71	0.47
Na_2O	6.60	6.78	6.71	6.91	6.77	6.40	6.18	6.07	6.40	6.45	5.66
K_2O	5.82	5.92	5.82	5.86	6.52	6.55	7.21	7.26	6.61	6.92	7.95
P_2O_5	0.00	0.02	0.08	0.02	0.03	0.10	0.04	0.01	0.02	0.01	0.07
Total	97.54	98.21	98.09	96.77	99.73	99.63	98.86	98.98	100.32	100.24	100.02
P.I.	0.97	1.00	0.99	1.03	1.01	0.94	0.99	0.98	0.95	0.98	0.96
Cl	3370	3440	3370	3240	2430	2220	1060				1100
F	590	540	730	500	1480						
S	bdl	bdl	bdl	bdl	bdl	bdl	bdl				bdl
Quartz	0.33		0.35								
Corundum											0.06
Orthoclase	35.26	35.62	35.06	35.79	39.30	39.50	43.82	43.98	39.58	41.47	47.63
Albite	57.25	57.63	57.88	55.08	53.41	53.50	49.56	50.59	53.23	52.72	48.55
Anorthite	1.63		0.42			3.21	0.61	0.91	2.40	0.77	1.90
Nepheline		0.36		1.48	2.45	0.96	2.28	1.12	0.89	1.42	
Diopside	2.06	3.78	2.82	3.59	3.60	0.51	2.47	2.22	2.68	2.34	
Hypersthene	1.77		1.56								0.70
Olivine		0.78		1.23	0.72	1.46	0.98	0.62	0.92	1.00	0.68
Magnetite	0.82	0.82	0.89		0.64	0.81	0.82	0.73	0.81	0.81	0.68
Ilmenite	0.88	0.86	0.84	0.87	1.09	1.50	1.03	1.27	1.11	1.09	1.03
Apatite		0.04	0.18	0.04	0.08	0.23	0.09	0.04	0.04	0.02	0.17
Acmite		0.10		1.79	0.44						
Leucite											
K-Metasilicate											
Na-Metasilicate				0.13							

Fe_2O_3/FeO ratio calculated following Kress & Carmichael (1991); P.I. = peralkalinity index. bdl = below detection limit. Volatiles given in ppm

5.5.5 Melt inclusions

A number of glassy melt inclusions hosted within both alkali feldspars and Fe-Ti oxides from each of the UFG and PIF units were analysed. Any inclusions that exhibited evidence of crystallisation or fracturing were not considered.

Representative analyses of alkali feldspar- and Fe-Ti oxide-hosted melt inclusions from the UFG lithologies are provided in Table 5.15. The entire dataset is reported in Appendix D. The analyses reveal relatively homogenous compositions that are similar to UFG whole rock and groundmass glass analyses. Silica contents lie between 60 and 64.5 wt. %, MgO abundances are exclusively below 0.55 wt. %, and total alkali contents range from 12.2 to 14 wt. %. The majority of analyses are mildly peralkaline, with peralkalinity indices up to 1.14, though a small number are metaluminous (PI = 0.94 to 0.99). Using the total alkali-silica of Le Bas *et al.* (1986), all samples can be classified as trachyte. Almost all of the analyses are silica undersaturated, with up to 6.17 wt. % normative nepheline. Two exceptions are instead observed to be hypersthene normative. Calculated normative mineralogies routinely comprise albite (~ 56 wt. %), orthoclase (~ 31 wt. %), diopside (~ 3 wt. %), olivine (~ 3 wt. %), ilmenite (~ 1 wt. %), apatite (~ 0.1 wt. %), acmite (~ 3 wt. %), and Na-metasilicate (~ 1 wt. %). More rarely, anorthite (~ 1 wt. %), magnetite (~ 1 wt. %), and, in one case, corundum (0.9 wt. %) are also predicted. Sulphur contents are extremely low, clustering around the detection limit (< 300 ppm). Contrastingly, the halogens Cl and F are found in significantly larger abundances (~ 3200 and 2000 ppm, respectively.

Table 5.16 reports quantitative analyses of glassy melt inclusions hosted in both alkali feldspar and Fe-Ti oxide crystals found within the PIF. As in the UFG, melt inclusion compositions are broadly similar to corresponding whole rock and groundmass glass analyses. Like the UFG, SiO_2 concentrations cluster around 62.5 wt. %, MgO contents do not exceed 0.5 wt. %, and total alkali contents range from 12 to 13.5 wt. %. All analyses are essentially metaluminous, with peralkalinity indices that lie between 0.93

Table 5.15 Representative melt inclusion analyses from the UFG

Unit	**Fur J**	**Fur J**	**Fur I**	**Fur I**	**Fur H**	**Fur H**	**Fur G**	**Fur F**	**Fur F**	**Fur E**	**Fur E**	**Fur C**	**Fur C**
Sample	MI01	MI06	MI05	MI09	MI03	MI07	MI01	MI02	MI03	MI06	MI02	MI01	MI01
Host	Fsp	Ox	Fsp	Fsp	Ox	Ox	Fsp	Ox	Ox	Fsp	Fsp	Ox	Fsp
SiO_2	60.24	62.02	60.54	63.94	63.15	62.74	61.23	60.66	64.05	62.42	62.69	63.79	60.17
TiO_2	0.62	0.71	0.48	0.37	0.56	0.64	0.40	0.47	0.65	0.40	0.49	0.63	0.38
Al_2O_3	15.90	18.35	16.81	17.77	17.40	17.31	16.94	19.37	17.25	17.03	16.82	17.70	16.78
Fe_2O_3	0.98	1.06	0.82	0.87	1.06	1.13	0.85	0.81	1.13	0.80	1.00	0.97	0.86
FeO	2.81	3.20	2.43	2.44	3.29	3.33	2.49	2.48	3.29	2.33	2.92	2.89	2.59
MnO	0.26	0.22	0.25	0.28	0.32	0.29	0.26	0.19	0.30	0.28	0.29	0.23	0.27
MgO	0.37	0.30	0.34	0.27	0.30	0.26	0.25	0.09	0.37	0.27	0.33	0.23	0.28
CaO	0.77	0.74	0.59	0.55	0.86	0.71	0.61	0.23	0.71	0.65	0.66	0.73	0.59
Na_2O	7.48	7.75	7.82	8.49	6.94	7.88	7.62	7.63	8.15	7.57	7.92	7.52	7.72
K_2O	5.37	5.20	4.16	5.51	5.21	5.33	4.86	5.22	5.28	5.18	5.00	5.59	4.11
P_2O_5	0.14	0.05	0.05	0.03	0.08	0.05	0.06	0.06	0.04	0.06	0.08	0.06	0.05
Total	94.92	99.60	94.29	100.52	99.17	99.66	95.57	97.21	101.22	96.99	98.21	100.33	93.79
P.I.	1.14	1.00	1.03	1.12	0.98	1.08	1.05	0.94	1.11	1.06	1.10	1.04	1.02
Cl	3190	3180	2780	3360	3820	3740	3390	4170	4040	3150	3810	2940	3300
F	1630	1770	2900	3250	1840	2130	2290	1940	2570	2350	2910	1600	3070
S	230	260	bdl	bdl	bdl	180	bdl	280	280	170	bdl	bdl	170
Quartz													
Corundum								0.90					
Orthoclase	33.43	30.85	26.07	32.39	31.05	31.61	30.05	31.73	30.83	31.56	30.09	32.93	25.90
Albite	53.15	54.30	62.08	53.52	59.22	52.83	57.93	55.43	54.47	57.51	57.14	54.07	62.77
Anorthite					0.95			0.82					
Nepheline	0.82	6.17	2.74	3.73		3.65	2.67	5.95	2.24	1.66	1.41	3.06	2.63
Diopside	2.67	2.91	2.38	2.22	2.49	2.81	2.39		2.84	2.53	2.47	2.82	2.43
Hypersthene					0.85								
Olivine	3.38	2.69	3.09	2.96	2.65	3.66	3.06	2.90	3.72	2.79	3.62	2.89	3.18
Magnetite		1.48			1.55			1.21					0.44
Ilmenite	1.24	1.35	0.97	0.70	1.07	1.22	0.79	0.92	1.23	0.78	0.95	1.19	0.76
Apatite	0.33	0.13	0.12	0.06	0.18	0.11	0.15	0.13	0.09	0.15	0.18	0.13	0.12
Acmite	2.99	0.13	2.52	2.50		3.28	2.57		3.23	2.39	2.95	2.80	1.78
Leucite													
K-Metasilicate													
Na-Metasilicate	2.01		0.04	1.91		0.84	0.39		1.36	0.64	1.20	0.12	

Fe_2O_3/FeO ratio calculated following Kress & Carmichael (1991); P.I. = peralkalinity index. bdl = below detection limit. Volatiles given in ppm

Table 5.16 Melt inclusion analyses from the PIF

Unit	**Povo fall**	**Povo fall**	**Povo fall**	**Povo fall**	**Povo fall**	**Povo ign**	**Povo ign**	**Povo ign**	**Povo ign**	**Povo ign**	**Povo ign**
Sample	EPFMI01	EPFMI5	MI03a	MI03b	MI11	MI01	MI03	MI04a	MI06	MI08	MI04b
Host	Fsp	Fsp	Ox	Ox	Ox	Ox	Ox	Ox	Ox	Ox	Ox
SiO_2	60.48	58.86	61.13	61.29	62.52	64.52	63.46	63.49	64.04	63.60	63.63
TiO_2	0.51	0.94	0.70	0.77	0.75	0.70	1.00	0.76	0.75	0.76	0.83
Al_2O_3	17.25	18.71	17.81	17.84	18.09	18.29	17.89	18.01	18.24	17.99	17.97
Fe_2O_3	0.53	0.71	0.68	0.70	0.86	0.62	0.89	0.81	0.84	0.76	0.88
FeO	1.58	2.07	2.06	2.10	2.63	1.85	2.63	2.40	2.52	2.23	2.65
MnO	0.12	0.15	0.11	0.12	0.15	0.12	0.17	0.12	0.13	0.14	0.10
MgO	0.31	0.49	0.44	0.42	0.43	0.02	0.36	0.35	0.40	0.40	0.35
CaO	0.96	1.33	1.27	1.37	1.52	0.30	1.21	1.25	1.19	1.53	1.36
Na_2O	6.13	6.72	5.89	5.77	6.50	6.49	6.68	6.60	6.55	6.60	6.42
K_2O	5.79	5.95	6.37	6.48	5.63	7.00	6.31	6.39	6.41	6.29	6.25
P_2O_5	0.08	0.13	0.07	0.10	0.07	0.08	0.05	0.11	0.08	0.04	0.07
Total	93.74	96.05	96.53	96.96	99.16	99.99	100.65	100.28	101.15	100.34	100.51
P.I.	0.95	0.94	0.93	0.93	0.93	1.00	1.00	0.99	0.97	0.98	0.96
Cl	1670	2900	2170	1940	2210	1960	2120	2080	2020	2380	2130
F	480	380	430	420	580	490	600	520	430	420	370
S	bdl	220	bdl	250	bdl	230	bdl	200	170	bdl	210
Quartz											
Corundum											
Orthoclase	36.50	36.61	39.00	39.49	33.55	41.37	37.05	37.66	37.45	37.04	36.75
Albite	55.34	45.49	50.26	49.70	54.22	53.17	51.15	51.14	51.67	50.89	52.33
Anorthite	2.61	3.45	3.46	3.75	3.58	0.10	0.19	0.64	1.42	0.88	1.75
Nepheline		7.43	0.74	0.35	0.67	0.95	2.71	2.47	1.69	2.58	0.93
Diopside	1.61	2.15	2.20	2.22	3.07	0.76	4.70	4.18	3.33	5.47	3.87
Hypersthene	1.64										
Olivine	0.23	1.65	1.76	1.70	2.05	1.24	0.92	1.08	1.63	0.50	1.39
Magnetite	0.82	1.07	1.02	1.05	1.26	0.90	1.28	1.17	1.20	1.10	1.27
Ilmenite	1.03	1.85	1.38	1.50	1.44	1.33	1.89	1.43	1.40	1.45	1.56
Apatite	0.20	0.30	0.17	0.24	0.16	0.18	0.11	0.24	0.19	0.09	0.16
Acmite											
Leucite											
K-Metasilicate											
Na-Metasilicate											

Fe_2O_3/FeO ratio calculated following Kress & Carmichael (1991); P.I. = peralkalinity index. bdl = below detection limit. Volatiles given in ppm

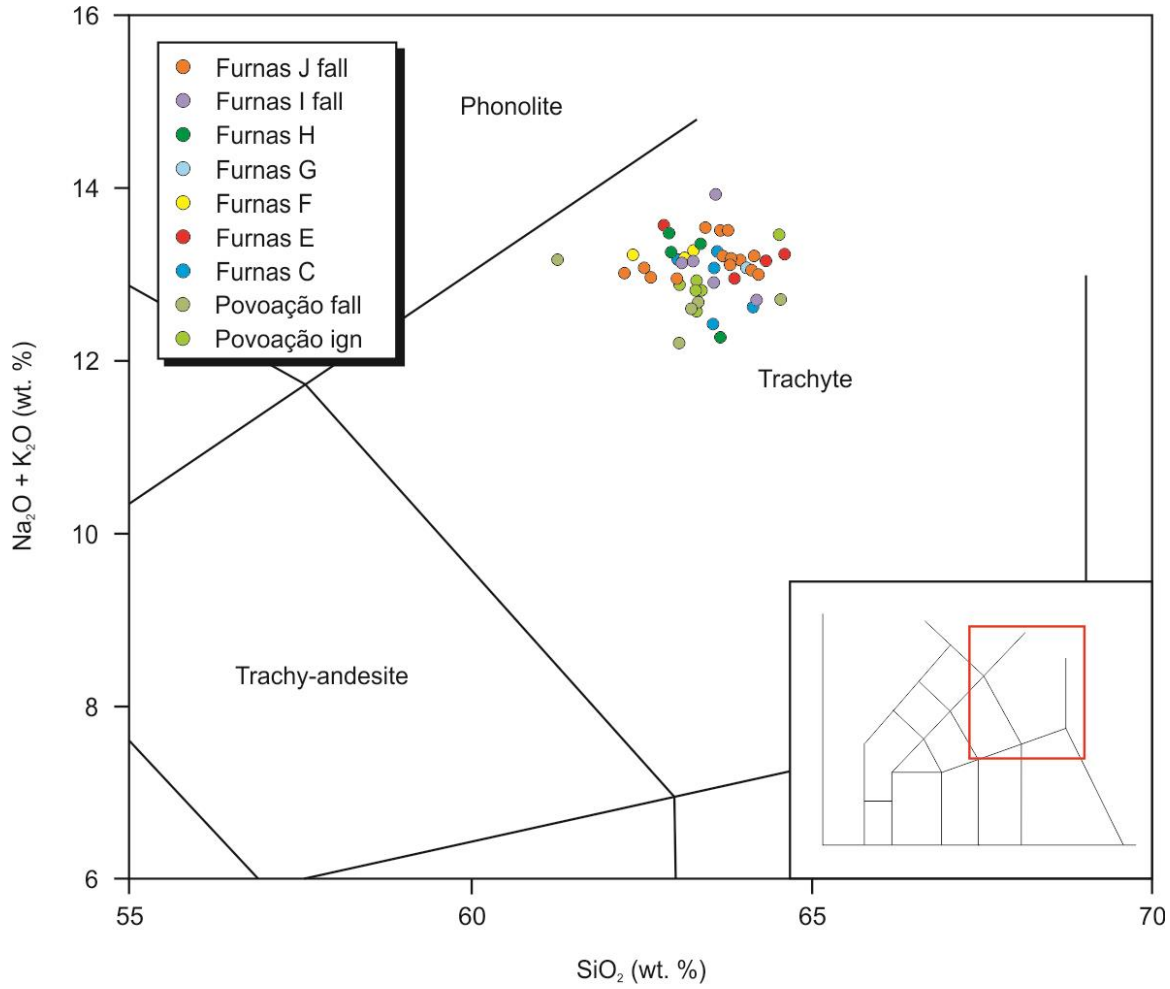

FIGURE 5.36: Melt inclusion analyses from the UFG and the PIF, plotted into the total alkali-silica classification diagram of Le Bas *et al.* (1986)

and 1.00. Melt inclusions from the Povoação fall are constrained to the lower limits of this range (≤ 0.95), whilst those of the Povoação ignimbrite are above 0.95. All analyses are classified as trachyte in the scheme of Le Bas *et al.* (1986) (Figure 5.36). Sulphur is present in trace levels (< 300 ppm), whilst Cl and F contents cluster around ~ 2100 and ~ 750 ppm, respectively. FTIR analyses of melt inclusions indicate high water contents of 3.2 and 5.0 wt. % (Table 5.17). In contrast, CO_2 was not present in sufficient quantities to be detected. All but one of the analyses are silica undersaturated, with up to 7.4 wt. % normative nepheline. The exception to this is instead hypersthene normative (1.6 wt. %). Excluding these minerals, all analyses have uniform normative mineralogies, including albite (~ 51 wt. %), orthoclase (~ 38 wt. %), diopside (~ 3 wt. %), olivine (~ 1 wt. %),

Table 5.17: FTIR analyses of alkali feldspar-hosted melt inclusions from Furnas J

Sample	Analysis no.	Peak height (cm^{-1})	Density (kg/m^3)	Thickness (cm)	Molar absorptivity (cm^{-1})	H_2O (wt. %)
Fur J MI04	1	0.776	2510	0.00240	73	3.18
Fur J MI04	2	0.791	2510	0.00240	73	3.24
Fur J MI03	1	0.918	2510	0.00180	73	5.01

ilmenite (~ 1.5 wt. %), apatite (~ 0.2 wt. %), and, unlike the UFG, ubiquitous anorthite (~ 2 wt. %) and magnetite (~ 1 wt. %).

5.6 Discussion

In this section, the combined dataset is used to provide insights into the pre-eruptive magmatic system of the young (< 5 ka), post-caldera, and the older, caldera-forming volcanic activity of Furnas, exploring first the pre-eruptive P-T-fO_2 conditions of the UFG and PIF trachytes, and the petrogenetic processes that generate them. Ultimately this allows the construction of a conceptual model for the magma plumbing system. Second, the compositional zonation patterns observed throughout the UFG, both within and between individual eruptions, are used to place constraints upon the temporal evolution of the magma reservoir from which the UFG eruptions were fed.

5.6.1 Pre-eruptive P-T-fO_2 conditions

5.6.1.1 Constraints upon the Upper Furnas Group

Due to the scarcity of ilmenite in the Furnas samples, temperature and fO_2 estimates for the trachytes, based upon two-oxide equilibria, could only be achieved for the Furnas J lava dome and the syenite ejecta. Ti-magnetite analyses from the Furnas J pumice fall were also tested for equilibrium with Furnas J dome ilmenite, and a single additional pairing was found to be suitable for calculation. Estimates for the Furnas J lava dome indicate a temperature range of ~ 80 °C between 814 and 897 °C and fO_2 values that are slightly above the FMQ buffer (Figure 5.37a). As the temperature decreases, the fO_2 values increase slightly, reaching approximately 0.5 log units above the FMQ curve at the lowest recorded temperatures. These values are representative of the final pre-eruptive magmatic temperatures and/or syn-eruptive conditions along the plumbing system, due to the rapid re-equilibration timescales of coexisting Fe-Ti oxides (e.g. Gardner *et al.* 1995; Venezky and Rutherford 1999; Pimentel *et al.*, 2015). The pre-eruptive redox conditions of the UFG trachytes appear to be more reducing than those of nearby Sete Cidades, where a total range of ~ FMQ + 1 to ~ MH – 1 was reported by Beier *et al.* (2006). Interestingly,

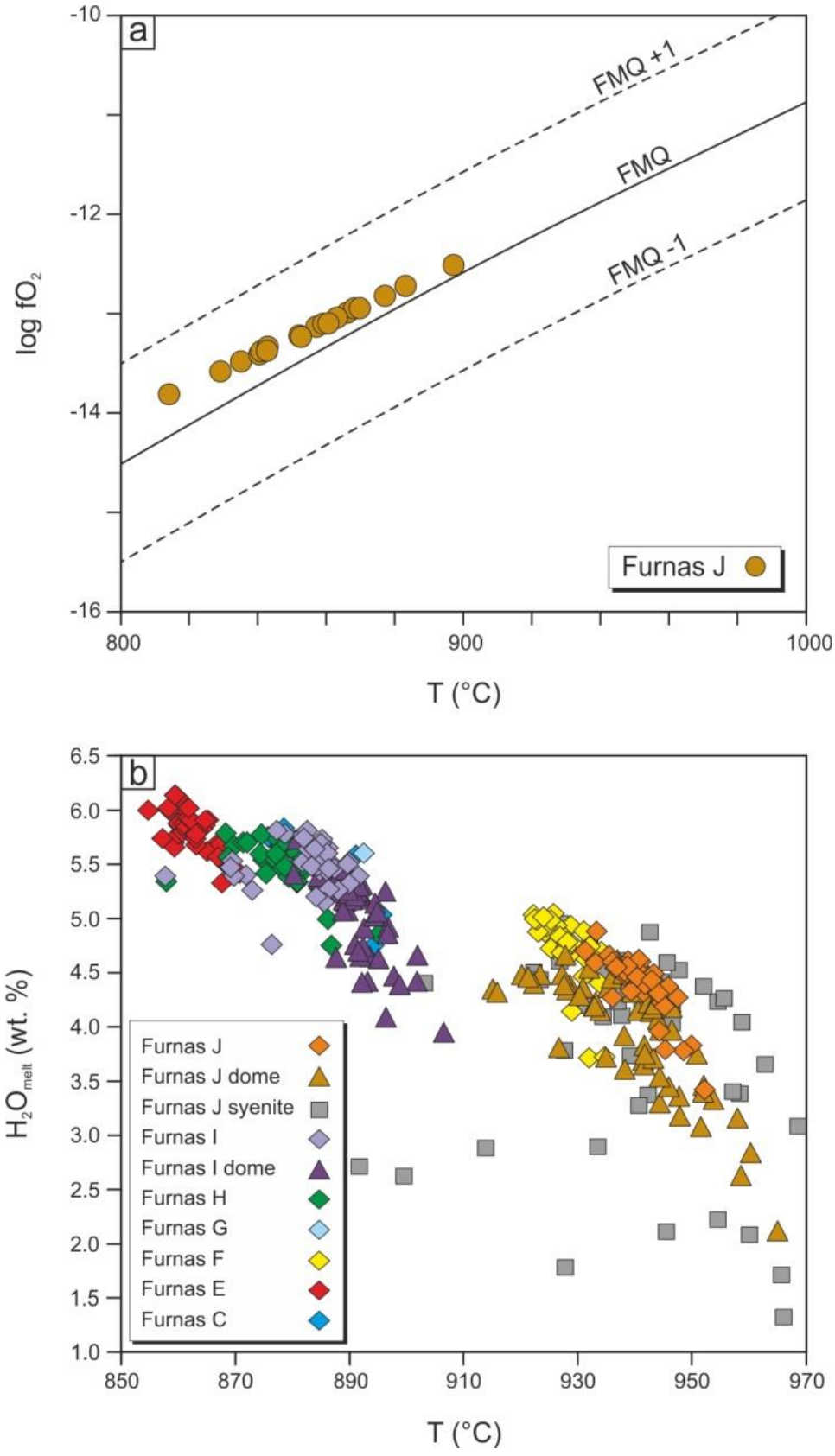

FIGURE 5.37: Summarised results of thermobarometry applied to the UFG **a)** T-fO_2 estimates derived from two-oxide models **b)** T-H_2O_{melt} estimates derived from alkali feldspar-melt thermometry and hygrometry

in the case of Sete Cidades volcano, both the caldera-forming and the post-caldera deposits (the latter being comparable to the UFG) record significantly more oxidising conditions than the UFG. This substantial variation may be linked to degassing of H_2 following the thermal disassociation of H_2O (cf. Mungall and Martin 1995), and would indicate a greater degree of magma degassing in the post-caldera magma system of Sete Cidades compared to that of Furnas. Equilibrium testing for the syenites indicates only four equilibrium pairs, yielding temperature between 621 and 780 °C, and fO_2 values that become more reduced at lower temperatures, ranging from 0.5 to 2 units below FMQ.

Pre-eruptive temperature estimates for the trachytes were also calculated via alkali feldspar-melt thermometry (Putirka 2008), using an initial estimated pressure input of 100 MPa. The effect of pressure is, in this case, negligible, with a change in calculated temperature of < 1 °C following a pressure increase of one order of magnitude. In each case, a range of up to 19 whole rock and groundmass glass compositions were used as potential equilibrium liquid compositions and the most suitable was identified using the $KD_{Or\text{-}Ab}$ equilibrium test presented by Mollo *et al.* (2015). In the majority of cases, all of the alkali feldspar analyses from a single eruption were found to be well equilibrated with a single groundmass glass or whole rock analysis from the same eruption. However, in the case of Furnas J, the most applicable equilibrium liquid for alkali feldspars from both the pumice fall and the lava dome was found to be a whole rock analysis of the lava dome (SM7-1).

Calculated temperature estimates for the UFG are summarised in Figure 5.37b and Table 5.18. The UFG exhibits a temperature range of 855 to 965 °C, with some fluctuation between individual eruptions. For example, the pumice fall and lava dome of Furnas J record temperatures in excess of 915 °C, whilst the majority of earlier UFG eruptions yield somewhat lower temperatures that are generally below 900 °C. Furnas F represents a notable exception to this, with a narrow range of hotter temperature estimates between 922 and 935 °C. Estimates derived from syenite ejecta are similar to those of the UFG falls and domes, but with greater scatter, ranging from 892 to 969 °C.

The limited available estimates for the enclaves yield temperatures that are not distinguishable from the host syenites. The comparatively wide range of temperature estimates observed in the syenites may reflect the temporal variation in feldspar nucleation that inevitably results from *in-situ* crystallisation.

Table 5.18 Summary or alkali feldspar-melt thermometry and hygrometry

Unit	No. of analyses	Temperature (°C)			H_2O_{melt} (wt. %)		
		Min	*Average*	*Max*	*Min*	*Average*	*Max*
Furnas J	40	931	941	952	3.4	4.4	4.9
Furnas J dome	67	915	939	965	2.1	4.0	4.7
Furnas I	39	858	882	892	4.8	5.5	5.8
Furnas I dome	67	880	891	907	4.0	5.1	5.7
Furnas H	38	859	880	896	4.8	5.5	5.8
Furnas G	1	n/a	893	n/a	n/a	5.6	n/a
Furnas F	36	922	927	935	3.7	4.7	5.0
Furnas E	46	855	863	871	5.3	5.8	6.1
Furnas C	17	876	885	896	4.8	5.5	5.8

Estimates of pre-eruptive H_2O contents (H_2O_{melt}) of the trachytes were determined for each unit of the UFG via alkali feldspar-melt equilibria (Mollo *et al.*, 2015). In each case, equilibrium liquid compositions were carried over from alkali feldspar-melt thermometry. Due to the dependency of calculated H_2O_{melt} values upon the input temperature, the average temperature estimate derived from alkali feldspar-melt thermometry was used as an input for each of the UFG units. Calculated H_2O_{melt} estimates for the UFG are summarised in Figure 5.37b. Results indicate that the UFG was hydrous, with average H_2O_{melt} values around 5 wt. %, and a total range from 2.4 to 6.1 wt. %. This range is consistent with the measured water contents of trachytic glass inclusions within alkali feldspars sampled from Furnas J (Table 5.17). The negative correlation between temperature and H_2O_{melt} indicate that the UFG trachytes were H_2O undersaturated prior to eruption. There is some evidence for variation in H_2O_{melt} within individual eruptions.

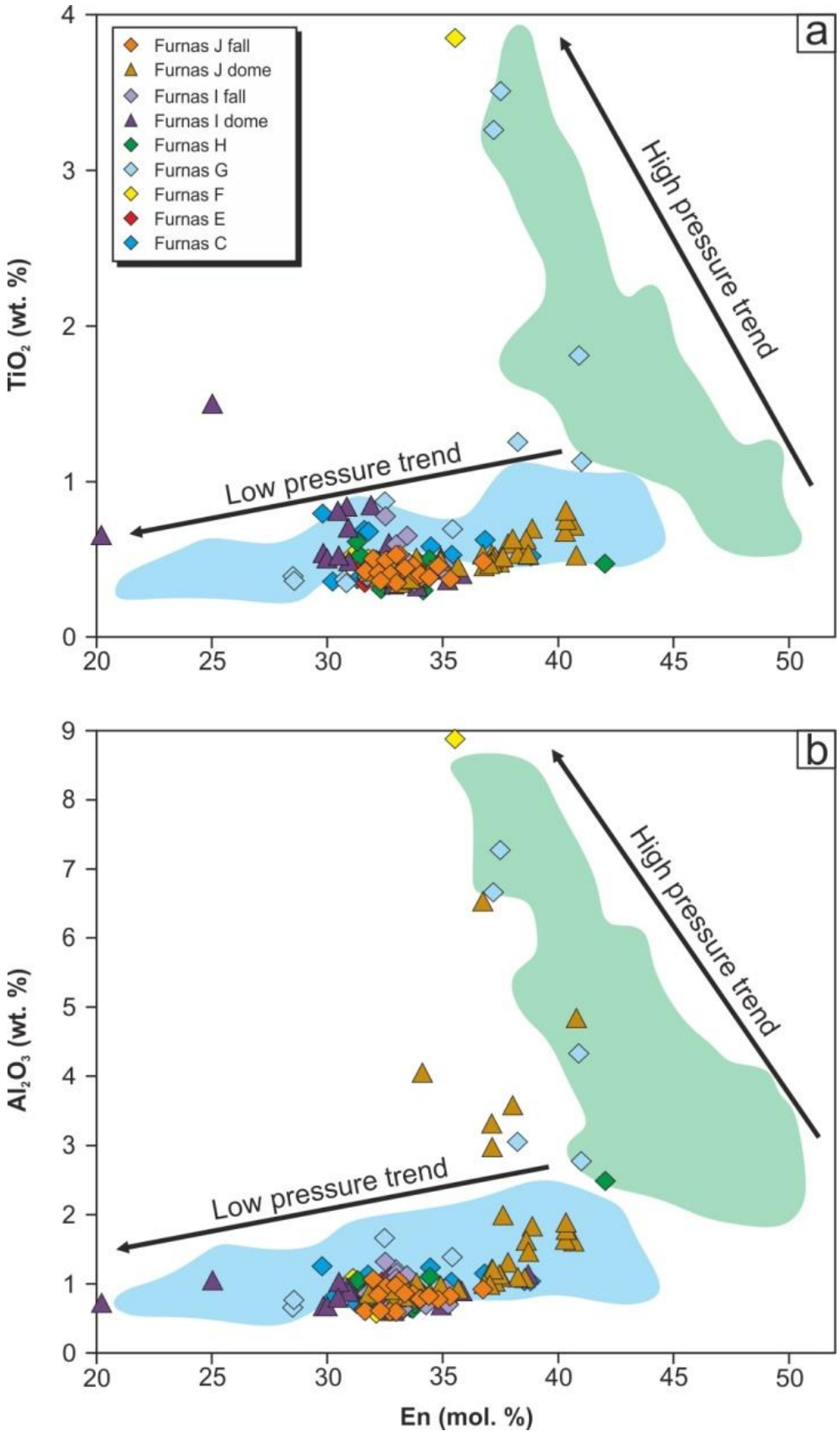

FIGURE 5.38: Variations in TiO_2 and Al_2O_3 content of UFG clinopyroxene, plotted with reference to the high and low pressure trends identified at nearby Sete Cidades (Beier *et al.,* 2006)

In the case of Furnas J and Furnas I, the late stage lava domes both yield H_2O_{melt} estimates that extend to somewhat lower values than the preceding pumice falls. This is most obvious for Furnas J, where the dome analyses return a range that extends as low as 2.4 wt. %, which is > 1 wt. % lower than the lowest estimate for the Furnas J pumice fall. Syenite ejecta and their enclaves yield a range of estimates that are comparable to those of Furnas J and Furnas F, but show substantial scatter, ranging from 1.3 to 5.3 wt. %.

Equilibrium testing of clinopyroxene indicated that none of the reported UFG clinopyroxenes were in equilibrium with their host trachytes, precluding quantitative estimation of pre-eruptive conditions. Beier *et al.* (2006) noted a similar lack of crystal-melt equilibrium in trachytes from Sete Cidades. Application of hypothetical liquid compositions derived from Rhyolite-MELTs modelling indicates that the most suitable equilibrium liquid compositions are broadly trachyandesitic. Despite the lack of equilibrium, clinopyroxene chemistry may still allow qualitative insights into the magma system. Beier *et al.* (2006) observed two trends in clinopyroxene Al_2O_3 and TiO_2 content at Sete Cidades: 1) high Al_2O_3 and TiO_2 in the mafic rocks, and 2) low Al_2O_3 and TiO_2 in the trachytes. These trends were attributed to high and low pressure crystallisation conditions, respectively. With the exception of a small number of clinopyroxenes from a number of the UFG units, the UFG clinopyroxene population adheres to the low Al_2O_3 and TiO_2 trend (Figure 5.38). On this basis, the bulk of clinopyroxene crystallisation may be constrained to shallow crystal conditions. The small number of high pressure clinopyroxenes may reflect an earlier high pressure fractionation step, similar to that of Sete Cidades, which is poorly represented in the UFG trachytes.

Further constraints can be placed upon the minimum depth of the magma reservoir through the calculation of saturation pressures of the melt. To achieve this, the solubility model of Di Matteo *et al.* (2004) was applied. This applies a polynominal fit of experimental data to parameterize H_2O solubility, and yields an estimated minimum pressure of 100 MPa ± 15 MPa, assuming water saturation at 5.0 wt. % (melt inclusion

water content), or 132 ± 15 MPa assuming water saturation at 6.1 wt. % (maximum hygrometry estimate).

5.6.1.2 Constraints upon the Povoação Ignimbrite Formation

Efforts to constrain the pre/syn-eruptive intensive variables of the PIF-forming magmas via two-oxide thermometry were more successful than for the UFG due to relative abundance of ilmenite. The Povoação pumice fall yields a narrow range of temperature estimates (905 to 916 °C, avg. = 910, *n* = 8), at redox conditions close to one log unit above the FMQ buffer reaction curve. In contrast, the Povoação ignimbrite yields a considerable range of 494 to 1289 °C (avg. = 883, *n* = 350), most likely reflecting the previously described rapid timescales of re-equilibration of Fe-Ti oxides. Despite this, more than 90 % of the results lie between ~ 950 and ~ 770 °C (Figure 5.39a). Within this range, and above it, predicted fO_2 values are predominantly one log unit above the FMQ buffer reaction curve. Below ~ 770 °C, fO_2 estimates decrease to values below two log units below the FMQ buffer reaction.

Calculated temperature estimates derived from alkali feldspar-melt thermometry are comparable with those of two-oxide models, with the Povoação fall and ignimbrite each presenting distinctive ranges of 875 to 860 °C (avg. = 867, *n* = 14), and 981 to 924 (avg. 936, *n* = 39), respectively. Pre-eruptive H_2O_{melt} estimates exhibit similar bimodality, with a range of 5.7 to 6.2 wt. % (avg. = 5.9, *n* = 14) for the Povoação fall, and a lower range of 3.8 to 4.9 wt. % (avg. = 4.5, *n* = 37) for the Povoação ignimbrite (Figure 5.39b**)**. These estimates were used to estimate the minimum depth of magma storage using the H_2O solubility model of Di Matteo *et al.* (2004), yielding a saturation pressure of 140 MPa, assuming water saturation at 6.2 wt. %.

Attempts to equilibrate clinopyroxene with any of the PIF whole rock, melt inclusion, or groundmass glass compositions were unsuccessful, indicating that the

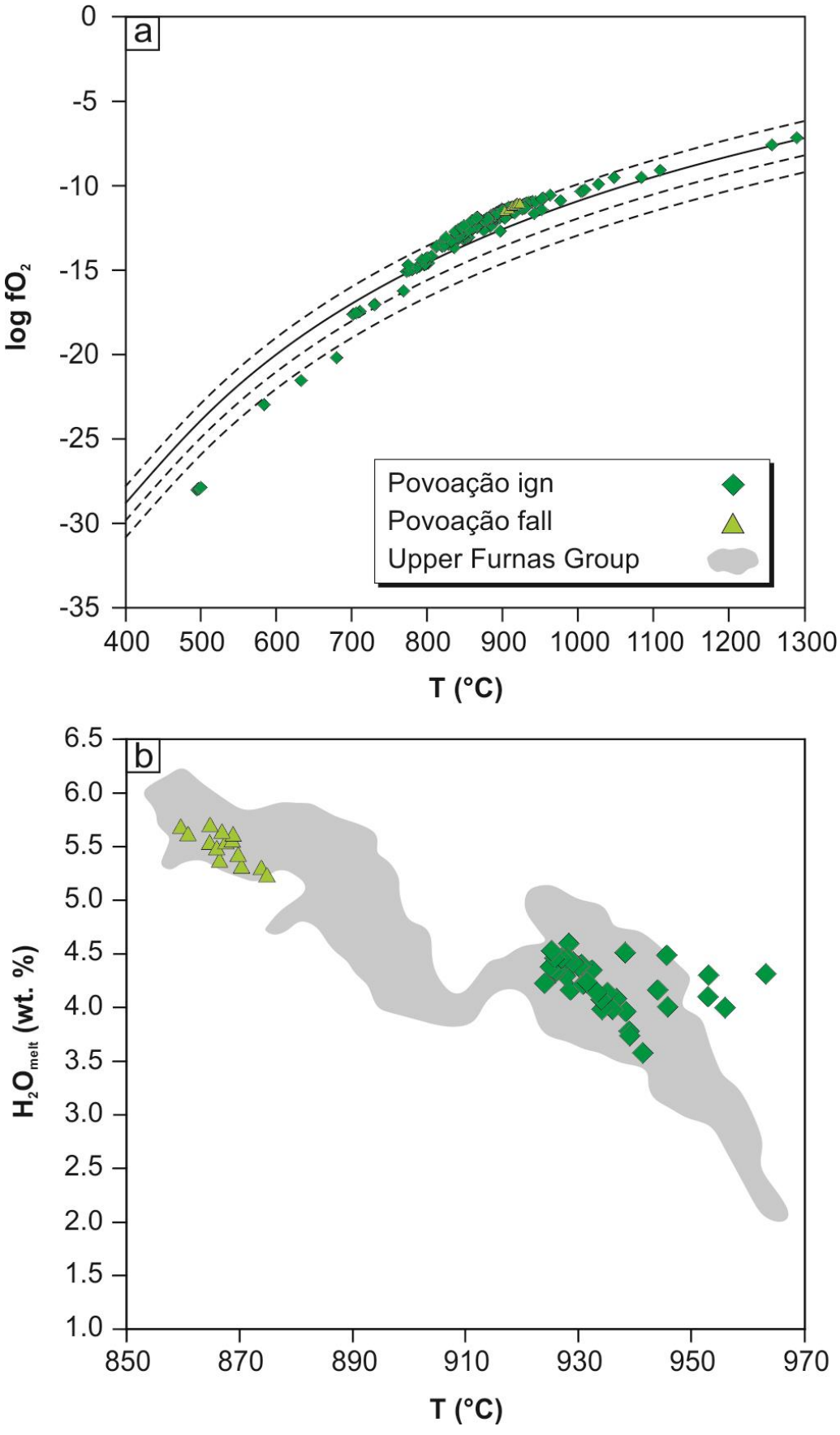

FIGURE 5.39: Summarised results of thermobarometry applied to the PIF **a)** T-fO_2 estimates derived from two-oxide models **b)** T-H_2O_{melt} estimates derived from alkali feldspar-melt thermometry and hygrometry

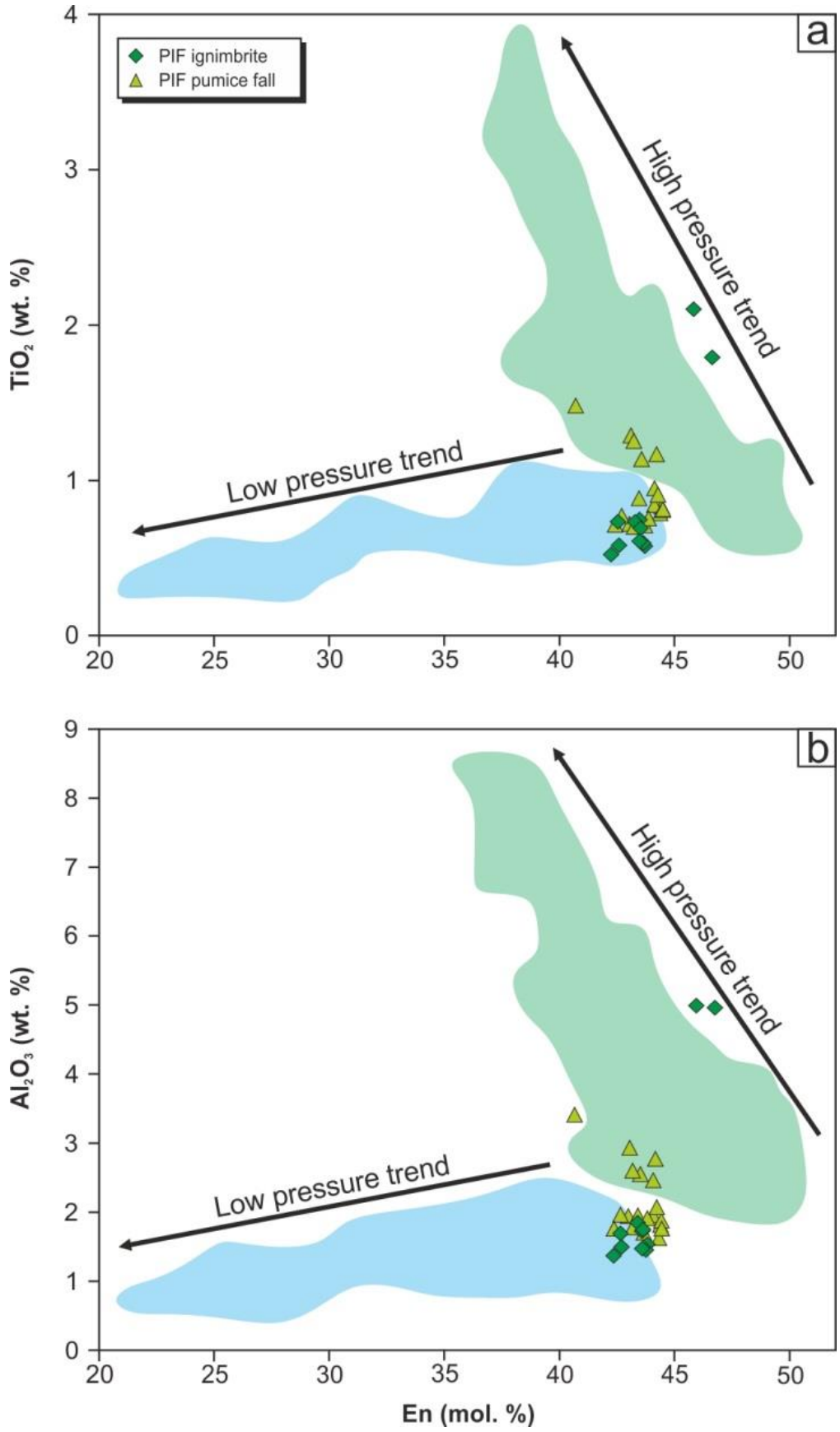

FIGURE 5.40: Variations in TiO_2 and Al_2O_3 content of PIF clinopyroxene, plotted with reference to the high and low pressure trends identified at nearby Sete Cidades (Beier *et al.*, 2006)

clinopyroxene population is not in equilibrium with the host trachytes, inhibiting the application of clinopyroxene-based models. Instead, the most suitable equilibrium composition was found to be a basaltic trachyandesitic composition taken from the most applicable, Rhyolite-MELTs modelled, liquid line of descent, though compositions ranging from basalt to trachyandesite are also close to equilibrium (within 10 %). Despite this, clinopyroxene geochemistry may provide some qualitative insights into the depth of crystallisation. As observed in the UFG, the majority of clinopyroxene phenocrysts from the PIF exhibit low TiO_2 and Al_2O_3 contents, suggesting shallow crustal crystallisation (Figure 5.40) (cf. Beier *et al.*, 2006). A minor number of of analyses adhere instead to the high pressure trend, exhibiting high En, TiO_2 and Al_2O_3 contents.

5.6.2 Establishing the liquid line of descent of Furnas magmas

5.6.2.1 Petrogenesis of the Upper Furnas Group magmas

To investigate the roles of fractional crystallisation and partial melting of crustal rocks in the generation of the UFG trachytes, Rayleigh fractionation and batch melting models are employed, using a young basaltic lava located ~ 6 km south west of Furnas village (sample 98SM33 of Elliott et al. 2007) as the parental magma, or a partially melted crustal gabbro, respectively. Suitable natural and experimental mineral-melt partition coefficients were selected from relevant lithologies from the GERM database (Nielsen 2006), and are reported in Table 5.19 (Paster *et al.*, 1974; Matsui *et al.*, 1977; McCallum and Charette 1978; Larsen 1979; Villemant *et al.*, 1981; Watson and Green 1981; Bacon and Druitt 1988; Mahood and Stimac 1990; McKenzie and O'Nions 1991; Nielsen, 1992; Ewart and Griffin 1994; Latourrette *et al.*, 1995; Wood and Trigila 2001; Klemme *et al.*, 2006). Modelling of compatible trace elements such as Sr, Ba, and Ni indicate that batch melting models of gabbroic crust with variable mineral assemblages are unable to reproduce the low concentrations observed in the dataset (Figure 5.41a, b, c). Instead, Rayleigh fractionation curves provide a better fit, and suggest that the compositional variability of

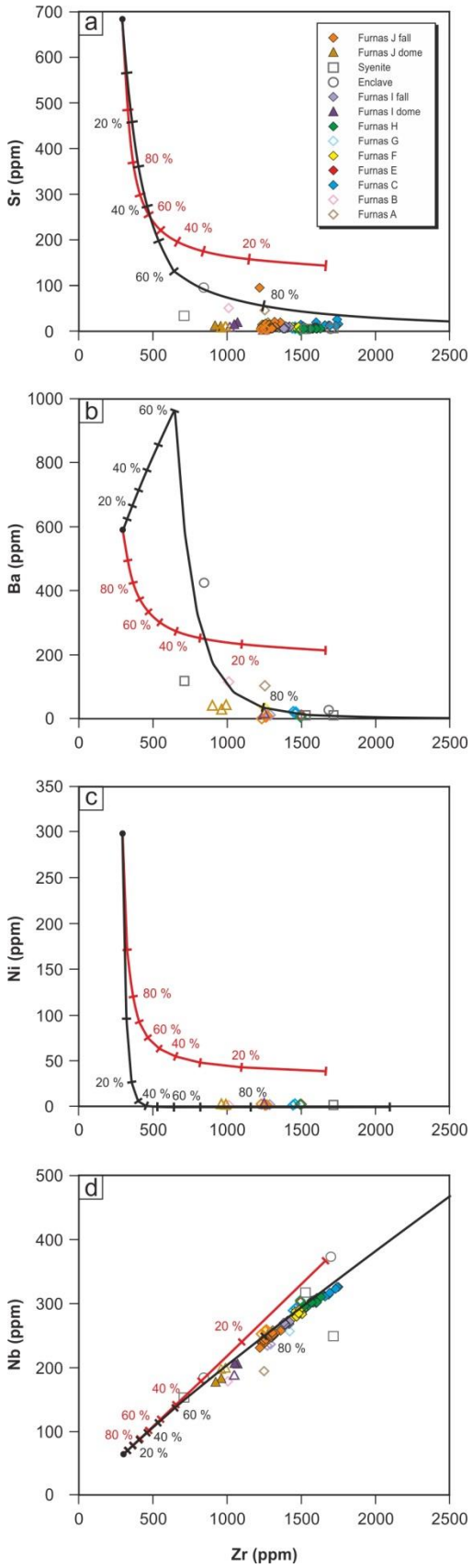

FIGURE 5.41: Results of trace element modelling. Calculated Rayleigh fractionation and batch melting curves are shown in black and red, respectively. Ticked intervals represent 10 % fractionation or partial melting. Analyses derived from ED-XRF are given with filled symbols, whilst those produced via WD-XRF are shown with open symbols. Parental compositions are shown with a black circle

Table 5.19 Partition coefficients used for trace element modelling

	Pl	Cpx	Ol	Mt	Bt	Ap	Alk fsp	Ilm
Step 1 RFC and batch melting								
Nb	0.010	0.100	0.010	0.900	0.088			
Zr	0.010	0.120	0.060	0.700	0.017			
Sr	10.000	0.700	0.020		0.700	1.200		
Ba	0.300	0.040	0.030		3.680	0.050		
Ni	0.270	2.500	34.000	48.00	23.90			
Step 2 RFC								
Nb				0.900	0.740		0.004	11.60
Zr				0.250	0.090		0.030	0.290
Sr					0.490	1.200	2.300	0.740
Ba				0.100	10.000	0.050	5.900	
Ni					89.625		0.905	6.200

All coefficients sourced from the GERM database (Nielsen, 2006). pl = plagioclase, cpx = clinopyroxene, ol = olivine, mt= Ti-magnetite, bt = Biotite, ap = apatite, alk fsp – alkali feldspar, ilm = ilmenite

the UFG trachytes (LET to MET) is largely controlled by ~ 75 to 85 % fractionation of an alkali basaltic parent. Modelled fractionation curves for incompatible elements such as Nb, and Zr indicate a similar range of fractionation values (~ 70 to 85 %) (Figure 5.41d). This is consistent with Sete Cidades (Beier *et al.*, 2006) and Fogo (e.g. Storey, 1982; Widom *et al.* 1992), as well as other notable peralkaline centres such as Terceira (e.g. Mungall and Martin, 1995) and Pantelleria (e.g. Neave *et al.,* 2012), where fractional crystallisation plays a dominant role in magma evolution.

To further investigate the role of fractional crystallisation, major element mass balance models were applied using the mineral compositions reported in Table 5.20. The results indicate that evolution from parental basalt to the least evolved trachyte (LET) (step 1) can be adequately explained ($\sum r^2 = 0.023$) by 87.5 % fractional crystallisation of a phase assemblage including clinopyroxene (45 %), plagioclase (24 %), Ti-magnetite (12 %), olivine (7 %), biotite (10 %), and apatite (2 %) (Table 5.21). The second evolutionary step (LET to the most evolved trachyte (MET)) can be achieved by a further 38 % fractional crystallisation of an assemblage dominated by alkali feldspar (94 %), with subsidiary Ti-magnetite (1 %), ilmenite (1 %), biotite (3 %), and apatite (1 %) ($\sum r^2 = 0.018$). Together, steps 1 and 2 indicate that the differentiation of parental basalt to the

Table 5.20 Mineral compositions used for major element mass balance modelling

Mineral	Pl	Alk fsp	Ol	Cpx	Mt-1	Mt-2	Ilm	Bt	Ap
SiO_2	54.71	65.15	40.44	52.26				36.70	
TiO_2		0.09		0.84	14.65	20.47	48.97	6.51	
Al_2O_3	29.28	19.00		2.21	0.99	4.39	0.03	13.30	
Fe_2O_3				3.37	40.01	26.61		6.85	
FeO	0.82	0.37	11.75	0.38	39.25	42.36	42.26	9.01	
MnO			0.22	0.12	2.63	0.52	3.93	0.41	
MgO		0.01	47.32	16.71	1.77	4.99	3.31	13.91	
CaO	10.30	0.54	0.28	22.37					55.70
Na_2O	4.83	6.87		0.28				0.97	
K_2O	0.43	6.69						8.71	
P_2O_5									41.82
H_2O									0.59

Mineral compositions for alkali feldspar (alk fsp), Ti-magnetite (Mt-1), and ilmenite (Ilm) were taken from the dataset of this study. Compositions for plagioclase (Pl), olivine (Ol), clinopyroxene (Cpx), Ti-magnetite (Mt-2), and biotite (Bt) were taken from Beier *et al.* (2006)

most evolved UFG trachyte can be accounted for by a total of 92 % fractional crystallisation of an assemblage that is dominated by clinopyroxene and plagioclase during basalt to trachyte evolution, and alkali feldspar during continued evolution within the trachytes. The predicted late stage prevalence of alkali feldspar fractionation is in agreement with the mineral assemblages of the trachytes, where alkali feldspar constitutes the dominant phenocryst phase. Predicted mafic to intermediate assemblages are broadly similar to available descriptions of mafic to intermediate rocks from across São Miguel (e.g. Moore 1991a; Beier *et al.*, 2006; Jeffery unpublished data).

The results of 150 Rhyolite-MELTs models indicate that a liquid of similar composition to the UFG trachytes (with respect to MgO, SiO_2, Al_2O_3, total alkalis, peralkalinity index, and H_2O_{melt}), can be produced via fractional crystallisation of a hydrous (1.5 wt. %) alkali basalt parent under low pressure (150 MPa), at redox conditions close to the FMQ buffer reaction curve (Figure 5.42). These conditions are consistent with those predicted via thermobarometrical models. This model predicts olivine as the liquidus phase (1,265 °C), followed by clinopyroxene and Ti-magnetite (1,115 °C), with clinopyroxene crystallisation ceasing at 905 ºC. This is followed by apatite (1,065 °C) plagioclase feldspar (985 ºC), biotite (900 ºC), and ilmenite (795 ºC). The model reaches compositions similar to the METs of the UFG at ~ 815 ºC, at which point the melt has undergone ~ 86 % fractionation of olivine (~ 10 %), clinopyroxene (~ 42 %), feldspar (~ 22

Table 5.21: Results of major element mass basalnce modelling for the UFG

Step 1: Alkali basalt to LET

Liquid Composition				Fractionating Phases	
Sample	Basalt		LET		
	98SM33		S022		
	Obs	Calc	Obs		
SiO_2	46.22	46.17	63.20	Cpx	45.1
TiO_2	3.41	3.29	0.57	Plg	23.9
Al_2O_3	10.89	10.93	17.83	Mt	12.3
FeO_t	11.44	11.48	3.34	Bt	10.2
MnO	0.17	0.19	0.22	Olv	7.1
MgO	11.53	11.53	0.38	Ap	1.6
CaO	12.01	12.04	0.88		
Na_2O	2.12	2.13	7.37		
K_2O	1.59	1.65	6.03		
P_2O_5	0.63	0.6	0.09		
$\sum r^2$	0.023				
F	0.125				

Step 2: LET to MET

Liquid Composition				Fractionating Phases	
Sample	LET		MET		
	S022		SM 1-2		
	Obs	Calc	Obs		
SiO_2	63.20	63.28	63.16	Alk fsp	94.1
TiO_2	0.57	0.57	0.42	Bt	3.2
Al_2O_3	17.83	17.86	17.40	Mt	1.4
FeO_t	3.34	3.44	4.21	Ap	0.7
MnO	0.22	0.22	0.30	Ilm	0.6
MgO	0.38	0.4	0.32		
CaO	0.88	0.83	0.77		
Na_2O	7.37	7.31	7.75		
K_2O	6.03	5.94	5.49		
P_2O_5	0.09	0.16	0.06		
$\sum r^2$	0.018				
F	0.618				

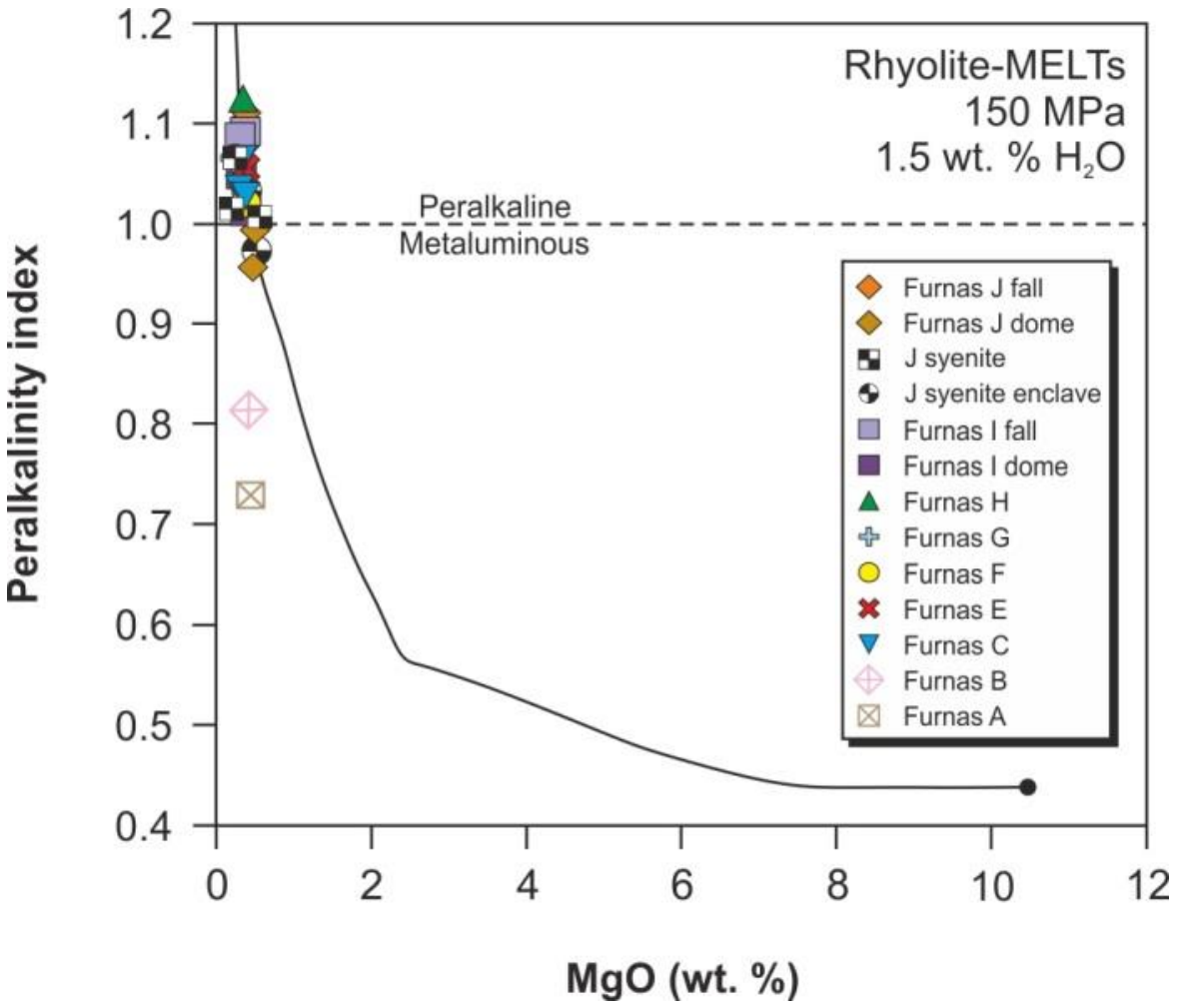

FIGURE 5.42: Results of Rhyolite-MELTs fractional crystallisation modelling from an alkali basalt (black circle). Modelled curved produced at 150 MPa, with an initial water content of 1.5 wt. %

%), Ti-magnetite (~ 10 %), apatite (~ 1 %), and biotite (~ 1 %). Higher pressure (300 and 500 MPa) models fail to reach the silica and total alkali values exhibited by the UFG, peaking at approximately trachyandesitic compositions. Lower pressure (50 MPa) models underestimate liquid Al_2O_3 contents due to the earlier crystallisation of feldspar, leading to higher peralkalinity indices than observed in the UFG. Polybaric models in which the pressure is changed from 500 to 150 MPa at arbitrarily selected temperature values of 1,100 ºC and 1,000 ºC also perform well, generating liquid compositions similar to the UFG when initial water content and redox conditions are set to 1.5 wt. % and the FMQ buffer, respectively. However, these models yield silica and total alkali contents that are slightly lower than the UFG. For models run at 150 MPa, olivine is the liquidus phase (1,200 to 1,260 ºC), regardless of initial water content or redox conditions. This is followed

by clinopyroxene, which crystallises at higher temperatures at lower water contents and more oxidising conditions. The crystallisation of feldspar is strongly controlled by initial melt water content, beginning at between 1,120 and 960 ºC, with the onset of crystallisation being favoured by lower water contents. Ti-magnetite shows a range of saturation temperatures that is slightly larger than that of feldspar (1,180 to 920 ºC), and is strongly affected by both initial water content and oxygen fugacity. As such, under relatively oxidising conditions (> FMQ buffer), Ti-magnetite crystallises before feldspar, regardless of initial water content, and may even form before clinopyroxene under highly oxidising, hydrous conditions (FMQ + 2, 4 wt. % H_2O). The conditions that yield the best results had initial melt water contents of 1.5 wt. %, and redox conditions defined by the FMQ buffer reaction.

In addition to the described petrogenetic models, geochemical characteristics of the UFG highlight the role of fractional crystallisation. The observed depletion of Ti and P indicate the fractionation of Fe-Ti oxides and apatite, respectively, whilst the extreme depletion of Sr and Ba, and the large negative Eu anomaly that is typical of Furnas trachytes, reflects extensive fractionation of both plagioclase and alkali feldspars. Based upon the presented evidence, it is suggested that the trachytes of the UFG are primarily derived from between ~ 70 and ~ 90 % low pressure fractional crystallisation of an alkali basaltic parental magma under redox conditions close to the FMQ buffer, although a minor contribution from crustal assimilation or partial melting of crustal lithologies cannot be ruled out entirely (e.g. Widom and Farquhar 2003; Snyder *et al.*, 2004; Genske *et al.* 2013, 2014; Larrea *et al.* 2014). These elevated fractionation values are compatible with estimates from other peralkaline systems such as Pantelleria (70 to 95 %, White *et al.* 2009; 76 to 96 %, Neave *et al.* 2012), Sete Cidades, Azores (~ 92 %, Renzulli and Santi 2000), Fogo, Azores (72-93 %, Widom *et al.* 1992) and the East African Rift (e.g. 95 to 99 %, Scaillet and Macdonald 2003; 50 to 85 %, Rooney *et al.* 2012).

5.6.2.2 Petrogenesis of the Povoação Ignimbrite Formation magmas

Mass balance models indicate that the least evolved trachytic compositions of the PIF can be generated by 82 % fractional crystallisation of an alkali basalt composition ($\sum r^2$ = 0.183) (Table 5.22). The predicted fractionating assemblage includes clinopyroxene (47 %) and plagioclase (25 %), with lesser Ti-magnetite (14 %), olivine (11 %), apatite (2 %), and ilmenite (1 %). In contrast, the second evolutionary step (LET to MET) is dominated by alkali feldspar (93 %), biotite (4 %), Ti-magnetite (2 %), and ilmenite (1 %), constituting 72 % fractionation ($\sum r^2$ = 0.691). Considered together, steps 1 and 2 indicate that the trachytic magmas of the PIF can be accounted for by 82 to 95 % fractional crystallisation of an alkali basalt, with clinopyroxene and plagioclase being the most significant fractionating phases during evolution from basalt to LET, and alkali feldspar being most important during evolution within the trachytes.

Trace element models for the incompatible elements Nb and Rb do not allow the differentiation of Rayleigh fractionation and batch melting, with both trends fitting well to the observed data from the PIF (Figure 5.43). The two models are relatively consistent, indicating that the Povoação ignimbrite can be generated by ~ 60 to 75 % fractionation, or high partial melt values of 15 to 30 %. The Povoação fall requires greater degrees of fractionation (~ 75 to 80 %), and lower partial melt values (~ 10 to 15 %). In contrast, models for Sr and Ba highlight the incompatibility of batch melting models, which overestimate elemental concentrations by 100 to 200 ppm. The modelled Rayleigh fractionation trend for Sr provides a good fit with the observed compositions, and indicates fractionation values of ~ 70 to 80 %. The Rayleigh fractionation trend for Ba also performs well, suggesting that the least evolved compositions of the PIF can be generated via ~ 70 to 75 % fractionation.

Table 5.22: Results of mass balance modelling for the PIF

Step 1: Alkali basalt to LET

	Liquid Composition			Fractionating Phases	
Sample	Basalt		LET		
	98SM33		AZ02-6		
	Obs	Calc	Obs		
SiO_2	46.22	46.56	63.25	Cpx	46.6
TiO_2	3.41	3.42	0.75	Plg	24.8
Al_2O_3	10.89	10.66	18.32	Mt	14.2
FeO_t	11.44	11.46	2.82	Ilm	1.2
MnO	0.17	0.19	0.13	Olv	11.1
MgO	11.53	11.5	0.50	Ap	2.0
CaO	12.01	11.96	1.29		
Na_2O	2.12	2.22	6.22		
K_2O	1.59	1.3	6.60		
P_2O_5	0.63	0.73	0.11		
$\sum r^2$	0.146				
F	0.183				

Step 2: LET to MET

	Liquid Composition			Fractionating Phases	
Sample	LET		MET		
	AZ02-6		S052B		
	Obs	Calc	Obs		
SiO_2	63.25	63.25	63.60	Alk fsp	93.2
TiO_2	0.75	0.77	0.58	Bt	4.3
Al_2O_3	18.32	18.42	18.09	Mt	2.3
FeO_t	2.82	2.85	2.60	Ilm	0.2
MnO	0.13	0.12	0.19		
MgO	0.50	0.65	0.58		
CaO	1.29	0.65	1.01		
Na_2O	6.22	6.71	7.19		
K_2O	6.60	6.53	6.10		
P_2O_5	0.11	0.01	0.05		
$\sum r^2$	0.691				
F	0.283				

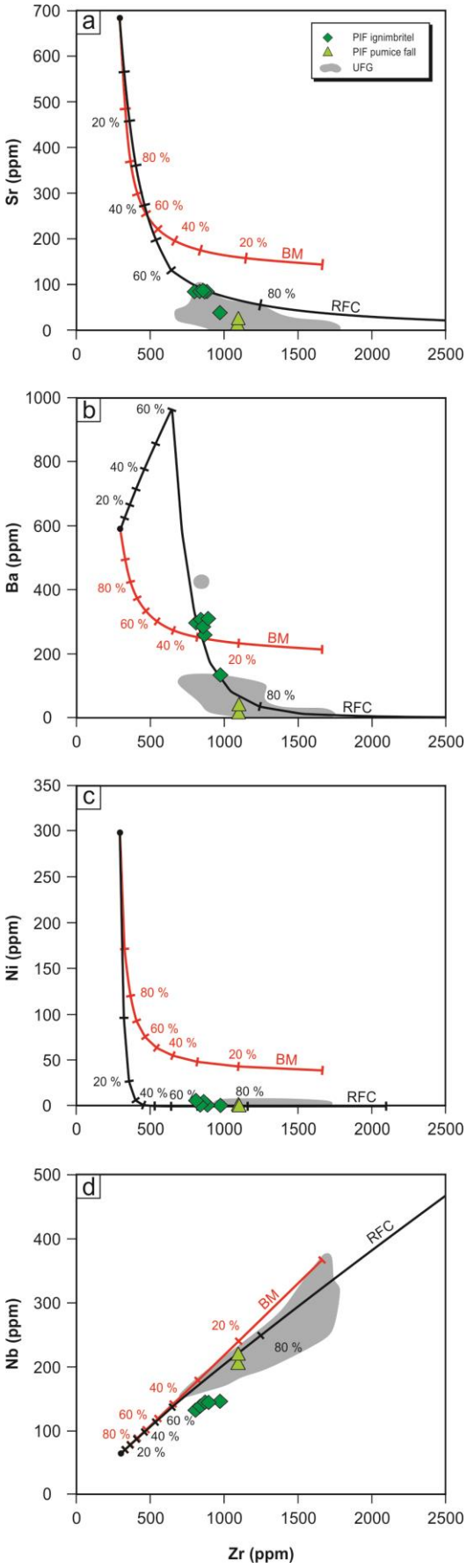

FIGURE 5.43: Results of trace element Rayleigh fractionation and batch melting models for the PIF. The compositions of the UFG are shown as a grey field

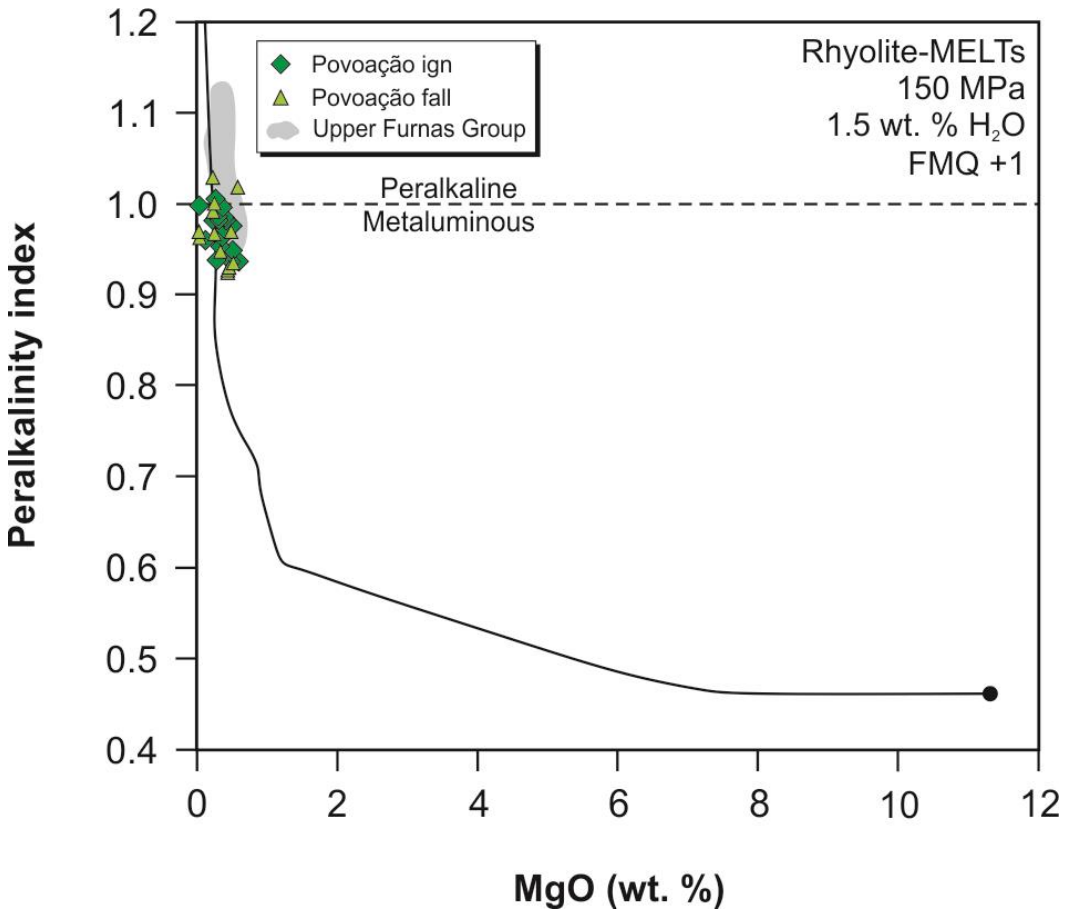

FIGURE 5.44: Results of Rhyolite-MELTs fractional crystallisation modelling from an alkali basalt (black circle). Modelled curved produced at 150 MPa, with an initial water content of 1.5 wt. %

Based upon geochemical characteristics such as MgO, Al_2O_3, SiO_2, total alkali content, peralkalinity index, and H_2O_{melt}, the results of Rhyolite-MELTs models indicate that the trachytic compositions of the PIF can be reproduced by extensive fractional crystallisation (~ 75 to ~ 90 %) of a hydrous (~ 1.5 wt. %) alkali basalt parental magma, at shallow crustal pressures (150 MPa) and redox conditions of FMQ+1 (Figure 5.44). The most applicable models predict the initial crystallisation of olivine (1250 °C), which is followed by clinopyroxene (1160 °C), apatite (1060 °C), Ti-magnetite (1140 °C), feldspar (970 °C), biotite (910 °C), and ilmenite (900 °C). The effect of oxygen fugacity is most pronounced on the crystallisation of ilmenite, which is predicted to occur sooner under more oxidising conditions. Olivine crystallisation ceases at between 1140 and 1120 °C, whilst clinopyroxene is predicted to stop crystallising at 920 to 910 °C. A fayalitic olivine is predicted to form at temperatures of approximately 750 °C. Clinopyroxene represents the

most significant fractionating phase (~ 47 %), followed by feldspar (~ 32 %), olivine (~ 10 %), Ti-magnetite (~ 8 %), biotite (~ 2 %), apatite (~ 1 %), and ilmenite (< 1 %).The results of petrogenetic modelling highlight the prominence of fractional crystallisation in the generation of the trachytic compositions of the PIF. Thermodynamic and mass balance models are in agreement, with total fractionation values between 75 and 95 %. Trace element models yield a similar range of fractionation values, though the modelled Zr-Nb trend extends this to ~ 60 %. The inability of Zr-Sr and Zr-Ba batch melting models to reproduce the compositions of the PIF suggests that any petrogenetic contribution from partial melting of gabbroic crust is minimal.

Further evidence for prevalent fractional crystallisation can be seen in geochemical characteristics such as the presence of significant depletions of Ba, Sr, Ti, and P, which likely reflect extensive fractionation of feldspar, Fe-Ti oxides, and apatite. Furthermore, the presence of a negative Eu anomaly in the Povoação fall is also likely to result from feldspar fractionation; however, this feature is significantly less pronounced in the Povoação ignimbrite. This suggests that either: 1) the negative anomaly observed in the Povoação fall was formed during evolution from LET to MET, rather than evolution from basalt to LET, or 2) the Povoação ignimbrite has been artificially enriched in Eu, effectively buffering the continued development of the anomaly, and potentially reversing it entirely. The latter model might be achieved through the accumulation and/or resorption of feldspars settling from higher levels of a zoned magma body. However, based upon the elevated concentrations of Ba and Sr in the PIF feldspars relative to the whole rock analyses, such a model might also be expected to yield similar enrichments in these elements. Despite this, the modelled Rayleigh fractionation trend for Sr accurately predicts the concentrations observed in the dataset, and the modelled trend for Ba overpredicts the observed abundance. Thus, whilst the accumulation and potential resorption of feldspar, as indicated by the presence of resorbed feldspar microphenocrysts, is likely to occur within the magma body, there is no evidence to suggest that it is a sufficient process to inhibit or counteract the development of the negative Eu anomaly.

It is therefore suggested that the contrasting size of the negative Eu anomaly between the Povoação ignimbrite and fall reflects its relatively late stage development. The thermodynamic model presented in this study suggests that the early crystallisation history of the trachytes is dominated by clinopyroxene, with lesser olivine. The precipitation of plagioclase feldspar is not predicted until trachyandesitic compositions, suggesting that, whilst the negative anomaly is still indicative of extensive feldspar fractionation, this fractionation does not occur until relatively late in the evolutionary history. As such, the observed disparity between the Povoação fall and ignimbrite is a reflection of the latter's relative 'evolutionary proximity' to the delayed saturation of feldspar in the melt.

5.6.2.3 Origin of syenite cognate xenoliths

Syenitic ejecta from the Furnas J eruption are considered to represent the final stages of crystallisation (< 800 ºC), characterised by an assemblage that, whilst still dominated by alkali feldspar, also includes a range of clinopyroxene compositions (diopside, augite, hedenbergite, aegirine-augite, aegirine), sodic amphiboles, Ti-magnetite and ilmenite. Amphiboles and clinopyroxenes of broadly similar composition were observed as interstitial phases in the Furnas I lava dome, suggesting that, like ilmenite, they only form at temperatures that are lower than those at which the UFG magmas were stored. Unlike reported syenitic ejecta from Terceira (Jeffery *et al.*, 2016a), Ascension (e.g. Harris, 1983), and nearby Fogo volcano (Ridolfi *et al.*, 2003), the Furnas syenites do not contain any of the Na-K-Ca-Ti-Zr silicate minerals that characterise agpaitic phase assemblages (e.g. aenigmatite, astrophyllite, eudialyte, cf. Marks *et al.*, 2011). Instead, Ti-magnetite, ilmenite, and trace amounts of zircon indicate that the syenites are miaskitic.

Based upon their geochemical and petrographical characteristics, the syenites are considered to represent *in-situ* crystallisation at the thermal boundary zone of a magma reservoir, rather than a cumulate from which significant melt volumes were extracted (cf.

Widom *et al.*, 1993). For example, evolution from LET to MET has been shown to be controlled by the fractionation of alkali feldspar, biotite, Ti-magnetite, and apatite. Neither Na-amphibole, nor Na-clinopyroxene are predicted in thermodynamic models, and both significantly decrease the fit of mass balance models when included, suggesting that the syenites cannot represent a cumulate from which the trachytes are derived. Similarly, the syenites and their enclaves show a wide range of trace element compositions that encompass those of the UFG, rendering many of the UFG eruptions less evolved than the syenites. If the syenite nodules did represent residual cumulates, they should be uniformly less evolved then the UFG trachytes. Furthermore, the syenites exhibit Eu anomalies that are comparable to, or greater than, those of the UFG trachytes. In the UFG rocks, a negative correlation is observed between Eu/Eu* and differentiation indices such as Zr and Nb, suggesting that the accumulation of feldspar could only result in a less negative, or even positive, Eu anomaly. As such, it is suggested that the syenites represent near-complete, *in-situ* crystallisation of unerupted trachytic magmas similar to those of the UFG. Their trace element variability is ultimately derived from the varying degrees of fractionation that also yield trace element diversity in the UFG trachytes, though hydrothermal alteration and the presence of accessory phases such as zircon also play a role.

5.6.2.4 The role of magma mixing/mingling processes

In addition to FC processes, a number of features of the UFG eruption products provide evidence for the role of replenishment and magma mingling between two variably evolved trachytes in the magma reservoir. For example, enclaves hosted in syenite ejecta display chilled margins, rounded, lobate forms, as well as large feldspar phenocrysts which exhibit similar compositions to host syenite feldspar and pronounced disequilibrium textures at their rims, suggesting that they are xenocrysts derived from the host syenite. These features are all indicative of liquid emplacement, suggesting that the enclaves represent

trachyte-syenite mingling in the highly crystalline mush zone at the margins of a magma reservoir.

Additionally, the presence of banded pumices in the uppermost pumice fall deposit of Furnas J (Lf) may provide direct evidence for mingling between two variably evolved trachytes during the later stages of the eruption, as has been described for the C11 explosive eruption (~ 1,000 ^{14}C y B.P.) of Caldeira volcano, Faial, Azores (Pimentel *et al.*, 2015). Grey bands within the predominantly white pumices of Lf exhibit markedly lower vesicularity, and thus may have been volatile poor (Cole *et al.*, 1995). The same study presented evidence for variable viscosity of the two types based upon deformation characteristics, as well as geochemical analyses for each type, which, on the basis of Zr content, suggest that the dense grey pumice may be marginally less evolved. However, it should be noted that both analyses are ~ 250 to 300 ppm lower in Zr than the Lf analyses of this study, and are instead comparable to the Furnas J lava dome analyses. This observation implies that there may be a relatively sharp geochemical transition from high Zr (~ 1200 ppm) to low Zr (~ 900 ppm) within the Lf unit. Additionally, the analyses of Cole *et al.* (1995) exhibit Ba contents an order of magnitude greater than typical UFG concentrations, which may indicate local resorption of feldspar. A single analysis within the dataset of this study reveals an anomalous enrichment of Sr (95 compared to < 10 ppm), which may reflect the same process.

5.6.3 Development of zoned magma bodies

Despite the apparent major element homogeneity and low eruptive volumes (generally ~ 0.1 km^3 DRE, Booth *et al.*, 1978) of the intra-caldera UFG trachytes, trace element compositions indicate substantial variation which, on the basis of Rayleigh fractionation models, equates to up to 50 % fractionation from LET to MET. Furthermore, despite their low eruptive volumes, the UFG deposits exhibit pronounced geochemical variation. For example, both the Furnas J and Furnas I eruptions began with an initial pumice fall,

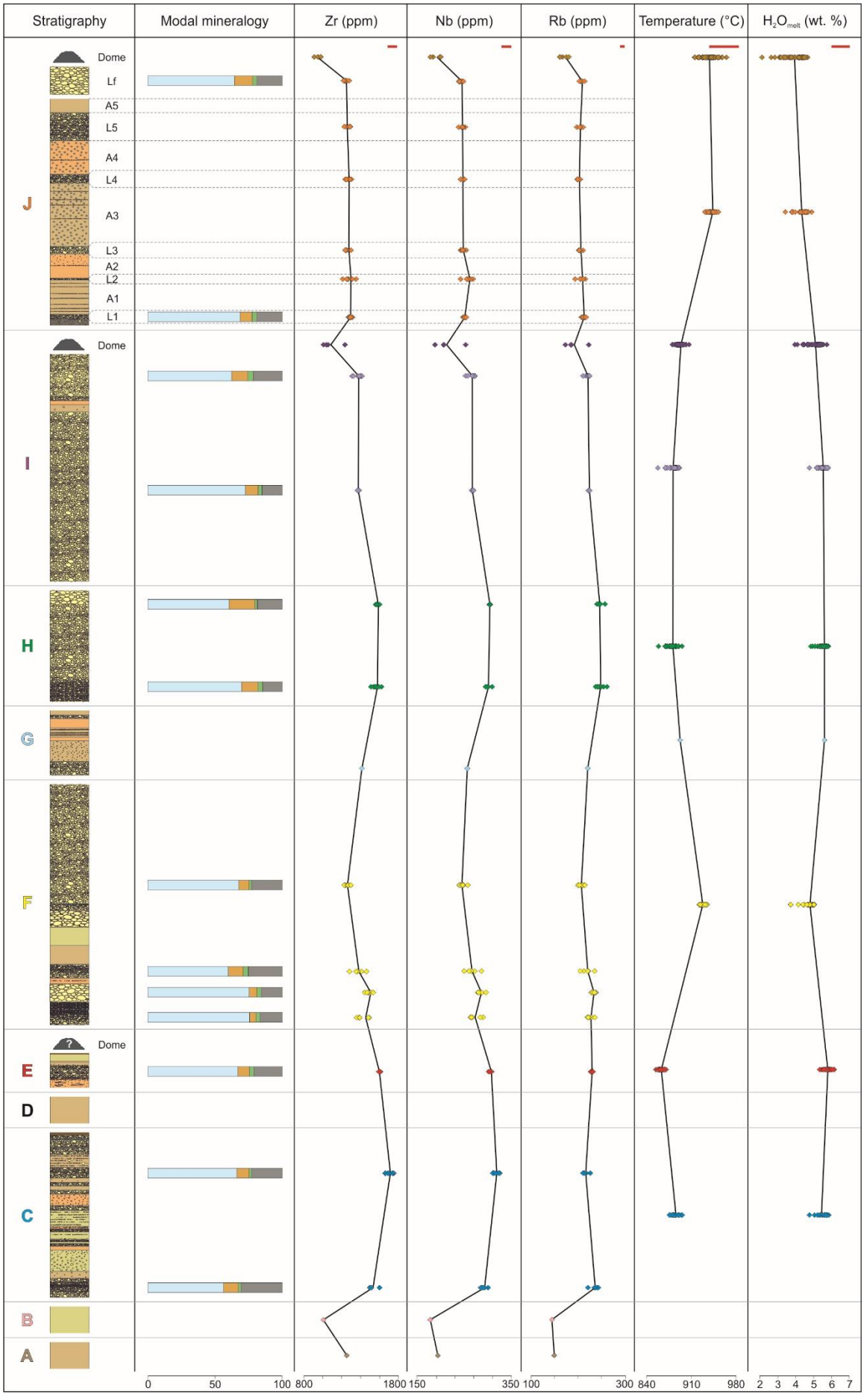
Stratigraphy
Modal mineralogy
Zr (ppm)
Nb (ppm)
Rb (ppm)
Temperature (°C)
H2Omelt (wt. %)
Dome
Lf
A5
L5
A4
L4
A3
L3
A2
L2
A1
L1
J
I
H
G
F
E
D
C
B
A
0
50
100
800
1800
150
350
100
300
840
910
980
2
3
4
5
6
7

◄ **FIGURE 5.45:** Variations in trace element concentrations, temperature estimates, and H_2O_{melt} estimates with stratigraphic height. Relevant errors are shown with red lines at the top of each column. Modal mineralogy: alkali feldspar = blue, biotite = orange, clinopyroxene = green, Fe-Ti oxides = grey

followed by a late stage lava dome; in both cases, the lava dome is, according to a variety of differentiation indices (Zr, Nb, REE, Eu/Eu*), less evolved than its respective pumice fall. This is particularly evident in the Furnas J deposits, where the individual pumice fall units (Cole *et al.*, 1995) combine to define a trend of decreasing Zr and Nb, culminatingin a large step-down (~ 250 ppm) to the less evolved lava dome (Figure 5.45**)**. Such phenomena are generally attributed to the development of a zoned magma reservoir prior to eruption (e.g. Hildreth, 1981), and suggest that the uppermost, eruptible region of the Furnas magma reservoir is able to develop rapidly and maintain compositional zonation over the timescales of the UFG. A variety of processes have been suggested to play a role in the development of zonation (e.g. Hildreth and Wilson, 2007); however, due to the described low magma viscosities development of extremely low viscosities in response to volatile accumulation and peralkalinity, it seems likely that zoning patterns in the UFG are the result of the efficient fractionation of alkali feldspar crystals, driving the melt towards MET compositions. The upwards increase in volatile content and associated decrease in viscosity may lead to a geochemical gradient via variably efficient fractionation (e.g. Furnas J, L1 to Lf). Additional processes that are considered to play a secondary role in the construction of a zoned cap include: 1) ascent of bubbles through volatile saturated magma which may lead to upward migration of alkalis, halogens, and other fluid mobile elements (Hildreth and Wilson, 2007), 2) generation of low density, hydrous melts via sidewall crystallisation (e.g. Huppert *et al.,* 1986), and 3) magma mixing in response to replenishment events. The presence of resorbed feldspars and banded pumices in the UFG provide evidence for the latter process.

The preservation of zonation in the UFG magmas until eruption indicates the absence of efficient convective cells able to rehomogenise the reservoir, which may be accounted for by a strong density gradient linked to the ~ 4 wt. % range in estimated melt

water contents (cf. Hildreth and Wilson, 2007). Alternatively, compositional zonation might be stabilised through the generation of multiple, individually convecting layers (e.g. Huppert and Sparks, 1984), though the applicability of such a model in a low volume of magma (< 0.3 km^3) may be restricted. If the zoning patterns of the UFG magmas are considered to have been largely unaltered by conduit processes during ascent, then the potentially sharp compositional contact between the pumice falls and lava domes of Furnas I and J may provide evidence for individual strata, reflecting a compositional discontinuity that was present in the magma reservoir between hydrous MET, and underlying, volatile-poor LET. This would also indicate that either a deeper part of the reservoir was tapped than in the majority of previous eruptions, or that the cap had not yet regenerated the comparatively large volumes of MET associated with older eruptions (e.g. Furnas C, ~ 0.3 km^3).

The zoning patterns observed in the Furnas C (and possibly F) deposits imply a more complex regime in which less evolved melts are capable of erupting prior to more evolved melts. The observed zoning patterns require more complex reservoir geometries, such as sequential eruption of multiple magma bodies, each acting as an independent evolving system (e.g. Cooper *et al.,* 2012; Zanon *et al.,* 2013; Pimentel *et al.,* 2015). Alternatively, this complex zonation might originate from an irregular chamber geometry which allows lower regions to be tapped first.

5.6.4 A model for the Furnas plumbing system

In this section, the results of thermobarometrical and petrogenetic models are consolidated to generate a conceptual model for the magmatic plumbing system which can account for the described petrographical, geochemical, and volcanological characteristics of Furnas. This model then acts as a framework for the development of a model for the temporal evolution of Furnas over a period of ~ 5,000 years.

5.6.4.1 The Upper Furnas Group magma system

Based upon the range of pressure estimates derived from H_2O solubility models and thermodynamic models (~ 122 to 156 MPa), the magma storage region of the UFG eruptions can be constrained to shallow crustal depths between ~ 2.7 and ~ 3.6 km (based upon an average crustal density of 2,800 kg/m^3). This range compares favourably with previous estimates of magma storage beneath Furnas volcano (Machado, 1972; Sigmundsson *et al.*, 1995; Blanco *et al.*, 1997; Camacho *et al.*, 1997; Montesinos *et al.*, 1999), and also the shallow magma reservoir of Sete Cidades (Beier *et al.*, 2006). The results of thermodynamic modelling, as well as the predominantly low Al_2O_3 and TiO_2 contents of clinopyroxene, suggest that much of the compositional range from basalt to MET is present at this depth (Figure 5.46).

Based upon the decreasing melt densities predicted by Rhyolite-MELTs from basalt to trachyte (~ 2580 to ~ 2230 kg/m^3), it is suggested that the reservoir beneath Furnas is compositionally zoned, with dense mafic magmas at the base, and low density, hydrous silicic magmas at the roof. Trachytic magmas at the roof may be further enriched in volatiles via upward migration of a vapour phase, further stabilising the density stratification. This configuration may account for the apparent Daly Gap observed at Furnas (Guest *et al.,* 1999), as ascending mafic magmas may stall in an established shallow crustal magma reservoir and differentiate, ultimately contributing relatively small volumes of residual trachytic liquid to the silicic cap of the reservoir rather than erupting themselves (e.g. Mahood, 1984; White *et al,.* 2009; Neave *et al,.* 2012). The likely presence of older, frozen reservoirs at this level is envisaged to further inhibit rapid magma ascent (e.g. Zanon and Pimentel, 2015). In contrast, basalts that ascend outside the confines of the caldera and avoid the shallow system, reached the surface and were erupted as the monogenetic cones and fissure eruptions that are typical of the volcano's flanks and the neighbouring Congro Fissure volcanic system (Zanon, 2015a).

The generation of crystal poor silicic magmas, such as those of the UFG, is commonly accounted for through the application of models which involve the extraction of interstitial melt from large crystal mush bodies, citing processes such as compaction, micro-settling, hindered settling, and gas-driven filter pressing (e.g. Sisson and Bacon, 1999; Bachmann and Bergantz, 2004; Hildreth, 2004; Pistone *et al.,* 2015). Such models are attractive primarily because of the difficulties associated with two-phase flow in relatively cool, high viscosity (~ $10^{4.5}$ Pa s) melts (Scaillet *et al.,* 1998). However, their application to peralkaline magmatic systems is complicated by the apparent absence of erupted crystal-rich melts (equivalent to the 'monotonous intermediates' associated with non-peralkaline systems, Macdonald, 2012), and also by the tendency of peralkaline melts to have lower viscosities than their metaluminous and peraluminous equivalents (e.g. Giordano *et al.,* 2006; Neave *et al.,* 2012). The efficiency of two-phase flow in the UFG trachytes was investigated through the estimation of crystal free melt viscosities. Application of the model of Giordano *et al.,* (2008) indicates that the trachytes, at a temperature of 908 °C and H_2O_{melt} values from 2.4 to 5.7 wt. %, have viscosities ranging from $10^{2.7}$ to $10^{4.1}$ Pa s. The UFG trachytes therefore had pre-eruptive viscosities that were up to two orders of magnitude lower than typical silicic melts (Scaillet *et al.,* 1998), which has implications for the dominant differentiation mechanism.

The efficiency of crystal settling was evaluated through the calculation of Stokes' settling velocities for alkali feldspar crystals (determined to be the most important crystallising phase during the later stages of magma evolution). This was supplemented with the hindered settling equation, which allows the determination of settling rates in polydispersed suspensions (Bachmann and Bergantz, 2004):

$$U_{hs} = U_{Stokes} \times f(c) \tag{5.1}$$

where U_{hs} is the hindered settling velocity, U_{Stokes} is Stokes settling velocity, and f(c) is a correction factor calculated as:

$$f(c) = \frac{(1 - c)^2}{(1 + c^{1/3})^{[\frac{5c}{3(1-c)}]}} \quad (5.2)$$

where c is equal to the crystal fraction. Crystal sizes were set to 2 mm, in accordance with petrographic observations. Results indicate that even for the highest viscosity estimate for the UFG, settling rates range from 0.51 m a^{-1} (hindered settling, 50 % crystallinity) to 1.76 m a^{-1} (unhindered). Settling rates for the lowest viscosity trachytes reach values as high as 13.7 m a^{-1} (hindered settling, 50 % crystallinity), and 47 m a^{-1} (unhindered). Assuming a volume of melt that is typical for the UFG eruptions (0.1 km^3 DRE; Booth *et al.,* 1978), and hypothetical magma reservoir aspect ratios of 1:1:1 and 8:1:1, alkali feldspar crystals would need to travel maximum distances of ~ 470 to 235 m to be removed from the volume of erupted melt. Available radiocarbon ages (and associated errors) for the UFG indicate that repose times do not exceed 918 years, but are likely to be ~ 190 years (Furnas I to J) or less (e.g. Furnas H to I, Guest *et al.,* 1999). Over such short timescales (190 years), alkali feldspar crystals are capable of settling ~ 100 m at the very least (highest viscosity), but are capable of settling far greater distances (up to 9600 m using the lowest calculated viscosity). It is therefore suggested that, unlike the rhyolitic systems to which crystal mush models may apply, crystal settling was a viable and efficient mechanism of differentiation in the UFG trachytes, and may account not only for the nearly aphyric nature of the erupted trachytes, but also for the rapid rates of differentiation implied by the wide range in their degree of evolution.

Syenitic ejecta are considered to represent a solidification front at the volatile rich cap of the reservoir, in which trachytic magmas near the margins of the reservoir solidify via *in-situ* crystallisation. Phase assemblages including aegirine, Na-amphibole and ilmenite are consistent with near-complete *in-situ* crystallisation, whilst the presence of miarolitic cavities and pyrrhotite indicate the accumulation of volatile phases. Crystallisation temperatures estimated from Ti-magnetite-ilmenite pairs are at least 70 °C lower than estimates for the UFG pumice falls. High temperature estimates derived from

alkali feldspar-melt equilibria (892 to 969 °C) are similar to those of Furnas J, and likely reflect the relatively early formation of feldspar compared to later ilmenite, aegirine, and amphibole. Enclaves within the syenites are considered to represent interaction between the upper thermal boundary layer and the crystal poor liquids in the underlying crystal poor cupola. Small volumes of crystal poor trachytes are inferred to have infiltrated the overlying crystal mush and been quenched. In Zr-Nb space, the majority of syenites and enclaves appear to lie along the same liquid line of descent as the UFG, implying a cogenetic association. Although Zr-Nb relationships could be uncoupled by the crystallisation of Zr-bearing phases, the observed rarity of zircon, as well as it's restriction to pore spaces, imply that late-stage zircon was retained rather than fractionated. The substantial range in the degree of evolution observed in their whole rock chemistry (~ 700 to 1700 ppm Zr) is likely to be a temporal effect, where the composition of a given syenite clast or enclave is related to the dominant melt composition in the roof zone of the reservoir, a feature which is shown to vary considerably. Additionally, it seems probable that this cupola would be zoned to some extent, exhibiting the same degree of composition variation as the UFG trachytes themselves. An 'onion-skin' arrangement, similar to that of Widom *et al.,* (1993) is therefore invoked, where random sampling of various layers of the roof zone yields a range of compositions. It should also be noted that a single syenite analysis appears to deviate from the UFG liquid line of descent in Zr-Nb space, suggesting that it may represent a fragment of an alternative liquid line of descent. It thus cannot be ruled out that some syenitic ejecta may instead represent the 'fossilised' remnants of a pre-UFG magmatic system, entrained pre- or syn-eruptively within the erupted trachyte.

Attempts to employ clinopyroxene thermobarometry revealed that the clinopyroxenes are not in equilibrium with the host trachytes (see above), instead being equilibrated with a broadly trachyandesitic composition. This is consistent with thermodynamic models, which suggest that clinopyroxene becomes saturated in the melt at 1115 ºC and crystallises until 905 ºC. Settling rates of clinopyroxene through the UFG

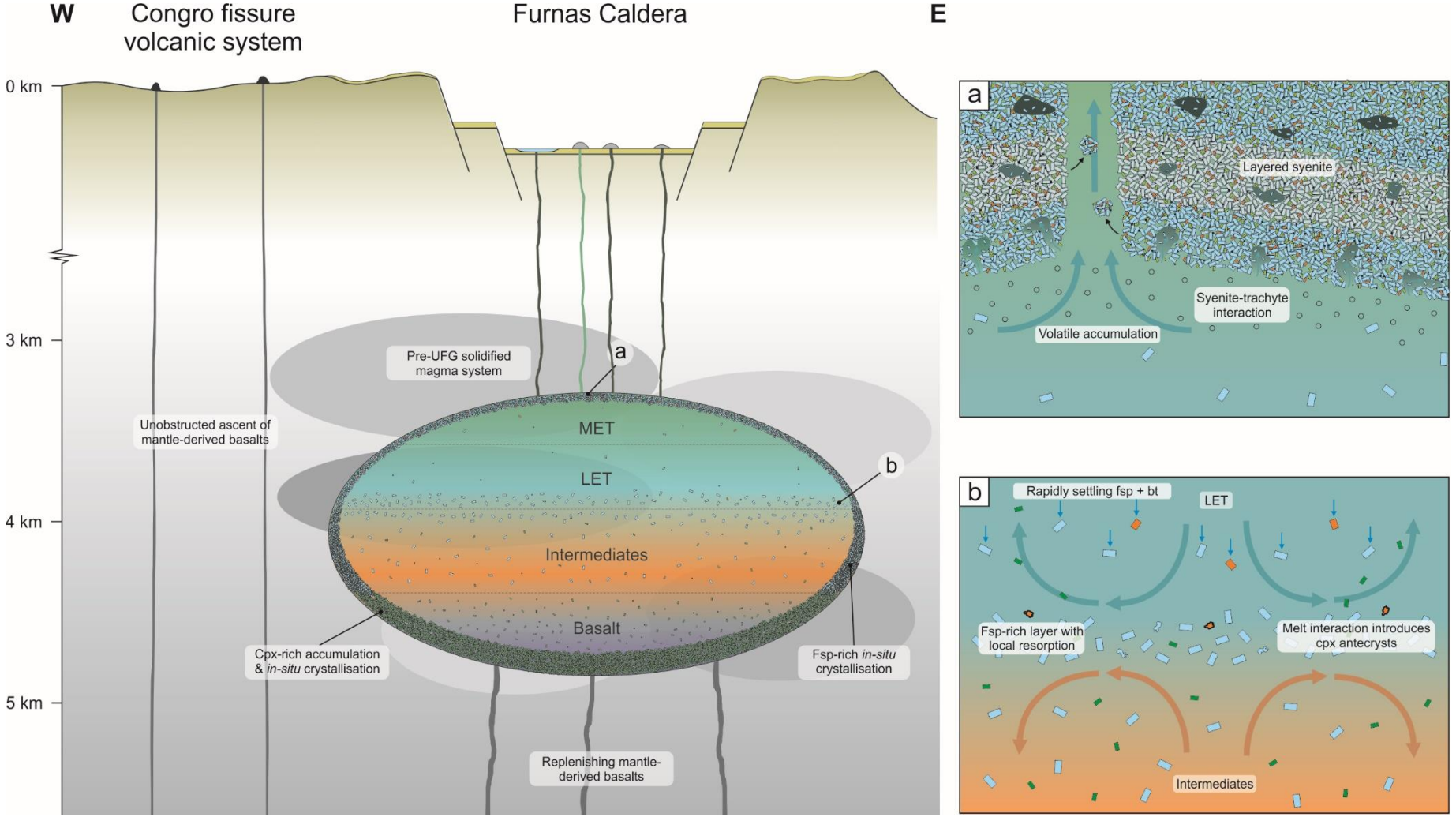
W
Congro fissure volcanic system
Furnas Caldera
E
0 km
3 km
4 km
5 km
Pre-UFG solidified magma system
a
Unobstructed ascent of mantle-derived basalts
MET
LET
Intermediates
Basalt
b
Cpx-rich accumulation & in-situ crystallisation
Fsp-rich in-situ crystallisation
Replenishing mantle-derived basalts
a
Layered syenite
Syenite-trachyte interaction
Volatile accumulation
b
Rapidly settling fsp + bt
LET
Fsp-rich layer with local resorption
Melt interaction introduces cpx antecrysts
Intermediates

◄ **FIGURE 5.46:** A schematic model for the structure of the shallow plumbing system of Furnas volcano. A density stratified magma reservoir with a trachytic cap is envisaged, at depths between 2.5 and 4 km a) Syenite ejecta derived from an upper solidification front may be sampled during eruption. The solidified remnants of pre-UFG magma systems may provide an additional source of syenitic xenoliths b) Interaction between individually convecting layers introduces an antecrystic clinopyroxene population to the cap, whilst rapidly settling feldspars form a Sr-, and Ba-rich feldspar layer. Settling biotite phenocrysts originating from uppermost METs are heavily resorbed by hotter underlying LETs and intermediates

trachytes are approximately three times faster than those of alkali feldspar, suggesting that the ubiquitous presence within the erupted trachytes requires a mechanism that is either continuous within the magma plumbing system, or occurs immediately prior to each eruption. Two possibilities for an origin are considered: (1) they are xenocrysts derived from the incorporation and assimilation of mafic wall rock material or (2) they are antecrystic relics derived from liquid-liquid interaction between the erupted trachytes and less evolved magmas. There is no petrographic evidence, such as crustal or cumulate xenoliths, to support the former hypothesis, and trace element models do not indicate partial melting as a significant petrogenetic process in the UFG. As such, the second hypothesis is favoured and, given the small but consistent presence of clinopyroxene throughout the UFG, implies the episodic interaction between trachytic and less-evolved, clinopyroxene-bearing magmas, most likely at an interface between strata with contrasting densities.

5.6.4.2 The Povoação Ignimbrite Formation magma system

The pre-eruptive magma system of the PIF exhibits a number of similarities with that of the younger UFG. For example, on the basis of thermodynamic and solubility modelling, the PIF-forming trachytes were stored at shallow crustal depths (~ 4 km, assuming a crustal density of 2,800 kg/m^3), at temperatures between 860 and 981 °C. Like the UFG eruptions, the pre-eruptive reservoir was undoubtedly zoned, with low temperature, low crystal content, high H_2O_{melt} METs (represented by the initial pumice fall), and comparatively high temperature, high crystal content, low H_2O_{melt} LETs (represented by the Povoação ignimbrite). The ubiquitous presence of a proportionally minor clinopyroxene population implies a similar regime of regular mixing between trachyte and

less evolved magmas, as suggested for the UFG (see above). The dominance of low TiO_2 and low Al_2O_3 clinopyroxenes, as well as the chemical disequilibrium between clinopyroxenes and host trachyte, suggest that a significant proportion of the compositional range exhibited by the liquid line of descent is present at this crustal level. However, the presence of rare, high TiO_2 and high Al_2O_3 clinopyroxenes, as seen in the UFG, implies that some clinopyroxenes from a deeper stage of crystallisation persist, even in the upper most eruptible cap of the shallow crustal reservoir. The results of petrogenetic modelling highlight the prevalence of fractional crystallisation as a process of magmatic differentiation, with the trachytes originating from protracted fractionation of a basaltic parental magma. Pre-eruptive magma viscosities were calculated as described above, assuming a crystal fraction of 0.2, range from $10^{2.9}$ to $10^{3.4}$ Pa s. Settling rates (calculated as above), both unhindered and hindered (assuming 50 % crystallinity), were calculated for alkali feldspar phenocrysts 2 mm in length, and range from 0.84 to 29.69 m a^{-1}. Based upon these values, it is suggested that, as in the UFG, crystal settling remains a viable and efficient process of magmatic differentiation in the PIF-forming trachytes.

Based upon these observations, it is suggested that the pre-eruptive magmatic system from which the PIF was derived was extremely similar to that of the UFG, comprising a shallow crustal magma reservoir in which mafic magmas evolved via fractional crystallisation to trachytic compositions. However, there are a number of key differences between the caldera-forming and the post-caldera phases of Furnas which must be accounted for. First, the eruptions of the UFG typically do not exceed 0.1 km^3 DRE (Guest *et al.*, 1999), whilst the PIF represents an eruption of at least 2 km^3 (Moore, 1990). Despite this disparity, the pre-eruptive magmatic systems of both stages in the history of Furnas appear to have been very similar in terms of their arrangement and the dominant processes occurring within them. It is therefore suggested that this contrast is likely to originate from larger scale processes such as magma supply rates and cyclic development of the magma system in which the comparatively large scale, caldera-

forming eruptions result from the slow expansion and eventual eruption of the shallow crustal system (see Chapter 6).

Second, the PIF is, on the basis of incompatible trace element abundances and peralkalinity, less differentiated than the UFG, being, at its most evolved, similar in composition to the UFG lava dome compositions. However, the calculated pre-eruptive magma viscosities of both the PIF and the UFG are similar, suggesting that their eruptive behaviours is unlikely to have been affected by this factor alone. Considering the contrasting eruptive volumes of the UFG and the PIF, it is likely that this compositional contrast simply reflects the tapping of deeper portions of the shallow crustal magma reservoir, as well as any higher order minor temporal variations in major element geochemistry. The former hypothesis may be supported by the generally higher temperatures recorded by the Povoação ignimbrite compared to many of the UFG eruptions; however, it should be noted that both Furnas J and Furnas F display similar temperatures to that of the Povoação ignimbrite. As such, the UFG eruptions may simply have been erupted from significantly smaller reservoirs, in which a significant temperature range is hosted within a smaller volume of magma.

Third, the PIF trachytes evolved under more oxidised conditions (FMQ +1) than the UFG (FMQ). The most pronounced effect of this contrast is the relative abundance of ilmenite in the PIF when compared to the UFG, where ilmenite is considerably less common. Rhyolite-MELTs models predict that increasing the oxygen fugacity to one log unit above FMQ leads to the saturation of ilmenite at 900 °C rather than 800 °C. Thus, considering the previously described temperature range of the PIF and UFG (~ 800 to ~ 980 °C), ilmenite might be expected to crystallise earlier in the more oxidised PIF trachytes, leading to its observe abundance. The origin of these contrasting oxygen fugacities may reflect variation in the mantle source, or alternatively, variable degrees of degassing. For example, thermal disassociation of H_2O, and subsequent degassing of H_2 has long been recognised as an oxidising process in magmas (e.g. Sato, 1978). However, it is apparent that the PIF and UFG trachytes lie along a single liquid line of descent. It is

therefore suggested that the minor shifts in fO_2 and mineral assemblage between caldera-forming and post-caldera eruptions reflect minor adjustment of the shallow crustal magma reservoir rather than a substantial alteration of the deep crustal/mantle magma system (e.g. Bachmann *et al.*, 2012).

5.6.5 Temporal evolution of the UFG magma reservoir

In addition to trace element zonation within individual eruptions, the UFG as a whole exhibits higher order variations which provide insights into the temporal evolution of the previously described eruptible cap of the shallow crustal reservoir. The complex trace element profiles of the UFG (Figure 5.45) are clearly inconsistent with the tapping of a single large magma batch, emplaced prior to the Furnas A eruption, and allowed to fractionate for ~ 5,000 years (maximum age of the UFG). Instead, the observed variability suggests a cyclical regime, in which a zoned, silicic cap forms at the top of the reservoir, and is partially erupted in one or more individual eruption events, before being re-established via continued fractionation and potentially mafic replenishment (Figure 5.47). This is consistent with neighbouring Fogo volcano, where a similar regime of zoned cap formation and tapping over the same time period has been suggested (Widom *et al.* 1992). At Furnas, four periods are recognised, during which a single zoned magma cap was erupted sequentially in up to three individual eruptive events, reforming after each period. Due to the relatively large errors and consequent degree of overlap in the radiocarbon ages of the UFG, the repose periods between individual eruptions cannot be determined accurately. However, it is suggested that the length of the repose time is likely to be linked to the temporal model of this study, with the longest repose times being associated with periods during which the zoned, eruptible cap was being reconstructed. The first zoned magma body of the UFG is the least constrained, but is inferred to have been tapped twice during the Furnas A and B eruptions, during a period of up to ~ 3,000 years, followed by a lengthy re-establishment phase, during which the reservoir cap

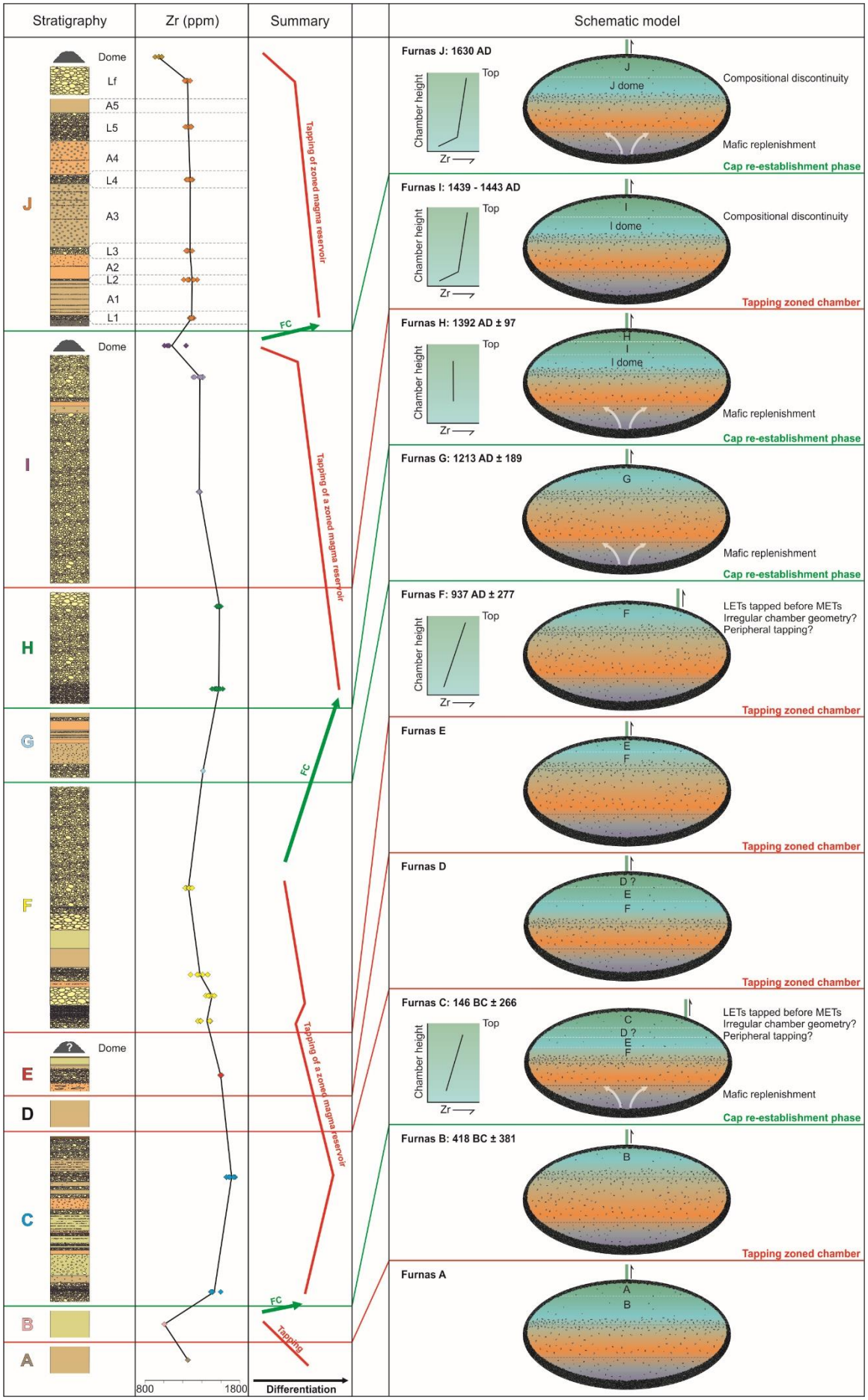
Stratigraphy
Zr (ppm)
Summary
Schematic model
Dome
Lf
A5
L5
A4
L4
A3
L3
A2
L2
A1
L1
J
I
H
G
F
E
D
C
B
A
Tapping of zoned magma reservoir
FC
Tapping of a zoned magma reservoir
Tapping
800
1800
Differentiation
Furnas J: 1630 AD
Chamber height
Top
Zr
J
J dome
Compositional discontinuity
Mafic replenishment
Cap re-establishment phase
Furnas I: 1439 - 1443 AD
I
I dome
Tapping zoned chamber
Furnas H: 1392 AD ± 97
H
Furnas G: 1213 AD ± 189
G
Furnas F: 937 AD ± 277
F
LETs tapped before METs
Irregular chamber geometry?
Peripheral tapping?
Furnas E
E
Furnas D
D ?
Furnas C: 146 BC ± 266
C
Furnas B: 418 BC ± 381
B
Furnas A
A

◄ **FIGURE 5.47:** A schematic model for cyclic replenishment and eruption phases throughout the UFG, based upon trace element chemistry. See text for discussion. FC = fractional crystallisation

evolved via 30 to 40 % fractionation prior to the Furnas C eruption. Available radiocarbon ages suggest that the Furnas B to C repose period may have been up to 918 years.

The Furnas C, E, and F eruptions together indicate a trend of progressively less evolved trachytes, suggesting that they represent sequential, and probably relatively rapid, tapping of a single zoned magma body that formed following Furnas B. This suggests that, despite the relatively substantial volume of the Furnas C eruption compared to the other UFG eruptions (0.3 km^3 DRE), the system was tapped a further three times prior to re-establishment, which may be linked to the repose time between eruptions, or the overall rate of trachyte replenishment in the cap. Small scale disruptions in the trend of decreasing evolution occur in Furnas C and F, where LETs are erupted prior to METs; however, these features can be attributed to complex magma withdrawal pathways and/or sequential tapping of multiple magma pockets (see above), and remain compatible with the model. The repose periods between these eruptions are likely to have been comparatively short, limiting the effects of continued differentiation between eruptions. This period was followed by a period of fractionation, which culminated in the Furnas H eruption, and equated to ~ 10 to 15 % fractionation. During this period, the reservoir was tapped once by the Furnas G eruption, but this did not inhibit continued fractionation prior to Furnas H.

The third zoned magma body is considered to have formed prior to Furnas H, and been sequentially tapped by the Furnas H and I eruptions. This is consistent with the comparatively short repose time between Furnas H and I (~ 20 years, Booth *et al.* 1978; Guest *et al.* 1999). Together, these eruptions define a trend of decreasing evolution that reverses the effect of fractional crystallisation by up to ~ 35 %. This was followed by a repose period of ~ 190 years, during which the system evolved by up to 20 % to produce the fourth zoned magma body, which was subsequently erupted in the Furnas J eruption. Based upon the similarity between the trace element profiles of the Furnas I and J

eruptions, it is possible that the shallow magmatic system of Furnas has entered a new repose period whilst the eruptible cap reforms, though it should be noted that the current repose time of 385 years is approximately twice that of the I to J repose time (~ 190 years).

5.6.6 Volatiles and degassing

Pre-eruptive water contents of the UFG and PIF trachytes correlate negatively with estimated temperatures (Figure 5.37, 5.39), and indicate that the magmas were stored under water-undersaturated conditions. This trend is also seen in halogen data for melt inclusions and groundmass glass, where both Cl and F correlate positively with peralkalinity indices (Figure 5.48). As such, the total volatile content of the Furnas trachytes was controlled primarily by fractionation, with little to no pre-eruptive degassing. Furthermore, melt inclusion analyses from both the UFG and the PIF contain Cl and F concentrations which are, on the basis of calculated 2-sigma standard deviations, indistinguishable from halogen concentrations of the groundmass glass. This suggests that, despite their high concentrations, neither Cl nor F was degassed to any significant extent during eruption, regardless of eruption style.

Table 5.23: Halogen contents from the UFG and PIF melt inclusions and groundmass glass

Unit	Analysis	Cl				F			
		Min	Average	Max	Stdev (2σ)	Min	Average	Max	Stdev (2σ)
UFG	Melt inclusion	2274	3203	4170	949	1196	2025	3252	929
	Groundmass glass	2183	3219	3647	599	1207	2027	2745	609
PIF	Melt inclusion	1669	2142	2900	617	365	466	602	155
	Groundmass glass	284	1727	3438	2617	495	768	1482	818

5.6.7 Implications for silicic volcanism on São Miguel

The magmatic system of Furnas shares a number of features with neighbouring Fogo and Sete Cidades volcanoes. For example, a prominent, sub-caldera, shallow crustal (~ 3 to 4 km) magma reservoir has been identified at each volcano, in which mafic to intermediate magmas differentiate primarily via fractional crystallisation to form a cap of variably evolved trachyte (e.g. Storey, 1982; Widom *et al.,* 1992; Renzulli and Santi, 2000; Beier *et al.,* 2006). Evidence for magma mingling and mixing, such as phenocryst textures (Beier *et al.*, 2006), hybrid magmas (Storey *et al.,* 1989), and banded pumices (Widom *et al.,* 1992; this study), is present at all three centres. However, felsic eruptive products are somewhat less dominant at Sete Cidades (~75 vol. %; Moore, 1991a) than at Furnas and

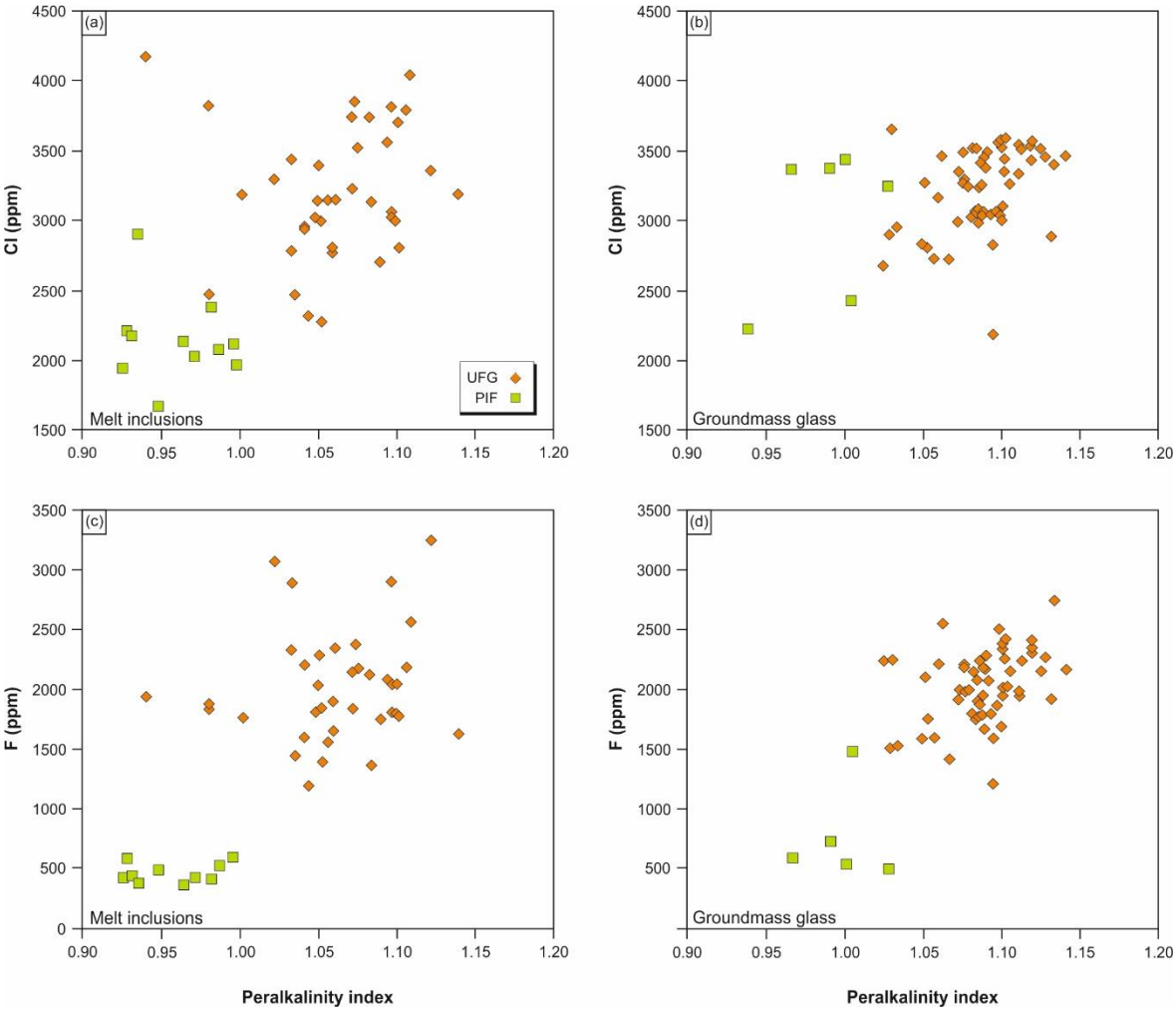

FIGURE 5.48: Variations in halogen concentration of melt inclusions and groundmass glass plotted against peralkalinity indices

Fogo (≥ 90 vol. %; Moore, 1991a), and the Daly gap observed at both Furnas and Fogo is absent (Beier *et al.,* 2006). One solution is that the upper, trachytic caps of the magma plumbing systems of both Furnas and Fogo are more developed, possibly due to periods of reduced basaltic input to the lower part of the systems (cf. Macdonald, 2012). They would therefore form a more significant barrier against the ascent and eruption of basaltic magmas. In contrast, the magma plumbing system of Sete Cidades may be somewhat less developed, and so unable to entirely prevent the ascent of basaltic magmas. This concept was first considered on São Miguel by Machado (1972) and Booth *et al.* (1978), who suggested that a laterally extensive felsic magma reservoir beneath the eastern end of the island could be responsible for the apparent cessation of basaltic activity in the Congro Fissure zone during the 5 ky. Additionally, the most recent eruptive products of the Congo Fissure zone are described by Moore (1990) as a trachytic dome and an associated pumice fall dated at 3.8 ± 0.4 ka (uncalibrated radiocarbon years B. P.). Furthermore, the same author describes a trachytic maar ~ 1 km south east of this dome which formed around the same time.

The apparent cessation of basaltic activity and the occurrence of felsic volcanism in the Congro Fissure zone may suggest that the shallow crustal magmatic plumbing system of either Fogo or Furnas (or both) may have expanded laterally and begun to encroach upon one another, expanding a shadow zone across the Congro Fissure zone which prevents ascending basalts from reaching the surface. If present, this expansion must have occurred very recently (< 5 ka), and represents only a minor portion of each volcano's eruptive history. However, it should be noted that a small number of effusive eruptions of trachytic magma have also occurred in the Picos Fissure zone. Due to its large size compared to the Congro Fissure zone, it is difficult to account for these eruptions using a model in which the shallow plumbing systems of Sete Cidades and Fogo expand laterally, eventually impinging upon one another. As such, the eruption of felsic magmas within the fissure zones may indicate that ascending basalts were able to stall in the crust and differentiate to produce trachytic residual melts, which are then

erupted. Alternatively, the erupted trachytes may represent the results of partial melting of crustal lithologies, with ascending basalts providing the heat source.

5.6.8 Caldera cycles at Furnas?

If the PIF and the UFG are considered to be representative of the caldera-forming and post-caldera activity of Furnas volcano, respectively, then the results of this study may provide some insights into the long-term temporal evolution of the volcano. The magmatic and volcanic behaviour of caldera-forming volcanoes is often recognised to be cyclic (e.g. Christiansen and Blank, 1972; Barberi *et al.*, 1991; Chesner and Rose, 1991; Houghton *et al.*, 1995; Wolff and Gardner, 1995; Lipman, 2000; Cole *et al.*, 1998, 2005; Bachmann *et al.*, 2012; Rubin *et al.*, 2016). The majority of studies have targeted large volume silicic systems such as Yellowstone, U.S.A., and the Taupo volcanic zone, New Zealand; however, the proposed models may still be applicable to the comparatively low volume, ocean island magmatic system of Furnas, where caldera-forming episodes appear to be more than one order of magnitude greater in eruptive volume than intra-caldera activity (Duncan *et al.*, 1999). Although the targets of this study (UFG and PIF) are not directly linked temporally, they may still act as representative periods within the volcano's history, allowing the construction of a general scheme for the evolution of the Furnas magmatic system.

Furnas volcano is considered to have undergone at least two caldera-forming eruptions during its subaerial activity, as well as more frequent, comparatively low volume eruptions which generated various ignimbrites, pumice falls, and surges (Guest *et al.*, 1999). It might therefore be suggested that Furnas has undergone at least two cycles of activity, each culminating in a caldera-forming eruption. Although such a model is not well constrained, its application may serve to guide the direction of future research. Within the framework of this scheme, the recent activity of Furnas, represented by the UFG, is considered to represent a resurgence of magmatism following the second caldera-forming

event, which will eventually culminate in a third caldera-forming eruption. Although the second caldera-forming eruption of Furnas is relatively poorly constrained to ~ 12 ka, the post-caldera period appears to lack any significant volcanism until the eruptions of the UFG (< 5 ka), suggesting that caldera formation may have been followed by up to ~ 7 ky of quiescence (Guest *et al.*, 1999). The only exception to this was the eruption of the Pico do Canário Formation (Guest *et al.*, 1999), a trachytic cone underlying the Fogo A deposit, which formed on the boundary between the Furnas and Povoação calderas, and which is dated indirectly at 6,600 B.P. by Moore (1991a, b).

The development of the small magma reservoir required to feed each of the UFG eruptions (≤ 0.3 km^3 DRE) within the shallow crust (< 5 km^3) requires relatively cold wall rocks with high effective viscosities (Jellinek and DePaolo, 2003; Gregg *et al.*, 2012; de Silva and Gregg, 2014; Degruyter and Huber, 2014). In contrast, a magma reservoir of sufficient size to generate eruptions on the scale of the PIF (> 2 km^3 DRE) would require relatively warm wall rocks with low effective viscosities. Thus, it might be suggested that prior to the eruption of the PIF, the shallow magma system of Furnas underwent a period of crustal heating (corresponding to the 'pre-heating' period of Jellinek and DePaolo, 2003), in which small bodies of magma were intruded into the shallow crust and warmed the surrounding country rock, whilst differentiating rapidly towards silicic compositions via fractional crystallisation, before being either solidified or erupted in response to fractional crystallisation-induced overpressure and/or magma replenishment (e.g. Jellinek and DePaolo, 2003; Degruyter and Huber, 2014). This stage is here termed 'Stage 1', and is considered to manifest itself as numerous low-volume eruptions of relatively chemically heterogeneous (e.g. LET to MET) material, such as that seen in the UFG. As this process continues, and the shallow crust is heated, the development of larger magma bodies is favoured, until such time as the numerous individual magma bodies present begin to encroach upon each other and interact. Eventually, as a result of continuing coalescence, the shallow crust is envisaged to contain a single dominant magma reservoir, in which the previously heterogeneous magma compositions of Stage 1 are homogenised to produce a

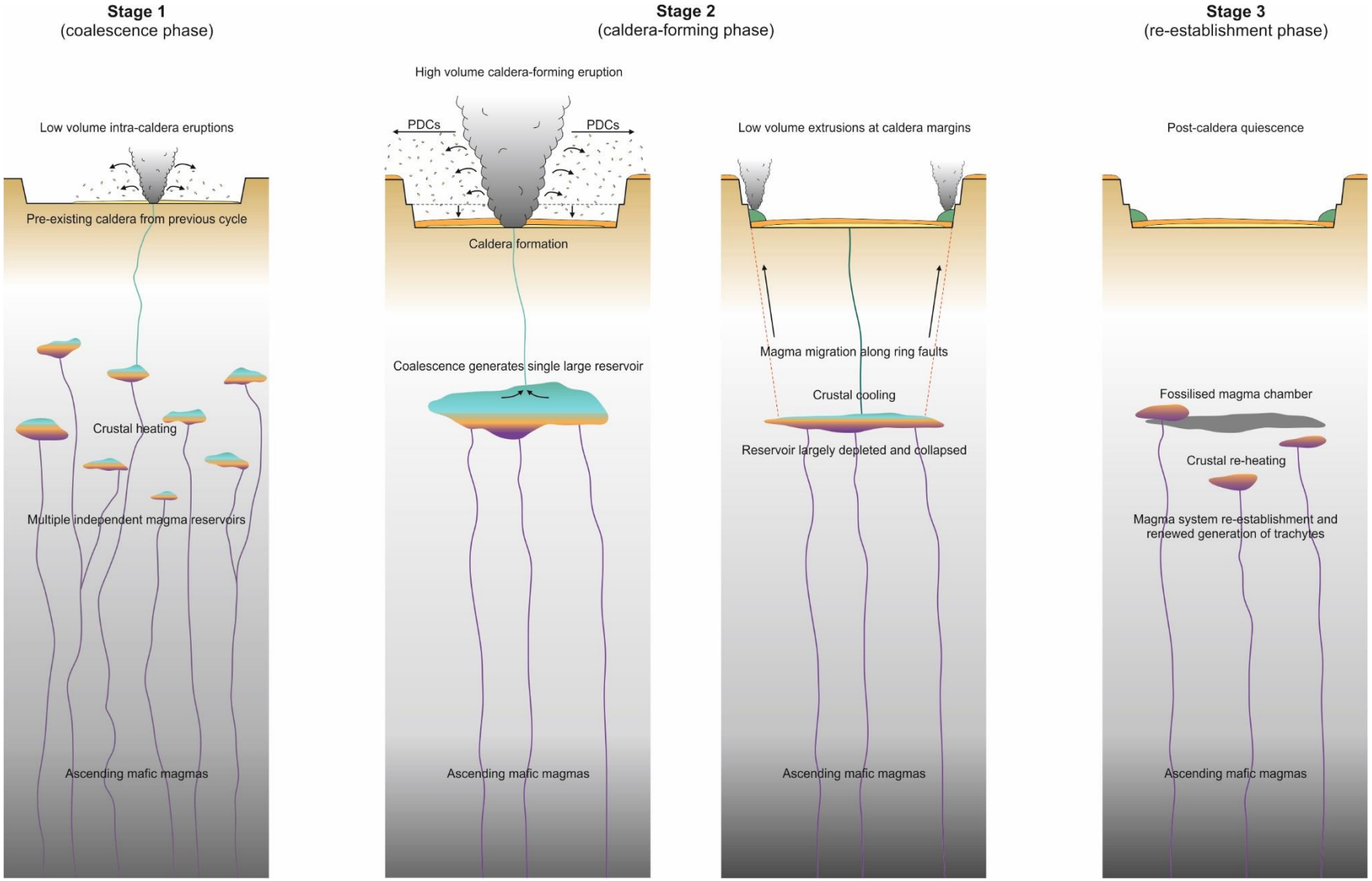
Stage 1
(coalescence phase)
Low volume intra-caldera eruptions
Pre-existing caldera from previous cycle
Crustal heating
Multiple independent magma reservoirs
Ascending mafic magmas
Stage 2
(caldera-forming phase)
High volume caldera-forming eruption
PDCs
PDCs
Caldera formation
Coalescence generates single large reservoir
Ascending mafic magmas
Low volume extrusions at caldera margins
Magma migration along ring faults
Crustal cooling
Reservoir largely depleted and collapsed
Ascending mafic magmas
Stage 3
(re-establishment phase)
Post-caldera quiescence
Fossilised magma chamber
Crustal re-heating
Magma system re-establishment and renewed generation of trachytes
Ascending mafic magmas

◄ **FIGURE 5.49:** A schematic model for caldera cycles at Furnas. See text for discussion

relatively uniform eruptible magma composition, such as that of the PIF. The compositional and lithological variability observed within the PIF (e.g. metaluminous vs. peralkaline, ignimbrite vs. pumice fall) may still result from the development of an uppermost cap of comparatively differentiated melt, as described above. Ascending mafic magmas are considered to be injected into the base of this reservoir, contributing heat and material to maintain it, but due to their inferred volumetric insignificance, they are not seen in the eruptive record and are effectively absorbed by the shallow crustal silicic system. At this point, the magma system is considered to have entered 'Stage 2', and is sufficiently developed to be capable of producing a caldera-forming eruption on the scale of the PIF.

At this stage, the overpressures required to initiate eruption are considered to be greater than in Stage 1, due to the viscoelastic behaviour of the heated crust (e.g. Folch and Marti, 1998; Jellinek and DePaolo, 2003). As such, eruptions become less frequent, and larger in scale. Potential triggers include: (1) the exsolution of a volatile phase in response to magmatic differentiation of both resident and replenishing magmas (e.g. Tait *et al.*, 1989a; Folch and Marti, 1998; Fowler and Spera, 2008), (2) an increase in the rate of magma replenishment (Degruyter and Huber, 2014), and (3) partial remelting of crystal mush (Huber *et al.*, 2011). Other processes, such as magma buoyancy and roof failure resulting from crustal thinning are less likely due to their general association with significantly larger volume magmatic reservoirs (e.g. Caricchi *et al.*, 2014; Malfait *et al.*, 2014). The PIF does not contain any textural evidence to indicate the rejuvenation and remelting of a substantial crystal mush (e.g. crystal rich 'monotonous intermediates; cf. Hildreth, 1981; Snyder, 2000; Couch *et al.*, 2001; Koyaguchi and Kaneko, 2001; Bachmann *et al.*, 2002, 2007), and melt inclusion and groundmass glass volatile contents suggest that the PIF-forming magmas were volatile-undersaturated, suggesting that the eruption was most likely triggered by magma replenishment.

Following a caldera-forming eruption, the shallow magma system is considered to have been largely depleted in eruptible magma. At this point, the magma system is considered to have entered a third stage (Stage 3). The absence of basaltic eruptions within the caldera suggests that any mafic magmas in the shallow system were either absorbed entirely by the prevailing felsic magmas, or were not eruptible. Alternatively, the presence of basaltic cones on the volcano's flanks may reflect the preferential eruption of remaining mafic magmas along the ring faults associated with the caldera, shortly after its formation. Due to the inferred removal of the majority of the silicic magma during eruption and caldera-collapse, Stage 3 is envisaged to represent a re-establishment phase, in which the shallow crustal magma storage system must be replenished via continued magma supply. During this stage, eruptions of silicic magmas are likely to halt until more silicic magmas have been generated by fractional crystallisation of basaltic parental magmas. Furthermore, the absence of a developed magmatic system is envisaged to promote cooling of the country rocks, further adding to the timescales required to re-establish the system to multiple reservoirs (Stage 1) and eventually, a single primary reservoir (Stage 2).

This model of the cyclical evolution of the Furnas magma plumbing system remains compatible with the results of this study and the magma chamber model presented in Section 5.6.4 (see above). Within the proposed framework, the eruptive products of the UFG are considered to represent Stage 1, in which the crust is being heated, and multiple magma pockets are present, each one an individual system which adheres to the schematic model presented in Section 5.6.4 (see above), in which mafic magmas fractionate to trachytic residual magmas. This also remains compatible with the model for the temporal development of the UFG magma plumbing system given in Section 5.6.5 (see above), requiring only a slight adjustment. The application of the cyclic scheme discussed here would imply that the trace element profile of the UFG is the result of the eruption of up to four individual magma chambers, each acting as an independent system, rather than the re-establishment of the silicic cap of a single reservoir. This may be

supported by taking into consideration the likely rates of fractionation. The repose intervals between the eruptions of the UFG are poorly constrained, but are unlikely to exceed ~ 1,000 years (see above). Assuming fractionation rates of between 0.2×10^{-4} and 2×10^{-4} (cf. Rogers *et al.*, 2004), the degree of fractionation required to produce the METs of Furnas from broadly intermediate magma compositions (~ 40 %) could be achieved between 2,000 and 8,000 years. These timescales imply that the repose intervals between the UFG eruptions may not have been sufficient to allow the reconstruction of a trachytic cupola, and provide further evidence for the presence of multiple magma bodies.

The PIF is considered to be representative of Stage 2, in which a consolidated magma reservoir had grown to a sufficient size to feed a caldera-forming eruption. Following a caldera-forming eruption, the shallow magma system is envisaged to be greatly depleted, leading to Stage 3, which may be represented by the apparent quiescence of Furnas following the second caldera-forming event and prior to the UFG eruptions. This time period is envisaged to represent the time required to re-establish the shallow magmatic system with trachytes derived from fractional crystallisation, which were then erupted as the UFG. The estimated length of this time period (~ 7,000 years) is largely compatible with the likely rates of fractionation from basalt to trachyte; between 3,000 and 18,000 years assuming fractionation rates of between 0.2×10^{-4} and 2×10^{-4} (cf. Rogers *et al.*, 2004).

In summary, the eruptive history of Furnas may exhibit a cyclic nature, in which (1) the shallow crustal magma system is developed as multiple discrete magma bodies evolving via fractional crystallisation towards trachytic compositions and erupting, (2) the individual magma bodies coalesce in response to crustal heating, forming a single larger reservoir which is then largely emptied during a caldera-forming eruption, and (3) a re-establishment phase of up to ~ 7,000 years rebuilds the shallow magma system via continued input and protracted fractional crystallisation of basaltic magmas, leading to a period of quiescence.

5.7 Conclusions

The compositional characteristics of both the young (< 5 ka), intra-caldera trachytes and the older, caldera-forming trachytes of Furnas volcano can be adequately accounted for by extended fractional crystallisation from an alkali basalt parental magma at minimum depths of ~ 2.5 to 4 km. Fractionation is initially dominated by clinopyroxene, which is eventually replaced by alkali feldspar in the latter stages of differentiation. Despite their major element homogeneity, trace element compositions highlight the prominent role of continued fractional crystallisation within the trachytes, revealing up to 50 % fractionation from the least evolved trachytes (LETs) to the most evolved trachytes (METs). This process is enhanced by the accumulation of water and the development of peralkalinity.

The magma plumbing system is shown to comprise a single prominent zone in which alkali basalts evolve through to trachytic residual liquids. Due to density variations, this reservoir is envisaged to be stratified, with high density mafic magmas at the base, and relatively cool, hydrous trachytes forming an upper cap. Rare syenitic ejecta are considered to represent *in-situ*, near-complete crystallisation of the trachytes in the roof zone of the reservoir, which is sampled randomly during eruption. Mingling and mixing within the trachytes is recorded by trachytic enclaves within the syenite ejecta, and by the presence of banded pumices in Furnas J. Further evidence for mixing can be seen in the ubiquitous presence of small quantities of clinopyroxene antecrysts within all of the UFG eruptions, which are likely to be introduced to the trachytes during interaction with underlying, hotter, intermediate magmas. The presence of such a shallow reservoir may account for the Daly Gap at Furnas, as ascending mafic magmas are intercepted before reaching the surface, instead ponding in the lower reservoir and fractionating towards felsic compositions. Volatile concentrations correlate negatively with temperature and positively with peralkalinity indices, indicating that the trachytes of Furnas were stored at volatile-undersaturated conditions. Melt inclusion and groundmass glass halogen

concentrations indicate that neither Cl nor F were degassed syn-eruptively, either during sub-Plinian UFG eruptions, or in the caldera-forming PIF eruption.

Despite the low volumes of the UFG eruptions (≤ 0.3 km^3), variations in trace element concentrations within individual eruptions indicate zonation of the upper cap of the reservoir prior to eruption, with the most evolved melts typically being the first to erupt. Evidence exists for the presence of both chemical gradients and relatively sharp compositional stratification, which, in the case of the latter, are considered to represent sharp compositional discontinuities in the pre-eruptive magma reservoir, providing direct evidence for the presence of density stratification. Less distinct gradients likely result from the accumulation of volatiles, as well as the associated increase in crystal settling rates. Overall, trace element profiles of the UFG are not compatible with continued fractionation and tapping of a single magma batch, and are instead indicative of a cyclic regime in which a compositionally stratified trachytic cap has formed and been sequentially erupted in up to three individual eruptions, before being re-established. This study suggests that up to there have been up to four such cycles of eruption and re-establishment within the UFG, with the 385 year repose time since the most recent eruption most likely representing a re-establishment phase.

The recent (< 5 ka) trachytic activity and the cessation of basaltic eruptive activity in the Congro Fissure zone may provide evidence for the lateral growth of the Furnas and/or Fogo shallow magma plumbing systems, leading to the formation of a shadow zone covering a substantial proportion of eastern São Miguel. However, rare trachytic eruptions in the Picos Fissure zone are more difficult to account for by lateral extension of the magma plumbing systems of Sete Cidades and/or Fogo. Instead, basaltic magmas ascending beneath the fissure zones may stall and fractionate towards trachytic compositions, or generate them directly via partial melting of crustal lithologies.

Finally, the eruptive history of Furnas may highlight a cyclic regime of evolution of the underlying magmatic system, in which the Upper Furnas Group (UFG) represents a developmental stage in which the shallow magma system comprises multiple discrete

magma chambers, each adhering to the model presented in Section 5.6.4. This regime is considered to evolve towards a single, comparatively large magma reservoir via coalescence of smaller magma bodies, which is then erupted in a caldera-forming event such as that which produced the Povoação Ignimbrite Formation (PIF). The apparent lack of eruptions during a period of up to ~ 7,000 years following the second caldera-forming event may indicate that the shallow crustal magma system is largely exhausted by the larger, caldera-forming eruptions, and requires a re-establishment phase. These timescales are compatible with published timescales of basalt to peralkaline trachyte fractionation.

CHAPTER 6: THE MAGMA SYSTEMS OF TERCEIRA ISLAND AND FURNAS VOLCANO, SÃO MIGUEL: IMPLICATIONS FOR THE EVOLUTION AND CONTRASTING ERUPTION STYLES OF PERALKALINE SILICIC MAGMAS

6.1 Chapter overview

In this chapter, the results of Chapters 4 and 5 are discussed, focussing on how the models presented in this study contribute to the greater understanding of the petrogenesis and eruption of peralkaline silicic magmas. First, the magmatic systems of both Pico Alto, Terceira, and Furnas, São Miguel, are compared directly, before being considered in the context of the magmatism of the Azores archipelago. They are then considered alongside a variety of peralkaline silicic centres such as the East Africa Rift and Pantelleria. Second, a detailed evaluation of the applicability of crystal mush extraction models to peralkaline silicic system is provided, in light of the major findings of this study. Third, the eruptive behaviour of peralkaline silicic magmas is discussed, linking features such as magma volatile content, magma viscosity, and interaction with external water, to the contrasting eruption styles observed in the Azores and globally. Finally, the implications of this study for future work within this area are considered, and a number of individual targets of interest are discussed in detail.

6.2 Genesis and evolution of peralkaline trachytes

The petrogenetic models presented in chapters 4 and 5 represent an original contribution to the understanding of peralkaline silicic magmatic systems, not only within the regional context of the Azores, but also in the global context of peralkaline silicic magmatism. As such, in this section the petrogenetic processes, pre-eruptive storage conditions, and proposed magma plumbing system models for both Pico Alto, Terceira, and Furnas, São Miguel are first compared with one another, second, with proposed models for other magmatic systems in the Azores archipelago, and third, with available petrogenetic models for prominent peralkaline silicic magma systems worldwide, including Pantelleria and the East African Rift (EAR).

6.2.1 Pico Alto and Furnas: a comparison

The magmatic plumbing systems of Pico Alto and Furnas each exhibit a number of similar features. For example, both centres have erupted exclusively peralkaline silicic trachytes from their central complexes, interpreted here as indicative of the presence of an established silicic reservoir in the shallow crust which actively inhibits the ascent of more mafic magma compositions (cf. Wolff 1987). In each case, the erupted trachytic magmas are crystal poor, with an assemblage dominated by alkali feldspar. Additional phases include comparatively rare clinopyroxene, Ti-magnetite, ilmenite, biotite, and apatite. Both systems have produced trachytes which contain cognate syenitic ejecta, considered here to represent bulk solidification of trachytic magmas at the margins of a reservoir (cf. Widom *et al.*, 1993; Ridolfi *et al.*, 2003). In both systems, the primary petrogenetic process involved in the derivation of the peralkaline trachytes has been shown to be fractional crystallisation rather than partial melting of crustal lithologies, though a secondary role of crustal assimilation cannot be ruled out. The fractionation histories of the peralkaline silicic magmas are similar between the two systems, comprising an initial stage in which clinopyroxene fractionation is dominant, with subsidiary olivine. This is followed by

relatively late stage plagioclase fractionation from intermediate magmas, and finally, fractionation of almost exclusively alkali feldspar at silicic compositions.

Clinopyroxene from the trachytic magmas of both centres is in demonstrable disequilibrium with its host rock, having last equilibrated with broadly intermediate compositions. However, its presence in both magma systems suggests that both systems involve a physical process of interaction and crystal exchange between magmas of contrasting compositions. Calculated estimates of pre-eruptive magma viscosity indicate that the peralkaline silicic magmas of both Pico Alto and Furnas were up to two orders of magnitude lower than might be expected for metaluminous silicic magmas (~ $10^{4.5}$ Pa s, Scaillet *et al.* 1998), and, based on modelling of two-phase flow, serve to highlight the viability of crystal settling as a dominant process of magmatic differentiation, even for the most evolved compositions of the suite. Furthermore, the ubiquitous presence of small proportions of disequilibrium clinopyroxene in both systems despite the rapid timescales of crystal settling suggests that the envisaged crystal exchange processes through which they are introduced is likely to occur immediately prior to the eruption.

Despite their major element homogeneity, individual eruptions typically contain pronounced trace element variations, which are suggestive of a zoned pre-eruptive magma reservoir. Where present, the degree of zonation is, on the basis of incompatible element concentrations, highly comparable between the magmatic systems, regardless of the eruptive volume of the deposit (Figure 6.1). Trace element Rayleigh fractionation models indicate that this range constitutes between 15 and 50 % fractionation from the least evolved trachyte (LET) to the most evolved trachyte (MET).

Estimates of pre-eruptive P-T-fO_2 conditions highlight a number of similarities and contrasts between the systems. Pre-eruptive temperatures estimated for Pico Alto and Furnas via two-oxide and alkali feldspar-melt models are highly compatible, and range from 773 to 936 °C, and 772 to 977 °C, respectively. If the syenite ejecta of each complex are included, these temperature ranges are extended down to 616 and 621 °C, respectively. Similarly, the pre-eruptive water contents of the erupted trachytes from both

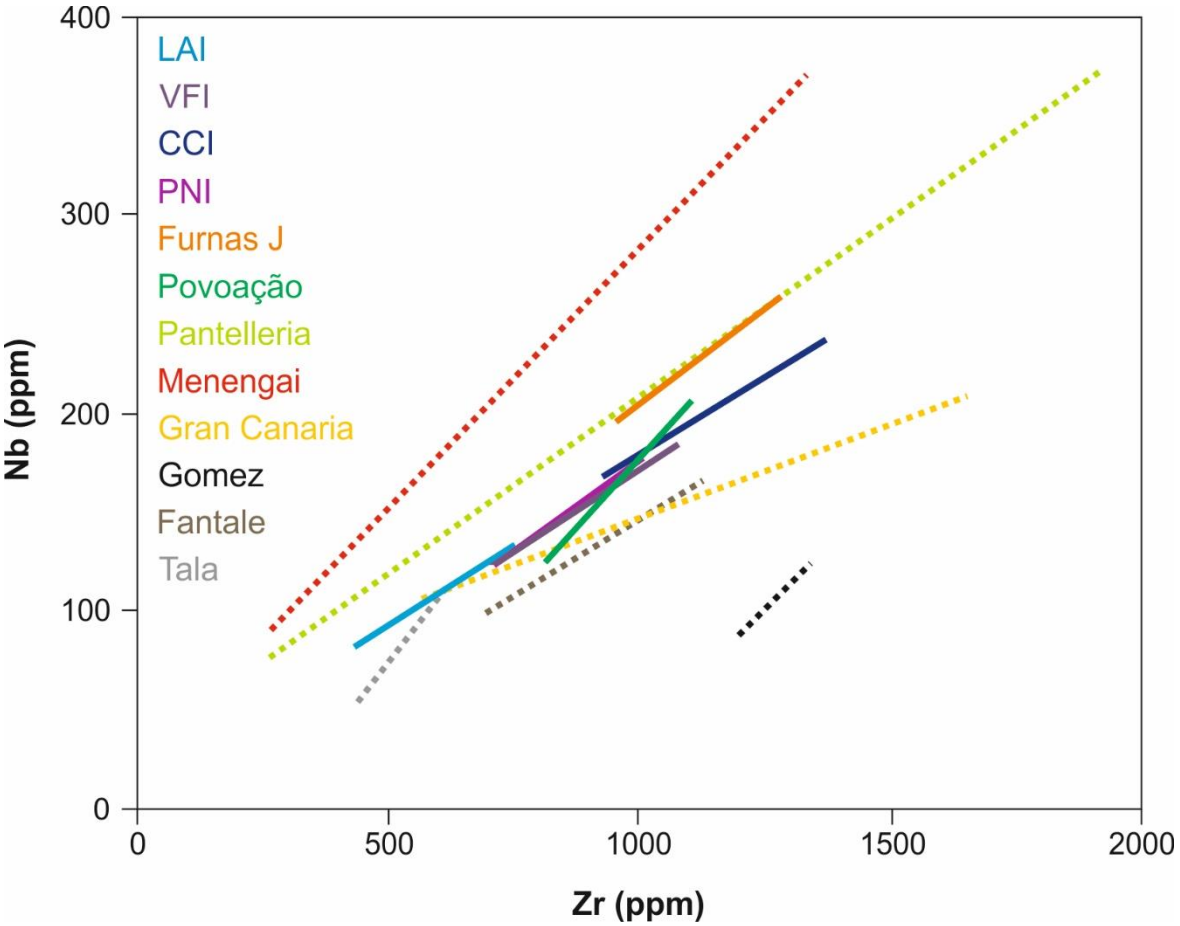

FIGURE 6.1: Degree of trace element zonation in a number of individual eruptions of peralkaline silicic magma. Data from: Ren *et al.* (2006), Scaillet and Macdonald (2006), Macdonald *et al.* (2011, 2012), Scaillet and Macdonald (2001), White *et al.* (2005), Di Carlo *et al.* (2010), White *et al.* (2006), Novak and Mahood (1986), this study. Figure after Macdonald (2012)

Pico Alto and Furnas exhibit very similar ranges of 2.5 to 6.0 wt. %, and 2.1 to 6.2 wt. %, respectively.

In contrast, estimates of pre-eruptive redox conditions calculated via two-oxide models show minor variation between the two volcanic centres. Available estimates for Pico Alto (this study) suggest that the silicic magmas were stored at relatively reducing conditions, close to one log unit below the fayalite-magnetite-quartz (FMQ) buffer reaction. In contrast, the silicic magmas of Furnas were evolved under more oxidising conditions, either close to the FMQ buffer (post-caldera eruptions of the Upper Furnas Group (UFG)), or, in the case of the caldera-forming Povoação Ignimbrite Formation, around one log unit above FMQ. Pre-eruptive water contents of the trachytes determined via analysis of melt inclusions, and estimated via alkali feldspar-melt hygrometry exhibit similar ranges,

suggesting that the observed variability in redox conditions is unlikely to be controlled by volatile content. Instead, this may reflect variable degrees of H_2 degassing following thermal dissociation of magmatic water (cf. Mungall and Martin, 1995). However, available volatile data for both Pico Alto and Furnas imply volatile undersaturated conditions. As such, the described variability may instead be linked to variations in the mantle source, whereby partial melting of variably oxidised mantle over time generates primary melts with variable redox states. This is consistent with the proposed models of mantle heterogeneity beneath the Azores (e.g. Dupré *et al.*, 1982; Haase and Beier, 2003; Beier *et al.*, 2007; Madureira *et al.*, 2011), and may account for the inter-island variability. However, the temporal redox variation exhibited by a single volcanic centre (Furnas) are less likely to be controlled by such a process, and are most liely linked to the temporal evolution of the magma plumbing system and its architechture.

The magmatic plumbing systems of Pico Alto and Furnas may also be similar in their overall structure. As discussed above, both systems exhibit abundant evidence for a prominent and well-established magma reservoir in the shallow crust (e.g. caldera-formation, low TiO_2 and low Al_2O_3 clinopyroxenes, miarolitic cavities), which feeds the eruptions of trachytic magmas at both volcanoes. The exclusively trachytic compositions of melt inclusions within the erupted trachytes suggests that at least the upper portion of these reservoirs comprises only trachytic magmas, which is consistent with the formation of a low density trachytic cap at the top of the magma system. However, the Pico Alto system also exhibits some evidence for a deeper portion of the magma system, in the form of high TiO_2 and high Al_2O_3 clinopyroxenes in the trachytes, and a population of Mg-rich olivine and Ca-rich plagioclase in the syenite-hosted enclaves. Furthermore, thermodynamic models provide a better fit to the data if the primary melt composition is allowed to fractionate to a hawaiitic composition at pressures representative of the lowermost crust (500 MPa, ~ 14 km), before ascending to shallow crustal conditions. In contrast, thermodynamic modelling of the Furnas magmas provides the best fit if only a single, shallow crustal stage is employed. Additionally, the syenite-hosted enclaves of

Table 6.1 Pre-eruptive temperature, fO_2, and H_2O_{melt} estimates for various Azorean trachytic magmas

Island	Volcano	Composition	T (°C)	fO_2	H_2O_{melt} (wt. %)	Reference
Faial	Caldeira	Trachyte	923 to 976	NNO		Pimentel *et al.* (2015)
		Trachyte	953 to 1040	NNO	3.3 to 5.2	
		Trachyte	953 ±22			Zanon *et al.* (2013)
São Miguel	Sete Cidades	Trachyte	736 to 784	FMQ		Renzulli and Santi (2000)
		Trachyte	695 to 702			
		Trachyte		FMQ to MH -1		Beier *et al.* (2006)
	Fogo	Trachyte	800 to 960	FMQ to FMQ +1	6.5 to 6.6	Wolff and Storey (1983); Wolff *et al.* (1990)
	Furnas	Trachyte	772 to 977	FMQ to FMQ +1	2.1 to 6.2	This study
		Syenite	621 to 969	FMQ to FMQ -2	1.3 to 4.9	This study
Terceira	Pico Alto	Trachyte	773 to 936	FMQ -1	2.5 to 6.0	This study
		Syenite	616 to 880	FMQ-1 to -2	3.1 to 5.7	This study
		Trachytic enclave	876 to 894		3.1 to 5.9	This study

Furnas are exlusively trachytic, with a range of compositions similar to, rather than less differentiated than, the erupted trachytes. Furthermore, they bear none of the mafic phases observed in the described syenite-hosted enclaves of Pico Alto. However, the presence of rare high TiO_2, high Al_2O_3 clinopyroxenes provides some evidence for a high pressure evolutionary step in the origin of the Furnas trachytes, though it may be rather less significant than that of Pico Alto.

6.2.2 Pico Alto and Furnas in the context of the Azores archipelago

The characterisation of the magmatic plumbing systems of Pico Alto and Furnas facilitates a direct and critical comparison with other Azorean magmatic systems. Focus is given here to those magma systems which have been most explored: Sete Cidades and Fogo, São Miguel (Wolff and Storey, 1983; Wolff *et al.,* 1990; Renzulli and Santi, 2000; Beier *et al.*, 2006), Caldeira, Faial (Zanon *et al.,* 2013; Zanon and Frezzotti, 2013; Pimentel *et al.,* 2015), Graciosa (Larrea *et al.*, 2014), Pico (França *et al.*, 2006; Zanon and Frezzotti, 2013), and Corvo (França *et al.*, 2003; Larrea *et al.*, 2013). This includes islands from each of the three geographical groups (western, central, and eastern), and also allows the comparison between islands which lie on the Terceira Rift and those which do not.

6.2.2.1 Pre-eruptive temperatures, H_2O_{melt}, and redox conditions

Available estimates of the pre-eruptive temperatures, water contents, and redox conditions of the silicic magmas from various Azorean volcanoes are given in Table 6.1. Pre-eruptive temperature estimates for Pico Alto and Furnas magmas fit well with those of Fogo and Sete Cidades on São Miguel, and also those of Caldeira volcano on Faial (Pimentel *et al.*, 2015) (Table 6.1) . Similarly, the range of water contents determined via FTIR analysis of melt inclusions, and estimated via alkali feldspar hygrometry, for both Pico Alto and Furnas magmas fit well with water contents estimated via amphibole hygrometry for Caldeira volcano, Faial. The water contents estimated for Fogo trachytes

by Wolff and Storey (1983) and Wolff *et al.* (1990) correlate with the uppermost portion of the ranges for Pico Alto and Furnas.

In contrast, the available estimates for pre-eruptive redox conditions indicate some variability, with values which range from around two log units below the fayalite-magnetite-quartz (FMQ) reaction curve to around one log unit below the magnetite-haematite reaction curve (Table 6.1). The most reducing conditions are recorded by the syenitic ejecta of this study, and may be linked to the crystallisation of aegirine and Na-amphibole, two phases which are not observed in the trachytes. Markl *et al.* (2010) showed that, in persodic melts, the crystallisation of aegirine invariably involves the reduction of the melt via the following reaction:

$$\underset{\text{(melt)}}{Na_2O + 2\,FeO + 4\,SiO_2 + \tfrac{1}{2}\,O_2} = \underset{\text{(aegirine)}}{2\,NaFeSi_2O_6} \qquad (6.1)$$

Similarly, the crystallisation of a sodic amphibole (in this case considered to be arfvedsonite) will have a similar effect via the following reaction:

$$\underset{\text{(melt)}}{3\,Na_2O + 10\,FeO + 16\,SiO_2 + O_2 + H_2O} = \underset{\text{(arfvedsonite)}}{2\,Na_3Fe^{2+}{}_4Fe^{3+}Si_8O_{22}(OH)_2} \qquad (6.2)$$

Thus, the final stages of crystallisation of the trachytic melts (< 800 °C), as represented by the syenite ejecta, are likely to be driven towards more reducing conditions when aegirine and Na-amphiboles become stable. The erupted trachytes do not record values this low because they have not yet reached the conditions which favour the crystallisation of these phases. This decrease in fO_2 is effectively a late-stage efffect which only occurs during the final stages magmatic solidification, overprinting any redox changes induced by mantle heterogeneity or degassing (see Section 6.2.1). This is applicable to Pico Alto and Furnas,

but may also apply to other Azorean volcanoes where similar syenitic ejecta have been reported (e.g. Fogo, Sete Cidades).

The majority of the available estimates for the erupted trachytic magmas of the Azores indicate redox conditions which approximate the FMQ buffer reaction curve, extending to around one log unit above and below it. Curiously, there appears to be some variation in redox conditions at individual volcanoes. For example, in chapter 5 the pre-eruptive redox conditions of the trachytes erupted at Furnas were shown to vary temporally, with the older, caldera-forming eruption recording less reducing conditions (FMQ +1) than the younger, post-caldera activity (FMQ). Similarly, Beier *et al.* (2006) identified significantly more oxidising pre-eruptive conditions (~ MH -1) for the caldera-forming and post-caldera deposits, compared with the pre-caldera deposits (~ FMQ) at Sete Cidades. These authors attributed this variation to a higher volatile content of the magmas, linked to a greater volatile component in the mantle source and the assimilation of crustal lithologies, noting the occurrence of crustal xenoliths in a number of lavas. A similar process may be invoked to account for the somewhat smaller range observed at Furnas. The time period that separates the caldera-forming eruption of the Povoação Ignimbrite Formation (PIF) and the much younger post-caldera activity of the Upper Furnas Group (UFG) is estimated to be ~ 30 to 35 kyr (based upon available radiocarbon ages for the PIF and the base of the UFG, calibrated using Intcal13, Reimer *et al.* (2013)), and is broadly comparable to the timescales of volcanic activity at Sete Cidades. As such, the variability in oxygen fugacity at Furnas may also be linked to variations in the volatile content of the mantle source. The potential role of crustal assimilation in the Furnas magmatic system cannot be ruled by the data of this study.

An alternative to this hypothesis is the role of variable degrees of degassing. Mungall and Martin (1995) suggested that the contrasting redox conditions recorded by the deposits of Pico Alto and Santa Bárbara could relate to the thermal disassociation of water and subsequent H_2 loss, resulting in an oxidation of the melt. The more oxidising conditions recorded by the caldera-forming and post-caldera deposits of Sete Cidades

may therefore reflect a greater degree of degassing compared to Furnas. This is most likely to be controlled by the precise depth of the shallow crustal magma reservoir, and the total volatile content of the magmas, which together control the point at which volatile saturation and subsequent volatile exsolution occurs. To a lesser extent, this may also be affected by the lithological and structural nature of the surrounding country rock, which may facilitate or inhibit volatile escape. Within this scheme, the temporal variation in redox conditions observed at both Furnas and Sete Cidades may reflect the adjustment of the shallow crustal magma system in response to caldera-forming events. During a caldera-forming eruption, the upper crustal magma reservoir is envisaged to be largely depleted, requiring the incremental construction of a new reservoir, which may then form at a different depth within the shallow crust. As such, the Povoação Ignimbrite-forming eruption of Furnas is likely to have been fed by a more degassed (and so potentially slightly shallower) magma reservoir than that of the UFG. Similarly, the caldera-forming and post-caldera eruptions of Sete Cidades may have been fed by a shallower magma reservoir than that which fed the pre-caldera activity.

6.2.2.2 The architecture of the magmatic plumbing systems

The schematic models of the magmatic plumbing systems of Pico Alto and Furnas volcanoes presented in this study are highly compatible with models that have been proposed at other Azorean volcanic centres. For example, Beier *et al.* (2006) suggested two dominant levels of magma storage beneath Sete Cidades, São Miguel; a lower crustal (~ 15 km) reservoir of mafic magmas, and an upper crustal (~ 3 km) reservoir comprising predominantly trachytic magmas. The same authors provided evidence for the mixing of ascending mafic magmas with trachytic magmas in the shallow crustal storage zone, as suggested here for Pico Alto, and attributed the caldera-forming eruptions of Sete Cidades to the same process. Furthermore, hybrid lavas erupted at Fogo volcano led Storey *et al.* (1989) to suggest that basaltic and trachytic magmas were mixing/mingling following a

replenishment event. As such, this general model of a mafic magma storage zone at the base of the crust and a periodically replenished, silicic storage zone in the shallow crust appears to be generally applicable to all three of the central volcanoes of São Miguel. However, such a model may also be applied to other Azorean volcanic centres. For example, this study has highlighted the presence of a polybaric magma system beneath Pico Alto, in which mafic magmas mix/mingle with silicic magmas prior to eruption (cf. Mungall, 1993), whilst Larrea *et al.* (2014) provided evidence for polybaric magma evolution beneath Graciosa island, with two discrete magma storage zones at very similar depths to those of Terceira and São Miguel (~ 15 and ~ 3 km). Furthermore, Zanon *et al.* (2013) suggested that a similar magmatic plumbing system exists beneath Faial island (~ 16 and ~ 5 km). In contrast, the magmatic plumbing system of Pico island does not appear to include a well defined shallow crustal storage zone, and has not produced trachytic magmas such as those of Terceira, São Miguel, and Graciosa (França *et al.*, 2006; Zanon and Frezzotti, 2013). Similarly, Larrea *et al.* (2013) showed that, although the trachytes associated with the syn-caldera phase of volcanic activity on Corvo island (França *et al.*, 2003) were stored in a shallow crustal reservoir, the predominantly mafic pre- and post-caldera magmas originated from a magma storage zone at ~ 15 km depth.

As such, although a zone of magma storage at the base of the crust (~ 15 km) appears to be typical of the Azorean magma systems, the presence of an established shallow crustal reservoir in which mafic magmas evolve towards silicic magmas is by no means ubiquitous. The presence of established shallow crustal reservoirs on São Miguel, Terceira, and Graciosa suggests that this may be tectonically controlled by the Terceira Rift, which passes through each of these islands. However, the presence of an established shallow system beneath Faial complicates this. Instead, the observed distribution of established shallow crustal reservoirs may relate to the age of the islands in question. Both Pico and Covo are considerably younger (~ 270 and 300 ka, respectively; Zanon, 2015b and references therein) than the islands of Terceira, São Miguel, Graciosa, and Faial (500 to 900 ka), suggesting that the establishment of a shallow crustal trachytic

reservoir may be restricted to the older, more matured islands, perhaps relating to the degree of crustal heating required to sustain a significant body of magma in the uppermost crust (e.g. Jellinek and DePaolo, 2003; Gregg *et al.*, 2012; de Silva and Gregg, 2014; Degruyter and Huber, 2014). At Corvo, the caldera-forming eruption of trachytic magma compositions, followed by resumed mafic eruptive products in the post-caldera phase, many imply that the underlying magma is approaching sufficient maturity to allow the construction of a shallow crustal reservoir, in which trachytic magmas can form.

6.2.3 Pico Alto and Furnas in the global context

The magmatic plumbing systems of both Pico Alto and Furnas present a variety of features which are characteristic of peralkaline silicic complexes (cf. Macdonald, 2012). For example, both exhibit eruptions of exclusively peralkaline silicic magmas within their central complexes, which range from larger volume (> 0.5 km^3 DRE) and caldera-forming (e.g. Self, 1976; Duncan *et al.*, 1999), to lower volume (< 0.5 km^3 DRE) eruptions which may be effusive, forming lava domes or coulées (e.g. Upper Terceira Group, Self, 1976), or sub-Plinian, forming pumice falls and pyroclastic surges (e.g. Furnas J, Cole *et al.*, 1995). Eruptions of mafic magmas are limited to the periphery of both volcanic centres, and intermediate compositions are scarce. The rocks considered in this study are not compatible with an origin through partial melting of crustal lithologies, and instead exhibit geochemical evidence for an origin through extended fractional crystallisation (60 to 95 %) of a basaltic parental magma (cf. Barberi *et al.*, 1975; Weaver, 1977; Novak and Mahood, 1986; Peccerillo *et al.*, 2003; Flude *et al.*, 2008; Parker and White, 2008; Macdonald, 2012). In this study, syenite-hosted trachytic enclaves have been shown to record evidence for mixing/mingling of trachytes with both mafic magmas and syenitic mush beneath Pico Alto, whilst banded pumices at Furnas imply the pre-eruptive mingling of two, variably hydrous trachytes. Similar styles of magma mingling/mixing, either between mafic and felsic, or felsic and felsic end members has been recorded in the deposits of

numerous peralkaline systems, such as Menengai, Kenya (Leat *et al.*, 1984; Macdonald *et al.*, 1994), Gedemsa, Ethiopia (Peccerillo *et al.*, 2003), Longonot, Kenya (Scott and Bailey, 1986), Gran Canaria, Canary Islands (Troll and Schmincke, 2002; Sumner and Wolff, 2003), Pantelleria, Italy (Ferla and Meli, 2006; Gioncada and Landi, 2010), Eburru, Kenya (Macdonald and Scaillet, 2006), Mayor Island, New Zealand (Houghton *et al.*, 1992), Emuruangogolak, Kenya (Dunkley *et al.*, 1993), Silali, Kenya (Macdonald *et al.* 1995), Olkaria, Kenya (Macdonald *et al.*, 2008). As such, the mixing of magmas appears to play a vital role in the pre-eruptive magma systems of peralkaline volcanoes, and may play a role in the generation of the compositional Daly gaps which are so often observed. Furthermore, the syenite-hosted enclaves reported in this study represent, to the author's knowledge, the first reported direct evidence for replenishment of a trachytic magma reservoir, with less evolved trachytic magma, through a syenitic crystal mush.

The enrichment in Ba observed throughout the Terceira suite, and to a lesser extent at Furnas, is also reported at other peralkaline volcanic centres (e.g. Sumner and Wolff, 2003; Macdonald *et al.*, 2008). This feature is generally attributed to the resorption of alkali feldspar xenocrysts (Macdonald *et al.*, 2008; Macdonald, 2012), and the presence of resorbed alkali feldspars in the ignimbrite-forming trachytes of Terceira and Furnas indicate that the same mechanism is likely to operate in each system. One solution is the gravitational settling of alkali feldspar phenocrysts into less evolved trachytes (Macdonald, 2012). However, the syenite-hosted enclaves of Pico Alto, which have the greatest enrichment of Ba in the entire suite (~ 1250 ppm), also include glomerocrysts of host syenite, suggesting that accumulation and assimilation of syenitic crystal mush during trachyte-syenite interaction also plays a role. Furthermore, the apparent enrichment of Ba throughout the Terceira suite, even amongst mafic lithologies, may indicate that assimilation of syenitic lithologies is not limited to the trachytic compositions. The presence of basaltic lava flows containing syenitic xenoliths on Terceira suggests that mafic magmas may also interact directly with partially or totally solidified syenitic mush prior to eruption (Mungall, 1993).

Another feature of the Pico Alto and Furnas magmatic systems which is typical of peralkaline silicic systems is the presence of a vertically zoned cap to the shallow crustal magma reservoir (Macdonald, 2012). Similarly zoned deposits have been identified at Olkaria, Kenya, (Marshall *et al.*, 2009), Menengai, Kenya (Leat *et al.*, 1984), Longonot, Kenya (Rogers *et al.*, 2004), Pantelleria, Italy (Mahood and Hildreth, 1986; Civetta *et al.*, 1998), Gran Canaria,Canary Islands (Sumner and Branney, 2002), Gedemsa, Ethiopia (Peccerillo *et al.*, 2003), Fantale, Ethiopia (Gibson, 1970), Kane Springs Wash caldera, USA (Novak and Mahood, 1986), Buckhorn caldera, USA (Parker and White, 2008), Sierra La Primavera, Mexico (Mahood, 1981). On the basis of Zr-Nb concentrations, the degree of zonation within individual deposits shows considerable variation, ranging from 1.1× to 7× (Macdonald, 2012) (Figure 6.1). The degree of enrichment (as determined via incompatible element enrichment), both in the available literature data, and in the data of this study, does not bear any relation to the erupted volumes (Macdonald, 2012). For example, the Funas J deposit shows a very similar degree of enrichment to the PIF, despite their contrasting eruptive volumes (~ 0.1 and > 2 km^3 DRE). Similarly, a number of the ignimbrites on Terceira exhibit the same degree of zonation (Figure 6.1). Macdonald (2012) attributed this feature to factors such as magma viscosity and chamber geometry. In contrast, available data for the Linhares-Matela Ignimbrite Formation (LMI) suggest that the pre-eruptive magma reservoir from which it was fed was not zoned. In this instance, the injection of mafic magmas into the erupted trachyte prior to eruption is envisaged to have promoted convection and removed any already-present compositional zonation. This is substantiated by the presence of olivine and plagioclase antecrysts, as well as resorbed alkali feldspars, throughout the deposit. The preservation of vertical zoning in at least four of the seven ignimbrite formations of Terceira suggests the eruption trigger may not have been mafic replenishment, or that they were erupted sufficiently rapidly following replenishment that the zoning patterns had not been re-homogenised by convection.

In terms of their geochemistry and the pre-eruptive conditions at which they were stored, the peralkaline trachytes of both Pico Alto and Furnas have much in common with

Table 6.2: Compositional data and estimates of pre-eruptive conditions of various peralkaline silicic rocks

Location	Rock	SiO_2	Peralkalinity index	Temperature (°C)	fO_2 (ΔFMQ)	Pressure (MPa)	Reference
Eburru 1	pt	65.3 to 66.4	1.24 to 1.25	705-715	-1	<100	1
Eburru 2	pt	67	1.69	790	-1	< 100	1
Eburru 3	pt	71	1.7	≤708	-0.6 to -0.7	100	1
Eburru 4	pt	71.3	1.96	<700	-1	150	2
Menengai	ct	62.5 to 64.2	1.1 to 1.2	854-870	-1.6 to -1.7	150	3
Olkaria	c	72.6 to 75.2	1.05 to 1.36	660-740	≈ 0	150	4
Pantelleria 1	pt-p	<64.8	<1.31	888-991	-0.7 to -1.1	150	5
Pantelleria 3	p	<67.8	1.55-1.63	756-764	-0.5 to -0.2	150	5
Pantelleria 5	p	69.7	1.94	<700	≈ 0	150	5
Pantelleria	p	70.4	1.4	730	-0.5	120	6
Pine Canyon	c	70.26	1.21	680-740	-1.7 to -1.9	100	7
Kane Springs	c	75	1.05	827	-0.1	190	8
Primavera	c	74.37	1.04	850	0	340?	9
Nemrut	t-r-c-p	68.77 to 75.50	0.87 to 1.37	721 to 898	0 to -1	10 to 360	10
Pico Alto Igns	ct	61.98 to 67.70	0.98 to 1.43	773 - 936	-1	≈ 130	This study
Pico Alto syenites	ct	64.49 to 65.56	1.08 to 1.14	616 - 880	-1 to -2	≈ 130	This study
UFG	ct	61.92 to 64.61	0.94 to 1.14	855-965	0	≈ 150	This study
UFG Syenite	ct	62.59 to 63.91	1.00 to 1.06	621-969	0 to -2	≈ 150	This study
PIF	ct	63.04 to 63.56	0.94 to 1.02	772 - 977	1	≈ 150	This study

Table after Macdonald (2012).Data from: (1) Ren *et al.* (2006); (2) Scaillet and Macdonald (2006); (3) Macdonald *et al.* (2011, 2012); (4) Scaillet and Macdonald (2001); (5) White *et al.* (2005); (6) Di Carlo *et al.* (2010); (7) White *et al.* (2006); (8) Novak and Mahood (1986); (9) Mahood (1981); (10) Macdonald *et al.* (2015). Eburru 1, 2, 3/4 represent the Older Trachyte, Younger Trachyte, and Pantellerite Formations, respectively. Pantelleria 1, 3, and 5 are from Associations 1, 3, and 5 of White *et al.* (2005), respectively. All literature T-fO_2 estimates derived from QUILF equilibria (Andersen *et al.* (1993), phase equilibrium experiments, or various formulations relating to two-oxide pairs. Literature pressure values are either assumed or derived from thermodynamic calculations. Abbreviations used: pt = pantelleritic trachyte; ct = comenditic trachyte; c = comendite; p = pantrellerite; t = trachyte; r = rhyolite

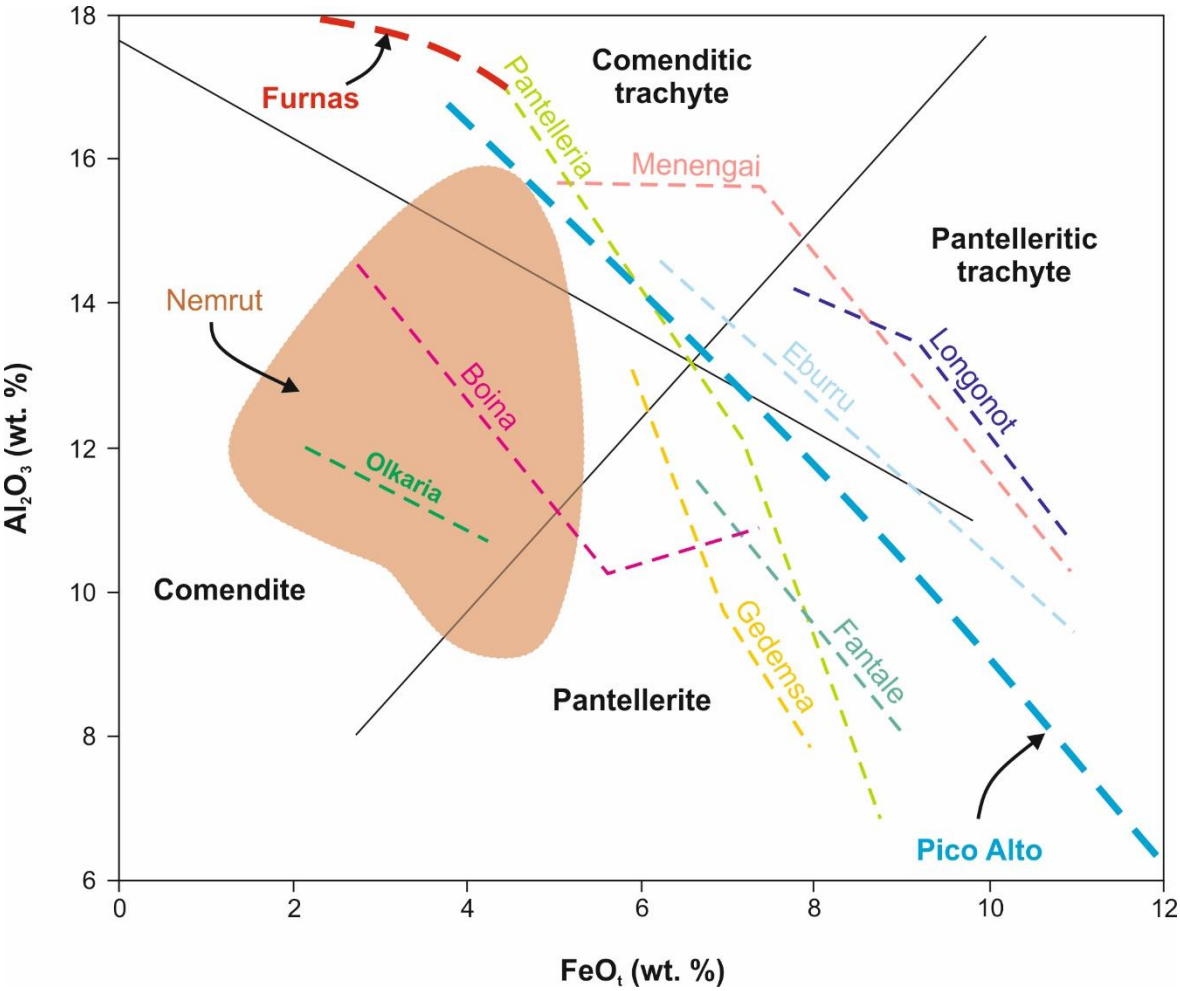

FIGURE 6.2: Summarised evolutionary trends for peralkaline silicic magmas from various volcanic centres. Figure after MacDonald *et al.* (2015). Classification scheme from Macdonald (1974a)

available data for other peralkaline centres (Table 6.2). Almost all of the erupted peralkaline silicic magmas were stored at shallow crustal conditions (< 200 MPa), at temperatures which range from 621 to 991 °C (if syenitic ejecta are included). As observed by Macdonald (2012), there is no clear relationship between pre-eruptive temperature, SiO_2 content, or peralkalinity index, which he relates to the importance of volatiles. The range of water contents provided by this study (2.1 to 6.2 wt. %) fall within, and slightly extend, the range of typical water contents for peralkaline silicic rocks (4 to 6 wt. %, e.g. Webster *et al.*, 1993; Barclay *et al.*, 1996; Scaillet andMacdonald, 2001, 2003, 2006; Gioncada and Landi, 2010), suggesting that it could strongly affect the liquid line of descent. This may also be seen in Figure 6.2, where the summarised liquid lines of descent from various peralkaline silicic centres are seen to vary in FeO_t-Al_2O_3 space.

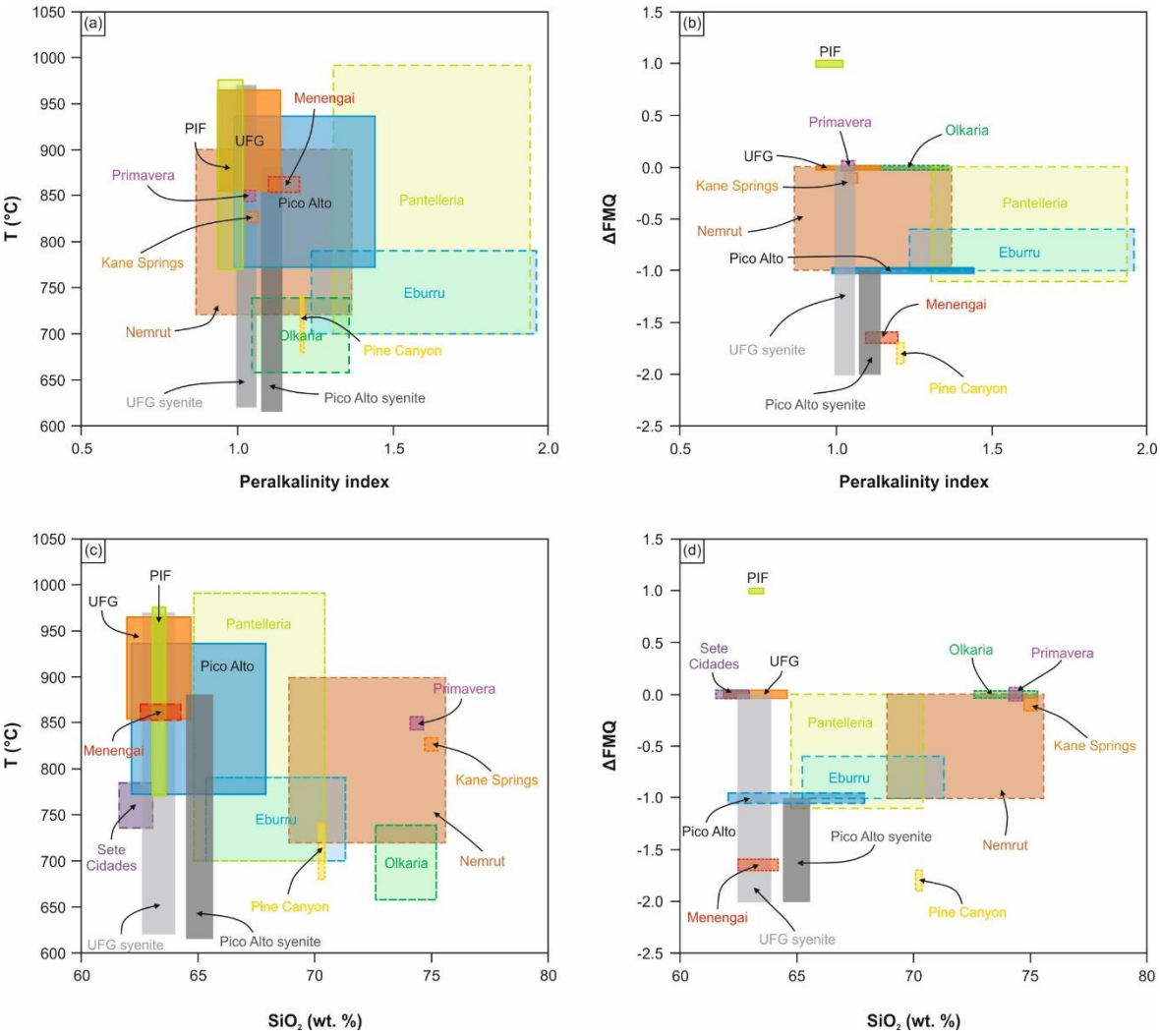

FIGURE 6.3: Summary figure of magma compositions and pre-eruptive intensive variables for various peralkaline silicic volcanic centres **a)** Peralkalinity indices plotted against predicted pre-eruptive temperatures **b)** Peralkalinity indices plotted against predicted oxygen fugacity (given as ΔFMQ) **c)** magma silica contents plotted against predicted pre-eruptive temperatures **d)** Magma silica contents plotted against estimated oxygen fugacity. Data from: Ren *et al.* (2006); Scaillet and Macdonald (2006); Macdonald *et al.* (2011, 2012); Scaillet and Macdonald (2001); White *et al.* (2005); Di Carlo *et al.* (2010); White *et al.* (2006); Novak and Mahood (1986), Renzulli and Santi (2000); Macdonald *et al.* (2015); this study

The pre-eruptive redox conditions determined for the Pico Alto and Furnas magmas generally adhere to those of other peralkaline silicic systems (Figure 6.3). For example, the trachytes of the UFG and the Terceiran ignimbrites were stored at redox conditions between FMQ and FMQ -1. The inclusion of the syenite ejecta extend this

range to FMQ -2; however, as discussed above, this is most likely to reflect the crystallisation of aegirine and Na-amphibole at low temperatures (< 800 °C). All of the available literature data (Table 6.2) suggests that other peralkaline silicic magmas evolved

under very similar redox conditions, with the minor variations between eruptive centres being attributable to variability in the mantle source, degassing histories, and potentially differing degrees of crustal assimilation. However, a notable exception to this is the PIF (this study), which records redox conditions around one log unit above the FMQ buffer reaction curve. As discussed above, this may reflect a temporal shift in the volatile content of the mantle source, a greater degree of degassing than is typical of peralkaline silicic centres, or crustal assimilation.

Finally, the trachytes of Pico Alto, and to a lesser extent Furnas, have been shown to have originated from a magmatic plumbing system comprising more than one storage depth (see Section 6.2.1). This model of a multi-stage magma ascent has been shown to be common in the Azores (see Section 6.2.2.2), but has also been invoked at other oceanic island volcanic centres. For example, Schwarz *et al.* (2004) proposed a multi-stage magma ascent model for the Madeira and Desertas rift zones, with magmas stalling at various levels in the mantle, at the Moho, and in the case of the Desertas Islands, at shallow crustal levels (2 to 4 km). Klügel *et al.* (2005) provided evidence for three distinct magma storage depths beneath the flanks of Cumbre Vieja volcano, Canary Islands: (1) uppermost mantle (430 to 780 MPa), (2) lowermost crust (180 to 420 MPa), and (3) shallow crust (100 to 150 MPa). A very similar magmatic plumbing system configuration to those of this study has been proposed for the Teide-Pico Viejo volcanic complex on Tenerife, Canary islands, in which phonolitic magmas occupy a shallow crustal magma storage region (~ 100 to ~ 150 MPa), and mafic to intermediate magmas are stored in the uppermost mantle/lowermost crust (600 to 1200 MPa) (Ablay *et al.*, 1998). Geist *et al.* (1998) showed that ascending magmas beneath the western Galápagos islands stalled first below the Moho, and second in the uppermost crust (< 300 MPa).

In contrast, the magmatic plumbing system model proposed for Pantelleria comprises only a prominent shallow crustal reservoir (~ 150 to 200 MPa), in which mafic, intermediate, and silicic magmas are present (Mahood and Baker, 1986; Neave *et al.*, 2012). Similarly, studies aimed at elucidating the magmatic plumbing systems of the

various peralkaline silicic centres of the EAR, such as Olkaria, Menengai, Silali, and Emuruangogolak, have highlighted a complex shallow crustal magma storage zone, in which the entire range of erupted magmas (mafic to peralkaline silicic) is stored (e.g. Leat *et al.*, 1984; Macdonald *et al.*, 1994; Smith *et al.*, 1995; Black *et al.*, 1998; Macdonald *et al.*, 2008). As such, in these systems the deep crustal/uppermost mantle magma storage zone suggested for many of the Azorean volcanoes is either not present, or is masked by the shallow crustal storage region. Although this may in part relate to the contrasting thickness of oceanic and continental crust, Geist *et al.* (1998) showed that the magmas feeding the Galápagos volcanic centres of Santa Cruz and Sierra Negra were stored at significantly different depths (30 km vs. 10 km), despite a relatively uniform crustal thickness of ~ 18 km. Instead, the depths of magma storage zones may be controlled by the precise, high resolution structure of the crust, or the rates of magma supply. For example, a prominent magma reservoir may form at the crust-mantle boundary due to a density contrast in the surrounding lithologies. Magma reservoirs in the upper crust are envisaged to form when the rates of magma supply are sufficiently high to thermally-maintain the reservoir in relatively cool, upper crustal conditions, but also low enough that the magmas stored in the upper crustal reservoirs are able to differentiate via closed-system fractionation towards peralkaline silicic compositions. As such, the apparent predominance of two-stage ascent models for Azorean volcanoes may reflect broadly similar magma production rates across the archipelago.

6.3 A note on the applicability of crystal mush extraction models to peralkaline silicic systems

The advent of the crystal mush extraction model as a source of silicic magmas (Bachmann and Bergantz, 2004; Hildreth, 2004) provided a mechanism which could account for a number of petrological problems, such as the extremely low crystal content of many rhyolitic magmas, despite the inherent difficulty of two-phase flow in liquids of such high viscosity. Similarly, the inability of crystals to separate from their host magmas, by crystal settling (e.g. Bowen, 1928), convective fractionation within a double-diffusive boundary layer (e.g. Chen and Turner, 1980; McBirney, 1980; Rice, 1981; McBirney *et al.*, 1985; Spera *et al.* 1995), or solidification front instabilities (Marsh, 2002), limits the efficiency of fractional crystallisation, yet many studies have highlighted the prominence of this process in the generation and evolution of silicic magmas (Weaver, 1977; Michael, 1983; Novak and Mahood, 1986; Bacon and Druitt, 1988; Mahood and Halliday, 1988; Hildreth *et al.*, 1991; DePaolo *et al.*, 1992; Macdonald *et al.*, 1995, 2008; Civetta *et al.*, 1998; Hildreth and Fierstein, 2000; Lindsay *et al.*, 2001; Clemens, 2003; Peccerillo *et al.*, 2003; Sumner and Wolff, 2003; Avanzinelli *et al.*, 2004; Lowenstern *et al.*, 2006; White *et al.*, 2006, 2009; Flude *et al.*, 2008; Parker and White, 2008; Marshall *et al.*, 2009). Crystal mush models account for these features by invoking the extraction and segregation of melt from a crystal mush via the upward migration of buoyant interstitial melt from a mush, driven by the exsolution of a gas phase (gas-driven filter pressing, Anderson *et al.*, 1984; Sisson and Bacon, 1999; Pistone *et al.*, 2015) and/or mush compaction (e.g. McKenzie, 1984; Shirley, 1986; Philpotts *et al.*, 1996; Rabinowicz *et al.*, 2001; Jackson *et al.*, 2003).

However, despite their attractiveness, the applicability of such models is not universal. For example, Streck (2014) highlighted a number of case studies, including ‘hot and dry’ (or A-type) and calc-alkaline rhyolites and granites, in which geochemical compositions of inferred crystal mushes and extracted melts were incompatible. Additionally, Macdonald (2012) noted that the application of such models to peralkaline

silicic systems may be hindered by the lack of evidence for a crystal mush (i.e. erupted crystal-rich intermediate magmas or 'monotonous intermediates', Hildreth, 1981). Macdonald *et al.* (1995, 2008) noted that the rarely erupted intermediate composition magmas of both Silali volcano and the Olkaria volcanic complex, Kenya, were similarly crystal poor to the erupted silicic magmas, suggesting that, at these centres at least, the presence of an intermediate crystal mush from which silicic magmas are extracted is unlikely (Macdonald, 2012).

The results of this study have highlighted the low pre-eruptive viscosities and ensuing efficiency of crystal settling within the trachytes of Pico Alto and Furnas, and suggest that this process remains a viable mechanism of two-phase flow even for the most evolved compositions. Furthermore, the lithologies that were considered in this study are almost exclusively crystal-poor, and provide two further examples of peralkaline silicic centres where the peralkaline equivalent of the monotonous intermediates remains absent. (cf. Macdonald, 2012). The syenite ejecta of both volcanoes has, on the basis of geochemistry and phase assemblages, been shown to reflect *in-situ* crystallisation of trachytic magmas similar to those of the various eruptions within a marginal thermal boundary layer, rather than a mush from which the trachytes were extracted. As such, there is no direct evidence to substantiate the application of a crystal mush extraction model for either Pico Alto or Furnas, and the generation of crystal-poor to aphyric magmas at each centre can be accounted for by rapid crystal settling. Instead, the models that are proposed in this study, whether polybaric or isobaric (and thus comprising either an entirely silicic magma chamber or a chamber with the entire compositional range, respectively), revolved around the mechanism of crystal settling, in which crystals (predominantly alkali feldspar) form and settle through a trachytic magma. As crystals settle, they move downwards through increasingly less evolved and hotter magmas and are resorbed back into the melt. In the context of a polybaric model (i.e. Pico Alto), this involves settling through trachytes of varying degrees of evolution, whilst for an isobaric model, this range is increased from the most evolved trachyte, through intermediate

compositions and eventually mafic magmas. The greatest rates of settling are shown to be in the most evolved trachytes, suggesting that with progressive depth within the magma body, the resident crystal population (and melt) of a given layer would become more contaminated by settling crystals, resulting in anomalous enrichments in Ba, K, Sr, and Eu. Over time, this is envisaged to lead to a crystal-poor, Ba-depleted cap at the top of the reservoir, and a comparatively crystal-rich (including resorbed antecrysts from above), Ba-enriched layer below (Figure 6.4). These layers may also be vertically zoned due to variable degrees of fractionation. As the deposits of the largest eruption of Furnas, the PIF may provide some evidence for this model. The initial pumice fall deposit is essentially aphyric and exhibits extremely low Ba contents (< 50 ppm). In contrast, the ignimbrite member is comparatively crystal-rich (though still crystal-poor), with higher Ba contents (up to ~ 310 ppm). Furthermore, the ignimbrite exhibits slightly higher K_2O and Al_2O_3 contents and a significantly smaller or absent negative Eu anomaly. In chapter 5, the latter feature is attributed to the relatively late crystallisation of plagioclase feldspar during the differentiation of mafic parental magmas; however, it could also reflect the accumulation and resorption of alkali feldspar in a deep layer which the PIF-forming eruption was able to tap. In contrast, the smaller UFG eruptions exhibit pronounced negative Eu-anomalies, low crystal contents, and similar K_2O and Al_2O_3 contents to the PIF pumice fall, suggesting that only the upper layer was tapped .

The scenario described above and the standard crystal mush extraction model should not be considered to be mutually exclusive, and may in fact be complementary. In Figure 6.5, a model is presented which reconciles the key features of the magma plumbing systems of Pico Alto and Furnas with those of the standard crystal mush extraction model (Bachmann and Bergantz, 2004; Hildreth, 2004). The first stage of the model involves the development of a magma reservoir in the upper crust, which proceeds to crystallise until it reaches a crystallinity of ~ 50 %, at which point crystals form a framework with a yield strength which prevents convection. Gas-driven filter pressing and compaction then extract interstitial melt from the mush generating a cupola of crystal-poor,

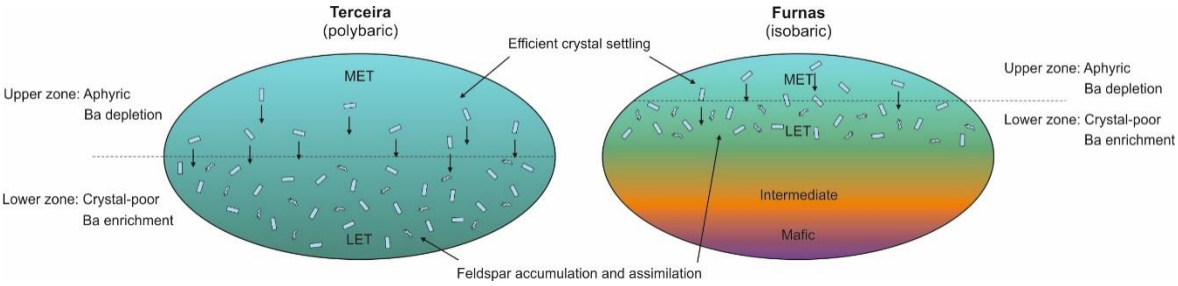

FIGURE 6.4: Schematic models for the general structure of the Pico Alto and Furnas shallow crustal magma reservoir in the context of the efficient crystal settling and its effect upon the compositional zonation of the system

hydrous, peralkaline silicic magma above the mush and below a thermal boundary zone at the top of the reservoir. Once the cupola has formed, the low viscosity of the peralkaline silicic magmas therein allows rapid and efficient fractional crystallisation, allowing the cupola magmas to differentiate further and generating vertical compositional zonation. Crystals settling from higher levels settle into lower levels, where they accumulate and are resorbed, enriching the lower level magmas in Ba and counteracting the development of a negative Eu anomaly. At this stage, the model presented in Figure 6.4 is effectively present within the cupola. The only key difference is that the lowermost layer, which grades into the crystal mush, is not only contaminated by settling crystals, but is also rejuvenated from below by melts which are periodically extracted from the crystal mush. The result is to generate a complex geochemical system in which the compositions of the lower portions of the cupola are driven towards more evolved compositions by limited fractional crystallisation, contaminated by crystals settling from above, and potentially dragged towards less evolved compositions by replenishment. In contrast, the upper portion of the cupola is able to fractionate to the most evolved and crystal-poor magmas in the system.

The compositional evolution of the lower layer of this scheme may be further complicated by the melting of the crystal mush in response to replenishment events. Wolff *et al.* (2015) showed that chemical zonation within the cupola of a crystal mush system could be generated in a closed system through the generation of a new melt within the

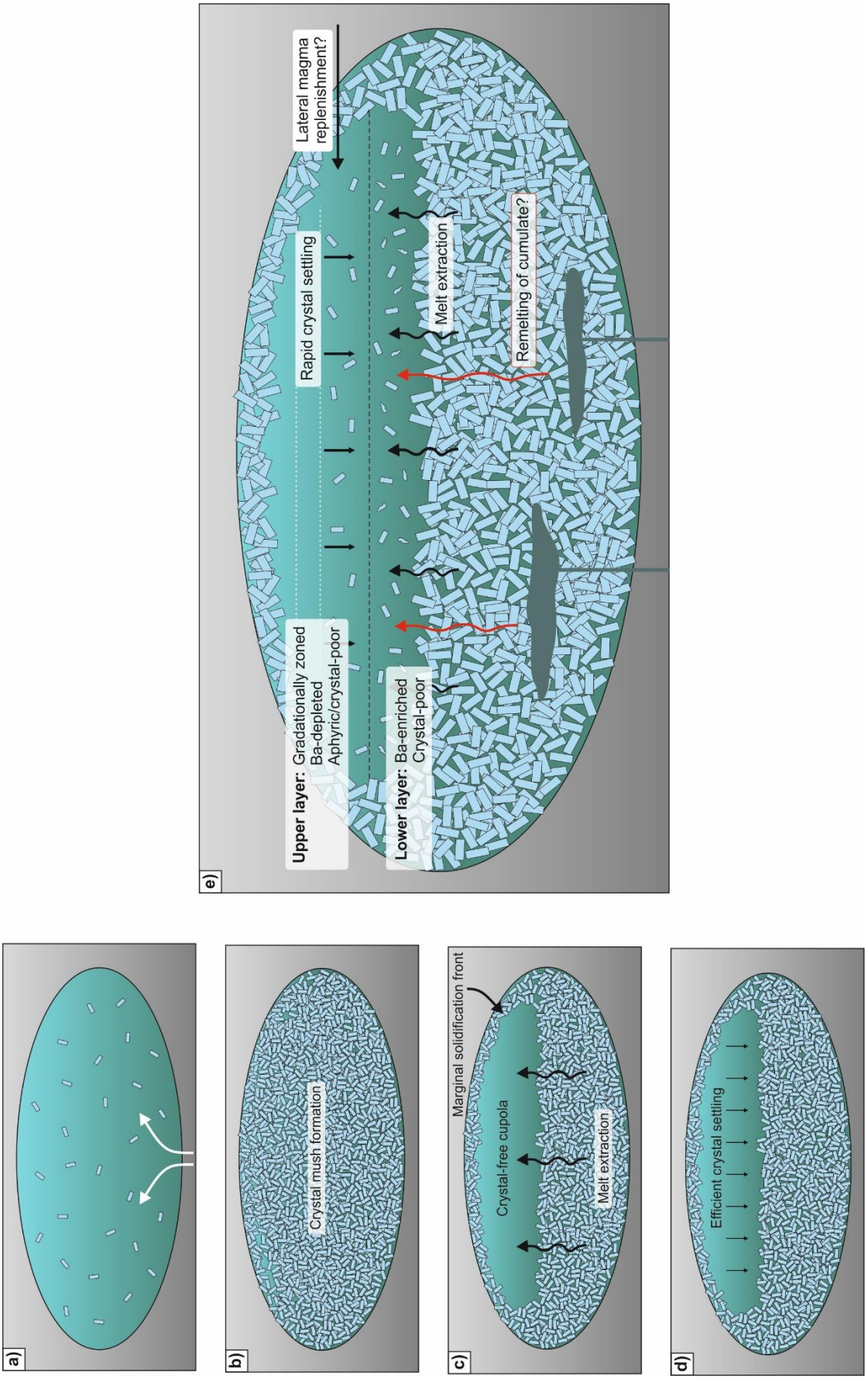
a)
b)
Crystal mush formation
c)
Marginal solidification front
Crystal-free cupola
Melt extraction
d)
Efficient crystal settling
e)
Lateral magma replenishment?
Rapid crystal settling
Melt extraction
Remelting of cumulate?
Upper layer: Gradationally zoned Ba-depleted Aphyric/crystal-poor
Lower layer: Ba-enriched Crystal-poor

◄ **FIGURE 6.5:** Schematic model reconciling the key features of the magmatic plumbing system of Pico Alto and Furnas, with those of the standard crystal mush extraction model (Bachmann and Bergantz, 2004) **a)** Generation of a magma reservoir in the shallow crust followed by crystallisation **b)** Continued crystallisation until critical threshold of ~ 45 to 50 % crystallinity, at which point the crystals form a rigid framework **c)** Interstitial melt is extracted from the crystal mush via compaction and gas-driven filter-pressing, forming a cupola of crystal-poor magma above the mush and below an upper solidification front **d)** Continued crystallisation within the low viscosity peralkaline magmas in the cupola leads to rapid rapid crystal settling and efficient fractional crystallisation **e)** Fractional crystallisation and continued periodic extraction of interstitial melt from the underlying mush leads to a double layer cupola. The upper layer is aphyric to crystal-poor, depleted in Ba, and vertically zoned due to variably efficient crystal settling associated with a downward increase in magme viscosity. The lower layer is enriched in Ba and contains antecrystic, resorbed feldspars as a result of crystal settling from overlying layers. Injection of new replenishing magmas into the crystal mush may provide a heat source for melting of the mush, generating a magma with a comparatively low water content, which may then be extracted and mixed with the low layer of the cupola. The smaller eruption of the UFG and Pico Alto are envisaged to tap only the upper layer, whilst the larger ignimbrite-forming phases may tap deeper portions of the cupola. Syenitic ejecta which are not representative of the mush itself may be sourced from the upper and side solidification fronts. Syenite-hosted hybridised trachytic enclaves may result from lateral replenishment, through the solidification front

crystal mush. They argue that the melting of the crystal mush leads to a melt with the same bulk composition as the mush. This composition is invariably less evolved and lower in water than the residual melts which are extracted from the mush to form the cupola. Their subsequent extraction and addition to the cupola forms a layer of less evolved, less hydrous silicic magma at the interface between the crystal mush and the cupola. The substantial range of pre-eruptive water contents predicted by alkali feldspar-hygrometry for both Pico Alto and Furnas may reflect this process, with the more hydrous magmas representing the residual melt from the mush, and the less hydrous magmas representing the remelting of the cumulate. This remains consistent with the description of the PIF above, where the contrasting compositions of the initial pumice fall and the ignimbrite may reflect this process. Although the syenite ejecta of both Terceira and Furnas are not considered to represent the crystal mush from which the erupted magmas were derived, the presence of clinopyroxene-, amphibole-, and aenigmatite-rich schlieren may provide some evidence for partial remelting melting of a crystal mush, representing portions where alkali feldspar has been melted out. Similarly, the granophyric patches found within the same lithologies may represent small accumulations of this melt, which were unable to migrate further and crystallised upon further cooling, or eruption.

A potential flaw in this model concerns the position of the syenitic thermal boundary zone. In the model presented in Chapter 4, enclave-bearing syenitic ejecta are

considered to record an injection of less evolved, hybridised trachyte into the base of a trachytic magma reservoir. In contrast, the model presented above limits the position of the marginal syenites to the upper and side margins of the cupola. Within the standard crystal mush extraction model, replenishing magmas are considered to be injected into the lower portion of the mush zone, where they then fractionate and may eventually contribute residual liquid to the cupola. The presence of less evolved, replenishing trachytes within the syenites, which, geochemically cannot represent the mush zone, implies that replenishing magmas were able to interact with the cupola directly. Realistically, the only means of achieving this is a more complex model involving lateral transportation of magma into the cupola.

In summary, the presented model provides a means of applying a crystal mush extraction model to the crystal-poor, peralkaline silicic magmas of peralkaline volcanic centres. Although a peralkaline equivalent of the monotonous intermediates has not yet been reported, and despite the low viscosities and high settling rates associated with peralkaline silicic magmas, the application of a crystal mush extraction model may still account for key features of peralkaline magmatic systems, such as the generation of strong compositional gradients in the pre-eruptive reservoir.

6.4 Eruption styles of peralkaline silicic magmas

Despite their broadly similar, peralkaline silicic compositions, the rocks that have formed the focus of this study were erupted via a wide range of mechanisms. For example, the ignimbrites of Terceira were erupted from explosive, 'boil-over' eruptions, some of which included a minor fall component which indicates the presence of an, at least briefly sustained, eruption column. These eruptions stand in stark contrast with the significantly more frequent but smaller scale effusive eruptions of Pico Alto, which generated peralkaline silicic lava domes and coulees, some of which also involved a minor fall component. The peralkaline silicic magmas of the UFG were erupted primarily as pumice falls derived from sustained eruption columns, with some dilute pyroclastic density currents (surges). At least three of the UFG eruptions terminated with the effusive eruption of a lava dome. In contrast, the older caldera-forming eruption of the PIF involved a briefly sustained eruption column and a comparatively voluminous pyroclastic density current.

The origins of such diversity in eruptive behaviour are not well understood, but are likely to be linked to magma composition, volatile content, supply, ascent rates and rheology (e.g. Jaupart and Allègre, 1991; Woods and Koyaguchi, 1994; Barclay *et al.*, 1996; Dingwell *et al.*, 1998; Andújar and Scaillet, 2012 and references therein), as well as physical factors such as vent geometry (e.g. Wilson *et al.*, 1980) and interaction with external water (Self and Sparks, 1978; Kokelaar, 1986). Here, the factors which are likely to play a role in the determination of eruption style of silicic magmas at Pico Alto and Furnas are explored, aiming to place constraints upon the primary processes which lead to this eruptive diversity.

6.4.1 Magma rheology

6.4.1.1 Magma composition

The development of peralkalinity has been shown to reduce melt viscosity (e.g. Dingwell *et al.*, 1998; Giordano *et al.*, 2006; Di Genova *et al.*, 2013; this study). Based upon the

range of peralkalinity indices observed in this study (0.95 to 1.43), eruptive behaviour may be linked directly to major element compositions. Furthermore, a compositional contrast may exist between the effusive and explosive eruptions of both Pico Alto and Furnas. For example, the majority of the effusive eruptions at Pico Alto have pantelleritic compositions (Self, 1974; Mungall and Martin, 1995). In contrast, the whole rock, melt inclusion, and groundmass glass compositions of the seven ignimbrite formations are almost exclusively comenditic trachyte (Self, 1974; Gertisser *et al.*, 2010; Tomlinson *et al.*,, 2015; this study). Similarly, the post-caldera eruptions of the UFG extend to more evolved compositions than those of the caldera-forming PIF. Pre-eruptive magma viscosities calculated for the compositions of this study, assuming a range of water contents (2.1 to 6.2 wt. %) and temperatures (824 to 981 °C), show a total range of $10^{2.7}$ to $10^{4.1}$ Pa s. The viscosity of the pre-eruptive pantelleritic magmas of Pico Alto was estimated using a pantelleritic composition taken from Mungall and Martin (1995), for the same range of water contents, assuming a temperature that is typical of pantelleritic magas (750 °C, cf. Macdonald, 2012), and range from $10^{3.7}$ to $10^{5.1}$ Pa s. This range is somewhat higher than that of the rocks of this study and indicates that any effect of composition and enhanced peralkalinity upon the rheology of the melt during evolution from comenditic trachyte to pantellerite is countered entirely by the associated decrease in temperature and associated melt polymerisation. Even if the water content of the melt is increased to a hypothetical value of 7 wt. %, melt viscosity remains higher than $10^{3.3}$ Pa s, suggesting that, on Terceira, the pre-eruptive viscosities of the effusively-erupted pantellerites were comparable to or somewhat greater than those of the explosively erupted comenditic trachytes. Similarly, the UFG trachytes extend to somewhat higher viscosities than the PIF-forming trachytes ($10^{2.7}$ to $10^{4.1}$ vs. $10^{2.9}$ to $10^{3.4}$ Pa s, respectively). As such, the most evolved compositions from both volcanic centres are likely to have had pre-eruptive magma viscosities that were similar to, or slightly greater than, those of the less evolved magmas. It is feasible that the potential transposition of the more evolved magmas towards higher viscosities may play a role in eruptive behaviour, by slowing magma ascent and enhancing the role of

outgassing through the conduit walls. However, the results of this study indicate that the pantellerites of Pico Alto are the product of continued differentiation of the comenditic trachytes, meaning that their pre-eruptive water contents are likely to be greater than , or at least equal to, those of the comenditic trachytes (~ 5 to 6 wt. %). As such, the lower portion of the calculated viscosity range is probably most applicable for the pantelleritic magmas, suggesting that the fractional crystallisation-induced increase in water content (and increasing peralkalinity) may counteract the effects of temperature decrease on viscosity, leaving the pantellerites with very similar viscosities to the ignimbrite-forming trachytes. The potential effects of magma composition alone are therefore considered to be limited, and of secondary importance.

6.4.1.2 Magma degassing

The viscosity of magma may be increased by decompression-induced degassing and associated crystallisation during ascent (e.g. Sparks, 1978; Papale, 1999), facilitating permeable outgassing. To investigate the rheological changes induced by degassing, isothermal magma viscosities were calculated for each of the ignimbrite-forming trachytes and a pantelleritic composition (taken from Mungall and Martin, 1995) from Pico Alto, and the trachytes of the UFG and the PIF from Furnas, over water contents ranging from 0 to 6 wt. %. Crystal fractions were set to 0.2. Results indicate that during degassing, the silicic magmas of both Pico Alto and Furnas increase in viscosity by up to ~ 4 orders of magnitude (Figure 6.6a, b). However, the maximum viscosity attained ($10^{7.5}$ Pa s) is below the typically applied threshold for brittle fragmentation (10^{8} to 10^{9} Pa s; Papale, 1999; Giordano *et al.*, 2009), suggesting that degassing alone cannot account for the explosive eruptions of Pico Alto and Furnas.

During degassing, the magma liquidus temperatures increase, promoting the crystallisation of microlites which leads to an increase in magma viscosity (e.g. Sparks

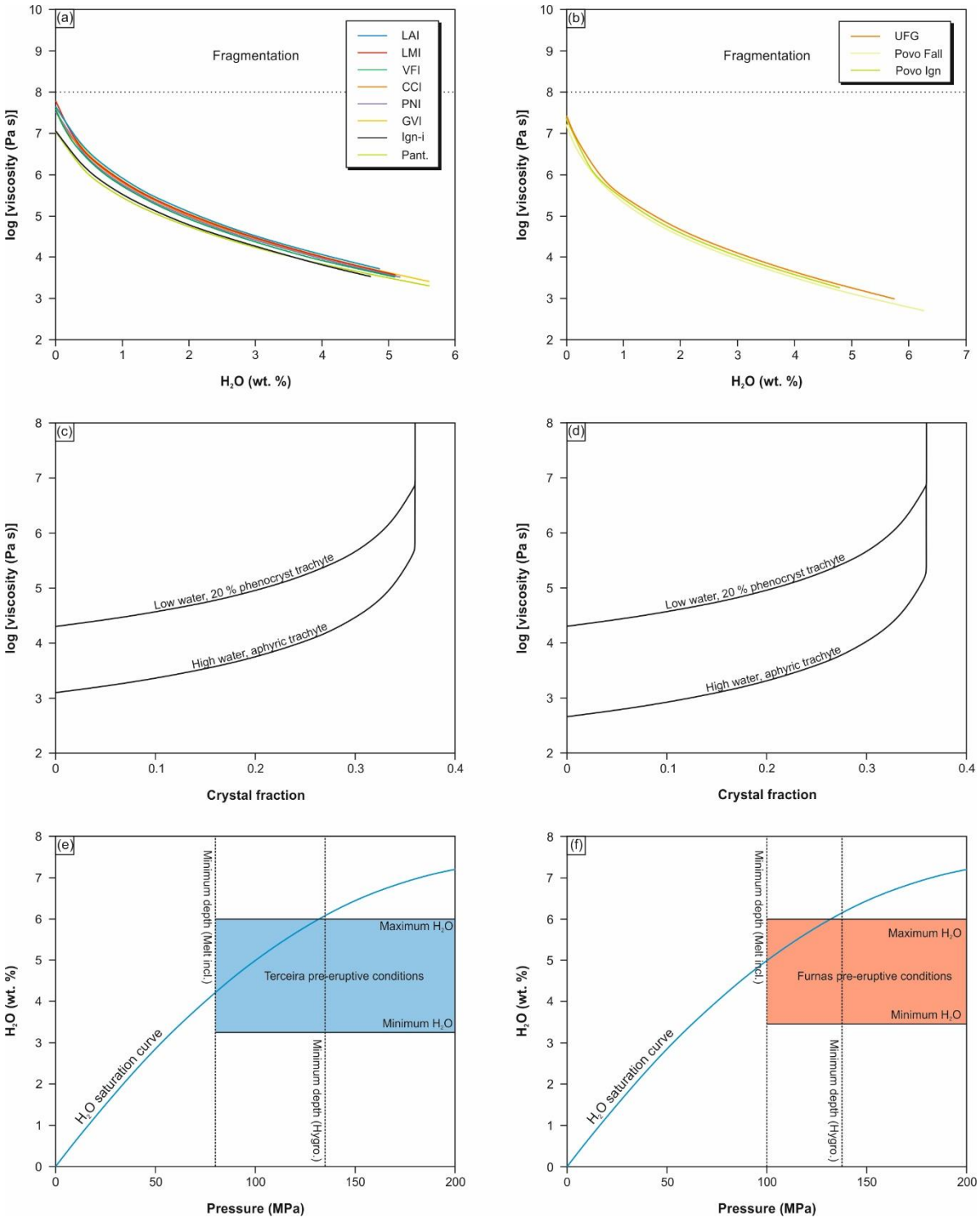

FIGURE 6.6: Results of rheological modelling **a)** Calculated magma viscosity changes during deagassing of Terceira trachytic and pantelleritic compositions, assuming a crystal fraction of 0.2 **b)** Calculated magma viscosity changes during degassing of Furnas trachytic compositions, assuming a crystal fraction of 0.2 **c)** Plot showing the increase in magma viscosity associated with microlite crystallisation for Terceira magmas, using the model of Vona *et al.*(2011) **d)** Plot showing the increase in magma viscosity associated with microlite crystallisation for Furnas magmas, using the model of Vona *et al.* (2011) **e)** The P-H_2O conditions of the Terceira lithologies in relation to the calculated H_2O solubility curve **f)** The P-H_2O conditions of the Furnas lithologies in relation to the calculated H_2O solubility curve

and Pinkerton, 1978). The effect of such crystallisation upon magma viscosity relates to crystal abundance, size, shape, packing density, and the shear strain of the magma (e.g. Llewellin *et al.*, 2002; Caricchi *et al.*, 2008; Costa *et al.*, 2009; Di Genova *et al.*, 2013). To explore the effects of syn-eruptive, degassing-induced crystallisation on the rheology of the comenditic trachytes of Pico Alto and Furnas, the viscosities of bubble-free, crystal-bearing magmas have been calculated using the model of Vona *et al.* (2011), following Di Genova *et al.* (2013). Models were run for the minimum and maximum pre-eruptive melt viscosity estimates from this study ($10^{2.7}$ and $10^{4.3}$ Pa s, respectively). In each case the strain rate was set to $\gamma = 1\ s^{-1}$, the crystal fraction was varied from 0 to 0.4, and the mean crystal aspect ratio was set to 7 (Hammer and Rutherford, 2002). Results indicate that during the course of crystallisation, magma viscosity increases by 2.6 log units before approaching infinite values at a crystal fraction of ~ 0.36 (Figure 6.6c, d). The rate of viscosity increase is non-linear and the greatest viscosity increase occurs above crystal fractions of ~ 0.3 (cf. Di Genova *et al.*, 2013). Although this increase in viscosity is insufficient to reach the thresholds of brittle fragmentation, when considered alongside the effects of degassing, as demonstrated above, the overall magma viscosity may reach values as high as ~ 10^{10} Pa s, facilitating brittle fragmentation.

6.4.2 Volatile saturation and magma ascent

Another potential factor which must be considered is the pre-eruptive water content of the magmas which, based upon melt inclusions and alkali feldspar-melt hygrometry, show a substantial range, both within and between individual eruptions (total range 2.1 to 6.2 wt. %). Considering the prevalence of fractional crystallisation as a late-stage differentiation mechanism within the trachytes (see above), as well as the highest predicted water contents being associated with the lowest estimated pre-erupted temperatures, it is likely that this range of water contents is attributable to the variable degree of crystal fractionation. This is consistent with the described evidence for pre-eruptive zonation in

the magma reservoir, and may be further enhanced by upward migration of a vapour phase. Such a process could also account for the transition from a stable eruption column to lava flow/dome formation (e.g Furnas J), implying the presence of a volatile-enriched cap in the reservoir. This could also account for the occurrence of minor basal pumice fall units associated with ignimbrite-forming episodes (cf. Gertisser *et al.*, 2010), as well as the highly evolved pantelleritic trachytic composition of the VFI basalt pumice fall.

Andújar and Scaillet (2012) concluded that the primary controlling factors in the determination of the eruptive behaviour of phonolitic and trachytic magmas are the water content of the magma, the depth of magma storage, and the relative distance of the magma from water-saturation. Although the precise depth of the shallow magma reservoirs of Pico Alto and Furnas cannot be constrained by the results of this study, their broad position within the crust can be restricted to shallow crustal pressures of at least ~ 80 or ~ 130 MPa for Pico Alto, and at least 100 or 132 MPa for Furnas. At these depths, the water contents of the magmas extend from the water saturation curve (calculated following Di Matteo *et al.*, 2004) to ~ 3 wt. % below it (Figure 6.6e, f). At Pico Alto, the pantelleritic magmas which were erupted effusively (with some associated pumice falls) are, as suggested by this study, the result of continued differentiation from less evolved comenditic trachytes (such as the ignimbrite-forming trachytes). Assuming no significant degassing (cf. Mungall and Martin, 1995), then it follows that they are, in contrast to the ignimbrite-forming trachytes, likely to have been restricted to near-water saturated conditions. As such, there may be a correlation between eruptive behaviour and distance to water saturation, in which the more differentiated and more hydrous magmas appear to have erupted primarily via effusive eruptions (and some associated initial pumice falls), and the less evolved, water-undersaturated to saturated magmas are erupted as comparatively large volume, explosive, ‘boil-over’ eruptions. Physical factors such as syn-eruptive vent-widening and interaction with external water are unlikely to account for this contrast. Instead, it is suggested here that the contrasting eruptive behaviour of these magmas is linked to their rates of ascent in the conduit, which is itself controlled by the

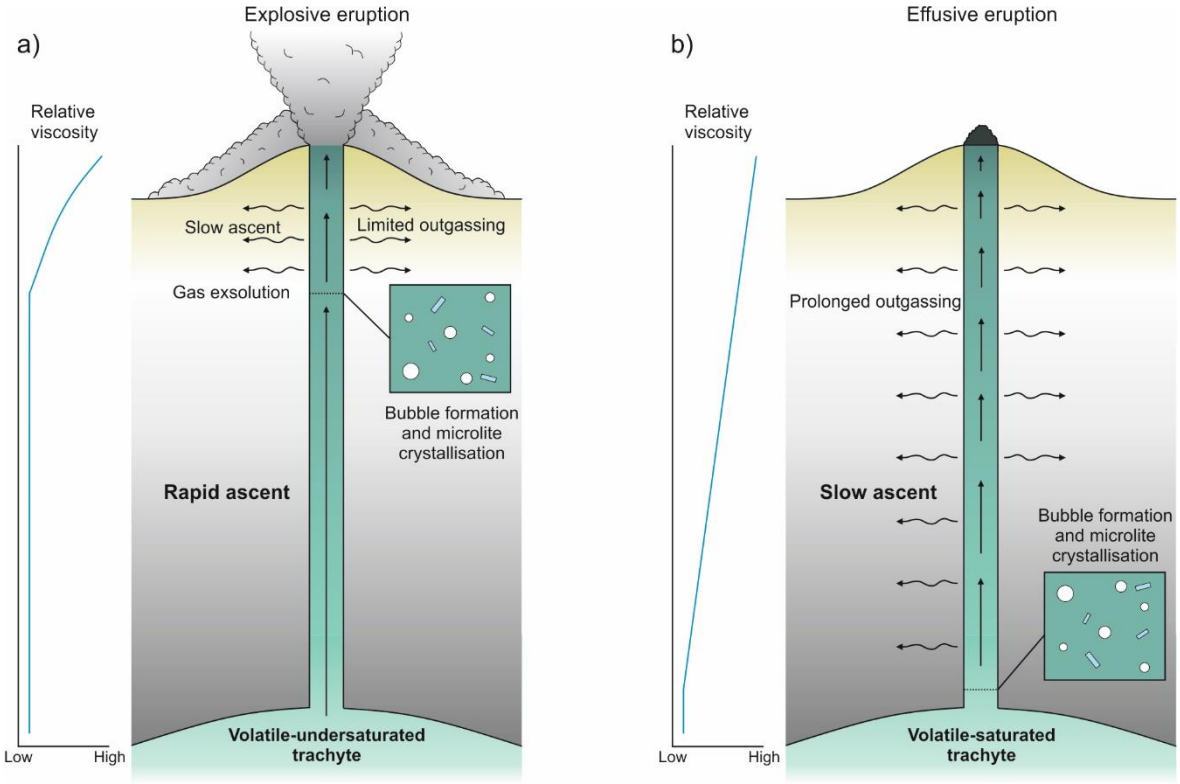

FIGURE 6.7: Schematic model for the contrasting eruptive behaviour of peralkaline silicic magmas in relation to their proximity to water saturation

degree of water undersaturation of the magma (Figure 6.7). The more evolved pantelleritic magmas are likely to be water saturated to oversaturated, and will therefore exsolve water rapidly in response to ascent. This is envisaged to promote a rapid increase in viscosity, due both to the loss of volatiles and degassing-induced crystallisation, which slows the rate of ascent. Furthermore, this process would effectively drive itself, as the slow ascent rates allow further degassing and associated crystallisation. In contrast, the ignimbrite-forming magmas are likely to have been undersaturated, delaying the initiation of water exsolution during ascent according to the degree of undersaturation. This delay is envisaged to allow rapid ascent with little outgassing, which allows the magmas to reach the surface with a greater proportion of their volatile budgets, and limited microlite crystallisation. This is consistent with the relative lack of microlites observed in the pumices of the ignimbrites. The apparent tendency for these eruptions to 'boil-over' may reflect the general difficulty of these magmas to achieve the viscosities required for fragmentation, due to the transposition of their viscosity range towards lower values than

those of metaluminous rhyolitic systems, despite the extremely late stage exsolution of bubbles and associated viscosity increase (e.g. Gonnermann and Manga, 2007).

Although this model can successfully account for the observed eruptive behaviour of Pico Alto, its application to Furnas is complicated by the almost exclusively explosive behaviour of the volcano. In contrast to the comparatively high-frequency, pantelleritic eruptions of Pico Alto, the high-frequency post-caldera eruptions of the UFG are likely to have been as explosive as the caldera-forming activity, albeit on a significantly smaller scale. As such, the magmatic system of Furnas clearly has an affinity for explosive activity compared to Pico Alto, which must be accounted for through some key difference in their magma plumbing system, magma composition, or external features. Despite their contrasting eruptive behaviour and scales, the eruptions of the UFG and the PIF exhibit a similar range of pre-eruptive water contents, and were similarly water-undersaturated to -saturated. Although the trachytes of the UFG have been shown to result from continued differentiation of PIF trachytes, the compositional contrast between them is less pronounced than that of the Pico Alto trachytes and pantellerites. Furthermore, calculated pre-eruptive viscosities for each formation span a similar range ($10^{2.7}$ to $10^{4.1}$ for the UFG, and $10^{2.9}$ to $10^{3.4}$ for the PIF), suggesting that the magmas of each formation were very similar in their compositions, volatile contents, and rheology. Thus, additional factors must be acting within the system to ensure regularly explosive behaviour.

One feature which should be considered is the depth to the shallow crustal magma storage zone. Although the results of this study have restricted shallow crustal magma storage beneath both Pico Alto and Furnas to pressures of ~ 100 to ~ 150 MPa, Andújar and Scaillet (2012) highlighted the strong control of depth over eruptive behaviour, even within the relatively restricted range of 0 to 200 MPa. As such, a small variation in the depth of the shallow storage zone that is below the resolution of this study may play a role in the eruptive dynamic of Furnas magmas, with shallower storage conditions favouring explosive eruptions.

An alternative to this hypothesis is the interaction of ascending magmas with external water. The deposits of the UFG exhibit abundant evidence for interaction with water during eruption, with only a single eruption comprising exclusively magmatic activity (Furnas H). This feature is generally attributed to the interaction of ascending magmas with one or more lakes within the caldera complex, and is considered to be somewhat characteristic of the volcano, at least during its most recent (< 5 ka) history (Cole *et al.*, 1999). However, this is also likely to include interaction with the hydrothermal system of the volcano (Ferreira and Oskarsson, 1999; Oskarsson *et al.*, 1999; Pasquier-Cardin *et al.*, 1999). Evidence for surface manifestations of hydrothermal activity are limited to a single locality on Pico Alto (Furnas do Enxofre, Henneberger *et al.*, 2004), suggesting that the subsurface hydrothermal system may be less developed compared to Furnas, where fumarole fields and soil degassing is comparatively abundant. Furthermore, the topographically-positive structure of Pico Alto stands in stark contrast with the lake-filled caldera of Furnas, preventing the accumulation of significant volumes of surface water. It is therefore suggested that the eruptive dynamic of Furnas is greatly affected by external factors, which are themselves a product of the topography and geography of the volcano. The implication is that any eruptive dynamic that has been pre-determined primarily by the volatile content, degree of volatile undersaturation, and storage depth, as well as secondary factors such as magma rheology, has been overprinted by the late-stage interaction with water. In contrast, the eruptions of Pico Alto are likely to better represent the eruptive dynamic brought about by the internal conditions of the magmatic system and the magmas stored therein. The transitions from explosive to effusive eruption styles observed in at least three of the UFG eruptions may therefore reflect a lower volatile content in the last-erupted trachytes (as suggested by zoned magma bodies), or the exhaustion of an external water supply which induced explosive behaviour, or a combination of the two.

6.5 Implications for future research

The results of this study have highlighted a number of additional research questions which may further contribute to the regional scale understanding of the magmatic plumbing systems of Terceira and São Miguel, and also to the wider implications for the structure and evolution of peralkaline magma systems and the petrogenesis of peralkaline silicic rocks. Here, a number of potential topics for future research are discussed in light of the results presented in this thesis.

6.5.1 Eruption styles of peralkaline silicic magmas

The results of this study indicate that the primary eruptive dynamic of the peralkaline silicic magmas of Pico Alto and Furnas is linked to the degree of pre-eruptive volatile saturation. The primary eruptive dynamic may then be overprinted by external factors such as interaction with external water, as proposed for Furnas. In addition to volatile content, the precise depth of magma storage is intrinsically linked to the degree of volatile undersaturation, and so the eruptive behaviour (Andújar and Scaillet, 2012). However, the level of precision required to adequately consider pressure variations as a controlling factor in the determination of eruption style of magmas ascending from a shallow crustal (< 200 MPa) reservoir cannot be achieved by conventional thermobarometric models, which frequently have uncertainties of ± 100 to 200 MPa (Putirka *et al.*, 1996; Putirka, 2008). Furthermore, the trachytes of both Pico Alto and Furnas (as well as Sete Cidades, Beier *et al.*, 2006) have been shown to contain clinopyroxene populations which are not suitable for thermobarometry due to clear disequilibrium with their host melt. A viable alternative which may provide high resolution barometric data is a detailed study of fluid inclusions in the trachyte-hosted alkali feldspars. This would allow the accurate (± 1 MPa, Zanon and Pimentel, 2015) reconstruction of the depths of the shallow crustal magma storage zone of both Pico Alto and Furnas, and could also be applied to the syenitic ejecta (Figure 6.8). Furthermore, the extension of this study to basaltic eruptive products from

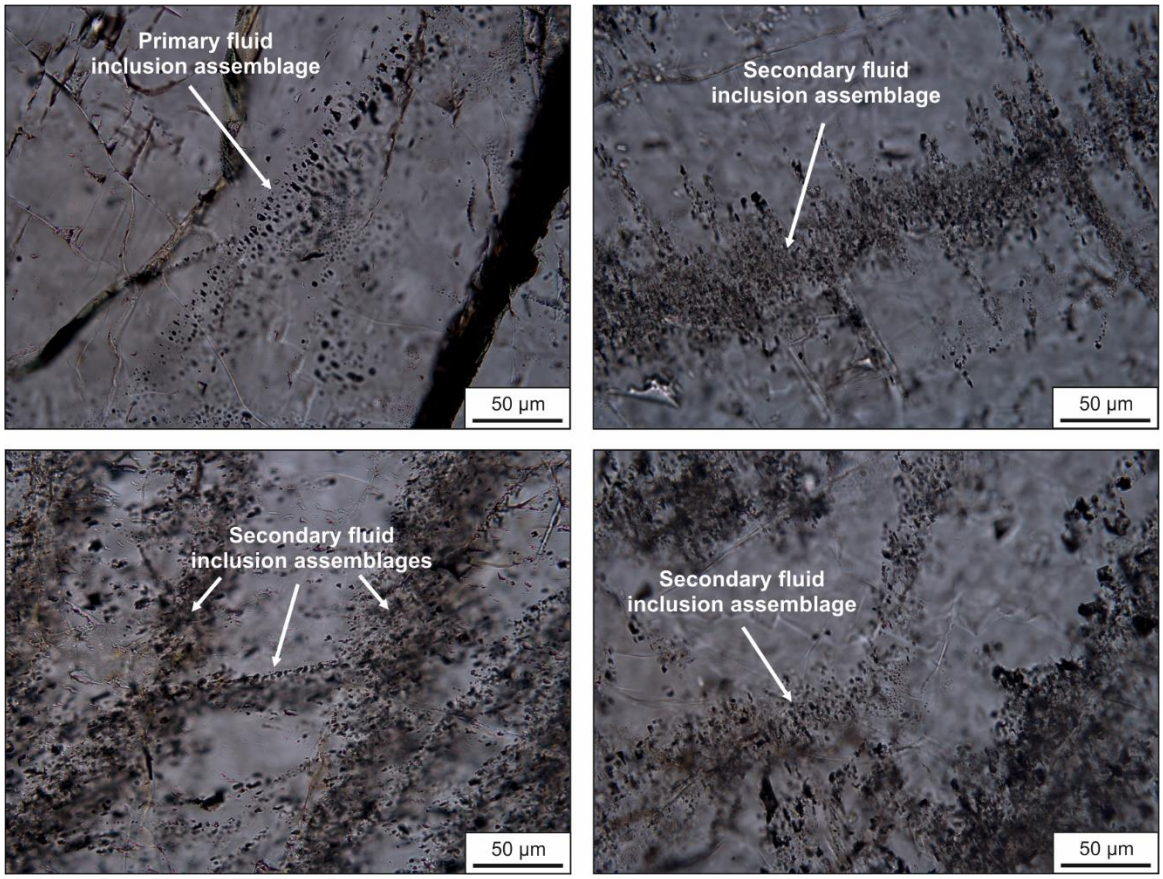

FIGURE 6.8: Examples of complex fluid inclusion assemblages in alkali feldspar crystals from the CCi syenite ejecta of Pico Alto

the flanks of Furnas may help to better characterise the architecture of the underlying magmatic system, beyond the constraints placed upon it by this study.

6.5.2 Quantifying the role of crustal assimilation

The results of this study indicate that the partial melting of crustal lithologies cannot account solely for the origins of the peralkaline trachytes of both Pico Alto and Furnas. However, a role for crustal assimilation during storage cannot be ruled out. Indeed, many studies have highlighted a role for crustal assimilation in the petrogenesis of peralkaline silicic rocks (e.g. Civetta *et al.*, 1984; Novak and Mahood, 1986; Davies and Macdonald, 1987; Macdonald *et al.*, 1994, 1995; Troll and Schmincke, 2002; Ayalew and Yirgu, 2003; Peccerillo *et al.*, 2003; Lowenstern *et al.*, 2006; White *et al.*, 2006). The investigation of the Sr-Nd-O isotopic compositions of the peralkaline rocks of Furnas and Pico Alto would

allow the identification and, via AFC modelling (DePaolo, 1981), quantification of any pre-eruptive crustal assimilation. For example, the Fogo A deposit was shown isotopically by Snyder *et al.* (2004) to have been contaminated by assimilation of seawater-altered syenitic wall rock, as well as to have gained xenocrystic feldspars. The general similarity between the magma systems of Furnas and Fogo, such as the occurrence of syenitic xenoliths, hybridised magmas, and shallow crustal reservoirs (e.g. Storey *et al.*, 1989; this study) suggests that similar processes are likely to be operating in the shallow crustal magma system, and may play a role in the evolution and eruption of the peralkaline silicic magmas of Furnas.

6.5.3 Late stage evolution of peralkaline magmas recorded by syenitic ejecta

The syenite ejecta of this study are considered to represent the near-complete solidification of peralkaline silicic magmas at shallow crustal depths. As shown by the complex mineral assemblages of the syenites, the continued differentiation of peralkaline silicic magmas leads to residual liquids that are enriched in volatiles, alkalis, REE, and HFSE. These elements may then be deposited as a variety of minerals such as dalyite, eudialyte, chevkinite-(Ce), britholite-(Ce), and pyrochlore (e.g. Ridolfi, 2004), by the late-stage release and migration of an orthomagmatic fluid into the roof zone of the magma reservoir, where mixing with resident fluids promotes precipitation (Mungall and Martin, 1996). The syenitic ejecta of Pico Alto and Furnas are likely to be representative of this roof zone, and may therefore be considered to be the active analogue of larger peralkaline intrusive complexes such as Tamazeght, Morocco (e.g. Salvi *et al.*, 2000), and Strange Lake, Canada (e.g. Mungall and Martin, 1996). As such, the detailed study and characterisation of the REE- and HFSE-bearing mineral assemblages of the Azorean syenites may provide insights into the processes through which such deposits form, which may then be related directly to overlying volcanism of the system, an approach which clearly cannot be applied to currently exposed intrusive complexes (e.g Macdonald *et al.*,

2014). In essence, the syenitic suite of both of the case studies applied in this work may record the late-stage magmatic to hydrothermal transition, and, when coupled with the magmatic petrogenetic schemes of this study, may allow the complete reconstruction of the magmas history, from primary basalt to syenitic intrusion.

6.5.4 Syn-eruptive processes of the Furnas J eruption

The eruptive sequence of the Furnas J eruption provides an ideal opportunity to investigate the syn-eruptive degassing processes of mildly peralkaline trachytic magma. As described above, the deposits of Furnas J comprise at least six discrete pumice falls, intercalated with ash-rich layers (Cole *et al.*, 1995). A detailed textural study of the pumices from each of the pumice fall units would provide insights into processes of decompression-driven gas exsolution, expansion, and escape which play a critical role in eruptive behaviour (e.g. Shea *et al.*, 2010a, 2010b; Houghton *et al.*, 2010), and as well as magma ascent rates and fragmentation. Critically, the investigation of each unit would allow these processes to be evaluated temporally, from the beginning to the final stages of the eruption. This could be easily supplemented by the detailed eruption narrative provided by Cole *et al.* (1995). Furthermore, the results presented in this study provide estimates for a number of pre-eruptive magmatic intensive variables (e.g. T, P, H_2O_{melt}, magma viscosity), which, through their control upon the growth and nucleation rates of exsolving gas bubbles, will not only contribute to the interpretation of vesicle size distributions, but could also provide primary inputs for 1-dimensional conduit modelling (e.g. Melnik and Sparks, 2002; Koyaguchi, 2005; Koyaguchi *et al.*, 2008; Kozono and Koyaguchi, 2009). Ultimately, this would allow further constraints to be placed upon the factors controlling transitions from variably explosive to effusive eruptive behaviour in peralkaline silicic magmas.

Preliminary textural investigation has already indicated a transition from lower to

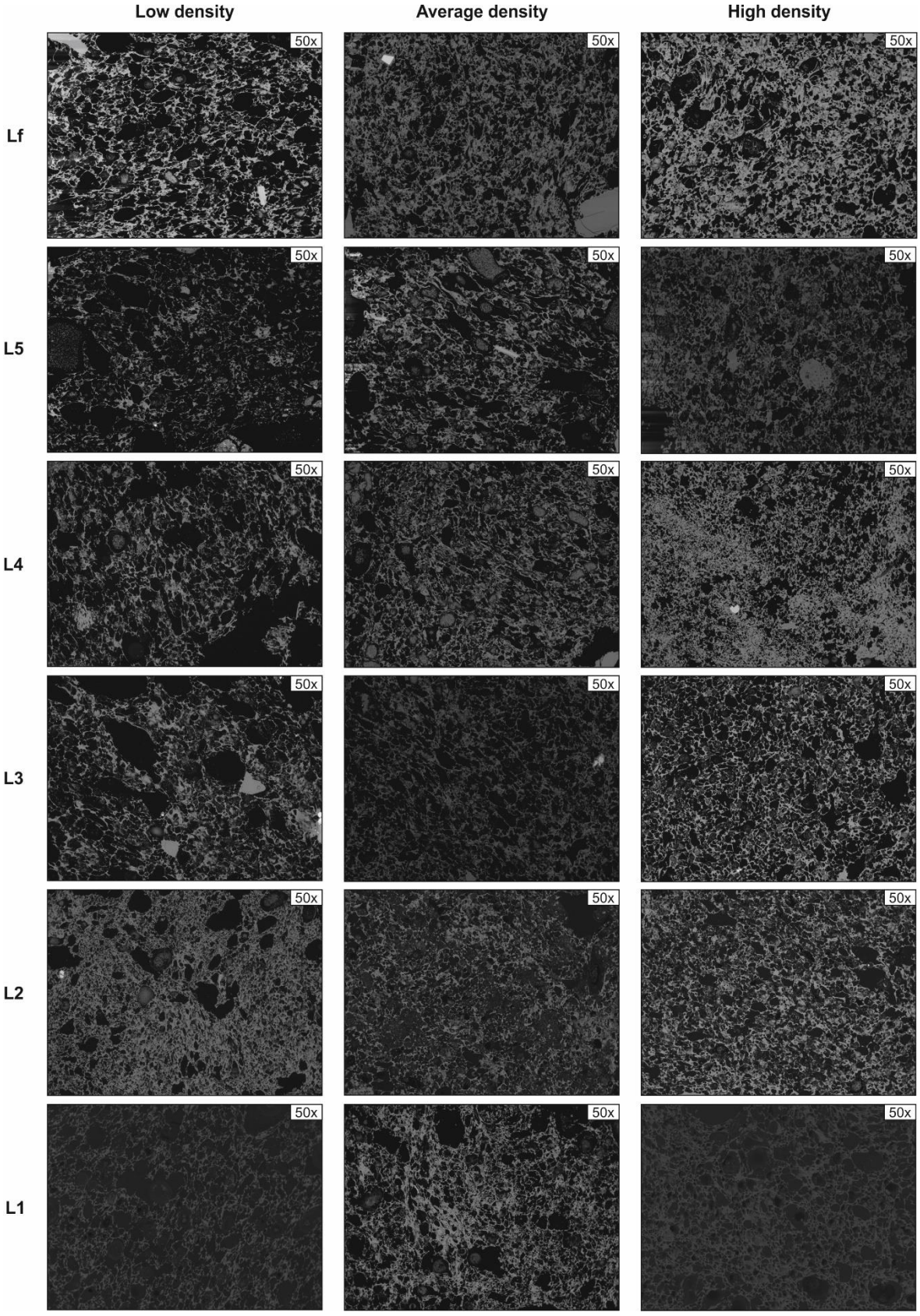

FIGURE 6.9: Representative BSE images of low, average, and high density pumice clasts from each of the pumice fall units of Furnas J. The density classiciations are based upon the histograms given in Figure 6.10, with the low and high density clasts being derived from the lowest and highest density bins of the relevant histogram, respectively.

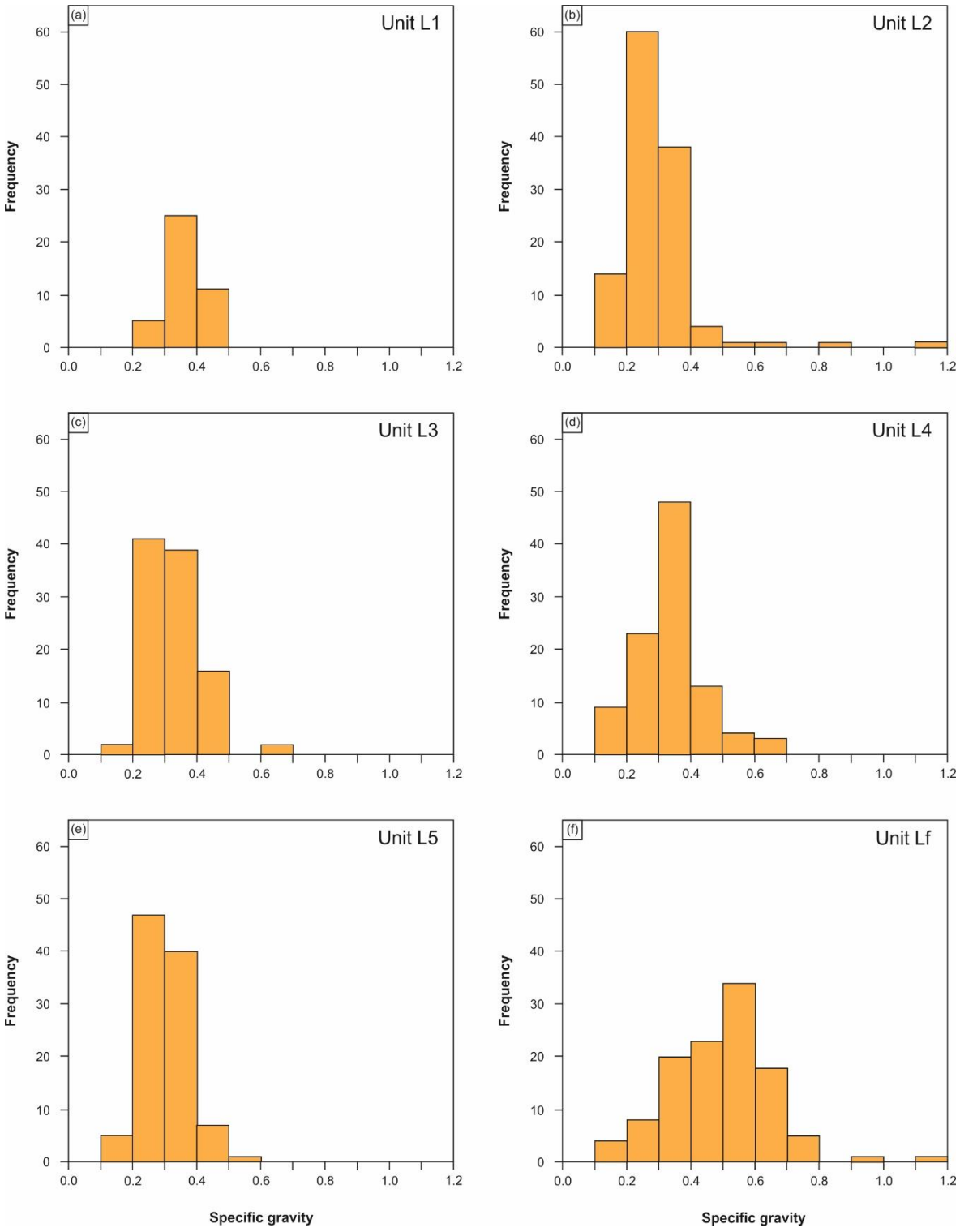

FIGURE 6.10: Density histograms for pumice clasts from each of the pumice fall units of the Furnas J eruption (Furnas L1 to Furnas Lf)

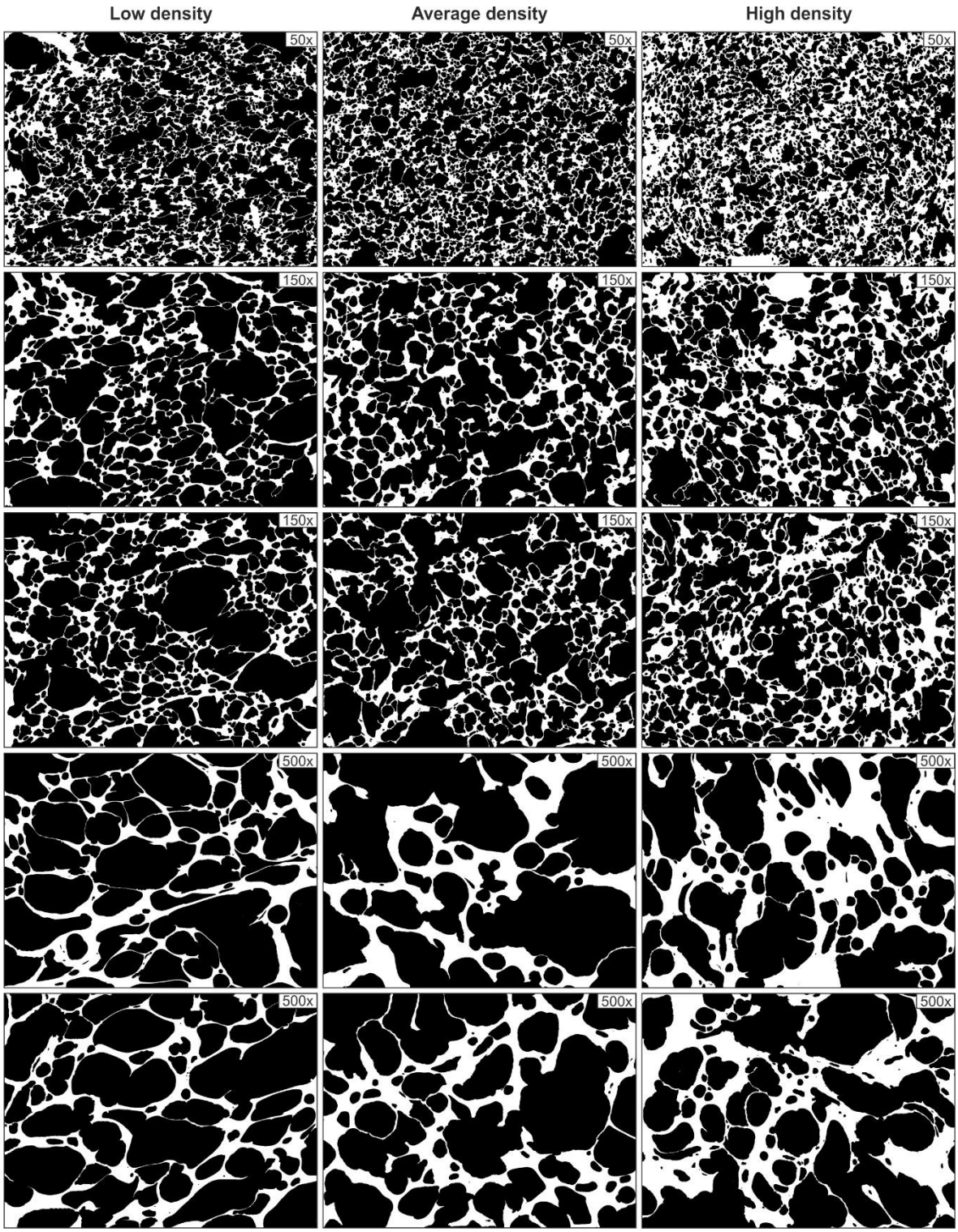

FIGURE 6.11: Representative, digitally reconstructed back-scattered electron images of variably dense pumice clasts from the Lf pumice fall unit of the Furnas J eruption. The density classiciations are based upon the histograms given in Figure 6.10, with the low and high density clasts being derived from the lowest and highest density bins of the relevant histogram, respectively.

higher density pumice clasts throughout the eruption, with the final unit (Lf) exhibiting a wider variety of pumice densities, which may reflect decreasing volatile content of the

tapped magma throughout the eruption (as proposed in Chapter 5) (Figures 6.9, 6.10). This density variation may correspond to a textural shift from highly vesicular pumices with significant bubble coalescence, towards lower vesicularity pumice clasts, with a lesser degree of bubble coalescence (Figure 6.11). These observations may be strongly linked to the temporal evolution of the eruptive behaviour through the increase in magma permeability and therefore outgassing during ascent (e.g. Stasiuk *et al.*, 1996; Melnik and Sparks, 1999; Tuffen *et al.*, 2003; Gonnermann and Manga, 2003, 2012; Mueller *et al.*, 2008). As such, a textural study of the Furnas J eruption may provide direct insights into the controls on eruptive behaviour, and feed directly into the models proposed in this work.

6.5.5 Trachytic eruptions of the Picos and Congro Fissure zones

During the course of this study, the theory of a shadow zone extending from Furnas to neighbouring Fogo has been discussed, based upon the apparent cessation of basaltic activity within the Congo Fissure zone during the last 5 ky (see Section 5.6.6; Machado, 1972; Booth *et al.*, 1978). The occurrence of a small number of young (~ 3.8 ka) trachytic eruptions within the same fissure zone may provide evidence for the lateral extension of the shallow crustal trachytic magma plumbing system of Furnas and/or Fogo into the Fissure zone (Moore, 1990). However, the occurrence of similarly limited trachytic eruptions within the considerably larger Picos Fissure zone is more difficult to account for using such a model (J. M. Pacheco, personal communication). The occurrence of trachytic magmas within the basaltic fissure systems therefore reflects an unanswered question, and may reflect either the capability of ascending basaltic magmas to stall and differentiate in the upper crust, or to generate silicic magmas by partially melting the crust. Furthermore, it is unclear why this occurrence of trachytic magmas appears to be limited to the most recent history of São Miguel, or how this phenomenon relates to the three trachytic centres of the island.

It is therefore suggested that a petrological study of the fissure zone trachytes, using a similar approach to that employed in Chapter 5, could place constraints upon their petrogenesis and conditions of storage, as well as allowing the direct comparison of the young trachytes of the three central volcanoes. This could have direct implications not only for the temporal evolution of the fissure zones themselves, but also for the evolution of the island as a whole. If ascending magmas are capable of stalling beneath the fissure zones, could the fissure zones plumbing systems begin to evolve into central caldera-forming volcanoes, such as Fogo, Furnas and Sete Cidades?

6.5.6 Caldera cyclity of Furnas volcano

In Section 5.6.7, a model was proposed in which the shallow crustal magmatic plumbing system of Furnas evolves in a cyclic manner, involving a developmental stage in which individual magma pockets form and erupt individually, a caldera-forming stage in which magma pockets coalesce and produce a single, larger eruption, and a re-establishment phase in which the plumbing system must be recharged with trachytic magmas derived from fractional crystallisation before any further eruptions. The validation of such a model will clearly require further research, and it is suggested here that the further petrological study of the deposits of the Middle and Lower Furnas Groups, and direct comparison with the Upper Furnas Group (UFG) represents the most promising approach. In particular, deposits which are representative of the three stages inferred in this study should be targeted. For example, the pre-Povoação Amoras, Albufeira, and Cavaleiro Formations include multiple units composed of stratified pumice and ash fall deposits similar to those of the UFG (Guest *et al.*, 1999). A stratigraphically constrained geochemical study of these fall units may identify similarly varied trace element compositions (interpreted here as indicative of either the cyclical formation, eruption, and reformation of an eruptible cupola of highly differentiated magma, or the sequential eruption of multiple discrete magma bodies), which would provide evidence for the magmatic plumbing system which

fed the majority of the LFG eruptions having been similar to that which fed the UFG eruptions. Similarly, a more detailed investigation of the Povoação Ignimbrite Formation (PIF), and potentially the less well understood ~12 ka caldera-forming event, would place greater constraints upon the compositional variability of the larger, caldera-forming episodes of Furnas, and allow the determination of whether they are erupted from single or multiple reservoirs.

CHAPTER 7: SUMMARY AND CONCLUSIONS

7.1 Chapter outline

The conclusions of this study are provided within the following three sections, where they are related directly to the four principal aims of the study, as given in Section 1.4. In Section 7.2, aims 1 and 2 are addressed with a summary of the results of a detailed petrological investigation into the petrogenetic processes and pre-eruptive P-T-fO_2-*X* conditions of the magmatic plumbing systems of Pico Alto and Furnas. Aim 3 is addressed in Section 7.3, where the results of a comparative study between both Pico Alto and Furnas, and other peralkaline silicic centres within the Azores archipelago and worldwide are summarised. Finally, Section 7.4 addresses aim 4 by summarising the proposed models for the eruptive behaviour of peralkaline silicic magmas.

7.2 The magmatic systems of Pico Alto and Furnas

The silicic magmas of Pico Alto and Furnas show a compositional range from metaluminous trachyte to comenditic trachytes and pantellerites, with peralkalinity indices between 0.94 and 1.43. In both cases, the least evolved trachytic magmas are generated primarily via extended (~ 65 % from parent) fractional crystallisation of a hydrous (~ 1.5 wt. %), mantle-derived basaltic parental magma, with crystallisation histories dominated by clinopyroxene at mafic compositions, and plagioclase feldspar at intermediate compositions. The most evolved compositions are then generated by continued fractionation (up to ~ 95 % from parent) of an assemblage which is invariably dominated by alkali feldspar. Pre-eruptive water contents range from 2.1 to 6.2 wt. %, and correlate negatively with temperature. Similarly, halogen concentrations in melt inclusions exhibit a positive correlation with both SiO_2 and calculated peralkalinity indices, indicating volatile undersaturated conditions in which volatile concentrations are controlled primarily by fractionation. Comparison of halogen concentrations within melt inclusions and groundmass glass suggest that Cl and F were generally not degassed during eruption.

The underlying magma plumbing system of both volcanic centres is shown to comprise a magma storage zone at shallow crustal depths (~ 2.5 to ~ 4 km), in which silicic magmas are stored and fractionate towards more evolved and more peralkaline compositions. The presence of these shallow reservoirs inhibits the ascent of mafic and intermediate magmas, generating a compositional Daly gap at both volcanic centres. The magmatic plumbing system of Pico Alto also includes a lower crustal (~ 14 km) magma storage zone, in which mantle-derived basalts fractionate towards broadly hawaiitic compositions prior to further ascent. Evidence of a similar lower crustal reservoir beneath Furnas is more limited, but its presence cannot be entirely discounted.

The eruptive products of both volcanoes contain variably abundant syenitic ejecta, which represent *in-situ* crystallisation of peralkaline silicic magmas in a thermal boundary zone at the margins of the shallow crustal magma reservoir. Phase assemblages of these

ejecta range from miaskitic to agpaitic, and include the rare zirconsilicate dalyite. Evaluation of dalyite's compositional variability, including published analyses from various lithologies, indicate the prevelence of Na↔K substitution in peralkaline granites and syenites, and the dominance of Ti↔Zr substitution in potassic peralkaline rocks. The degree of observed Na↔K substitution within the dalyite of this study is linked to a K-enrichment trend of interstitial melt induced by pore wall crystallisation of Na-rich alkali feldspars and sub-solidus albitisation, coupled with the variation in nucleation delay that is introduced by variation in pore volume.

The eruptive products of both volcanoes provide abundant evidence for the prominent role of magma mingling and mixing, including banded pumices and mixed crystal populations. Mixing and hybridisation is shown to occur between variably evolved trachytes, as well as trachytes and more mafic magmas. The presence of trachytic enclaves within syenite ejecta records the mingling of trachytic magmas with syenitic crystal mushes, most likely during a replenishment event. As such, the magmatic systems of both Furnas and Pico Alto are undoubtedly open, and the mingling/mixing of magmas of varying composition plays a key role in the petrogenesis of the observed rocks, and may even act as an eruption trigger.

The pre-eruptive magma reservoirs of both Pico Alto and Furnas were compositionally and thermally zoned, with colder, more differentiated, and more hydrous magmas overlying comparatively hot, less differentiated magmas with lower water contents. The degree of zonation does not correlate with eruptive volume, despite a range of ~ 0.1 to > 2 km^3. The compositional zonation observed within individual ignimbrite formations is highly variable, corresponding to between 15 and 50 % fractionation. The nature of the boundaries between compositional zones appears primarily to be gradational; however, a single eruption of Furnas provides evidence for a sharp compositional contrast within the pre-eruptive magma reservoir.

The trace element compositions of the youngest activity of Furnas (< 5 ka), are not compatible with the periodic tapping of a single magma body evolving continuously via

fractional crystallisation. Instead, a cyclical regime is proposed, in which a chemically-stratified cap of trachytic magmas of varying degrees of differentiation forms at the top of the shallow crustal reservoir, before being erupted in one or more individual eruptions, and reforming. The results of this study indicate that up to four such cycles have occurred within this relatively short time period of ~ 5,000 years. Within the same period of time, the eruptions of basaltic magmas within the Congro Fissure zone between Furnas and neighbouring Fogo have ceased, and may have been replaced by rare, low-volume trachytic eruptions. This may indicate the lateral extension of the Furnas (and/or Fogo) magma systems, the development of a new shallow crustal reservoir beneath the fissure zone, or the partial melting of crustal rocks.

The eruptive history of Furnas may indicate a cyclic regime in which the shallow crustal magma system evolves from a developmental stage, to a caldera-forming phase, and finally, to a re-establishment phase. The developmental phase is represented by the young (< 5 ka) intra-caldera eruptions, at which point the shallow magma system comprises multiple individual magma reservoirs, which feed one or more eruptions and may account for the trace element variations observed throughout the deposits. Continued addition of magma to the system generates more individual reservoirs, until they impinge upon one another and coagulate to form a single, relatively homogenised magma reservoir, which then feeds a caldera-forming eruption, such as that of the Povoação Ignimbrite Formation (PIF). Following a caldera-forming phase, the magma system is envisaged to enter a re-establishment phase, in which eruptible peralkaline silicic magmas must be generated prior to further eruptions. The apparent lack of volcanic activity for ~ 7,000 years following the second caldera-forming eruption of Furnas may provide evidence for this phase. Published timescales of fractionation from basalt to trachytes are consistent with this hypothesis.

Pre-eruptive magma viscosities calculated for the peralkaline silicic rocks of this study indicate viscosities up to two orders of magnitude lower than those typical of metaluminous rhyolitic magmas. Based upon these values, calculated settling rates of

alkali feldspar crystals reach 47.00 m a^{-1}, suggesting that, within the magmatic systems of both volcanic centres, crystal settling remains an efficient and viable mechanism for two phase flow and not only facilitates rapid differentiation, but also accounts for the low crystal contents of the erupted magmas. The upper caps of the magma reservoirs are therefore envisaged to comprise an upper, vertically-zoned layer which is crystal poor, and a lower layer which contains alkali feldspar crystals grown *in-situ*, as well as crystals settling down from higher levels. As such, the lower layer is feldspar accumulative, and comparatively enriched in elements such as Ba, K, and Al. The development of low magma viscosities, and the application of the model described above, may seem to preclude the application of models which account for the low crystal contents of silicic magmas via the extraction and segregation of melt from crystal mush bodies, suggesting that they may not be applicable to peralkaline systems. However, the two models are not mutually exclusive, and may be complementary. The double-layered model described above can be readily applied to the cupola of a standard mush extraction model, with the lower layer being extracted from the underlying mush (and potentially being contributed to by melting of the mush during basalt replenishment), and the upper layer resulting from efficient fractional crystallisation of the lower layer. Despite these reconciliatory features, the peralkaline equivalents of the crystal-rich monotonous intermediates, which represent the crystal mush itself, have not yet been recognised, either in the Azores, or at other peralkaline centres. Syenitic nodules are frequently more evolved than their host magmas, and cannot reflect a cumulate from which the trachytic liquids were derived.

7.3 Pico Alto and Furnas in the context of peralkaline silicic magmatism

In terms of their architecture, the magmatic systems of Pico Alto and Furnas share a number of features with other peralkaline silicic centres, both within the Azores and worldwide. The proposed models for the magmatic plumbing systems of Pico Alto and Furnas, in which magma storage zones are positioned within the upper crust (i.e. ~ 3 to 4 km) and the base of the crust (i.e. ~ 14 km), are generally compatible with other volcanic centres in the Azores, including Sete Cidades and Fogo on São Miguel, Caldeira volcano on Faial, Corvo island, and Graciosa island. However, the presence of an upper crustal magma storage zone is not ubiquitous. Although the presence of major tectonic features such as the Terceira Rift may play a role, this likely reflects the age of the island in question. For example, those islands where a shallow crustal magma storage zone is absent, or less established (Pico and Corvo, respectively), are also the youngest islands in the archipelago, and may therefore be considered to be at an earlier stage in their evolution. Models for peralkaline magma systems outside of the Azores such as Pantelleria, and the East African Rift volcanoes, may not necessarily include a lower crustal evolutionary step, but almost invariably include an established shallow crustal reservoir, such as those of Pico Alto or Furnas. A two-level magma plumbing system may therefore be considered to be typical of Azorean volcanic centres, and may be controlled by the overall crustal structure of the region.

The magmatic systems of Pico Alto and Furnas also exhibit similar T-fO_2-X conditions to other peralkaline silicic centres. The peralkalinity indices of the Pico Alto and Furnas trachytes range from 0.94 to 1.43, which is similar to the available estimates for other peralkaline magma systems worldwide (0.87 to 1.96). Similarly, the total pre-eruptive temperature range of the Pico Alto and Furnas trachytes is 772 to 977 °C (which is extended to 621 to 977 °C if syenitic ejecta are considered), which is compatible with available estimates from similar systems (608 to 991 °C). Pre-eruptive water contents for the Pico Alto and Furnas systems range from 2.1 to 6.2 wt. %, which compares well with

the typical range of peralkaline silicic magmas (4 to 6 wt. %). In contrast, pre-eruptive redox conditions show a marked variability, ranging from two log units below the fayalite-magnetite-quartz buffer reaction (FMQ -2) to one log unit below the magnetite-hematite buffer reaction (MH -1). This diversity results from varying degrees of degassing and crustal assimilation in each system, and varies temporally at individual volcanic centres, most likely in response to minor changes in the configuration of the shallow crustal magmatic system in response to caldera-forming eruptive events. The lowest oxygen fugacities of this range are restricted to the syenitic ejecta of this study, and reflect the locally reducing conditions induced by the crystallisation of aegirine and Na-amphibole.

Additional features which Pico Alto and Furnas share with other peralkaline silicic centres are the development of compositionally zoned magma bodies, the predominance of fractional crystallisation as a petrogenetic process, the presence of a shadow zone which prevents the eruption of mafic or intermediate magmas, and the occurrence of magma mingling/mixing processes between magmas of variable composition.

7.4 Eruption styles of peralkaline silicic magmas

Despite their broadly similar compositions, the peralkaline silicic magmas of Pico Alto and Furnas were erupted via a spectrum of different mechanisms, ranging from effusive and dome-forming eruptions, to explosive eruptions. Furthermore, explosive activity ranges from intra-caldera, sub-Plinian eruptions, to caldera-forming eruptions which may include a briefly sustained Plinian eruption column as well as a pyroclastic density current-generating, 'boil-over' phase. The reduced pre-eruptive viscosities of peralkaline silicic magmas inhibit the attainment of viscosities required for magmatic fragmentation during ascent, suggesting that such magma compositions should tend towards more effusive activity. Modelling of isothermal degassing and crystallisation indicate that sufficiently high viscosities may be reached through the combined effects of extensive decompression-driven degassing and degassing induced crystallisation. As such, the primary controls on the eruptive dynamic of peralkaline silicic magmas are proposed to be the volatile content of the magma, and its relative distance from volatile saturated conditions. The effect of major element composition appears to be negligible. Volatile saturated or oversaturated magmas begin to degas and crystallise rapidly following ascent, increasing their viscosity, slowing their ascent, and allowing more time for permeable outgassing. This process is self-driven, with increasing viscosities allowing more degassing, and continued degassing driving the viscosity upwards. The result is the effusive eruption of degassed magma, forming a lava dome such as is typical of Pico Alto. In contrast, a volatile undersaturated magma can ascend further through the conduit prior to degassing and crystallisation, giving it less time to degas, and allowing it to reach the surface with a greater proportion of its volatile budget, where it erupts explosively. This model is highly applicable to Pico Alto, where the lava dome-forming magmas appear to be uniformly more evolved in composition (pantellerite) than the ignimbrite-forming magmas (comenditic trachyte). The two compositions are shown to be related via fractional crystallisation, and so the more evolved compositions are likely to be closer to volatile saturation. The apparent difficulty of

sustaining a Plinian eruption column, as indicated by the ‘boil-over’ eruptions of Pico Alto, likely reflects the transposition of pre-eruptive magma viscosities towards lower values.

The application of this model to Furnas is complicated by the volcano’s history of explosive activity. Effusive activity at Furnas is limited to the latter stages of explosive eruptions, where it can be accounted for by the eruption of the least evolved, least hydrous trachytes of the reservoir, either through the main conduit (as seen for the UFG), or via the ring dykes associated with episodes of caldera collapse. The apparent affinity for explosive eruptive activity is considered to reflect the interaction of ascending magmas with external water. Unlike Pico Alto, Furnas volcano comprises a topographic low, in which one or more lakes have formed throughout its history. Furthermore, the hydrothermal system of Furnas is well developed compared to that of Pico Alto. As such, the eruption styles determined by the pre-eruptive conditions of the magmatic system of Furnas are effectively overprinted by a late-stage effect during magma ascent, yielding predominantly explosive activity. The late stage extrusion of lava domes either reflects the low volatile content of the last magmas to erupt, or the exhaustion of the external water supply.

REFERENCES

Abdel-Monem, A. A., Fernandez, L. A., Boone, G., M. (1975) K/Ar ages from the eastern Azores group (Santa Maria, São Miguel and the Formigas Islands). Lithos, 8:247-254

Ablay, G. J., Carroll, M. R., Palmer, M. R., Martí, J., Sparks, R. S. J. (1998) Basanite-phonolite lineages of the Tiede-Pico Viejo Volcanic Complex, Tenerife, Canary islands. Journal of Petrology, 39: 905-936

Adam, J., Green, T. (2006) Trace element partitioning between mica- and amphibole-bearing garnet lherzolite and hydrous basanitic melt: 1. Experimental results and the investigation of controls on partitioning behaviour. Contributions to Mineralogy and Petrology, 152: 1-17

Agostinho, J. (1931) Volcanoes of the Açores Islands. Bulletin of Volcanology, 14: 123-138

Akhtar, M. J., Waseem, S. (2001) Atomistic simulation studies of zircon. Chemical Physics**,** 274: 109-120

Allègre, C. J., Hamelin, B., Provost, A., Dupré, B. (1987) Topology in isotopic multispace and origin of mantle chemical heterogeneities. Earth and Planetary Science Letters, 81: 319-337

Andersen, D. J., Lindsley, D. H., Davidson, P. M. (1993) QUILF: A Pascal program to assess equilibria among Fe-Mg-Mn-Ti oxides, pyroxenes, olivine and quartz. Computers and Geosciences, 19: 1333-1350

Andersen, T., Erambert, M., Larsen, A. O., Selbekk, R. S. (2010) Petrology of nepheline syenite pegmatites in the Oslo Rift, Norway: ziconium silicate mineral assemblages as indicators of alkalinity and volatile fugacity in mildly agpaitic magma. Journal of Petrology, 51: 2303-2325

Anderson, A. T., Swihart, G. H., Artioli, G., Geiger, C. A. (1984) Segregation vesicles, gas filter-pressing, and igneous differentiation. Journal of Geology, 92: 55-72

Anderson, D. L. (2006) Speculations on the nature and cause of mantle heterogeneity. Tectonophysics, 416: 7-22

Anderson, D. L. (2013) The persistent mantle plume myth. Australian Journal of Earth Sciences, 60: 657-673

Anderson, D. L., Natland, J. H. (2005) A brief history of the plume hypothesis and its xcompetitors: concept and controversy. In: Foulger, G. R., Natland, J. H., Presnall, D. C., Anderson, D. L. (eds.) Plates, Plumes, and Paradigms. Geological Society of America Special Paper, 388: 119-145

Anderson, R. N., McKenzie, D., Sclater, J. G. (1973) Gravity, bathymetry and convection in the Earth. Earth and Planetary Science Letters, 18: 391-407

Andújar, J., Scaillet, B. (2012) Relationships between pre-eruptive conditions and eruptive styles of phonolite-trachyte magmas. Lithos, 152: 122-131

Aoki, K. (1959) Petrology of alkali rocks of the Iki islands and Higashi-Masuura district, Japan. Tohoku University Scientific Report, 3: 261-310

Aoki, K. (1964) Clinopyroxene from the alkali rocks of Japan. American Mineralogist, 49: 1199-1223

Araña, V., Badiola, E. R., Hernán, F. (1973) Peralkaline acid tendencies in Gran Canaria (Canary islands). Contributions to Mineralogy and Petrology, 40: 53-62

Araña, V., Barberi, F., Santacroce, R. (1974) Some data on the comendite type area of S. Pietro and S. Antioco, Sardinia. Bulletin of Volcanology, 38: 726-736

Asimow, P. D., Ghiorso, M. S. (1998) Algorithmic modifications extending MELTS to calculate subsolidus phase relations. American Mineralogist, 83: 1127-1132

Atkins, F. B., Baker, P. E., Bell, J. D., Smith, D. G. W. (1964) Oxford expedition to Ascension island, 1964. Nature, 204: 721-724

Avanzinelli, R., Bindi, L., Menchetti, S., Conticelli, S. (2004) Crystallisation and genesis of peralkaline magmas from Pantelleria volcano, Italy: an integrated petrological and crystal-chemical study. Lithos, 73: 41-69

Ayalew, D., Yirgu, G. (2003) Crustal contribution to the genesis of Ethiopian plateau rhyolitic ignimbrites: basalt and rhyolite geochemical provinciality. Journal of the Geological Society of London, 160: 47-56

Bachmann, O., Bergantz, G. W. (2004) On the origin of crystal-poor rhyolites: extracted from batholithic crystal mushes. Journal of Petrology, 45: 1565-1582

Bachmann, O., Charlier, B. L. A., Lowenstern, J. B. (2007) Zircon crystallisation and recycling in the magma chamber of the rhyolitic Kos Plateau Tuff (Agean arc). Geology, 35: 73-76

Bachmann, O., Deering, C. D., Ruprecht, J. S., Huber, C., Skopelitis, A., Schnyder, C. (2012) Evolution of silicic magmas in the Kos-Nisyros volcanic center, Greece: a petrological cycle associated with caldera collapse. Contributions to Mineralogy and Petrology, 163: 151-166

Bachmann, O., Dungan, M. A., Lipman, P. W. (2002) The Fish Canyon magma body, San Juan volcanic field, Colorado: rejuvenation and eruption of an upper crustal batholith. Journal of Petrology, 43: 1469-1503

Bacon, C. R., Druitt, T. H. (1988) Compositional evolution of the zoned calcalkaline magma chamber of Mount Mazama, Crater Lake, Oregon. Contributions to Mineralogy and Petrology, 98: 224-256

Bacon, C. R., Hirschmann, M. M. (1988) Mg/Mn partitioning as a test for equilibrium between coexisting Fe-Ti oxides. American Mineralogist, 73: 57-61

Bailey, D. K. (1974) Experimental petrology relating to oversaturated peralkaline volcanics. A review. Bulletin of Volcanology, 38: 637-652

Bailey, D. K., Macdonald, R. (1970) Petrochemical variations among mildly peralkaline (comendite) obsidians from the oceans and continents. Contributions to Mineralogy and Petrology, 28: 340-351

Bailey, D. K., Macdonald, R. (1975) Fluorine and chlorine in peralkaline liquids and the need for magma generation in an open system. Mineralogical Magazine, 40: 405-414

Bailey, D. K., Macdonald, R. (1987) Dry peralkaline felsic liquids and carbon dioxide flux through the Kenya rift zone. In: Mysen, B. (ed.) Magmatic processes: physiochemical principles. Geochemical Society, Special Publication, 1: 91-105

Baker, P. E. (1967) Historical and geological notes on Bouvetøya. British Antarctic Survey Bulletin, 13: 71-84

Baker, P. E. (1974) Peralkaline acid volcanic rocks of oceanic islands. Bulletin of Volcanology, 38: 737-754

Baker, P. E., Buckley, F., Holland, J. G. (1974) Petrology and geochemistry of Easter island. Contributions to Mineralogy and Petrology, 44: 85-100

Barberi, F., Cassano, E., La Torre P., Sbrana, A. (1991) Structural evolution of Campi Flegrei caldera in light of volcanological and geophysical data. Journal of Volcanology and Geothermal Research, 48: 33-49

Barberi, F., Santacroce, R., Varet, J. (1974) Silicic peralkaline volcanic rocks of the Afar Depression (Ethiopia). Bulletin of Volcanology, 38: 755-790

Barberi, F., Ferrara, G., Santacroce, R., Treuil, M., Varet, J. (1975) A transitional basalt-pantellerite sequence of fractional crystallisation, the Boina Centre (Afar Rift, Ethiopia). Journal of Petrology, 16:22-56

Barclay, J., Carroll, M. R., Houghton, B. F., Wilson, C. J. N. (1996) Pre-eruptive volatile content and degassing history of an evolving peralkaline volcano. Journal of Volcanology and Geothermal Research, 74: 75-87

Barker, A. K., Troll, V. R., Ellam, R. M., Hansteen, T. H., Harris, C., Stillman, C. J., Andersson, A. (2012) Magmatic evolution of the Cadamosto Seamount, Cape Verde: beyond the spatial extent of EM1. Contributions to Mineralogy and Petrology, 163:949-965

Beier, C., Haase, K. M., Abouchami, W., Krienitz, M. S., Hauff, F. (2008) Magma genesis by rifting of oceanic lithosphere above anomalous mantle: Terceira Rift, Azores. Geochemistry, Geophysics, Geosystems, 9: Q12013

Beier, C., Haase, K. M., Hansteen, T. H. (2006) Magma evolution of the Sete Cidades volcano, São Miguel, Azores. Journal of Petrology, 47: 1375-1411

Beier, C., Haase, K. M., Turner, S. P. (2012) Conditions of melting beneath the Azores. Lithos, 144-145: 1-11

Beier, C., Mata, J.,Stöckhert, F., Mattielli, N., Brandl, P. A., Madureira, P., Genske, F. Martins, S., Madeira, J., Haase, K. M. (2013) Geochemical evidence for melting of carbonated peridotite on Santa Maria island, Azores. Contributions to Mineralogy and Petrology, 165: 823-841

Beier, C., Stracke, A., Haase, K. M. (2007) The peculiar geochemical signatures of São Miguel lavas: metasomatised or recycled sources? Earth and Planetary Science Letters, 259: 186-199

Beier, C., Turner, S., Plank, T., White, W. (2010) A preliminary assessment of the symmetry of source composition and melting dynamics across the Azores plume. Geochemistry, Geophysics, Geosystems, 9: Q12013

Bergman, S. C. (1987) Lamproites and other potassium-rich igneous rocks: a review of their occurrence, mineralogy and geochemistry. In: Fitton, J. G., Upton, B. G. J. (eds.) (1974) Alkaline igneous rocks. Geological Society Special Publication No. 30, 103-190

Bernth, U., Brousse, R., Frei, R., Sørensen, H. (2002) The origin of phonolites and trachytes from the Col de Guéry area, le Mont-Dore, Massif Central, France. Matematisk-fysiske Meddelelser, 50, The Royal Danish Academy of Sciences and Letters, 61 pp.

Berthois, L. (1953) Contribution à l'étude lithologique de l'Archipel des Açores. Comunicaçoes dos serviços Geológicos de Portugal, 34: 1-198

Bigg, E. K. (1953) The supercooling of water. Proceedings of the Physical Society (London), 66B: 688-694

Birkett, T. C., Miller, R. R., Roberts, A. C., Mariano, A. N. (1992) Zirconium-bearing minerals of the Strange Lake Intrusive Complex, Quebec-Labrador. Canadian Mineralogist, 30: 191-205

Black, S., Macdonald, R., Barreiro, B. A., Dunkley, P. N., Smith, M. (1998) Open system alkaline magmatism in northern Kenya: evidence from U-series disequilibria and radiogenic isotopes. Contributions to Mineralogy and Petrology, 131: 364-378

Black, S., Macdonald, R., Kelly, M. R. (1997) Crustal origin for peralkaline rhyolites from Kenya: evidence from U-series disequilibria and Th-isotopes. Journal of Petrology, 38: 277-297

Blanco, I., García, A., Torta, J. M. (1997) Magnetic study of the Furnas caldera (Azores). Annali di Geofisica, 40: 341-359

Bohrson, W. A., Reid, M. R. (1997) Genesis of silicic peralkaline volcanic rocks in an oceanic island setting by crustal melting and open-system processes: Socorro Island, Mexico. Journal of Petrology, 38: 1137-1166

Bohrson, W. A., Reid, M. R. (1998) Genesis of evolved ocean island magmas by deep- and shallow-level basement recycling, Socorro island, Mexico: constraints from Th and other isotope signatures. Journal of Petrology, 39: 995-1008

Bohrson, W. A., Reid, M. R., Grunder, A. L., Heizler, M. T., Harrison, T. M., Lee, J. (1996) Prolonged history of silicic peralkaline volcanism in the eastern Pacific Ocean. Journal of Geophysical Research, 101: 11,457-11,474

Bonatti, E. (1971) Ancient continental mantle beneath oceanic ridges. Journal of Geophysical Research, 76: 3825-3831

Bonin, B., Grelou-Orsini, C., Vialette, Y. (1978) Age, origin and evolution of the anorogenic complex of Evisa (Corsica): a K-Li-Rb-Sr study. Contributions to Mineralogy and Petrology, 65: 425-432

Booth, B., Croasdale, R., Walker, G. P. L. (1978) A quantitative study of five thousand years of volcanism on São Miguel, Azores. Philosophical transactions of the Royal Society of London, Series A, Mathematical and Physical Sciences, 288: 271-319

Borley, G. D. (1963) Amphiboles from the Younger Granites of Nigeria. I. Chemical classification. Mineralogical Magazine, 33: 358-376

Bottinga, Y., Weill, D. (1972) The viscosity of magmatic silicate liquids: a model for calculation. American Journal of Science, 272: 438-475

Bourdon, B., Turner, S. P., Ribe, N. M. (2005) Partial melting and upwelling rates beneath the Azores from a U-series isotope perspective. Earth and Planetary Science Letters, 239: 42-56

Bowen, N. L. (1928) The evolution of igneous rocks. New York: Dover, 332 pp.

Bowen, N. L. (1937) Recent high temperature research on silicates and its significance in igneous geology. American Journal of Science, 33: 1-21

Bowin, C., Thompson, G., Schilling, J. G. (1984) Residual geoid anomalies in Atlantic Ocean Basin: relationship to mantle plumes. Journal of Geophysical Research, 89: 9905-9918

Brenan, J. M., Neroda, E., Lundstrom, C. C., Shaw, H. F., Ryerson, F. J., Phinney, D. L. (1998) Behaviour of boron, beryllium, and lithium during melting and crystallization: constraints from mineral-melt partitioning experiments. Geochimica et Cosmochimica Acta, 62: 2129-2141

Broch, O. A. (1946) Lavas of Bouvet island. In: Two contributions to Antarctic petrography. Scientific results of the Norwegian Antarctic expedition, 25: 3-26

Brod, J. A. (1999) Petrology and geochemistry of the tapira alkaline complex, minas gerais state, Brazil. [Ph.D. thesis]. Durham University, U.K., 486 pp.

Brousse, R., Varet, J. (1966) Les trachytes du Mont-Dore et du Cantal septentrional et leurs enclaves. Bulletin de la Societe Geologique de France, 8: 246-262

Bryan, W. B. (1966) History and mechanism of eruption of soda-rhyolite and alkali basalt, Socorro island, Mexico. Bulletin of Volcanology, 29: 453-479

Bryan, W. B., Finger, L. W., Chayes, F. (1969) Estimating proportions in petrographic mixing equations by least-squares approximation. Science, 163: 926-927

Calvert, A. T., Moore, R. B., McGeehin, J. P., Rodrigues da Silva, A. M. (2006) Volcanic history and $^{40}Ar/^{39}Ar$ and ^{14}C geochronology of Terceira Island, Azores, Portugal. Journal of Volcanology and Geothermal Research, 156: 103-115

Camacho, A. G., Montesinos, F. G., Vieira, R. (1997) A three-dimensional gravity inversion applied to São Miguel Island (Azores). Journal of Geophysical Research, 102: 7717-7730

Cann, J. R. (1967) A second occurrence of dalyite and the petrology of some ejected syenite blocks from São Miguel, Azores. Mineralogical Magazine, 36: 227-232

Cannat, M., Briais, A., Deplus, C., Escartín, J., Georgen, J., Lin, J., Mercouriev, S., Meyzen, C., Muller, M., Pouliquen, G., Rabain, A., da Silva, P. (1999) Mid-Atlantic Ridge – Azores hotspot interactions: along-axis migration of a hotspot-derived event of enhanced magmatism 10 to 4 Ma ago. Earth and Planetary Science Letters, 173: 257-269

Caricchi, L., Annen, C., Blundy, J. D., Simpson, G., Pinel, V. (2014) Frequency and magnitude of volcanic eruptions controlled by magma injection and buoyancy. Nature Geoscience, 7: 126-130

Caricchi, L., Giordano, D., Burlini, L., Ulmer, P., Romano, C. (2008) Rheological properties of magma from the 1538 eruption of Monte Nuovo (Phlegre Fields, Italy): an experimental study. Chemical Geology, 256: 158-171

Carmichael, I. S. E. (1962) Pantelleritic liquids and their phenocrysts. Mineralogical Magazine, 33: 86-113

Carmichael, I. S. E. (1964) The petrology of Thingmuli, a Tertiary volcano in eastern Iceland. Journal of Petrology, 5: 435-460

Carter, R. M. (1967) The geology of Pitcairn island, south Pacific. Bishop Museum Bulletin, 231: 1-38

Cazenave, A., Houry, S., Lago, B., Dominh, K. (1992) Geosat-derived geoid anomalies at medium wavelength. Journal of Geophysical Research, 97: 7081-7096

Chakhmouradian, A. R., Mitchell, R. H. (2002) The mineralogy of Ba- and Zr-rich alkaline pegmatites from Gordon Butte, Crazy Mountains (Montana, USA): comparisons between potassic and sodic agpaitic pegmatites. Contributions to Mineralogy and Petrology, 143: 93-114

Chayes, F. (1963) Relative abundance of intermediate members of the oceanic basalt-trachyte association. Journal of Geophysical Research, 68: 1519-1534

Chen, C. F., Turner, J. S. (1980) Crystallisation in a double-diffusive system. Journal of Geophysical Research, 85: 2573-2593

Chesner, C., Rose, W. (1991) Stratigraphy of the Toba Tuffs and the evolution of the Toba Caldera Complex, Sumatra, Indonesia. Bulletin of Volcanology, 53: 343-356

Chester, D. K., Dibben, J. L., Duncan, A. M. (2002) Volcanic hazard assessment in western Europe. Journal of Volcanology and Geothermal Research, 115: 411-435

Christiansen, R. L., Blank, H. R. (1972) Volcanic stratigraphy of the Quaternary rhyolite plateau in Yellowstone National Park. U.S. Government Printing Office

Civetta, L., Cornette, Y., Crisci, G., Gillot, P. Y., Orsi, G., Requejo, C. S. (1984) Geology, geochronology and chemical evolution of the island of Pantelleria. Geological Magazine, 121: 541-668

Civetta, L., D'antonio, M., Orsi, G., Tilton, G. R. (1998) The geochemistry of volcanic rocks from Pantelleria Island, Sicily Channel: petrogenesis and characteristics of the mantle source region. Journal of Petrology, 39: 1453-1491

Clague, D. A., Dalrymple, G. B. (1987) The Hawaiian-Emperor volcanic chan: Part I, Geologic evolution. In: Decker, R. W., Wright, T. L., Stauffer, P. H. (eds.) Volcanism in Hawaii. U.S. Geological Survey Professional Paper, 1350, 5-73

Clague, D. A., Dalrymple, G. B. (1989) Tectonics, geochronology and origin of the Hawaiian-Emperor volcanic chain. In: Winterer, E. L., Hussong, D. M., Decker, R. W. (eds.) The geology of North America, Volume N: The Eastern Pacific Ocean and Hawaii. Boulder, CO: Geological Society of America, 188-217

Claude-Ivanaj, C., Joron, J. L., Allègre, C. J. (2001) ^{238}U-^{230}Th-^{226}Ra fractionation in historical lavas from the Azores: long-lived source heterogeneity v. metasomatism fingerprints. Chemical Geology, 176: 295-310

Clemens, J. D. (2003) S-type granite – petrogenetic issues, models and evidence. Earth Science Reviews, 61: 1-18

Cole, J. W., Brown, S. J. A., Burt, R. M., Beresford, S. W., Wilson, C. J. N. (1998) Lithic types in ignimbrites as a guide to the evolution of a caldera complex, Taupo volcanic centre, New Zealand. Journal of Volcanology and Geothermal Research, 80: 217-237

Cole, J. W., Milner, D. M., Spinks, K. D. (2005) Calderas and caldera structures: a review. Earth Science Reviews, 69: 1-26

Cole, P. D., Guest, J. E., Queiroz, G., Wallenstein, N., Pacheco, J. -M., Gaspar, J. L., Ferreira, T., Duncan, A. M. (1999) Styles of volcanism and volcanic hazards on Furnas volcano, São Miguel, Azores. Journal of Volcanology and Geothermal Research, 92: 39-53

Cole, P. D., Queiroz, G., Wallenstein, N., Gaspar, J. L., Duncan, A. M., Guest, J. E. (1995) An historic subplinian/phreatomagmatic eruption: the 1630 AD eruption of Furnas volcano, São Miguel, Azores. Journal of Volcanology and Geothermal Research, 69: 117-135

Cooper, G. F., Wilson, C. J., Millet, M., Baker, J. A., Smith, E. G. (2012) Systematic tapping of independent magma chambers during the 1 Ma Kidnappers super eruption. Earth and Planetary Science Letters, 313: 23-33

Costa, A., Carricchi, L., Bagdassarov, N. S. (2009) A model for the rheology of particle-bearing suspensions and partially molten rocks. Geochemistry, Geophysics, Geosystems, 10: 1-13

Couch, S., Sparks, R. S. J., Carroll, M. R. (2001) Mineral disequilibrium in lavas explained by convective self-mixing in open magma chambers. Nature, 411: 1037-1039

Courtillot, V., Davaille, A., Besse, J., Stock, J. (2003) Three distinct types of hotspots in the Earth's mantle. Earth and Planetary Science Letters, 205: 295-308

Cronin, S. J., Neall, V. E., Lecointre, J. A., Hedley, M. J., Loganathan, P. (2003) Environmental hazards of fluoride in volcanic ash: a case study from Ruapehu volcano, New Zealand. Journal of Volcanology and Geothermal Research, 121: 271-291

Dahren, B., Troll, V. R., Andersson, U. B., Chadwick, J. P., Gardner, M. F., Jaxybulatov, K., Koulakov, I. (2012) Magma plumbing beneath Anak Krakatau volcano, Indonesia: evidence for multiple magma storage regions. Contributions to Mineralogy and Petrology, 163:631-651

Daly, R. A. (1925) The geology of Ascension island. Proceedings of the American Academy of Arts and Sciences, 60: 1-80

Davies, G. R., Macdonald, R. (1987) Crustal influences in the petrogenesis of the Naivasha basalt-comendite complex: combined trace element and Sr-Nd-Pb isotope constraints. Journal of Petrology, 28: 1009-1031

Deer, W. A., Howie, R. A., Zussman, J. (1992) An introduction to the rock-forming minerals. 2nd edition, Harlow: Longman, 696 pp.

Degruyter, W., Huber, C. (2014) A model for eruption frequency of upper crustal silicic magma chambers. Earth and Planetary Science Letters, 403: 117-130

DePaolo, D. J. (1981) Trace element and isotopic effects of combined wall rock assimilation and fractional crystallisation. Earth and Planetary Science Letters, 53: 189-202

DePaolo, D. J., Perry, F. V., Baldridge, W. S. (1992) Crustal versus mantle sources in granitic magmas: a two-parameter model based on Nd isotope studies. Transactions of the Royal Society of Edinburgh, 83: 439-446

de Silva, S. L., Gregg, P. M. (2014) Thermomechanical feedbacks in magmatic systems: Implications for growth, longevity, and evolution of large caldera-forming magmareservoirs and their supereruptions. Journal of Volcanology and Geothermal Research, 282: 77-91

Di Carlo, I., Rotolo, S. G., Scaillet, B., Buccheri, V., Pichavant, M. (2010) Phase equilibrium constraints on pre-eruptive conditions of recent felsic explosive volcanism at Pantelleria Island, Italy. Journal of Petrology, 51: 2245-2276

Di Genova, D., Romano, C., Hess, K. -U., Vona, A., Poe, B. T., Giordano, D., Dingwell, D. B., Behrens, H. (2013) The rheology of peralkaline rhyolites from Pantelleria island. Journal of Volcanology and Geothermal Research, 249: 201-216

Di Matteo, V., Carroll, M. R., Behrens, H., Vetere, F., Brooker, R. A. (2004) Water solubility in trachytic melts. Chemical Geology, 213: 187-196

Dingwell, D. B., Bagdassarov, N. S., Bussod, J., Webb, S. L. (1993) Magma rheology. In: Luth, R. W. (ed.) Short handbook on experiments at high pressure and applications to the Earth's mantle. Mineralogical Association of Canada, Ontario, 21: 131-196

Dingwell, D. B., Hess, K. U. (1998) Melt viscosities in the system Na-Fe-Si-O-F-Cl: contrasting effects of F and Cl in alkaline melts. American Mineralogist, 83: 1016-1021

Dingwell, D. B., Hess, K. –U., Romano, C. (1998) Extremely fluid behaviour of hydrous peralkaline rhyolites. Earth and Planetary Science Letters, 158: 31-38

Dingwell, D. B., Romano, C., Hess, K. U. (1996) The effect of water on the viscosity of a haplogranitic melt under P-T-*X* conditions relevant to silicic volcanism. Contributions to Mineralogy and Petrology, 124: 19-28

Dingwell, D. B., Scarfe, C. M., Cronin, D. J. (1985) The effect of fluorine on viscosities in the system Na_2O-Al_2O_3-SiO_2: implications for phonolites, trachytes and rhyolites. American Mineralogist, 70: 80-87

Dolivo-Dobrovol'skiy, D. V., Yevdokimov, M. D. (1991) Zirconium mineralisation of the alkali metasomatites of the Murun Complex. International Geology Review, 33: 490-496

Duncan, A. M., Queiroz, G., Guest, J. E., Cole, P. D., Wallenstein, N., Pacheco, J. M. (1999) The Povoação Ignimbrite, Furnas volcano, São Miguel, Azores. Journal of Volcanology and Geothermal Research, 92: 55-65

Dunkley, P. N., Smith, M., Allen, D. J., Darling, W. G. (1993) The geothermal activity and geology of the northern sector of the Kenya Rift Valley. British Geological Survey Research Report, SC93/1

Duprè, B., Allégre, C. J. (1980) Pb-Sr-Nd isotopic correlation and the chemistry of the North Atlantic mantle. Nature, 286: 17-22

Dupré, B., Lambret, B., Allègre, C. J. (1982) Isotopic variations within a single oceanic island: the Terceira case. Nature, 299: 620-622

Eggins, S. M., Woodhead, J. D., Kinsley, L. P. J., Mortimer, G. E., Sylvester, P., McCulloch, M. T., Hergt, J. M., Handler, M. R. (1997) A simple method for the precise determination of ≥ 40 trace elements in geological samples by ICPMS using enriched isotope internal standardisation. Chemical Geology, 134: 311-326

Elliott, T., Blichert-Toft, J., Heumann, A., Koetsier, G., Forjaz, V. (2007) The origin of enriched mantle beneath São Miguel, Azores. Geochimica et Cosmochimica Acta, 71: 219-240

Escartín, J., Cannat, M., Pouliquen, G., Rabain, A., Lin, J. (2001) Crustal thickness of V-shaped ridges south of the Azores: interaction of the Mid-Atlantic Ridge (36°-39°N) and the Azores hot spot. Journal of Geophysical Research, 106: 21719-21735

Esenwein, P. (1929) Zur petrographie der Azoren. Zeitschrift für Vulkanologie, 12: 108-227

Esperança, S., Carlson, R. W., Shirey, S. B., Smith, D. (1997) Dating crust-mantle separation: Re-OS isotopic study of mafic xenoliths from central Arizona. Geology, 25: 651-654

Ewart, A., Griffin, W. L. (1994) Application of Proton-Microprobe Data to Trace-Element Partitioning in Volcanic-Rocks. Chemical Geology, 117: 251-284

Ewart, A., Taylor, S. R., Capp, A. C. (1968) Geochemistry of the pantellerites of Mayor island, New Zealand. Contributions to Mineralogy and Petrology, 17: 116-140

Féraud, G., Kaneoka, I., Allègre, C. -J. (1980) K/Ar ages and stress pattern in the Azores: geodynamic implications. Earth and Planetary Science Letters, 46: 275-286

Ferguson, A. K. (1978) The crystallisation of pyroxenes and amphiboles in some alkaline rocks and the presence of a pyroxene compositional gap. Contributions to Mineralogy and Petrology, 67: 11-15

Ferla, P., Meli, C. (2006) Evidence of magma mixing in the 'Daly Gap' of alkaline suites: a case study from the enclaves of Pantelleria (Italy). Journal of Petrology, 47: 1467-1507

Fernandez, L. A. (1980) Geology and petrology of the Nordeste volcanic complex, São Miguel, Azores. Geological Society of America Bulletin, 91: 2457-2557

Ferreira, M. P., Azevedo, J. M. (1995) Evolucão geologica do arquipelago dos Acores baseada na geocronologia: Seminario "Geologia Atlantica". Associacao Portuguesa de Geologos, Ponta Delgada: 9 p.

Ferreira, T., Oskarsson, N. (1999) Chemistry and isotopic composition of fumarole discharges of Furnas caldera. Journal of Volcanology and Geothermal Reseach, 92: 169-179

Finch, R. J., Hanchar, J. M. (2003) Structure and chemistry of zircon and zircon-group minerals. In: Hanchar, J. M., Hoskin, P. W. O. (eds.) Zircon. Mineralogical Society of America, Reviews in Mineralogy and Geochemistry, 53: 1-25

Fitton, J. G. (2007) The OIB paradox. In: Foulger, G., R., Jurdy, D., M., (eds.) Plates, plumes and planetary processes. Geological society of America, Special Paper 430, 387-412 pp.

Fleet, S. G. (1965) The crystal structure of dalyite. Zeitschrift für Kristallographie 121: 349-368

Flude, S., Burgess, R., McGarvie, D. W. (2008) Silicic volcanism at Ljósufjöll, Iceland: insights into evolution and eruptive history from Ar-Ar dating. Journal of Volcanology and Geothermal Research, 169: 154-175

Foerstner, H. (1881) Nota preliminare sulla geologia dell'isola di Pantelleria secundo gli studi fatti negli anni 1874 e 1881. Bolletino di Rendi Conti Geologia Italia, 12: 523-556

Folch, A., Marti, J. (1998) The generation of overpressure in felsic magma chambers by replenishment. Earth and Planetary Science Letters, 164: 301-314

Foulger, G. R. (2012) Are 'hot spots' hot spots? Journal of Geodynamics, 58: 1-28

Fouqué, F. (1883) Un feldspath triclinique de Quatre Riberias, Isle de Terceira, Açores. Bulletin of the French Mineralogy and Crystallography Society

Fowler, S. J., Spera, F. J. (2008) Phase equilibria trigger for explosive volcanic eruptions. Geophysical Research Letters, 35: L08309

França, Z., Nunes, J. C., Cruz, J. V., Duarte, H. F., Forjaz, V. H. (2003) Estudo preliminar do vulcanismo da ilha do Corvo, Açores. In: Garcia, F. G., Valero, J. L. (eds.) Proceedings da 3a Assembleia Luso-Espanhola de Geodesia e Geofisica. Valencia: Univ. Politécnica de Valencia, 2:: 727-730

França, Z. T. M., Tassinari, C. C. G., Cruz, J. V., Aparicio, A. Y., Araña, V., Rodrigues, B. N. (2006) Petrology, geochemistry and Sr-Nd-Pb isotopes of the volcanic rocks from Pico Island – Azores (Portugal). Journal of Volcanology and Geothermal Research, 156: 71-89

Freire Luis, J., Miranda, J. M., Galdeano, A., Patriat, P., Rossignol, J. C., Mendes Victor, L. A. (1994) The Azores triple junction evolution since 10 Ma from an aeromagnetic survey of the Mid-Atlantic Ridge. Earth and Planetary Science Letters, 125: 439-459

Freire Luis, J., Neves, M. C. (2006) The isostatic compensation of the Azores Plateau: A 3D admittance and coherence analysis. Journal of Volcanology and Geothermal Research, 156: 10-22

Friedlander, I. (1929) Die Azoren. Zeitschrift für Vulkanologie, 13: 77-109

Furnes, H., Mitchell, J. G., Robins, B., Ryan, P., Skjerlie, F. J. (1982) Petrography and geochemistry of peralkaline, ultrapotassic syenite dykes of Middle Permian age, Sunnfjord, West Norway. Norsk Geologisk Tidsskrift, 62: 147-159

Gale, J. D. (1997) GULP: A computer program for the symmetry-adapted simulation of solids. Journal of the Chemical Society, Faraday Transactions, 93: 629-637

Gandino, A., Guidi, M., Merlo, C., Mete, L., Rossi, R., Zan, L. (1985) Preliminary model for the Ribeira Grande geothermal field (Azores isnalds). Geothermics, 14: 91-105

Gardner, J. E., Rutherford, M., Carey, S., Sigurdsson, H. (1995) Experimental constraints on pre-eruptive water contents and changing magma storage prior to explosive eruptions of Mount St Helens volcano. Bulletin Volcanology, 57: 1-17

Gaspar, J. L. (1996) Ilha Graciosa (Açores). História vulcanológica e avaliação do hazard. Unpublished PhD thesis, Universidade dos Açores

Gaspar, J. L., Queiroz, G., Pacheco, J. M., Ferreira, T., Wallenstein, N., Almeida, M. H., Coutinho, R. (2003) Serreta submarine ridge eruption (Azores). In: White, J. D. L., Smellie, J. L., Clague, D. A. (eds.) Explosive subaqueous volcanism. American Geophysical Union Geophysical Monograph, 140: 205-212

Gaspar, J. L., Guest, J. E., Duncan, A. M., Barriga, F. J. A. S., Chester, D. K. (eds) (2015) Volcanic geology of São Miguel island (Azores archipelago). Geological Society of London Memoirs: 44 125-134

Gast, P. W., Hedge, C., Tilton, G. R. (1964) Isotopic composition of lead and strontium from Ascension and Gough Islands. Science, 145: 1181-1185

Geist, D., Naumann, T., Larson, P. (1998) Evolution of Galápagos magmas: mantle and crustal fractionation without assimilation. Journal of Petrology, 39: 953-971

Genske, F. S., Beier, C., Haase, K. M., Turner, S. P., Krumm, S., Brandl, P. A. (2013) Oxygen isotopes in the Azores islands: crustal assimilation recorded in olivine. Geology, 41: 491-494

Genske, F. S., Turner, S. P., Beier, C., Chu, M. F., Tonarini, S., Pearson, N. J., Haase, K. M. (2014) Lithium and boron isotope systematics in lavas from the Azores islands reveal crustal assimilation. Chemical Geology, 373: 27-36

Genske, F. S., Turner, S. P., Beier, C., Scaefer, B. F. (2012) The petrology and geochemistry of lavas from the western Azores islands of Flores and Corvo. Journal of Petrology, 53: 1673-1708

Gente, P., Dyment, J., Maia, M., Goslin, J. (2003) Interaction between the Mid-Atlantic Ridge and the Azores hot spot during the last 85 Myr: emplacement and rifting of the hotspot derived plateaus. Geochemistry, Geophysics, Geosystems, 4: 8514, doi: 10.1029/2003GC000527

Gertisser, R., Self, S., Gaspar, J. L., Kelley, S. P., Pimentel, A., Eikenberg, J., Barry, T. L., Pacheco, J. M., Queiroz, G., Vespa, M. (2010) Ignimbrite stratigraphy and chronology on Terceira Island, Azores. Geological Society of America Special Paper 464, 133-154

Gertisser, R., Self, S., Thomas, L. E., Handley, H. K., Van Calsteren, P., Wolff, J. A. (2012) Processes and timescales of magma genesis and differentiation leading to the Great Tambora eruption in 1815. Journal of Petrology, 53: 271-297

Ghiorso, M. S., Sack, R. O. (1995) Chemical mass transfer in magmatic processes IV. A revised and internally consistent thermodynamic model for the interpolation and extrapolation of liquid-solid equilibria in magmatic systems at elevated temperatures and pressures. Contributions to Mineralogy and Petrology, 119: 197-212

Gibson, I. L. (1970) A pantelleritic welded ash-flow from the Ethiopian Rift Valley. Contributions to Mineralogy and Petrology, 28: 89-111

Gioncada, A., Landi, P. (2010) The pre-eruptive volatile contents of recent basaltic and pantelleritic magmas at Pantelleria (Italy). Journal of Volcanology and Geothermal Research, 189: 191-201

Giordano, D., Ardia, P., Romano, C., Dingwell, D. B., Di Muro, A., Schmidt, M W., Mangiacapra, A., Hess, K. U. (2009) The rheological evolution of alkaline Vesuvius magmas and comparison with alkaline series from the Phlegrean Fields, Etna, Stromboli and Teide. Geochimica et Cosmochimica Acta, 73: 6613-6630

Giordano, D., Dingwell, D. B. (2003) Viscosity of hydrous Etna basalt: implications for Plinian-style basaltic eruptions. Bulletin of Volcanology, 65: 8-14

Giordano, D., Mangiacapra, A., Potuzak, M., Russell, J. K., Romano, C., Dingwell, D. B., Di Muro, A. (2006) An expanded non-Arrhenian model for silicate melt viscosity: A treatment for metaluminous, peraluminous and peralkaline liquids. Chemical Geology, 229: 42-56

Giordano, D., Romano, C., Dingwell, D. B., Poe, B., Behrens, H. (2004) The combined effects of water and fluorine on the viscosity of silicic magmas. Geochimica et Cosmochimica Acta, 68: 5159-5168

Giordano, D., Russell, J. K., Dingwell, D. B. (2008) Viscosity of magmatic liquids: a model. Earth and Planetary Science Letters, 271: 123-134

Gonnermann, H. M., Manga, M. (2007) The fluid mechanics inside a volcano. Annual Review of Fluid Mechanics, 39: 321-356

Gonnermann, H. M., Manga, M. (2003) Explosive volcanism may not be an inevitable consequence of magma fragmentation. Nature, 426: 432-435

Gonnermann, H. M., Manga, M. (2012) Dynamics of magma ascent in the volcanic conduit. In: Fagents, S. A., Gregg, T. K. P., Lopes, R. M. C. (eds.) Modelling volcanic processes: the physics and mathematics of volcanism. Cambridge, Cambridge University Press: 55-84

Goslin, J., Thirot, J. -L., Noël, O., Francheteau, J. (1998) Slow-ridge/hotspot interactions from global gravity, seismic tomography and $^{87}Sr/^{86}Sr$ isotope data. Geophysical Journal International, 135: 700-710

Gottsmann, J., Dingwell, D. B. (2002) Thermal expansivities of supercooled haplobasaltic liquids. Geochimica et Cosmochimica Acta, 66: 2231-2238

Greenough, J. D., Dostal, J., Mallory-Greenough, L. M. (2005) Oceanic island volcanism II: Mantle processes. Geoscience Canada, 32: 77-90

Gregg, P. M., De Silva, S. L., Grosfils, E. B., Parmigiani, J. P. (2012) Catastrophic caldera-forming eruptions: Thermomechanics and implications for eruption triggering and maximum caldera dimensions on Earth. Journal of Volcanology and Geothermal Research, 241: 1-12

Gualda, G. A. R., Ghiorso, M. S., Lemons, R. V., Carley, T. L. (2012) Rhyolite-MELTS: a modified calibration of MELTS optimized for silica-rich, fluid-bearing magmatic systems. Journal of Petrology, 53: 875-890

Guest, J. E., Gaspar, J. L., Cole, P. D., Queiroz, G., Duncan, A. M., Wallenstein, N., Ferreira, T., Pacheco, J. M. (1999) Volcanic geology of Furnas volcano, São Miguel, Azores. Journal of Volcanology and Geothermal Research, 92: 1-29

Guest, J. E., Pacheco, J. M., Cole, P. D., Duncan, A. M., Wallenstein, N., Queiroz, G., Gaspar, J. L., Ferreira, T. (2015) The volcanic history of Furnas Volcano, São Miguel, Azores. In: Gaspar, J. L., Guest, J. E., Duncan, A. M., Barriga, F. J. A. S., Chester, D. K. (eds.) 2015, Volcanic geology of São Miguel island (Azores archipelago). Geological Society of London Memoirs, 44: 125-134

Haase, K. M., Beier, C. (2003) Tectonic control of ocean island basalt sources on São Miguel, Azores? Geophysical Research Letters, 30: 1856

Halama, R., Vennemann, T., Siebel, W., Markl, G. (2005) The Grønnedal-Ika carbonatite-syenite complex, South Greenland: carbonatite formation by liquid immiscibility. Journal of Petrology, 46: 191-217

Hammer, J. E., Rutherford, M. J. (2002) An experimental study of the kinetics of decompression-induced crystallisation in silicic melt. Journal of Geophysical Research, B: Solid Earth, 107

Hanan, B. B., Graham, D. W. (1996) Lead and helium isotope evidence from oceanic basalts for a common deep source of mantle plumes. Science, 272: 991-995

Harris, C. (1983) The petrology of lavas and associated plutonic inclusions of Ascension Island. Journal of Petrology, 24: 424-470

Harris, C. (1986) A quantitative study of magmatic inclusions in the plutonic ejecta of Ascension island. Journal of Petrology, 27, 251-276

Harris, C., Rickard, R. S. (1987) Rare-earth-rich eudialyte and dalyite from a peralkaline granite dyke at Straumsvola, Dronning Maud Land, Antarctica. Canadian Mineralogist, 25: 755-762

Hart, S. R. (1988) Heterogeneous mantle domains: signatures, genesis and mixing chronologies. Earth and Planetary Science Letters, 90: 273-296

Hauri, E. H. (1996) Major element variability in the Hawaiian mantle plume. Nature, 382: 415-419

Hawthorne, F. C., Oberti, R., Ottolini, L., Foord, E. E. (1996) Lithium-bearing fluor-arfvedsonite from Hurricane Mountain, New Hampshire: a crystal-chemical study. The Canadian Mineralogist, 34: 1015-1019

Hawthorne, F. C., Oberti, R., Cannillo, E., Ottolini, L., Roelofsen, J. N., Martin, R. F. (2001) Li-bearing arfvedsonitic amphiboles from the Strange Lake peralkaline granite, Quebec. The Canadian Mineralogist, 39: 1161-1170

Henneberger, R., Cabeças, R., Martins, R., Granados, E. (2004) Pico Alto, Terceira: a new geothermal field in the Azores. Geothermal Resources Council Transactions, 28: 345-349

Hildenbrand, A., Madureira, P., Ornelas Marques, F., Cruz, I., Henry, B., Silva, P. (2008) Multi-stage evolution of a subaerial volcanic ridge over the last 1.3 Myr: S Jorge island, Azores triple junction. Earth and Planetary Science Letters, 273: 289-298

Hildner, E., Klügel, A., Hauff, F. (2011) Magma storage and ascent during the 1995 eruption of Fogo, Cape Verde Archipelago. Contributions to Mineralogy and Petrology, 162:751-772

Hildreth, W. (1981) Gradients in silicic magma chambers: Implications for lithospheric magmatism. Journal of Geophysical Research, 86: 10153-10192

Hildreth, W. (2004) Volcanological perspectives on Long Valley, Mammoth Mountain, and Mono Craters: several contiguous but discrete systems. Journal of Volcanology and Geothermal Research, 136: 169-198

Hildreth, W., Fierstein, J. (2000) Katmai volcanic cluster and the great eruption of 1912. Geological Society of America Bulletin, 112: 1594-1620

Hildreth, W., Halliday, A. N., Christiansen, R. L. (1991) Isotopic and chemical evidence concerning the genesis and contamination of basaltic and rhyolitic magma beneath the Yellowstone Plateau volcanic field. Journal of Petrology, 32: 63-137

Hildreth, W., Wilson, C. J. N. (2007) Compositional zoning of the Bishop Tuff. Journal of Petrology, 48: 951-999

Hofmann, A. W. (1997) Mantle geochemistry: the message from oceanic volcanism. Nature, 385: 219-229

Hofmann, A. W. (2003) Sampling mantle heterogeneity through oceanic basalts: isotopes and trace elements. Treatise on Geochmistry, 2: 61-101

Hofmann, A. W., Jochum, K. P. (1996) Source characteristics derived from very incompatible trace elements in Mauna Loa and Mauna Kea basalts., Hawaii Scientific Drilling Project. Journal of Geophysical Research, 101: 11831-11893

Hogarth, D. D., Chao, G. Y., Townsend, M. G. (1987) Potassium- and fluorine-rich amphiboles from the Gatineau area, Quebec. Canadian Mineraologist, 25: 739-753

Holness, M. B., Anderson, A. T., Martin, V. M., Maclennan, J., Passmore, E., Schwindinger, K. (2007) Textures in partially solidified crystalline nodules: a window into the pore structure of slowly cooled mafic intrusions. Journal of Petrology, 48: 1243-1264

Holness, M. B., Sawyer, E. W. (2008) On the pseudomorphing of melt-filled pores during crystallization of migmatites. Journal of Petrology, 49: 1343-1363

Horn, I., Foley, S. F., Jackson, S. E., Jenner, G. A. (1994) Experimentally determined partitioning of high field strength- and selected transition elements between spinel and basaltic melt. Chemical Geology, 117: 193-218

Houghton, B. F., Carey, R. J., Cashman, K. V., Wilson, C. J. N., Hobden, B. J., Hammer, J. E. (2010) Diverse patterns of ascent, degassing, and eruption of rhyolite magma during the 1.8 ka Taupo eruption, New Zealand: evidence from clast vesicularity. Journal of Volcanology and Geothermal Research, 195: 31-47

Houghton, B. F., Weaver, S. D., Wilson, C. J. N., Lanphere, M. A. (1992) Evolution of a Quaternary peralkaline volcano: Mayor Island, New Zealand. Journal of Volcanology and Geothermal Research, 51: 217-236

Houghton, B. F., Wilson, C. J. N., McWilliams, M., Lanphere, M. A., Weaver, S. D., Briggs, R. M., Pringle, M. S. (1995) Chronology and dynamics of a large silicic magmatic system: central Taupo Volcanic Zone, New Zealand. Geology, 23: 13-16

Howie, R. A., Walsh, J. N. (1981) Riebeckitic arfvedsonite and aenigmatite from the Ailsa Craig microgranite. Scottish Journal of Geology, 17:123-128

Huber, C., Bachmann, O., Dufek, J. (2011) Thermo-mechanical reactivation of locked crystal mushes: Melting-induced internal fracturing and assimilation processes in magmas. Earth and Planetary Science Letters, 304: 443-454

Hui, H., Zhang, Y. (2007) Toward a general viscosity equation for natural anhydrous and hydrous silicate melts. Geochimica et Cosmochimica Acta, 71: 403-416

Huppert, H. E., Sparks, R. S. J. (1984) Double diffusive convection due to crystallisation in magmas. Annual Review of Earth and Planetary Sciences, 12: 11-37

Huppert, H. E., Sparks, R. S. J., Wilson, J. R., Hallworth, M. A. (1986) Cooling and crystallisation at an inclined plane. Earth and Planetary Science Letters, 79: 319-328

Illies, J. H. (1969) An intercontinental belt of the world rift system. Tectonophysics, 8: 5-29

Ito, E., White, W. M., Goepel, C. (1987) The O, Sr, Nd and Pb isotope geochemistry of MORB. Chemical Geology, 62: 157-176

Jackson, M. D., Cheadle, M. J., Atherton, M. P. (2003) Quantitative modelling of granitic melt generation and segregation in the continental crust. Journal of Geophysical Research, 108: 2332

Jaupart, C., Allègre, C. J (1991) Gas content, eruption rate and instabilities of eruption regime in silicic volcanoes. Earth and Planetary Science Letters, 102: 413-429

Jean-Baptiste, P., Allard, P., Coutinho, R., Ferreira, T., Fourré, E., Queiroz, G., Gaspar, J. L. (2009) Helium isotopes in hydrothermal volcanic fluids of the Azores archipelago. Earth and Planetary Science Letters, 281: 70-80

Jeffery, A. J., Gertisser, R., Jackson, R. A., O'Driscoll, B., Kronz, A. (2016a) On the compositional variability of dalyite, $K_2ZrSi_6O_{15}$: a new occurrence from Terceira, Azores. Mineralogical Magazine, 80: 547-565

Jeffery, A. J., Gertisser, R., O'Driscoll, B., Pacheco, J. M., Whitley, S., Pimentel, A., Self, S. (2016c) Temporal evolution of a post-caldera, mildly peralkaline magmatic system: Furnas volcano, São Miguel, Azores. Contributions to Mineralogy and Petrology, 171: 42

Jeffery, A. J., Gertisser, R., Pacheco, J. M., Pimentel, A., O'Driscoll, B., Self, S. (2016d) Caldera-forming vs. intra-caldera volcanism at Furnas volcano, São Miguel, Azores: petrological insights from the Povoação Ignimbrite. Journal of Volcanology and Geothermal Research, In Prep

Jeffery, A. J., Gertisser, R., Self, S., Pimentel, A., O'Driscoll, B., Pachco, J. M. (2016b) Petrogenesis of the peralkaline ignimbrites of Tercaira, Azores. Journal of Petrology, In Prep

Jeffery, A. J., Gertisser, R., Troll, V. R., Jolis, E. M., Dahren, B., Harris, C., Tindle, A. G., Preece, K., O'Driscoll, B., Humaida, H., Chadwick, J. P. (2013) The pre-eruptive magma plumbing system of the 2007-2008 dome-forming eruption of Kelut volcano, East Java, Indonesia. Contributions to Mineralogy and Petrology, 166: 275-308

Jellinek, A. M., DePaolo, D. J. (2003) A model for the origin of large silicic magma chambers: precursors of caldera-forming eruptions. Bulletin of Volcanology, 65: 363-381

Johnson, C. L., Wijbrans, J. R., Constable, C. G., Gee, J., Staudigel, H., Tauxe, L., Forjaz, V. H., Salgueiro, M. (1998) 40Ar-39Ar ages and paleomagnetism of São Miguel lavas, Azores. Earth and Planetary Science Letters, 160: 637-649

Jones, G., Chester, D. K., Shooshtariam, F. (1999) Statistical analysis of the frequency of eruptions at Furnas Volcano, São Miguel, Azores. Journal of Volcanology and Geothermal Research, 92: 31-38

Jørgensen, K. A. (1980) The Thórsmörk ignimbrite: an unusual comenditic pyroclastic flow in southern Iceland. Journal of Volcanology and Geothermal Research, 8: 7-22

Kaula, W. M. (1970) Earth's gravity field: relation to global tectonics. Science, 169: 982-985

Kelsey, C. H. (1965) Calculation of the C.I.P.W. norm. Mineralogical Magazine, 34: 276-282

Khomyakov, A. P. (1995) Mineralogy of hyperagpaitic alkaline rocks. Oxford Science Publications, Oxford, UK. 222 pp.

Klemme, S., Gunther, D., Hametner, K., Prowatke, S., Zack, T. (2006) The partitioning of trace elements between ilmenite, ulvospinel, armalcolite and silicate melts with implications for the early differentiation of the moon. Chemical Geology, 234: 251-263

Klügel, A., Hansteen, T. H., Galipp, K. (2005) Magma storage and underplating beneath Cumbre Vieja volcano, La Palma (Canary Islands). Earth and Planetary Science Letters, 236: 211-226

Klügel, A., Hoernle, K. A., Schmincke, H. –U., White, J. D. L. (2000) The chemically zoned 1949 eruption on La Palma (Canary Islands): Petrologic evolution and magma supply dynamics of a rift zone eruption. Journal of Geophysical Research, 105: 5997-6016

Kokelaar, B. P. (1986) Magma-water interactions in subaqueous and emergent basaltic volcanism. Bulletin of Volcanology, 48: 275-290

Konev, A. A., Vorob'ev, E. I., Lasebnik, K. A. (1996) The mineralogy of the Murun alkaline massif. Siberian Branch of the Russian Academy, Scientific Press, Novosibirsk, (in Russ.)

Koppers, A. A. P., Phipps Morgan, J., Morgan, W. J., Staudigel, H. (2001) Testing the fixed hotspot hypothesis using $^{40}Ar/^{39}Ar$ age progressions along seamount trails. Earth and Planetary Science Letters, 185: 237-252

Korenaga, J., Kelemen, P. B. (2000) Major element heterogeneity in the mantle source of the north Atlantic igneous province. Earth and Planetary Science Letters, 184: 251-268

Koyaguchi, T. (2005) An analytical study for 1-dimensional steady flow in volcanic conduits. Journal of Volcanology and Geothermal Research, 143: 29-52

Koyaguchi, T., Kaneko, K. (2001) Thermal evolution of silicic magma chambers after basalt replenishment. Transactions of the Royal Society of Edinburgh, 91: 47-60

Koyaguchi, T., Scheu, B., Mitani, N. K., Melnik, O. (2008) A fragmentation criterion for highly viscous bubbly magmas estimated from shock tube experiments. Journal of Volcanology and Geothermal Research, 178: 58-71

Kozono, T., Koyaguchi, T. (2009) Effects of relative motion between gas and liquid on 1-dimensional steady flow in silicic volcanic conduits: 2. Origin of diversity of eruption styles. Journal of Volcanology and Geothermal Research, 180: 37-49

Krause, D. C. (1966) Tectonics, marine geology, and bathymetry of the Celebes Sea-Sulu Sea region. Geological Society of America Bulletin, 77: 813-832

Krause, D. C., Watkins, N. D. (1970) North Atlantic crustal genesis in the vicinity of the Azores. Geophysical Journal of the Royal Astronomical Society, 19: 261-283

Kress, V. C., Carmichael, I. S. E. (1991) The compressibility of silicate liquids containing Fe_2O_3 and the effect of composition, temperature, oxygen fugacity and pressure on their redox states. Contributions to Mineralogy and Petrology, 108: 82-92

Kröger, F. A., Vink, H. J. (1956) Relations between the concentrations of imperfections in crystalline solids. Solid State Physics, 3, 307-435

Kunzmann, T. (1999) The aenigmatite-rhönite mineral group. European Journal of Mineralogy, 11: 743-756

Kurz, M. D., Jenkins, W. J., Schilling, J. G., Hart, S. R. (1982) Helium isotopic variations in the mantle beneath the central North Atlantic Ocean. Earth and Planetary Science Letters, 58: 1-14

Lange, R. A. (1994) The effect of H_2O, CO_2 and F on the density and viscosity of silicate melts. In: Carroll, M. R., Holloway, J. R. (eds.) Volatiles in Magmas. Mineralogical Society of America, Reviews in Mineralogy, 30: 331-365

Larrea, P., França, Z., Lago, M., Widom, E., Galé, C., Ubide, T. (2013) Magmatic processes and the role of antecrysts in the genesis of Corvo island (Azores archipelago), Portugal. Journal of Petrology, 54: 769-793

Larrea, P., Galé, C., Ubide, T., Widom, E., Lago, M., França, Z. (2014) Magmatic evolution of Graciosa (Azores, Portugal). Journal of Petrology, 55: 2125-2154

Larsen, L. M. (1976) Clinopyroxenes and coexisting mafic minerals from the alkaline Ilímaussaq intrusion, South Greenland. Journal of Petrology, 17: 258-290

Larsen, L. M. (1979) Distribution of Ree and Other Trace-Elements between Phenocrysts and Peralkaline Undersaturated Magmas, Exemplified by Rocks from the Gardar Igneous Province, South Greenland. Lithos, 12: 303-315

Latourrette, T., Hervig, R. L., Holloway, J. R. (1995) Trace-Element Partitioning between Amphibole, Phlogopite, and Basanite Melt. Earth and Planetary Science Letters, 135: 13-30

Lazebnik, K. A., Makhotko, V. F. (1982) Dalyite, the first finding in the USSR. Zapiski Vsesoyuznogo Mineralogicheskogo Obschestva, 111: 587-593

Leake, B. E., Woolley, A. R., Arps, C. E. S., Birch, W. D., Gilbert, M. C., Grice, J. D., Hawthorne, F. C., Kato, A., Kisch, H. J., Krivovichev, V. G., Linthout, K., Laird, J., Mandarino, J. A., Maresch, W. V., Nickel, E. H., Rock, N. M. S., Schumacher, J. C., Smith, D. C., Stephenson, N. C. N., Ungaretti, L., Whittaker, E. J. W., Youzhi, G. (1997) Nomenclature of amphiboles: report of the subcommittee on amphiboles of the international mineralogical

association, commission on new minerals and mineral names. The Canadian Mineralogist, 35: 219-246

Leat, P. T., Macdonald, R., Smith, R. L. (1984) Geochemical evolution of the Menengai caldera volcano, Kenya. Journal of Geophysical Research, 89: 8571-8592

Le Bas, M. J., Le Maitre, R. W., Streckeisen, A., Zanettin, B. (1986) A chemical classification of volcanic rocks based on the Total Alkali-Silica diagram. Journal of Petrology, 27: 745-750

Le Douaran, S., Francheteau, J. (1981) Axial depth anomalies from 10 to 50° north along the Mid-Atlantic Ridge: correlation with other mantle properties. Earth and Planetary Science Letters, 54: 29-47

Lee, M. R., Parsons, I. (1997) Dislocation formation and albitisation in alkali feldspars from the Shap granite. American Mineralogist, 82: 557-570

Lemarchand, F., Benoit, V., Calais, G. (1987) Trace element distribution coefficients in alkaline series. Geochimica et Cosmochimica Acta, 51: 1071-1081

Lepage, L. D. (2003) ILMAT: an excel worksheet for ilmenite-magnetite geothermometry and geobarometry. Computers and Geosciences, 29: 673-678

Lindsay, J. M., Schmitt, A. K., Trumbull, R. B., De Silva, S. L., Siebel, W., Emmermann, R. (2001) Magmatic evolution of the La Pacana caldera system, Central Andes, Chile: compositional variation of two cogenetic, large-volume felsic ignimbrites. Journal of Petrology, 42: 459-486

Linthout, K., Nobel, F. A., Lustenhouwer, W. J. (1988) First occurrence of dalyite in extrusive rock. Mineralogical Magazine, 52: 705-708

Lipman, P. W. (2000) Calderas. In: Sigurdsson, H. (ed.) Encyclopedia of Volcanoes. Academic Press, London, 643-662:

Llewellin, E. W., Mader, H. M., Wilson, S. D. R. (2002) The constitutive equation and flow dynamics of bubbly magmas. Geophysical Research Letters, 29: 24

Lloyd, E. F., Collis, S. K. (1981) Geothermal prospection-Ilha Terceira, Acores: Geological report: Geothermal Energy New Zealand Ltd., under contract to the Secretaria Regional do Comercio e Industria, Governo Regional dos Acores, 96 p.

Longpré, M. A., Troll, V. R., Hansteen, T. H. (2008) Upper mantle magma storage and transport under a Canarian shield-volcano, Teno, Tenerife (Spain). Journal of Geophysical Research, 113:B08203

Lourenço, N., Miranda, J. M., Luis, J. F., Ribeiro, A., Mendes Victor, L. A., Madeira, J., Needham, H. D. (1998) Morpho-tectonic of the Azores Volcanic Plateau from a new bathymetric compilation of the area. Marine Geophysical Researches, 20: 141-156

Lowenstern, J. B. (1994) Chlorine, fluid immiscibility, and degassing in peralkaline magmas from Pantelleria, Italy. American Mineralogist, 79: 353-369

Lowenstern, J. B., Charlier, B. L. A., Clynne, M. A., Wooden, J. L. (2006) Extreme U-Th disequilibrium in rift-related basalts, rhyolites and granophyric granite and the timescale of rhyolite generation, intrusion and crystallisation at Alid volcanic center, Eritrea. Journal of Petrology, 47: 2105-2122

Lowenstern, J. B., Mahood, G. A. (1991) New data on magmatic H_2O contents of pantellerites, with implications for petrogenesis and eruptive dynamics at Pantelleria. Bulletin of Volcanology, 54: 78-83

Luhr, J. F., Carmichael, I. S. E., Varekamp, J. C. (1984) The 1982 eruptions of El Chichon volcano, Chiapas, Mexico: mineralogy and petrology of the anhydrite-bearing pumices. Journal of Volcanology and Geothermal Research, 23: 69-108

Luis, J. F., Miranda, J. M. (2008) Reevaluation of magnetic chrons in the North Atlantic between 35°N and 47°N: implications for the formation of the Azores Triple Junction and associated plateau. Journal of Geophysical Research, 113: B10105

Luis, J. F., Miranda, J. M., Galdeano, A., Patriat, P., Rossignol, J. C., Mendes Victor, L. A. (1994) The Azores triple junction evolution since 10 Ma from an aeromagnetic survey of the Mid-Atlantic Ridge. Earth and Planetary Science Letters, 125: 439-459

Macdonald, R. (1974a) Nomenclature and Petrochemistry of the peralkaline oversaturated extrusive rocks. Bulletin of Volcanology, 38: 498-505

Macdonald, R. (1974b) Tectonic settings and magma associations. Bulletin of Volcanology, 38: 575-593

Macdonald, R. (2012) Evolution of peralkaline silicic complexes: lessons from the extrusive rocks. Lithos, 152: 11-22

Macdonald, R., Bagiński, B., Leat, P. T., White, J. C., Dzierżanowski, P. (2011) Mineral stability in peralkaline silicic rocks: information from trachytes of the Menengai volcano, Kenya. Lithos, 125: 553-568

Macdonald, R., Bagiński, B., Ronga, F., Dzierżanowski, P., Lustrini, M., Marzoli, A., Meluso, L. (2012) Evidence for extreme fractionation of peralkaline silicic magmas, the Boseti volcanic complex, Main Ethiopian Rift. Mineralogy and Petrology, 104: 163-175

Macdonald, R., Bagiński, B., Upton, B. G. J. (2014) The volcano-pluton interface; The Longonot (Kenya) and Kûngnât (Greenland) peralkaline complexes. Lithos, 196-197

Macdonald, R., Belkin, H. E., Fitton, J. G., Rogers, N. W., Nejbert, K., Tindle, A. G., Marshall, A. S. (2008) The roles of fractional crystallisation, magma mixing, crystal mush remobilisation and volatile-melt interactions in the genesis of a young basalt-peralkaline rhyolite suite, the Greater Olkaria Volcanic Complex, Kenya Rift Valley. Journal of Petrology, 49: 1515-1547

Macdonald, R., Davies, G. R., Bliss, C. M., Leat, P. T., Bailey, D. K., Smith, R. L. (1987) Geochemistry of high-silica peralkaline rhyolites, Naivasha, Kenya Rift Valley. Journal of Petrology, 28: 979-1008

Macdonald, R., Davies, G. R., Upton, B. G. J., Dunkley, P. N., Smith, M., Leat, P. T. (1995) Petrogenesis of Silali volcano, Gregory Rift, Kenya. Journal of the Geological Society of London, 152: 703-720

Macdonald, R., McGarvie, D. W., Pinkerton, H., Smith, R. L., Palacz, Z. A. (1989) Petrogenetic evolution of the Torfajökull volcanic complex, Iceland I. Relationship between the magma types. Journal of Petrology, 31: 429-459

Macdonald, R., Navarro, J. M., Upton, B. G. J., Davies, G. R. (1994) Strong compositional zonation in peralkaline magma: Menengai, Kenya Rift Valley. Journal of Volcanology and Geothermal Research, 60: 301-325

Macdonald, R., Scaillet, B. (2006) The central Kenya peralkaline province: insights into the evolution of peralkalinesalic magmas. Lithos, 91: 59-73

Macdonald, R., Sumita, M., Schmincke, H. –U., Bagiński, B., White, J. C., Ilnicki, S. S. (2015) Peralkaline felsic magmatism at the Nemrut volcano, Turkey: impact of volcanism on the evolution of Lake Van (Anatolia) IV. Contributions to Mineralogy and Petrology, 169: 34

Machado, F. (1955) The fracture pattern of Azorean volcanoes. Bulletin of Volcanology, 17: 119-125

Machado, F. (1967) Active volcanoes of the Azores. Catalogue of the Active Volcanoes of the World, part 21, Atlantic Ocean, International Association of Volcanology, Rome: 9-52

Machado, F. (1972) Acid volcanoes of San Miguel, Azores. Bulletin of Volcanology, 36: 319-327

Madeira, J., Ribeiro, A. (1990) Geodynamic models for the Azores triple junction: a contribution from tectonics. Tectonophysics, 184: 405-415

Madureira, P., Mata, J., Mattielli, N., Queiroz, G., Silva, P. (2011) Mantle source heterogeneity, magma generation and magmatic evolution at Terceira Island (Azores archipelago): Constraints from elemental and isotopic (Sr, Nd, Hf, and Pb) data. Lithos, 126: 402-418

Madureira, P., Moreira, M., Mata, J., Allègre, C. -J. (2005) Primitive neon isotopes in Terceira Island (Azores archipelago). Earth and Planetary Science Letters, 233: 429-440

Mahood, G. A. (1981) Chemical evolution of a Pleistocene rhyolitic center: Sierra La Primavera, Jalisco, México. Contributions to Mineralogy and Petrology, 77: 129-149

Mahood, G. A. (1984) Pyroclastic rocks and calderas associated with strongly peralkaline magmatism. Journal of Geophysical Research, 89: 8540-8552

Mahood, G. A., Baker, D. R. (1986) Experimental constraints on depths of fractionation of mildly alkalic basalts and associated felsic rocks: Pantelleria, Strait of Sicily. Contributions to Mineralogy and Petrology, 93: 251-264

Mahood, G. A., Halliday, A. N. (1988) Generation of high-silica rhyolite: a Nd, Sr, and O isotopic study of Sierra La Primavera, Mexican neovolcanic belt. Contributions to Mineralogy and Petrology, 100: 183-191

Mahood, G. A., Halliday, A. N., Hildreth, W. (1990) Isotopic evidence for the origin of pantellerites in a rift-related alkalic suite: Pantelleria, Italy. IAVCEI Abstracts, International Volcanological Congress, Mainz

Mahood, G. A., Hildreth, W. (1986) Geology of the peralkaline volcano at Pantelleria, Strait of Sicily. Bulletin of Volcanology, 48: 143-172

Mahood, G. A., Stimac, J. A. (1990) Trace element partitioning in pantellerites and trachytes. Geochimica et Cosmochimica Acta, 54: 2257-2276

Malfait, W. J., Seifert, R., Petitgirard, S., Perrillat, J. –P., Mezouar, M., Ota, T., Nakamura, E., Lerch, P., Sanchez-Valle, C. (2014) Supervolcano eruptions driven by melt buoyancy in large silicic magma chambers. Nature Geoscience, 7: 122-125

Mandeville, C. W., Webster, J. D., Rutherford, M. J., Taylor, B. E., Timbal, A., Faure, K. (2002) Determination of molar absorptivities for infrared absorption bands of H2O in andesitic glasses. American Mineralogist, 87: 813-821

Mann, U., Marks, M., Markl, G. (2006) Influence of oxygen fugacity on mineral compositions in peralkaline melts: The Katzenbuckel volcano, Southwest Germany. Lithos, 91: 262-285

Manning, D. A. C. (1981) The effect of fluorine on liquidus phase relationships in the system Qz-Ab-Or with excess water. Contributions to Mineralogy and Petrology, 76: 206-215

Mariano, A. N., Francis, C. A. (1989) Dalyite from fenites in carbonatite complexes of the Minas Gerais – Goias belt, Brazil. Geological Society of America Abstract Programs, 21: A46

Mariano, A. N., Marchetto, M. (1991) Serra Negra and Salitre – carbonatite alkaline igneous complex. In: Leonardos, O. H., Meyer, H. O. A., Gaspar, J. C. (eds.) 5th International Kimberlite Conference (Field Guide Book). Araxá, Brazil, CPRM, Special publication, 3/91: 75-79

Markl, G., Marks, M. A. W., Frost, B. R. (2010) On the controls of oxygen fugacity in the generation and crystallisation of peralkaline melts. Journal of Petrology, 51, 1831-1847

Markl, G., Marks, M., Schwinn, G., Sommer, H. (2001) Phase equilibrium constraints upon intensive crystallisation parameters of the Ilímaussaq complex, South Greenland. Journal of Petrology, 42: 2231-2258

Marks, M. A. W., Halama, R., Wenzel, T., Markl, G. (2004) Trace element variations in clinopyroxene and amphibole from alkaline to peralkaline syenites and granites: implications for mineral-melt trace-element partitioning. Chemical Geology, 211: 185-215

Marks, M. A. W., Hettmann, K., Schilling, J., Frost, B. R., Markl, G. (2011) The mineralogical diversity of alkaline igneous rocks: critical factors for the transition from miaskitic to agpaitic phase assemblages. Journal of Petrology, 52: 439-455

Marks, M. A. W., Markl, G. (2015) The Ilímaussaq alkaline complex, South Greenland. In: Charlier, B., Manur, O., Latypov, R., Tegner, C. (eds.) Layered Intrusions. Springer, Dordrecht, 649-692

Marks, M. A. W., Rudnik, R. L., Ludwig, T., Marschall, H., Zack, T., Halama, R., McDonough, W. F., Rost, D., Wenzel, T., Vicenzi, E. P., Savov, I. P., Altherr, R., Markl, G. (2008) Sodic pyroxene and sodic amphibole as potential reference materials for *in situ* lithium isotope determinations by SIMS. Geostandards and Geoanalytical Research, 32: 295-310

Marks, M. A. W., Schilling, J., Coulson, I. M., Wenzel, T., Markl, G. (2008) The alkaline-peralkaline Tamazeght complex, High Atlas Mountains, Morocco: mineral chemistry and petrological constraints for derivation from a compositionally heterogeneous mantle source. Journal of Petrology, 49: 1097-1131

Marks, M., Vennemann, T., Siebel, W., Markl, G. (2003) Quantification of magmatic and hydrothermal processes in a peralkaline syenite-alkali granite complex based on textures, phase equilibria, and stable and radiogenic isotopes. Journal of Petrology, 44: 1247-1280

Marques, F. O., Catalão, J. C., DeMets, C., Costa, A. C. G., Hildenbrand, A. (2013) GPS and tectonic evidence for a diffuse plate boundary at the Azores triple junction. Earth and Planetary Science Letters, 281: 177-187

Marsh, B. D. (1981) On the crystallinity, probability of occurrence, and rheology of lava and magma. Contributions to Mineralogy and Petrology, 78: 85-98

Marsh, B. D. (2002) On bimodal differentiation by solidification front instability in basaltic magmas, part 1: basic mechanics. Geochimica et Cosmochimica Acta, 66: 2211-2229

Marsh, J. S. (1975) Aenigmatite stability in silica-undersaturated rocks. Contributions to Mineralogy and Petrology, 50: 135-144

Marshall, A. S., Macdonald, R., Rogers, N. W., Fitton, J. G., Tindle, A. G., Nejbert, K., Hinton, R. W. (2009) Fractionation of peralkaline silicic magmas: the Greater Olkaria Volcanic Complex, Kenya Rift Valley. Journal of Petrology, 50: 323-359

Matsui, Y., Onuma, N., Nagasawa, H., Higuchi, H., Banno, S. (1977) Crystal structure control in trace element partition between crystal and magma. Tectonics, 100: 315-324

Mattsson, H. B. (2010) Textural variation in juvenile pyroclasts from an emergent Surtseyan-type, volcanic eruption: the Capelas tuff cone, São Miguel (Azores). Journal of Volcanology and Geothermal Research, 189: 81-91

McBirney, A. R., Gass, I. G. (1967) Relations of oceanic volcanic rocks to mid-oceanic rises and heat flow. Earth and Planetary Science Letters, 2: 265-276

McBirney, A. R. (1980) Mixing and unmixing of magmas. Journal of Volcanology and Geothermal Research, 7: 357-371

McBirney, A. R., Baker, B. H., Nilson, R. H. (1985) Liquid fractionation. Part 1: Basic Principles and experimental simulations. Journal of Volcanology and Geothemal Research, 24: 1-24

McCallum, I. S., Charette, M. P. (1978) Zr and Nb partition coefficients: implications for the genesis of mare basalts, kreep, and sea floor basalts. Geochimica et Cosmochimica Acta, 42: 859-869

McDougall, I., Schmincke, H.-U. (1976) Geochronology of Gran Canaria, Canary islands: age of shield building volcanism and other magmatic phases. Bulletin of Volcanology, 40: 57-77

McKenzie, D. (1984) The generation and compaction of partially molton rock. Journal of Petrology, 25: 713-765

McKenzie, D., O'Nions, R. K. (1983) Mantle reservoirs and ocean island basalts. Nature, 301, 229-231

McKenzie, D., O'Nions, R. K. (1991) Partial melt distributions from inversion of rare Earth element concentrations. Journal of Petrology, 32: 1021-1091

McKenzie, D., O'Nions, R. K. (1995) The source regions of ocean island basalts. Journal of Petrology, 36: 133-159

Melia, T. P., Moffitt, W. P. (1964) Crystallisation from aqueous solution. Journal of Colloid Science, 19: 433-447

Melnik, O., Sparks, R. S. J. (1999) Nonlinear dynamics of lava dome extrusion. Nature, 402: 37-41

Melnik, O., Sparks, R. S. J. (2002) Modelling of conduit flow dynamics during explosive activity at Soufrière Hills volcano, Montserrat. Geological Society of London Memoirs, 21: 307-317

Menard, H. W., Atwater, T. (1968) Changes in direction of sea-floor spreading. Nature, 219: 463-467

Métrich, N., Zanon, V., Créon, L., Hildenbrand, A., Moreira, M., Marques, F. O. (2014) Is the 'Azores Hotspot' a wetspot? Insights from the geochemistry of fluid and melt inclusions in olivine of Pico basalts. Journal of Petrology, 55: 377-393

Michael, P. J. (1983) Chemical differentiation of the Bishop Tuff and other high-silica magmas through crystallisation processes. Geology, 11: 31-34

Millard, G. A., Mather, T. A., Pyle, D. M., Rose, W. I., Thornton, B. F. (2006) Halogen emissions from a small volcanic eruption: modelling the peak concentrations, dispersion and volcanically induced ozone loss in the stratosphere. Geophysical Research Letters, 33: L19815

Millet, M. A., Doucelance, R., Baker, J. A., Schiano, P. (2009) Reconsidering the origins of isotopic variations in ocean island basalts: insights from fine-scale study of São Jorge island, Azores archipelago. Chemical Geology, 265: 289-302

Mitchell, R. H., Bergman, S. C. (1991) Petrology of Lamproites. Plenum Press New York. 410 pp.

Mollo, S., Masotta, M., Forni, F., Bachmann, O., De Astis, G., Moore, G., Scarlato, P. (2015) A K-feldspar-liquid hygrometer specific to alkaline differentiated magmas. Chemical Geology, 392: 1-8

Montesinos, F. G., Camacho, A. G., Vieira, R. (1999) Analysis of gravimetric anomalies in Furnas caldera (São Miguel, Azores). Journal of Volcanology and Geothermal Research, 92: 67-81

Moore, R. B. (1990) Volcanic geology and eruption frequency, São Miguel, Azores. Bulletin of Volcanology, 52: 602-614

Moore, R. B. (1991a) Geology of three Late Quaternary stratovolcanoes on São Miguel, Azores. U.S. Geological Survey Bulletin 1900, 1-46

Moore, R. B. (1991b) Geologic map of São Miguel, Azores. United States Geological Survey Miscellaneous Investigations Series, Denver, Map I-2007

Moore, R. B., Rubin, M. (1991) Radiocarbon dates for lava flows and pyroclastic deposits on São Miguel, Azores. Radiocarbon, 33: 151-164

Moreira, M., Doucelance, R., Kurz, M. D., Dupré, B., Allègre, C. -J. (1999) Helium and lead isotope geochemistry of the Azores archipelago. Earth and Planetary Science Letters, 169: 189-205

Morey, G. W., Hesselgesser, J. M. (1952) The system H_2O-Na_2O-SiO_2 at 400 °C. American Journal of Science, Bowen Volume, 343-372

Morgan, W. J. (1971) Convection plumes in the lower mantle. Nature, 42: 42-43

Morimoto, N., Fabries, J., Ferguson, A. K., Ginzburg, I. V., Ross, M., Seifert, F. A., Zussman, J., Aoki, K., Gottardi, G. (1988) Nomenclature of pyroxenes. Mineralogical Magazone, 52:535-550

Morra, V., Secchi, F. A., Assorgia, A. (1994) Petrogenetic significance of peralkaline rocks from Cenozoic calc-alkaline volcanism from SW Sardinia, Italy. Chemical Geology, 118: 109-142

Mueller, S., Scheu, B.,Spieler, O., Dingwell, D. B. (2008) Permeability control on magma fragmentation. Geology, 36: 399-402

Mujaji, M., Burrows, J., Jackson, R. A. (2014) Optical spectroscopy of the Nd^{3+} and Nd^{3+} - Gd^{3+}/Yb^{3+} centres in BaF_2 single crystals and calculations on lanthanide-doped BaF_2. Journal of Luminescence, 151: 106-110

Mungall, J. E. (1993) Compositional effects of magma mixing and diffusive mass transport on a basalt-pantellerite suite, Terceira, Azores. [Ph.D. thesis] McGill University, Montreal, 385 p.

Mungall, J. E., Martin, R. F. (1995) Petrogenesis of basalt-comendite and basalt-pantellerite suites, Terceira, Azores, and some implications for the origin of oceanic-island rhyolites. Contributions to Mineralogy and Petrology, 119: 43-55

Mungall, J. E., Martin, R. F. (1996) Extreme differentiation of peralkaline rhyolite, Terceira, Azores: a modern analogue of Strange Lake, Labrador? The Canadian Mineralogist, 34: 769-777

Mysen, B. O., Kushiro, I., Nicholls, I. A., Ringwood, A. E. (1974) A possible mantle origin for andesitic magmas: a discussion of a paper by Nicholls and Ringwood. Earth and Planetary Science Letters, 21: 221-229

Neave, D. A., Fabbro, G., Herd, R. A., Petrone, C. M., Edmonds, M. (2012) Melting, differentiation and degassing at the Pantelleria volcano, Italy. Journal of Petrology, 53: 637-663

Neumann, E. -R., Olsen, K. H., Baldridge, W. S., Sundvoll, B. (1992) The Oslo Rift: a review. Tectonphysics, 208: 1-18

Nicholls, J., Carmichael, I. S. E. (1969) Peralkaline acid liquids: a petrological study. Contributions to Mineralogy and Petrology, 20: 268-294

Nielsen, R. L. (1992) BIGD: a FORTRAN program to calculate trace-element partition coefficients for natural mafic and intermediate composition magmas. Computers and Geosciences, 18: 773-788

Nielsen, R. L. (2006) Geochemical Earth Reference Model (GERM) partition coefficient (Kd) database. Available at: www.earthref.org/KDD/

Nielsen, R. L., Gallahan, W. E., Newberger, F. (1992) Experimentally determined mineral-melt partition coefficients for Sc, Y and REE for olivine, orthopyroxene, pigeonite, magnetite and ilmenite. Contributions to Mineralogy and Petrology, 110: 488-499

Nimis, P. (1995) A clinopyroxene geobarometer for basaltic systems based on crystal-structure modelling. Contributions to Mineralogy and Petrology, 121:115-125

Nimis, P., Taylor, W. R. (2000) Single clinopyroxene thermobarometry for garnet peridotites. part I. Calibration and testing of a Cr-in-Cpx barometer and an enstatite-in-Cpx thermometer. Contributions to Mineralogy and Petrology, 139:541-554

Noble, D. C., Parker, D. F. (1974) Peralkaline silicic volcanic rocks of western United States. Bulletin of Volcanology, 38: 803-827

Nougier, J. (1970) Contribution à l'étude géologique et géomorphologique des îles Kerguelen (TAAF). CFNRA, Paris, 27: 246 pp.

Novak, S. W., Mahood, G. A. (1986) Rise and fall of a basalt-trachyte-rhyolite magma system at the Kane Springs Wash Caldera, Nevada. Contributions to Mineralogy and Petrology, 94: 353-373

Nunes, J. C. (1999) Actividade vulcânica na ilha do PicoPlistocénico superior ao Holocénico: mecanismo eruptive e hazard vulcânico. Unpublished Ph.D thesis, University of the Azores, Ponta Delgada

Nunes, J. C., Forjaz, V. H., Alves, J. L., Bernardes, A. C. (2003) Caracterização 886 vulcanológica do Banco D. João de Castro (Açores): novos dados. Ciências da Terra (UNL), V(CD-ROM), D55-D58.

Nyonfang, E., Nono, A. (2003) Clinopyroxenes from some felsic alkaline rocks of the Cameroon Line, central Africa: petrological implications. European Journal of Mineralogy, 15: 527-542

Nystuen, J. P. (1975) Plutonic and subvolcanic intrusions in the Hurdal area, Oslo region. Norges Geologiske Undersokelse Bulletin, 317: 1-21

Oberti, R., Ungaretti, L., Cannillo, E., Hawthorne, F. C. (1992) The behaviour of Ti in amphiboles: I. Four- and six-coordinate Ti in richterite. European Journal of Mineraology, 4: 425-439

Oskarsson, N., Pálsson, K., Ólafsson, H., Ferreira, T. (1999) Experimental monitoring of carbon dioxide by low power IR-sensors: soil degassing in the Furnas Volcanic Centre, Azores. Journal of Volcanology and Geothermal Research, 92: 121-193

Pacheco, J. M. (2001) Processos associados ao desenvolvimento de erupções vulcânicas hidromagmáticas explosivas na ilha do Faial e sua interpretação numa perspectiva de avaliação do hazard e minimização do risco. Unpublished PhD thesis, Universidade dos Açores

Papale, P. (1999) Strain-induced magma fragmentation in explosive eruptions. Nature, 397: 425-428

Parker, D. F., White, J. C. (2008) Large-scale silicic alkalic magmatism associated with the Buckhorn Caldera, Trans-Pecos Texas, USA: comparison with Pantelleria, Italy. Bulletin of Volcanology, 70: 403-415

Pasquier-Cardin, A., Allard, P., Ferreira, T., Hatte, C., Coutinho, R., Fontugne, M., Jaudon, M. (1999) Magma-derived CO_2 emissions recorded in ^{14}C and ^{13}C content of plants growing in Furnas caldera, Azores. Journal of Volcanology and Geothermal Research, 92: 195-207

Paster, T. P., Schauwecker, D. S., Haskin, L. A. (1974) The behavior of some trace elements during solidification of the Skaergaard layered series. Geochimica et Cosmochimica Acta, 38: 1549-1577

Peccerillo, A., Barberio, M. R., Yirgu, G., Ayalew, D., Barbieri, M., Wu, T. W. (2003) Relationships between mafic and peralkaline silicic magmatism in continental rift settings: a petrological, geochemical and isotopic study of Gedemsa volcano, Central Ethiopian Rift. Journal of Petrology, 44: 2003-2032

Peccerillo, A., Donati, C., Santo, A. P., Orlando, A., Yirgu, G., Ayalew, D. (2007) Petrogenesis of silicic peralkaline rocks in the Ethiopian rift: geochemical evidence and volcanological implications. Journal of African Sciences 48: 161-173

Pensa, A., Giordano, G., Cas, R. A. F., Porreca, M. (2015) Thermal state and implications for eruptive styles of the intra-Plinian and climactic ignimbrites of the 4.6 ka Fogo A eruption sequence, São Miguel, Azores. Bulletin of Volccanology, 77: 99

Petford, N., Lister, J. R., Kerr, R. C. (1994) The ascent of felsic magmas in dyke. Lithos, 32: 161-168

Pfänder, J. A., Münker, C., Stracke, A., Mezger, K. (2007) Nb/Ta and Zr/Hf in ocean island basalts – implications for crust-mantle differentiation and the fate of niobium. Earth and Planetary Science Letters, 254: 158-172

Phemister, J., Harvey, C. O., Sabine, P. A. (1950) The riebeckite-bearing dikes of Shetland. Mineralogical Magazine, 29: 359-373

Philpotts, A. R., Carrol, M., Hill, J. M. (1996) Crystal-mush compaction and the origin of pegmatitic segregation sheets in a thick flood-basalt flow in the Mesozoic Hartford Basin, Connecticut. Journal of Petrology, 37: 811-836

Pimentel, A. (2006) Domos e coulées da ilha Terceira: contribuição por o estudo dos mecanismos de instalação. Unpublished M.Sc thesis, Departamento de Geociêcias, Ponta Delgada, Universidade dos Açores

Pimentel, A., Pacheco, J., Self, S. (2015) The ~1000-years BP explosive eruption of Caldeira Volcano (Faial, Azores): the first stage of incremental caldera formation. Bulletin of Volcanology, 77:42

Pistone, M., Arzilli, F., Dobson, K. J., Cordonnier, B., Reusser, E., Ulmer, P., Marone, F., Whittington, A. G., Mancini, L., Fife, J. L., Blundy, J. D. (2015) Gas-driven filter pressing in magmas: Insights into *in-situ* melt segregation from crystal mushes. Geology, 43: 699-702

Prytulak, J., Elliot, T. (2009) Determining melt productivity of mantle sources from ^{238}U-^{230}Th and ^{235}U-^{231}Pa disequilibria; an example from Pico Island, Azores. Geochimica et Cosmochimica Acta, 73: 2103-2122

Putirka, K. D. (2008) Thermometers and barometers for volcanic systems. Reviews in Mineralogy and Geochemistry, 69:61-120

Putirka, K., Johnson, M., Kinzler, R., Longhi, J., Walker, D. (1996) Thermobarometry of mafic igneous rocks based on clinopyroxene-liquid equilibria, 0-30 kbar. Contributions to Mineralogy and Petrology, 123: 92-108

Putirka, K. D., Mikaelian, H., Ryerson, F., Shaw, H. (2003) New clinopyroxene-liquid thermobarometers for mafic, evolved, and volatile-bearing lava compositions, with applications to lavas from Tibet and the Snake River Plain, Idaho. American Mineralogist, 88: 1542-1554

Putnis, A., Mauthe, G. (2001) The effect of pore size on cementation in porous rocks. Geofluids, 1: 37-41

Putnis, A., Prieto, M., Fernandez-Diaz, L. (1995) Supersaturation and crystallisation in porous media. Geological Magazine, 132: 1-13

Pyle, D. M., Mather, T. A. (2009) Halogens in igneous processes and their fluxes to the atmosphere and oceans from volcanic activity: A review. Chemical Geology, 263: 110-121

Queiroz, G. (1998) Vulcão das Sete Cidades (S. Miguel, Açores) historia eruptive e avaliação do hazard. [Ph.D Thesis] University of the Azores.

Quin, J. P. (1962) La lindinosite (granite mesocrate à riebeckite) du massif d'Evisa. Bulletin de la Societe Geologique de France, 4: 380-383

Raade, G., Mladeck, M. H. (1983) Janhaugite, $Na_3Mn_3Ti_2Si_4O_{15}(OH,F,O)_3$, a new mineral from Norway. American Mineralogist, 68: 1216-1219

Rabinowicz, M., Genthon, P., Ceuleneer, G., Hillairet, M. (2001) Compaction in a mantle mush with high melt concentrations and the generation of magma chambers. Earth and Planetary Science Letters, 188: 313-328

Rasmussen, E., Neumann, E. -R., Andersen, T., Sundvoll, B., Fjerdingstad, V., Stabel, A. (1988) Petrogenetic processes associated with intermediate and silicic magmatism in the Oslo Rift, south-east Norway. Mineralogical Magazine, 52: 293-307

Reguir, E. (2001) Aspects of the mineralogy of the Murun alkaline complex, Yakutia, Russia. [M.Sc thesis]. Lakehead University, Canada, 193 pp.

Reimer, P. J., Bard, E., Bayliss, A., Beck, J. W., Blackwell, P. G., Bronk Ramsey, C., Buck, C. E., Cheng, H., Edwards, R. L., Friedrich, M. (2013) IntCal13 and Marine13 radiocarbon age calibration curves 0-50,000 years cal BP. Radiocarbon, 55: 1869-1887

Ren, M., Omenda P. A., Anthony, E. Y., White, J. C., Macdonald, R., Bailey, D. K. (2006) Application of the QUILF thermobarometer to the peralkaline trachytes and pantellerites of the Eburru volcanic complex, East African Rift, Kenya. Lithos, 91: 109-124

Renzulli, A., Santi, P. (2000) Two-stage fractionation history of the alkali basalt-trachyte series of Sete Cidades volcano (São Miguel island, Azores). European Journal of Mineralogy, 12: 469-494

Ribeiro, A. (2002) Soft Plate and Impact Tectonics. Springer-Verlag, 324 pp.

Rice, A. (1981) Convective fractionation: a mechanism to provide cryptic zoning (macrosegregation), layering crescumulates, banded tuffs and explosive volcanism in igneous processes. Journal of Geophysical Research, 86: 405-417

Richards, A. F. (1966) Geology of the islas Revillagigedo, Mexico, 2. Geology and petrography of isla San Benedicto. Proceedings of the Californian Academy of Sciences, 33: 361-414

Ridley, W. I., Watkins, N. D., MacFarlane, D. J. (1974). Chapter 12: The Oceanic Islands: Azores. In: Nairn, A., E., M., Stehli, F., G., (eds.) The Ocean Basins and Margins, Volume 2: The North Atlantic. London: *New-York/London: Plenum Press*. 445-484

Ridolfi, F. (2004) REE-and HFSE-minerals in peralkaline syenites: crystal chemistry and petrogenetic significance. SIMP, Plinius, 30: 202-206

Ridolfi, F., Renzulli, A., Santi, P., Upton, B. G. J. (2003) Evolutionary stages of crystallization of weakly peralkaline syenites: evidence from ejecta in the plinian deposits of Agua de Pau volcano (São Miguel, Azores Islands). Mineralogical Magazine, 67: 749-767

Ritsema, J., Allen, R. M. (2003) The elusive mantle plume. Earth and Planetary Science Letters, 207: 1-12

Robins, B., Furnes, H., Ryan, P. (1983) A new occurrence of dalyite. Mineralogical Magazine, 47: 93-94

Rogers, N. W., Evans, P. J., Blake, S., Scott, S. C., Hawkesworth, C. J. (2004) Rates and timescales of fractional crystallisation from ^{238}U-^{230}-Th-^{226}Ra disequilibria in trachyte lavas from Longonot volcano, Kenya. Journal of Petrology, 45: 1747-1776

Rooney, T. O., Hart, W. K., Hall, C. M., Ayalew, D., Ghiorso, M. S., Hidalgo, P., Yirgu, G. (2012) Peralkaline magma evolution and the tephra record in the Ethiopian Rift. Contributions to Mineralogy and Petrology, 164: 407-426

Rose, W. I., Millard, G. A., Mather, T. A., Hunton, D. E., Anderson, B., Oppenheimer, C., Thornton, B. F., Gerlach, T. M., Viggiano, A. A., Kondo, Y., Miller, T. M., Ballenthin, J. O. (2006) The atmospheric chemistry of a 33-34 hour old volcanic cloud from Hekla Volcano (Iceland): insights from direct sampling and the application of chemical box modelling. Journal of Geophysical Research – Atmospheres, 111: D20206

Roux, J., Varet, V. (1975) Alkali feldspar liquid equilibrium relationships in peralkaline oversaturated systems and volcanic rocks. Contributions to Mineralogy and Petrology, 49: 67-81

Rubin, A., Cooper, K. M., Leever, M., Wimpenny, J., Deering, C., Rooney, T., Gravley, D., Yin, Q. (2016) Changes in magma storage conditions following caldera collapse at Okataina Volcanic Center, New Zealand. Contributions to Mineralogy and Petrology, 171: 4

Sabine, P. A. (1960) The geology of Rockall, north Atlantic. Bulletin of the Geological Survey of Great Britain, 16: 156-178

Saleh, G. M. (2006) Geologic relationships and mineralisation of peralkaline/alkaline granite-syenite of the Zargat Na'am ring complex, Southeastern Desert, Egypt. Chinese Journal of Geochemistry, 25: 97-111

Salters, V. J. M., Dick, B. J. B. (2002) Mineralogy of the mid-ocean ridge basalt source from neodymium isotopic composition of abyssal peridotites. Nature, 418: 68-72

Salvi, S., Fontan, F., Monchoux, P., Williams-Jones, A. E., Moine, B. (2000) Hydrothermal mobilisation of high field strength elements in alkaline igneous systems: evidence from the Tamazeght Complex (Morocco). Economic Geology, 95: 559-576

Salvi, S., Williams-Jones, A. E. (1995) Zirconosilicate phase relations in the Strange Lake (Lac Brisson) pluton, Quebec-Labrador, Canada. American Mineralogist, 80: 1031-1040

Salvioli-Mariani, E., Venturelli, G. (1996) Temperature of crystallisation and evolution of the Jumilla and Cancarix lamproites (SE Spain) as suggested by melt and solid inclusions in minerals. European Journal of Mineralogy, 8: 1027-1039

Sato, M. (1978) Oxygen fugacity of basaltic magmas and the role of gas-forming elements. Geophysical Research Letters, 5: 447-449

Scaillet, B., Holtz, F., Pichavant, M. (1998) Phase equilibrium constraints on the viscosity of silicic magmas 1. Volcanic-plutonic comparison. Journal of Geophysical Research, 103: 27257-27266

Scaillet, B., Macdonald, R. (2001) Phase relations of peralkaline silicic magmas and petrogenetic implications. Journal of Petrology, 42: 825-845

Scaillet, B., Macdonald, R. (2003) Experimental constraints on the relationships between peralkaline rhyolites of the Kenya Rift Valley. Journal of Petrology, 44: 1867-1894

Scaillet, B., Macdonald, R. (2006) Experimental constraints on pre-eruption conditions of pantelleritic magmas: evidence from the Eburru complex, Kenya Rift. Lithos, 91: 95-108

Sceal, J. S. C., Weaver, S. D. (1971) Trace element data bearing on the origin of salic rocks from the Quaternary volcano Paka, Gregory Rift, Kenya. Earth and Planetary Science Letters, 12: 327-331

Scherer, G. W. (1999) Crystallization in pores. Cement and Concrete Research, 29:1347-1358

Schilling, J. -G. (1975) Azores mantle blob - rare earth evidence. Earth and Planetary Science Letters, 25: 103-115

Schilling, J. -G. (1991) Fluxes and excess temperatures of mantle plumes inferred from their interaction with migrating mid-ocean ridges. Nature, 352: 397-403

Schmincke, H. -U. (1973) Magmatic evolution and tectonic regime in the Canary, Madeira, and Azores Island Groups. Geological Society of America Bulletin, 84: 633-648

Schmincke, H. -U. (1974) Volcanological aspects of peralkaline silicic welded ash-flow tuffs. Bulletin of Volcanology, 38: 594-636

Schmincke, H. -U., Weibel, M. (1972) Chemical study of rocks from Madeira, Porto Santo and São Miguel, Terceira (Azores). Neues Jahrbuch Fur Mineralogie-Abhandlungen, 117: 253-281

Schmitt, A. K., Emmermann, R., Trumbull, R. B., Bühn, B., Henjes-Kunst, F. (2000) Petrogenesis and $^{40}Ar/^{39}Ar$ geochronology of the Brandberg complex, Namibia: evidence for a major mantle contribution in metaluminous and peralkaline granites. Journal of Petrology, 41: 1207-1239

Schönenberger, J., Marks, M., Wagner, T., Markl, G. (2006) Fluid-rock interaction in autoliths of agpaitic nepheline syenites in the Ilímaussaq intrusions, South Greenland. Lithos, 91: 331-351

Schwarz, S., Klügel, A., Wohlgemuth, U. C. (2004) Melt extraction pathways and stagnation depths beneath the Madeira and Desertas rift zones (NE Atlantic) inferred from barometric studies. Contributions to Mineralogy and Petrology, 147: 228-240

Scott, S. C., Bailey, D. K. (1986) Coeruption of contrasting magmas and temporal variations in magma chemistry at Longonot volcano, Central Kenya. Bulletin of Volcanology, 47: 849-873

Searle, R. (1980) Tectonic pattern of the Azores spreading centre and triple junction. Earth and Planetary Science Letters, 51: 415-434

Seaman, S., J., Dyar, M., D., Marinkovic, N. (2009) The effects of heterogeneity in magma water concentration on the development of flow banding and spherulites in rhyolitic lava. Journal of Volcanology and Geothermal Research, 183: 157-169

Self, S. (1971) The Lajes Ignimbrite, Ilha Terceira, Acores. Communicações dos Serviços Geólogicos de Portugal, 55: 165-184

Self, S. (1974) Recent volcanism on Terceira, Azores. [Ph.D. thesis] London, Imperial College, 236 p.

Self, S. (1976) The Recent Volcanology of Terceira, Azores. Journal of the Geological Society of London, 132: 645-666

Self, S., Gunn, B. M. (1976) Petrology, volume and age relations of alkaline and saturated peralkaline volcanics from Terceira, Azores. Contributions to Mineralogy and Petrology, 54: 293-313

Self, S., Sparks, R. S. J. (1978) Characteristics of widespread pyroclastic deposits formed by the interaction of silicic magma and water. Bulletin of Volcanology, 41: 196-212

Serralheiro, A., Forjaz, V. H., Alves, C. A. M., Rodrigues, B. (1989) Carta vulcanológica dos Açores, ilha do Faial (1:15000). Ed. Serviço Regional de Protecção Civil, Universidade dos Açores e Centro de Vulcanologia do INIC, 4 sheets, Ponta Delgada

Shaw, H. R. (1972) Viscosities of magmatic silicate liquids – empirical method of prediction. American Journal of Science, 272: 870

Shea, T., Gurioli, L., Larsen, J. F., Houghton, B. F., Hammer, J. E., Cashman, K. V. (2010a) Linking experimental and natural vesicle textures in Vesuvius 79AD white pumice. Journal of Volcanology and Geothermal Research, 192: 69-84

Shea, T., Houghton, B. F., Gurioli, L., Cashman, K. V., Hammer, J. E., Hobden, B. J. (2010b) Textural studies of vesicles in volcanic rocks: An integrated methodology. Journal of Volcanology and Geothermal Research, 190: 271-289

Shimizu, H. (1980) Experimental study on rare-earth element partitioning in minerals formed at 20 and 30kb for basaltic systems. Geochemical Journal, 14: 185-202

Shinohara, H. (1991) Pressure dependence of water/rock reaction and control of HCl/NaCl ratio. In: Matsuhisa, Y., Aoki, M., Hedenquist, J. W. (eds.) High temperature acid fluids and associated alteration and mineralisation. Report of the Geological Survey of Japan, 277: 97-99

Shirley, D. N. (1986) Compaction in igneous cumulates. Journal of Geology, 94: 795-809

Sibrant, A. L. R., Hildenbrand, A., Margues, F. O., Wiess, B., Boulesteix, T., Hübscher, C., Lüdmann, T., Costa, A. C. G., Catalão, J. C. (2015) Morpho-structural evolution of a volcanic island developed inside an active oceanic rift: S. Miguel Island (Terceira Rift, Azores). Journal of Volcanology and Geothermal Research, 301: 90-106

Sigmundsson, F., Tryggvason, E., Alves, M. M., Alves, J. L., Pálsson, K., Ólafsson, H. (1995) Slow inflation of the Furnas volcano, São Miguel, Azores, suggested from initial levelling and Global Positining System measurements. Geophysical Research Letters, 22: 1681-1684

Sigurdsson, H. (1970) The petrology and chemistry of the Setberg volcanic region and of the intermediate and acid rocks of Iceland. Unpublished Ph.D thesis, Durham University

Silveira, G., Stutzmann, E., Davaille, A., Montagner, J. -P., Mendes-Victor, L., Sebai, A. (2006) Azores hotspot signature in the upper mantle. Journal of Volcanology and Geothermal Research, 156: 23-34

Sisson, T. W., Bacon C. R. (1999) Gas-driven filter pressing in magmas. Geology, 27: 613-616

Sleep, N. H. (1984) Tapping of magmas from ubiquitous mantle heterogeneities – an alternative to mantle plumes. Journal of Geophysical Research, 89: 29-41

Smith, R. L. (1960) Zones and zonal variations in welded ash flows. U.S. Geological Survey Professional Paper 354-F, 149-159

Smith, M., Dunkley, P. N., Deino, A., Williams, L. A. J., McCall, G. J. H. (1995) Geochronology, stratigraphy and structural evolution of Silali volcano, Gregory Rift, Kenya. Journal of the Geological Society of London, 152: 297-310

Snyder, D. (2000) Thermal effects of the intrusion of basaltic magma into a more silicic magma chamber and implications for eruption triggering. Earth and Planetary Science Letters, 175: 257-273

Snyder, D. C., Widom, E., Pietruszka, A. J., Carlson, R. W. (2004) The role of open-system processes in the development of silicic magma chambers: a chemical and isotopic investigation of the Fogo A trachyte deposit, São Miguel, Azores. Journal of Petrology, 45: 723-738

Snyder, D. C., Widom, E., Pietruszka, A. J., Carlson, R. W., Schmincke, H. –U. (2007) Time scales of formation of zoned magma chambers: U-series disequilibria in the Fogo A and 1563 A. D. trachyte deposits, São Miguel, Azores. Chemical Geology, 239, 138-155

Solgevik, H., Mattsson, H. B., Hermelin, O. (2007) Growth of an emergent tuff cone: fragmentation and depositional processes recorded in the Capelas tuff cone, São Miguel, Azores. Journal of Volcanology and Geothermal Research, 159: 246-266

Sparks, R. S. J. (1978) The dynamics of bubble formation and growth in magmas: a review and analysis. Journal of Volcanology and Geothermal Research, 3: 1-37

Sparks, R. S. J., Pinkerton, H. (1978) Effects of degassing on rheology of basaltic lava. Nature, 276: 385-386

Sparks, R. S. J., Self, S., Walker, G. P. L. (1973) Products of ignimbrite eruptions. Geology, 1:115-118

Spera, F. J., Oldenburg, C. M., Christensen, C., Todesco, M. (1995) Simulations of convection with crystallisation in the system $KAlSi_2O_6$-$CaMgSi_2O_6$: implications for compositionally zoned magma bodies. American Mineralogist, 80: 1188-1207

Stasiuk, M., Barclay, J., Caroll, M., Jaupart, C, Ratt, J., Sparks, R. S., Tait, S. (1996) Degassing during magma ascent in the Mule Creek vent (USA). Bulletin of Volcanology, 58: 117-130

Stepnova, Yu. A., Zalishchak, B. L., Pakhomova, V. A. (2013) Rare-earth mineralisation of alkali magma of the Russian Far East: on the example of the Shibanovsky massif. Геология, Вестник, 3: 44-51 (in Russ.)

Storey, M. (1982) Trachytic pyroclasts from Agua de Pau volcano, São Miguel, Azores: evolution of a magma body over 4,000 years. Contributions to Mineralogy and Petrology, 78: 423-432

Storey, M., Wolff, J. A., Norry, M. J., Marriner, G. F. (1989) Origin of hybrid lavas from Agua de Pau volcano, São Miguel, Azores. In: Saunders, A. D., Norry, M. J. (eds.) Magmatism in the Ocean Basins. Blackwell, London, pp. 161-180

Stormer Jr, J. C. (1983) The effects of recalculation on estimates of temperature and oxygen fugacity from analyses of multi-componant iron-titanium oxides. American Mineralogist, 68: 586-594

Streck, M. J. (2014) Evaluation of crystal mush extraction models to explain crystal-poor rhyolites. Journal of Volcanology and Geothermal Research, 284: 79-94

Stroncik, N. A., Klügel, A., Hansteen, T. H. (2009) The magmatic plumbing system beneath El Hierro (Canary Islands): constraints from phenocrysts and naturally quenched basaltic glasses in submarine rocks. Contributions to Mineralogy and Petrology, 157:593-607

Sumner, J. M., Branney, M. J. (2002) The emplacement history of a remarkable heterogeneous, chemically zoned, rheomorphic and locally lave-like ignimbrite: 'TL' on Gran Canaria. Journal of Volcanology and Geothermal Research, 115: 109-138

Sumner, J. M., Wolff, J. (2003) Petrogenesis of mixed-magma, high-grade, peralkaline ignimbrite 'TL' (Gran Canaria): diverse styles of mixing in a replenished, zoned magma chamber. Journal of Volcanology and Geothermal Research, 126: 109-126

Sun, S., McDonough, W. F. (1989) Chemical and isotopic systematics of ocean basins: implications for mantle composition and processes. In: Saunders, A. D., Norry, M. J. (eds.) Magmatism in the Ocean Basins, Geological Society of London Special Publication, 42:313-346

Sutherland, D. S. (1974) Petrography and mineralogy of the peralkaline silicic rocks. Bulletin of Volcanology, 38: 518-547

Symonds, R. B., Reed, M. H., Rose, W. I. (1992) Origin, speciation, and fluxes of trace-element gases at Augustine volcano, Alaska: insights into magma degassing and fumurolic processes. Geochimica et Cosmochimica Acta, 56: 633-657

Symonds, R. B., Rose, W. I., Bluth, G. J. S., Gerlach, T. M. (1994) Volcanic gas studies – methods, results, and applications. Reviews in Mineralogy, 30: 1-66

Tait, S., Jaupart, C., Vergniolle, S. (1989a) Pressure, gas content and eruption periodicity of a shallow, crystallising magma chamber. Earth and Planetary Science Letters, 92: 107-123

Tait, S. R., Wörner, G., Van Den Bogaard, P., Schmincke, H. –U. (1989b) Cumulate nodules as evidence for convective fractionation in a phonolite magma chamber. Journal of Volcanology and Geothermal Research, 37: 21-37

Thibaud, R., Gente, P., Maia, M. (1998) A systematic analysis of the Mid-Atlantic Ridge morphology and gravity between 15°N and 40°N: constraints of the thermal structure. Journal of Geophysical Research, 103: 24223-24243

Thompson, R. N. (1969) Tertiary granites and associated rocks of the Marsco area, Isle of Skye. Quarterly Journal of the Geological Society of London, 124: 349-385

Thompson, R. N. (1974) Some high-pressure clinopyroxenes. Mineralogical Magazine, 39: 768-787

Thorarinsson, S. (1967) Hekla and Katla. The share of acid and intermediate lava and tephra in the volcanic products through the geological history of Iceland. In: Bjornsson, S., (ed.) Iceland and mid-ocean ridges. Reykjavik: 190-199

Tindle, A. G., Webb, P. C. (1990) Estimation of lithium contents in trioctahedral micas using microprobe data: application to micas from granitic rocks. European Journal of Mineralogy, 2: 595-610

Tolstoy, I. (1951) Submarine topography in the North Atlantic. Bulletin of the Geological Society of America, 62: 441-450

Tomlinson, E. L., Smith, V. C., Albert, P. G., Aydar, E., Civetta, L., Cioni, R., Çubukçu, E., Gertisser, R., Isaia, R., Menzies, M. A., Orsi, G., Rosi, M., Zanchetta, G. (2015) The major and trace element glass compositions of the productive Mediterranean volcanic sources: tools for correlating distal tephra layers in and around Europe. Quaternary Science Reviews, 118: 48-66

Troll, V. R., Schmincke, H. -U. (2002) Magma mixing and crustal recycling recorded in ternary feldspar from compositionally zoned peralkaline ignimbrite 'A', Gran Canaria, Canary islands. Journal of Petrology, 43: 243-270

Trua, T., Deniel, C., Mazzuoli, R. (1999) Crustal control in the genesis of Plio-Quaternary bimodal magmatism of the Main Ethiopian Rift (MER): geochemical and isotopic (Sr, Nd, Pb) evidence. Chemical Geology 155: 201-231

Tuffen, H., Dingwell, D. B., Pinkerton, H. (2003) Repeated fracture and healing of silicic magma generate flow banding and earthquakes? Geology, 31: 1089-1092

Turbeville, B. N. (1993) Sidewall differentiation in an alkalic magma chamber: evidence from syenite xenoliths in tuffs of the Latera caldera, Italy. Geological Magazine, 130: 453-470

Turner, S., Hawkesworth, C., Rogers, N., King, P. (1997) U-Th isotope disequilibria and ocean island basalt generation in the Azores. Chemical Geology, 139: 145-164

Upton, B. G. J. (1974) The alkaline province of south-west Greenland. In: Sørensen, H. (ed.) The alkaline rocks. London: Wiley and Sons, 221-238

Upton, B. G. J., Emeleus, C. H., Heaman, L. M., Goodenough, K. M., Finch, A. A. (2003) Magmatism of the mid-Proterozoic Gardar province, south Greenland: chronology, petrogenesis and geological setting. Lithos, 68: 43-65

Upton, B. G. J., Wadsworth, W. J. (1972) Aspects of magmatic evolution on Reunion island. Philosophical Transactions of the Royal Society of London, Series A, Mathematical and Physical Sciences, 271: 105-130

Urabe, T. (1985) Aluminous granite as a source magma of hydrothermal ore deposits: an experimental study. Economic Geology, 80: 148-724

Van Tassel, R. (1952) Dalyite, a new potassium zirconium silicate, from Ascension Island, Atlantic. Mineralogical Magazine, 29: 850-857

Venezky, D. Y., Rutherford, M. J. (1999) Petrology and Fe-Ti oxide reequilibration of the 1991 Mount Unzen mixed magma. Journal of Volcanology and Geothermal Research, 89: 213-230

Venturelli, G., Capedri, S., Di Battistini, G., Crawford, A., Kogarko, L. N., Celestini, S. (1984) The ultrapotassic rocks from southeastern Spain. Lithos, 17: 37-54

Villemant, B. (1988) Trace-Element Evolution in the Phlegrean Fields (Central-Italy) - Fractional Crystallization and Selective Enrichment. Contributions to Mineralogy and Petrology, 98: 169-183

Villemant, B., Jaffrezic, H., Joron, J. L., Treuil, M. (1981) Distribution Coefficients of Major and Trace-Elements - Fractional Crystallization in the Alkali Basalt Series of Chaine-Des-Puys (Massif Central, France). Geochimica et Cosmochimica Acta, 45: 1997-2016

Vogt, P. R., Jung, W. Y. (2004) The Terceira Rift as hyper-slow, hotspot-dominated oblique speeding axis: a comparison with other slow-spreading plate boundaries. Earth and Planetary Science Letters, 218: 77-90

Vona, A., Romano, C., Dingwell, D. B., Giordano, D. (2011) The rheology of crystal-bearing basaltic magmas from Stromboli and Etna. Geochimica et Cosmochimica Acta, 75: 3214-3236

Wagner, C., Velde, D., Mokhtari, A. (1987) Sector-zoned phlogopites in igneous rocks. Contributions to Mineralogy and Petrology, 96: 186-191

Walker, G. P. L. (1989) Gravitational (density) controls on volcanism, magma chambers and intrusions. Australian Journal of Earth Sciences, 36: 149-165

Walker, G. P. L. Croasdale, R., (1971) Two plinian-type eruptions in the Azores. Journal of the Geological Society of London, 127: 17-55

Wallenstein, N. (1999) Estudo da história recente e do comportamento eruptivo do vulcão do Fogo (S.Miguel, Açores). A valiação preliminar do hazard. Unpublished PhD thesis, Departamento de Geociências Universidades dos Açores, São Miguel Island (Portugal)

Washington, H. S. (1913a) The volcanoes and rocks of Pantelleria: I. Journal of Geology, 21: 653-670

Washington, H. S. (1913b) The volcanoes and rocks of Pantelleria: II. Journal of Geology, 21: 683-719

Washington, H. S. (1914) The volcanoes and rocks of Pantelleria: III. Journal of Geology, 22: 16-27

Watson, E. B., Green, T. H. (1981) Apatite/liquid partition coefficients for the rare earth elements and strontium. Earth and Planetary Science Letters, 56: 405-421

Weaver, B. L. (1991) Trace element evidence for the origin of ocean-island basalts. Geology, 19: 123-126

Weaver, S. D. (1977) The Quaternary caldera volcano Emuruangogolak, Kenya Rift, and the petrology of a bimodal ferrobasalt-pantelleritic trachyte association. Bulletin Volcanologique, 40: 209-230

Weaver, S. D., Sceal, J. S. C., Gibson, I. L. (1972) Trace-element data relevant to the origin of trachytic and pantelleritic lavas in the East African Rift System. Contributions to Mineralogy and Petrology, 36: 181-194

Webster, J. D., Taylor, R. P., Bean, C. (1993) Pre-eruptive melt composition amd constraints on degassing of water-rich pantellerite magma, Fantale volcano, Ethiopia. Contributions to Mineralogy and Petrology, 114: 53-62

White, J. C., Benker, S. C., Ren, M., Urbanczyk, K. M., Corrick, D. W. (2006) Petrogenesis and tectonic setting of the peralkaline Pine Canyon caldera, Trans-Pecos Texas, USA. Lithos, 91: 74-94

White, J. C., Parker, D. F., Ren, M. (2009) The origin of trachyte and pantellerite from Pantelleria, Italy: insights from major element, trace element, and thermodynamic modelling. Journal of Volcanology and Geothermal research, 179: 33-55

White, J. C., Ren, M., Parker, D. F. (2005) Variation in mineralogy, temperature, and oxygen fugacity in a suite of strongly peralkaline lavas and tuffs, Pantelleria, Italy. The Canadian Mineralogist, 43: 1331-1347

White, W. M. (1985) Sources of oceanic basalts: radiogenic isotope evidence. Geology, 13: 115-118

White, W. (2010) Oceanic island basalts and mantle plumes: the geochemical perspective. Annual Reviews in Earth and Planetary Sciences, 38: 133-160

White, W. M., Hart, S. R., Schilling, J. -G. (1975) Geochemistry of the Azores and the Mid-Atlantic Ridge; 29°N to 60°N. Carnegie Institute of Washington Year Book, 74: 224-234

White, W. M., Schilling, J. -G., Hart, S. R. (1976) Evidence for the Azores mantle plume from strontium isotope geochemistry of the central North Atlantic. Nature, 263: 659-663

White, W. M., Tapia, M. D. M., Schilling, J. –G. (1979) The petrology and geochemistry of the Azores islands. Contributions to Mineralogy and Petrology, 69: 201-213

Whittington, A. G., Richet, P., Linard, Y., Holtz, F. (2001) The viscosity of hydrous phonolites and trachytes. Chemical Geology, 174: 209-223

Widom, E., Carlson, R. W., Gill, J. B., Schmincke, H. -U. (1997) Th-Sr-Nd-Pb isotope and trace element evidence for the origin of the São Miguel, Azores, enriched mantle source. Chemical Geology, 140: 49-68

Widom, E., Farquhar, J. (2003) Oxygen isotope signatures in olivines from São Miguel (Azores) basalts: implications for crustal and mantle processes. Chemical Geology, 193: 237-255

Widom, E., Gill, J. B., Schmincke, H. -U. (1992) Syenite nodules as a long-term record of magmatic activity in Agua de Pau volcano, São Miguel, Azores. Journal of Petrology, 34: 929-953

Widom, E., Schmincke, H. –U., Gill, J. B. (1993) Processes and timescales in the evolution of a chemically zoned trachyte: Fogo A, São Miguel, Azores. Contributions to Mineralogy and Petrology, 111: 311-328

Widom, E., Shirey, S. B. (1996) Os isotope systematics in the Azores: implications for mantle plume sources. Earth and Planetary Science Letters, 142: 451-465

Wilding, M. C., Macdonald, R., Davies, J. R., Fallick, A. E. (1993) Volatile characteristics or peralkaline rhyolites from Kenya: an ion microprobe, infrared spectroscopic and hydrogen isotope study. Contributions to Mineralogy and Petrology, 144: 264-275

Wilson, L., Sparks, R. S. J., Walker, G. P. L. (1980) Explosive volcanic eruptions – IV. The control of magma properties and conduit geometry on eruption column behaviour. Geophysical Journal of the Royal Astronomical Society, 63: 117-148

Wimmenauer, W. (1974) Chapter 4.4: The alkaline province of central Europe and France. In: Sørensen, H. (ed.) The alkaline rocks. London: Wiley and Sons, 238-271

Wolff, J. A. (1987) Crystallisation of nepheline syenite in a subvolcanic magma system: Tenerife, Canary Islands. Lithos, 20: 207-223

Wolff, J. A. (2015) Remelting of cumulates as a process for producing chemical zoning in silicic tuffs: a comparison of cool, wet and hot, dry rhyolitic magma systems. Lithos, 236-237: 275-286

Wolff, J. A., Gardner, J. N. (1995) Is the Valles caldera entering a new cycle of activity? Geology, 23: 411-414

Wolff, J. A., Storey, M. (1983) The volatile component of some pumice-forming alkaline magmas from the Azores and Canary islands. Contributions to Mineralogy and Petrology, 82: 66-74

Wolff, J. A., Wörner, G., Blake, S. (1990) Gradients in physical parameters in zoned felsic magma bodies: implications for evolution and eruptive withdrawl. Journal of Volcanology and Geothermal Research, 43: 37-55

Wood, B., Trigila, R. (2001) Experimental determination of aluminour clinopyroxene-melt partition coefficients for potassic liquids, with application to the evolution of the Roman province potassic magmas. Chemical Geology, 172: 213-223

Woods, A. W., Koyaguchi, T. (1994) Transitions between explosive and effusive eruptions of silicic magmas. Nature, 370: 641-644

Wyllie, P. J., Tuttle, O. F. (1961) Experimental investigation of silicate systems containing two volatile components. Part II. The effects of NH_3 and HF in addition to water on the melting temperatures of granite and albite. American Journal of Science, 259: 128-143

Zanon, V. (2015a) Conditions for mafic magma storage beneath fissure zones at oceanic islands. The case of São Miguel island (Azores archipelago). In: Caricchi, L,, Blundy, J. D. (eds.) Chemical, physical and temporal evolution of magmatic systems, Geological Society, London, Special Publications, 422, doi: 10.1144/SP422.4

Zanon, V. (2015b) The magmatism of the Azores islands. In: Gaspar, J. L., Guest, J. E., Duncan, A. M., Barriga, F. J. A. S., Chester, D. K. (eds.) 2015, Volcanic geology of São Miguel island (Azores archipelago). Geological Society of London Memoirs, 44: 51-64

Zanon, V., Frezzotti, M. L. (2013) Magma storage and ascent conditions beneath Pico and Faial islands (Azores archipelago): a study on fluid inclusions. Geochemistry, Geophysics, Geosystems, 14: 3494-3514

Zanon, V., Kueppers, U., Pacheco, J. M., Cruz, I. (2013) Volcanism from fissure zones and the Caldeira central volcano of Faial Island, Azores archipelago: geochemical processes in multiple feeding systems. Geological Magazine, 150: 536-555

Zanon, V., Pacheco, J., Pimentel, A. (2009) Growth and evolution of an emergent tuff cone: considerations from structural geology, geomorphology and facies analysis of São Roque volcano, São Miguel, Azores. Journal of Volcanology and Geothermal Research, 180: 277-291

Zanon, V., Pimentel, A. (2015) Spatio-temporal constraints on magma storage and ascent conditions in a transtensional tectonic setting: the case of the Terceira island (Azores). American Mineralogist, 100: 795-805

Zbyszewski, G. (1966) As observações de F. Fouqué sobre o vulcanismo dos Açores. Boletim do Núcleo Cultural da Horta, 4: 17-95

Zbyszewski, G., Cândido de Medeiros, A., da Veiga Ferreira, O., Torre de Assuncão, C. (1971) Carta geologica de Portugal, 1:50,000. Noticia explicativa da folha Ilha Terceira, Lisbon 1971

Zeis, E. G. (1960) Chemical analyses of two pantellerites. Journal of Petrology, 1:304-308

Zimova, M., Webb, S. L. (2006) The combined effects of chlorine and fluorine on the viscosity of aluminosilicate melts. Geochimica et Cosmochimica Acta, 71: 1553-1562

Zindler, A., Hart, S. R. (1986) Chemical geodynamics. Annual Review of Earth and Planetary Sciences, 14: 493-571

Petrogenesis and contrasting eruption styles of peralkaline silicic magmas from Terceira and São Miguel, Azores

Adam John Jeffery

Vol. II Appendices

Thesis submitted for the degree of Doctor of Philosophy in Earth Sciences

October 2016

Keele University

PREFACE

This thesis represents an original contribution to science, and has been divided into two seperate volumes. The first volume comprises the main body of the thesis, including an introductory chapter, a literature review and context chapter, and a chapter detailing the various methods and analytical techniques used. This is followed by two main body chapters, in which the scientific results of two individual studies are provided and discussed. This culminates in a synthesis chapter, in which the implications of this work are considered in both a regional and a global context. Finally, the primary conlusions and research implications are detailed in a conclusions chapter. The second volume of this work comprises various appendices, providing in full the datasets employed throughout this work, including: a list of sampling locations, a list of samples, mineral chemical data, whole rock and glass chemical data, test of data quality, and results of thermobarometry.

CONTENTS

VOLUME II. APPENDICES

APPENDIX A: LOCATION LIST

Table A1: List of sampling locations

Location no.	Location	Units	Easting	Northing
1	São Miguel	Fur-H	0649916	4181064
2	São Miguel	Fur-H	0649645	4181031
3	São Miguel	Fur-J	0648191	4178878
4	São Miguel	Fur-J	0646536	4177754
5	São Miguel	Fur-G	0647121	4181607
6	São Miguel	Fur-G	0647111	4181610
7	São Miguel	12 ka ign	0646698	4181922
8	São Miguel	Fur-C, E	0648475	4184411
9	São Miguel	Fur-J	0647044	4178096
10	São Miguel	Fur-J dome	0647262	4178572
11	São Miguel	Fur-I dome	0648661	4180453
12	São Miguel	Fur-J	0649036	4177270
13	São Miguel	Fur-F	0647845	4180829
14	São Miguel	Fur-I	0647856	4180852
15	São Miguel	Povo Fm.	0654221	4179197
16	São Miguel	Povo Fm.	0654340	4179238
17a	São Miguel	Povo Fm.	0654252	4179256
17b	São Miguel	Povo Fm.	0654110	4179236
18	Terceira	Ign-I, CCI	0489169	4292517
19	Terceira	CCI	0488363	4293063
20	Terceira	CCI	0488199	4293112
21	Terceira	PNI	0486860	4293046
22	Terceira	LAI	0487899	4292724
23a	Terceira	CCI,VFI	0487685	4292725
23b	Terceira	VFI, LAI	0474469	4279091
24	Terceira	LAI	0489678	4291770
25a	Terceira	CCI, VFI	0487125	4293028
25b	Terceira	VFI	0487072	4293020
25c	Terceira	VFI	0487055	4293002
26	Terceira	LAI	0481453	4280143
27a	Terceira	GVI	0482863	4278212
27b	Terceira	GVI	0482395	4278386
28	Terceira	CCI, VFI	0480069	4278481
29	Terceira	LAI	0481625	4278203
30	Terceira	LAI	0475995	4278281
31	Terceira	LAI	0475972	4278280
32	Terceira	LAI	0490056	4292299
33	Terceira	LAI	0482025	4293744
34	Terceira	LAI	0484308	4292647
35	Terceira	LAI	0485139	4293306
36	Terceira	LAI	0486507	4292857
37	Terceira	LAI	0490448	4292913
38	Terceira	LAI	0491962	4292057
39	Terceira	CCI	0483731	4293966
40	Terceira	LAI	0474429	4279086
41	Terceira	-	-	-
42	Terceira	LAI	0490153	4291502

Table A1 continued

Location no.	Location	Units	Easting	Northing
43	Terceira	LAI	0489918	4277637
44	São Miguel	Furnas basalt	0650881	4180004
45	São Miguel	Furnas basalt	0650714	4181118
46	São Miguel	Furnas basalt	0647860	4182893
47	São Miguel	Furnas basalt	0644124	4181506
48	São Miguel	Furnas basalt	0642432	4181434
49	São Miguel	Furnas basalt	0642501	4181452
50	São Miguel	Furnas basalt	0642848	4180012
51	São Miguel	Furnas basalt	0646344	4183100
52	Terceira	LMI	0481607	4280134

APPENDIX B: SAMPLE LISTS

Table B1: List of samples from Terceira and São Miguel

Sample	Island	Location	Unit	Description
T001	Terceira	18	Ign-i	Ign
T002	Terceira	18	CCI lower flow	Light Pumice
T003	Terceira	18	CCI lower flow	Dark Glassy Clasts
T004	Terceira	18	CCI middle flow	Light + Dark pumice
T005	Terceira	19	CCI fall	Pumice + 1 syenite
T006	Terceira	19	CCI	Syenite
T007	Terceira	19	CCI	Obsidian chips
T008	Terceira	19	CCI lower	Pumice
T009	Terceira	20	CCI upper/middle	Syenite
T010	Terceira	20	CCI upper/middle	Dark pumice
T011	Terceira	20	CCI upper/middle	Light pumice
T012	Terceira	21	PNI base	Ign
T013	Terceira	21	Early VFI fall	Pumice
T014 (I)	Terceira	21	CCI	Syenite
T014 (II)	Terceira	22	Pre-Lajes	Vesicular lava
T015	Terceira	22	Pre-Lajes	Pumice
T016	Terceira	22	Pre-Lajes	Lithic
T017	Terceira	22	Pre-Lajes	Pumice
T018	Terceira	22	Pre-Lajes	Pumice
T019	Terceira	22	Lajes	Charcol
T020	Terceira	22	Lajes	Dark Pumice
T021	Terceira	23	CCI	Light Pumice
T022	Terceira	23	CCI	Dark Pumice
T023	Terceira	23	Pre-CCI	Tuff nodules?'
T024 (I)	Terceira	19	CCI Surge	Fine Pumice
T024 (II)	Terceira	23	Pre-VFI fall	Pumice
T025	Terceira	23	VFI (Flow 1)	Lower light pumice
T026	Terceira	23	VFI (Flow 1)	Lower dark pumice
T027	Terceira	23	VFI (Flow 1)	Lower glass chips
T028	Terceira	23	VFI (Flow 1)	Upper Pumice
T029	Terceira	23	VFI (Flow 2)	Lower Pumice
T030	Terceira	23	VFI (Flow 2)	Lower glass chips
T031	Terceira	23	VFI (Flow 2)	Upper Pumice
T032	Terceira	23	VFI (Flow 3)	Lower Pumice
T033	Terceira	24	Pre-Lajes	Pumice + 1 syenite
T034	Terceira	24	Lajes	Lower Pumice
T035	Terceira	24	Lajes	Middle Pumice
T036	Terceira	24	Lajes	Middle Glassy Pumice
T037	Terceira	24	Lajes	Upper light pumice
T038 (I)	Terceira	24	Lajes	Basal crystal layer
T038 (II)	Terceira	25	Top CCI	Pumice
T039	Terceira	25	VFI	Red ash
T040	Terceira	25	VFI fall	Glassy chips
T041	Terceira	25	Lower VFI	Pumice
T042	Terceira	25	VFI (Flow 1?)	Bottom pumice
T043	Terceira	25	VFI (Flow 1?)	Glassy chips
T044 (I)	Terceira	25	VFI (Flow 1?)	Upper pumice
T044 (II)	Terceira	25	VFI	Pumice
T045	Terceira	25	VFI	Pumice
T046	Terceira	25	VFI	Pumice
T047	Terceira	25	VFI	Pumice
T048	Terceira	25	VFI	Glassy chips
T049	Terceira	26	Angra	Pumice

Table B1 continued

Sample	Island	Location	Unit	Description
T050	Terceira	27	GVI	Base Ign
T051	Terceira	27	GVI	Ign
T052	Terceira	27	GVI	Ign
T053	Terceira	27	GVI	Top Ign
T054	Terceira	28	CCI Top	Pumice
T055	Terceira	28	CCI Top	Pumice
T056	Terceira	28	VFI fall	Pumice
T057	Terceira	28	VFI	Pumice
T058	Terceira	29	Angra	Pumice
T059	Terceira	30	Lajes	Pumice
T060	Terceira	29	LAI	Lower Angra
T061	Terceira	29	Basalt beneath Angra	Basalt beneath Angra
T062	Terceira	26	Angra	Angra
T063	Terceira	27	GVI	Welded base
T064	Terceira	19	CCI	Basal pumice fall
T065	Terceira	19	CCI	Basal pumice surge
T066	Terceira	19	CCI	Base of CCI
T067	Terceira	20	CCI	Lower CCI flow unit
T068	Terceira	20	CCI	Middle/upper flow unit
T069	Terceira	20	CCI	Middle/upper flow unit
T070	Terceira	20	CCI	Basal pumice surge
T071	Terceira	23	CCI	P. Vila Nova CCI
T072	Terceira	25	VFI	Early VFI fall
T073	Terceira	25	CCI	Various syenite nodules
T074	Terceira	24	LAI	Lajes syenite nodules
T075	Terceira	18	Ign-i	Welded ignimbrite
T076	Terceira	18	CCI	Lower flow unit
T077	Terceira	18	CCI	Lower flow unit
T078	Terceira	18	CCI	Mid/upper flow unit
T079	Terceira	18	Basalt opposite CCI	Base of basalt flow
T080	Terceira	33	Lajes?	Syenite? + Lithics
T081	Terceira	33	Lajes?	Black vesicular pumice
T082	Terceira	35	Lajes?	Syenite?
T083	Terceira	35	Lajes?	Black glassy fragments
T084	Terceira	24	Lajes	Upper light pumice
T085	Terceira	24	Lajes	Lower dark pumice
T086	Terceira	37	Lajes	Zr pumice 0-1.5m
T087	Terceira	37	Lajes	Zr pumice 1.5-2.5m
T088	Terceira	37	Lajes	Zr pumice 2.5-3.5m
T089	Terceira	37	Lajes	Zr pumice 3.5>
T090	Terceira	37	Lajes	Black pumice
T091	Terceira	37	Lava	Lava at base of lajes
T092	Terceira	39	Debris flow?	Syenite boulder
T093	Terceira	21	PNI	Dense pumice clasts
T094	Terceira	25	VFI	Outcrop 2 VFI
T095	Terceira	25	VFI	Outcrop 3 VFI
T096	Terceira	25	VFI	Outcrop 2 VFI
T097	Terceira	30	Lajes	São mateus low flow
T098	Terceira	30	Lava	Lava below lajes
T099	Terceira	38	Lajes	Lower light pumice
T100	Terceira	38	Lajes	Flattened pumice
T101	Terceira	38	Lajes	K-fsp rich layer
T102	Terceira	23	Lajes	Black pumice

Table B1 continued

Sample	Island	Location	Unit	Description
T103	Terceira	23	VFI	Flow unit 1 light pumice
T104	Terceira	23	VFI	Flow unit 2 light pumice
T105	Terceira	23	VFI	Flow unit 3 light pumice
T106	Terceira	23	VFI	Flow unit 4 light pumice
T107	Terceira	23	VFI	Flow unit 5 light pumice
T108	Terceira	23	VFI	VFI base light pumice
T109	Terceira	23	VFI	VFI flow above base
T110	Terceira	41	Misterios negros	Dome near W footpath
T111	Terceira	28	CCI	Light pumice
T112	Terceira	28	VFI fall	Fine pumice fall
T113	Terceira	28	VFI	Light pumice
S001	São miguel	1	Furnas H	Pumice
S002	São miguel	2	Furnas H	Pumice
S003	São miguel	3	Furnas H	Banded Pumice
S004	São miguel	3	Furnas H	White Pumice
S005	São miguel	4	Furnas J	Pumice
S006	São miguel	5	Furnas G?	Lower Pumice
S007	São miguel	5	Furnas G?	Upper Pumice
S008	São miguel	6	Furnas G?	Pumice
S009	São miguel	7	Caldera wall Ign	Ign
S010	São miguel	8	Furnas C	Pumice
S011	São miguel	8	Furnas C	Grey ash
S012a	São miguel	8	Furnas E	Grey ash
S012b	São miguel	9	Furnas E	Pumice
S013	São miguel	8	Furnas E	Grey ash
S014	São miguel	8	Fogo 1563	Pumice
S015	São miguel	8	Fogo 1563	Pumice
S016	São miguel	8	Furnas C	Big Pumice
S018	São miguel	9	Furnas J	White Pumice
S019	São miguel	9	Furnas J	Lithics
S020	São miguel	9	Furnas J	Fine Pumice
S021	São miguel	10	Furnas J Dome	Outer Dome
S022	São miguel	10	Furnas J Dome	Top of Dome
S023	São miguel	11	Furnas I Dome	Outer Dome
S024	São miguel	12	Furnas J Flows/Falls	Pumice
S025	São miguel	12	Furnas J Flows/Falls	Pumice
S026	São miguel	12	Furnas J Flows/Falls	Fine Pumice
S027	São miguel	12	Furnas J Flows/Falls	Lapillli
S028	São miguel	12	Furnas J Flows/Falls	Pumice
S029	São miguel	12	Furnas J Flows/Falls	Grey ash + acc. Lapili
S030	São miguel	12	Furnas J Flows/Falls	Pumice
S031	São miguel	12	Furnas J Flows/Falls	Pumice
S032	São miguel	12	Furnas J Flows/Falls	Pumice
S033	São miguel	12	Furnas J Flows/Falls	Pumice
S034	São miguel	12	Furnas J Flows/Falls	Pumice
S035	São miguel	12	Top Furnas J	Syenite
S036	São miguel	14	Furnas I	White Pumice
S037	São miguel	14	Furnas I (Bottom)	Pumice
S038	São miguel	14	Furnas I (Top)	Pumice
S039	São miguel	14	Furnas I	Lapilli
S040	São miguel	14	Furnas I	Pumice
S041	São miguel	13	Furnas F	Pumice
S042	São miguel	13	Furnas F	Pumice

Table B1 continued

Sample	Island	Location	Unit	Description
S043	São miguel	13	Furnas F	Ash
S044	São miguel	13	Furnas F	Lapilli
S045	São miguel	13	Furnas F	Ash
S046	São miguel	13	Furnas F	Pumice
S047	São miguel	15	Povoacao	Ign
S048	São miguel	15	Povoacao	Fiamme
S049	São miguel	16	Povoacao	Dark Pumice
S050	São miguel	16	Povoacao	Orange Pumice
S051	São miguel	16	Povoacao	Fiamme
S052	São miguel	16	Povoacao fall	White Pumice
S053	São miguel	16/17	Povoacao fall	White Pumice
S054	São miguel	16/17	Povoacao fall	White Pumice
S055	São miguel	9	Furnas J	Coarse pumice (lower)
S056	São miguel	9	Furnas J	Pumice above S055
S057	São miguel	13	Furnas F	Pumice
S058	São miguel	13	Furnas F	Pumice
S059	São miguel	13	Furnas F	Pumice
S060	São miguel	13	Furnas F	Pumice
S061	São miguel	14	Furnas I	Lower Pumice
S062	São miguel	12	Furnas J	Syenite
S063	São miguel	12	Furnas J	Banded pumice
S064	São miguel	8	Furnas E	Pumice
S065	São miguel	8	Furnas C	Pumice (upper)
S066	São miguel	8	Furnas C	Pumice (lower)
S067	São miguel	44	Basalt	Basalt
S068	São miguel	45	Basalt	Basalt
S069	São miguel	46	Basalt	Basalt
S070	São miguel	47	Basalt	Scoria
S071	São miguel	48	Basalt	Scoria
S072	São miguel	49	Basalt	Scoria
S073	São miguel	50	Basalt	Scoria
S074	São miguel	3	Furnas J (Lf)	White pumice
S075	São miguel	3	Furnas J (Lf)	Banded or grey Pumice
S076	São miguel	3	Furnas J (A5)	Pumice
S077	São miguel	17	Povoacao Ign	Pumice
S078	São miguel	17	Below Povoacao Ign	Porphyritic rock
S079	São miguel	17	Povo pumice fall?	Pumice
S080	São miguel	12	Furnas J L1	Pumice
S081	São miguel	12	Furnas J L2	Pumice
S082	São miguel	12	Furnas J L3	Pumice
S083	São miguel	12	Furnas J A2	Pumice
S084	São miguel	12	Furnas J A3	Pumice
S085	São miguel	12	Furnas J A3	Pumice
S086	São miguel	12	Furnas J A3	Pumice
S087	São miguel	12	Furnas J A3	Pumice
S088	São miguel	12	Furnas J L4	Pumice
S089	São miguel	12	Furnas J L5	Pumice
S090	São miguel	12	Furnas J syenite	Pumice
S091	São miguel	12	Furnas J syenite	Pumice
S092	São miguel	2	Furnas H	Pumice
S093	São miguel	51	Basalt	Basalt
S094	São miguel	4	Furnas J L1	Pumice

APPENDIX C: MINERAL CHEMISTRY

Table C1: Alkali feldspar analyses from the Terceira ignimbrite formations and associated lithologies

Unit	**LAI**	**LAI**	**LAI**	**LAI**	**LAI**	**LAI**	**LAI**	**LAI**	**LAI**	**LAI**	**LAI**	**LAI**	**LAI**	**LAI**
Sample	TER1-1	TER1-1	TER1-1	TER1-1	TER1-1	TER1-1	TER1-1	TER1-1	TER1-1	TER1-1	TER1-1	TER1-1	TER1-1	TER1-1
No.	19 / 1 .	20 / 1 .	21 / 1 .	22 / 1 .	23 / 1 .	24 / 1 .	25 / 1 .	27 / 1 .	28 / 1 .	29 / 1 .	30 / 1 .	31 / 1 .	32 / 1 .	33 / 1 .
Notes	Pheno	Pheno	Pheno	Pheno	Pheno	Pheno	Pheno	Pheno	Pheno	Pheno	Pheno	Pheno	Pheno	Pheno
SiO_2	66.18	66.38	66.45	66.23	66.68	65.42	64.09	66.59	66.45	66.47	64.50	66.28	66.54	66.39
TiO_2	0.06	0.04	0.04	0.04	0.02	0.01	0.07	0.04	0.07	0.04	0.04	0.05	0.05	0.05
Al_2O_3	18.75	18.93	18.65	18.91	18.88	18.63	20.74	19.08	19.22	18.97	20.54	19.18	19.15	18.82
BaO	0.07	0.05	0.02	0.04	0.02	0.09	0.87	0.08	0.16	0.10	0.04	0.11	0.05	0.02
FeO	0.49	0.35	0.38	0.33	0.43	0.36	0.39	0.31	0.37	0.32	0.34	0.29	0.30	0.37
SrO	0.03	0.03	0.04	0.02	bdl	0.04	0.05	bdl	bdl	0.03	0.02	0.03	0.03	bdl
MgO	0.01	0.00	0.00	0.00	bdl	0.01	0.01	0.01	bdl	0.01	0.01	bdl	bdl	bdl
CaO	0.29	0.20	0.14	0.18	0.13	0.20	1.87	0.27	0.30	0.28	0.21	0.34	0.29	0.17
Na_2O	7.82	7.71	7.61	7.64	7.72	7.61	8.53	7.84	7.63	7.77	7.11	7.91	7.84	7.71
K_2O	5.47	5.58	5.70	5.69	5.57	5.67	2.87	5.36	5.39	5.56	5.66	5.39	5.43	5.66
Total	99.16	99.26	99.03	99.09	99.45	98.03	99.49	99.57	99.59	99.53	98.46	99.59	99.68	99.19
Si	2.984	2.986	2.996	2.985	2.992	2.985	2.884	2.983	2.978	2.983	2.925	2.973	2.979	2.989
Ti	0.002	0.001	0.001	0.001	0.001	0.000	0.002	0.001	0.002	0.001	0.001	0.002	0.002	0.002
Al	0.996	1.003	0.991	1.005	0.998	1.002	1.100	1.007	1.015	1.003	1.098	1.014	1.010	0.999
Ba	0.001	0.001	0.000	0.001	0.000	0.002	0.015	0.001	0.003	0.002	0.001	0.002	0.001	0.000
Fe	0.018	0.013	0.014	0.012	0.016	0.014	0.015	0.011	0.014	0.012	0.013	0.011	0.011	0.014
Sr	0.001	0.001	0.001	0.001		0.001	0.001			0.001	0.000	0.001	0.001	
Mg	0.001	0.000	0.000	0.000		0.000	0.001	0.001		0.001	0.000			
Ca	0.014	0.010	0.007	0.009	0.006	0.010	0.090	0.013	0.014	0.013	0.010	0.016	0.014	0.008
Na	0.683	0.672	0.665	0.668	0.671	0.673	0.744	0.681	0.663	0.676	0.625	0.688	0.680	0.673
K	0.315	0.320	0.328	0.327	0.319	0.330	0.165	0.306	0.308	0.318	0.327	0.309	0.310	0.325
Sum	5.015	5.007	5.004	5.009	5.003	5.016	5.018	5.005	4.997	5.011	5.001	5.016	5.009	5.010
Ab	67.5	67.1	66.5	66.5	67.4	66.4	74.5	68.1	67.2	67.1	65.0	67.9	67.7	66.9
An	1.4	1.0	0.7	0.9	0.6	1.0	9.0	1.3	1.5	1.3	1.0	1.6	1.4	0.8
Or	31.1	31.9	32.8	32.6	32.0	32.6	16.5	30.6	31.3	31.6	34.0	30.5	30.9	32.3

Table C1 continued

Unit	**LAI**	**LAI**	**LAI**	**LAI**	**LAI**	**LAI**	**LAI**	**LAI**	**LAI**	**LAI**	**LAI**	**LAI**	**LAI**	**LAI**
Sample	TER1-1	TER1-2	TER1-2	TER1-2	TER1-2	TER1-2	TER1-2	TER1-2	TER1-2	TER1-2	TER1-2	TER1-2	TER1-2	TER1-2
No.	34 / 1 .	1 / 1 .	2 / 1 .	3 / 1 .	4 / 1 .	5 / 1 .	6 / 1 .	7 / 1 .	8 / 1 .	9 / 1 .	10 / 1 .	11 / 1 .	12 / 1 .	13 / 1 .
Notes	Pheno	Pheno	Pheno	Pheno	Pheno	Pheno	Pheno	Pheno	Pheno	Pheno	Pheno	Pheno	Pheno	Pheno
SiO_2	66.30	67.11	67.43	67.59	67.47	67.24	67.37	67.15	66.62	67.06	66.88	67.34	66.83	66.42
TiO_2	0.05	0.03	0.05	0.03	0.05	0.03	0.03	0.02	0.03	0.03	0.04	0.04	0.03	0.08
Al_2O_3	18.88	19.30	19.17	19.11	19.07	18.97	19.17	18.85	19.21	19.06	19.16	19.07	19.11	19.19
BaO	0.09	0.06	0.02	0.02	0.02	0.04	0.06	0.04	0.13	0.05	0.06	0.05	0.12	0.16
FeO	0.35	0.33	0.38	0.42	0.38	0.37	0.39	0.44	0.29	0.32	0.31	0.34	0.33	0.30
SrO	0.01	0.02	0.03	0.05	0.01	bdl	0.06	0.01	0.03	0.01	0.04	bdl	bdl	bdl
MgO	bdl	0.01	bdl	0.01	0.01	0.01	0.02		0.01	0.01	0.01	0.01	bdl	0.01
CaO	0.23	0.22	0.15	0.13	0.16	0.15	0.19	0.17	0.31	0.22	0.29	0.18	0.22	0.46
Na_2O	7.66	7.83	7.90	7.69	7.90	7.81	7.80	7.93	7.79	7.91	7.94	7.82	7.83	7.99
K_2O	5.53	5.58	5.76	5.85	5.74	5.95	5.76	5.76	5.54	5.68	5.49	5.77	5.67	5.25
Total	99.09	100.48	100.90	100.91	100.82	100.57	100.87	100.37	99.94	100.35	100.22	100.64	100.15	99.87
Si	2.987	2.981	2.986	2.991	2.989	2.989	2.985	2.991	2.978	2.985	2.980	2.989	2.982	2.972
Ti	0.002	0.001	0.002	0.001	0.002	0.001	0.001	0.001	0.001	0.001	0.001	0.001	0.001	0.003
Al	1.003	1.010	1.001	0.997	0.996	0.994	1.001	0.990	1.012	1.000	1.006	0.998	1.005	1.012
Ba	0.002	0.001	0.000	0.000	0.000	0.001	0.001	0.001	0.002	0.001	0.001	0.001	0.002	0.003
Fe	0.013	0.012	0.014	0.016	0.014	0.014	0.014	0.016	0.011	0.012	0.012	0.013	0.012	0.011
Sr	0.000	0.001	0.001	0.001	0.000		0.002	0.000	0.001	0.000	0.001			
Mg		0.000		0.001	0.001	0.001	0.001		0.000	0.000	0.001	0.001		0.000
Ca	0.011	0.010	0.007	0.006	0.008	0.007	0.009	0.008	0.015	0.010	0.014	0.008	0.011	0.022
Na	0.669	0.674	0.678	0.660	0.679	0.673	0.670	0.685	0.675	0.683	0.686	0.673	0.678	0.693
K	0.318	0.316	0.325	0.331	0.325	0.338	0.326	0.327	0.316	0.323	0.312	0.327	0.323	0.300
Sum	5.004	5.008	5.014	5.004	5.013	5.018	5.011	5.019	5.010	5.016	5.014	5.011	5.014	5.016
Ab	67.1	67.4	67.1	66.2	67.1	66.1	66.7	67.1	67.1	67.2	67.8	66.8	67.0	68.3
An	1.1	1.0	0.7	0.6	0.8	0.7	0.9	0.8	1.5	1.0	1.4	0.8	1.0	2.2
Or	31.8	31.6	32.2	33.2	32.1	33.2	32.4	32.1	31.4	31.8	30.9	32.4	31.9	29.5

Table C1 continued

Unit	**LAI**	**LAI**	**LAI**	**LAI**	**LAI**	**LAI**	**LAI**	**LAI**	**LAI**	**LAI**	**LAI**	**LAI**	**LAI**	**LAI**
Sample	TER1-2	TER1-2	TER1-2	TER1-2	TER1-2	TER1-2	TER1-2	TER1-2	TER1-2	TER1-2	TER1-2	TER1-2	TER1-2	TER1-2
No.	14 / 1 .	15 / 1 .	16 / 1 .	17 / 1 .	18 / 1 .	19 / 1 .	20 / 1 .	21 / 1 .	22 / 1 .	24 / 1 .	25 / 1 .	26 / 1 .	27 / 1 .	28 / 1 .
Notes	Pheno	Pheno	Pheno	Pheno	Pheno	Pheno	Pheno	Pheno	Pheno	Pheno	Pheno	Pheno	Pheno	Pheno
SiO_2	66.46	67.20	66.80	67.11	66.32	66.52	65.42	65.99	67.12	65.55	66.67	66.73	67.33	66.60
TiO_2	0.03	0.03	0.02	0.03	0.07	0.06	0.07	0.08	0.06	0.07	0.05	0.05	0.04	0.07
Al_2O_3	18.92	19.03	18.66	18.70	19.68	19.02	20.23	20.07	19.26	19.27	18.96	18.89	19.17	18.91
BaO	0.07	0.08	0.05	0.05	0.71	0.36	0.68	0.73	0.32	0.41	0.17	0.18	0.14	0.13
FeO	0.33	0.34	0.49	0.42	0.29	0.29	0.30	0.29	0.29	0.27	0.30	0.30	0.27	0.29
SrO	0.04	0.04	0.03	0.01	0.06	0.03	0.02	0.04	0.02	0.03	0.02	0.03	0.04	0.05
MgO	bdl	bdl	0.01	bdl	bdl	0.01	0.01	bdl	0.02	bdl	0.01	0.01	0.01	bdl
CaO	0.22	0.22	0.17	0.14	0.91	0.53	1.24	1.23	0.47	0.85	0.40	0.41	0.41	0.42
Na_2O	7.85	7.74	7.64	7.69	8.18	7.94	8.25	8.32	7.93	8.08	7.84	7.80	7.99	7.93
K_2O	5.68	5.73	5.85	5.99	4.40	5.22	4.01	3.92	5.35	4.68	5.60	5.48	5.42	5.50
Total	99.60	100.42	99.72	100.15	100.61	99.98	100.24	100.66	100.83	99.21	100.01	99.88	100.81	99.92
Si	2.983	2.990	2.996	2.997	2.951	2.977	2.921	2.933	2.977	2.956	2.982	2.986	2.983	2.981
Ti	0.001	0.001	0.001	0.001	0.002	0.002	0.002	0.003	0.002	0.002	0.002	0.002	0.001	0.002
Al	1.001	0.998	0.986	0.984	1.032	1.003	1.065	1.051	1.007	1.024	0.999	0.996	1.001	0.998
Ba	0.001	0.001	0.001	0.001	0.012	0.006	0.012	0.013	0.006	0.007	0.003	0.003	0.002	0.002
Fe	0.012	0.013	0.018	0.016	0.011	0.011	0.011	0.011	0.011	0.010	0.011	0.011	0.010	0.011
Sr	0.001	0.001	0.001	0.000	0.002	0.001	0.000	0.001	0.001	0.001	0.000	0.001	0.001	0.001
Mg			0.000			0.001	0.001		0.001		0.000	0.001	0.000	
Ca	0.011	0.010	0.008	0.007	0.043	0.026	0.059	0.059	0.022	0.041	0.019	0.020	0.020	0.020
Na	0.683	0.668	0.664	0.666	0.706	0.689	0.714	0.716	0.682	0.706	0.680	0.677	0.686	0.688
K	0.325	0.325	0.335	0.341	0.250	0.298	0.228	0.222	0.303	0.269	0.319	0.313	0.306	0.314
Sum	5.019	5.007	5.010	5.013	5.009	5.013	5.015	5.008	5.010	5.017	5.016	5.009	5.011	5.019
Ab	67.0	66.6	65.9	65.7	70.7	68.0	71.3	71.9	67.7	69.5	66.7	67.1	67.8	67.3
An	1.0	1.0	0.8	0.7	4.3	2.5	5.9	5.9	2.2	4.0	1.9	2.0	1.9	2.0
Or	31.9	32.4	33.3	33.7	25.0	29.4	22.8	22.3	30.1	26.5	31.4	31.0	30.3	30.7

Table C1 continued

Unit	**LAI**	**LAI**	**LAI**	**LAI**	**LAI**	**LAI**	**LAI**	**LAI**	**LAI**	**LAI**	**LAI**	**LAI**	**LAI**	**LAI**
Sample	TER1-2	TER1-2	TER3-1	TER3-1	TER3-1	TER3-1	TER3-1	TER3-1	TER3-1	TER3-1	TER3-1	TER3-1	TER3-1	TER3-1
No.	29 / 1 .	30 / 1 .	54 / 1 .	55 / 1 .	56 / 1 .	57 / 1 .	58 / 1 .	60 / 1 .	63 / 1 .	64 / 1 .	65 / 1 .	66 / 1 .	67 / 1 .	68 / 1 .
Notes	Pheno	Pheno	Pheno	Pheno	Pheno	Pheno	Pheno	Pheno	Pheno	Pheno	Pheno	Pheno	Pheno	Pheno
SiO_2	67.31	67.58	66.29	66.16	66.42	66.48	66.43	65.11	66.27	66.15	66.89	66.29	65.61	65.91
TiO_2	0.05	0.03	0.04	0.05	0.04	0.03	0.07	0.12	0.04	0.05	0.01	0.06	0.04	0.05
Al_2O_3	18.65	19.01	19.00	18.93	19.06	19.19	18.97	19.65	19.06	18.82	18.60	19.18	18.84	19.07
BaO	0.08	0.10	0.18	0.15	0.13	0.15	0.12	0.85	0.22	0.17	0.09	0.26	0.24	0.28
FeO	0.34	0.34	0.27	0.30	0.28	0.28	0.29	0.38	0.29	0.30	0.49	0.28	0.27	0.29
SrO	0.01	0.04	0.02	0.02	0.02	0.04	0.03	0.02	0.06	0.02	0.03	0.02	0.02	0.02
MgO	bdl	0.02	0.01	0.01	bdl	bdl	0.01	bdl	bdl	bdl	0.02	bdl	bdl	bdl
CaO	0.26	0.25	0.48	0.46	0.47	0.50	0.43	1.06	0.51	0.33	0.18	0.53	0.57	0.54
Na_2O	7.75	7.84	7.95	7.80	7.92	7.98	7.94	8.19	7.94	7.89	7.54	7.96	7.93	7.92
K_2O	5.72	5.70	5.14	5.32	5.38	5.31	5.38	4.25	5.20	5.49	5.95	5.16	5.15	5.29
Total	100.17	100.92	99.37	99.20	99.71	99.96	99.65	99.64	99.58	99.22	99.78	99.73	98.69	99.36
Si	3.001	2.992	2.979	2.980	2.977	2.973	2.979	2.933	2.975	2.982	2.999	2.971	2.974	2.969
Ti	0.002	0.001	0.002	0.002	0.001	0.001	0.002	0.004	0.001	0.002	0.000	0.002	0.002	0.002
Al	0.980	0.992	1.006	1.005	1.007	1.011	1.003	1.043	1.008	1.000	0.983	1.013	1.006	1.013
Ba	0.001	0.002	0.003	0.003	0.002	0.003	0.002	0.015	0.004	0.003	0.002	0.005	0.004	0.005
Fe	0.013	0.013	0.010	0.011	0.010	0.011	0.011	0.014	0.011	0.011	0.018	0.010	0.010	0.011
Sr	0.000	0.001	0.001	0.001	0.000	0.001	0.001	0.000	0.002	0.000	0.001	0.001	0.001	0.001
Mg		0.001	0.000	0.001			0.000				0.001			
Ca	0.012	0.012	0.023	0.022	0.022	0.024	0.021	0.051	0.025	0.016	0.008	0.025	0.027	0.026
Na	0.670	0.673	0.692	0.681	0.689	0.692	0.690	0.716	0.691	0.689	0.655	0.692	0.696	0.692
K	0.325	0.322	0.294	0.306	0.307	0.303	0.308	0.244	0.298	0.316	0.340	0.295	0.298	0.304
Sum	5.005	5.009	5.010	5.010	5.016	5.018	5.016	5.021	5.014	5.019	5.007	5.014	5.019	5.021
Ab	66.5	66.8	68.6	67.5	67.6	67.9	67.8	70.8	68.2	67.5	65.3	68.4	68.2	67.7
An	1.2	1.2	2.3	2.2	2.2	2.3	2.0	5.1	2.4	1.6	0.8	2.5	2.7	2.5
Or	32.3	32.0	29.2	30.3	30.2	29.7	30.2	24.1	29.4	30.9	33.9	29.1	29.2	29.7

Table C1 continued

Unit	**LAI**	**LAI**	**LAI**	**LAI**	**LAI**	**LAI**	**LAI**	**LAI**	**LAI**	**LAI**	**LAI**	**LAI**	**LAI**	**LAI**
Sample	TER3-1	TER3-1	TER3-1	TER3-1	TER3-1	TER3-1	TER3-1	TER3-2	TER3-2	TER3-2	TER3-2	TER3-2	TER3-2	TER3-2
No.	69 / 1 .	70 / 1 .	71 / 1 .	72 / 1 .	73 / 1 .	74 / 1 .	75 / 1 .	1 / 1 .	2 / 1 .	3 / 1 .	4 / 1 .	5 / 1 .	6 / 1 .	7 / 1 .
Notes	Pheno	Pheno	Pheno	Pheno	Pheno	Pheno	Pheno	Pheno	Pheno	Pheno	Pheno	Pheno	Pheno	Pheno
SiO_2	66.45	66.70	67.00	66.12	66.90	66.83	67.20	66.83	67.70	67.52	66.86	67.27	66.67	66.23
TiO_2	0.05	0.04	0.03	0.06	0.05	0.05	0.04	0.04	0.03	0.07	0.03	0.03	0.08	0.08
Al_2O_3	19.42	19.26	19.28	19.09	19.01	19.03	18.89	19.42	19.29	18.82	18.95	19.14	19.72	19.75
BaO	0.24	0.26	0.23	0.25	0.11	0.11	0.12	0.12	0.06	0.15	0.14	0.05	0.29	0.54
FeO	0.31	0.29	0.26	0.29	0.28	0.32	0.27	0.29	0.31	0.64	0.34	0.36	0.24	0.29
SrO	0.04	0.01	0.03	0.04	0.03	0.01	0.02	0.05	0.01	0.02	0.04	0.03	0.03	0.04
MgO	bdl	bdl	0.01	0.01	0.02	0.01	bdl	0.01	bdl	0.03	bdl	0.01	bdl	0.01
CaO	0.58	0.51	0.58	0.62	0.33	0.35	0.37	0.42	0.16	0.37	0.27	0.23	0.67	0.87
Na_2O	7.94	7.90	7.98	7.98	7.76	7.93	7.90	8.06	7.71	7.55	7.91	7.80	8.12	8.18
K_2O	5.03	5.19	5.04	5.08	5.58	5.57	5.53	5.35	5.83	5.54	5.53	5.71	4.68	4.53
Total	100.07	100.16	100.45	99.53	100.07	100.21	100.35	100.58	101.09	100.70	100.07	100.63	100.51	100.50
Si	2.966	2.975	2.977	2.970	2.986	2.981	2.991	2.970	2.989	2.996	2.986	2.986	2.959	2.948
Ti	0.002	0.002	0.001	0.002	0.002	0.002	0.001	0.001	0.001	0.002	0.001	0.001	0.003	0.003
Al	1.021	1.012	1.010	1.011	1.000	1.000	0.991	1.017	1.004	0.984	0.998	1.002	1.032	1.036
Ba	0.004	0.004	0.004	0.004	0.002	0.002	0.002	0.002	0.001	0.003	0.002	0.001	0.005	0.009
Fe	0.011	0.011	0.010	0.011	0.011	0.012	0.010	0.011	0.011	0.024	0.013	0.013	0.009	0.011
Sr	0.001	0.000	0.001	0.001	0.001	0.000	0.001	0.001	0.000	0.001	0.001	0.001	0.001	0.001
Mg			0.001	0.000	0.001	0.000		0.001		0.002		0.000		0.000
Ca	0.028	0.025	0.028	0.030	0.016	0.017	0.018	0.020	0.008	0.017	0.013	0.011	0.032	0.041
Na	0.687	0.683	0.687	0.695	0.671	0.686	0.681	0.694	0.660	0.649	0.685	0.671	0.699	0.706
K	0.287	0.296	0.286	0.291	0.318	0.317	0.314	0.303	0.328	0.313	0.315	0.323	0.265	0.257
Sum	5.008	5.007	5.004	5.016	5.007	5.018	5.010	5.020	5.002	4.991	5.014	5.009	5.004	5.013
Ab	68.6	68.1	68.7	68.4	66.8	67.3	67.3	68.2	66.3	66.2	67.6	66.8	70.2	70.3
An	2.8	2.4	2.8	2.9	1.6	1.7	1.8	2.0	0.8	1.8	1.3	1.1	3.2	4.1
Or	28.6	29.5	28.6	28.7	31.6	31.1	31.0	29.8	33.0	32.0	31.1	32.2	26.6	25.6

Table C1 continued

Unit	**LAl**	**LAl**	**LAl**	**LAl**	**LAl**	**LAl**	**LAl**	**LAl**	**LAl**	**LAl**	**LAl**	**LAl**	**LAl**	**LAl**
Sample	TER3-2	TER3-2	TER3-2	TER3-2	TER3-2	TER3-2	TER3-2	TER4-1	TER4-1	TER4-1	TER4-1	TER4-1	TER4-1	TER4-1
No.	8 / 1 .	9 / 1 .	13 / 1 .	15 / 1 .	16 / 1 .	17 / 1 .	18 / 1 .	76 / 1 .	77 / 1 .	78 / 1 .	79 / 1 .	80 / 1 .	81 / 1 .	82 / 1 .
Notes	Pheno	Pheno	Pheno	Pheno	Pheno	Pheno	Pheno	Pheno	Pheno	Pheno	Pheno	Pheno	Pheno	Pheno
SiO_2	67.56	67.67	67.15	67.68	67.60	67.64	67.42	67.06	66.25	66.88	66.48	67.64	66.93	67.20
TiO_2	0.02	0.04	0.04	0.02	0.02	0.03	0.03	0.03	0.05	0.04	0.02	0.02	0.06	0.04
Al_2O_3	18.80	19.42	18.85	19.04	19.02	19.12	19.24	18.85	19.35	19.06	18.66	19.18	19.37	19.31
BaO	bdl	0.09	bdl	0.01	0.05	0.06	0.11	0.03	0.13	0.05	0.02	0.02	0.17	0.11
FeO	0.46	0.38	0.47	0.45	0.46	0.38	0.37	0.45	0.29	0.35	0.42	0.43	0.35	0.35
SrO	bdl	0.02	0.05	0.06	0.05	0.01	bdl	0.02	0.03	0.05	0.02	0.02	0.01	0.03
MgO	0.01	bdl	0.01	0.01	0.01	bdl	0.01	0.01	0.01	bdl	0.01	bdl	bdl	bdl
CaO	0.11	0.24	0.05	0.14	0.13	0.13	0.17	0.11	0.38	0.20	0.12	0.14	0.28	0.24
Na_2O	7.46	7.84	7.83	7.74	7.61	7.65	7.81	7.72	8.01	8.11	7.80	7.92	8.05	7.94
K_2O	6.00	5.60	5.95	5.71	6.00	5.84	5.73	6.03	5.43	5.70	5.95	6.04	5.54	5.69
Total	100.43	101.31	100.40	100.87	100.95	100.86	100.89	100.31	99.94	100.46	99.50	101.40	100.74	100.89
Si	3.003	2.982	2.992	2.995	2.994	2.994	2.985	2.991	2.965	2.979	2.990	2.985	2.972	2.978
Ti	0.001	0.001	0.001	0.001	0.001	0.001	0.001	0.001	0.002	0.001	0.001	0.001	0.002	0.001
Al	0.985	1.009	0.990	0.993	0.993	0.997	1.004	0.991	1.021	1.001	0.989	0.997	1.013	1.008
Ba		0.002		0.000	0.001	0.001	0.002	0.001	0.002	0.001	0.000	0.000	0.003	0.002
Fe	0.017	0.014	0.017	0.017	0.017	0.014	0.014	0.017	0.011	0.013	0.016	0.016	0.013	0.013
Sr		0.000	0.001	0.002	0.001	0.000		0.000	0.001	0.001	0.000	0.000	0.000	0.001
Mg	0.001		0.001	0.001	0.000		0.001	0.001	0.001		0.001			
Ca	0.005	0.011	0.002	0.007	0.006	0.006	0.008	0.005	0.018	0.010	0.006	0.007	0.013	0.011
Na	0.643	0.670	0.676	0.664	0.654	0.656	0.670	0.668	0.695	0.701	0.680	0.677	0.693	0.682
K	0.340	0.315	0.338	0.323	0.339	0.330	0.324	0.343	0.310	0.324	0.342	0.340	0.314	0.322
Sum	4.995	5.004	5.019	5.001	5.006	5.000	5.009	5.018	5.025	5.031	5.025	5.024	5.023	5.018
Ab	65.0	67.2	66.5	66.9	65.4	66.1	66.9	65.7	67.9	67.7	66.2	66.1	68.0	67.2
An	0.5	1.1	0.2	0.7	0.6	0.6	0.8	0.5	1.8	0.9	0.6	0.6	1.3	1.1
Or	34.4	31.6	33.3	32.5	34.0	33.3	32.3	33.8	30.3	31.3	33.2	33.2	30.8	31.7

Table C1 continued

Unit	**LAl**	**LAl**	**LAl**	**LAl**	**LAl**	**LAl**	**LAl**	**LAl**	**LAl**	**LAl**	**LAl**	**LAl**	**LAl**	**LAl**
Sample	TER4-1	TER4-1	TER4-1	TER4-1	TER4-1	TER4-1	TER4-1	TER4-1	TER4-1	TER4-1	TER4-1	TER4-1	TER4-1	TER4-1
No.	83 / 1 .	84 / 1 .	85 / 1 .	86 / 1 .	87 / 1 .	88 / 1 .	89 / 1 .	90 / 1 .	91 / 1 .	92 / 1 .	94 / 1 .	95 / 1 .	96 / 1 .	97 / 1 .
Notes	Pheno	Pheno	Pheno	Pheno	Pheno	Pheno	Pheno	Pheno	Pheno	Pheno	Pheno	Pheno	Pheno	Pheno
SiO_2	66.72	65.72	66.37	65.93	67.04	66.60	66.58	66.87	65.83	65.20	66.00	65.81	65.84	66.05
TiO_2	0.06	0.03	0.03	0.04	0.04	0.02	0.05	0.02	0.03	0.04	0.06	0.04	0.02	0.03
Al_2O_3	18.91	18.81	18.41	18.91	18.93	18.94	19.29	19.04	18.86	19.19	18.84	18.81	18.67	19.12
BaO	0.06	0.06	0.05	0.05	0.03	0.06	0.09	0.01	0.03	0.13	0.13	0.10	0.04	0.04
FeO	0.32	0.38	0.46	0.37	0.46	0.43	0.32	0.42	0.44	0.29	0.32	0.35	0.39	0.39
SrO	0.04	0.05	0.06	0.04	0.03	0.01	0.03	0.01	0.01	0.03	0.03	0.02	0.02	0.01
MgO	0.02	0.01	0.01	bdl	bdl	bdl	bdl	0.01	0.01	bdl	bdl	bdl	bdl	0.01
CaO	0.22	0.15	0.16	0.18	0.13	0.16	0.21	0.11	0.11	0.33	0.28	0.23	0.17	0.15
Na_2O	7.86	7.81	7.61	7.58	7.93	7.83	7.76	7.84	7.66	7.92	7.89	7.87	7.86	7.87
K_2O	5.84	5.95	6.19	6.15	5.91	5.92	5.82	5.92	5.95	5.55	5.67	5.72	5.86	5.93
Total	100.04	98.96	99.35	99.27	100.51	99.96	100.15	100.25	98.93	98.68	99.22	98.95	98.88	99.59
Si	2.984	2.976	2.995	2.977	2.986	2.983	2.974	2.983	2.979	2.959	2.978	2.978	2.982	2.971
Ti	0.002	0.001	0.001	0.001	0.001	0.001	0.002	0.001	0.001	0.001	0.002	0.001	0.001	0.001
Al	0.997	1.004	0.979	1.006	0.994	1.000	1.015	1.001	1.006	1.027	1.002	1.003	0.997	1.013
Ba	0.001	0.001	0.001	0.001	0.000	0.001	0.002	0.000	0.000	0.002	0.002	0.002	0.001	0.001
Fe	0.012	0.014	0.017	0.014	0.017	0.016	0.012	0.016	0.017	0.011	0.012	0.013	0.015	0.015
Sr	0.001	0.001	0.002	0.001	0.001	0.000	0.001	0.000	0.000	0.001	0.001	0.001	0.001	0.000
Mg	0.001	0.000	0.001					0.001	0.001					0.000
Ca	0.010	0.007	0.008	0.009	0.006	0.008	0.010	0.005	0.005	0.016	0.013	0.011	0.008	0.007
Na	0.681	0.686	0.666	0.663	0.685	0.680	0.672	0.678	0.672	0.697	0.691	0.690	0.690	0.687
K	0.333	0.344	0.356	0.355	0.336	0.338	0.331	0.337	0.343	0.321	0.326	0.330	0.339	0.340
Sum	5.023	5.036	5.025	5.028	5.027	5.026	5.019	5.023	5.025	5.035	5.028	5.029	5.033	5.035
Ab	66.5	66.1	64.7	64.6	66.7	66.3	66.3	66.4	65.8	67.4	67.0	66.9	66.5	66.4
An	1.0	0.7	0.7	0.9	0.6	0.7	1.0	0.5	0.5	1.6	1.3	1.1	0.8	0.7
Or	32.5	33.2	34.6	34.5	32.7	33.0	32.7	33.0	33.6	31.1	31.7	32.0	32.7	32.9

Table C1 continued

Unit	**LAl**	**LAl**	**LAl**	**LAl**	**LAl**	**LAl**	**LAl**	**LAl**	**LAl**	**LAl**	**LAl**	**LAl**	**LAl**	**LAl**
Sample	TER4-1	TER6-1	TER6-1	TER6-1	TER6-1	TER6-1	TER6-1	TER6-1	TER6-1	TER6-1	TER6-1	TER6-1	TER6-1	TER7-1
No.	98 / 1 .	36 / 1 .	37 / 1 .	38 / 1 .	39 / 1 .	40 / 1 .	41 / 1 .	42 / 1 .	43 / 1 .	44 / 1 .	45 / 1 .	46 / 1 .	47 / 1 .	31 / 1 .
Notes	Pheno	Pheno	Pheno	Pheno	Pheno	Pheno	Pheno	Pheno	Pheno	Pheno	Pheno	Pheno	Pheno	Pheno
SiO_2	65.93	67.12	65.85	66.18	66.33	66.98	67.33	66.08	65.42	67.14	66.20	67.41	66.95	66.28
TiO_2	0.05	0.04	0.06	0.03	0.05	0.01	0.04	0.06	0.07	0.04	0.04	0.04	0.04	0.07
Al_2O_3	18.95	19.25	19.97	19.73	19.61	19.03	19.36	19.51	20.26	18.98	19.00	19.08	19.43	20.24
BaO	0.04	0.11	0.13	0.14	0.03	0.07	0.09	0.11	0.35	0.06	0.06	0.03	0.09	0.68
FeO	0.39	0.32	0.27	0.30	0.37	0.44	0.34	0.28	0.38	0.43	0.35	0.37	0.34	0.29
SrO	0.02	0.04	0.03	0.01	0.04	0.05	0.02	0.06	0.06	0.04	0.06	0.03	bdl	0.04
MgO	0.01	bdl	0.01	bdl	bdl	bdl	bdl	bdl	0.01	bdl	0.02	0.01	bdl	bdl
CaO	0.18	0.22	0.46	0.34	0.24	0.15	0.26	0.48	0.51	0.15	0.23	0.18	0.24	1.34
Na_2O	7.88	7.86	7.83	7.84	7.65	7.99	7.95	8.01	8.02	7.59	7.75	7.83	8.08	8.58
K_2O	5.86	5.64	5.16	5.65	5.82	5.83	5.52	5.30	4.87	5.83	5.56	5.87	5.57	3.48
Total	99.32	100.59	99.76	100.23	100.14	100.55	100.91	99.88	99.96	100.25	99.27	100.87	100.74	100.99
Si	2.974	2.981	2.947	2.955	2.962	2.982	2.979	2.958	2.929	2.992	2.980	2.988	2.971	2.931
Ti	0.002	0.001	0.002	0.001	0.002	0.000	0.001	0.002	0.002	0.001	0.001	0.001	0.001	0.002
Al	1.007	1.008	1.053	1.038	1.032	0.999	1.010	1.029	1.069	0.997	1.008	0.997	1.016	1.055
Ba	0.001	0.002	0.002	0.002	0.001	0.001	0.002	0.002	0.006	0.001	0.001	0.001	0.002	0.012
Fe	0.015	0.012	0.010	0.011	0.014	0.016	0.013	0.011	0.014	0.016	0.013	0.014	0.013	0.011
Sr	0.001	0.001	0.001	0.000	0.001	0.001	0.001	0.002	0.002	0.001	0.002	0.001		0.001
Mg	0.001		0.000						0.001		0.001	0.000		
Ca	0.009	0.011	0.022	0.016	0.011	0.007	0.012	0.023	0.024	0.007	0.011	0.009	0.011	0.063
Na	0.689	0.676	0.679	0.679	0.662	0.690	0.682	0.695	0.697	0.656	0.677	0.673	0.695	0.735
K	0.337	0.319	0.294	0.322	0.332	0.331	0.311	0.303	0.278	0.331	0.319	0.332	0.316	0.196
Sum	5.034	5.011	5.011	5.025	5.017	5.028	5.011	5.024	5.022	5.002	5.013	5.015	5.025	5.006
Ab	66.6	67.2	68.2	66.7	65.9	67.1	67.8	68.1	69.7	66.0	67.2	66.4	68.0	73.9
An	0.8	1.0	2.2	1.6	1.1	0.7	1.2	2.2	2.4	0.7	1.1	0.9	1.1	6.4
Or	32.6	31.7	29.6	31.6	33.0	32.2	31.0	29.7	27.8	33.3	31.7	32.7	30.9	19.7

Table C1 continued

Unit	**LAl**	**LAl**	**LAl**	**LAl**	**LAl**	**LAl**	**LAl**	**LAl**	**LAl**	**LAl**	**LAl**	**LAl**	**LAl**	**LAl**
Sample	TER7-1	TER7-1	TER7-1	TER7-1	TER7-1	TER7-1	TER7-1	TER7-1	TER7-1	TER7-1	TER7-1	TER7-1	TER7-1	TER7-1
No.	32 / 1 .	33 / 1 .	34 / 1 .	35 / 1 .	36 / 1 .	37 / 1 .	38 / 1 .	39 / 1 .	40 / 1 .	41 / 1 .	42 / 1 .	43 / 1 .	44 / 1 .	45 / 1 .
Notes	Pheno	Pheno	Pheno	Pheno	Pheno	Pheno	Pheno	Pheno	Pheno	Pheno	Pheno	Pheno	Pheno	Pheno
SiO_2	64.49	67.97	67.82	67.55	67.62	67.41	67.39	67.52	67.44	66.29	66.50	66.43	66.30	66.70
TiO_2	0.09	0.04	0.02	0.03	0.04	0.04	0.04	0.04	0.05	0.04	0.04	0.02	0.04	0.04
Al_2O_3	20.22	18.98	19.01	18.95	18.88	18.89	19.09	18.98	19.11	18.72	18.64	18.73	18.72	18.83
BaO	0.86	0.06	0.04	0.07	0.04	0.06	0.08	0.06	0.06	0.10	0.11	0.11	0.05	0.03
FeO	0.29	0.29	0.34	0.30	0.34	0.31	0.32	0.33	0.32	0.31	0.32	0.34	0.30	0.31
SrO	0.05	0.02	0.04	0.02	0.02	0.04	0.02	0.01	bdl	0.03	0.03	0.01	0.03	0.07
MgO	0.02	bdl	0.02	bdl	bdl	0.02	0.01	0.02	bdl	0.01	bdl	0.01	0.01	bdl
CaO	1.57	0.19	0.21	0.21	0.18	0.20	0.22	0.21	0.27	0.22	0.24	0.20	0.27	0.31
Na_2O	8.59	7.99	7.75	7.89	7.73	7.78	7.88	7.79	7.83	7.86	7.86	7.88	8.02	8.03
K_2O	3.22	5.71	5.71	5.69	5.77	5.70	5.71	5.67	5.74	5.60	5.68	5.66	5.45	5.59
Total	99.39	101.26	100.96	100.71	100.61	100.45	100.76	100.62	100.82	99.19	99.43	99.38	99.20	99.92
Si	2.906	2.997	2.997	2.995	2.999	2.996	2.988	2.995	2.988	2.988	2.991	2.989	2.986	2.985
Ti	0.003	0.001	0.001	0.001	0.001	0.001	0.001	0.001	0.002	0.001	0.001	0.001	0.001	0.001
Al	1.074	0.986	0.990	0.990	0.987	0.990	0.998	0.992	0.998	0.994	0.988	0.993	0.994	0.993
Ba	0.015	0.001	0.001	0.001	0.001	0.001	0.001	0.001	0.001	0.002	0.002	0.002	0.001	0.001
Fe	0.011	0.011	0.013	0.011	0.013	0.012	0.012	0.012	0.012	0.012	0.012	0.013	0.011	0.012
Sr	0.001	0.001	0.001	0.001	0.000	0.001	0.000	0.000		0.001	0.001	0.000	0.001	0.002
Mg	0.001		0.001			0.001	0.001	0.001		0.001		0.000	0.001	
Ca	0.076	0.009	0.010	0.010	0.008	0.009	0.010	0.010	0.013	0.011	0.012	0.010	0.013	0.015
Na	0.750	0.683	0.664	0.678	0.665	0.670	0.677	0.670	0.673	0.687	0.686	0.687	0.701	0.696
K	0.185	0.321	0.322	0.322	0.326	0.323	0.323	0.321	0.324	0.322	0.326	0.325	0.313	0.319
Sum	5.022	5.011	5.000	5.009	5.001	5.004	5.012	5.003	5.010	5.018	5.019	5.020	5.022	5.025
Ab	74.2	67.4	66.7	67.2	66.5	66.8	67.0	67.0	66.6	67.4	67.0	67.3	68.2	67.6
An	7.5	0.9	1.0	1.0	0.8	0.9	1.0	1.0	1.3	1.0	1.1	1.0	1.3	1.4
Or	18.3	31.7	32.3	31.9	32.6	32.2	31.9	32.1	32.1	31.6	31.8	31.8	30.5	31.0

Table C1 continued

Unit	**LAI**	**LAI**	**LAI**	**LAI**	**LAI**	**LAI**	**LAI**	**LAI**	**LAI**	**LAI**	**LAI**	**LAI**	**LAI**	**LAI**
Sample	TER7-1	TER7-1	TER7-1	TER7-1	TER7-1	TER7-1	TER7-1	TER7-1	TER10-3	TER10-3	TER10-3	TER10-3	TER10-3	TER10-3
No.	46 / 1 .	47 / 1 .	48 / 1 .	49 / 1 .	50 / 1 .	51 / 1 .	52 / 1 .	53 / 1 .	35 / 1 .	35 / 2 .	35 / 3 .	35 / 4 .	35 / 5 .	35 / 6 .
Notes	Pheno	Pheno	Pheno	Pheno	Pheno	Pheno	Pheno	Pheno	Pheno	Pheno	Pheno	Pheno	Pheno	Pheno
SiO_2	66.57	66.77	66.68	66.23	66.58	66.61	66.63	66.64	67.15	66.14	66.77	67.14	67.06	66.80
TiO_2	0.04	0.03	0.04	0.05	0.04	0.05	0.04	0.07	0.04	0.05	0.05	0.02	0.02	0.02
Al_2O_3	18.71	18.84	18.85	18.70	18.77	18.96	18.82	18.77	19.14	19.60	19.11	18.95	19.23	18.81
BaO	0.10	0.08	0.05	0.06	0.07	0.07	0.06	0.06	0.05	0.07	0.08	0.04	0.01	0.01
FeO	0.31	0.30	0.32	0.29	0.33	0.28	0.32	0.31	0.34	0.35	0.31	0.43	0.36	0.39
SrO	0.03	0.02	bdl	0.03	0.05	0.01	0.03	0.02	0.03	0.05	0.05	0.07	0.02	0.01
MgO	0.01	bdl	bdl	bdl	0.01	bdl	bdl	0.01	0.01	0.01	bdl	0.01	bdl	bdl
CaO	0.24	0.21	0.21	0.25	0.25	0.26	0.23	0.24	0.18	0.20	0.19	0.10	0.12	0.10
Na_2O	7.89	7.90	8.00	8.05	8.00	8.00	7.91	7.89	7.92	7.29	7.84	7.63	7.83	7.65
K_2O	5.53	5.72	5.71	5.60	5.47	5.56	5.65	5.60	5.65	5.65	5.72	5.89	5.88	5.92
Total	99.44	99.87	99.87	99.26	99.56	99.80	99.68	99.61	100.52	99.40	100.12	100.27	100.52	99.71
Si	2.991	2.989	2.986	2.985	2.988	2.983	2.988	2.989	2.984	2.968	2.981	2.992	2.982	2.993
Ti	0.001	0.001	0.001	0.002	0.001	0.002	0.001	0.002	0.001	0.002	0.002	0.001	0.001	0.001
Al	0.991	0.994	0.995	0.993	0.993	1.001	0.995	0.992	1.003	1.037	1.005	0.996	1.008	0.994
Ba	0.002	0.001	0.001	0.001	0.001	0.001	0.001	0.001	0.001	0.001	0.001	0.001	0.000	0.000
Fe	0.012	0.011	0.012	0.011	0.013	0.010	0.012	0.012	0.013	0.013	0.011	0.016	0.013	0.015
Sr	0.001	0.000		0.001	0.001	0.000	0.001	0.000	0.001	0.001	0.001	0.002	0.000	0.000
Mg	0.001				0.001			0.000	0.000	0.001		0.000		
Ca	0.012	0.010	0.010	0.012	0.012	0.012	0.011	0.012	0.009	0.009	0.009	0.005	0.006	0.005
Na	0.688	0.685	0.695	0.704	0.696	0.694	0.687	0.686	0.683	0.634	0.679	0.659	0.675	0.664
K	0.317	0.327	0.326	0.322	0.313	0.318	0.323	0.320	0.320	0.324	0.326	0.335	0.334	0.338
Sum	5.014	5.019	5.026	5.030	5.019	5.021	5.019	5.015	5.015	4.990	5.016	5.006	5.018	5.011
Ab	67.7	67.0	67.4	67.8	68.1	67.8	67.3	67.4	67.5	65.6	66.9	66.0	66.5	65.9
An	1.1	1.0	1.0	1.2	1.2	1.2	1.1	1.1	0.8	1.0	0.9	0.5	0.6	0.5
Or	31.2	32.0	31.6	31.0	30.7	31.0	31.7	31.5	31.7	33.5	32.1	33.5	32.9	33.6

Table C1 continued

Unit	**LAI**	**LAI**	**LAI**	**LAI**	**LAI**	**LAI**	**LAI**	**LAI**	**LAI**	**LAI**	**LAI**	**LAI**
Sample	TER10-3	TER10-3	TER10-3	TER10-3	TER10-3	TER10-3	TER10-3	TER10-3	TER10-3	TER10-3	TER10-3	TER10-3
No.	35 / 7 .	35 / 8 .	35 / 9 .	35 / 10 .	35 / 11 .	35 / 12 .	35 / 13 .	35 / 15 .	35 / 16 .	35 / 18 .	35 / 19 .	35 / 20 .
Notes	Pheno	Pheno	Pheno	Pheno	Pheno	Pheno	Pheno	Pheno	Pheno	Pheno	Pheno	Pheno
SiO_2	64.56	67.01	67.01	67.14	66.49	66.82	66.77	66.77	67.03	65.06	66.82	66.39
TiO_2	0.05	0.01	0.03	0.02	0.05	0.02	0.02	0.03	0.02	0.02	0.05	0.03
Al_2O_3	20.89	18.92	18.89	19.09	19.43	18.92	19.04	18.91	18.81	20.99	19.07	19.12
BaO	0.04	0.01	0.02	0.01	0.03	0.01	0.01	0.01	0.02	0.01	0.08	0.07
FeO	0.51	0.46	0.41	0.45	0.39	0.38	0.38	0.38	0.37	0.42	0.33	0.32
SrO	0.03	0.08	0.03	bdl	0.02	0.02	0.03	0.01	0.03	0.01	0.05	0.04
MgO	0.01	bdl	bdl	0.02	bdl	bdl	bdl	0.01	0.01	bdl	bdl	bdl
CaO	0.17	0.10	0.09	0.12	0.12	0.11	0.12	0.11	0.10	0.18	0.19	0.23
Na_2O	7.33	7.56	7.78	7.61	7.68	7.84	7.72	7.78	7.68	7.40	7.87	7.77
K_2O	5.68	5.89	5.88	5.88	5.78	5.88	5.82	5.81	5.81	5.57	5.71	5.63
Total	99.26	100.03	100.13	100.34	100.00	100.01	99.93	99.81	99.88	99.65	100.17	99.58
Si	2.910	2.993	2.991	2.989	2.971	2.988	2.986	2.989	2.996	2.915	2.982	2.979
Ti	0.002	0.000	0.001	0.001	0.002	0.001	0.001	0.001	0.001	0.001	0.002	0.001
Al	1.110	0.996	0.994	1.002	1.023	0.997	1.004	0.997	0.991	1.108	1.003	1.011
Ba	0.001	0.000	0.000	0.000	0.001	0.000	0.000	0.000	0.000	0.000	0.001	0.001
Fe	0.019	0.017	0.015	0.017	0.015	0.014	0.014	0.014	0.014	0.016	0.012	0.012
Sr	0.001	0.002	0.001		0.001	0.001	0.001	0.000	0.001	0.000	0.001	0.001
Mg	0.000			0.001				0.001	0.001			
Ca	0.008	0.005	0.004	0.006	0.006	0.005	0.006	0.005	0.005	0.009	0.009	0.011
Na	0.641	0.655	0.673	0.657	0.666	0.679	0.669	0.675	0.666	0.643	0.681	0.676
K	0.326	0.336	0.335	0.334	0.330	0.335	0.332	0.332	0.331	0.318	0.325	0.322
Sum	5.017	5.004	5.015	5.005	5.013	5.021	5.013	5.015	5.006	5.010	5.018	5.014
Ab	65.7	65.8	66.5	65.9	66.5	66.6	66.4	66.7	66.5	66.3	67.1	67.0
An	0.8	0.5	0.4	0.6	0.6	0.5	0.6	0.5	0.5	0.9	0.9	1.1
Or	33.5	33.7	33.1	33.5	32.9	32.9	33.0	32.8	33.1	32.8	32.0	31.9

Table C1 continued

Unit	**LMI**	**LMI**	**LMI**	**LMI**	**LMI**	**LMI**	**LMI**	**LMI**	**LMI**	**LMI**	**LMI**	**LMI**	**LMI**	**LMI**
Sample	TER5-2	TER5-2	TER5-2	TER5-2	TER5-2	TER5-2	TER5-2	TER5-2	TER5-2	TER5-2	TER5-2	TER5-2	TER5-2	TER5-2
No.	101 / 1 .	102 / 1 .	103 / 1 .	104 / 1 .	1 / 1 .	2 / 1 .	3 / 1 .	4 / 1 .	5 / 1 .	6 / 1 .	7 / 1 .	8 / 1 .	9 / 1 .	10 / 1 .
Notes	Pheno	Pheno	Pheno	Pheno	Pheno	Pheno	Pheno	Pheno	Pheno	Pheno	Pheno	Pheno	Pheno	Pheno
SiO_2	53.35	52.92	52.45	52.26	65.85	66.15	65.98	65.87	67.72	67.12	63.69	65.79	65.73	67.82
TiO_2	0.12	0.13	0.11	0.11	0.06	0.07	0.07	0.05	0.03	0.07	0.15	0.08	0.08	0.04
Al_2O_3	28.78	29.03	28.72	28.65	20.76	20.52	20.38	20.61	18.98	18.98	21.85	20.35	20.47	18.88
BaO					0.36	0.35	0.36	0.37	0.12	0.13	0.31	0.34	0.32	0.15
FeO	0.73	0.74	0.71	0.72	0.28	0.31	0.30	0.28	0.31	0.33	0.39	0.31	0.51	0.35
SrO					0.10	0.07	0.09	0.10	bdl	0.03	0.18	0.08	0.08	0.01
MgO	0.11	0.11	0.11	0.10	0.01	bdl	0.01	bdl	bdl	bdl	0.01	bdl	bdl	0.01
CaO	12.60	12.60	12.75	12.77	2.14	2.01	1.88	2.02	0.46	0.44	3.59	1.85	2.11	0.30
Na_2O	4.39	4.36	4.24	4.26	9.05	8.94	8.85	8.95	8.33	8.33	8.60	9.06	9.04	8.08
K_2O	0.20	0.21	0.20	0.21	2.33	2.39	2.57	2.56	4.78	4.74	1.70	2.52	2.31	5.21
Total	100.28	100.11	99.28	99.09	100.95	100.82	100.48	100.81	100.73	100.18	100.47	100.38	100.65	100.85
Si	2.419	2.405	2.405	2.402	2.903	2.916	2.920	2.909	2.994	2.986	2.830	2.916	2.907	2.999
Ti	0.004	0.005	0.004	0.004	0.002	0.002	0.002	0.002	0.001	0.002	0.005	0.003	0.003	0.001
Al	1.538	1.555	1.552	1.552	1.078	1.066	1.063	1.072	0.989	0.995	1.144	1.063	1.067	0.984
Ba	0.000	0.000	0.000	0.000	0.006	0.006	0.006	0.006	0.002	0.002	0.005	0.006	0.006	0.003
Fe	0.028	0.028	0.027	0.028	0.010	0.011	0.011	0.010	0.012	0.012	0.014	0.012	0.019	0.013
Sr	0.000	0.000	0.000	0.000	0.003	0.002	0.002	0.003		0.001	0.005	0.002	0.002	0.000
Mg	0.007	0.007	0.007	0.007	0.000		0.000				0.001			0.000
Ca	0.612	0.613	0.626	0.629	0.101	0.095	0.089	0.096	0.022	0.021	0.171	0.088	0.100	0.014
Na	0.386	0.384	0.377	0.380	0.774	0.764	0.759	0.766	0.714	0.719	0.741	0.778	0.776	0.693
K	0.012	0.012	0.011	0.012	0.131	0.134	0.145	0.144	0.269	0.269	0.096	0.142	0.130	0.294
Sum	5.006	5.011	5.010	5.014	5.009	4.998	4.999	5.008	5.002	5.008	5.012	5.010	5.009	5.001
Ab	38.2	38.0	37.1	37.2	76.9	76.9	76.4	76.2	71.0	71.3	73.5	77.2	77.1	69.2
An	60.6	60.7	61.7	61.6	10.0	9.6	9.0	9.5	2.2	2.1	17.0	8.7	9.9	1.4
Or	1.2	1.2	1.1	1.2	13.0	13.5	14.6	14.3	26.8	26.7	9.5	14.1	12.9	29.4

Table C1 continued

Unit	**LMI**	**LMI**	**LMI**	**LMI**	**LMI**	**LMI**	**LMI**	**LMI**	**LMI**	**LMI**	**LMI**	**LMI**	**LMI**	**LMI**
Sample	TER5-2	TER5-2	TER5-2	TER5-2	TER5-2	TER5-2	TER5-2	TER5-2	TER5-2	TER5-2	TER5-2	TER5-2	TER5-2	TER5-2
No.	11 / 1 .	12 / 1 .	13 / 1 .	14 / 1 .	15 / 1 .	16 / 1 .	1 / 1 .	2 / 1 .	3 / 1 .	4 / 1 .	5 / 1 .	6 / 1 .	7 / 1 .	8 / 1 .
Notes	Pheno	Pheno	Pheno	Pheno	Pheno	Pheno	Pheno	Pheno	Pheno	Pheno	Pheno	Pheno	Pheno	Pheno
SiO_2	67.78	64.03	63.97	66.35	66.95	52.79	65.80	66.01	65.45	65.50	67.22	67.16	63.64	65.67
TiO_2	0.06	0.07	0.08	0.04	0.05	0.12	0.06	0.06	0.06	0.07	0.05	0.04	0.14	0.06
Al_2O_3	18.97	21.49	21.49	18.76	19.20	28.84	20.39	20.10	20.05	20.22	18.78	18.80	21.99	20.54
BaO	0.18	0.33	0.28	0.18	0.18	0.01	0.35	0.35	0.34	0.33	0.15	0.13	0.11	0.35
FeO	0.33	0.36	0.34	0.29	0.30	0.72	0.29	0.30	0.29	0.29	0.34	0.33	0.45	0.30
SrO	0.01	0.15	0.18	0.03	0.05	0.14	0.09	0.10	0.08	0.09	0.05	0.02	0.18	0.09
MgO	bdl	0.02	0.02	bdl	bdl	0.10	bdl	bdl	0.02	0.01	bdl	bdl	0.03	0.01
CaO	0.27	3.17	3.38	0.50	0.65	12.71	2.01	1.73	2.01	1.92	0.47	0.43	3.87	2.08
Na_2O	7.98	8.79	8.84	8.35	8.54	4.33	8.94	9.00	8.93	8.80	8.27	8.29	8.64	8.93
K_2O	5.21	1.79	1.66	4.54	4.28	0.21	2.36	2.62	2.59	2.59	4.70	4.79	1.43	2.47
Total	100.79	100.21	100.25	99.05	100.20	99.96	100.30	100.27	99.83	99.81	100.02	99.99	100.47	100.50
Si	2.998	2.849	2.846	2.986	2.976	2.406	2.916	2.928	2.919	2.919	2.994	2.993	2.823	2.908
Ti	0.002	0.002	0.003	0.001	0.002	0.004	0.002	0.002	0.002	0.002	0.002	0.001	0.005	0.002
Al	0.989	1.127	1.127	0.995	1.006	1.549	1.065	1.051	1.054	1.062	0.986	0.987	1.150	1.072
Ba	0.003	0.006	0.005	0.003	0.003	0.000	0.006	0.006	0.006	0.006	0.003	0.002	0.002	0.006
Fe	0.012	0.013	0.013	0.011	0.011	0.027	0.011	0.011	0.011	0.011	0.013	0.012	0.017	0.011
Sr	0.000	0.004	0.005	0.001	0.001	0.004	0.002	0.003	0.002	0.002	0.001	0.000	0.005	0.002
Mg		0.001	0.001			0.006			0.001	0.000			0.002	0.001
Ca	0.013	0.151	0.161	0.024	0.031	0.621	0.095	0.082	0.096	0.092	0.022	0.021	0.184	0.099
Na	0.684	0.759	0.763	0.729	0.736	0.383	0.768	0.774	0.772	0.760	0.714	0.716	0.743	0.767
K	0.294	0.102	0.094	0.261	0.243	0.012	0.133	0.148	0.147	0.147	0.267	0.272	0.081	0.140
Sum	4.995	5.015	5.017	5.010	5.009	5.013	5.000	5.005	5.011	5.002	5.002	5.006	5.010	5.008
Ab	69.1	75.0	74.9	71.9	72.9	37.7	77.1	77.0	76.0	76.1	71.2	71.0	73.7	76.3
An	1.3	14.9	15.8	2.4	3.1	61.1	9.6	8.2	9.4	9.2	2.2	2.0	18.3	9.8
Or	29.7	10.1	9.3	25.7	24.0	1.2	13.4	14.8	14.5	14.8	26.6	27.0	8.0	13.9

Table C1 continued

Unit	**LMI**	**LMI**	**LMI**	**LMI**	**LMI**	**LMI**	**LMI**	**LMI**	**LMI**	**LMI**	**LMI**	**LMI**	**LMI**	**LMI**
Sample	TER5-2	TER5-2	TER5-2	TER5-2	TER5-2	TER5-2	TER5-2	TER5-2	TER5-2-rim	TER5-2	TER5-2	TER5-2	TER5-2	TER5-2
No.	10 / 1 .	11 / 1 .	12 / 1 .	13 / 1 .	14 / 1 .	15 / 1 .	16 / 1 .	17 / 1 .	18 / 1 .	19 / 1 .	20 / 1 .	21 / 1 .	22 / 1 .	23 / 1 .
Notes	Pheno	Pheno	Pheno	Pheno	Pheno	Pheno	Pheno	Pheno	Pheno	Pheno	Pheno	Pheno	Pheno	Pheno
SiO_2	67.45	67.41	63.88	63.98	66.88	66.84	52.79	52.64	60.16	52.79	52.81	65.81	65.58	66.26
TiO_2	0.04	0.03	0.09	0.07	0.06	0.04	0.13	0.13	0.15	0.10	0.10	0.03	0.04	0.04
Al_2O_3	18.78	18.66	21.46	21.35	19.02	18.95	28.77	28.94	23.94	28.95	28.86	20.23	20.41	20.09
BaO	0.17	0.14	0.31	0.29	0.23	0.17	0.02	bdl	0.06	bdl	0.01	0.35	0.37	0.36
FeO	0.33	0.34	0.34	0.35	0.28	0.29	0.71	0.68	0.61	0.68	0.68	0.29	0.32	0.32
SrO	0.04	bdl	0.15	0.15	0.01	0.01	0.12	0.13	0.19	0.15	0.13	0.07	0.08	0.09
MgO	bdl	0.01	0.01	0.01	0.01	bdl	0.12	0.10	0.04	0.11	0.12	bdl	0.01	bdl
CaO	0.28	0.27	3.37	3.26	0.50	0.70	12.59	12.77	6.44	12.79	12.83	1.88	2.02	1.56
Na_2O	7.89	7.96	8.71	8.71	8.30	8.42	4.19	4.22	7.66	4.13	4.14	8.96	8.97	8.82
K_2O	5.25	5.34	1.66	1.72	4.61	4.21	0.20	0.21	0.76	0.20	0.21	2.48	2.42	2.95
Total	100.23	100.16	99.96	99.90	99.90	99.64	99.65	99.83	100.00	99.92	99.89	100.11	100.23	100.50
Si	3.001	3.002	2.848	2.854	2.983	2.985	2.411	2.402	2.698	2.405	2.407	2.923	2.912	2.934
Ti	0.001	0.001	0.003	0.002	0.002	0.001	0.004	0.004	0.005	0.003	0.003	0.001	0.001	0.001
Al	0.985	0.980	1.128	1.122	1.000	0.997	1.549	1.556	1.265	1.555	1.550	1.059	1.068	1.049
Ba	0.003	0.002	0.005	0.005	0.004	0.003	0.000		0.001		0.000	0.006	0.006	0.006
Fe	0.012	0.013	0.013	0.013	0.010	0.011	0.027	0.026	0.023	0.026	0.026	0.011	0.012	0.012
Sr	0.001		0.004	0.004	0.000	0.000	0.003	0.003	0.005	0.004	0.004	0.002	0.002	0.002
Mg		0.000	0.000	0.001	0.001		0.008	0.007	0.003	0.008	0.008		0.000	
Ca	0.013	0.013	0.161	0.156	0.024	0.034	0.616	0.624	0.310	0.625	0.627	0.089	0.096	0.074
Na	0.680	0.687	0.753	0.753	0.718	0.729	0.371	0.373	0.666	0.365	0.365	0.771	0.773	0.757
K	0.298	0.303	0.094	0.098	0.262	0.240	0.012	0.012	0.043	0.011	0.012	0.141	0.137	0.167
Sum	4.995	5.002	5.009	5.008	5.005	5.000	5.002	5.009	5.019	5.002	5.003	5.003	5.008	5.002
Ab	68.6	68.5	74.7	74.8	71.5	72.7	37.2	36.9	65.4	36.5	36.4	77.0	76.8	75.9
An	1.3	1.3	16.0	15.5	2.4	3.4	61.7	61.8	30.4	62.4	62.4	8.9	9.5	7.4
Or	30.0	30.2	9.4	9.7	26.1	23.9	1.2	1.2	4.2	1.1	1.2	14.1	13.6	16.7

Table C1 continued

Unit	**LMI**	**LMI**	**LMI**	**LMI**	**LMI**	**LMI**	**LMI**	**LMI**	**LMI**	**LMI**	**LMI**	**LMI**	**LMI**
Sample	TER5-2	TER5-2	TER5-2	TER5-2	TER5-2	TER5-2	TER5-2	TER5-2	TER5-2	TER5-2	TER5-2	TER5-2	TER5-2-strongly resorbed
No.	24 / 1 .	25 / 1 .	26 / 1 .	27 / 1 .	28 / 1 .	29 / 1 .	30 / 1 .	31 / 1 .	32 / 1 .	33 / 1 .	34 / 1 .	35 / 1 .	36 / 1 .
Notes	Pheno	Pheno	Pheno	Pheno	Pheno	Pheno	Pheno	Pheno	Pheno	Pheno	Pheno	Pheno	Pheno
SiO_2	65.65	66.05	64.87	65.32	67.40	66.25	66.08	52.90	67.47	67.08	65.03	64.83	63.07
TiO_2	0.05	0.05	0.05	0.05	0.11	0.10	0.04	0.11	0.03	0.04	0.06	0.06	0.09
Al_2O_3	20.42	20.28	20.15	19.89	18.49	19.89	20.33	28.62	19.09	19.04	20.15	20.19	22.27
BaO	0.36	0.35	0.34	0.32	0.06	0.28	0.29	bdl	0.15	0.12	0.33	0.34	0.25
FeO	0.29	0.31	0.29	0.30	0.59	0.46	0.32	0.68	0.29	0.29	0.29	0.27	0.38
SrO	0.07	0.07	0.09	0.08	0.02	0.05	0.09	0.14	0.05	0.01	0.10	0.10	0.19
MgO	bdl	0.01	0.01	bdl	0.02	bdl	bdl	0.12	bdl	0.01	bdl	bdl	0.02
CaO	1.88	1.78	1.94	1.75	0.16	1.43	1.73	12.39	0.49	0.50	1.92	1.94	4.13
Na_2O	8.89	8.88	8.73	8.92	7.97	8.62	9.01	4.34	8.29	8.44	8.85	8.77	8.63
K_2O	2.66	2.74	2.59	2.72	5.41	3.51	2.70	0.21	4.64	4.51	2.63	2.53	1.15
Total	100.28	100.55	99.07	99.36	100.23	100.59	100.59	99.51	100.50	100.04	99.37	99.05	100.17
Si	2.914	2.923	2.914	2.927	3.003	2.937	2.922	2.418	2.989	2.985	2.914	2.912	2.808
Ti	0.002	0.002	0.002	0.002	0.004	0.003	0.001	0.004	0.001	0.001	0.002	0.002	0.003
Al	1.068	1.058	1.067	1.050	0.971	1.039	1.060	1.542	0.997	0.999	1.064	1.069	1.168
Ba	0.006	0.006	0.006	0.006	0.001	0.005	0.005		0.003	0.002	0.006	0.006	0.004
Fe	0.011	0.012	0.011	0.011	0.022	0.017	0.012	0.026	0.011	0.011	0.011	0.010	0.014
Sr	0.002	0.002	0.002	0.002	0.000	0.001	0.002	0.004	0.001	0.000	0.003	0.003	0.005
Mg		0.001	0.000		0.001			0.008		0.000			0.001
Ca	0.089	0.085	0.093	0.084	0.008	0.068	0.082	0.607	0.023	0.024	0.092	0.094	0.197
Na	0.765	0.762	0.760	0.775	0.689	0.741	0.773	0.384	0.712	0.728	0.769	0.764	0.745
K	0.151	0.155	0.148	0.156	0.308	0.198	0.152	0.012	0.262	0.256	0.150	0.145	0.065
Sum	5.008	5.005	5.005	5.012	5.006	5.010	5.009	5.005	4.999	5.006	5.011	5.006	5.010
Ab	76.1	76.1	75.9	76.4	68.6	73.6	76.7	38.3	71.4	72.2	76.0	76.2	74.0
An	8.9	8.4	9.3	8.3	0.8	6.8	8.1	60.5	2.3	2.4	9.1	9.3	19.6
Or	15.0	15.5	14.8	15.3	30.6	19.7	15.1	1.2	26.3	25.4	14.8	14.5	6.5

Table C1 continued

Unit	**VFI**	**VFI**	**VFI**	**VFI**	**VFI**	**VFI**	**VFI**	**VFI**	**VFI**	**VFI**	**VFI**	**VFI**
Sample	TER2-2	TER2-2	TER2-2	TER2-2	TER2-2	TER2-2	TER2-2	TER2-2	TER2-2	TER2-2	TER2-2	TER2-2
No.	55 / 1 .	56 / 1 .	57 / 1 .	58 / 1 .	59 / 1 .	60 / 1 .	61 / 1 .	62 / 1 .	63 / 1 .	64 / 1 .	65 / 1 .	66 / 1 .
Notes	Pheno	Pheno	Pheno	Pheno	Pheno	Pheno	Pheno	Pheno	Pheno	Pheno	Pheno	Pheno
SiO_2	66.37	66.46	66.27	63.11	62.81	64.02	64.02	66.81	66.69	63.15	66.59	66.70
TiO_2	0.05	0.05	0.06	0.07	0.08	0.05	0.10	0.03	0.04	0.09	0.03	0.04
Al_2O_3	19.59	18.64	18.68	21.94	21.49	20.59	20.80	18.68	18.89	21.46	18.86	18.92
BaO	0.48	0.29	0.24	0.52	0.65	0.65	0.68	0.11	0.31	0.56	0.25	0.21
FeO	0.22	0.25	0.25	0.24	0.24	0.23	0.21	0.25	0.28	0.30	0.24	0.25
SrO	0.04	0.05	bdl	0.16	0.13	0.09	0.12	bdl	0.04	0.12	0.03	0.07
MgO	0.01	0.01	0.01	0.01	0.01	0.01	0.01	0.01	0.01	bdl	bdl	0.02
CaO	0.99	0.40	0.40	3.68	3.35	2.20	2.29	0.29	0.39	3.08	0.40	0.39
Na_2O	8.26	7.74	7.80	8.45	8.41	8.39	8.45	7.66	7.63	8.46	8.09	7.96
K_2O	4.17	5.32	5.33	1.73	1.85	2.84	2.74	5.56	5.49	2.11	5.34	5.40
Total	100.16	99.22	99.05	99.91	99.01	99.07	99.42	99.41	99.77	99.34	99.84	99.98
Si	2.957	2.993	2.989	2.823	2.836	2.888	2.879	2.999	2.988	2.842	2.983	2.983
Ti	0.002	0.002	0.002	0.002	0.003	0.002	0.003	0.001	0.001	0.003	0.001	0.001
Al	1.028	0.989	0.993	1.157	1.144	1.095	1.102	0.988	0.998	1.138	0.996	0.998
Ba	0.008	0.005	0.004	0.009	0.011	0.011	0.012	0.002	0.005	0.010	0.004	0.004
Fe	0.008	0.009	0.009	0.009	0.009	0.009	0.008	0.009	0.010	0.011	0.009	0.009
Sr	0.001	0.001		0.004	0.003	0.002	0.003		0.001	0.003	0.001	0.002
Mg	0.000	0.001	0.001	0.000	0.001	0.000	0.001	0.000	0.001			0.001
Ca	0.047	0.019	0.019	0.176	0.162	0.106	0.111	0.014	0.019	0.149	0.019	0.019
Na	0.713	0.676	0.682	0.733	0.736	0.734	0.737	0.667	0.663	0.738	0.703	0.691
K	0.237	0.306	0.307	0.099	0.107	0.164	0.157	0.318	0.314	0.121	0.305	0.308
Sum	5.002	5.001	5.007	5.012	5.011	5.012	5.013	4.999	5.000	5.016	5.022	5.016
Ab	71.5	67.5	67.7	72.7	73.3	73.1	73.3	66.8	66.6	73.3	68.4	67.9
An	4.7	1.9	1.9	17.5	16.1	10.6	11.0	1.4	1.9	14.7	1.9	1.8
Or	23.8	30.6	30.4	9.8	10.6	16.3	15.7	31.9	31.5	12.0	29.7	30.3

Table C1 continued

Unit	**VFI**	**VFI**	**VFI**	**VFI**	**VFI**	**VFI**	**VFI**	**VFI**	**VFI**	**VFI**	**VFI**	**VFI**
Sample	TER2-2	TER2-2	TER2-2	TER2-2	TER2-2	TER2-2	TER2-2	TER2-2	TER2-2	TER2-2	TER2-2	TER2-2
No.	67 / 1 .	68 / 1 .	69 / 1 .	70 / 1 .	71 / 1 .	72 / 1 .	73 / 1 .	74 / 1 .	75 / 1 .	76 / 1 .	77 / 1 .	78 / 1 .
Notes	Pheno	Pheno	Pheno	Pheno	Pheno	Pheno	Pheno	Pheno	Pheno	Pheno	Pheno	Pheno
SiO_2	66.30	66.14	66.25	66.02	65.88	66.23	65.69	66.81	66.98	66.82	66.53	66.79
TiO_2	0.04	0.06	0.06	0.02	0.04	0.05	0.04	0.02	0.03	0.04	0.03	0.03
Al_2O_3	18.79	18.90	18.88	19.25	19.25	19.20	19.14	18.59	18.37	18.45	18.30	18.76
BaO	0.26	0.32	0.22	0.33	0.45	0.44	0.50	0.11	0.01	0.02	0.04	0.18
FeO	0.26	0.28	0.26	0.24	0.24	0.23	0.24	0.33	0.36	0.35	0.32	0.26
SrO	0.03	0.02	0.02	bdl	0.03	0.04	0.04	0.01	0.06	0.01	0.02	0.01
MgO	0.01	bdl	0.01	0.01	0.01	bdl	bdl	bdl	bdl	0.01	bdl	bdl
CaO	0.49	0.50	0.41	0.76	0.79	0.74	0.80	0.25	0.20	0.17	0.20	0.37
Na_2O	7.89	7.77	7.95	7.98	8.00	8.05	7.95	7.74	7.57	7.60	7.61	8.03
K_2O	5.25	5.18	5.30	4.73	4.67	4.74	4.67	5.91	5.86	5.88	5.85	5.36
Total	99.30	99.15	99.35	99.34	99.36	99.71	99.07	99.76	99.43	99.36	98.91	99.78
Si	2.984	2.981	2.980	2.967	2.963	2.968	2.965	2.996	3.009	3.004	3.006	2.990
Ti	0.001	0.002	0.002	0.001	0.001	0.002	0.001	0.001	0.001	0.001	0.001	0.001
Al	0.997	1.004	1.001	1.020	1.021	1.014	1.018	0.983	0.972	0.977	0.974	0.990
Ba	0.005	0.006	0.004	0.006	0.008	0.008	0.009	0.002	0.000	0.000	0.001	0.003
Fe	0.010	0.010	0.010	0.009	0.009	0.009	0.009	0.012	0.014	0.013	0.012	0.010
Sr	0.001	0.001	0.001		0.001	0.001	0.001	0.000	0.002	0.000	0.001	0.000
Mg	0.000		0.001	0.000	0.001					0.001		
Ca	0.023	0.024	0.020	0.037	0.038	0.035	0.039	0.012	0.009	0.008	0.010	0.018
Na	0.689	0.679	0.694	0.695	0.698	0.699	0.696	0.673	0.659	0.663	0.667	0.697
K	0.301	0.298	0.304	0.271	0.268	0.271	0.269	0.338	0.336	0.337	0.337	0.306
Sum	5.011	5.004	5.016	5.006	5.008	5.008	5.007	5.017	5.002	5.006	5.008	5.015
Ab	67.9	67.9	68.2	69.3	69.5	69.5	69.3	65.8	65.6	65.7	65.8	68.3
An	2.3	2.4	1.9	3.6	3.8	3.5	3.8	1.2	0.9	0.8	1.0	1.7
Or	29.7	29.8	29.9	27.0	26.7	26.9	26.8	33.0	33.4	33.5	33.3	30.0

Table C1 continued

Unit	**VFI**	**VFI**	**VFI**	**VFI**	**VFI**	**VFI**	**VFI**	**VFI**	**VFI**	**VFI**	**VFI**	**VFI**
Sample	TER11-2B	TER11-2B	TER11-2B	TER11-2B	TER11-2B	TER11-2B	TER11-2B	TER11-2B	TER11-2B	TER11-2B	TER11-2B	TER11-2B
No.	1 / 1 .	2 / 1 .	3 / 1 .	4 / 1 .	5 / 1 .	6 / 1 .	7 / 1 .	8 / 1 .	9 / 1 .	10 / 1 .	11 / 1 .	12 / 1 .
Notes	Pheno	Pheno	Pheno	Pheno	Pheno	Pheno	Pheno	Pheno	Pheno	Pheno	Pheno	Pheno
SiO_2	66.47	66.66	66.82	66.47	66.32	66.82	66.86	66.75	66.64	66.42	66.62	65.72
TiO_2	0.06	0.05	0.08	0.06	0.06	0.05	0.04	0.04	0.03	0.06	0.06	0.04
Al_2O_3	19.59	19.54	19.41	19.50	20.04	20.06	19.68	19.48	19.50	19.59	19.43	19.33
BaO	0.50	0.37	0.38	0.36	0.53	0.42	0.37	0.43	0.37	0.48	0.44	0.46
FeO	0.24	0.23	0.26	0.25	0.22	0.24	0.23	0.24	0.24	0.25	0.27	0.24
SrO	0.05	bdl	0.03	0.04	0.05	bdl	0.04	0.02	0.04	0.01	0.04	0.02
MgO	0.01	bdl	0.01	0.01	0.01	0.01	0.02	bdl	0.01	0.01	0.01	bdl
CaO	0.76	0.63	0.58	0.67	0.94	0.77	0.72	0.64	0.71	0.81	0.73	0.68
Na_2O	8.12	8.14	8.14	8.14	8.27	8.16	8.15	8.03	7.99	8.00	7.98	7.95
K_2O	4.63	4.84	4.85	4.78	4.36	4.54	4.62	4.86	4.83	4.74	4.78	4.76
Total	100.41	100.45	100.55	100.27	100.82	101.07	100.73	100.49	100.37	100.36	100.34	99.20
Si	2.959	2.964	2.969	2.962	2.941	2.950	2.962	2.967	2.966	2.958	2.967	2.961
Ti	0.002	0.002	0.003	0.002	0.002	0.002	0.001	0.001	0.001	0.002	0.002	0.001
Al	1.028	1.024	1.016	1.024	1.047	1.044	1.028	1.021	1.022	1.028	1.019	1.027
Ba	0.009	0.006	0.007	0.006	0.009	0.007	0.006	0.007	0.007	0.008	0.008	0.008
Fe	0.009	0.008	0.010	0.009	0.008	0.009	0.009	0.009	0.009	0.009	0.010	0.009
Sr	0.001		0.001	0.001	0.001		0.001	0.001	0.001	0.000	0.001	0.001
Mg	0.000		0.001	0.001	0.001	0.001	0.001		0.001	0.000	0.000	
Ca	0.036	0.030	0.028	0.032	0.045	0.036	0.034	0.031	0.034	0.039	0.035	0.033
Na	0.700	0.701	0.701	0.703	0.711	0.699	0.700	0.692	0.690	0.691	0.689	0.695
K	0.263	0.274	0.275	0.272	0.247	0.256	0.261	0.276	0.274	0.269	0.272	0.273
Sum	5.007	5.010	5.009	5.012	5.012	5.003	5.003	5.005	5.004	5.006	5.002	5.008
Ab	70.1	69.7	69.8	69.8	70.9	70.5	70.3	69.3	69.1	69.2	69.2	69.4
An	3.6	3.0	2.7	3.2	4.5	3.7	3.4	3.1	3.4	3.9	3.5	3.3
Or	26.3	27.3	27.4	27.0	24.6	25.8	26.2	27.6	27.5	26.9	27.3	27.3

Table C1 continued

Unit	**VFI**	**VFI**	**VFI**	**VFI**	**VFI**	**VFI**	**VFI**	**VFI**	**VFI**	**VFI**	**VFI**	**VFI**
Sample	TER11-2B	TER11-2B	TER11-2B	TER11-2B	TER11-2B	TER11-2B	TER11-2B	TER11-2B	TER11-2B	TER11-2B	TER11-2B	TER11-2B
No.	13 / 1 .	14 / 1 .	15 / 1 .	16 / 1 .	17 / 1 .	18 / 1 .	20 / 1 .	21 / 1 .	22 / 1 .	23 / 1 .	24 / 1 .	25 / 1 .
Notes	Pheno	Pheno	Pheno	Pheno	Pheno	Pheno	Pheno	Pheno	Pheno	Pheno	Pheno	Pheno
SiO_2	66.05	66.58	66.06	65.98	66.25	65.96	66.39	66.42	66.46	66.71	67.10	67.11
TiO_2	0.04	0.03	0.04	0.06	0.03	0.06	0.03	0.05	0.04	0.05	0.01	0.02
Al_2O_3	19.45	19.38	19.41	19.53	19.41	19.70	19.11	19.13	19.22	18.90	18.77	18.69
BaO	0.41	0.42	0.38	0.42	0.40	0.43	0.42	0.36	0.40	0.15	0.02	0.04
FeO	0.24	0.23	0.24	0.24	0.22	0.23	0.25	0.25	0.27	0.33	0.35	0.38
SrO	bdl	0.02	0.05	0.05	0.02	0.04	0.02	0.05	0.05	bdl	0.06	0.03
MgO	0.01	bdl	bdl	bdl	bdl	0.01	0.01	0.01	0.01	bdl	bdl	0.01
CaO	0.77	0.80	0.80	0.81	0.78	0.96	0.44	0.43	0.49	0.30	0.09	0.12
Na_2O	8.09	7.99	8.06	8.15	8.17	8.38	7.93	8.02	8.02	8.01	7.75	7.78
K_2O	4.54	4.62	4.66	4.51	4.58	4.18	5.16	5.15	5.18	5.37	5.90	5.81
Total	99.61	100.07	99.69	99.76	99.86	99.94	99.75	99.87	100.15	99.82	100.05	99.99
Si	2.960	2.969	2.960	2.955	2.963	2.947	2.976	2.974	2.970	2.985	2.997	2.999
Ti	0.001	0.001	0.001	0.002	0.001	0.002	0.001	0.002	0.001	0.002	0.000	0.001
Al	1.028	1.019	1.025	1.031	1.023	1.037	1.010	1.009	1.013	0.997	0.988	0.984
Ba	0.007	0.007	0.007	0.007	0.007	0.008	0.007	0.006	0.007	0.003	0.000	0.001
Fe	0.009	0.009	0.009	0.009	0.008	0.009	0.009	0.010	0.010	0.012	0.013	0.014
Sr		0.001	0.001	0.001	0.000	0.001	0.000	0.001	0.001		0.002	0.001
Mg	0.000					0.000	0.001	0.000	0.000			0.001
Ca	0.037	0.038	0.039	0.039	0.037	0.046	0.021	0.021	0.024	0.015	0.004	0.006
Na	0.703	0.691	0.700	0.707	0.708	0.726	0.689	0.696	0.695	0.695	0.671	0.674
K	0.260	0.263	0.266	0.258	0.261	0.239	0.295	0.294	0.295	0.307	0.336	0.331
Sum	5.006	4.997	5.009	5.010	5.009	5.014	5.010	5.015	5.017	5.015	5.012	5.011
Ab	70.3	69.6	69.7	70.5	70.4	71.8	68.6	68.8	68.5	68.4	66.3	66.7
An	3.7	3.8	3.8	3.9	3.7	4.6	2.1	2.1	2.3	1.4	0.4	0.6
Or	26.0	26.5	26.5	25.7	25.9	23.6	29.3	29.1	29.1	30.2	33.3	32.7

Table C1 continued

Unit	CCI	CCI	CCI	CCI	CCI	CCI	CCI	CCI	CCI	CCI	CCI
Sample	TER2-1	TER2-1	TER2-1	TER2-1	TER2-1	TER2-1	TER2-1	TER2-1	TER2-1	TER2-1	TER2-1
No.	79 / 1 .	80 / 1 .	81 / 1 .	82 / 1 .	83 / 1 .	84 / 1 .	85 / 1 .	86 / 1 .	87 / 1 .	88 / 1 .	89 / 1 .
Notes	Pheno	Pheno	Pheno	Pheno	Pheno	Pheno	Pheno	Pheno	Pheno	Pheno	Pheno
SiO_2	67.15	67.55	67.26	67.10	67.34	67.09	68.05	67.34	67.58	67.48	67.88
TiO_2	0.04	bdl	0.01	0.01	0.02	0.03	0.01	0.02	0.02	0.03	0.02
Al_2O_3	18.77	18.88	18.63	18.67	18.72	18.75	19.03	19.64	18.68	18.92	18.69
BaO	0.02	0.02	0.02	bdl	0.01	0.04	bdl	0.03	0.01	0.02	0.01
FeO	0.28	0.27	0.32	0.30	0.32	0.32	0.29	0.32	0.30	0.29	0.33
SrO	0.05	0.05	0.01	0.05	0.01	0.01	0.01	bdl	0.01	0.04	0.02
MgO	bdl	0.01	0.01	bdl	0.02	bdl	0.01	bdl	0.01	bdl	0.01
CaO	0.25	0.23	0.15	0.17	0.29	0.19	0.20	0.29	0.17	0.27	0.18
Na_2O	7.92	7.98	7.88	7.95	7.87	7.82	7.86	7.76	7.72	7.75	7.74
K_2O	5.95	5.95	5.95	5.87	5.76	5.80	5.84	5.65	5.90	5.83	5.93
Total	100.43	100.93	100.22	100.12	100.35	100.05	101.30	101.06	100.40	100.62	100.81
Si	2.992	2.993	3.000	2.997	2.998	2.996	2.998	2.974	3.005	2.995	3.007
Ti	0.001		0.000	0.000	0.001	0.001	0.000	0.001	0.001	0.001	0.001
Al	0.986	0.986	0.980	0.983	0.982	0.987	0.988	1.022	0.979	0.990	0.976
Ba	0.000	0.000	0.000		0.000	0.001		0.001	0.000	0.000	0.000
Fe	0.010	0.010	0.012	0.011	0.012	0.012	0.011	0.012	0.011	0.011	0.012
Sr	0.001	0.001	0.000	0.001	0.000	0.000	0.000		0.000	0.001	0.000
Mg		0.000	0.000		0.001		0.000		0.000		0.001
Ca	0.012	0.011	0.007	0.008	0.014	0.009	0.009	0.014	0.008	0.013	0.008
Na	0.684	0.686	0.681	0.688	0.679	0.677	0.672	0.664	0.666	0.667	0.665
K	0.338	0.336	0.339	0.334	0.327	0.330	0.328	0.318	0.335	0.330	0.335
Sum	5.025	5.024	5.020	5.023	5.014	5.013	5.007	5.006	5.005	5.008	5.005
Ab	66.2	66.4	66.3	66.8	66.6	66.6	66.6	66.7	66.0	66.0	65.9
An	1.1	1.0	0.7	0.8	1.3	0.9	0.9	1.4	0.8	1.3	0.8
Or	32.7	32.6	33.0	32.4	32.1	32.5	32.5	31.9	33.2	32.7	33.2

Table C1 continued

Unit	**CCI**	**CCI**	**CCI**	**CCI**	**CCI**	**CCI**	**CCI**	**CCI**	**CCI**	**CCI**
Sample	TER2-1	TER2-1	TER2-1	TER2-1	TER2-1	TER2-1	TER2-1	TER2-1	TER2-1	TER2-1
No.	90 / 1 .	91 / 1 .	92 / 1 .	93 / 1 .	94 / 1 .	95 / 1 .	96 / 1 .	97 / 1 .	98 / 1 .	99 / 1 .
Notes	Pheno	Pheno	Pheno	Pheno	Pheno	Pheno	Pheno	Pheno	Pheno	Pheno
SiO_2	67.63	67.48	67.54	67.74	67.62	66.87	67.26	67.20	67.84	67.53
TiO_2	0.05	0.01	0.01	0.05	0.04	0.03	0.03	0.05	0.03	0.03
Al_2O_3	18.74	18.77	18.73	18.69	18.49	18.68	18.86	18.76	18.78	18.80
BaO	0.01	bdl	0.02	0.05	0.03	bdl	0.03	0.04	0.02	0.03
FeO	0.28	0.29	0.29	0.27	0.30	0.30	0.28	0.28	0.29	0.27
SrO	0.01	0.02	0.03	bdl	bdl	0.02	0.02	bdl	0.05	0.01
MgO	0.02	bdl	0.01	0.01	bdl	bdl	bdl	0.01	0.01	0.01
CaO	0.20	0.18	0.17	0.16	0.15	0.25	0.25	0.24	0.20	0.20
Na_2O	7.86	7.82	7.76	7.80	7.79	7.80	7.77	7.77	7.74	7.76
K_2O	5.82	5.86	5.87	5.83	5.87	5.72	5.72	6.04	5.80	5.91
Total	100.61	100.44	100.43	100.61	100.29	99.67	100.21	100.39	100.76	100.56
Si	3.001	3.000	3.003	3.005	3.010	2.996	2.996	2.994	3.004	3.000
Ti	0.002	0.000	0.000	0.002	0.001	0.001	0.001	0.002	0.001	0.001
Al	0.980	0.983	0.981	0.977	0.970	0.987	0.990	0.985	0.980	0.984
Ba	0.000		0.000	0.001	0.000		0.001	0.001	0.000	0.001
Fe	0.010	0.011	0.011	0.010	0.011	0.011	0.010	0.011	0.011	0.010
Sr	0.000	0.000	0.001			0.000	0.000		0.001	0.000
Mg	0.001		0.001	0.000				0.000	0.001	0.000
Ca	0.009	0.009	0.008	0.008	0.007	0.012	0.012	0.011	0.009	0.010
Na	0.677	0.674	0.669	0.671	0.672	0.678	0.671	0.671	0.665	0.668
K	0.330	0.332	0.333	0.330	0.334	0.327	0.325	0.343	0.328	0.335
Sum	5.010	5.011	5.007	5.005	5.006	5.012	5.006	5.019	5.000	5.009
Ab	66.6	66.4	66.2	66.5	66.4	66.7	66.6	65.4	66.4	66.0
An	0.9	0.9	0.8	0.8	0.7	1.2	1.2	1.1	0.9	0.9
Or	32.5	32.7	33.0	32.7	32.9	32.1	32.2	33.5	32.7	33.1

Table C1 continued

Unit	**CCI**	**CCI**	**CCI**	**CCI**	**CCI**	**CCI**	**CCI**	**CCI**	**CCI**	**CCI**
Sample	TER2-1	TER2-2	TER2-2	TER2-2	TER2-3	TER2-4	TER2-5	TER2-6	TER2-7	TER2-8
No.	100 / 1 .	76 / 1 .	77 / 1 .	78 / 1 .	CCIMI01Fsp	CCIMI02Fsp	CCIMI03Fsp	CCIMI04Fsp	CCIMI05Fsp	CCIMI06Fsp
Notes	Pheno	Pheno	Pheno	Pheno	Pheno	Pheno	Pheno	Pheno	Pheno	Pheno
SiO_2	66.86	66.82	66.53	66.79	67.18	67.46	66.85	67.56	66.96	67.62
TiO_2	0.06	0.04	0.03	0.03						
Al_2O_3	18.62	18.45	18.30	18.76	18.90	19.29	19.36	19.35	19.12	19.23
BaO	0.04	0.02	0.04	0.18	0.02	0.05	0.03	0.02	0.03	0.02
FeO	0.28	0.35	0.32	0.26	0.33	0.25	0.22	0.29	0.31	0.23
SrO	0.04	0.01	0.02	0.01	bdl	bdl	bdl	bdl	bdl	bdl
MgO	bdl	0.01	bdl	bdl						
CaO	0.26	0.17	0.20	0.37	0.15	0.23	0.35	0.14	0.11	0.17
Na_2O	7.73	7.60	7.61	8.03	7.57	7.73	7.83	7.21	7.65	7.78
K_2O	5.97	5.68	5.65	5.16	5.98	5.78	5.50	6.06	6.20	5.95
Total	99.86	99.16	98.71	99.58	100.13	100.79	100.13	100.62	100.38	101.00
Si	2.995	3.006	3.008	2.992	2.996	2.987	2.978	2.993	2.985	2.989
Ti	0.002	0.001	0.001	0.001						
Al	0.983	0.978	0.975	0.990	0.993	1.007	1.016	1.010	1.004	1.002
Ba	0.001	0.000	0.001	0.003	0.000	0.001	0.000	0.000	0.000	0.000
Fe	0.010	0.013	0.012	0.010	0.012	0.009	0.008	0.011	0.012	0.008
Sr	0.001	0.000	0.001	0.000						
Mg		0.001								
Ca	0.012	0.008	0.010	0.018	0.007	0.011	0.017	0.006	0.005	0.008
Na	0.671	0.663	0.667	0.698	0.655	0.664	0.676	0.619	0.661	0.667
K	0.341	0.326	0.326	0.295	0.340	0.326	0.313	0.343	0.353	0.336
Sum	5.017	4.998	5.000	5.008	5.004	5.005	5.008	4.983	5.020	5.011
Ab	65.5	66.5	66.5	69.1	65.3	66.3	67.3	64.0	64.9	66.0
An	1.2	0.8	1.0	1.8	0.7	1.1	1.6	0.7	0.5	0.8
Or	33.3	32.7	32.5	29.2	33.9	32.6	31.1	35.4	34.6	33.2

Table C1 continued

Unit	**CCl sy**	**CCl sy**	**CCl sy**	**CCl sy**	**CCl sy**	**CCl sy**	**CCl sy**	**CCl sy**	**CCl sy**	**CCl sy**	**CCl sy**	**CCl sy**	**CCl sy**
Sample	TER30-6	TER30-6	TER30-6	TER30-6	TER30-6	TER30-6	TER30-6	TER30-6	TER30-6	TER30-6	TER30-6	TER30-6	TER30-6
No.	Fsp2	Fsp2	Fsp3	Fsp3	Fsp4	Fsp4	Fsp5	Fsp5	Fsp6	Fsp6	Fsp8	Fp8	Fsp9
Notes	Core	Rim	Core	Rim	Core	Rim	Core	Rim	Core	Rim	Core	Rim	Core
SiO_2	67.14	68.06	66.39	68.97	67.85	67.23	67.17	66.37	64.54	66.37	66.85	66.57	66.95
TiO_2													
Al_2O_3	19.32	19.46	19.65	18.36	19.35	19.50	19.46	19.07	18.47	18.51	19.89	19.73	20.07
BaO	0.02	0.03	0.08	0.04	0.03	bdl	bdl	0.10	0.02	bdl	0.27	0.25	0.23
FeO	0.24	0.22	0.23	0.95	0.36	0.29	0.25	0.04	0.11	0.55	0.24	0.22	0.24
SrO	0.03	0.04	bdl	bdl	bdl	bdl	bdl	bdl	bdl	0.04	bdl	0.01	bdl
MgO													
CaO	0.77	0.15	0.37	bdl	0.04	0.11	0.14	0.01	bdl	bdl	0.59	0.45	0.52
Na_2O	8.00	7.64	7.70	11.41	7.88	7.56	7.68	3.23	0.53	2.92	8.17	8.22	7.94
K_2O	5.17	6.08	5.78	0.54	5.73	6.07	6.17	12.48	16.00	12.74	4.82	4.86	5.14
Total	100.69	101.68	100.20	100.27	101.24	100.76	100.87	101.30	99.67	101.13	100.83	100.31	101.09
Si	2.975	2.989	2.962	3.021	2.990	2.980	2.977	2.989	2.992	3.001	2.958	2.961	2.956
Ti													
Al	1.009	1.007	1.033	0.948	1.005	1.019	1.017	1.012	1.009	0.987	1.037	1.034	1.044
Ba	0.000	0.001	0.001	0.001	0.001			0.002	0.000		0.005	0.004	0.004
Fe	0.009	0.008	0.009	0.035	0.013	0.011	0.009	0.002	0.004	0.021	0.009	0.008	0.009
Sr	0.001	0.001								0.001		0.000	
Mg													
Ca	0.037	0.007	0.018		0.002	0.005	0.007	0.000			0.028	0.021	0.025
Na	0.687	0.650	0.666	0.969	0.673	0.650	0.660	0.282	0.048	0.256	0.701	0.709	0.680
K	0.292	0.341	0.329	0.030	0.322	0.343	0.349	0.717	0.946	0.735	0.272	0.276	0.289
Sum	5.010	5.003	5.019	5.004	5.006	5.007	5.019	5.004	5.000	5.001	5.010	5.014	5.007
Ab	67.6	65.2	65.8	97.0	67.5	65.1	65.0	28.2	4.8	25.8	70.0	70.5	68.4
An	3.6	0.7	1.7	0.0	0.2	0.5	0.7	0.0	0.0	0.0	2.8	2.1	2.5
Or	28.8	34.1	32.5	3.0	32.3	34.4	34.4	71.7	95.2	74.2	27.2	27.4	29.1

Table C1 continued

Unit	**CCl sy**	**CCl sy**	**CCl sy**	**CCl sy**	**CCl sy**	**CCl sy**	**CCl sy**	**CCl sy**	**CCl sy**	**CCl sy**	**CCl sy**	**CCl sy**	**CCl sy**
Sample	TER30-6	TER30-6	TER30-6	TER30-6	TER30-6	TER30-6	TER30-6	TER30-6	TER30-6	TER30-6	TER30-6	TER30-6	TER30-6
No.	Fsp9	Fsp10	Fsp10	Fsp11	Fsp11	Fsp12	Fsp12	Fsp13	Fsp13	Fsp14	Fsp14	Fsp15	Fsp15
Notes	Rim	Core	Rim	Core	Rim	Core	Rim	Core	Rim	Core	Rim	Core	Rim
SiO_2	66.86	67.54	67.73	67.58	67.81	67.12	68.86	66.83	66.42	67.54	67.35	67.62	67.58
TiO_2													
Al_2O_3	19.15	19.61	19.22	19.70	19.18	19.78	18.71	18.13	18.23	19.23	18.58	19.85	19.22
BaO	0.02	0.16	bdl	0.17	0.02	0.11	0.02	0.01	0.05	0.04	bdl	0.10	bdl
FeO	0.29	0.28	0.34	0.21	0.43	0.25	1.08	0.91	0.96	0.23	1.12	0.20	0.36
SrO	0.04	bdl	0.01	bdl	0.01	bdl	0.02	bdl	bdl	0.03	0.03	bdl	bdl
MgO													
CaO	0.10	0.33	0.02	0.37	0.02	0.39	bdl	bdl	bdl	0.10	0.02	0.48	0.04
Na_2O	7.63	7.81	7.47	8.03	7.88	8.04	11.63	4.59	4.61	8.09	6.87	8.19	7.91
K_2O	5.89	5.39	6.08	5.03	5.91	4.98	0.40	10.18	10.33	5.59	6.83	4.91	5.74
Total	99.98	101.12	100.87	101.09	101.26	100.67	100.72	100.65	100.60	100.85	100.80	101.35	100.85
Si	2.986	2.978	2.996	2.977	2.992	2.969	3.006	3.013	3.003	2.988	3.001	2.970	2.990
Ti													
Al	1.008	1.019	1.002	1.023	0.997	1.031	0.963	0.963	0.971	1.003	0.976	1.028	1.002
Ba	0.000	0.003		0.003	0.000	0.002	0.000	0.000	0.001	0.001		0.002	
Fe	0.011	0.010	0.013	0.008	0.016	0.009	0.039	0.034	0.036	0.009	0.042	0.007	0.013
Sr	0.001		0.000		0.000		0.001			0.001	0.001		
Mg													
Ca	0.005	0.016	0.001	0.017	0.001	0.018				0.005	0.001	0.023	0.002
Na	0.661	0.668	0.641	0.686	0.674	0.690	0.984	0.401	0.404	0.694	0.594	0.698	0.679
K	0.336	0.303	0.343	0.283	0.333	0.281	0.022	0.586	0.596	0.316	0.388	0.275	0.324
Sum	5.008	4.997	4.995	4.996	5.013	5.001	5.016	4.998	5.011	5.015	5.002	5.002	5.010
Ab	66.0	67.7	65.1	69.6	66.9	69.7	97.8	40.7	40.4	68.4	60.4	70.1	67.6
An	0.5	1.6	0.1	1.8	0.1	1.9	0.0	0.0	0.0	0.5	0.1	2.3	0.2
Or	33.5	30.7	34.8	28.7	33.0	28.4	2.2	59.3	59.6	31.1	39.5	27.6	32.3

Table C1 continued

Unit	**CCl sy**	**CCl sy**	**CCl sy**	**CCl sy**	**CCl sy**	**CCl sy**	**CCl sy**	**CCl sy**	**CCl sy**	**CCl sy**	**CCl sy**	**CCl sy**	**CCl sy**
Sample	TER30-6	TER30-6	TER30-6	TER30-6	TER30-6	TER30-6	TER30-6	TER30-6	TER30-6	TER30-6	TER30-6	TER30-6	TER30-6
No.	Fsp16	Fsp16	Fsp17	Fsp17	Fsp18	Fsp18	Fsp19	Fsp19	Fsp20	Fsp20	Fsp21	Fsp21	Fsp22
Notes	Core	Rim	Core	Rim	Core	Rim	Core	Rim	Core	Rim	Core	Rim	Core
SiO_2	67.89	67.22	67.21	67.00	67.17	68.06	67.28	67.87	67.35	67.85	67.35	67.63	67.87
TiO_2													
Al_2O_3	19.05	18.17	19.58	18.35	20.03	18.73	19.19	18.22	19.18	18.37	19.50	18.93	19.21
BaO	0.02	0.02	0.18	0.02	0.26	bdl	bdl	bdl	0.04	0.03	0.09	0.02	0.01
FeO	0.33	1.25	0.33	0.97	0.26	0.70	0.26	1.32	0.31	1.17	0.24	0.31	0.26
SrO	bdl	0.09	bdl	0.03	bdl	bdl	bdl	bdl	bdl	bdl	bdl	0.02	0.05
MgO													
CaO	0.02	bdl	0.29	bdl	0.46	0.04	0.20	bdl	0.11	bdl	0.22	0.16	0.15
Na_2O	7.92	5.76	7.88	4.31	8.21	7.73	7.58	7.83	7.57	7.75	7.53	7.78	7.77
K_2O	5.71	8.89	5.45	10.83	4.94	6.17	5.89	5.71	6.03	5.73	6.01	5.81	5.83
Total	100.94	101.40	100.92	101.51	101.33	101.43	100.40	100.95	100.59	100.90	100.94	100.66	101.15
Si	2.999	3.006	2.974	3.005	2.958	3.003	2.990	3.012	2.990	3.010	2.980	2.999	2.994
Ti													
Al	0.992	0.957	1.021	0.970	1.040	0.974	1.005	0.953	1.004	0.960	1.017	0.989	0.999
Ba	0.000	0.000	0.003	0.000	0.004				0.001	0.001	0.002	0.000	0.000
Fe	0.012	0.047	0.012	0.036	0.010	0.026	0.010	0.049	0.012	0.043	0.009	0.011	0.010
Sr		0.002		0.001								0.001	0.001
Mg													
Ca	0.001		0.014		0.022	0.002	0.010		0.005		0.010	0.008	0.007
Na	0.678	0.499	0.676	0.375	0.701	0.661	0.653	0.674	0.652	0.667	0.646	0.669	0.665
K	0.322	0.507	0.308	0.620	0.278	0.347	0.334	0.323	0.342	0.324	0.339	0.329	0.328
Sum	5.005	5.019	5.008	5.007	5.012	5.014	5.001	5.010	5.005	5.005	5.004	5.005	5.003
Ab	67.8	49.6	67.8	37.7	70.1	65.4	65.5	67.6	65.3	67.3	64.9	66.5	66.5
An	0.1	0.0	1.4	0.0	2.2	0.2	1.0	0.0	0.5	0.0	1.0	0.8	0.7
Or	32.1	50.4	30.8	62.3	27.7	34.4	33.5	32.4	34.2	32.7	34.1	32.7	32.8

Table C1 continued

Unit	**CCl sy**	**CCl sy**	**CCl sy**	**CCl sy**	**CCl sy**	**CCl sy**	**CCl sy**	**CCl sy**	**CCl sy**	**CCl sy**	**CCl sy**	**CCl sy**	**CCl sy**
Sample	TER30-6	TER30-6	TER30-6	TER30-6	TER30-6	TER30-6	TER30-6	TER30-1	TER30-1	TER30-1	TER30-1	TER30-1	TER30-1
No.	Fsp22	Fsp23	Fsp23	Fsp24	Fsp24	Fsp25	Fsp25	Fsp1	Fsp2	Fsp4	Fsp5	Fsp6	Fsp7
Notes	Rim	Core	Rim	Core	Rim	Core	Rim	Pheno	Pheno	Pheno	Pheno	Pheno	Pheno
SiO_2	66.94	68.51	68.37	67.63	66.62	67.47	67.09	67.07	66.89	65.81	67.32	66.68	65.11
TiO_2													
Al_2O_3	18.06	18.67	18.54	19.50	18.10	18.83	18.91	18.53	18.90	19.55	19.31	19.03	19.60
BaO	bdl	bdl	bdl	bdl	0.02	0.00	0.06	0.01	0.02	0.20	0.05	bdl	0.22
FeO	1.00	1.17	1.18	0.22	1.08	0.50	0.64	0.77	0.70	0.22	0.21	0.31	0.17
SrO	bdl	bdl	bdl	bdl	0.01	bdl	bdl	bdl	bdl	bdl	bdl	bdl	bdl
MgO													
CaO	bdl	0.02	bdl	0.26	bdl	0.03	0.01	0.08	0.02	0.49	0.23	0.09	0.54
Na_2O	4.59	9.85	9.73	8.00	4.64	7.84	7.71	7.86	8.10	8.39	8.11	7.58	8.07
K_2O	10.33	3.05	3.07	5.19	10.41	5.93	5.70	5.91	5.60	4.80	5.36	6.16	5.15
Total	100.92	101.27	100.89	100.80	100.88	100.60	100.12	100.23	100.23	99.46	100.60	99.85	98.86
Si	3.014	3.003	3.007	2.985	3.006	2.998	2.994	2.997	2.986	2.955	2.984	2.986	2.946
Ti													
Al	0.958	0.964	0.961	1.014	0.963	0.986	0.994	0.976	0.994	1.035	1.009	1.004	1.045
Ba					0.000	0.000	0.001	0.000	0.000	0.004	0.001		0.004
Fe	0.038	0.043	0.043	0.008	0.041	0.019	0.024	0.029	0.026	0.008	0.008	0.011	0.006
Sr					0.000								
Mg													
Ca		0.001		0.012		0.001	0.000	0.004	0.001	0.023	0.011	0.004	0.026
Na	0.401	0.837	0.830	0.685	0.406	0.675	0.667	0.681	0.701	0.730	0.697	0.658	0.708
K	0.593	0.171	0.172	0.292	0.599	0.336	0.324	0.337	0.319	0.275	0.303	0.352	0.297
Sum	5.004	5.019	5.013	4.996	5.015	5.015	5.005	5.024	5.027	5.030	5.012	5.017	5.034
Ab	40.3	83.0	82.8	69.2	40.4	66.7	67.2	66.7	68.7	71.0	68.9	64.9	68.6
An	0.0	0.1	0.0	1.2	0.0	0.1	0.0	0.4	0.1	2.3	1.1	0.4	2.6
Or	59.7	16.9	17.2	29.5	59.6	33.2	32.7	33.0	31.2	26.7	30.0	34.7	28.8

Table C1 continued

Unit	**CCI sy**	**CCI sy**	**CCI sy**	**CCI sy**	**CCI sy**	**CCI sy**	**CCI sy**	**CCI sy**	**CCI sy**	**CCI sy**	**CCI sy**
Sample	TER30-1	TER30-7	TER30-7	TER30-7	TER30-7	TER30-7	TER29-1	TER29-1	TER29-1	TER29-1	TER29-1
No.	Fsp8	Fsp1	Fsp5	Fsp6	Fsp7	Fsp8	Fsp2	Fsp3	Fsp4	Fsp6	Fsp7
Notes	Pheno	Pheno	Pheno	Pheno	Pheno	Pheno	Pheno	Pheno	Pheno	Pheno	Pheno
SiO_2	66.99	66.71	67.24	67.21	67.26	67.25	66.99	66.69	67.17	66.88	66.74
TiO_2											
Al_2O_3	18.89	18.56	18.17	19.32	18.23	19.20	19.16	18.85	19.09	19.22	19.15
BaO	bdl	bdl	bdl	0.06	0.02	0.03	0.03	bdl	bdl	0.02	0.01
FeO	0.40	0.90	1.02	0.20	0.93	0.24	0.24	0.51	0.29	0.26	0.25
SrO	bdl	bdl	bdl	bdl	bdl	bdl	bdl	bdl	bdl	bdl	bdl
MgO											
CaO	0.06	bdl	bdl	0.29	bdl	0.08	0.17	0.15	0.29	0.21	0.18
Na_2O	7.94	7.27	7.12	8.18	7.44	7.62	7.68	7.93	7.89	7.67	7.34
K_2O	5.78	6.46	6.70	5.22	6.31	6.10	6.07	5.75	5.52	6.03	6.47
Total	100.06	99.90	100.25	100.48	100.18	100.52	100.34	99.89	100.26	100.29	100.14
Si	2.991	2.996	3.011	2.982	3.010	2.989	2.985	2.986	2.988	2.981	2.983
Ti											
Al	0.994	0.982	0.959	1.010	0.961	1.006	1.006	0.995	1.001	1.010	1.009
Ba				0.001	0.000	0.001	0.001			0.000	0.000
Fe	0.015	0.034	0.038	0.007	0.035	0.009	0.009	0.019	0.011	0.010	0.010
Sr											
Mg											
Ca	0.003			0.014		0.004	0.008	0.007	0.014	0.010	0.008
Na	0.687	0.633	0.618	0.704	0.646	0.657	0.663	0.688	0.681	0.663	0.636
K	0.329	0.370	0.383	0.295	0.360	0.346	0.345	0.328	0.313	0.343	0.369
Sum	5.020	5.015	5.010	5.013	5.012	5.010	5.017	5.025	5.008	5.017	5.015
Ab	67.4	63.1	61.8	69.5	64.2	65.2	65.3	67.2	67.5	65.3	62.8
An	0.3	0.0	0.0	1.3	0.0	0.4	0.8	0.7	1.4	1.0	0.8
Or	32.3	36.9	38.2	29.2	35.8	34.4	33.9	32.1	31.1	33.8	36.4

Table C1 continued

Unit	**CCl enc**	**CCl enc**	**CCl enc**	**CCl enc**	**CCl enc**	**CCl enc**	**CCl enc**	**CCl enc**	**CCl enc**	**CCl enc**	**CCl enc**	**CCl enc**	**CCl enc**
Sample	Spec 1	Spec 1	Spec 1	Spec 1	Spec 1	Spec 1	Spec 1	Spec 1	Spec 1	Spec 1	Spec 1	Spec 1	Spec 1
No.	Pheno1	Pheno1	Pheno1	Pheno2	Pheno2	Pheno2	Pheno2	Pheno3	Pheno3	Pheno3	Pheno4	Pheno4	Pheno4
Notes	Core	Core	Rim	Core	Core	Rim	Rim	Core	Core	Rim	Core	Core	Rim
SiO_2	62.68	62.54	64.22	64.44	63.29	62.85	63.09	63.39	63.29	63.52	66.02	64.13	63.99
TiO_2													
Al_2O_3	20.67	20.83	21.55	19.46	21.01	21.13	21.46	21.33	21.24	21.50	19.84	20.58	21.03
BaO	0.68	0.70	0.58	0.39	0.51	0.72	0.75	0.69	0.72	0.62	0.15	0.59	0.72
FeO	0.25	0.25	0.11	0.27	0.24	0.22	0.23	0.22	0.24	0.26	0.20	0.19	0.24
SrO	0.04	0.08	0.07	0.03	0.04	0.03	0.02	0.07	0.09	0.09	0.03	bdl	0.08
MgO													
CaO	1.97	1.97	2.27	0.58	2.20	2.35	2.45	2.34	2.35	2.49	0.77	1.53	2.11
Na_2O	9.31	9.46	10.17	7.80	8.90	9.36	9.50	9.64	9.79	9.81	10.63	9.07	9.63
K_2O	2.34	1.84	0.77	5.51	2.42	1.95	1.25	1.32	1.39	1.04	1.43	2.88	1.56
Total	97.93	97.66	99.73	98.47	98.62	98.62	98.76	99.00	99.11	99.34	99.07	98.96	99.37
Si	2.865	2.861	2.860	2.940	2.866	2.851	2.847	2.854	2.852	2.848	2.944	2.894	2.871
Ti													
Al	1.114	1.123	1.131	1.046	1.121	1.130	1.141	1.132	1.128	1.136	1.043	1.094	1.112
Ba	0.012	0.012	0.010	0.007	0.009	0.013	0.013	0.012	0.013	0.011	0.003	0.010	0.013
Fe	0.009	0.009	0.004	0.010	0.009	0.008	0.009	0.008	0.009	0.010	0.007	0.007	0.009
Sr	0.001	0.002	0.002	0.001	0.001	0.001	0.001	0.002	0.002	0.002	0.001		0.002
Mg													
Ca	0.097	0.097	0.108	0.028	0.107	0.114	0.119	0.113	0.114	0.119	0.037	0.074	0.101
Na	0.825	0.839	0.878	0.690	0.781	0.823	0.832	0.842	0.855	0.853	0.919	0.793	0.838
K	0.136	0.107	0.044	0.321	0.140	0.113	0.072	0.076	0.080	0.060	0.082	0.166	0.089
Sum	5.059	5.051	5.036	5.043	5.034	5.052	5.034	5.039	5.052	5.040	5.035	5.039	5.036
Ab	78.0	80.4	85.3	66.4	76.0	78.4	81.4	81.7	81.5	82.6	88.6	76.8	81.5
An	9.1	9.3	10.5	2.7	10.4	10.9	11.6	11.0	10.8	11.6	3.5	7.2	9.9
Or	12.9	10.3	4.2	30.9	13.6	10.8	7.0	7.4	7.6	5.8	7.9	16.0	8.7

Table C1 continued

Unit	CCl enc	CCl enc	CCl enc	CCl enc	CCl enc	CCl enc	CCl enc	CCl enc	CCl enc	CCl enc	CCl enc	CCl enc	CCl enc
Sample	Spec 1	Spec 1	Spec 1	Spec 1	Spec 1	Spec 1	T073A3	T073A4	T073A5	T073A6	T073A7	T073A8	T073A9
No.	Pheno5	Pheno5	Pheno5	Pheno6	Pheno6	Pheno6	Pheno1	Pheno1	Pheno1	Pheno1	Pheno1	Pheno2	Pheno2
Notes	Core	Core	Rim	Core	Core	Rim	Core	Core	Core	Rim	Rim	Core	Core
SiO_2	66.01	66.84	63.55	65.62	64.59	66.19	62.60	62.94	63.63	62.68	63.45	47.11	46.34
TiO_2													
Al_2O_3	19.72	19.55	20.98	19.53	19.15	18.54	18.75	20.82	20.39	20.94	21.08	31.45	32.16
BaO	0.25	0.26	0.70	0.26	0.21	0.02	0.72	0.71	0.66	0.71	0.77	bdl	bdl
FeO	0.10	0.04	0.26	0.24	0.22	0.46	0.87	0.20	0.21	0.31	0.26	0.54	0.48
SrO	0.07	bdl	0.08	0.01	bdl	bdl	bdl	0.05	0.03	0.07	0.04	0.11	0.10
MgO													
CaO	0.63	0.30	2.02	0.58	0.53	0.08	0.23	1.89	1.42	2.22	2.12	15.32	16.00
Na_2O	10.37	8.41	9.54	8.39	8.37	8.26	4.16	8.86	8.81	9.35	9.21	2.75	2.47
K_2O	2.19	5.02	1.39	4.50	4.81	5.41	10.99	2.59	3.16	1.63	1.93	0.15	0.06
Total	99.35	100.42	98.52	99.13	97.87	98.96	98.32	98.07	98.31	97.91	98.86	97.43	97.61
Si	2.946	2.970	2.872	2.954	2.952	2.990	2.935	2.870	2.895	2.858	2.865	2.223	2.186
Ti													
Al	1.038	1.024	1.117	1.036	1.031	0.987	1.036	1.119	1.093	1.126	1.122	1.749	1.788
Ba	0.004	0.005	0.012	0.005	0.004	0.000	0.013	0.013	0.012	0.013	0.014		
Fe	0.004	0.002	0.010	0.009	0.009	0.017	0.034	0.008	0.008	0.012	0.010	0.021	0.019
Sr	0.002		0.002	0.000				0.001	0.001	0.002	0.001	0.003	0.003
Mg													
Ca	0.030	0.014	0.098	0.028	0.026	0.004	0.011	0.092	0.069	0.108	0.103	0.775	0.809
Na	0.897	0.724	0.836	0.733	0.741	0.724	0.378	0.784	0.777	0.827	0.807	0.251	0.226
K	0.125	0.284	0.080	0.259	0.280	0.312	0.657	0.151	0.183	0.095	0.111	0.009	0.003
Sum	5.046	5.023	5.028	5.023	5.043	5.034	5.065	5.038	5.039	5.040	5.032	5.032	5.034
Ab	85.3	70.8	82.4	71.9	70.7	69.6	36.1	76.3	75.5	80.3	79.0	24.3	21.7
An	2.9	1.4	9.6	2.8	2.5	0.4	1.1	9.0	6.7	10.5	10.1	74.8	77.9
Or	11.9	27.8	7.9	25.4	26.8	30.0	62.8	14.7	17.8	9.2	10.9	0.9	0.3

Table C1 continued

Unit	**CCl enc**	**CCl enc**	**CCl enc**	**CCl enc**	**CCl enc**	**CCl enc**	**CCl enc**	**CCl enc**	**CCl enc**	**CCl enc**	**CCl enc**	**CCl enc**	**CCl enc**
Sample	T073A10	T073A11	T073A12	T073A13	T073A14	T073A15	T073A16	T073A17	T073A18	T073A19	T073A20	T073A21	T073A22
No.	Pheno2	Pheno2	Pheno2	Pheno2	Pheno3	Pheno3	Pheno3	Pheno3	Pheno3	Pheno3	Pheno4	Pheno4	Pheno5
Notes	Core	Rim	Rim	Rim	Core	Core	Core	Rim	Rim	Rim	Core	Core	Core
SiO_2	46.93	46.19	45.73	47.13	64.33	62.81	64.51	64.79	64.96	64.82	64.11	63.50	64.61
TiO_2													
Al_2O_3	32.15	32.73	32.73	32.14	20.36	21.34	19.97	19.01	18.69	19.22	19.81	19.48	19.26
BaO	bdl	bdl	bdl	bdl	0.39	0.70	0.41	0.08	0.11	0.16	0.51	0.52	0.21
FeO	0.55	0.34	0.49	0.37	0.26	0.25	0.32	0.38	0.34	0.30	0.29	0.26	0.23
SrO	0.12	0.13	0.15	0.12	0.05	0.06	bdl	bdl	bdl	bdl	0.02	bdl	0.01
MgO													
CaO	15.99	16.61	16.76	15.81	1.48	2.51	1.03	0.10	0.14	0.38	1.26	0.87	0.56
Na_2O	2.53	2.10	2.05	2.72	9.41	9.38	8.58	8.44	7.62	8.34	8.80	6.55	8.08
K_2O	0.12	0.00	0.02	0.03	2.50	1.54	3.90	5.31	6.38	5.08	3.45	7.34	5.02
Total	98.41	98.10	97.93	98.31	98.78	98.60	98.71	98.10	98.23	98.31	98.24	98.54	98.00
Si	2.197	2.168	2.155	2.204	2.902	2.845	2.921	2.958	2.972	2.952	2.918	2.922	2.950
Ti													
Al	1.774	1.811	1.817	1.771	1.082	1.139	1.066	1.023	1.008	1.032	1.063	1.057	1.036
Ba					0.007	0.012	0.007	0.001	0.002	0.003	0.009	0.009	0.004
Fe	0.021	0.013	0.019	0.014	0.010	0.009	0.012	0.014	0.013	0.012	0.011	0.010	0.009
Sr	0.003	0.003	0.004	0.003	0.001	0.001					0.000		0.000
Mg													
Ca	0.802	0.836	0.846	0.792	0.071	0.122	0.050	0.005	0.007	0.019	0.061	0.043	0.028
Na	0.230	0.191	0.187	0.246	0.823	0.824	0.753	0.747	0.676	0.737	0.777	0.585	0.716
K	0.007	0.000	0.001	0.002	0.144	0.089	0.225	0.309	0.372	0.295	0.200	0.431	0.293
Sum	5.035	5.022	5.031	5.034	5.041	5.042	5.035	5.058	5.049	5.048	5.039	5.057	5.036
Ab	22.1	18.6	18.1	23.7	79.3	79.6	73.2	70.4	64.1	70.1	74.8	55.2	69.1
An	77.2	81.4	81.8	76.2	6.9	11.8	4.8	0.5	0.6	1.8	5.9	4.1	2.7
Or	0.7	0.0	0.1	0.2	13.9	8.6	21.9	29.1	35.3	28.1	19.3	40.7	28.2

Table C1 continued

Unit	CCl enc	CCl enc	CCl enc	CCl enc	CCl enc	CCl enc	CCl enc	CCl enc	CCl enc	CCl enc	CCl enc	CCl enc	CCl enc
Sample	T073A23	T073A24	T073A25	T073A26	T073A27	T073A28	T073A29	T073A30	T073A31	T073A32	T073A33	T073A34	T073A35
No.	Pheno5	Pheno5	Pheno5	Pheno5	Pheno6	Pheno6	Pheno6	Pheno6	Pheno6	Pheno7	Pheno7	Pheno7	Pheno7
Notes	Core	Core	Rim	Rim	Core	Core	Core	Rim	Rim	Core	Core	Core	Rim
SiO_2	64.89	64.79	65.69	65.20	64.80	64.89	64.87	66.11	65.96	65.51	65.97	64.78	65.88
TiO_2													
Al_2O_3	19.24	19.36	18.78	18.75	19.52	19.48	19.53	18.54	18.72	18.96	19.29	19.22	19.18
BaO	0.24	0.22	0.03	0.05	0.31	0.36	0.29	0.06	0.07	0.08	0.07	0.21	0.09
FeO	0.27	0.22	0.33	0.42	0.19	0.20	0.26	0.47	0.42	0.18	0.23	0.21	0.16
SrO	bdl	0.04	bdl	bdl	bdl	0.04	0.03	0.02	bdl	bdl	bdl	0.02	0.02
MgO													
CaO	0.52	0.62	0.12	0.04	0.70	0.75	0.79	0.02	0.02	0.35	0.37	0.48	0.34
Na_2O	8.26	8.37	8.22	8.07	8.36	8.31	8.38	8.10	8.04	8.09	8.21	8.83	8.81
K_2O	4.95	4.60	5.58	5.84	4.68	4.76	4.67	5.69	5.57	5.45	5.34	4.09	4.26
Total	98.36	98.20	98.76	98.37	98.57	98.80	98.82	99.01	98.80	98.62	99.49	97.84	98.75
Si	2.952	2.948	2.977	2.972	2.941	2.942	2.939	2.989	2.985	2.971	2.964	2.953	2.970
Ti													
Al	1.032	1.038	1.003	1.007	1.044	1.041	1.043	0.988	0.998	1.014	1.022	1.033	1.019
Ba	0.004	0.004	0.001	0.001	0.006	0.006	0.005	0.001	0.001	0.001	0.001	0.004	0.002
Fe	0.010	0.008	0.013	0.016	0.007	0.008	0.010	0.018	0.016	0.007	0.009	0.008	0.006
Sr		0.001				0.001	0.001	0.000				0.001	0.001
Mg													
Ca	0.025	0.030	0.006	0.002	0.034	0.037	0.038	0.001	0.001	0.017	0.018	0.023	0.017
Na	0.729	0.739	0.722	0.713	0.736	0.730	0.736	0.710	0.706	0.711	0.716	0.780	0.770
K	0.287	0.267	0.323	0.340	0.271	0.275	0.270	0.328	0.322	0.315	0.306	0.238	0.245
Sum	5.040	5.036	5.044	5.051	5.040	5.040	5.042	5.036	5.029	5.036	5.036	5.040	5.028
Ab	70.0	71.3	68.7	67.6	70.7	70.1	70.5	68.3	68.6	68.2	68.8	74.9	74.6
An	2.4	2.9	0.6	0.2	3.3	3.5	3.7	0.1	0.1	1.6	1.7	2.2	1.6
Or	27.6	25.8	30.7	32.2	26.0	26.4	25.9	31.6	31.3	30.2	29.4	22.8	23.8

Table C1 continued

Unit	**CCI enc**	**CCI enc**	**CCI enc**	**CCI enc**	**CCI enc**	**CCI enc**	**CCI enc**	**CCI enc**	**CCI enc**	**CCI enc**	**CCI enc**	**CCI enc**	**CCI enc**
Sample	T073A36	Spec1	Spec2	Spec3	Spec 1	Spec 1	Spec 1	Spec 1	Spec 1	Spec 1	Spec 1	Spec 1	Spec 1
No.	Pheno7	Pheno7	Pheno7	Pheno7	Fspar 1	Fspar 2	Fspar 3	Fspar 4	Fspar 5	Fspar 7	Fspar 8	Fspar 9	Fspar 12
Notes	Rim	Core	Core	Rim	Gm	Gm	Gm	Gm	Gm	Gm	Gm	Gm	Gm
SiO_2	65.85	48.52	50.33	47.17	65.51	66.23	65.91	66.78	66.18	66.68	67.09	65.93	66.27
TiO_2		0.05	0.08	0.08									
Al_2O_3	17.83	31.52	30.80	32.24	19.36	19.19	19.32	18.39	19.62	19.24	19.42	19.14	19.16
BaO	0.02				0.18	0.14	0.12	bdl	0.06	0.06	0.01	0.09	0.06
FeO	1.46	0.09	0.09	0.14	0.82	0.35	0.23	0.81	0.27	0.11	0.17	0.27	0.35
SrO	bdl				bdl	bdl	bdl	bdl	0.02	bdl	bdl	bdl	bdl
MgO													
CaO	bdl	14.39	13.15	15.54	0.24	0.17	0.29	0.02	0.07	0.04	0.11	0.18	0.04
Na_2O	8.42	3.47	4.44	2.96	8.75	8.57	8.69	7.68	9.81	8.20	10.46	8.79	8.03
K_2O	5.21	0.05	0.05	0.04	4.36	4.85	4.46	6.26	3.29	5.52	2.44	4.66	6.08
Total	98.80	98.08	98.94	98.18	99.22	99.50	99.02	99.94	99.32	99.83	99.69	99.06	99.99
Si	2.994	2.260	2.317	2.205	2.952	2.971	2.966	2.998	2.958	2.980	2.974	2.969	2.971
Ti		0.002	0.003	0.003									
Al	0.955	1.731	1.672	1.776	1.028	1.015	1.024	0.973	1.034	1.013	1.015	1.016	1.013
Ba	0.000				0.003	0.002	0.002		0.001	0.001	0.000	0.002	0.001
Fe	0.056	0.004	0.003	0.006	0.031	0.013	0.009	0.030	0.010	0.004	0.006	0.010	0.013
Sr		0.000	0.000	0.000					0.001				
Mg													
Ca		0.718	0.649	0.778	0.012	0.008	0.014	0.001	0.004	0.002	0.005	0.009	0.002
Na	0.743	0.313	0.396	0.269	0.764	0.745	0.758	0.668	0.850	0.711	0.899	0.768	0.698
K	0.302	0.003	0.003	0.002	0.251	0.277	0.256	0.359	0.188	0.314	0.138	0.268	0.348
Sum	5.051	5.031	5.044	5.039	5.041	5.033	5.029	5.029	5.044	5.026	5.037	5.041	5.046
Ab	71.1	30.3	37.8	25.6	74.4	72.3	73.8	65.0	81.6	69.2	86.3	73.5	66.6
An	0.0	69.4	61.9	74.2	1.1	0.8	1.3	0.1	0.3	0.2	0.5	0.8	0.2
Or	28.9	0.3	0.3	0.2	24.4	26.9	24.9	34.9	18.0	30.6	13.2	25.6	33.2

Table C1 continued

Unit	CCl enc	CCl enc	CCl enc	CCl enc	CCl enc	CCl enc	CCl enc	CCl enc	CCl enc	CCl enc	CCl enc	CCl enc	CCl enc
Sample	Spec 1	Spec 1	Spec 1	Spec 1	Spec 1	Spec 1	Spec 1	T073 A3	T073 A3	T073 A3	T073 A3	T073 A3	T073 A3
No.	Fspar 13	Fspar 14	Fspar 15	Fspar 16	Fspar 18	Fspar 19	Fspar 20	Fspar 1	Fspar 2	Fspar 3	Fspar 4	Fspar 5	Fspar 7
Notes	Gm	Gm	Gm	Gm	Gm	Gm	Gm	Gm	Gm	Gm	Gm	Gm	Gm
SiO_2	67.74	65.35	68.35	64.94	66.22	66.78	66.37	66.24	66.73	67.62	65.99	67.13	66.82
TiO_2													
Al_2O_3	18.85	19.25	19.43	18.66	19.16	19.21	19.22	19.44	19.22	19.49	19.31	19.48	19.24
BaO	bdl	0.19	0.01	0.18	0.01	0.01	0.06	bdl	bdl	bdl	0.03	0.02	bdl
FeO	0.45	0.25	0.15	0.24	0.86	0.92	0.45	0.11	0.11	0.12	0.11	0.06	0.13
SrO	0.01	0.03	bdl	bdl	0.05	0.03	0.02	bdl	bdl	0.01	0.03	bdl	0.03
MgO													
CaO	0.02	0.30	0.14	0.03	0.11	0.07	0.51	0.16	0.15	0.10	0.18	0.20	0.16
Na_2O	11.40	8.26	11.54	3.25	11.58	11.14	9.32	11.49	11.52	11.57	11.07	11.66	11.80
K_2O	0.95	5.19	0.69	12.69	0.55	0.99	4.10	0.64	0.42	0.55	1.12	0.36	0.40
Total	99.44	98.82	100.30	99.98	98.55	99.16	100.05	98.09	98.14	99.48	97.82	98.90	98.57
Si	2.996	2.959	2.989	2.979	2.964	2.971	2.961	2.966	2.980	2.981	2.968	2.975	2.976
Ti													
Al	0.983	1.027	1.001	1.009	1.011	1.007	1.011	1.026	1.012	1.013	1.024	1.018	1.010
Ba		0.003	0.000	0.003	0.000	0.000	0.001				0.000	0.000	
Fe	0.017	0.009	0.005	0.009	0.032	0.034	0.017	0.004	0.004	0.005	0.004	0.002	0.005
Sr	0.000	0.001			0.001	0.001	0.000				0.001		0.001
Mg													
Ca	0.001	0.015	0.007	0.001	0.005	0.004	0.025	0.008	0.007	0.005	0.008	0.009	0.007
Na	0.978	0.725	0.979	0.289	1.005	0.961	0.806	0.997	0.997	0.989	0.965	1.002	1.019
K	0.054	0.300	0.038	0.743	0.031	0.056	0.233	0.036	0.024	0.031	0.064	0.020	0.023
Sum	5.029	5.039	5.019	5.033	5.049	5.034	5.054	5.038	5.024	5.023	5.035	5.027	5.040
Ab	94.7	69.8	95.6	28.0	96.5	94.2	75.8	95.8	97.0	96.5	93.0	97.1	97.1
An	0.1	1.4	0.7	0.1	0.5	0.3	2.3	0.8	0.7	0.5	0.8	0.9	0.7
Or	5.2	28.8	3.7	71.9	3.0	5.5	21.9	3.5	2.3	3.0	6.2	2.0	2.2

Table C1 continued

Unit	**CCI enc**	**CCI enc**	**CCI enc**	**CCI enc**	**CCI enc**	**CCI enc**	**CCI enc**	**CCI enc**	**CCI enc**	**CCI enc**	**CCI enc**	**CCI enc**
Sample	T073 A3	T073 A3	T073 A3	T073 A3	T073 A3	T073 A3	T073 A3	T073 A3	T073 A3	T073 A3	T073 A3	T073 A3
No.	Fspar 8	Fspar 9	Fspar 10	Fspar 12	Fspar 13	Fspar 14	Fspar 15	Fspar 16	Fspar 17	Fspar 18	Fspar 19	Fspar 20
Notes	Gm	Gm	Gm	Gm	Gm	Gm	Gm	Gm	Gm	Gm	Gm	Gm
SiO_2	67.46	65.76	64.89	65.36	66.24	65.38	65.44	64.16	65.06	64.86	65.76	65.07
TiO_2												
Al_2O_3	19.39	19.27	19.05	18.75	19.05	18.91	18.38	20.44	18.47	19.47	18.92	18.58
BaO	bdl	0.13	0.12	0.03	0.07	0.05	0.01	0.38	0.04	0.21	0.05	0.03
FeO	0.12	0.17	0.11	0.41	0.37	0.36	0.70	0.40	0.58	0.32	0.33	0.55
SrO	0.03	bdl	0.01	bdl	bdl	bdl	bdl	0.04	bdl	bdl	0.01	bdl
MgO												
CaO	0.26	0.24	0.05	0.09	0.13	0.12	bdl	1.22	0.04	0.48	0.09	bdl
Na_2O	11.60	10.64	8.36	8.05	8.23	8.07	7.83	9.53	8.13	9.37	8.40	7.92
K_2O	0.51	1.94	5.52	5.67	5.15	5.59	5.91	2.54	5.77	3.33	5.46	5.95
Total	99.37	98.16	98.12	98.35	99.24	98.50	98.29	98.72	98.10	98.04	99.02	98.10
Si	2.979	2.962	2.962	2.975	2.979	2.971	2.986	2.898	2.976	2.945	2.972	2.976
Ti												
Al	1.009	1.023	1.024	1.006	1.010	1.013	0.989	1.088	0.996	1.042	1.008	1.002
Ba		0.002	0.002	0.000	0.001	0.001	0.000	0.007	0.001	0.004	0.001	0.001
Fe	0.004	0.007	0.004	0.015	0.014	0.014	0.027	0.015	0.022	0.012	0.013	0.021
Sr	0.001		0.000					0.001			0.000	
Mg												
Ca	0.012	0.012	0.003	0.005	0.006	0.006		0.059	0.002	0.023	0.004	
Na	0.993	0.929	0.740	0.711	0.717	0.711	0.693	0.834	0.721	0.825	0.736	0.702
K	0.029	0.112	0.322	0.329	0.296	0.324	0.344	0.146	0.337	0.193	0.315	0.347
Sum	5.027	5.047	5.057	5.042	5.023	5.040	5.038	5.048	5.055	5.043	5.049	5.048
Ab	96.0	88.3	69.5	68.1	70.4	68.3	66.8	80.2	68.0	79.3	69.8	66.9
An	1.2	1.1	0.2	0.4	0.6	0.6	0.0	5.7	0.2	2.2	0.4	0.0
Or	2.8	10.6	30.2	31.5	29.0	31.1	33.2	14.1	31.8	18.5	29.8	33.1

Table C1 continued

Unit	**PNI**	**PNI**	**PNI**	**PNI**	**PNI**	**PNI**	**PNI**	**PNI**	**PNI**	**PNI**	**PNI**	**PNI**	**PNI**	**PNI**
Sample	T012	T012	T012	T012	T012	T012	T012	T012	T012	T012	T012	T012	T012	T012
No.	Fsp2	Fsp3	Fsp4	Fsp5	Fsp6	Fsp7	Fsp8	Fsp9	Fsp10	Fsp11	Fsp12	Fsp13	Fsp14	Fsp15
Notes	Pheno	Pheno	Pheno	Pheno	Pheno	Pheno	Pheno	Pheno	Pheno	Pheno	Pheno	Pheno	Pheno	Pheno
SiO_2	64.82	64.76	63.83	66.07	65.98	65.95	66.33	63.89	66.16	66.65	65.81	65.16	65.35	59.77
TiO_2														
Al_2O_3	19.46	19.37	19.56	19.07	18.74	19.04	20.24	19.38	19.39	19.40	19.39	19.44	19.24	18.67
BaO	0.24	0.20	0.28	0.07	0.06	0.14	0.27	0.16	0.19	0.16	0.18	0.28	0.21	0.23
FeO	0.26	0.27	0.27	0.23	0.29	0.26	0.29	0.28	0.31	0.29	0.30	0.28	0.26	0.28
SrO	bdl	bdl	bdl	bdl	bdl	0.01	bdl	0.04	bdl	bdl	bdl	bdl	bdl	bdl
MgO														
CaO	0.85	0.70	0.95	0.39	0.37	0.50	0.95	0.69	0.74	0.55	0.71	0.93	0.64	0.74
Na_2O	8.66	8.53	8.59	8.35	8.73	8.54	8.46	8.81	8.86	8.35	8.69	8.83	8.48	9.02
K_2O	4.01	4.42	3.99	5.01	4.87	4.64	3.86	4.15	4.07	4.66	4.22	3.96	4.37	4.02
Total	98.30	98.25	97.47	99.19	99.04	99.07	100.40	97.40	99.71	100.06	99.31	98.88	98.56	92.73
Si	2.943	2.945	2.927	2.973	2.977	2.971	2.940	2.933	2.958	2.970	2.956	2.943	2.958	2.898
Ti														
Al	1.041	1.038	1.057	1.011	0.996	1.011	1.057	1.048	1.022	1.019	1.026	1.035	1.027	1.067
Ba	0.004	0.004	0.005	0.001	0.001	0.002	0.005	0.003	0.003	0.003	0.003	0.005	0.004	0.004
Fe	0.010	0.010	0.010	0.009	0.011	0.010	0.011	0.011	0.011	0.011	0.011	0.011	0.010	0.011
Sr						0.000		0.001						
Mg														
Ca	0.041	0.034	0.047	0.019	0.018	0.024	0.045	0.034	0.035	0.026	0.034	0.045	0.031	0.039
Na	0.762	0.752	0.764	0.729	0.764	0.746	0.727	0.784	0.768	0.721	0.757	0.773	0.744	0.848
K	0.232	0.256	0.233	0.288	0.280	0.267	0.218	0.243	0.232	0.265	0.242	0.228	0.252	0.249
Sum	5.034	5.040	5.043	5.029	5.047	5.030	5.004	5.057	5.031	5.014	5.030	5.040	5.027	5.116
Ab	73.6	72.1	73.2	70.4	71.9	72.0	73.4	73.9	74.2	71.3	73.3	73.9	72.4	74.7
An	4.0	3.3	4.5	1.8	1.7	2.3	4.6	3.2	3.4	2.6	3.3	4.3	3.0	3.4
Or	22.4	24.6	22.4	27.8	26.4	25.7	22.0	22.9	22.4	26.2	23.4	21.8	24.6	21.9

Table C1 continued

Unit	**PNI**	**PNI**	**PNI**	**PNI**	**PNI**	**PNI**	**PNI**	**PNI**	**PNI**	**PNI**	**PNI**	**PNI**	**PNI**	**PNI**
Sample	T012	T012	T012	T012	T012	T012	T012	T012	T012	T012	T012	T012	T012	T012
No.	Fsp16	Fsp17	Fsp18	Fsp19	Fsp20	Fsp21	Fsp22	Fsp23	Fsp24	Fsp25	Fsp26	Fsp27	Fsp28	Fsp29
Notes	Pheno	Pheno	Pheno	Pheno	Pheno	Pheno	Pheno	Pheno	Pheno	Pheno	Pheno	Pheno	Pheno	Pheno
SiO_2	66.09	66.32	65.50	66.14	66.45	66.52	65.49	65.78	66.19	65.71	65.92	66.53	65.68	64.63
TiO_2														
Al_2O_3	19.46	19.27	19.74	19.36	19.24	19.63	19.92	19.35	19.83	19.69	19.69	19.27	19.52	19.17
BaO	0.16	0.10	0.27	0.15	0.10	0.17	0.27	0.12	0.20	0.22	0.20	0.09	0.17	0.12
FeO	0.26	0.27	0.25	0.25	0.30	0.27	0.26	0.28	0.31	0.28	0.29	0.29	0.31	0.29
SrO	bdl	bdl	0.01	bdl	bdl	bdl	bdl	0.01	bdl	bdl	bdl	bdl	bdl	0.02
MgO														
CaO	0.62	0.41	0.97	0.61	0.42	0.56	0.83	0.62	0.68	0.73	0.61	0.48	0.55	0.36
Na_2O	8.12	8.26	8.61	8.52	8.08	8.46	8.61	8.40	8.44	8.75	8.54	8.58	8.51	8.08
K_2O	4.60	4.74	3.93	4.40	4.95	4.63	4.01	4.46	4.29	4.17	4.25	4.74	4.30	4.98
Total	99.31	99.37	99.27	99.43	99.53	100.24	99.40	99.02	99.93	99.55	99.50	99.98	99.04	97.65
Si	2.965	2.973	2.942	2.964	2.976	2.960	2.938	2.961	2.951	2.945	2.953	2.969	2.956	2.957
Ti														
Al	1.029	1.018	1.045	1.023	1.015	1.029	1.053	1.027	1.042	1.040	1.039	1.014	1.035	1.034
Ba	0.003	0.002	0.005	0.003	0.002	0.003	0.005	0.002	0.004	0.004	0.003	0.002	0.003	0.002
Fe	0.010	0.010	0.009	0.009	0.011	0.010	0.010	0.011	0.011	0.010	0.011	0.011	0.012	0.011
Sr			0.000					0.000						0.000
Mg														
Ca	0.030	0.020	0.047	0.029	0.020	0.027	0.040	0.030	0.032	0.035	0.029	0.023	0.027	0.018
Na	0.706	0.718	0.750	0.740	0.702	0.730	0.749	0.733	0.730	0.760	0.742	0.742	0.742	0.717
K	0.263	0.271	0.225	0.252	0.283	0.263	0.230	0.256	0.244	0.238	0.243	0.270	0.247	0.291
Sum	5.006	5.012	5.023	5.020	5.009	5.022	5.024	5.020	5.014	5.034	5.020	5.030	5.021	5.030
Ab	70.7	71.2	73.4	72.5	69.9	71.6	73.5	72.0	72.5	73.5	73.2	71.7	73.1	69.9
An	3.0	1.9	4.6	2.9	2.0	2.6	3.9	2.9	3.2	3.4	2.9	2.2	2.6	1.7
Or	26.3	26.9	22.0	24.6	28.2	25.8	22.5	25.1	24.3	23.1	24.0	26.1	24.3	28.4

Table C1 continued

Unit	**PNI**	**PNI**	**PNI**	**PNI**	**PNI**	**PNI**	**PNI**	**PNI**	**PNI**	**PNI**	**PNI**	**PNI**	**PNI**	**PNI**
Sample	T012	T012	T012	T012	T012	T012	T012	T012	T012	T012	T012	T012	T012	T012
No.	Fsp30	Fsp31	Fsp32	Fsp33	Fsp34	Fsp35	Fsp36	Fsp37	Fsp38	Fsp39	Fsp40	Fsp41	MI01-fsp	MI02-fsp
Notes	Pheno	Pheno	Pheno	Pheno	Pheno	Pheno	Pheno	Pheno	Pheno	Pheno	Pheno	Pheno	Pheno	Pheno
SiO_2	64.13	65.31	65.33	64.69	66.76	66.55	66.41	65.42	66.09	66.30	64.75	66.92	67.43	67.01
TiO_2														
Al_2O_3	19.38	19.88	19.52	19.43	19.25	19.88	19.70	20.42	19.30	19.84	21.05	19.52	19.57	19.40
BaO	0.18	0.20	0.24	0.23	0.11	0.13	0.19	0.31	0.12	0.23	0.36	bdl	0.15	0.09
FeO	0.28	0.26	0.30	0.28	0.29	0.27	0.25	0.30	0.29	0.27	0.26	0.25	0.29	0.30
SrO	0.01	0.03	bdl	bdl	bdl	bdl	0.01	0.05	bdl	bdl	0.03	bdl	bdl	bdl
MgO														
CaO	0.57	0.92	0.64	0.77	0.38	0.62	0.63	1.45	0.49	0.65	1.68	0.37	0.47	0.40
Na_2O	8.40	8.61	8.62	8.71	8.31	8.32	8.40	8.82	8.31	8.40	8.85	6.92	8.24	8.19
K_2O	4.47	3.86	4.27	4.19	4.98	4.24	4.49	3.05	4.73	4.46	2.75	6.84	4.81	4.89
Total	97.43	99.07	98.92	98.29	100.08	100.01	100.08	99.82	99.33	100.16	99.73	100.82	100.96	100.28
Si	2.941	2.937	2.948	2.941	2.976	2.959	2.958	2.917	2.967	2.952	2.890	2.974	2.975	2.977
Ti														
Al	1.047	1.054	1.038	1.041	1.011	1.042	1.034	1.073	1.021	1.041	1.107	1.022	1.018	1.016
Ba	0.003	0.003	0.004	0.004	0.002	0.002	0.003	0.005	0.002	0.004	0.006		0.003	0.002
Fe	0.011	0.010	0.011	0.010	0.011	0.010	0.009	0.011	0.011	0.010	0.010	0.009	0.011	0.011
Sr	0.000	0.001					0.000	0.001			0.001			
Mg														
Ca	0.028	0.044	0.031	0.038	0.018	0.029	0.030	0.069	0.024	0.031	0.080	0.018	0.022	0.019
Na	0.747	0.751	0.754	0.768	0.718	0.717	0.725	0.763	0.723	0.725	0.766	0.596	0.705	0.705
K	0.262	0.221	0.246	0.243	0.283	0.240	0.255	0.174	0.271	0.253	0.157	0.388	0.271	0.277
Sum	5.039	5.022	5.033	5.044	5.019	4.999	5.015	5.014	5.019	5.017	5.017	5.007	5.004	5.007
Ab	72.1	73.9	73.1	73.2	70.5	72.7	71.8	75.9	71.1	71.8	76.4	59.5	70.6	70.4
An	2.7	4.3	3.0	3.6	1.8	3.0	3.0	6.9	2.3	3.1	8.0	1.8	2.2	1.9
Or	25.2	21.8	23.8	23.2	27.8	24.4	25.2	17.3	26.6	25.1	15.6	38.7	27.1	27.7

Table C1 continued

Unit	**PNI**	**PNI**	**PNI**	**PNI**	**PNI**	**PNI**	**PNI**	**PNI**	**PNI**	**PNI**	**PNI**	**PNI**	**PNI**
Sample	T012	T012	T012	T012	T012	T012	T012	T012	T093	T093	T093	T093	T093
No.	MI03-fsp	MI04-fsp	MI05-fsp	MI06-fsp	MI07-fsp	MI08-fsp	MI09-fsp	MI10-fsp	Fsp1	Fsp2	Fsp3	Fsp4	Fsp5
Notes	Pheno	Pheno	Pheno	Pheno	Pheno	Pheno	Pheno	Pheno	Pheno	Pheno	Pheno	Pheno	Pheno
SiO_2	67.05	65.68	66.13	64.55	64.91	67.20	65.86	67.63	66.83	67.27	66.81	65.09	66.76
TiO_2													
Al_2O_3	19.40	19.51	18.81	18.60	19.62	19.72	19.60	19.81	19.47	19.52	19.51	20.69	19.34
BaO	0.08	0.17	0.09	0.04	0.11	0.10	0.15	0.16	0.14	0.09	0.11	0.33	0.08
FeO	0.34	0.29	0.31	0.27	0.26	0.26	0.32	0.32	0.32	0.33	0.29	0.27	0.27
SrO	bdl	bdl	bdl	bdl	bdl	0.02	bdl	bdl	bdl	bdl	bdl	bdl	bdl
MgO													
CaO	0.41	0.71	0.31	0.32	0.47	0.51	0.46	0.59	0.47	0.42	0.47	1.75	0.47
Na_2O	8.06	8.45	8.50	8.66	8.56	8.30	8.15	8.28	8.47	8.24	8.48	8.82	8.37
K_2O	4.90	4.36	4.94	5.02	4.58	4.54	4.69	4.61	4.52	4.96	4.64	2.79	4.81
Total	100.25	99.17	99.09	97.46	98.52	100.64	99.23	101.40	100.22	100.83	100.31	99.74	100.10
Si	2.978	2.954	2.980	2.965	2.942	2.970	2.959	2.969	2.970	2.974	2.968	2.904	2.973
Ti												0.002	0.003
Al	1.016	1.034	0.999	1.007	1.048	1.027	1.038	1.025	1.020	1.017	1.022	1.088	1.015
Ba	0.001	0.003	0.002	0.001	0.002	0.002	0.003	0.003	0.002	0.002	0.002	0.006	0.001
Fe	0.013	0.011	0.012	0.010	0.010	0.010	0.012	0.012	0.012	0.012	0.011	0.010	0.010
Sr						0.000							
Mg													
Ca	0.019	0.034	0.015	0.016	0.023	0.024	0.022	0.028	0.022	0.020	0.022	0.084	0.022
Na	0.694	0.737	0.743	0.771	0.752	0.711	0.710	0.705	0.730	0.706	0.730	0.763	0.723
K	0.278	0.250	0.284	0.294	0.265	0.256	0.269	0.258	0.256	0.280	0.263	0.159	0.273
Sum	5.000	5.023	5.034	5.064	5.042	5.000	5.012	5.000	5.013	5.011	5.018	5.013	5.018
Ab	70.0	72.2	71.3	71.3	72.3	71.8	70.9	71.1	72.4	70.2	71.9	75.9	71.0
An	2.0	3.3	1.4	1.5	2.2	2.4	2.2	2.8	2.2	2.0	2.2	8.3	2.2
Or	28.0	24.5	27.3	27.2	25.5	25.8	26.9	26.1	25.4	27.8	25.9	15.8	26.8

Table C1 continued

Unit	**GVI**	**GVI**	**GVI**	**GVI**	**GVI**	**GVI**	**GVI**	**GVI**	**GVI**	**GVI**	**GVI**	**GVI**	**GVI**	**GVI**
Sample	TER13-1	TER13-1	TER13-1	TER13-1	TER13-1	TER13-1	TER13-1	TER13-1	TER13-1	TER13-1	TER13-1	TER13-1	TER13-1	TER13-1
No.	Fsp1	Fsp2	Fsp3	Fsp4	Fsp6	Fsp7	Fsp8	Fsp11	Fsp12	Fsp13	Fsp14	Fsp15	Fsp16	Fsp17
Notes	Pheno	Pheno	Pheno	Pheno	Pheno	Pheno	Pheno	Pheno	Pheno	Pheno	Pheno	Pheno	Pheno	Pheno
SiO_2	64.83	65.99	66.68	66.52	67.84	67.59	67.76	67.40	66.55	66.17	66.71	66.26	66.42	66.40
TiO_2														
Al_2O_3	18.44	19.71	19.46	19.42	19.62	19.85	19.75	19.67	19.65	19.48	19.40	19.35	19.34	19.70
BaO	0.08	0.20	0.20	0.24	0.18	0.18	0.21	0.22	0.19	0.21	0.22	0.19	0.13	0.31
FeO	0.32	0.41	0.31	0.34	0.30	0.31	0.34	0.33	0.32	0.33	0.29	0.31	0.30	0.27
SrO	bdl	bdl	bdl	bdl	bdl	bdl	bdl	bdl	bdl	bdl	bdl	bdl	bdl	bdl
MgO														
CaO	0.41	0.72	0.58	0.53	0.47	0.56	0.52	0.56	0.57	0.57	0.61	0.65	0.45	0.64
Na_2O	7.90	8.26	8.11	8.17	7.81	7.94	7.95	7.79	7.84	7.96	7.85	8.19	8.08	8.19
K_2O	5.07	4.56	4.96	4.81	4.95	4.91	5.08	4.82	4.57	4.73	4.71	4.82	4.94	4.65
Total	97.04	99.85	100.30	100.02	101.18	101.33	101.61	100.79	99.69	99.46	99.78	99.76	99.66	100.16
Si	2.983	2.950	2.968	2.968	2.983	2.971	2.973	2.976	2.969	2.966	2.976	2.965	2.972	2.958
Ti														
Al	1.000	1.039	1.021	1.021	1.017	1.028	1.021	1.024	1.033	1.029	1.020	1.021	1.020	1.034
Ba	0.001	0.004	0.003	0.004	0.003	0.003	0.004	0.004	0.003	0.004	0.004	0.003	0.002	0.005
Fe	0.012	0.015	0.012	0.013	0.011	0.011	0.012	0.012	0.012	0.012	0.011	0.011	0.011	0.010
Sr														
Mg														
Ca	0.020	0.034	0.028	0.025	0.022	0.026	0.025	0.026	0.027	0.028	0.029	0.031	0.022	0.031
Na	0.705	0.716	0.700	0.707	0.666	0.677	0.676	0.667	0.678	0.692	0.679	0.711	0.701	0.707
K	0.298	0.260	0.282	0.274	0.278	0.275	0.284	0.272	0.260	0.270	0.268	0.275	0.282	0.264
Sum	5.019	5.018	5.013	5.012	4.980	4.991	4.996	4.981	4.983	5.001	4.987	5.017	5.010	5.010
Ab	68.9	70.9	69.4	70.3	68.9	69.2	68.6	69.1	70.2	69.9	69.6	69.9	69.8	70.6
An	2.0	3.4	2.7	2.5	2.3	2.7	2.5	2.7	2.8	2.8	3.0	3.1	2.1	3.1
Or	29.1	25.7	27.9	27.2	28.8	28.1	28.9	28.1	26.9	27.3	27.5	27.1	28.1	26.4

Table C1 continued

Unit	**GVI**	**GVI**	**GVI**	**GVI**	**GVI**	**GVI**	**GVI**	**GVI**	**GVI**	**GVI**	**GVI**	**GVI**	**GVI**	**GVI**
Sample	TER13-1	TER13-1	TER13-1	TER13-1	TER13-1	TER13-1	TER13-1	TER13-1	TER13-1	TER13-1	TER13-1	TER13-1	TER13-1	TER13-1
No.	Fsp18	Fsp19	Fsp20	92 / 2 .	92 / 3 .	92 / 4 .	92 / 5 .	92 / 6 .	92 / 7 .	92 / 8 .	92 / 9 .	92 / 10 .	93 / 1 .	93 / 2 .
Notes	Pheno	Pheno	Pheno	Pheno	Pheno	Pheno	Pheno	Pheno	Pheno	Pheno	Pheno	Pheno	Pheno	Pheno
SiO_2	66.27	66.51	66.49	63.64	64.91	65.34	64.79	64.02	63.17	65.38	66.03	65.43	67.22	66.46
TiO_2				0.08	0.04	0.07	0.06	0.07	0.05	0.06	0.08	0.05	0.06	0.07
Al_2O_3	19.25	19.71	19.36	17.08	17.37	17.15	16.93	16.95	16.65	17.34	17.32	17.37	17.76	18.13
BaO	0.10	0.22	0.16	0.22	0.17	0.17	0.17	0.19	0.17	0.20	0.16	0.12	0.45	0.37
FeO	0.35	0.33	0.31	0.30	0.31	0.31	0.33	0.33	0.28	0.32	0.30	0.31	0.25	0.26
SrO	bdl	bdl	bdl	0.05	0.03	0.03	0.02	0.04	bdl	0.02	0.01	0.01	0.03	bdl
MgO				bdl	bdl	0.01	0.01	bdl	bdl	bdl	bdl	bdl	0.01	bdl
CaO	0.37	0.47	0.49	0.51	0.50	0.48	0.49	0.55	0.47	0.53	0.51	0.44	0.64	0.63
Na_2O	7.90	8.12	8.05	7.89	8.07	7.94	7.74	7.63	7.51	7.85	8.10	8.05	8.10	8.13
K_2O	5.15	4.85	5.00	4.73	4.81	4.94	4.93	4.81	4.73	4.93	4.81	4.98	4.60	4.46
Total	99.40	100.21	99.85	94.50	96.20	96.44	95.47	94.58	93.03	96.62	97.30	96.78	99.11	98.51
Si	2.974	2.961	2.971	3.009	3.013	3.025	3.028	3.021	3.027	3.020	3.026	3.018	3.025	3.007
Ti				0.003	0.001	0.002	0.002	0.003	0.002	0.002	0.003	0.002	0.002	0.002
Al	1.018	1.034	1.020	0.952	0.950	0.936	0.933	0.942	0.940	0.944	0.935	0.945	0.942	0.966
Ba	0.002	0.004	0.003	0.004	0.003	0.003	0.003	0.004	0.003	0.004	0.003	0.002	0.008	0.007
Fe	0.013	0.012	0.011	0.012	0.012	0.012	0.013	0.013	0.011	0.012	0.011	0.012	0.009	0.010
Sr				0.001	0.001	0.001	0.000	0.001		0.001	0.000	0.000	0.001	
Mg						0.000	0.001						0.000	
Ca	0.018	0.022	0.023	0.026	0.025	0.024	0.025	0.028	0.024	0.026	0.025	0.022	0.031	0.031
Na	0.687	0.701	0.697	0.723	0.726	0.713	0.701	0.698	0.698	0.703	0.720	0.720	0.706	0.713
K	0.295	0.275	0.285	0.285	0.285	0.292	0.294	0.290	0.289	0.290	0.281	0.293	0.264	0.257
Sum	5.008	5.010	5.010	5.016	5.016	5.007	5.000	4.999	4.995	5.002	5.004	5.014	4.988	4.993
Ab	68.7	70.2	69.3	69.9	70.1	69.3	68.8	68.8	69.0	69.0	70.2	69.5	70.6	71.2
An	1.8	2.2	2.3	2.5	2.4	2.3	2.4	2.7	2.4	2.6	2.4	2.1	3.1	3.1
Or	29.5	27.6	28.3	27.6	27.5	28.4	28.8	28.5	28.6	28.5	27.4	28.3	26.4	25.7

Table C1 continued

Unit	GVI	GVI	GVI	GVI	GVI	GVI	GVI	GVI	GVI	GVI	GVI	GVI	GVI
Sample	TER13-1	TER13-1	TER13-1	TER13-1	TER13-1	TER13-1	TER13-1	TER13-1	TER13-1	TER13-1	TER13-1	TER13-1	TER13-1
No.	93 / 3 .	93 / 4 .	93 / 5 .	93 / 6 .	93 / 7 .	93 / 8 .	93 / 9 .	93 / 10 .	94 / 1 .	96 / 3 .	96 / 4 .	96 / 5 .	96 / 7 .
Notes	Pheno	Pheno	Pheno	Pheno	Pheno	Pheno	Pheno	Pheno	Pheno	Pheno	Pheno	Pheno	Pheno
SiO_2	68.03	66.14	66.36	66.94	66.81	66.52	67.28	67.58	66.82	65.16	65.50	65.70	65.20
TiO_2	0.07	0.06	0.06	0.06	0.07	0.07	0.08	0.06	0.06	0.11	0.04	0.07	0.08
Al_2O_3	18.31	17.94	18.12	18.21	18.08	18.18	18.18	18.21	17.64	17.03	17.07	17.30	17.33
BaO	0.40	0.41	0.39	0.38	0.31	0.33	0.38	0.41	0.13	0.14	0.14	0.16	0.12
FeO	0.34	0.26	0.28	0.27	0.25	0.30	0.28	0.26	0.31	0.31	0.34	0.31	0.31
SrO	0.01	0.02	0.03	0.04	0.01	0.03	0.04	0.02	bdl	0.02	0.01	0.01	0.03
MgO	0.01	0.01	0.01	bdl	0.01	bdl	bdl	bdl	0.02	bdl	0.01	bdl	0.01
CaO	0.64	0.63	0.71	0.63	0.64	0.69	0.62	0.67	0.47	0.45	0.49	0.54	0.39
Na_2O	7.37	7.94	8.03	8.07	8.27	8.16	8.13	8.05	7.95	7.98	7.94	8.05	7.93
K_2O	4.34	4.77	4.51	4.61	4.51	4.39	4.53	4.45	5.06	5.07	4.97	4.98	5.07
Total	99.52	98.17	98.49	99.20	98.95	98.66	99.51	99.71	98.45	96.27	96.52	97.12	96.46
Si	3.031	3.008	3.005	3.009	3.009	3.005	3.013	3.017	3.025	3.024	3.029	3.021	3.018
Ti	0.002	0.002	0.002	0.002	0.002	0.002	0.003	0.002	0.002	0.004	0.001	0.002	0.003
Al	0.961	0.962	0.967	0.965	0.960	0.968	0.960	0.958	0.941	0.931	0.930	0.937	0.945
Ba	0.007	0.007	0.007	0.007	0.006	0.006	0.007	0.007	0.002	0.003	0.003	0.003	0.002
Fe	0.013	0.010	0.010	0.010	0.009	0.011	0.010	0.010	0.012	0.012	0.013	0.012	0.012
Sr	0.000	0.001	0.001	0.001	0.000	0.001	0.001	0.001		0.000	0.000	0.000	0.001
Mg	0.000	0.000	0.001		0.000				0.001		0.001		0.001
Ca	0.030	0.031	0.035	0.030	0.031	0.033	0.030	0.032	0.023	0.022	0.024	0.027	0.020
Na	0.637	0.700	0.705	0.703	0.722	0.714	0.706	0.697	0.698	0.718	0.712	0.718	0.712
K	0.247	0.277	0.260	0.264	0.259	0.253	0.259	0.253	0.292	0.300	0.293	0.292	0.299
Sum	4.929	4.997	4.992	4.990	4.999	4.993	4.987	4.977	4.996	5.015	5.007	5.013	5.012
Ab	69.7	69.5	70.5	70.5	71.4	71.4	71.0	71.0	68.9	69.0	69.1	69.3	69.1
An	3.3	3.0	3.5	3.1	3.1	3.3	3.0	3.3	2.2	2.1	2.4	2.6	1.9
Or	27.0	27.5	26.1	26.5	25.6	25.3	26.0	25.8	28.8	28.8	28.5	28.2	29.0

Table C1 continued

Unit	**GVI**	**GVI**	**GVI**	**GVI**	**GVI**	**GVI**	**GVI**	**GVI**	**GVI**	**GVI**	**GVI**	**GVI**	**GVI**
Sample	TER13-1	TER13-1	TER13-1	TER13-1	TER13-1	TER13-1	TER13-1	TER13-1	TER13-1	TER13-1	TER13-1	TER13-1	TER13-1
No.	96 / 8 .	96 / 9 .	96 / 10 .	103 / 1 .	103 / 2 .	103 / 3 .	103 / 4 .	103 / 5 .	103 / 6 .	103 / 7 .	103 / 8 .	103 / 9 .	103 / 10 .
Notes	Pheno	Pheno	Pheno	Pheno	Pheno	Pheno	Pheno	Pheno	Pheno	Pheno	Pheno	Pheno	Pheno
SiO_2	65.61	65.64	67.47	65.57	67.40	66.63	66.83	67.99	67.84	67.56	67.86	67.60	67.82
TiO_2	0.08	0.05	0.07	0.10	0.08	0.09	0.06	0.08	0.07	0.07	0.07	0.05	0.06
Al_2O_3	17.62	18.34	17.91	18.06	17.97	17.99	17.82	17.87	17.74	18.18	18.34	18.42	18.44
BaO	0.14	0.13	0.14	0.14	0.16	0.16	0.14	0.16	0.17	0.17	0.15	0.20	0.17
FeO	0.28	0.32	0.30	0.44	0.35	0.32	0.35	0.36	0.33	0.31	0.30	0.32	0.33
SrO	0.02	0.01	0.03	bdl	0.02	0.04	0.01	0.01	0.03	0.04	bdl	0.04	0.03
MgO	bdl	0.01	bdl	0.02	0.01	bdl	bdl	bdl	bdl	bdl	bdl	bdl	0.01
CaO	0.42	0.49	0.45	0.61	0.52	0.41	0.41	0.41	0.51	0.52	0.54	0.58	0.61
Na_2O	7.91	7.89	7.93	7.69	8.06	8.02	7.82	7.81	7.96	7.94	8.07	8.10	8.14
K_2O	5.10	5.08	5.01	4.67	4.93	5.02	5.14	5.22	4.99	4.98	4.90	4.78	4.78
Total	97.15	97.96	99.32	97.28	99.49	98.67	98.57	99.91	99.63	99.76	100.22	100.08	100.38
Si	3.014	2.991	3.025	3.002	3.019	3.012	3.022	3.032	3.033	3.017	3.015	3.009	3.009
Ti	0.003	0.002	0.002	0.003	0.003	0.003	0.002	0.003	0.002	0.002	0.002	0.002	0.002
Al	0.954	0.985	0.947	0.974	0.949	0.959	0.950	0.939	0.935	0.957	0.961	0.966	0.964
Ba	0.003	0.002	0.003	0.002	0.003	0.003	0.002	0.003	0.003	0.003	0.003	0.004	0.003
Fe	0.011	0.012	0.011	0.017	0.013	0.012	0.013	0.013	0.012	0.012	0.011	0.012	0.012
Sr	0.000	0.000	0.001		0.001	0.001	0.000	0.000	0.001	0.001		0.001	0.001
Mg		0.001		0.001	0.001								
Ca	0.021	0.024	0.022	0.030	0.025	0.020	0.020	0.020	0.025	0.025	0.026	0.028	0.029
Na	0.705	0.697	0.690	0.682	0.700	0.703	0.685	0.675	0.690	0.687	0.695	0.699	0.700
K	0.299	0.295	0.286	0.273	0.282	0.290	0.297	0.297	0.284	0.284	0.278	0.271	0.271
Sum	5.008	5.010	4.987	4.985	4.994	5.002	4.992	4.982	4.985	4.988	4.989	4.991	4.992
Ab	68.8	68.6	69.1	69.3	69.6	69.4	68.4	68.1	69.1	69.0	69.6	70.0	70.0
An	2.0	2.3	2.2	3.0	2.5	1.9	2.0	2.0	2.5	2.5	2.6	2.8	2.9
Or	29.2	29.1	28.7	27.7	28.0	28.6	29.6	29.9	28.5	28.5	27.8	27.2	27.1

Table C1 continued

Unit	**Ign-i**	**Ign-i**	**Ign-i**	**Ign-i**	**Ign-i**	**Ign-i**	**Ign-i**	**Ign-i**	**Ign-i**	**Ign-i**	**Ign-i**	**Ign-i**	**Ign-i**
Sample	T001	T001	T001	T001	T001	T001	T001	T001	T001	T001	T001	T001	T001
No.	Fsp1	Fsp2	Fsp3	Fsp4	Fsp5	Fsp6	Fsp7	Fsp8	Fsp9	Fsp10	Fsp11	Fsp12	Fsp13
Notes	Pheno	Pheno	Pheno	Pheno	Pheno	Pheno	Pheno	Pheno	Pheno	Pheno	Pheno	Pheno	Pheno
SiO_2	65.62	67.34	66.72	66.77	66.66	66.42	65.68	65.42	66.80	65.94	67.31	67.30	67.30
TiO_2													
Al_2O_3	19.15	19.13	19.12	19.05	18.93	18.99	18.86	18.77	18.85	19.15	19.11	19.03	19.33
BaO	0.02	bdl	bdl	bdl	0.03	bdl	bdl	0.02	0.01	0.01	0.02	bdl	0.08
FeO	0.29	0.31	0.28	0.30	0.28	0.29	0.29	0.32	0.25	0.28	0.27	0.30	0.27
SrO	bdl	bdl	bdl	0.04	bdl	bdl	bdl	bdl	0.01	bdl	bdl	bdl	bdl
MgO													
CaO	0.13	0.13	0.24	0.13	0.11	0.11	0.11	0.06	0.09	0.10	0.13	0.12	0.20
Na_2O	7.50	7.57	7.78	7.48	7.59	7.91	7.75	7.65	7.65	7.83	7.64	7.54	7.93
K_2O	6.16	6.35	5.96	6.25	6.09	5.83	6.08	6.13	6.16	6.18	6.07	6.14	5.76
Total	98.87	100.83	100.10	100.02	99.69	99.56	98.77	98.37	99.83	99.49	100.55	100.43	100.86
Si	2.971	2.988	2.981	2.986	2.989	2.982	2.978	2.979	2.992	2.970	2.991	2.994	2.981
Ti													
Al	1.022	1.000	1.007	1.004	1.001	1.005	1.008	1.007	0.995	1.017	1.001	0.998	1.009
Ba	0.000				0.001			0.000	0.000	0.000	0.000		0.001
Fe	0.011	0.012	0.010	0.011	0.011	0.011	0.011	0.012	0.009	0.011	0.010	0.011	0.010
Sr				0.001					0.000				
Mg	0.000	0.000	0.000	0.000	0.000	0.000	0.000	0.000	0.000	0.000	0.000	0.000	0.000
Ca	0.007	0.006	0.011	0.006	0.005	0.005	0.005	0.003	0.004	0.005	0.006	0.006	0.009
Na	0.658	0.651	0.674	0.649	0.660	0.689	0.681	0.675	0.664	0.684	0.658	0.650	0.681
K	0.356	0.359	0.340	0.357	0.348	0.334	0.352	0.356	0.352	0.355	0.344	0.348	0.326
Sum	5.025	5.017	5.023	5.014	5.015	5.026	5.035	5.033	5.018	5.041	5.010	5.007	5.018
Ab	64.5	64.0	65.8	64.1	65.1	67.0	65.6	65.3	65.1	65.5	65.3	64.7	67.0
An	0.6	0.6	1.1	0.6	0.5	0.5	0.5	0.3	0.4	0.4	0.6	0.6	0.9
Or	34.9	35.3	33.1	35.3	34.4	32.5	33.9	34.4	34.5	34.0	34.1	34.7	32.0

Table C1 continued

Unit	**Ign-i**	**Ign-i**	**Ign-i**	**Ign-i**	**Ign-i**	**Ign-i**	**Ign-i**	**Ign-i**	**Ign-i**	**Ign-i**	**Ign-i**	**Ign-i**
Sample	T001	T001	T001	T001	T001	T001	T001	T001	T001	T001	T001	T001
No.	Fsp14	Fsp15	MI01-fsp	Fsp16	Fsp17	Fsp18	Fsp19	Fsp20	Fsp21	Fsp22	Fsp23	Fsp24
Notes	Pheno	Pheno	Pheno	Pheno	Pheno	Pheno	Pheno	Pheno	Pheno	Pheno	Pheno	Pheno
SiO_2	67.66	66.98	65.84	65.40	65.79	66.33	65.76	66.55	66.21	65.80	66.77	64.23
TiO_2												
Al_2O_3	19.11	19.08	18.58	20.73	19.79	20.10	20.72	19.65	18.82	20.43	19.70	21.17
BaO	0.01	0.01	bdl	0.85	0.32	0.48	0.71	0.24	0.01	0.63	0.24	1.25
FeO	0.29	0.26	0.39	0.24	0.22	0.22	0.18	0.21	0.33	0.23	0.22	0.29
SrO	bdl	bdl	bdl	0.01	bdl	bdl	0.01	bdl	bdl	bdl	bdl	bdl
MgO												
CaO	0.09	0.14	0.07	1.63	0.94	0.98	1.43	0.70	0.11	1.33	0.73	2.22
Na_2O	7.55	7.79	7.89	9.40	8.50	8.98	8.76	8.53	7.50	9.17	9.09	9.25
K_2O	6.15	5.95	5.92	2.07	4.28	3.50	3.14	4.22	6.07	2.84	3.28	1.80
Total	100.86	100.21	98.69	100.32	99.84	100.59	100.71	100.11	99.05	100.44	100.04	100.21
Si	2.996	2.987	2.987	2.904	2.943	2.939	2.913	2.961	2.989	2.920	2.962	2.869
Ti												
Al	0.997	1.003	0.993	1.085	1.043	1.050	1.082	1.030	1.001	1.068	1.030	1.114
Ba	0.000	0.000		0.015	0.006	0.008	0.012	0.004	0.000	0.011	0.004	0.022
Fe	0.011	0.010	0.015	0.009	0.008	0.008	0.007	0.008	0.013	0.009	0.008	0.011
Sr				0.000			0.000					
Mg	0.000	0.000	0.000	0.000	0.000	0.000	0.000	0.000	0.000	0.000	0.000	0.000
Ca	0.004	0.007	0.003	0.078	0.045	0.047	0.068	0.034	0.005	0.063	0.035	0.106
Na	0.648	0.673	0.694	0.809	0.737	0.771	0.752	0.736	0.656	0.789	0.782	0.801
K	0.347	0.338	0.343	0.117	0.244	0.198	0.177	0.240	0.350	0.161	0.186	0.103
Sum	5.003	5.018	5.035	5.017	5.026	5.021	5.011	5.012	5.014	5.021	5.007	5.026
Ab	64.8	66.1	66.7	80.6	71.8	75.9	75.4	72.9	64.9	77.9	78.0	79.3
An	0.4	0.7	0.3	7.7	4.4	4.6	6.8	3.3	0.5	6.3	3.5	10.5
Or	34.7	33.2	32.9	11.7	23.8	19.5	17.8	23.7	34.6	15.9	18.5	10.2

Table C2: Clinopyroxene analyses from the Terceira ignimbrite formations and associated lithologies

Unit	**LAI**	**LAI**	**LAI**	**LAI**	**LAI**	**LAI**	**LAI**	**LAI**	**LAI**	**LAI**	**LAI**	**LAI**	**LAI**	**LAI**
Sample	TER1-1	TER1-1	TER1-1	TER1-1	TER1-1	TER1-1	TER1-1	TER1-1	TER1-1	TER1-1	TER1-1	TER1-1	TER1-1	TER1-1
No.	1 / 1 .	2 / 1 .	3 / 1 .	4 / 1 .	5 / 1 .	7 / 1 .	8 / 1 .	9 / 1 .	10 / 1 .	11 / 1 .	12 / 1 .	13 / 1 .	14 / 1 .	15 / 1 .
Notes	Pheno	Pheno	Pheno	Pheno	Pheno	Pheno	Pheno	Pheno	Pheno	Pheno	Pheno	Pheno	Pheno	Pheno
SiO_2	50.52	51.52	51.37	50.44	50.62	50.76	50.61	50.08	50.66	50.50	48.80	50.59	50.91	50.43
TiO_2	0.39	0.39	0.38	0.34	0.43	0.65	0.39	0.48	0.38	0.40	1.68	0.40	0.40	0.37
Al_2O_3	1.86	0.46	0.48	0.38	0.47	0.69	0.57	0.41	0.44	0.46	2.91	0.40	0.42	0.41
Cr_2O_3	0.01	0.02	bdl	0.04	bdl	0.01	bdl	0.01	bdl	bdl	bdl	0.04	0.01	0.02
FeO	15.94	15.58	15.85	17.69	16.05	16.13	15.88	19.48	15.82	15.72	11.68	16.99	16.90	16.43
MnO	1.33	1.35	1.34	1.39	1.36	1.46	1.35	1.69	1.36	1.37	0.64	1.45	1.41	1.38
MgO	10.05	10.47	10.56	8.98	10.20	10.39	9.96	8.51	10.30	10.26	12.33	9.77	9.53	9.75
CaO	19.89	20.04	19.82	19.34	19.60	18.58	19.71	18.02	19.71	19.21	19.86	19.18	19.77	19.77
Na_2O	0.87	0.78	0.82	1.00	0.92	0.94	0.93	1.09	0.85	0.82	0.76	0.88	0.92	0.88
K_2O	bdl	bdl	0.01	bdl	bdl	0.05	0.07	0.01	bdl	0.01	0.06	0.01	0.01	bdl
Total	100.86	100.61	100.64	99.61	99.67	99.66	99.47	99.78	99.50	98.75	98.72	99.69	100.27	99.45
Si	1.916	1.960	1.953	1.955	1.945	1.951	1.949	1.949	1.949	1.959	1.859	1.953	1.954	1.948
Ti	0.011	0.011	0.011	0.010	0.012	0.019	0.011	0.014	0.011	0.012	0.048	0.012	0.012	0.011
Al	0.083	0.020	0.022	0.017	0.021	0.031	0.026	0.019	0.020	0.021	0.130	0.018	0.019	0.019
Cr	0.000	0.001		0.001		0.000		0.000				0.001	0.000	0.001
Fe^{2+}	0.379	0.403	0.393	0.446	0.384	0.417	0.387	0.497	0.386	0.410	0.258	0.430	0.424	0.403
Fe^{3+}	0.126	0.093	0.111	0.127	0.132	0.101	0.125	0.137	0.123	0.100	0.114	0.118	0.119	0.128
Mn	0.043	0.044	0.043	0.046	0.044	0.047	0.044	0.056	0.044	0.045	0.021	0.047	0.046	0.045
Mg	0.568	0.594	0.599	0.519	0.585	0.595	0.572	0.494	0.591	0.593	0.700	0.562	0.545	0.561
Ca	0.808	0.817	0.807	0.803	0.807	0.765	0.813	0.751	0.813	0.798	0.811	0.793	0.813	0.818
Na	0.064	0.057	0.061	0.075	0.069	0.070	0.069	0.082	0.063	0.062	0.056	0.066	0.068	0.066
K			0.000			0.002	0.003	0.000		0.000	0.003	0.000	0.001	
Sum	4.000	4.000	4.000	4.000	4.000	4.000	4.000	4.000	4.000	4.000	4.000	4.000	4.000	4.000
Aegirine	6.4	5.7	6.1	7.5	6.9	7.0	6.9	8.2	6.3	6.2	5.6	6.6	6.8	6.6
Ferri-Tschermak	3.1	1.8	2.5	2.6	3.2	1.5	2.8	2.7	3.0	1.9	2.9	2.6	2.5	3.1
Jadeite	0.0	0.0	0.0	0.0	0.0	0.0	0.0	0.0	0.0	0.0	0.0	0.0	0.0	0.0
Ti-Aegirine	0.0	0.0	0.0	0.0	0.0	0.0	0.0	0.0	0.0	0.0	0.0	0.0	0.0	0.0
Ti-Tschermak	1.1	1.0	1.1	0.9	1.1	1.6	1.1	0.9	1.0	1.1	4.8	0.9	0.9	0.9
Al-Tschermak	0.0	0.0	0.0	0.0	0.0	0.0	0.0	0.0	0.0	0.0	0.0	0.0	0.0	0.0
Diopside	44.0	45.0	44.6	39.5	44.1	41.2	44.2	33.7	44.7	43.5	52.5	41.0	41.8	43.3
Hedenbergite	32.6	33.8	32.5	37.4	32.3	32.2	33.2	37.7	32.6	33.3	20.9	34.8	36.0	34.5
Enstatite	6.4	7.2	7.6	6.2	7.2	9.2	6.5	7.8	7.2	7.9	8.8	7.6	6.4	6.4
Ferrosilite	4.8	5.4	5.5	5.9	5.2	7.2	4.9	8.8	5.2	6.1	3.5	6.5	5.5	5.1

Table C2 continued

Unit	**LAI**	**LAI**	**LAI**	**LAI**	**LAI**	**LAI**	**LAI**	**LAI**	**LAI**	**LAI**	**LAI**	**LAI**	**LAI**	**LAI**
Sample	TER1-1	TER1-1	TER1-1	TER1-1	TER1-2	TER1-2	TER1-2	TER1-2	TER1-2	TER1-2	TER1-2	TER3-1	TER3-1	TER3-1
No.	16 / 1 .	17 / 1 .	19 / 1 .	20 / 1 .	85 / 1 .	96 / 1 .	95 / 1 .	86 / 1 .	82 / 1 .	84 / 1 .	83 / 1 .	127 / 1 .	128 / 1 .	129 / 1 .
Notes	Pheno	Pheno	Pheno	Pheno	Pheno	Pheno	Pheno	Pheno	Pheno	Pheno	Pheno	Pheno	Pheno	Pheno
SiO_2	50.59	50.71	48.71	51.03	51.04	51.35	51.41	51.50	51.52	51.57	51.60	50.86	50.99	50.07
TiO_2	0.40	0.35	1.57	0.38	0.47	0.58	0.39	0.59	0.47	0.52	0.47	0.53	0.40	0.47
Al_2O_3	0.44	0.51	2.72	0.39	0.53	0.73	0.42	0.76	0.63	0.70	0.67	0.61	0.49	0.50
Cr_2O_3	0.01	0.01	0.02	0.01	bdl	0.01	bdl	bdl	0.01	bdl	0.01			bdl
FeO	15.71	16.01	10.88	16.25	16.06	15.33	15.62	13.40	12.99	13.77	13.31	14.75	15.20	15.41
MnO	1.37	1.39	0.58	1.36	1.41	1.26	1.33	1.13	1.09	1.12	1.11	1.29	1.36	1.35
MgO	10.46	10.04	12.66	10.03	10.40	10.67	10.30	12.15	12.23	11.57	12.12	11.40	10.70	10.78
CaO	19.71	19.58	20.99	19.65	19.02	19.66	20.02	19.58	20.19	20.00	19.92	19.73	20.04	20.02
Na_2O	0.87	0.90	0.68	0.91	0.79	0.86	0.78	0.71	0.69	0.74	0.68	0.72	0.82	0.75
K_2O	bdl	0.04	0.01	0.01	0.01	0.01	0.02	bdl	bdl	bdl	0.01	0.01	bdl	bdl
Total	99.57	99.53	98.81	100.02	99.71	100.47	100.29	99.80	99.82	100.00	99.89	99.90	99.99	99.36
Si	1.943	1.952	1.849	1.957	1.962	1.953	1.963	1.954	1.951	1.958	1.955	1.939	1.947	1.925
Ti	0.012	0.010	0.045	0.011	0.013	0.017	0.011	0.017	0.013	0.015	0.013	0.015	0.012	0.014
Al	0.020	0.023	0.121	0.018	0.024	0.033	0.019	0.034	0.028	0.031	0.030	0.027	0.022	0.022
Cr	0.000	0.000	0.001	0.000		0.000			0.000		0.000	0.000	0.000	
Fe^{2+}	0.370	0.395	0.204	0.406	0.432	0.395	0.408	0.348	0.318	0.359	0.340	0.351	0.365	0.340
Fe^{3+}	0.134	0.121	0.141	0.115	0.084	0.092	0.091	0.077	0.093	0.078	0.082	0.119	0.121	0.156
Mn	0.045	0.045	0.019	0.044	0.046	0.041	0.043	0.036	0.035	0.036	0.036	0.042	0.044	0.044
Mg	0.599	0.576	0.716	0.574	0.596	0.605	0.586	0.687	0.691	0.655	0.685	0.648	0.609	0.618
Ca	0.811	0.808	0.854	0.807	0.783	0.801	0.819	0.796	0.819	0.814	0.809	0.806	0.820	0.825
Na	0.065	0.067	0.050	0.068	0.059	0.063	0.058	0.052	0.051	0.054	0.050	0.053	0.060	0.056
K		0.002	0.000	0.001	0.000	0.000	0.001				0.000	0.000		
Sum	4.000	4.000	4.000	4.000	4.000	4.000	4.000	4.000	4.000	4.000	4.000	4.000	4.000	4.000
Aegirine	6.5	6.7	5.0	6.8	5.9	6.3	5.8	5.2	5.1	5.4	5.0	5.3	6.0	5.6
Ferri-Tschermak	3.5	2.7	4.6	2.4	1.3	1.4	1.6	1.3	2.1	1.2	1.6	3.3	3.0	5.0
Jadeite	0.0	0.0	0.0	0.0	0.0	0.0	0.0	0.0	0.0	0.0	0.0	0.0	0.0	0.0
Ti-Aegirine	0.0	0.0	0.0	0.0	0.0	0.0	0.0	0.0	0.0	0.0	0.0	0.0	0.0	0.0
Ti-Tschermak	1.0	1.0	4.5	0.9	1.2	1.6	0.9	1.7	1.3	1.5	1.3	1.4	1.1	1.1
Al-Tschermak	0.0	0.0	0.0	0.0	0.0	0.0	0.0	0.0	0.0	0.0	0.0	0.0	0.0	0.0
Diopside	45.3	43.7	58.2	43.4	42.1	44.8	44.9	49.2	51.9	49.1	50.3	47.3	46.6	47.1
Hedenbergite	31.4	33.4	18.1	34.1	33.8	32.2	34.5	27.5	26.6	29.6	27.6	28.7	31.3	29.3
Enstatite	7.3	7.0	6.7	7.0	8.7	7.9	6.9	9.8	8.6	8.2	9.1	8.8	7.2	7.3
Ferrosilite	5.1	5.3	2.1	5.5	7.0	5.7	5.3	5.5	4.4	5.0	5.0	5.3	4.8	4.6

Table C2 continued

Unit	LAI	LAI	LAI	LAI	LAI	LAI	LAI	LAI	LAI	LAI	LAI	LAI	LAI	LAI
Sample	TER3-1	TER3-1	TER3-1	TER3-1	TER3-1	TER3-1	TER3-1	TER3-1	TER3-1	TER3-1	TER1-1	TER1-1	TER1-1	TER1-1
No.	130 / 1 .	131 / 1 .	132 / 1 .	133 / 1 .	134 / 1 .	135 / 1 .	137 / 1 .	138 / 1 .	139 / 1 .	140 / 1 .	1 / 1 .	2 / 1 .	3 / 1 .	4 / 1 .
Notes	Pheno	Pheno	Pheno	Pheno	Pheno	Pheno	Pheno	Pheno	Pheno	Pheno	Pheno	Pheno	Pheno	Pheno
SiO_2	50.04	50.38	49.48	50.73	51.06	51.55	51.48	51.36	51.33	51.31	50.52	51.52	51.37	50.44
TiO_2	0.47	0.39	0.38	0.37	0.44	0.43	0.46	0.47	0.48	0.43	0.39	0.39	0.38	0.34
Al_2O_3	0.52	0.52	0.44	0.59	0.57	0.50	0.57	0.65	0.62	0.56	1.86	0.46	0.48	0.38
Cr_2O_3	0.01	0.02	0.02	0.02	bdl	0.01	0.04	bdl	0.02	0.01	0.01	0.02	bdl	0.04
FeO	15.18	14.77	16.02	16.08	14.19	14.61	13.77	13.65	13.85	14.11	15.94	15.58	15.85	17.69
MnO	1.31	1.25	1.44	1.37	1.21	1.23	1.18	1.17	1.21	1.23	1.33	1.35	1.34	1.39
MgO	10.72	11.05	10.48	10.31	11.52	11.40	11.97	12.07	11.86	11.56	10.05	10.47	10.56	8.98
CaO	20.44	20.47	20.14	20.00	20.38	20.47	20.51	20.24	20.12	20.42	19.89	20.04	19.82	19.34
Na_2O	0.76	0.69	0.80	0.87	0.70	0.69	0.72	0.71	0.75	0.72	0.87	0.78	0.82	1.00
K_2O	bdl	0.01	bdl	0.01	bdl	bdl	bdl	bdl	0.01	0.01	bdl	bdl	0.01	bdl
Total	99.46	99.55	99.20	100.34	100.07	100.90	100.70	100.33	100.25	100.36	100.86	100.61	100.64	99.61
Si	1.921	1.929	1.909	1.936	1.939	1.945	1.938	1.939	1.942	1.942	1.916	1.960	1.953	1.955
Ti	0.014	0.011	0.011	0.011	0.012	0.012	0.013	0.013	0.014	0.012	0.011	0.011	0.011	0.010
Al	0.024	0.023	0.020	0.027	0.025	0.022	0.025	0.029	0.028	0.025	0.083	0.020	0.022	0.017
Cr	0.000	0.001	0.001	0.001		0.000	0.001		0.000	0.000	0.000	0.001		0.001
Fe^{2+}	0.324	0.326	0.317	0.368	0.327	0.348	0.310	0.312	0.321	0.328	0.379	0.403	0.393	0.446
Fe^{3+}	0.164	0.147	0.200	0.145	0.124	0.113	0.124	0.119	0.117	0.119	0.126	0.093	0.111	0.127
Mn	0.043	0.041	0.047	0.044	0.039	0.039	0.038	0.037	0.039	0.039	0.043	0.044	0.043	0.046
Mg	0.614	0.631	0.603	0.587	0.652	0.641	0.672	0.679	0.669	0.653	0.568	0.594	0.599	0.519
Ca	0.841	0.840	0.832	0.818	0.829	0.827	0.827	0.819	0.816	0.828	0.808	0.817	0.807	0.803
Na	0.057	0.052	0.060	0.064	0.052	0.051	0.052	0.052	0.055	0.053	0.064	0.057	0.061	0.075
K		0.000		0.000					0.000	0.000			0.000	
Sum	4.000	4.000	4.000	4.000	4.000	4.000	4.000	4.000	4.000	4.000	4.000	4.000	4.000	4.000
Aegirine	5.7	5.2	6.0	6.4	5.2	5.1	5.2	5.2	5.5	5.3	6.4	5.7	6.1	7.5
Ferri-Tschermak	5.3	4.8	7.0	4.0	3.6	3.1	3.6	3.3	3.1	3.3	3.1	1.8	2.5	2.6
Jadeite	0.0	0.0	0.0	0.0	0.0	0.0	0.0	0.0	0.0	0.0	0.0	0.0	0.0	0.0
Ti-Aegirine	0.0	0.0	0.0	0.0	0.0	0.0	0.0	0.0	0.0	0.0	0.0	0.0	0.0	0.0
Ti-Tschermak	1.2	1.1	1.0	1.1	1.2	1.1	1.3	1.3	1.4	1.2	1.1	1.0	1.1	0.9
Al-Tschermak	0.0	0.0	0.0	0.0	0.0	0.0	0.0	0.0	0.0	0.0	0.0	0.0	0.0	0.0
Diopside	48.6	49.4	46.9	45.0	50.0	48.9	51.3	51.0	50.1	50.1	44.0	45.0	44.6	39.5
Hedenbergite	29.0	28.7	28.3	31.7	28.1	29.6	26.5	26.2	27.0	28.2	32.6	33.8	32.5	37.4
Enstatite	6.4	6.9	6.7	6.8	7.6	7.6	7.9	8.5	8.4	7.6	6.4	7.2	7.6	6.2
Ferrosilite	3.8	4.0	4.0	4.8	4.3	4.6	4.1	4.4	4.5	4.3	4.8	5.4	5.5	5.9

Table C2 continued

Unit	**LAI**	**LAI**	**LAI**	**LAI**	**LAI**	**LAI**	**LAI**	**LAI**	**LAI**	**LAI**	**LAI**	**LAI**	**LAI**	**LAI**
Sample	TER1-1	TER1-1	TER1-1	TER1-1	TER1-1	TER1-1	TER1-1	TER1-1	TER1-1	TER1-1	TER4-1	TER4-1	TER4-1	TER4-1
No.	5 / 1 .	7 / 1 .	8 / 1 .	9 / 1 .	10 / 1 .	11 / 1 .	12 / 1 .	13 / 1 .	14 / 1 .	15 / 1 .	99 / 1 .	100 / 1 .	101 / 1 .	102 / 1 .
Notes	Pheno	Pheno	Pheno	Pheno	Pheno	Pheno	Pheno	Pheno	Pheno	Pheno	Pheno	Pheno	Pheno	Pheno
SiO_2	50.62	50.76	50.61	50.08	50.66	50.50	48.80	50.59	50.91	50.43	50.39	50.65	50.94	51.77
TiO_2	0.43	0.65	0.39	0.48	0.38	0.40	1.68	0.40	0.40	0.37	0.45	0.50	0.48	0.39
Al_2O_3	0.47	0.69	0.57	0.41	0.44	0.46	2.91	0.40	0.42	0.41	0.53	0.60	0.52	0.47
Cr_2O_3	bdl	0.01	bdl	0.01	bdl	bdl	bdl	0.04	0.01	0.02	0.02	0.01	0.01	0.01
FeO	16.05	16.13	15.88	19.48	15.82	15.72	11.68	16.99	16.90	16.43	15.40	14.62	15.37	15.66
MnO	1.36	1.46	1.35	1.69	1.36	1.37	0.64	1.45	1.41	1.38	1.44	1.29	1.30	1.36
MgO	10.20	10.39	9.96	8.51	10.30	10.26	12.33	9.77	9.53	9.75	10.99	11.46	10.92	10.70
CaO	19.60	18.58	19.71	18.02	19.71	19.21	19.86	19.18	19.77	19.77	19.62	19.90	20.18	20.40
Na_2O	0.92	0.94	0.93	1.09	0.85	0.82	0.76	0.88	0.92	0.88	0.77	0.73	0.79	0.81
K_2O	bdl	0.05	0.07	0.01	bdl	0.01	0.06	0.01	0.01	bdl	0.01	bdl	0.01	bdl
Total	99.67	99.66	99.47	99.78	99.50	98.75	98.72	99.69	100.27	99.45	99.61	99.76	100.52	101.57
Si	1.945	1.951	1.949	1.949	1.949	1.959	1.859	1.953	1.954	1.948	1.931	1.932	1.935	1.949
Ti	0.012	0.019	0.011	0.014	0.011	0.012	0.048	0.012	0.012	0.011	0.013	0.014	0.014	0.011
Al	0.021	0.031	0.026	0.019	0.020	0.021	0.130	0.018	0.019	0.019	0.024	0.027	0.023	0.021
Cr		0.000		0.000				0.001	0.000	0.001	0.001	0.000	0.000	0.000
Fe^{2+}	0.384	0.417	0.387	0.497	0.386	0.410	0.258	0.430	0.424	0.403	0.349	0.330	0.350	0.376
Fe^{3+}	0.132	0.101	0.125	0.137	0.123	0.100	0.114	0.118	0.119	0.128	0.144	0.136	0.138	0.118
Mn	0.044	0.047	0.044	0.056	0.044	0.045	0.021	0.047	0.046	0.045	0.047	0.042	0.042	0.044
Mg	0.585	0.595	0.572	0.494	0.591	0.593	0.700	0.562	0.545	0.561	0.628	0.652	0.619	0.601
Ca	0.807	0.765	0.813	0.751	0.813	0.798	0.811	0.793	0.813	0.818	0.806	0.813	0.821	0.823
Na	0.069	0.070	0.069	0.082	0.063	0.062	0.056	0.066	0.068	0.066	0.057	0.054	0.058	0.059
K		0.002	0.003	0.000		0.000	0.003	0.000	0.001		0.000		0.000	
Sum	4.000	4.000	4.000	4.000	4.000	4.000	4.000	4.000	4.000	4.000	4.000	4.000	4.000	4.000
Aegirine	6.9	7.0	6.9	8.2	6.3	6.2	5.6	6.6	6.8	6.6	5.7	5.4	5.8	5.9
Ferri-Tschermak	3.2	1.5	2.8	2.7	3.0	1.9	2.9	2.6	2.5	3.1	4.4	4.1	4.0	2.9
Jadeite	0.0	0.0	0.0	0.0	0.0	0.0	0.0	0.0	0.0	0.0	0.0	0.0	0.0	0.0
Ti-Aegirine	0.0	0.0	0.0	0.0	0.0	0.0	0.0	0.0	0.0	0.0	0.0	0.0	0.0	0.0
Ti-Tschermak	1.1	1.6	1.1	0.9	1.0	1.1	4.8	0.9	0.9	0.9	1.2	1.3	1.2	1.0
Al-Tschermak	0.0	0.0	0.0	0.0	0.0	0.0	0.0	0.0	0.0	0.0	0.0	0.0	0.0	0.0
Diopside	44.1	41.2	44.2	33.7	44.7	43.5	52.5	41.0	41.8	43.3	46.0	48.3	47.1	46.1
Hedenbergite	32.3	32.2	33.2	37.7	32.6	33.3	20.9	34.8	36.0	34.5	29.0	27.6	29.8	32.2
Enstatite	7.2	9.2	6.5	7.8	7.2	7.9	8.8	7.6	6.4	6.4	8.4	8.4	7.4	7.0
Ferrosilite	5.2	7.2	4.9	8.8	5.2	6.1	3.5	6.5	5.5	5.1	5.3	4.8	4.7	4.9

Table C2 continued

Unit	**LAI**	**LAI**	**LAI**	**LAI**	**LAI**	**LAI**	**LAI**	**LAI**	**LAI**	**LAI**	**LAI**	**LAI**	**LAI**	**LAI**
Sample	TER4-1	TER4-1	TER4-1	TER4-1	TER4-1	TER4-1	TER4-1	TER4-1	TER4-1	TER4-1	TER4-1	TER4-1	TER4-1	TER4-1
No.	103 / 1 .	104 / 1 .	105 / 1 .	106 / 1 .	107 / 1 .	108 / 1 .	109 / 1 .	110 / 1 .	111 / 1 .	113 / 1 .	114 / 1 .	115 / 1 .	116 / 1 .	117 / 1 .
Notes	Pheno	Pheno	Pheno	Pheno	Pheno	Pheno	Pheno	Pheno	Pheno	Pheno	Pheno	Pheno	Pheno	Pheno
SiO_2	51.51	51.43	50.40	50.76	51.03	50.66	50.50	51.01	50.83	51.44	50.66	51.36	50.59	50.82
TiO_2	0.39	0.35	0.39	0.40	0.38	0.40	0.37	0.41	0.44	0.40	0.38	0.40	0.72	0.38
Al_2O_3	0.40	0.44	0.42	0.42	0.42	0.42	0.41	0.51	0.50	0.40	1.18	0.45	2.30	0.42
Cr_2O_3	0.01	0.02	0.02	0.01	0.02	0.01	0.01	0.02	0.02	0.01	0.03	bdl	0.02	0.01
FeO	16.12	16.68	16.73	17.45	16.31	16.67	16.41	15.03	15.70	16.19	16.12	17.33	15.30	16.20
MnO	1.40	1.42	1.38	1.52	1.40	1.42	1.40	1.31	1.34	1.35	1.41	1.39	1.37	1.36
MgO	10.31	9.92	9.94	9.68	10.21	10.02	10.13	11.09	10.51	10.30	9.88	9.24	9.70	10.31
CaO	20.20	19.79	20.17	19.38	19.83	19.64	19.91	20.21	20.09	20.18	19.65	19.93	17.93	20.05
Na_2O	0.87	0.84	0.86	0.90	0.88	0.91	0.91	0.70	0.75	0.88	0.77	0.98	1.59	0.87
K_2O	bdl	bdl	bdl	0.01	bdl	bdl	bdl	0.01	bdl	bdl	0.01	bdl	0.32	0.01
Total	101.22	100.88	100.31	100.52	100.47	100.16	100.04	100.30	100.18	101.18	100.10	101.08	99.84	100.43
Si	1.950	1.960	1.930	1.945	1.947	1.942	1.935	1.940	1.942	1.948	1.942	1.959	1.928	1.939
Ti	0.011	0.010	0.011	0.011	0.011	0.012	0.011	0.012	0.013	0.012	0.011	0.011	0.021	0.011
Al	0.018	0.020	0.019	0.019	0.019	0.019	0.018	0.023	0.023	0.018	0.053	0.020	0.103	0.019
Cr	0.000	0.001	0.001	0.000	0.000	0.000	0.000	0.000	0.001	0.000	0.001		0.001	0.000
Fe^{2+}	0.387	0.428	0.374	0.424	0.391	0.393	0.369	0.354	0.379	0.386	0.420	0.441	0.355	0.370
Fe^{3+}	0.123	0.103	0.162	0.135	0.130	0.142	0.157	0.124	0.123	0.127	0.097	0.112	0.132	0.147
Mn	0.045	0.046	0.045	0.049	0.045	0.046	0.045	0.042	0.043	0.043	0.046	0.045	0.044	0.044
Mg	0.582	0.563	0.567	0.553	0.581	0.573	0.579	0.629	0.599	0.582	0.565	0.525	0.551	0.586
Ca	0.819	0.808	0.827	0.796	0.811	0.807	0.818	0.823	0.822	0.819	0.807	0.814	0.732	0.820
Na	0.064	0.062	0.064	0.067	0.065	0.068	0.067	0.051	0.056	0.065	0.057	0.072	0.117	0.065
K				0.000				0.000			0.001		0.016	0.000
Sum	4.000	4.000	4.000	4.000	4.000	4.000	4.000	4.000	4.000	4.000	4.000	4.000	4.000	4.000
Aegirine	6.4	6.2	6.4	6.7	6.5	6.8	6.7	5.1	5.6	6.5	5.7	7.2	11.7	6.5
Ferri-Tschermak	3.0	2.0	4.9	3.4	3.2	3.7	4.5	3.6	3.4	3.1	2.0	2.0	0.8	4.1
Jadeite	0.0	0.0	0.0	0.0	0.0	0.0	0.0	0.0	0.0	0.0	0.0	0.0	0.0	0.0
Ti-Aegirine	0.0	0.0	0.0	0.0	0.0	0.0	0.0	0.0	0.0	0.0	0.0	0.0	0.0	0.0
Ti-Tschermak	0.9	1.0	0.9	1.0	0.9	1.0	0.9	1.1	1.1	0.9	1.1	1.0	2.1	0.9
Al-Tschermak	0.0	0.0	0.0	0.0	0.0	0.0	0.0	0.0	0.0	0.0	0.0	0.0	3.1	0.0
Diopside	44.8	42.2	44.2	40.5	43.9	43.0	44.5	47.6	45.6	44.8	42.6	40.8	39.0	45.1
Hedenbergite	33.3	35.5	32.7	34.7	33.0	33.0	31.9	30.0	32.2	33.1	35.1	37.7	28.3	31.8
Enstatite	6.7	7.0	6.3	7.4	7.1	7.1	6.7	7.7	7.1	6.7	7.0	5.9	8.0	6.8
Ferrosilite	5.0	5.9	4.6	6.3	5.3	5.5	4.8	4.8	5.0	4.9	5.7	5.4	5.8	4.8

Table C2 continued

Unit	**LAI**	**LAI**	**LAI**	**LAI**	**LAI**	**LAI**	**LAI**	**LAI**	**LAI**	**LAI**	**LAI**	**LAI**	**LAI**	**LAI**
Sample	TER4-1	TER4-1	TER4-1	TER4-1	TER4-1	TER4-1	TER4-1	TER4-1	TER4-1	TER6-1	TER6-1	TER7-1	TER7-1	TER7-1
No.	118 / 1 .	119 / 1 .	120 / 1 .	121 / 1 .	122 / 1 .	123 / 1 .	124 / 1 .	125 / 1 .	126 / 1 .	36 / 1 .	37 / 1 .	79 / 1 .	80 / 1 .	65 / 1 .
Notes	Pheno	Pheno	Pheno	Pheno	Pheno	Pheno	Pheno	Pheno	Pheno	Pheno	Pheno	Pheno	Pheno	Pheno
SiO_2	50.42	51.14	51.36	50.41	51.32	51.39	51.56	51.45	50.62	50.62	50.67	51.01	51.02	51.04
TiO_2	0.39	0.36	0.32	0.41	0.38	0.42	0.36	0.34	0.35	0.46	0.43	0.32	0.35	0.33
Al_2O_3	0.40	0.39	0.35	0.48	0.48	0.45	0.39	0.35	0.29	0.87	0.57	0.33	0.38	0.39
Cr_2O_3	bdl	bdl	bdl	bdl	0.02	0.01	bdl	bdl	0.01	0.01	bdl	0.02	0.01	0.01
FeO	16.08	16.95	17.16	17.21	17.19	16.95	16.31	17.22	17.39	15.47	15.19	17.71	16.59	17.12
MnO	1.39	1.50	1.39	1.54	1.44	1.41	1.36	1.45	1.52	1.34	1.32	1.43	1.38	1.44
MgO	10.11	10.04	9.50	9.97	9.48	9.77	10.14	9.49	9.43	10.61	10.68	8.98	9.74	9.35
CaO	20.22	19.55	20.01	18.99	19.87	20.13	20.30	20.13	19.84	19.75	19.69	19.47	19.69	19.39
Na_2O	0.84	0.84	0.92	0.94	0.94	0.92	0.83	0.85	0.81	0.78	0.80	1.02	0.86	0.94
K_2O	0.01	0.01	0.01	0.01	bdl	bdl	bdl	bdl	bdl	bdl	0.01	0.01	bdl	0.01
Total	99.85	100.77	101.02	99.96	101.12	101.45	101.25	101.29	100.27	99.90	99.37	100.29	100.02	100.03
Si	1.936	1.951	1.958	1.938	1.955	1.948	1.954	1.958	1.948	1.937	1.947	1.964	1.961	1.966
Ti	0.011	0.010	0.009	0.012	0.011	0.012	0.010	0.010	0.010	0.013	0.012	0.009	0.010	0.010
Al	0.018	0.017	0.016	0.022	0.022	0.020	0.017	0.016	0.013	0.039	0.026	0.015	0.017	0.018
Cr					0.001	0.000			0.000	0.000		0.001	0.000	0.000
Fe^{2+}	0.367	0.418	0.428	0.406	0.431	0.410	0.401	0.436	0.429	0.376	0.374	0.455	0.429	0.450
Fe^{3+}	0.150	0.123	0.119	0.148	0.116	0.127	0.116	0.112	0.131	0.118	0.114	0.116	0.104	0.101
Mn	0.045	0.048	0.045	0.050	0.046	0.045	0.044	0.047	0.050	0.043	0.043	0.046	0.045	0.047
Mg	0.579	0.571	0.540	0.571	0.538	0.552	0.573	0.538	0.541	0.605	0.612	0.515	0.558	0.537
Ca	0.832	0.799	0.817	0.783	0.811	0.817	0.824	0.821	0.818	0.810	0.811	0.803	0.811	0.800
Na	0.062	0.062	0.068	0.070	0.069	0.067	0.061	0.063	0.061	0.058	0.060	0.076	0.064	0.070
K	0.000	0.001	0.000	0.000							0.000	0.000		0.000
Sum	4.000	4.000	4.000	4.000	4.000	4.000	4.000	4.000	4.000	4.000	4.000	4.000	4.000	4.000
Aegirine	6.2	6.2	6.8	7.0	6.9	6.7	6.1	6.3	6.1	5.8	6.0	7.6	6.4	7.0
Ferri-Tschermak	4.4	3.0	2.6	3.9	2.3	3.0	2.7	2.5	3.5	3.0	2.7	2.0	2.0	1.5
Jadeite	0.0	0.0	0.0	0.0	0.0	0.0	0.0	0.0	0.0	0.0	0.0	0.0	0.0	0.0
Ti-Aegirine	0.0	0.0	0.0	0.0	0.0	0.0	0.0	0.0	0.0	0.0	0.0	0.0	0.0	0.0
Ti-Tschermak	0.9	0.9	0.8	1.1	1.1	1.0	0.9	0.8	0.7	1.3	1.2	0.7	0.9	0.9
Al-Tschermak	0.0	0.0	0.0	0.0	0.0	0.0	0.0	0.0	0.0	0.0	0.0	0.0	0.0	0.0
Diopside	45.5	41.8	41.8	40.7	41.1	42.6	44.4	41.6	41.2	45.2	45.9	39.3	42.3	40.3
Hedenbergite	32.4	34.2	36.6	32.5	36.5	35.1	34.4	37.2	36.4	31.4	31.2	38.2	35.9	37.3
Enstatite	6.2	7.6	6.1	8.2	6.3	6.3	6.5	6.1	6.4	7.6	7.7	6.1	6.8	6.7
Ferrosilite	4.4	6.2	5.3	6.5	5.6	5.2	5.0	5.5	5.7	5.3	5.2	5.9	5.7	6.2

Table C2 continued

Unit	**LAI**	**LAI**	**LAI**	**LAI**	**LAI**	**LAI**	**LAI**	**LAI**	**LAI**	**LAI**	**LAI**	**LAI**	**LAI**
Sample	TER7-1	TER7-1	TER7-1	TER7-1	TER7-1	TER7-1	TER10-3	TER10-3	TER10-3	TER10-3	TER10-3	TER10-3	TER10-3
No.	67 / 1 .	81 / 1 .	64 / 1 .	76 / 1 .	66 / 1 .	75 / 1 .	38 / 1 .	39 / 1 .	40 / 1 .	42 / 1 .	43 / 1 .	44 / 1 .	47 / 1 .
Notes	Pheno	Pheno	Pheno	Pheno	Pheno	Pheno	Pheno	Pheno	Pheno	Pheno	Pheno	Pheno	Pheno
SiO_2	51.19	51.21	51.41	51.41	51.42	51.47	50.06	50.86	50.73	50.94	51.03	51.03	51.96
TiO_2	0.36	0.36	0.34	0.38	0.35	0.38	0.31	0.36	0.38	0.43	0.40	0.41	0.53
Al_2O_3	0.38	0.45	0.64	0.45	0.34	0.40	0.29	0.37	0.40	0.42	0.68	0.37	2.80
Cr_2O_3	0.02	0.02	0.02	0.01	0.01	bdl	0.01	bdl	bdl	0.02	bdl	0.01	0.02
FeO	17.09	15.66	17.51	15.91	16.16	15.92	19.20	16.47	15.64	16.14	15.73	15.82	13.61
MnO	1.41	1.34	1.39	1.32	1.38	1.37	1.46	1.37	1.32	1.41	1.35	1.35	1.21
MgO	9.20	10.12	8.90	10.05	10.08	10.13	7.57	9.62	10.10	10.13	9.99	10.09	9.18
CaO	19.08	19.68	18.44	19.73	19.53	19.53	19.00	19.67	19.79	19.67	19.39	19.56	17.30
Na_2O	0.97	0.87	1.00	0.89	0.84	0.82	1.25	0.91	0.85	0.88	0.99	0.85	1.66
K_2O	bdl	0.06	0.26	0.01	bdl	bdl	bdl	bdl	0.01	bdl	0.06	0.02	0.64
Total	99.70	99.77	99.91	100.15	100.09	100.03	99.15	99.63	99.20	100.03	99.63	99.52	98.90
Si	1.979	1.966	1.986	1.968	1.971	1.973	1.963	1.962	1.959	1.953	1.961	1.966	1.992
Ti	0.010	0.010	0.010	0.011	0.010	0.011	0.009	0.010	0.011	0.012	0.012	0.012	0.015
Al	0.017	0.020	0.029	0.020	0.015	0.018	0.013	0.017	0.018	0.019	0.031	0.017	0.126
Cr	0.000	0.001	0.000	0.000	0.000		0.000			0.000		0.000	0.000
Fe^{2+}	0.477	0.408	0.499	0.421	0.434	0.436	0.493	0.424	0.399	0.401	0.405	0.418	0.424
Fe^{3+}	0.076	0.094	0.067	0.088	0.084	0.074	0.137	0.107	0.107	0.116	0.101	0.092	0.012
Mn	0.046	0.044	0.045	0.043	0.045	0.044	0.048	0.045	0.043	0.046	0.044	0.044	0.039
Mg	0.531	0.579	0.513	0.573	0.576	0.579	0.443	0.553	0.581	0.579	0.572	0.579	0.525
Ca	0.790	0.809	0.763	0.809	0.802	0.802	0.798	0.813	0.819	0.808	0.798	0.807	0.711
Na	0.073	0.065	0.075	0.066	0.062	0.061	0.095	0.068	0.064	0.066	0.074	0.064	0.123
K		0.003	0.013	0.000					0.000		0.003	0.001	0.031
Sum	4.000	4.000	4.000	4.000	4.000	4.000	4.000	4.000	4.000	4.000	4.000	4.000	4.000
Aegirine	7.3	6.5	6.7	6.6	6.2	6.1	9.5	6.8	6.4	6.6	7.4	6.4	1.2
Ferri-Tschermak	0.1	1.5	0.0	1.1	1.1	0.7	2.1	1.9	2.1	2.5	1.3	1.4	0.0
Jadeite	0.0	0.0	0.8	0.0	0.0	0.0	0.0	0.0	0.0	0.0	0.0	0.0	11.1
Ti-Aegirine	0.0	0.0	0.0	0.0	0.0	0.0	0.0	0.0	0.0	0.0	0.0	0.0	0.0
Ti-Tschermak	0.9	1.0	0.7	1.0	0.8	0.9	0.7	0.9	0.9	0.9	1.2	0.8	0.4
Al-Tschermak	0.0	0.0	0.0	0.0	0.0	0.0	0.0	0.0	0.0	0.0	0.0	0.0	0.0
Diopside	39.3	44.1	36.7	43.6	42.8	43.0	34.7	42.5	44.8	43.7	43.3	43.7	37.6
Hedenbergite	38.7	34.4	38.9	35.2	35.6	35.7	42.4	36.0	34.0	33.7	34.0	34.8	33.1
Enstatite	6.9	6.9	7.3	6.9	7.4	7.5	4.8	6.4	6.7	7.1	6.9	7.1	7.5
Ferrosilite	6.8	5.4	7.7	5.6	6.2	6.2	5.9	5.4	5.1	5.5	5.4	5.7	6.6

Table C2 continued

Unit	**LMI**	**LMI**	**LMI**	**LMI**	**LMI**	**LMI**	**LMI**	**LMI**	**LMI**	**LMI**	**LMI**	**LMI**	**LMI**	**LMI**
Sample	TER5-2	TER5-2	TER5-2	TER5-2	TER5-2	TER5-2	TER5-2	TER5-2	TER5-2	TER5-2	TER5-2	TER5-2	TER5-2	TER5-2
No.	105 / 1 .	106 / 1 .	107 / 1 .	109 / 1 .	110 / 1 .	111 / 1 .	112 / 1 .	113 / 1 .	114 / 1 .	115 / 1 .	116 / 1 .	117 / 1 .	118 / 1 .	120 / 1 .
Notes	Pheno	Pheno	Pheno	Pheno	Pheno	Pheno	Pheno	Pheno	Pheno	Pheno	Pheno	Pheno	Pheno	Pheno
SiO_2	51.08	51.18	50.73	51.02	50.86	50.81	50.83	50.34	50.03	50.34	51.24	51.38	51.57	45.78
TiO_2	0.44	0.47	0.50	0.47	0.58	0.45	0.49	0.66	1.71	1.50	0.44	0.49	0.39	3.50
Al_2O_3	0.77	0.81	0.86	0.70	0.96	0.78	0.80	0.81	3.02	2.83	0.63	0.79	0.57	5.94
Cr_2O_3	bdl	0.02	0.02	0.02	0.02	bdl	0.03	0.02	0.06	0.01	0.01	0.01	0.01	0.09
FeO	12.74	13.10	13.19	13.35	12.69	12.85	12.95	17.74	10.44	9.54	14.60	13.06	15.19	10.41
MnO	0.97	1.00	0.98	1.01	1.00	0.98	1.01	1.34	0.36	0.40	1.09	1.03	1.11	0.25
MgO	12.66	12.33	12.36	12.21	12.68	12.56	12.44	9.50	14.12	13.99	11.47	12.35	10.93	12.86
CaO	20.19	20.34	20.40	20.33	20.05	20.30	20.15	19.02	19.64	21.29	20.04	20.11	20.27	20.48
Na_2O	0.69	0.64	0.59	0.67	0.65	0.64	0.69	0.84	0.58	0.59	0.72	0.69	0.68	0.59
K_2O	bdl	bdl	0.01	bdl	0.01	0.01	0.01	bdl	0.05	0.02	bdl	bdl	bdl	0.02
Total	99.55	99.91	99.64	99.79	99.49	99.40	99.38	100.29	100.04	100.51	100.25	99.92	100.71	99.92
Si	1.934	1.936	1.925	1.934	1.927	1.929	1.931	1.937	1.866	1.865	1.944	1.943	1.955	1.716
Ti	0.013	0.013	0.014	0.013	0.016	0.013	0.014	0.019	0.048	0.042	0.013	0.014	0.011	0.099
Al	0.034	0.036	0.038	0.031	0.043	0.035	0.036	0.037	0.133	0.123	0.028	0.035	0.025	0.262
Cr		0.001	0.001	0.001	0.001		0.001	0.001	0.002	0.000	0.000	0.000	0.000	0.003
Fe^{2+}	0.280	0.303	0.291	0.301	0.284	0.278	0.286	0.457	0.243	0.190	0.352	0.311	0.390	0.178
Fe^{3+}	0.123	0.111	0.127	0.122	0.118	0.130	0.125	0.114	0.082	0.106	0.111	0.102	0.091	0.148
Mn	0.031	0.032	0.032	0.033	0.032	0.031	0.032	0.044	0.011	0.013	0.035	0.033	0.036	0.008
Mg	0.715	0.695	0.699	0.690	0.716	0.711	0.704	0.545	0.785	0.773	0.649	0.696	0.618	0.719
Ca	0.819	0.824	0.829	0.826	0.814	0.826	0.820	0.784	0.785	0.845	0.815	0.815	0.823	0.823
Na	0.051	0.047	0.044	0.049	0.048	0.047	0.051	0.063	0.042	0.042	0.053	0.051	0.050	0.043
K			0.000		0.001	0.000	0.000		0.002	0.001				0.001
Sum	4.000	4.000	4.000	4.000	4.000	4.000	4.000	4.000	4.000	4.000	4.000	4.000	4.000	4.000
Aegirine	5.1	4.7	4.4	4.9	4.8	4.7	5.1	6.3	4.2	4.2	5.3	5.1	5.0	4.3
Ferri-Tschermak	3.6	3.2	4.2	3.7	3.5	4.1	3.7	2.5	2.0	3.2	2.9	2.6	2.1	5.3
Jadeite	0.0	0.0	0.0	0.0	0.0	0.0	0.0	0.0	0.0	0.0	0.0	0.0	0.0	0.0
Ti-Aegirine	0.0	0.0	0.0	0.0	0.0	0.0	0.0	0.0	0.0	0.0	0.0	0.0	0.0	0.0
Ti-Tschermak	1.3	1.3	1.4	1.3	1.6	1.3	1.4	1.8	4.8	4.2	1.3	1.4	1.1	9.9
Al-Tschermak	0.0	0.0	0.0	0.0	0.0	0.0	0.0	0.0	0.0	0.0	0.0	0.0	0.0	0.0
Diopside	53.6	52.6	52.9	52.3	52.9	53.8	52.9	38.6	54.1	61.2	48.4	51.9	46.8	53.4
Hedenbergite	23.4	25.3	24.4	25.3	23.4	23.4	23.9	35.5	17.6	16.0	28.9	25.6	32.3	13.8
Enstatite	8.9	8.5	8.5	8.4	9.4	8.7	8.7	8.0	12.2	8.1	8.2	8.9	7.5	9.2
Ferrosilite	3.9	4.1	3.9	4.0	4.1	3.8	4.0	7.3	4.0	2.1	4.9	4.4	5.2	2.4

Table C2 continued

Unit	VFI	VFI	VFI	VFI	VFI	VFI	VFI	VFI	VFI	VFI	VFI	VFI	VFI	VFI
Sample	TM-1(1)	TM-1(1)	TM-1(1)	TM-1(1)	TM-1(1)	TM-1(1)	TM-2(1)	TM-2(1)	TM-2(1)	TM-2(1)	TM-2(1)	TER2-2	TER2-2	TER2-2
No.	Px1	Px2	Px3	Px4	Px5	Px6	Px1	Px2	Px3	Px4	Px5	13 / 1 .	14 / 1 .	15 / 1 .
Notes	Pheno	Pheno	Pheno	Pheno	Pheno	Pheno	Pheno	Pheno	Pheno	Pheno	Pheno	Pheno	Pheno	Pheno
SiO_2	51.43	49.62	50.99	50.35	49.99	49.30	51.03	51.13	51.13	51.69	48.69	50.49	50.51	50.23
TiO_2	0.48	0.41	0.39	0.43	0.44	0.51	0.38	0.41	0.40	0.37	0.40	0.52	0.84	0.41
Al_2O_3	0.57	0.36	0.44	0.60	0.56	0.58	0.39	0.51	0.48	0.57	0.43	0.68	1.14	0.52
Cr_2O_3	bdl	bdl	bdl	bdl	bdl	bdl	bdl	bdl	0.01	bdl	bdl	bdl	0.01	0.03
FeO	18.11	19.18	17.97	15.03	15.72	17.30	18.26	16.25	18.11	16.28	16.87	17.31	15.59	17.67
MnO	1.27	1.26	1.27	1.05	1.08	1.23	1.38	1.11	1.26	1.08	1.15	1.19	1.05	1.18
MgO	8.21	6.90	8.42	9.72	9.41	8.62	8.02	9.39	8.23	9.53	8.19	9.38	10.39	8.79
CaO	20.01	19.70	20.03	20.21	19.69	19.41	19.86	20.31	20.00	20.46	21.74	20.04	19.93	20.08
Na_2O	0.77	0.85	0.69	0.65	0.66	0.69	0.66	0.70	0.68	0.69	0.62	0.69	0.79	0.70
K_2O	0.01	0.01	bdl	bdl	0.01	bdl	bdl	bdl	bdl	0.01	bdl	0.01	0.01	bdl
Total	100.85	98.29	100.20	98.05	97.57	97.65	99.98	99.81	100.31	100.67	98.09	100.32	100.27	99.62
Si	1.981	1.975	1.975	1.970	1.971	1.955	1.987	1.973	1.981	1.976	1.923	1.942	1.928	1.952
Ti	0.014	0.012	0.011	0.013	0.013	0.015	0.011	0.012	0.012	0.011	0.012	0.015	0.024	0.012
Al	0.026	0.017	0.020	0.028	0.026	0.027	0.018	0.023	0.022	0.026	0.020	0.031	0.051	0.024
Cr									0.000				0.000	0.001
Fe^{2+}	0.540	0.563	0.524	0.436	0.461	0.488	0.560	0.464	0.543	0.468	0.399	0.451	0.394	0.475
Fe^{3+}	0.043	0.075	0.058	0.056	0.057	0.085	0.035	0.060	0.043	0.053	0.158	0.106	0.104	0.100
Mn	0.042	0.043	0.042	0.035	0.036	0.041	0.046	0.036	0.042	0.035	0.039	0.039	0.034	0.039
Mg	0.471	0.409	0.486	0.567	0.553	0.510	0.466	0.540	0.475	0.543	0.482	0.538	0.591	0.509
Ca	0.826	0.840	0.831	0.847	0.832	0.825	0.829	0.840	0.830	0.838	0.920	0.826	0.815	0.836
Na	0.057	0.065	0.052	0.049	0.051	0.053	0.050	0.052	0.051	0.051	0.047	0.051	0.058	0.052
K	0.000	0.001			0.000					0.001		0.000	0.000	
Sum	4.000	4.000	4.000	4.000	4.000	4.000	4.000	4.000	4.000	4.000	4.000	4.000	4.000	4.000
Aegirine	4.3	6.5	5.2	4.9	5.1	5.3	3.5	5.2	4.3	5.1	4.7	5.1	5.8	5.2
Ferri-Tschermak	0.0	0.5	0.3	0.4	0.3	1.6	0.0	0.4	0.0	0.1	5.5	2.7	2.3	2.4
Jadeite	0.6	0.0	0.0	0.0	0.0	0.0	0.5	0.0	0.3	0.0	0.0	0.0	0.0	0.0
Ti-Aegirine	0.8	0.0	0.0	0.0	0.0	0.0	1.0	0.0	0.5	0.0	0.0	0.0	0.0	0.0
Ti-Tschermak	1.0	0.8	1.0	1.3	1.3	1.4	0.6	1.2	0.9	1.1	1.0	1.5	2.4	1.2
Al-Tschermak	0.0	0.0	0.0	0.0	0.0	0.0	0.0	0.0	0.0	0.2	0.0	0.0	0.0	0.0
Diopside	36.5	33.3	37.8	45.4	42.9	39.0	35.7	42.8	36.8	42.8	44.8	41.0	44.6	39.9
Hedenbergite	45.1	49.3	44.0	37.7	38.6	40.5	46.5	39.6	45.3	39.7	40.7	37.4	32.3	40.2
Enstatite	5.2	3.8	5.4	5.6	6.2	6.0	5.3	5.6	5.3	5.7	1.7	6.4	7.3	5.5
Ferrosilite	6.4	5.6	6.3	4.7	5.6	6.2	6.9	5.2	6.5	5.3	1.6	5.8	5.3	5.6

Table C2 continued

Unit	**VFI**	**VFI**	**VFI**	**VFI**	**VFI**	**VFI**	**VFI**	**VFI**	**VFI**	**VFI**	**VFI**	**VFI**	**VFI**	**VFI**
Sample	TER2-2	TER2-2	TER2-2	TER2-2	TER2-2	TER2-2	TER2-2	TER2-2	TER2-2	TER2-2	TER2-2	TER2-2	TER2-2	TER2-2
No.	16 / 1 .	17 / 1 .	19 / 1 .	20 / 1 .	85 / 1 .	96 / 1 .	95 / 1 .	86 / 1 .	82 / 1 .	84 / 1 .	83 / 1 .	127 / 1 .	128 / 1 .	129 / 1 .
Notes	Pheno	Pheno	Pheno	Pheno	Pheno	Pheno	Pheno	Pheno	Pheno	Pheno	Pheno	Pheno	Pheno	Pheno
SiO_2	49.50	49.72	49.94	51.23	50.88	50.10	51.46	50.61	50.19	50.16	49.91	51.37	49.92	50.70
TiO_2	0.61	0.45	0.50	0.42	0.41	0.40	0.41	0.57	0.39	0.43	0.43	0.44	0.39	0.42
Al_2O_3	1.49	0.51	0.55	0.53	0.43	0.51	0.55	0.83	0.47	0.50	0.52	1.27	0.49	0.47
Cr_2O_3	0.01	0.01	0.01	0.02	0.02	0.01	0.01	0.01	0.03	0.02	0.03	0.03	0.02	0.01
FeO	18.04	19.01	18.28	17.88	18.71	18.21	16.90	16.66	18.15	17.86	18.19	17.40	18.17	18.88
MnO	1.27	1.24	1.26	1.19	1.28	1.26	1.14	1.13	1.18	1.19	1.23	1.14	1.21	1.32
MgO	8.62	8.14	8.67	8.70	8.60	8.71	9.65	9.91	8.42	8.83	8.29	8.52	8.32	8.34
CaO	19.20	19.62	19.19	19.75	19.86	19.59	19.99	19.77	19.74	19.72	19.96	19.23	19.86	19.57
Na_2O	0.74	0.79	0.76	0.74	0.69	0.70	0.68	0.67	0.77	0.73	0.70	1.05	0.72	0.71
K_2O	bdl	bdl	0.02	0.01	bdl	0.01	bdl	0.01	0.01	bdl	0.01	0.19	0.01	bdl
Total	99.50	99.50	99.20	100.47	100.88	99.52	100.79	100.18	99.35	99.46	99.28	100.64	99.12	100.44
Si	1.927	1.944	1.952	1.976	1.959	1.952	1.967	1.943	1.960	1.953	1.953	1.970	1.955	1.964
Ti	0.018	0.013	0.015	0.012	0.012	0.012	0.012	0.016	0.011	0.013	0.013	0.013	0.011	0.012
Al	0.068	0.024	0.025	0.024	0.020	0.023	0.025	0.038	0.021	0.023	0.024	0.057	0.023	0.021
Cr	0.000	0.000	0.000	0.001	0.000	0.000	0.000	0.000	0.001	0.001	0.001	0.001	0.001	0.000
Fe^{2+}	0.490	0.500	0.499	0.521	0.514	0.491	0.472	0.441	0.498	0.480	0.497	0.494	0.497	0.532
Fe^{3+}	0.097	0.121	0.099	0.055	0.089	0.103	0.068	0.094	0.094	0.101	0.098	0.064	0.098	0.080
Mn	0.042	0.041	0.042	0.039	0.042	0.042	0.037	0.037	0.039	0.039	0.041	0.037	0.040	0.043
Mg	0.500	0.475	0.505	0.500	0.494	0.506	0.550	0.567	0.490	0.512	0.483	0.487	0.486	0.482
Ca	0.801	0.822	0.804	0.816	0.819	0.818	0.818	0.813	0.826	0.823	0.837	0.790	0.833	0.812
Na	0.056	0.060	0.058	0.055	0.051	0.053	0.051	0.050	0.058	0.055	0.053	0.078	0.055	0.053
K			0.001	0.001		0.001		0.001	0.001		0.000	0.009	0.000	
Sum	4.000	4.000	4.000	4.000	4.000	4.000	4.000	4.000	4.000	4.000	4.000	4.000	4.000	4.000
Aegirine	5.6	6.0	5.8	5.5	5.1	5.3	5.1	5.0	5.8	5.5	5.3	6.4	5.5	5.3
Ferri-Tschermak	2.1	3.1	2.1	0.0	1.9	2.5	0.9	2.2	1.8	2.3	2.2	0.0	2.2	1.3
Jadeite	0.0	0.0	0.0	0.0	0.0	0.0	0.0	0.0	0.0	0.0	0.0	1.4	0.0	0.0
Ti-Aegirine	0.0	0.0	0.0	0.0	0.0	0.0	0.0	0.0	0.0	0.0	0.0	0.0	0.0	0.0
Ti-Tschermak	1.8	1.2	1.3	1.2	1.0	1.2	1.2	1.6	1.1	1.1	1.2	1.3	1.1	1.1
Al-Tschermak	0.0	0.0	0.0	0.0	0.0	0.0	0.0	0.0	0.0	0.0	0.0	0.5	0.0	0.0
Diopside	36.9	36.4	37.2	37.9	37.2	38.1	41.4	42.0	38.0	39.1	38.0	37.0	38.0	35.9
Hedenbergite	39.3	41.5	39.8	42.5	41.8	40.1	38.3	35.4	41.7	39.7	42.3	40.3	42.0	42.9
Enstatite	6.5	5.5	6.7	6.0	6.1	6.2	6.8	7.3	5.5	6.1	5.2	5.9	5.3	6.1
Ferrosilite	7.0	6.3	7.1	6.8	6.8	6.6	6.3	6.2	6.0	6.1	5.8	6.4	5.9	7.3

Table C2 continued

Unit	CCI	CCI	CCI	CCI	CCI	CCI	CCI	CCI	CCI	CCI	CCI	CCI	CCI	CCI	CCI	CCI
Sample	TM-1(2)	TM-1(2)	TM-1(2)	TM-1(2)	TM-1(2)	TM-1(2)	TM-1(2)	TM-2(2)	TM-2(2)	TM-2(2)	TM-2(2)	TM-2(2)	TM-2(2)	TM-2(2)	TM-2(2)	TM-2(2)
No.	Px1	Px3	Px6	Px7	Px8	Px9	Px10	Px1	Px2	Px5	Px6	Px9	Px11	Px12	Px13	Px15
Notes	Pheno	Pheno	Pheno	Pheno	Pheno	Pheno	Pheno	Pheno	Pheno	Pheno	Pheno	Pheno	Pheno	Pheno	Pheno	Pheno
SiO_2	50.70	51.42	51.11	51.21	51.42	51.46	51.52	51.23	51.47	51.47	51.01	51.22	51.20	50.83	50.29	50.70
TiO_2	0.36	0.30	0.32	0.36	0.34	0.30	0.41	0.30	0.34	0.34	0.36	0.32	0.35	0.33	0.32	0.33
Al_2O_3	0.35	0.36	0.36	0.42	0.34	0.37	0.48	0.34	0.38	0.37	0.43	0.41	0.39	0.35	0.36	0.35
Cr_2O_3	bdl	bdl	bdl	bdl	0.03	0.01	bdl	bdl	bdl	bdl	0.02	bdl	bdl	bdl	bdl	0.01
FeO	18.75	17.99	17.83	18.07	18.46	17.49	17.12	18.63	18.67	19.04	16.86	18.06	17.50	18.08	17.80	17.82
MnO	1.22	1.26	1.25	1.28	1.22	1.18	1.27	1.28	1.33	1.26	1.23	1.23	1.21	1.37	1.20	1.27
MgO	7.34	7.94	7.97	7.76	7.48	8.26	8.77	7.61	7.86	7.26	8.63	7.83	8.26	8.00	7.96	8.05
CaO	20.27	19.96	19.98	20.14	20.16	20.26	19.98	19.99	19.85	19.89	20.14	19.99	20.03	19.60	20.01	20.01
Na_2O	0.91	0.91	0.96	1.03	1.04	0.88	0.88	1.05	1.04	1.06	0.89	1.05	0.90	0.81	0.97	0.99
K_2O	bdl	bdl	bdl	bdl	bdl	bdl	bdl	bdl	bdl	bdl	bdl	0.01	bdl	bdl	bdl	bdl
Total	99.90	100.14	99.78	100.27	100.49	100.21	100.44	100.43	100.94	100.69	99.56	100.12	99.84	99.37	98.91	99.53
Si	1.978	1.994	1.987	1.983	1.990	1.989	1.982	1.983	1.981	1.992	1.979	1.985	1.986	1.988	1.971	1.975
Ti	0.011	0.009	0.009	0.010	0.010	0.009	0.012	0.009	0.010	0.010	0.011	0.009	0.010	0.010	0.009	0.010
Al	0.016	0.017	0.017	0.019	0.015	0.017	0.022	0.015	0.017	0.017	0.019	0.019	0.018	0.016	0.017	0.016
Cr					0.001	0.000					0.001					0.000
Fe^{2+}	0.537	0.537	0.515	0.513	0.536	0.512	0.494	0.524	0.523	0.558	0.480	0.513	0.512	0.542	0.487	0.490
Fe^{3+}	0.075	0.047	0.064	0.072	0.062	0.053	0.057	0.079	0.078	0.058	0.067	0.073	0.056	0.049	0.096	0.090
Mn	0.040	0.041	0.041	0.042	0.040	0.039	0.041	0.042	0.043	0.041	0.040	0.040	0.040	0.045	0.040	0.042
Mg	0.427	0.459	0.462	0.448	0.432	0.476	0.503	0.439	0.451	0.419	0.499	0.452	0.478	0.466	0.465	0.467
Ca	0.847	0.829	0.832	0.835	0.836	0.839	0.823	0.829	0.819	0.825	0.837	0.830	0.833	0.821	0.840	0.835
Na	0.069	0.068	0.073	0.077	0.078	0.066	0.066	0.079	0.077	0.079	0.067	0.079	0.067	0.061	0.074	0.075
K												0.001				
Sum	4.000	4.000	4.000	4.000	4.000	4.000	4.000	4.000	4.000	4.000	4.000	4.000	4.000	4.000	4.000	4.000
Aegirine	6.9	4.7	6.4	7.2	6.2	5.3	5.7	7.9	7.7	5.8	6.7	7.3	5.6	4.9	7.4	7.5
Ferri-Tschermak	0.3	0.0	0.0	0.0	0.0	0.0	0.0	0.0	0.0	0.0	0.0	0.0	0.0	0.0	1.1	0.8
Jadeite	0.0	1.0	0.3	0.2	0.6	0.6	0.4	0.0	0.0	0.9	0.0	0.3	0.4	0.4	0.0	0.0
Ti-Aegirine	0.0	1.1	0.5	0.4	1.1	0.7	0.6	0.0	0.0	1.2	0.0	0.3	0.7	0.8	0.0	0.0
Ti-Tschermak	0.8	0.3	0.7	0.9	0.4	0.5	0.9	0.8	0.9	0.4	1.0	0.8	0.7	0.6	0.8	0.8
Al-Tschermak	0.0	0.0	0.0	0.0	0.0	0.0	0.0	0.0	0.0	0.0	0.0	0.0	0.0	0.0	0.0	0.0
Diopside	35.6	36.6	37.4	36.9	35.6	38.6	39.4	35.9	35.9	33.8	40.5	37.0	38.3	36.1	38.5	38.3
Hedenbergite	48.0	46.0	45.1	45.8	47.5	44.7	42.0	46.2	45.1	48.3	42.2	45.2	44.2	45.5	43.6	43.6
Enstatite	3.6	4.5	4.3	3.9	3.7	4.4	5.4	4.0	4.6	3.9	4.7	4.1	4.6	5.2	4.0	4.2
Ferrosilite	4.8	5.7	5.2	4.8	4.9	5.1	5.7	5.2	5.8	5.6	4.9	5.0	5.4	6.5	4.5	4.8

Table C2 continued

Unit	**CCI sy**	**CCI sy**	**CCI sy**	**CCI sy**	**CCI sy**	**CCI sy**	**CCI sy**	**CCI sy**	**CCI sy**	**CCI sy**	**CCI sy**	**CCI sy**	**CCI sy**	**CCI sy**	**CCI sy**
Sample	TER30-1	TER30-1	TER30-1	TER30-1	TER30-1	TER30-1	TER30-1	TER30-1	TER30-1	TER30-1	TER30-1	TER30-1	TER30-1	TER30-1	TER30-1
No.	Px1	Px2	Px3	Px4	Px5	Px6	Px7	Px8	Px9	Px10	Px11	Px12	Px13	Px14	Px15
Notes	Intercum.	Intercum.	Intercum.	Intercum.	Intercum.	Intercum.	Intercum.	Intercum.	Intercum.	Intercum.	Intercum.	Intercum.	Intercum.	Intercum.	Intercum.
SiO_2	52.75	52.33	52.03	52.12	52.70	53.08	50.52	49.81	52.28	52.30	52.18	52.48	52.01	51.94	52.54
TiO_2	1.99	2.20	3.36	5.02	4.99	1.53	0.25	0.34	1.35	2.01	3.97	4.89	2.67	5.65	2.36
Al_2O_3	0.34	0.30	0.25	0.20	0.24	0.41	0.26	0.26	0.12	0.23	0.24	0.25	0.11	0.22	0.21
Cr_2O_3	bdl	bdl	0.01	0.02	0.03	bdl	bdl	0.02	bdl	bdl	bdl	bdl	0.04	bdl	bdl
FeO	27.40	26.94	26.09	25.57	25.57	28.19	23.93	22.43	26.75	27.59	26.25	25.32	25.69	24.97	27.32
MnO	0.70	0.83	0.71	0.46	0.46	0.73	1.25	1.29	0.78	0.53	0.60	0.56	0.63	0.51	0.52
MgO	0.13	0.15	0.09	0.03	0.02	0.17	2.94	4.47	0.08	0.08	0.04	0.03	0.01	0.04	0.11
CaO	1.79	0.89	1.76	1.58	1.51	0.85	17.85	18.94	3.34	1.96	2.27	1.45	2.40	1.38	1.74
Na_2O	12.47	13.14	12.64	12.63	12.73	13.12	2.98	1.70	11.33	12.28	12.41	12.90	12.36	12.77	12.53
K_2O	bdl	0.03	bdl	0.01	bdl	0.03	0.02	0.02	0.01	bdl	0.01	bdl	bdl	bdl	bdl
Total	97.57	96.81	96.94	97.65	98.25	98.10	100.00	99.27	96.03	96.98	97.96	97.87	95.92	97.48	97.33
Si	2.020	2.008	2.005	2.001	2.010	2.012	1.993	1.982	2.047	2.019	1.998	2.005	2.025	1.996	2.017
Ti	0.057	0.063	0.097	0.145	0.143	0.044	0.008	0.010	0.040	0.058	0.114	0.140	0.078	0.163	0.068
Al	0.015	0.013	0.011	0.009	0.011	0.018	0.012	0.012	0.005	0.010	0.011	0.011	0.005	0.010	0.009
Cr			0.000	0.000	0.001			0.000					0.001		
Fe^{2+}	0.122	0.041	0.113	0.182	0.193	0.057	0.574	0.612	0.195	0.136	0.154	0.155	0.115	0.180	0.125
Fe^{3+}	0.756	0.823	0.728	0.639	0.623	0.837	0.216	0.135	0.681	0.755	0.686	0.654	0.721	0.622	0.752
Mn	0.023	0.027	0.023	0.015	0.015	0.023	0.042	0.043	0.026	0.017	0.019	0.018	0.021	0.017	0.017
Mg	0.007	0.008	0.005	0.002	0.001	0.010	0.173	0.265	0.005	0.005	0.002	0.002	0.001	0.002	0.007
Ca	0.073	0.037	0.073	0.065	0.062	0.034	0.754	0.808	0.140	0.081	0.093	0.059	0.100	0.057	0.072
Na	0.926	0.977	0.944	0.940	0.942	0.964	0.228	0.131	0.860	0.919	0.921	0.956	0.933	0.952	0.933
K		0.002		0.001		0.001	0.001	0.001	0.000		0.000				
Sum	4.000	4.000	4.000	4.000	4.000	4.000	4.000	4.000	4.000	4.000	4.000	4.000	4.000	4.000	4.000
Aegirine	75.6	82.3	72.8	63.9	62.3	83.7	21.6	13.1	68.1	75.5	68.6	65.4	72.1	62.2	75.2
Ferri-Tschermak	0.0	0.0	0.0	0.0	0.0	0.0	0.0	0.2	0.0	0.0	0.0	0.0	0.0	0.0	0.0
Jadeite	3.6	2.1	1.6	1.1	2.1	3.0	0.5	0.0	5.3	2.9	0.9	1.6	3.0	0.6	2.7
Ti-Aegirine	11.5	12.7	19.5	29.0	28.6	8.7	0.7	0.0	7.9	11.7	22.6	28.1	15.6	32.3	13.6
Ti-Tschermak	0.0	0.0	0.0	0.0	0.0	0.0	0.4	0.6	0.0	0.0	0.1	0.0	0.0	0.2	0.0
Al-Tschermak	0.0	0.0	0.0	0.0	0.0	0.0	0.0	0.0	0.0	0.0	0.0	0.0	0.0	0.0	0.0
Diopside	0.4	0.1	0.2	0.1	0.0	0.4	16.5	23.0	0.3	0.2	0.1	0.0	0.0	0.0	0.3
Hedenbergite	7.0	1.1	4.2	5.4	6.1	3.1	58.6	56.9	13.7	7.9	6.2	3.4	5.8	3.7	6.8
Enstatite	0.1	0.0	0.0	0.0	0.0	0.1	0.4	1.7	0.0	0.0	0.0	0.0	0.0	0.0	0.0
Ferrosilite	1.0	0.0	0.0	0.0	0.2	0.5	1.3	4.3	2.2	0.9	0.0	0.0	0.0	0.0	0.4

Table C2 continued

Unit	**CCI sy**	**CCI sy**	**CCI sy**	**CCI sy**	**CCI sy**	**CCI sy**	**CCI sy**	**CCI sy**	**CCI sy**	**CCI sy**	**CCI sy**	**CCI sy**	**CCI sy**	**CCI sy**	**CCI sy**
Sample	TER30-1	TER30-1	TER30-7	TER30-7	TER30-7	TER30-7	TER30-7	TER30-7	TER30-7	TER30-7	TER30-7	TER29-1	TER29-1	TER29-1	TER29-1
No.	Px16	Px17	Px1	Px2	Px3	Px4	Px5	Px6	Px7	Px9	Px10	Px1	Px2	Px3	Px4
Notes	Intercum.	Intercum.	Intercum.	Intercum.	Intercum.	Intercum.	Intercum.	Intercum.	Intercum.	Intercum.	Intercum.	Intercum.	Intercum.	Intercum.	Intercum.
SiO_2	52.37	52.08	52.56	52.57	40.92	52.78	52.22	52.20	52.46	52.64	52.11	51.73	51.95	51.95	51.27
TiO_2	1.76	1.93	5.97	1.80	8.15	4.68	3.58	1.80	6.24	3.01	5.09	2.53	2.25	2.24	2.40
Al_2O_3	0.18	0.12	0.25	0.40	0.48	0.29	0.24	0.38	0.26	0.30	0.21	0.15	0.20	0.13	0.15
Cr_2O_3	bdl	bdl	0.01	bdl	bdl	0.01	0.01	0.01	bdl	0.03	bdl	bdl	bdl	bdl	bdl
FeO	27.48	25.84	24.03	26.68	40.21	25.87	26.61	28.00	24.19	26.63	24.97	26.71	27.68	27.09	26.52
MnO	0.74	0.84	0.49	0.60	1.69	0.68	0.46	0.29	0.57	0.57	0.56	0.55	0.48	0.69	0.84
MgO	0.03	0.07	0.04	0.05	0.21	0.04	0.02	0.12	0.05	0.08	0.09	0.28	0.30	0.32	0.50
CaO	1.03	2.83	1.55	0.97	0.42	1.25	1.19	1.37	0.98	1.23	1.08	3.29	3.65	2.46	7.05
Na_2O	12.92	12.11	12.32	12.82	7.28	12.80	12.62	12.76	13.19	12.92	12.89	11.24	11.42	12.02	9.54
K_2O	0.06	0.02	0.03	bdl	0.02	bdl	bdl	0.01	0.01	0.03	0.01	0.01	bdl	0.02	0.01
Total	96.56	95.83	97.24	95.89	99.39	98.41	96.96	96.94	97.95	97.44	97.01	96.50	97.92	96.92	98.28
Si	2.018	2.030	2.031	2.038	1.677	2.009	2.016	2.006	2.001	2.014	2.007	2.021	2.000	2.008	1.992
Ti	0.051	0.057	0.174	0.052	0.251	0.134	0.104	0.052	0.179	0.087	0.147	0.074	0.065	0.065	0.070
Al	0.008	0.006	0.011	0.018	0.023	0.013	0.011	0.017	0.012	0.014	0.010	0.007	0.009	0.006	0.007
Cr			0.000			0.000	0.000	0.000		0.001					
Fe^{2+}	0.065	0.105	0.273	0.100	0.679	0.178	0.165	0.083	0.167	0.108	0.161	0.219	0.177	0.127	0.274
Fe^{3+}	0.821	0.738	0.503	0.765	0.700	0.645	0.694	0.817	0.605	0.744	0.644	0.654	0.714	0.749	0.588
Mn	0.024	0.028	0.016	0.020	0.059	0.022	0.015	0.009	0.018	0.019	0.018	0.018	0.016	0.022	0.028
Mg	0.001	0.004	0.002	0.003	0.013	0.003	0.001	0.007	0.003	0.004	0.005	0.016	0.017	0.019	0.029
Ca	0.042	0.118	0.064	0.040	0.019	0.051	0.049	0.056	0.040	0.050	0.045	0.138	0.151	0.102	0.293
Na	0.966	0.915	0.923	0.964	0.579	0.945	0.944	0.951	0.975	0.958	0.963	0.852	0.852	0.901	0.719
K	0.003	0.001	0.001		0.001			0.000	0.000	0.001	0.000	0.001		0.001	0.000
Sum	4.000	4.000	4.000	4.000	4.000	4.000	4.000	4.000	4.000	4.000	4.000	4.000	4.000	4.000	4.000
Aegirine	82.1	73.8	50.3	76.5	57.9	64.5	69.4	81.7	60.5	74.4	64.4	65.4	71.4	74.9	58.8
Ferri-Tschermak	0.0	0.0	0.0	0.0	6.1	0.0	0.0	0.0	0.0	0.0	0.0	0.0	0.0	0.0	0.0
Jadeite	2.7	3.5	4.3	5.6	0.0	2.2	2.7	2.3	1.2	2.8	1.7	2.8	0.8	1.4	0.0
Ti-Aegirine	10.2	11.3	34.7	10.5	0.0	26.8	20.8	10.4	35.8	17.3	29.5	14.9	13.0	13.0	13.1
Ti-Tschermak	0.0	0.0	0.0	0.0	1.9	0.0	0.0	0.0	0.0	0.0	0.0	0.0	0.0	0.0	0.3
Al-Tschermak	0.0	0.0	0.0	0.0	0.0	0.0	0.0	0.0	0.0	0.0	0.0	0.0	0.0	0.0	0.0
Diopside	0.1	0.2	0.1	0.1	0.0	0.1	0.0	0.3	0.0	0.1	0.1	0.9	1.2	1.1	2.3
Hedenbergite	3.9	7.7	6.4	3.9	0.0	5.0	4.9	4.4	0.9	4.3	3.5	12.9	13.3	9.1	24.2
Enstatite	0.0	0.0	0.0	0.0	0.6	0.0	0.0	0.0	0.0	0.0	0.0	0.1	0.0	0.0	0.0
Ferrosilite	0.0	0.0	2.7	1.5	36.9	0.9	1.4	0.0	0.0	0.0	0.0	1.9	0.0	0.0	0.0

Table C2 continued

Unit	**CCI sy**	**CCI sy**	**CCI sy**	**CCI sy**	**CCI sy**	**CCI sy**	**CCI sy**	**CCI sy**	**CCI sy**	**CCI sy**	**CCI sy**	**CCI sy**	**CCI sy**	**CCI sy**	**CCI sy**
Sample	TER29-1	TER29-1	TER29-1	TER29-1	TER29-1	TER29-1	TER30-1	TER30-1	TER30-1	TER30-1	TER30-1	TER30-1	TER30-1	TER30-1	TER30-1
No.	Px5	Px6	Px7	Px8	Px9	Px10	Px1	Px2	Px5	Px9a	Px9b	Pz13a	Px13b	Px16	Px17a
Notes	Intercum.	Intercum.	Intercum.	Intercum.	Intercum.	Intercum.	Intercum.	Intercum.	Intercum.	Intercum.	Intercum.	Intercum.	Intercum.	Intercum.	Intercum.
SiO_2	52.06	52.84	51.68	52.15	51.97	51.71	52.26	50.95	51.39	51.59	52.04	51.43	51.40	52.74	52.37
TiO_2	2.14	2.40	2.48	2.79	2.37	2.22	2.82	1.65	1.46	1.44	3.02	3.09	3.78	2.01	1.86
Al_2O_3	0.16	0.23	0.12	0.22	0.26	0.13	0.14	0.12	0.17	0.12	0.25	0.14	0.20	0.44	0.21
Cr_2O_3	bdl	0.01	bdl	bdl	bdl	bdl	bdl	bdl	0.01	0.01	bdl	bdl	bdl	0.01	bdl
FeO	26.99	28.51	26.36	26.97	27.54	27.14	26.25	24.71	27.04	26.73	26.75	26.13	25.88	27.50	27.60
MnO	0.53	0.45	0.88	0.55	0.47	0.87	1.06	1.02	0.58	0.78	0.54	0.58	0.58	0.70	0.66
MgO	0.30	0.16	0.26	0.15	0.26	0.26	0.06	0.03	0.17	0.06	0.06	0.02	0.05	0.08	0.09
CaO	3.01	0.51	4.13	2.98	3.03	4.69	3.33	2.37	2.13	2.69	2.00	1.35	1.95	0.68	2.24
Na_2O	11.78	13.20	11.01	11.82	11.68	10.51	11.93	11.94	12.35	11.71	12.21	12.95	12.39	13.18	12.16
K_2O	0.01	bdl	0.01	bdl	bdl	0.02	0.01	bdl	0.01	bdl	0.01	bdl	0.01	bdl	0.02
Total	96.97	98.30	96.92	97.63	97.58	97.54	97.86	92.79	95.32	95.12	96.88	95.69	96.23	97.35	97.21
Si	2.014	2.003	2.014	2.009	2.003	2.013	2.006	2.046	2.009	2.033	2.014	2.000	2.000	2.013	2.018
Ti	0.062	0.068	0.073	0.081	0.069	0.065	0.081	0.050	0.043	0.043	0.088	0.090	0.111	0.058	0.054
Al	0.007	0.010	0.005	0.010	0.012	0.006	0.006	0.006	0.008	0.005	0.011	0.006	0.009	0.020	0.010
Cr		0.000							0.000	0.000				0.000	
Fe^{2+}	0.149	0.087	0.205	0.174	0.171	0.251	0.136	0.098	0.060	0.143	0.165	0.061	0.137	0.065	0.134
Fe^{3+}	0.724	0.817	0.654	0.694	0.717	0.633	0.707	0.732	0.824	0.738	0.701	0.789	0.705	0.813	0.756
Mn	0.017	0.014	0.029	0.018	0.015	0.029	0.034	0.035	0.019	0.026	0.018	0.019	0.019	0.023	0.021
Mg	0.017	0.009	0.015	0.009	0.015	0.015	0.003	0.002	0.010	0.003	0.003	0.001	0.003	0.004	0.005
Ca	0.125	0.021	0.172	0.123	0.125	0.196	0.137	0.102	0.089	0.114	0.083	0.056	0.081	0.028	0.092
Na	0.884	0.970	0.832	0.883	0.873	0.793	0.888	0.930	0.936	0.895	0.916	0.977	0.935	0.976	0.909
K	0.000		0.001			0.001	0.000		0.000		0.000		0.000		0.001
Sum	4.000	4.000	4.000	4.000	4.000	4.000	4.000	4.000	4.000	4.000	4.000	4.000	4.000	4.000	4.000
Aegirine	72.4	81.7	65.4	69.4	71.7	63.3	70.7	73.2	82.4	73.8	70.1	78.9	70.5	81.3	75.6
Ferri-Tschermak	0.0	0.0	0.0	0.0	0.0	0.0	0.0	0.0	0.0	0.0	0.0	0.0	0.0	0.0	0.0
Jadeite	2.1	1.3	1.9	1.8	1.5	1.9	1.3	5.2	1.7	3.8	2.5	0.7	0.9	3.3	2.8
Ti-Aegirine	12.5	13.7	14.5	16.2	13.7	13.0	16.3	10.0	8.6	8.5	17.6	18.1	22.1	11.5	10.8
Ti-Tschermak	0.0	0.0	0.0	0.0	0.0	0.0	0.0	0.0	0.0	0.0	0.0	0.0	0.0	0.0	0.0
Al-Tschermak	0.0	0.0	0.0	0.0	0.0	0.0	0.0	0.0	0.0	0.0	0.0	0.0	0.0	0.0	0.0
Diopside	1.1	0.2	1.0	0.5	0.9	1.0	0.2	0.1	0.5	0.2	0.2	0.0	0.1	0.1	0.3
Hedenbergite	11.0	1.9	16.2	11.5	11.6	18.6	9.0	8.4	4.2	11.1	8.1	0.0	4.8	2.7	8.9
Enstatite	0.0	0.1	0.0	0.0	0.0	0.1	0.0	0.0	0.0	0.0	0.0	0.0	0.0	0.0	0.0
Ferrosilite	0.0	1.0	0.2	0.0	0.3	1.6	0.0	0.0	0.0	0.8	0.7	0.0	0.0	0.3	0.7

Table C2 continued

Unit	**CCI sy**	**CCI sy**	**CCI sy**	**CCI sy**	**CCI sy**	**CCI sy**	**CCI sy**	**CCI sy**	**CCI sy**	**CCI sy**	**CCI sy**	**CCI sy**	**CCI sy**	**CCI sy**
Sample	TER30-1	TER30-7	TER29-1	TER29-1	TER29-1	TER29-1	TER29-1	TER29-1	TER30-3	TER30-3	TER30-3	TER30-3	TER30-3	TER30-3
No.	Px17b	Px3	Px1	Px4a	Px4b	Px7a	Px7b	Px10	Px1	Px2	Px3a	Px4	Px5	Px3b
Notes	Intercum.	Intercum.	Intercum.	Intercum.	Intercum.	Intercum.	Intercum.	Intercum.	Intercum.	Intercum.	Intercum.	Intercum.	Intercum.	Intercum.
SiO_2	52.74	52.71	52.17	51.80	52.33	52.34	52.80	52.12	48.63	53.02	51.73	52.29	52.60	50.11
TiO_2	4.12	6.12	2.44	4.38	2.94	3.96	0.93	2.90	2.19	4.84	0.35	0.37	1.07	0.38
Al_2O_3	0.25	0.21	0.22	0.23	0.18	0.19	0.62	0.19	4.94	0.26	0.42	0.54	0.46	0.25
Cr_2O_3	0.04	0.02	0.01	bdl	bdl	bdl	bdl	bdl	bdl	bdl	bdl	bdl	bdl	0.01
FeO	25.99	24.65	27.85	25.55	25.21	25.43	28.65	26.59	8.06	25.35	17.19	14.41	28.00	27.01
MnO	0.65	0.62	0.47	0.56	0.61	0.58	0.27	0.59	0.18	0.48	1.15	1.07	1.29	1.47
MgO	0.05	0.07	0.27	0.27	0.46	0.23	0.22	0.29	13.61	0.00	8.46	10.60	0.17	1.54
CaO	1.87	0.77	2.25	3.68	3.42	2.55	1.17	2.72	21.53	1.24	20.14	20.70	0.49	16.00
Na_2O	12.52	13.05	12.12	11.39	11.57	11.98	12.94	11.96	0.48	12.74	0.92	0.70	13.04	3.14
K_2O	0.01	bdl	0.01	0.01	bdl	0.01	bdl	bdl	bdl	bdl	0.02	bdl	0.01	0.01
Total	98.23	98.22	97.80	97.87	96.72	97.27	97.60	97.35	99.62	97.93	100.38	100.69	97.14	99.92
Si	2.013	2.009	2.001	1.999	2.030	2.021	2.010	2.009	1.813	2.028	1.993	1.982	2.013	2.003
Ti	0.118	0.175	0.070	0.127	0.086	0.115	0.027	0.084	0.061	0.139	0.010	0.011	0.031	0.012
Al	0.011	0.009	0.010	0.010	0.008	0.009	0.028	0.009	0.217	0.012	0.019	0.024	0.021	0.012
Cr	0.001	0.001	0.000											0.000
Fe^{2+}	0.177	0.200	0.145	0.235	0.186	0.203	0.058	0.157	0.183	0.211	0.509	0.415	0.036	0.700
Fe^{3+}	0.652	0.586	0.749	0.590	0.631	0.618	0.854	0.700	0.069	0.600	0.045	0.041	0.860	0.203
Mn	0.021	0.020	0.015	0.018	0.020	0.019	0.009	0.019	0.006	0.015	0.038	0.034	0.042	0.050
Mg	0.003	0.004	0.016	0.015	0.027	0.013	0.013	0.016	0.756	0.000	0.486	0.599	0.010	0.092
Ca	0.076	0.032	0.092	0.152	0.142	0.105	0.048	0.112	0.860	0.051	0.831	0.841	0.020	0.685
Na	0.926	0.964	0.901	0.852	0.870	0.897	0.955	0.894	0.035	0.945	0.069	0.052	0.967	0.243
K	0.000		0.000	0.001		0.001					0.001		0.000	0.001
Sum	4.000	4.000	4.000	4.000	4.000	4.000	4.000	4.000	4.000	4.000	4.000	4.000	4.000	4.000
Aegirine	65.2	58.6	74.9	59.0	63.1	61.8	85.4	70.0	3.5	60.0	4.5	4.1	86.0	20.3
Ferri-Tschermak	0.0	0.0	0.0	0.0	0.0	0.0	0.0	0.0	1.7	0.0	0.0	0.0	0.0	0.0
Jadeite	2.4	1.8	1.1	1.0	3.8	2.9	3.8	1.7	0.0	3.9	1.2	0.7	3.3	1.5
Ti-Aegirine	23.6	35.1	14.1	25.3	17.1	23.0	5.3	16.8	0.0	27.8	1.2	0.4	6.2	2.3
Ti-Tschermak	0.0	0.0	0.0	0.0	0.0	0.0	0.0	0.0	6.1	0.0	0.4	0.9	0.0	0.0
Al-Tschermak	0.0	0.0	0.0	0.0	0.0	0.0	0.0	0.0	3.0	0.0	0.0	0.0	0.0	0.0
Diopside	0.1	0.1	0.8	0.8	1.6	0.6	0.8	0.9	60.2	0.0	38.9	47.5	0.2	7.5
Hedenbergite	7.5	3.1	8.4	13.4	12.6	10.0	4.0	10.0	15.0	5.1	43.8	35.7	1.8	61.1
Enstatite	0.0	0.0	0.1	0.0	0.0	0.0	0.0	0.0	7.7	0.0	4.7	6.1	0.2	0.8
Ferrosilite	0.3	0.8	0.6	0.0	0.2	0.7	0.2	0.0	1.9	1.8	5.3	4.6	1.6	6.5

Table C2 continued

Unit	**CCI enc**	**CCI enc**	**CCI enc**	**CCI enc**	**CCI enc**	**CCI enc**	**CCI enc**	**CCI enc**	**CCI enc**	**CCI enc**	**CCI enc**	**CCI enc**	**CCI enc**	**CCI enc**
Sample	Spec 1	Spec 1	Spec 1	Spec 1	Spec 1	Spec 1	Spec 1	Spec 1	Spec 1	Spec 1	Spec 1	Spec 1	Spec 1	Spec 1
No.	Pheno2	Pheno2	Pheno2	Pheno 3	Pheno3	Pheno3	Pheno4	Pheno4	Pheno4	Pheno5	Pheno6	Pheno7	Pheno7	Pheno8
Notes	Core	Core	Core	Core	Core	Rim	Core	Core	Rim	Core	Core	Core	Core	Core
SiO_2	48.99	49.19	49.79	49.05	49.74	47.53	48.53	48.47	47.02	48.45	45.88	48.47	48.97	50.69
TiO_2	1.22	1.20	1.28	1.36	1.31	1.95	1.78	1.73	1.64	1.60	2.57	1.83	1.55	0.50
Al_2O_3	4.31	4.33	2.85	4.02	2.78	4.40	4.71	4.49	3.46	4.31	6.59	5.22	4.29	0.78
Cr_2O_3	0.43	0.60	bdl	0.25	0.02	0.03	0.22	0.29	0.11	0.16	0.02	0.27	0.26	bdl
FeO	5.64	5.31	7.78	5.53	6.95	13.11	6.45	6.09	16.10	6.20	7.34	6.45	6.28	13.76
MnO	0.08	0.10	0.36	0.11	0.21	0.56	0.14	0.13	0.74	0.09	0.11	0.11	0.14	1.05
MgO	14.85	15.57	14.23	14.76	15.24	10.39	14.65	14.89	8.47	14.53	13.32	14.15	14.90	11.44
CaO	22.23	22.36	21.44	22.80	21.40	18.05	21.92	22.30	17.13	22.27	21.52	22.08	21.95	20.36
Na_2O	0.34	0.35	0.93	0.31	0.43	2.24	0.42	0.37	2.49	0.35	0.44	0.38	0.38	0.64
K_2O	0.01	bdl	bdl	bdl	bdl	0.34	0.01	0.02	0.53	0.03	0.03	bdl	0.03	bdl
Total	98.08	99.01	98.66	98.19	98.08	98.59	98.82	98.78	97.69	97.99	97.83	98.94	98.74	99.20
Si	1.836	1.821	1.863	1.838	1.868	1.807	1.810	1.806	1.826	1.822	1.737	1.809	1.826	1.941
Ti	0.034	0.034	0.036	0.038	0.037	0.056	0.050	0.048	0.048	0.045	0.073	0.051	0.044	0.014
Al	0.190	0.189	0.126	0.177	0.123	0.197	0.207	0.197	0.158	0.191	0.294	0.230	0.189	0.035
Cr	0.013	0.017		0.007	0.001	0.001	0.006	0.009	0.004	0.005	0.001	0.008	0.008	
Fe^{2+}	0.096	0.054	0.099	0.087	0.122	0.157	0.103	0.077	0.220	0.099	0.114	0.132	0.104	0.338
Fe^{3+}	0.081	0.110	0.144	0.086	0.096	0.259	0.098	0.113	0.303	0.096	0.119	0.069	0.092	0.102
Mn	0.002	0.003	0.011	0.004	0.007	0.018	0.004	0.004	0.024	0.003	0.004	0.003	0.004	0.034
Mg	0.830	0.859	0.794	0.825	0.853	0.589	0.815	0.827	0.491	0.815	0.752	0.787	0.828	0.653
Ca	0.893	0.887	0.859	0.915	0.861	0.735	0.876	0.891	0.713	0.897	0.873	0.883	0.877	0.835
Na	0.024	0.025	0.068	0.023	0.031	0.165	0.031	0.027	0.187	0.025	0.033	0.028	0.027	0.047
K	0.000					0.017	0.000	0.001	0.026	0.001	0.001		0.001	
Sum	4.000	4.000	4.000	4.000	4.000	4.000	4.000	4.000	4.000	4.000	4.000	4.000	4.000	4.000
Aegirine	2.4	2.5	6.8	2.3	3.1	16.5	3.1	2.7	18.7	2.5	3.3	2.8	2.7	4.7
Ferri-Tschermak	2.8	4.2	3.8	3.2	3.3	4.7	3.4	4.3	5.8	3.5	4.3	2.1	3.3	2.7
Jadeite	0.0	0.0	0.0	0.0	0.0	0.0	0.0	0.0	0.0	0.0	0.0	0.0	0.0	0.0
Ti-Aegirine	0.0	0.0	0.0	0.0	0.0	0.0	0.0	0.0	0.0	0.0	0.0	0.0	0.0	0.0
Ti-Tschermak	3.4	3.4	3.6	3.8	3.7	5.6	5.0	4.8	4.8	4.5	7.3	5.1	4.4	1.4
Al-Tschermak	2.7	1.0	0.0	1.5	0.0	0.4	1.7	0.4	0.0	1.3	3.1	3.9	1.5	0.0
Diopside	71.8	75.1	68.9	74.8	68.8	48.4	68.5	72.5	40.5	71.4	62.8	65.9	69.5	50.5
Hedenbergite	8.5	5.0	9.6	8.2	10.4	14.4	9.0	7.1	20.2	8.9	9.8	11.3	9.1	28.8
Enstatite	5.6	5.4	5.2	3.8	8.3	5.2	6.5	5.1	4.3	5.0	6.2	6.4	6.6	7.4
Ferrosilite	0.7	0.4	0.7	0.4	1.3	1.6	0.8	0.5	2.1	0.6	1.0	1.1	0.9	4.2

Table C2 continued

Unit	**CCl enc**	**CCl enc**	**CCl enc**	**CCl enc**	**CCl enc**	**CCl enc**	**CCl enc**	**CCl enc**	**CCl enc**	**CCl enc**	**CCl enc**	**CCl enc**	**CCl enc**
Sample	Spec 1	T073 A3	T073 A3	T073 A3	T073 A3	T073 A3	T073 A3	T073 A3	T073 A3	T073 A3	T073 A3	T073 A3	T073 A3
No.	Pheno9	Pheno1	Pheno1	Pheno1	Pheno1	Pheno1	Pheno1	Pheno1	Pheno2	Pheno2	Pheno3	Pheno4	Pheno5
Notes	Core	Core	Core	Core	Core	Rim	Rim	Rim	Core	Core	Core	Core	Core
SiO_2	50.82	49.51	46.77	48.09	49.69	47.62	47.58	49.11	50.21	50.39	49.82	47.69	48.82
TiO_2	0.49	1.50	2.53	1.93	1.55	2.10	2.09	1.58	0.56	0.52	0.55	1.88	1.12
Al_2O_3	0.77	3.83	5.55	4.82	3.40	4.74	4.92	3.15	0.66	0.56	0.93	4.54	4.61
Cr_2O_3	bdl	0.22	0.23	0.28	0.14	0.11	0.15	0.04	0.02	bdl	bdl	0.06	0.76
FeO	12.69	6.77	7.76	7.08	7.07	7.44	7.45	9.06	14.67	14.96	13.13	7.53	4.92
MnO	0.97	0.15	0.13	0.15	0.17	0.17	0.11	0.33	1.07	1.10	0.88	0.19	0.11
MgO	12.03	15.14	13.50	13.77	15.07	14.15	14.15	14.00	10.60	10.56	11.90	14.28	15.71
CaO	20.88	21.56	21.89	21.86	21.34	22.06	21.94	21.08	20.17	20.38	20.30	21.86	21.55
Na_2O	0.58	0.42	0.39	0.45	0.39	0.50	0.45	0.56	0.69	0.60	0.52	0.41	0.41
K_2O	bdl	bdl	0.01	0.04	bdl	0.02	bdl	bdl	0.04	bdl	0.01	bdl	0.02
Total	99.22	99.11	98.76	98.48	98.83	98.92	98.84	98.91	98.71	99.07	98.05	98.44	98.02
Si	1.937	1.840	1.759	1.808	1.855	1.781	1.781	1.845	1.942	1.945	1.924	1.792	1.821
Ti	0.014	0.042	0.071	0.055	0.043	0.059	0.059	0.045	0.016	0.015	0.016	0.053	0.032
Al	0.034	0.168	0.246	0.214	0.150	0.209	0.217	0.140	0.030	0.026	0.042	0.201	0.203
Cr		0.006	0.007	0.008	0.004	0.003	0.004	0.001	0.001			0.002	0.022
Fe^{2+}	0.297	0.119	0.129	0.136	0.143	0.087	0.103	0.165	0.368	0.384	0.307	0.099	0.054
Fe^{3+}	0.107	0.092	0.115	0.086	0.077	0.146	0.131	0.120	0.107	0.099	0.117	0.137	0.100
Mn	0.031	0.005	0.004	0.005	0.005	0.005	0.004	0.010	0.035	0.036	0.029	0.006	0.003
Mg	0.683	0.839	0.757	0.772	0.839	0.789	0.789	0.784	0.611	0.608	0.685	0.800	0.873
Ca	0.853	0.859	0.882	0.881	0.854	0.884	0.880	0.849	0.836	0.843	0.840	0.880	0.861
Na	0.043	0.031	0.029	0.032	0.029	0.036	0.032	0.041	0.052	0.045	0.039	0.030	0.029
K			0.000	0.002		0.001			0.002		0.001		0.001
Sum	4.000	4.000	4.000	4.000	4.000	4.000	4.000	4.000	4.000	4.000	4.000	4.000	4.000
Aegirine	4.3	3.1	2.9	3.2	2.9	3.6	3.2	4.1	5.2	4.5	3.9	3.0	2.9
Ferri-Tschermak	3.2	3.1	4.3	2.7	2.4	5.5	4.9	4.0	2.7	2.7	3.9	5.4	3.5
Jadeite	0.0	0.0	0.0	0.0	0.0	0.0	0.0	0.0	0.0	0.0	0.0	0.0	0.0
Ti-Aegirine	0.0	0.0	0.0	0.0	0.0	0.0	0.0	0.0	0.0	0.0	0.0	0.0	0.0
Ti-Tschermak	1.4	4.2	7.1	5.5	4.3	5.9	5.9	4.5	1.5	1.3	1.6	5.3	3.2
Al-Tschermak	0.0	0.8	0.5	2.2	0.5	0.0	0.0	0.0	0.0	0.0	0.0	0.0	2.4
Diopside	54.5	67.8	64.8	65.7	66.3	69.0	68.0	62.5	47.8	47.5	52.7	68.3	72.3
Hedenbergite	26.2	10.0	11.4	12.0	11.8	8.1	9.1	14.0	31.5	32.8	25.8	9.0	4.7
Enstatite	6.9	8.0	5.5	5.8	8.8	5.0	5.5	8.0	6.7	6.6	7.9	5.8	7.5
Ferrosilite	3.3	1.2	1.0	1.0	1.6	0.6	0.7	1.8	4.4	4.6	3.9	0.8	0.5

Table C2 continued

Unit	**CCI enc**	**CCI enc**	**CCI enc**	**CCI enc**	**CCI enc**	**CCI enc**	**CCI enc**	**CCI enc**	**CCI enc**	**CCI enc**	**CCI enc**	**CCI enc**	**CCI enc**	**CCI enc**
Sample	Spec 1	Spec 1	Spec 1	Spec 1	Spec 1	Spec 1	Spec 1	Spec 1	Spec 1	Spec 1	Spec 1	Spec 1	Spec 1	Spec 1
No.	Cpx 1	Cpx 2	Cpx 3	Cpx 4	Cpx 5	Cpx 6	Cpx 7	Cpx 8	Cpx 9	Cpx 10	Cpx 11	Cpx 12	Cpx 13	Cpx 14
Notes	Gm	Gm	Gm	Gm	Gm	Gm	Gm	Gm	Gm	Gm	Gm	Gm	Gm	Gm
SiO_2	50.54	47.55	49.98	50.10	46.67	50.70	50.31	50.54	50.50	50.81	49.97	50.30	50.45	49.98
TiO_2	0.31	1.47	0.34	0.45	2.96	0.30	0.35	0.40	0.39	0.33	0.32	0.34	0.35	0.35
Al_2O_3	0.33	2.69	0.46	0.38	0.46	0.48	0.42	0.56	0.46	0.58	0.36	0.35	2.17	0.41
Cr_2O_3	bdl	0.01	0.02	bdl	0.01	bdl	bdl	0.01	0.02	bdl	bdl	bdl	0.01	0.01
FeO	18.48	18.93	16.07	16.40	19.31	14.75	15.73	15.33	18.16	18.38	16.58	16.64	16.57	16.49
MnO	1.21	0.87	1.02	1.10	1.05	1.03	1.02	1.06	1.13	1.11	1.09	1.09	0.90	1.07
MgO	6.98	7.32	8.76	8.40	8.99	9.91	8.80	9.09	7.03	6.84	8.15	8.41	6.87	8.67
CaO	19.75	15.58	20.86	20.25	18.38	20.51	20.37	20.49	20.24	19.61	20.45	20.43	17.54	20.61
Na_2O	1.23	2.29	0.91	1.07	0.81	0.86	0.94	1.17	1.28	1.42	0.99	1.01	2.26	0.93
K_2O	0.01	0.59	0.02	0.01	bdl	0.02	0.04	0.06	0.05	0.10	0.01	bdl	0.08	0.01
Total	98.84	97.30	98.44	98.14	98.63	98.55	97.97	98.72	99.26	99.20	97.92	98.58	97.20	98.54
Si	1.989	1.880	1.954	1.968	1.846	1.966	1.975	1.961	1.977	1.990	1.971	1.969	1.990	1.955
Ti	0.009	0.044	0.010	0.013	0.088	0.009	0.010	0.012	0.012	0.010	0.009	0.010	0.010	0.010
Al	0.015	0.125	0.021	0.017	0.021	0.022	0.019	0.026	0.021	0.027	0.017	0.016	0.101	0.019
Cr		0.000	0.001		0.000			0.000	0.001				0.000	0.000
Fe^{2+}	0.526	0.393	0.406	0.437	0.466	0.384	0.433	0.377	0.493	0.515	0.447	0.442	0.472	0.419
Fe^{3+}	0.082	0.233	0.120	0.101	0.173	0.094	0.084	0.120	0.101	0.087	0.099	0.102	0.074	0.121
Mn	0.040	0.029	0.034	0.037	0.035	0.034	0.034	0.035	0.037	0.037	0.037	0.036	0.030	0.036
Mg	0.410	0.431	0.511	0.492	0.530	0.573	0.515	0.526	0.410	0.399	0.479	0.491	0.404	0.505
Ca	0.833	0.660	0.874	0.852	0.779	0.852	0.857	0.852	0.849	0.823	0.864	0.857	0.741	0.864
Na	0.094	0.175	0.069	0.081	0.062	0.065	0.072	0.088	0.097	0.108	0.076	0.076	0.173	0.070
K	0.001	0.030	0.001	0.000		0.001	0.002	0.003	0.003	0.005	0.001		0.004	0.001
Sum	4.000	4.000	4.000	4.000	4.000	4.000	4.000	4.000	4.000	4.000	4.000	4.000	4.000	4.000
Aegirine	8.2	17.5	6.9	8.1	6.2	6.5	7.2	8.8	9.7	8.7	7.6	7.6	7.4	7.0
Ferri-Tschermak	0.0	2.9	2.5	1.0	5.5	1.5	0.6	1.6	0.2	0.0	1.2	1.3	0.0	2.5
Jadeite	0.5	0.0	0.0	0.0	0.0	0.0	0.0	0.0	0.0	1.7	0.0	0.0	9.1	0.0
Ti-Aegirine	0.7	0.0	0.0	0.0	0.0	0.0	0.0	0.0	0.0	0.4	0.0	0.0	0.7	0.0
Ti-Tschermak	0.5	4.4	1.0	0.9	1.1	0.9	1.0	1.2	1.1	0.5	0.8	0.8	0.5	1.0
Al-Tschermak	0.0	0.5	0.0	0.0	0.0	0.0	0.0	0.0	0.0	0.0	0.0	0.0	0.0	0.0
Diopside	34.7	29.4	45.1	42.4	36.6	47.9	44.1	46.2	36.4	34.3	42.0	42.3	32.8	43.7
Hedenbergite	48.0	28.8	38.8	40.9	34.6	35.0	40.0	36.2	47.2	47.4	42.4	41.2	40.8	39.2
Enstatite	3.1	6.8	3.0	3.4	8.2	4.7	3.7	3.2	2.3	2.8	3.0	3.4	3.7	3.4
Ferrosilite	4.2	6.7	2.6	3.2	7.7	3.4	3.3	2.5	2.9	3.8	3.0	3.3	4.6	3.1

Table C2 continued

Unit	**CCI enc**	**CCI enc**	**CCI enc**	**CCI enc**	**CCI enc**	**CCI enc**	**CCI enc**	**CCI enc**	**CCI enc**	**CCI enc**	**CCI enc**	**CCI enc**	**CCI enc**	**CCI enc**
Sample	Spec 1	Spec 1	Spec 1	Spec 1	Spec 1	Spec 1	T073 A3	T073 A3	T073 A3	T073 A3	T073 A3	T073 A3	T073 A3	T073 A3
No.	Cpx 15	Cpx 16	Cpx 17	Cpx 18	Cpx 19	Cpx 20	Cpx 1	Cpx 2	Cpx 4	Cpx 5	Cpx 6	Cpx 7	Cpx 8	Cpx 9
Notes	Gm	Gm	Gm	Gm	Gm	Gm	Gm	Gm	Gm	Gm	Gm	Gm	Gm	Gm
SiO_2	50.04	48.19	49.03	49.32	49.14	48.89	50.66	50.17	48.35	47.57	48.83	50.60	50.05	50.13
TiO_2	0.23	0.33	0.31	0.38	0.35	0.42	0.24	0.44	0.43	0.41	0.81	0.41	0.32	0.39
Al_2O_3	0.35	0.56	0.32	0.32	0.41	0.35	0.38	0.52	0.19	0.23	0.18	0.59	0.33	0.35
Cr_2O_3	bdl	bdl	0.01	bdl	bdl	0.01	0.02	bdl	0.02	0.02	bdl	0.02	bdl	bdl
FeO	17.98	21.78	19.47	22.42	17.58	22.50	16.24	13.61	26.84	25.26	27.25	13.67	17.83	16.56
MnO	1.12	1.06	1.17	1.05	1.10	1.11	1.08	1.05	1.18	1.28	0.91	1.00	1.25	1.20
MgO	7.34	4.06	6.29	3.63	7.65	3.84	9.51	10.75	1.43	2.25	0.69	11.12	7.97	9.27
CaO	20.00	20.38	19.78	16.90	19.66	17.36	20.19	20.50	13.71	15.89	10.52	20.66	19.93	20.13
Na_2O	1.25	1.53	1.42	3.32	1.24	2.75	0.82	0.76	5.00	3.28	7.18	0.71	1.19	0.77
K_2O	0.01	0.05	0.01	0.03	bdl	0.01	0.03	bdl	bdl	bdl	bdl	0.03	0.03	0.01
Total	98.32	97.94	97.81	97.37	97.14	97.23	99.16	97.82	97.14	96.19	96.37	98.81	98.91	98.82
Si	1.974	1.944	1.956	1.981	1.958	1.974	1.963	1.951	1.956	1.959	1.964	1.946	1.958	1.954
Ti	0.007	0.010	0.009	0.012	0.011	0.013	0.007	0.013	0.013	0.013	0.024	0.012	0.010	0.011
Al	0.016	0.026	0.015	0.015	0.019	0.017	0.017	0.024	0.009	0.011	0.009	0.027	0.015	0.016
Cr			0.000			0.000	0.001		0.000	0.001		0.001		
Fe^{2+}	0.475	0.548	0.486	0.493	0.445	0.535	0.422	0.337	0.464	0.564	0.342	0.329	0.443	0.428
Fe^{3+}	0.118	0.187	0.164	0.260	0.141	0.225	0.105	0.105	0.444	0.306	0.574	0.111	0.141	0.112
Mn	0.037	0.036	0.039	0.036	0.037	0.038	0.035	0.034	0.040	0.045	0.031	0.032	0.042	0.040
Mg	0.432	0.244	0.374	0.217	0.455	0.231	0.549	0.623	0.087	0.138	0.041	0.637	0.465	0.539
Ca	0.845	0.881	0.846	0.727	0.839	0.751	0.838	0.854	0.594	0.701	0.453	0.851	0.835	0.841
Na	0.095	0.120	0.110	0.258	0.096	0.215	0.062	0.057	0.392	0.262	0.560	0.053	0.090	0.058
K	0.000	0.002	0.001	0.001		0.000	0.001					0.001	0.002	0.001
Sum	4.000	4.000	4.000	4.000	4.000	4.000	4.000	4.000	4.000	4.000	4.000	4.000	4.000	4.000
Aegirine	9.5	12.0	11.0	25.8	9.6	21.5	6.2	5.7	39.2	26.2	56.0	5.3	9.0	5.8
Ferri-Tschermak	1.1	3.3	2.7	0.1	2.2	0.5	2.2	2.4	2.6	2.2	0.7	2.9	2.5	2.7
Jadeite	0.0	0.0	0.0	0.0	0.0	0.0	0.0	0.0	0.0	0.0	0.0	0.0	0.0	0.0
Ti-Aegirine	0.0	0.0	0.0	0.0	0.0	0.0	0.0	0.0	0.0	0.0	0.0	0.0	0.0	0.0
Ti-Tschermak	0.7	1.0	0.8	0.7	1.0	0.8	0.7	1.2	0.4	0.6	0.4	1.2	0.8	0.8
Al-Tschermak	0.0	0.0	0.0	0.0	0.0	0.0	0.0	0.0	0.0	0.0	0.0	0.0	0.0	0.0
Diopside	37.8	24.4	33.7	20.9	39.2	21.2	44.2	51.3	8.3	12.5	4.1	51.7	39.3	43.1
Hedenbergite	44.9	58.4	47.4	50.9	41.5	52.6	36.8	30.6	48.1	54.9	37.3	29.3	40.9	37.5
Enstatite	2.7	0.0	1.8	0.4	3.1	0.9	5.4	5.5	0.2	0.7	0.0	6.0	3.6	5.4
Ferrosilite	3.2	0.0	2.6	1.0	3.3	2.4	4.5	3.3	1.1	3.0	0.0	3.4	3.7	4.7

Table C2 continued

Unit	**CCI enc**	**CCI enc**	**CCI enc**	**CCI enc**	**CCI enc**	**CCI enc**	**CCI enc**	**CCI enc**	**CCI enc**	**CCI enc**	**CCI enc**	**CCI enc**	**CCI enc**	**CCI enc**
Sample	T073 A3	T073 A3	T073 A3	T073 A3	T073 A3	T073 A3	T073 A3	T073 A3	T073 A3	T073 A3	T073 A3	T073 A3	T073 A3	T073 A3
No.	Cpx 10	Cpx 11	Cpx 12	Cpx 13	Cpx 14	Cpx 15	Cpx 16	Cpx 17	Cpx 18	Cpx 19	Cpx 20	Cpx 21	Cpx 22	Cpx 23
Notes	Gm	Gm	Gm	Gm	Gm	Gm	Gm	Gm	Gm	Gm	Gm	Gm	Gm	Gm
SiO_2	48.27	48.86	48.12	49.14	48.85	49.74	49.87	50.99	49.66	48.86	49.69	50.91	50.28	50.51
TiO_2	1.73	1.58	1.48	0.30	0.33	0.34	0.41	0.51	0.38	0.41	0.38	0.58	0.46	0.38
Al_2O_3	4.23	3.89	4.35	0.49	0.28	0.46	0.37	0.68	0.41	0.21	0.50	0.89	0.51	0.38
Cr_2O_3	0.11	0.22	0.39	bdl	bdl	0.01	0.04	0.03	0.01	bdl	bdl	bdl	bdl	bdl
FeO	6.56	6.40	6.20	20.08	21.94	14.95	20.43	13.24	16.34	24.75	15.58	13.26	15.46	17.33
MnO	0.12	0.13	0.14	1.05	1.30	1.02	0.98	0.89	1.11	1.24	1.15	0.93	1.09	1.10
MgO	14.29	14.73	15.05	5.50	4.86	9.80	5.43	11.54	8.82	2.89	9.65	11.89	9.96	8.24
CaO	22.42	22.04	22.20	20.24	18.66	20.17	16.73	20.36	19.98	16.09	20.31	20.32	20.38	19.61
Na_2O	0.40	0.37	0.37	1.51	1.98	0.84	3.31	0.75	1.23	3.43	0.81	0.58	0.63	1.07
K_2O	0.01	0.01	bdl	0.04	bdl	0.01	bdl	0.02	0.01	0.01	0.01	bdl	bdl	0.01
Total	98.15	98.24	98.29	98.35	98.20	97.33	97.56	99.00	97.94	97.90	98.09	99.36	98.77	98.62
Si	1.815	1.834	1.801	1.956	1.955	1.955	1.975	1.951	1.947	1.966	1.943	1.941	1.953	1.980
Ti	0.049	0.045	0.042	0.009	0.010	0.010	0.012	0.015	0.011	0.013	0.011	0.017	0.013	0.011
Al	0.187	0.172	0.192	0.023	0.013	0.021	0.017	0.031	0.019	0.010	0.023	0.040	0.023	0.017
Cr	0.003	0.006	0.012			0.000	0.001	0.001	0.000					
Fe^{2+}	0.097	0.108	0.055	0.503	0.524	0.378	0.416	0.331	0.378	0.533	0.378	0.335	0.411	0.486
Fe^{3+}	0.110	0.093	0.139	0.165	0.210	0.113	0.261	0.093	0.158	0.300	0.132	0.088	0.092	0.083
Mn	0.004	0.004	0.004	0.035	0.044	0.034	0.033	0.029	0.037	0.042	0.038	0.030	0.036	0.036
Mg	0.801	0.824	0.839	0.326	0.290	0.574	0.321	0.658	0.515	0.173	0.563	0.676	0.577	0.482
Ca	0.904	0.886	0.890	0.863	0.800	0.849	0.710	0.835	0.839	0.694	0.851	0.830	0.848	0.824
Na	0.029	0.027	0.027	0.116	0.153	0.064	0.254	0.055	0.094	0.268	0.062	0.043	0.047	0.081
K	0.001	0.001		0.002		0.000		0.001	0.000	0.000	0.000			0.000
Sum	4.000	4.000	4.000	4.000	4.000	4.000	4.000	4.000	4.000	4.000	4.000	4.000	4.000	4.000
Aegirine	2.9	2.7	2.7	11.6	15.3	6.4	25.4	5.5	9.4	26.8	6.2	4.3	4.7	8.1
Ferri-Tschermak	4.0	3.3	5.6	2.4	2.8	2.4	0.3	1.9	3.2	1.6	3.5	2.2	2.2	0.1
Jadeite	0.0	0.0	0.0	0.0	0.0	0.0	0.0	0.0	0.0	0.0	0.0	0.0	0.0	0.0
Ti-Aegirine	0.0	0.0	0.0	0.0	0.0	0.0	0.0	0.0	0.0	0.0	0.0	0.0	0.0	0.0
Ti-Tschermak	4.9	4.5	4.2	0.9	0.7	1.0	0.9	1.5	0.9	0.5	1.1	1.7	1.2	0.9
Al-Tschermak	0.3	0.6	0.0	0.0	0.0	0.0	0.0	0.0	0.0	0.0	0.0	0.0	0.0	0.0
Diopside	72.1	70.7	74.0	31.3	25.8	47.5	29.1	51.8	44.2	15.6	46.3	51.4	45.9	39.1
Hedenbergite	9.1	9.6	5.2	51.7	50.7	34.0	40.7	28.3	35.6	51.7	34.2	27.8	35.5	42.4
Enstatite	4.0	5.9	5.0	0.7	1.6	5.0	1.5	7.0	3.7	0.9	5.0	8.1	5.9	4.5
Ferrosilite	0.5	0.8	0.4	1.1	3.1	3.6	2.1	3.8	3.0	2.9	3.7	4.4	4.6	4.9

Table C2 continued

Unit	**CCI enc**	**CCI enc**	**CCI enc**	**CCI enc**	**CCI enc**	**CCI enc**	**CCI enc**	**CCI enc**	**CCI enc**	**CCI enc**	**CCI enc**	**CCI enc**
Sample	T073 A3	T073 A3	Spec 1	Spec 1	Spec 1	Spec 1	Spec 1	Spec 1	Spec 1	Spec 1	Spec 1	Spec 1
No.	Cpx 24	Cpx 25	Cpx 21	Cpx 22	Cpx 23	Cpx 24	Cpx 25	Cpx 26	Cpx 26b	Cpx 27	Cpx 28	Cpx 29
Notes	Gm	Gm	Gm	Gm	Gm	Gm	Gm	Gm	Gm	Gm	Gm	Gm
SiO_2	48.74	47.87	50.31	50.67	48.47	47.76	48.29	50.49	49.90	50.32	49.00	50.28
TiO_2	1.44	1.94	0.42	0.52	1.72	1.90	1.13	0.37	0.69	0.38	0.35	0.39
Al_2O_3	4.77	5.03	0.63	0.69	3.91	4.41	1.09	0.47	0.78	0.34	0.19	0.46
Cr_2O_3	0.35	0.18	bdl	bdl	0.16	0.18	bdl	bdl	0.01	bdl	bdl	bdl
FeO	6.53	7.80	14.25	13.15	7.16	7.66	20.81	14.91	17.07	18.18	23.96	16.16
MnO	0.15	0.15	1.13	0.98	0.18	0.16	1.15	1.05	1.13	1.12	1.11	1.11
MgO	14.57	13.55	10.82	11.39	14.23	14.05	6.42	9.99	8.18	7.68	3.01	9.16
CaO	21.40	21.23	20.51	20.79	21.81	21.62	15.07	20.45	19.02	20.04	16.05	20.32
Na_2O	0.44	0.53	0.60	0.64	0.61	0.76	3.08	0.81	1.63	1.27	3.74	0.90
K_2O	bdl	0.31	0.02	bdl	0.01	bdl	0.41	0.03	0.10	0.01	bdl	bdl
Total	98.38	98.60	98.69	98.84	98.26	98.50	97.44	98.58	98.52	99.34	97.40	98.79
Si	1.825	1.799	1.944	1.945	1.822	1.791	1.912	1.959	1.948	1.963	1.972	1.957
Ti	0.041	0.055	0.012	0.015	0.049	0.054	0.034	0.011	0.020	0.011	0.011	0.011
Al	0.210	0.223	0.029	0.031	0.173	0.195	0.051	0.021	0.036	0.016	0.009	0.021
Cr	0.010	0.005			0.005	0.005			0.000			
Fe^{2+}	0.125	0.128	0.356	0.326	0.099	0.075	0.376	0.383	0.402	0.460	0.489	0.417
Fe^{3+}	0.080	0.118	0.105	0.096	0.126	0.165	0.313	0.101	0.155	0.133	0.317	0.109
Mn	0.005	0.005	0.037	0.032	0.006	0.005	0.038	0.035	0.037	0.037	0.038	0.037
Mg	0.813	0.759	0.623	0.652	0.797	0.786	0.379	0.578	0.476	0.447	0.180	0.531
Ca	0.859	0.855	0.849	0.855	0.878	0.869	0.639	0.850	0.796	0.837	0.692	0.848
Na	0.032	0.039	0.045	0.048	0.045	0.055	0.236	0.061	0.123	0.096	0.292	0.068
K		0.015	0.001		0.000		0.021	0.001	0.005	0.001		
Sum	4.000	4.000	4.000	4.000	4.000	4.000	4.000	4.000	4.000	4.000	4.000	4.000
Aegirine	3.2	3.9	4.5	4.8	4.5	5.5	23.6	6.1	12.3	9.6	29.2	6.8
Ferri-Tschermak	2.4	3.9	3.0	2.4	4.1	5.5	3.9	2.0	1.6	1.9	1.3	2.1
Jadeite	0.0	0.0	0.0	0.0	0.0	0.0	0.0	0.0	0.0	0.0	0.0	0.0
Ti-Aegirine	0.0	0.0	0.0	0.0	0.0	0.0	0.0	0.0	0.0	0.0	0.0	0.0
Ti-Tschermak	4.1	5.5	1.2	1.5	4.9	5.4	2.5	1.1	1.8	0.8	0.4	1.1
Al-Tschermak	3.6	2.2	0.0	0.0	0.0	0.0	0.0	0.0	0.0	0.0	0.0	0.0
Diopside	65.4	62.9	49.5	52.7	69.7	69.0	27.5	47.6	39.6	38.4	17.2	44.0
Hedenbergite	10.4	11.0	31.2	28.9	9.2	7.0	30.1	34.4	36.6	42.7	50.3	37.6
Enstatite	7.9	6.5	6.4	6.3	5.0	4.8	5.2	5.1	4.0	3.1	0.4	4.5
Ferrosilite	1.3	1.1	4.0	3.4	0.7	0.5	5.7	3.7	3.7	3.5	1.2	3.9

Table C2 continued

Unit	**PNI**	**PNI**	**PNI**	**PNI**	**PNI**	**PNI**	**PNI**	**PNI**	**PNI**	**PNI**	**PNI**	**PNI**	**PNI**	**PNI**	**PNI**
Sample	T012	T012	T012	T012	T012	T012	T012	T012	T012	T012	T012	T012	T012	T012	T012
No.	1 / 1 .	2 / 1 .	3 / 1 .	4 / 1 .	5 / 1 .	9 / 1 .	10 / 1 .	11 / 1 .	12 / 1 .	13 / 1 .	14 / 1 .	15 / 1 .	16 / 1 .	17 / 1 .	18 / 1 .
Notes	Pheno	Pheno	Pheno	Pheno	Pheno	Pheno	Pheno	Pheno	Pheno	Pheno	Pheno	Pheno	Pheno	Pheno	Pheno
SiO_2	52.43	52.51	52.44	52.23	47.56	52.42	52.47	53.11	52.64	52.72	52.75	51.51	52.46	52.52	52.14
TiO_2	0.44	0.43	0.35	0.47	3.18	0.40	0.37	0.62	0.71	0.48	0.41	0.64	0.38	0.39	0.47
Al_2O_3	0.55	0.53	0.48	0.49	5.98	0.44	0.43	3.31	3.31	0.77	0.48	0.83	0.47	0.49	0.53
Cr_2O_3	bdl	0.01	0.02	bdl	0.06	bdl	0.02	0.49	0.70	0.04	bdl	bdl	0.02	bdl	bdl
FeO	15.63	15.98	16.10	15.54	9.25	15.47	15.88	3.96	3.93	13.53	15.12	16.84	15.28	15.84	15.49
MnO	1.26	1.24	1.20	1.15	0.22	1.22	1.33	0.07	0.07	1.01	1.21	1.40	1.21	1.23	1.17
MgO	10.05	9.94	9.98	10.09	12.84	10.20	10.14	17.04	16.74	11.37	10.58	9.50	10.60	9.81	9.88
CaO	20.19	19.83	19.47	19.89	20.95	20.11	19.83	21.96	22.32	20.34	19.87	18.85	20.13	20.07	19.95
Na_2O	0.67	0.75	0.66	0.65	0.56	0.62	0.66	0.26	0.29	0.64	0.66	0.88	0.73	0.77	0.68
K_2O	bdl	bdl	bdl	bdl	0.01	bdl	bdl	bdl	bdl	bdl	bdl	bdl	bdl	bdl	bdl
Total	101.22	101.22	100.68	100.50	100.60	100.87	101.12	100.80	100.70	100.89	101.06	100.45	101.28	101.12	100.31
Si	1.988	1.993	2.002	1.995	1.767	1.994	1.993	1.920	1.907	1.986	1.998	1.975	1.981	1.995	1.996
Ti	0.013	0.012	0.010	0.013	0.089	0.011	0.010	0.017	0.019	0.013	0.012	0.018	0.011	0.011	0.014
Al	0.025	0.024	0.021	0.022	0.262	0.020	0.019	0.141	0.141	0.034	0.021	0.038	0.021	0.022	0.024
Cr		0.000	0.000		0.002		0.001	0.014	0.020	0.001			0.000		
Fe^{2+}	0.473	0.486	0.512	0.486	0.223	0.477	0.482	0.120	0.113	0.415	0.470	0.500	0.435	0.481	0.489
Fe^{3+}	0.023	0.021	0.002	0.010	0.064	0.015	0.022	0.000	0.006	0.012	0.008	0.040	0.048	0.022	0.007
Mn	0.040	0.040	0.039	0.037	0.007	0.039	0.043	0.002	0.002	0.032	0.039	0.045	0.039	0.040	0.038
Mg	0.568	0.562	0.568	0.575	0.711	0.579	0.574	0.918	0.904	0.639	0.598	0.543	0.597	0.556	0.564
Ca	0.821	0.806	0.796	0.814	0.834	0.820	0.807	0.850	0.866	0.821	0.806	0.775	0.815	0.817	0.818
Na	0.049	0.055	0.049	0.048	0.040	0.046	0.048	0.018	0.020	0.047	0.048	0.066	0.054	0.056	0.050
K					0.000										
Sum	4.000	4.000	4.000	4.000	4.000	4.000	4.000	4.000	4.000	4.000	4.000	4.000	4.000	4.000	4.000
Aegirine	2.3	2.1	0.2	1.0	4.0	1.5	2.2	0.0	0.6	1.2	0.8	4.0	4.8	2.2	0.7
Ferri-Tschermak	0.0	0.0	0.0	0.0	1.2	0.0	0.0	0.0	0.0	0.0	0.0	0.0	0.0	0.0	0.0
Jadeite	1.3	1.7	2.4	1.6	0.0	1.4	1.2	1.8	1.5	2.0	1.9	1.3	0.2	1.7	2.0
Ti-Aegirine	1.4	1.7	2.0	2.1	0.0	1.7	1.4	0.0	0.0	1.4	2.1	1.2	0.3	1.8	2.3
Ti-Tschermak	0.6	0.4	0.0	0.3	8.9	0.3	0.3	1.7	1.9	0.6	0.1	1.2	0.9	0.2	0.2
Al-Tschermak	0.0	0.0	0.0	0.0	2.9	0.0	0.0	4.2	3.4	0.0	0.0	0.0	0.0	0.0	0.0
Diopside	42.8	41.5	40.4	42.5	53.2	43.2	42.0	69.9	72.1	47.9	43.5	38.1	44.9	42.0	42.2
Hedenbergite	38.7	38.8	39.2	38.7	17.2	38.5	38.4	9.3	9.2	33.5	37.0	38.2	35.6	39.4	39.4
Enstatite	6.8	7.2	7.9	7.2	9.0	7.1	7.5	11.0	9.2	7.8	7.9	8.0	7.3	6.5	6.8
Ferrosilite	6.2	6.7	7.7	6.6	2.9	6.4	6.9	1.5	1.2	5.4	6.7	8.0	5.8	6.1	6.3

Table C2 continued

Unit	**GVI**	**GVI**	**GVI**	**GVI**	**GVI**	**GVI**	**GVI**	**GVI**	**GVI**	**Ign-i**	**Ign-i**	**Ign-i**	**Ign-i**	**Ign-i**	**Ign-i**	**Ign-i**
Sample	TER13-1	TER13-1	TER13-1	TER13-1	TER13-1	TER13-1	TER13-1	TER13-1	TER13-1	T001	T001	T001	T001	T001	T001	T001
No.	64 / 1 .	65 / 1 .	66 / 1 .	67 / 1 .	82 / 1 .	83 / 1 .	95 / 1 .	101 / 1 .	102 / 1 .	35 / 1 .	37 / 1 .	39 / 1 .	40 / 1 .	43 / 1 .	47 / 1 .	48 / 1 .
Notes	Pheno	Pheno	Pheno	Pheno	Pheno	Pheno	Pheno	Pheno	Pheno	Pheno	Pheno	Pheno	Pheno	Pheno	Pheno	Pheno
SiO_2	51.03	51.84	51.59	52.90	51.96	51.91	53.15	52.76	53.60	52.04	51.52	51.52	52.13	51.44	52.03	51.67
TiO_2	0.43	0.43	0.48	0.44	0.44	0.51	0.46	0.47	0.44	0.36	0.89	0.26	0.40	0.26	0.28	0.36
Al_2O_3	0.54	0.55	0.68	0.58	0.59	0.69	0.60	0.59	0.50	0.33	1.05	0.39	0.43	0.35	0.24	0.45
Cr_2O_3	bdl	bdl	bdl	bdl	bdl	0.02	bdl	bdl	bdl	bdl	0.02	0.02	0.03	bdl	0.02	0.01
FeO	10.45	10.96	10.52	10.78	11.34	12.38	10.32	10.87	11.13	19.10	17.06	18.44	17.58	18.06	17.89	18.20
MnO	1.19	1.17	1.25	1.21	1.23	1.05	1.17	1.21	1.24	1.35	1.24	1.28	1.23	1.38	1.24	1.29
MgO	14.38	13.87	14.43	14.09	13.48	13.19	14.39	13.81	13.82	7.34	9.37	7.80	8.47	7.92	8.13	7.91
CaO	20.27	20.33	20.04	20.25	20.22	20.06	20.40	20.15	19.99	19.61	19.19	20.08	20.43	19.71	20.24	19.44
Na_2O	0.74	0.81	0.83	0.79	0.81	0.72	0.78	0.88	0.78	1.11	0.85	0.88	0.90	0.99	0.98	0.94
K_2O	bdl	bdl	bdl	bdl	bdl	bdl	bdl	bdl	bdl	bdl	bdl	bdl	bdl	bdl	bdl	bdl
Total	99.03	99.96	99.81	101.03	100.07	100.53	101.27	100.74	101.51	101.23	101.18	100.66	101.59	100.11	101.04	100.25
Si	1.920	1.938	1.925	1.956	1.945	1.942	1.957	1.958	1.977	2.003	1.964	1.990	1.987	1.995	1.996	2.002
Ti	0.012	0.012	0.014	0.012	0.012	0.014	0.013	0.013	0.012	0.010	0.025	0.008	0.011	0.008	0.008	0.011
Al	0.024	0.024	0.030	0.025	0.026	0.030	0.026	0.026	0.022	0.015	0.047	0.018	0.019	0.016	0.011	0.020
Cr						0.001					0.001	0.001	0.001		0.001	0.000
Fe^{2+}	0.163	0.209	0.175	0.239	0.237	0.278	0.227	0.241	0.289	0.574	0.508	0.543	0.510	0.531	0.521	0.566
Fe^{3+}	0.166	0.134	0.153	0.095	0.118	0.109	0.091	0.096	0.055	0.041	0.036	0.053	0.050	0.054	0.053	0.024
Mn	0.038	0.037	0.040	0.038	0.039	0.033	0.036	0.038	0.039	0.044	0.040	0.042	0.040	0.045	0.040	0.042
Mg	0.806	0.773	0.803	0.776	0.752	0.736	0.790	0.764	0.760	0.421	0.533	0.449	0.481	0.458	0.465	0.457
Ca	0.817	0.814	0.801	0.802	0.811	0.804	0.805	0.801	0.790	0.809	0.784	0.831	0.834	0.819	0.832	0.807
Na	0.054	0.059	0.060	0.057	0.059	0.052	0.056	0.063	0.056	0.082	0.063	0.066	0.066	0.074	0.073	0.070
K																
Sum	4.000	4.000	4.000	4.000	4.000	4.000	4.000	4.000	4.000	4.000	4.000	4.000	4.000	4.000	4.000	4.000
Aegirine	5.4	5.9	6.0	5.7	5.9	5.2	5.6	6.3	5.5	4.1	3.6	5.3	5.0	5.4	5.3	2.4
Ferri-Tschermak	5.6	3.8	4.6	1.9	2.9	2.8	1.7	1.6	0.0	0.0	0.0	0.0	0.0	0.0	0.0	0.0
Jadeite	0.0	0.0	0.0	0.0	0.0	0.0	0.0	0.0	0.0	1.8	1.1	0.8	0.6	1.1	0.7	2.3
Ti-Aegirine	0.0	0.0	0.0	0.0	0.0	0.0	0.0	0.0	0.1	2.1	1.5	0.6	1.0	1.0	1.3	2.1
Ti-Tschermak	1.2	1.2	1.4	1.2	1.2	1.4	1.3	1.3	1.1	0.0	1.8	0.5	0.6	0.3	0.2	0.0
Al-Tschermak	0.0	0.0	0.0	0.0	0.0	0.0	0.0	0.0	0.0	0.0	0.0	0.0	0.0	0.0	0.0	0.0
Diopside	60.0	58.0	58.4	56.8	56.3	53.5	58.1	56.5	54.5	32.8	37.8	35.9	38.6	36.1	37.6	34.6
Hedenbergite	15.0	18.4	15.7	20.2	20.7	22.7	19.4	20.6	23.5	48.1	38.9	46.8	44.2	45.5	45.4	46.1
Enstatite	10.3	9.7	10.9	10.4	9.5	10.0	10.4	9.9	10.8	4.5	7.6	4.4	4.6	4.7	4.3	5.3
Ferrosilite	2.6	3.1	2.9	3.7	3.5	4.3	3.5	3.6	4.6	6.6	7.8	5.8	5.3	6.0	5.2	7.1

Table C3: Ti-magnetite analyses from the Terceira ignimbrite formations and associated lithologies

Unit	**LAI**	**LAI**	**LAI**	**LAI**	**LAI**	**LAI**	**LAI**	**LAI**	**LAI**	**LAI**	**LAI**	**LAI**	**LAI**	**LAI**
Sample	TER1-1	TER1-1	TER1-1	TER1-1	TER1-1	TER1-1	TER1-1	TER1-1	TER1-1	TER1-2	TER1-2	TER1-2	TER1-2	TER1-2
No.	48 / 1 .	49 / 1 .	50 / 1 .	51 / 1 .	53 / 1 .	54 / 1 .	59 / 1 .	60 / 1 .	61 / 1 .	97 / 1 .	100 / 1 .	99 / 1 .	98 / 1 .	90 / 1 .
Notes	Mph	Mph	Mph	Mph	Mph	Mph	Mph	Mph	Mph	Mph	Mph	Mph	Mph	Mph
TiO_2	22.56	22.07	22.24	22.38	22.37	22.39	22.42	22.31	22.37	22.14	22.33	22.49	22.58	22.72
Al_2O_3	0.60	0.61	0.62	0.61	0.62	0.63	0.58	0.61	0.59	0.55	0.55	0.56	0.55	0.76
Cr_2O_3	0.02	0.01	bdl	bdl	0.03	0.01	0.03	0.01	0.03	bdl	0.02	0.03	bdl	0.01
FeO	71.78	71.51	71.88	71.90	72.25	71.87	71.77	71.84	71.99	72.22	72.44	72.19	72.17	71.36
MnO	1.78	1.79	1.77	1.81	1.81	1.82	1.79	1.77	1.78	1.82	1.85	1.82	1.84	1.77
MgO	1.12	1.12	1.08	1.14	1.10	1.11	1.12	1.06	1.16	1.03	1.07	1.09	1.08	1.40
Total	97.85	97.10	97.59	97.85	98.19	97.82	97.71	97.59	97.93	97.76	98.25	98.18	98.22	98.01
Ti	0.629	0.620	0.622	0.624	0.622	0.625	0.626	0.624	0.623	0.618	0.620	0.625	0.628	0.631
Al	0.026	0.027	0.027	0.027	0.027	0.027	0.026	0.027	0.026	0.024	0.024	0.024	0.024	0.033
Cr	0.001	0.000			0.001	0.000	0.001	0.000	0.001		0.000	0.001		0.000
Fe^{2+}	1.512	1.501	1.506	1.504	1.504	1.506	1.508	1.510	1.503	1.504	1.504	1.508	1.511	1.498
Fe^{3+}	0.715	0.733	0.729	0.725	0.729	0.723	0.721	0.725	0.727	0.739	0.735	0.724	0.721	0.705
Mn	0.056	0.057	0.056	0.057	0.057	0.057	0.056	0.056	0.056	0.057	0.058	0.057	0.058	0.055
Mg	0.062	0.062	0.060	0.063	0.061	0.061	0.062	0.059	0.064	0.057	0.059	0.060	0.059	0.077
Sum	3.000	3.000	3.000	3.000	3.000	3.000	3.000	3.000	3.000	3.000	3.000	3.000	3.000	3.000
Usp	62.9	62.0	62.2	62.4	62.2	62.5	62.7	62.4	62.3	61.8	62.1	62.6	62.8	63.1
Mt	35.8	36.7	36.5	36.3	36.5	36.2	36.1	36.3	36.4	37.0	36.7	36.2	36.0	35.3
Sp	1.3	1.3	1.4	1.3	1.4	1.4	1.3	1.3	1.3	1.2	1.2	1.2	1.2	1.7

Table C3 continued

Unit	**LAI**	**LAI**	**LAI**	**LAI**	**LAI**	**LAI**	**LAI**	**LAI**	**LAI**	**LAI**	**LAI**	**LAI**	**LAI**	**LAI**
Sample	TER1-2	TER1-2	TER1-2	TER3-1	TER3-1	TER3-1	TER3-1	TER3-1	TER3-1	TER3-1	TER3-1	TER3-2	TER3-2	TER3-2
No.	91 / 1 .	88 / 1 .	89 / 1 .	146 / 1 .	147 / 1 .	148 / 1 .	149 / 1 .	150 / 1 .	151 / 1 .	152 / 1 .	153 / 1 .	62 / 1 .	64 / 1 .	65 / 1 .
Notes	Mph	Mph	Mph	Mph	Mph	Mph	Mph	Mph	Mph	Mph	Mph	Mph	Mph	Mph
TiO_2	22.83	22.86	22.87	23.60	22.12	23.31	21.76	21.27	22.83	22.07	24.23	22.54	22.43	22.57
Al_2O_3	0.74	0.74	0.78	0.83	0.88	0.93	0.88	0.95	0.97	0.88	0.97	0.50	0.56	0.54
Cr_2O_3	0.03	0.03	bdl	0.01	0.01	0.01	0.01	0.01	0.01	0.02	bdl	0.03	0.02	0.02
FeO	71.60	71.40	71.51	70.58	71.16	69.91	70.95	71.17	70.25	71.80	69.46	71.80	71.89	71.95
MnO	1.78	1.76	1.79	1.76	1.51	1.63	1.77	2.18	1.67	1.69	1.78	1.81	1.80	1.84
MgO	1.37	1.38	1.41	1.57	1.55	1.64	1.44	1.45	1.51	1.56	1.56	0.99	1.06	1.09
Total	98.34	98.16	98.35	98.35	97.22	97.43	96.81	97.03	97.24	98.02	98.00	97.66	97.76	98.00
Ti	0.632	0.634	0.633	0.653	0.618	0.650	0.611	0.595	0.638	0.611	0.673	0.631	0.626	0.629
Al	0.032	0.032	0.034	0.036	0.038	0.041	0.039	0.042	0.042	0.038	0.042	0.022	0.025	0.023
Cr	0.001	0.001		0.000	0.000	0.000	0.000	0.000	0.000	0.001		0.001	0.001	0.001
Fe^{2+}	1.501	1.503	1.500	1.512	1.485	1.508	1.475	1.446	1.502	1.473	1.531	1.519	1.511	1.511
Fe^{3+}	0.703	0.699	0.701	0.658	0.726	0.659	0.740	0.768	0.681	0.739	0.613	0.716	0.722	0.719
Mn	0.056	0.055	0.056	0.055	0.048	0.051	0.056	0.069	0.053	0.053	0.055	0.057	0.057	0.058
Mg	0.075	0.076	0.078	0.086	0.086	0.091	0.080	0.080	0.084	0.086	0.086	0.055	0.059	0.060
Sum	3.000	3.000	3.000	3.000	3.000	3.000	3.000	3.000	3.000	3.000	3.000	3.000	3.000	3.000
Usp	63.2	63.4	63.3	65.3	61.8	65.0	61.1	59.5	63.8	61.1	67.3	63.1	62.7	62.9
Mt	35.2	35.0	35.0	32.9	36.3	33.0	37.0	38.4	34.1	37.0	30.6	35.8	36.1	35.9
Sp	1.6	1.6	1.7	1.8	1.9	2.0	1.9	2.1	2.1	1.9	2.1	1.1	1.2	1.2

Table C3 continued

Unit	**LAI**	**LAI**	**LAI**	**LAI**	**LAI**	**LAI**	**LAI**	**LAI**	**LAI**	**LAI**	**LAI**	**LAI**	**LAI**	**LAI**
Sample	TER3-2	TER3-2	TER3-2	TER3-2	TER3-2	TER3-2	TER3-2	TER3-2	TER3-2	TER3-2	TER3-2	TER3-2	TER4-1	TER4-1
No.	66 / 1 .	67 / 1 .	68 / 1 .	69 / 1 .	70 / 1 .	71 / 1 .	72 / 1 .	73 / 1 .	74 / 1 .	75 / 1 .	76 / 1 .	77 / 1 .	156 / 1 .	157 / 1 .
Notes	Mph	Mph	Mph	Mph	Mph	Mph	Mph	Mph	Mph	Mph	Mph	Mph	Mph	Mph
TiO_2	22.50	22.58	22.58	22.68	22.58	22.58	22.39	22.36	22.56	22.86	22.91	22.53	22.19	22.39
Al_2O_3	0.54	0.55	0.55	0.50	0.51	0.82	0.74	0.65	0.58	0.58	0.61	0.62	0.52	0.53
Cr_2O_3	0.01	0.01	0.01	0.01	0.01	0.04	0.01	0.02	0.01	bdl	0.01	0.03	0.02	0.01
FeO	72.24	72.27	72.18	71.91	72.22	71.61	71.93	72.19	72.14	71.56	71.65	71.64	71.79	72.31
MnO	1.87	1.82	1.80	1.82	1.85	1.86	1.81	1.86	1.80	1.84	1.84	1.78	1.82	1.83
MgO	1.08	1.07	1.11	1.04	1.06	1.20	1.17	1.03	1.08	1.12	1.12	1.06	1.01	0.96
Total	98.24	98.30	98.24	97.95	98.23	98.11	98.05	98.11	98.16	97.96	98.15	97.66	97.34	98.02
Ti	0.625	0.627	0.627	0.633	0.628	0.627	0.623	0.622	0.627	0.637	0.637	0.630	0.623	0.624
Al	0.024	0.024	0.024	0.022	0.022	0.036	0.032	0.028	0.025	0.025	0.027	0.027	0.023	0.023
Cr	0.000	0.000	0.000	0.000	0.000	0.001	0.000	0.001	0.000		0.000	0.001	0.001	0.000
Fe^{2+}	1.507	1.511	1.510	1.518	1.511	1.503	1.501	1.507	1.512	1.518	1.517	1.515	1.509	1.514
Fe^{3+}	0.725	0.721	0.721	0.713	0.722	0.709	0.723	0.727	0.720	0.700	0.699	0.712	0.731	0.728
Mn	0.058	0.057	0.056	0.057	0.058	0.058	0.057	0.058	0.056	0.058	0.058	0.056	0.057	0.057
Mg	0.060	0.059	0.061	0.057	0.059	0.066	0.064	0.057	0.059	0.062	0.062	0.059	0.056	0.053
Sum	3.000	3.000	3.000	3.000	3.000	3.000	3.000	3.000	3.000	3.000	3.000	3.000	3.000	3.000
Usp	62.5	62.7	62.8	63.3	62.8	62.7	62.3	62.2	62.8	63.7	63.7	63.0	62.3	62.4
Mt	36.3	36.1	36.0	35.6	36.1	35.5	36.1	36.4	36.0	35.0	34.9	35.6	36.6	36.4
Sp	1.2	1.2	1.2	1.1	1.1	1.8	1.6	1.4	1.3	1.3	1.3	1.4	1.1	1.2

Table C3 continued

Unit	**LAI**	**LAI**	**LAI**	**LAI**	**LAI**	**LAI**	**LAI**	**LAI**	**LAI**	**LAI**	**LAI**	**LAI**	**LAI**	**LAI**
Sample	TER4-1	TER4-1	TER4-1	TER4-1	TER4-1	TER4-1	TER4-1	TER4-1	TER4-1	TER4-1	TER4-1	TER4-1	TER4-1	TER4-1
No.	159 / 1 .	160 / 1 .	161 / 1 .	163 / 1 .	164 / 1 .	167 / 1 .	168 / 1 .	169 / 1 .	170 / 1 .	171 / 1 .	172 / 1 .	173 / 1 .	174 / 1 .	175 / 1 .
Notes	Mph	Mph	Mph	Mph	Mph	Mph	Mph	Mph	Mph	Mph	Mph	Mph	Mph	Mph
TiO_2	22.55	22.72	22.34	22.41	22.33	22.71	22.30	22.22	22.52	22.14	22.39	22.52	22.62	22.36
Al_2O_3	0.56	0.55	0.56	0.52	0.51	0.53	0.52	0.50	0.54	0.55	0.51	0.57	0.52	0.55
Cr_2O_3	0.01	0.01	bdl	0.01	0.01	0.02	0.02	bdl	0.02	0.01	0.01	0.01	0.02	0.01
FeO	72.36	72.08	71.73	72.33	71.81	72.09	72.05	72.02	72.23	72.05	72.25	72.18	72.12	72.23
MnO	1.81	1.83	1.84	1.87	1.84	1.83	1.85	1.82	1.80	1.84	1.84	1.80	1.82	1.83
MgO	0.99	0.99	1.04	0.96	1.03	0.99	1.02	0.95	1.01	1.04	1.01	1.02	1.02	1.07
Total	98.28	98.16	97.52	98.10	97.53	98.17	97.75	97.52	98.11	97.63	98.00	98.10	98.12	98.04
Ti	0.627	0.632	0.626	0.624	0.625	0.632	0.623	0.623	0.627	0.619	0.624	0.627	0.630	0.623
Al	0.025	0.024	0.025	0.023	0.022	0.023	0.023	0.022	0.023	0.024	0.022	0.025	0.023	0.024
Cr	0.000	0.000		0.000	0.000	0.000	0.001		0.001	0.000	0.000	0.000	0.000	0.000
Fe^{2+}	1.515	1.521	1.510	1.513	1.510	1.520	1.509	1.512	1.515	1.503	1.511	1.514	1.516	1.506
Fe^{3+}	0.721	0.711	0.724	0.728	0.727	0.712	0.730	0.733	0.722	0.737	0.729	0.721	0.717	0.730
Mn	0.057	0.057	0.058	0.059	0.058	0.057	0.058	0.058	0.056	0.058	0.058	0.057	0.057	0.057
Mg	0.055	0.054	0.058	0.053	0.057	0.055	0.056	0.053	0.056	0.058	0.056	0.056	0.056	0.059
Sum	3.000	3.000	3.000	3.000	3.000	3.000	3.000	3.000	3.000	3.000	3.000	3.000	3.000	3.000
Usp	62.7	63.3	62.6	62.4	62.5	63.2	62.3	62.3	62.7	61.9	62.4	62.7	63.0	62.3
Mt	36.1	35.6	36.2	36.4	36.3	35.6	36.5	36.6	36.1	36.9	36.5	36.1	35.9	36.5
Sp	1.2	1.2	1.2	1.1	1.1	1.1	1.1	1.1	1.2	1.2	1.1	1.2	1.1	1.2

Table C3 continued

Unit	**LAI**	**LAI**	**LAI**	**LAI**	**LAI**	**LAI**	**LAI**	**LAI**	**LAI**	**LAI**	**LAI**	**LAI**	**LAI**	**LAI**
Sample	TER4-1	TER4-1	TER4-1	TER4-1	TER6-1	TER6-1	TER6-1	TER6-1	TER6-1	TER7-1	TER7-1	TER7-1	TER7-1	TER10-3
No.	177 / 1 .	178 / 1 .	179 / 1 .	180 / 1 .	78 / 1 .	79 / 1 .	80 / 1 .	81 / 1 .	82 / 1 .	71 / 1 .	72 / 1 .	74 / 1 .	73 / 1 .	85 / 1 .
Notes	Mph	Mph	Mph	Mph	Mph	Mph	Mph	Mph	Mph	Mph	Mph	Mph	Mph	Mph
TiO_2	22.65	22.75	22.58	22.41	22.75	22.73	22.80	22.16	22.23	22.44	22.50	22.71	22.73	22.05
Al_2O_3	0.49	0.50	0.54	0.46	0.55	0.54	0.49	0.57	0.62	0.55	0.56	0.49	0.52	0.77
Cr_2O_3	0.04	0.01	bdl	0.02	0.01	bdl	0.01	0.02	0.01	0.02	0.02	bdl	0.01	0.01
FeO	72.19	72.19	72.30	71.73	71.62	71.58	71.84	71.67	71.63	72.14	72.11	72.24	72.25	71.70
MnO	1.84	1.83	1.81	1.84	1.84	1.83	1.83	1.83	1.82	1.84	1.83	1.84	1.82	1.80
MgO	0.95	0.97	0.98	0.96	1.10	1.09	1.16	1.07	1.09	1.04	1.08	1.10	1.08	1.31
Total	98.16	98.25	98.21	97.43	97.86	97.78	98.11	97.33	97.41	98.03	98.09	98.38	98.41	97.63
Ti	0.631	0.633	0.628	0.629	0.635	0.635	0.634	0.622	0.623	0.625	0.626	0.630	0.631	0.615
Al	0.022	0.022	0.023	0.020	0.024	0.024	0.021	0.025	0.027	0.024	0.024	0.021	0.023	0.034
Cr	0.001	0.000		0.001	0.000		0.000	0.001	0.000	0.001	0.001		0.000	0.000
Fe^{2+}	1.520	1.522	1.518	1.517	1.516	1.517	1.513	1.504	1.505	1.510	1.510	1.512	1.514	1.486
Fe^{3+}	0.716	0.712	0.720	0.721	0.706	0.707	0.710	0.731	0.727	0.725	0.722	0.718	0.715	0.737
Mn	0.058	0.057	0.057	0.058	0.058	0.058	0.057	0.058	0.058	0.058	0.057	0.057	0.057	0.056
Mg	0.053	0.054	0.054	0.053	0.061	0.060	0.064	0.060	0.061	0.057	0.059	0.061	0.060	0.073
Sum	3.000	3.000	3.000	3.000	3.000	3.000	3.000	3.000	3.000	3.000	3.000	3.000	3.000	3.000
Usp	63.1	63.3	62.8	62.9	63.5	63.5	63.4	62.2	62.3	62.5	62.7	63.0	63.1	61.5
Mt	35.8	35.6	36.0	36.1	35.3	35.3	35.5	36.6	36.4	36.3	36.1	35.9	35.8	36.9
Sp	1.1	1.1	1.2	1.0	1.2	1.2	1.1	1.3	1.4	1.2	1.2	1.1	1.1	1.7

Table C3 continued

Unit	**LAI**	**LAI**	**LAI**	**LAI**	**LAI**	**LAI**	**LAI**	**LAI**	**LAI**	**LAI**	**LAI**	**LAI**	**LAI**	**LAI**
Sample	TER10-3	TER10-3	TER10-3	TER10-3	TER10-3	TER10-3	TER10-3	TER10-3	TER10-3	TER10-3	TER10-3	TER10-3	TER10-3	TER10-3
No.	86 / 1 .	87 / 1 .	88 / 1 .	89 / 1 .	90 / 1 .	91 / 1 .	92 / 1 .	93 / 1 .	94 / 1 .	95 / 1 .	96 / 1 .	97 / 1 .	98 / 1 .	100 / 1 .
Notes	Mph	Mph	Mph	Mph	Mph	Mph	Mph	Mph	Mph	Mph	Mph	Mph	Mph	Mph
TiO_2	22.26	22.19	22.27	22.19	22.17	22.64	22.52	22.12	22.11	22.16	22.40	22.49	22.49	22.14
Al_2O_3	0.78	1.42	0.82	0.59	0.61	0.51	0.51	0.51	0.46	0.53	0.56	0.52	0.58	0.57
Cr_2O_3	bdl	bdl	bdl	0.04	0.01	0.01	0.01	bdl	0.01	0.01	0.02	0.01	0.02	0.01
FeO	71.81	71.90	71.79	72.08	72.04	72.09	72.27	72.08	71.96	72.06	72.15	72.24	72.33	72.10
MnO	1.77	1.77	1.76	1.79	1.80	1.82	1.84	1.83	1.81	1.80	1.83	1.83	1.82	1.79
MgO	1.31	1.27	1.27	1.12	1.10	1.08	1.06	1.11	1.09	1.08	1.11	1.08	1.10	1.08
Total	97.93	98.55	97.90	97.82	97.73	98.14	98.20	97.64	97.44	97.62	98.07	98.17	98.35	97.69
Ti	0.619	0.611	0.619	0.619	0.619	0.630	0.626	0.618	0.619	0.620	0.623	0.626	0.624	0.619
Al	0.034	0.061	0.036	0.026	0.027	0.022	0.022	0.022	0.020	0.023	0.024	0.023	0.025	0.025
Cr				0.001	0.000	0.000	0.000		0.000	0.000	0.001	0.000	0.000	0.000
Fe^{2+}	1.491	1.487	1.494	1.500	1.501	1.513	1.510	1.499	1.502	1.503	1.505	1.509	1.507	1.502
Fe^{3+}	0.728	0.716	0.726	0.735	0.735	0.718	0.725	0.741	0.741	0.737	0.728	0.726	0.726	0.738
Mn	0.055	0.055	0.055	0.056	0.057	0.057	0.058	0.058	0.057	0.057	0.057	0.057	0.057	0.056
Mg	0.072	0.069	0.070	0.062	0.061	0.060	0.059	0.062	0.061	0.060	0.061	0.060	0.061	0.060
Sum	3.000	3.000	3.000	3.000	3.000	3.000	3.000	3.000	3.000	3.000	3.000	3.000	3.000	3.000
Usp	61.9	61.1	61.9	61.9	61.9	63.0	62.6	61.8	61.9	62.0	62.4	62.6	62.4	61.9
Mt	36.4	35.8	36.3	36.8	36.8	35.9	36.3	37.1	37.0	36.9	36.4	36.3	36.3	36.9
Sp	1.7	3.1	1.8	1.3	1.3	1.1	1.1	1.1	1.0	1.2	1.2	1.1	1.3	1.2

Table C3 continued

Unit	**LMI**	**LMI**	**LMI**	**LMI**	**LMI**	**LMI**	**LMI**	**LMI**	**LMI**	**LMI**	**LMI**	**LMI**	**LMI**	**LMI**	**LMI**	**LMI**
Sample	TER5-2	TER5-2	TER5-2	TER5-2	TER5-2	TER5-2	TER5-2	TER5-2	TER5-2	TER5-2	TER5-2	TER5-2	TER5-2	TER5-2	TER5-2	TER5-2
No.	158 / 1 .	159 / 1 .	160 / 1 .	161 / 1 .	162 / 1 .	163 / 1 .	164 / 1 .	165 / 1 .	168 / 1 .	169 / 1 .	170 / 1 .	171 / 1 .	172 / 1 .	173 / 1 .	174 / 1 .	175 / 1 .
Notes	Mph	Mph	Mph	Mph	Mph	Mph	Mph	Mph	Mph	Mph	Mph	Mph	Mph	Mph	Mph	Mph
TiO_2	21.58	21.53	21.61	19.35	21.85	21.68	22.04	21.85	22.32	21.53	21.08	21.15	21.08	21.03	22.34	22.44
Al_2O_3	0.71	0.69	0.73	1.18	0.68	0.69	0.65	0.64	0.73	0.72	1.10	1.12	1.13	1.12	0.72	1.15
Cr_2O_3	0.02	0.01	0.02	0.02	0.01	0.01	0.01	0.02	0.03	0.01	0.01	0.01	bdl	0.02	0.01	0.02
FeO	72.48	72.35	71.50	73.89	72.24	72.40	72.23	72.50	71.84	72.38	72.41	72.61	72.45	72.57	71.28	70.88
MnO	1.64	1.54	1.56	1.26	1.57	1.57	1.59	1.55	1.53	1.63	1.45	1.45	1.44	1.49	1.68	1.64
MgO	0.82	1.19	1.02	1.62	0.97	1.13	1.01	0.87	0.93	0.87	1.51	1.45	1.54	1.38	1.07	1.23
Total	97.25	97.30	96.44	97.32	97.32	97.49	97.52	97.42	97.37	97.14	97.55	97.78	97.64	97.60	97.09	97.35
Ti	0.606	0.603	0.611	0.537	0.613	0.606	0.617	0.613	0.626	0.605	0.586	0.586	0.585	0.585	0.628	0.627
Al	0.031	0.030	0.032	0.052	0.030	0.030	0.028	0.028	0.032	0.032	0.048	0.049	0.049	0.049	0.032	0.050
Cr	0.001	0.000	0.001	0.000	0.000	0.000	0.000	0.000	0.001	0.000	0.000	0.000		0.001	0.000	0.000
Fe^{2+}	1.509	1.488	1.504	1.409	1.509	1.494	1.511	1.516	1.526	1.505	1.457	1.461	1.456	1.462	1.515	1.507
Fe^{3+}	0.755	0.764	0.744	0.873	0.744	0.757	0.737	0.746	0.715	0.757	0.780	0.778	0.781	0.781	0.712	0.695
Mn	0.052	0.049	0.050	0.039	0.050	0.050	0.050	0.049	0.048	0.052	0.045	0.045	0.045	0.047	0.053	0.052
Mg	0.046	0.066	0.057	0.089	0.054	0.063	0.056	0.048	0.052	0.048	0.083	0.080	0.085	0.076	0.060	0.068
Sum	3.000	3.000	3.000	3.000	3.000	3.000	3.000	3.000	3.000	3.000	3.000	3.000	3.000	3.000	3.000	3.000
Usp	60.6	60.3	61.2	53.7	61.3	60.6	61.7	61.3	62.6	60.5	58.6	58.7	58.5	58.5	62.8	62.7
Mt	37.8	38.2	37.2	43.7	37.2	37.9	36.9	37.3	35.8	37.9	39.0	38.9	39.0	39.1	35.6	34.8
Sp	1.6	1.5	1.6	2.6	1.5	1.5	1.4	1.4	1.6	1.6	2.4	2.4	2.5	2.4	1.6	2.5

Table C3 continued

Unit	**VFI**	**VFI**	**VFI**	**VFI**	**VFI**	**VFI**	**VFI**	**VFI**	**VFI**	**VFI**	**VFI**	**VFI**	**CCI**
Sample	TER2-2	TER2-2	TER2-2	TER2-2	TER2-2	TER2-2	TER2-2	TER2-2	TER11-2B	TER11-2B	TER11-2B	TER11-2B	TER2-1
No.	196 / 1 .	197 / 1 .	198 / 1 .	199 / 1 .	200 / 1 .	201 / 1 .	202 / 1 .	203 / 1 .	156 / 1 .	158 / 1 .	159 / 1 .	160 / 1 .	204 / 1 .
Notes	Mph	Mph	Mph	Mph	Mph	Mph	Mph	Mph	Mph	Mph	Mph	Mph	Mph
TiO_2	23.17	23.26	23.17	23.14	22.97	23.51	23.56	23.57	22.38	22.70	22.52	22.62	22.91
Al_2O_3	0.66	0.64	0.64	0.60	0.62	0.67	0.63	0.66	0.46	0.43	0.85	2.96	0.51
Cr_2O_3	0.02	0.02	bdl	0.02	0.01	0.01	0.02	0.02	0.01	0.02	0.01	bdl	0.02
FeO	71.13	71.37	70.83	71.00	71.06	71.24	71.33	71.46	72.03	72.12	70.96	69.18	71.08
MnO	1.63	1.66	1.61	1.62	1.64	1.63	1.67	1.63	1.59	1.64	1.61	1.54	1.77
MgO	0.84	0.76	0.81	0.80	0.81	0.79	0.82	0.76	0.75	0.72	0.81	0.85	0.73
Total	97.45	97.70	97.06	97.17	97.11	97.85	98.03	98.09	97.23	97.62	96.75	97.15	97.02
Ti	0.651	0.652	0.654	0.652	0.647	0.658	0.658	0.658	0.631	0.637	0.636	0.630	0.647
Al	0.029	0.028	0.028	0.026	0.027	0.029	0.028	0.029	0.020	0.019	0.038	0.129	0.023
Cr	0.001	0.001		0.001	0.000	0.000	0.001	0.001	0.000	0.001	0.000		0.001
Fe^{2+}	1.552	1.558	1.557	1.556	1.550	1.563	1.560	1.565	1.538	1.545	1.540	1.535	1.550
Fe^{3+}	0.669	0.667	0.665	0.669	0.678	0.654	0.656	0.654	0.718	0.706	0.690	0.610	0.683
Mn	0.051	0.052	0.051	0.051	0.052	0.051	0.053	0.051	0.051	0.052	0.051	0.048	0.056
Mg	0.047	0.042	0.045	0.045	0.045	0.044	0.045	0.042	0.042	0.040	0.045	0.047	0.041
Sum	3.000	3.000	3.000	3.000	3.000	3.000	3.000	3.000	3.000	3.000	3.000	3.000	3.000
Usp	65.1	65.2	65.4	65.2	64.7	65.8	65.8	65.8	63.1	63.7	63.6	63.0	64.7
Mt	33.5	33.4	33.2	33.5	33.9	32.7	32.8	32.7	35.9	35.3	34.5	30.5	34.1
Sp	1.5	1.4	1.4	1.3	1.4	1.5	1.4	1.5	1.0	0.9	1.9	6.5	1.1

Table C3 continued

Unit	**PNI**	**PNI**	**PNI**	**PNI**	**PNI**	**PNI**	**PNI**	**PNI**	**PNI**	**PNI**	**PNI**	**PNI**	**PNI**
Sample	T012	T012	T012	T012	T012	T012	T012	T012	T012	T012	T012	T012	T012
No.	19 / 1 .	20 / 1 .	21 / 1 .	22 / 1 .	23 / 1 .	24 / 1 .	25 / 1 .	27 / 1 .	28 / 1 .	29 / 1 .	30 / 1 .	31 / 1 .	32 / 1 .
Notes	Mph	Mph	Mph	Mph	Mph	Mph	Mph	Mph	Mph	Mph	Mph	Mph	Mph
TiO_2	22.40	22.90	22.19	22.53	22.83	22.58	22.54	20.54	22.94	22.97	24.01	22.93	23.36
Al_2O_3	0.74	0.84	0.66	0.84	0.82	0.95	0.84	0.66	0.77	0.76	0.72	0.72	0.68
Cr_2O_3	0.03	bdl	bdl	bdl	bdl	bdl	bdl	bdl	bdl	bdl	bdl	bdl	bdl
FeO	69.48	68.53	70.88	69.28	69.90	68.78	68.68	70.74	68.86	67.68	66.76	68.55	68.72
MnO	1.51	1.70	1.63	1.53	1.58	1.72	1.67	1.45	1.91	1.66	1.81	1.80	1.76
MgO	0.97	0.68	0.84	0.88	0.88	0.67	0.73	0.97	0.66	1.42	0.45	0.73	0.72
Total	95.12	94.64	96.20	95.06	96.01	94.70	94.45	94.36	95.15	94.49	93.75	94.72	95.24
Ti	0.643	0.663	0.631	0.648	0.650	0.652	0.653	0.594	0.661	0.662	0.704	0.663	0.672
Al	0.033	0.038	0.030	0.038	0.037	0.043	0.038	0.030	0.035	0.034	0.033	0.032	0.031
Cr	0.001												
Fe^{2+}	1.540	1.569	1.532	1.548	1.550	1.558	1.557	1.491	1.561	1.527	1.618	1.563	1.574
Fe^{3+}	0.679	0.637	0.709	0.667	0.663	0.652	0.656	0.783	0.644	0.642	0.559	0.642	0.625
Mn	0.049	0.055	0.052	0.050	0.051	0.056	0.054	0.047	0.062	0.054	0.060	0.059	0.057
Mg	0.055	0.039	0.047	0.050	0.050	0.038	0.042	0.056	0.038	0.081	0.026	0.042	0.041
Sum	3.000	3.000	3.000	3.000	3.000	3.000	3.000	3.000	3.000	3.000	3.000	3.000	3.000
Usp	64.4	66.3	63.1	64.8	65.0	65.3	65.3	59.4	66.1	66.2	70.4	66.3	67.2
Mt	34.0	31.8	35.4	33.3	33.2	32.6	32.8	39.1	32.2	32.1	27.9	32.1	31.2
Sp	1.7	1.9	1.5	1.9	1.8	2.1	1.9	1.5	1.7	1.7	1.7	1.6	1.5

Table C3 continued

Unit	**GVI**	**GVI**	**GVI**	**GVI**	**GVI**	**GVI**	**GVI**	**GVI**	**GVI**	**GVI**	**GVI**	**GVI**
Sample	TER13-1	TER13-1	TER13-1	TER13-1	TER13-1	TER13-1	TER13-1	TER13-1	TER13-1	TER13-1	TER13-1	TER13-1
No.	73 / 1 .	74 / 1 .	77 / 1 .	78 / 1 .	79 / 1 .	80 / 1 .	81 / 1 .	87 / 1 .	88 / 1 .	89 / 1 .	90 / 1 .	91 / 1 .
Notes	Mph	Mph	Mph	Mph	Mph	Mph	Mph	Mph	Mph	Mph	Mph	Mph
TiO_2	18.63	19.69	23.47	23.98	21.02	26.68	25.63	22.17	18.86	32.15	21.87	15.60
Al_2O_3	0.79	0.73	0.71	0.69	0.72	0.70	0.69	0.69	0.82	0.45	0.73	0.81
Cr_2O_3	bdl	0.01	0.01	0.01	0.01	bdl	0.01	bdl	bdl	0.01	0.01	0.01
FeO	71.32	70.73	66.92	66.23	68.51	61.89	67.27	67.32	71.43	56.40	68.13	74.62
MnO	1.77	1.95	1.70	1.76	1.76	2.39	2.23	2.02	1.72	2.40	1.84	1.81
MgO	1.63	1.69	1.80	1.82	1.73	2.10	1.91	1.70	1.55	2.09	1.70	1.23
Total	94.14	94.80	94.60	94.49	93.74	93.76	97.74	93.89	94.38	93.50	94.28	94.08
Ti	0.535	0.562	0.674	0.690	0.608	0.774	0.713	0.641	0.541	0.942	0.630	0.448
Al	0.036	0.033	0.032	0.031	0.033	0.032	0.030	0.031	0.037	0.020	0.033	0.036
Cr		0.000	0.000	0.000	0.000		0.000			0.000	0.000	0.000
Fe^{2+}	1.385	1.404	1.517	1.529	1.451	1.575	1.538	1.478	1.397	1.741	1.473	1.320
Fe^{3+}	0.894	0.843	0.620	0.589	0.752	0.421	0.544	0.687	0.881	0.096	0.708	1.066
Mn	0.057	0.063	0.055	0.057	0.057	0.078	0.070	0.066	0.056	0.079	0.060	0.059
Mg	0.093	0.096	0.102	0.104	0.099	0.121	0.105	0.097	0.088	0.121	0.097	0.070
Sum	3.000	3.000	3.000	3.000	3.000	3.000	3.000	3.000	3.000	3.000	3.000	3.000
Usp	53.5	56.2	67.4	69.0	60.8	77.4	71.3	64.1	54.1	94.2	63.0	44.9
Mt	44.7	42.1	31.0	29.5	37.6	21.0	27.2	34.3	44.1	4.8	35.4	53.3
Sp	1.8	1.6	1.6	1.5	1.6	1.6	1.5	1.6	1.8	1.0	1.6	1.8

Table C3 continued

Unit	**Ign-i**	**Ign-i**	**Ign-i**	**Ign-i**	**Ign-i**	**Ign-i**	**Ign-i**	**Ign-i**	**Ign-i**	**Ign-i**	**Ign-i**	**Ign-i**	**Ign-i**	**Ign-i**
Sample	T001	T001	T001	T001	T001	T001	T001	T001	T001	T001	T001	T001	T001	T001
No.	49 / 1 .	50 / 1 .	51 / 1 .	52 / 1 .	53 / 1 .	54 / 1 .	55 / 1 .	56 / 1 .	57 / 1 .	58 / 1 .	59 / 1 .	60 / 1 .	61 / 1 .	62 / 1 .
Notes	Mph	Mph	Mph	Mph	Mph	Mph	Mph	Mph	Mph	Mph	Mph	Mph	Mph	Mph
TiO_2	23.72	23.17	23.30	22.68	23.79	23.05	23.58	24.49	23.84	24.89	23.29	23.49	23.38	22.89
Al_2O_3	0.40	0.39	0.37	0.40	0.40	0.36	0.29	0.38	0.49	0.36	0.44	0.32	0.35	0.33
Cr_2O_3	bdl	bdl	0.02	0.02	0.01	bdl	0.01	bdl	bdl	0.03	0.01	0.03	bdl	bdl
FeO	70.39	70.70	70.16	71.18	70.01	70.46	70.38	65.45	69.93	66.82	69.79	70.41	70.43	70.55
MnO	1.84	1.81	1.97	1.87	1.89	1.83	1.88	1.41	1.91	1.82	1.76	1.90	1.87	1.81
MgO	0.50	0.59	0.44	0.43	0.59	0.45	0.42	0.25	0.65	0.45	0.66	0.49	0.60	0.52
Total	96.84	96.66	96.26	96.58	96.68	96.14	96.56	91.98	96.82	94.36	95.95	96.64	96.63	96.11
Ti	0.673	0.658	0.666	0.645	0.676	0.659	0.672	0.735	0.676	0.727	0.666	0.668	0.664	0.654
Al	0.018	0.017	0.017	0.018	0.018	0.016	0.013	0.018	0.022	0.016	0.020	0.014	0.016	0.015
Cr			0.001	0.001	0.000		0.000			0.001	0.000	0.001		
Fe^{2+}	1.587	1.567	1.577	1.561	1.583	1.575	1.588	1.672	1.578	1.641	1.572	1.580	1.571	1.567
Fe^{3+}	0.635	0.666	0.652	0.691	0.630	0.666	0.643	0.512	0.626	0.529	0.648	0.648	0.656	0.676
Mn	0.059	0.058	0.064	0.060	0.060	0.059	0.060	0.048	0.061	0.060	0.057	0.061	0.060	0.058
Mg	0.028	0.033	0.025	0.024	0.033	0.025	0.024	0.015	0.036	0.026	0.037	0.028	0.034	0.029
Sum	3.000	3.000	3.000	3.000	3.000	3.000	3.000	3.000	3.000	3.000	3.000	3.000	3.000	3.000
Usp	67.3	65.8	66.6	64.5	67.6	65.9	67.2	73.5	67.6	72.7	66.6	66.9	66.4	65.4
Mt	31.8	33.3	32.6	34.6	31.5	33.3	32.1	25.6	31.3	26.5	32.4	32.4	32.8	33.8
Sp	0.9	0.9	0.8	0.9	0.9	0.8	0.6	0.9	1.1	0.8	1.0	0.7	0.8	0.7

Table C3 continued

Unit	**CCI Sy**	**CCI Sy**	**CCI Sy**	**CCI Sy**	**CCI Sy**	**CCI Sy**	**CCI Sy**	**CCI Sy**	**CCI Sy**	**CCI Sy**	**CCI Sy**
Sample	TER30-3	TER30-3	TER30-3	TER30-3	TER30-3	TER30-3	TER30-3	TER30-3	TER30-3	TER30-3	TER30-3
No.	MAG 1	MAG 2	MAG 3	MAG 4	MAG 5	MAG 6	MAG 7	MAG 8	MAG 9	MAG 10	MAG 11
Notes	Mph	Mph	Mph	Mph	Mph	Mph	Mph	Mph	Mph	Mph	Mph
TiO_2	16.68	16.71	16.71	16.81	14.94	14.93	15.01	15.00	15.07	15.12	20.81
Al_2O_3	0.13	0.15	0.16	0.13	0.06	0.10	0.11	0.09	0.08	0.07	0.15
Cr_2O_3	0.01	0.01	bdl	bdl	bdl	0.01	0.01	0.01	bdl	bdl	bdl
FeO	74.92	74.28	74.19	73.36	77.66	78.01	77.23	76.64	77.00	77.70	73.60
MnO	2.23	2.06	2.18	2.11	2.18	2.26	2.21	2.26	2.10	2.20	2.08
MgO	0.10	0.04	0.06	0.04	0.06	0.04	0.03	0.04	0.03	0.04	0.11
Total	94.06	93.25	93.30	92.45	94.90	95.36	94.60	94.04	94.28	95.13	96.75
Ti	0.486	0.492	0.491	0.499	0.431	0.429	0.435	0.437	0.438	0.435	0.592
Al	0.006	0.007	0.007	0.006	0.003	0.005	0.005	0.004	0.004	0.003	0.007
Cr	0.000	0.000				0.000	0.000	0.000			
Fe^{2+}	1.407	1.421	1.416	1.426	1.357	1.353	1.361	1.360	1.368	1.362	1.519
Fe^{3+}	1.021	1.009	1.010	0.996	1.135	1.138	1.126	1.122	1.120	1.126	0.809
Mn	0.073	0.068	0.072	0.071	0.071	0.073	0.072	0.074	0.069	0.071	0.067
Mg	0.006	0.002	0.004	0.002	0.003	0.002	0.002	0.003	0.002	0.002	0.006
Sum	3.000	3.000	3.000	3.000	3.000	3.000	3.000	3.000	3.000	3.000	3.000
Usp	48.6	49.2	49.1	49.9	43.1	42.9	43.5	43.7	43.8	43.5	59.2
Mt	51.1	50.5	50.5	49.8	56.8	56.9	56.3	56.1	56.0	56.3	40.5
Sp	0.3	0.3	0.4	0.3	0.1	0.2	0.3	0.2	0.2	0.2	0.3

Table C3 continued

Unit	**CCI Sy**	**CCI Sy**	**CCI Sy**	**CCI Sy**	**CCI Sy**	**CCI Sy**	**CCI Sy**	**CCI Sy**	**CCI Sy**	**CCI Sy**
Sample	TER30-6	TER30-6	TER30-6	TER30-6	TER30-6	TER30-6	TER30-6	TER30-6	TER30-6	TER30-6
No.	MAG 12	MAG 13	MAG 14	MAG 15	MAG 16	MAG 17	MAG 18	MAG 19	MAG 20	MAG 21
Notes	Mph	Mph	Mph	Mph	Mph	Mph	Mph	Mph	Mph	Mph
TiO_2	23.76	14.99	15.93	19.60	18.80	23.01	21.34	22.69	21.29	20.69
Al_2O_3	0.08	0.06	0.03	0.12	0.11	0.11	0.08	0.05	0.14	0.09
Cr_2O_3	bdl	bdl	bdl	bdl	bdl	bdl	bdl	bdl	bdl	0.01
FeO	71.40	77.91	76.83	74.60	74.98	71.94	73.60	71.89	72.88	73.95
MnO	1.95	1.65	1.62	1.98	1.98	1.90	1.93	2.45	2.17	2.10
MgO	0.01	0.00	0.05	0.08	0.00	0.01	0.03	0.04	0.12	0.10
Total	97.20	94.61	94.45	96.37	95.87	96.97	96.98	97.12	96.60	96.94
Ti	0.676	0.434	0.463	0.559	0.539	0.655	0.607	0.645	0.607	0.588
Al	0.004	0.003	0.001	0.005	0.005	0.005	0.004	0.002	0.006	0.004
Cr										0.000
Fe^{2+}	1.612	1.380	1.407	1.491	1.475	1.594	1.543	1.564	1.531	1.515
Fe^{3+}	0.645	1.129	1.074	0.876	0.917	0.684	0.783	0.708	0.780	0.821
Mn	0.062	0.054	0.053	0.064	0.064	0.061	0.062	0.078	0.070	0.067
Mg	0.001	0.000	0.003	0.004	0.000	0.001	0.002	0.002	0.007	0.006
Sum	3.000	3.000	3.000	3.000	3.000	3.000	3.000	3.000	3.000	3.000
Usp	67.6	43.4	46.3	55.9	53.9	65.5	60.7	64.5	60.7	58.8
Mt	32.3	56.5	53.7	43.8	45.8	34.2	39.2	35.4	39.0	41.0
Sp	0.2	0.1	0.1	0.3	0.2	0.3	0.2	0.1	0.3	0.2

Table C4: Ilmenite analyses from the Terceira ignimbrite formations and associated lithologies

Unit	**LAI**	**LAI**	**LAI**	**LAI**	**LAI**	**LAI**	**LAI**	**LAI**	**Ign-i**	**CCI Sy**	**CCI Sy**	**CCI Sy**	**CCI Sy**	**CCI Sy**	**CCI Sy**	**CCI Sy**	**CCI Sy**
Sample	TER3-2	TER4-1	TER4-1	TER7-1	TER7-1	TER7-1	TER10-3	TER10-3	T001	TER30-3	TER30-3	TER30-3	TER30-3	TER30-6	TER30-6	TER30-6	TER30-6
No.	63 / 1 .	154 / 1 .	155 / 1 .	68 / 1 .	69 / 1 .	70 / 1 .	83 / 1 .	84 / 1 .	63 / 1 .	ILM 1	ILM 2	ILM 3	ILM 4	ILM 5	ILM 6	ILM 7	ILM 8
Notes	Mph	Mph	Mph	Mph	Mph	Mph	Mph	Mph	Mph	Mph	Mph	Mph	Mph	Mph	Mph	Mph	Mph
TiO_2	51.10	51.10	51.03	50.12	50.44	51.25	51.09	51.14	50.41	50.64	50.44	51.13	50.19	50.32	51.05	50.46	50.20
Al_2O_3	0.07	0.04	0.04	0.07	0.07	0.05	0.05	0.06	0.01	0.02	0.05	bdl	0.01	bdl	bdl	0.02	0.04
Cr_2O_3	0.02	0.01	0.02	0.01	bdl	0.02	0.01	0.03	bdl	0.01	bdl	bdl	bdl	bdl	bdl	bdl	bdl
FeO	45.00	45.55	45.56	45.00	45.09	44.92	45.33	45.42	44.67	44.31	45.56	45.62	45.11	45.85	43.94	46.30	45.89
MnO	2.30	2.32	2.32	2.30	2.28	2.28	2.28	2.28	2.25	3.58	2.67	2.66	2.81	2.86	2.73	2.69	2.31
MgO	1.68	1.59	1.55	1.65	1.62	1.66	1.76	1.68	0.91	0.09	0.20	0.21	0.15	0.11	bdl	0.04	0.05
Total	100.17	100.61	100.52	99.15	99.50	100.17	100.50	100.61	98.23	98.65	98.92	99.62	98.27	99.14	97.72	99.51	98.49
Ti	0.954	0.950	0.950	0.944	0.948	0.957	0.949	0.950	0.965	0.972	0.965	0.971	0.967	0.961	0.991	0.960	0.965
Al	0.002	0.001	0.001	0.002	0.002	0.001	0.001	0.002	0.000	0.001	0.001		0.000			0.001	0.001
Cr	0.000	0.000	0.000	0.000		0.000	0.000	0.001		0.000							
Fe^{2+}	0.843	0.843	0.844	0.834	0.839	0.847	0.837	0.840	0.882	0.892	0.899	0.907	0.900	0.895	0.932	0.901	0.914
Fe^{3+}	0.091	0.099	0.099	0.109	0.103	0.085	0.100	0.098	0.069	0.055	0.070	0.057	0.066	0.079	0.017	0.079	0.068
Mn	0.048	0.049	0.049	0.049	0.048	0.048	0.048	0.048	0.048	0.077	0.058	0.057	0.061	0.062	0.060	0.058	0.050
Mg	0.062	0.059	0.057	0.062	0.060	0.061	0.065	0.062	0.035	0.003	0.008	0.008	0.006	0.004		0.002	0.002
Sum	2.000	2.000	2.000	2.000	2.000	2.000	2.000	2.000	2.000	2.000	2.000	2.000	2.000	2.000	2.000	2.000	2.000
Ilm	91.1	90.6	90.6	90.2	90.5	91.4	90.7	90.8	92.1	90.3	91.3	91.9	91.1	90.5	93.5	90.8	92.0
Hem	4.3	4.7	4.7	5.2	4.9	4.1	4.8	4.7	3.3	2.5	3.3	2.7	3.1	3.7	0.8	3.7	3.2
Pyr	4.6	4.6	4.6	4.7	4.6	4.6	4.6	4.6	4.6	7.2	5.4	5.4	5.7	5.8	5.6	5.5	4.8

Table C5: Olivine analyses from the Terceira ignimbrite formations

Unit	**LAI**	**LAI**	**LAI**	**LAI**	**LAI**	**LAI**	**LAI**	**LAI**	**LAI**	**LMI**	**LMI**	**CCI**	**CCI**	**CCI**	**CCI**
Sample	TER1-1	TER1-1	TER1-2-ol	TER1-2-ol	TER3-1	TER3-1	TER3-1	TER3-1	TER3-1	TER5-2	TER5-2	TM-1(2)	TM-1(2)	TM-1(2)	TM-1(2)
No.	56 / 1 .	57 / 1 .	93 / 1 .	92 / 1 .	136 / 1 .	142 / 1 .	143 / 1 .	144 / 1 .	145 / 1 .	166 / 1 .	167 / 1 .	POl2	Ol4	Ol5	Ol11
Notes	Pheno	Pheno	Pheno	Pheno	Pheno	Pheno	Pheno	Pheno	Pheno	Pheno	Pheno	Pheno	Pheno	Pheno	Pheno
SiO_2	33.10	33.16	33.94	33.94	34.17	33.81	33.69	33.89	33.18	33.01	32.82	31.69	32.40	31.51	31.83
TiO_2	0.04	0.02	0.03	0.03	0.03	0.03	0.03	0.03	0.04	0.03	0.03	0.04	0.06	0.02	0.09
Al_2O_3	0.03	0.01	0.01	0.01	0.01	bdl	bdl	0.01	0.01	0.01	0.02	bdl	bdl	bdl	0.01
Cr_2O_3	0.02	bdl	0.03	bdl	0.02	0.02	0.02	0.03	0.02	0.03	bdl	bdl	0.02	0.03	0.02
FeO	50.39	50.61	47.11	46.55	47.50	47.21	47.27	47.16	46.05	53.01	52.90	55.70	54.45	57.56	56.71
MnO	3.48	3.49	2.96	2.98	3.04	3.05	3.04	3.05	2.98	3.45	3.43	3.95	3.65	4.25	4.05
MgO	14.28	14.24	17.54	17.89	17.22	16.85	16.95	17.19	16.84	12.35	12.28	8.97	10.28	7.30	8.09
CaO	0.26	0.27	0.28	0.27	0.30	0.28	0.29	0.30	0.30	0.32	0.31	0.34	0.33	0.34	0.29
Na_2O												bdl	0.03	0.01	0.01
K_2O												0.01	bdl	bdl	bdl
Total	101.60	101.81	101.89	101.66	102.29	101.24	101.28	101.64	99.41	102.20	101.81	100.69	101.22	101.02	101.12
Si	0.996	0.996	0.996	0.996	1.000	1.001	0.997	0.998	0.999	0.999	0.998	0.997	1.003	1.000	1.002
Ti	0.001	0.000	0.001	0.001	0.001	0.001	0.001	0.001	0.001	0.001	0.001	0.001	0.001	0.001	0.002
Al	0.001	0.000	0.000	0.000	0.000			0.000	0.000	0.000	0.001				0.000
Cr	0.000		0.001		0.000	0.000	0.001	0.001	0.000	0.001			0.001	0.001	0.001
Fe	1.268	1.271	1.156	1.142	1.162	1.168	1.170	1.161	1.159	1.342	1.346	1.466	1.409	1.527	1.493
Mn	0.089	0.089	0.074	0.074	0.075	0.077	0.076	0.076	0.076	0.089	0.088	0.105	0.096	0.114	0.108
Mg	0.640	0.637	0.767	0.782	0.751	0.743	0.748	0.755	0.755	0.557	0.557	0.421	0.474	0.345	0.380
Ca	0.009	0.009	0.009	0.008	0.009	0.009	0.009	0.009	0.010	0.010	0.010	0.011	0.011	0.012	0.010
Na													0.002	0.001	0.001
K															
Sum	3.003	3.003	3.003	3.003	2.999	2.999	3.002	3.001	3.000	2.999	3.001	3.002	2.997	3.000	2.996
Fo	33.57	33.40	39.90	40.66	39.26	38.88	38.99	39.38	39.46	29.33	29.27	22.30	25.18	18.44	20.27
Fa	66.43	66.60	60.10	59.34	60.74	61.12	61.01	60.62	60.54	70.67	70.73	77.70	74.82	81.56	79.73

Table C5 continued

Unit	**CCI**	**CCI**	**CCI**	**CCI**	**CCI**	**CCI**	**CCI**	**PNI**	**PNI**	**Ign-i**	**Ign-i**	**Ign-i**	**Ign-i**	**Ign-i**
Sample	TM-1(2)	TM-2(2)	TM-2(2)	TM-2(2)	TM-2(2)	TM-2(2)	TM-2(2)	PNI-7	PNI-8	IGI-1	IGI-5	IGI-8	IGI-9	IGI-13
No.	Ol12	Ol3	Ol4	Ol7	Ol8	Ol10	Ol14	7 / 1 .	8 / 1 .	34 / 1 .	38 / 1 .	41 / 1 .	42 / 1 .	46 / 1 .
Notes	Pheno	Pheno	Pheno	Pheno	Pheno	Pheno	Pheno	Pheno	Pheno	Pheno	Pheno	Pheno	Pheno	Pheno
SiO_2	31.44	31.82	32.03	31.77	31.83	31.16	31.38	33.09	33.28	32.92	39.03	32.23	32.07	32.07
TiO_2	0.05	0.07	0.00	0.00	0.05	0.00	0.00	0.03	0.03	0.05	0.04	0.00	0.00	0.02
Al_2O_3	0.02	bdl	0.02	0.01	0.01	bdl	bdl	bdl	bdl	bdl	bdl	bdl	bdl	bdl
Cr_2O_3	bdl	bdl	bdl	bdl	bdl	bdl	0.02	0.02	0.01	0.01	bdl	0.01	bdl	bdl
FeO	57.30	56.10	55.02	55.93	56.68	56.02	57.10	50.41	50.37	50.79	22.58	54.13	54.32	55.27
MnO	4.01	3.93	3.77	3.92	4.14	4.05	4.10	3.30	3.19	3.20	0.36	3.65	3.65	3.79
MgO	8.18	9.02	9.73	8.82	7.50	7.78	7.54	13.56	13.56	13.13	38.59	9.93	10.04	9.00
CaO	0.33	0.35	0.34	0.34	0.33	0.31	0.35			0.34	0.25	0.34	0.37	0.33
Na_2O	bdl	0.02	0.02	0.01	0.04	bdl	0.04	0.04	0.03	0.02	0.01	0.04	bdl	0.02
K_2O	bdl	bdl	bdl	0.01	bdl	bdl	bdl	bdl	bdl	bdl	bdl	bdl	bdl	bdl
Total	101.34	101.30	100.92	100.81	100.58	99.32	100.52	100.79	100.82	100.46	100.86	100.32	100.45	100.50
Si	0.991	0.996	0.999	0.999	1.009	1.001	0.999	1.005	1.009	1.005	1.006	1.007	1.002	1.007
Ti	0.001	0.002	0.000	0.000	0.001	0.000	0.000	0.001	0.001	0.001	0.001	0.000	0.000	0.001
Al	0.001		0.001	0.000	0.000									
Cr							0.001	0.001	0.000	0.000		0.000		
Fe	1.511	1.468	1.436	1.471	1.502	1.505	1.520	1.280	1.277	1.296	0.487	1.414	1.419	1.451
Mn	0.107	0.104	0.100	0.104	0.111	0.110	0.111	0.085	0.082	0.083	0.008	0.097	0.097	0.101
Mg	0.384	0.421	0.453	0.414	0.354	0.373	0.358	0.614	0.613	0.598	1.484	0.462	0.468	0.421
Ca	0.011	0.012	0.011	0.011	0.011	0.011	0.012	0.000	0.000	0.011	0.007	0.011	0.012	0.011
Na		0.001	0.001	0.001	0.002		0.002	0.002	0.002	0.001	0.001	0.002		0.001
K				0.000										
Sum	3.007	3.003	3.001	3.001	2.991	2.999	3.002	2.995	2.991	2.995	2.993	2.994	2.998	2.993
Fo	20.29	22.28	23.97	21.94	19.09	19.84	19.05	32.41	32.43	31.55	75.29	24.64	24.78	22.49
Fa	79.71	77.72	76.03	78.06	80.91	80.16	80.95	67.59	67.57	68.45	24.71	75.36	75.22	77.51

Table C6: Biotite analyses from the Grota do Vale Ignimbrite Formation (GVI)

Unit	**GVI**	**GVI**	**GVI**	**GVI**	**GVI**	**GVI**	**GVI**	**GVI**	**GVI**
Sample	TER131-min	TER131-min	TER131-min	TER131-min	TER131-min	TER131-min	TER131-min	TER131-min	TER131-min
No.	84 / 1 .	85 / 1 .	86 / 1 .	97 / 1 .	98 / 1 .	104 / 1 .	105 / 1 .	106 / 1 .	107 / 1 .
Notes	Pheno	Pheno	Pheno	Pheno	Pheno	Pheno	Pheno	Pheno	Pheno
SiO_2	39.30	38.60	39.26	38.45	37.63	38.45	38.01	36.65	36.63
TiO_2	6.02	5.91	5.95	5.79	5.77	5.84	5.97	5.72	5.87
Al_2O_3	10.89	10.95	11.04	10.89	10.47	11.77	10.66	10.16	10.25
BaO	0.23	0.25	0.24	0.15	0.16	0.25	0.13	0.17	0.14
FeO	13.87	13.76	13.90	13.56	13.70	13.28	13.99	13.68	13.66
MnO	0.34	0.30	0.34	0.37	0.33	0.54	0.33	0.30	0.31
MgO	14.61	14.29	14.46	14.16	14.47	13.76	13.96	13.91	14.38
ZnO	0.05	0.06	0.05	0.05	0.06	0.06	0.04	0.06	0.06
CaO	0.04	0.04	0.04	0.07	0.34	0.13	0.11	0.06	0.06
Na_2O	1.12	1.14	1.08	0.94	1.02	0.87	0.78	1.04	1.07
K_2O	8.47	8.17	8.30	8.08	8.30	7.74	7.53	8.20	8.34
F	1.33	1.56	1.50	1.56	1.46	1.69	1.58	1.34	1.77
Cl	0.04	0.05	0.04	0.04	0.04	0.05	0.04	0.04	0.03
Total	99.96	98.53	99.73	97.51	97.18	97.78	96.49	94.71	95.73
Si	5.873	5.856	5.877	5.880	5.809	5.849	5.872	5.812	5.763
Ti	0.676	0.675	0.670	0.666	0.670	0.668	0.694	0.682	0.694
Al^{IV}	1.918	1.958	1.948	1.963	1.906	2.111	1.940	1.900	1.900
Al^{VI}	0.000	0.000	0.000	0.000	0.000	0.000	0.000	0.000	0.000
Ba	0.014	0.015	0.014	0.009	0.010	0.015	0.008	0.010	0.009
Fe	1.734	1.746	1.740	1.735	1.769	1.690	1.808	1.815	1.797
Mn	0.043	0.039	0.043	0.047	0.043	0.069	0.043	0.040	0.041
Mg	3.253	3.231	3.226	3.229	3.329	3.121	3.216	3.290	3.373
Zn	0.006	0.007	0.006	0.006	0.007	0.006	0.005	0.007	0.007
Ca	0.006	0.007	0.006	0.011	0.056	0.020	0.019	0.009	0.010
Na	0.326	0.336	0.314	0.278	0.306	0.256	0.234	0.319	0.326
K	1.615	1.580	1.584	1.575	1.635	1.502	1.483	1.660	1.673
OH	3.361	3.241	3.279	3.237	3.278	3.175	3.217	3.318	3.110
F	0.630	0.747	0.712	0.754	0.713	0.813	0.773	0.673	0.881
Cl	0.009	0.013	0.009	0.009	0.009	0.013	0.010	0.010	0.009
Sum	19.463	19.449	19.428	19.400	19.539	19.306	19.322	19.545	19.593

Table C7: Amphibole analyses from the CCI syenite ejecta and syenite-hosted enclaves

Unit	**CCI Sy**	**CCI Sy**	**CCI Sy**	**CCI Sy**	**CCI Sy**	**CCI Sy**	**CCI Sy**	**CCI Sy**	**CCI Sy**	**CCI Sy**	**CCI Sy**	**CCI Sy**	**CCI Sy**
Sample	TER30-3	TER30-3	TER30-3	TER30-3	TER30-3	TER30-3	TER30-3	TER30-3	TER30-3	TER30-3	TER30-3	TER30-3	TER30-3
No.	Amph1	Amph1	Amph2	Amph2	Amph3	Amph4	Amph5	Amph6	Amph6	Amph7	Amph7	Amph8	Amph9
Notes	Core	Rim	Core	Rim	Core	Core	Core	Core	Rim	Core	Rim	Core	Core
SiO_2	48.64	47.67	48.32	47.75	53.22	52.80	48.44	47.85	50.08	47.49	48.69	48.21	47.72
TiO_2	1.75	2.27	1.80	2.59	3.83	3.17	1.83	2.04	1.89	2.55	2.19	2.52	1.96
Al_2O_3	3.08	2.15	3.08	1.74	0.33	0.27	3.07	3.17	0.38	1.82	1.04	1.43	3.08
FeO	21.81	29.92	23.26	31.80	27.16	27.41	23.16	23.68	34.00	32.94	33.16	33.48	24.91
MnO	0.92	1.37	1.01	1.44	0.43	0.41	0.97	1.00	1.60	1.47	1.49	1.53	1.05
MgO	8.48	2.71	7.62	1.57	0.03	0.00	7.92	7.36	0.19	1.05	0.64	0.69	6.99
CaO	7.33	5.44	7.23	4.39	1.40	3.26	7.36	7.25	2.20	4.62	3.40	3.91	7.37
Na_2O	5.35	5.90	4.89	6.39	12.48	11.53	4.62	5.07	7.29	6.16	7.01	6.06	4.63
K_2O	1.15	1.27	1.09	1.26	0.00	0.02	1.15	1.14	1.55	1.28	1.42	1.27	1.23
F													
Cl													
Total	98.51	98.70	98.30	98.94	98.88	98.87	98.52	98.56	99.18	99.38	99.03	99.09	98.94
Si	7.417	7.545	7.393	7.578	8.188	8.161	7.371	7.340	7.938	7.537	7.767	7.633	7.302
Ti	0.201	0.270	0.207	0.309	0.443	0.369	0.209	0.235	0.225	0.304	0.263	0.300	0.226
Al^{IV}	0.554	0.401	0.555	0.326	0.000	0.000	0.551	0.573	0.062	0.340	0.195	0.266	0.555
Al^{VI}	0.000	0.000	0.000	0.000	0.059	0.050	0.000	0.000	0.008	0.000	0.000	0.000	0.000
Fe^{2+}	2.771	3.904	2.765	4.036	3.494	3.543	2.644	2.876	4.204	4.121	4.296	4.009	2.827
Fe^{3+}	0.010	0.056	0.211	0.184	0.000	0.000	0.303	0.162	0.303	0.251	0.128	0.424	0.360
Mn	0.119	0.184	0.131	0.194	0.056	0.053	0.125	0.130	0.215	0.198	0.201	0.205	0.135
Mg	1.928	0.639	1.738	0.372	0.007	0.000	1.797	1.683	0.045	0.249	0.151	0.162	1.594
Ca	1.198	0.923	1.185	0.746	0.231	0.540	1.200	1.192	0.374	0.786	0.581	0.663	1.208
Na	1.582	1.811	1.451	1.966	3.723	3.456	1.363	1.508	2.240	1.896	2.168	1.860	1.374
K	0.223	0.256	0.213	0.255	0.000	0.003	0.222	0.222	0.313	0.259	0.289	0.257	0.240
OH	2.000	2.000	2.000	2.000	2.000	2.000	2.000	2.000	2.000	2.000	2.000	2.000	2.000
F													
Cl													
Sum	18.002	17.848	18.201	18.175	17.785	17.922	17.940	17.780	17.822	18.063	18.144	17.930	17.795

Table C7 continued

Unit	CCI Sy	CCI Sy	CCI Sy	CCI Sy	CCI Sy	CCI Sy	CCI Sy	CCI Sy	CCI Sy	CCI Sy	CCI Sy	CCI Sy	CCI Sy
Sample No.	TER30-3 Amph10	TER30-3 Amph 10	TER30-6 Amph 11	TER30-6 Amph11	TER30-6 Amph 12	TER30-6 Amph 13	TER30-6 Amph13	TER30-6 Amph 14	TER30-6 Amph14	TER30-6 Amph 15	TER30-6 Amph 16	TER30-6 Amph 17	TER30-6 Amph17
Notes	Core	Rim	Core	Rim	Core	Core	Rim	Core	Rim	Core	Core	Core	Rim
SiO_2	49.97	52.13	47.67	49.14	47.58	47.99	49.80	46.82	47.88	47.80	52.51	47.32	49.49
TiO_2	1.69	2.56	2.25	1.29	2.14	1.89	1.41	2.04	2.29	1.85	0.74	1.97	1.36
Al_2O_3	0.23	0.17	2.71	0.73	3.07	3.46	0.56	3.73	2.62	2.84	0.16	3.40	0.47
FeO	34.29	26.87	25.24	33.75	24.74	22.14	34.67	23.89	26.10	25.20	27.60	22.13	34.65
MnO	1.44	1.06	1.02	1.53	1.09	0.97	1.51	1.06	1.26	1.06	2.52	1.03	1.55
MgO	0.05	0.29	5.93	0.57	7.13	8.89	0.27	7.71	6.15	6.40	3.10	8.55	0.16
CaO	0.86	5.27	6.89	3.02	7.20	7.74	2.48	7.81	6.72	7.17	0.32	7.72	2.10
Na_2O	8.40	10.38	5.05	6.97	4.69	4.54	7.49	4.46	5.14	4.87	9.47	4.43	7.44
K_2O	1.56	0.00	1.27	1.41	1.16	1.13	1.58	1.09	1.20	1.18	1.61	1.13	1.58
F													
Cl													
Total	98.49	98.73	98.03	98.41	98.80	98.75	99.77	98.62	99.36	98.37	98.02	97.67	98.79
Si	7.972	8.106	7.433	7.854	7.273	7.248	7.876	7.150	7.344	7.393	8.216	7.243	7.886
Ti	0.203	0.299	0.264	0.156	0.246	0.215	0.168	0.234	0.264	0.215	0.087	0.227	0.163
Al^{IV}	0.028	0.000	0.498	0.137	0.553	0.616	0.104	0.671	0.474	0.518	0.000	0.613	0.088
Al^{VI}	0.016	0.031	0.000	0.000	0.000	0.000	0.000	0.000	0.000	0.000	0.029	0.000	0.000
Fe^{2+}	4.178	3.494	3.265	4.150	2.728	2.389	4.234	2.581	3.011	3.065	3.546	2.452	4.140
Fe^{3+}	0.397	0.000	0.026	0.362	0.435	0.407	0.352	0.470	0.337	0.195	0.065	0.380	0.478
Mn	0.195	0.139	0.135	0.207	0.141	0.124	0.202	0.138	0.164	0.139	0.334	0.133	0.209
Mg	0.012	0.068	1.378	0.135	1.625	2.002	0.064	1.755	1.406	1.476	0.723	1.951	0.037
Ca	0.147	0.878	1.151	0.517	1.179	1.252	0.420	1.278	1.104	1.188	0.053	1.266	0.359
Na	2.598	3.129	1.527	2.160	1.390	1.329	2.297	1.321	1.529	1.460	2.873	1.315	2.299
K	0.318	0.000	0.253	0.288	0.226	0.218	0.319	0.213	0.235	0.234	0.321	0.220	0.321
OH	2.000	2.000	2.000	2.000	2.000	2.000	2.000	2.000	2.000	2.000	2.000	2.000	2.000
F													
Cl													
Sum	17.800	17.812	17.882	18.247	17.801	17.837	18.015	17.990	17.968	17.927	18.038	17.965	18.036

Table C7 continued

Unit	**CCI Sy**	**CCI Sy**	**CCI Sy**	**CCI Sy**	**CCI Sy**	**CCI Sy**	**CCI Sy**	**CCI Sy**	**CCI Sy**	**CCI Sy**	**Sy enc**	**Sy enc**	**Sy enc**
Sample	TER30-6	TER30-6	TER30-1	TER30-1	TER30-1	TER30-1	TER30-1	TER30-1	TER30-1	TER30-1	Spec 1	Spec 1	Spec 1
No.	Amph 18	Amph 19	Amph1	Amph2	Amph3	Amph4	Amph5	Amph6	Amph7	Amph8	Amph 1	Amph 2	Amph 3
Notes	Core	Core	Core	Core	Core	Core	Core	Core	Core	Core	Gm	Gm	Gm
SiO_2	47.81	47.52	48.12	47.22	47.35	47.91	47.88	47.56	47.49	48.08	45.47	46.71	45.40
TiO_2	1.92	1.79	2.07	2.24	2.34	2.30	1.66	2.25	2.41	2.00	2.07	2.31	2.24
Al_2O_3	3.21	3.00	2.87	2.57	2.34	2.67	2.69	2.81	2.24	2.97	2.71	2.51	4.20
FeO	23.78	23.77	24.63	28.21	28.60	26.83	24.22	26.73	29.05	23.95	26.52	24.04	20.07
MnO	1.06	1.09	1.04	1.18	1.23	1.16	1.08	1.14	1.25	1.14	1.14	1.02	0.82
MgO	7.58	7.08	6.43	4.20	3.83	4.93	6.93	5.35	3.41	7.35	4.95	6.54	9.39
CaO	7.36	7.15	7.02	6.76	6.32	6.82	7.25	6.80	6.08	7.44	6.78	6.26	8.62
Na_2O	4.74	5.30	5.35	4.94	5.38	5.39	5.20	5.30	5.47	4.71	5.60	5.79	4.83
K_2O	1.17	1.17	1.14	1.21	1.23	1.20	1.07	1.20	1.20	1.13	1.23	1.37	1.12
F			1.98	1.62	1.61	1.72	2.15	1.79	1.43	1.98	1.94	2.04	2.39
Cl			0.04	0.05	0.05	0.05	0.04	0.05	0.05	0.05	0.04	0.03	0.04
Total	98.64	97.87	100.69	100.20	100.28	100.97	100.16	100.98	100.07	100.79	98.45	98.62	99.11
Si	7.301	7.375	7.432	7.415	7.458	7.442	7.428	7.373	7.494	7.350	7.321	7.395	7.068
Ti	0.221	0.209	0.240	0.265	0.277	0.269	0.193	0.262	0.286	0.230	0.251	0.275	0.262
Al^{IV}	0.578	0.549	0.522	0.476	0.434	0.489	0.492	0.513	0.417	0.535	0.514	0.467	0.772
Al^{VI}	0.000	0.000	0.000	0.000	0.000	0.000	0.000	0.000	0.000	0.000	0.000	0.000	0.000
Fe^{2+}	2.700	3.007	3.181	3.560	3.695	3.485	3.062	3.338	3.782	2.811	3.569	3.166	2.601
Fe^{3+}	0.337	0.079	0.000	0.144	0.073	0.000	0.081	0.127	0.052	0.251	0.002	0.017	0.011
Mn	0.137	0.144	0.136	0.157	0.164	0.152	0.142	0.150	0.167	0.147	0.155	0.136	0.108
Mg	1.726	1.638	1.480	0.983	0.899	1.142	1.603	1.236	0.802	1.675	1.188	1.544	2.178
Ca	1.204	1.189	1.162	1.137	1.067	1.135	1.205	1.129	1.028	1.219	1.170	1.061	1.438
Na	1.404	1.595	1.602	1.504	1.643	1.623	1.564	1.593	1.674	1.396	1.747	1.776	1.459
K	0.229	0.231	0.225	0.242	0.247	0.237	0.211	0.238	0.241	0.220	0.253	0.278	0.223
OH	2.000	2.000	1.023	1.183	1.185	1.143	0.935	1.110	1.273	1.030	1.000	0.972	0.813
F			0.967	0.805	0.802	0.845	1.055	0.878	0.714	0.957	0.989	1.021	1.178
Cl			0.010	0.012	0.013	0.012	0.010	0.013	0.013	0.012	0.011	0.007	0.009
Sum	17.868	17.978	17.980	17.884	17.957	17.975	17.980	17.960	17.942	17.835	18.171	18.115	18.119

Table C7 continued

Unit	Sy enc	Sy enc	Sy enc	Sy enc	Sy enc	Sy enc	Sy enc	Sy enc	Sy enc	Sy enc	Sy enc	Sy enc	Sy enc
Sample	Spec 1	Spec 1	Spec 1	Spec 1	Spec 1	Spec 1	Spec 1	Spec 1	Spec 1	Spec 1	Spec 1	Spec 1	Spec 1
No.	Amph 4	Amph 5	Amph 6	Amph 7	Amph 8	Amph 9	Amph 10	Amph 11	Amph 12	Amph 13	Amph 14	Amph 15	Amph 16
Notes	Gm	Gm	Gm	Gm	Gm	Gm	Gm	Gm	Gm	Gm	Gm	Gm	Gm
SiO_2	44.45	47.52	47.33	45.73	46.09	46.81	46.70	46.21	46.46	45.51	45.60	46.31	47.06
TiO_2	2.20	2.42	2.39	2.27	2.16	2.27	2.24	2.32	2.03	2.24	2.43	2.36	2.54
Al_2O_3	4.18	1.41	1.54	4.07	3.93	2.27	2.16	2.38	2.78	2.34	2.27	2.06	1.50
FeO	24.31	28.49	27.81	22.64	22.45	27.31	27.78	27.20	23.49	26.78	29.11	28.71	29.55
MnO	0.94	1.28	1.25	0.90	0.95	1.15	1.13	1.13	1.03	1.14	1.22	1.26	1.30
MgO	6.33	3.54	3.88	7.39	7.61	4.41	4.38	4.58	7.21	4.86	3.37	3.69	2.91
CaO	7.91	4.86	5.28	8.32	8.21	5.96	6.07	6.23	7.27	6.32	5.95	5.61	4.96
Na_2O	4.78	6.01	6.11	4.65	4.79	5.71	5.45	5.43	5.23	5.53	5.73	5.61	6.00
K_2O	1.05	1.32	1.33	1.19	1.21	1.32	1.42	1.24	1.19	1.11	1.29	1.30	1.34
F	1.89	1.37	1.35	1.81	0.98	1.75	1.89	1.76	2.22	1.93	1.41	1.81	1.61
Cl	0.04	0.05	0.03	0.04	0.04	0.04	0.04	0.04	0.05	0.04	0.04	0.04	0.04
Total	98.08	98.27	98.29	99.01	98.42	98.99	99.25	98.52	98.95	97.79	98.43	98.75	98.80
Si	7.082	7.608	7.586	7.157	7.186	7.460	7.436	7.390	7.319	7.343	7.363	7.424	7.563
Ti	0.263	0.291	0.289	0.267	0.253	0.273	0.268	0.279	0.241	0.271	0.296	0.284	0.307
Al^{IV}	0.786	0.267	0.290	0.750	0.723	0.426	0.405	0.448	0.516	0.446	0.433	0.390	0.284
Al^{VI}	0.000	0.000	0.000	0.000	0.000	0.000	0.000	0.000	0.000	0.000	0.000	0.000	0.000
Fe^{2+}	3.110	3.683	3.728	2.963	2.927	3.598	3.553	3.497	3.019	3.431	3.802	3.592	3.846
Fe^{3+}	0.130	0.132	0.000	0.000	0.000	0.042	0.146	0.141	0.076	0.183	0.129	0.256	0.125
Mn	0.126	0.173	0.169	0.120	0.125	0.155	0.153	0.152	0.137	0.156	0.167	0.171	0.177
Mg	1.503	0.846	0.926	1.724	1.769	1.047	1.039	1.093	1.693	1.170	0.810	0.882	0.697
Ca	1.351	0.834	0.907	1.395	1.372	1.017	1.035	1.067	1.226	1.092	1.030	0.963	0.854
Na	1.478	1.866	1.899	1.412	1.448	1.765	1.682	1.684	1.596	1.730	1.794	1.745	1.868
K	0.213	0.270	0.272	0.239	0.241	0.268	0.289	0.254	0.240	0.228	0.266	0.266	0.274
OH	1.038	1.291	1.307	1.095	1.507	1.108	1.038	1.099	0.883	1.005	1.269	1.073	1.172
F	0.950	0.696	0.684	0.895	0.483	0.880	0.952	0.890	1.105	0.984	0.721	0.915	0.819
Cl	0.011	0.013	0.009	0.010	0.010	0.011	0.010	0.011	0.012	0.011	0.011	0.012	0.010
Sum	18.042	17.969	18.066	18.026	18.044	18.050	18.006	18.005	18.062	18.050	18.090	17.974	17.996

Table C7 continued

Unit	**Sy enc**	**Sy enc**	**Sy enc**	**Sy enc**	**Sy enc**	**Sy enc**	**Sy enc**	**Sy enc**	**Sy enc**	**Sy enc**	**Sy enc**	**Sy enc**	**Sy enc**
Sample	Spec 1	Spec 1	Spec 1	Spec 1	Spec 1	T073 A3	T073 A3	T073 A3	T073 A3	T073 A3	T073 A3	T073 A3	T073 A3
No.	Amph 17	Amph 18	Amph 19	Amph 20	Amph 21	Amph 1	Amph 2	Amph 3	Amph 4	Amph 5	Amph 6	Amph 7	Amph 8
Notes	Gm	Gm	Gm	Gm	Gm	Gm	Gm	Gm	Gm	Gm	Gm	Gm	Gm
SiO_2	45.26	46.53	45.83	46.09	45.54	48.23	46.42	45.15	45.06	46.34	46.72	45.47	46.13
TiO_2	2.47	2.23	2.30	2.35	2.35	1.15	2.74	2.11	2.03	2.60	2.74	2.80	2.08
Al_2O_3	1.35	2.22	2.15	2.30	2.41	0.89	1.83	3.82	3.68	1.36	1.78	1.73	3.82
FeO	29.78	26.83	27.39	28.19	27.27	27.16	30.25	21.57	23.99	30.65	30.49	30.02	20.73
MnO	1.31	1.21	1.19	1.19	1.16	1.19	1.44	0.95	1.00	1.21	1.24	1.31	0.88
MgO	2.89	4.82	4.58	4.15	4.74	1.47	2.29	8.49	6.65	2.46	2.71	2.78	9.27
CaO	4.87	6.39	6.11	6.04	6.43	12.43	5.25	8.20	7.92	4.50	5.43	5.34	8.27
Na_2O	6.26	5.45	5.51	5.80	5.58	5.16	5.82	4.68	4.80	6.24	5.80	5.98	4.70
K_2O	1.37	1.30	1.31	1.15	1.19	0.24	1.27	1.08	1.11	1.36	1.32	1.27	1.14
F	1.66	1.86	1.74	1.80	2.07	0.18	1.20	2.51	1.85	1.04	1.23	1.32	2.15
Cl	0.04	0.05	0.05	0.04	0.04	0.01	0.05	0.04	0.04	0.04	0.05	0.05	0.04
Total	97.26	98.89	98.14	99.11	98.78	98.12	98.55	98.60	98.13	97.81	99.50	98.08	99.20
Si	7.445	7.425	7.371	7.366	7.309	7.695	7.491	7.093	7.165	7.509	7.456	7.392	7.131
Ti	0.305	0.267	0.278	0.283	0.283	0.138	0.333	0.249	0.242	0.317	0.328	0.342	0.241
Al^{IV}	0.261	0.417	0.407	0.433	0.455	0.167	0.348	0.708	0.690	0.259	0.334	0.332	0.696
Al^{VI}	0.000	0.000	0.000	0.000	0.000	0.000	0.000	0.000	0.000	0.000	0.000	0.000	0.000
Fe^{2+}	3.858	3.521	3.480	3.601	3.495	3.624	3.973	2.627	3.098	3.871	3.893	3.890	2.492
Fe^{3+}	0.238	0.059	0.204	0.167	0.166	0.000	0.109	0.208	0.092	0.283	0.176	0.191	0.187
Mn	0.183	0.164	0.162	0.161	0.158	0.161	0.196	0.126	0.135	0.167	0.168	0.180	0.115
Mg	0.709	1.147	1.099	0.989	1.133	0.351	0.551	1.989	1.577	0.595	0.645	0.673	2.137
Ca	0.859	1.093	1.053	1.034	1.106	2.125	0.907	1.380	1.349	0.781	0.928	0.931	1.369
Na	1.996	1.688	1.718	1.799	1.737	1.596	1.821	1.425	1.480	1.962	1.796	1.886	1.408
K	0.287	0.265	0.268	0.235	0.243	0.049	0.262	0.215	0.225	0.282	0.269	0.263	0.226
OH	1.124	1.049	1.103	1.080	0.938	1.903	1.377	0.742	1.057	1.456	1.366	1.306	0.940
F	0.865	0.938	0.885	0.909	1.051	0.093	0.611	1.247	0.931	0.532	0.621	0.680	1.049
Cl	0.011	0.013	0.012	0.011	0.011	0.004	0.012	0.011	0.012	0.011	0.013	0.014	0.010
Sum	18.141	18.046	18.039	18.068	18.087	17.906	17.990	18.021	18.055	18.025	17.993	18.079	18.003

Table C7 continued

Unit	**Sy enc**	**Sy enc**	**Sy enc**	**Sy enc**	**Sy enc**	**Sy enc**	**Sy enc**	**Sy enc**	**Sy enc**	**Sy enc**	**Sy enc**	**Sy enc**
Sample	T073 A3	T073 A3	T073 A3	T073 A3	T073 A3	T073 A3	T073 A3	T073 A3	T073 A3	T073 A3	T073 A3	T073 A3
No.	Amph 9	Amph 10	Amph 11	Amph 12	Amph 13	Amph 14	Amph 15	Amph 16	Amph 17	Amph 18	Amph 19	Amph 20
Notes	Gm	Gm	Gm	Gm	Gm	Gm	Gm	Gm	Gm	Gm	Gm	Gm
SiO_2	46.01	45.73	45.46	45.36	45.93	44.99	45.49	46.65	46.03	46.00	46.13	46.34
TiO_2	2.18	2.24	1.97	2.17	2.00	2.09	2.71	2.09	2.10	2.34	2.03	2.13
Al_2O_3	4.16	3.32	2.98	3.45	3.81	4.05	1.58	3.22	2.82	2.53	3.44	4.26
FeO	19.27	26.67	28.39	25.61	21.11	22.52	29.97	24.62	24.45	27.06	22.52	19.36
MnO	0.85	1.11	1.20	1.08	0.91	0.92	1.25	0.99	1.05	1.14	0.98	0.86
MgO	9.99	5.16	3.89	5.69	8.74	7.63	2.59	6.83	6.69	4.64	8.13	9.81
CaO	8.58	7.12	7.09	6.78	8.15	8.46	4.90	7.39	7.12	6.55	7.67	8.37
Na_2O	4.79	5.16	5.06	4.99	4.77	4.71	6.24	5.01	5.29	5.41	5.09	4.80
K_2O	1.09	1.11	1.10	1.14	1.08	1.19	1.30	1.04	1.15	1.20	1.11	1.11
F	2.10	1.23	1.51	1.85	2.06	2.11	1.27	1.84	1.90	1.63	2.20	2.15
Cl	0.04	0.04	0.04	0.05	0.04	0.04	0.04	0.05	0.04	0.04	0.05	0.04
Total	99.07	98.89	98.69	98.15	98.61	98.71	97.34	99.72	98.66	98.51	99.35	99.22
Si	7.097	7.226	7.294	7.203	7.161	7.104	7.450	7.252	7.276	7.361	7.183	7.129
Ti	0.253	0.266	0.238	0.259	0.235	0.248	0.333	0.245	0.250	0.282	0.238	0.246
Al^{IV}	0.757	0.618	0.563	0.645	0.700	0.753	0.305	0.590	0.525	0.477	0.631	0.772
Al^{VI}	0.000	0.000	0.000	0.000	0.000	0.000	0.000	0.000	0.000	0.000	0.000	0.000
Fe^{2+}	2.425	3.344	3.675	3.041	2.622	2.974	3.953	2.965	3.076	3.551	2.719	2.423
Fe^{3+}	0.060	0.180	0.135	0.360	0.129	0.000	0.152	0.236	0.156	0.070	0.214	0.068
Mn	0.111	0.149	0.164	0.145	0.121	0.123	0.174	0.130	0.140	0.154	0.129	0.112
Mg	2.297	1.217	0.930	1.348	2.032	1.797	0.632	1.582	1.577	1.106	1.887	2.250
Ca	1.418	1.206	1.219	1.153	1.361	1.432	0.860	1.232	1.206	1.124	1.279	1.380
Na	1.433	1.581	1.574	1.536	1.443	1.441	1.983	1.511	1.623	1.677	1.535	1.431
K	0.214	0.224	0.225	0.231	0.216	0.240	0.272	0.206	0.233	0.244	0.221	0.217
OH	0.964	1.376	1.220	1.057	0.972	0.937	1.334	1.084	1.037	1.166	0.903	0.943
F	1.027	0.613	0.769	0.931	1.016	1.052	0.655	0.904	0.952	0.824	1.085	1.047
Cl	0.009	0.011	0.011	0.012	0.011	0.012	0.011	0.012	0.012	0.010	0.012	0.010
Sum	18.065	18.011	18.017	17.919	18.019	18.112	18.115	17.949	18.062	18.045	18.035	18.029

Table C8: Aenigmatite analyses from the CCI syenite ejecta

Unit	**Syenite**	**Syenite**	**Syenite**	**Syenite**	**Syenite**	**Syenite**	**Syenite**	**Syenite**	**Syenite**	**Syenite**	**Syenite**	**Syenite**	**Syenite**	**Syenite**	**Syenite**	**Syenite**
Sample	TER30-3	TER30-3	TER30-3	TER30-6	TER30-6	TER30-6	TER30-6	TER30-6	TER30-6	TER30-6	TER30-7	TER30-7	TER30-7	TER30-7	TER30-7	TER30-7
No.	Aenig1	Aenig2	Aenig3	Aenig4	Aenig5	Aenig6	Aenig7	Aenig8	Aenig9	Aenig10	Aenig1	Aenig2	Aenig3	Aenig4	Aenig5	Aenig6
Notes	Int	Int	Int	Int	Int	Int	Int	Int	Int	Int	Int	Int	Int	Int	Int	Int
SiO_2	41.19	40.52	41.53	40.46	40.43	40.22	40.87	40.51	40.49	40.78	40.43	38.82	40.55	39.56	39.84	39.92
TiO_2	8.55	8.37	8.58	8.32	8.68	8.37	8.28	8.54	8.70	8.32	8.85	8.66	9.40	8.64	8.61	8.60
Al_2O_3	0.50	0.87	0.38	0.97	0.90	1.18	0.73	0.99	0.69	0.83	0.40	0.76	0.00	0.76	0.68	0.35
FeO	41.73	42.13	41.64	41.15	41.72	42.31	41.49	41.23	41.70	41.54	40.79	41.33	38.28	41.75	41.44	41.23
MnO	1.66	1.53	1.74	2.04	1.37	1.46	1.45	1.48	1.53	1.41	1.62	1.51	2.90	1.53	1.62	1.69
MgO	0.21	0.19	0.24	0.18	0.38	0.28	0.33	0.29	0.26	0.31	0.23	0.35	0.08	0.37	0.32	0.16
CaO	0.31	0.42	0.24	0.74	0.78	0.81	0.64	0.71	0.60	0.71	0.22	0.68	0.00	0.53	0.54	0.17
Na_2O	7.41	6.85	7.15	7.21	7.11	7.14	7.12	6.92	7.07	7.00	7.21	6.85	7.45	7.06	7.06	7.28
K_2O	0.01	bdl	0.01	0.01	0.02	bdl	bdl	0.02	bdl	bdl	bdl	bdl	bdl	bdl	bdl	bdl
Total	**101.56**	**100.93**	**101.52**	**101.08**	**101.41**	**101.80**	**100.91**	**100.70**	**101.04**	**100.90**	**99.75**	**98.96**	**98.65**	**100.21**	**100.11**	**99.39**
Si	5.794	5.764	5.861	5.718	5.700	5.649	5.788	5.759	5.740	5.782	5.798	5.625	5.874	5.653	5.698	5.747
Ti	0.905	0.896	0.911	0.884	0.921	0.884	0.882	0.913	0.928	0.887	0.954	0.945	1.024	0.929	0.926	0.931
Al	0.083	0.145	0.062	0.162	0.149	0.196	0.121	0.166	0.116	0.139	0.068	0.129	0.000	0.129	0.114	0.060
Fe^{2+}	4.366	4.590	4.561	4.254	4.362	4.289	4.419	4.502	4.453	4.477	4.460	4.353	4.340	4.324	4.359	4.346
Fe^{3+}	0.543	0.421	0.353	0.610	0.557	0.681	0.495	0.400	0.491	0.448	0.432	0.656	0.297	0.666	0.597	0.617
Mn	0.198	0.184	0.208	0.244	0.164	0.174	0.174	0.178	0.184	0.169	0.197	0.185	0.355	0.185	0.196	0.206
Mg	0.043	0.040	0.050	0.039	0.081	0.058	0.069	0.062	0.054	0.065	0.050	0.076	0.016	0.078	0.068	0.034
Ca	0.047	0.065	0.036	0.111	0.118	0.122	0.096	0.108	0.091	0.108	0.034	0.105	0.000	0.081	0.083	0.026
Na	2.021	1.889	1.956	1.976	1.944	1.944	1.955	1.907	1.943	1.924	2.006	1.925	2.093	1.957	1.959	2.033
K	0.001		0.002	0.001	0.004			0.003								
Sum	14.000	14.000	14.000	14.000	14.000	14.000	14.000	14.000	14.000	14.000	14.000	14.000	14.000	14.000	14.000	14.000

Table C9 Feldapr analyses from the UFG and the PIF

Unit	**Fur J**	**Fur J**	**Fur J**	**Fur J**	**Fur J**	**Fur J**	**Fur J**	**Fur J**	**Fur J**	**Fur J**	**Fur J**	**Fur J**	**Fur J**	**Fur J**
Sample	S018	S018	S018	S018	S018	S018	S018	S018	S018	S018	S018	S018	S018	S018
No.	Fsp1	Fsp2	Fsp3	Fsp4	Fsp5	Fsp6	Fsp7	Fsp8	Fsp9	Fsp10	Fsp11	Fsp12	Fsp13	Fsp14
Notes	Pheno	Pheno	Pheno	Pheno	Pheno	Pheno	Pheno	Pheno	Pheno	Pheno	Pheno	Pheno	Pheno	Pheno
SiO_2	64.75	64.56	64.90	64.18	64.52	64.47	65.19	65.00	64.84	65.63	66.14	65.51	64.58	64.77
TiO_2														
Al_2O_3	18.75	18.99	18.96	19.05	19.07	19.52	19.00	19.45	19.57	18.93	19.01	19.30	19.32	19.09
BaO	bdl	0.01	0.01	bdl	bdl	0.01	bdl	0.01	0.01	bdl	0.02	0.02	bdl	bdl
FeO	0.24	0.21	0.23	0.24	0.27	0.21	0.23	0.28	0.34	0.21	0.25	0.21	0.23	0.22
SrO	bdl	0.01	bdl	bdl	bdl	bdl	bdl	bdl	bdl	bdl	bdl	bdl	bdl	bdl
MgO														
CaO	0.31	0.45	0.40	0.42	0.48	0.85	0.42	0.84	1.02	0.40	0.33	0.51	0.60	0.43
Na_2O	6.87	6.80	6.79	7.09	6.68	7.42	6.71	7.17	7.29	6.76	6.68	6.72	6.99	6.95
K_2O	7.10	7.00	7.17	6.63	6.65	6.10	6.97	6.04	5.59	6.87	7.10	7.25	6.51	6.78
Total	98.01	98.04	98.46	97.61	97.67	98.58	98.52	98.79	98.66	98.80	99.52	99.52	98.22	98.23
Si	2.971	2.961	2.965	2.954	2.963	2.937	2.971	2.949	2.942	2.979	2.982	2.961	2.951	2.961
Ti														
Al	1.014	1.027	1.021	1.033	1.032	1.048	1.020	1.040	1.047	1.013	1.010	1.028	1.040	1.029
Ba		0.000	0.000			0.000		0.000	0.000		0.000	0.000		
Fe	0.009	0.008	0.009	0.009	0.010	0.008	0.009	0.010	0.013	0.008	0.010	0.008	0.009	0.008
Sr		0.000												
Mg														
Ca	0.015	0.022	0.020	0.021	0.024	0.042	0.021	0.041	0.049	0.020	0.016	0.024	0.029	0.021
Na	0.611	0.605	0.601	0.633	0.595	0.655	0.593	0.631	0.641	0.595	0.584	0.589	0.619	0.616
K	0.416	0.410	0.418	0.389	0.390	0.354	0.405	0.350	0.324	0.398	0.408	0.418	0.380	0.395
Sum	5.036	5.033	5.034	5.040	5.013	5.044	5.018	5.021	5.017	5.011	5.009	5.029	5.028	5.030
Ab	58.7	58.3	57.9	60.7	59.0	62.3	58.2	61.8	63.2	58.8	57.9	57.1	60.2	59.7
An	1.4	2.2	1.9	2.0	2.4	4.0	2.0	4.0	4.9	1.9	1.6	2.4	2.8	2.0
Or	39.9	39.5	40.2	37.3	38.6	33.7	39.8	34.2	31.9	39.3	40.5	40.5	36.9	38.3

Table C9 continued

Unit	**Fur J**	**Fur J**	**Fur J**	**Fur J**	**Fur J**	**Fur J**	**Fur J**	**Fur J**	**Fur J**	**Fur J**	**Fur J**	**Fur J**	**Fur J**
Sample	S018	S018	S018	S018	S018	S018	S018	S018	S018	S018	S018	S018	S018
No.	Fsp15	Fsp16	Fsp17	Fsp18	Fsp19	Fsp20	Fsp21	Fsp22	Fsp23	Fsp24	Fsp25	Fsp26	Fsp27
Notes	Pheno	Pheno	Pheno	Pheno	Pheno	Pheno	Pheno	Pheno	Pheno	Pheno	Pheno	Pheno	Pheno
SiO_2	65.64	65.73	65.19	65.72	65.94	65.04	64.99	66.07	66.49	66.41	65.91	66.38	66.32
TiO_2													
Al_2O_3	18.89	19.09	19.20	19.06	18.83	19.03	19.04	19.04	19.34	19.27	19.63	19.25	19.30
BaO	bdl	bdl	bdl	bdl	bdl	bdl	0.01	bdl	bdl	bdl	bdl	0.02	bdl
FeO	0.24	0.31	0.22	0.27	0.28	0.25	0.26	0.27	0.19	0.29	0.30	0.21	0.26
SrO	bdl	bdl	bdl	bdl	bdl	bdl	bdl	bdl	bdl	bdl	bdl	bdl	bdl
MgO													
CaO	0.40	0.44	0.63	0.36	0.29	0.42	0.42	0.43	0.36	0.37	0.88	0.39	0.49
Na_2O	6.64	6.73	6.95	6.61	6.62	6.68	6.83	6.88	6.33	6.66	6.87	6.76	6.89
K_2O	6.82	7.00	6.39	7.03	7.14	6.96	6.76	6.87	7.30	7.09	6.09	6.91	6.58
Total	98.63	99.30	98.58	99.04	99.10	98.38	98.31	99.56	100.01	100.09	99.68	99.93	99.83
Si	2.982	2.972	2.963	2.977	2.986	2.968	2.967	2.977	2.980	2.976	2.958	2.977	2.974
Ti													
Al	1.011	1.017	1.029	1.017	1.005	1.024	1.024	1.011	1.022	1.018	1.038	1.018	1.020
Ba							0.000					0.000	
Fe	0.009	0.012	0.008	0.010	0.011	0.009	0.010	0.010	0.007	0.011	0.011	0.008	0.010
Sr													
Mg													
Ca	0.020	0.021	0.030	0.017	0.014	0.021	0.020	0.021	0.017	0.018	0.042	0.019	0.023
Na	0.585	0.590	0.613	0.580	0.581	0.591	0.605	0.601	0.550	0.579	0.598	0.588	0.599
K	0.395	0.404	0.371	0.406	0.412	0.405	0.394	0.395	0.417	0.405	0.349	0.395	0.376
Sum	5.002	5.016	5.014	5.008	5.009	5.018	5.020	5.015	4.993	5.007	4.996	5.005	5.003
Ab	58.5	58.1	60.4	57.8	57.7	58.1	59.3	59.1	55.9	57.8	60.5	58.7	60.0
An	2.0	2.1	3.0	1.7	1.4	2.0	2.0	2.1	1.8	1.8	4.3	1.9	2.3
Or	39.5	39.8	36.6	40.5	40.9	39.8	38.6	38.8	42.4	40.5	35.3	39.5	37.7

Table C9 continued

Unit	**Fur J**	**Fur J**	**Fur J**	**Fur J**	**Fur J**	**Fur J**	**Fur J**	**Fur J**	**Fur J**	**Fur J**	**Fur J**	**Fur J**	**Fur J**
Sample	S018	S018	S018	S018	S018	S018	S018	S018	S018	S018	S018	S018	S018
No.	Fsp28	Fsp29	Fsp30	Fsp31	Fsp32	Fsp33	Fsp34	Fsp35	Fsp36	Fsp37	Fsp38	Fsp39	Fsp40
Notes	Pheno	Pheno	Pheno	Pheno	Pheno	Pheno	Pheno	Pheno	Pheno	Pheno	Pheno	Pheno	Pheno
SiO_2	66.26	66.37	66.34	66.37	65.24	66.53	65.96	65.95	66.19	66.10	66.04	66.21	66.57
TiO_2													
Al_2O_3	19.26	19.01	19.21	19.30	18.98	19.15	19.04	19.12	19.00	19.54	19.10	19.33	19.00
BaO	0.01	bdl	0.02	bdl	bdl	0.01	0.01	bdl	0.03	bdl	0.01	0.02	bdl
FeO	0.27	0.28	0.26	0.25	0.24	0.27	0.22	0.29	0.25	0.29	0.25	0.29	0.28
SrO	bdl	bdl	bdl	bdl	bdl	bdl	bdl	bdl	bdl	bdl	bdl	bdl	bdl
MgO													
CaO	0.41	0.35	0.42	0.38	0.49	0.37	0.42	0.35	0.38	0.75	0.39	0.62	0.35
Na_2O	6.61	6.61	6.65	6.58	7.15	6.94	6.46	6.36	6.19	6.85	6.41	6.40	6.49
K_2O	6.99	7.07	6.80	6.95	6.44	6.86	7.15	7.37	7.34	6.29	7.05	6.84	7.10
Total	99.81	99.69	99.70	99.83	98.54	100.14	99.25	99.44	99.38	99.82	99.24	99.71	99.79
Si	2.976	2.985	2.980	2.978	2.969	2.979	2.981	2.978	2.987	2.963	2.982	2.974	2.989
Ti													
Al	1.020	1.008	1.017	1.021	1.018	1.011	1.014	1.017	1.011	1.032	1.016	1.023	1.006
Ba	0.000		0.000			0.000	0.000		0.001		0.000	0.000	
Fe	0.010	0.011	0.010	0.009	0.009	0.010	0.008	0.011	0.009	0.011	0.009	0.011	0.011
Sr													
Mg													
Ca	0.020	0.017	0.020	0.018	0.024	0.018	0.020	0.017	0.018	0.036	0.019	0.030	0.017
Na	0.576	0.576	0.579	0.572	0.631	0.603	0.566	0.557	0.542	0.595	0.561	0.557	0.565
K	0.401	0.406	0.390	0.398	0.374	0.392	0.412	0.425	0.423	0.360	0.406	0.392	0.407
Sum	5.002	5.002	4.996	4.997	5.024	5.013	5.001	5.004	4.990	4.998	4.994	4.989	4.994
Ab	57.8	57.7	58.5	57.9	61.3	59.5	56.7	55.8	55.1	60.1	56.9	56.9	57.2
An	2.0	1.7	2.1	1.9	2.3	1.8	2.0	1.7	1.9	3.6	1.9	3.1	1.7
Or	40.2	40.6	39.4	40.2	36.4	38.7	41.3	42.5	43.0	36.3	41.2	40.0	41.2

Table C9 continued

Unit	Fur J dome	Fur J dome	Fur J dome	Fur J dome	Fur J dome	Fur J dome	Fur J dome	Fur J dome	Fur J dome	Fur J dome	Fur J dome	Fur J dome
Sample	SM7-1	SM7-1	SM7-1	SM7-1	SM7-1	SM7-1	SM7-1	SM7-1	SM7-1	SM7-1	SM7-1	SM7-1
No.	Fsp3	Fsp3	Fsp4	Fsp4	Fsp5	Fsp5	Fsp6	Fsp6	Fsp7	Fsp7	Fsp8	Fsp8
Notes	Core	Rim	Core	Rim	Core	Rim	Core	Rim	Core	Rim	Core	Rim
SiO_2	66.71	66.56	66.46	65.93	66.29	62.00	66.64	66.53	66.16	65.80	66.18	65.94
TiO_2												
Al_2O_3	19.39	19.40	19.89	19.33	20.03	19.08	19.47	19.93	19.82	20.31	19.81	20.27
BaO	bdl	0.03	0.02	0.01	0.02	0.04	0.01	bdl	0.03	0.08	0.04	bdl
FeO	0.26	0.59	0.25	0.31	0.21	0.30	0.25	0.32	0.20	0.30	0.23	0.31
SrO	bdl	bdl	bdl	0.01	bdl	0.04	bdl	bdl	bdl	bdl	bdl	0.06
MgO												
CaO	0.35	0.60	0.82	0.52	0.92	0.73	0.49	0.91	0.85	1.29	0.75	1.31
Na_2O	6.62	6.83	6.96	6.56	6.54	6.82	6.30	6.65	5.90	6.67	6.01	7.14
K_2O	7.21	6.72	6.32	7.20	7.00	6.58	7.79	6.64	7.84	6.33	7.71	5.71
Total	100.55	100.73	100.72	99.87	101.02	95.59	100.96	100.98	100.80	100.77	100.73	100.73
Si	2.976	2.967	2.954	2.966	2.947	2.924	2.970	2.953	2.954	2.930	2.956	2.931
Ti												
Al	1.020	1.019	1.042	1.025	1.049	1.061	1.023	1.043	1.043	1.066	1.043	1.062
Ba		0.001	0.000	0.000	0.000	0.001	0.000		0.001	0.001	0.001	
Fe	0.010	0.022	0.009	0.012	0.008	0.012	0.009	0.012	0.007	0.011	0.009	0.011
Sr				0.000		0.001						0.001
Mg												
Ca	0.017	0.028	0.039	0.025	0.044	0.037	0.023	0.043	0.041	0.062	0.036	0.062
Na	0.573	0.590	0.600	0.572	0.564	0.624	0.544	0.572	0.511	0.576	0.520	0.615
K	0.410	0.382	0.358	0.413	0.397	0.396	0.443	0.376	0.447	0.360	0.439	0.324
Sum	5.005	5.010	5.004	5.014	5.009	5.055	5.013	5.000	5.003	5.005	5.003	5.007
Ab	57.3	59.0	60.1	56.6	56.1	59.0	53.9	57.7	51.2	57.8	52.3	61.5
An	1.7	2.8	3.9	2.5	4.4	3.5	2.3	4.4	4.1	6.2	3.6	6.2
Or	41.0	38.2	35.9	40.9	39.5	37.5	43.8	37.9	44.7	36.1	44.1	32.3

Table C9 continued

Unit	**Fur J dome**	**Fur J dome**	**Fur J dome**	**Fur J dome**	**Fur J dome**	**Fur J dome**	**Fur J dome**	**Fur J dome**	**Fur J dome**	**Fur J dome**	**Fur J dome**
Sample	SM7-1	SM7-1	SM7-1	SM7-1	SM7-1	SM7-1	SM7-1	SM7-1	SM7-1	SM7-1	SM7-1
No.	Fsp9	Fsp9	Fsp10	Fsp10	Fsp11	Fsp11	Fsp12	Fsp12	18 / 1 .	18 / 2 .	18 / 3 .
Notes	Core	Rim	Core	Rim	Core	Rim	Core	Rim	Pheno	Pheno	Pheno
SiO_2	66.18	67.06	65.57	65.43	66.67	65.91	65.77	66.21	65.45	63.56	65.13
TiO_2									0.06	0.11	0.13
Al_2O_3	19.55	19.57	19.97	20.43	19.40	19.96	20.14	20.01	19.44	19.01	18.90
BaO	0.02	bdl	0.15	0.19	bdl	0.01	bdl	0.04	bdl	bdl	bdl
FeO	0.25	0.25	0.22	0.24	0.30	0.49	0.20	0.39	0.36	0.68	0.64
SrO	0.04	bdl	0.05	0.06	bdl	bdl	bdl	0.02	0.03	0.03	bdl
MgO									bdl	0.19	0.01
CaO	0.55	0.45	1.02	1.38	0.45	1.25	1.07	1.11	0.85	0.96	0.72
Na_2O	7.12	7.07	5.72	6.20	6.53	6.93	5.65	6.55	6.95	7.05	7.13
K_2O	6.50	6.77	8.04	7.03	7.15	5.94	7.80	6.73	6.61	5.48	6.40
Total	100.22	101.17	100.75	100.96	100.50	100.49	100.63	101.06	99.72	97.06	99.02
Si	2.961	2.971	2.939	2.920	2.975	2.940	2.941	2.943	2.949	2.937	2.958
Ti									0.002	0.004	0.004
Al	1.031	1.022	1.055	1.075	1.020	1.049	1.061	1.048	1.032	1.035	1.012
Ba	0.000		0.003	0.003		0.000		0.001			
Fe	0.009	0.009	0.008	0.009	0.011	0.018	0.007	0.015	0.014	0.026	0.024
Sr	0.001		0.001	0.001				0.001	0.001	0.001	
Mg										0.013	0.001
Ca	0.026	0.021	0.049	0.066	0.022	0.060	0.051	0.053	0.041	0.048	0.035
Na	0.618	0.607	0.497	0.536	0.565	0.599	0.490	0.564	0.607	0.631	0.628
K	0.371	0.383	0.460	0.400	0.407	0.338	0.445	0.382	0.380	0.323	0.371
Sum	5.018	5.013	5.012	5.011	5.001	5.004	4.996	5.006	5.026	5.018	5.032
Ab	60.9	60.1	49.4	53.5	56.9	60.1	49.7	56.5	59.1	63.0	60.7
An	2.6	2.1	4.9	6.6	2.2	6.0	5.2	5.3	4.0	4.7	3.4
Or	36.6	37.8	45.7	39.9	41.0	33.9	45.1	38.2	37.0	32.3	35.9

Table C9 continued

Unit	Fur J dome	Fur J dome	Fur J dome	Fur J dome	Fur J dome	Fur J dome	Fur J dome	Fur J dome	Fur J dome	Fur J dome	Fur J dome
Sample	SM7-1	SM7-1	SM7-1	SM7-1	SM7-1	SM7-1	SM7-1	SM7-1	SM7-1	SM7-1	SM7-1
No.	18 / 4 .	18 / 5 .	18 / 6 .	18 / 7 .	18 / 8 .	18 / 9 .	18 / 10 .	19 / 1 .	19 / 2 .	19 / 3 .	19 / 4 .
Notes	Pheno	Pheno	Pheno	Pheno	Pheno	Pheno	Pheno	Pheno	Pheno	Pheno	Pheno
SiO_2	65.04	64.82	64.74	65.59	61.39	65.28	65.03	65.66	65.77	65.87	63.39
TiO_2	0.11	0.10	0.08	0.09	0.12	0.08	0.12	0.10	0.05	0.06	0.08
Al_2O_3	19.26	19.36	19.21	18.91	18.93	19.46	18.73	19.24	19.18	19.16	18.87
BaO	bdl	bdl	bdl	0.02	bdl	bdl	0.01	0.02	0.01	0.01	0.03
FeO	0.44	0.41	0.40	0.40	0.91	0.47	0.43	0.43	0.22	0.21	0.26
SrO	bdl	0.01	bdl	0.04	0.02	bdl	bdl	bdl	bdl	bdl	0.01
MgO	bdl	0.01	bdl	0.01	0.14	0.01	bdl	bdl	bdl	bdl	bdl
CaO	0.86	1.04	0.99	0.49	1.38	1.02	0.46	0.84	0.63	0.51	0.48
Na_2O	7.42	7.07	6.88	7.17	7.21	8.00	6.54	7.04	7.06	7.04	6.19
K_2O	5.85	6.25	6.42	6.57	3.85	5.51	7.51	6.53	6.56	6.90	7.17
Total	98.96	99.05	98.72	99.26	93.95	99.80	98.80	99.84	99.46	99.74	96.48
Si	2.948	2.941	2.948	2.968	2.918	2.937	2.968	2.956	2.966	2.966	2.955
Ti	0.004	0.004	0.003	0.003	0.004	0.003	0.004	0.003	0.002	0.002	0.003
Al	1.029	1.035	1.031	1.008	1.060	1.032	1.007	1.021	1.019	1.017	1.037
Ba				0.000			0.000	0.000	0.000	0.000	0.000
Fe	0.017	0.015	0.015	0.015	0.036	0.018	0.016	0.016	0.008	0.008	0.010
Sr		0.000		0.001	0.001						0.000
Mg		0.001		0.000	0.010	0.000					
Ca	0.042	0.051	0.048	0.024	0.070	0.049	0.022	0.041	0.030	0.024	0.024
Na	0.652	0.622	0.607	0.629	0.664	0.697	0.578	0.614	0.617	0.615	0.560
K	0.338	0.362	0.373	0.379	0.233	0.316	0.437	0.375	0.377	0.397	0.427
Sum	5.029	5.030	5.024	5.029	4.997	5.052	5.033	5.025	5.020	5.029	5.016
Ab	63.2	60.1	59.0	60.9	68.6	65.6	55.7	59.7	60.2	59.4	55.4
An	4.0	4.9	4.7	2.3	7.3	4.6	2.1	3.9	3.0	2.4	2.4
Or	32.8	35.0	36.3	36.8	24.1	29.8	42.1	36.4	36.8	38.3	42.2

Table C9 continued

Unit	Fur J dome	Fur J dome	Fur J dome	Fur J dome	Fur J dome	Fur J dome	Fur J dome	Fur J dome	Fur J dome	Fur J dome	Fur J dome
Sample	SM7-1	SM7-1	SM7-1	SM7-1	SM7-1	SM7-1	SM7-1	SM7-1	SM7-1	SM7-1	SM7-1
No.	19 / 5 .	19 / 6 .	19 / 7 .	19 / 8 .	19 / 9 .	19 / 10 .	20 / 1 .	20 / 2 .	20 / 3 .	20 / 4 .	20 / 5 .
Notes	Pheno	Pheno	Pheno	Pheno	Pheno	Pheno	Pheno	Pheno	Pheno	Pheno	Pheno
SiO_2	65.59	65.66	65.37	64.65	65.04	64.81	64.67	65.23	65.25	65.31	65.50
TiO_2	0.10	0.06	0.05	0.11	0.04	0.07	0.11	0.03	0.08	0.08	0.05
Al_2O_3	18.88	19.05	18.98	19.27	18.99	18.90	19.00	19.16	18.93	19.09	19.00
BaO	0.01	bdl	bdl	bdl	bdl	bdl	bdl	bdl	bdl	bdl	0.01
FeO	0.28	0.25	0.22	0.30	0.24	0.26	0.42	0.26	0.31	0.25	0.26
SrO	0.02	0.04	0.05	0.02	0.01	0.03	bdl	0.05	0.02	bdl	0.04
MgO	bdl	bdl	bdl	0.01	bdl	bdl	0.01	bdl	0.01	bdl	bdl
CaO	0.41	0.55	0.63	0.62	0.53	0.66	0.82	0.61	0.62	0.65	0.51
Na_2O	6.70	6.89	6.80	6.79	6.81	6.98	6.90	6.92	6.95	6.99	7.04
K_2O	7.14	6.94	6.87	6.76	6.82	6.67	6.58	6.68	6.51	6.64	6.70
Total	99.12	99.43	98.95	98.50	98.46	98.37	98.48	98.93	98.66	99.00	99.10
Si	2.974	2.968	2.968	2.950	2.966	2.961	2.953	2.961	2.967	2.962	2.968
Ti	0.003	0.002	0.002	0.004	0.001	0.002	0.004	0.001	0.003	0.003	0.002
Al	1.009	1.015	1.016	1.036	1.021	1.018	1.022	1.025	1.015	1.021	1.015
Ba	0.000										0.000
Fe	0.011	0.010	0.009	0.012	0.009	0.010	0.016	0.010	0.012	0.009	0.010
Sr	0.000	0.001	0.001	0.001	0.000	0.001		0.001	0.000		0.001
Mg				0.001			0.001		0.000		
Ca	0.020	0.027	0.031	0.030	0.026	0.032	0.040	0.030	0.030	0.032	0.025
Na	0.589	0.604	0.598	0.600	0.602	0.618	0.611	0.609	0.613	0.614	0.618
K	0.413	0.400	0.398	0.393	0.397	0.389	0.383	0.387	0.378	0.384	0.387
Sum	5.019	5.025	5.021	5.026	5.022	5.031	5.029	5.023	5.018	5.025	5.026
Ab	57.6	58.6	58.3	58.6	58.8	59.5	59.1	59.4	60.1	59.6	60.0
An	1.9	2.6	3.0	2.9	2.5	3.1	3.9	2.9	3.0	3.1	2.4
Or	40.4	38.8	38.7	38.4	38.7	37.4	37.0	37.7	37.0	37.3	37.6

Table C9 continued

Unit	Fur J dome	Fur J dome	Fur J dome	Fur J dome	Fur J dome	Fur J dome	Fur J dome	Fur J dome	Fur J dome	Fur J dome	Fur J dome
Sample	SM7-1	SM7-1	SM7-1	SM7-1	SM7-1	SM7-1	SM7-1	SM7-1	SM7-1	SM7-1	SM7-1
No.	20 / 7 .	20 / 10 .	21 / 1 .	21 / 2 .	21 / 3 .	21 / 4 .	21 / 5 .	21 / 7 .	21 / 8 .	21 / 9 .	21 / 10 .
Notes	Pheno	Pheno	Pheno	Pheno	Pheno	Pheno	Pheno	Pheno	Pheno	Pheno	Pheno
SiO_2	64.74	65.36	64.73	64.36	64.60	63.63	64.41	64.59	65.02	64.90	65.17
TiO_2	0.07	0.07	0.05	0.04	0.06	0.05	0.05	0.06	0.05	0.06	0.06
Al_2O_3	18.89	19.14	19.08	19.01	19.17	18.92	19.26	19.10	19.08	19.09	19.31
BaO	0.01	bdl	bdl	0.02	0.06	bdl	0.02	0.01	bdl	0.02	bdl
FeO	0.23	0.25	0.21	0.22	0.21	0.19	0.22	0.22	0.19	0.23	0.21
SrO	bdl	0.01	0.04	0.03	0.01	0.03	0.01	bdl	0.05	0.03	0.01
MgO	bdl	bdl	bdl	bdl	bdl	bdl	bdl	bdl	bdl	bdl	0.01
CaO	0.51	0.62	0.76	0.81	0.77	0.83	0.85	0.73	0.74	0.75	0.83
Na_2O	6.78	7.03	6.40	6.48	6.34	6.19	6.45	6.29	6.24	6.24	6.41
K_2O	6.97	6.64	7.31	7.10	7.49	7.31	7.05	7.55	7.55	7.51	7.33
Total	98.20	99.09	98.56	98.07	98.69	97.15	98.32	98.55	98.89	98.82	99.32
Si	2.964	2.961	2.957	2.955	2.951	2.951	2.948	2.954	2.961	2.958	2.953
Ti	0.002	0.002	0.002	0.001	0.002	0.002	0.002	0.002	0.002	0.002	0.002
Al	1.019	1.022	1.027	1.028	1.032	1.034	1.039	1.030	1.024	1.026	1.031
Ba	0.000			0.000	0.001		0.000	0.000		0.000	
Fe	0.009	0.009	0.008	0.008	0.008	0.007	0.009	0.009	0.007	0.009	0.008
Sr		0.000	0.001	0.001	0.000	0.001	0.000		0.001	0.001	0.000
Mg											0.000
Ca	0.025	0.030	0.037	0.040	0.038	0.041	0.042	0.036	0.036	0.037	0.040
Na	0.601	0.617	0.567	0.577	0.561	0.556	0.572	0.558	0.551	0.552	0.563
K	0.407	0.384	0.426	0.416	0.436	0.433	0.412	0.440	0.438	0.437	0.424
Sum	5.028	5.026	5.024	5.026	5.030	5.025	5.023	5.028	5.020	5.021	5.022
Ab	58.2	59.8	55.0	55.9	54.2	54.0	55.8	53.9	53.7	53.8	54.8
An	2.4	2.9	3.6	3.8	3.6	4.0	4.1	3.5	3.5	3.6	3.9
Or	39.4	37.2	41.4	40.3	42.1	42.0	40.1	42.6	42.8	42.6	41.3

Table C9 continued

Unit	Fur J dome	Fur J dome	Fur J dome	Fur J dome	Fur J dome	Fur J dome	Fur J dome	Fur J dome	Fur J dome	Fur J dome	Fur J dome
Sample	SM7-1	SM7-1	SM7-1	SM7-1	SM7-1	SM7-1	SM7-1	SM7-1	SM7-1	SM7-1	SM7-1
No.	22 / 1 .	23 / 1 .	24 / 1 .	25 / 1 .	26 / 1 .	27 / 1 .	28 / 1 .	29 / 1 .	30 / 1 .	31 / 1 .	32 / 1 .
Notes	Pheno	Pheno	Pheno	Pheno	Pheno	Pheno	Mph	Mph	Mph	Mph	Mph
SiO_2	64.02	65.79	64.36	65.00	65.15	65.46	64.26	63.94	64.84	65.51	64.44
TiO_2	0.03	0.05	0.07	0.07	0.03	0.06	0.11	0.15	0.08	0.15	0.12
Al_2O_3	18.65	18.81	19.14	19.34	18.83	18.81	19.29	19.50	18.88	19.02	19.79
BaO	bdl	0.02	0.02	bdl	bdl	bdl	bdl	0.02	bdl	0.02	0.09
FeO	0.28	0.26	0.20	0.20	0.24	0.30	0.58	0.64	0.44	0.59	0.37
SrO	0.04	0.03	0.01	0.01	0.03	bdl	0.03	bdl	bdl	bdl	0.03
MgO	bdl	bdl	0.01	bdl	bdl	bdl	0.01	0.01	0.01	bdl	bdl
CaO	0.38	0.36	0.86	0.83	0.42	0.47	1.14	1.41	0.52	0.68	1.41
Na_2O	6.89	6.86	6.04	5.99	6.94	7.16	7.08	7.72	7.33	7.41	7.81
K_2O	6.88	7.11	7.77	7.84	6.86	6.56	5.77	4.87	6.18	5.98	4.76
Total	97.18	99.29	98.48	99.27	98.48	98.83	98.25	98.25	98.24	99.34	98.81
Si	2.964	2.978	2.949	2.952	2.972	2.973	2.937	2.919	2.962	2.960	2.921
Ti	0.001	0.002	0.002	0.002	0.001	0.002	0.004	0.005	0.003	0.005	0.004
Al	1.017	1.004	1.034	1.035	1.012	1.007	1.039	1.049	1.017	1.013	1.057
Ba		0.000	0.000					0.000		0.000	0.002
Fe	0.011	0.010	0.008	0.008	0.009	0.012	0.022	0.025	0.017	0.022	0.014
Sr	0.001	0.001	0.000	0.000	0.001		0.001				0.001
Mg			0.001				0.000	0.001	0.000		
Ca	0.019	0.017	0.042	0.041	0.020	0.023	0.056	0.069	0.025	0.033	0.068
Na	0.619	0.602	0.536	0.528	0.613	0.630	0.627	0.683	0.649	0.649	0.686
K	0.406	0.411	0.454	0.454	0.399	0.380	0.336	0.284	0.360	0.345	0.275
Sum	5.039	5.025	5.027	5.019	5.028	5.027	5.022	5.035	5.032	5.026	5.028
Ab	59.3	58.4	51.9	51.6	59.4	61.0	61.5	66.0	62.7	63.2	66.7
An	1.8	1.7	4.1	4.0	2.0	2.2	5.5	6.7	2.5	3.2	6.6
Or	38.9	39.9	44.0	44.4	38.6	36.8	33.0	27.4	34.8	33.6	26.7

Table C9 continued

Unit	**Fur I**	**Fur I**	**Fur I**	**Fur I**	**Fur I**	**Fur I**	**Fur I**	**Fur I**	**Fur I**	**Fur I**	**Fur I**	**Fur I**	**Fur I**	**Fur I**
Sample	S038	S038	S038	S038	S038	S038	S038	S038	S038	S038	S038	S038	S038	S038
No.	Fsp1	Fsp2	Fsp3	Fsp4	Fsp5	Fsp6	Fsp7	Fsp8	Fsp9	Fsp10	Fsp11	Fsp12	Fsp13	Fsp14
Notes	Pheno	Pheno	Pheno	Pheno	Pheno	Pheno	Pheno	Pheno	Pheno	Pheno	Pheno	Pheno	Pheno	Pheno
SiO_2	65.00	65.01	50.07	64.78	64.67	64.59	65.05	64.95	65.80	65.55	66.21	65.77	66.22	65.82
TiO_2														
Al_2O_3	18.68	18.67	0.83	18.61	18.49	18.70	18.50	18.62	18.76	19.11	19.10	18.87	19.26	18.84
BaO	0.01	bdl	bdl	bdl	bdl	0.01	0.01	0.03	bdl	bdl	0.01	bdl	bdl	0.01
FeO	0.24	0.29	14.18	0.27	0.23	0.26	0.34	0.30	0.25	0.28	0.27	0.28	0.22	0.31
SrO	bdl	bdl	bdl	bdl	bdl	bdl	bdl	bdl	bdl	bdl	bdl	bdl	bdl	bdl
MgO														
CaO	0.55	0.42	20.37	0.36	0.37	0.40	0.31	0.30	0.27	0.56	0.36	0.41	0.56	0.38
Na_2O	7.03	7.05	1.36	6.92	7.06	7.51	7.44	7.19	6.99	7.13	6.87	7.20	6.98	6.96
K_2O	6.88	6.87	0.00	6.94	6.89	6.59	6.81	6.95	7.03	6.56	7.05	6.84	7.04	7.01
Total	98.39	98.31	86.81	97.88	97.71	98.07	98.45	98.35	99.10	99.20	99.88	99.37	100.28	99.33
Si	2.971	2.973	2.932	2.975	2.976	2.963	2.974	2.972	2.982	2.966	2.976	2.974	2.967	2.978
Ti														
Al	1.006	1.006	0.057	1.007	1.003	1.011	0.997	1.004	1.002	1.019	1.012	1.006	1.017	1.005
Ba	0.000					0.000	0.000	0.001			0.000			0.000
Fe	0.009	0.011	0.694	0.010	0.009	0.010	0.013	0.012	0.009	0.011	0.010	0.010	0.008	0.012
Sr														
Mg														
Ca	0.027	0.020	1.278	0.018	0.018	0.020	0.015	0.015	0.013	0.027	0.017	0.020	0.027	0.018
Na	0.623	0.625	0.154	0.616	0.630	0.668	0.660	0.638	0.614	0.625	0.599	0.631	0.606	0.611
K	0.401	0.401	0.000	0.407	0.404	0.386	0.397	0.406	0.406	0.379	0.404	0.395	0.402	0.405
Sum	5.038	5.037	5.116	5.033	5.040	5.058	5.056	5.047	5.027	5.027	5.019	5.036	5.029	5.028
Ab	59.3	59.7	10.8	59.2	59.8	62.2	61.5	60.3	59.4	60.6	58.7	60.4	58.5	59.1
An	2.6	2.0	89.2	1.7	1.7	1.8	1.4	1.4	1.3	2.6	1.7	1.9	2.6	1.8
Or	38.2	38.3	0.0	39.1	38.4	35.9	37.1	38.3	39.3	36.7	39.6	37.7	38.9	39.2

Table C9 continued

Unit	**Fur I**	**Fur I**	**Fur I**	**Fur I**	**Fur I**	**Fur I**	**Fur I**	**Fur I**	**Fur I**	**Fur I**	**Fur I**	**Fur I**	**Fur I**
Sample	S038	S038	S038	S038	S038	S038	S038	S038	S038	S038	S038	S038	S038
No.	Fsp15	Fsp16	Fsp17	Fsp18	Fsp19	Fsp20	Fsp21	Fsp22	Fsp23	Fsp24	Fsp25	Fsp26	Fsp27
Notes	Pheno	Pheno	Pheno	Pheno	Pheno	Pheno	Pheno	Pheno	Pheno	Pheno	Pheno	Pheno	Pheno
SiO_2	65.82	65.79	66.12	65.47	66.37	36.50	65.69	64.59	66.12	65.96	66.01	64.92	66.02
TiO_2													
Al_2O_3	18.81	18.86	18.88	19.38	18.96	6.91	19.73	20.11	18.98	19.06	18.85	19.51	18.96
BaO	0.01	0.03	bdl	0.01	0.02	bdl	0.03	0.05	bdl	bdl	bdl	bdl	bdl
FeO	0.25	0.24	0.26	0.21	0.28	0.00	0.20	0.21	0.25	0.26	0.27	0.23	0.24
SrO	bdl	bdl	bdl	bdl	bdl	bdl	bdl	bdl	bdl	bdl	bdl	bdl	bdl
MgO													
CaO	0.37	0.38	0.32	0.80	0.39	0.16	0.91	1.47	0.32	0.35	0.23	0.91	0.28
Na_2O	7.36	6.56	6.57	6.23	7.00	5.07	6.30	6.40	7.00	6.96	6.81	6.18	6.82
K_2O	6.70	7.31	7.55	7.74	6.98	2.33	7.42	6.50	7.03	6.82	7.30	7.55	7.18
Total	99.32	99.17	99.70	99.85	100.00	50.97	100.28	99.32	99.70	99.41	99.47	99.29	99.50
Si	2.976	2.981	2.982	2.955	2.980	3.181	2.948	2.922	2.978	2.976	2.982	2.946	2.980
Ti													
Al	1.002	1.007	1.004	1.031	1.003	0.710	1.044	1.072	1.008	1.014	1.004	1.043	1.009
Ba	0.000	0.001		0.000	0.000		0.001	0.001					
Fe	0.009	0.009	0.010	0.008	0.010	0.000	0.007	0.008	0.010	0.010	0.010	0.009	0.009
Sr													
Mg													
Ca	0.018	0.018	0.015	0.039	0.019	0.015	0.044	0.071	0.015	0.017	0.011	0.044	0.013
Na	0.645	0.576	0.575	0.545	0.609	0.857	0.548	0.561	0.611	0.609	0.597	0.544	0.597
K	0.387	0.423	0.434	0.446	0.400	0.259	0.425	0.375	0.404	0.393	0.421	0.437	0.413
Sum	5.038	5.015	5.020	5.025	5.023	5.022	5.017	5.010	5.026	5.018	5.024	5.023	5.021
Ab	61.5	56.7	56.1	52.9	59.3	75.7	53.9	55.7	59.3	59.8	58.0	53.1	58.3
An	1.7	1.8	1.5	3.8	1.8	1.4	4.3	7.1	1.5	1.7	1.1	4.3	1.3
Or	36.8	41.5	42.4	43.3	38.9	22.9	41.8	37.2	39.2	38.5	40.9	42.6	40.4

Table C9 continued

Unit	**Fur I**	**Fur I**	**Fur I**	**Fur I**	**Fur I**	**Fur I**	**Fur I**	**Fur I**	**Fur I**	**Fur I**	**Fur I**	**Fur I**	**Fur I**	**Fur I**
Sample	S038	S038	S038	S038	S038	S038	S038	S038	S038	S038	S038	S038	S038	S038
No.	Fsp28	Fsp29	Fsp30	Fsp31	Fsp32	Fsp33	Fsp34	Fsp35	Fsp36	Fsp37	Fsp38	Fsp39	Fsp40	Fsp41
Notes	Pheno	Pheno	Pheno	Pheno	Pheno	Pheno	Pheno	Pheno	Pheno	Pheno	Pheno	Pheno	Pheno	Pheno
SiO_2	64.83	65.88	65.99	65.11	66.17	66.10	66.71	66.92	66.19	66.17	66.15	66.39	66.00	65.86
TiO_2														
Al_2O_3	18.98	19.30	19.32	19.58	19.04	19.08	19.12	19.40	19.15	19.35	19.84	19.06	19.92	19.73
BaO	0.02	0.01	0.02	0.02	bdl	bdl	0.01	0.03	bdl	bdl	0.02	0.02	0.01	bdl
FeO	0.49	0.24	0.43	0.23	0.29	0.31	0.27	0.25	0.24	0.27	0.20	0.27	0.22	0.20
SrO	bdl	bdl	bdl	bdl	bdl	bdl	bdl	bdl	bdl	bdl	bdl	bdl	bdl	bdl
MgO														
CaO	0.67	0.55	0.38	0.98	0.26	0.41	0.38	0.51	0.43	0.63	0.89	0.28	0.84	0.84
Na_2O	5.61	6.74	6.95	6.28	7.18	6.93	6.78	6.90	6.93	7.03	6.15	6.78	6.87	6.79
K_2O	8.50	6.96	6.87	7.20	6.65	7.09	7.02	6.59	7.01	6.62	7.59	7.22	6.38	6.47
Total	99.10	99.68	99.96	99.40	99.59	99.92	100.29	100.60	99.94	100.07	100.84	100.02	100.23	99.89
Si	2.960	2.967	2.965	2.947	2.978	2.973	2.983	2.978	2.973	2.966	2.951	2.981	2.949	2.954
Ti														
Al	1.021	1.024	1.023	1.044	1.010	1.011	1.008	1.017	1.014	1.022	1.043	1.009	1.049	1.043
Ba	0.000	0.000	0.000	0.000			0.000	0.001			0.000	0.000	0.000	
Fe	0.019	0.009	0.016	0.009	0.011	0.012	0.010	0.009	0.009	0.010	0.007	0.010	0.008	0.008
Sr														
Mg														
Ca	0.033	0.027	0.018	0.047	0.013	0.020	0.018	0.024	0.021	0.030	0.043	0.013	0.040	0.040
Na	0.497	0.588	0.606	0.551	0.627	0.604	0.588	0.595	0.604	0.611	0.532	0.590	0.595	0.590
K	0.495	0.400	0.394	0.416	0.382	0.407	0.400	0.374	0.402	0.379	0.432	0.414	0.364	0.370
Sum	5.025	5.015	5.023	5.014	5.021	5.027	5.007	4.998	5.022	5.018	5.009	5.017	5.006	5.005
Ab	48.5	58.0	59.5	54.3	61.4	58.6	58.4	59.9	58.8	59.9	52.9	58.0	59.6	59.0
An	3.2	2.6	1.8	4.7	1.2	1.9	1.8	2.4	2.0	2.9	4.2	1.3	4.0	4.0
Or	48.3	39.4	38.7	41.0	37.4	39.5	39.8	37.7	39.2	37.1	42.9	40.7	36.4	37.0

Table C9 continued

Unit	**Fur I dome**	**Fur I dome**	**Fur I dome**	**Fur I dome**	**Fur I dome**	**Fur I dome**	**Fur I dome**	**Fur I dome**	**Fur I dome**	**Fur I dome**	**Fur I dome**	**Fur I dome**
Sample	SM5-1	SM5-1	SM5-1	SM5-1	SM5-1	SM5-1	SM5-1	SM5-1	SM5-1	SM5-1	SM5-1	SM5-1
No.	Fsp13	Fsp13	Fsp14	Fsp14	Fsp15	Fsp15	Fsp19	Fsp19	Fsp20	Fsp20	Fsp21	Fsp21
Notes	Core	Rim	Core	Rim	Core	Rim	Core	Rim	Core	Rim	Core	Rim
SiO_2	65.50	66.99	67.16	67.32	65.93	66.20	67.32	67.39	67.01	66.80	66.47	64.48
TiO_2												
Al_2O_3	19.62	19.64	19.54	19.64	19.77	19.44	19.43	19.19	19.50	19.24	19.59	18.65
BaO	0.01	bdl	0.01	bdl	0.04	bdl	0.02	bdl	0.05	0.03	bdl	0.06
FeO	0.26	0.33	0.30	0.26	0.20	0.47	0.28	0.48	0.26	0.52	0.23	0.48
SrO	0.02	bdl	0.02	bdl	bdl	bdl	0.01	bdl	bdl	bdl	0.02	bdl
MgO												
CaO	0.59	0.51	0.43	0.37	0.64	0.61	0.34	0.18	0.35	0.40	0.62	0.15
Na_2O	7.13	7.53	7.41	7.40	6.97	7.40	6.88	7.26	7.13	7.47	6.75	7.52
K_2O	6.38	5.85	6.37	5.92	6.51	6.07	7.00	6.45	6.88	6.11	7.11	6.02
Total	99.51	100.85	101.25	100.91	100.06	100.19	101.27	100.95	101.18	100.57	100.79	97.36
Si	2.952	2.968	2.971	2.977	2.953	2.961	2.980	2.988	2.971	2.975	2.962	2.971
Ti												
Al	1.042	1.026	1.019	1.023	1.044	1.025	1.014	1.003	1.019	1.010	1.029	1.013
Ba	0.000		0.000		0.001		0.000		0.001	0.000		0.001
Fe	0.010	0.012	0.011	0.010	0.007	0.018	0.010	0.018	0.010	0.020	0.009	0.019
Sr	0.001		0.001				0.000				0.001	
Mg												
Ca	0.028	0.024	0.020	0.018	0.031	0.029	0.016	0.009	0.017	0.019	0.030	0.007
Na	0.623	0.647	0.636	0.634	0.605	0.642	0.590	0.624	0.613	0.645	0.583	0.672
K	0.367	0.331	0.359	0.334	0.372	0.346	0.395	0.365	0.389	0.347	0.404	0.354
Sum	5.022	5.008	5.017	4.996	5.013	5.021	5.006	5.006	5.020	5.016	5.017	5.036
Ab	61.2	64.6	62.6	64.3	60.0	63.1	58.9	62.6	60.2	63.8	57.3	65.0
An	2.8	2.4	2.0	1.8	3.1	2.9	1.6	0.9	1.6	1.9	2.9	0.7
Or	36.0	33.0	35.4	33.9	36.9	34.1	39.5	36.6	38.2	34.3	39.7	34.3

Table C9 continued

Unit	Fur I dome	Fur I dome	Fur I dome	Fur I dome	Fur I dome	Fur I dome	Fur I dome	Fur I dome	Fur I dome	Fur I dome	Fur I dome
Sample	SM5-1	SM5-1	SM5-1	SM5-1	SM5-1	SM5-1	SM5-1	SM5-1	SM5-1	SM5-1	SM5-1
No.	Fsp22	Fsp22	1 / 1 .	1 / 2 .	1 / 3 .	1 / 4 .	1 / 5 .	1 / 6 .	1 / 7 .	1 / 8 .	1 / 9 .
Notes	Core	Rim	Pheno	Pheno	Pheno	Pheno	Pheno	Pheno	Pheno	Pheno	Pheno
SiO_2	66.80	66.95	66.42	66.27	66.41	66.06	66.09	66.08	65.08	64.15	65.67
TiO_2			0.06	0.04	0.05	0.06	0.03	0.03	0.04	0.01	0.06
Al_2O_3	19.62	19.36	18.81	18.96	19.09	19.04	18.94	18.93	18.86	18.64	18.84
BaO	0.02	bdl	bdl	bdl	bdl	bdl	bdl	bdl	0.03	0.02	0.01
FeO	0.29	0.25	0.51	0.35	0.28	0.28	0.31	0.29	0.30	0.28	0.29
SrO	bdl	0.01	0.04	0.04	0.04	bdl	bdl	bdl	0.04	0.03	0.07
MgO			bdl	bdl	bdl	bdl	bdl	bdl	bdl	bdl	0.01
CaO	0.45	0.27	0.19	0.38	0.35	0.37	0.36	0.33	0.36	0.38	0.40
Na_2O	6.89	6.57	7.42	7.20	7.27	7.14	7.22	7.15	6.96	6.97	7.30
K_2O	6.79	7.13	6.65	6.66	6.51	6.53	6.65	6.83	6.64	6.40	6.37
Total	100.86	100.54	100.09	99.87	99.98	99.46	99.57	99.60	98.29	96.88	99.02
Si	2.968	2.983	2.981	2.978	2.977	2.976	2.977	2.978	2.972	2.970	2.975
Ti			0.002	0.001	0.002	0.002	0.001	0.001	0.001	0.000	0.002
Al	1.028	1.017	0.995	1.004	1.009	1.011	1.006	1.005	1.015	1.017	1.006
Ba	0.000								0.000	0.000	0.000
Fe	0.011	0.009	0.019	0.013	0.011	0.011	0.012	0.011	0.011	0.011	0.011
Sr		0.000	0.001	0.001	0.001				0.001	0.001	0.002
Mg											0.000
Ca	0.021	0.013	0.009	0.018	0.017	0.018	0.018	0.016	0.018	0.019	0.020
Na	0.594	0.568	0.645	0.627	0.631	0.624	0.630	0.625	0.616	0.625	0.641
K	0.385	0.405	0.380	0.382	0.372	0.375	0.382	0.393	0.387	0.378	0.368
Sum	5.007	4.995	5.033	5.023	5.019	5.016	5.025	5.027	5.021	5.022	5.025
Ab	59.4	57.6	62.4	61.0	61.9	61.3	61.2	60.5	60.4	61.2	62.3
An	2.1	1.3	0.9	1.8	1.6	1.8	1.7	1.5	1.7	1.9	1.9
Or	38.5	41.1	36.8	37.2	36.5	36.9	37.1	38.0	37.9	37.0	35.8

Table C9 continued

Unit	Fur I dome	Fur I dome	Fur I dome	Fur I dome	Fur I dome	Fur I dome	Fur I dome	Fur I dome	Fur I dome	Fur I dome	Fur I dome
Sample	SM5-1	SM5-1	SM5-1	SM5-1	SM5-1	SM5-1	SM5-1	SM5-1	SM5-1	SM5-1	SM5-1
No.	1 / 10 .	1 / 12 .	1 / 13 .	1 / 14 .	1 / 15 .	1 / 16 .	1 / 17 .	1 / 18 .	1 / 19 .	1 / 20 .	1 / 21 .
Notes	Pheno	Pheno	Pheno	Pheno	Pheno	Pheno	Pheno	Pheno	Pheno	Pheno	Pheno
SiO_2	66.10	65.76	65.78	65.53	65.56	65.74	65.69	65.60	66.00	65.97	65.65
TiO_2	0.05	0.04	0.03	0.04	0.05	0.06	0.04	0.06	0.05	0.04	0.04
Al_2O_3	19.07	18.73	18.85	18.89	18.69	18.86	18.87	18.69	18.85	18.95	18.87
BaO	bdl	bdl	bdl	0.01	bdl	bdl	0.02	0.01	bdl	0.01	0.01
FeO	0.29	0.29	0.33	0.34	0.39	0.43	0.31	0.33	0.30	0.36	0.38
SrO	bdl	0.01	0.04	0.04	0.04	0.02	0.01	0.06	0.01	0.04	0.01
MgO	bdl	bdl	bdl	bdl	bdl	bdl	bdl	bdl	0.01	bdl	bdl
CaO	0.42	0.36	0.36	0.35	0.35	0.35	0.32	0.36	0.29	0.37	0.43
Na_2O	7.35	7.17	7.29	7.21	7.32	7.44	7.28	7.24	7.28	7.51	7.61
K_2O	6.41	6.63	6.58	6.63	6.71	6.44	6.48	6.56	6.64	6.27	6.00
Total	99.67	98.97	99.23	99.04	99.10	99.31	99.00	98.90	99.42	99.51	99.00
Si	2.973	2.981	2.975	2.971	2.975	2.972	2.976	2.978	2.979	2.973	2.972
Ti	0.002	0.001	0.001	0.001	0.002	0.002	0.001	0.002	0.002	0.001	0.001
Al	1.011	1.001	1.005	1.010	0.999	1.005	1.008	1.000	1.003	1.007	1.007
Ba				0.000			0.000	0.000		0.000	0.000
Fe	0.011	0.011	0.012	0.013	0.015	0.016	0.012	0.013	0.011	0.014	0.014
Sr		0.000	0.001	0.001	0.001	0.000	0.000	0.002	0.000	0.001	0.000
Mg									0.000		
Ca	0.020	0.018	0.018	0.017	0.017	0.017	0.015	0.017	0.014	0.018	0.021
Na	0.641	0.630	0.639	0.634	0.644	0.652	0.640	0.637	0.637	0.656	0.668
K	0.367	0.383	0.380	0.383	0.388	0.371	0.375	0.380	0.382	0.361	0.347
Sum	5.024	5.024	5.030	5.031	5.040	5.035	5.026	5.028	5.028	5.030	5.031
Ab	62.3	61.1	61.7	61.3	61.4	62.7	62.1	61.6	61.6	63.4	64.5
An	1.9	1.7	1.7	1.7	1.6	1.6	1.5	1.7	1.4	1.7	2.0
Or	35.7	37.2	36.6	37.0	37.0	35.7	36.4	36.7	37.0	34.9	33.5

Table C9 continued

Unit	Fur I dome	Fur I dome	Fur I dome	Fur I dome	Fur I dome	Fur I dome	Fur I dome	Fur I dome	Fur I dome	Fur I dome	Fur I dome
Sample	SM5-1	SM5-1	SM5-1	SM5-1	SM5-1	SM5-1	SM5-1	SM5-1	SM5-1	SM5-1	SM5-1
No.	1 / 22 .	1 / 23 .	1 / 24 .	1 / 25 .	1 / 26 .	1 / 27 .	1 / 28 .	1 / 29 .	1 / 30 .	2 / 1 .	2 / 2 .
Notes	Pheno	Pheno	Pheno	Pheno	Pheno	Pheno	Pheno	Pheno	Pheno	Pheno	Pheno
SiO_2	65.73	65.55	65.60	65.26	65.47	65.65	65.46	65.42	65.73	65.45	65.81
TiO_2	0.06	0.05	0.04	0.04	0.07	0.04	0.06	0.09	0.05	0.07	0.03
Al_2O_3	18.75	18.77	18.72	18.68	18.70	18.69	18.71	18.45	18.42	19.02	18.70
BaO	bdl	bdl	bdl	bdl	bdl	0.01	0.01	0.01	bdl	bdl	bdl
FeO	0.34	0.31	0.29	0.31	0.29	0.28	0.35	0.65	0.48	0.27	0.26
SrO	0.03	0.02	bdl	0.03	0.04	0.03	0.01	0.01	0.02	0.03	bdl
MgO	bdl	bdl	bdl	bdl	bdl	0.01	bdl	bdl	bdl	bdl	bdl
CaO	0.29	0.30	0.29	0.32	0.32	0.28	0.32	0.34	0.19	0.51	0.38
Na_2O	7.14	7.16	7.19	7.06	7.11	7.21	7.28	7.34	7.36	7.15	7.19
K_2O	6.91	6.80	6.80	6.69	6.80	6.77	6.60	6.27	6.70	6.58	6.74
Total	99.24	98.93	98.92	98.36	98.78	98.97	98.80	98.57	98.94	99.08	99.10
Si	2.977	2.976	2.978	2.978	2.977	2.979	2.975	2.980	2.986	2.966	2.981
Ti	0.002	0.002	0.002	0.001	0.002	0.001	0.002	0.003	0.002	0.002	0.001
Al	1.001	1.004	1.002	1.005	1.002	0.999	1.002	0.991	0.986	1.016	0.998
Ba						0.000	0.000	0.000			
Fe	0.013	0.012	0.011	0.012	0.011	0.011	0.013	0.025	0.018	0.010	0.010
Sr	0.001	0.001		0.001	0.001	0.001	0.000	0.000	0.000	0.001	
Mg						0.001					
Ca	0.014	0.015	0.014	0.016	0.015	0.014	0.016	0.017	0.009	0.025	0.018
Na	0.627	0.630	0.633	0.625	0.627	0.635	0.642	0.648	0.648	0.628	0.631
K	0.399	0.394	0.394	0.390	0.394	0.392	0.383	0.365	0.388	0.380	0.389
Sum	5.034	5.032	5.033	5.026	5.030	5.033	5.034	5.028	5.038	5.028	5.029
Ab	60.3	60.7	60.8	60.7	60.5	61.0	61.7	63.0	62.0	60.8	60.8
An	1.4	1.4	1.4	1.5	1.5	1.3	1.5	1.6	0.9	2.4	1.8
Or	38.4	37.9	37.8	37.8	38.1	37.7	36.8	35.4	37.1	36.8	37.5

Table C9 continued

Unit	**Fur I dome**	**Fur I dome**	**Fur I dome**	**Fur I dome**	**Fur I dome**	**Fur I dome**	**Fur I dome**	**Fur I dome**	**Fur I dome**	**Fur I dome**	**Fur I dome**
Sample	SM5-1	SM5-1	SM5-1	SM5-1	SM5-1	SM5-1	SM5-1	SM5-1	SM5-1	SM5-1	SM5-1
No.	2 / 3 .	2 / 4 .	2 / 5 .	2 / 6 .	2 / 7 .	2 / 9 .	2 / 10 .	4 / 1 .	5 / 1 .	6 / 1 .	7 / 1 .
Notes	Pheno	Pheno	Pheno	Pheno	Pheno	Pheno	Pheno	Pheno	Pheno	Pheno	Pheno
SiO_2	65.80	65.77	65.67	65.78	65.32	65.65	65.70	66.60	65.26	65.64	65.53
TiO_2	0.04	0.03	0.06	0.05	0.04	0.03	0.06	0.06	0.04	0.02	0.03
Al_2O_3	19.01	18.83	18.94	18.70	19.58	18.87	18.84	19.02	18.72	18.85	18.86
BaO	bdl	0.01	bdl	bdl	bdl	bdl	bdl	0.01	bdl	0.02	bdl
FeO	0.25	0.27	0.26	0.28	0.31	0.25	0.34	0.31	0.29	0.27	0.27
SrO	0.04	bdl	0.04	0.02	0.02	0.06	0.01	0.04	0.02	0.03	0.04
MgO	bdl	bdl	bdl	bdl	bdl	bdl	bdl	0.01	bdl	bdl	bdl
CaO	0.43	0.38	0.45	0.26	0.37	0.41	0.52	0.41	0.43	0.38	0.44
Na_2O	7.23	7.40	7.33	7.19	7.48	7.22	7.17	6.78	7.26	7.39	7.23
K_2O	6.65	6.43	6.54	6.75	6.20	6.44	6.51	6.11	6.41	6.47	6.55
Total	99.44	99.08	99.29	99.01	99.31	98.89	99.13	99.35	98.39	99.07	98.92
Si	2.970	2.977	2.970	2.982	2.949	2.976	2.974	2.991	2.975	2.974	2.973
Ti	0.001	0.001	0.002	0.002	0.001	0.001	0.002	0.002	0.001	0.001	0.001
Al	1.012	1.004	1.010	0.999	1.042	1.008	1.005	1.007	1.006	1.006	1.008
Ba		0.000						0.000		0.000	
Fe	0.010	0.010	0.010	0.011	0.012	0.010	0.013	0.011	0.011	0.010	0.010
Sr	0.001		0.001	0.001	0.001	0.002	0.000	0.001	0.000	0.001	0.001
Mg								0.000			
Ca	0.021	0.018	0.022	0.013	0.018	0.020	0.025	0.020	0.021	0.018	0.021
Na	0.633	0.649	0.643	0.632	0.655	0.635	0.629	0.591	0.642	0.649	0.636
K	0.383	0.371	0.377	0.390	0.357	0.372	0.376	0.350	0.373	0.374	0.379
Sum	5.030	5.030	5.034	5.028	5.034	5.022	5.024	4.974	5.028	5.034	5.029
Ab	61.1	62.5	61.7	61.0	63.6	61.8	61.1	61.5	62.0	62.4	61.4
An	2.0	1.8	2.1	1.2	1.7	1.9	2.4	2.1	2.0	1.7	2.1
Or	36.9	35.7	36.2	37.7	34.7	36.3	36.5	36.4	36.0	35.9	36.6

Table C9 continued

Unit	**Fur I dome**	**Fur I dome**	**Fur I dome**	**Fur I dome**	**Fur I dome**	**Fur I dome**	**Fur I dome**	**Fur I dome**	**Fur I dome**	**Fur I dome**	**Fur I dome**
Sample	SM5-1	SM5-1	SM5-1	SM5-1	SM5-1	SM5-1-mph	SM5-1-mph	SM5-1-mph	SM5-1-mph	SM5-1-mph	SM5-1
No.	8 / 1 .	9 / 1 .	10 / 1 .	11 / 1 .	12 / 1 .	13 / 1 .	14 / 1 .	15 / 1 .	16 / 1 .	17 / 1 .	167 / 1 .
Notes	Pheno	Pheno	Pheno	Pheno	Pheno	Mph	Mph	Mph	Mph	Mph	Pheno
SiO_2	65.80	66.00	65.54	65.79	65.73	66.29	66.48	66.31	66.40	66.15	64.72
TiO_2	0.05	0.05	0.05	0.04	0.04	0.10	0.08	0.09	0.08	0.07	0.06
Al_2O_3	18.38	18.98	18.86	19.19	18.96	18.72	18.86	18.61	18.65	18.95	18.43
BaO	0.02	bdl	bdl	0.01	bdl	bdl	bdl	0.02	bdl	bdl	bdl
FeO	0.50	0.29	0.28	0.30	0.29	0.70	0.53	0.74	0.58	0.59	0.53
SrO	0.03	0.01	0.04	0.02	0.04	0.03	bdl	bdl	0.02	bdl	
MgO	bdl	bdl	0.01	bdl	bdl	bdl	bdl	bdl	bdl	bdl	bdl
CaO	0.20	0.43	0.45	0.65	0.49	0.42	0.43	0.24	0.17	0.35	0.17
Na_2O	7.32	7.11	7.27	7.91	7.50	8.00	7.83	7.55	7.36	7.79	6.78
K_2O	6.58	6.74	6.56	5.39	6.07	5.06	5.52	6.14	6.56	5.93	6.58
Total	98.88	99.61	99.05	99.30	99.11	99.32	99.73	99.67	99.82	99.81	97.25
Si	2.989	2.974	2.971	2.963	2.972	2.982	2.981	2.984	2.986	2.971	2.984
Ti	0.002	0.002	0.002	0.001	0.001	0.003	0.003	0.003	0.003	0.002	0.002
Al	0.984	1.008	1.008	1.019	1.010	0.993	0.997	0.987	0.989	1.003	1.002
Ba	0.000			0.000				0.000			
Fe	0.019	0.011	0.011	0.011	0.011	0.026	0.020	0.028	0.022	0.022	0.020
Sr	0.001	0.000	0.001	0.000	0.001	0.001			0.001		
Mg			0.000								
Ca	0.010	0.021	0.022	0.031	0.024	0.020	0.020	0.012	0.008	0.017	0.008
Na	0.645	0.622	0.639	0.691	0.657	0.697	0.681	0.659	0.642	0.679	0.606
K	0.381	0.387	0.379	0.310	0.350	0.291	0.316	0.352	0.377	0.340	0.387
Sum	5.030	5.025	5.033	5.027	5.026	5.012	5.017	5.025	5.026	5.034	5.009
Ab	62.3	60.4	61.4	67.0	63.7	69.2	66.9	64.4	62.5	65.5	60.5
An	0.9	2.0	2.1	3.0	2.3	2.0	2.0	1.1	0.8	1.6	0.8
Or	36.8	37.6	36.5	30.0	34.0	28.8	31.0	34.4	36.7	32.8	38.6

Table C9 continued

Unit	**Fur H**	**Fur H**	**Fur H**	**Fur H**	**Fur H**	**Fur H**	**Fur H**	**Fur H**	**Fur H**	**Fur H**	**Fur H**	**Fur H**	**Fur H**	**Fur H**
Sample	S003	S003	S003	S003	S003	S003	S003	S003	S003	S003	S003	S003	S003	S003
No.	Fsp1	Fsp2	Fsp3	Fsp4	Fsp5	Fsp6	Fsp7	Fsp8	Fsp9	Fsp10	Fsp11	Fsp12	Fsp13	Fsp14
Notes	Pheno	Pheno	Pheno	Pheno	Pheno	Pheno	Pheno	Pheno	Pheno	Pheno	Pheno	Pheno	Pheno	Pheno
SiO_2	65.28	65.42	64.82	64.12	61.16	64.00	65.32	65.07	64.40	65.20	65.63	65.08	65.84	66.36
TiO_2														
Al_2O_3	18.92	18.99	18.70	19.01	19.34	19.30	19.25	19.16	19.73	19.46	19.04	19.52	19.21	19.39
BaO	bdl	0.03	bdl	bdl	bdl	bdl	bdl	bdl	0.03	0.01	bdl	0.01	bdl	bdl
FeO	0.26	0.27	0.27	0.30	0.21	0.24	0.29	0.27	0.20	0.23	0.32	0.25	0.26	0.28
SrO	bdl	bdl	bdl	bdl	bdl	bdl	bdl	bdl	bdl	bdl	bdl	bdl	bdl	bdl
MgO														
CaO	0.41	0.38	0.21	0.43	0.79	0.60	0.40	0.26	1.03	0.52	0.31	0.58	0.42	0.46
Na_2O	7.55	7.10	6.85	6.94	6.22	7.31	6.55	6.91	5.83	6.36	6.88	6.62	6.69	7.00
K_2O	6.48	6.99	7.21	6.95	7.50	6.58	7.30	7.42	8.02	7.63	7.37	7.16	7.22	6.49
Total	98.90	99.19	98.06	97.75	95.22	98.03	99.11	99.09	99.25	99.40	99.55	99.22	99.64	99.98
Si	2.965	2.967	2.974	2.953	2.906	2.938	2.963	2.959	2.932	2.954	2.968	2.950	2.969	2.972
Ti														
Al	1.013	1.015	1.011	1.032	1.083	1.044	1.029	1.027	1.059	1.039	1.015	1.043	1.021	1.023
Ba		0.001							0.001	0.000		0.000		
Fe	0.010	0.010	0.010	0.012	0.008	0.009	0.011	0.010	0.008	0.009	0.012	0.010	0.010	0.011
Sr														
Mg														
Ca	0.020	0.019	0.010	0.021	0.040	0.030	0.019	0.013	0.050	0.025	0.015	0.028	0.020	0.022
Na	0.665	0.624	0.609	0.620	0.573	0.651	0.576	0.609	0.515	0.559	0.603	0.582	0.585	0.608
K	0.376	0.404	0.422	0.408	0.455	0.385	0.422	0.430	0.466	0.441	0.425	0.414	0.415	0.371
Sum	5.048	5.040	5.037	5.045	5.066	5.058	5.021	5.048	5.029	5.026	5.039	5.027	5.021	5.006
Ab	62.7	59.6	58.5	59.1	53.7	61.1	56.6	57.9	49.9	54.5	57.8	56.8	57.3	60.7
An	1.9	1.8	1.0	2.0	3.8	2.8	1.9	1.2	4.9	2.5	1.4	2.7	2.0	2.2
Or	35.4	38.6	40.5	38.9	42.6	36.2	41.5	40.9	45.2	43.0	40.8	40.4	40.7	37.1

Table C9 continued

Unit	**Fur H**	**Fur H**	**Fur H**	**Fur H**	**Fur H**	**Fur H**	**Fur H**	**Fur H**	**Fur H**	**Fur H**	**Fur H**	**Fur H**	**Fur H**
Sample	S003	S003	S003	S003	S003	S003	S003	S003	S003	S003	S003	S003	S003
No.	Fsp15	Fsp16	Fsp17	Fsp18	Fsp19	Fsp20	Fsp21	Fsp22	Fsp23	Fsp24	Fsp25	Fsp26	Fsp27
Notes	Pheno	Pheno	Pheno	Pheno	Pheno	Pheno	Pheno	Pheno	Pheno	Pheno	Pheno	Pheno	Pheno
SiO_2	66.19	66.54	67.15	66.09	65.97	66.02	66.89	66.84	66.89	66.83	66.13	65.59	65.67
TiO_2													
Al_2O_3	19.17	18.96	19.48	19.32	19.49	19.49	19.36	19.53	19.27	19.67	19.58	19.41	19.51
BaO	bdl	0.01	bdl	0.01	bdl	0.03	bdl	bdl	0.02	bdl	bdl	bdl	0.01
FeO	0.29	0.25	0.31	0.25	0.29	0.26	0.31	0.24	0.25	0.25	0.30	0.24	0.25
SrO	bdl	bdl	bdl	bdl	bdl	bdl	bdl	bdl	bdl	bdl	bdl	bdl	bdl
MgO													
CaO	0.25	0.27	0.38	0.41	0.45	0.40	0.33	0.35	0.31	0.34	0.54	0.43	0.34
Na_2O	7.16	6.72	6.98	6.20	7.28	6.45	6.99	6.43	6.95	6.78	7.57	6.86	6.81
K_2O	6.93	7.37	6.35	7.70	6.08	7.64	6.49	7.24	6.94	6.90	5.63	6.75	6.91
Total	99.99	100.12	100.65	99.98	99.56	100.29	100.38	100.62	100.63	100.77	99.75	99.28	99.50
Si	2.972	2.985	2.981	2.972	2.964	2.963	2.980	2.977	2.980	2.970	2.962	2.963	2.961
Ti													
Al	1.015	1.002	1.019	1.024	1.032	1.031	1.017	1.025	1.012	1.030	1.033	1.033	1.037
Ba		0.000		0.000		0.000			0.000				0.000
Fe	0.011	0.009	0.012	0.009	0.011	0.010	0.012	0.009	0.009	0.009	0.011	0.009	0.009
Sr													
Mg													
Ca	0.012	0.013	0.018	0.020	0.022	0.019	0.016	0.016	0.015	0.016	0.026	0.021	0.016
Na	0.623	0.585	0.601	0.541	0.634	0.561	0.604	0.555	0.600	0.584	0.657	0.601	0.595
K	0.397	0.422	0.360	0.442	0.348	0.437	0.369	0.411	0.394	0.391	0.322	0.389	0.397
Sum	5.031	5.017	4.990	5.007	5.011	5.021	4.998	4.994	5.011	5.002	5.011	5.016	5.017
Ab	60.4	57.3	61.4	53.9	63.1	55.1	61.1	56.5	59.5	58.9	65.4	59.5	59.0
An	1.2	1.3	1.8	2.0	2.2	1.9	1.6	1.7	1.5	1.7	2.6	2.0	1.6
Or	38.4	41.4	36.8	44.1	34.7	43.0	37.3	41.8	39.1	39.4	32.0	38.5	39.4

Table C9 continued

Unit	**Fur H**	**Fur H**	**Fur H**	**Fur H**	**Fur H**	**Fur H**	**Fur H**	**Fur H**	**Fur H**	**Fur H**	**Fur H**	**Fur H**	**Fur H**
Sample	S003	S003	S003	S003	S003	S003	S003	S003	S003	S003	S003	S003	S003
No.	Fsp28	Fsp29	Fsp30	Fsp31	Fsp32	Fsp33	Fsp34	Fsp35	Fsp36	Fsp37	Fsp38	Fsp39	Fsp40
Notes	Pheno	Pheno	Pheno	Pheno	Pheno	Pheno	Pheno	Pheno	Pheno	Pheno	Pheno	Pheno	Pheno
SiO_2	65.37	65.73	65.31	65.72	65.75	65.57	61.69	65.21	66.82	65.54	65.58	66.34	66.92
TiO_2													
Al_2O_3	19.42	19.25	19.42	19.47	19.63	19.51	22.97	19.93	19.46	20.10	19.28	19.54	19.52
BaO	bdl	bdl	0.02	bdl	bdl	0.01	0.92	bdl	0.03	bdl	bdl	0.02	bdl
FeO	0.25	0.29	0.22	0.26	0.21	0.28	0.22	0.19	0.29	0.26	0.29	0.22	0.25
SrO	bdl	bdl	bdl	bdl	bdl	bdl	0.07	0.02	bdl	bdl	bdl	bdl	bdl
MgO													
CaO	0.54	0.49	0.52	0.54	0.53	0.40	3.86	0.81	0.31	0.92	0.28	0.71	0.37
Na_2O	6.69	6.33	6.44	6.88	6.75	6.67	7.28	7.05	6.60	7.08	6.33	6.19	6.92
K_2O	6.78	7.75	7.14	6.79	6.74	6.96	2.75	6.05	7.15	5.92	7.50	7.35	6.84
Total	99.05	99.85	99.07	99.66	99.61	99.40	99.76	99.25	100.66	99.82	99.26	100.37	100.82
Si	2.960	2.965	2.960	2.959	2.958	2.960	2.780	2.941	2.977	2.938	2.969	2.967	2.974
Ti													
Al	1.036	1.023	1.037	1.033	1.041	1.038	1.220	1.059	1.022	1.062	1.029	1.030	1.022
Ba			0.000			0.000	0.016		0.000			0.000	
Fe	0.009	0.011	0.008	0.010	0.008	0.011	0.008	0.007	0.011	0.010	0.011	0.008	0.009
Sr							0.002	0.000					
Mg													
Ca	0.026	0.024	0.025	0.026	0.026	0.019	0.186	0.039	0.015	0.044	0.013	0.034	0.018
Na	0.587	0.554	0.566	0.601	0.589	0.584	0.636	0.616	0.570	0.615	0.556	0.537	0.596
K	0.392	0.446	0.413	0.390	0.387	0.401	0.158	0.348	0.406	0.339	0.433	0.419	0.388
Sum	5.011	5.023	5.010	5.019	5.009	5.013	5.007	5.012	5.001	5.008	5.011	4.996	5.007
Ab	58.4	54.1	56.4	59.1	58.8	58.2	64.9	61.4	57.5	61.7	55.4	54.2	59.5
An	2.6	2.3	2.5	2.6	2.6	1.9	19.0	3.9	1.5	4.4	1.3	3.4	1.8
Or	39.0	43.6	41.1	38.4	38.6	39.9	16.1	34.7	41.0	33.9	43.2	42.4	38.7

Table C9 continued

Unit	**Fur G**	**Fur F**	**Fur F**	**Fur F**	**Fur F**	**Fur F**	**Fur F**	**Fur F**	**Fur F**	**Fur F**	**Fur F**	**Fur F**	**Fur F**	**Fur F**
Sample	MI01	S042	S042	S042	S042	S042	S042	S042	S042	S042	S042	S042	S042	S042
No.	Fsp1	Fsp 1	Fsp 3	Fsp 4	Fsp 5	Fsp 6	Fsp 7	Fsp 8	Fsp 9	Fsp 10	Fsp 11	Fsp 12	Fsp 13	Fsp 14
Notes	Pheno	Pheno	Pheno	Pheno	Pheno	Pheno	Pheno	Pheno	Pheno	Pheno	Pheno	Pheno	Pheno	Pheno
SiO_2	67.05	63.34	64.54	63.03	63.69	63.49	63.34	63.56	64.53	65.34	64.59	65.23	65.16	64.59
TiO_2														
Al_2O_3	19.38	18.97	18.47	18.74	18.89	18.78	18.91	19.21	18.71	18.78	19.03	19.17	18.91	18.92
BaO	0.02	0.02	bdl	bdl	0.02	bdl	bdl	bdl	bdl	bdl	bdl	bdl	bdl	bdl
FeO	0.26	0.26	0.48	0.24	0.28	0.31	0.27	0.25	0.26	0.57	0.28	0.24	0.30	0.24
SrO	bdl	bdl	bdl	bdl	bdl	bdl	bdl	bdl	bdl	bdl	bdl	bdl	bdl	bdl
MgO														
CaO	0.36	0.34	0.19	0.29	0.32	0.33	0.32	0.47	0.24	0.14	0.37	0.29	0.28	0.36
Na_2O	6.93	7.17	7.01	6.54	7.10	6.93	7.19	6.95	6.78	7.20	6.80	7.05	6.84	6.67
K_2O	6.72	6.75	6.86	7.15	6.93	6.71	6.92	6.95	7.19	6.73	6.68	6.84	7.01	7.03
Total	100.71	96.85	97.55	95.99	97.22	96.55	96.95	97.39	97.71	98.76	97.75	98.82	98.50	97.81
Si	2.980	2.945	2.976	2.956	2.951	2.957	2.945	2.940	2.971	2.974	2.964	2.964	2.972	2.967
Ti		0.000	0.000	0.000	0.000	0.000	0.000	0.000	0.000	0.000	0.000	0.000	0.000	0.000
Al	1.015	1.040	1.004	1.036	1.032	1.031	1.036	1.047	1.015	1.007	1.029	1.027	1.016	1.024
Ba	0.000	0.000			0.000									
Fe	0.010	0.010	0.019	0.009	0.011	0.012	0.011	0.010	0.010	0.022	0.011	0.009	0.012	0.009
Sr		0.000	0.000	0.000	0.000	0.000	0.000	0.000	0.000	0.000	0.000	0.000	0.000	0.000
Mg		0.000	0.000	0.000	0.000	0.000	0.000	0.000	0.000	0.000	0.000	0.000	0.000	0.000
Ca	0.017	0.017	0.009	0.015	0.016	0.016	0.016	0.023	0.012	0.007	0.018	0.014	0.014	0.018
Na	0.597	0.646	0.627	0.595	0.638	0.626	0.648	0.623	0.605	0.635	0.605	0.621	0.605	0.594
K	0.381	0.400	0.403	0.428	0.410	0.399	0.410	0.410	0.422	0.391	0.391	0.397	0.408	0.412
Sum	5.001	5.059	5.038	5.038	5.057	5.040	5.066	5.053	5.035	5.036	5.019	5.031	5.026	5.024
Ab	60.0	60.8	60.3	57.3	60.0	60.1	60.3	59.0	58.2	61.5	59.6	60.2	58.9	58.0
An	1.7	1.6	0.9	1.4	1.5	1.6	1.5	2.2	1.1	0.7	1.8	1.4	1.3	1.7
Or	38.3	37.6	38.8	41.2	38.5	38.3	38.2	38.8	40.6	37.8	38.6	38.4	39.7	40.2

Table C9 continued

Unit	**Fur F**	**Fur F**	**Fur F**	**Fur F**	**Fur F**	**Fur F**	**Fur F**	**Fur F**	**Fur F**	**Fur F**	**Fur F**	**Fur F**	**Fur F**	**Fur F**
Sample	S042	S042	S042	S042	S042	S042	S042	S042	S042	S042	S042	S042	S042	S042
No.	Fsp 15	Fsp 16	Fsp 17	Fsp 18	Fsp 19	Fsp 20	Fsp 21	Fsp 22	Fsp 23	Fsp 24	Fsp 25	Fsp 26	Fsp 27	Fsp 28
Notes	Pheno	Pheno	Pheno	Pheno	Pheno	Pheno	Pheno	Pheno	Pheno	Pheno	Pheno	Pheno	Pheno	Pheno
SiO_2	65.06	63.83	65.59	64.92	63.85	64.90	65.88	64.38	65.32	65.47	65.66	65.62	65.25	65.70
TiO_2														
Al_2O_3	19.23	18.99	19.24	19.07	18.95	19.13	19.43	19.03	19.11	19.19	18.98	19.02	19.06	18.98
BaO	bdl	0.02	0.01	0.03	bdl	0.01	0.02	bdl	0.02	0.02	0.01	bdl	bdl	0.03
FeO	0.25	0.27	0.29	0.23	0.25	0.26	0.32	0.24	0.24	0.23	0.51	0.33	0.24	0.27
SrO	bdl	bdl	bdl	bdl	bdl	bdl	bdl	bdl	bdl	bdl	bdl	bdl	bdl	bdl
MgO														
CaO	0.51	0.29	0.37	0.31	0.26	0.32	0.51	0.40	0.33	0.44	0.11	0.29	0.24	0.30
Na_2O	6.86	6.92	7.00	7.18	6.96	7.31	7.19	6.84	6.84	6.69	7.31	7.01	6.86	6.86
K_2O	6.88	6.90	6.82	6.68	7.07	6.43	6.53	7.07	7.18	6.97	6.54	6.99	7.04	7.13
Total	98.79	97.21	99.32	98.42	97.34	98.36	99.88	97.97	99.04	99.01	99.13	99.26	98.69	99.27
Si	2.959	2.954	2.965	2.962	2.954	2.961	2.960	2.957	2.966	2.968	2.973	2.971	2.969	2.974
Ti	0.000	0.000	0.000	0.000	0.000	0.000	0.000	0.000	0.000	0.000	0.000	0.000	0.000	0.000
Al	1.031	1.036	1.025	1.026	1.033	1.028	1.029	1.030	1.023	1.025	1.013	1.015	1.022	1.013
Ba		0.000	0.000	0.001		0.000	0.000		0.000	0.000	0.000			0.001
Fe	0.009	0.010	0.011	0.009	0.010	0.010	0.012	0.009	0.009	0.009	0.019	0.012	0.009	0.010
Sr	0.000	0.000	0.000	0.000	0.000	0.000	0.000	0.000	0.000	0.000	0.000	0.000	0.000	0.000
Mg	0.000	0.000	0.000	0.000	0.000	0.000	0.000	0.000	0.000	0.000	0.000	0.000	0.000	0.000
Ca	0.025	0.014	0.018	0.015	0.013	0.016	0.025	0.020	0.016	0.022	0.005	0.014	0.012	0.015
Na	0.605	0.621	0.614	0.635	0.624	0.647	0.626	0.609	0.602	0.588	0.642	0.615	0.605	0.602
K	0.399	0.407	0.393	0.389	0.417	0.374	0.374	0.414	0.416	0.403	0.378	0.404	0.409	0.412
Sum	5.028	5.042	5.026	5.037	5.051	5.036	5.026	5.040	5.032	5.015	5.030	5.031	5.027	5.026
Ab	58.8	59.6	59.9	61.1	59.2	62.4	61.1	58.4	58.2	58.1	62.6	59.6	59.0	58.5
An	2.4	1.4	1.7	1.5	1.2	1.5	2.4	1.9	1.6	2.1	0.5	1.3	1.2	1.4
Or	38.8	39.1	38.4	37.4	39.6	36.1	36.5	39.7	40.2	39.8	36.9	39.1	39.8	40.0

Table C9 continued

Unit	**Fur F**	**Fur F**	**Fur F**	**Fur F**	**Fur F**	**Fur F**	**Fur F**	**Fur F**	**Fur F**	**Fur F**	**Fur F**	**Fur F**
Sample	S042	S042	S042	S042	S042	S042	S042	S042	S042	S042	S042	S042
No.	Fsp 29	Fsp 30	Fsp 31	Fsp 32	Fsp 33	Fsp 34	Fsp 35	Fsp 36	Fsp 37	Fsp 38	Fsp 39	Fsp 40
Notes	Pheno	Pheno	Pheno	Pheno	Pheno	Pheno	Pheno	Pheno	Pheno	Pheno	Pheno	Pheno
SiO_2	65.29	64.91	65.47	65.64	65.76	66.37	66.19	66.41	67.28	67.20	66.70	66.88
TiO_2												
Al_2O_3	19.28	19.03	19.13	18.99	19.32	19.59	19.16	19.13	19.64	19.38	19.42	19.42
BaO	bdl	0.01	bdl	0.01	bdl	bdl	bdl	bdl	bdl	bdl	0.03	bdl
FeO	0.26	0.25	0.27	0.29	0.28	0.21	0.26	0.28	0.26	0.26	0.25	0.29
SrO	bdl	bdl	bdl	bdl	bdl	bdl	bdl	bdl	bdl	bdl	bdl	bdl
MgO												
CaO	0.41	0.26	0.31	0.31	0.31	0.44	0.26	0.23	0.63	0.41	0.30	0.41
Na_2O	7.12	6.81	7.27	6.64	6.82	6.73	6.71	6.65	7.01	7.05	6.64	7.07
K_2O	6.41	7.04	6.65	7.07	6.82	7.09	7.28	7.22	5.94	6.81	6.97	6.44
Total	98.77	98.31	99.10	98.95	99.31	100.43	99.86	99.92	100.76	101.11	100.30	100.51
Si	2.963	2.967	2.966	2.977	2.969	2.965	2.977	2.982	2.978	2.979	2.978	2.977
Ti	0.000	0.000	0.000	0.000	0.000	0.000	0.000	0.000	0.000	0.000	0.000	0.000
Al	1.031	1.025	1.021	1.015	1.028	1.032	1.015	1.012	1.024	1.012	1.022	1.019
Ba		0.000		0.000							0.000	
Fe	0.010	0.010	0.010	0.011	0.010	0.008	0.010	0.010	0.010	0.010	0.009	0.011
Sr	0.000	0.000	0.000	0.000	0.000	0.000	0.000	0.000	0.000	0.000	0.000	0.000
Mg	0.000	0.000	0.000	0.000	0.000	0.000	0.000	0.000	0.000	0.000	0.000	0.000
Ca	0.020	0.013	0.015	0.015	0.015	0.021	0.013	0.011	0.030	0.019	0.014	0.019
Na	0.626	0.603	0.639	0.584	0.597	0.583	0.585	0.579	0.602	0.606	0.575	0.610
K	0.371	0.410	0.384	0.409	0.393	0.404	0.418	0.414	0.335	0.385	0.397	0.366
Sum	5.021	5.028	5.035	5.012	5.012	5.013	5.017	5.008	4.978	5.011	4.996	5.002
Ab	61.6	58.8	61.5	57.9	59.4	57.8	57.6	57.7	62.2	60.0	58.3	61.3
An	2.0	1.2	1.4	1.5	1.5	2.1	1.3	1.1	3.1	1.9	1.4	1.9
Or	36.5	40.0	37.0	40.6	39.1	40.1	41.1	41.2	34.7	38.1	40.3	36.7

Table C9 continued

Unit	**Fur E**	**Fur E**	**Fur E**	**Fur E**	**Fur E**	**Fur E**	**Fur E**	**Fur E**	**Fur E**	**Fur E**	**Fur E**	**Fur E**	**Fur E**	**Fur E**	**Fur E**
Sample	S012	S012	S012	S012	S012	S012	S012	S012	S012	S012	S012	S012	S012	S012	S012
No.	Fsp3	Fsp4	Fsp6	Fsp7	Fsp8	Fsp9	Fsp10	Fsp11	Fsp12	Fsp13	Fsp14	Fsp15	Fsp16	Fsp17	Fsp18
Notes	Pheno	Pheno	Pheno	Pheno	Pheno	Pheno	Pheno	Pheno	Pheno	Pheno	Pheno	Pheno	Pheno	Pheno	Pheno
SiO_2	65.27	66.04	66.25	65.86	65.87	65.80	65.98	65.92	64.96	64.74	65.40	65.70	65.86	66.11	65.48
TiO_2															
Al_2O_3	18.99	18.78	19.04	19.32	19.33	19.25	18.91	19.04	18.40	18.68	18.91	19.21	19.08	19.10	19.02
BaO	bdl	0.02	0.02	0.01	bdl	bdl	bdl	bdl	0.02	bdl	bdl	bdl	bdl	0.01	bdl
FeO	0.28	0.26	0.23	0.23	0.24	0.23	0.28	0.30	0.32	0.25	0.30	0.18	0.28	0.25	0.26
SrO	bdl	bdl	bdl	bdl	bdl	bdl	bdl	bdl	bdl	bdl	bdl	bdl	bdl	bdl	bdl
MgO															
CaO	0.33	0.37	0.28	0.64	0.62	0.67	0.38	0.35	0.30	0.24	0.47	0.56	0.35	0.35	0.34
Na_2O	7.00	6.81	6.88	6.68	6.77	6.84	6.96	7.06	6.94	7.04	7.39	7.03	7.21	7.27	7.18
K_2O	6.86	6.86	7.10	6.68	7.06	6.81	7.07	6.96	7.14	6.59	6.32	6.68	6.44	6.80	6.79
Total	98.74	99.14	99.80	99.42	99.89	99.60	99.57	99.62	98.08	97.54	98.79	99.36	99.22	99.89	99.08
Si	2.969	2.987	2.980	2.969	2.963	2.965	2.977	2.973	2.981	2.977	2.970	2.966	2.974	2.972	2.969
Ti	0.000	0.000	0.000	0.000	0.000	0.000	0.000	0.000	0.000	0.000	0.000	0.000	0.000	0.000	0.000
Al	1.018	1.001	1.009	1.026	1.025	1.022	1.006	1.012	0.995	1.012	1.012	1.022	1.015	1.012	1.016
Ba		0.000	0.000	0.000					0.000					0.000	
Fe	0.011	0.010	0.009	0.009	0.009	0.009	0.010	0.011	0.012	0.010	0.011	0.007	0.011	0.009	0.010
Sr															
Mg	0.000	0.000	0.000	0.000	0.000	0.000	0.000	0.000	0.000	0.000	0.000	0.000	0.000	0.000	0.000
Ca	0.016	0.018	0.013	0.031	0.030	0.032	0.018	0.017	0.015	0.012	0.023	0.027	0.017	0.017	0.017
Na	0.617	0.597	0.600	0.584	0.590	0.598	0.609	0.617	0.617	0.628	0.651	0.615	0.631	0.634	0.631
K	0.398	0.396	0.407	0.384	0.405	0.392	0.407	0.400	0.418	0.387	0.366	0.385	0.371	0.390	0.393
Sum	5.030	5.009	5.019	5.002	5.022	5.018	5.028	5.030	5.039	5.024	5.033	5.023	5.019	5.034	5.035
Ab	59.8	59.1	58.8	58.5	57.6	58.5	58.9	59.7	58.8	61.2	62.6	59.9	61.9	60.9	60.7
An	1.6	1.8	1.3	3.1	2.9	3.1	1.8	1.6	1.4	1.1	2.2	2.6	1.7	1.6	1.6
Or	38.6	39.1	39.9	38.5	39.5	38.3	39.4	38.7	39.8	37.7	35.2	37.5	36.4	37.5	37.7

Table C9 continued

Unit	**Fur E**	**Fur E**	**Fur E**	**Fur E**	**Fur E**	**Fur E**	**Fur E**	**Fur E**	**Fur E**	**Fur E**	**Fur E**	**Fur E**	**Fur E**	**Fur E**
Sample	S012	S012	S012	S012	S012	S012	S012	S012	S012	S012	S012	S012	S012	S012
No.	Fsp19	Fsp20	Fsp21	Fsp22	Fsp23	Fsp24	Fsp25	Fsp26	Fsp27	Fsp28	Fsp29	Fsp30	Fsp31	Fsp32
Notes	Pheno	Pheno	Pheno	Pheno	Pheno	Pheno	Pheno	Pheno	Pheno	Pheno	Pheno	Pheno	Pheno	Pheno
SiO_2	66.25	66.27	66.52	65.88	65.74	65.94	66.45	65.93	65.83	66.29	65.12	66.27	65.63	66.81
TiO_2														
Al_2O_3	19.04	18.93	19.12	19.18	19.42	19.31	19.20	19.05	18.96	19.13	18.89	18.95	18.97	19.04
BaO	0.02	bdl	0.01	bdl	bdl	0.01	bdl	0.01	bdl	bdl	bdl	bdl	0.03	0.02
FeO	0.30	0.28	0.29	0.28	0.23	0.24	0.29	0.29	0.27	0.27	0.32	0.30	0.29	0.30
SrO	bdl	bdl	bdl	bdl	bdl	bdl	bdl	bdl	bdl	bdl	bdl	bdl	bdl	bdl
MgO														
CaO	0.35	0.36	0.34	0.39	0.58	0.44	0.34	0.36	0.37	0.31	0.27	0.34	0.34	0.31
Na_2O	6.90	6.77	7.08	7.41	7.06	6.63	6.77	7.15	6.92	6.79	6.96	6.90	7.03	6.88
K_2O	6.72	6.90	6.80	6.55	6.36	7.39	6.92	6.90	6.92	7.18	7.09	6.87	6.83	6.88
Total	99.57	99.51	100.16	99.68	99.39	99.97	99.97	99.69	99.26	99.96	98.64	99.62	99.12	100.23
Si	2.981	2.985	2.979	2.966	2.963	2.966	2.979	2.971	2.977	2.977	2.969	2.983	2.973	2.987
Ti	0.000	0.000	0.000	0.000	0.000	0.000	0.000	0.000	0.000	0.000	0.000	0.000	0.000	0.000
Al	1.010	1.005	1.009	1.018	1.031	1.024	1.015	1.012	1.010	1.013	1.015	1.005	1.013	1.003
Ba	0.000		0.000			0.000		0.000					0.001	0.000
Fe	0.011	0.010	0.011	0.010	0.009	0.009	0.011	0.011	0.010	0.010	0.012	0.011	0.011	0.011
Sr														
Mg	0.000	0.000	0.000	0.000	0.000	0.000	0.000	0.000	0.000	0.000	0.000	0.000	0.000	0.000
Ca	0.017	0.017	0.016	0.019	0.028	0.021	0.017	0.018	0.018	0.015	0.013	0.016	0.017	0.015
Na	0.602	0.591	0.615	0.647	0.617	0.578	0.589	0.625	0.607	0.591	0.615	0.602	0.617	0.596
K	0.386	0.397	0.388	0.376	0.366	0.424	0.396	0.397	0.399	0.411	0.412	0.395	0.395	0.392
Sum	5.008	5.006	5.018	5.036	5.013	5.023	5.006	5.033	5.021	5.018	5.037	5.013	5.026	5.006
Ab	59.9	58.8	60.3	62.1	61.1	56.5	58.8	60.1	59.3	58.1	59.1	59.4	60.0	59.4
An	1.7	1.7	1.6	1.8	2.8	2.1	1.7	1.7	1.7	1.5	1.3	1.6	1.6	1.5
Or	38.4	39.4	38.1	36.1	36.2	41.4	39.5	38.2	39.0	40.4	39.6	38.9	38.4	39.1

Table C9 continued

Unit	**Fur E**	**Fur E**	**Fur E**	**Fur E**	**Fur E**	**Fur E**	**Fur E**	**Fur E**	**Fur E**	**Fur E**	**Fur E**	**Fur E**	**Fur E**	**Fur E**
Sample	S012	S012	S012	S012	S012	S012	S012	S012	S012	S012	S012	S012	S012	S012
No.	Fsp33	Fsp34	Fsp35	Fsp36	Fsp37	Fsp38	Fsp39	Fsp40	MI01	MI02	MI03	MI04	MI05	MI06
Notes	Pheno	Pheno	Pheno	Pheno	Pheno	Pheno	Pheno	Pheno	Pheno	Pheno	Pheno	Pheno	Pheno	Pheno
SiO_2	66.03	66.08	66.03	66.29	65.56	66.06	65.52	65.86	65.75	65.32	63.93	65.79	65.44	66.48
TiO_2														
Al_2O_3	19.33	19.00	18.89	19.32	19.19	19.14	19.05	18.94	18.81	18.86	18.87	18.95	18.96	19.25
BaO	0.03	0.01	bdl	0.02	bdl	bdl	0.01	0.02	bdl	bdl	bdl	bdl	bdl	bdl
FeO	0.30	0.26	0.26	0.29	0.29	0.26	0.27	0.24	0.31	0.42	0.29	0.22	0.30	0.25
SrO	bdl	bdl	bdl	bdl	bdl	bdl	bdl	bdl	bdl	bdl	bdl	bdl	0.01	bdl
MgO														
CaO	0.44	0.32	0.43	0.52	0.38	0.31	0.29	0.22	0.28	0.34	0.42	0.38	0.44	0.25
Na_2O	7.16	6.81	6.96	7.63	7.11	6.97	7.03	6.61	7.12	7.44	7.66	7.29	7.29	6.98
K_2O	6.83	7.22	6.67	6.16	6.84	6.93	6.94	6.92	6.92	6.56	6.51	6.78	6.44	6.97
Total	100.11	99.70	99.24	100.22	99.37	99.67	99.11	98.81	99.19	98.94	97.69	99.41	98.88	100.19
Si	2.963	2.978	2.982	2.965	2.964	2.974	2.970	2.986	2.978	2.968	2.948	2.972	2.969	2.976
Ti	0.000	0.000	0.000	0.000	0.000	0.000	0.000	0.000	0.000	0.000	0.000	0.000	0.000	0.000
Al	1.022	1.009	1.005	1.018	1.023	1.016	1.018	1.012	1.004	1.010	1.025	1.009	1.014	1.016
Ba	0.001	0.000		0.000			0.000	0.000						
Fe	0.011	0.010	0.010	0.011	0.011	0.010	0.010	0.009	0.012	0.016	0.011	0.008	0.011	0.009
Sr													0.000	
Mg	0.000	0.000	0.000	0.000	0.000	0.000	0.000	0.000	0.000	0.000	0.000	0.000	0.000	0.000
Ca	0.021	0.015	0.021	0.025	0.018	0.015	0.014	0.011	0.014	0.016	0.021	0.019	0.022	0.012
Na	0.623	0.595	0.609	0.662	0.623	0.608	0.618	0.581	0.625	0.655	0.685	0.639	0.641	0.606
K	0.391	0.415	0.384	0.351	0.395	0.398	0.401	0.400	0.400	0.380	0.383	0.391	0.373	0.398
Sum	5.032	5.023	5.012	5.032	5.034	5.021	5.031	4.999	5.033	5.045	5.073	5.038	5.031	5.018
Ab	60.2	58.0	60.1	63.7	60.2	59.6	59.8	58.6	60.2	62.3	62.9	60.9	61.9	59.6
An	2.0	1.5	2.0	2.4	1.8	1.5	1.4	1.1	1.3	1.6	1.9	1.8	2.1	1.2
Or	37.8	40.5	37.9	33.9	38.1	39.0	38.8	40.3	38.5	36.1	35.2	37.3	36.0	39.2

Table C9 continued

Unit	**Fur C**	**Fur C**	**Fur C**	**Fur C**	**Fur C**	**Fur C**	**Fur C**	**Fur C**	**Fur C**	**Fur C**	**Fur C**	**Fur C**	**Fur C**	**Fur C**	**Fur C**	**Fur C**	**Fur C**
Sample	S016	S016	S016	S016	S016	S016	S016	S016	S016	S016	S016	S016	S016	S016	S016	S016	S016
No.	Fsp2	Fsp5	Fsp6	Fsp7	Fsp8	Fsp9	Fsp10	Fsp11	Fsp12	Fsp13	Fsp14	Fsp15	MI01	MI02	MI03	MI04	MI05
Notes	Pheno	Pheno	Pheno	Pheno	Pheno	Pheno	Pheno	Pheno	Pheno	Pheno	Pheno	Pheno	Pheno	Pheno	Pheno	Pheno	Pheno
SiO_2	66.31	66.34	66.78	67.51	65.15	67.10	66.89	63.80	67.19	68.09	66.78	66.62	66.06	67.50	67.39	66.02	67.40
TiO_2																	
Al_2O_3	19.55	19.26	19.31	19.45	19.55	19.63	19.78	19.89	19.36	19.56	19.77	19.51	20.07	19.91	20.07	19.87	19.70
BaO	bdl	0.03	0.02	bdl	bdl	0.01	0.01	bdl	bdl	bdl	0.01	bdl	bdl	0.01	0.04	bdl	bdl
FeO	0.19	0.24	0.25	0.22	0.24	0.24	0.26	0.24	0.26	0.25	0.15	0.24	0.23	0.24	0.21	0.23	0.19
SrO	bdl	bdl	bdl	bdl	bdl	bdl	bdl	bdl	bdl	0.03	bdl	bdl	0.01	bdl	bdl	bdl	bdl
MgO																	
CaO	0.55	0.41	0.21	0.40	0.39	0.55	0.41	0.86	0.41	0.23	0.58	0.34	0.61	0.62	0.66	0.41	0.45
Na_2O	7.31	7.29	7.14	6.60	6.47	6.95	6.86	7.38	6.68	6.48	6.47	6.79	7.42	6.86	6.98	6.75	6.63
K_2O	6.55	6.70	6.46	7.09	7.52	6.65	6.79	5.74	7.03	7.35	7.40	6.82	5.81	6.48	6.05	6.96	6.90
Total	100.47	100.26	100.16	101.27	99.32	101.13	101.00	97.91	100.93	101.99	101.16	100.33	100.22	101.62	101.40	100.24	101.28
Si	2.960	2.970	2.982	2.985	2.952	2.971	2.966	2.922	2.983	2.990	2.964	2.974	2.947	2.969	2.966	2.954	2.977
Ti																	
Al	1.029	1.016	1.016	1.014	1.044	1.024	1.034	1.073	1.013	1.012	1.034	1.026	1.055	1.032	1.041	1.048	1.026
Ba		0.000	0.000			0.000	0.000				0.000			0.000	0.001		
Fe	0.007	0.009	0.009	0.008	0.009	0.009	0.010	0.009	0.010	0.009	0.005	0.009	0.009	0.009	0.008	0.009	0.007
Sr										0.001			0.000				
Mg																	
Ca	0.027	0.020	0.010	0.019	0.019	0.026	0.019	0.042	0.020	0.011	0.028	0.016	0.029	0.029	0.031	0.020	0.021
Na	0.633	0.633	0.618	0.566	0.568	0.597	0.590	0.655	0.575	0.552	0.557	0.588	0.642	0.585	0.596	0.586	0.568
K	0.373	0.383	0.368	0.400	0.435	0.376	0.384	0.335	0.398	0.412	0.419	0.388	0.331	0.364	0.340	0.397	0.389
Sum	5.028	5.030	5.003	4.991	5.027	5.003	5.004	5.037	4.998	4.986	5.007	5.001	5.012	4.989	4.981	5.013	4.988
Ab	61.3	61.1	62.1	57.5	55.6	59.8	59.4	63.4	57.9	56.6	55.5	59.2	64.1	59.8	61.6	58.4	58.1
An	2.6	1.9	1.0	1.9	1.9	2.6	2.0	4.1	2.0	1.1	2.7	1.7	2.9	3.0	3.2	2.0	2.2
Or	36.1	37.0	36.9	40.6	42.5	37.6	38.7	32.5	40.1	42.3	41.8	39.1	33.0	37.2	35.2	39.6	39.8

Table C10: Clinopyroxene analyses from the UFG and the PIF

Unit	**Fur J**	**Fur J**	**Fur J**	**Fur J**	**Fur J**	**Fur J**	**Fur J**	**Fur J**	**Fur J**	**Fur J**
Sample	FM-1(1)	FM-1(1)	FM-1(1)	FM-1(1)	FM-1(1)	FM-1(1)	FM-1(1)	FM-1(1)	FM-1(1)	FM-1(1)
No.	Px1	Px2	Px3	Px4	Px5	Px6	Px7	Px8	Px9	Px10
Notes	Pheno	Pheno	Pheno	Pheno	Pheno	Pheno	Pheno	Pheno	Pheno	Pheno
SiO_2	52.85	52.33	53.01	51.99	52.74	52.92	52.43	52.52	52.54	52.52
TiO_2	0.48	0.50	0.39	0.38	0.39	0.43	0.42	0.53	0.37	0.49
Al_2O_3	0.93	1.07	0.78	0.79	0.80	0.89	0.61	1.04	0.82	0.96
Cr_2O_3	bdl	bdl	0.01	bdl	bdl	bdl	bdl	bdl	bdl	bdl
FeO	10.56	12.30	11.33	11.68	11.46	11.73	12.73	11.84	11.11	12.10
MnO	1.17	1.49	1.41	1.48	1.41	1.52	1.65	1.45	1.36	1.66
MgO	12.78	10.86	11.62	11.87	11.66	11.27	10.92	11.15	12.16	11.03
CaO	21.46	21.37	21.45	21.69	21.59	21.10	21.60	20.97	21.25	21.07
Na_2O	0.64	1.07	0.94	0.93	0.96	0.99	0.87	0.99	0.79	1.18
K_2O	0.01	bdl	0.02	bdl	bdl	0.01	bdl	bdl	0.01	0.01
Total	100.88	100.99	100.97	100.82	101.01	100.87	101.23	100.49	100.42	101.03
Si	1.968	1.962	1.980	1.944	1.969	1.983	1.967	1.977	1.970	1.966
Ti	0.014	0.014	0.011	0.011	0.011	0.012	0.012	0.015	0.010	0.014
Al	0.041	0.047	0.034	0.035	0.035	0.039	0.027	0.046	0.036	0.043
Cr			0.000							
Fe^{2+}	0.286	0.309	0.302	0.242	0.284	0.326	0.321	0.329	0.288	0.294
Fe^{3+}	0.043	0.077	0.052	0.123	0.074	0.042	0.078	0.043	0.061	0.085
Mn	0.037	0.047	0.045	0.047	0.045	0.048	0.052	0.046	0.043	0.053
Mg	0.709	0.607	0.647	0.662	0.649	0.630	0.611	0.626	0.680	0.615
Ca	0.856	0.859	0.859	0.869	0.864	0.847	0.868	0.846	0.854	0.845
Na	0.046	0.077	0.068	0.068	0.069	0.072	0.063	0.072	0.057	0.086
K	0.001		0.001			0.000			0.001	0.000
Sum	4.000	4.000	4.000	4.000	4.000	4.000	4.000	4.000	4.000	4.000
Aegirine	4.3	7.7	5.2	6.8	6.9	4.2	6.3	4.3	5.7	8.5
Ferri-Tschermak	0.0	0.0	0.0	2.8	0.2	0.0	0.7	0.0	0.2	0.0
Jadeite	0.3	0.0	1.5	0.0	0.0	2.3	0.0	2.3	0.0	0.1
Ti-Aegirine	0.0	0.0	0.2	0.0	0.0	0.7	0.0	0.6	0.0	0.0
Ti-Tschermak	1.4	1.4	1.0	1.1	1.1	0.8	1.2	1.2	1.0	1.4
Al-Tschermak	0.5	0.9	0.0	0.0	0.4	0.0	0.0	0.0	0.6	0.7
Diopside	57.6	52.6	55.3	57.8	56.2	52.6	52.7	52.1	56.2	52.7
Hedenbergite	26.2	30.9	29.6	25.2	28.4	31.2	32.2	31.3	27.3	29.7
Enstatite	6.7	4.0	4.7	4.2	4.4	5.1	4.2	5.1	5.9	4.4
Ferrosilite	3.0	2.4	2.5	1.8	2.2	3.0	2.6	3.1	2.9	2.5

Table C10 continued

Unit	**Fur J**	**Fur J**	**Fur J**	**Fur J**	**Fur J**	**Fur J**	**Fur J**	**Fur J**	**Fur J**	**Fur J**
Sample	FM-2(1)	FM-2(1)	FM-2(1)	FM-2(1)	FM-2(1)	FM-2(1)	FM-2(1)	FM-2(1)	FM-2(1)	FM-2(1)
No.	Px1	Px2	Px3	Px4	Px5	Px6	Px7	Px8	Px9	Px10
Notes	Pheno	Pheno	Pheno	Pheno	Pheno	Pheno	Pheno	Pheno	Pheno	Pheno
SiO_2	52.62	52.79	52.09	52.41	52.18	52.41	52.93	52.33	53.16	52.99
TiO_2	0.46	0.40	0.41	0.40	0.53	0.35	0.36	0.46	0.38	0.44
Al_2O_3	0.86	0.78	0.85	0.60	0.98	0.60	0.61	0.78	0.83	0.87
Cr_2O_3	bdl	bdl	bdl	bdl	bdl	bdl	0.01	0.01	bdl	0.02
FeO	11.56	11.40	12.20	12.38	11.75	11.80	12.17	10.94	11.23	11.47
MnO	1.44	1.44	1.54	1.60	1.53	1.56	1.61	1.34	1.38	1.50
MgO	11.67	11.71	10.84	11.22	11.17	11.26	11.09	11.76	11.81	11.37
CaO	21.78	21.57	21.02	21.18	21.23	21.40	21.59	21.07	21.49	21.48
Na_2O	0.97	0.87	1.16	0.82	1.10	0.87	0.90	0.91	0.96	0.98
K_2O	bdl	0.01	bdl	bdl	bdl	0.01	bdl	0.02	bdl	0.01
Total	101.35	100.98	100.10	100.62	100.47	100.26	101.28	99.61	101.24	101.13
Si	1.958	1.973	1.969	1.975	1.962	1.978	1.981	1.979	1.979	1.979
Ti	0.013	0.011	0.012	0.011	0.015	0.010	0.010	0.013	0.011	0.012
Al	0.038	0.035	0.038	0.027	0.043	0.027	0.027	0.035	0.036	0.038
Cr							0.000	0.000		0.001
Fe^{2+}	0.270	0.294	0.300	0.330	0.287	0.310	0.325	0.298	0.295	0.309
Fe^{3+}	0.090	0.062	0.086	0.061	0.083	0.062	0.056	0.048	0.054	0.050
Mn	0.045	0.046	0.049	0.051	0.049	0.050	0.051	0.043	0.044	0.047
Mg	0.648	0.652	0.611	0.630	0.626	0.634	0.619	0.663	0.655	0.633
Ca	0.869	0.864	0.851	0.855	0.855	0.865	0.866	0.854	0.857	0.860
Na	0.070	0.063	0.085	0.060	0.080	0.064	0.065	0.066	0.069	0.071
K		0.001				0.000		0.001		0.000
Sum	4.000	4.000	4.000	4.000	4.000	4.000	4.000	4.000	4.000	4.000
Aegirine	7.0	6.2	8.5	6.0	8.0	6.2	5.6	4.8	5.4	5.0
Ferri-Tschermak	1.0	0.0	0.1	0.0	0.1	0.0	0.0	0.0	0.0	0.0
Jadeite	0.0	0.2	0.0	0.0	0.0	0.2	0.8	1.4	1.5	1.7
Ti-Aegirine	0.0	0.0	0.0	0.0	0.0	0.0	0.1	0.4	0.0	0.4
Ti-Tschermak	1.3	1.1	1.2	1.1	1.5	1.0	0.9	1.0	1.1	1.0
Al-Tschermak	0.0	0.5	0.7	0.2	0.5	0.2	0.0	0.0	0.0	0.0
Diopside	56.9	55.7	53.0	52.5	54.3	54.4	53.3	55.7	55.8	54.3
Hedenbergite	27.7	29.0	30.3	31.7	29.1	30.9	32.3	28.6	28.8	30.6
Enstatite	3.9	4.8	4.1	5.3	4.2	4.5	4.3	5.2	4.9	4.4
Ferrosilite	1.9	2.5	2.3	3.2	2.2	2.5	2.6	2.7	2.5	2.5

Table C10 continued

Unit	Fur J dome	Fur J dome	Fur J dome	Fur J dome	Fur J dome	Fur J dome	Fur J dome	Fur J dome	Fur J dome	Fur J dome	Fur J dome	Fur J dome
Sample	SM 7-1	SM 7-1	SM 7-1	SM 7-1	SM 7-1	SM 7-1	SM7-1	SM7-1	SM7-1	SM7-1	SM7-1	SM7-1
No.	Clino01	Clino02	Clino03	Clino04	Clino05	Clino05	73 / 1 .	73 / 2 .	73 / 3 .	73 / 4 .	73 / 5 .	73 / 6 .
Notes	Pheno	Pheno	Pheno	Pheno	*Core*	*Rim*	Pheno	Pheno	Pheno	Pheno	Pheno	Pheno
SiO_2	52.08	52.47	52.35	52.63	52.31	52.13	51.37	50.98	51.43	50.83	46.64	50.74
TiO_2	0.51	0.72	0.68	0.56	0.42	0.49	0.38	0.35	0.60	0.53	0.53	0.70
Al_2O_3	1.02	1.62	1.64	1.09	0.86	0.98	0.81	0.93	1.31	1.22	6.53	1.83
Cr_2O_3	bdl	bdl	0.02	bdl	bdl	0.03	bdl	bdl	bdl	0.01	0.02	bdl
FeO	11.95	8.80	8.85	9.95	12.89	11.46	12.00	11.75	9.68	9.93	11.09	9.48
MnO	1.34	0.77	0.79	1.02	1.58	1.30	1.49	1.47	1.11	1.22	0.87	0.90
MgO	11.51	14.01	13.94	13.43	10.65	11.76	11.08	11.11	13.00	12.69	11.74	13.31
CaO	20.90	20.95	21.19	21.21	20.48	20.54	20.82	20.86	21.30	21.19	18.79	21.00
Na_2O	0.86	0.64	0.64	0.62	1.23	0.81	0.99	0.97	0.75	0.75	0.63	0.67
K_2O	0.03	bdl	bdl	0.01	bdl	bdl	bdl	0.01	0.01	bdl	bdl	bdl
Total	100.20	99.97	100.10	100.52	100.42	99.50	98.89	98.43	99.19	98.37	96.84	98.62
Si	1.964	1.952	1.946	1.959	1.975	1.977	1.964	1.957	1.938	1.935	1.800	1.919
Ti	0.014	0.020	0.019	0.016	0.012	0.014	0.011	0.010	0.017	0.015	0.015	0.020
Al	0.045	0.071	0.072	0.048	0.038	0.044	0.036	0.042	0.058	0.055	0.297	0.082
Cr			0.000			0.001				0.000	0.000	
Fe^{2+}	0.316	0.243	0.231	0.261	0.329	0.331	0.297	0.280	0.219	0.216	0.240	0.210
Fe^{3+}	0.061	0.031	0.044	0.049	0.078	0.033	0.086	0.097	0.086	0.101	0.118	0.090
Mn	0.043	0.024	0.025	0.032	0.051	0.042	0.048	0.048	0.035	0.039	0.028	0.029
Mg	0.647	0.777	0.773	0.745	0.599	0.665	0.632	0.635	0.730	0.720	0.676	0.751
Ca	0.845	0.835	0.844	0.846	0.828	0.835	0.853	0.858	0.860	0.864	0.777	0.851
Na	0.063	0.046	0.046	0.045	0.090	0.059	0.073	0.072	0.055	0.055	0.047	0.049
K	0.001			0.001				0.000	0.000			
Sum	4.000	4.000	4.000	4.000	4.000	4.000	4.000	4.000	4.000	4.000	4.000	4.000
Aegirine	6.1	3.1	4.4	4.5	7.8	3.3	7.3	7.2	5.5	5.5	4.7	4.9
Ferri-Tschermak	0.0	0.0	0.0	0.2	0.0	0.0	0.7	1.2	1.5	2.3	3.5	2.0
Jadeite	0.2	1.6	0.2	0.0	1.2	2.1	0.0	0.0	0.0	0.0	0.0	0.0
Ti-Aegirine	0.0	0.0	0.0	0.0	0.0	0.6	0.0	0.0	0.0	0.0	0.0	0.0
Ti-Tschermak	1.4	2.0	1.9	1.6	1.2	1.1	1.1	1.0	1.7	1.5	1.5	2.0
Al-Tschermak	0.7	0.8	1.6	0.6	0.1	0.0	0.1	0.0	0.0	0.0	9.8	0.1
Diopside	53.0	60.1	60.8	59.0	49.9	52.8	54.0	55.1	61.4	61.0	45.0	61.4
Hedenbergite	29.4	20.7	20.1	23.2	31.6	29.6	29.5	28.4	21.4	21.6	17.9	19.6
Enstatite	5.9	8.8	8.2	7.8	5.0	6.8	4.6	4.2	5.8	5.5	11.3	6.8
Ferrosilite	3.3	3.0	2.7	3.1	3.2	3.8	2.5	2.2	2.0	1.9	4.5	2.2

Table C10 continued

Unit	**Fur J dome**	**Fur J dome**	**Fur J dome**	**Fur J dome**	**Fur J dome**	**Fur J dome**	**Fur J dome**	**Fur J dome**	**Fur J dome**	**Fur J dome**	**Fur J dome**	**Fur J dome**
Sample	SM7-1	SM7-1	SM7-1	SM7-1	SM7-1	SM7-1	SM7-1	SM7-1	SM7-1	SM7-1	SM7-1	SM7-1
No.	73 / 7 .	73 / 8 .	73 / 9 .	73 / 10 .	73 / 11 .	73 / 12 .	73 / 13 .	73 / 14 .	73 / 15 .	73 / 16 .	73 / 17 .	73 / 18 .
Notes	Pheno	Pheno	Pheno	Pheno	Pheno	Pheno	Pheno	Pheno	Pheno	Pheno	Pheno	Pheno
SiO_2	51.32	51.75	51.28	51.48	52.63	51.58	49.65	49.68	50.68	51.80	50.39	51.58
TiO_2	0.63	0.54	0.51	0.52	0.48	0.50	0.48	0.48	0.51	0.53	0.63	0.53
Al_2O_3	1.63	1.10	1.10	1.03	1.14	1.21	3.32	2.98	2.00	1.47	3.59	4.85
Cr_2O_3	bdl	bdl	0.01	bdl	0.02	bdl	bdl	bdl	bdl	bdl	bdl	bdl
FeO	9.96	10.01	10.41	10.60	10.95	10.61	10.27	10.03	10.06	9.79	9.55	9.06
MnO	0.97	1.05	1.08	1.13	1.15	1.11	1.07	1.03	1.05	0.99	0.93	0.88
MgO	13.38	13.16	12.94	12.83	13.00	12.78	12.31	12.22	12.68	13.33	12.70	13.85
CaO	21.05	20.92	21.00	20.88	20.75	20.89	20.14	20.14	20.58	20.93	20.62	20.22
Na_2O	0.69	0.66	0.69	0.65	0.73	0.68	0.65	0.62	0.65	0.65	0.67	0.67
K_2O	bdl	0.01	0.01	0.01	0.01	0.01	0.01	0.01	bdl	bdl	bdl	bdl
Total	99.60	99.18	99.03	99.11	100.85	99.34	97.90	97.15	98.19	99.46	99.08	101.61
Si	1.924	1.952	1.940	1.949	1.958	1.948	1.898	1.915	1.932	1.946	1.898	1.882
Ti	0.018	0.015	0.015	0.015	0.013	0.014	0.014	0.014	0.015	0.015	0.018	0.014
Al	0.072	0.049	0.049	0.046	0.050	0.054	0.150	0.135	0.090	0.065	0.159	0.208
Cr			0.000		0.001							
Fe^{2+}	0.218	0.251	0.237	0.261	0.281	0.261	0.253	0.268	0.256	0.246	0.243	0.231
Fe^{3+}	0.094	0.065	0.093	0.075	0.059	0.074	0.076	0.055	0.065	0.061	0.058	0.045
Mn	0.031	0.034	0.034	0.036	0.036	0.036	0.035	0.034	0.034	0.032	0.030	0.027
Mg	0.748	0.740	0.730	0.724	0.721	0.719	0.702	0.702	0.721	0.746	0.713	0.754
Ca	0.846	0.846	0.851	0.847	0.827	0.845	0.825	0.831	0.841	0.842	0.832	0.791
Na	0.050	0.048	0.051	0.048	0.053	0.050	0.048	0.046	0.048	0.047	0.049	0.047
K		0.000	0.001	0.000	0.000	0.000	0.000	0.001				
Sum	4.000	4.000	4.000	4.000	4.000	4.000	4.000	4.000	4.000	4.000	4.000	4.000
Aegirine	5.0	4.8	5.1	4.8	5.3	5.0	4.8	4.6	4.8	4.7	4.9	4.5
Ferri-Tschermak	2.2	0.8	2.1	1.4	0.3	1.2	1.4	0.5	0.9	0.7	0.4	0.0
Jadeite	0.0	0.0	0.0	0.0	0.0	0.0	0.0	0.0	0.0	0.0	0.0	0.2
Ti-Aegirine	0.0	0.0	0.0	0.0	0.0	0.0	0.0	0.0	0.0	0.0	0.0	0.0
Ti-Tschermak	1.8	1.5	1.5	1.5	1.3	1.4	1.4	1.4	1.5	1.5	1.8	1.4
Al-Tschermak	0.0	0.1	0.0	0.0	0.8	0.1	4.8	5.0	2.2	1.1	5.7	8.9
Diopside	60.5	59.3	59.5	58.1	55.7	57.9	53.2	53.4	56.8	59.0	54.4	51.2
Hedenbergite	20.1	22.8	22.1	23.8	24.5	23.9	21.8	22.9	22.8	22.0	20.8	17.5
Enstatite	7.1	7.4	6.8	7.2	8.2	7.0	8.5	8.4	7.6	7.8	8.5	12.1
Ferrosilite	2.4	2.8	2.5	2.9	3.6	2.9	3.5	3.6	3.1	2.9	3.2	4.1

Table C10 continued

Unit	**Fur J dome**	**Fur J dome**	**Fur J dome**	**Fur J dome**	**Fur J dome**	**Fur J dome**	**Fur J dome**	**Fur J dome**	**Fur J dome**	**Fur J dome**	**Fur J dome**
Sample	SM7-1	SM7-1	SM7-1	SM7-1	SM7-1	SM7-1	SM7-1	SM7-1	SM7-1	SM7-1	SM7-1
No.	73 / 19 .	73 / 20 .	73 / 21 .	73 / 22 .	73 / 23 .	73 / 24 .	73 / 25 .	74 / 1 .	75 / 1 .	76 / 1 .	77 / 1 .
Notes	Pheno	Pheno	Pheno	Pheno	Pheno	Pheno	Pheno	Pheno	Pheno	Pheno	Pheno
SiO_2	51.02	51.10	51.45	51.81	49.27	53.23	51.68	51.94	51.68	51.14	51.65
TiO_2	0.75	0.81	0.37	0.39	0.41	0.46	0.45	0.47	0.37	0.43	0.43
Al_2O_3	1.78	1.89	0.93	0.84	4.06	1.00	0.93	0.99	0.82	0.92	0.86
Cr_2O_3	bdl	0.02	bdl	bdl	bdl	bdl	bdl	bdl	0.02	bdl	0.02
FeO	8.47	8.23	11.67	11.92	11.00	10.98	10.86	10.42	11.80	11.70	11.47
MnO	0.71	0.70	1.47	1.51	1.31	1.30	1.27	1.16	1.53	1.46	1.41
MgO	13.89	13.84	11.24	11.30	11.16	12.72	12.15	12.75	11.42	11.07	11.70
CaO	21.39	21.50	20.87	20.81	20.36	20.80	21.01	21.12	20.96	21.12	20.90
Na_2O	0.66	0.66	0.96	1.04	0.81	0.84	0.79	0.69	0.94	1.04	0.98
K_2O	bdl	bdl	bdl	bdl	bdl	bdl	bdl	bdl	bdl	bdl	bdl
Total	98.67	98.75	98.94	99.60	98.36	101.29	99.14	99.51	99.53	98.86	99.43
Si	1.920	1.921	1.964	1.965	1.883	1.974	1.961	1.958	1.961	1.954	1.958
Ti	0.021	0.023	0.011	0.011	0.012	0.013	0.013	0.013	0.011	0.012	0.012
Al	0.079	0.084	0.042	0.038	0.183	0.044	0.041	0.044	0.037	0.041	0.039
Cr		0.001							0.000		0.001
Fe^{2+}	0.180	0.183	0.291	0.290	0.264	0.296	0.276	0.264	0.287	0.271	0.270
Fe^{3+}	0.086	0.075	0.081	0.088	0.088	0.045	0.069	0.065	0.088	0.103	0.093
Mn	0.022	0.022	0.047	0.049	0.042	0.041	0.041	0.037	0.049	0.047	0.045
Mg	0.779	0.776	0.640	0.639	0.636	0.703	0.687	0.717	0.646	0.630	0.661
Ca	0.863	0.866	0.854	0.845	0.834	0.826	0.854	0.853	0.852	0.865	0.849
Na	0.048	0.048	0.071	0.077	0.060	0.060	0.058	0.051	0.069	0.077	0.072
K											
Sum	4.000	4.000	4.000	4.000	4.000	4.000	4.000	4.000	4.000	4.000	4.000
Aegirine	4.8	4.8	7.1	7.7	6.0	4.5	5.8	5.1	6.9	7.7	7.2
Ferri-Tschermak	1.9	1.4	0.5	0.6	1.4	0.0	0.6	0.7	0.9	1.3	1.1
Jadeite	0.0	0.0	0.0	0.0	0.0	1.5	0.0	0.0	0.0	0.0	0.0
Ti-Aegirine	0.0	0.0	0.0	0.0	0.0	0.0	0.0	0.0	0.0	0.0	0.0
Ti-Tschermak	2.1	2.3	1.1	1.1	1.2	1.3	1.3	1.3	1.1	1.2	1.2
Al-Tschermak	0.0	0.5	0.5	0.2	6.6	0.1	0.2	0.2	0.0	0.0	0.0
Diopside	65.3	65.2	54.4	54.0	50.1	55.0	57.1	58.5	54.7	55.7	55.9
Hedenbergite	17.0	17.3	28.8	28.6	24.1	26.3	26.3	24.6	28.5	28.2	26.7
Enstatite	6.3	6.2	4.8	4.9	6.7	7.7	5.8	6.6	4.9	3.6	5.1
Ferrosilite	1.6	1.6	2.5	2.6	3.2	3.7	2.7	2.8	2.6	1.8	2.4

Table C10 continued

Unit	**Fur I**	**Fur I**	**Fur I**	**Fur I**	**Fur I**	**Fur I**	**Fur I**	**Fur I**	**Fur I**	**Fur I**
Sample	FM-1(2)	FM-1(2)	FM-1(2)	FM-1(2)	FM-1(2)	FM-1(2)	FM-1(2)	FM-1(2)	FM-1(2)	FM-1(2)
No.	Px1	Px2	Px3	Px4	Px5	Px6	Px7	Px8	Px9	Px10
Notes	Pheno	Pheno	Pheno	Pheno	Pheno	Pheno	Pheno	Pheno	Pheno	Pheno
SiO_2	52.20	52.97	51.69	52.65	52.47	53.15	52.34	52.83	52.74	52.37
TiO_2	0.38	0.44	0.77	0.45	0.49	0.41	0.48	0.40	0.39	0.48
Al_2O_3	0.86	0.84	1.32	0.93	0.82	0.78	0.95	0.70	0.69	0.85
Cr_2O_3	bdl	bdl	bdl	0.01	bdl	0.02	0.05	bdl	bdl	bdl
FeO	12.25	11.39	12.67	10.92	11.95	11.65	12.14	11.32	11.50	11.72
MnO	1.57	1.50	1.66	1.37	1.54	1.47	1.58	1.39	1.55	1.61
MgO	10.66	11.52	10.87	11.91	11.21	11.71	11.14	12.29	11.78	11.33
CaO	21.13	21.45	20.20	21.02	21.10	21.48	20.42	21.49	21.24	21.12
Na_2O	1.11	1.02	1.27	0.84	1.06	1.02	1.17	0.80	0.98	1.11
K_2O	bdl	bdl	bdl	0.01	0.01	bdl	bdl	bdl	bdl	bdl
Total	100.16	101.12	100.45	100.12	100.65	101.69	100.26	101.22	100.87	100.59
Si	1.974	1.976	1.948	1.981	1.971	1.972	1.973	1.966	1.972	1.966
Ti	0.011	0.012	0.022	0.013	0.014	0.011	0.014	0.011	0.011	0.014
Al	0.038	0.037	0.059	0.041	0.036	0.034	0.042	0.031	0.030	0.038
Cr				0.000		0.001	0.001			
Fe^{2+}	0.315	0.296	0.306	0.311	0.303	0.289	0.314	0.279	0.285	0.283
Fe^{3+}	0.072	0.059	0.094	0.032	0.072	0.072	0.068	0.074	0.075	0.084
Mn	0.050	0.047	0.053	0.044	0.049	0.046	0.050	0.044	0.049	0.051
Mg	0.601	0.641	0.611	0.668	0.628	0.648	0.626	0.682	0.657	0.634
Ca	0.856	0.857	0.816	0.847	0.849	0.854	0.825	0.857	0.851	0.849
Na	0.081	0.073	0.092	0.061	0.077	0.073	0.086	0.058	0.071	0.081
K				0.001	0.001					
Sum	4.000	4.000	4.000	4.000	4.000	4.000	4.000	4.000	4.000	4.000
Aegirine	7.2	5.9	9.2	3.2	7.2	7.2	6.8	5.8	7.1	8.1
Ferri-Tschermak	0.0	0.0	0.1	0.0	0.0	0.0	0.0	0.8	0.2	0.2
Jadeite	0.9	1.3	0.0	2.2	0.5	0.1	1.5	0.0	0.0	0.0
Ti-Aegirine	0.0	0.1	0.0	0.6	0.0	0.0	0.2	0.0	0.0	0.0
Ti-Tschermak	1.1	1.2	2.2	1.0	1.4	1.1	1.3	1.1	1.1	1.4
Al-Tschermak	0.4	0.0	0.7	0.0	0.2	0.5	0.0	0.0	0.2	0.3
Diopside	52.3	55.1	49.5	54.7	53.4	55.2	51.3	56.9	55.4	54.4
Hedenbergite	31.8	29.5	29.1	29.1	30.0	28.6	29.9	26.9	28.2	28.7
Enstatite	3.9	4.5	5.8	5.9	4.7	4.8	5.6	5.6	5.1	4.5
Ferrosilite	2.4	2.4	3.4	3.2	2.6	2.5	3.3	2.7	2.6	2.4

Table C10 continued

Unit	**Fur I**	**Fur I**	**Fur I**	**Fur I**	**Fur I**	**Fur I**	**Fur I**	**Fur I**	**Fur I**	**Fur I**
Sample	FM-2(2)	FM-2(2)	FM-2(2)	FM-2(2)	FM-2(2)	FM-2(2)	FM-2(2)	FM-2(2)	FM-2(2)	FM-2(2)
No.	Px1	Px2	Px3	Px4	Px5	Px6	Px7	Px8	Px9	Px10
Notes	Pheno	Pheno	Pheno	Pheno	Pheno	Pheno	Pheno	Pheno	Pheno	Pheno
SiO_2	52.67	52.48	52.17	52.53	51.69	51.69	51.63	52.26	52.04	52.34
TiO_2	0.40	0.35	0.52	0.39	0.47	0.59	0.49	0.48	0.65	0.43
Al_2O_3	0.67	0.78	1.16	0.64	0.82	1.08	0.94	0.89	1.13	0.80
Cr_2O_3	bdl	bdl	bdl	bdl	0.02	bdl	0.03	0.03	bdl	bdl
FeO	11.84	11.49	12.32	11.66	12.42	12.38	12.22	11.62	11.98	11.92
MnO	1.60	1.52	1.57	1.53	1.51	1.64	1.58	1.43	1.54	1.52
MgO	11.07	11.41	11.26	11.38	10.82	11.07	11.06	11.38	11.37	11.20
CaO	21.18	20.98	20.94	21.45	21.21	20.34	21.00	21.18	20.91	20.86
Na_2O	0.90	1.05	1.17	0.93	1.19	1.19	1.22	1.13	1.11	1.19
K_2O	0.01	bdl	bdl	0.01	0.01	bdl	bdl	bdl	bdl	0.03
Total	100.33	100.05	101.11	100.52	100.16	99.98	100.17	100.40	100.73	100.29
Si	1.988	1.979	1.949	1.975	1.953	1.955	1.948	1.963	1.951	1.970
Ti	0.011	0.010	0.015	0.011	0.013	0.017	0.014	0.013	0.018	0.012
Al	0.030	0.035	0.051	0.028	0.037	0.048	0.042	0.039	0.050	0.035
Cr					0.000		0.001	0.001		
Fe^{2+}	0.337	0.298	0.279	0.299	0.276	0.297	0.262	0.277	0.284	0.288
Fe^{3+}	0.037	0.065	0.106	0.068	0.117	0.095	0.123	0.088	0.092	0.087
Mn	0.051	0.049	0.050	0.049	0.048	0.053	0.050	0.046	0.049	0.048
Mg	0.623	0.641	0.627	0.638	0.609	0.624	0.622	0.637	0.636	0.629
Ca	0.857	0.848	0.838	0.864	0.859	0.824	0.849	0.853	0.840	0.841
Na	0.066	0.077	0.085	0.068	0.087	0.087	0.089	0.082	0.081	0.087
K	0.000			0.000	0.000					0.001
Sum	4.000	4.000	4.000	4.000	4.000	4.000	4.000	4.000	4.000	4.000
Aegirine	3.7	6.5	8.5	6.8	8.7	8.7	8.9	8.2	8.1	8.7
Ferri-Tschermak	0.0	0.0	1.0	0.0	1.5	0.4	1.7	0.3	0.6	0.0
Jadeite	1.8	1.2	0.0	0.0	0.0	0.0	0.0	0.0	0.0	0.0
Ti-Aegirine	1.1	0.0	0.0	0.0	0.0	0.0	0.0	0.0	0.0	0.0
Ti-Tschermak	0.6	1.0	1.5	1.1	1.3	1.7	1.4	1.3	1.8	1.2
Al-Tschermak	0.0	0.1	0.0	0.3	0.0	0.3	0.0	0.3	0.1	0.5
Diopside	52.4	54.3	53.3	55.0	54.2	51.3	54.4	55.3	53.5	53.7
Hedenbergite	32.6	29.3	28.0	30.0	28.8	28.7	27.3	28.0	28.0	28.7
Enstatite	4.8	4.9	4.7	4.4	3.4	5.6	3.9	4.2	5.0	4.6
Ferrosilite	3.0	2.7	2.5	2.4	1.8	3.1	2.0	2.1	2.6	2.5

Table C10 continued

Unit	Fur I dome	Fur I dome	Fur I dome	Fur I dome	Fur I dome	Fur I dome	Fur I dome	Fur I dome	Fur I dome	Fur I dome	Fur I dome	Fur I dome
Sample	SM 5-1	SM 5-1	SM 5-1	SM 5-1	SM 5-1	SM 5-1	SM 5-1	SM5-1	SM5-1	SM5-1	SM5-1	SM5-1
No.	Clino10	Clino11	Clino12	Clino13	Clino14	Clino15	Clino15	53 / 1 .	54 / 1 .	55 / 1 .	56 / 1 .	57 / 1 .
Notes	Pheno	Pheno	Pheno	Pheno	Pheno	Core	Rim	Pheno	Pheno	Pheno	Gm	Pheno
SiO_2	52.63	51.83	51.64	52.32	51.90	52.43	52.88	51.14	50.74	50.24	50.52	51.27
TiO_2	0.53	0.46	0.60	0.36	0.49	0.42	0.51	0.54	0.85	0.84	1.50	0.43
Al_2O_3	1.14	1.01	1.16	0.85	0.94	0.86	0.69	0.68	0.97	0.94	1.05	0.87
Cr_2O_3	bdl	bdl	bdl	0.01	bdl	bdl	0.04	bdl	bdl	bdl	bdl	0.02
FeO	9.80	13.11	12.45	11.53	13.39	11.96	11.69	13.89	13.68	13.62	22.30	12.09
MnO	0.93	1.65	1.61	1.21	1.74	1.52	1.54	1.74	1.71	1.68	1.77	1.54
MgO	13.44	10.73	10.94	12.09	10.28	11.60	11.88	9.67	10.14	9.98	5.75	11.11
CaO	21.25	20.43	20.39	21.00	20.12	20.62	20.47	19.46	18.11	19.16	5.19	20.66
Na_2O	0.63	1.25	1.22	0.67	1.24	1.07	1.34	1.95	2.42	1.97	7.92	1.12
K_2O	bdl	bdl	0.01	bdl	0.01	bdl	0.02	0.01	0.03	bdl	0.61	0.01
Total	100.34	100.47	100.02	100.04	100.11	100.47	101.05	99.07	98.65	98.43	96.63	99.12
Si	1.961	1.955	1.953	1.973	1.971	1.969	1.969	1.958	1.939	1.932	1.956	1.954
Ti	0.015	0.013	0.017	0.010	0.014	0.012	0.014	0.015	0.024	0.024	0.044	0.012
Al	0.050	0.045	0.052	0.038	0.042	0.038	0.030	0.031	0.044	0.043	0.048	0.039
Cr				0.000			0.001					0.000
Fe^{2+}	0.261	0.303	0.296	0.318	0.345	0.298	0.264	0.277	0.227	0.246	0.145	0.275
Fe^{3+}	0.044	0.111	0.098	0.046	0.080	0.078	0.100	0.168	0.210	0.192	0.577	0.111
Mn	0.029	0.053	0.052	0.039	0.056	0.048	0.049	0.056	0.055	0.055	0.058	0.050
Mg	0.746	0.603	0.617	0.680	0.582	0.649	0.659	0.552	0.578	0.572	0.332	0.632
Ca	0.848	0.826	0.826	0.848	0.819	0.830	0.816	0.798	0.741	0.789	0.215	0.844
Na	0.045	0.092	0.089	0.049	0.091	0.078	0.097	0.144	0.180	0.147	0.594	0.083
K			0.000		0.000		0.001	0.000	0.001		0.030	0.001
Sum	4.000	4.000	4.000	4.000	4.000	4.000	4.000	4.000	4.000	4.000	4.000	4.000
Aegirine	4.4	9.2	8.9	4.6	8.0	7.8	9.7	14.4	18.0	14.7	57.7	8.3
Ferri-Tschermak	0.0	1.0	0.4	0.0	0.0	0.0	0.2	1.2	1.5	2.3	0.0	1.4
Jadeite	0.1	0.0	0.0	0.4	1.1	0.0	0.0	0.0	0.0	0.0	0.4	0.0
Ti-Aegirine	0.0	0.0	0.0	0.0	0.0	0.0	0.0	0.0	0.0	0.0	1.3	0.0
Ti-Tschermak	1.5	1.3	1.7	1.0	1.4	1.2	1.4	1.5	2.2	2.1	2.2	1.2
Al-Tschermak	1.0	0.0	0.5	0.6	0.2	0.7	0.0	0.0	0.0	0.0	0.0	0.0
Diopside	59.3	50.5	51.2	54.5	47.5	52.9	54.3	48.1	47.3	48.9	12.0	54.0
Hedenbergite	23.1	29.8	28.8	28.6	32.8	28.2	25.7	29.0	23.1	25.7	7.3	27.7
Enstatite	7.7	4.9	5.2	6.7	5.3	6.0	5.8	3.6	5.2	4.2	10.4	4.6
Ferrosilite	3.0	2.9	2.9	3.5	3.7	3.2	2.8	2.1	2.6	2.2	6.4	2.4

Table C10 continued

Unit	Fur I dome	Fur I dome	Fur I dome	Fur I dome	Fur I dome	Fur I dome	Fur I dome	Fur I dome	Fur I dome	Fur I dome	Fur I dome	Fur I dome
Sample	SM5-1	SM5-1	SM5-1	SM5-1	SM5-1	SM5-1	SM5-1	SM5-1	SM5-1	SM5-1	SM5-1	SM5-1
No.	58 / 1 .	59 / 1 .	60 / 1 .	61 / 1 .	62 / 1 .	63 / 1 .	65 / 1 .	66 / 1 .	67 / 1 .	68 / 1 .	70 / 1 .	71 / 1 .
Notes	Pheno	Pheno	Pheno	Pheno	Pheno	Pheno	Pheno	Pheno	Pheno	Pheno	Pheno	Gm
SiO_2	51.37	50.85	50.85	51.56	51.84	51.20	51.12	51.50	51.01	51.70	50.74	49.67
TiO_2	0.40	0.70	0.42	0.42	0.33	0.50	0.40	0.37	0.52	0.34	0.81	0.65
Al_2O_3	0.84	0.89	0.85	0.82	0.81	0.68	0.90	0.82	1.03	0.61	0.80	0.73
Cr_2O_3	bdl	bdl	bdl	0.01	0.02	bdl	bdl	bdl	bdl	bdl	bdl	bdl
FeO	11.87	13.57	12.26	12.21	11.62	13.97	10.72	12.33	13.10	12.05	13.85	18.31
MnO	1.54	1.66	1.55	1.48	1.45	1.64	1.21	1.56	1.55	1.70	1.66	1.70
MgO	11.04	9.93	10.95	10.91	11.48	9.69	12.24	11.14	10.15	11.21	9.70	5.92
CaO	20.82	18.97	20.65	20.88	20.92	19.30	21.19	20.86	20.74	21.09	18.72	16.90
Na_2O	1.14	2.14	1.08	1.05	1.01	2.00	0.74	1.08	1.10	0.98	2.18	3.43
K_2O	bdl	0.02	bdl	bdl	bdl	bdl	bdl	bdl	bdl	bdl	0.06	bdl
Total	99.01	98.73	98.59	99.34	99.47	98.97	98.50	99.66	99.21	99.65	98.52	97.32
Si	1.960	1.947	1.951	1.964	1.966	1.961	1.951	1.954	1.955	1.963	1.949	1.960
Ti	0.012	0.020	0.012	0.012	0.009	0.015	0.012	0.011	0.015	0.010	0.023	0.019
Al	0.038	0.040	0.038	0.037	0.036	0.031	0.040	0.037	0.047	0.027	0.036	0.034
Cr				0.000	0.001							
Fe^{2+}	0.275	0.248	0.278	0.302	0.281	0.281	0.252	0.278	0.324	0.283	0.262	0.335
Fe^{3+}	0.104	0.186	0.115	0.087	0.087	0.166	0.090	0.113	0.096	0.100	0.183	0.269
Mn	0.050	0.054	0.050	0.048	0.047	0.053	0.039	0.050	0.050	0.055	0.054	0.057
Mg	0.628	0.567	0.626	0.620	0.649	0.553	0.696	0.630	0.580	0.634	0.556	0.348
Ca	0.851	0.778	0.849	0.852	0.850	0.792	0.866	0.848	0.852	0.858	0.771	0.715
Na	0.084	0.159	0.080	0.077	0.074	0.148	0.055	0.079	0.082	0.072	0.162	0.262
K		0.001									0.003	
Sum	4.000	4.000	4.000	4.000	4.000	4.000	4.000	4.000	4.000	4.000	4.000	4.000
Aegirine	8.4	15.9	8.0	7.7	7.4	14.8	5.5	7.9	8.2	7.2	16.2	26.2
Ferri-Tschermak	1.0	1.4	1.7	0.5	0.7	0.9	1.7	1.7	0.7	1.4	1.0	0.3
Jadeite	0.0	0.0	0.0	0.0	0.0	0.0	0.0	0.0	0.0	0.0	0.0	0.0
Ti-Aegirine	0.0	0.0	0.0	0.0	0.0	0.0	0.0	0.0	0.0	0.0	0.0	0.0
Ti-Tschermak	1.2	2.0	1.2	1.2	0.9	1.5	1.2	1.1	1.5	1.0	1.8	1.7
Al-Tschermak	0.0	0.0	0.0	0.1	0.2	0.0	0.0	0.0	0.1	0.0	0.0	0.0
Diopside	54.7	48.6	53.7	53.3	55.3	47.9	59.0	53.9	50.3	54.5	47.3	32.7
Hedenbergite	28.3	25.9	28.2	30.1	27.9	28.9	24.7	28.1	32.5	29.0	26.9	36.7
Enstatite	4.0	4.0	4.4	4.3	4.8	3.7	5.3	4.5	3.8	4.5	4.1	1.1
Ferrosilite	2.1	2.2	2.3	2.4	2.4	2.2	2.2	2.4	2.5	2.4	2.4	1.2

Table C10 continued

Unit	**Fur H**	**Fur H**	**Fur H**	**Fur H**	**Fur H**	**Fur H**	**Fur H**	**Fur H**	**Fur H**	**Fur H**
Sample	FM-1(3)	FM-1(3)	FM-1(3)	FM-1(3)	FM-1(3)	FM-1(3)	FM-1(3)	FM-1(3)	FM-1(3)	FM-1(3)
No.	Px1	Px2	Px3	Px4	Px5	Px6	Px7	Px8	Px9	Px10
Notes	Pheno	Pheno	Pheno	Pheno	Pheno	Pheno	Pheno	Pheno	Pheno	Pheno
SiO_2	52.19	52.98	52.42	53.04	52.04	52.16	52.17	52.45	52.10	52.05
TiO_2	0.40	0.35	0.40	0.40	0.49	0.40	0.47	0.49	0.50	0.47
Al_2O_3	0.82	0.64	0.92	0.82	0.93	0.85	0.86	0.93	1.10	2.49
Cr_2O_3	0.03	bdl	0.01	bdl	bdl	0.03	0.01	bdl	bdl	0.01
FeO	12.31	11.43	12.23	12.26	12.60	11.89	12.13	11.63	11.58	8.95
MnO	1.50	1.46	1.54	1.56	1.62	1.52	1.53	1.40	1.36	0.54
MgO	10.89	11.54	11.05	11.22	10.93	11.18	10.93	11.58	11.79	14.64
CaO	21.04	21.54	21.06	21.42	21.02	21.03	20.97	21.20	21.14	20.69
Na_2O	1.05	0.95	1.14	1.13	1.11	1.08	1.10	0.87	0.93	0.38
K_2O	0.02	0.01	0.01	0.01	0.01	bdl	bdl	bdl	bdl	bdl
Total	100.25	100.90	100.78	101.86	100.76	100.14	100.16	100.54	100.50	100.22
Si	1.972	1.982	1.967	1.969	1.956	1.968	1.971	1.970	1.954	1.928
Ti	0.011	0.010	0.011	0.011	0.014	0.011	0.013	0.014	0.014	0.013
Al	0.037	0.028	0.041	0.036	0.041	0.038	0.038	0.041	0.049	0.109
Cr	0.001		0.000			0.001	0.000			0.000
Fe^{2+}	0.315	0.300	0.296	0.294	0.296	0.294	0.310	0.311	0.281	0.240
Fe^{3+}	0.074	0.058	0.087	0.087	0.100	0.081	0.073	0.054	0.083	0.037
Mn	0.048	0.046	0.049	0.049	0.052	0.049	0.049	0.045	0.043	0.017
Mg	0.613	0.644	0.618	0.621	0.613	0.629	0.616	0.648	0.659	0.808
Ca	0.852	0.863	0.847	0.852	0.847	0.850	0.849	0.853	0.850	0.821
Na	0.077	0.069	0.083	0.082	0.081	0.079	0.080	0.063	0.068	0.027
K	0.001	0.000	0.001	0.000	0.001					
Sum	4.000	4.000	4.000	4.000	4.000	4.000	4.000	4.000	4.000	4.000
Aegirine	7.4	5.8	8.3	8.2	8.1	7.9	7.3	5.4	6.8	2.7
Ferri-Tschermak	0.0	0.0	0.2	0.3	0.9	0.1	0.0	0.0	0.7	0.5
Jadeite	0.3	1.0	0.0	0.0	0.0	0.0	0.7	0.9	0.0	0.0
Ti-Aegirine	0.0	0.1	0.0	0.0	0.0	0.0	0.0	0.0	0.0	0.0
Ti-Tschermak	1.1	0.9	1.1	1.1	1.4	1.1	1.3	1.4	1.4	1.3
Al-Tschermak	0.5	0.0	0.7	0.4	0.0	0.6	0.2	0.2	0.3	3.6
Diopside	52.4	55.5	53.0	53.7	52.5	53.8	52.6	54.1	55.3	58.2
Hedenbergite	31.0	29.9	29.6	29.7	29.8	29.3	30.7	29.7	27.2	18.5
Enstatite	4.4	4.4	4.4	4.2	4.4	4.5	4.5	5.4	5.3	11.3
Ferrosilite	2.6	2.4	2.5	2.3	2.5	2.5	2.6	3.0	2.6	3.6

Table C10 continued

Unit	**Fur H**	**Fur H**	**Fur H**	**Fur H**	**Fur H**	**Fur H**	**Fur H**	**Fur H**	**Fur H**	**Fur H**
Sample	FM-2(3)	FM-2(3)	FM-2(3)	FM-2(3)	FM-2(3)	FM-2(3)	FM-2(3)	FM-2(3)	FM-2(3)	FM-2(3)
No.	Px1	Px2	Px3	Px4	Px5	Px6	Px7	Px8	Px9	Px10
Notes	Pheno	Pheno	Pheno	Pheno	Pheno	Pheno	Pheno	Pheno	Pheno	Pheno
SiO_2	52.34	52.69	52.37	52.32	52.90	52.46	52.62	52.30	52.35	51.39
TiO_2	0.41	0.36	0.38	0.44	0.42	0.30	0.37	0.31	0.52	0.61
Al_2O_3	0.76	0.60	0.75	0.87	0.71	0.80	0.71	0.69	0.99	1.05
Cr_2O_3	0.01	bdl	0.01	bdl	bdl	0.01	bdl	0.02	bdl	0.01
FeO	12.37	12.41	12.29	12.48	11.99	11.55	11.29	12.07	13.06	12.92
MnO	1.54	1.70	1.53	1.54	1.44	1.48	1.46	1.56	1.64	1.65
MgO	10.64	11.11	10.69	10.96	11.65	11.75	11.85	11.02	10.57	10.52
CaO	21.05	21.30	21.24	21.01	21.30	21.34	21.64	21.44	20.61	20.76
Na_2O	0.99	0.89	1.12	1.20	0.74	1.00	0.78	0.96	1.22	1.16
K_2O	bdl	bdl	bdl	bdl	bdl	0.02	bdl	bdl	bdl	0.02
Total	100.12	101.06	100.38	100.81	101.16	100.70	100.72	100.36	100.97	100.09
Si	1.984	1.977	1.976	1.964	1.979	1.963	1.971	1.973	1.967	1.949
Ti	0.012	0.010	0.011	0.012	0.012	0.008	0.010	0.009	0.015	0.017
Al	0.034	0.027	0.033	0.038	0.031	0.035	0.031	0.031	0.044	0.047
Cr	0.000		0.000			0.000		0.001		0.000
Fe^{2+}	0.344	0.326	0.314	0.295	0.335	0.267	0.292	0.304	0.329	0.303
Fe^{3+}	0.048	0.063	0.074	0.097	0.040	0.094	0.062	0.076	0.081	0.107
Mn	0.049	0.054	0.049	0.049	0.046	0.047	0.046	0.050	0.052	0.053
Mg	0.601	0.622	0.601	0.613	0.650	0.656	0.662	0.620	0.592	0.595
Ca	0.855	0.856	0.859	0.845	0.854	0.856	0.869	0.867	0.830	0.843
Na	0.073	0.064	0.082	0.087	0.054	0.072	0.056	0.070	0.089	0.085
K						0.001				0.001
Sum	4.000	4.000	4.000	4.000	4.000	4.000	4.000	4.000	4.000	4.000
Aegirine	4.8	6.3	7.4	8.7	4.0	7.2	5.6	7.0	8.1	8.5
Ferri-Tschermak	0.0	0.0	0.0	0.5	0.0	1.1	0.3	0.3	0.0	1.1
Jadeite	1.7	0.1	0.8	0.0	1.0	0.0	0.0	0.0	0.8	0.0
Ti-Aegirine	0.7	0.0	0.0	0.0	0.3	0.0	0.0	0.0	0.0	0.0
Ti-Tschermak	0.8	1.0	1.1	1.2	1.1	0.8	1.0	0.9	1.5	1.7
Al-Tschermak	0.0	0.2	0.2	0.2	0.0	0.0	0.3	0.3	0.3	0.0
Diopside	51.2	52.3	52.8	52.9	53.2	56.5	56.4	54.2	49.4	51.0
Hedenbergite	33.5	32.0	31.8	29.7	31.1	27.1	28.8	31.0	31.8	30.5
Enstatite	4.4	4.9	3.7	4.2	5.8	4.5	4.9	3.9	4.9	4.2
Ferrosilite	2.8	3.0	2.2	2.4	3.4	2.2	2.5	2.2	3.2	2.5

Table C10 continued

Unit	**Fur G**	**Fur G**	**Fur G**	**Fur G**	**Fur G**	**Fur G**	**Fur G**	**Fur G**	**Fur G**	**Fur G**	**Fur G**	**Fur G**	**Fur G**	**Fur G**
Sample	FM-1(4)	FM-1(4)	FM-1(4)	FM-1(4)	FM-1(4)	FM-1(4)	FM-1(4)	FM-1(4)	FM-2(4)	FM-2(4)	FM-2(4)	FM-2(4)	FM-2(4)	FM-2(4)
No.	Px1	Px2	Px3	Px4	Px5	Px7	Px8	Px9	Px1	Px2	Px3	Px4	Px5	Px6
Notes	Pheno	Pheno	Pheno	Pheno	Pheno	Pheno	Pheno	Pheno	Pheno	Pheno	Pheno	Pheno	Pheno	Pheno
SiO_2	52.62	52.09	51.92	51.72	52.00	52.27	45.64	45.57	50.34	52.05	49.76	52.80	50.81	50.57
TiO_2	0.48	0.37	0.51	0.69	0.39	0.36	3.51	3.26	1.25	0.35	1.81	0.40	0.87	1.13
Al_2O_3	0.85	0.92	1.21	1.38	0.65	0.76	7.27	6.66	3.05	0.95	4.33	0.78	1.66	2.77
Cr_2O_3	0.02	0.02	0.01	0.02	bdl	bdl	0.06	0.01	bdl	bdl	bdl	0.02	0.01	0.01
FeO	10.78	12.87	11.95	10.02	13.91	14.39	8.53	8.32	8.57	13.06	7.59	11.87	11.87	7.54
MnO	1.30	1.58	1.14	1.09	1.52	1.60	0.14	0.17	0.47	1.63	0.25	1.52	1.30	0.36
MgO	11.66	10.23	11.33	12.07	9.68	9.65	12.42	12.45	13.08	10.24	14.15	11.15	10.85	14.13
CaO	22.18	20.78	21.80	21.93	21.71	21.08	22.03	22.60	22.32	20.49	22.32	21.31	21.07	22.10
Na_2O	0.88	1.67	0.85	0.87	0.98	1.03	0.51	0.41	0.61	1.49	0.51	1.03	1.05	0.58
K_2O	bdl	bdl	0.02	0.01	bdl	0.03	0.01	0.02	0.01	bdl	bdl	0.01	0.01	0.01
Total	100.76	100.53	100.74	99.80	100.85	101.17	100.11	99.48	99.70	100.26	100.72	100.89	99.50	99.20
Si	1.968	1.960	1.948	1.945	1.970	1.976	1.702	1.710	1.881	1.967	1.830	1.979	1.931	1.887
Ti	0.013	0.010	0.014	0.020	0.011	0.010	0.098	0.092	0.035	0.010	0.050	0.011	0.025	0.032
Al	0.037	0.041	0.053	0.061	0.029	0.034	0.320	0.295	0.134	0.042	0.188	0.034	0.074	0.122
Cr	0.001	0.001	0.000	0.000			0.002	0.000				0.001	0.000	0.000
Fe^{2+}	0.274	0.265	0.290	0.242	0.360	0.384	0.151	0.129	0.189	0.300	0.144	0.313	0.285	0.153
Fe^{3+}	0.063	0.140	0.084	0.074	0.081	0.070	0.115	0.132	0.078	0.113	0.090	0.059	0.092	0.082
Mn	0.041	0.050	0.036	0.035	0.049	0.051	0.004	0.006	0.015	0.052	0.008	0.048	0.042	0.011
Mg	0.650	0.574	0.634	0.677	0.547	0.544	0.691	0.697	0.729	0.577	0.776	0.623	0.615	0.786
Ca	0.889	0.838	0.876	0.884	0.881	0.854	0.880	0.909	0.894	0.830	0.879	0.856	0.858	0.884
Na	0.064	0.122	0.062	0.064	0.072	0.075	0.037	0.030	0.044	0.109	0.037	0.075	0.078	0.042
K			0.001	0.000		0.001	0.000	0.001	0.001			0.000	0.000	0.000
Sum	4.000	4.000	4.000	4.000	4.000	4.000	4.000	4.000	4.000	4.000	4.000	4.000	4.000	4.000
Aegirine	6.3	12.2	6.2	6.4	7.2	7.0	3.7	3.0	4.4	10.9	3.7	5.9	7.8	4.2
Ferri-Tschermak	0.0	0.9	1.1	0.5	0.4	0.0	3.9	5.1	1.7	0.2	2.7	0.0	0.7	2.0
Jadeite	0.1	0.0	0.0	0.0	0.0	0.5	0.0	0.0	0.0	0.0	0.0	1.4	0.0	0.0
Ti-Aegirine	0.0	0.0	0.0	0.0	0.0	0.0	0.0	0.0	0.0	0.0	0.0	0.2	0.0	0.0
Ti-Tschermak	1.3	1.0	1.4	2.0	1.1	1.0	9.8	9.2	3.5	1.0	5.0	1.0	2.5	3.2
Al-Tschermak	0.4	0.0	0.1	0.6	0.0	0.4	2.2	0.5	1.5	0.9	1.7	0.0	0.5	0.9
Diopside	58.6	52.8	56.0	60.6	49.5	46.6	58.9	63.8	64.5	50.2	65.7	53.5	53.6	68.0
Hedenbergite	28.4	29.0	28.9	24.7	37.1	37.3	13.3	12.4	18.1	30.6	12.8	31.0	28.5	14.2
Enstatite	3.2	2.3	3.7	3.5	2.6	3.9	5.1	2.9	4.2	3.7	5.9	4.4	4.0	5.3
Ferrosilite	1.5	1.3	1.9	1.4	1.9	3.1	1.1	0.6	1.2	2.3	1.2	2.5	2.1	1.1

Table C10 continued

Unit	**Fur F**	**Fur F**	**Fur F**	**Fur F**	**Fur F**	**Fur F**	**Fur F**	**Fur F**	**Fur F**	**Fur F**	**Fur F**
Sample	FM-1(5)	FM-1(5)	FM-1(5)	FM-1(5)	FM-1(5)	FM-1(5)	FM-1(5)	FM-1(5)	FM-1(5)	FM-1(5)	FM-1(5)
No.	Px1	Px2	Px3	Px4	Px5	Px6	Px7	Px8	Px9	Px10	Px11
Notes	Pheno	Pheno	Pheno	Pheno	Pheno	Pheno	Pheno	Pheno	Pheno	Pheno	Pheno
SiO_2	52.30	52.52	52.72	52.51	52.52	51.77	52.55	52.42	52.59	52.16	44.14
TiO_2	0.39	0.40	0.41	0.39	0.38	0.53	0.44	0.33	0.39	0.48	3.85
Al_2O_3	0.85	0.86	0.67	0.80	0.62	1.08	0.79	0.77	0.83	0.88	8.88
Cr_2O_3	bdl	bdl	bdl	bdl	bdl	bdl	bdl	bdl	bdl	bdl	0.03
FeO	12.13	12.13	11.90	12.29	12.35	13.01	12.42	12.27	11.77	12.06	8.50
MnO	1.51	1.56	1.59	1.59	1.66	1.67	1.53	1.59	1.43	1.54	0.10
MgO	11.05	11.19	11.28	11.03	10.95	10.45	10.85	11.16	10.98	11.22	11.53
CaO	20.94	21.21	21.33	21.03	21.33	20.71	21.11	21.16	21.22	20.91	22.39
Na_2O	1.01	1.24	1.01	1.11	0.97	1.31	1.18	0.99	0.98	1.11	0.47
K_2O	0.01	bdl	0.02	bdl	bdl	bdl	bdl	bdl	bdl	0.01	0.01
Total	100.19	101.11	100.93	100.75	100.78	100.53	100.87	100.70	100.19	100.37	99.90
Si	1.976	1.961	1.975	1.972	1.976	1.953	1.972	1.970	1.986	1.964	1.653
Ti	0.011	0.011	0.011	0.011	0.011	0.015	0.012	0.009	0.011	0.013	0.108
Al	0.038	0.038	0.030	0.035	0.028	0.048	0.035	0.034	0.037	0.039	0.392
Cr											0.001
Fe^{2+}	0.320	0.272	0.301	0.307	0.318	0.298	0.308	0.307	0.331	0.292	0.147
Fe^{3+}	0.064	0.107	0.072	0.079	0.070	0.113	0.082	0.079	0.041	0.088	0.119
Mn	0.048	0.049	0.050	0.051	0.053	0.053	0.049	0.051	0.046	0.049	0.003
Mg	0.622	0.623	0.630	0.618	0.614	0.588	0.607	0.625	0.618	0.630	0.644
Ca	0.847	0.849	0.856	0.846	0.860	0.837	0.849	0.852	0.859	0.843	0.898
Na	0.074	0.090	0.073	0.081	0.071	0.096	0.086	0.072	0.072	0.081	0.034
K	0.001		0.001							0.001	0.001
Sum	4.000	4.000	4.000	4.000	4.000	4.000	4.000	4.000	4.000	4.000	4.000
Aegirine	6.4	9.0	7.2	7.9	7.0	9.6	8.2	7.2	4.1	8.1	3.4
Ferri-Tschermak	0.0	0.8	0.0	0.0	0.0	0.8	0.0	0.3	0.0	0.4	4.3
Jadeite	1.0	0.0	0.1	0.2	0.1	0.0	0.4	0.0	2.3	0.0	0.0
Ti-Aegirine	0.0	0.0	0.0	0.0	0.0	0.0	0.0	0.0	0.8	0.0	0.0
Ti-Tschermak	1.1	1.1	1.1	1.1	1.1	1.5	1.2	0.9	0.7	1.3	10.8
Al-Tschermak	0.2	0.0	0.2	0.6	0.3	0.1	0.3	0.5	0.0	0.3	4.5
Diopside	52.4	54.7	54.1	52.5	52.7	50.9	52.5	53.1	52.9	53.4	57.0
Hedenbergite	31.0	28.2	30.2	30.4	31.9	30.4	30.8	30.4	32.2	28.9	13.3
Enstatite	4.9	3.8	4.4	4.6	4.3	3.9	4.1	4.7	4.3	4.8	3.7
Ferrosilite	2.9	2.0	2.5	2.7	2.6	2.4	2.4	2.7	2.6	2.6	0.9

Table C10 continued

Unit	**Fur F**	**Fur F**	**Fur F**	**Fur F**	**Fur F**	**Fur F**	**Fur F**	**Fur F**	**Fur F**	**Fur F**
Sample	FM-2(5)	FM-2(5)	FM-2(5)	FM-2(5)	FM-2(5)	FM-2(5)	FM-2(5)	FM-2(5)	FM-2(5)	FM-2(5)
No.	Px1	Px2	Px3	Px4	Px5	Px6	Px7	Px8	Px9	Px10
Notes	Pheno	Pheno	Pheno	Pheno	Pheno	Pheno	Pheno	Pheno	Pheno	Pheno
SiO_2	51.97	51.47	52.95	52.16	52.61	52.13	52.03	51.92	52.42	52.76
TiO_2	0.50	0.43	0.42	0.38	0.44	0.36	0.41	0.42	0.35	0.37
Al_2O_3	0.99	0.88	0.81	0.81	0.85	0.69	0.84	0.83	0.67	0.57
Cr_2O_3	bdl	bdl	0.01	bdl	0.01	bdl	bdl	bdl	bdl	0.01
FeO	12.62	12.13	11.99	12.30	11.95	11.91	11.86	12.35	12.32	12.24
MnO	1.58	1.50	1.48	1.48	1.52	1.49	1.51	1.53	1.56	1.60
MgO	10.69	10.68	11.23	10.90	11.13	11.34	11.09	11.12	11.30	11.01
CaO	20.86	21.13	21.69	21.60	21.19	21.68	21.17	21.27	21.57	21.55
Na_2O	1.17	1.09	1.02	1.21	1.16	0.99	1.05	1.18	0.98	0.94
K_2O	bdl	bdl	0.01	0.01	bdl	0.02	0.01	bdl	bdl	0.01
Total	100.39	99.32	101.61	100.85	100.87	100.61	99.97	100.62	101.17	101.06
Si	1.962	1.962	1.971	1.956	1.971	1.958	1.967	1.950	1.960	1.979
Ti	0.014	0.012	0.012	0.011	0.012	0.010	0.012	0.012	0.010	0.010
Al	0.044	0.040	0.035	0.036	0.038	0.031	0.037	0.037	0.030	0.025
Cr			0.000		0.000					0.000
Fe^{2+}	0.308	0.295	0.299	0.266	0.294	0.267	0.293	0.263	0.284	0.319
Fe^{3+}	0.090	0.092	0.074	0.120	0.080	0.107	0.082	0.125	0.101	0.065
Mn	0.051	0.048	0.047	0.047	0.048	0.047	0.048	0.049	0.049	0.051
Mg	0.602	0.607	0.623	0.609	0.622	0.635	0.625	0.623	0.630	0.616
Ca	0.844	0.863	0.865	0.868	0.850	0.872	0.858	0.856	0.864	0.866
Na	0.086	0.081	0.074	0.088	0.084	0.072	0.077	0.086	0.071	0.069
K			0.000	0.001		0.001	0.000			0.000
Sum	4.000	4.000	4.000	4.000	4.000	4.000	4.000	4.000	4.000	4.000
Aegirine	8.6	8.1	7.4	8.8	8.0	7.2	7.7	8.6	7.1	6.5
Ferri-Tschermak	0.2	0.6	0.0	1.6	0.0	1.7	0.2	2.0	1.5	0.0
Jadeite	0.0	0.0	0.0	0.0	0.4	0.0	0.0	0.0	0.0	0.4
Ti-Aegirine	0.0	0.0	0.0	0.0	0.0	0.0	0.0	0.0	0.0	0.0
Ti-Tschermak	1.4	1.2	1.2	1.1	1.2	1.0	1.2	1.2	1.0	1.0
Al-Tschermak	0.6	0.2	0.6	0.0	0.4	0.0	0.5	0.0	0.0	0.0
Diopside	51.5	53.9	54.5	55.6	53.8	56.5	54.2	55.0	54.9	53.4
Hedenbergite	30.7	30.5	30.2	28.5	29.6	28.0	29.6	27.5	29.1	32.1
Enstatite	4.3	3.4	3.9	2.7	4.2	3.5	4.1	3.7	4.1	4.1
Ferrosilite	2.6	1.9	2.2	1.4	2.3	1.7	2.3	1.8	2.1	2.4

Table C10 continued

Unit	**Fur E**	**Fur E**	**Fur E**	**Fur E**	**Fur E**	**Fur E**	**Fur E**	**Fur E**	**Fur E**	**Fur E**
Sample	AM-1(3)	AM-1(3)	AM-1(3)	AM-1(3)	AM-1(3)	AM-1(3)	AM-1(3)	AM-1(3)	AM-1(3)	AM-1(3)
No.	Px1	Px2	Px3	Px4	Px5	Px6	Px7	Px8	Px9	Px10
Notes	Pheno	Pheno	Pheno	Pheno	Pheno	Pheno	Pheno	Pheno	Pheno	Pheno
SiO_2	51.85	52.33	52.47	52.26	52.69	52.71	52.82	52.73	52.64	52.71
TiO_2	0.48	0.44	0.41	0.42	0.36	0.36	0.37	0.36	0.40	0.35
Al_2O_3	0.90	0.64	0.89	0.84	0.84	0.63	0.67	0.65	0.90	0.63
Cr_2O_3	bdl	bdl	bdl	0.03	bdl	bdl	bdl	bdl	0.02	bdl
FeO	12.51	12.26	12.11	11.76	12.29	11.97	12.02	11.84	12.02	12.58
MnO	1.56	1.40	1.57	1.56	1.47	1.60	1.61	1.51	1.55	1.72
MgO	10.75	11.29	11.20	10.99	11.09	11.18	11.29	11.71	11.14	10.84
CaO	20.99	21.66	20.97	21.45	21.54	21.36	21.60	21.74	21.02	21.46
Na_2O	1.08	0.60	1.14	1.13	0.94	0.92	0.92	0.74	1.11	1.00
K_2O	bdl	bdl	0.01	0.01	0.01	0.01	0.01	bdl	bdl	bdl
Total	100.11	100.62	100.77	100.45	101.24	100.74	101.30	101.28	100.80	101.30
Si	1.963	1.974	1.968	1.966	1.971	1.981	1.973	1.969	1.974	1.974
Ti	0.014	0.013	0.012	0.012	0.010	0.010	0.010	0.010	0.011	0.010
Al	0.040	0.028	0.039	0.037	0.037	0.028	0.029	0.029	0.040	0.028
Cr				0.001					0.001	
Fe^{2+}	0.310	0.344	0.294	0.281	0.315	0.319	0.305	0.303	0.307	0.317
Fe^{3+}	0.086	0.043	0.085	0.089	0.069	0.057	0.070	0.067	0.070	0.077
Mn	0.050	0.045	0.050	0.050	0.047	0.051	0.051	0.048	0.049	0.055
Mg	0.607	0.635	0.626	0.616	0.618	0.626	0.629	0.652	0.623	0.605
Ca	0.851	0.875	0.843	0.865	0.863	0.860	0.865	0.870	0.845	0.861
Na	0.079	0.044	0.083	0.082	0.068	0.067	0.066	0.054	0.081	0.073
K			0.000	0.001	0.000	0.001	0.001			
Sum	4.000	4.000	4.000	4.000	4.000	4.000	4.000	4.000	4.000	4.000
Aegirine	7.9	4.3	8.3	8.2	6.8	5.7	6.6	5.4	7.0	7.3
Ferri-Tschermak	0.3	0.0	0.1	0.3	0.1	0.0	0.2	0.7	0.0	0.2
Jadeite	0.0	0.1	0.0	0.0	0.0	0.9	0.0	0.0	1.1	0.0
Ti-Aegirine	0.0	0.0	0.0	0.0	0.0	0.1	0.0	0.0	0.0	0.0
Ti-Tschermak	1.4	1.3	1.2	1.2	1.0	1.0	1.0	1.0	1.1	1.0
Al-Tschermak	0.3	0.1	0.7	0.3	0.8	0.0	0.3	0.0	0.3	0.2
Diopside	52.2	53.4	53.1	55.0	53.3	53.5	54.2	55.5	52.8	52.5
Hedenbergite	31.0	32.7	29.2	29.6	31.2	31.6	30.7	29.8	30.2	32.2
Enstatite	4.3	5.0	4.8	3.3	4.3	4.6	4.3	4.9	4.7	4.0
Ferrosilite	2.5	3.1	2.6	1.8	2.5	2.7	2.5	2.6	2.7	2.5

Table C10 continued

Unit	**Fur E**	**Fur E**	**Fur E**	**Fur E**	**Fur E**	**Fur E**	**Fur E**	**Fur E**	**Fur E**	**Fur E**
Sample	AM-2(3)	AM-2(3)	AM-2(3)	AM-2(3)	AM-2(3)	AM-2(3)	AM-2(3)	AM-2(3)	AM-2(3)	AM-2(3)
No.	Px1	Px2	Px3	Px4	Px5	Px6	Px7	Px8	Px9	Px10
Notes	Pheno	Pheno	Pheno	Pheno	Pheno	Pheno	Pheno	Pheno	Pheno	Pheno
SiO_2	52.25	51.61	52.67	52.29	52.07	52.43	52.15	52.42	51.94	52.43
TiO_2	0.37	0.47	0.36	0.43	0.45	0.40	0.41	0.42	0.48	0.38
Al_2O_3	0.79	1.03	0.60	0.79	0.85	0.78	0.88	0.88	0.90	0.90
Cr_2O_3	0.03	bdl	bdl	bdl	0.01	0.01	bdl	bdl	bdl	0.03
FeO	11.88	12.45	11.83	12.04	12.20	11.71	12.44	11.77	12.60	11.99
MnO	1.57	1.66	1.61	1.50	1.58	1.51	1.53	1.35	1.64	1.59
MgO	11.17	10.69	11.25	10.86	11.09	11.47	11.08	11.44	10.47	11.08
CaO	20.67	20.01	20.96	20.93	20.94	21.00	21.01	20.78	20.68	20.61
Na_2O	1.02	1.16	0.93	1.07	1.14	1.00	1.05	0.77	1.15	1.04
K_2O	bdl	0.01	0.02	bdl	bdl	bdl	0.01	0.01	0.02	bdl
Total	99.75	99.09	100.23	99.91	100.33	100.31	100.56	99.84	99.88	100.06
Si	1.980	1.973	1.988	1.981	1.962	1.973	1.963	1.986	1.973	1.982
Ti	0.011	0.014	0.010	0.012	0.013	0.011	0.012	0.012	0.014	0.011
Al	0.035	0.046	0.027	0.035	0.038	0.035	0.039	0.039	0.040	0.040
Cr	0.001				0.000	0.000				0.001
Fe^{2+}	0.320	0.331	0.329	0.324	0.289	0.300	0.303	0.350	0.328	0.330
Fe^{3+}	0.057	0.067	0.045	0.057	0.096	0.069	0.088	0.023	0.072	0.049
Mn	0.050	0.054	0.051	0.048	0.050	0.048	0.049	0.043	0.053	0.051
Mg	0.631	0.609	0.633	0.613	0.623	0.644	0.622	0.646	0.593	0.624
Ca	0.839	0.820	0.848	0.850	0.845	0.847	0.847	0.843	0.842	0.835
Na	0.075	0.086	0.068	0.079	0.084	0.073	0.076	0.057	0.085	0.077
K		0.000	0.001				0.000	0.001	0.001	
Sum	4.000	4.000	4.000	4.000	4.000	4.000	4.000	4.000	4.000	4.000
Aegirine	5.7	6.7	4.5	5.7	8.4	6.9	7.6	2.3	7.2	4.9
Ferri-Tschermak	0.0	0.0	0.0	0.0	0.6	0.0	0.6	0.0	0.0	0.0
Jadeite	1.6	1.9	1.5	1.6	0.0	0.4	0.0	2.5	1.2	2.2
Ti-Aegirine	0.2	0.0	0.8	0.5	0.0	0.0	0.0	0.9	0.0	0.5
Ti-Tschermak	0.9	1.4	0.6	0.9	1.3	1.1	1.2	0.7	1.4	0.8
Al-Tschermak	0.0	0.0	0.0	0.0	0.0	0.4	0.2	0.0	0.0	0.0
Diopside	52.3	49.4	52.6	52.3	53.5	54.0	52.8	52.0	50.4	51.3
Hedenbergite	30.7	31.2	31.6	31.7	29.1	29.2	29.9	31.7	32.4	31.3
Enstatite	5.4	5.8	5.2	4.5	4.4	5.2	4.7	6.2	4.4	5.5
Ferrosilite	3.1	3.6	3.1	2.7	2.4	2.8	2.6	3.8	2.8	3.3

Table C10 continued

Unit	**Fur C**	**Fur C**	**Fur C**	**Fur C**	**Fur C**	**Fur C**	**Fur C**	**Fur C**	**Fur C**	**Fur C**	**Fur C**	**Fur C**	**Fur C**	**Fur C**	**Fur C**	**Fur C**	**Fur C**
Sample	FM-1(6)	FM-1(6)	FM-1(6)	FM-1(6)	FM-1(6)	FM-1(6)	FM-1(6)	FM-2(6)	FM-2(6)	FM-2(6)	FM-2(6)	FM-2(6)	FM-2(6)	FM-2(6)	FM-2(6)	FM-2(6)	FM-2(6)
No.	Px1	Px2	Px4	Px6	Px8	Px9	Px10	Px1	Px2	Px3	Px4	Px5	Px6	Px7	Px8	Px9	Px10
Notes	Pheno	Pheno	Pheno	Pheno	Pheno	Pheno	Pheno	Pheno	Pheno	Pheno	Pheno	Pheno	Pheno	Pheno	Pheno	Pheno	Pheno
SiO_2	49.43	52.51	51.88	50.88	51.61	52.33	51.59	52.12	51.99	51.62	51.75	52.48	51.77	52.44	52.36	53.16	52.99
TiO_2	0.36	0.58	0.42	0.79	0.59	0.52	0.69	0.49	0.62	0.48	0.50	0.49	0.68	0.53	0.37	0.38	0.44
Al_2O_3	0.78	1.23	0.68	1.25	1.04	1.04	1.00	0.93	1.15	0.82	0.84	0.90	1.13	1.03	0.71	0.83	0.87
Cr_2O_3	bdl	0.01	bdl	bdl	0.01	bdl	bdl	0.01	bdl	bdl	bdl	0.03	bdl	bdl	bdl	bdl	0.02
FeO	11.35	11.54	12.26	13.68	9.81	9.86	12.76	12.75	10.85	11.90	11.97	12.79	13.61	10.28	12.85	11.23	11.47
MnO	1.31	1.19	1.44	1.45	0.98	1.01	1.52	1.31	1.18	1.29	1.35	1.40	1.79	1.07	1.36	1.38	1.50
MgO	10.49	11.88	10.88	9.93	13.42	13.54	10.61	10.95	12.73	11.45	11.44	11.32	10.68	12.39	10.78	11.81	11.37
CaO	23.82	21.48	21.27	20.76	21.34	21.21	20.82	21.13	21.00	21.42	21.65	20.96	19.88	22.62	21.85	21.49	21.48
Na_2O	0.75	0.83	0.74	1.06	0.69	0.65	1.08	0.80	0.71	0.78	0.76	0.81	1.28	0.78	0.82	0.96	0.98
K_2O	0.01	0.01	0.03	bdl	0.01	0.01	0.01	0.01	bdl	0.02	bdl	0.01	0.02	bdl	0.01	bdl	0.01
Total	98.30	101.27	99.60	99.80	99.49	100.17	100.08	100.50	100.22	99.78	100.25	101.20	100.83	101.13	101.11	101.24	101.13
Si	1.904	1.955	1.977	1.943	1.938	1.952	1.956	1.969	1.949	1.956	1.953	1.967	1.949	1.947	1.967	1.979	1.979
Ti	0.010	0.016	0.012	0.023	0.017	0.015	0.020	0.014	0.018	0.014	0.014	0.014	0.019	0.015	0.010	0.011	0.012
Al	0.035	0.054	0.030	0.056	0.046	0.046	0.045	0.041	0.051	0.037	0.037	0.040	0.050	0.045	0.031	0.036	0.038
Cr		0.000			0.000			0.000				0.001					0.001
Fe^{2+}	0.173	0.296	0.343	0.347	0.213	0.238	0.322	0.350	0.272	0.296	0.294	0.343	0.322	0.231	0.331	0.295	0.309
Fe^{3+}	0.193	0.063	0.048	0.090	0.095	0.069	0.083	0.053	0.068	0.082	0.084	0.057	0.107	0.089	0.073	0.054	0.050
Mn	0.602	0.659	0.618	0.565	0.751	0.753	0.600	0.617	0.711	0.647	0.644	0.632	0.600	0.686	0.604	0.655	0.633
Mg	0.043	0.037	0.046	0.047	0.031	0.032	0.049	0.042	0.037	0.041	0.043	0.044	0.057	0.034	0.043	0.044	0.047
Ca	0.983	0.857	0.869	0.850	0.859	0.848	0.846	0.855	0.843	0.870	0.876	0.842	0.802	0.900	0.880	0.857	0.860
Na	0.056	0.060	0.055	0.078	0.050	0.047	0.079	0.059	0.051	0.057	0.055	0.059	0.093	0.056	0.060	0.069	0.071
K	0.000	0.000	0.002		0.000	0.001	0.001	0.001		0.001		0.000	0.001		0.000		0.000
Sum	4.000	4.000	4.000	4.000	4.000	4.000	4.000	4.000	4.000	4.000	4.000	4.000	4.000	4.000	4.000	4.000	4.000
Aegirine	5.6	6.0	4.8	7.8	5.0	4.7	7.9	5.3	5.1	5.7	5.5	5.7	9.3	5.6	6.0	5.4	5.0
Ferri-Tschermak	6.8	0.1	0.0	0.6	2.3	1.1	0.2	0.0	0.9	1.2	1.4	0.0	0.7	1.6	0.7	0.0	0.0
Jadeite	0.0	0.0	0.7	0.0	0.0	0.0	0.0	0.6	0.0	0.0	0.0	0.1	0.0	0.0	0.0	1.5	1.7
Ti-Aegirine	0.0	0.0	0.0	0.0	0.0	0.0	0.0	0.0	0.0	0.0	0.0	0.0	0.0	0.0	0.0	0.0	0.4
Ti-Tschermak	1.0	1.6	1.1	2.3	1.7	1.5	2.0	1.4	1.8	1.4	1.4	1.4	1.9	1.5	1.0	1.1	1.0
Al-Tschermak	0.0	0.9	0.0	0.0	0.0	0.0	0.1	0.4	0.0	0.0	0.0	0.5	0.0	0.0	0.0	0.0	0.0
Diopside	60.2	55.1	52.6	48.4	61.9	60.5	50.9	51.2	57.0	55.5	55.6	51.0	47.6	62.7	53.3	55.8	54.3
Hedenbergite	21.6	27.9	33.1	33.7	20.1	21.7	31.4	32.6	24.7	28.9	29.1	31.3	30.0	24.2	33.0	28.8	30.6
Enstatite	0.0	5.4	4.6	4.1	6.6	7.4	4.5	5.2	7.1	4.6	4.4	6.1	6.2	2.9	3.6	4.9	4.4
Ferrosilite	0.0	2.7	2.9	2.8	2.2	2.7	2.8	3.3	3.1	2.4	2.3	3.8	3.9	1.1	2.2	2.5	2.5

Table C11: Ti-magnetite analyses from the UFG and the PIF

Unit	**Fur J**	**Fur J**	**Fur J**	**Fur J**	**Fur J**	**Fur J**	**Fur J**	**Fur J**	**Fur J**	**Fur J**	**Fur J dome**	**Fur J dome**	**Fur J dome**	**Fur J dome**
Sample	FM-1(1)	FM-1(1)	FM-1(1)	FM-1(1)	FM-1(1)	FM-1(1)	FM-1(1)	FM-2(1)	FM-2(1)	FM-2(1)	SM 7-1	SM 7-1	SM 7-1	SM 7-1
No.	Ox1	Ox2	Ox3	Ox4	Ox5	Ox6	Ox7	Ox1	Ox2	Ox3	Oxide02	Oxide03	Oxide04	Oxide05
Notes	Mph	Mph	Mph	Mph	Mph	Mph	Mph	Mph	Mph	Mph	Mph	Mph	Mph	Mph
TiO_2	17.21	17.23	16.97	18.43	16.81	17.21	17.03	17.96	18.16	17.88	19.42	16.41	16.92	16.77
Al_2O_3	0.97	0.97	0.98	1.31	0.97	1.01	0.96	0.97	0.95	0.99	0.45	0.93	0.87	0.74
Cr_2O_3	bdl	bdl	bdl	bdl	bdl	bdl	bdl	bdl	bdl	bdl	bdl	bdl	bdl	0.02
FeO	74.08	73.97	73.70	71.59	73.43	73.67	73.87	74.27	74.37	73.56	70.79	73.31	72.77	73.49
MnO	2.60	2.61	2.50	2.17	2.66	2.67	2.69	2.63	2.59	2.60	3.44	3.06	2.97	2.80
MgO	1.34	1.36	1.43	1.83	1.42	1.42	1.33	1.41	1.39	1.40	2.29	2.03	2.17	1.95
NiO	bdl	0.01	0.01	bdl	0.01	bdl	bdl	bdl	bdl	bdl				
V_2O_3	0.01	0.01	0.02	0.01	0.01	0.02	bdl	0.02	0.01	0.03				
SiO_2	0.03	0.05	0.04	0.06	0.07	0.04	0.03	0.07	0.06	0.04				
ZnO	0.26	0.28	0.24	0.22	0.22	0.26	0.23	0.26	0.24	0.23				
Total	96.50	96.49	95.88	95.62	95.59	96.30	96.15	97.59	97.77	96.72	96.39	95.74	95.70	95.77
Ti	0.483	0.483	0.478	0.519	0.475	0.483	0.479	0.498	0.503	0.500	0.543	0.461	0.475	0.472
Al	0.042	0.043	0.043	0.058	0.043	0.044	0.042	0.042	0.041	0.043	0.020	0.041	0.038	0.033
Cr														0.001
Fe^{2+}	1.320	1.319	1.314	1.344	1.307	1.314	1.314	1.334	1.341	1.336	1.308	1.251	1.260	1.274
Fe^{3+}	0.990	0.987	0.997	0.899	1.001	0.986	0.997	0.956	0.949	0.953	0.894	1.038	1.012	1.024
Mn	0.082	0.082	0.079	0.069	0.085	0.084	0.085	0.082	0.081	0.082	0.108	0.097	0.094	0.089
Mg	0.074	0.076	0.080	0.102	0.079	0.079	0.074	0.077	0.077	0.078	0.127	0.113	0.121	0.109
Ni		0.000	0.000		0.000									
V	0.000	0.000	0.001	0.000	0.000	0.001		0.001	0.000	0.001				
Si	0.001	0.002	0.001	0.002	0.002	0.002	0.001	0.003	0.002	0.001				
Zn	0.007	0.008	0.007	0.006	0.006	0.007	0.006	0.007	0.007	0.006				
Sum	3.000	3.000	3.000	3.000	3.000	3.000	3.000	3.000	3.000	3.000	3.000	3.000	3.000	3.000
Usp	48.3	48.4	47.9	52.1	47.6	48.4	48.0	49.9	50.4	50.1	54.3	46.1	47.5	47.2
Mt	49.6	49.5	49.9	45.1	50.2	49.4	49.9	47.9	47.5	47.7	44.7	51.9	50.6	51.2
Sp	2.1	2.1	2.2	2.9	2.1	2.2	2.1	2.1	2.1	2.2	1.0	2.0	1.9	1.6

Table C11 continued

Unit	**Fur J dome**	**Fur J dome**	**Fur J dome**	**Fur J dome**	**Fur J dome**	**Fur J dome**	**Fur J dome**	**Fur J dome**	**Fur J dome**	**Fur J dome**	**Fur J dome**	**Fur J dome**	**Fur J dome**	**Fur J dome**
Sample	SM7-1	SM7-1	SM7-1	SM7-1	SM7-1	SM7-1	SM7-1	SM7-1	SM7-1	SM7-1	SM7-1	SM7-1	SM7-1	SM7-1
No.	118 / 1 .	119 / 1 .	120 / 1 .	121 / 1 .	122 / 1 .	123 / 1 .	124 / 1 .	125 / 1 .	126 / 1 .	127 / 1 .	128 / 1 .	129 / 1 .	132 / 1 .	133 / 1 .
Notes	Mph	Mph	Mph	Mph	Mph	Mph	Mph	Mph	Mph	Mph	Mph	Mph	Mph	Mph
TiO_2	17.51	15.77	15.66	15.55	15.81	17.72	16.79	16.72	14.74	14.68	15.73	17.00	13.64	14.77
Al_2O_3	1.24	0.67	0.73	0.76	0.77	1.21	1.33	1.29	1.69	1.41	1.24	1.31	0.56	0.65
Cr_2O_3	0.02	bdl	bdl	bdl	bdl	bdl	bdl	0.02	bdl	bdl	bdl	bdl	bdl	bdl
FeO	71.37	73.39	73.44	73.09	73.46	71.52	71.31	71.72	73.37	73.85	71.15	71.42	74.92	74.06
MnO	2.86	2.97	3.03	2.98	3.05	2.61	2.91	2.95	2.71	2.78	2.90	2.90	2.80	2.89
MgO	2.17	1.90	1.90	1.96	1.91	2.03	2.17	2.20	2.11	2.01	1.98	2.20	1.79	1.85
NiO														
V_2O_3														
SiO_2														
ZnO														
Total	95.18	94.69	94.76	94.34	95.00	95.07	94.50	94.90	94.60	94.71	92.97	94.83	93.69	94.18
Ti	0.494	0.448	0.445	0.443	0.448	0.501	0.476	0.472	0.416	0.415	0.454	0.481	0.392	0.422
Al	0.055	0.030	0.033	0.034	0.034	0.054	0.059	0.057	0.075	0.062	0.056	0.058	0.025	0.029
Cr	0.000							0.000						
Fe^{2+}	1.281	1.246	1.241	1.237	1.243	1.304	1.261	1.255	1.212	1.214	1.246	1.265	1.200	1.224
Fe^{3+}	0.957	1.074	1.078	1.080	1.070	0.945	0.989	0.998	1.093	1.108	1.037	0.981	1.192	1.128
Mn	0.091	0.095	0.097	0.096	0.097	0.083	0.093	0.094	0.086	0.088	0.094	0.092	0.090	0.093
Mg	0.121	0.107	0.107	0.111	0.107	0.114	0.122	0.123	0.118	0.113	0.113	0.123	0.102	0.105
Ni														
V														
Si														
Zn														
Sum	3.000	3.000	3.000	3.000	3.000	3.000	3.000	3.000	3.000	3.000	3.000	3.000	3.000	3.000
Usp	49.4	44.8	44.5	44.3	44.8	50.1	47.6	47.3	41.6	41.5	45.4	48.1	39.2	42.2
Mt	47.9	53.7	53.9	54.0	53.5	47.2	49.4	49.9	54.6	55.4	51.8	49.0	59.6	56.4
Sp	2.7	1.5	1.6	1.7	1.7	2.7	3.0	2.8	3.7	3.1	2.8	2.9	1.3	1.5

Table C11 continued

Unit	**Fur J sy**	**Fur J sy**	**Fur J sy**	**Fur J sy**	**Fur J sy**	**Fur J sy**	**Fur J sy**	**Fur I**	**Fur I**	**Fur I**	**Fur I**	**Fur I**	**Fur I**	**Fur I**
Sample	Fur-JSyB	Fur-JSyB	Fur-JSyB	Fur-JSyB	Fur-JSyB	Fur-JSyB	Fur-JSyB	FM-1(2)	FM-1(2)	FM-1(2)	FM-1(2)	FM-1(2)	FM-1(2)	FM-1(2)
No.	Ox1	Ox2	Ox3	Ox4	Ox5	Ox6	Ox7	Ox8	Ox9	Ox10	Ox11	Ox12	Ox13	Ox14
Notes	Mph	Mph	Mph	Mph	Mph	Mph	Mph	Mph	Mph	Mph	Mph	Mph	Mph	Mph
TiO_2	12.01	11.21	16.29	16.99	16.94	17.56	16.64	16.10	19.91	19.65	20.51	16.11	16.21	16.45
Al_2O_3	0.06	0.11	0.09	0.14	0.14	0.31	0.17	0.87	0.95	1.37	1.23	0.89	0.88	0.87
Cr_2O_3	bdl	0.01	bdl	bdl	bdl	bdl	bdl	bdl	bdl	bdl	bdl	bdl	bdl	bdl
FeO	78.36	77.94	72.69	73.19	73.50	73.45	75.33	74.89	71.07	70.98	71.64	75.26	74.44	75.45
MnO	4.28	4.51	4.31	2.29	2.30	3.93	4.02	2.73	2.55	2.32	2.42	2.65	2.68	2.71
MgO	0.05	0.08	0.00	0.00	0.03	0.04	0.03	1.29	1.39	1.79	2.03	1.29	1.25	1.27
NiO	bdl	bdl	bdl	bdl	bdl	bdl	bdl	0.01	0.01	0.01	0.01	bdl	0.02	bdl
V_2O_3	bdl	0.01	0.02	bdl	0.01	0.01	0.01	bdl	0.01	0.02	0.01	0.02	0.02	bdl
SiO_2	0.01	0.02	0.13	0.05	0.14	0.06	0.06	0.08	0.06	0.06	0.05	0.07	0.06	0.06
ZnO	0.79	1.02	0.56	0.37	0.31	0.35	0.41	0.24	0.26	0.25	0.22	0.27	0.28	0.27
Total	95.56	94.91	94.09	93.03	93.37	95.70	96.66	96.20	96.21	96.46	98.12	96.56	95.84	97.07
Ti	0.343	0.322	0.475	0.502	0.498	0.503	0.472	0.453	0.561	0.550	0.564	0.451	0.458	0.459
Al	0.003	0.005	0.004	0.007	0.007	0.014	0.007	0.038	0.042	0.060	0.053	0.039	0.039	0.038
Cr		0.000												
Fe^{2+}	1.181	1.143	1.322	1.416	1.416	1.367	1.333	1.290	1.397	1.372	1.374	1.291	1.296	1.298
Fe^{3+}	1.310	1.349	1.035	0.987	0.986	0.975	1.044	1.051	0.831	0.836	0.816	1.053	1.041	1.041
Mn	0.138	0.146	0.142	0.076	0.076	0.127	0.128	0.086	0.081	0.073	0.075	0.084	0.085	0.085
Mg	0.003	0.005	0.000	0.000	0.002	0.002	0.002	0.072	0.078	0.099	0.111	0.072	0.070	0.070
Ni								0.000	0.000	0.000	0.000		0.001	
V		0.000	0.001		0.000	0.000	0.000		0.000	0.001	0.000	0.001	0.001	
Si	0.000	0.001	0.005	0.002	0.005	0.002	0.002	0.003	0.002	0.002	0.002	0.003	0.002	0.002
Zn	0.022	0.029	0.016	0.011	0.009	0.010	0.011	0.007	0.007	0.007	0.006	0.007	0.008	0.007
Sum	3.000	3.000	3.000	3.000	3.000	3.000	3.000	3.000	3.000	3.000	3.000	3.000	3.000	3.000
Usp	34.3	32.3	47.8	50.3	50.1	50.5	47.3	45.4	56.3	55.1	56.5	45.2	45.9	46.0
Mt	65.5	67.5	52.0	49.4	49.6	48.9	52.3	52.7	41.6	41.9	40.9	52.8	52.2	52.2
Sp	0.1	0.2	0.2	0.3	0.3	0.7	0.4	1.9	2.1	3.0	2.7	2.0	2.0	1.9

Table C11 continued

Unit	**Fur I**	**Fur I**	**Fur I**	**Fur I dome**	**Fur I dome**	**Fur I dome**	**Fur I dome**	**Fur I dome**	**Fur I dome**	**Fur I dome**	**Fur I dome**	**Fur I dome**	**Fur I dome**	**Fur I dome**
Sample	FM-1(2)	FM-1(2)	FM-2(2)	SM 5-1	SM 5-1	SM 5-1	SM 5-1	SM 5-1	SM5-1	SM5-1	SM5-1	SM5-1	SM5-1	SM5-1
No.	Ox15	Ox16	Ox17	Oxide16	Oxide17	Oxide18	Oxide19	Oxide20	106 / 1 .	107 / 1 .	108 / 1 .	109 / 1 .	110 / 1 .	111 / 1 .
Notes	Mph	Mph	Mph	Mph	Mph	Mph	Mph	Mph	Mph	Mph	Mph	Mph	Mph	Mph
TiO_2	16.26	19.58	16.73	15.38	15.09	15.94	15.23	15.02	14.80	14.89	15.08	14.54	14.33	14.38
Al_2O_3	0.88	1.08	0.91	0.45	0.41	0.28	0.47	0.49	0.29	0.26	0.28	0.40	0.52	0.51
Cr_2O_3	0.01	bdl	bdl	bdl	bdl	bdl	bdl	0.01	bdl	bdl	bdl	0.03	bdl	bdl
FeO	75.40	72.04	75.12	76.68	76.66	76.09	76.10	76.23	75.66	75.45	74.77	76.47	76.48	76.26
MnO	2.72	2.53	2.63	3.12	3.16	3.30	3.20	3.06	3.22	3.37	3.49	3.08	3.00	2.99
MgO	1.21	1.51	1.28	0.49	0.46	0.28	0.51	0.57	0.21	0.17	0.17	0.37	0.53	0.53
NiO	bdl	bdl	bdl											
V_2O_3	0.02	0.01	bdl											
SiO_2	0.06	0.07	0.03											
ZnO	0.27	0.24	0.26											
Total	96.83	97.05	96.96	96.12	95.78	95.89	95.50	95.37	94.16	94.14	93.77	94.87	94.85	94.65
Ti	0.454	0.546	0.467	0.436	0.429	0.454	0.434	0.429	0.429	0.432	0.440	0.418	0.411	0.413
Al	0.039	0.047	0.040	0.020	0.018	0.013	0.021	0.022	0.013	0.012	0.013	0.018	0.024	0.023
Cr	0.000							0.000				0.001		
Fe^{2+}	1.297	1.379	1.307	1.309	1.302	1.332	1.303	1.298	1.312	1.312	1.315	1.297	1.284	1.286
Fe^{3+}	1.047	0.855	1.024	1.108	1.123	1.079	1.111	1.121	1.129	1.124	1.109	1.146	1.155	1.151
Mn	0.086	0.079	0.083	0.100	0.101	0.106	0.103	0.098	0.105	0.110	0.115	0.100	0.097	0.097
Mg	0.067	0.083	0.071	0.027	0.026	0.016	0.029	0.032	0.012	0.010	0.010	0.021	0.030	0.030
Ni														
V	0.001	0.000												
Si	0.002	0.003	0.001											
Zn	0.007	0.006	0.007											
Sum	3.000	3.000	3.000	3.000	3.000	3.000	3.000	3.000	3.000	3.000	3.000	3.000	3.000	3.000
Usp	45.6	54.8	46.7	43.6	42.9	45.4	43.4	42.9	42.9	43.2	43.9	41.8	41.1	41.3
Mt	52.5	42.9	51.3	55.4	56.2	53.9	55.5	56.0	56.4	56.2	55.4	57.3	57.7	57.5
Sp	1.9	2.4	2.0	1.0	0.9	0.6	1.0	1.1	0.7	0.6	0.6	0.9	1.2	1.2

Table C11 continued

Unit	**Fur I dome**	**Fur I dome**	**Fur I dome**	**Fur H**	**Fur H**	**Fur H**	**Fur H**	**Fur H**	**Fur H**	**Fur H**	**Fur H**	**Fur H**	**Fur H**	**Fur G**
Sample	SM5-1	SM5-1	SM5-1	FM-1(3)	FM-1(3)	FM-1(3)	FM-1(3)	FM-1(3)	FM-1(3)	FM-1(3)	FM-1(3)	FM-2(1)	FM-2(3)	FM-1(4)
No.	112 / 1 .	113 / 1 .	114 / 1 .	Ox1	Ox2	Ox3	Ox4	Ox5	Ox6	Ox7	Ox8	Ox1	Ox2	Ox1
Notes	Mph	Mph	Mph	Mph	Mph	Mph	Mph	Mph	Mph	Mph	Mph	Mph	Mph	Mph
TiO_2	14.32	14.32	14.15	16.65	16.88	16.88	16.37	17.05	16.53	17.30	16.26	17.96	17.12	20.72
Al_2O_3	0.35	0.38	0.28	0.80	0.81	0.80	0.80	0.82	0.80	0.77	0.81	0.97	0.80	0.85
Cr_2O_3	bdl	0.01	0.02	bdl	bdl	bdl	bdl	0.01	bdl	bdl	bdl	bdl	bdl	bdl
FeO	76.40	76.30	76.40	74.99	74.95	74.38	75.29	75.27	74.85	74.83	74.95	74.27	74.54	72.31
MnO	3.12	3.28	3.14	2.80	2.82	2.84	2.76	2.80	2.72	2.84	2.69	2.63	2.90	2.67
MgO	0.30	0.21	0.20	1.13	1.08	1.15	1.08	1.04	1.13	1.18	1.14	1.41	1.16	1.13
NiO				bdl	bdl	bdl	bdl	0.02	bdl	bdl	bdl	bdl	bdl	bdl
V_2O_3				0.01	bdl	0.02	0.01	0.01	0.01	0.04	bdl	0.02	0.01	bdl
SiO_2				0.07	0.07	0.07	0.06	0.04	0.05	0.09	0.10	0.07	0.08	0.06
ZnO				0.26	0.28	0.24	0.25	0.24	0.25	0.25	0.23	0.26	0.26	0.27
Total	94.48	94.49	94.20	96.70	96.90	96.39	96.61	97.30	96.34	97.30	96.18	97.59	96.87	98.01
Ti	0.413	0.413	0.410	0.467	0.472	0.475	0.459	0.475	0.465	0.482	0.458	0.498	0.479	0.575
Al	0.016	0.017	0.013	0.035	0.035	0.035	0.035	0.036	0.035	0.034	0.036	0.042	0.035	0.037
Cr		0.000	0.001					0.000						
Fe^{2+}	1.295	1.295	1.296	1.311	1.318	1.316	1.308	1.324	1.311	1.324	1.307	1.334	1.319	1.425
Fe^{3+}	1.158	1.155	1.166	1.026	1.014	1.010	1.041	1.010	1.031	0.995	1.041	0.956	1.000	0.808
Mn	0.101	0.107	0.103	0.088	0.089	0.090	0.087	0.088	0.086	0.089	0.085	0.082	0.091	0.083
Mg	0.017	0.012	0.011	0.063	0.060	0.064	0.060	0.058	0.063	0.065	0.064	0.077	0.064	0.062
Ni								0.001						
V				0.000		0.000	0.000	0.000	0.000	0.001		0.001	0.000	
Si				0.002	0.003	0.002	0.002	0.002	0.002	0.003	0.004	0.003	0.003	0.002
Zn				0.007	0.008	0.007	0.007	0.007	0.007	0.007	0.006	0.007	0.007	0.007
Sum	3.000	3.000	3.000	3.000	3.000	3.000	3.000	3.000	3.000	3.000	3.000	3.000	3.000	3.000
Usp	41.3	41.4	41.0	46.8	47.4	47.6	46.0	47.6	46.6	48.4	46.0	49.9	48.1	57.6
Mt	57.9	57.8	58.3	51.5	50.9	50.6	52.2	50.6	51.6	49.9	52.2	47.9	50.2	40.5
Sp	0.8	0.9	0.6	1.8	1.8	1.8	1.8	1.8	1.8	1.7	1.8	2.1	1.8	1.9

Table C11 continued

Unit	**Fur G**	**Fur G**	**Fur G**	**Fur G**	**Fur G**	**Fur G**	**Fur G**	**Fur G**	**Fur F**	**Fur F**	**Fur F**	**Fur F**	**Fur F**	**Fur F**
Sample	FM-1(4)	FM-1(4)	FM-1(4)	FM-1(4)	FM-1(4)	FM-1(4)	FM-1(4)	FM-1(4)	FM-1(5)	FM-1(5)	FM-1(5)	FM-1(5)	FM-1(5)	FM-1(5)
No.	Ox2	Ox3	Ox4	Ox5	Ox6	Ox8	Ox9	Ox10	Ox1	Ox2	Ox3	Ox4	Ox5	Ox6
Notes	Mph	Mph	Mph	Mph	Mph	Mph	Mph	Mph	Mph	Mph	Mph	Mph	Mph	Mph
TiO_2	18.76	16.31	15.19	17.41	19.32	21.41	18.22	18.08	16.28	17.26	15.86	20.66	16.16	18.21
Al_2O_3	0.86	1.39	1.94	3.56	0.79	1.26	0.82	0.84	0.86	0.84	0.84	1.07	0.90	0.91
Cr_2O_3	bdl	bdl	0.06	bdl	bdl	bdl	bdl	bdl	bdl	bdl	bdl	bdl	0.01	bdl
FeO	74.07	74.93	75.53	70.84	72.85	70.68	74.28	73.49	75.13	74.15	75.65	72.06	75.60	73.67
MnO	2.65	2.35	1.41	0.77	2.65	2.31	2.66	2.65	2.76	2.69	2.61	2.52	2.74	2.66
MgO	1.00	1.65	2.06	4.58	1.09	1.36	0.94	1.00	1.18	1.22	1.12	1.43	1.14	1.23
NiO	bdl	bdl	0.01	0.01	0.02	bdl	0.01	bdl	bdl	0.02	bdl	bdl	bdl	0.01
V_2O_3	0.01	0.07	0.29	0.24	bdl	0.01	0.01	0.01	bdl	bdl	bdl	bdl	0.01	0.01
SiO_2	0.07	0.05	0.03	0.07	0.07	0.08	0.05	0.07	0.07	0.08	0.05	0.08	0.08	0.06
ZnO	0.24	0.21	0.20	0.15	0.22	0.26	0.22	0.23	0.26	0.21	0.27	0.26	0.25	0.24
Total	97.65	96.96	96.72	97.64	97.01	97.37	97.21	96.38	96.54	96.48	96.40	98.08	96.88	97.01
Ti	0.522	0.453	0.420	0.465	0.541	0.597	0.510	0.510	0.457	0.485	0.446	0.571	0.452	0.509
Al	0.037	0.060	0.084	0.149	0.035	0.055	0.036	0.037	0.038	0.037	0.037	0.046	0.039	0.040
Cr			0.002										0.000	
Fe^{2+}	1.380	1.284	1.258	1.198	1.393	1.445	1.369	1.366	1.299	1.328	1.295	1.410	1.298	1.352
Fe^{3+}	0.913	1.028	1.064	0.908	0.877	0.745	0.941	0.938	1.044	0.988	1.068	0.806	1.051	0.937
Mn	0.083	0.073	0.044	0.023	0.084	0.073	0.084	0.084	0.087	0.085	0.083	0.078	0.086	0.084
Mg	0.055	0.091	0.113	0.243	0.060	0.075	0.052	0.056	0.066	0.068	0.062	0.079	0.063	0.068
Ni			0.000	0.000	0.000		0.000			0.001				0.000
V	0.000	0.002	0.009	0.007		0.000	0.000	0.000					0.000	0.000
Si	0.002	0.002	0.001	0.003	0.003	0.003	0.002	0.003	0.002	0.003	0.002	0.003	0.003	0.002
Zn	0.006	0.006	0.006	0.004	0.006	0.007	0.006	0.006	0.007	0.006	0.007	0.007	0.007	0.007
Sum	3.000	3.000	3.000	3.000	3.000	3.000	3.000	3.000	3.000	3.000	3.000	3.000	3.000	3.000
Usp	52.4	45.4	42.3	46.8	54.3	59.8	51.1	51.1	45.8	48.6	44.6	57.3	45.3	51.0
Mt	45.8	51.6	53.5	45.7	44.0	37.4	47.1	47.0	52.3	49.5	53.5	40.4	52.7	47.0
Sp	1.9	3.0	4.2	7.5	1.7	2.8	1.8	1.9	1.9	1.9	1.9	2.3	2.0	2.0

Table C11 continued

Unit	**Fur F**	**Fur F**	**Fur F**	**Fur F**	**Fur E**	**Fur E**	**Fur E**	**Fur E**	**Fur E**	**Fur E**	**Fur E**	**Fur E**	**Fur E**	**Fur E**
Sample	FM-1(5)	FM-1(5)	FM-1(5)	FM-2(5)	AM-2(3)	AM-2(3)	AM-2(3)	AM-2(3)	AM-2(3)	AM-2(3)	AM-2(3)	AM-2(3)	AM-2(3)	AM-2(3)
No.	Ox7	Ox8	Ox9	Ox1	Ox1	Ox2	Ox3	Ox4	Ox5	Ox6	Ox7	Ox8	Ox9	Ox10
Notes	Mph	Mph	Mph	Mph	Mph	Mph	Mph	Mph	Mph	Mph	Mph	Mph	Mph	Mph
TiO_2	19.35	20.72	16.41	15.91	19.70	18.62	16.16	15.85	16.38	20.23	15.29	19.17	16.55	17.79
Al_2O_3	0.99	0.93	0.79	0.85	1.07	1.01	0.87	0.83	0.83	0.93	0.57	0.87	0.84	0.85
Cr_2O_3	bdl	bdl	bdl	bdl	bdl	bdl	bdl	bdl	0.02	bdl	bdl	bdl	bdl	bdl
FeO	72.50	72.16	75.57	76.16	72.88	72.83	76.39	75.90	75.11	72.73	76.64	73.28	75.33	75.19
MnO	2.62	2.64	2.79	2.82	2.41	2.53	2.73	2.68	2.80	2.81	2.92	2.71	2.77	2.84
MgO	1.48	1.21	1.15	1.33	1.48	1.62	1.19	1.20	1.18	1.37	0.54	1.19	1.14	1.15
NiO	bdl	bdl	bdl	bdl	bdl	bdl	bdl	0.01	0.01	bdl	0.01	0.01	0.01	bdl
V_2O_3	bdl	0.01	bdl	0.01	0.02	0.01	0.01	0.01	0.01	bdl	bdl	0.01	0.02	0.01
SiO_2	0.06	0.07	0.06	0.06	0.07	0.08	0.05	0.05	0.04	0.08	0.10	0.09	0.03	0.05
ZnO	0.25	0.25	0.25	0.27	0.21	0.26	0.28	0.26	0.30	0.27	0.28	0.23	0.26	0.26
Total	97.26	97.99	97.03	97.41	97.84	96.97	97.68	96.79	96.69	98.42	96.34	97.55	96.94	98.14
Ti	0.539	0.575	0.458	0.441	0.545	0.519	0.448	0.443	0.459	0.558	0.432	0.533	0.463	0.492
Al	0.043	0.040	0.035	0.037	0.046	0.044	0.038	0.037	0.036	0.040	0.025	0.038	0.037	0.037
Cr									0.000					
Fe^{2+}	1.370	1.422	1.302	1.275	1.385	1.346	1.291	1.287	1.298	1.391	1.305	1.379	1.306	1.335
Fe^{3+}	0.875	0.804	1.044	1.076	0.858	0.911	1.063	1.073	1.042	0.839	1.103	0.889	1.036	0.976
Mn	0.082	0.082	0.088	0.088	0.075	0.079	0.085	0.084	0.088	0.087	0.093	0.085	0.087	0.088
Mg	0.082	0.067	0.064	0.073	0.081	0.090	0.065	0.066	0.066	0.075	0.030	0.066	0.063	0.063
Ni								0.000	0.000		0.000	0.000	0.000	
V		0.000		0.000	0.000	0.000	0.000	0.000	0.000			0.000	0.000	0.000
Si	0.002	0.003	0.002	0.002	0.002	0.003	0.002	0.002	0.002	0.003	0.004	0.003	0.001	0.002
Zn	0.007	0.007	0.007	0.007	0.006	0.007	0.008	0.007	0.008	0.007	0.008	0.006	0.007	0.007
Sum	3.000	3.000	3.000	3.000	3.000	3.000	3.000	3.000	3.000	3.000	3.000	3.000	3.000	3.000
Usp	54.0	57.6	45.9	44.3	54.7	52.1	44.9	44.4	46.0	55.9	43.4	53.5	46.3	49.3
Mt	43.8	40.3	52.3	53.9	43.0	45.7	53.2	53.8	52.2	42.1	55.4	44.6	51.9	48.9
Sp	2.2	2.0	1.7	1.8	2.3	2.2	1.9	1.8	1.8	2.0	1.3	1.9	1.8	1.9

Table C11 continued

Unit	**Fur C**	**Fur C**	**Fur C**	**Fur C**	**Fur C**	**Fur C**	**Fur C**	**Fur C**	**Fur C**	**Fur C**	**Povo fall**	**Povo fall**	**Povo fall**	**Povo fall**
Sample	FM-1(6)	FM-1(6)	FM-1(6)	FM-1(6)	FM-1(6)	FM-1(6)	FM-1(6)	FM-1(6)	FM-1(6)	FM-2(6)	AM-2(4)	AM-2(4)	AM-2(4)	AM-2(4)
No.	Ox1	Ox2	Ox3	Ox4	Ox5	Ox6	Ox7	Ox8	Ox9	Ox1	Ox1	Ox2	Ox4	Ox5
Notes	Mph	Mph	Mph	Mph	Mph	Mph	Mph	Mph	Mph	Mph	Mph	Mph	Mph	Mph
TiO_2	18.73	21.93	21.40	21.51	22.79	21.53	20.25	21.17	21.06	21.66	13.58	13.71	13.67	13.75
Al_2O_3	0.92	1.01	0.93	0.90	0.93	1.47	0.99	0.91	0.96	0.90	2.12	2.46	2.06	2.11
Cr_2O_3	bdl	bdl	bdl	bdl	bdl	bdl	0.01	bdl	0.01	bdl	bdl	0.02	0.03	0.01
FeO	74.12	70.73	71.71	71.90	71.08	70.89	72.52	71.95	72.07	71.33	75.83	75.37	76.48	76.42
MnO	2.56	2.51	2.58	2.59	2.58	2.07	2.60	2.70	2.66	2.61	1.34	1.18	1.37	1.25
MgO	1.20	1.29	1.28	1.11	1.22	2.12	1.32	1.12	1.26	1.09	2.61	2.97	2.45	2.60
NiO	bdl	bdl	bdl	0.01	bdl	0.01	bdl	0.01	bdl	bdl	0.01	0.01	bdl	bdl
V_2O_3	bdl	bdl	bdl	0.01	0.02	0.03	bdl	bdl	bdl	0.03	0.28	0.28	0.25	0.26
SiO_2	0.08	0.06	0.06	0.03	0.03	0.05	0.05	0.03	0.07	0.04	0.03	0.09	0.04	0.05
ZnO	0.28	0.23	0.24	0.22	0.23	0.21	0.24	0.27	0.29	0.23	0.20	0.15	0.15	0.19
Total	97.88	97.75	98.20	98.27	98.88	98.39	97.98	98.16	98.39	97.88	96.00	96.24	96.50	96.64
Ti	0.519	0.610	0.592	0.596	0.628	0.590	0.561	0.587	0.582	0.603	0.376	0.377	0.377	0.378
Al	0.040	0.044	0.040	0.039	0.040	0.063	0.043	0.039	0.042	0.039	0.092	0.106	0.089	0.091
Cr							0.000		0.000			0.000	0.001	0.000
Fe^{2+}	1.369	1.456	1.438	1.449	1.476	1.406	1.403	1.435	1.425	1.456	1.186	1.177	1.198	1.194
Fe^{3+}	0.916	0.732	0.770	0.766	0.702	0.753	0.831	0.784	0.789	0.751	1.147	1.126	1.146	1.142
Mn	0.080	0.079	0.080	0.081	0.080	0.064	0.081	0.084	0.083	0.082	0.042	0.037	0.043	0.039
Mg	0.066	0.071	0.070	0.061	0.067	0.115	0.072	0.062	0.069	0.060	0.143	0.162	0.134	0.142
Ni				0.000		0.000		0.000			0.000	0.000		
V				0.000	0.000	0.001				0.001	0.008	0.008	0.007	0.008
Si	0.003	0.002	0.002	0.001	0.001	0.002	0.002	0.001	0.003	0.002	0.001	0.003	0.002	0.002
Zn	0.007	0.006	0.007	0.006	0.006	0.006	0.006	0.007	0.008	0.006	0.005	0.004	0.004	0.005
Sum	3.000	3.000	3.000	3.000	3.000	3.000	3.000	3.000	3.000	3.000	3.000	3.000	3.000	3.000
Usp	52.1	61.1	59.4	59.7	62.9	59.1	56.2	58.8	58.3	60.4	37.8	38.0	37.9	38.0
Mt	45.9	36.7	38.6	38.4	35.1	37.7	41.6	39.3	39.6	37.6	57.6	56.7	57.6	57.4
Sp	2.0	2.2	2.0	2.0	2.0	3.2	2.1	2.0	2.1	2.0	4.6	5.3	4.5	4.6

Table C11 continued

Unit	**Povo fall**	**Povo fall**	**Povo fall**	**Povo fall**	**Povo fall**	**Povo ign**	**Povo ign**	**Povo ign**	**Povo ign**	**Povo ign**	**Povo ign**	**Povo ign**	**Povo ign**	**Povo ign**
Sample	AM-2(4)	AM-2(4)	AM-2(4)	AM-2(4)	AM-2(4)	SM9-1	SM9-1	SM9-1	SM9-1	SM9-1	SM9-1	SM9-1	SM9-1	SM9-1
No.	Ox6	Ox7	Ox8	Ox9	Ox10	19 / 1 .	20 / 1 .	21 / 1 .	23 / 1 .	24 / 1 .	29 / 1 .	30 / 1 .	35 / 1 .	36 / 1 .
Notes	Mph	Mph	Mph	Mph	Mph	Mph	Mph	Mph	Mph	Mph	Mph	Mph	Mph	Mph
TiO_2	14.11	14.11	13.84	13.97	14.21	13.27	14.81	14.39	12.61	14.05	13.86	14.59	14.80	13.18
Al_2O_3	2.28	2.36	2.16	2.12	2.27	1.90	1.96	2.01	2.03	1.92	1.91	1.78	1.87	1.82
Cr_2O_3	0.01	0.01	bdl	bdl	0.01	0.02	0.01	0.01	0.02	0.04	0.03	bdl	0.03	0.01
FeO	76.14	75.70	76.47	76.19	75.89	74.33	73.25	74.00	75.75	73.91	74.58	73.92	73.50	74.56
MnO	1.26	1.29	1.35	1.37	1.26	1.81	1.64	1.54	1.79	1.89	1.82	1.69	1.72	1.85
MgO	2.73	2.92	2.54	2.47	2.74	2.35	2.25	2.23	2.24	2.27	2.25	2.31	2.44	2.24
NiO	bdl	bdl	bdl	bdl	0.01									
V_2O_3	0.26	0.28	0.26	0.26	0.26									
SiO_2	0.06	0.06	0.06	0.05	0.04									
ZnO	0.13	0.16	0.16	0.17	0.16									
Total	96.98	96.88	96.85	96.60	96.85	93.67	93.91	94.16	94.44	94.07	94.45	94.27	94.35	93.66
Ti	0.386	0.386	0.380	0.385	0.389	0.377	0.420	0.407	0.355	0.398	0.391	0.413	0.418	0.375
Al	0.098	0.101	0.093	0.091	0.097	0.085	0.087	0.089	0.090	0.085	0.084	0.079	0.083	0.081
Cr	0.000	0.000			0.000	0.000	0.000	0.000	0.001	0.001	0.001		0.001	0.000
Fe^{2+}	1.198	1.186	1.198	1.205	1.198	1.187	1.242	1.233	1.173	1.211	1.207	1.229	1.227	1.189
Fe^{3+}	1.118	1.115	1.135	1.128	1.113	1.161	1.072	1.096	1.200	1.118	1.132	1.096	1.081	1.169
Mn	0.039	0.040	0.042	0.042	0.039	0.058	0.052	0.049	0.057	0.060	0.058	0.054	0.055	0.059
Mg	0.148	0.158	0.138	0.135	0.149	0.132	0.126	0.125	0.125	0.127	0.126	0.129	0.137	0.127
Ni					0.000									
V	0.008	0.008	0.008	0.008	0.008									
Si	0.002	0.002	0.002	0.002	0.001									
Zn	0.003	0.004	0.004	0.005	0.004									
Sum	3.000	3.000	3.000	3.000	3.000	3.000	3.000	3.000	3.000	3.000	3.000	3.000	3.000	3.000
Usp	38.8	38.8	38.2	38.7	39.1	37.7	42.1	40.7	35.5	39.8	39.1	41.3	41.8	37.5
Mt	56.2	56.1	57.1	56.7	56.0	58.1	53.6	54.8	60.0	55.9	56.6	54.8	54.1	58.5
Sp	4.9	5.1	4.7	4.6	4.9	4.2	4.4	4.5	4.5	4.3	4.2	3.9	4.1	4.1

Table C11 continued

Unit	**Povo ign**	**Povo ign**	**Povo ign**	**Povo ign**	**Povo ign**	**Povo ign**	**Povo ign**	**Povo ign**	**Povo ign**	**Povo ign**	**Povo ign**	**Povo ign**	**Povo ign**	**Povo ign**
Sample	SM9-1	SM9-1	AZ02-6	AZ02-6	AZ02-6	AZ02-6	AZ02-6	AZ02-6	AZ02-6	AZ02-6	SM10-1	SM10-1	SM10-1	SM10-1
No.	38 / 1 .	42 / 1 .	44 / 1 .	45 / 1 .	47 / 1 .	51 / 1 .	52 / 1 .	53 / 1 .	54 / 1 .	55 / 1 .	154 / 1 .	155 / 1 .	157 / 1 .	158 / 1 .
Notes	Mph	Mph	Mph	Mph	Mph	Mph	Mph	Mph	Mph	Mph	Mph	Mph	Mph	Mph
TiO_2	13.74	13.33	17.21	12.91	14.58	10.63	10.75	11.90	14.81	11.71	12.46	13.49	14.84	13.92
Al_2O_3	1.86	4.10	2.07	1.88	1.79	2.12	1.76	2.68	2.53	1.76	1.51	1.40	2.19	1.84
Cr_2O_3	0.01	0.02	0.01	0.01	bdl	0.01	0.01	bdl	0.04	bdl	0.03	0.03	0.03	bdl
FeO	74.89	72.84	67.33	72.15	70.60	73.55	73.91	72.86	69.82	72.96	76.29	75.38	72.05	72.09
MnO	1.80	1.73	1.98	2.17	1.98	2.14	2.27	1.69	2.11	2.17	2.25	2.20	1.90	2.42
MgO	2.22	2.21	1.48	1.13	1.29	1.28	1.30	1.55	1.14	1.43	1.64	1.51	1.71	1.40
NiO														
V_2O_3														
SiO_2														
ZnO														
Total	94.51	94.22	90.07	90.24	90.24	89.72	89.99	90.68	90.45	90.02	94.17	94.01	92.72	91.68
Ti	0.387	0.373	0.514	0.384	0.434	0.317	0.320	0.350	0.439	0.348	0.354	0.385	0.428	0.408
Al	0.082	0.180	0.097	0.088	0.083	0.099	0.082	0.123	0.118	0.082	0.067	0.063	0.099	0.084
Cr	0.000	0.001	0.000	0.000		0.000	0.000		0.001		0.001	0.001	0.001	
Fe^{2+}	1.206	1.196	1.360	1.245	1.292	1.169	1.167	1.204	1.302	1.191	1.190	1.229	1.269	1.246
Fe^{3+}	1.143	1.073	0.876	1.144	1.048	1.268	1.278	1.177	1.002	1.222	1.223	1.166	1.044	1.100
Mn	0.057	0.055	0.066	0.073	0.066	0.072	0.076	0.056	0.071	0.073	0.072	0.071	0.062	0.080
Mg	0.124	0.123	0.087	0.067	0.076	0.075	0.076	0.090	0.067	0.084	0.092	0.086	0.098	0.081
Ni														
V														
Si														
Zn														
Sum	3.000	3.000	3.000	3.000	3.000	3.000	3.000	3.000	3.000	3.000	3.000	3.000	3.000	3.000
Usp	38.7	37.3	51.4	38.4	43.4	31.7	32.0	35.0	44.0	34.8	35.5	38.6	42.8	40.8
Mt	57.1	53.7	43.8	57.2	52.4	63.4	63.9	58.9	50.1	61.1	61.2	58.3	52.2	55.0
Sp	4.1	9.0	4.8	4.4	4.2	5.0	4.1	6.2	5.9	4.1	3.4	3.1	5.0	4.2

Table C11 continued

Unit	**Povo ign**	**Povo ign**	**Povo ign**	**Povo ign**	**Povo ign**	**Povo ign**	**Povo ign**	**Povo ign**	**Povo ign**	**Povo ign**	**Povo ign**	**Povo ign**	**Povo ign**	**Povo ign**
Sample	SM10-1	SM10-1	SM10-1	SM10-1	SM10-1	SM10-1	SM10-1	SM10-1	SM10-1	AM-2(1)	AM-2(2)	AM-1(1)	AM-1(1)	AM-1(1)
No.	162 / 1 .	Oxides29	Oxides30	Oxides33	Oxides38	Oxides39	Oxides40	Oxides45	Oxides46	Ox2	Ox3	Ox2	Ox3	Ox4
Notes	Mph	Mph	Mph	Mph	Mph	Mph	Mph	Mph	Mph	Mph	Mph	Mph	Mph	Mph
TiO_2	13.39	13.30	12.27	9.14	13.23	13.17	10.78	21.52	24.51	13.04	8.42	14.42	14.53	20.40
Al_2O_3	2.72	1.95	1.76	1.50	1.77	1.39	2.01	0.52	0.49	2.04	2.52	1.87	1.91	1.95
Cr_2O_3	bdl	bdl	bdl	bdl	0.01	bdl	bdl	bdl	bdl	0.02	bdl	bdl	bdl	bdl
FeO	73.30	73.73	74.50	80.67	75.50	76.56	77.06	65.23	63.95	76.09	78.70	75.89	75.66	68.85
MnO	1.56	2.29	3.25	2.16	2.07	2.16	2.01	2.96	2.60	1.73	2.17	1.91	1.87	1.52
MgO	3.04	1.98	1.38	1.19	2.51	1.75	2.03	1.24	1.05	2.18	2.66	2.45	2.48	2.07
NiO										bdl	0.01	bdl	bdl	bdl
V_2O_3										0.15	0.14	0.15	0.14	0.15
SiO_2										0.07	0.04	0.05	0.06	0.06
ZnO										0.30	0.28	0.23	0.22	0.18
Total	94.01	93.25	93.15	94.66	95.09	95.03	93.89	91.48	92.60	95.61	94.93	96.96	96.88	95.18
Ti	0.376	0.381	0.353	0.259	0.370	0.371	0.305	0.641	0.725	0.363	0.234	0.396	0.399	0.576
Al	0.120	0.087	0.079	0.066	0.078	0.061	0.089	0.024	0.023	0.089	0.110	0.080	0.082	0.086
Cr					0.000					0.000				
Fe^{2+}	1.157	1.194	1.169	1.123	1.166	1.205	1.127	1.469	1.577	1.183	1.013	1.199	1.203	1.409
Fe^{3+}	1.129	1.152	1.215	1.416	1.182	1.196	1.300	0.693	0.527	1.174	1.416	1.119	1.110	0.753
Mn	0.049	0.074	0.105	0.069	0.065	0.069	0.064	0.099	0.087	0.054	0.068	0.059	0.058	0.048
Mg	0.169	0.112	0.078	0.067	0.139	0.098	0.114	0.073	0.062	0.120	0.146	0.133	0.135	0.116
Ni											0.000			
V										0.004	0.004	0.004	0.004	0.005
Si										0.003	0.001	0.002	0.002	0.002
Zn										0.008	0.008	0.006	0.006	0.005
Sum	3.000	3.000	3.000	3.000	3.000	3.000	3.000	3.000	3.000	3.000	3.000	3.000	3.000	3.000
Usp	37.6	38.1	35.3	25.9	37.0	37.1	30.5	64.1	72.5	36.5	23.4	39.8	40.1	57.9
Mt	56.5	57.6	60.7	70.8	59.1	59.8	65.0	34.7	26.4	59.0	71.1	56.2	55.8	37.8
Sp	6.0	4.4	4.0	3.3	3.9	3.1	4.5	1.2	1.1	4.5	5.5	4.0	4.1	4.3

Table C12: Ilmenite analyses from the UFG and PIF

Unit	**Fur J dome**	**Fur J sy**	**Fur J sy**	**Fur J sy**	**Fur J sy**	**Fur J sy**	**Fur J sy**	**Fur J sy**	**Fur J sy**	**Fur J sy**	**Fur J sy**
Sample	SM 7-1	Fur-JSyB	Fur-JSyB	Fur-JSyB	Fur-JSyCZ1	Fur-JSyCZ1	Fur-JSyCZ1	Fur-JSyCZ1	Fur-JSyCZ1	Fur-JSyCZ2	Fur-JSyCZ3
No.	Oxide02	Ox1	Ox3	Ox5	Ox1	Ox2	Ox3	Ox4	Ox5	Ox6	Ox7
Notes	Mph	Mph	Mph	Mph	Mph	Mph	Mph	Mph	Mph	Mph	Mph
TiO_2	48.97	51.81	51.93	51.14	48.71	46.57	48.64	47.26	48.87	49.48	49.88
Al_2O_3	0.03	bdl	bdl	0.02	bdl	0.01	0.02	bdl	bdl	0.03	0.01
Cr_2O_3	bdl	bdl	bdl	bdl	bdl	bdl	bdl	bdl	bdl	bdl	bdl
FeO	42.26	27.57	34.05	35.07	38.15	36.89	37.55	37.12	36.96	33.63	35.54
MnO	3.93	21.23	14.39	13.13	10.53	10.78	10.73	10.64	11.73	14.03	12.52
MgO	3.31	0.09	0.12	0.18	0.07	0.04	0.04	0.06	0.02	0.07	0.03
NiO		bdl	bdl	bdl	0.01	bdl	bdl	bdl	0.01	bdl	0.01
V_2O_3		bdl	bdl	0.02	0.02	0.02	0.01	0.07	0.03	bdl	0.02
SiO_2		0.02	0.01	bdl	0.03	0.02	0.03	bdl	bdl	0.03	0.05
ZnO		0.06	0.07	0.03	0.08	0.08	0.07	0.09	0.10	0.26	0.10
Total	98.50	100.78	100.57	99.59	97.60	94.41	97.10	95.24	97.72	97.53	98.16
Ti	0.915	0.972	0.977	0.971	0.943	0.932	0.947	0.938	0.946	0.959	0.961
Al	0.001			0.001		0.000	0.001			0.001	0.000
Cr											
Fe^{2+}	0.710	0.519	0.666	0.682	0.710	0.687	0.710	0.696	0.687	0.646	0.687
Fe^{3+}	0.168	0.056	0.046	0.058	0.111	0.134	0.104	0.123	0.108	0.079	0.074
Mn	0.083	0.448	0.305	0.281	0.230	0.243	0.235	0.238	0.256	0.306	0.272
Mg	0.123	0.003	0.005	0.007	0.003	0.001	0.002	0.002	0.001	0.003	0.001
Ni					0.000				0.000		0.000
V				0.000	0.000	0.000	0.000	0.001	0.001		0.000
Si		0.001	0.000		0.001	0.001	0.001			0.001	0.001
Zn		0.001	0.001	0.001	0.001	0.001	0.001	0.002	0.002	0.005	0.002
Sum	2.000	2.000	2.000	2.000	2.000	2.000	2.000	2.000	2.000	2.000	2.000
Ilm	77.6	53.5	68.3	70.4	75.3	73.7	75.0	74.3	72.8	67.7	71.6
Pyr	9.0	46.2	31.2	28.9	24.4	26.1	24.9	25.4	27.1	32.1	28.3
Geik	13.4	0.4	0.5	0.7	0.3	0.2	0.2	0.2	0.1	0.3	0.1

Table C12 continued

Unit	**Povo fall**	**Povo ign**	**Povo ign**	**Povo ign**	**Povo ign**	**Povo ign**	**Povo ign**	**Povo ign**	**Povo ign**	**Povo ign**	**Povo ign**
Sample	AM-2(4)	SM9-1	SM9-1	SM9-1	SM9-1	SM9-1	SM9-1	SM9-1	SM9-1	SM9-1	SM9-1
No.	Ox3	22 / 1 .	25 / 1 .	26 / 1 .	27 / 1 .	28 / 1 .	31 / 1 .	32 / 1 .	33 / 1 .	34 / 1 .	39 / 1 .
Notes	Mph	Mph	Mph	Mph	Mph	Mph	Mph	Mph	Mph	Mph	Mph
TiO_2	44.99	45.05	44.46	44.51	44.58	44.25	44.92	44.89	45.71	46.12	44.22
Al_2O_3	0.24	0.22	0.20	0.21	0.18	0.20	0.22	0.19	0.22	0.23	0.20
Cr_2O_3	bdl	bdl	bdl	0.04	bdl	0.03	bdl	0.02	0.03	bdl	bdl
FeO	46.49	44.61	45.65	45.91	45.14	45.80	44.75	44.98	43.98	42.99	44.72
MnO	1.47	2.00	2.06	2.10	1.91	2.10	2.42	2.40	2.35	2.26	2.31
MgO	3.93	3.78	3.45	3.49	3.57	3.48	3.86	3.79	3.66	3.67	3.84
NiO	bdl										
V_2O_3	0.14										
SiO_2	0.01										
ZnO	0.05										
Total	97.32	95.66	95.81	96.25	95.38	95.85	96.16	96.26	95.94	95.25	95.27
Ti	0.843	0.860	0.849	0.846	0.855	0.845	0.852	0.852	0.872	0.886	0.847
Al	0.007	0.007	0.006	0.006	0.005	0.006	0.006	0.006	0.006	0.007	0.006
Cr				0.001		0.001		0.000	0.001		
Fe^{2+}	0.666	0.674	0.674	0.670	0.678	0.668	0.656	0.658	0.683	0.698	0.651
Fe^{3+}	0.303	0.273	0.296	0.301	0.285	0.304	0.289	0.291	0.250	0.221	0.301
Mn	0.031	0.043	0.044	0.045	0.041	0.045	0.052	0.051	0.050	0.049	0.050
Mg	0.146	0.143	0.131	0.131	0.136	0.132	0.145	0.143	0.138	0.140	0.146
Ni											
V	0.003										
Si	0.000										
Zn	0.001										
Sum	2.000	2.000	2.000	2.000	2.000	2.000	2.000	2.000	2.000	2.000	2.000
Ilm	79.0	78.4	79.4	79.2	79.3	79.1	76.9	77.2	78.4	78.7	76.9
Pyr	3.7	5.0	5.2	5.3	4.8	5.3	6.1	6.0	5.8	5.5	5.9
Geik	17.3	16.6	15.4	15.5	15.9	15.6	17.0	16.7	15.9	15.8	17.2

Table C12 continued

Unit	**Povo ign**	**Povo ign**	**Povo ign**	**Povo ign**	**Povo ign**	**Povo ign**	**Povo ign**	**Povo ign**	**Povo ign**	**Povo ign**	**Povo ign**
Sample	SM9-1	SM9-1	AZ02-6	AZ02-6	AZ02-6	AZ02-6	AZ02-6	AZ02-6	AZ02-6	SM10-1	SM10-1
No.	40 / 1 .	41 / 1 .	46 / 1 .	48 / 1 .	49 / 1 .	50 / 1 .	56 / 1 .	57 / 1 .	58 / 1 .	149 / 1 .	150 / 1 .
Notes	Mph	Mph	Mph	Mph	Mph	Mph	Mph	Mph	Mph	Mph	Mph
TiO_2	43.37	46.14	43.38	47.66	41.84	43.99	47.72	49.26	49.61	43.99	44.01
Al_2O_3	0.88	0.21	0.22	0.22	0.20	0.24	0.14	0.17	0.22	0.18	0.21
Cr_2O_3	bdl	bdl	0.01	0.03	bdl	bdl	bdl	0.03	bdl	0.01	bdl
FeO	43.60	43.09	44.70	39.58	45.53	41.59	40.35	37.87	38.12	45.80	45.88
MnO	1.75	1.95	1.61	2.80	2.71	2.62	2.47	2.32	2.75	2.50	2.51
MgO	3.05	3.31	2.20	1.37	2.54	2.38	2.37	2.90	1.88	3.23	3.30
NiO											
V_2O_3											
SiO_2											
ZnO											
Total	92.64	94.69	92.12	91.65	92.80	90.81	93.05	92.54	92.56	95.70	95.91
Ti	0.857	0.895	0.871	0.974	0.830	0.895	0.952	0.985	1.001	0.842	0.841
Al	0.027	0.006	0.007	0.007	0.006	0.008	0.005	0.005	0.007	0.005	0.006
Cr			0.000	0.001				0.001		0.000	
Fe^{2+}	0.698	0.725	0.747	0.854	0.670	0.739	0.803	0.818	0.855	0.666	0.662
Fe^{3+}	0.259	0.204	0.251	0.045	0.335	0.202	0.092	0.024	0.000	0.309	0.313
Mn	0.039	0.043	0.036	0.064	0.061	0.060	0.056	0.052	0.063	0.054	0.054
Mg	0.120	0.127	0.088	0.055	0.100	0.096	0.094	0.115	0.075	0.123	0.125
Ni											
V											
Si											
Zn											
Sum	2.000	2.000	2.000	2.000	2.000	2.000	2.000	2.000	2.000	2.000	2.000
Ilm	81.5	81.0	85.8	87.7	80.7	82.6	84.3	83.0	86.1	79.1	78.7
Pyr	4.5	4.8	4.2	6.6	7.3	6.7	5.8	5.3	6.3	6.4	6.4
Geik	14.0	14.2	10.1	5.7	12.0	10.7	9.8	11.7	7.6	14.6	14.9

Table C12 continued

Unit	**Povo ign**	**Povo ign**	**Povo ign**	**Povo ign**	**Povo ign**	**Povo ign**	**Povo ign**	**Povo ign**	**Povo ign**	**Povo ign**	**Povo ign**
Sample	SM10-1	SM10-1	SM10-1	SM10-1	SM10-1	SM10-1	SM10-1	SM10-1	SM10-1	SM10-1	SM10-1
No.	151 / 1 .	152 / 1 .	153 / 1 .	156 / 1 .	159 / 1 .	160 / 1 .	163 / 1 .	164 / 1 .	165 / 1 .	Ox32	Ox34
Notes	Mph	Mph	Mph	Mph	Mph	Mph	Mph	Mph	Mph	Mph	Mph
TiO_2	44.06	43.90	44.02	45.27	44.15	44.02	44.36	44.29	44.22	46.04	47.94
Al_2O_3	0.15	0.22	0.20	0.20	0.21	0.18	0.19	0.18	0.20	0.19	0.17
Cr_2O_3	bdl	bdl	0.02	0.02	0.02	bdl	bdl	0.03	bdl	bdl	bdl
FeO	45.91	46.11	46.34	43.98	46.24	46.05	45.91	45.44	45.71	45.55	43.86
MnO	2.55	2.45	2.45	2.38	2.18	2.14	2.62	2.69	2.70	3.10	2.25
MgO	3.21	3.14	3.17	3.58	3.31	3.42	3.25	3.05	3.30	2.94	2.49
NiO											
V_2O_3											
SiO_2											
ZnO											
Total	95.88	95.82	96.21	95.43	96.10	95.78	96.28	95.68	96.10	97.82	96.71
Ti	0.843	0.840	0.839	0.868	0.842	0.841	0.845	0.850	0.843	0.866	0.918
Al	0.005	0.007	0.006	0.006	0.006	0.005	0.006	0.006	0.006	0.006	0.005
Cr			0.000	0.000	0.000			0.001			
Fe^{2+}	0.666	0.668	0.666	0.681	0.670	0.666	0.666	0.676	0.660	0.691	0.775
Fe^{3+}	0.310	0.313	0.316	0.257	0.310	0.313	0.306	0.294	0.309	0.262	0.159
Mn	0.055	0.053	0.053	0.051	0.047	0.046	0.056	0.058	0.058	0.066	0.049
Mg	0.122	0.119	0.120	0.136	0.125	0.129	0.123	0.116	0.125	0.110	0.095
Ni											
V											
Si											
Zn											
Sum	2.000	2.000	2.000	2.000	2.000	2.000	2.000	2.000	2.000	2.000	2.000
Ilm	79.0	79.5	79.4	78.4	79.6	79.1	78.8	79.5	78.3	79.8	84.4
Pyr	6.5	6.3	6.3	5.9	5.6	5.5	6.7	6.8	6.9	7.6	5.3
Geik	14.5	14.2	14.3	15.7	14.8	15.4	14.5	13.6	14.8	12.7	10.3

Table C12 continued

Unit	**Povo ign**	**Povo ign**	**Povo ign**	**Povo ign**	**Povo ign**	**Povo ign**	**Povo ign**	**Povo ign**	**Povo ign**	**Povo ign**	**Povo ign**
Sample	SM10-1	SM10-1	SM10-1	SM10-1	SM10-1	SM10-1	SM10-1	AM-2(2)	AM-1(1)	SM9-1	SM9-1
No.	Ox35	Ox36	Ox37	Ox41	Ox42	Ox44	Ox47	Ox1	Ox1	17 / 1 .	18 / 1 .
Notes	Mph	Mph	Mph	Mph	Mph	Mph	Mph	Mph	Mph	Mph	Mph
TiO_2	47.58	46.22	46.08	46.44	46.35	46.21	47.35	52.27	49.20	44.86	46.39
Al_2O_3	0.17	0.16	0.18	0.11	0.18	0.10	0.15	0.16	0.17	0.20	0.31
Cr_2O_3	bdl	bdl	bdl	bdl	bdl	bdl	bdl	bdl	bdl	0.03	0.02
FeO	43.89	45.79	45.46	44.08	44.78	45.80	44.23	38.43	45.64	44.40	44.23
MnO	3.01	2.63	2.89	4.85	3.31	3.65	3.16	1.94	2.49	2.25	0.98
MgO	2.77	3.38	3.06	2.58	3.48	1.65	3.32	3.17	3.58	4.10	1.66
NiO								bdl	bdl		
V_2O_3								0.09	0.05		
SiO_2								0.01	0.02		
ZnO								0.02	0.11		
Total	97.42	98.18	97.67	98.06	98.10	97.41	98.21	96.09	101.26	95.84	93.58
Ti	0.902	0.863	0.867	0.875	0.866	0.883	0.886	1.007	0.892	0.853	0.923
Al	0.005	0.005	0.005	0.003	0.005	0.003	0.004	0.005	0.005	0.006	0.010
Cr										0.001	0.000
Fe^{2+}	0.733	0.683	0.692	0.675	0.667	0.742	0.696	0.823	0.711	0.650	0.836
Fe^{3+}	0.192	0.268	0.260	0.248	0.263	0.231	0.224	0.000	0.209	0.288	0.143
Mn	0.064	0.055	0.061	0.103	0.070	0.079	0.067	0.042	0.051	0.048	0.022
Mg	0.104	0.125	0.114	0.096	0.129	0.062	0.123	0.121	0.129	0.154	0.065
Ni										0.000	0.000
V								0.002	0.001		
Si								0.000	0.000		
Zn								0.000	0.002		
Sum	2.000	2.000	2.000	2.000	2.000	2.000	2.000	2.000	2.000	2.000	2.000
Ilm	81.3	79.1	79.8	77.2	77.1	84.0	78.6	83.5	79.8	76.2	90.5
Pyr	7.1	6.4	7.1	11.8	8.0	8.9	7.5	4.3	5.7	5.7	2.4
Geik	11.5	14.5	13.2	11.0	14.9	7.1	13.9	12.3	14.4	18.1	7.1

Table C13: Biotite analyses from the UFG and the PIF

Unit	**Fur J**	**Fur J**	**Fur J**	**Fur J**	**Fur J**	**Fur J**	**Fur J dome**	**Fur J dome**	**Fur J dome**	**Fur J dome**	**Fur J dome**
Sample	S005	S005	S005	S005	S005	S005	SM 7-1	SM 7-1	SM 7-1	SM 7-1	SM 7-1
No.	Bio1	Bio2	Bio3	Bio4	Bio5	Bio6	Bio01	Bio02	Bio03	Bio04	Bio05
Notes	Mph	Mph	Mph	Mph	Mph	Mph	Mph	Mph	Mph	Mph	Mph
SiO_2	37.52	36.59	35.86	36.56	37.18	36.90	37.34	37.34	37.55	37.88	37.57
TiO_2	5.43	7.39	8.12	7.79	5.89	6.30	7.25	7.37	6.11	5.56	5.40
Al_2O_3	12.09	13.00	12.95	12.84	12.35	12.49	13.18	13.16	12.69	12.65	12.38
FeO	16.35	17.46	17.13	16.98	16.56	16.48	15.45	14.51	16.55	16.27	17.39
MnO	0.58	0.60	0.53	0.63	0.54	0.56	0.41	0.32	0.51	0.48	0.58
MgO	13.40	11.97	11.38	11.58	13.08	12.99	13.58	13.95	13.54	13.55	13.71
CaO	bdl	0.01	bdl	bdl	bdl	bdl	0.01	bdl	bdl	0.02	0.01
Na_2O	0.90	0.91	0.98	0.84	0.96	0.87	0.94	0.89	0.92	1.09	0.88
K_2O	8.87	8.62	8.55	8.69	8.83	8.68	8.91	8.87	8.96	8.82	9.03
F	1.37	1.01	0.90	0.96	1.32	1.26					
Cl	0.04	0.03	0.03	0.03	0.04	0.03					
Total	96.55	97.59	96.43	96.90	96.74	96.55	97.06	96.41	96.83	96.32	96.95
Si	5.683	5.490	5.442	5.513	5.625	5.585	5.511	5.522	5.590	5.654	5.612
Ti	0.619	0.834	0.927	0.883	0.670	0.717	0.805	0.820	0.684	0.624	0.607
Al^{IV}	2.158	2.299	2.316	2.282	2.202	2.228	2.293	2.294	2.227	2.225	2.180
Al^{VI}	0.000	0.000	0.000	0.000	0.000	0.000	0.000	0.000	0.000	0.000	0.000
Fe	2.071	2.191	2.174	2.141	2.095	2.086	1.907	1.795	2.060	2.031	2.172
Mn	0.074	0.076	0.068	0.080	0.069	0.071	0.051	0.040	0.064	0.061	0.074
Mg	3.025	2.677	2.574	2.603	2.950	2.931	2.988	3.075	3.005	3.015	3.053
Ca		0.001					0.001			0.003	0.002
Na	0.265	0.265	0.289	0.247	0.281	0.254	0.268	0.257	0.266	0.316	0.253
K	1.714	1.650	1.655	1.671	1.704	1.676	1.677	1.673	1.701	1.679	1.720
OH	3.335	3.512	3.560	3.537	3.359	3.389					
F	0.656	0.479	0.433	0.456	0.632	0.603					
Cl	0.009	0.008	0.007	0.007	0.009	0.008					
Sum	19.609	19.484	19.446	19.422	19.596	19.549	19.508	19.476	19.596	19.607	19.678

Table C13 continued

Unit	Fur J dome	Fur J dome	Fur J dome	Fur J dome	Fur J dome	Fur J dome	Fur J dome	Fur J dome	Fur J sy	Fur J sy	Fur J sy
Sample	SM 7-1	SM 7-1	SM 7-1	SM 7-1	SM 7-1	SM 7-1	SM 7-1	SM 7-1	S035	S035	S035
No.	78 / 1 .	79 / 1 .	80 / 1 .	80 / 1 .	78 / 1 .	79 / 1 .	168 / 1 .	169 / 1 .	Bio1	Bio2	Bio4
Notes	Mph	Mph	Mph	Mph	Mph	Mph	Mph	Mph	Gm	Gm	Gm
SiO_2	37.18	37.90	37.67	38.23	37.74	38.47	37.37	37.52	37.35	37.86	36.52
TiO_2	5.80	5.69	5.26	5.34	5.89	5.78	5.13	5.29	3.85	3.72	6.84
Al_2O_3	12.22	12.05	12.18	12.36	12.40	12.23	11.95	12.18	11.36	11.24	12.54
FeO	16.42	16.12	16.67	16.91	16.67	16.36	17.33	16.84	23.78	22.07	21.35
MnO	0.50	0.49	0.62	0.63	0.51	0.50	0.58	0.62	1.91	1.64	0.86
MgO	13.42	13.87	13.31	13.51	13.62	14.08	13.28	13.71	8.94	10.11	8.52
CaO	0.02	0.02	0.03	0.03	0.02	0.02	0.05	bdl	bdl	bdl	bdl
Na_2O	0.92	0.97	0.88	0.89	0.93	0.99	1.03	0.90	0.52	0.49	1.07
K_2O	8.78	8.77	8.50	8.63	8.91	8.90	8.32	8.62	9.26	9.22	8.73
F							3.40	1.71	1.53	2.14	1.78
Cl							0.05	0.04	0.01	0.01	0.03
Total	95.27	95.89	95.10	96.53	96.70	97.33	98.47	97.42	98.51	98.49	98.24
Si	5.627	5.680	5.700	5.699	5.626	5.679	5.679	5.654	5.794	5.847	5.603
Ti	0.660	0.641	0.599	0.599	0.660	0.641	0.587	0.600	0.449	0.432	0.789
Al^{IV}	2.180	2.129	2.172	2.172	2.179	2.129	2.140	2.163	2.077	2.046	2.268
Al^{VI}	0.000	0.000	0.000	0.000	0.000	0.000	0.000	0.000	0.000	0.000	0.000
Fe	2.079	2.020	2.109	2.109	2.078	2.020	2.202	2.122	3.085	2.850	2.740
Mn	0.064	0.062	0.079	0.079	0.064	0.062	0.075	0.078	0.251	0.215	0.111
Mg	3.029	3.099	3.003	3.003	3.028	3.099	3.007	3.079	2.067	2.327	1.949
Ca	0.004	0.004	0.005	0.005	0.004	0.004	0.007				
Na	0.270	0.283	0.257	0.257	0.270	0.283	0.302	0.263	0.155	0.146	0.319
K	1.695	1.676	1.640	1.640	1.695	1.676	1.612	1.656	1.832	1.816	1.708
OH							2.353	3.172	3.246	2.953	3.128
F							1.633	0.816	0.751	1.045	0.864
Cl							0.014	0.011	0.004	0.001	0.008
Sum	19.606	19.593	19.564	19.564	19.606	19.594	19.621	19.625	19.712	19.679	19.488

Table C13 continued

Unit	Fur J sy	Fur J sy	Fur J sy	Fur J sy	Fur J sy	Fur I	Fur I	Fur I	Fur I	Fur I	Fur I
Sample	S035	S035	S035	S035	S035	S036	S036	S036	S036	S036	S036
No.	Bio5	Bio6	Bio7	Bio8	Bio9	Bio1	Bio2	Bio3	Bio4	Bio5	Bio6
Notes	Gm	Gm	Gm	Gm	Gm	Mph	Mph	Mph	Mph	Mph	Mph
SiO_2	37.60	36.65	36.66	36.82	36.23	36.78	36.83	36.41	36.82	36.89	37.08
TiO_2	5.88	7.37	4.63	4.60	3.44	6.71	4.99	7.77	8.33	5.99	8.36
Al_2O_3	12.44	12.94	11.45	9.70	10.75	12.46	11.70	12.96	13.14	12.43	13.26
FeO	17.09	18.99	25.82	27.36	28.58	16.57	15.84	14.24	13.21	16.78	13.18
MnO	0.61	0.69	1.31	1.30	1.48	0.61	0.57	0.31	0.26	0.66	0.23
MgO	12.17	10.19	7.36	6.40	6.12	12.63	13.64	13.16	13.67	13.09	13.84
CaO	bdl	0.07	bdl	bdl	0.09	0.02	bdl	bdl	bdl	0.02	bdl
Na_2O	0.93	1.00	0.62	0.53	0.59	0.90	0.78	0.86	0.82	0.94	0.86
K_2O	9.10	8.88	8.87	8.72	8.69	8.76	8.72	8.76	8.95	8.64	8.90
F	2.34	1.94	1.94	1.59	1.60	1.25	1.66	0.75	0.69	1.37	0.72
Cl	0.04	0.03	0.04	0.01	0.04	0.03	0.03	0.02	0.02	0.03	0.02
Total	98.21	98.75	98.70	97.03	97.61	96.72	94.76	95.24	95.90	96.83	96.45
Si	5.677	5.537	5.742	5.900	5.812	5.567	5.697	5.500	5.490	5.585	5.492
Ti	0.668	0.837	0.545	0.554	0.415	0.764	0.580	0.883	0.934	0.682	0.931
Al^{IV}	2.214	2.304	2.114	1.832	2.033	2.223	2.133	2.308	2.309	2.218	2.315
Al^{VI}	0.000	0.000	0.000	0.000	0.000	0.000	0.000	0.000	0.000	0.000	0.000
Fe	2.158	2.399	3.382	3.666	3.835	2.097	2.049	1.799	1.647	2.125	1.633
Mn	0.079	0.088	0.174	0.176	0.201	0.079	0.074	0.040	0.032	0.084	0.028
Mg	2.739	2.295	1.718	1.529	1.464	2.850	3.145	2.964	3.039	2.954	3.056
Ca		0.011			0.015	0.003				0.002	
Na	0.273	0.293	0.189	0.164	0.185	0.263	0.233	0.251	0.236	0.275	0.246
K	1.753	1.711	1.772	1.782	1.778	1.691	1.720	1.688	1.702	1.669	1.681
OH	2.872	3.065	3.029	3.191	3.178	3.393	3.180	3.635	3.671	3.336	3.656
F	1.117	0.927	0.961	0.806	0.812	0.598	0.812	0.359	0.324	0.656	0.338
Cl	0.011	0.009	0.010	0.003	0.011	0.008	0.008	0.006	0.005	0.008	0.006
Sum	19.561	19.476	19.636	19.603	19.738	19.535	19.633	19.433	19.390	19.595	19.383

Table C13 continued

Unit	Fur H	Fur H	Fur H	Fur H	Fur H	Fur H	Fur H	Povo Fall	Povo Fall	Povo Fall	Povo Fall
Sample	S001	S001	S001	S001	S001	S001	S001	S052	S052	S052	S052
No.	Bio1	Bio2	Bio3	Bio4	Bio6	Bio7	Bio8	Bio1	Bio2	Bio3	Bio4
Notes	Mph	Mph	Mph	Mph	Mph	Mph	Mph	Mph	Mph	Mph	Mph
SiO_2	37.46	37.88	37.56	37.31	36.81	37.05	37.76	36.23	36.27	34.24	34.46
TiO_2	5.08	5.09	5.06	5.60	5.52	5.01	4.94	7.31	7.32	8.27	8.24
Al_2O_3	12.03	12.13	11.90	12.19	12.05	11.76	11.90	13.63	13.65	14.00	13.73
FeO	17.48	17.38	17.51	17.38	17.20	17.16	17.70	14.18	14.62	15.07	14.88
MnO	0.70	0.65	0.67	0.65	0.59	0.64	0.68	0.24	0.25	0.25	0.30
MgO	13.25	13.39	13.27	12.87	12.86	12.72	13.40	13.65	13.59	12.24	12.30
CaO	0.01	0.02	0.02	bdl	0.01	0.05	0.06	0.00	0.00	0.00	0.01
Na_2O	0.90	0.87	0.93	0.88	0.91	0.90	0.96	0.77	0.69	0.70	0.71
K_2O	8.68	8.66	8.86	8.67	8.79	8.54	8.87	9.55	8.82	8.24	8.22
F	1.50	1.51	1.46	1.40	1.23	1.35	1.48	0.54	0.52	0.42	0.41
Cl	0.04	0.04	0.04	0.04	0.05	0.05	0.03	0.03	0.03	0.03	0.03
Total	97.13	97.62	97.29	96.99	96.02	95.23	97.79	96.13	95.77	93.47	93.30
Si	5.675	5.696	5.685	5.651	5.632	5.714	5.690	5.429	5.440	5.280	5.318
Ti	0.579	0.576	0.576	0.638	0.635	0.581	0.560	0.824	0.826	0.959	0.956
Al^{IV}	2.148	2.150	2.123	2.176	2.173	2.138	2.114	2.408	2.413	2.545	2.497
Al^{VI}	0.000	0.000	0.000	0.000	0.000	0.000	0.000	0.000	0.000	0.000	0.000
Fe	2.215	2.186	2.217	2.202	2.201	2.213	2.231	1.777	1.834	1.943	1.920
Mn	0.090	0.083	0.086	0.084	0.077	0.084	0.087	0.030	0.032	0.033	0.039
Mg	2.992	3.002	2.994	2.906	2.933	2.924	3.010	3.049	3.039	2.814	2.829
Ca	0.002	0.003	0.004		0.002	0.009	0.010	0.000	0.000	0.000	0.002
Na	0.264	0.255	0.274	0.258	0.269	0.268	0.281	0.225	0.201	0.210	0.213
K	1.677	1.661	1.711	1.675	1.715	1.680	1.705	1.825	1.687	1.621	1.618
OH	3.272	3.272	3.290	3.319	3.392	3.328	3.286	3.736	3.744	3.785	3.789
F	0.719	0.718	0.699	0.671	0.595	0.658	0.705	0.255	0.248	0.206	0.202
Cl	0.010	0.010	0.011	0.010	0.013	0.013	0.009	0.008	0.009	0.008	0.008
Sum	19.643	19.611	19.669	19.589	19.638	19.610	19.686	19.568	19.472	19.404	19.393

Table C13 continued

Unit	Povo Fall	Povo Fall	Povo Ign	Povo Ign	Povo Ign	Povo Ign	Povo Ign	Povo Ign	Povo Ign	Povo Ign	Povo Ign
Sample	S052	S052	SM10-1Biot01	SM10-1Biot02	SM10-1Biot03	SM10-1Biot04	SM10-1Biot05	SM10-1Biot06	SM10-1Biot07	SM10-1Biot08	SM10-1Biot09_core
No.	Bio5	Bio6	Bio1	Bio2	Bio3	Bio4	Bio5	Bio6	Bio7	Bio8	Bio9
Notes	Mph	Mph	Mph	Mph	Mph	Mph	Mph	Mph	Mph	Mph	Mph
SiO_2	34.67	34.86	36.85	37.17	36.84	37.32	37.09	37.70	37.44	37.11	37.23
TiO_2	8.06	7.81	7.25	7.28	7.26	7.29	6.51	6.91	7.13	7.44	7.27
Al_2O_3	14.12	13.85	13.71	13.38	13.98	13.57	13.57	13.72	13.74	13.66	13.79
FeO	14.74	14.85	14.02	14.34	14.25	14.21	14.00	14.07	14.34	14.19	14.36
MnO	0.24	0.30	0.29	0.37	0.39	0.31	0.36	0.35	0.39	0.38	0.34
MgO	12.67	12.67	14.42	14.22	13.79	14.28	14.28	14.44	14.38	14.26	13.98
CaO	0.00	0.00	0.05	0.01	0.01	0.00	0.06	0.01	0.02	0.01	0.02
Na_2O	0.72	0.67	0.88	0.82	0.71	0.80	0.87	0.80	0.77	0.81	0.81
K_2O	8.19	8.38	9.03	9.04	8.85	9.04	9.07	9.01	9.00	9.22	9.04
F	0.45	0.49									
Cl	0.03	0.03	0.05	0.04	0.04	0.05	0.03	0.04	0.05	0.03	0.03
Total	93.89	93.91	96.55	96.67	96.12	96.86	95.85	97.05	97.26	97.11	96.87
Si	5.306	5.344	5.441	5.487	5.459	5.488	5.514	5.523	5.484	5.454	5.479
Ti	0.928	0.900	0.805	0.808	0.809	0.806	0.728	0.761	0.785	0.822	0.805
Al^{IV}	2.547	2.503	2.386	2.328	2.442	2.352	2.378	2.369	2.372	2.366	2.392
Al^{VI}	0.000	0.000	0.000	0.000	0.000	0.000	0.000	0.000	0.000	0.000	0.000
Fe	1.886	1.904	1.731	1.771	1.766	1.748	1.741	1.724	1.757	1.744	1.767
Mn	0.031	0.039	0.037	0.046	0.049	0.039	0.046	0.043	0.048	0.047	0.043
Mg	2.890	2.895	3.174	3.129	3.046	3.130	3.165	3.153	3.140	3.124	3.067
Ca	0.000	0.000	0.008	0.002	0.002	0.000	0.009	0.002	0.003	0.002	0.003
Na	0.213	0.199	0.251	0.234	0.203	0.227	0.252	0.228	0.219	0.231	0.231
K	1.599	1.639	1.701	1.702	1.673	1.696	1.720	1.684	1.682	1.728	1.697
OH	3.774	3.754									
F	0.218	0.237									
Cl	0.009	0.009	0.012	0.010	0.010	0.012	0.008	0.011	0.013	0.008	0.007
Sum	19.399	19.423	19.536	19.508	19.449	19.489	19.555	19.487	19.493	19.520	19.484

Table C13 continued

Unit	**Povo Ign**	**Povo Ign**	**Povo Ign**	**Povo Ign**	**Povo Ign**	**Povo Ign**	**Povo Ign**	**Povo Ign**	**Povo Ign**	**Povo Ign**	**Povo Ign**
Sample	SM10-1Biot10	SM10-1Biot09_rim	SM10-1	SM10-1	SM10-1	SM10-1	SM10-1	SM10-1	SM10-1	SM10-1	SM9-1
No.	Bio10	Bio11	170 / 1 .	170 / 2 .	170 / 3 .	170 / 4 .	170 / 8 .	170 / 9 .	170 / 10 .	171 / 1 .	59 / 1 .
Notes	Mph	Mph	Mph	Mph	Mph	Mph	Mph	Mph	Mph	Mph	Mph
SiO_2	36.83	37.33	36.47	34.62	34.19	34.22	33.93	36.25	36.79	36.70	37.11
TiO_2	7.38	7.35	7.66	8.55	8.58	8.37	8.10	7.68	7.23	7.08	7.37
Al_2O_3	13.55	13.81	13.59	14.31	14.09	14.09	13.88	13.65	13.27	13.49	13.49
FeO	14.17	14.00	14.34	14.78	14.92	14.91	14.66	14.32	14.61	14.39	14.14
MnO	0.39	0.38	0.36	0.37	0.37	0.36	0.35	0.36	0.34	0.37	0.36
MgO	14.15	14.18	13.74	12.49	12.24	12.56	12.36	13.75	14.01	14.10	14.10
CaO	0.01	0.03	0.02	0.01	0.02	0.00	0.01	0.00	0.02	0.02	0.02
Na_2O	0.74	0.89	0.81	0.74	0.78	0.75	0.68	0.76	0.80	0.81	0.83
K_2O	9.18	9.16	8.74	7.78	7.74	7.78	7.63	8.48	8.69	8.77	8.85
F			0.66	0.53	0.41	0.50	0.78	0.70	0.60	0.79	0.72
Cl	0.03	0.03	0.03	0.04	0.02	0.03	0.08	0.03	0.03	0.04	0.04
Total	96.43	97.15	96.42	94.22	93.35	93.57	92.44	95.97	96.37	96.56	97.04
Si	5.453	5.473	5.424	5.229	5.216	5.214	5.242	5.407	5.479	5.462	5.484
Ti	0.822	0.810	0.857	0.971	0.985	0.959	0.941	0.862	0.810	0.793	0.819
Al^{IV}	2.365	2.387	2.382	2.548	2.533	2.531	2.527	2.399	2.329	2.367	2.349
Al^{VI}	0.000	0.000	0.000	0.000	0.000	0.000	0.000	0.000	0.000	0.000	0.000
Fe	1.755	1.717	1.784	1.868	1.903	1.900	1.894	1.786	1.820	1.791	1.748
Mn	0.049	0.047	0.045	0.048	0.048	0.046	0.045	0.045	0.042	0.047	0.045
Mg	3.123	3.099	3.045	2.812	2.783	2.852	2.846	3.059	3.109	3.129	3.107
Ca	0.001	0.004	0.002	0.002	0.003	0.000	0.001	0.000	0.003	0.004	0.003
Na	0.213	0.253	0.234	0.216	0.230	0.220	0.203	0.220	0.230	0.235	0.238
K	1.734	1.713	1.658	1.499	1.506	1.512	1.503	1.613	1.651	1.665	1.668
OH			3.681	3.737	3.799	3.749	3.598	3.662	3.712	3.621	3.654
F			0.311	0.252	0.195	0.242	0.381	0.331	0.280	0.370	0.337
Cl	0.007	0.007	0.008	0.011	0.006	0.009	0.021	0.007	0.007	0.009	0.009
Sum	19.516	19.506	19.474	19.383	19.400	19.428	19.407	19.448	19.488	19.512	19.476

Unit	**Povo Ign**	**Povo Ign**	**Povo Ign**	**Povo Ign**	**Povo Ign**	**Povo Ign**	**Povo Ign**	**Povo Ign**	**Povo Ign**	**Povo Ign**	**Povo Ign**
Sample	SM9-1	SM9-1	SM9-1	SM9-1	SM9-1	SM9-1	SM9-1	SM9-1	SM9-1	SM9-1	SM9-1
No.	60 / 1 .	61 / 1 .	62 / 1 .	63 / 1 .	64 / 1 .	65 / 1 .	66 / 1 .	67 / 1 .	68 / 1 .	121 / 1 .	121 / 2 .
Notes	Mph	Mph	Mph	Mph	Mph	Mph	Mph	Mph	Mph	Mph	Mph
SiO_2	37.27	36.74	36.97	36.64	35.70	37.03	36.34	36.80	36.83	37.04	36.78
TiO_2	7.33	6.96	6.99	7.11	6.87	6.96	6.93	7.14	6.69	7.48	7.27
Al_2O_3	13.49	13.35	13.56	13.17	12.71	13.62	13.39	13.36	13.28	13.62	13.23
FeO	13.89	14.03	13.84	13.87	13.14	13.69	13.89	13.75	13.39	14.36	14.26
MnO	0.34	0.35	0.37	0.35	0.33	0.34	0.35	0.37	0.33	0.36	0.36
MgO	14.28	14.16	14.21	14.26	13.51	13.87	13.63	14.07	13.65	14.29	14.39
CaO	0.03	0.03	0.03	0.03	0.02	0.02	0.03	0.03	0.04	0.04	0.05
Na_2O	0.82	0.80	0.78	0.77	0.74	0.72	0.75	0.86	0.83	0.81	0.82
K_2O	8.82	8.83	8.81	8.73	8.50	8.65	8.85	8.85	8.55	8.89	8.90
F	0.83	0.60	0.71	0.68	0.69	0.75	0.76	0.77	0.93		
Cl	0.03	0.05	0.05	0.04	0.07	0.03	0.05	0.05	0.07		
Total	97.13	95.91	96.33	95.63	92.26	95.67	94.97	96.03	94.57	96.89	96.07
Si	5.496	5.490	5.495	5.489	5.537	5.528	5.495	5.495	5.572	5.450	5.464
Ti	0.813	0.782	0.782	0.801	0.801	0.782	0.788	0.801	0.761	0.828	0.812
Al^{IV}	2.345	2.352	2.376	2.325	2.324	2.396	2.385	2.351	2.368	2.362	2.316
Al^{VI}	0.000	0.000	0.000	0.000	0.000	0.000	0.000	0.000	0.000	0.000	0.000
Fe	1.713	1.753	1.721	1.738	1.704	1.709	1.756	1.717	1.695	1.767	1.772
Mn	0.043	0.044	0.046	0.045	0.043	0.042	0.044	0.047	0.043	0.045	0.045
Mg	3.139	3.155	3.148	3.185	3.124	3.087	3.072	3.131	3.078	3.134	3.187
Ca	0.004	0.005	0.005	0.004	0.003	0.003	0.005	0.005	0.006	0.006	0.008
Na	0.233	0.233	0.225	0.223	0.222	0.210	0.219	0.250	0.244	0.232	0.237
K	1.658	1.682	1.671	1.668	1.681	1.647	1.707	1.685	1.649	1.668	1.686
OH	3.605	3.703	3.653	3.668	3.644	3.639	3.624	3.624	3.541		
F	0.388	0.284	0.336	0.322	0.338	0.353	0.364	0.363	0.443		
Cl	0.008	0.013	0.011	0.010	0.019	0.008	0.012	0.012	0.017		
Sum	19.464	19.510	19.483	19.492	19.451	19.420	19.487	19.496	19.429	19.491	19.528

Table C13 continued

Unit	**Povo Ign**	**Povo Ign**	**Povo Ign**	**Povo Ign**	**Povo Ign**	**Povo Ign**	**Povo Ign**	**Povo Ign**	**Povo Ign**	**Povo Ign**	**Povo Ign**
Sample	SM9-1	SM9-1	SM9-1	SM9-1	SM9-1	SM9-1	SM9-1	SM9-1	SM9-1	SM9-1	SM9-1
No.	121 / 3 .	121 / 4 .	121 / 5 .	124 / 1 .	125 / 1 .	126 / 1 .	127 / 1 .	129 / 1 .	131 / 1 .	132 / 1 .	133 / 1 .
Notes	Mph	Mph	Mph	Mph	Mph	Mph	Mph	Mph	Mph	Mph	Mph
SiO_2	36.81	36.90	36.43	36.79	37.12	36.91	37.03	37.12	37.02	35.82	36.21
TiO_2	7.03	7.20	7.44	7.36	7.42	7.37	7.25	7.44	6.95	7.61	7.74
Al_2O_3	13.25	13.28	13.27	13.44	13.25	13.44	13.24	13.52	13.37	13.41	13.37
FeO	14.37	14.44	14.74	14.46	14.42	14.29	14.34	14.39	14.39	14.52	14.57
MnO	0.36	0.38	0.37	0.36	0.37	0.35	0.36	0.36	0.38	0.36	0.36
MgO	14.54	14.43	14.04	14.42	14.28	14.28	14.44	14.50	14.62	13.93	14.01
CaO	0.02	0.05	0.06	0.00	0.00	0.02	0.02	0.03	0.03	0.00	0.01
Na_2O	0.80	0.84	0.81	0.80	0.79	0.79	0.86	0.84	0.82	0.87	0.82
K_2O	9.03	9.01	8.91	8.94	9.03	8.82	8.95	8.92	8.99	8.81	8.93
F											
Cl											
Total	96.20	96.51	96.07	96.56	96.67	96.27	96.48	97.11	96.56	95.32	96.03
Si	5.465	5.462	5.428	5.440	5.481	5.463	5.477	5.450	5.472	5.380	5.398
Ti	0.784	0.802	0.834	0.819	0.823	0.820	0.806	0.822	0.772	0.859	0.868
Al^{IV}	2.318	2.317	2.331	2.342	2.305	2.344	2.307	2.340	2.330	2.374	2.349
Al^{VI}	0.000	0.000	0.000	0.000	0.000	0.000	0.000	0.000	0.000	0.000	0.000
Fe	1.785	1.787	1.837	1.788	1.780	1.769	1.774	1.766	1.778	1.823	1.816
Mn	0.045	0.047	0.047	0.044	0.046	0.044	0.045	0.045	0.048	0.046	0.046
Mg	3.218	3.183	3.118	3.179	3.143	3.150	3.184	3.174	3.221	3.119	3.113
Ca	0.004	0.009	0.010	0.000	0.000	0.003	0.003	0.004	0.005	0.000	0.002
Na	0.230	0.240	0.234	0.230	0.225	0.228	0.245	0.240	0.235	0.254	0.238
K	1.709	1.700	1.693	1.686	1.700	1.666	1.688	1.670	1.695	1.688	1.697
OH											
F											
Cl											
Sum	19.560	19.547	19.534	19.528	19.505	19.490	19.530	19.512	19.556	19.544	19.527

Table C13 continued

Unit	**Povo Ign**	**Povo Ign**	**Povo Ign**	**Povo Ign**	**Povo Ign**	**Povo Ign**	**Povo Ign**	**Povo Ign**	**Povo Ign**	**Povo Ign**
Sample	SM9-1	SM9-1	SM9-1	SM9-1	SM9-1	SM9-1	SM9-1	SM9-1	AZ02-6	AZ02-6
No.	134 / 1 .	135 / 1 .	136 / 1 .	137 / 1 .	138 / 1 .	139 / 1 .	140 / 1 .	141 / 1 .	152 / 1 .	153 / 1 .
Notes	Mph	Mph	Mph	Mph	Mph	Mph	Mph	Mph	Mph	Mph
SiO_2	36.71	36.60	36.73	36.55	35.98	36.74	36.62	36.70	36.58	37.24
TiO_2	7.32	7.64	7.16	7.55	7.47	7.65	7.66	7.61	7.18	7.46
Al_2O_3	13.19	13.22	13.24	13.56	13.22	13.36	13.33	13.35	13.18	13.37
FeO	14.36	14.56	14.33	14.10	14.26	14.55	14.44	14.40	14.92	14.45
MnO	0.36	0.36	0.35	0.38	0.37	0.36	0.34	0.37	0.43	0.34
MgO	14.30	14.08	14.51	13.97	13.92	14.28	14.13	14.03	14.11	14.61
CaO	0.01	0.01	0.03	0.05	0.04	0.02	0.03	0.02	0.03	0.01
Na_2O	0.85	0.82	0.84	0.81	0.81	0.82	0.88	0.82	0.83	0.84
K_2O	9.06	9.01	8.88	8.75	8.79	8.98	8.87	9.02	9.00	9.01
F										
Cl										
Total	96.16	96.28	96.05	95.71	94.85	96.77	96.29	96.31	96.24	97.32
Si	5.457	5.436	5.457	5.441	5.421	5.428	5.433	5.445	5.448	5.459
Ti	0.818	0.853	0.800	0.845	0.847	0.850	0.854	0.849	0.804	0.822
Al^{IV}	2.311	2.314	2.318	2.378	2.349	2.326	2.330	2.334	2.314	2.310
Al^{VI}	0.000	0.000	0.000	0.000	0.000	0.000	0.000	0.000	0.000	0.000
Fe	1.786	1.809	1.781	1.755	1.797	1.798	1.791	1.786	1.859	1.772
Mn	0.046	0.045	0.044	0.048	0.047	0.045	0.043	0.046	0.054	0.042
Mg	3.170	3.117	3.215	3.099	3.127	3.144	3.126	3.104	3.134	3.193
Ca	0.001	0.001	0.004	0.007	0.006	0.003	0.004	0.004	0.004	0.002
Na	0.244	0.236	0.241	0.235	0.237	0.234	0.253	0.234	0.239	0.240
K	1.717	1.706	1.683	1.660	1.689	1.692	1.678	1.707	1.710	1.685
OH										
F										
Cl										
Sum	19.550	19.522	19.545	19.471	19.520	19.522	19.513	19.510	19.565	19.526

Table C14: Amphibole analyses from the UFG

Unit	**Fur I**	**Fur I**	**Fur I**	**Fur I**	**Fur I**	**Fur J Sy**	**Fur J Sy**	**Fur J Sy**	**Fur J Sy**	**Fur J Sy**	**Fur J Sy**	**Fur J Sy**	**Fur J Sy**
Sample	SM 5-1	SM 5-1	SM 5-1	SM 5-1	SM 5-1	S035	S035	S035	S035	S035	S035	S035	S035
No.	Amph6	Amph7	Amph8	Amph9	Amph10	Amph1	Amph2	Amph3	Amph4	Amph5	Amph6	Amph7	Amph8
Notes	Gm	Gm	Gm	Gm	Gm	Gm	Gm	Gm	Gm	Gm	Gm	Gm	Gm
SiO_2	50.63	50.20	50.45	49.78	50.34	51.16	48.28	46.05	45.31	45.18	45.94	47.46	45.49
TiO_2	1.55	1.33	1.06	1.37	1.42	1.04	1.48	2.42	2.24	2.41	2.33	2.02	2.30
Al_2O_3	3.09	2.69	2.43	3.08	2.46	1.95	4.09	3.87	3.93	4.47	3.76	2.66	4.05
FeO	12.61	16.07	16.99	14.03	16.47	20.47	21.94	29.70	28.83	27.39	29.12	31.70	29.12
MnO	1.16	1.58	1.67	1.32	1.63	2.41	2.21	1.92	1.92	1.93	2.21	1.96	2.04
MgO	14.82	12.41	11.49	13.61	11.81	8.08	7.41	2.21	2.84	3.56	2.50	1.08	2.63
CaO	7.59	6.96	6.47	7.38	6.54	2.49	3.87	3.27	3.88	5.32	3.07	0.85	4.21
Na_2O	5.20	5.41	5.74	5.33	5.70	8.15	7.20	7.24	6.83	6.07	7.19	8.72	6.75
K_2O	1.24	1.33	1.36	1.32	1.30	1.50	1.53	1.54	1.58	1.58	1.62	1.57	1.60
F						2.51	2.25	1.10	1.12	1.21	1.07	1.16	1.09
Cl	0.01	0.01	bdl	0.01	bdl	bdl	0.01	0.01	0.01	0.01	bdl	0.01	0.01
Total	97.91	97.99	97.66	97.23	97.67	99.76	100.26	99.33	98.49	99.13	98.81	99.18	99.29
Si	7.389	7.446	7.550	7.385	7.515	7.784	7.343	7.284	7.219	7.153	7.276	7.533	7.212
Ti	0.170	0.148	0.119	0.153	0.160	0.119	0.169	0.288	0.268	0.287	0.278	0.241	0.274
Al^{IV}	0.531	0.470	0.429	0.539	0.433	0.216	0.657	0.716	0.738	0.834	0.702	0.467	0.757
Al^{VI}	0.000	0.000	0.000	0.000	0.000	0.133	0.076	0.005	0.000	0.000	0.000	0.031	0.000
Fe^{2+}	1.267	1.671	1.895	1.487	1.830	2.267	2.228	3.433	3.309	3.329	3.245	3.545	3.420
Fe^{3+}	0.272	0.322	0.232	0.254	0.226	0.338	0.562	0.496	0.532	0.298	0.613	0.664	0.441
Mn	0.144	0.198	0.212	0.166	0.206	0.311	0.285	0.257	0.259	0.259	0.296	0.264	0.274
Mg	3.224	2.744	2.563	3.010	2.628	1.833	1.680	0.521	0.675	0.840	0.590	0.256	0.622
Ca	1.187	1.106	1.037	1.173	1.046	0.406	0.631	0.554	0.662	0.902	0.521	0.144	0.715
Na	1.471	1.556	1.666	1.533	1.650	2.404	2.123	2.220	2.110	1.863	2.208	2.684	2.075
K	0.231	0.252	0.260	0.250	0.248	0.291	0.297	0.311	0.321	0.319	0.327	0.318	0.324
F						1.208	1.082	0.550	0.564	0.606	0.536	0.582	0.547
Cl	0.003	0.003	0.000	0.002	0.000	0.000	0.002	0.001	0.002	0.002	0.000	0.001	0.002
OH*	1.997	1.997	2.000	1.998	2.000	0.792	0.916	1.448	1.434	1.392	1.464	1.416	1.451
Sum	17.889	17.914	17.963	17.956	17.944	18.101	18.051	18.085	18.093	18.085	18.056	18.146	18.114

Table C14 continued

Unit	Fur J Sy	Fur J Sy	Fur J Sy	Fur J Sy	Fur J Sy	Fur J Sy	Fur J Sy	Fur J Sy	Fur J Sy	Fur J Sy	Fur J Sy	Fur J Sy	Fur J Sy
Sample	S035	S035	S035	S035	S035	S035	S035	S035	S035	S035	S035	S035	S035
No.	Amph9	Amph10	Amph11	Amph12	Amph13	Amph14	Amph15	Amph16	Amph17	Amph18	Amph19	Amph20	Amph21
Notes	Gm	Gm	Gm	Gm	Gm	Gm	Gm	Gm	Gm	Gm	Gm	Gm	Gm
SiO_2	45.70	45.32	46.65	45.76	45.39	45.65	45.83	45.45	46.34	46.38	45.36	46.83	45.23
TiO_2	2.19	2.18	1.68	2.47	2.51	2.32	1.99	2.27	1.71	2.42	2.38	2.32	2.65
Al_2O_3	3.69	3.67	3.42	3.81	3.84	3.64	3.61	3.95	3.40	3.24	3.37	3.66	3.87
FeO	28.69	30.77	27.47	28.20	31.12	32.26	28.49	28.76	27.48	32.08	32.42	28.44	32.30
MnO	2.17	2.47	2.21	2.21	2.02	1.89	2.24	2.15	2.27	1.73	1.88	1.92	1.97
MgO	2.53	1.34	3.84	3.46	1.26	0.83	3.27	3.17	3.74	0.51	0.65	3.10	0.77
CaO	4.33	3.77	5.08	4.80	2.71	1.55	4.76	4.89	4.82	0.96	1.51	1.45	1.71
Na_2O	6.71	6.76	6.21	6.32	7.20	7.99	6.20	6.36	6.34	8.58	7.97	8.42	7.76
K_2O	1.54	1.54	1.55	1.50	1.61	1.67	1.58	1.60	1.62	1.57	1.66	1.63	1.58
F	1.18	0.92	1.34	1.20	0.91	0.93	1.24	1.15	1.31	0.94	0.89	1.47	0.89
Cl	bdl	0.02	0.01	0.01	0.01	0.01	0.01	0.01	0.01	bdl	0.01	bdl	0.01
Total	98.73	98.76	99.46	99.74	98.57	98.73	99.22	99.76	99.04	98.42	98.10	99.24	98.74
Si	7.308	7.264	7.350	7.191	7.248	7.281	7.250	7.170	7.336	7.436	7.299	7.342	7.205
Ti	0.263	0.263	0.199	0.292	0.301	0.278	0.237	0.269	0.204	0.292	0.288	0.274	0.318
Al^{IV}	0.692	0.693	0.635	0.706	0.723	0.684	0.673	0.734	0.634	0.564	0.639	0.658	0.727
Al^{VI}	0.003	0.000	0.000	0.000	0.000	0.000	0.000	0.000	0.000	0.049	0.000	0.018	0.000
Fe^{2+}	3.552	3.581	3.276	3.221	3.462	3.448	3.249	3.326	3.262	3.689	3.523	3.009	3.375
Fe^{3+}	0.284	0.543	0.344	0.485	0.694	0.855	0.520	0.468	0.377	0.612	0.840	0.720	0.928
Mn	0.294	0.335	0.295	0.294	0.273	0.255	0.300	0.287	0.304	0.235	0.256	0.255	0.266
Mg	0.603	0.320	0.902	0.811	0.299	0.197	0.771	0.745	0.883	0.123	0.156	0.725	0.183
Ca	0.742	0.647	0.858	0.808	0.464	0.265	0.807	0.826	0.818	0.165	0.260	0.244	0.292
Na	2.080	2.101	1.897	1.926	2.229	2.471	1.902	1.945	1.946	2.667	2.486	2.559	2.397
K	0.314	0.315	0.312	0.301	0.328	0.340	0.319	0.322	0.327	0.321	0.341	0.326	0.321
F	0.597	0.466	0.668	0.596	0.458	0.467	0.620	0.574	0.656	0.477	0.454	0.729	0.449
Cl	0.000	0.005	0.002	0.002	0.003	0.003	0.002	0.003	0.003	0.000	0.001	0.000	0.003
OH*	1.403	1.529	1.330	1.401	1.539	1.530	1.378	1.424	1.341	1.523	1.545	1.271	1.548
Sum	18.136	18.063	18.066	18.035	18.021	18.076	18.027	18.094	18.091	18.154	18.088	18.129	18.010

Table C14 continued

Unit	**Fur J Sy**	**Fur J Sy**	**Fur J Sy**	**Fur J Sy**	**Fur J Sy**	**Fur J Sy**	**Fur J Sy**	**Fur J Sy**	**Fur J Sy**	**Fur J Sy**	**Fur J Sy**	**Fur J Sy**	**Fur J Sy**
Sample	S035	S035	S035	S035	S035	S035	S035	S035	S035	S035	S035	S035	S035
No.	Amph22	Amph23	Amph24	Amph25	Amph26	Amph27	Amph28	Amph29	Amph30	Amph31	Amph32	Amph33	Amph34
Notes	Gm	Gm	Gm	Gm	Gm	Gm	Gm	Gm	Gm	Gm	Gm	Gm	Gm
SiO_2	46.14	45.40	44.98	44.89	45.55	44.85	45.53	45.41	44.84	45.67	44.85	45.78	45.42
TiO_2	2.04	2.16	2.11	2.06	2.15	1.94	2.28	2.30	2.57	2.03	2.36	2.26	2.38
Al_2O_3	3.29	3.75	3.70	3.62	3.84	3.81	3.56	3.67	3.84	3.71	4.01	3.55	3.38
FeO	33.30	28.35	31.64	31.95	30.41	30.94	32.04	31.93	32.39	30.45	31.40	28.42	32.94
MnO	1.86	2.21	2.39	2.46	2.31	2.39	2.06	2.03	1.90	2.08	2.03	2.26	1.86
MgO	0.40	3.11	1.51	1.12	1.83	1.87	1.11	1.12	0.72	2.05	1.14	3.06	0.49
CaO	0.99	4.78	4.37	4.21	3.00	5.19	2.16	2.12	1.74	3.37	2.49	4.00	1.26
Na_2O	8.26	6.23	6.19	6.37	7.39	5.89	7.78	7.68	8.07	6.84	7.46	6.74	8.26
K_2O	1.64	1.60	1.52	1.46	1.62	1.48	1.52	1.47	1.42	1.54	1.65	1.50	1.49
F	0.98	1.22	1.02	0.94	1.03	1.03	0.96	0.93	0.84	1.06	0.94	1.21	0.89
Cl	bdl	0.01	0.01	0.01	0.01	0.01	0.01	bdl	bdl	0.01	0.01	0.01	bdl
Total	98.90	98.82	99.44	99.09	99.14	99.40	99.01	98.66	98.33	98.81	98.34	98.79	98.37
Si	7.353	7.227	7.161	7.188	7.238	7.155	7.250	7.239	7.191	7.253	7.195	7.266	7.286
Ti	0.245	0.259	0.253	0.248	0.257	0.233	0.273	0.276	0.310	0.243	0.285	0.270	0.287
Al^{IV}	0.618	0.704	0.694	0.683	0.719	0.716	0.668	0.689	0.726	0.694	0.758	0.664	0.639
Al^{VI}	0.000	0.000	0.000	0.000	0.000	0.000	0.000	0.000	0.000	0.000	0.000	0.000	0.000
Fe^{2+}	3.478	3.328	3.444	3.556	3.378	3.518	3.430	3.371	3.470	3.296	3.445	3.246	3.509
Fe^{3+}	0.961	0.446	0.769	0.723	0.664	0.610	0.837	0.885	0.874	0.748	0.767	0.526	0.910
Mn	0.251	0.298	0.322	0.334	0.311	0.323	0.278	0.274	0.258	0.280	0.276	0.304	0.253
Mg	0.095	0.738	0.358	0.268	0.434	0.445	0.263	0.266	0.171	0.485	0.273	0.724	0.117
Ca	0.170	0.815	0.745	0.722	0.511	0.887	0.369	0.362	0.299	0.573	0.428	0.680	0.216
Na	2.552	1.923	1.911	1.978	2.277	1.822	2.402	2.374	2.509	2.106	2.321	2.074	2.569
K	0.333	0.325	0.309	0.298	0.328	0.301	0.309	0.299	0.291	0.312	0.338	0.304	0.305
F	0.493	0.614	0.514	0.476	0.518	0.520	0.483	0.471	0.426	0.532	0.479	0.607	0.453
Cl	0.000	0.001	0.003	0.003	0.002	0.003	0.002	0.000	0.000	0.002	0.002	0.003	0.000
OH*	1.507	1.384	1.483	1.521	1.481	1.477	1.515	1.529	1.574	1.466	1.519	1.389	1.547
Sum	18.056	18.063	17.965	17.998	18.116	18.010	18.080	18.035	18.099	17.992	18.086	18.058	18.090

APPENDIX D: WHOLE ROCK AND GLASS DATA

Table D1: Whole rock major element compositions of Terceira Ignimbrite formations, analysed by WD-XRF

Source	**University of East Anglia**															
Sample no.	T034	T035	T036	T037	T013	T025	T026	T028	T029	T031	T005	T024	T002	T003	T010	T011
Unit	LAI	LAI	LAI	LAI	VFI	VFI	VFI	VFI	VFI	VFI	CCI	CCI	CCI	CCI	CCI	CCI
Type	Ign	Ign	Ign	Ign	Fall	Ign	Ign	Ign	Ign	Ign	Fall	Surge	Ign	Ign	Ign	Ign
Major elements (wt. %)																
SiO_2	64.46	62.78	64.81	62.30	60.78	61.99	63.23	62.21	61.93	61.95	61.39	62.06	61.76	62.61	63.29	62.11
TiO_2	0.61	0.59	0.59	0.67	0.46	0.57	0.57	0.57	0.56	0.61	0.46	0.45	0.58	0.62	0.61	0.47
Al_2O_3	15.29	15.91	15.36	16.02	13.32	14.84	15.51	15.28	14.94	15.28	14.79	14.82	15.04	15.49	16.10	14.04
$Fe_2O_3^T$	5.10	5.04	5.04	4.81	7.93	5.86	5.73	5.82	5.83	5.75	5.16	5.16	5.82	5.72	5.12	6.20
MnO	0.21	0.21	0.20	0.19	0.28	0.22	0.22	0.23	0.22	0.22	0.21	0.21	0.22	0.21	0.19	0.25
MgO	0.36	0.35	0.34	0.41	0.17	0.30	0.31	0.33	0.32	0.37	0.37	0.35	0.34	0.40	0.48	0.24
CaO	0.68	0.65	0.66	0.79	0.47	0.90	0.95	0.92	0.90	1.06	0.63	0.61	0.94	1.11	0.99	0.55
Na_2O	7.37	6.90	7.52	6.72	6.03	6.92	7.29	7.09	6.91	7.03	6.95	7.45	6.91	7.22	7.43	6.81
K_2O	5.02	4.80	5.05	4.77	4.04	4.78	4.82	4.76	4.75	4.72	4.92	4.91	4.73	4.74	4.94	4.70
P_2O_5	0.09	0.09	0.08	0.11	0.04	0.08	0.09	0.09	0.09	0.10	0.05	0.05	0.10	0.10	0.08	0.04
LOI	0.76	2.54	0.12	3.20	6.39	3.16	0.76	2.34	3.17	2.86	5.00	4.04	3.21	1.29	0.29	4.46
Total	99.95	99.86	99.77	99.99	99.91	99.62	99.48	99.64	99.62	99.95	99.93	100.11	99.65	99.51	99.52	99.87
P.I.	1.15	1.04	1.16	1.01	1.07	1.12	1.11	1.10	1.11	1.09	1.13	1.19	1.10	1.10	1.09	1.16

Table D2: Whole rock trace element compositions of Terceira Ignimbrite formations, analysed by WD-XRF

Source	**University of East Anglia**															
Sample no.	T034	T035	T036	T037	T013	T025	T026	T028	T029	T031	T005	T024	T002	T003	T010	T011
Unit	LAI	LAI	LAI	LAI	VFI	VFI	VFI	VFI	VFI	VFI	CCI	CCI	CCI	CCI	CCI	CCI
Type	Ign	Ign	Ign	Ign	Fall	Ign	Ign	Ign	Ign	Ign	Fall	Surge	Ign	Ign	Ign	Ign
Trace elements (ppm)																
Sc	bdl	bdl	bdl	bdl	bdl	bdl	bdl	bdl	bdl	bdl	bdl	bdl	bdl	bdl	bdl	bdl
V	bdl	bdl	bdl	bdl	bdl	bdl	bdl	bdl	bdl	bdl	bdl	bdl	bdl	bdl	bdl	bdl
Cr	bdl	bdl	bdl	bdl	bdl	bdl	bdl	bdl	bdl	bdl	bdl	bdl	bdl	bdl	bdl	bdl
Ni	bdl	bdl	bdl	bdl	bdl	bdl	bdl	bdl	bdl	bdl	bdl	bdl	bdl	bdl	bdl	bdl
Cu	bdl	bdl	bdl	bdl	bdl	bdl	bdl	bdl	bdl	bdl	bdl	bdl	bdl	bdl	bdl	bdl
Zn	156	205	154	133	315	163	155	157	160	151	179	184	158	149	144	241
As	10	11	bdl	bdl	26	11	bdl	bdl	bdl	bdl	11	12	bdl	bdl	bdl	17
Rb	102	93	102	73	192	100	93	94	99	89	133	135	94	89	94	174
Sr	bdl	12	bdl	16	bdl	20	26	23	22	36	bdl	bdl	24	36	18	bdl
Y	58	55	57	45	131	62	57	58	61	56	78	78	59	55	56	108
Zr	686	664	693	491	2258	772	706	701	762	678	1043	1073	714	666	674	1550
Nb	118	113	118	88	354	129	119	118	127	115	176	180	121	113	121	255
Mo	bdl	bdl	bdl	bdl	17	bdl	bdl	bdl	bdl	bdl	11	11	bdl	bdl	bdl	14
Ba	243	309	239	524	bdl	502	746	605	531	714	bdl	bdl	596	799	315	bdl
La	87	90	83	71	239	106	90	100	97	96	137	140	98	86	90	194
Ce	139	139	133	121	340	166	158	158	166	161	191	193	163	155	142	261
Pb	bdl	bdl	bdl	bdl	26	bdl	bdl	bdl	bdl	bdl	bdl	bdl	bdl	bdl	bdl	bdl
Th	13	12	14	10	40	15	13	13	14	13	18	19	13	13	13	26
U	bdl	bdl	bdl	bdl	11	bdl	bdl	bdl	bdl	bdl	bdl	bdl	bdl	bdl	bdl	bdl

Table D3: Whole rock trace element compositions of Terceira lithologies, analysed by ICP-AES

Source	**Bureau Veritas Laboratories**					
Sample no.	T001	TO73SY	T073EA	T073EB	T073A1	T073A3
Unit	Ign-i	Syenite	Sy-enc	Sy-enc	Sy-enc	Sy-enc
Notes	Ign	Ejecta	Enclave	Enclave	Enclave	Enclave
SiO_2	61.31	64.23	60.13	61.4	60.91	60.56
TiO_2	0.99	0.48	1.03	0.85	0.89	0.97
Al_2O_3	15.40	15.92	16.00	16.19	16.05	16.18
Fe_2O_3	6.56	4.68	6.5	6.03	6.18	6.18
MnO	0.21	0.19	0.22	0.22	0.22	0.2
MgO	1.26	0.24	1.54	1.07	1.43	1.53
CaO	1.98	0.58	2.51	1.94	2.2	2.29
Na_2O	7.01	7.32	6.77	7.18	6.99	6.94
K_2O	4.03	5.03	4.12	4.25	4.13	3.91
P_2O_5	0.18	0.05	0.19	0.15	0.15	0.16
LOI	0.70	1	0.6	0.4	0.5	0.7
Total	98.97	99.25	98.96	99.08	99.03	99.00
P.I.	1.03	1.10	0.97	1.01	0.99	0.97

Table D4: Trace element compositions of Terceira lithologies, analysed via ICP-MS

Source	**Bureau Veritas Laboratories**															
Sample no.	TER10-3	TER5-2	TER11-2B	TER35-2	TER56-1	TER10-2	T001	TER13-1	TER30-1	TER35-1	TER30-6	TO73SY	T073EA	T073EB	T073A1	T073A3
Unit	LAI	LMI	VFI	CCI	PNI	Ign-i	Ign-i	GVI	Syenite	Syenite	Syenite	Syenite	Sy-enc	Sy-enc	Sy-enc	Sy-enc
Notes	Ign	Ign	Ign	Ign	Ign	Ign	Ign	Ign	Ejecta	Ejecta	Ejecta	Ejecta	Enclave	Enclave	Enclave	Enclave
Ba	371	586	701	33	472	534	1545.00	348.00	345	67	282	181	1236	1216	1235	1234
Be	5	5	5	7	6	5	6.00	4.00	4	6	4	4	3	3	3	2
Co	0.3	3	0.8	0.8	3	0.5	5.60	0.90	1.1	1	1.5	0.8	5.7	3.1	4.9	6.3
Cs	0.8	0.9	0.8	1.4	1.1	0.9	0.10	1.60	0.6	0.8	0.8	0.8	0.9	0.4	0.6	2.6
Ga	31.4	29.3	30.3	33.4	30.2	29.6	32.20	30.40	33	36.1	32.5	34.1	28.4	27.4	27	28.3
Hf	14.3	18.5	16.9	26.9	20.7	16.8	16.80	20.50	21	20.4	21.2	22	13.8	11.3	13.1	13.7
Nb	127.7	160.6	147.2	237	185.8	146.9	133.60	151.40	169.6	159.5	183.5	180	111.3	101	115.1	113.8
Rb	94.9	100.9	97.3	145	105.3	98.5	89.50	109.60	110.6	120.9	107.2	112.2	93.4	82.9	93.8	139.6
Sn	5	6	6	10	7	6	3.00	5.00	6	7	6	8	2	2	2	3
Sr	11.3	111.3	29.6	7.8	89.1	20.6	77.10	23.60	12.9	2.6	11.5	10.6	139.9	109.1	125.6	136.9
Ta	6.9	8.9	7.9	12.7	10.1	8.1	7.70	9.10	9.4	9.4	10.8	9.9	6.5	5.8	6.7	6.4
Th	10	13.4	12.3	18.2	14.5	12.1	10.40	15.20	12.6	12.9	13.2	15	7	5.4	7.7	8.5
U	3.4	4.5	4.5	6.5	6.1	4.3	2.50	4.70	4.1	4.3	4.8	5.5	2.7	1.7	2.3	2.7
V	<8	14	<8	<8	11	<8	58.00	<8	<8	<8	<8	<8	48	21	31	43
W	1.6	2.3	1.9	3.3	2.3	1.8	1.90	2.00	<0.5	0.8	<0.5	0.6	2.5	1	1	1.3
Zr	610.1	773.2	719.1	1149.6	882.7	721.8	716.90	904.30	812.6	832.3	863.2	961.8	583.9	467.3	576.5	590.7
Y	52.6	61.9	60.5	87.6	84.2	61.2	45.90	58.10	63.4	18.7	62.8	51.4	44.3	32.5	41.5	45.3
La	67.8	86.1	81.9	124.7	137.6	83.4	73.80	97.10	89.7	72.2	80.2	91.8	70.5	59.1	66.7	65.7
Ce	143.7	167.6	168.6	250.7	186.5	175	153.70	199.00	185.6	139.2	167.7	180.8	141.2	125.9	136.6	137.3
Pr	15.49	18.71	18.76	26.77	29.38	18.97	16.71	19.87	20.14	14.22	17.86	18.04	15.86	13.89	15.46	15.03
Nd	59.8	70.7	72.5	102.1	114.1	74.7	64.50	71.90	68.6	46.9	64.7	67.7	60.6	54.9	58.9	57.2
Sm	11.19	12.96	13.06	17.33	19.54	13.53	11.46	12.81	12.8	7.12	11.81	10.74	11.45	9.46	10.73	10.48
Eu	2.06	2.58	2.66	1.69	3.36	2.49	3.03	2.44	2.09	0.85	1.94	1.44	2.8	2.52	2.62	2.65

Table D4 continued

Source	**Bureau Veritas Laboratories**															
Sample no.	TER10-3	TER5-2	TER11-2B	TER35-2	TER56-1	TER10-2	T001	TER13-1	TER30-1	TER35-1	TER30-6	TO73SY	T073EA	T073EB	T073A1	T073A3
Unit	LAI	LMI	VFI	CCI	PNI	Ign-i	Ign-i	GVI	Syenite	Syenite	Syenite	Syenite	Sy-enc	Sy-enc	Sy-enc	Sy-enc
Notes	Ign	Ign	Ign	Ign	Ign	Ign	Ign	Ign	Ejecta	Ejecta	Ejecta	Ejecta	Enclave	Enclave	Enclave	Enclave
Gd	9.87	11.4	11.63	15.42	16.85	12.1	10.61	12.19	11.17	4.78	10.73	10.31	10.14	8.16	9.88	9.57
Tb	1.76	1.96	1.98	2.69	2.83	2.04	1.59	1.90	1.98	0.73	1.89	1.71	1.57	1.24	1.51	1.5
Dy	9.71	10.95	11.07	15.7	15.67	11.6	8.76	10.73	10.37	3.39	10.91	10.85	8.84	6.78	8.25	8.56
Ho	1.95	2.21	2.23	3.13	2.99	2.23	1.80	2.25	2.11	0.75	2.27	2.17	1.63	1.25	1.57	1.7
Er	5.6	6.36	6.46	9.32	8.61	6.36	4.88	6.40	6.24	2.79	6.7	5.93	4.74	3.57	4.59	4.57
Tm	0.82	0.96	0.92	1.38	1.26	0.96	0.75	0.95	1	0.59	1.09	0.9	0.71	0.55	0.7	0.74
Yb	5.31	5.97	5.72	8.59	7.95	6.01	4.60	6.47	6.56	4.72	6.95	6.35	5.06	4.06	4.89	4.92
Lu	0.77	0.9	0.85	1.3	1.14	0.88	0.79	0.94	0.98	0.83	1.07	1.01	0.76	0.69	0.75	0.73
Mo	0.2	1.3	0.2	0.4	0.4	0.2	2.00	0.20	0.3	0.2	0.3					
Cu	0.5	3.3	0.9	2	2.8	0.7	4.70	4.70	1.3	0.5	0.8					
Pb	0.2	1.0	0.2	0.4	1.0	0.2	2.5	2.0	2.9	0.9	1.6					
Zn	12	49	12	13	42	12	61	34	21	7	18					
Ni	bdl	3.0	0.2	0.2	2.6	0.1	5.5	0.2	bdl	bdl	bdl	bdl	bdl	bdl	bdl	bdl
As	bdl	bdl	bdl	bdl	bdl	bdl	0.7	bdl	bdl	bdl	bdl					
Cd	bdl	0.1	bdl	bdl	bdl	bdl	bdl	0.2	0.1	bdl	bdl					
Sb	bdl	bdl	bdl	bdl	bdl	bdl	bdl	bdl	bdl	bdl	bdl					
Bi	bdl	bdl	bdl	bdl	bdl	bdl	bdl	bdl	bdl	bdl	bdl					
Ag	bdl	bdl	bdl	bdl	bdl	bdl	bdl	bdl	bdl	bdl	bdl					
Au	0.7	bdl	bdl	1.3	0.5	0.6	1.6	0.6	bdl	bdl	bdl					
Hg	bdl	bdl	bdl	bdl	bdl	bdl	bdl	bdl	bdl	bdl	bdl					
Tl	bdl	bdl	bdl	bdl	bdl	bdl	bdl	bdl	bdl	bdl	bdl					
Se	bdl	bdl	bdl	bdl	bdl	bdl	bdl	bdl	bdl	bdl	bdl					

Table D5: Electron microprobe analyses of Terceira melt inclusions

Source	Sample	Unit	Identifier	SiO_2	TiO_2	Al_2O_3	FeO_t	MnO	MgO	CaO	Na_2O	K_2O	P_2O_5	Total	Peralkalinity	Cl	F	S
University of Goettingen	T038IIb	LAI	MI01	63.93	0.66	14.68	4.59	0.20	0.37	0.62	6.56	4.97	0.09	96.67	1.10	2795	2022	151
	T0382	LAI	MI01	63.23	0.69	15.51	4.10	0.20	0.44	0.77	6.63	4.94	0.13	96.64	1.05	1511	857	171
	T0382	LAI	MI02	64.56	0.52	14.46	4.55	0.22	0.31	0.50	6.70	4.97	0.06	96.85	1.13	2763	1469	192
	T0382	LAI	MI03	62.60	0.45	13.74	4.57	0.22	0.24	0.58	6.39	4.80	0.06	93.65	1.14	2444	1823	244
	T0382	LAI	MI04	64.03	0.55	15.69	4.02	0.18	0.37	0.65	6.95	5.05	0.06	97.55	1.08	1683	968	97
	T0382	LAI	MI05	64.92	0.55	15.09	4.24	0.21	0.39	0.65	7.04	4.69	0.06	97.84	1.10	2053	1444	238
	T0382	LAI	MI06	64.52	0.55	14.96	4.25	0.18	0.31	0.59	6.98	4.73	0.09	97.17	1.11	2448	1278	192
	T0382	LAI	MI07	62.84	0.51	13.87	4.48	0.24	0.36	0.49	6.24	4.61	0.06	93.69	1.10	2651	1836	226
	T0352	LAI	MI08	64.80	0.50	14.36	4.34	0.21	0.27	0.62	6.74	4.86	0.08	96.78	1.14	2452	1492	187
	T0383	LAI	MI01	63.99	0.66	15.01	4.49	0.21	0.48	0.91	6.71	4.82	0.09	97.37	1.08	1539	1383	187
	T0383	LAI	MI02	64.46	0.72	15.43	4.28	0.21	0.46	0.70	7.10	5.00	0.12	98.48	1.11	1946	1310	175
	T0383	LAI	MI03	63.98	0.70	15.04	4.12	0.21	0.41	0.67	6.83	4.82	0.11	96.88	1.09	1970	1278	289
	T0383	LAI	MI04	63.84	0.62	14.97	4.02	0.18	0.41	0.64	6.83	5.03	0.11	96.64	1.11	1960	1305	199
	T0383	LAI	MI05	63.90	0.60	14.99	4.18	0.24	0.39	0.68	6.98	4.59	0.10	96.65	1.10	1921	1130	215
	T0383	LAI	MI06	64.31	0.61	15.26	4.28	0.23	0.41	0.65	7.08	4.74	0.11	97.69	1.10	1905	1159	173
	T0383	LAI	MI07	63.98	0.64	15.17	4.15	0.18	0.42	0.71	6.96	4.53	0.06	96.80	1.08	1893	1494	197
	T0383	LAI	MI08	61.89	0.57	14.95	4.18	0.19	0.41	0.68	6.78	4.44	0.09	94.18	1.07	1892	1563	169
	T0383	LAI	MI09	63.77	0.62	15.19	4.22	0.21	0.41	0.63	6.96	4.59	0.10	96.70	1.08	1918	1468	177
	T0383	LAI	MI10	63.97	0.59	15.12	4.38	0.24	0.39	0.67	6.83	4.64	0.08	96.91	1.08	1901	1253	161
	T0383	LAI	MI11	64.53	0.54	14.47	4.29	0.21	0.33	0.60	6.86	4.90	0.02	96.76	1.15	2437	1479	213
	T0383	LAI	MI12	64.50	0.48	14.52	4.20	0.23	0.30	0.58	6.65	4.79	0.05	96.30	1.11	2458	1495	163
	T0383	LAI	MI13	64.73	0.51	14.40	4.31	0.18	0.30	0.56	6.75	4.87	0.05	96.66	1.14	2565	1588	202
	T0383	LAI	MI14	64.76	0.51	14.50	4.38	0.21	0.31	0.56	6.88	4.80	0.06	96.96	1.14	2563	1413	232
	T0383	LAI	MI15	64.38	0.53	14.56	4.39	0.20	0.32	0.55	6.80	4.85	0.06	96.64	1.13	2530	1450	192
	T0383	LAI	MI16	64.70	0.50	14.55	4.38	0.20	0.32	0.55	6.80	4.91	0.07	96.97	1.13	2417	1481	167

Table D5 continued

Source	Sample	Unit	Identifier	SiO_2	TiO_2	Al_2O_3	FeO_t	MnO	MgO	CaO	Na_2O	K_2O	P_2O_5	Total	Peralkalinity	Cl	F	S
University of Goettingen	T0383	LAI	MI17	62.41	0.76	14.30	4.93	0.28	0.47	0.67	7.02	4.36	0.12	95.32	1.14	2278	1789	282
	T0383	LAI	MI18	65.07	0.51	14.83	4.32	0.21	0.35	0.62	7.10	4.81	0.07	97.88	1.14	2524	1366	178
	T0383	LAI	MI19	64.76	0.54	14.95	4.39	0.24	0.41	0.67	7.18	4.52	0.05	97.71	1.12	2096	1469	155
	T0383	LAI	MI20	64.24	0.56	15.12	4.29	0.22	0.35	0.61	7.38	4.20	0.06	97.04	1.10	2279	1986	193
	T0383	LAI	MI21	65.43	0.40	14.59	4.29	0.22	0.29	0.54	6.85	4.94	0.05	97.59	1.14	2556	1505	135
	TM-1(1)	VFI	MI01	63.51	0.75	16.04	5.14	0.19	0.28	0.91	7.13	5.11	0.05	99.11	1.08	2889	1179	472
	TM-1(1)	VFI	MI02	64.15	0.76	14.94	5.87	0.26	0.30	0.91	7.39	4.75	0.08	99.40	1.16	2653	1128	452
	TM-2(1)	VFI	MI01	64.55	0.79	15.53	5.37	0.21	0.33	0.90	7.30	4.79	0.10	99.87	1.11	2124	1315	527
	TER27-1II	VFI	MI01	59.16	0.96	14.96	6.13	0.31	0.46	1.07	6.58	4.49	0.15	94.28	1.05	3990	2116	358
	TER27-1II	VFI	MI02	62.49	0.49	14.87	4.70	0.22	0.32	0.84	6.75	4.47	0.06	95.21	1.07	2623	2105	241
	TER27-1II	VFI	MI04	61.94	0.50	14.39	4.84	0.21	0.29	0.66	5.25	5.06	0.07	93.22	0.98	2990	2198	233
	TER27-1II	VFI	MI05	62.26	0.52	14.67	4.69	0.21	0.28	0.74	6.73	4.69	0.07	94.86	1.10	2696	2311	250
	TER27-1II	VFI	MI06	60.02	0.71	14.51	5.52	0.27	0.39	0.97	6.50	4.98	0.11	93.96	1.11	3085	1855	264
	TER27-1II	VFI	MI07	60.70	0.56	14.31	5.24	0.24	0.38	0.88	6.19	5.07	0.11	93.68	1.10	2829	1944	252
	TER27-1II	VFI	MI08	61.02	0.62	14.51	5.19	0.24	0.36	0.90	6.87	4.31	0.08	94.11	1.10	2783	2133	246
	TER27-1II	VFI	MI09	62.85	0.51	14.86	4.67	0.18	0.33	0.71	6.94	4.67	0.03	95.75	1.11	2360	1335	190
	TER27-1II	VFI	MI10	62.96	0.57	14.93	5.00	0.20	0.28	0.86	7.10	4.69	0.10	96.70	1.12	2581	1413	214
	TER27-1II	VFI	MI11	63.65	0.48	14.99	4.96	0.22	0.33	0.81	6.68	4.66	0.04	96.82	1.07	2522	1379	203
	TER27-1II	VFI	MI12	62.44	0.58	14.89	5.03	0.23	0.35	0.92	6.74	4.63	0.07	95.89	1.08	2536	1527	199
	TER27-1II	VFI	MI13	62.54	0.58	15.08	4.74	0.22	0.30	0.88	6.68	4.71	0.08	95.82	1.07	2304	1291	214
	TER27-1I	VFI	MI01	61.78	0.56	14.65	5.01	0.20	0.32	0.79	6.91	4.58	0.07	94.87	1.11	2788	2039	312
	TER27-1I	VFI	MI02	63.21	0.59	14.65	5.35	0.26	0.35	0.65	7.07	4.73	0.07	96.92	1.14	2658	1556	241
	TER27-1I	VFI	MI03	62.79	0.66	15.09	5.22	0.23	0.46	0.95	6.72	4.58	0.13	96.83	1.06	2279	1348	254
	TER27-1I	VFI	MI04	63.22	0.43	14.72	5.00	0.22	0.24	0.73	6.72	4.80	0.04	96.12	1.10	2826	1201	163
	TER27-1I	VFI	MI05	62.48	0.42	14.94	4.60	0.20	0.31	0.87	6.74	4.75	0.05	95.35	1.09	2306	1501	220

Table D5 continued

Source	Sample	Unit	Identifier	SiO_2	TiO_2	Al_2O_3	FeO_t	MnO	MgO	CaO	Na_2O	K_2O	P_2O_5	Total	Peralkalinity	Cl	F	S
University of Goettingen	TER27-1I	VFI	MI06	61.00	0.71	14.38	5.76	0.27	0.46	1.09	6.41	4.09	0.08	94.25	1.04	2399	1550	261
	TER27-1I	VFI	MI07	61.37	0.49	14.50	4.84	0.23	0.28	0.80	5.63	4.76	0.05	92.96	0.99	2624	1453	210
	TER27-1I	VFI	MI09	62.08	0.42	15.01	4.56	0.21	0.26	0.78	6.18	4.67	0.09	94.26	1.01	2489	1771	217
	TER2-2II	VFI	MI01	62.92	0.66	15.28	4.98	0.21	0.39	0.96	6.71	4.60	0.11	96.81	1.05	2209	1635	229
	TER2-2II	VFI	MI02	63.86	0.47	15.71	4.42	0.19	0.25	0.75	7.24	4.86	0.05	97.80	1.09	2455	1325	243
	TER2-2II	VFI	MI03	64.19	0.45	15.28	4.37	0.20	0.26	0.78	7.32	4.82	0.04	97.71	1.13	2415	1474	287
	TER2-2II	VFI	MI04	63.53	0.45	15.19	4.47	0.21	0.27	0.75	7.07	4.75	0.02	96.72	1.10	2508	1328	193
	TER2-2II	VFI	MI06	63.69	0.58	15.72	4.81	0.21	0.35	0.96	7.34	4.93	0.09	98.67	1.11	2015	1197	242
	VFI_2	VFI	01_A	62.46	0.47	15.24	4.51	0.21	0.26	0.79	6.16	4.84	0.08	95.02	1.01	2539	1571	130
	VFI_2	VFI	01_B	63.11	0.51	15.34	4.65	0.19	0.26	0.83	6.58	5.08	0.07	96.62	1.06	2797	1289	134
	VFI_2	VFI	02_A	63.08	0.60	14.76	5.54	0.25	0.34	0.79	6.08	5.05	0.10	96.59	1.05	2574	1526	268
	VFI_2	VFI	02_B	62.21	0.70	15.02	5.51	0.23	0.44	0.90	6.56	4.43	0.12	96.12	1.04	2488	2094	160
	VFI_2	VFI	03_A	61.66	0.58	14.63	5.08	0.23	0.35	0.87	6.36	4.81	0.09	94.67	1.07	2478	1258	303
	VFI_2	VFI	04_A	61.93	0.68	15.01	5.51	0.28	0.43	0.96	6.74	4.71	0.10	96.34	1.08	2664	1586	268
	VFI_3	VFI	01_A	61.99	0.58	14.80	5.01	0.20	0.29	0.77	5.87	5.04	0.07	94.61	1.02	3018	1209	195
	VFI_3	VFI	02_A	62.01	0.65	14.86	5.43	0.22	0.33	0.87	6.64	4.67	0.07	95.75	1.08	3150	1848	234
	VFI_3	VFI	02_B	61.56	0.50	14.92	5.11	0.24	0.35	0.80	5.95	5.01	0.08	94.52	1.02	3124	2388	273
	VFI_3	VFI	02_C	62.37	0.67	13.87	6.17	0.28	0.38	0.99	6.35	4.47	0.08	95.63	1.10	4881	2252	220
	VFI_3	VFI	03_A	61.49	0.59	14.70	5.37	0.25	0.39	0.93	6.20	4.67	0.09	94.68	1.04	2925	1016	441
	VFI_3	VFI	03_B	61.14	0.62	14.84	5.48	0.23	0.38	0.93	6.15	4.59	0.12	94.48	1.02	2827	1151	251
	VFI_4	VFI	01_A	63.25	0.44	15.82	4.03	0.17	0.22	0.64	6.42	4.73	0.00	95.73	0.99	2198	1625	191
	VFI_4	VFI	03_A	62.85	0.64	14.80	5.39	0.23	0.37	0.94	6.56	4.66	0.07	96.51	1.07	2761	1890	303
	VFI_4	VFI	04_A	61.88	0.53	14.84	4.93	0.21	0.30	0.75	6.08	4.95	0.06	94.53	1.04	3145	1906	208
	VFI_4	VFI	05_A	62.43	0.48	15.05	4.84	0.22	0.29	0.76	6.06	4.88	0.06	95.06	1.01	2791	1445	212
	VFI_4	VFI	06_A	63.61	0.48	15.54	4.37	0.18	0.26	0.74	6.80	5.20	0.01	97.19	1.08	2025	1009	182

Table D5 continued

Source	Sample	Unit	Identifier	SiO_2	TiO_2	Al_2O_3	FeO_t	MnO	MgO	CaO	Na_2O	K_2O	P_2O_5	Total	Peralkalinity	Cl	F	S
University of Goettingen	VFI_4	VFI	07_A	61.71	0.57	14.63	4.82	0.26	0.34	0.81	6.22	4.55	0.08	93.99	1.04	2533	1928	213
	VFI_4	VFI	09_A	62.21	0.48	15.09	4.84	0.22	0.32	0.83	6.22	4.89	0.08	95.19	1.03	2436	1461	173
	VFI_2	VFI	01_C	61.36	0.52	14.84	4.85	0.18	0.31	0.73	6.43	4.77	0.05	94.04	1.06	2791	1352	208
	VFI_2	VFI	01_D	63.70	0.54	14.43	5.23	0.23	0.36	0.75	6.35	4.53	0.11	96.22	1.06	3653	1752	291
	VFI_2	VFI	03_B	62.00	0.65	15.10	5.11	0.20	0.43	0.92	6.39	4.76	0.09	95.65	1.04	2471	1657	247
	VFI_2	VFI	03_C	62.75	0.60	15.16	4.98	0.21	0.38	0.88	6.75	4.53	0.09	96.33	1.06	2502	1646	316
	VFI_2	VFI	03_D	62.49	0.63	15.12	5.47	0.20	0.41	0.80	6.48	5.10	0.09	96.79	1.07	3061	1295	286
	VFI_2	VFI	03_E	61.90	0.56	14.91	5.07	0.20	0.35	0.87	6.39	4.86	0.08	95.19	1.06	2491	1264	177
	VFI_2	VFI	03_F	63.52	0.60	15.33	5.25	0.20	0.37	0.92	7.02	5.25	0.12	98.58	1.12	2820	1638	238
	VFI_2	VFI	03_G	61.15	0.61	14.71	5.36	0.22	0.39	0.86	6.89	4.90	0.08	95.18	1.13	2997	2044	217
	VFI_2	VFI	04_B	62.78	0.65	15.05	5.24	0.24	0.39	0.93	6.61	4.94	0.06	96.90	1.08	2537	1308	243
	VFI_2	VFI	04_C	61.81	0.66	14.65	5.45	0.23	0.40	0.85	6.14	4.71	0.07	94.98	1.04	2800	1718	152
	VFI_2	VFI	04_D	62.76	0.63	14.90	5.34	0.21	0.41	0.84	6.29	5.10	0.08	96.56	1.06	2577	1637	74
	VFI_3	VFI	01_B	62.16	0.49	14.93	4.55	0.18	0.23	0.67	6.10	4.82	0.06	94.19	1.02	2897	2089	161
	VFI_3	VFI	01_C	62.53	0.55	14.96	4.81	0.20	0.29	0.76	6.78	4.51	0.11	95.50	1.07	2850	1707	390
	VFI_4	VFI	03_B	62.65	0.56	14.90	5.40	0.25	0.34	0.93	6.67	4.75	0.06	96.52	1.08	2910	1564	208
	VFI_4	VFI	06_B	64.15	0.50	15.35	4.48	0.18	0.29	0.67	6.46	4.87	0.04	96.98	1.04	2242	633	204
	VFI_4	VFI	07_B	61.88	0.52	14.63	4.93	0.19	0.36	0.79	6.11	4.35	0.09	93.85	1.01	2514	2011	260
	CCI I	CCI	MI01	63.57	0.43	14.65	4.70	0.24	0.21	0.43	7.41	4.97	0.02	96.63	1.20	4627	1767	138
	CCI I	CCI	MI2	63.42	0.41	14.74	4.44	0.19	0.24	0.46	7.30	4.93	0.03	96.16	1.18	4180	2104	166
	CCI I	CCI	MI3a	63.21	0.51	16.16	3.73	0.18	0.26	0.72	6.53	4.96	0.08	96.34	1.00	1852	821	141
	CCI I	CCI	MI3b	62.11	0.53	15.67	3.61	0.15	0.30	0.69	7.00	4.97	0.08	95.11	1.08	1813	624	157
	CCI I	CCI	MI3c	62.91	0.56	15.71	4.13	0.19	0.35	0.85	7.16	4.96	0.07	96.89	1.09	1729	841	183
	CCI I	CCI	MI3d	63.35	0.52	16.15	3.91	0.18	0.32	0.74	7.30	5.12	0.08	97.68	1.09	1662	1073	229
	CCI I	CCI	MI4	62.42	0.35	14.58	4.36	0.19	0.21	0.40	7.17	4.85	0.07	94.59	1.17	4556	1995	187

Table D5 continued

Source	Sample	Unit	Identifier	SiO_2	TiO_2	Al_2O_3	FeO_t	MnO	MgO	CaO	Na_2O	K_2O	P_2O_5	Total	Peralkalinity	Cl	F	S
University of Goettingen	CCI I	CCI	MI5a	62.31	0.40	14.82	4.47	0.20	0.23	0.52	7.55	4.86	0.03	95.40	1.19	3919	1878	108
	CCI I	CCI	MI5b	61.53	0.42	14.89	4.50	0.20	0.27	0.63	7.26	4.79	0.03	94.52	1.15	3515	2042	207
	CCI I	CCI	MI6	63.55	0.41	14.98	4.46	0.24	0.24	0.45	7.44	4.88	0.05	96.70	1.17	4207	2203	141
	TM-1(2)	CCI	MI04	64.22	0.61	15.51	4.58	0.20	0.29	0.77	7.33	4.80	0.04	98.34	1.11	3893	1774	710
	TM-2(2)	CCI	MI05	64.92	0.80	14.95	5.64	0.21	0.24	0.71	8.01	4.51	0.01	100.00	1.21	6850	2613	1046
	TM-2(2)	CCI	MI06	64.99	0.78	14.91	5.22	0.21	0.21	0.59	7.84	4.76	0.04	99.55	1.21	5817	3142	1258
	TER2-1II	CCI	MI02	64.39	0.47	15.32	4.30	0.20	0.28	0.58	7.24	4.93	0.07	97.79	1.13	1737		171
	TER2-1II	CCI	MI03	63.84	0.35	14.84	4.03	0.20	0.21	0.41	7.21	4.76	0.01	95.87	1.15	1820		187
	TER2-1II	CCI	MI06	65.01	0.38	11.91	6.43	0.33	0.07	0.41	7.39	4.45	0.06	96.44	1.43	4660		119
	TM-1(5)	PNI	MI01	66.99	0.46	16.99	1.90	0.05	0.03	0.09	7.94	4.51	0.00	98.95	1.06	3619	2965	50
	T012I	PNI	MI04	65.47	0.37	16.30	3.48	0.13	0.24	0.54	7.34	5.15	0.06	99.09	1.08	913	1222	216
	TM-1(6)	Ign-i	MI03	61.69	0.89	13.59	5.35	0.18	0.20	0.64	8.07	4.53	0.05	95.19	1.34	6398	4751	129
	TM-2(6)	Ign-i	MI01	66.12	0.75	15.65	4.50	0.17	0.25	0.74	8.47	4.77	0.04	101.46	1.22	6959	2611	155
	TM-2(6)	Ign-i	MI03	65.93	0.76	15.14	4.83	0.19	0.21	0.65	8.61	4.78	0.03	101.12	1.28	6567	3658	174
	AM-2(5)	GVI	MI01	65.04	0.89	16.08	4.76	0.16	0.45	0.87	8.35	4.81	0.08	101.48	1.18	3673	2150	257

Table D6: Electron microprobe analyses of Terceira groundmass glass

Source	Sample	Unit	Identifier	SiO_2	TiO_2	Al_2O_3	FeO_t	MnO	MgO	CaO	Na_2O	K_2O	P_2O_5	Total	Peralkalinity	Cl	F	S
University of Goettingen	TER1-1-gm	Angra Ign	26 / 1 .	66.37	0.58	15.15	4.69	0.20	0.34	0.63	6.90	4.93	0.08	99.88	1.10			
	TER1-1-gm	Angra Ign	27 / 1 .	66.55	0.61	15.00	4.44	0.25	0.36	0.59	6.77	4.93	0.08	99.58	1.10			
	TER1-1-gm	Angra Ign	28 / 1 .	66.34	0.57	15.19	4.61	0.23	0.34	0.66	7.13	5.02	0.10	100.18	1.13			
	TER1-2-gm	Angra Ign	21 / 1 .	65.56	0.63	15.50	4.35	0.18	0.40	0.71	7.28	5.22	0.13	99.95	1.14			
	TER1-2-gm	Angra Ign	22 / 1 .	65.29	0.57	15.71	4.42	0.22	0.38	0.63	6.96	4.97	0.11	99.25	1.07			
	TER1-2-gm	Angra Ign	23 / 1 .	65.73	0.58	15.66	4.28	0.23	0.36	0.68	7.17	5.13	0.11	99.93	1.11			
	TER1-2-gm	Angra Ign	24 / 1 .	65.84	0.59	15.29	4.45	0.23	0.36	0.64	7.37	5.06	0.07	99.91	1.15			
	TER1-2-gm	Angra Ign	25 / 1 .	65.61	0.52	15.26	4.66	0.22	0.34	0.61	7.34	4.79	0.04	99.36	1.13			
	TER6-1-gm	Angra Ign	4 / 1 .	66.49	0.59	14.94	4.64	0.22	0.37	0.59	6.69	4.97	0.04	99.54	1.10			
	TER6-1-gm	Angra Ign	5 / 1 .	66.40	0.54	15.22	4.68	0.19	0.36	0.65	6.72	5.10	0.05	99.91	1.09			
	TER6-1-gm	Angra Ign	6 / 1 .	66.79	0.57	15.06	4.51	0.19	0.33	0.59	6.83	5.08	0.07	100.02	1.11			
	TER7-1-gm	Angra Ign	37 / 1 .	66.21	0.56	14.93	4.71	0.22	0.38	0.58	7.37	5.05	0.09	100.09	1.18			
	TER7-1-gm	Angra Ign	39 / 1 .	66.36	0.57	14.69	4.65	0.22	0.36	0.54	7.46	4.98	0.10	99.92	1.20			
	TER7-1-gm	Angra Ign	40 / 1 .	66.67	0.56	14.76	4.57	0.22	0.37	0.53	7.65	5.16	0.02	100.50	1.23			
	TER3-1-gm	Lajes Ign	26 / 1 .	64.50	0.61	15.48	4.33	0.19	0.41	0.73	7.15	5.01	0.11	98.53				
	TER3-1-gm	Lajes Ign	28 / 1 .	63.67	0.65	15.47	4.18	0.17	0.45	0.80	6.74	4.92	0.11	97.18	1.11			
	TER3-1-gm	Lajes Ign	29 / 1 .	64.37	0.64	15.51	4.18	0.19	0.44	0.81	7.12	5.10	0.07	98.42	1.11			
	TER3-1-gm	Lajes Ign	30 / 1 .	64.20	0.64	15.42	4.21	0.20	0.45	0.79	7.08	4.89	0.08	97.97	1.10			
	TER3-2-gm	Lajes Ign	1 / 1 .	66.37	0.60	15.09	4.51	0.24	0.32	0.49	7.08	5.14	0.06	99.91	1.14			
	TER3-2-gm	Lajes Ign	2 / 1 .	67.08	0.63	15.20	4.65	0.20	0.36	0.54	6.95	5.03	0.10	100.73	1.11			
	TER3-2-gm	Lajes Ign	3 / 1 .	66.43	0.57	14.87	4.37	0.21	0.36	0.64	7.45	4.99	0.07	99.96	1.19			
	TER4-1-gm	Lajes Ign	31 / 1 .	65.56	0.59	14.76	4.87	0.22	0.34	0.56	7.32	4.64	0.11	98.96	1.16			
	TER4-1-gm	Lajes Ign	32 / 1 .	65.46	0.53	14.52	4.56	0.21	0.35	0.56	7.17	5.32	0.07	98.77	1.21			
	TER4-1-gm	Lajes Ign	33 / 1 .	65.34	0.55	14.56	4.47	0.20	0.36	0.59	7.31	5.51	0.05	98.94	1.24			

Table D6 continued

Source	Sample	Unit	Identifier	SiO_2	TiO_2	Al_2O_3	FeO_t	MnO	MgO	CaO	Na_2O	K_2O	P_2O_5	Total	Peralkalinity	Cl	F	S
University of Goettingen	TER4-1-gm	Lajes lgn	34 / 1 .	66.01	0.55	14.90	4.57	0.22	0.36	0.59	7.72	4.89	0.11	99.91	1.21			
	TER4-1-gm	Lajes lgn	35 / 1 .	65.64	0.55	14.74	4.50	0.23	0.30	0.68	7.38	5.02	0.09	99.12	1.19			
	TER10-3-gm	Lajes lgn	23 / 1 .	65.75	0.56	15.18	4.64	0.21	0.41	0.62	6.71	4.83	0.05	98.96	1.07			
	TER10-3-gm	Lajes lgn	24 / 1 .	66.37	0.58	15.34	4.51	0.19	0.38	0.63	7.34	4.97	0.10	100.41	1.14			
	TER10-3-gm	Lajes lgn	25 / 1 .	66.24	0.60	15.25	4.55	0.18	0.33	0.57	7.03	5.02	0.07	99.84	1.11			
	TER5-2-gm	LMI	217 / 1 .	64.36	0.59	15.32	4.62	0.17	0.41	1.05	6.21	6.33	0.06	99.12				
	TER5-2-gm	LMI	218 / 1 .	64.92	0.56	15.27	4.98	0.20	0.40	1.26	5.92	6.25	0.06	99.82	1.11			
	TER5-2-gm	LMI	220 / 1 .	64.40	0.68	15.98	4.88	0.17	0.50	1.04	8.14	4.37	0.14	100.30	1.13			
	TER5-2-gm	LMI	221 / 1 .	63.92	0.67	15.88	4.79	0.17	0.44	1.10	9.02	2.90	0.13	99.02	1.13			
	TER5-2LMIGG01	LMI	1	64.31	0.67	15.70	4.85	0.16	0.47	0.99	8.74	2.62	0.12	98.64	1.10	1665	583	111
	TER5-2LMIGG02	LMI	2	64.95	0.57	15.50	4.83	0.18	0.41	0.96	7.22	4.94	0.09	99.65	1.11	2331	306	238
	TER5-2LMIGG03	LMI	3	64.23	0.63	15.64	4.68	0.17	0.44	1.08	7.48	4.52	0.09	98.97	1.10	2125	882	110
	TER5-2LMIGG04	LMI	4	64.21	0.63	15.69	4.95	0.20	0.50	1.06	7.02	5.50	0.14	99.91	1.12	2282	883	135
	TER5-2LMIGG05	LMI	5	63.87	0.69	15.61	4.98	0.18	0.51	1.15	7.16	5.26	0.14	99.56	1.12	2336	876	188
	TER5-2LMIGG06	LMI	6	64.65	0.69	15.54	4.95	0.20	0.51	1.00	8.47	3.18	0.14	99.33	1.12	1707	1009	113
	TER2-2-gm	VFI	229 / 1 .	64.07	0.49	15.16	5.17	0.22	0.30	0.82	7.56	4.73	0.08	98.59				
	TER2-2-gm	VFI	230 / 1 .	64.34	0.54	15.24	5.35	0.21	0.28	0.86	7.74	4.85	0.05	99.45	1.16			
	TER2-2-gm	VFI	231 / 1 .	64.83	0.50	15.12	5.22	0.24	0.30	0.80	7.39	4.93	0.05	99.38	1.16			
	TER11-2B-gm	VFI	61 / 1 .	65.34	0.50	15.24	4.81	0.24	0.31	0.87	7.29	5.27	0.07	99.93	1.16			
	TER11-2B-gm	VFI	63 / 1 .	65.14	0.53	15.48	4.77	0.20	0.37	0.96	7.30	4.83	0.05	99.63	1.11			
	TER2-1-gm	CCI	233 / 1 .	64.43	0.45	15.65	4.71	0.23	0.28	0.65	7.17	4.84	0.05	98.46				
	TER2-1-gm	CCI	235 / 1 .	64.44	0.47	14.91	4.90	0.23	0.27	0.63	7.09	4.96	0.02	97.92	1.09			
	TER2-1-gm	CCI	236 / 1 .	63.89	0.42	15.06	4.88	0.16	0.26	0.62	7.40	5.16	0.05	97.90	1.18			
	TER10-2-gm	CCI	2 / 1 .	65.99	0.51	14.77	5.44	0.22	0.31	0.84	7.10	4.88	0.03	100.09	1.15			
	TER10-2-gm	CCI	3 / 1 .	65.76	0.53	14.89	5.65	0.24	0.25	0.84	7.21	4.99	0.06	100.42	1.16			

Table D6 continued

Source	Sample	Unit	Identifier	SiO_2	TiO_2	Al_2O_3	FeO_t	MnO	MgO	CaO	Na_2O	K_2O	P_2O_5	Total	Peralkalinity	Cl	F	S
University of Goettingen	TER10-2-gm	CCI	4 / 1 .	65.56	0.51	14.91	5.51	0.23	0.24	0.85	7.07	4.93	0.10	99.91	1.14			
	TER10-2-gm	CCI	5 / 1 .	66.06	0.55	15.08	5.46	0.23	0.27	0.80	7.15	4.85	0.07	100.52	1.13			
	TER10-2-gm	CCI	6 / 1 .	65.59	0.47	15.04	5.35	0.21	0.33	0.78	7.28	4.90	0.09	100.05	1.15			
	TER10-2-gm	CCI	7 / 1 .	65.33	0.55	14.90	5.47	0.24	0.31	0.82	7.31	4.90	0.08	99.92	1.16			
	TER10-2-gm	CCI	8 / 1 .	65.91	0.52	14.88	5.43	0.25	0.27	0.82	7.15	4.82	0.02	100.09	1.14			
	TER10-2-gm-hell	CCI	9 / 1 .	65.31	0.54	14.92	5.57	0.23	0.28	0.77	7.62	4.77	0.11	100.12	1.19			
	TER11-1A-gm	CCI	12 / 1 .	61.86	1.17	16.22	6.42	0.22	0.86	1.97	7.20	3.64	0.26	99.81	0.97			
	TER11-1A-gm	CCI	13 / 1 .	62.69	1.09	16.00	5.96	0.19	0.88	2.15	6.99	3.68	0.24	99.88	0.97			
	TER11-1A-gm	CCI	14 / 1 .	58.85	1.67	15.88	8.02	0.27	1.29	2.84	7.20	3.64	0.43	100.10	0.99			
	TER11-1A-gm	CCI	15 / 1 .	61.24	1.32	15.92	6.97	0.28	1.24	2.95	6.39	3.72	0.28	100.30	0.91			
	TER11-1A-gm	CCI	16 / 1 .	60.45	1.53	16.02	6.31	0.21	1.27	3.09	7.00	3.39	0.31	99.59	0.95			
	TER11-1A-gm	CCI	17 / 1 .	61.67	1.59	16.44	5.63	0.17	1.14	2.50	7.22	3.85	0.34	100.55	0.98			
	TER11-1A-gm	CCI	19 / 1 .	61.84	1.33	15.91	6.39	0.22	1.04	2.38	7.36	3.11	0.30	99.87	0.97			
	TER11-1A-gm	CCI	20 / 1 .	62.94	1.02	15.52	6.36	0.20	0.99	2.19	7.07	3.82	0.16	100.27	1.02			
	CCIGG01	CCI	1	64.53	0.51	15.50	4.88	0.25	0.30	0.88	7.27	4.87	0.05	99.03	1.11			
	CCIGG02	CCI	2	64.50	0.52	15.58	4.96	0.22	0.32	0.85	7.53	4.89	0.08	99.45	1.13			
	CCIGG03	CCI	3	64.04	0.49	15.50	5.06	0.23	0.32	0.85	7.19	4.89	0.07	98.64	1.10			
	CCIGG04	CCI	4	64.26	0.53	15.56	5.17	0.23	0.30	0.91	7.15	4.90	0.04	99.04	1.10			
	CCIGG05	CCI	5	64.52	0.55	15.68	4.91	0.20	0.30	0.82	7.21	5.04	0.09	99.31	1.10			
	CCIGG06	CCI	6	64.69	0.52	15.34	4.87	0.20	0.29	0.80	7.23	5.04	0.09	99.07	1.13			
	CCIGG07	CCI	7	63.90	0.55	15.70	4.92	0.26	0.34	0.93	7.06	4.95	0.08	98.69	1.08			
	CCIGG08	CCI	8	64.51	0.53	15.59	5.06	0.23	0.30	0.84	7.18	4.93	0.05	99.22	1.10			
	CCIGG09	CCI	9	64.65	0.53	15.58	4.86	0.24	0.31	0.90	7.05	4.86	0.05	99.04	1.08			
	CCIGG10	CCI	10	63.77	0.53	15.50	4.86	0.23	0.31	0.85	6.91	4.84	0.07	97.87	1.07			
	CCIGG11	CCI	11	64.06	0.52	15.53	5.07	0.27	0.29	0.87	7.49	4.97	0.08	99.15	1.14			

Table D6 continued

Source	Sample	Unit	Identifier	SiO_2	TiO_2	Al_2O_3	FeO_t	MnO	MgO	CaO	Na_2O	K_2O	P_2O_5	Total	Peralkalinity	Cl	F	S
University of Goettingen	CCIGG12	CCI	12	64.58	0.52	15.60	4.80	0.22	0.32	0.86	7.08	5.04	0.06	99.08	1.10			
	CCIGG13	CCI	13	63.87	0.50	15.65	4.83	0.22	0.28	0.85	7.04	4.88	0.06	98.19	1.08			
	CCIGG14	CCI	14	64.04	0.53	15.59	4.96	0.22	0.32	0.94	7.45	4.97	0.06	99.07	1.13			
	CCIGG15	CCI	15	64.49	0.56	15.74	4.77	0.22	0.31	0.87	7.09	4.90	0.07	99.02	1.08			
	PNIGG01	PNI	1	64.80	0.64	15.47	5.03	0.22	0.44	0.99	7.58	4.35	0.10	99.62		1493	343	218
	PNIGG02	PNI	2	64.59	0.63	15.64	4.70	0.21	0.43	0.98	7.38	4.43	0.12	99.11	1.11			
	PNIGG03	PNI	3	63.91	0.64	15.52	4.95	0.20	0.43	1.00	7.06	5.03	0.08	98.82	1.10	1472	470	256
	PNIGG04	PNI	4	63.84	0.73	15.76	4.86	0.20	0.50	1.23	7.26	4.66	0.09	99.12	1.08			
	PNIGG05	PNI	5	64.95	0.59	15.29	5.09	0.24	0.40	0.98	7.86	3.95	0.05	99.39	1.13	1831	249	202
	PNIGG06	PNI	6	64.75	0.62	15.58	4.88	0.22	0.44	0.99	7.59	4.49	0.12	99.68	1.11	1812	860	169
	PNIGG07	PNI	7	65.15	0.54	15.56	4.92	0.23	0.41	0.88	7.64	4.38	0.07	99.79	1.11	1995	287	211
	PNIGG08	PNI	8	65.27	0.57	15.43	4.75	0.21	0.37	0.84	7.28	4.93	0.09	99.75	1.12	1464	179	229
	PNIGG09	PNI	9	64.43	0.60	15.50	5.08	0.23	0.42	1.13	7.51	4.54	0.12	99.57	1.11	2264	183	270
	PNIGG10	PNI	10	64.13	0.65	15.79	4.91	0.20	0.48	1.05	7.71	4.53	0.10	99.55	1.11	1511	1420	175
	GVIGG01	GVI	1	62.82	0.64	15.10	3.92	0.20	0.47	0.60	5.76	5.88	0.09	95.48		2469	1937	177
	GVIGG02	GVI	2	62.76	0.62	15.45	3.90	0.21	0.47	0.34	6.69	5.49	0.11	96.03	1.05	2859	2128	229
	GVIGG04	GVI	3	64.67	0.63	15.99	4.03	0.24	0.44	0.37	8.12	5.08	0.10	99.66	1.18	3371	2119	140
	GVIGG05	GVI	4	64.61	0.61	16.03	3.93	0.21	0.48	0.45	7.70	5.16	0.10	99.28	1.14	3120	2608	160
	GVIGG06	GVI	5	64.14	0.63	15.92	3.98	0.26	0.48	0.48	8.01	5.12	0.06	99.09	1.18	3184	2104	105
	GVIGG07	GVI	6	63.86	0.64	15.86	3.36	0.21	0.42	0.26	7.53	5.12	0.10	97.36	1.13	2645	1906	107
	GVIGG13	GVI	7	63.38	0.63	15.63	3.51	0.21	0.37	0.49	6.94	5.32	0.05	96.54	1.10	2740	1755	213
	GVIGG14	GVI	8	62.84	0.61	15.21	4.09	0.23	0.46	0.64	6.66	5.38	0.05	96.17	1.10	2271	1702	109
	GVIGG15	GVI	9	63.85	0.63	15.86	3.59	0.21	0.45	0.45	7.53	4.98	0.07	97.63	1.12	2795	2022	151

Table D7: Whole rock analyses of Furnas lithologies, analysed via WD-XRF

Source	**Open University**									
Sample	FUR-2	FUR-3	SM1-2	SM3-1	SM1-1	SM1-3	SM4-1	SM2-1	SM4-2	SM5-1
Unit	Furnas A	Furnas B	Furnas C	Furnas C	Furnas C	Furnas E	Furnas F	Furnas H	Furnas I	Furnas I
Type	Fall	Fall	Fall	Fall	Fall	Fall	Fall	Fall	Fall	Dome
Major elements (wt. %)										
SiO_2	57.69	58.25	61.24	60.78	61.04	61.04	63.11	61.59	61.95	63.42
TiO_2	0.71	0.69	0.41	0.41	0.44	0.47	0.51	0.44	0.47	0.46
Al_2O_3	19.51	18.39	16.87	17.10	17.43	17.50	17.57	16.90	17.18	17.55
$Fe_2O_3^T$	3.44	2.86	4.54	4.30	4.38	4.25	4.06	4.12	4.01	3.96
MnO	0.11	0.10	0.29	0.27	0.27	0.27	0.25	0.27	0.26	0.24
MgO	0.41	0.39	0.31	0.30	0.34	0.37	0.39	0.33	0.37	0.34
CaO	0.98	0.92	0.75	0.72	0.76	0.72	0.83	0.70	0.75	0.76
Na_2O	5.31	5.63	7.51	7.44	7.47	7.71	7.04	7.98	7.74	7.39
K_2O	5.10	5.30	5.32	5.13	5.30	5.39	5.87	5.46	5.64	5.78
P_2O_5	0.18	0.22	0.06	0.05	0.06	0.06	0.07	0.06	0.07	0.07
LOI	6.35	6.86	2.31	3.10	2.49	2.00	0.54	2.29	1.89	0.49
Total	99.79	99.60	99.61	99.60	99.98	99.79	100.24	100.14	100.32	100.45
Peralkalinity	0.73	0.82	1.07	1.04	1.03	1.06	1.02	1.13	1.10	1.05
Na + K	11.14	11.79	13.19	13.02	13.10	13.40	12.95	13.74	13.59	13.17
Trace elements (ppm)										
Rb	149	144	230	225	226	228	212	238	212	223
Sr	46	51	6	5	10	4	8	2	4	4
Y	49	40	76	75	76	79	69	79	68	67
Zr	1254	1010	1443	1461	1460	1498	1253	1494	1288	1248
Nb	193	177	289	292	293	302	255	303	261	253
Ba	103	115	21	17	20	11	33	5	11	17
Pb	15	11	15	15	16	13	14	16	13	13
Th	31	24	30	29	29	32	24	30	26	26
U	8	6	8	7	9	8	7	8	6	8
Sc	2	1	2	1	2	3	3	3	3	2
V	11	17	bdl	1	5	3	6	bdl	bdl	3
Cr	5	5	4	4	6	5	5	2	5	6
Co	2	bdl	1	bdl	bdl	1	bdl	1	bdl	bdl
Ni	4	3	4	4	4	4	3	3	2	5
Cu	5	5	3	4	5	5	4	3	2	4
Zn	103	90	189	194	190	190	186	188	170	139
Ga	31	31	32	33	32	33	31	33	30	32
Mo	13	25	12	13	11	14	4	13	11	1
As	12	12	10	8	7	8	7	8	4	4
S	305	488	52	50	51	49	26	59	48	18

Table D7 continued

Source	Open University					University of East Anglia					
Sample	AZ02-4	SM6-1	SM8-1	SM7-1	SM7-2	S008	S037	S038	S023	S022	S035
Unit	Furnas J	Furnas J	Furnas J	Furnas J	Furnas J	Furnas G	Furnas I	Furnas I	Fur-I	Fur-J	Furnas J
Type	Fall	Fall	Surge	Dome	Dome	Fall	Fall	Fall	Dome	Dome	Syenite
Major elements (wt. %)											
SiO_2	61.00	61.50	61.40	62.64	62.88	61.13	61.26	61.35	62.69	62.52	61.06
TiO_2	0.47	0.48	0.48	0.57	0.57	0.41	0.47	0.47	0.55	0.56	0.56
Al_2O_3	17.04	17.02	17.03	17.58	17.88	16.89	17.01	17.04	17.71	17.64	17.49
$Fe_2O_3^T$	4.00	3.98	3.96	3.94	4.17	4.08	3.76	3.79	3.70	3.67	3.76
MnO	0.25	0.25	0.24	0.24	0.20	0.27	0.25	0.25	0.22	0.22	0.25
MgO	0.36	0.38	0.37	0.47	0.46	0.25	0.31	0.31	0.39	0.38	0.23
CaO	0.76	0.79	0.78	0.88	0.90	0.71	0.71	0.70	0.82	0.87	0.85
Na_2O	7.78	7.83	7.47	6.61	6.44	7.42	7.63	7.64	7.00	7.29	7.02
K_2O	5.56	5.59	5.59	5.97	5.95	5.40	5.60	5.59	5.95	5.96	5.69
P_2O_5	0.06	0.07	0.07	0.09	0.09	0.05	0.07	0.07	0.08	0.09	0.05
LOI	1.92	2.15	2.51	0.96	0.75	2.92	2.77	2.29	0.54	0.21	2.28
Total	99.21	100.03	99.89	99.96	100.29	99.22	99.55	99.21	99.37	99.13	98.95
Peralkalinity	1.10	1.11	1.08	0.99	0.95	1.07	1.09	1.09	1.01	1.05	1.01
Na + K	13.71	13.71	13.41	12.71	12.45	13.31	13.67	13.65	13.10	13.39	13.15
Trace elements (ppm)											
Rb	211	209	204	180	161	221	205	206	173	161	267
Sr	3	5	4	8	11	bdl	bdl	bdl	10	11	bdl
Y	68	68	66	63	70	66	61	62	52	70	71
Zr	1267	1258	1230	961	991	1424	1275	1296	1021	991	1733
Nb	259	257	251	197	199	256	233	235	187	199	238
Ba	9	5	bdl	30	44	bdl	bdl	bdl	bdl	44	bdl
Pb	12	15	11	8	8	21	20	bdl	bdl	8	bdl
Th	28	26	25	20	18	29	26	26	22	18	40
U	7	6	4	5	7	bdl	bdl	bdl	bdl	7	bdl
Sc	bdl	2	2	bdl	1	bdl	bdl	bdl	bdl	1	bdl
V	2	bdl	6	2	2	bdl	bdl	bdl	bdl	2	bdl
Cr	3	6	4	5	3	bdl	bdl	bdl	bdl	3	bdl
Co	bdl	1	bdl	2	bdl					bdl	
Ni	2	1	5	4	3	bdl	bdl	bdl	bdl	3	bdl
Cu	4	4	4	6	2	bdl	bdl	bdl	bdl	2	bdl
Zn	170	169	164	143	327	175	161	162	126	327	173
Ga	30	30	28	29	29					29	
Mo	11	10	11	5	3	12	11	11	bdl	3	14
As	10	8	5	3	2	13	14	11	10	2	12
S	61	53	77	29	23					23	

Table D8: Selected trace element analyses of Furnas lithologies, analysed by ED-XRF

Source	**Keele University**														
Sample	S022	S022	S074	S074	S074	S074	S074	S074	S074	S074	S074	S074	S089	S089	S089
Unit	Fur J	Fur J	Fur J	Fur J	Fur J	Fur J	Fur J	Fur J	Fur J	Fur J	Fur J	Fur J	Fur J	Fur J	Fur J
Notes	Dome	Dome	Lf	Lf	Lf	Lf	Lf	Lf	Lf	Lf	Lf	Lf	L5	L5	L5
Trace elements (ppm)															
Nb	183	177	241	245	244	241	238	239	243	240	239	248	244	252	237
Zr	961	923	1256	1253	1247	1250	1235	1250	1269	1243	1233	1291	1261	1300	1239
Sr	12	13	bdl	bdl	bdl	bdl	bdl	bdl	bdl	bdl	bdl	bdl	bdl	bdl	bdl
Rb	167	175	205	207	206	206	209	206	209	205	203	214	207	211	197

Source	**Keele University**														
Sample	S089	S089	S089	S088	S088	S088	S088	S088	S082	S082	S082	S082	S082	S082	S081
Unit	Fur J	Fur J	Fur J	Fur J	Fur J	Fur J	Fur J	Fur J	Fur J	Fur J	Fur J	Fur J	Fur J	Fur J	Fur J
Notes	L5	L5	L5	L4	L4	L4	L4	L4	L3	L3	L3	L3	L3	L3	L2
Trace elements (ppm)															
Nb	247	246	246	249	246	242	250	241	248	243	240	237	239	241	257
Zr	1304	1289	1300	1316	1277	1251	1301	1262	1311	1268	1258	1251	1260	1249	1363
Sr	bdl	bdl	bdl	13	12	12	bdl	13	13	14	12	14	15	12	19
Rb	204	204	204	205	200	198	203	199	211	205	203	202	203	203	216

Source	**Keele University**														
Sample	S081	S081	S081	S081	S081	S005	S005	S005	S005	S005	S005	S005	S005	S005	S005
Unit	Fur J	Fur J	Fur J	Fur J	Fur J	Fur J	Fur J	Fur J	Fur J	Fur J	Fur J	Fur J	Fur J	Fur J	Fur J
Notes	L2	L2	L2	L2	L2	L1	L1	L1	L1	L1	L1	L1	L1	L1	L1
Trace elements (ppm)															
Nb	252	244	247	230	243	248	247	248	247	253	251	253	252	253	249
Zr	1324	1282	1274	1222	1263	1284	1287	1297	1297	1301	1297	1303	1302	1326	1297
Sr	20	14	12	95	17	bdl	14	bdl	bdl	bdl	bdl	bdl	bdl	bdl	bdl
Rb	211	206	210	194	204	212	211	211	207	214	212	210	210	213	210

Table D8: continued

Source	Keele University														
Sample	S005	S005	S023	S023	S061	S061	S061	S061	S061	S061	S061	S061	S037	S037	S037
Unit	Fur J	Fur J	Fur I	Fur I	Fur I	Fur I	Fur I	Fur I	Fur I	Fur I	Fur I	Fur I	Fur I	Fur I	Fur I
Notes	L1	L1	Dome	Dome	Upper	Upper	Upper	Upper	Upper	Upper	Upper	Upper	Lower	Lower	Lower
Trace elements (ppm)															
Nb	251	254	205	206	266	272	252	267	269	257	271	266	266	265	269
Zr	1311	1306	1070	1050	1383	1412	1323	1423	1421	1336	1425	1400	1387	1379	1394
Sr	bdl	bdl	21	16	bdl	bdl	bdl	bdl	bdl	bdl	bdl	bdl	bdl	bdl	bdl
Rb	215	217	186	184	221	222	216	223	222	211	222	225	224	223	224

Source	Keele University														
Sample	S037	S037	S001	S001	S001	S001	S001	S092	S092	S092	S092	S092	S092	S092	S092
Unit	Fur I	Fur I	Fur H	Fur H	Fur H	Fur H	Fur H	Fur H	Fur H	Fur H	Fur H	Fur H	Fur H	Fur H	Fur H
Notes	Lower	Lower	Upper	Upper	Upper	Upper	Upper	Lower	Lower	Lower	Lower	Lower	Lower	Lower	Lower
Trace elements (ppm)															
Nb	267	269	303	304	305	303	304	300	300	296	301	309	301	301	295
Zr	1395	1386	1568	1580	1611	1584	1582	1580	1562	1548	1567	1633	1605	1569	1522
Sr	bdl	bdl	bdl	bdl	bdl	bdl	bdl	bdl	bdl	bdl	bdl	bdl	bdl	bdl	bdl
Rb	222	224	246	241	258	244	248	249	243	246	243	262	255	241	238

Source	Keele University														
Sample	S060	S060	S060	S060	S060	S060	S060	S060	S059	S059	S059	S059	S059	S058	S058
Unit	Fur F	Fur F	Fur F	Fur F	Fur F	Fur F	Fur F	Fur F	Fur F	Fur F	Fur F	Fur F	Fur F	Fur F	Fur F
Notes	Upper	Upper	Upper	Upper	Upper	Upper	Upper	Upper	Mid-2	Mid-2	Mid-2	Mid-2	Mid-2	Mid-1	Mid-1
Trace elements (ppm)															
Nb	247	241	239	239	244	247	247	257	272	286	264	260	249	282	276
Zr	1280	1252	1242	1238	1272	1286	1277	1308	1408	1462	1367	1352	1282	1506	1443
Sr	bdl	13	12	13	bdl	13	18	bdl	bdl	bdl	12	bdl	bdl	bdl	bdl
Rb	206	207	213	200	200	210	203	215	222	235	213	221	205	233	228

Table D8: continued

Source	Keele University														
Sample	S058	S058	S058	S058	S057	S057	S057	S057	S057	S057	S064	S064	S064	S065	S065
Unit	Fur F	Fur F	Fur F	Fur F	Fur F	Fur F	Fur F	Fur F	Fur F	Fur F	Fur E	Fur E	Fur E	Fur C	Fur C
Notes	Mid-1	Mid-1	Mid-1	Mid-1	Lower	Lower	Lower	Lower	Lower	Lower				Upper	Upper
Trace elements (ppm)															
Nb	284	285	294	278	264	290	267	284	263	265	308	305	302	325	325
Zr	1478	1482	1532	1469	1386	1490	1388	1482	1360	1389	1608	1593	1598	1751	1742
Sr	bdl	bdl	bdl	bdl	bdl	bdl	bdl	bdl	bdl	bdl	bdl	bdl	bdl	15	26
Rb	238	232	237	235	223	229	223	236	220	222	227	230	232	217	226

Source	Keele University											
Sample	S065	S065	S065	S065	S065	S065	S066	S066	S066	S066	S066	S066
Unit	Fur C	Fur C	Fur C	Fur C	Fur C	Fur C	Fur C	Fur C	Fur C	Fur C	Fur C	Fur C
Notes	Upper	Upper	Upper	Upper	Upper	Upper	Lower	Lower	Lower	Lower	Lower	Lower
Trace elements (ppm)												
Nb	311	322	313	311	310	316	289	284	300	293	291	286
Zr	1659	1732	1684	1660	1661	1693	1515	1497	1601	1516	1514	1504
Sr	12	12	13	bdl	13	12	bdl	14	19	bdl	bdl	bdl
Rb	217	217	211	214	212	211	243	235	221	240	243	236

Table D9: Whole rock compositions of Furnas lithologies, analysed by ICP-AES

Source	**Bureau Veritas Laboratories**			
Sample	S062	S091SY	S091ENC	FJSY
Unit	Furnas J	Furnas J	Furnas J	Furnas J
Type	Syenite	Syenite	Enclave	Enclave
Major elements (wt. %)				
SiO_2	61.80	62.68	62.37	62.47
TiO_2	0.76	0.45	0.65	0.57
Al_2O_3	17.84	17.10	18.00	17.33
$Fe_2O_3^T$	3.63	4.10	3.79	4.41
MnO	0.19	0.28	0.21	0.29
MgO	0.56	0.26	0.51	0.38
CaO	1.03	0.54	0.96	0.56
Na_2O	6.68	7.33	6.96	7.66
K_2O	6.41	5.65	5.60	4.90
P_2O_5	0.12	0.02	0.12	0.09
LOI	0.8	1.3	0.5	0.9
Total	99.53	99.38	99.67	99.56
Peralkalinity	1.00	1.06	0.97	1.03
Total alkali	13.26	13.23	12.67	12.73

Table D10: Whole rock trace element data for Furnas lithologies, analysed by ICP-MS

Source	**Open University**						**Bureau Veritas Laboratories**			
Sample	SM1-2	SM1-3	SM4-1	SM2-1	SM4-2	SM6-1	S062	S091SY	S091ENC	FJSY
Unit	Furnas C	Furnas E	Furnas F	Furnas H	Furnas I	Furnas J	Furnas J	Furnas J	Furnas J	Furnas J
Type	Fall	Fall	Fall	Fall	Fall	Fall	Syenite	Syenite	Enclave	Enclave
Trace elements (ppm)										
Li	26.3	27.6	21.9	25.5	25.6	23.2				
Sc	3	3	2	2	2	2			2	2
V	1	2	1	0	0	1	bdl	bdl	bdl	bdl
Cr	2.8	1.0	0.7	0.3	0.4	1.3				
Co	1.2	0.3	0.1	0.1	0.1	0.3	bdl	bdl	bdl	0.4
Ni	2.0	0.6	0.2	0.2	0.1	0.7			bdl	bdl
Cu	3.9	3.2	2.8	2.6	2.7	4.4				
Zn	178	182	167	173	171	163				
Rb	229.3	223.1	135.6	214.3	215.3	202.0	150.7	235.9	280.6	270.6
Sr	5.9	3.8	4.5	1.1	4.5	4.2	34.2	5.4	95.5	12.4
Y	78.0	81.1	42.7	74.9	73.5	67.1	29.3	46.2	49.6	64.8
Zr	1621.0	1678.0	1409.0	1544.0	1500.0	1391.0	709.6	1528.2	843.5	1685.0
Nb	314.2	327.8	277.2	301.7	294.1	275.0	152.3	316.3	181.9	369.9
Mo	12.3	11.8	4.5	11.3	11.0	10.5				
Sn	9	9	8	9	8	8	3	11	6	10
Sb	0.5	0.5	0.4	0.5	0.4	0.4				
Cs	2.3	2.3	1.4	2.2	2.2	2.0	1.2	1.3	2.7	2.5
Ba	11	8	23	2	12	6	117	10	424	27
La	179.3	185.4	86.0	170.8	167.9	154.7	95.5	95.8	159.6	166.1
Ce	349.9	360.4	188.6	334.0	332.7	302.6	167.2	219.9	300.9	342.6
Pr	38.27	39.34	20.71	36.14	35.89	33.31	16.61	22.58	29.82	35.11
Nd	121.6	127.4	69.1	116.4	116.6	108.3	57.1	79.4	99.1	119.5
Sm	19.64	20.58	11.56	18.79	18.73	17.49	8.80	13.36	14.53	18.95
Eu	0.69	0.92	0.76	0.82	1.01	0.95	1.90	0.62	2.40	1.18
Gd	16.36	17.11	9.82	15.61	15.60	14.45	6.98	10.87	12.26	15.53
Tb	2.50	2.62	1.58	2.40	2.38	2.21	1.02	1.73	1.81	2.44
Dy	13.44	14.14	8.76	12.93	12.73	11.85	5.38	10.16	9.93	13.83
Ho	2.64	2.78	1.76	2.55	2.50	2.32	1.03	1.93	1.84	2.55
Er	7.45	7.78	5.05	7.16	6.99	6.51	2.99	5.55	4.74	7.22
Yb	6.53	6.82	4.53	6.27	6.12	5.69	3.14	5.94	4.46	7.06
Lu	0.97	1.01	0.68	0.93	0.91	0.84	0.44	0.89	0.68	1.04
Hf	30.6	31.8	26.7	29.5	28.4	26.6	16.1	34.5	18.7	36.2
Ta	19.4	20.1	16.9	18.7	18.0	17.2	6.3	19.7	11.4	20.5
Pb	14.5	14.9	9.1	13.6	13.5	12.7				
Th	34.0	34.8	14.2	31.9	30.6	27.8	16.0	16.3	22.1	31.2
U	7.8	8.2	4.5	7.4	7.2	6.6	3.6	11.8	5.7	9.8
Sc							2	1		
Be							5	7	3	7
Ga							26.2	35.6	25.9	33.2
W							0.9	2.1	1.5	2.6
Tm							0.4	0.8	0.7	1.1

Table D11: Electron microprobe analyses of melt inclusions from Furnas lithologies

Source	Sample	Unit	Identifier	SiO_2	TiO_2	Al_2O_3	FeO_t	MnO	MgO	CaO	Na_2O	K_2O	P_2O_5	Total	Peralkalinity	Cl	F	S
University of Goettingen	Fur-J 1	Furnas J	MI01	60.24	0.62	15.90	3.69	0.26	0.37	0.77	7.48	5.37	0.14	94.92	1.14	3187	1630	229
	Fur-J 1	Furnas J	MI2	60.17	0.99	16.23	4.13	0.31	0.54	0.95	7.47	4.98	0.15	96.04	1.09	2697	1752	261
	Fur-J 1	Furnas J	MI3	61.68	0.50	16.76	3.16	0.26	0.30	0.65	8.38	4.32	0.04	96.13	1.10	2802	1775	211
	Fur-J 1	Furnas J	MI4	61.45	0.50	16.63	3.35	0.25	0.28	0.67	7.45	5.56	0.10	96.33	1.10	2999	1799	198
	Fur-J 1	Furnas J	MI5	60.50	0.57	16.44	3.38	0.25	0.36	0.70	8.11	4.33	0.08	94.81	1.10	3061	2045	205
	Fur-J 1	Furnas J	MI6	62.49	0.47	17.41	3.25	0.25	0.30	0.67	7.61	5.29	0.06	97.88	1.05	3017	1813	171
	Fur-J 1	Furnas J	MI07a	61.85	0.49	17.20	3.29	0.27	0.32	0.66	7.42	5.40	0.09	97.08	1.05	3138	2040	98
	Fur-J 1	Furnas J	MI07b	62.20	0.52	16.96	3.18	0.25	0.35	0.72	7.35	5.31	0.08	97.00	1.05	2994	1853	221
	Fur-J 1	Furnas J	MI08	61.83	0.46	17.08	3.11	0.23	0.36	0.74	7.19	5.54	0.04	96.66	1.04	2315	1196	155
	S018II	Furnas J	MI07	60.82	0.47	16.71	3.11	0.23	0.30	0.63	7.26	5.04	0.05	94.70	1.04	2950	2213	74
	S018II	Furnas J	IMI10	61.06	0.42	16.91	3.19	0.22	0.30	0.68	7.64	5.32	0.04	95.88	1.08	3130	1369	193
	FM-2(1)	Furnas J	MI01	63.15	0.88	17.39	4.82	0.27	0.31	0.74	7.73	5.47	0.08	100.95	1.07	3226	1840	121
	FM-2(1)	Furnas J	MI05	63.66	0.72	17.52	4.43	0.27	0.30	0.84	7.74	5.33	0.05	100.97	1.06	3144	1559	205
	FM-2(1)	Furnas J	MI06	62.02	0.71	18.35	4.15	0.22	0.30	0.74	7.75	5.20	0.05	99.60	1.00	3182	1767	264
	FM-1(2)	Furnas I	MI01	64.11	0.67	17.55	4.52	0.27	0.26	0.69	7.88	5.46	0.04	101.57	1.08	3518	2176	105
	FM-1(1)	Furnas I	MI03	64.43	0.85	17.71	3.98	0.21	0.21	0.75	7.42	5.66	0.03	101.35	1.04	2464	1448	123
	FM-2(2)	Furnas I	MI01	63.66	0.58	17.45	4.23	0.30	0.28	0.70	7.78	5.45	0.05	100.59	1.07	3739	2152	169
	S038I	Furnas I	MI05	60.54	0.48	16.81	3.17	0.25	0.34	0.59	7.82	4.16	0.05	94.29	1.03	2780	2896	142
	S038I	Furnas I	MI09	63.94	0.37	17.77	3.22	0.28	0.27	0.55	8.49	5.51	0.03	100.52	1.12	3360	3252	146

Table D11 continued

Source	Sample	Unit	Identifier	SiO_2	TiO_2	Al_2O_3	FeO_t	MnO	MgO	CaO	Na_2O	K_2O	P_2O_5	Total	Peralkalinity	Cl	F	S
University of Goettingen	FM-1(3)	Furnas H	MI01	63.04	0.64	17.37	4.23	0.28	0.28	0.68	8.15	5.36	0.04	100.18	1.11	3796	2185	93
	FM-1(3)	Furnas H	MI03	63.15	0.56	17.40	4.24	0.32	0.30	0.86	6.94	5.21	0.08	99.17	0.98	3818	1842	163
	FM-2(3)	Furnas H	MI05	63.56	0.51	17.47	3.86	0.28	0.30	0.75	8.41	4.98	0.05	100.28	1.10	3703	2050	68
	FM-2(3)	Furnas H	MI07	62.74	0.64	17.31	4.35	0.29	0.26	0.71	7.88	5.33	0.05	99.66	1.08	3740	2130	179
	S008	Furnas G	MI01	61.23	0.40	16.94	3.25	0.26	0.25	0.61	7.62	4.86	0.06	95.57	1.05	3393	2288	119
	FM-1(5)	Furnas F	MI01	64.46	0.61	17.81	4.36	0.26	0.26	0.73	8.08	5.38	0.02	102.09	1.07	3847	2379	121
	FM-2(5)	Furnas F	MI02	60.66	0.47	19.37	3.21	0.19	0.09	0.23	7.63	5.22	0.06	97.21	0.94	4170	1940	279
	FM-2(5)	Furnas F	MI03	64.05	0.65	17.25	4.31	0.30	0.37	0.71	8.15	5.28	0.04	101.22	1.11	4037	2571	279
	AM-2(3)	Furnas E	MI02	63.55	0.71	17.80	3.40	0.18	0.29	0.80	7.55	5.83	0.06	100.27	1.05	2274	1395	285
	AM-2(3)	Furnas E	MI03	62.15	0.43	17.17	3.59	0.28	0.28	0.63	7.27	5.33	0.05	97.28	1.03	3434	2344	150
	S012I	Furnas E	MI01	63.45	0.49	16.79	3.10	0.28	0.27	0.69	7.75	5.23	0.07	98.20	1.10	3023	1807	167
	S012I	Furnas E	MI02	62.69	0.49	16.82	3.82	0.29	0.33	0.66	7.92	5.00	0.08	98.21	1.10	3812	2906	150
	S012I	Furnas E	MI04	62.75	0.59	17.65	3.81	0.27	0.44	0.64	8.27	5.27	0.06	99.84	1.09	3558	2084	135
	S012I	Furnas E	MI06	62.42	0.40	17.03	3.05	0.28	0.27	0.65	7.57	5.18	0.06	96.99	1.06	3149	2348	171
	FM-1(6)	Furnas C	MI02	63.67	0.54	17.57	3.73	0.19	0.27	0.71	7.56	5.70	0.02	100.06	1.06	2770	1898	121
	FM-1(6)	Furnas C	MI03	64.53	0.83	18.03	4.21	0.20	0.24	0.73	7.18	5.42	0.04	101.51	0.98	2472	1877	104
	FM-1(6)	Furnas C	MI04	63.15	0.72	17.74	4.00	0.22	0.25	0.75	8.04	5.14	0.03	100.14	1.06	2798	1656	167
	FM-2(6)	Furnas C	MI01	63.79	0.63	17.70	3.76	0.23	0.23	0.73	7.52	5.59	0.06	100.33	1.04	2939	1600	142
	S016I	Furnas C	MI01	60.17	0.38	16.78	3.36	0.27	0.28	0.59	7.72	4.11	0.05	93.79	1.02	3295	3074	174

Table D12: Electron microprobe analyses of groundmass glass from Furnas lithologies

Source	Sample	Unit	Identifier	SiO_2	TiO_2	Al_2O_3	FeO_t	MnO	MgO	CaO	Na_2O	K_2O	P_2O_5	Total	Peralkalinity	Cl	F	S
University of Goettingen	S005	Furnas J	GG02	62.59	0.44	17.34	3.32	0.30	0.31	0.76	7.62	5.82	0.04	98.62	1.09	3075	1877	68
	S005	Furnas J	GG03	62.93	0.46	17.23	3.26	0.28	0.32	0.74	7.62	5.95	0.03	98.92	1.10	3101	2016	149
	S005	Furnas J	GG04	62.84	0.49	17.24	3.19	0.24	0.35	0.70	7.72	5.74	0.06	98.66	1.10	3062	1870	
	S005	Furnas J	GG05	62.35	0.49	17.32	3.34	0.27	0.32	0.81	7.61	5.74	0.07	98.43	1.08	3024	1799	60
	S005	Furnas J	GG06	62.82	0.45	17.12	3.21	0.27	0.28	0.78	7.57	5.89	0.06	98.55	1.10	3037	1693	70
	S005	Furnas J	GG07	62.40	0.48	17.19	3.35	0.28	0.31	0.79	7.62	5.70	0.10	98.32	1.09	3410	1790	58
	S005	Furnas J	GG08	62.65	0.46	17.22	3.31	0.25	0.33	0.81	7.66	5.87	0.05	98.70	1.10	3006	1955	
	S005	Furnas J	GG09	62.98	0.45	17.36	3.30	0.22	0.33	0.76	7.66	5.90	0.06	99.11	1.09	3041	1796	90
	S005	Furnas J	GG10	62.90	0.48	17.27	3.28	0.29	0.30	0.75	7.57	5.86	0.04	98.84	1.09	3036	1955	164
	S005	Furnas J	GG11	62.99	0.48	17.20	3.26	0.26	0.29	0.77	7.46	5.92	0.06	98.78	1.09	2980	1772	
	S005	Furnas J	GG12	62.83	0.49	17.41	3.29	0.24	0.31	0.80	7.71	5.80	0.03	98.99	1.09	3059	1670	
	S005	Furnas J	GG13	62.45	0.47	17.28	3.27	0.24	0.32	0.75	7.67	5.66	0.01	98.21	1.08	3051	1905	112
	S005	Furnas J	GG14	62.99	0.50	17.22	3.28	0.29	0.31	0.71	7.55	5.77	0.08	98.79	1.08	3066	1749	110
	S036	Furnas I	GG01	63.57	0.47	17.48	3.33	0.23	0.34	0.69	7.26	5.61	0.08	99.16	1.03	3647	2251	53
	S036	Furnas I	GG02	63.21	0.45	17.34	3.36	0.29	0.34	0.74	7.35	5.68	0.05	98.91	1.05	3267	2105	68
	S036	Furnas I	GG04	62.91	0.47	17.17	3.31	0.29	0.33	0.72	7.74	5.61	0.06	98.71	1.10	2822	1589	57
	S036	Furnas I	GG05	62.59	0.45	16.98	3.40	0.26	0.33	0.77	7.58	5.55	0.07	98.07	1.09	3254	2189	128
	S036	Furnas I	GG06	63.33	0.44	17.37	3.39	0.23	0.33	0.68	7.72	5.54	0.03	99.14	1.08	3268	2207	
	S036	Furnas I	GG07	62.93	0.41	17.38	3.32	0.30	0.32	0.75	7.76	5.65	0.07	98.98	1.09	3233	2245	
	S036	Furnas I	GG08	63.10	0.49	17.33	3.37	0.21	0.34	0.73	7.44	5.67	0.05	98.82	1.06	3162	2217	121

Table D12 continued

Source	Sample	Unit	Identifier	SiO_2	TiO_2	Al_2O_3	FeO_t	MnO	MgO	CaO	Na_2O	K_2O	P_2O_5	Total	Peralkalinity	Cl	F	S
University of Goettingen	S002	Furnas H	GG01	64.47	0.52	17.85	3.35	0.26	0.38	0.83	7.45	5.73	0.05	100.98	1.03	2949	1528	51
	S002	Furnas H	GG02	64.29	0.49	17.85	3.46	0.29	0.35	0.87	7.28	5.91	0.09	100.98	1.03	2897	1511	40
	S002	Furnas H	GG03	64.69	0.49	17.69	3.36	0.25	0.34	0.82	7.66	5.89	0.06	101.34	1.07	2989	1920	40
	S002	Furnas H	GG04	63.99	0.46	17.31	3.28	0.26	0.35	0.74	7.30	5.97	0.06	99.82	1.07	2719	1415	116
	S002	Furnas H	GG05	63.79	0.44	17.43	3.23	0.24	0.34	0.71	7.42	5.63	0.06	99.38	1.05	2830	1587	40
	S002	Furnas H	GG06	64.15	0.47	17.59	3.37	0.26	0.34	0.74	7.52	5.76	0.05	100.34	1.06	2727	1599	143
	S002	Furnas H	GG07	62.17	0.50	17.11	3.15	0.24	0.33	0.72	7.13	5.37	0.09	96.89	1.03	2675	2243	133
	S008	Furnas G	GG01	63.55	0.39	17.34	3.57	0.30	0.26	0.68	7.89	5.48	0.04	99.60	1.09	3378	2288	148
	S008	Furnas G	GG02	62.82	0.39	17.11	3.53	0.27	0.26	0.66	8.06	5.54	0.04	98.78	1.13	3513	2152	88
	S008	Furnas G	GG03	63.42	0.39	17.19	3.73	0.24	0.29	0.71	8.10	5.61	0.04	99.82	1.13	3455	2272	
	S008	Furnas G	GG04	63.37	0.42	17.32	3.57	0.29	0.26	0.79	7.88	5.49	0.02	99.50	1.09	3490	2072	101
	S008	Furnas G	GG05	62.31	0.41	17.07	3.45	0.29	0.24	0.73	7.86	5.44	0.05	97.93	1.10	3440	2027	126
	S008	Furnas G	GG06	62.92	0.41	17.28	3.49	0.31	0.28	0.73	8.43	5.41	0.08	99.44	1.14	3460	2168	167
	S008	Furnas G	GG07	63.29	0.40	17.37	3.71	0.23	0.32	0.71	7.78	5.58	0.01	99.51	1.08	3516	2086	128
	S008	Furnas G	GG08	63.28	0.44	17.27	3.49	0.31	0.25	0.73	7.98	5.46	0.05	99.35	1.10	3350	2255	62
	S008	Furnas G	GG09	62.93	0.42	17.12	3.64	0.34	0.28	0.67	7.79	5.39	0.05	98.72	1.09	3451	2174	165
	S008	Furnas G	GG10	62.52	0.33	16.98	3.61	0.27	0.29	0.70	7.86	5.40	0.06	98.11	1.11	3260	2153	85
	S042	Furnas F	GG01	61.79	0.40	16.72	3.47	0.30	0.31	0.75	7.90	5.51	0.03	97.26	1.13	3399	2745	82
	S042	Furnas F	GG02	62.54	0.37	17.04	3.44	0.25	0.31	0.66	7.90	5.52	0.04	98.16	1.11	3508	2244	87
	S042	Furnas F	GG03	60.55	0.42	16.60	3.30	0.24	0.31	0.59	7.58	5.33	0.00	95.01	1.10	3561	2508	53

Table D12 continued

Source	Sample	Unit	Identifier	SiO_2	TiO_2	Al_2O_3	FeO_t	MnO	MgO	CaO	Na_2O	K_2O	P_2O_5	Total	Peralkalinity	Cl	F	S
University of Goettingen	S042	Furnas F	GG04	62.28	0.50	17.06	3.36	0.33	0.31	0.71	7.65	5.43	0.09	97.80	1.08	3520	2151	62
	S042	Furnas F	GG05	61.14	0.47	16.73	3.31	0.30	0.33	0.72	7.34	5.48	0.05	95.97	1.08	3488	2194	66
	S042	Furnas F	GG06	61.72	0.42	16.92	3.21	0.30	0.30	0.70	7.40	5.36	0.06	96.48	1.06	3457	2549	68
	S042	Furnas F	GG07	62.22	0.43	17.06	3.38	0.27	0.31	0.66	7.92	5.48	0.03	97.85	1.11	3544	1988	95
	S042	Furnas F	GG08	61.76	0.49	16.94	3.33	0.20	0.36	0.75	7.57	5.39	0.04	96.91	1.08	3240	2001	
	S012b	Furnas E	GG01	63.48	0.40	17.24	3.46	0.24	0.31	0.68	7.95	5.49	0.07	99.41	1.10	3589	2426	127
	S012b	Furnas E	GG02	63.03	0.48	17.04	3.44	0.26	0.32	0.68	7.92	5.59	0.10	98.95	1.12	3565	2369	69
	S012b	Furnas E	GG03	63.18	0.41	17.30	3.50	0.24	0.31	0.67	7.96	5.50	0.04	99.21	1.10	3523	2339	
	S012b	Furnas E	GG04	63.41	0.44	17.31	3.50	0.28	0.33	0.68	7.98	5.48	0.09	99.59	1.10	3582	2383	80
	S012b	Furnas E	GG05	64.16	0.50	17.55	3.13	0.24	0.22	0.85	8.05	5.17	0.11	100.05	1.07			
	S012b	Furnas E	GG06	63.55	0.41	17.46	3.12	0.23	0.27	0.79	8.14	5.29	0.08	99.42	1.09	2183	1207	120
	S012b	Furnas E	GG07	62.68	0.45	17.02	3.43	0.25	0.32	0.68	7.97	5.49	0.00	98.39	1.12	3430	2311	160
	S012b	Furnas E	GG09	62.68	0.40	16.95	3.37	0.28	0.31	0.70	7.91	5.50	0.07	98.26	1.12	3537	2411	
	S012b	Furnas E	GG10	63.42	0.46	16.94	3.52	0.28	0.30	0.72	8.13	5.36	0.08	99.30	1.13	2888	1923	158
	S010	Furnas C	GG02	63.15	0.40	17.53	3.68	0.25	0.32	0.74	7.89	5.45	0.02	99.53	1.08	3290	1986	154
	S010	Furnas C	GG07	62.17	0.41	17.33	3.44	0.27	0.28	0.73	7.77	5.38	0.06	97.92	1.07	3349	2001	
	S010	Furnas C	GG08	63.44	0.40	17.60	3.57	0.25	0.26	0.70	7.69	5.44	0.01	99.45	1.05	2803	1754	67
	S010	Furnas C	GG10	63.41	0.40	17.30	3.56	0.32	0.26	0.77	7.99	5.62	0.03	99.75	1.11	3334	1948	145

APPENDIX E: DATA QUALITY

Table E1: Primary major element standard analyses for WD-XRF

Standard	No. analyses		SiO_2	TiO_2	Al_2O_3	Fe_2O_3	MnO	MgO	CaO	Na_2O	K_2O	P_2O_5	LOI	Total
WS-E	14	Expected	51.10	2.40	13.78	13.15	0.17	5.55	8.95	2.47	1.00	0.30	0.85	99.72
		Avg	51.11	2.41	13.88	13.17	0.17	5.58	8.98	2.43	0.99	0.30	0.85	99.87
		Stdev	0.14	0.01	0.05	0.02	0.00	0.03	0.03	0.02	0.01	0.01	0.00	0.26
OUG94	14	Expected	69.95	0.31	14.66	3.05	0.08	1.04	1.34	4.60	2.96	0.17	1.97	100.12
		Avg	69.91	0.32	14.63	3.05	0.08	1.04	1.37	4.60	2.96	0.17	1.97	100.10
		Stdev	0.07	0.00	0.04	0.01	0.00	0.01	0.00	0.03	0.02	0.00	0.00	0.11
GSP-2	2	Expected	66.60	0.66	14.90	4.90	0.03	0.96	2.10	2.78	5.38	0.29		98.60
		Avg	66.17	0.66	14.97	4.91	0.04	1.01	2.02	3.62	5.43	0.33		99.15
		Stdev	0.08	0.00	0.02	0.00	0.00	0.01	0.00	0.04	0.00	0.00		0.16
W2a	2	Expected	52.68	1.06	15.45	10.83	0.17	6.37	10.86	2.20	0.63	0.14		100.38
		Avg	52.01	1.04	15.29	10.83	0.16	6.29	10.63	2.57	0.65	0.15		99.60
		Stdev	0.06	0.00	0.11	0.00	0.00	0.01	0.01	0.01	0.01	0.00		0.21
AC-E	2	Expected	70.35	0.11	14.70	2.53	0.06	0.03	0.34	6.54	4.49	0.01		99.16
		Avg	69.93	0.10	14.83	2.46	0.06	0.04	0.37	6.78	4.47	0.04		99.06
		Stdev	0.01	0.00	0.08	0.00	0.00	0.01	0.01	0.04	0.00	0.00		0.14

Table E2: Primary trace element standard analyses for WD-XRF

Standard:	No. analyses:		Rb	Sr	Y	Zr	Nb	Ba	Sc	V	Cr	Co	Ni	Cu	Zn	Ga	La	Ce	S	TiO_2 wt. %	Fe_2O_3 wt. %
BHVO-1	12	Expected	11.0	403.0	27.6	179.0	19.0	139.0	31.8	317.0	289.0	45.0	121.0	136.0	105.0	21.0			102.0	2.71	12.23
		Avg	9.4	403.7	27.7	178.0	18.2	143.7	33.5	317.6	290.5	43.0	120.8	136.6	104.7	21.5			88.0	2.73	12.34
		Stdev	0.6	2.4	0.5	1.4	0.5	4.9	1.7	5.4	1.7	3.8	1.9	1.8	2.7	1.2			20.7	0.02	0.06
QLO-1	12	Expected	74.0	336.0	24.0	185.0	10.3	1370.0	8.9	54.0	3.2	7.2	5.8	29.0	61.0	17.0			30.0	0.6	4.4
		Avg	72.5	331.5	24.0	188.8	10.1	1388.1	8.2	48.5	4.8	7.5	4.6	26.3	59.8	15.8			51.6	0.7	4.0
		Stdev	0.8	2.2	0.8	1.3	0.5	18.1	1.2	3.0	1.6	1.4	1.0	1.3	1.5	0.7			3.5	0.0	0.0
DNC-1	12	Expected	4.5	145.0	18.0	41.0	3.0	114.0	31.0	148.0	285.0	54.7	247.0	96.0	66.0	15.0				0.5	9.9
		Avg	3.9	146.3	18.2	38.8	2.0	107.2	30.7	147.2	281.1	55.2	241.8	86.8	64.3	14.1				0.5	9.8
		Stdev	0.4	1.0	0.4	0.5	0.5	4.1	1.8	2.5	5.2	2.4	1.7	1.2	1.0	0.9				0.0	0.0
W-2	12	Expected	20.0	194.0	24.0	94.0	7.9	182.0	35.0	262.0	93.0	44.0	70.0	103.0	77.0	20.0				1.1	10.7
		Avg	20.4	198.8	22.5	94.1	7.3	180.8	36.1	266.2	94.2	41.7	68.4	103.0	77.0	18.2				1.1	10.5
		Stdev	0.5	1.6	0.6	0.8	0.7	6.8	1.9	2.9	2.1	2.9	2.0	1.1	1.0	1.0				0.0	0.0
AGV-2	6	Expected	69.0	658.0	20.0	230.0	15.0	1140.0	13.0	120.0	17.0	16.0	19.0	53.0	86.0	20.0				1.1	6.7
		Avg	69.2	657.8	19.7	239.7	13.0	1141.4	15.5	121.7	17.8	15.5	20.7	51.7	87.7	18.2				1.1	6.4
		Stdev	0.4	2.0	0.4	2.0	0.5	17.1	2.2	2.4	0.5	0.8	1.2	1.4	1.0	0.8				0.0	0.0

Table E2 continued

Standard:	No. analyses:		Rb	Sr	Y	Zr	Nb	Ba	Sc	V	Cr	Co	Ni	Cu	Zn	Ga	La	Ce	S	TiO_2 wt. %	Fe_2O_3 wt. %
BCR-2	6	Expected	48.0	346.0	37.0	188.0	-	683.0	33.0	416.0	18.0	37.0	-	19.0	127.0	23.0			-	2.3	13.8
		Avg	49.4	351.6	37.3	193.3		708.6	34.8	426.4	19.5	33.1		21.4	127.5	21.3				2.4	13.6
		Stdev	0.8	1.9	0.5	0.9		13.7	1.6	9.7	0.9	1.7		1.7	1.8	1.3				0.0	0.1
SDO-1	2	Expected	126	75.1	40.6	165	36.6	397	13.2	160	66.4		99.5	60.2	64.1		38.5	79.3			
		Avg	129.5	71.5	38.5	161.5	15.0	391.0	12.5	174.5	48.5		89.0	61.5	58.0		46.0	84.50			
		Stdev	0.7	0.7	0.7	0.7	0.0	2.8	0.7	0.7	2.1		1.4	0.7	0.0		4.2	0.71			
Mess-2	2	Expected	n/a	125	n/a	n/a	n/a	n/a	n/a	252	106		49.3	39.3	172		n/a	n/a			
		Avg	141.5	130.0	25.0	139.5	16.5	1026.5	14.0	246.5	92.0		47.0	43.5	144.5		48.0	108.50			
		Stdev	0.7	1.4	0.0	0.7	0.7	2.1	0.0	2.1	1.4		0.0	0.7	2.1		4.2	2.12			
STSD-2	2	Expected	104	400	37	185	20	540	16	101	116		53	47	246		59	93			
		Avg	99.0	410.0	35.5	181.0	20.5	523.0	14.0	104.5	100.5		57.0	45.0	236.0		56.5	120.00			
		Stdev	0.0	0.0	0.7	0.0	0.7	2.8	1.4	2.1	2.1		0.0	1.4	1.4		0.7	1.41			
W2a	2	Expected	21	190	23	100	7.9	170	36	260	92		70	110	80		10	23			
		Avg	22.0	188.5	21.0	92.5	10.0	134.0	33.0	266.5	63.5		66.5	116.5	73.5		6.5	43.50			
		Stdev	0.0	0.7	0.0	0.7	0.0	1.4	0.0	0.7	0.7		0.7	2.1	0.7		4.9	4.95			

Table E3: Primary trace element standard analyses for ED-XRF

Sample	Expected values				Measured values			
	Rb	Sr	Zr	Nb	Rb	Sr	Zr	Nb
ace-1	62		175	90	152		780	110
agv-1	26	472	46	9	67	662	225	15
an-g		53	2			76	15	
bcr-1	19	233	38	8	47	330	190	14
t-1	19	980	54	87	47		265	100
agv-1	3	278	35	14	11	403	179	19
g-2		75	3			108	22	
glo-1	19	951	54	85	47		250	98
ac-e		103	7			145	41	
ma-n	28	278	23	5	73	400	125	8
g-1	88	185	44	16	215	249	201	20
g-2	69	347	65	10	170	478	300	13
ga	70	218	28	10	175	310	150	12
gh	160	6	35	71	390	10	150	85
gs-n	77	422	46	18	185	570	235	21
gsp-1	105	171	111	21	254	234	530	26
jg-1	73	133	22	8	181	184	108	13
ma-n	1546	68	4	153		84	27	173
mrg-1	3	188	22	20	9	266	108	20
nim-d		2				3		
nim-g	131	7	58	41	325	10	300	53
nim-n		183	2			260	14	
nim-p		23	3			32	15	
nim-s	214	45	3		530	62	20	
ph-8	31	39	67	29	67	76	320	
qlo-1	28	239	38	7	74	336	185	10
rgm-1	62	75	47	6	149	108	219	9
stm-1	48	516	270	210	118	700	1210	268
sy-1	29	141	667	81		286	2978	
sy-2	86	193	58	18	217	271	280	
sy-3	80	225	66	178	206	302	320	
t-1	12	272	32	10	34	408	140	12
w-1	9	131	19	6	21	187	100	8
w-2	8	133	19	5	20	194	94	8

Table E4: Secondary trace element analyses for ED-XRF

Sample	Expected values				Measured values				Percentage difference			
	Rb	Sr	Zr	Nb	Rb	Sr	Zr	Nb	Rb	Sr	Zr	Nb
S053	146	359	815	117	144	350	782	118	1	2	4	1
S035	267	bdl	1733	238	254	bdl	1725	248	5		0	4
S037	205	bdl	1275	233	192	bdl	1208	237	6		5	2
S008	221	bdl	1424	256	209	bdl	1330	259	5		7	1
S023	173	bdl	1021	187	166	bdl	964	184	4		6	1
T005	133	bdl	1043	176	124	bdl	979	174	6		6	1
T002	94	24	714	121	86	23	668	120	8	5	6	1
T010	94	18	674	121	88	16	632	117	7	11	6	3
T050	45	142	971	173	44	135	912	169	2	5	6	3
T014	19	580	243	53	18	528	219	52	6	9	10	3
T037	73	16	491	88	66	12	458	86	9	23	7	2
T036	102	bdl	693	118	93	bdl	642	114	9		7	3
T035	93	12	664	113	84	10	614	110	10	16	8	3
T035	102	bdl	686	118	94	bdl	642	116	8		6	2
T031	89	36	678	115	85	32	643	112	4	11	5	3
T013	192	bdl	2258	354	177	bdl	2111	350	8		7	1
T026	93	26	706	119	87	22	664	118	7	14	6	1
T025	100	20	772	129	90	18	728	126	10	11	6	3
T028	94	23	701	118	88	20	652	115	6	14	7	2
T029	99	22	762	127	94	19	715	126	5	12	6	0
T024	135	bdl	1073	180	130	bdl	1007	175	4		6	3
T011	174	bdl	1550	255	161	bdl	1453	248	8		6	3
T003	89	36	666	113	83	33	623	111	7	9	6	1

Table E5: Repeat analyses for ED-XRF

Sample:	Analysis no.	Nb	Zr	Rb	Sr
S092	1	247	318	97	
	2	245	312	95	
	3	243	312	92	
	4	242	313	94	
	5	239	311	95	
	6	242	311	95	
	7	246	310	95	
	8	242	309	95	
	9	240	309	95	
	10	241	313	95	
	11	241	311	94	
	12	242	310	94	
	13	243	311	94	
	14	245	313	95	
	15	246	311	95	
	16	243	311	93	
	17	246	313	95	
	18	245	312	95	
	19	244	313	95	
	20	241	311	94	
	Avg	243	312	95	
	Stdev	2	2	1	
STM-1	1	209	269	48	514
	2	211	272	48	513
	3	211	273	49	514
	4	212	269	49	519
	5	215	272	47	518
	6	212	271	47	520
	7	208	273	48	526
	8	212	273	49	516
	9	209	270	49	518
	10	212	269	48	515
	11	211	271	47	518
	12	209	273	48	517
	13	209	270	47	510
	14	212	273	49	517
	15	211	272	48	517
	16	212	273	48	521
	17	212	273	48	521
	18	209	271	48	518
	19	210	272	49	520
	20	211	271	47	518
	Avg	211	272	48	517
	Stdev	2	1	1	3

Table E6: Primary standard analyses for ICP-AES

Standard:	No. analyses:		Expected	1	2	Avg	Stdev
SO-18	2	SiO_2	58.47	58.33	58.55	58.44	0.16
		TiO_2	0.69	0.69	0.69	0.69	0.00
		Al_2O_3	14.23	14.11	14.07	14.09	0.03
		Fe_2O_3	7.67	7.53	7.45	7.49	0.06
		MnO	0.39	0.39	0.39	0.39	0.00
		MgO	3.35	3.36	3.32	3.34	0.03
		CaO	6.42	6.31	6.32	6.32	0.01
		Na_2O	3.71	3.62	3.6	3.61	0.01
		K_2O	2.17	2.12	2.1	2.11	0.01
		P_2O_5	0.83	0.8	0.78	0.79	0.01
		Cr_2O_3	0.55	0.541	0.539	0.54	0.00
		LOI		1.9	1.9	1.90	0.00
		Total	98.48	99.70	99.71	99.71	0.32
		Ni	44	51	47	49.0	2.8
		Sc	25	24	23	23.5	0.7

Table E7: Primary standard analyses for ICP-MS

Standard	AGV-1		BCR-2		BHVO-1			BHVO-2			BIR-1		RGM-1			
Element	Exp.	Mes.	Exp.	Mes.	Exp.	Mes.	Mes.	Exp.	Mes.	Mes.	Exp.	Mes.	Exp.	Mes.	Mes.	Mes.
Li	12.0	10.8	9.0	9.7	4.6	4.9	5.2	5.0	4.8	4.9	3.6	3.2	57.0	65.6	66.7	67.6
Sc	12.0	12.5	33.0	34.7	31.8	34.5	34.4	32.0	34.5	33.7	44.0	44.2	4.4	5.3	5.1	5.3
Ti	6295.0	6427.0	13548.0	14195.3	16246.0	17322.3	17543.7	16366.0	17367.1	16837.7	5755.0	5954.2	1619.0	1727.1	1663.5	1723.6
V	120.0	120.2	416.0	428.5	317.0	326.2	332.4	11.0	330.0	323.6	310.0	329.1	13.0	12.3	11.9	12.1
Cr	10.0	9.0	18.0	16.9		297.5	297.7	280.0	301.5	293.8	370.0	405.7	3.7	2.1	2.0	2.0
Co	15.0	15.8	37.0	39.5	45.0	47.3	48.0	45.0	47.4	45.8	52.0	55.2	2.0	2.3	2.2	2.2
Ni	16.0	16.0		13.2		121.3	120.6	119.0	122.9	119.2	170.0	172.5		1.8	1.7	1.7
Cu	60.0	60.1	19.0	21.5	136.0	144.3	143.1	127.0	135.0	131.2		125.7	12.0	14.1	13.6	13.9
Zn	88.0	88.8	127.0	136.6	105.0	108.4	109.5	103.0	106.9	104.7	70.0	71.8	32.0	36.3	34.6	34.9
Rb	67.0	65.4	48.0	47.7	11.0	9.6	10.2	9.8	9.8	9.8		0.2	150.0	152.3	154.1	156.1
Sr	660.0	645.9	346.0	342.8	403.0	397.4	422.2	389.0	405.2	405.4	110.0	108.6	110.0	108.6	109.2	108.9
Y	20.0	19.9	37.0	37.4	28.0	27.3	29.2	26.0	27.5	27.7	16.0	16.0	25.0	25.0	25.3	25.3
Zr	227.0	238.5	188.0	199.5	179.0	181.5	192.6	172.0	183.0	184.3	18.0	15.1	220.0	249.0	249.5	249.6
Nb	15.0	14.3		13.0	19.0	19.0	20.3	18.0	19.2	19.3	0.6	0.5	8.9	9.2	9.3	9.3
Mo	2.7	2.0	248.0	255.3		1.0	1.1		3.2	3.3		0.1	2.3	2.5	2.6	2.5
Sn	4.2	4.4		2.3		2.0	2.1	1.9	1.8	1.8		0.7	4.1	4.4	4.4	4.4
Sb	4.3	4.4		0.4		0.2	0.2		0.1	0.1	0.6	0.6	1.3	1.4	1.3	1.3
Cs	1.3	1.3	1.1	1.2	0.1	0.1	0.1		0.1	0.1		0.0	9.6	10.8	11.0	11.2
Ba	1230.0	1158.2	683.0	652.4	139.0	134.3	144.8	130.0	130.9	133.5	7.0	6.3	810.0	806.6	841.9	860.5
La	38.0	37.7	25.0	25.2	16.0	16.0	16.2	15.0	15.7	15.6	0.6	0.6	24.0	23.7	23.6	24.5
Ce	67.0	66.4	53.0	52.1	39.0	37.6	40.1	38.0	37.5	38.4	1.9	1.9	47.0	45.6	47.0	47.6
Pr	7.6	8.4	6.8	6.8	18.0	5.4	5.7		5.4	5.4		0.4		5.3	5.4	5.5
Nd	33.0	31.1	28.0	28.4	25.0	24.9	25.5	25.0	24.7	24.4	2.5	2.4	19.0	19.2	19.2	19.8
Sm	5.9	5.7	6.7	6.6	6.2	6.2	6.4	6.2	6.2	6.1	1.1	1.1	4.3	4.0	4.0	4.0
Eu	1.6	1.6	2.0	1.9	2.1	2.0	2.1		2.0	2.0	0.6	0.5	0.7	0.6	0.6	0.7
Gd	5.0	4.8	6.8	6.8	6.4	6.4	6.7	6.3	6.3	6.4	1.8	1.8	3.7	3.8	3.8	3.9
Tb	0.7	0.7	1.1	1.1	1.0	1.0	1.0	0.9	1.0	1.0		0.4		0.6	0.6	0.6
Dy	3.6	3.4		6.2	5.2	5.3	5.5		5.2	5.3		2.5	4.1	3.6	3.6	3.7
Ho		0.7	1.3	1.3	1.0	1.0	1.0	1.0	1.0	1.0		0.6		0.8	0.8	0.8
Er	1.7	1.8		3.7	2.4	2.6	2.7		2.6	2.6		1.7		2.4	2.4	2.4
Yb	1.7	1.6	3.5	3.3	2.0	2.0	2.1	2.0	2.0	2.0	1.7	1.6		2.5	2.5	2.5
Lu	0.3	0.2	0.5	0.5	0.3	0.3	0.3	0.3	0.3	0.3	0.3	0.2	0.4	0.4	0.4	0.4
Hf	5.1	4.9	4.8	4.8	4.4	4.3	4.4	4.1	4.3	4.2	0.6	0.5		5.9	5.9	5.9
Ta	0.9	0.9		0.8	1.2	1.2	1.3	1.4	1.2	1.2		0.0	1.0	1.0	1.0	1.0
Pb	36.0	35.6	11.0	10.4	2.6	2.2	2.3		1.9	1.9	3.0	3.3	24.0	24.5	24.6	25.3
Th	6.5	6.5	6.2	6.2	1.1	1.3	1.4	1.2	1.3	1.3		0.0	15.0	16.9	17.1	16.1
U	1.9	1.9	1.7	1.7		0.4	0.4		0.4	0.4		0.0	5.8	5.8	5.8	5.9

Table E7 continued

Standard	WS-E		JB2		JB3		SO-18			DS9		OREAS45EA	
Element	Exp.	Mes.	Exp.	Mes.	Exp.	Mes.	Exp.	Avg.	Stdev	Exp.	Mes.	Exp.	Mes.
Li	13.6	13.9	7.8	8.8	7.2	8.5							
Sc	28.0	28.9	53.5	56.8	33.8	43.0							
Ti	14388.0	14481.2	7134.0	7406.6	8633.0	8951.9							
V	340.0	330.9	575.0	599.5	372.0	398.1	200	197.8	6.8				
Cr	99.0	94.8	28.1	27.7	58.1	61.6							
Co	44.0	45.5	38.0	39.2	34.3	37.4	26.2	26.5	0.7				
Ni	55.0	146.8	16.6	15.0	36.2	40.6				40.3	39.6	357	351.3
Cu	65.0	66.4	225.0	231.3	194.0	195.4				108	114.7	709	640.4
Zn	117.0	116.9	108.0	109.7	100.0	106.9				317	309	30.6	29
Rb	25.0	25.4	7.4	6.5	15.1	15.7	28.7	27.8	0.9				
Sr	410.0	398.1	178.0	184.0	4.3	4.3	407.4	413.0	12.3				
Y	30.4	31.5	24.9	25.1	26.9	29.8	31	30.4	0.4				
Zr	195.0	208.9	51.2	51.2	97.8	99.4	280	289.7	4.0				
Nb	18.0	18.2	1.6	0.5	2.5	2.0	21.3	19.0	0.4				
Mo	3.7	3.1	1.1	1.9	1.1	1.1				12.84	12.2	1.78	1.6
Sn	18.0	30.5	1.0	0.6	0.9	1.0	15	13.8	1.1				
Sb	0.1	0.1	0.3	0.2	0.1	0.1				4.94	5.2	0.64	0.4
Cs	0.5	0.5	0.9	0.9	0.9	1.1	7.1	6.8	0.1				
Ba	338.0	326.6	222.0	220.2	245.0	241.6	514	498.4	7.1				
La	27.0	27.0	2.4	2.3	8.8	9.3	12.3	12.6	0.3				
Ce	61.0	57.7	6.8	6.6	21.5	22.5	27.1	27.4	0.6				
Pr	7.8	7.9	1.0	1.2	3.1	3.4	3.45	3.3	0.1				
Nd	33.0	32.8	6.6	6.4	15.6	16.7	14	13.3	0.7				
Sm	8.8	8.6	2.3	2.3	4.3	4.6	3	2.8	0.2				
Eu	2.3	2.1	0.9	0.8	1.3	1.4	0.89	0.9	0.0				
Gd	7.2	7.1	3.3	3.2	4.7	5.0	2.93	3.0	0.2				
Tb	1.1	1.1	0.6	0.6	0.7	0.8	0.53	0.5	0.0				
Dy	6.0	5.9	3.7	3.9	4.5	4.8	3	3.3	0.2				
Ho	1.2	1.1	0.8	0.9	0.8	1.0	0.62	0.6	0.0				
Er	3.0	3.0	2.6	2.6	2.5	2.9	1.84	1.8	0.1				
Yb	2.5	2.4	2.6	2.5	2.6	2.7	1.79	1.8	0.1				
Lu	0.4	0.4	0.4	0.4	0.4	0.4	0.27	0.3	0.0				
Hf	5.3	5.0	1.5	1.4	2.7	2.6	9.8	9.6	0.7				
Ta	1.2	1.1	0.1	0.0	0.2	0.1	7.4	6.9	0.4				
Pb	13.8	13.1	5.4	5.2	5.6	5.1				126	125.3	14.3	13.8
Th	3.0	3.1	0.4	0.3	1.3	1.5	9.9	10.0	0.5				
U	0.7	0.6	0.2	0.2	0.5	0.5	16.4	15.9	0.3				

Table E7 continued

Standard:		SO-18		DS9		OREAS45EA	
Element	Exp.	Avg.	Stdev	Exp.	Mes.	Exp.	Mes.
Be		1.7	0.6				
Ga	17.6	17.1	1.0				
W	14.8	13.8	0.5				
Tm	0.27	0.3	0.0				
As				25.5	25.4	11.4	10.1
Cd				1.4	2.3	0.03	<0.1
Bi				6.32	6	0.23	0.2
Ag				1.83	1.7	0.311	0.3
Au				118	109	53	60.5
Hg				0.2	0.2	0.34	0.02
Tl				5.3	5	0.072	<0.1
Se				5.2	4.7	2.09	0.9

Table E8: Calibration standards for electron microprobe analyses

Standard:	No. analyses:		SiO_2	TiO_2	Cr_2O_3	Al_2O_3	NiO	FeO	MnO	MgO	CaO	Na_2O	K_2O	ZnO	V_2O_3	P_2O_5	BaO	SrO	F	Cl	S	Total
Albite	46	Expected	68.67			19.50						11.74	0.11									100.02
		Average	68.31			19.53						11.72	0.13									99.68
		Stdev	0.30			0.12						0.11	0.02									0.38
Sanidine	49	Expected	64.70			18.60						1.65	14.24									99.19
		Average	64.36			18.70						1.66	14.17									98.89
		Stdev	0.42			0.15						0.05	0.18									0.56
Anorthite	47	Expected	44.00			36.03					19.09	0.53	0.03									99.68
		Average	43.82			35.41					19.12	0.54	0.01									98.90
		Stdev	0.34			0.27					0.28	0.03	0.01									0.72
Wollastonite	27	Expected	51.51					0.35			47.74											99.60
		Average	51.87					0.36			47.73											99.96
		Stdev	0.27					0.03			0.36											0.45
TiO_2	31	Expected		100.00																		100.00
		Average		99.95																		99.95
		Stdev		0.75																		0.75
Rhodonite	20	Expected	46.27					1.02	43.49	1.63	7.28											99.69
		Average	47.70					0.97	42.24	1.87	7.23											100.01
		Stdev	0.27					0.04	0.40	0.04	0.10											3.28
Haematite	58	Expected						89.98														89.98
		Average						89.78														89.78
		Stdev						0.47														0.47
Olivine	29	Expected	40.81					9.55		49.42												99.78
		Average	40.69					9.38		49.08												99.15
		Stdev	0.27					0.11		0.22												0.42
Apatite	23	Expected									55.6					42.23			3.77			101.60
		Average									54.22					40.07			4.59			98.88
		Stdev									0.52					0.55			0.17			1.98
NaCl	21	Expected										39.34								60.66		100.00
		Average										56.54								60.51		117.05
		Stdev										0.40								0.47		0.59

Table E8 continued

Standard:	No. analyses:		SiO_2	TiO_2	Cr_2O_3	Al_2O_3	NiO	FeO	MnO	MgO	CaO	Na_2O	K_2O	ZnO	V_2O_3	P_2O_5	BaO	SrO	F	Cl	S	Total
ZnS	20	Expected																			32.90	32.90
		Average																			30.41	30.41
		Stdev																			1.17	1.17
Al_2O_3	13	Expected				100.00																100.00
		Average				101.35																101.35
		Stdev				0.89																0.89
Celsian	16	Expected	33.77			27.46											39.25					100.48
		Average	33.74			28.71											38.93					101.37
		Stdev	0.20			0.18											0.54					0.65
$SrTiO_3$	11	Expected																56.46				56.46
		Average																55.96				55.96
		Stdev																0.56				0.56
Cr_2O_3	11	Expected			100.00																	100.00
		Average			99.77																	99.77
		Stdev			0.50																	0.50
NiO	4	Expected					100.00															100.00
		Average					100.47															100.47
		Stdev					0.57															0.57
MgO	6	Expected								100.00												100.00
		Average								99.56												99.56
		Stdev								0.95												0.95
V	4	Expected													100.00							100.00
		Average													148.36							148.36
		Stdev													0.43							0.43
Gahnite	4	Expected				55.32		1.97	0.34					42.5								100.13
		Average				55.41		1.91	0.35					42.72								100.38
		Stdev				0.43		0.04	0.02					0.56								0.95
Celestine	3	Expected																56.41				56.41
		Average																56.49				56.49
		Stdev																0.24				0.24

APPENDIX F: THERMOBAROMETRY RESULTS

Table F1: Results of alkali feldspar-melt thermometry and hygrometry for Terceira lithologies

Unit	Liquid composition											Feldspar composition							Equilibrium	T	H_2O
	Sample	SiO_2	TiO_2	Al_2O_3	FeO_t	MnO	MgO	CaO	Na_2O	K_2O	P_2O_5	Sample	SiO_2	Al_2O_3	FeO_t	CaO	Na_2O	K_2O	ΔKd_{Or-Ab}	(°C)	(wt. %)
LAI	TER53-2	65.28	0.62	15.76	4.61	0.21	0.39	0.76	7.20	5.07	0.10	19 / 1 .	66.81	18.93	0.49	0.29	7.89	5.52	-0.02	874	4.51
LAI	TER53-2	65.28	0.62	15.76	4.61	0.21	0.39	0.76	7.20	5.07	0.10	20 / 1 .	66.93	19.08	0.36	0.20	7.77	5.62	0.00	874	4.89
LAI	TER53-2	65.28	0.62	15.76	4.61	0.21	0.39	0.76	7.20	5.07	0.10	21 / 1 .	67.14	18.84	0.38	0.14	7.69	5.76	0.02	872	4.75
LAI	TER53-2	65.28	0.62	15.76	4.61	0.21	0.39	0.76	7.20	5.07	0.10	22 / 1 .	66.88	19.10	0.33	0.18	7.72	5.75	0.00	872	5.00
LAI	TER53-2	65.28	0.62	15.76	4.61	0.21	0.39	0.76	7.20	5.07	0.10	23 / 1 .	67.07	18.99	0.44	0.13	7.76	5.60	0.03	874	4.47
LAI	TER53-2	65.28	0.62	15.76	4.61	0.21	0.39	0.76	7.20	5.07	0.10	24 / 1 .	66.82	19.03	0.36	0.21	7.77	5.80	0.00	872	4.91
LAI	TER53-2	65.28	0.62	15.76	4.61	0.21	0.39	0.76	7.20	5.07	0.10	27 / 1 .	66.94	19.17	0.31	0.27	7.88	5.38	-0.01	875	4.98
LAI	TER53-2	65.28	0.62	15.76	4.61	0.21	0.39	0.76	7.20	5.07	0.10	28 / 1 .	66.84	19.33	0.37	0.30	7.67	5.42	-0.03	874	4.84
LAI	TER53-2	65.28	0.62	15.76	4.61	0.21	0.39	0.76	7.20	5.07	0.10	29 / 1 .	66.86	19.08	0.32	0.28	7.82	5.59	-0.02	874	5.01
LAI	TER53-2	65.28	0.62	15.76	4.61	0.21	0.39	0.76	7.20	5.07	0.10	30 / 1 .	65.55	20.87	0.35	0.21	7.23	5.75	-0.02	869	5.03
LAI	TER53-2	65.28	0.62	15.76	4.61	0.21	0.39	0.76	7.20	5.07	0.10	31 / 1 .	66.65	19.29	0.30	0.34	7.95	5.42	0.67	875	4.97
LAI	TER53-2	65.28	0.62	15.76	4.61	0.21	0.39	0.76	7.20	5.07	0.10	32 / 1 .	66.81	19.22	0.30	0.29	7.87	5.45	-0.02	875	5.01
LAI	TER53-2	65.28	0.62	15.76	4.61	0.21	0.39	0.76	7.20	5.07	0.10	33 / 1 .	66.94	18.98	0.37	0.17	7.78	5.71	0.01	873	4.82
LAI	TER53-2	65.28	0.62	15.76	4.61	0.21	0.39	0.76	7.20	5.07	0.10	34 / 1 .	66.97	19.08	0.35	0.23	7.74	5.58	0.00	873	4.91
LAI	TER53-2	65.28	0.62	15.76	4.61	0.21	0.39	0.76	7.20	5.07	0.10	1 / 1 .	66.84	19.22	0.33	0.21	7.80	5.56	0.00	874	4.98
LAI	TER53-2	65.28	0.62	15.76	4.61	0.21	0.39	0.76	7.20	5.07	0.10	2 / 1 .	66.87	19.01	0.38	0.15	7.83	5.71	0.02	873	4.75
LAI	TER53-2	65.28	0.62	15.76	4.61	0.21	0.39	0.76	7.20	5.07	0.10	3 / 1 .	67.02	18.95	0.42	0.13	7.63	5.81	0.01	872	4.64
LAI	TER53-2	65.28	0.62	15.76	4.61	0.21	0.39	0.76	7.20	5.07	0.10	4 / 1 .	66.94	18.92	0.38	0.16	7.84	5.70	0.02	874	4.77
LAI	TER53-2	65.28	0.62	15.76	4.61	0.21	0.39	0.76	7.20	5.07	0.10	5 / 1 .	66.88	18.87	0.37	0.15	7.76	5.92	0.01	872	4.84
LAI	TER53-2	65.28	0.62	15.76	4.61	0.21	0.39	0.76	7.20	5.07	0.10	6 / 1 .	66.88	19.03	0.39	0.19	7.74	5.72	0.67	873	4.81
LAI	TER53-2	65.28	0.62	15.76	4.61	0.21	0.39	0.76	7.20	5.07	0.10	7 / 1 .	66.94	18.79	0.44	0.17	7.90	5.74	0.01	874	4.60
LAI	TER53-2	65.28	0.62	15.76	4.61	0.21	0.39	0.76	7.20	5.07	0.10	8 / 1 .	66.76	19.25	0.29	0.31	7.80	5.55	-0.03	874	5.07
LAI	TER53-2	65.28	0.62	15.76	4.61	0.21	0.39	0.76	7.20	5.07	0.10	9 / 1 .	66.86	19.01	0.32	0.22	7.89	5.66	0.00	874	5.02
LAI	TER53-2	65.28	0.62	15.76	4.61	0.21	0.39	0.76	7.20	5.07	0.10	10 / 1 .	66.80	19.14	0.31	0.29	7.93	5.49	-0.02	875	4.97
LAI	TER53-2	65.28	0.62	15.76	4.61	0.21	0.39	0.76	7.20	5.07	0.10	11 / 1 .	66.95	18.96	0.34	0.18	7.78	5.74	0.01	873	4.96
LAI	TER53-2	65.28	0.62	15.76	4.61	0.21	0.39	0.76	7.20	5.07	0.10	12 / 1 .	66.81	19.11	0.33	0.22	7.83	5.67	0.00	873	5.00
LAI	TER53-2	65.28	0.62	15.76	4.61	0.21	0.39	0.76	7.20	5.07	0.10	13 / 1 .	66.62	19.25	0.30	0.46	8.01	5.27	-0.07	876	4.81
LAI	TER53-2	65.28	0.62	15.76	4.61	0.21	0.39	0.76	7.20	5.07	0.10	14 / 1 .	66.80	19.02	0.33	0.22	7.89	5.71	0.00	873	5.00
LAI	TER53-2	65.28	0.62	15.76	4.61	0.21	0.39	0.76	7.20	5.07	0.10	15 / 1 .	67.01	18.97	0.34	0.21	7.72	5.71	0.00	872	4.99
LAI	TER53-2	65.28	0.62	15.76	4.61	0.21	0.39	0.76	7.20	5.07	0.10	16 / 1 .	67.04	18.73	0.49	0.17	7.66	5.88	0.00	871	4.50
LAI	TER53-2	65.28	0.62	15.76	4.61	0.21	0.39	0.76	7.20	5.07	0.10	17 / 1 .	67.05	18.68	0.42	0.14	7.68	5.98	0.01	871	4.68
LAI	TER53-2	65.28	0.62	15.76	4.61	0.21	0.39	0.76	7.20	5.07	0.10	18 / 1 .	66.42	19.71	0.29	0.91	8.19	4.40	-0.28	881	4.16
LAI	TER53-2	65.28	0.62	15.76	4.61	0.21	0.39	0.76	7.20	5.07	0.10	19 / 1 .	66.79	19.10	0.29	0.54	7.97	5.24	-0.09	875	4.78
LAI	TER53-2	65.28	0.62	15.76	4.61	0.21	0.39	0.76	7.20	5.07	0.10	20 / 1 .	65.72	20.32	0.31	1.25	8.29	4.03	-0.52	882	3.73
LAI	TER53-2	65.28	0.62	15.76	4.61	0.21	0.39	0.76	7.20	5.07	0.10	21 / 1 .	66.06	20.09	0.29	1.23	8.32	3.92	-0.54	883	3.72

Table F1 continued

Unit		Liquid composition											Feldspar composition						Equilibrium	T	H_2O
	Sample	SiO_2	TiO_2	Al_2O_3	FeO_t	MnO	MgO	CaO	Na_2O	K_2O	P_2O_5	Sample	SiO_2	Al_2O_3	FeO_t	CaO	Na_2O	K_2O	ΔKd_{Or-Ab}	(°C)	(wt. %)
LAI	TER53-2	65.28	0.62	15.76	4.61	0.21	0.39	0.76	7.20	5.07	0.10	22 / 1 .	66.79	19.16	0.29	0.47	7.89	5.32	-0.07	875	4.87
LAI	TER53-2	65.28	0.62	15.76	4.61	0.21	0.39	0.76	7.20	5.07	0.10	24 / 1 .	66.36	19.51	0.28	0.86	8.18	4.74	-0.23	878	4.34
LAI	TER53-2	65.28	0.62	15.76	4.61	0.21	0.39	0.76	7.20	5.07	0.10	25 / 1 .	66.79	18.99	0.30	0.40	7.85	5.61	-0.05	873	4.98
LAI	TER53-2	65.28	0.62	15.76	4.61	0.21	0.39	0.76	7.20	5.07	0.10	26 / 1 .	66.95	18.95	0.30	0.42	7.83	5.50	-0.06	873	4.95
LAI	TER53-2	65.28	0.62	15.76	4.61	0.21	0.39	0.76	7.20	5.07	0.10	27 / 1 .	66.91	19.05	0.26	0.41	7.94	5.38	-0.05	875	5.00
LAI	TER53-2	65.28	0.62	15.76	4.61	0.21	0.39	0.76	7.20	5.07	0.10	28 / 1 .	66.78	18.96	0.29	0.43	7.95	5.52	-0.06	874	4.95
LAI	TER53-2	65.28	0.62	15.76	4.61	0.21	0.39	0.76	7.20	5.07	0.10	29 / 1 .	67.26	18.64	0.34	0.25	7.75	5.71	-0.01	872	5.00
LAI	TER53-2	65.28	0.62	15.76	4.61	0.21	0.39	0.76	7.20	5.07	0.10	30 / 1 .	67.05	18.86	0.34	0.25	7.78	5.66	-0.01	873	4.97
LAI	TER53-2	65.28	0.62	15.76	4.61	0.21	0.39	0.76	7.20	5.07	0.10	54 / 1 .	66.85	19.15	0.28	0.48	8.01	5.18	-0.07	876	4.83
LAI	TER53-2	65.28	0.62	15.76	4.61	0.21	0.39	0.76	7.20	5.07	0.10	55 / 1 .	66.81	19.12	0.30	0.46	7.88	5.37	0.67	874	4.87
LAI	TER53-2	65.28	0.62	15.76	4.61	0.21	0.39	0.76	7.20	5.07	0.10	56 / 1 .	66.72	19.14	0.28	0.47	7.96	5.40	-0.07	874	4.91
LAI	TER53-2	65.28	0.62	15.76	4.61	0.21	0.39	0.76	7.20	5.07	0.10	57 / 1 .	66.63	19.23	0.28	0.50	8.00	5.32	-0.08	875	4.84
LAI	TER53-2	65.28	0.62	15.76	4.61	0.21	0.39	0.76	7.20	5.07	0.10	58 / 1 .	66.76	19.07	0.29	0.43	7.97	5.40	-0.06	875	4.91
LAI	TER53-2	65.28	0.62	15.76	4.61	0.21	0.39	0.76	7.20	5.07	0.10	60 / 1 .	65.93	19.90	0.38	1.07	8.30	4.30	-0.37	881	3.87
LAI	TER53-2	65.28	0.62	15.76	4.61	0.21	0.39	0.76	7.20	5.07	0.10	63 / 1 .	66.73	19.19	0.29	0.52	8.00	5.23	-0.09	876	4.78
LAI	TER53-2	65.28	0.62	15.76	4.61	0.21	0.39	0.76	7.20	5.07	0.10	64 / 1 .	66.80	19.00	0.30	0.34	7.96	5.55	-0.03	874	5.00
LAI	TER53-2	65.28	0.62	15.76	4.61	0.21	0.39	0.76	7.20	5.07	0.10	65 / 1 .	67.11	18.66	0.49	0.18	7.56	5.97	0.00	870	4.56
LAI	TER53-2	65.28	0.62	15.76	4.61	0.21	0.39	0.76	7.20	5.07	0.10	66 / 1 .	66.65	19.29	0.28	0.53	8.00	5.18	-0.09	876	4.78
LAI	TER53-2	65.28	0.62	15.76	4.61	0.21	0.39	0.76	7.20	5.07	0.10	67 / 1 .	66.67	19.14	0.28	0.58	8.05	5.24	0.67	876	4.75
LAI	TER53-2	65.28	0.62	15.76	4.61	0.21	0.39	0.76	7.20	5.07	0.10	68 / 1 .	66.53	19.25	0.29	0.54	7.99	5.34	-0.09	875	4.79
LAI	TER53-2	65.28	0.62	15.76	4.61	0.21	0.39	0.76	7.20	5.07	0.10	69 / 1 .	66.60	19.46	0.31	0.58	7.96	5.04	-0.11	876	4.65
LAI	TER53-2	65.28	0.62	15.76	4.61	0.21	0.39	0.76	7.20	5.07	0.10	70 / 1 .	66.77	19.28	0.29	0.51	7.91	5.20	-0.09	875	4.80
LAI	TER53-2	65.28	0.62	15.76	4.61	0.21	0.39	0.76	7.20	5.07	0.10	71 / 1 .	66.87	19.25	0.26	0.58	7.96	5.03	-0.11	877	4.74
LAI	TER53-2	65.28	0.62	15.76	4.61	0.21	0.39	0.76	7.20	5.07	0.10	72 / 1 .	66.62	19.24	0.29	0.62	8.05	5.12	-0.12	876	4.65
LAI	TER53-2	65.28	0.62	15.76	4.61	0.21	0.39	0.76	7.20	5.07	0.10	73 / 1 .	66.95	19.03	0.28	0.33	7.76	5.58	-0.03	873	5.10
LAI	TER53-2	65.28	0.62	15.76	4.61	0.21	0.39	0.76	7.20	5.07	0.10	74 / 1 .	66.77	19.01	0.32	0.35	7.92	5.56	-0.04	874	4.93
LAI	TER53-2	65.28	0.62	15.76	4.61	0.21	0.39	0.76	7.20	5.07	0.10	75 / 1 .	67.06	18.86	0.27	0.37	7.88	5.52	-0.04	874	5.05
LAI	TER53-2	65.28	0.62	15.76	4.61	0.21	0.39	0.76	7.20	5.07	0.10	1 / 1 .	66.56	19.34	0.29	0.42	8.02	5.33	-0.05	876	4.90
LAI	TER53-2	65.28	0.62	15.76	4.61	0.21	0.39	0.76	7.20	5.07	0.10	2 / 1 .	67.01	19.10	0.31	0.16	7.63	5.77	0.01	872	5.10
LAI	TER53-2	65.28	0.62	15.76	4.61	0.21	0.39	0.76	7.20	5.07	0.10	3 / 1 .	67.16	18.72	0.64	0.37	7.51	5.51	-0.05	872	4.31
LAI	TER53-2	65.28	0.62	15.76	4.61	0.21	0.39	0.76	7.20	5.07	0.10	4 / 1 .	66.93	18.97	0.34	0.27	7.92	5.54	-0.01	874	4.92
LAI	TER53-2	65.28	0.62	15.76	4.61	0.21	0.39	0.76	7.20	5.07	0.10	5 / 1 .	66.91	19.04	0.35	0.23	7.76	5.68	-0.01	873	4.93
LAI	TER53-2	65.28	0.62	15.76	4.61	0.21	0.39	0.76	7.20	5.07	0.10	6 / 1 .	66.55	19.68	0.24	0.67	8.11	4.68	-0.16	879	4.56
LAI	TER53-2	65.28	0.62	15.76	4.61	0.21	0.39	0.76	7.20	5.07	0.10	7 / 1 .	66.28	19.76	0.29	0.87	8.18	4.53	-0.25	880	4.23

Table F1 continued

Unit		Liquid composition											Feldspar composition						Equilibrium	T	H_2O
	Sample	SiO_2	TiO_2	Al_2O_3	FeO_t	MnO	MgO	CaO	Na_2O	K_2O	P_2O_5	Sample	SiO_2	Al_2O_3	FeO_t	CaO	Na_2O	K_2O	ΔKd_{Or-Ab}	(°C)	(wt. %)
LAI	TER53-2	65.28	0.62	15.76	4.61	0.21	0.39	0.76	7.20	5.07	0.10	8 / 1 .	67.27	18.72	0.46	0.11	7.43	5.98	0.01	869	4.47
LAI	TER53-2	65.28	0.62	15.76	4.61	0.21	0.39	0.76	7.20	5.07	0.10	9 / 1 .	66.87	19.19	0.37	0.24	7.74	5.54	-0.01	874	4.84
LAI	TER53-2	65.28	0.62	15.76	4.61	0.21	0.39	0.76	7.20	5.07	0.10	13 / 1 .	66.92	18.79	0.46	0.05	7.80	5.93	0.04	872	3.82
LAI	TER53-2	65.28	0.62	15.76	4.61	0.21	0.39	0.76	7.20	5.07	0.10	15 / 1 .	67.14	18.88	0.45	0.14	7.68	5.67	0.02	873	4.51
LAI	TER53-2	65.28	0.62	15.76	4.61	0.21	0.39	0.76	7.20	5.07	0.10	16 / 1 .	67.03	18.86	0.46	0.12	7.55	5.95	0.01	870	4.51
LAI	TER53-2	65.28	0.62	15.76	4.61	0.21	0.39	0.76	7.20	5.07	0.10	17 / 1 .	67.11	18.97	0.37	0.13	7.59	5.80	0.01	871	4.80
LAI	TER53-2	65.28	0.62	15.76	4.61	0.21	0.39	0.76	7.20	5.07	0.10	18 / 1 .	66.90	19.09	0.37	0.17	7.75	5.69	0.01	873	4.83
LAI	TER53-2	65.28	0.62	15.76	4.61	0.21	0.39	0.76	7.20	5.07	0.10	76 / 1 .	66.89	18.80	0.44	0.11	7.70	6.01	0.02	871	4.48
LAI	TER53-2	65.28	0.62	15.76	4.61	0.21	0.39	0.76	7.20	5.07	0.10	77 / 1 .	66.40	19.40	0.29	0.38	8.03	5.44	-0.04	875	4.94
LAI	TER53-2	65.28	0.62	15.76	4.61	0.21	0.39	0.76	7.20	5.07	0.10	78 / 1 .	66.64	18.99	0.35	0.20	8.08	5.68	0.67	875	4.87
LAI	TER53-2	65.28	0.62	15.76	4.61	0.21	0.39	0.76	7.20	5.07	0.10	79 / 1 .	66.84	18.76	0.42	0.12	7.84	5.98	0.02	872	4.59
LAI	TER53-2	65.28	0.62	15.76	4.61	0.21	0.39	0.76	7.20	5.07	0.10	80 / 1 .	66.73	18.92	0.42	0.14	7.81	5.96	0.01	871	4.63
LAI	TER53-2	65.28	0.62	15.76	4.61	0.21	0.39	0.76	7.20	5.07	0.10	81 / 1 .	66.56	19.26	0.35	0.27	8.00	5.51	-0.01	875	4.87
LAI	TER53-2	65.28	0.62	15.76	4.61	0.21	0.39	0.76	7.20	5.07	0.10	82 / 1 .	66.69	19.16	0.34	0.24	7.88	5.65	-0.01	874	4.94
LAI	TER53-2	65.28	0.62	15.76	4.61	0.21	0.39	0.76	7.20	5.07	0.10	83 / 1 .	66.76	18.92	0.32	0.22	7.86	5.85	0.00	872	5.08
LAI	TER53-2	65.28	0.62	15.76	4.61	0.21	0.39	0.76	7.20	5.07	0.10	84 / 1 .	66.48	19.03	0.38	0.16	7.90	6.02	0.01	871	4.82
LAI	TER53-2	65.28	0.62	15.76	4.61	0.21	0.39	0.76	7.20	5.07	0.10	85 / 1 .	66.88	18.55	0.46	0.16	7.67	6.24	0.00	868	4.65
LAI	TER53-2	65.28	0.62	15.76	4.61	0.21	0.39	0.76	7.20	5.07	0.10	86 / 1 .	66.48	19.07	0.38	0.18	7.64	6.21	-0.01	868	4.96
LAI	TER53-2	65.28	0.62	15.76	4.61	0.21	0.39	0.76	7.20	5.07	0.10	87 / 1 .	66.74	18.85	0.45	0.13	7.90	5.88	0.67	873	4.46
LAI	TER53-2	65.28	0.62	15.76	4.61	0.21	0.39	0.76	7.20	5.07	0.10	88 / 1 .	66.67	18.96	0.43	0.16	7.84	5.92	0.01	872	4.65
LAI	TER53-2	65.28	0.62	15.76	4.61	0.21	0.39	0.76	7.20	5.07	0.10	89 / 1 .	66.56	19.28	0.32	0.21	7.75	5.82	0.00	872	5.07
LAI	TER53-2	65.28	0.62	15.76	4.61	0.21	0.39	0.76	7.20	5.07	0.10	90 / 1 .	66.71	19.00	0.42	0.11	7.82	5.91	0.02	872	4.56
LAI	TER53-2	65.28	0.62	15.76	4.61	0.21	0.39	0.76	7.20	5.07	0.10	91 / 1 .	66.57	19.07	0.44	0.11	7.75	6.01	0.02	871	4.50
LAI	TER53-2	65.28	0.62	15.76	4.61	0.21	0.39	0.76	7.20	5.07	0.10	92 / 1 .	66.18	19.48	0.30	0.34	8.04	5.63	-0.03	874	5.00
LAI	TER53-2	65.28	0.62	15.76	4.61	0.21	0.39	0.76	7.20	5.07	0.10	94 / 1 .	66.63	19.02	0.32	0.28	7.97	5.72	-0.02	873	5.01
LAI	TER53-2	65.28	0.62	15.76	4.61	0.21	0.39	0.76	7.20	5.07	0.10	95 / 1 .	66.59	19.03	0.35	0.23	7.96	5.78	0.00	873	4.92
LAI	TER53-2	65.28	0.62	15.76	4.61	0.21	0.39	0.76	7.20	5.07	0.10	96 / 1 .	66.63	18.90	0.40	0.17	7.95	5.94	0.01	872	4.76
LAI	TER53-2	65.28	0.62	15.76	4.61	0.21	0.39	0.76	7.20	5.07	0.10	97 / 1 .	66.35	19.20	0.40	0.15	7.91	5.96	0.01	872	4.73
LAI	TER53-2	65.28	0.62	15.76	4.61	0.21	0.39	0.76	7.20	5.07	0.10	98 / 1 .	66.42	19.09	0.39	0.18	7.94	5.91	0.01	872	4.77
LAI	TER53-2	65.28	0.62	15.76	4.61	0.21	0.39	0.76	7.20	5.07	0.10	36 / 1 .	66.82	19.17	0.32	0.22	7.82	5.61	0.00	874	5.03
LAI	TER53-2	65.28	0.62	15.76	4.61	0.21	0.39	0.76	7.20	5.07	0.10	37 / 1 .	66.12	20.05	0.27	0.46	7.86	5.18	-0.07	876	4.88
LAI	TER53-2	65.28	0.62	15.76	4.61	0.21	0.39	0.76	7.20	5.07	0.10	38 / 1 .	66.13	19.71	0.30	0.34	7.84	5.65	-0.04	873	5.03
LAI	TER53-2	65.28	0.62	15.76	4.61	0.21	0.39	0.76	7.20	5.07	0.10	39 / 1 .	66.29	19.59	0.37	0.24	7.64	5.82	-0.01	871	4.94
LAI	TER53-2	65.28	0.62	15.76	4.61	0.21	0.39	0.76	7.20	5.07	0.10	40 / 1 .	66.69	18.95	0.44	0.15	7.95	5.80	0.02	873	4.54
LAI	TER53-2	65.28	0.62	15.76	4.61	0.21	0.39	0.76	7.20	5.07	0.10	41 / 1 .	66.79	19.21	0.34	0.25	7.89	5.47	-0.01	875	4.90

Table F1 continued

Unit		Liquid composition										Feldspar composition							Equilibrium	T	H_2O
	Sample	SiO_2	TiO_2	Al_2O_3	FeO_t	MnO	MgO	CaO	Na_2O	K_2O	P_2O_5	Sample	SiO_2	Al_2O_3	FeO_t	CaO	Na_2O	K_2O	ΔKd_{Or-Ab}	(°C)	(wt. %)
LAI	TER53-2	65.28	0.62	15.76	4.61	0.21	0.39	0.76	7.20	5.07	0.10	42 / 1 .	66.27	19.56	0.28	0.48	8.03	5.32	-0.07	875	4.85
LAI	TER53-2	65.28	0.62	15.76	4.61	0.21	0.39	0.76	7.20	5.07	0.10	43 / 1 .	65.72	20.35	0.38	0.51	8.06	4.89	-0.09	879	4.47
LAI	TER53-2	65.28	0.62	15.76	4.61	0.21	0.39	0.76	7.20	5.07	0.10	44 / 1 .	67.03	18.95	0.43	0.15	7.58	5.82	0.01	871	4.66
LAI	TER53-2	65.28	0.62	15.76	4.61	0.21	0.39	0.76	7.20	5.07	0.10	45 / 1 .	66.77	19.16	0.35	0.23	7.82	5.61	0.00	874	4.90
LAI	TER53-2	65.28	0.62	15.76	4.61	0.21	0.39	0.76	7.20	5.07	0.10	46 / 1 .	66.88	18.93	0.37	0.18	7.77	5.82	0.00	872	4.88
LAI	TER53-2	65.28	0.62	15.76	4.61	0.21	0.39	0.76	7.20	5.07	0.10	47 / 1 .	66.52	19.30	0.34	0.24	8.03	5.54	0.00	875	4.90
LAI	TER53-2	65.28	0.62	15.76	4.61	0.21	0.39	0.76	7.20	5.07	0.10	31 / 1 .	66.10	20.18	0.29	1.34	8.56	3.47	-0.84	887	3.41
LAI	TER53-2	65.28	0.62	15.76	4.61	0.21	0.39	0.76	7.20	5.07	0.10	32 / 1 .	65.48	20.53	0.30	1.59	8.72	3.27	-1.20	887	3.11
LAI	TER53-2	65.28	0.62	15.76	4.61	0.21	0.39	0.76	7.20	5.07	0.10	33 / 1 .	67.18	18.76	0.29	0.18	7.90	5.65	0.67	874	5.11
LAI	TER53-2	65.28	0.62	15.76	4.61	0.21	0.39	0.76	7.20	5.07	0.10	34 / 1 .	67.23	18.85	0.34	0.20	7.69	5.66	0.00	873	5.00
LAI	TER53-2	65.28	0.62	15.76	4.61	0.21	0.39	0.76	7.20	5.07	0.10	35 / 1 .	67.14	18.83	0.30	0.20	7.84	5.65	0.00	874	5.09
LAI	TER53-2	65.28	0.62	15.76	4.61	0.21	0.39	0.76	7.20	5.07	0.10	36 / 1 .	67.24	18.77	0.34	0.18	7.69	5.74	0.01	872	4.97
LAI	TER53-2	65.28	0.62	15.76	4.61	0.21	0.39	0.76	7.20	5.07	0.10	37 / 1 .	67.18	18.83	0.31	0.20	7.75	5.68	0.00	873	5.07
LAI	TER53-2	65.28	0.62	15.76	4.61	0.21	0.39	0.76	7.20	5.07	0.10	38 / 1 .	66.95	18.97	0.32	0.21	7.83	5.67	0.00	873	5.02
LAI	TER53-2	65.28	0.62	15.76	4.61	0.21	0.39	0.76	7.20	5.07	0.10	39 / 1 .	67.15	18.87	0.33	0.21	7.75	5.64	0.00	873	5.00
LAI	TER53-2	65.28	0.62	15.76	4.61	0.21	0.39	0.76	7.20	5.07	0.10	40 / 1 .	66.93	18.96	0.32	0.27	7.77	5.70	-0.02	872	5.04
LAI	TER53-2	65.28	0.62	15.76	4.61	0.21	0.39	0.76	7.20	5.07	0.10	41 / 1 .	66.92	18.90	0.31	0.22	7.93	5.66	0.00	874	5.03
LAI	TER53-2	65.28	0.62	15.76	4.61	0.21	0.39	0.76	7.20	5.07	0.10	42 / 1 .	66.98	18.77	0.33	0.24	7.92	5.72	0.67	873	5.01
LAI	TER53-2	65.28	0.62	15.76	4.61	0.21	0.39	0.76	7.20	5.07	0.10	43 / 1 .	66.93	18.87	0.34	0.20	7.94	5.70	0.01	874	4.94
LAI	TER53-2	65.28	0.62	15.76	4.61	0.21	0.39	0.76	7.20	5.07	0.10	44 / 1 .	66.89	18.89	0.30	0.27	8.09	5.50	-0.01	876	5.00
LAI	TER53-2	65.28	0.62	15.76	4.61	0.21	0.39	0.76	7.20	5.07	0.10	45 / 1 .	66.83	18.86	0.31	0.31	8.04	5.60	-0.02	874	4.98
LAI	TER53-2	65.28	0.62	15.76	4.61	0.21	0.39	0.76	7.20	5.07	0.10	46 / 1 .	67.04	18.84	0.32	0.24	7.95	5.56	0.00	875	5.00
LAI	TER53-2	65.28	0.62	15.76	4.61	0.21	0.39	0.76	7.20	5.07	0.10	47 / 1 .	66.92	18.88	0.30	0.21	7.91	5.73	0.00	873	5.09
LAI	TER53-2	65.28	0.62	15.76	4.61	0.21	0.39	0.76	7.20	5.07	0.10	48 / 1 .	66.81	18.89	0.32	0.21	8.02	5.72	0.00	874	4.99
LAI	TER53-2	65.28	0.62	15.76	4.61	0.21	0.39	0.76	7.20	5.07	0.10	49 / 1 .	66.78	18.86	0.29	0.25	8.12	5.64	0.00	875	5.06
LAI	TER53-2	65.28	0.62	15.76	4.61	0.21	0.39	0.76	7.20	5.07	0.10	50 / 1 .	66.95	18.87	0.34	0.25	8.04	5.50	0.00	876	4.90
LAI	TER53-2	65.28	0.62	15.76	4.61	0.21	0.39	0.76	7.20	5.07	0.10	51 / 1 .	66.80	19.02	0.28	0.26	8.02	5.58	-0.01	875	5.10
LAI	TER53-2	65.28	0.62	15.76	4.61	0.21	0.39	0.76	7.20	5.07	0.10	52 / 1 .	66.90	18.90	0.32	0.23	7.94	5.68	0.00	874	5.02
LAI	TER53-2	65.28	0.62	15.76	4.61	0.21	0.39	0.76	7.20	5.07	0.10	53 / 1 .	66.95	18.86	0.32	0.24	7.92	5.62	-0.01	874	5.02
LAI	TER53-2	65.28	0.62	15.76	4.61	0.21	0.39	0.76	7.20	5.07	0.10	35 / 1 .	66.85	19.06	0.34	0.18	7.89	5.63	0.01	874	4.91
LAI	TER53-2	65.28	0.62	15.76	4.61	0.21	0.39	0.76	7.20	5.07	0.10	35 / 2 .	66.61	19.74	0.35	0.20	7.34	5.69	-0.01	870	5.00
LAI	TER53-2	65.28	0.62	15.76	4.61	0.21	0.39	0.76	7.20	5.07	0.10	35 / 3 .	66.78	19.11	0.31	0.19	7.84	5.72	0.01	873	5.08
LAI	TER53-2	65.28	0.62	15.76	4.61	0.21	0.39	0.76	7.20	5.07	0.10	35 / 4 .	67.03	18.92	0.43	0.10	7.62	5.88	0.02	871	4.46
LAI	TER53-2	65.28	0.62	15.76	4.61	0.21	0.39	0.76	7.20	5.07	0.10	35 / 5 .	66.73	19.13	0.36	0.12	7.79	5.85	0.02	872	4.79
LAI	TER53-2	65.28	0.62	15.76	4.61	0.21	0.39	0.76	7.20	5.07	0.10	35 / 6 .	67.01	18.87	0.40	0.10	7.67	5.94	0.02	871	4.62

Table F1 continued

Unit		Liquid composition										Feldspar composition							Equilibrium	T	H_2O
	Sample	SiO_2	TiO_2	Al_2O_3	FeO_t	MnO	MgO	CaO	Na_2O	K_2O	P_2O_5	Sample	SiO_2	Al_2O_3	FeO_t	CaO	Na_2O	K_2O	ΔKd_{Or-Ab}	(°C)	(wt. %)
LAI	TER53-2	65.28	0.62	15.76	4.61	0.21	0.39	0.76	7.20	5.07	0.10	35 / 7 .	65.09	21.06	0.52	0.17	7.39	5.72	0.00	871	4.42
LAI	TER53-2	65.28	0.62	15.76	4.61	0.21	0.39	0.76	7.20	5.07	0.10	35 / 8 .	67.05	18.93	0.46	0.10	7.56	5.89	0.02	871	4.38
LAI	TER53-2	65.28	0.62	15.76	4.61	0.21	0.39	0.76	7.20	5.07	0.10	35 / 9 .	66.96	18.87	0.41	0.09	7.77	5.87	0.03	872	4.44
LAI	TER53-2	65.28	0.62	15.76	4.61	0.21	0.39	0.76	7.20	5.07	0.10	35 / 10 .	66.92	19.03	0.44	0.12	7.59	5.86	0.02	871	4.50
LAI	TER53-2	65.28	0.62	15.76	4.61	0.21	0.39	0.76	7.20	5.07	0.10	35 / 11 .	66.53	19.44	0.39	0.12	7.69	5.79	0.02	872	4.65
LAI	TER53-2	65.28	0.62	15.76	4.61	0.21	0.39	0.76	7.20	5.07	0.10	35 / 12 .	66.84	18.93	0.38	0.11	7.84	5.88	0.02	872	4.67
LAI	TER53-2	65.28	0.62	15.76	4.61	0.21	0.39	0.76	7.20	5.07	0.10	35 / 13 .	66.85	19.07	0.38	0.12	7.73	5.83	0.02	872	4.70
LAI	TER53-2	65.28	0.62	15.76	4.61	0.21	0.39	0.76	7.20	5.07	0.10	35 / 15 .	66.91	18.95	0.38	0.11	7.80	5.82	0.67	873	4.67
LAI	TER53-2	65.28	0.62	15.76	4.61	0.21	0.39	0.76	7.20	5.07	0.10	35 / 16 .	67.14	18.85	0.37	0.10	7.70	5.82	0.02	872	4.70
LAI	TER53-2	65.28	0.62	15.76	4.61	0.21	0.39	0.76	7.20	5.07	0.10	35 / 18 .	65.30	21.07	0.42	0.18	7.42	5.59	0.00	872	4.69
LAI	TER53-2	65.28	0.62	15.76	4.61	0.21	0.39	0.76	7.20	5.07	0.10	35 / 19 .	66.79	19.06	0.33	0.19	7.87	5.71	0.01	873	4.97
LAI	TER53-2	65.28	0.62	15.76	4.61	0.21	0.39	0.76	7.20	5.07	0.10	35 / 20 .	66.74	19.22	0.33	0.23	7.81	5.65	0.00	873	5.01
LMI	MIGG05	64.16	0.70	15.68	5.00	0.18	0.52	1.16	7.19	5.28	0.14	5 / 1 .	67.72	18.98	0.31	0.46	8.33	4.78	-0.06	932	3.38
LMI	MIGG05	64.16	0.70	15.68	5.00	0.18	0.52	1.16	7.19	5.28	0.14	6 / 1 .	67.12	18.98	0.33	0.44	8.33	4.74	-0.05	933	3.34
LMI	MIGG05	64.16	0.70	15.68	5.00	0.18	0.52	1.16	7.19	5.28	0.14	10 / 1 .	67.82	18.88	0.35	0.30	8.08	5.21	0.00	929	3.57
LMI	MIGG05	64.16	0.70	15.68	5.00	0.18	0.52	1.16	7.19	5.28	0.14	11 / 1 .	67.78	18.97	0.33	0.27	7.98	5.21	0.01	928	3.65
LMI	MIGG05	64.16	0.70	15.68	5.00	0.18	0.52	1.16	7.19	5.28	0.14	14 / 1 .	66.35	18.76	0.29	0.50	8.35	4.54	-0.08	934	3.29
LMI	MIGG05	64.16	0.70	15.68	5.00	0.18	0.52	1.16	7.19	5.28	0.14	15 / 1 .	66.95	19.20	0.30	0.65	8.54	4.28	-0.18	936	3.04
LMI	MIGG05	64.16	0.70	15.68	5.00	0.18	0.52	1.16	7.19	5.28	0.14	5 / 1 .	67.22	18.78	0.34	0.47	8.27	4.70	-0.06	933	3.31
LMI	MIGG05	64.16	0.70	15.68	5.00	0.18	0.52	1.16	7.19	5.28	0.14	6 / 1 .	67.16	18.80	0.33	0.43	8.29	4.79	-0.05	932	3.37
LMI	MIGG05	64.16	0.70	15.68	5.00	0.18	0.52	1.16	7.19	5.28	0.14	10 / 1 .	67.45	18.78	0.33	0.28	7.89	5.25	0.01	927	3.65
LMI	MIGG05	64.16	0.70	15.68	5.00	0.18	0.52	1.16	7.19	5.28	0.14	11 / 1 .	67.41	18.66	0.34	0.27	7.96	5.34	0.01	927	3.65
LMI	MIGG05	64.16	0.70	15.68	5.00	0.18	0.52	1.16	7.19	5.28	0.14	14 / 1 .	66.88	19.02	0.28	0.50	8.30	4.61	-0.08	933	3.37
LMI	MIGG05	64.16	0.70	15.68	5.00	0.18	0.52	1.16	7.19	5.28	0.14	15 / 1 .	66.84	18.95	0.29	0.70	8.42	4.21	-0.21	936	3.00
LMI	MIGG05	64.16	0.70	15.68	5.00	0.18	0.52	1.16	7.19	5.28	0.14	28 / 1 .	67.40	18.49	0.59	0.16	7.97	5.41	0.04	927	2.84
LMI	MIGG05	64.16	0.70	15.68	5.00	0.18	0.52	1.16	7.19	5.28	0.14	32 / 1 .	67.47	19.09	0.29	0.49	8.29	4.64	-0.07	933	3.37
LMI	MIGG05	64.16	0.70	15.68	5.00	0.18	0.52	1.16	7.19	5.28	0.14	33 / 1 .	67.08	19.04	0.29	0.50	8.44	4.51	-0.09	935	3.29
VFI	231 / 1 .	65.23	0.50	15.21	5.25	0.25	0.30	0.81	7.44	4.96	0.05	55 / 1 .	66.37	19.59	0.22	0.99	8.26	4.17	-0.30	881	4.22
VFI	231 / 1 .	65.23	0.50	15.21	5.25	0.25	0.30	0.81	7.44	4.96	0.05	56 / 1 .	66.46	18.64	0.25	0.40	7.74	5.32	-0.01	874	5.17
VFI	231 / 1 .	65.23	0.50	15.21	5.25	0.25	0.30	0.81	7.44	4.96	0.05	57 / 1 .	66.27	18.68	0.25	0.40	7.80	5.33	0.00	874	5.17
VFI	231 / 1 .	65.23	0.50	15.21	5.25	0.25	0.30	0.81	7.44	4.96	0.05	62 / 1 .	66.81	18.68	0.25	0.29	7.66	5.56	0.02	872	5.37
VFI	231 / 1 .	65.23	0.50	15.21	5.25	0.25	0.30	0.81	7.44	4.96	0.05	63 / 1 .	66.69	18.89	0.28	0.39	7.63	5.49	-0.01	872	5.18
VFI	231 / 1 .	65.23	0.50	15.21	5.25	0.25	0.30	0.81	7.44	4.96	0.05	65 / 1 .	66.59	18.86	0.24	0.40	8.09	5.34	0.00	875	5.14
VFI	231 / 1 .	65.23	0.50	15.21	5.25	0.25	0.30	0.81	7.44	4.96	0.05	66 / 1 .	66.70	18.92	0.25	0.39	7.96	5.40	0.00	874	5.17
VFI	231 / 1 .	65.23	0.50	15.21	5.25	0.25	0.30	0.81	7.44	4.96	0.05	67 / 1 .	66.30	18.79	0.26	0.49	7.89	5.25	-0.03	874	5.02

Table F1 continued

Unit		Liquid composition										Feldspar composition							Equilibrium	T	H_2O
	Sample	SiO_2	TiO_2	Al_2O_3	FeO_t	MnO	MgO	CaO	Na_2O	K_2O	P_2O_5	Sample	SiO_2	Al_2O_3	FeO_t	CaO	Na_2O	K_2O	ΔKd_{Or-Ab}	(°C)	(wt. %)
VFI	231 / 1 .	65.23	0.50	15.21	5.25	0.25	0.30	0.81	7.44	4.96	0.05	68 / 1 .	66.14	18.90	0.28	0.50	7.77	5.18	-0.03	874	4.97
VFI	231 / 1 .	65.23	0.50	15.21	5.25	0.25	0.30	0.81	7.44	4.96	0.05	69 / 1 .	66.25	18.88	0.26	0.41	7.95	5.30	0.00	875	5.11
VFI	231 / 1 .	65.23	0.50	15.21	5.25	0.25	0.30	0.81	7.44	4.96	0.05	70 / 1 .	66.02	19.25	0.24	0.76	7.98	4.73	-0.13	877	4.63
VFI	231 / 1 .	65.23	0.50	15.21	5.25	0.25	0.30	0.81	7.44	4.96	0.05	71 / 1 .	65.88	19.25	0.24	0.79	8.00	4.67	-0.15	877	4.56
VFI	231 / 1 .	65.23	0.50	15.21	5.25	0.25	0.30	0.81	7.44	4.96	0.05	72 / 1 .	66.23	19.20	0.23	0.74	8.05	4.74	-0.13	878	4.65
VFI	231 / 1 .	65.23	0.50	15.21	5.25	0.25	0.30	0.81	7.44	4.96	0.05	73 / 1 .	65.69	19.14	0.24	0.80	7.95	4.67	-0.15	877	4.58
VFI	231 / 1 .	65.23	0.50	15.21	5.25	0.25	0.30	0.81	7.44	4.96	0.05	74 / 1 .	66.81	18.59	0.33	0.25	7.74	5.91	0.03	870	5.19
VFI	231 / 1 .	65.23	0.50	15.21	5.25	0.25	0.30	0.81	7.44	4.96	0.05	75 / 1 .	66.98	18.37	0.36	0.20	7.57	5.86	0.04	870	5.08
VFI	231 / 1 .	65.23	0.50	15.21	5.25	0.25	0.30	0.81	7.44	4.96	0.05	76 / 1 .	66.82	18.45	0.35	0.17	7.60	5.88	0.04	870	5.09
VFI	231 / 1 .	65.23	0.50	15.21	5.25	0.25	0.30	0.81	7.44	4.96	0.05	77 / 1 .	66.53	18.30	0.32	0.20	7.61	5.85	0.04	870	5.22
VFI	231 / 1 .	65.23	0.50	15.21	5.25	0.25	0.30	0.81	7.44	4.96	0.05	78 / 1 .	66.79	18.76	0.26	0.37	8.03	5.36	0.01	875	5.15
VFI	231 / 1 .	65.23	0.50	15.21	5.25	0.25	0.30	0.81	7.44	4.96	0.05	1 / 1 .	66.47	19.59	0.24	0.76	8.12	4.63	-0.14	879	4.58
VFI	231 / 1 .	65.23	0.50	15.21	5.25	0.25	0.30	0.81	7.44	4.96	0.05	2 / 1 .	66.66	19.54	0.23	0.63	8.14	4.84	-0.08	878	4.79
VFI	231 / 1 .	65.23	0.50	15.21	5.25	0.25	0.30	0.81	7.44	4.96	0.05	3 / 1 .	66.82	19.41	0.26	0.58	8.14	4.85	-0.06	878	4.78
VFI	231 / 1 .	65.23	0.50	15.21	5.25	0.25	0.30	0.81	7.44	4.96	0.05	4 / 1 .	66.47	19.50	0.25	0.67	8.14	4.78	-0.10	878	4.68
VFI	231 / 1 .	65.23	0.50	15.21	5.25	0.25	0.30	0.81	7.44	4.96	0.05	5 / 1 .	66.32	20.04	0.22	0.94	8.27	4.36	-0.24	880	4.32
VFI	231 / 1 .	65.23	0.50	15.21	5.25	0.25	0.30	0.81	7.44	4.96	0.05	6 / 1 .	66.82	20.06	0.24	0.77	8.16	4.54	-0.15	879	4.53
VFI	231 / 1 .	65.23	0.50	15.21	5.25	0.25	0.30	0.81	7.44	4.96	0.05	7 / 1 .	66.86	19.68	0.23	0.72	8.15	4.62	-0.13	879	4.62
VFI	231 / 1 .	65.23	0.50	15.21	5.25	0.25	0.30	0.81	7.44	4.96	0.05	8 / 1 .	66.75	19.48	0.24	0.64	8.03	4.86	-0.09	877	4.78
VFI	231 / 1 .	65.23	0.50	15.21	5.25	0.25	0.30	0.81	7.44	4.96	0.05	9 / 1 .	66.64	19.50	0.24	0.71	7.99	4.83	-0.11	877	4.71
VFI	231 / 1 .	65.23	0.50	15.21	5.25	0.25	0.30	0.81	7.44	4.96	0.05	10 / 1 .	66.42	19.59	0.25	0.81	8.00	4.74	-0.15	877	4.57
VFI	231 / 1 .	65.23	0.50	15.21	5.25	0.25	0.30	0.81	7.44	4.96	0.05	11 / 1 .	66.62	19.43	0.27	0.73	7.98	4.78	-0.12	877	4.63
VFI	231 / 1 .	65.23	0.50	15.21	5.25	0.25	0.30	0.81	7.44	4.96	0.05	12 / 1 .	65.72	19.33	0.24	0.68	7.95	4.76	-0.11	877	4.71
VFI	231 / 1 .	65.23	0.50	15.21	5.25	0.25	0.30	0.81	7.44	4.96	0.05	13 / 1 .	66.05	19.45	0.24	0.77	8.09	4.54	-0.15	879	4.54
VFI	231 / 1 .	65.23	0.50	15.21	5.25	0.25	0.30	0.81	7.44	4.96	0.05	14 / 1 .	66.58	19.38	0.23	0.80	7.99	4.62	-0.16	878	4.58
VFI	231 / 1 .	65.23	0.50	15.21	5.25	0.25	0.30	0.81	7.44	4.96	0.05	15 / 1 .	66.06	19.41	0.24	0.80	8.06	4.66	-0.16	878	4.54
VFI	231 / 1 .	65.23	0.50	15.21	5.25	0.25	0.30	0.81	7.44	4.96	0.05	16 / 1 .	65.98	19.53	0.24	0.81	8.15	4.51	-0.17	879	4.48
VFI	231 / 1 .	65.23	0.50	15.21	5.25	0.25	0.30	0.81	7.44	4.96	0.05	17 / 1 .	66.25	19.41	0.22	0.78	8.17	4.58	-0.15	879	4.56
VFI	231 / 1 .	65.23	0.50	15.21	5.25	0.25	0.30	0.81	7.44	4.96	0.05	18 / 1 .	65.96	19.70	0.23	0.96	8.38	4.18	-0.29	882	4.20
VFI	231 / 1 .	65.23	0.50	15.21	5.25	0.25	0.30	0.81	7.44	4.96	0.05	20 / 1 .	66.385	19.107	0.245	0.442	7.931	5.155	-0.01	875	5.07
VFI	231 / 1 .	65.23	0.50	15.21	5.25	0.25	0.30	0.81	7.44	4.96	0.05	21 / 1 .	66.416	19.125	0.254	0.434	8.021	5.151	-0.01	876	5.03
VFI	231 / 1 .	65.23	0.50	15.21	5.25	0.25	0.30	0.81	7.44	4.96	0.05	22 / 1 .	66.464	19.224	0.271	0.492	8.019	5.179	-0.03	875	4.95
VFI	231 / 1 .	65.23	0.50	15.21	5.25	0.25	0.30	0.81	7.44	4.96	0.05	23 / 1 .	66.709	18.898	0.329	0.304	8.007	5.372	0.03	875	4.99
VFI	231 / 1 .	65.23	0.50	15.21	5.25	0.25	0.30	0.81	7.44	4.96	0.05	24 / 1 .	67.102	18.772	0.349	0.09	7.745	5.903	0.07	871	4.84
VFI	231 / 1 .	65.23	0.50	15.21	5.25	0.25	0.30	0.81	7.44	4.96	0.05	25 / 1 .	67.11	18.694	0.375	0.122	7.782	5.805	0.07	872	4.85

Table F1 continued

Unit	Liquid composition											Feldspar composition							Equilibrium	T	H_2O
	Sample	SiO_2	TiO_2	Al_2O_3	FeO_t	MnO	MgO	CaO	Na_2O	K_2O	P_2O_5	Sample	SiO_2	Al_2O_3	FeO_t	CaO	Na_2O	K_2O	ΔKd_{Or-Ab}	(°C)	(wt. %)
CCl	TER10-1	64.30	0.52	16.26	4.67	0.18	0.47	0.86	7.65	5.00	0.07	79 / 1 .	67.15	18.77	0.28	0.25	7.92	5.95	-0.04	875	5.09
CCl	TER10-1	64.30	0.52	16.26	4.67	0.18	0.47	0.86	7.65	5.00	0.07	80 / 1 .	67.55	18.88	0.27	0.23	7.98	5.95	-0.04	875	5.13
CCl	TER10-1	64.30	0.52	16.26	4.67	0.18	0.47	0.86	7.65	5.00	0.07	81 / 1 .	67.26	18.63	0.32	0.15	7.88	5.95	-0.02	875	4.92
CCl	TER10-1	64.30	0.52	16.26	4.67	0.18	0.47	0.86	7.65	5.00	0.07	82 / 1 .	67.10	18.67	0.30	0.17	7.95	5.87	-0.02	876	4.98
CCl	TER10-1	64.30	0.52	16.26	4.67	0.18	0.47	0.86	7.65	5.00	0.07	83 / 1 .	67.34	18.72	0.32	0.29	7.87	5.76	-0.05	876	4.93
CCl	TER10-1	64.30	0.52	16.26	4.67	0.18	0.47	0.86	7.65	5.00	0.07	84 / 1 .	67.09	18.75	0.32	0.19	7.82	5.80	-0.03	876	4.92
CCl	TER10-1	64.30	0.52	16.26	4.67	0.18	0.47	0.86	7.65	5.00	0.07	85 / 1 .	68.05	19.03	0.29	0.20	7.86	5.84	-0.03	876	5.05
CCl	TER10-1	64.30	0.52	16.26	4.67	0.18	0.47	0.86	7.65	5.00	0.07	86 / 1 .	67.34	19.64	0.32	0.29	7.76	5.65	-0.06	876	4.92
CCl	TER10-1	64.30	0.52	16.26	4.67	0.18	0.47	0.86	7.65	5.00	0.07	87 / 1 .	67.58	18.68	0.30	0.17	7.72	5.90	-0.03	875	5.05
CCl	TER10-1	64.30	0.52	16.26	4.67	0.18	0.47	0.86	7.65	5.00	0.07	88 / 1 .	67.48	18.92	0.29	0.27	7.75	5.83	-0.05	875	5.07
CCl	TER10-1	64.30	0.52	16.26	4.67	0.18	0.47	0.86	7.65	5.00	0.07	89 / 1 .	67.88	18.69	0.33	0.18	7.74	5.93	-0.03	875	4.93
CCl	TER10-1	64.30	0.52	16.26	4.67	0.18	0.47	0.86	7.65	5.00	0.07	90 / 1 .	67.63	18.74	0.28	0.20	7.86	5.82	-0.03	876	5.11
CCl	TER10-1	64.30	0.52	16.26	4.67	0.18	0.47	0.86	7.65	5.00	0.07	91 / 1 .	67.48	18.77	0.29	0.18	7.82	5.86	-0.03	876	5.04
CCl	TER10-1	64.30	0.52	16.26	4.67	0.18	0.47	0.86	7.65	5.00	0.07	92 / 1 .	67.54	18.73	0.29	0.17	7.76	5.87	-0.02	875	5.07
CCl	TER10-1	64.30	0.52	16.26	4.67	0.18	0.47	0.86	7.65	5.00	0.07	93 / 1 .	67.74	18.69	0.27	0.16	7.80	5.83	-0.02	876	5.13
CCl	TER10-1	64.30	0.52	16.26	4.67	0.18	0.47	0.86	7.65	5.00	0.07	94 / 1 .	67.62	18.49	0.30	0.15	7.79	5.87	-0.02	875	5.00
CCl	TER10-1	64.30	0.52	16.26	4.67	0.18	0.47	0.86	7.65	5.00	0.07	95 / 1 .	66.87	18.68	0.30	0.25	7.80	5.72	-0.04	876	4.98
CCl	TER10-1	64.30	0.52	16.26	4.67	0.18	0.47	0.86	7.65	5.00	0.07	96 / 1 .	67.26	18.86	0.28	0.25	7.77	5.72	-0.04	876	5.08
CCl	TER10-1	64.30	0.52	16.26	4.67	0.18	0.47	0.86	7.65	5.00	0.07	97 / 1 .	67.20	18.76	0.28	0.24	7.77	6.04	-0.05	873	5.13
CCl	TER10-1	64.30	0.52	16.26	4.67	0.18	0.47	0.86	7.65	5.00	0.07	98 / 1 .	67.84	18.78	0.29	0.20	7.74	5.80	-0.03	875	5.05
CCl	TER10-1	64.30	0.52	16.26	4.67	0.18	0.47	0.86	7.65	5.00	0.07	99 / 1 .	67.53	18.80	0.27	0.20	7.76	5.91	-0.03	875	5.16
CCl	TER10-1	64.30	0.52	16.26	4.67	0.18	0.47	0.86	7.65	5.00	0.07	100 / 1 .	66.86	18.62	0.28	0.26	7.73	5.97	-0.05	874	5.12
CCl	TER10-1	64.30	0.52	16.26	4.67	0.18	0.47	0.86	7.65	5.00	0.07	76 / 1 .	66.82	18.45	0.35	0.17	7.60	5.68	-0.02	876	4.80
CCl	TER10-1	64.30	0.52	16.26	4.67	0.18	0.47	0.86	7.65	5.00	0.07	77 / 1 .	66.53	18.30	0.32	0.20	7.61	5.65	-0.03	876	4.93
CCl	TER10-1	64.30	0.52	16.26	4.67	0.18	0.47	0.86	7.65	5.00	0.07	78 / 1 .	66.79	18.76	0.26	0.37	8.03	5.16	-0.07	881	4.86
CCl	TER10-1	64.30	0.52	16.26	4.67	0.18	0.47	0.86	7.65	5.00	0.07	CCIMI01Fsp	67.18	18.90	0.33	0.15	7.57	5.98	-0.03	873	4.96
CCl	TER10-1	64.30	0.52	16.26	4.67	0.18	0.47	0.86	7.65	5.00	0.07	CCIMI02Fsp	67.46	19.29	0.25	0.23	7.73	5.78	-0.04	875	5.20
CCl	TER10-1	64.30	0.52	16.26	4.67	0.18	0.47	0.86	7.65	5.00	0.07	CCIMI03Fsp	66.85	19.36	0.22	0.35	7.83	5.50	-0.07	877	5.13
CCl	TER10-1	64.30	0.52	16.26	4.67	0.18	0.47	0.86	7.65	5.00	0.07	CCIMI04Fsp	67.56	19.35	0.29	0.14	7.21	6.06	-0.03	870	5.18
CCl	TER10-1	64.30	0.52	16.26	4.67	0.18	0.47	0.86	7.65	5.00	0.07	CCIMI05Fsp	66.96	19.12	0.31	0.11	7.65	6.20	-0.02	872	4.93
CCl	TER10-1	64.30	0.52	16.26	4.67	0.18	0.47	0.86	7.65	5.00	0.07	CCIMI06Fsp	67.62	19.23	0.23	0.17	7.78	5.95	-0.03	875	5.35
Sy	TER30-1	64.71	0.59	15.90	4.85	0.21	0.36	0.83	7.51	4.97	0.08	KFsp02_core	67.14	19.32	0.24	0.77	8.00	5.17	-0.21	874	4.76
Sy	TER30-1	64.71	0.59	15.90	4.85	0.21	0.36	0.83	7.51	4.97	0.08	KFsp02_rim	68.06	19.46	0.22	0.15	7.64	6.08	-0.03	869	5.68
Sy	TER30-1	64.71	0.59	15.90	4.85	0.21	0.36	0.83	7.51	4.97	0.08	KFsp04_core	67.85	19.35	0.36	0.04	7.88	5.73	0.02	874	4.21
Sy	TER30-1	64.71	0.59	15.90	4.85	0.21	0.36	0.83	7.51	4.97	0.08	KFsp04_rim	67.23	19.50	0.29	0.11	7.56	6.07	-0.02	869	5.27

Table F1 continued

Unit	Liquid composition											Feldspar composition							Equilibrium	T	H_2O
	Sample	SiO_2	TiO_2	Al_2O_3	FeO_t	MnO	MgO	CaO	Na_2O	K_2O	P_2O_5	Sample	SiO_2	Al_2O_3	FeO_t	CaO	Na_2O	K_2O	ΔKd_{Or-Ab}	(°C)	(wt. %)
Sy	TER30-1	64.71	0.59	15.90	4.85	0.21	0.36	0.83	7.51	4.97	0.08	KFsp06_rim(light)	66.37	18.51	0.55	0.00	2.92	12.74	0.13	757	
Sy	TER30-1	64.71	0.59	15.90	4.85	0.21	0.36	0.83	7.51	4.97	0.08	KFsp08_core	66.85	19.89	0.24	0.59	8.17	4.82	-0.16	879	4.79
Sy	TER30-1	64.71	0.59	15.90	4.85	0.21	0.36	0.83	7.51	4.97	0.08	KFsp08_rim	66.57	19.73	0.22	0.45	8.22	4.86	-0.11	880	4.98
Sy	TER30-1	64.71	0.59	15.90	4.85	0.21	0.36	0.83	7.51	4.97	0.08	KFsp09_core	66.95	20.07	0.24	0.52	7.94	5.14	-0.13	875	5.00
Sy	TER30-1	64.71	0.59	15.90	4.85	0.21	0.36	0.83	7.51	4.97	0.08	KFsp09_rim	66.86	19.15	0.29	0.10	7.63	5.89	-0.01	871	5.18
Sy	TER30-1	64.71	0.59	15.90	4.85	0.21	0.36	0.83	7.51	4.97	0.08	KFsp10_core	67.54	19.61	0.28	0.33	7.81	5.39	-0.07	874	5.17
Sy	TER30-1	64.71	0.59	15.90	4.85	0.21	0.36	0.83	7.51	4.97	0.08	KFsp10_rim	67.73	19.22	0.34	0.02	7.47	6.08	0.00	869	3.89
Sy	TER30-1	64.71	0.59	15.90	4.85	0.21	0.36	0.83	7.51	4.97	0.08	KFsp11_core	67.58	19.70	0.21	0.37	8.03	5.03	-0.08	878	5.20
Sy	TER30-1	64.71	0.59	15.90	4.85	0.21	0.36	0.83	7.51	4.97	0.08	KFsp11_rim	67.81	19.18	0.43	0.02	7.88	5.91	0.02	872	3.33
Sy	TER30-1	64.71	0.59	15.90	4.85	0.21	0.36	0.83	7.51	4.97	0.08	TER30-6_13_rim	66.42	18.23	0.96	0.00	4.61	10.33	0.00	808	
Sy	TER30-1	64.71	0.59	15.90	4.85	0.21	0.36	0.83	7.51	4.97	0.08	TER30-6_14_core	67.54	19.23	0.23	0.10	8.09	5.59	0.01	876	5.36
Sy	TER30-1	64.71	0.59	15.90	4.85	0.21	0.36	0.83	7.51	4.97	0.08	TER30-6_14_rim	67.35	18.58	1.12	0.02	6.87	6.83	-0.03	859	
Sy	TER30-1	64.71	0.59	15.90	4.85	0.21	0.36	0.83	7.51	4.97	0.08	TER30-6_15_core	67.62	19.85	0.20	0.48	8.19	4.91	-0.12	879	5.04
Sy	TER30-1	64.71	0.59	15.90	4.85	0.21	0.36	0.83	7.51	4.97	0.08	TER30-6_15_rim	67.58	19.22	0.36	0.04	7.91	5.74	0.02	874	4.20
Sy	TER30-1	64.71	0.59	15.90	4.85	0.21	0.36	0.83	7.51	4.97	0.08	TER30-6_16_rim	67.22	18.17	1.25	0.00	5.76	8.89	-0.04	833	
Sy	TER30-1	64.71	0.59	15.90	4.85	0.21	0.36	0.83	7.51	4.97	0.08	TER30-6_17_rim	67.00	18.35	0.97	0.00	4.31	10.83	0.02	800	
Sy	TER30-1	64.71	0.59	15.90	4.85	0.21	0.36	0.83	7.51	4.97	0.08	TER30-6_18_core	67.17	20.03	0.26	0.46	8.21	4.94	-0.11	879	4.91
Sy	TER30-1	64.71	0.59	15.90	4.85	0.21	0.36	0.83	7.51	4.97	0.08	TER30-6_18_rim	68.06	18.73	0.70	0.04	7.73	6.17	0.00	870	3.10
Sy	TER30-1	64.71	0.59	15.90	4.85	0.21	0.36	0.83	7.51	4.97	0.08	TER30-6_19_rim	67.87	18.22	1.32	0.00	7.83	5.71	0.03	874	
Sy	TER30-1	64.71	0.59	15.90	4.85	0.21	0.36	0.83	7.51	4.97	0.08	TER30-6_20_rim	67.85	18.37	1.17	0.00	7.75	5.73	0.02	873	
Sy	TER30-1	64.71	0.59	15.90	4.85	0.21	0.36	0.83	7.51	4.97	0.08	TER30-6_21_core	67.35	19.50	0.24	0.22	7.53	6.01	-0.05	868	5.58
Sy	TER30-1	64.71	0.59	15.90	4.85	0.21	0.36	0.83	7.51	4.97	0.08	TER30-6_21_rim	67.63	18.93	0.31	0.16	7.78	5.81	-0.02	872	5.20
Sy	TER30-1	64.71	0.59	15.90	4.85	0.21	0.36	0.83	7.51	4.97	0.08	TER30-6_22_rim	66.94	18.06	1.00	0.00	4.59	10.33	0.00	808	
Sy	TER30-1	64.71	0.59	15.90	4.85	0.21	0.36	0.83	7.51	4.97	0.08	TER30-6_23_rim	68.37	18.54	1.18	0.00	9.73	3.07	-0.55	902	
Sy	TER30-1	64.71	0.59	15.90	4.85	0.21	0.36	0.83	7.51	4.97	0.08	TER30-6_24_rim	66.62	18.10	1.08	0.00	4.64	10.41	0.00	808	
Sy	TER30-1	64.71	0.59	15.90	4.85	0.21	0.36	0.83	7.51	4.97	0.08	TER30-6_25_core	67.47	18.83	0.50	0.03	7.84	5.93	0.01	872	3.41
Sy	TER30-1	64.71	0.59	15.90	4.85	0.21	0.36	0.83	7.51	4.97	0.08	TER30-6_25_rim	67.09	18.91	0.64	0.01	7.71	5.70	0.02	873	
Sy	TER30-1	64.71	0.59	15.90	4.85	0.21	0.36	0.83	7.51	4.97	0.08	TER30-1Fsp01	67.07	18.53	0.77	0.08	7.86	5.91	0.00	872	3.38
Sy	TER30-1	64.71	0.59	15.90	4.85	0.21	0.36	0.83	7.51	4.97	0.08	TER30-1Fsp02	66.89	18.90	0.70	0.02	8.10	5.60	0.03	876	
Sy	TER30-1	64.71	0.59	15.90	4.85	0.21	0.36	0.83	7.51	4.97	0.08	TER30-1Fsp04	65.81	19.55	0.22	0.49	8.39	4.80	-0.13	880	4.89
Sy	TER30-1	64.71	0.59	15.90	4.85	0.21	0.36	0.83	7.51	4.97	0.08	TER30-1Fsp05	67.32	19.31	0.21	0.23	8.11	5.36	-0.03	876	5.41
Sy	TER30-1	64.71	0.59	15.90	4.85	0.21	0.36	0.83	7.51	4.97	0.08	TER30-1Fsp06	66.68	19.03	0.31	0.09	7.58	6.16	-0.02	868	5.12
Sy	TER30-1	64.71	0.59	15.90	4.85	0.21	0.36	0.83	7.51	4.97	0.08	TER30-1Fsp07	65.11	19.60	0.17	0.54	8.07	5.15	-0.13	876	5.10
Sy	TER30-1	64.71	0.59	15.90	4.85	0.21	0.36	0.83	7.51	4.97	0.08	TER30-7Fsp05	67.24	18.17	1.02	0.00	7.12	6.70	-0.02	862	
Sy	TER30-1	64.71	0.59	15.90	4.85	0.21	0.36	0.83	7.51	4.97	0.08	TER30-7Fsp07	67.26	18.23	0.93	0.00	7.44	6.31	0.00	867	

Table F1 continued

Unit	Liquid composition											Feldspar composition							Equilibrium	T	H_2O
	Sample	SiO_2	TiO_2	Al_2O_3	FeO_t	MnO	MgO	CaO	Na_2O	K_2O	P_2O_5	Sample	SiO_2	Al_2O_3	FeO_t	CaO	Na_2O	K_2O	$\Delta Kd_{Or\text{-}Ab}$	(°C)	(wt. %)
Sy	TER30-1	64.71	0.59	15.90	4.85	0.21	0.36	0.83	7.51	4.97	0.08	TER30-7Fsp08	67.25	19.20	0.24	0.08	7.62	6.10	-0.01	869	5.44
Sy	TER30-1	64.71	0.59	15.90	4.85	0.21	0.36	0.83	7.51	4.97	0.08	TER29-1Fsp02	66.99	19.16	0.24	0.17	7.68	6.07	-0.03	869	5.56
Sy	TER30-1	64.71	0.59	15.90	4.85	0.21	0.36	0.83	7.51	4.97	0.08	TER29-1Fsp03	66.69	18.85	0.51	0.15	7.93	5.75	-0.02	873	4.44
Sy	TER30-1	64.71	0.59	15.90	4.85	0.21	0.36	0.83	7.51	4.97	0.08	TER29-1Fsp04	67.17	19.09	0.29	0.29	7.89	5.52	-0.05	874	5.17
Sy	TER30-1	64.71	0.59	15.90	4.85	0.21	0.36	0.83	7.51	4.97	0.08	TER29-1Fsp06	66.88	19.22	0.26	0.21	7.67	6.03	-0.04	869	5.46
Sy	TER30-1	64.71	0.59	15.90	4.85	0.21	0.36	0.83	7.51	4.97	0.08	TER29-1Fsp07	66.74	19.15	0.25	0.18	7.34	6.47	-0.05	864	5.64
Enc	TER10-1	64.30	0.52	16.26	4.67	0.18	0.47	0.86	7.65	5.00	0.07	Fspar 1	65.51	19.36	0.82	0.24	8.75	4.36	-0.06	891	3.18
Enc	TER10-1	64.30	0.52	16.26	4.67	0.18	0.47	0.86	7.65	5.00	0.07	Fspar 2	66.23	19.19	0.35	0.17	8.57	4.85	-0.01	887	4.44
Enc	TER10-1	64.30	0.52	16.26	4.67	0.18	0.47	0.86	7.65	5.00	0.07	Fspar 3	65.91	19.32	0.23	0.29	8.69	4.46	-0.07	890	4.71
Enc	TER10-1	64.30	0.52	16.26	4.67	0.18	0.47	0.86	7.65	5.00	0.07	Fspar 5	66.18	19.62	0.27	0.07	9.81	3.29	-0.44	904	3.68
Enc	TER10-1	64.30	0.52	16.26	4.67	0.18	0.47	0.86	7.65	5.00	0.07	Fspar 6	64.01	18.47	0.19	1.38	8.24	5.30	-0.40	875	4.09
Enc	TER10-1	64.30	0.52	16.26	4.67	0.18	0.47	0.86	7.65	5.00	0.07	Fspar 7	66.68	19.24	0.11	0.04	8.20	5.52	0.03	881	5.83
Enc	TER10-1	64.30	0.52	16.26	4.67	0.18	0.47	0.86	7.65	5.00	0.07	Fspar 12	66.27	19.16	0.35	0.04	8.03	6.08	0.01	876	4.09
Enc	TER10-1	64.30	0.52	16.26	4.67	0.18	0.47	0.86	7.65	5.00	0.07	Fspar 14	65.35	19.25	0.25	0.30	8.26	5.19	-0.05	882	4.93
Enc	TER10-1	64.30	0.52	16.26	4.67	0.18	0.47	0.86	7.65	5.00	0.07	Fspar 16	64.94	18.66	0.24	0.03	3.25	12.69	0.10	769	6.02
Enc	TER10-1	64.30	0.52	16.26	4.67	0.18	0.47	0.86	7.65	5.00	0.07	Fspar 20	66.37	19.22	0.45	0.51	9.32	4.10	-0.27	894	3.78
Enc	TER10-1	64.30	0.52	16.26	4.67	0.18	0.47	0.86	7.65	5.00	0.07	Fspar 6	64.71	19.23	0.07	0.11	9.11	4.43	-0.02	893	5.78
Enc	TER10-1	64.30	0.52	16.26	4.67	0.18	0.47	0.86	7.65	5.00	0.07	Fspar 10	64.89	19.05	0.11	0.05	8.36	5.52	0.03	882	5.87
Enc	TER10-1	64.30	0.52	16.26	4.67	0.18	0.47	0.86	7.65	5.00	0.07	Fspar 11	62.94	18.55	0.08	0.01	2.42	13.99	0.18	737	7.73
Enc	TER10-1	64.30	0.52	16.26	4.67	0.18	0.47	0.86	7.65	5.00	0.07	Fspar 12	65.36	18.75	0.41	0.09	8.05	5.67	0.01	879	4.30
Enc	TER10-1	64.30	0.52	16.26	4.67	0.18	0.47	0.86	7.65	5.00	0.07	Fspar 13	66.24	19.05	0.37	0.13	8.23	5.15	0.01	883	4.42
Enc	TER10-1	64.30	0.52	16.26	4.67	0.18	0.47	0.86	7.65	5.00	0.07	Fspar 14	65.38	18.91	0.36	0.12	8.07	5.59	0.00	879	4.58
Enc	TER10-1	64.30	0.52	16.26	4.67	0.18	0.47	0.86	7.65	5.00	0.07	Fspar 15	65.44	18.38	0.70	0.00	7.83	5.91	0.02	876	0.02
Enc	TER10-1	64.30	0.52	16.26	4.67	0.18	0.47	0.86	7.65	5.00	0.07	Fspar 17	65.06	18.47	0.58	0.04	8.13	5.77	0.02	879	3.11
Enc	TER10-1	64.30	0.52	16.26	4.67	0.18	0.47	0.86	7.65	5.00	0.07	Fspar 19	65.76	18.92	0.33	0.09	8.40	5.46	0.02	882	4.47
Enc	TER10-1	64.30	0.52	16.26	4.67	0.18	0.47	0.86	7.65	5.00	0.07	Fspar 20	65.07	18.58	0.55	0.00	7.92	5.95	0.02	877	
PNI	PNIGG08	65.44	0.58	15.47	4.76	0.21	0.37	0.84	7.30	4.94	0.09	T012Fsp2	64.82	19.46	0.26	0.85	8.66	4.01	-0.41	886	3.87
PNI	PNIGG08	65.44	0.58	15.47	4.76	0.21	0.37	0.84	7.30	4.94	0.09	T012Fsp3	64.76	19.37	0.27	0.70	8.53	4.42	-0.26	883	4.16
PNI	PNIGG08	65.44	0.58	15.47	4.76	0.21	0.37	0.84	7.30	4.94	0.09	T012Fsp4	63.83	19.56	0.27	0.95	8.59	3.99	-0.46	885	3.77
PNI	PNIGG08	65.44	0.58	15.47	4.76	0.21	0.37	0.84	7.30	4.94	0.09	T012Fsp5	66.07	19.07	0.23	0.39	8.35	5.01	-0.09	880	4.80
PNI	PNIGG08	65.44	0.58	15.47	4.76	0.21	0.37	0.84	7.30	4.94	0.09	T012Fsp6	65.98	18.74	0.29	0.37	8.73	4.87	-0.09	883	4.54
PNI	PNIGG08	65.44	0.58	15.47	4.76	0.21	0.37	0.84	7.30	4.94	0.09	T012Fsp7	65.95	19.04	0.26	0.50	8.54	4.64	-0.15	883	4.46
PNI	PNIGG08	65.44	0.58	15.47	4.76	0.21	0.37	0.84	7.30	4.94	0.09	T012Fsp8	66.33	20.24	0.29	0.95	8.46	3.86	-0.50	885	3.74
PNI	PNIGG08	65.44	0.58	15.47	4.76	0.21	0.37	0.84	7.30	4.94	0.09	T012Fsp9	63.89	19.38	0.28	0.69	8.81	4.15	-0.31	886	3.99
PNI	PNIGG08	65.44	0.58	15.47	4.76	0.21	0.37	0.84	7.30	4.94	0.09	T012Fsp10	66.16	19.39	0.31	0.74	8.86	4.07	-0.36	887	3.90

Table F1 continued

Unit	Liquid composition											Feldspar composition							Equilibrium	T	H_2O
	Sample	SiO_2	TiO_2	Al_2O_3	FeO_t	MnO	MgO	CaO	Na_2O	K_2O	P_2O_5	Sample	SiO_2	Al_2O_3	FeO_t	CaO	Na_2O	K_2O	ΔKd_{Or-Ab}	(°C)	(wt. %)
PNI	PNIGG08	65.44	0.58	15.47	4.76	0.21	0.37	0.84	7.30	4.94	0.09	T012Fsp11	66.65	19.40	0.29	0.55	8.35	4.66	-0.17	881	4.40
PNI	PNIGG08	65.44	0.58	15.47	4.76	0.21	0.37	0.84	7.30	4.94	0.09	T012Fsp13	65.16	19.44	0.28	0.93	8.83	3.96	-0.49	886	3.73
PNI	PNIGG08	65.44	0.58	15.47	4.76	0.21	0.37	0.84	7.30	4.94	0.09	T012Fsp14	65.35	19.24	0.26	0.64	8.48	4.37	-0.24	883	4.23
PNI	PNIGG08	65.44	0.58	15.47	4.76	0.21	0.37	0.84	7.30	4.94	0.09	T012Fsp16	66.09	19.46	0.26	0.62	8.12	4.60	-0.20	880	4.40
PNI	PNIGG08	65.44	0.58	15.47	4.76	0.21	0.37	0.84	7.30	4.94	0.09	T012Fsp17	66.32	19.27	0.27	0.41	8.26	4.74	-0.11	881	4.62
PNI	PNIGG08	65.44	0.58	15.47	4.76	0.21	0.37	0.84	7.30	4.94	0.09	T012Fsp18	65.50	19.74	0.25	0.97	8.61	3.93	-0.49	885	3.78
PNI	PNIGG08	65.44	0.58	15.47	4.76	0.21	0.37	0.84	7.30	4.94	0.09	T012Fsp19	66.14	19.36	0.25	0.61	8.52	4.40	-0.22	884	4.30
PNI	PNIGG08	65.44	0.58	15.47	4.76	0.21	0.37	0.84	7.30	4.94	0.09	T012Fsp20	66.45	19.24	0.30	0.42	8.08	4.95	-0.10	879	4.63
PNI	PNIGG08	65.44	0.58	15.47	4.76	0.21	0.37	0.84	7.30	4.94	0.09	T012Fsp21	66.52	19.63	0.27	0.56	8.46	4.63	-0.18	882	4.40
PNI	PNIGG08	65.44	0.58	15.47	4.76	0.21	0.37	0.84	7.30	4.94	0.09	T012Fsp22	65.49	19.92	0.26	0.83	8.61	4.01	-0.40	886	3.91
PNI	PNIGG08	65.44	0.58	15.47	4.76	0.21	0.37	0.84	7.30	4.94	0.09	T012Fsp23	65.78	19.35	0.28	0.62	8.40	4.46	-0.21	883	4.26
PNI	PNIGG08	65.44	0.58	15.47	4.76	0.21	0.37	0.84	7.30	4.94	0.09	T012Fsp24	66.19	19.83	0.31	0.68	8.44	4.29	-0.26	884	4.11
PNI	PNIGG08	65.44	0.58	15.47	4.76	0.21	0.37	0.84	7.30	4.94	0.09	T012Fsp25	65.71	19.69	0.28	0.73	8.75	4.17	-0.33	886	4.00
PNI	PNIGG08	65.44	0.58	15.47	4.76	0.21	0.37	0.84	7.30	4.94	0.09	T012Fsp26	65.92	19.69	0.29	0.61	8.54	4.25	-0.24	885	4.16
PNI	PNIGG08	65.44	0.58	15.47	4.76	0.21	0.37	0.84	7.30	4.94	0.09	T012Fsp27	66.53	19.27	0.29	0.48	8.58	4.74	-0.14	882	4.44
PNI	PNIGG08	65.44	0.58	15.47	4.76	0.21	0.37	0.84	7.30	4.94	0.09	T012Fsp28	65.68	19.52	0.31	0.55	8.51	4.30	-0.21	885	4.19
PNI	PNIGG08	65.44	0.58	15.47	4.76	0.21	0.37	0.84	7.30	4.94	0.09	T012Fsp29	64.63	19.17	0.29	0.36	8.08	4.98	-0.08	879	4.67
PNI	PNIGG08	65.44	0.58	15.47	4.76	0.21	0.37	0.84	7.30	4.94	0.09	T012Fsp30	64.13	19.38	0.28	0.57	8.40	4.47	-0.19	883	4.28
PNI	PNIGG08	65.44	0.58	15.47	4.76	0.21	0.37	0.84	7.30	4.94	0.09	T012Fsp31	65.31	19.88	0.26	0.92	8.61	3.86	-0.49	886	3.78
PNI	PNIGG08	65.44	0.58	15.47	4.76	0.21	0.37	0.84	7.30	4.94	0.09	T012Fsp32	65.33	19.52	0.30	0.64	8.62	4.27	-0.26	885	4.10
PNI	PNIGG08	65.44	0.58	15.47	4.76	0.21	0.37	0.84	7.30	4.94	0.09	T012Fsp33	64.69	19.43	0.28	0.77	8.71	4.19	-0.34	885	3.97
PNI	PNIGG08	65.44	0.58	15.47	4.76	0.21	0.37	0.84	7.30	4.94	0.09	T012Fsp34	66.76	19.25	0.29	0.38	8.31	4.98	-0.09	880	4.65
PNI	PNIGG08	65.44	0.58	15.47	4.76	0.21	0.37	0.84	7.30	4.94	0.09	T012Fsp35	66.55	19.88	0.27	0.62	8.32	4.24	-0.24	884	4.23
PNI	PNIGG08	65.44	0.58	15.47	4.76	0.21	0.37	0.84	7.30	4.94	0.09	T012Fsp36	66.41	19.70	0.25	0.63	8.40	4.49	-0.22	882	4.33
PNI	PNIGG08	65.44	0.58	15.47	4.76	0.21	0.37	0.84	7.30	4.94	0.09	T012Fsp38	66.09	19.30	0.29	0.49	8.31	4.73	-0.14	881	4.46
PNI	PNIGG08	65.44	0.58	15.47	4.76	0.21	0.37	0.84	7.30	4.94	0.09	T012Fsp39	66.30	19.84	0.27	0.65	8.40	4.46	-0.23	882	4.26
PNI	PNIGG08	65.44	0.58	15.47	4.76	0.21	0.37	0.84	7.30	4.94	0.09	S003Fsp40	66.92	19.52	0.25	0.37	6.92	6.84	-0.11	857	5.45
PNI	PNIGG08	65.44	0.58	15.47	4.76	0.21	0.37	0.84	7.30	4.94	0.09	T012IMI01_fsp	67.43	19.57	0.29	0.47	8.24	4.81	-0.13	880	4.54
PNI	PNIGG08	65.44	0.58	15.47	4.76	0.21	0.37	0.84	7.30	4.94	0.09	T012IMI02_fsp	67.01	19.40	0.30	0.40	8.19	4.89	-0.10	880	4.62
PNI	PNIGG08	65.44	0.58	15.47	4.76	0.21	0.37	0.84	7.30	4.94	0.09	T012IMI03_fsp	67.05	19.40	0.34	0.41	8.06	4.90	-0.10	879	4.52
PNI	PNIGG08	65.44	0.58	15.47	4.76	0.21	0.37	0.84	7.30	4.94	0.09	T012IMI04_fsp	65.68	19.51	0.29	0.71	8.45	4.36	-0.27	883	4.13
PNI	PNIGG08	65.44	0.58	15.47	4.76	0.21	0.37	0.84	7.30	4.94	0.09	T012IMI05_fsp	66.13	18.81	0.31	0.31	8.50	4.94	-0.06	881	4.60
PNI	PNIGG08	65.44	0.58	15.47	4.76	0.21	0.37	0.84	7.30	4.94	0.09	T012IMI07_fsp	64.91	19.62	0.26	0.47	8.56	4.58	-0.15	883	4.44
PNI	PNIGG08	65.44	0.58	15.47	4.76	0.21	0.37	0.84	7.30	4.94	0.09	T012IMI08_fsp	67.20	19.72	0.26	0.51	8.30	4.54	-0.16	882	4.49
PNI	PNIGG08	65.44	0.58	15.47	4.76	0.21	0.37	0.84	7.30	4.94	0.09	T012IMI09_fsp	65.86	19.60	0.32	0.46	8.15	4.69	-0.13	881	4.45

Table F1 continued

Unit	Liquid composition											Feldspar composition							Equilibrium	T	H_2O
	Sample	SiO_2	TiO_2	Al_2O_3	FeO_t	MnO	MgO	CaO	Na_2O	K_2O	P_2O_5	Sample	SiO_2	Al_2O_3	FeO_t	CaO	Na_2O	K_2O	ΔKd_{Or-Ab}	(°C)	(wt. %)
PNI	PNIGG08	65.44	0.58	15.47	4.76	0.21	0.37	0.84	7.30	4.94	0.09	T012IMI10_fsp	67.63	19.81	0.32	0.59	8.28	4.61	-0.19	881	4.31
PNI	PNIGG08	65.44	0.58	15.47	4.76	0.21	0.37	0.84	7.30	4.94	0.09	PNIFsp01	66.83	19.47	0.32	0.47	8.47	4.52	-0.15	883	4.33
PNI	PNIGG08	65.44	0.58	15.47	4.76	0.21	0.37	0.84	7.30	4.94	0.09	PNIFsp02	67.27	19.52	0.33	0.42	8.24	4.96	-0.10	879	4.53
PNI	PNIGG08	65.44	0.58	15.47	4.76	0.21	0.37	0.84	7.30	4.94	0.09	PNIFsp03	66.81	19.51	0.29	0.47	8.48	4.64	-0.14	883	4.45
PNI	PNIGG08	65.44	0.58	15.47	4.76	0.21	0.37	0.84	7.30	4.94	0.09	PNIFsp05	66.76	19.34	0.27	0.47	8.37	4.81	-0.13	881	4.56
GVI	GVIGG15	65.40	0.65	16.25	3.68	0.21	0.46	0.46	7.71	5.10	0.07	GVIFsp1	64.83	18.44	0.32	0.41	7.90	5.07	0.26	820	5.82
GVI	GVIGG15	65.40	0.65	16.25	3.68	0.21	0.46	0.46	7.71	5.10	0.07	GVIFsp2	65.99	19.71	0.41	0.72	8.26	4.56	0.18	824	5.23
GVI	GVIGG15	65.40	0.65	16.25	3.68	0.21	0.46	0.46	7.71	5.10	0.07	GVIFsp3	66.68	19.46	0.31	0.58	8.11	4.96	0.22	821	5.67
GVI	GVIGG15	65.40	0.65	16.25	3.68	0.21	0.46	0.46	7.71	5.10	0.07	GVIFsp4	66.52	19.42	0.34	0.53	8.17	4.81	0.25	822	5.59
GVI	GVIGG15	65.40	0.65	16.25	3.68	0.21	0.46	0.46	7.71	5.10	0.07	GVIFsp6	67.84	19.62	0.30	0.47	7.81	4.95	0.24	820	5.85
GVI	GVIGG15	65.40	0.65	16.25	3.68	0.21	0.46	0.46	7.71	5.10	0.07	GVIFsp7	67.59	19.85	0.31	0.56	7.94	4.91	0.22	821	5.72
GVI	GVIGG15	65.40	0.65	16.25	3.68	0.21	0.46	0.46	7.71	5.10	0.07	GVIFsp8	67.76	19.75	0.34	0.52	7.95	5.08	0.23	820	5.74
GVI	GVIGG15	65.40	0.65	16.25	3.68	0.21	0.46	0.46	7.71	5.10	0.07	GVIFsp11	67.40	19.67	0.33	0.56	7.79	4.82	0.22	820	5.67
GVI	GVIGG15	65.40	0.65	16.25	3.68	0.21	0.46	0.46	7.71	5.10	0.07	GVIFsp12	66.55	19.65	0.32	0.57	7.84	4.57	0.22	822	5.58
GVI	GVIGG15	65.40	0.65	16.25	3.68	0.21	0.46	0.46	7.71	5.10	0.07	GVIFsp13	66.17	19.48	0.33	0.57	7.96	4.73	0.22	822	5.58
GVI	GVIGG15	65.40	0.65	16.25	3.68	0.21	0.46	0.46	7.71	5.10	0.07	GVIFsp14	66.71	19.40	0.29	0.61	7.85	4.71	0.20	821	5.66
GVI	GVIGG15	65.40	0.65	16.25	3.68	0.21	0.46	0.46	7.71	5.10	0.07	GVIFsp15	66.26	19.35	0.31	0.65	8.19	4.82	0.20	822	5.56
GVI	GVIGG15	65.40	0.65	16.25	3.68	0.21	0.46	0.46	7.71	5.10	0.07	GVIFsp01	66.42	19.34	0.30	0.45	8.08	4.94	0.27	822	5.79
GVI	GVIGG15	65.40	0.65	16.25	3.68	0.21	0.46	0.46	7.71	5.10	0.07	GVIFsp02	66.40	19.70	0.27	0.64	8.19	4.65	0.21	823	5.58
GVI	GVIGG15	65.40	0.65	16.25	3.68	0.21	0.46	0.46	7.71	5.10	0.07	GVIFsp03	66.27	19.25	0.35	0.37	7.90	5.15	0.27	820	5.81
GVI	GVIGG15	65.40	0.65	16.25	3.68	0.21	0.46	0.46	7.71	5.10	0.07	GVIFsp04	66.51	19.71	0.33	0.47	8.12	4.85	0.27	822	5.67
GVI	GVIGG15	65.40	0.65	16.25	3.68	0.21	0.46	0.46	7.71	5.10	0.07	GVIFsp05	66.49	19.36	0.31	0.49	8.05	5.00	0.25	821	5.78
GVI	GVIGG15	65.40	0.65	16.25	3.68	0.21	0.46	0.46	7.71	5.10	0.07	93 / 1 .	67.22	17.76	0.25	0.64	8.10	4.60	0.20	823	5.62
GVI	GVIGG15	65.40	0.65	16.25	3.68	0.21	0.46	0.46	7.71	5.10	0.07	93 / 2 .	66.46	18.13	0.26	0.63	8.13	4.46	0.21	824	5.55
GVI	GVIGG15	65.40	0.65	16.25	3.68	0.21	0.46	0.46	7.71	5.10	0.07	93 / 3 .	68.03	18.31	0.34	0.64	7.37	4.34	0.18	821	5.53
GVI	GVIGG15	65.40	0.65	16.25	3.68	0.21	0.46	0.46	7.71	5.10	0.07	93 / 4 .	66.14	17.94	0.26	0.63	7.94	4.77	0.20	821	5.69
GVI	GVIGG15	65.40	0.65	16.25	3.68	0.21	0.46	0.46	7.71	5.10	0.07	93 / 5 .	66.36	18.12	0.28	0.71	8.03	4.51	0.17	823	5.49
GVI	GVIGG15	65.40	0.65	16.25	3.68	0.21	0.46	0.46	7.71	5.10	0.07	93 / 6 .	66.94	18.21	0.27	0.63	8.07	4.61	0.21	823	5.60
GVI	GVIGG15	65.40	0.65	16.25	3.68	0.21	0.46	0.46	7.71	5.10	0.07	93 / 7 .	66.81	18.08	0.25	0.64	8.27	4.51	0.21	824	5.56
GVI	GVIGG15	65.40	0.65	16.25	3.68	0.21	0.46	0.46	7.71	5.10	0.07	93 / 8 .	66.52	18.18	0.30	0.69	8.16	4.39	0.19	824	5.41
GVI	GVIGG15	65.40	0.65	16.25	3.68	0.21	0.46	0.46	7.71	5.10	0.07	93 / 9 .	67.28	18.18	0.28	0.62	8.13	4.53	0.22	824	5.57
GVI	GVIGG15	65.40	0.65	16.25	3.68	0.21	0.46	0.46	7.71	5.10	0.07	93 / 10 .	67.58	18.21	0.26	0.67	8.05	4.45	0.19	824	5.55
GVI	GVIGG15	65.40	0.65	16.25	3.68	0.21	0.46	0.46	7.71	5.10	0.07	94 / 1 .	66.82	17.64	0.31	0.47	7.95	5.06	0.25	820	5.82
GVI	GVIGG15	65.40	0.65	16.25	3.68	0.21	0.46	0.46	7.71	5.10	0.07	96 / 5 .	65.70	17.30	0.31	0.54	8.05	4.98	0.23	821	5.71
GVI	GVIGG15	65.40	0.65	16.25	3.68	0.21	0.46	0.46	7.71	5.10	0.07	96 / 8 .	65.61	17.62	0.28	0.42	7.91	5.10	0.26	820	5.94

Table F1 continued

Unit	Liquid composition											Feldspar composition							Equilibrium	T	H_2O
	Sample	SiO_2	TiO_2	Al_2O_3	FeO_t	MnO	MgO	CaO	Na_2O	K_2O	P_2O_5	Sample	SiO_2	Al_2O_3	FeO_t	CaO	Na_2O	K_2O	ΔKd_{Or-Ab}	(°C)	(wt. %)
GVI	GVIGG15	65.40	0.65	16.25	3.68	0.21	0.46	0.46	7.71	5.10	0.07	96 / 9 .	65.64	18.34	0.32	0.49	7.89	5.08	0.24	819	5.79
GVI	GVIGG15	65.40	0.65	16.25	3.68	0.21	0.46	0.46	7.71	5.10	0.07	96 / 10 .	67.47	17.91	0.30	0.45	7.93	5.01	0.25	820	5.86
GVI	GVIGG15	65.40	0.65	16.25	3.68	0.21	0.46	0.46	7.71	5.10	0.07	103 / 1 .	65.57	18.06	0.44	0.61	7.69	4.67	0.20	821	5.39
GVI	GVIGG15	65.40	0.65	16.25	3.68	0.21	0.46	0.46	7.71	5.10	0.07	103 / 2 .	67.40	17.97	0.35	0.52	8.06	4.93	0.24	821	5.65
GVI	GVIGG15	65.40	0.65	16.25	3.68	0.21	0.46	0.46	7.71	5.10	0.07	103 / 3 .	66.63	17.99	0.32	0.41	8.02	5.02	0.27	821	5.82
GVI	GVIGG15	65.40	0.65	16.25	3.68	0.21	0.46	0.46	7.71	5.10	0.07	103 / 4 .	66.83	17.82	0.35	0.41	7.82	5.14	0.25	819	5.82
GVI	GVIGG15	65.40	0.65	16.25	3.68	0.21	0.46	0.46	7.71	5.10	0.07	103 / 5 .	67.99	17.87	0.36	0.41	7.81	5.22	0.25	819	5.84
GVI	GVIGG15	65.40	0.65	16.25	3.68	0.21	0.46	0.46	7.71	5.10	0.07	103 / 6 .	67.84	17.74	0.33	0.51	7.96	4.99	0.24	820	5.73
GVI	GVIGG15	65.40	0.65	16.25	3.68	0.21	0.46	0.46	7.71	5.10	0.07	103 / 7 .	67.56	18.18	0.31	0.52	7.94	4.98	0.23	820	5.77
GVI	GVIGG15	65.40	0.65	16.25	3.68	0.21	0.46	0.46	7.71	5.10	0.07	103 / 8 .	67.86	18.34	0.30	0.54	8.07	4.90	0.23	821	5.74
GVI	GVIGG15	65.40	0.65	16.25	3.68	0.21	0.46	0.46	7.71	5.10	0.07	103 / 9 .	67.60	18.42	0.32	0.58	8.10	4.78	0.22	822	5.62
GVI	GVIGG15	65.40	0.65	16.25	3.68	0.21	0.46	0.46	7.71	5.10	0.07	103 / 10 .	67.82	18.44	0.33	0.61	8.14	4.78	0.21	822	5.57
Ign-i	TER10-2	64.56	0.58	15.47	5.39	0.23	0.37	0.97	7.43	4.93	0.09	T001Fsp1	65.62	19.15	0.29	0.13	7.50	6.16	-0.10	881	4.89
Ign-i	TER10-2	64.56	0.58	15.47	5.39	0.23	0.37	0.97	7.43	4.93	0.09	T001Fsp2	67.34	19.13	0.31	0.13	7.57	6.35	-0.10	880	4.83
Ign-i	TER10-2	64.56	0.58	15.47	5.39	0.23	0.37	0.97	7.43	4.93	0.09	T001Fsp3	66.72	19.12	0.28	0.24	7.78	5.96	-0.12	883	4.91
Ign-i	TER10-2	64.56	0.58	15.47	5.39	0.23	0.37	0.97	7.43	4.93	0.09	T001Fsp4	66.77	19.05	0.30	0.13	7.48	6.25	-0.10	880	4.88
Ign-i	TER10-2	64.56	0.58	15.47	5.39	0.23	0.37	0.97	7.43	4.93	0.09	T001Fsp5	66.66	18.93	0.28	0.11	7.59	6.09	-0.09	882	4.82
Ign-i	TER10-2	64.56	0.58	15.47	5.39	0.23	0.37	0.97	7.43	4.93	0.09	T001Fsp6	66.42	18.99	0.29	0.11	7.91	5.83	-0.09	886	4.69
Ign-i	TER10-2	64.56	0.58	15.47	5.39	0.23	0.37	0.97	7.43	4.93	0.09	T001Fsp7	65.68	18.86	0.29	0.11	7.75	6.08	-0.09	883	4.77
Ign-i	TER10-2	64.56	0.58	15.47	5.39	0.23	0.37	0.97	7.43	4.93	0.09	T001Fsp8	65.42	18.77	0.32	0.06	7.65	6.13	-0.08	882	4.38
Ign-i	TER10-2	64.56	0.58	15.47	5.39	0.23	0.37	0.97	7.43	4.93	0.09	T001Fsp9	66.80	18.85	0.25	0.09	7.65	6.16	-0.09	882	4.96
Ign-i	TER10-2	64.56	0.58	15.47	5.39	0.23	0.37	0.97	7.43	4.93	0.09	T001Fsp10	65.94	19.15	0.28	0.10	7.83	6.18	-0.09	883	4.76
Ign-i	TER10-2	64.56	0.58	15.47	5.39	0.23	0.37	0.97	7.43	4.93	0.09	T001Fsp11	67.31	19.11	0.27	0.13	7.64	6.07	-0.10	882	4.95
Ign-i	TER10-2	64.56	0.58	15.47	5.39	0.23	0.37	0.97	7.43	4.93	0.09	T001Fsp12	67.30	19.03	0.30	0.12	7.54	6.14	-0.10	881	4.83
Ign-i	TER10-2	64.56	0.58	15.47	5.39	0.23	0.37	0.97	7.43	4.93	0.09	T001Fsp13	67.30	19.33	0.27	0.20	7.93	5.76	-0.11	886	4.89
Ign-i	TER10-2	64.56	0.58	15.47	5.39	0.23	0.37	0.97	7.43	4.93	0.09	T001Fsp14	67.66	19.11	0.29	0.09	7.55	6.15	-0.09	882	4.77
Ign-i	TER10-2	64.56	0.58	15.47	5.39	0.23	0.37	0.97	7.43	4.93	0.09	T001Fsp15	66.98	19.08	0.26	0.14	7.79	5.95	-0.10	884	4.96
Ign-i	TER10-2	64.56	0.58	15.47	5.39	0.23	0.37	0.97	7.43	4.93	0.09	T001IMI01_fsp	65.84	18.58	0.39	0.07	7.89	5.92	-0.08	886	4.01
Ign-i	TER10-2	64.56	0.58	15.47	5.39	0.23	0.37	0.97	7.43	4.93	0.09	Ig-iFsp05	66.55	19.65	0.21	0.70	8.53	4.22	-0.41	898	4.01
Ign-i	TER10-2	64.56	0.58	15.47	5.39	0.23	0.37	0.97	7.43	4.93	0.09	Ig-iFsp06	66.21	18.82	0.33	0.11	7.50	6.07	-0.10	882	4.64

Table F2: Results of two-oxide thermometry for trhe Lajes-Angra Ignimbrite Formation (LAI)

LAI Pair identifier	Phase	TiO_2	Al_2O_3	Fe_2O_3	FeO	MnO	MgO	Cr_2O_3	Sum	log(Mg/Mn)	T	fO_2
A1	Magnetite	22.56	0.60	25.60	48.74	1.78	1.12	0.02	100.43	0.043	813	-15.43
	Ilmenite	51.10	0.07	4.84	40.64	2.30	1.68	0.02	100.66	0.107		
A2	Magnetite	22.56	0.60	25.60	48.74	1.78	1.12	0.02	100.43	0.043	837	-14.78
	Ilmenite	51.10	0.07	5.30	40.78	2.32	1.59	0.01	101.17	0.080		
A3	Magnetite	22.56	0.60	25.60	48.74	1.78	1.12	0.02	100.43	0.043	837	-14.77
	Ilmenite	51.03	0.04	5.30	40.79	2.32	1.55	0.02	101.05	0.070		
A4	Magnetite	22.56	0.60	25.60	48.74	1.78	1.12	0.02	100.43	0.043	866	-14.03
	Ilmenite	50.12	0.07	5.76	39.82	2.30	1.65	0.01	99.73	0.102		
A5	Magnetite	22.56	0.60	25.60	48.74	1.78	1.12	0.02	100.43	0.043	849	-14.46
	Ilmenite	50.44	0.07	5.46	40.18	2.28	1.62	0.00	100.05	0.098		
A6	Magnetite	22.56	0.60	25.60	48.74	1.78	1.12	0.02	100.43	0.043	794	-15.95
	Ilmenite	51.25	0.05	4.54	40.83	2.28	1.66	0.02	100.63	0.109		
A7	Magnetite	22.56	0.60	25.60	48.74	1.78	1.12	0.02	100.43	0.043	841	-14.67
	Ilmenite	51.09	0.05	5.35	40.51	2.28	1.76	0.01	101.06	0.134		
A8	Magnetite	22.56	0.60	25.60	48.74	1.78	1.12	0.02	100.43	0.043	834	-14.84
	Ilmenite	51.14	0.06	5.25	40.70	2.28	1.68	0.03	101.14	0.112		
B1	Magnetite	22.07	0.61	26.06	48.06	1.79	1.12	0.01	99.72	0.043	806	-15.57
	Ilmenite	51.10	0.07	4.84	40.64	2.30	1.68	0.02	100.66	0.107		
B2	Magnetite	22.07	0.61	26.06	48.06	1.79	1.12	0.01	99.72	0.043	829	-14.92
	Ilmenite	51.10	0.07	5.30	40.78	2.32	1.59	0.01	101.17	0.080		
B3	Magnetite	22.07	0.61	26.06	48.06	1.79	1.12	0.01	99.72	0.043	829	-14.92
	Ilmenite	51.03	0.04	5.30	40.79	2.32	1.55	0.02	101.05	0.070		
B4	Magnetite	22.07	0.61	26.06	48.06	1.79	1.12	0.01	99.72	0.043	857	-14.18
	Ilmenite	50.12	0.07	5.76	39.82	2.30	1.65	0.01	99.73	0.102		
B5	Magnetite	22.07	0.61	26.06	48.06	1.79	1.12	0.01	99.72	0.043	841	-14.61
	Ilmenite	50.44	0.07	5.46	40.18	2.28	1.62	0.00	100.05	0.098		
B6	Magnetite	22.07	0.61	26.06	48.06	1.79	1.12	0.01	99.72	0.043	787	-16.09
	Ilmenite	51.25	0.05	4.54	40.83	2.28	1.66	0.02	100.63	0.109		
B7	Magnetite	22.07	0.61	26.06	48.06	1.79	1.12	0.01	99.72	0.043	833	-14.82
	Ilmenite	51.09	0.05	5.35	40.51	2.28	1.76	0.01	101.06	0.134		
B8	Magnetite	22.07	0.61	26.06	48.06	1.79	1.12	0.01	99.72	0.043	827	-14.99
	Ilmenite	51.14	0.06	5.25	40.70	2.28	1.68	0.03	101.14	0.112		
C1	Magnetite	22.24	0.62	26.04	48.45	1.77	1.08	0.00	100.20	0.031	807	-15.54
	Ilmenite	51.10	0.07	4.84	40.64	2.30	1.68	0.02	100.66	0.107		
C2	Magnetite	22.24	0.62	26.04	48.45	1.77	1.08	0.00	100.20	0.031	831	-14.88
	Ilmenite	51.10	0.07	5.30	40.78	2.32	1.59	0.01	101.17	0.080		
C3	Magnetite	22.24	0.62	26.04	48.45	1.77	1.08	0.00	100.20	0.031	831	-14.88
	Ilmenite	51.03	0.04	5.30	40.79	2.32	1.55	0.02	101.05	0.070		

Table F2 continued

LAI Pair identifier	Phase	TiO_2	Al_2O_3	Fe_2O_3	FeO	MnO	MgO	Cr_2O_3	Sum	log(Mg/Mn)	T	fO_2
C4	Magnetite	22.24	0.62	26.04	48.45	1.77	1.08	0.00	100.20	0.031	860	-14.14
	Ilmenite	50.12	0.07	5.76	39.82	2.30	1.65	0.01	99.73	0.102		
C5	Magnetite	22.24	0.62	26.04	48.45	1.77	1.08	0.00	100.20	0.031	843	-14.57
	Ilmenite	50.44	0.07	5.46	40.18	2.28	1.62	0.00	100.05	0.098		
C6	Magnetite	22.24	0.62	26.04	48.45	1.77	1.08	0.00	100.20	0.031	789	-16.06
	Ilmenite	51.25	0.05	4.54	40.83	2.28	1.66	0.02	100.63	0.109		
C7	Magnetite	22.24	0.62	26.04	48.45	1.77	1.08	0.00	100.20	0.031	835	-14.78
	Ilmenite	51.09	0.05	5.35	40.51	2.28	1.76	0.01	101.06	0.134		
C8	Magnetite	22.24	0.62	26.04	48.45	1.77	1.08	0.00	100.20	0.031	829	-14.95
	Ilmenite	51.14	0.06	5.25	40.70	2.28	1.68	0.03	101.14	0.112		
D1	Magnetite	22.38	0.61	25.98	48.52	1.81	1.14	0.00	100.44	0.042	808	-15.52
	Ilmenite	51.10	0.07	4.84	40.64	2.30	1.68	0.02	100.66	0.107		
D2	Magnetite	22.38	0.61	25.98	48.52	1.81	1.14	0.00	100.44	0.042	832	-14.87
	Ilmenite	51.10	0.07	5.30	40.78	2.32	1.59	0.01	101.17	0.080		
D3	Magnetite	22.38	0.61	25.98	48.52	1.81	1.14	0.00	100.44	0.042	832	-14.86
	Ilmenite	51.03	0.04	5.30	40.79	2.32	1.55	0.02	101.05	0.070		
D4	Magnetite	22.38	0.61	25.98	48.52	1.81	1.14	0.00	100.44	0.042	861	-14.12
	Ilmenite	50.12	0.07	5.76	39.82	2.30	1.65	0.01	99.73	0.102		
D5	Magnetite	22.38	0.61	25.98	48.52	1.81	1.14	0.00	100.44	0.042	844	-14.55
	Ilmenite	50.44	0.07	5.46	40.18	2.28	1.62	0.00	100.05	0.098		
D6	Magnetite	22.38	0.61	25.98	48.52	1.81	1.14	0.00	100.44	0.042	790	-16.04
	Ilmenite	51.25	0.05	4.54	40.83	2.28	1.66	0.02	100.63	0.109		
D7	Magnetite	22.38	0.61	25.98	48.52	1.81	1.14	0.00	100.44	0.042	836	-14.76
	Ilmenite	51.09	0.05	5.35	40.51	2.28	1.76	0.01	101.06	0.134		
D8	Magnetite	22.38	0.61	25.98	48.52	1.81	1.14	0.00	100.44	0.042	830	-14.93
	Ilmenite	51.14	0.06	5.25	40.70	2.28	1.68	0.03	101.14	0.112		
E1	Magnetite	22.37	0.62	26.19	48.69	1.81	1.10	0.03	100.80	0.030	807	-15.54
	Ilmenite	51.10	0.07	4.84	40.64	2.30	1.68	0.02	100.66	0.107		
E2	Magnetite	22.37	0.62	26.19	48.69	1.81	1.10	0.03	100.80	0.030	831	-14.88
	Ilmenite	51.10	0.07	5.30	40.78	2.32	1.59	0.01	101.17	0.080		
E3	Magnetite	22.37	0.62	26.19	48.69	1.81	1.10	0.03	100.80	0.030	831	-14.88
	Ilmenite	51.03	0.04	5.30	40.79	2.32	1.55	0.02	101.05	0.070		
E4	Magnetite	22.37	0.62	26.19	48.69	1.81	1.10	0.03	100.80	0.030	860	-14.14
	Ilmenite	50.12	0.07	5.76	39.82	2.30	1.65	0.01	99.73	0.102		
E5	Magnetite	22.37	0.62	26.19	48.69	1.81	1.10	0.03	100.80	0.030	843	-14.57
	Ilmenite	50.44	0.07	5.46	40.18	2.28	1.62	0.00	100.05	0.098		
E6	Magnetite	22.37	0.62	26.19	48.69	1.81	1.10	0.03	100.80	0.030	789	-16.06
	Ilmenite	51.25	0.05	4.54	40.83	2.28	1.66	0.02	100.63	0.109		

Table F2 continued

LAI Pair identifier	Phase	TiO_2	Al_2O_3	Fe_2O_3	FeO	MnO	MgO	Cr_2O_3	Sum	log(Mg/Mn)	T	fO_2
D7	Magnetite	22.37	0.62	26.19	48.69	1.81	1.10	0.03	100.80	0.030	835	-14.78
	Ilmenite	51.09	0.05	5.35	40.51	2.28	1.76	0.01	101.06	0.134		
E8	Magnetite	22.37	0.62	26.19	48.69	1.81	1.10	0.03	100.80	0.030	829	-14.95
	Ilmenite	51.14	0.06	5.25	40.70	2.28	1.68	0.03	101.14	0.112		
F1	Magnetite	22.39	0.63	25.90	48.56	1.82	1.11	0.01	100.43	0.030	809	-15.50
	Ilmenite	51.10	0.07	4.84	40.64	2.30	1.68	0.02	100.66	0.107		
F2	Magnetite	22.39	0.63	25.90	48.56	1.82	1.11	0.01	100.43	0.030	833	-14.84
	Ilmenite	51.10	0.07	5.30	40.78	2.32	1.59	0.01	101.17	0.080		
F3	Magnetite	22.39	0.63	25.90	48.56	1.82	1.11	0.01	100.43	0.030	833	-14.84
	Ilmenite	51.03	0.04	5.30	40.79	2.32	1.55	0.02	101.05	0.070		
F4	Magnetite	22.39	0.63	25.90	48.56	1.82	1.11	0.01	100.43	0.030	862	-14.10
	Ilmenite	50.12	0.07	5.76	39.82	2.30	1.65	0.01	99.73	0.102		
F5	Magnetite	22.39	0.63	25.90	48.56	1.82	1.11	0.01	100.43	0.030	845	-14.53
	Ilmenite	50.44	0.07	5.46	40.18	2.28	1.62	0.00	100.05	0.098		
F6	Magnetite	22.39	0.63	25.90	48.56	1.82	1.11	0.01	100.43	0.030	791	-16.02
	Ilmenite	51.25	0.05	4.54	40.83	2.28	1.66	0.02	100.63	0.109		
F7	Magnetite	22.39	0.63	25.90	48.56	1.82	1.11	0.01	100.43	0.030	837	-14.74
	Ilmenite	51.09	0.05	5.35	40.51	2.28	1.76	0.01	101.06	0.134		
F8	Magnetite	22.39	0.63	25.90	48.56	1.82	1.11	0.01	100.43	0.030	831	-14.91
	Ilmenite	51.14	0.06	5.25	40.70	2.28	1.68	0.03	101.14	0.112		
G1	Magnetite	22.42	0.58	25.80	48.56	1.79	1.12	0.03	100.29	0.042	810	-15.48
	Ilmenite	51.10	0.07	4.84	40.64	2.30	1.68	0.02	100.66	0.107		
G2	Magnetite	22.42	0.58	25.80	48.56	1.79	1.12	0.03	100.29	0.042	834	-14.83
	Ilmenite	51.10	0.07	5.30	40.78	2.32	1.59	0.01	101.17	0.080		
G3	Magnetite	22.42	0.58	25.80	48.56	1.79	1.12	0.03	100.29	0.042	834	-14.82
	Ilmenite	51.03	0.04	5.30	40.79	2.32	1.55	0.02	101.05	0.070		
G4	Magnetite	22.42	0.58	25.80	48.56	1.79	1.12	0.03	100.29	0.042	863	-14.08
	Ilmenite	50.12	0.07	5.76	39.82	2.30	1.65	0.01	99.73	0.102		
G5	Magnetite	22.42	0.58	25.80	48.56	1.79	1.12	0.03	100.29	0.042	846	-14.51
	Ilmenite	50.44	0.07	5.46	40.18	2.28	1.62	0.00	100.05	0.098		
G6	Magnetite	22.42	0.58	25.80	48.56	1.79	1.12	0.03	100.29	0.042	792	-16.01
	Ilmenite	51.25	0.05	4.54	40.83	2.28	1.66	0.02	100.63	0.109		
G7	Magnetite	22.42	0.58	25.80	48.56	1.79	1.12	0.03	100.29	0.042	838	-14.73
	Ilmenite	51.09	0.05	5.35	40.51	2.28	1.76	0.01	101.06	0.134		
G8	Magnetite	22.42	0.58	25.80	48.56	1.79	1.12	0.03	100.29	0.042	831	-14.90
	Ilmenite	51.14	0.06	5.25	40.70	2.28	1.68	0.03	101.14	0.112		
H1	Magnetite	22.31	0.61	25.89	48.54	1.77	1.06	0.01	100.19	0.022	809	-15.50
	Ilmenite	51.10	0.07	4.84	40.64	2.30	1.68	0.02	100.66	0.107		

Table F2 continued

LAI Pair identifier	Phase	TiO_2	Al_2O_3	Fe_2O_3	FeO	MnO	MgO	Cr_2O_3	Sum	log(Mg/Mn)	T	fO_2
H2	Magnetite	22.31	0.61	25.89	48.54	1.77	1.06	0.01	100.19	0.022	833	-14.85
	Ilmenite	51.10	0.07	5.30	40.78	2.32	1.59	0.01	101.17	0.080		
H3	Magnetite	22.31	0.61	25.89	48.54	1.77	1.06	0.01	100.19	0.022	833	-14.84
	Ilmenite	51.03	0.04	5.30	40.79	2.32	1.55	0.02	101.05	0.070		
H4	Magnetite	22.31	0.61	25.89	48.54	1.77	1.06	0.01	100.19	0.022	861	-14.10
	Ilmenite	50.12	0.07	5.76	39.82	2.30	1.65	0.01	99.73	0.102		
H5	Magnetite	22.31	0.61	25.89	48.54	1.77	1.06	0.01	100.19	0.022	845	-14.53
	Ilmenite	50.44	0.07	5.46	40.18	2.28	1.62	0.00	100.05	0.098		
H6	Magnetite	22.31	0.61	25.89	48.54	1.77	1.06	0.01	100.19	0.022	791	-16.03
	Ilmenite	51.25	0.05	4.54	40.83	2.28	1.66	0.02	100.63	0.109		
H7	Magnetite	22.31	0.61	25.89	48.54	1.77	1.06	0.01	100.19	0.022	837	-14.75
	Ilmenite	51.09	0.05	5.35	40.51	2.28	1.76	0.01	101.06	0.134		
H8	Magnetite	22.31	0.61	25.89	48.54	1.77	1.06	0.01	100.19	0.022	830	-14.92
	Ilmenite	51.14	0.06	5.25	40.70	2.28	1.68	0.03	101.14	0.112		
I1	Magnetite	22.37	0.59	26.07	48.53	1.78	1.16	0.03	100.53	0.059	808	-15.53
	Ilmenite	51.10	0.07	4.84	40.64	2.30	1.68	0.02	100.66	0.107		
I2	Magnetite	22.37	0.59	26.07	48.53	1.78	1.16	0.03	100.53	0.059	831	-14.88
	Ilmenite	51.10	0.07	5.30	40.78	2.32	1.59	0.01	101.17	0.080		
I3	Magnetite	22.37	0.59	26.07	48.53	1.78	1.16	0.03	100.53	0.059	832	-14.87
	Ilmenite	51.03	0.04	5.30	40.79	2.32	1.55	0.02	101.05	0.070		
I4	Magnetite	22.37	0.59	26.07	48.53	1.78	1.16	0.03	100.53	0.059	860	-14.13
	Ilmenite	50.12	0.07	5.76	39.82	2.30	1.65	0.01	99.73	0.102		
I5	Magnetite	22.37	0.59	26.07	48.53	1.78	1.16	0.03	100.53	0.059	843	-14.56
	Ilmenite	50.44	0.07	5.46	40.18	2.28	1.62	0.00	100.05	0.098		
I6	Magnetite	22.37	0.59	26.07	48.53	1.78	1.16	0.03	100.53	0.059	790	-16.05
	Ilmenite	51.25	0.05	4.54	40.83	2.28	1.66	0.02	100.63	0.109		
I7	Magnetite	22.37	0.59	26.07	48.53	1.78	1.16	0.03	100.53	0.059	835	-14.78
	Ilmenite	51.09	0.05	5.35	40.51	2.28	1.76	0.01	101.06	0.134		
I8	Magnetite	22.37	0.59	26.07	48.53	1.78	1.16	0.03	100.53	0.059	829	-14.95
	Ilmenite	51.14	0.06	5.25	40.70	2.28	1.68	0.03	101.14	0.112		
J1	Magnetite	22.14	0.55	26.43	48.43	1.82	1.03	0.00	100.41	-0.004	803	-15.62
	Ilmenite	51.10	0.07	4.84	40.64	2.30	1.68	0.02	100.66	0.107		
J2	Magnetite	22.14	0.55	26.43	48.43	1.82	1.03	0.00	100.41	-0.004	827	-14.97
	Ilmenite	51.10	0.07	5.30	40.78	2.32	1.59	0.01	101.17	0.080		
J3	Magnetite	22.14	0.55	26.43	48.43	1.82	1.03	0.00	100.41	-0.004	827	-14.96
	Ilmenite	51.03	0.04	5.30	40.79	2.32	1.55	0.02	101.05	0.070		
J4	Magnetite	22.14	0.55	26.43	48.43	1.82	1.03	0.00	100.41	-0.004	855	-14.22
	Ilmenite	50.12	0.07	5.76	39.82	2.30	1.65	0.01	99.73	0.102		

Table F2 continued

LAI Pair identifier	Phase	TiO_2	Al_2O_3	Fe_2O_3	FeO	MnO	MgO	Cr_2O_3	Sum	log(Mg/Mn)	T	fO_2
J5	Magnetite	22.14	0.55	26.43	48.43	1.82	1.03	0.00	100.41	-0.004	839	-14.65
	Ilmenite	50.44	0.07	5.46	40.18	2.28	1.62	0.00	100.05	0.098		
J6	Magnetite	22.14	0.55	26.43	48.43	1.82	1.03	0.00	100.41	-0.004	786	-16.14
	Ilmenite	51.25	0.05	4.54	40.83	2.28	1.66	0.02	100.63	0.109		
J7	Magnetite	22.14	0.55	26.43	48.43	1.82	1.03	0.00	100.41	-0.004	831	-14.86
	Ilmenite	51.09	0.05	5.35	40.51	2.28	1.76	0.01	101.06	0.134		
J8	Magnetite	22.14	0.55	26.43	48.43	1.82	1.03	0.00	100.41	-0.004	824	-15.03
	Ilmenite	51.14	0.06	5.25	40.70	2.28	1.68	0.03	101.14	0.112		
K1	Magnetite	22.33	0.55	26.41	48.67	1.85	1.07	0.02	100.91	0.009	805	-15.59
	Ilmenite	51.10	0.07	4.84	40.64	2.30	1.68	0.02	100.66	0.107		
K2	Magnetite	22.33	0.55	26.41	48.67	1.85	1.07	0.02	100.91	0.009	828	-14.94
	Ilmenite	51.10	0.07	5.30	40.78	2.32	1.59	0.01	101.17	0.080		
K3	Magnetite	22.33	0.55	26.41	48.67	1.85	1.07	0.02	100.91	0.009	829	-14.93
	Ilmenite	51.03	0.04	5.30	40.79	2.32	1.55	0.02	101.05	0.070		
K4	Magnetite	22.33	0.55	26.41	48.67	1.85	1.07	0.02	100.91	0.009	857	-14.19
	Ilmenite	50.12	0.07	5.76	39.82	2.30	1.65	0.01	99.73	0.102		
K5	Magnetite	22.33	0.55	26.41	48.67	1.85	1.07	0.02	100.91	0.009	840	-14.62
	Ilmenite	50.44	0.07	5.46	40.18	2.28	1.62	0.00	100.05	0.098		
K6	Magnetite	22.33	0.55	26.41	48.67	1.85	1.07	0.02	100.91	0.009	787	-16.11
	Ilmenite	51.25	0.05	4.54	40.83	2.28	1.66	0.02	100.63	0.109		
K7	Magnetite	22.33	0.55	26.41	48.67	1.85	1.07	0.02	100.91	0.009	832	-14.83
	Ilmenite	51.09	0.05	5.35	40.51	2.28	1.76	0.01	101.06	0.134		
K8	Magnetite	22.33	0.55	26.41	48.67	1.85	1.07	0.02	100.91	0.009	826	-15.00
	Ilmenite	51.14	0.06	5.25	40.70	2.28	1.68	0.03	101.14	0.112		
L1	Magnetite	22.49	0.56	26.01	48.79	1.82	1.09	0.03	100.79	0.025	809	-15.50
	Ilmenite	51.10	0.07	4.84	40.64	2.30	1.68	0.02	100.66	0.107		
L2	Magnetite	22.49	0.56	26.01	48.79	1.82	1.09	0.03	100.79	0.025	833	-14.85
	Ilmenite	51.10	0.07	5.30	40.78	2.32	1.59	0.01	101.17	0.080		
L3	Magnetite	22.49	0.56	26.01	48.79	1.82	1.09	0.03	100.79	0.025	833	-14.84
	Ilmenite	51.03	0.04	5.30	40.79	2.32	1.55	0.02	101.05	0.070		
L4	Magnetite	22.49	0.56	26.01	48.79	1.82	1.09	0.03	100.79	0.025	861	-14.10
	Ilmenite	50.12	0.07	5.76	39.82	2.30	1.65	0.01	99.73	0.102		
L5	Magnetite	22.49	0.56	26.01	48.79	1.82	1.09	0.03	100.79	0.025	845	-14.53
	Ilmenite	50.44	0.07	5.46	40.18	2.28	1.62	0.00	100.05	0.098		
L6	Magnetite	22.49	0.56	26.01	48.79	1.82	1.09	0.03	100.79	0.025	791	-16.03
	Ilmenite	51.25	0.05	4.54	40.83	2.28	1.66	0.02	100.63	0.109		
L7	Magnetite	22.49	0.56	26.01	48.79	1.82	1.09	0.03	100.79	0.025	837	-14.75
	Ilmenite	51.09	0.05	5.35	40.51	2.28	1.76	0.01	101.06	0.134		

Table F2 continued

LAI Pair identifier	Phase	TiO_2	Al_2O_3	Fe_2O_3	FeO	MnO	MgO	Cr_2O_3	Sum	log(Mg/Mn)	T	fO_2
L8	Magnetite	22.49	0.56	26.01	48.79	1.82	1.09	0.03	100.79	0.025	830	-14.92
	Ilmenite	51.14	0.06	5.25	40.70	2.28	1.68	0.03	101.14	0.112		
M1	Magnetite	22.58	0.55	25.89	48.87	1.84	1.08	0.00	100.81	0.011	810	-15.48
	Ilmenite	51.10	0.07	4.84	40.64	2.30	1.68	0.02	100.66	0.107		
M2	Magnetite	22.58	0.55	25.89	48.87	1.84	1.08	0.00	100.81	0.011	834	-14.83
	Ilmenite	51.10	0.07	5.30	40.78	2.32	1.59	0.01	101.17	0.080		
M3	Magnetite	22.58	0.55	25.89	48.87	1.84	1.08	0.00	100.81	0.011	834	-14.82
	Ilmenite	51.03	0.04	5.30	40.79	2.32	1.55	0.02	101.05	0.070		
M4	Magnetite	22.58	0.55	25.89	48.87	1.84	1.08	0.00	100.81	0.011	863	-14.08
	Ilmenite	50.12	0.07	5.76	39.82	2.30	1.65	0.01	99.73	0.102		
M5	Magnetite	22.58	0.55	25.89	48.87	1.84	1.08	0.00	100.81	0.011	846	-14.51
	Ilmenite	50.44	0.07	5.46	40.18	2.28	1.62	0.00	100.05	0.098		
M6	Magnetite	22.58	0.55	25.89	48.87	1.84	1.08	0.00	100.81	0.011	792	-16.00
	Ilmenite	51.25	0.05	4.54	40.83	2.28	1.66	0.02	100.63	0.109		
M7	Magnetite	22.58	0.55	25.89	48.87	1.84	1.08	0.00	100.81	0.011	838	-14.72
	Ilmenite	51.09	0.05	5.35	40.51	2.28	1.76	0.01	101.06	0.134		
M8	Magnetite	22.58	0.55	25.89	48.87	1.84	1.08	0.00	100.81	0.011	832	-14.89
	Ilmenite	51.14	0.06	5.25	40.70	2.28	1.68	0.03	101.14	0.112		
V1	Magnetite	21.27	0.95	27.43	46.49	2.18	1.45	0.01	99.78	0.069	790	-15.88
	Ilmenite	51.10	0.07	4.84	40.64	2.30	1.68	0.02	100.66	0.107		
V2	Magnetite	21.27	0.95	27.43	46.49	2.18	1.45	0.01	99.78	0.069	813	-15.24
	Ilmenite	51.10	0.07	5.30	40.78	2.32	1.59	0.01	101.17	0.080		
V4	Magnetite	21.27	0.95	27.43	46.49	2.18	1.45	0.01	99.78	0.069	840	-14.50
	Ilmenite	50.12	0.07	5.76	39.82	2.30	1.65	0.01	99.73	0.102		
V5	Magnetite	21.27	0.95	27.43	46.49	2.18	1.45	0.01	99.78	0.069	824	-14.92
	Ilmenite	50.44	0.07	5.46	40.18	2.28	1.62	0.00	100.05	0.098		
V6	Magnetite	21.27	0.95	27.43	46.49	2.18	1.45	0.01	99.78	0.069	773	-16.39
	Ilmenite	51.25	0.05	4.54	40.83	2.28	1.66	0.02	100.63	0.109		
V7	Magnetite	21.27	0.95	27.43	46.49	2.18	1.45	0.01	99.78	0.069	816	-15.14
	Ilmenite	51.09	0.05	5.35	40.51	2.28	1.76	0.01	101.06	0.134		
V8	Magnetite	21.27	0.95	27.43	46.49	2.18	1.45	0.01	99.78	0.069	810	-15.30
	Ilmenite	51.14	0.06	5.25	40.70	2.28	1.68	0.03	101.14	0.112		
Z1	Magnetite	22.54	0.50	25.55	48.81	1.81	0.99	0.03	100.23	-0.016	813	-15.43
	Ilmenite	51.10	0.07	4.84	40.64	2.30	1.68	0.02	100.66	0.107		
Z2	Magnetite	22.54	0.50	25.55	48.81	1.81	0.99	0.03	100.23	-0.016	837	-14.78
	Ilmenite	51.10	0.07	5.30	40.78	2.32	1.59	0.01	101.17	0.080		
Z3	Magnetite	22.54	0.50	25.55	48.81	1.81	0.99	0.03	100.23	-0.016	837	-14.77
	Ilmenite	51.03	0.04	5.30	40.79	2.32	1.55	0.02	101.05	0.070		

Table F2 continued

LAI Pair identifier	Phase	TiO_2	Al_2O_3	Fe_2O_3	FeO	MnO	MgO	Cr_2O_3	Sum	log(Mg/Mn)	T	fO_2
Z4	Magnetite	22.54	0.50	25.55	48.81	1.81	0.99	0.03	100.23	-0.016	866	-14.03
	Ilmenite	50.12	0.07	5.76	39.82	2.30	1.65	0.01	99.73	0.102		
Z5	Magnetite	22.54	0.50	25.55	48.81	1.81	0.99	0.03	100.23	-0.016	849	-14.46
	Ilmenite	50.44	0.07	5.46	40.18	2.28	1.62	0.00	100.05	0.098		
Z6	Magnetite	22.54	0.50	25.55	48.81	1.81	0.99	0.03	100.23	-0.016	794	-15.95
	Ilmenite	51.25	0.05	4.54	40.83	2.28	1.66	0.02	100.63	0.109		
Z7	Magnetite	22.54	0.50	25.55	48.81	1.81	0.99	0.03	100.23	-0.016	841	-14.67
	Ilmenite	51.09	0.05	5.35	40.51	2.28	1.76	0.01	101.06	0.134		
Z8	Magnetite	22.54	0.50	25.55	48.81	1.81	0.99	0.03	100.23	-0.016	834	-14.84
	Ilmenite	51.14	0.06	5.25	40.70	2.28	1.68	0.03	101.14	0.112		
AA1	Magnetite	22.43	0.56	25.82	48.66	1.80	1.06	0.02	100.35	0.016	810	-15.48
	Ilmenite	51.10	0.07	4.84	40.64	2.30	1.68	0.02	100.66	0.107		
AA2	Magnetite	22.43	0.56	25.82	48.66	1.80	1.06	0.02	100.35	0.016	834	-14.83
	Ilmenite	51.10	0.07	5.30	40.78	2.32	1.59	0.01	101.17	0.080		
AA3	Magnetite	22.43	0.56	25.82	48.66	1.80	1.06	0.02	100.35	0.016	834	-14.82
	Ilmenite	51.03	0.04	5.30	40.79	2.32	1.55	0.02	101.05	0.070		
AA4	Magnetite	22.43	0.56	25.82	48.66	1.80	1.06	0.02	100.35	0.016	863	-14.08
	Ilmenite	50.12	0.07	5.76	39.82	2.30	1.65	0.01	99.73	0.102		
AA5	Magnetite	22.43	0.56	25.82	48.66	1.80	1.06	0.02	100.35	0.016	846	-14.51
	Ilmenite	50.44	0.07	5.46	40.18	2.28	1.62	0.00	100.05	0.098		
AA6	Magnetite	22.43	0.56	25.82	48.66	1.80	1.06	0.02	100.35	0.016	792	-16.01
	Ilmenite	51.25	0.05	4.54	40.83	2.28	1.66	0.02	100.63	0.109		
AA7	Magnetite	22.43	0.56	25.82	48.66	1.80	1.06	0.02	100.35	0.016	838	-14.73
	Ilmenite	51.09	0.05	5.35	40.51	2.28	1.76	0.01	101.06	0.134		
AA8	Magnetite	22.43	0.56	25.82	48.66	1.80	1.06	0.02	100.35	0.016	831	-14.90
	Ilmenite	51.14	0.06	5.25	40.70	2.28	1.68	0.03	101.14	0.112		
AB1	Magnetite	22.57	0.54	25.75	48.78	1.84	1.09	0.02	100.59	0.019	811	-15.46
	Ilmenite	51.10	0.07	4.84	40.64	2.30	1.68	0.02	100.66	0.107		
AB2	Magnetite	22.57	0.54	25.75	48.78	1.84	1.09	0.02	100.59	0.019	835	-14.81
	Ilmenite	51.10	0.07	5.30	40.78	2.32	1.59	0.01	101.17	0.080		
AB3	Magnetite	22.57	0.54	25.75	48.78	1.84	1.09	0.02	100.59	0.019	835	-14.80
	Ilmenite	51.03	0.04	5.30	40.79	2.32	1.55	0.02	101.05	0.070		
AB4	Magnetite	22.57	0.54	25.75	48.78	1.84	1.09	0.02	100.59	0.019	864	-14.06
	Ilmenite	50.12	0.07	5.76	39.82	2.30	1.65	0.01	99.73	0.102		
AB5	Magnetite	22.57	0.54	25.75	48.78	1.84	1.09	0.02	100.59	0.019	847	-14.49
	Ilmenite	50.44	0.07	5.46	40.18	2.28	1.62	0.00	100.05	0.098		
AB6	Magnetite	22.57	0.54	25.75	48.78	1.84	1.09	0.02	100.59	0.019	793	-15.99
	Ilmenite	51.25	0.05	4.54	40.83	2.28	1.66	0.02	100.63	0.109		

Table F2 continued

LAI Pair identifier	Phase	TiO_2	Al_2O_3	Fe_2O_3	FeO	MnO	MgO	Cr_2O_3	Sum	log(Mg/Mn)	T	fO_2
AB7	Magnetite	22.57	0.54	25.75	48.78	1.84	1.09	0.02	100.59	0.019	839	-14.71
	Ilmenite	51.09	0.05	5.35	40.51	2.28	1.76	0.01	101.06	0.134		
AB8	Magnetite	22.57	0.54	25.75	48.78	1.84	1.09	0.02	100.59	0.019	833	-14.87
	Ilmenite	51.14	0.06	5.25	40.70	2.28	1.68	0.03	101.14	0.112		
AC1	Magnetite	22.50	0.54	26.07	48.78	1.87	1.08	0.01	100.85	0.009	808	-15.52
	Ilmenite	51.10	0.07	4.84	40.64	2.30	1.68	0.02	100.66	0.107		
AC2	Magnetite	22.50	0.54	26.07	48.78	1.87	1.08	0.01	100.85	0.009	832	-14.87
	Ilmenite	51.10	0.07	5.30	40.78	2.32	1.59	0.01	101.17	0.080		
AC3	Magnetite	22.50	0.54	26.07	48.78	1.87	1.08	0.01	100.85	0.009	832	-14.86
	Ilmenite	51.03	0.04	5.30	40.79	2.32	1.55	0.02	101.05	0.070		
AC4	Magnetite	22.50	0.54	26.07	48.78	1.87	1.08	0.01	100.85	0.009	860	-14.12
	Ilmenite	50.12	0.07	5.76	39.82	2.30	1.65	0.01	99.73	0.102		
AC5	Magnetite	22.50	0.54	26.07	48.78	1.87	1.08	0.01	100.85	0.009	844	-14.55
	Ilmenite	50.44	0.07	5.46	40.18	2.28	1.62	0.00	100.05	0.098		
AC6	Magnetite	22.50	0.54	26.07	48.78	1.87	1.08	0.01	100.85	0.009	790	-16.04
	Ilmenite	51.25	0.05	4.54	40.83	2.28	1.66	0.02	100.63	0.109		
AC7	Magnetite	22.50	0.54	26.07	48.78	1.87	1.08	0.01	100.85	0.009	836	-14.77
	Ilmenite	51.09	0.05	5.35	40.51	2.28	1.76	0.01	101.06	0.134		
AC8	Magnetite	22.50	0.54	26.07	48.78	1.87	1.08	0.01	100.85	0.009	829	-14.93
	Ilmenite	51.14	0.06	5.25	40.70	2.28	1.68	0.03	101.14	0.112		
AD1	Magnetite	22.58	0.55	25.93	48.93	1.82	1.07	0.01	100.90	0.013	810	-15.48
	Ilmenite	51.10	0.07	4.84	40.64	2.30	1.68	0.02	100.66	0.107		
AD2	Magnetite	22.58	0.55	25.93	48.93	1.82	1.07	0.01	100.90	0.013	834	-14.83
	Ilmenite	51.10	0.07	5.30	40.78	2.32	1.59	0.01	101.17	0.080		
AD3	Magnetite	22.58	0.55	25.93	48.93	1.82	1.07	0.01	100.90	0.013	834	-14.82
	Ilmenite	51.03	0.04	5.30	40.79	2.32	1.55	0.02	101.05	0.070		
AD4	Magnetite	22.58	0.55	25.93	48.93	1.82	1.07	0.01	100.90	0.013	863	-14.08
	Ilmenite	50.12	0.07	5.76	39.82	2.30	1.65	0.01	99.73	0.102		
AD5	Magnetite	22.58	0.55	25.93	48.93	1.82	1.07	0.01	100.90	0.013	846	-14.51
	Ilmenite	50.44	0.07	5.46	40.18	2.28	1.62	0.00	100.05	0.098		
AD6	Magnetite	22.58	0.55	25.93	48.93	1.82	1.07	0.01	100.90	0.013	792	-16.00
	Ilmenite	51.25	0.05	4.54	40.83	2.28	1.66	0.02	100.63	0.109		
AD7	Magnetite	22.58	0.55	25.93	48.93	1.82	1.07	0.01	100.90	0.013	838	-14.73
	Ilmenite	51.09	0.05	5.35	40.51	2.28	1.76	0.01	101.06	0.134		
AD8	Magnetite	22.58	0.55	25.93	48.93	1.82	1.07	0.01	100.90	0.013	832	-14.89
	Ilmenite	51.14	0.06	5.25	40.70	2.28	1.68	0.03	101.14	0.112		
AE1	Magnetite	22.58	0.55	25.91	48.87	1.80	1.11	0.01	100.83	0.037	810	-15.48
	Ilmenite	51.10	0.07	4.84	40.64	2.30	1.68	0.02	100.66	0.107		

Table F2 continued

LAI Pair identifier	Phase	TiO_2	Al_2O_3	Fe_2O_3	FeO	MnO	MgO	Cr_2O_3	Sum	log(Mg/Mn)	T	fO_2
AE2	Magnetite	22.58	0.55	25.91	48.87	1.80	1.11	0.01	100.83	0.037	834	-14.83
	Ilmenite	51.10	0.07	5.30	40.78	2.32	1.59	0.01	101.17	0.080		
AE3	Magnetite	22.58	0.55	25.91	48.87	1.80	1.11	0.01	100.83	0.037	834	-14.82
	Ilmenite	51.03	0.04	5.30	40.79	2.32	1.55	0.02	101.05	0.070		
AE4	Magnetite	22.58	0.55	25.91	48.87	1.80	1.11	0.01	100.83	0.037	863	-14.08
	Ilmenite	50.12	0.07	5.76	39.82	2.30	1.65	0.01	99.73	0.102		
AE5	Magnetite	22.58	0.55	25.91	48.87	1.80	1.11	0.01	100.83	0.037	846	-14.51
	Ilmenite	50.44	0.07	5.46	40.18	2.28	1.62	0.00	100.05	0.098		
AE6	Magnetite	22.58	0.55	25.91	48.87	1.80	1.11	0.01	100.83	0.037	792	-16.00
	Ilmenite	51.25	0.05	4.54	40.83	2.28	1.66	0.02	100.63	0.109		
AE7	Magnetite	22.58	0.55	25.91	48.87	1.80	1.11	0.01	100.83	0.037	838	-14.72
	Ilmenite	51.09	0.05	5.35	40.51	2.28	1.76	0.01	101.06	0.134		
AE8	Magnetite	22.58	0.55	25.91	48.87	1.80	1.11	0.01	100.83	0.037	832	-14.89
	Ilmenite	51.14	0.06	5.25	40.70	2.28	1.68	0.03	101.14	0.112		
AF1	Magnetite	22.68	0.50	25.52	48.95	1.82	1.04	0.01	100.52	0.003	814	-15.41
	Ilmenite	51.10	0.07	4.84	40.64	2.30	1.68	0.02	100.66	0.107		
AF2	Magnetite	22.68	0.50	25.52	48.95	1.82	1.04	0.01	100.52	0.003	838	-14.76
	Ilmenite	51.10	0.07	5.30	40.78	2.32	1.59	0.01	101.17	0.080		
AF3	Magnetite	22.68	0.50	25.52	48.95	1.82	1.04	0.01	100.52	0.003	838	-14.75
	Ilmenite	51.03	0.04	5.30	40.79	2.32	1.55	0.02	101.05	0.070		
AF4	Magnetite	22.68	0.50	25.52	48.95	1.82	1.04	0.01	100.52	0.003	867	-14.01
	Ilmenite	50.12	0.07	5.76	39.82	2.30	1.65	0.01	99.73	0.102		
AF5	Magnetite	22.68	0.50	25.52	48.95	1.82	1.04	0.01	100.52	0.003	850	-14.44
	Ilmenite	50.44	0.07	5.46	40.18	2.28	1.62	0.00	100.05	0.098		
AF6	Magnetite	22.68	0.50	25.52	48.95	1.82	1.04	0.01	100.52	0.003	795	-15.94
	Ilmenite	51.25	0.05	4.54	40.83	2.28	1.66	0.02	100.63	0.109		
AF7	Magnetite	22.68	0.50	25.52	48.95	1.82	1.04	0.01	100.52	0.003	842	-14.66
	Ilmenite	51.09	0.05	5.35	40.51	2.28	1.76	0.01	101.06	0.134		
AF8	Magnetite	22.68	0.50	25.52	48.95	1.82	1.04	0.01	100.52	0.003	835	-14.83
	Ilmenite	51.14	0.06	5.25	40.70	2.28	1.68	0.03	101.14	0.112		
AG1	Magnetite	22.58	0.51	25.93	48.89	1.85	1.06	0.01	100.83	0.004	810	-15.49
	Ilmenite	51.10	0.07	4.84	40.64	2.30	1.68	0.02	100.66	0.107		
AG2	Magnetite	22.58	0.51	25.93	48.89	1.85	1.06	0.01	100.83	0.004	834	-14.84
	Ilmenite	51.10	0.07	5.30	40.78	2.32	1.59	0.01	101.17	0.080		
AG3	Magnetite	22.58	0.51	25.93	48.89	1.85	1.06	0.01	100.83	0.004	834	-14.83
	Ilmenite	51.03	0.04	5.30	40.79	2.32	1.55	0.02	101.05	0.070		
AG4	Magnetite	22.58	0.51	25.93	48.89	1.85	1.06	0.01	100.83	0.004	862	-14.09
	Ilmenite	50.12	0.07	5.76	39.82	2.30	1.65	0.01	99.73	0.102		

Table F2 continued

LAI Pair identifier	Phase	TiO_2	Al_2O_3	Fe_2O_3	FeO	MnO	MgO	Cr_2O_3	Sum	log(Mg/Mn)	T	fO_2
AG5	Magnetite	22.58	0.51	25.93	48.89	1.85	1.06	0.01	100.83	0.004	846	-14.52
	Ilmenite	50.44	0.07	5.46	40.18	2.28	1.62	0.00	100.05	0.098		
AG6	Magnetite	22.58	0.51	25.93	48.89	1.85	1.06	0.01	100.83	0.004	791	-16.01
	Ilmenite	51.25	0.05	4.54	40.83	2.28	1.66	0.02	100.63	0.109		
AG7	Magnetite	22.58	0.51	25.93	48.89	1.85	1.06	0.01	100.83	0.004	837	-14.73
	Ilmenite	51.09	0.05	5.35	40.51	2.28	1.76	0.01	101.06	0.134		
AG8	Magnetite	22.58	0.51	25.93	48.89	1.85	1.06	0.01	100.83	0.004	831	-14.90
	Ilmenite	51.14	0.06	5.25	40.70	2.28	1.68	0.03	101.14	0.112		
AH1	Magnetite	22.58	0.82	25.50	48.67	1.86	1.20	0.04	100.66	0.057	815	-15.38
	Ilmenite	51.10	0.07	4.84	40.64	2.30	1.68	0.02	100.66	0.107		
AH2	Magnetite	22.58	0.82	25.50	48.67	1.86	1.20	0.04	100.66	0.057	840	-14.72
	Ilmenite	51.10	0.07	5.30	40.78	2.32	1.59	0.01	101.17	0.080		
AH3	Magnetite	22.58	0.82	25.50	48.67	1.86	1.20	0.04	100.66	0.057	840	-14.72
	Ilmenite	51.03	0.04	5.30	40.79	2.32	1.55	0.02	101.05	0.070		
AH4	Magnetite	22.58	0.82	25.50	48.67	1.86	1.20	0.04	100.66	0.057	869	-13.97
	Ilmenite	50.12	0.07	5.76	39.82	2.30	1.65	0.01	99.73	0.102		
AH5	Magnetite	22.58	0.82	25.50	48.67	1.86	1.20	0.04	100.66	0.057	852	-14.40
	Ilmenite	50.44	0.07	5.46	40.18	2.28	1.62	0.00	100.05	0.098		
AH6	Magnetite	22.58	0.82	25.50	48.67	1.86	1.20	0.04	100.66	0.057	797	-15.90
	Ilmenite	51.25	0.05	4.54	40.83	2.28	1.66	0.02	100.63	0.109		
AH7	Magnetite	22.58	0.82	25.50	48.67	1.86	1.20	0.04	100.66	0.057	843	-14.62
	Ilmenite	51.09	0.05	5.35	40.51	2.28	1.76	0.01	101.06	0.134		
AH8	Magnetite	22.58	0.82	25.50	48.67	1.86	1.20	0.04	100.66	0.057	837	-14.79
	Ilmenite	51.14	0.06	5.25	40.70	2.28	1.68	0.03	101.14	0.112		
AI1	Magnetite	22.39	0.74	25.96	48.57	1.81	1.17	0.01	100.65	0.056	810	-15.49
	Ilmenite	51.10	0.07	4.84	40.64	2.30	1.68	0.02	100.66	0.107		
AI2	Magnetite	22.39	0.74	25.96	48.57	1.81	1.17	0.01	100.65	0.056	834	-14.84
	Ilmenite	51.10	0.07	5.30	40.78	2.32	1.59	0.01	101.17	0.080		
AI3	Magnetite	22.39	0.74	25.96	48.57	1.81	1.17	0.01	100.65	0.056	834	-14.83
	Ilmenite	51.03	0.04	5.30	40.79	2.32	1.55	0.02	101.05	0.070		
AI4	Magnetite	22.39	0.74	25.96	48.57	1.81	1.17	0.01	100.65	0.056	862	-14.09
	Ilmenite	50.12	0.07	5.76	39.82	2.30	1.65	0.01	99.73	0.102		
AI5	Magnetite	22.39	0.74	25.96	48.57	1.81	1.17	0.01	100.65	0.056	846	-14.52
	Ilmenite	50.44	0.07	5.46	40.18	2.28	1.62	0.00	100.05	0.098		
AI6	Magnetite	22.39	0.74	25.96	48.57	1.81	1.17	0.01	100.65	0.056	791	-16.01
	Ilmenite	51.25	0.05	4.54	40.83	2.28	1.66	0.02	100.63	0.109		
AI7	Magnetite	22.39	0.74	25.96	48.57	1.81	1.17	0.01	100.65	0.056	837	-14.73
	Ilmenite	51.09	0.05	5.35	40.51	2.28	1.76	0.01	101.06	0.134		

Table F2 continued

LAI Pair identifier	Phase	TiO_2	Al_2O_3	Fe_2O_3	FeO	MnO	MgO	Cr_2O_3	Sum	log(Mg/Mn)	T	fO_2
AI8	Magnetite	22.39	0.74	25.96	48.57	1.81	1.17	0.01	100.65	0.056	831	-14.90
	Ilmenite	51.14	0.06	5.25	40.70	2.28	1.68	0.03	101.14	0.112		
AJ1	Magnetite	22.36	0.65	26.09	48.71	1.86	1.03	0.02	100.72	-0.012	808	-15.51
	Ilmenite	51.10	0.07	4.84	40.64	2.30	1.68	0.02	100.66	0.107		
AJ2	Magnetite	22.36	0.65	26.09	48.71	1.86	1.03	0.02	100.72	-0.012	832	-14.86
	Ilmenite	51.10	0.07	5.30	40.78	2.32	1.59	0.01	101.17	0.080		
AJ3	Magnetite	22.36	0.65	26.09	48.71	1.86	1.03	0.02	100.72	-0.012	832	-14.85
	Ilmenite	51.03	0.04	5.30	40.79	2.32	1.55	0.02	101.05	0.070		
AJ4	Magnetite	22.36	0.65	26.09	48.71	1.86	1.03	0.02	100.72	-0.012	861	-14.11
	Ilmenite	50.12	0.07	5.76	39.82	2.30	1.65	0.01	99.73	0.102		
AJ5	Magnetite	22.36	0.65	26.09	48.71	1.86	1.03	0.02	100.72	-0.012	844	-14.54
	Ilmenite	50.44	0.07	5.46	40.18	2.28	1.62	0.00	100.05	0.098		
AJ6	Magnetite	22.36	0.65	26.09	48.71	1.86	1.03	0.02	100.72	-0.012	790	-16.04
	Ilmenite	51.25	0.05	4.54	40.83	2.28	1.66	0.02	100.63	0.109		
AJ7	Magnetite	22.36	0.65	26.09	48.71	1.86	1.03	0.02	100.72	-0.012	836	-14.76
	Ilmenite	51.09	0.05	5.35	40.51	2.28	1.76	0.01	101.06	0.134		
AJ8	Magnetite	22.36	0.65	26.09	48.71	1.86	1.03	0.02	100.72	-0.012	830	-14.93
	Ilmenite	51.14	0.06	5.25	40.70	2.28	1.68	0.03	101.14	0.112		
AK1	Magnetite	22.56	0.58	25.85	48.88	1.80	1.08	0.01	100.76	0.024	811	-15.47
	Ilmenite	51.10	0.07	4.84	40.64	2.30	1.68	0.02	100.66	0.107		
AK2	Magnetite	22.56	0.58	25.85	48.88	1.80	1.08	0.01	100.76	0.024	835	-14.81
	Ilmenite	51.10	0.07	5.30	40.78	2.32	1.59	0.01	101.17	0.080		
AK3	Magnetite	22.56	0.58	25.85	48.88	1.80	1.08	0.01	100.76	0.024	835	-14.81
	Ilmenite	51.03	0.04	5.30	40.79	2.32	1.55	0.02	101.05	0.070		
AK4	Magnetite	22.56	0.58	25.85	48.88	1.80	1.08	0.01	100.76	0.024	864	-14.06
	Ilmenite	50.12	0.07	5.76	39.82	2.30	1.65	0.01	99.73	0.102		
AK5	Magnetite	22.56	0.58	25.85	48.88	1.80	1.08	0.01	100.76	0.024	847	-14.49
	Ilmenite	50.44	0.07	5.46	40.18	2.28	1.62	0.00	100.05	0.098		
AK6	Magnetite	22.56	0.58	25.85	48.88	1.80	1.08	0.01	100.76	0.024	793	-15.99
	Ilmenite	51.25	0.05	4.54	40.83	2.28	1.66	0.02	100.63	0.109		
AK7	Magnetite	22.56	0.58	25.85	48.88	1.80	1.08	0.01	100.76	0.024	839	-14.71
	Ilmenite	51.09	0.05	5.35	40.51	2.28	1.76	0.01	101.06	0.134		
AK8	Magnetite	22.56	0.58	25.85	48.88	1.80	1.08	0.01	100.76	0.024	832	-14.88
	Ilmenite	51.14	0.06	5.25	40.70	2.28	1.68	0.03	101.14	0.112		
AL1	Magnetite	22.86	0.58	25.10	48.97	1.84	1.12	0.00	100.48	0.031	818	-15.32
	Ilmenite	51.10	0.07	4.84	40.64	2.30	1.68	0.02	100.66	0.107		
AL2	Magnetite	22.86	0.58	25.10	48.97	1.84	1.12	0.00	100.48	0.031	843	-14.66
	Ilmenite	51.10	0.07	5.30	40.78	2.32	1.59	0.01	101.17	0.080		

Table F2 continued

LAI Pair identifier	Phase	TiO_2	Al_2O_3	Fe_2O_3	FeO	MnO	MgO	Cr_2O_3	Sum	log(Mg/Mn)	T	fO_2
AL3	Magnetite	22.86	0.58	25.10	48.97	1.84	1.12	0.00	100.48	0.031	843	-14.66
	Ilmenite	51.03	0.04	5.30	40.79	2.32	1.55	0.02	101.05	0.070		
AL4	Magnetite	22.86	0.58	25.10	48.97	1.84	1.12	0.00	100.48	0.031	872	-13.91
	Ilmenite	50.12	0.07	5.76	39.82	2.30	1.65	0.01	99.73	0.102		
AL5	Magnetite	22.86	0.58	25.10	48.97	1.84	1.12	0.00	100.48	0.031	855	-14.34
	Ilmenite	50.44	0.07	5.46	40.18	2.28	1.62	0.00	100.05	0.098		
AL6	Magnetite	22.86	0.58	25.10	48.97	1.84	1.12	0.00	100.48	0.031	800	-15.85
	Ilmenite	51.25	0.05	4.54	40.83	2.28	1.66	0.02	100.63	0.109		
AL7	Magnetite	22.86	0.58	25.10	48.97	1.84	1.12	0.00	100.48	0.031	847	-14.56
	Ilmenite	51.09	0.05	5.35	40.51	2.28	1.76	0.01	101.06	0.134		
AL8	Magnetite	22.86	0.58	25.10	48.97	1.84	1.12	0.00	100.48	0.031	840	-14.73
	Ilmenite	51.14	0.06	5.25	40.70	2.28	1.68	0.03	101.14	0.112		
AM1	Magnetite	22.91	0.61	25.08	49.08	1.84	1.12	0.01	100.64	0.031	819	-15.30
	Ilmenite	51.10	0.07	4.84	40.64	2.30	1.68	0.02	100.66	0.107		
AM2	Magnetite	22.91	0.61	25.08	49.08	1.84	1.12	0.01	100.64	0.031	844	-14.64
	Ilmenite	51.10	0.07	5.30	40.78	2.32	1.59	0.01	101.17	0.080		
AM3	Magnetite	22.91	0.61	25.08	49.08	1.84	1.12	0.01	100.64	0.031	844	-14.63
	Ilmenite	51.03	0.04	5.30	40.79	2.32	1.55	0.02	101.05	0.070		
AM4	Magnetite	22.91	0.61	25.08	49.08	1.84	1.12	0.01	100.64	0.031	873	-13.89
	Ilmenite	50.12	0.07	5.76	39.82	2.30	1.65	0.01	99.73	0.102		
AM5	Magnetite	22.91	0.61	25.08	49.08	1.84	1.12	0.01	100.64	0.031	856	-14.32
	Ilmenite	50.44	0.07	5.46	40.18	2.28	1.62	0.00	100.05	0.098		
AM6	Magnetite	22.91	0.61	25.08	49.08	1.84	1.12	0.01	100.64	0.031	800	-15.83
	Ilmenite	51.25	0.05	4.54	40.83	2.28	1.66	0.02	100.63	0.109		
AM7	Magnetite	22.91	0.61	25.08	49.08	1.84	1.12	0.01	100.64	0.031	848	-14.54
	Ilmenite	51.09	0.05	5.35	40.51	2.28	1.76	0.01	101.06	0.134		
AM8	Magnetite	22.91	0.61	25.08	49.08	1.84	1.12	0.01	100.64	0.031	841	-14.71
	Ilmenite	51.14	0.06	5.25	40.70	2.28	1.68	0.03	101.14	0.112		
AN1	Magnetite	22.53	0.62	25.45	48.74	1.78	1.06	0.03	100.21	0.020	814	-15.40
	Ilmenite	51.10	0.07	4.84	40.64	2.30	1.68	0.02	100.66	0.107		
AN2	Magnetite	22.53	0.62	25.45	48.74	1.78	1.06	0.03	100.21	0.020	838	-14.74
	Ilmenite	51.10	0.07	5.30	40.78	2.32	1.59	0.01	101.17	0.080		
AN3	Magnetite	22.53	0.62	25.45	48.74	1.78	1.06	0.03	100.21	0.020	839	-14.74
	Ilmenite	51.03	0.04	5.30	40.79	2.32	1.55	0.02	101.05	0.070		
AN4	Magnetite	22.53	0.62	25.45	48.74	1.78	1.06	0.03	100.21	0.020	868	-13.99
	Ilmenite	50.12	0.07	5.76	39.82	2.30	1.65	0.01	99.73	0.102		
AN5	Magnetite	22.53	0.62	25.45	48.74	1.78	1.06	0.03	100.21	0.020	851	-14.42
	Ilmenite	50.44	0.07	5.46	40.18	2.28	1.62	0.00	100.05	0.098		

Table F2 continued

LAI Pair identifier	Phase	TiO_2	Al_2O_3	Fe_2O_3	FeO	MnO	MgO	Cr_2O_3	Sum	log(Mg/Mn)	T	fO_2
AN6	Magnetite	22.53	0.62	25.45	48.74	1.78	1.06	0.03	100.21	0.020	796	-15.92
	Ilmenite	51.25	0.05	4.54	40.83	2.28	1.66	0.02	100.63	0.109		
AN7	Magnetite	22.53	0.62	25.45	48.74	1.78	1.06	0.03	100.21	0.020	842	-14.64
	Ilmenite	51.09	0.05	5.35	40.51	2.28	1.76	0.01	101.06	0.134		
AN8	Magnetite	22.53	0.62	25.45	48.74	1.78	1.06	0.03	100.21	0.020	836	-14.81
	Ilmenite	51.14	0.06	5.25	40.70	2.28	1.68	0.03	101.14	0.112		
AO1	Magnetite	22.19	0.52	26.03	48.37	1.82	1.01	0.02	99.96	-0.011	806	-15.56
	Ilmenite	51.10	0.07	4.84	40.64	2.30	1.68	0.02	100.66	0.107		
AO2	Magnetite	22.19	0.52	26.03	48.37	1.82	1.01	0.02	99.96	-0.011	830	-14.90
	Ilmenite	51.10	0.07	5.30	40.78	2.32	1.59	0.01	101.17	0.080		
AO3	Magnetite	22.19	0.52	26.03	48.37	1.82	1.01	0.02	99.96	-0.011	830	-14.90
	Ilmenite	51.03	0.04	5.30	40.79	2.32	1.55	0.02	101.05	0.070		
AO4	Magnetite	22.19	0.52	26.03	48.37	1.82	1.01	0.02	99.96	-0.011	858	-14.16
	Ilmenite	50.12	0.07	5.76	39.82	2.30	1.65	0.01	99.73	0.102		
AO5	Magnetite	22.19	0.52	26.03	48.37	1.82	1.01	0.02	99.96	-0.011	842	-14.59
	Ilmenite	50.44	0.07	5.46	40.18	2.28	1.62	0.00	100.05	0.098		
AO6	Magnetite	22.19	0.52	26.03	48.37	1.82	1.01	0.02	99.96	-0.011	788	-16.08
	Ilmenite	51.25	0.05	4.54	40.83	2.28	1.66	0.02	100.63	0.109		
AO7	Magnetite	22.19	0.52	26.03	48.37	1.82	1.01	0.02	99.96	-0.011	834	-14.80
	Ilmenite	51.09	0.05	5.35	40.51	2.28	1.76	0.01	101.06	0.134		
AO8	Magnetite	22.19	0.52	26.03	48.37	1.82	1.01	0.02	99.96	-0.011	828	-14.97
	Ilmenite	51.14	0.06	5.25	40.70	2.28	1.68	0.03	101.14	0.112		
AP1	Magnetite	22.39	0.53	26.09	48.83	1.83	0.96	0.01	100.64	-0.036	808	-15.52
	Ilmenite	51.10	0.07	4.84	40.64	2.30	1.68	0.02	100.66	0.107		
AP2	Magnetite	22.39	0.53	26.09	48.83	1.83	0.96	0.01	100.64	-0.036	832	-14.87
	Ilmenite	51.10	0.07	5.30	40.78	2.32	1.59	0.01	101.17	0.080		
AP3	Magnetite	22.39	0.53	26.09	48.83	1.83	0.96	0.01	100.64	-0.036	832	-14.87
	Ilmenite	51.03	0.04	5.30	40.79	2.32	1.55	0.02	101.05	0.070		
AP4	Magnetite	22.39	0.53	26.09	48.83	1.83	0.96	0.01	100.64	-0.036	860	-14.12
	Ilmenite	50.12	0.07	5.76	39.82	2.30	1.65	0.01	99.73	0.102		
AP5	Magnetite	22.39	0.53	26.09	48.83	1.83	0.96	0.01	100.64	-0.036	844	-14.55
	Ilmenite	50.44	0.07	5.46	40.18	2.28	1.62	0.00	100.05	0.098		
AP6	Magnetite	22.39	0.53	26.09	48.83	1.83	0.96	0.01	100.64	-0.036	790	-16.05
	Ilmenite	51.25	0.05	4.54	40.83	2.28	1.66	0.02	100.63	0.109		
AP7	Magnetite	22.39	0.53	26.09	48.83	1.83	0.96	0.01	100.64	-0.036	836	-14.77
	Ilmenite	51.09	0.05	5.35	40.51	2.28	1.76	0.01	101.06	0.134		
AP8	Magnetite	22.39	0.53	26.09	48.83	1.83	0.96	0.01	100.64	-0.036	829	-14.94
	Ilmenite	51.14	0.06	5.25	40.70	2.28	1.68	0.03	101.14	0.112		

Table F2 continued

LAI Pair identifier	Phase	TiO_2	Al_2O_3	Fe_2O_3	FeO	MnO	MgO	Cr_2O_3	Sum	log(Mg/Mn)	T	fO_2
AQ1	Magnetite	22.55	0.56	25.92	49.03	1.81	0.99	0.01	100.88	-0.017	811	-15.47
	Ilmenite	51.10	0.07	4.84	40.64	2.30	1.68	0.02	100.66	0.107		
AQ2	Magnetite	22.55	0.56	25.92	49.03	1.81	0.99	0.01	100.88	-0.017	835	-14.82
	Ilmenite	51.10	0.07	5.30	40.78	2.32	1.59	0.01	101.17	0.080		
AQ3	Magnetite	22.55	0.56	25.92	49.03	1.81	0.99	0.01	100.88	-0.017	835	-14.81
	Ilmenite	51.03	0.04	5.30	40.79	2.32	1.55	0.02	101.05	0.070		
AQ4	Magnetite	22.55	0.56	25.92	49.03	1.81	0.99	0.01	100.88	-0.017	863	-14.07
	Ilmenite	50.12	0.07	5.76	39.82	2.30	1.65	0.01	99.73	0.102		
AQ5	Magnetite	22.55	0.56	25.92	49.03	1.81	0.99	0.01	100.88	-0.017	847	-14.50
	Ilmenite	50.44	0.07	5.46	40.18	2.28	1.62	0.00	100.05	0.098		
AQ6	Magnetite	22.55	0.56	25.92	49.03	1.81	0.99	0.01	100.88	-0.017	792	-15.99
	Ilmenite	51.25	0.05	4.54	40.83	2.28	1.66	0.02	100.63	0.109		
AQ7	Magnetite	22.55	0.56	25.92	49.03	1.81	0.99	0.01	100.88	-0.017	838	-14.72
	Ilmenite	51.09	0.05	5.35	40.51	2.28	1.76	0.01	101.06	0.134		
AQ8	Magnetite	22.55	0.56	25.92	49.03	1.81	0.99	0.01	100.88	-0.017	832	-14.88
	Ilmenite	51.14	0.06	5.25	40.70	2.28	1.68	0.03	101.14	0.112		
AR1	Magnetite	22.72	0.55	25.51	49.13	1.83	0.99	0.01	100.74	-0.022	815	-15.39
	Ilmenite	51.10	0.07	4.84	40.64	2.30	1.68	0.02	100.66	0.107		
AR2	Magnetite	22.72	0.55	25.51	49.13	1.83	0.99	0.01	100.74	-0.022	839	-14.73
	Ilmenite	51.10	0.07	5.30	40.78	2.32	1.59	0.01	101.17	0.080		
AR3	Magnetite	22.72	0.55	25.51	49.13	1.83	0.99	0.01	100.74	-0.022	839	-14.73
	Ilmenite	51.03	0.04	5.30	40.79	2.32	1.55	0.02	101.05	0.070		
AR4	Magnetite	22.72	0.55	25.51	49.13	1.83	0.99	0.01	100.74	-0.022	868	-13.98
	Ilmenite	50.12	0.07	5.76	39.82	2.30	1.65	0.01	99.73	0.102		
AR5	Magnetite	22.72	0.55	25.51	49.13	1.83	0.99	0.01	100.74	-0.022	851	-14.41
	Ilmenite	50.44	0.07	5.46	40.18	2.28	1.62	0.00	100.05	0.098		
AR6	Magnetite	22.72	0.55	25.51	49.13	1.83	0.99	0.01	100.74	-0.022	796	-15.91
	Ilmenite	51.25	0.05	4.54	40.83	2.28	1.66	0.02	100.63	0.109		
AR7	Magnetite	22.72	0.55	25.51	49.13	1.83	0.99	0.01	100.74	-0.022	843	-14.63
	Ilmenite	51.09	0.05	5.35	40.51	2.28	1.76	0.01	101.06	0.134		
AR8	Magnetite	22.72	0.55	25.51	49.13	1.83	0.99	0.01	100.74	-0.022	836	-14.80
	Ilmenite	51.14	0.06	5.25	40.70	2.28	1.68	0.03	101.14	0.112		
AS1	Magnetite	22.34	0.56	25.83	48.49	1.84	1.04	0.00	100.10	-0.002	809	-15.50
	Ilmenite	51.10	0.07	4.84	40.64	2.30	1.68	0.02	100.66	0.107		
AS2	Magnetite	22.34	0.56	25.83	48.49	1.84	1.04	0.00	100.10	-0.002	833	-14.85
	Ilmenite	51.10	0.07	5.30	40.78	2.32	1.59	0.01	101.17	0.080		
AS3	Magnetite	22.34	0.56	25.83	48.49	1.84	1.04	0.00	100.10	-0.002	833	-14.84
	Ilmenite	51.03	0.04	5.30	40.79	2.32	1.55	0.02	101.05	0.070		

Table F2 continued

LAI Pair identifier	Phase	TiO_2	Al_2O_3	Fe_2O_3	FeO	MnO	MgO	Cr_2O_3	Sum	log(Mg/Mn)	T	fO_2
AS4	Magnetite	22.34	0.56	25.83	48.49	1.84	1.04	0.00	100.10	-0.002	861	-14.10
	Ilmenite	50.12	0.07	5.76	39.82	2.30	1.65	0.01	99.73	0.102		
AS5	Magnetite	22.34	0.56	25.83	48.49	1.84	1.04	0.00	100.10	-0.002	845	-14.53
	Ilmenite	50.44	0.07	5.46	40.18	2.28	1.62	0.00	100.05	0.098		
AS6	Magnetite	22.34	0.56	25.83	48.49	1.84	1.04	0.00	100.10	-0.002	791	-16.03
	Ilmenite	51.25	0.05	4.54	40.83	2.28	1.66	0.02	100.63	0.109		
AS7	Magnetite	22.34	0.56	25.83	48.49	1.84	1.04	0.00	100.10	-0.002	837	-14.75
	Ilmenite	51.09	0.05	5.35	40.51	2.28	1.76	0.01	101.06	0.134		
AS8	Magnetite	22.34	0.56	25.83	48.49	1.84	1.04	0.00	100.10	-0.002	830	-14.92
	Ilmenite	51.14	0.06	5.25	40.70	2.28	1.68	0.03	101.14	0.112		
AT1	Magnetite	22.41	0.52	26.11	48.83	1.87	0.96	0.01	100.72	-0.044	808	-15.53
	Ilmenite	51.10	0.07	4.84	40.64	2.30	1.68	0.02	100.66	0.107		
AT2	Magnetite	22.41	0.52	26.11	48.83	1.87	0.96	0.01	100.72	-0.044	831	-14.88
	Ilmenite	51.10	0.07	5.30	40.78	2.32	1.59	0.01	101.17	0.080		
AT3	Magnetite	22.41	0.52	26.11	48.83	1.87	0.96	0.01	100.72	-0.044	832	-14.87
	Ilmenite	51.03	0.04	5.30	40.79	2.32	1.55	0.02	101.05	0.070		
AT4	Magnetite	22.41	0.52	26.11	48.83	1.87	0.96	0.01	100.72	-0.044	860	-14.13
	Ilmenite	50.12	0.07	5.76	39.82	2.30	1.65	0.01	99.73	0.102		
AT5	Magnetite	22.41	0.52	26.11	48.83	1.87	0.96	0.01	100.72	-0.044	843	-14.56
	Ilmenite	50.44	0.07	5.46	40.18	2.28	1.62	0.00	100.05	0.098		
AT6	Magnetite	22.41	0.52	26.11	48.83	1.87	0.96	0.01	100.72	-0.044	790	-16.05
	Ilmenite	51.25	0.05	4.54	40.83	2.28	1.66	0.02	100.63	0.109		
AT7	Magnetite	22.41	0.52	26.11	48.83	1.87	0.96	0.01	100.72	-0.044	835	-14.77
	Ilmenite	51.09	0.05	5.35	40.51	2.28	1.76	0.01	101.06	0.134		
AT8	Magnetite	22.41	0.52	26.11	48.83	1.87	0.96	0.01	100.72	-0.044	829	-14.94
	Ilmenite	51.14	0.06	5.25	40.70	2.28	1.68	0.03	101.14	0.112		
AU1	Magnetite	22.33	0.51	25.91	48.50	1.84	1.03	0.01	100.13	-0.006	808	-15.52
	Ilmenite	51.10	0.07	4.84	40.64	2.30	1.68	0.02	100.66	0.107		
AU2	Magnetite	22.33	0.51	25.91	48.50	1.84	1.03	0.01	100.13	-0.006	832	-14.87
	Ilmenite	51.10	0.07	5.30	40.78	2.32	1.59	0.01	101.17	0.080		
AU3	Magnetite	22.33	0.51	25.91	48.50	1.84	1.03	0.01	100.13	-0.006	832	-14.86
	Ilmenite	51.03	0.04	5.30	40.79	2.32	1.55	0.02	101.05	0.070		
AU4	Magnetite	22.33	0.51	25.91	48.50	1.84	1.03	0.01	100.13	-0.006	860	-14.12
	Ilmenite	50.12	0.07	5.76	39.82	2.30	1.65	0.01	99.73	0.102		
AU5	Magnetite	22.33	0.51	25.91	48.50	1.84	1.03	0.01	100.13	-0.006	844	-14.55
	Ilmenite	50.44	0.07	5.46	40.18	2.28	1.62	0.00	100.05	0.098		
AU6	Magnetite	22.33	0.51	25.91	48.50	1.84	1.03	0.01	100.13	-0.006	790	-16.05
	Ilmenite	51.25	0.05	4.54	40.83	2.28	1.66	0.02	100.63	0.109		

Table F2 continued

LAI Pair identifier	Phase	TiO_2	Al_2O_3	Fe_2O_3	FeO	MnO	MgO	Cr_2O_3	Sum	log(Mg/Mn)	T	fO_2
AU7	Magnetite	22.33	0.51	25.91	48.50	1.84	1.03	0.01	100.13	-0.006	836	-14.77
	Ilmenite	51.09	0.05	5.35	40.51	2.28	1.76	0.01	101.06	0.134		
AU8	Magnetite	22.33	0.51	25.91	48.50	1.84	1.03	0.01	100.13	-0.006	829	-14.94
	Ilmenite	51.14	0.06	5.25	40.70	2.28	1.68	0.03	101.14	0.112		
AV1	Magnetite	22.71	0.53	25.54	49.11	1.83	0.99	0.02	100.73	-0.020	814	-15.40
	Ilmenite	51.10	0.07	4.84	40.64	2.30	1.68	0.02	100.66	0.107		
AV2	Magnetite	22.71	0.53	25.54	49.11	1.83	0.99	0.02	100.73	-0.020	839	-14.74
	Ilmenite	51.10	0.07	5.30	40.78	2.32	1.59	0.01	101.17	0.080		
AV3	Magnetite	22.71	0.53	25.54	49.11	1.83	0.99	0.02	100.73	-0.020	839	-14.74
	Ilmenite	51.03	0.04	5.30	40.79	2.32	1.55	0.02	101.05	0.070		
AV4	Magnetite	22.71	0.53	25.54	49.11	1.83	0.99	0.02	100.73	-0.020	868	-13.99
	Ilmenite	50.12	0.07	5.76	39.82	2.30	1.65	0.01	99.73	0.102		
AV5	Magnetite	22.71	0.53	25.54	49.11	1.83	0.99	0.02	100.73	-0.020	851	-14.42
	Ilmenite	50.44	0.07	5.46	40.18	2.28	1.62	0.00	100.05	0.098		
AV6	Magnetite	22.71	0.53	25.54	49.11	1.83	0.99	0.02	100.73	-0.020	796	-15.92
	Ilmenite	51.25	0.05	4.54	40.83	2.28	1.66	0.02	100.63	0.109		
AV7	Magnetite	22.71	0.53	25.54	49.11	1.83	0.99	0.02	100.73	-0.020	842	-14.64
	Ilmenite	51.09	0.05	5.35	40.51	2.28	1.76	0.01	101.06	0.134		
AV8	Magnetite	22.71	0.53	25.54	49.11	1.83	0.99	0.02	100.73	-0.020	836	-14.81
	Ilmenite	51.14	0.06	5.25	40.70	2.28	1.68	0.03	101.14	0.112		
AW1	Magnetite	22.30	0.52	26.11	48.55	1.85	1.02	0.02	100.38	-0.014	807	-15.55
	Ilmenite	51.10	0.07	4.84	40.64	2.30	1.68	0.02	100.66	0.107		
AW2	Magnetite	22.30	0.52	26.11	48.55	1.85	1.02	0.02	100.38	-0.014	830	-14.90
	Ilmenite	51.10	0.07	5.30	40.78	2.32	1.59	0.01	101.17	0.080		
AW3	Magnetite	22.30	0.52	26.11	48.55	1.85	1.02	0.02	100.38	-0.014	830	-14.89
	Ilmenite	51.03	0.04	5.30	40.79	2.32	1.55	0.02	101.05	0.070		
AW4	Magnetite	22.30	0.52	26.11	48.55	1.85	1.02	0.02	100.38	-0.014	859	-14.15
	Ilmenite	50.12	0.07	5.76	39.82	2.30	1.65	0.01	99.73	0.102		
AW5	Magnetite	22.30	0.52	26.11	48.55	1.85	1.02	0.02	100.38	-0.014	842	-14.58
	Ilmenite	50.44	0.07	5.46	40.18	2.28	1.62	0.00	100.05	0.098		
AW6	Magnetite	22.30	0.52	26.11	48.55	1.85	1.02	0.02	100.38	-0.014	789	-16.07
	Ilmenite	51.25	0.05	4.54	40.83	2.28	1.66	0.02	100.63	0.109		
AW7	Magnetite	22.30	0.52	26.11	48.55	1.85	1.02	0.02	100.38	-0.014	834	-14.80
	Ilmenite	51.09	0.05	5.35	40.51	2.28	1.76	0.01	101.06	0.134		
AW8	Magnetite	22.30	0.52	26.11	48.55	1.85	1.02	0.02	100.38	-0.014	828	-14.97
	Ilmenite	51.14	0.06	5.25	40.70	2.28	1.68	0.03	101.14	0.112		
AX1	Magnetite	22.22	0.50	26.10	48.53	1.82	0.95	0.00	100.13	-0.037	806	-15.56
	Ilmenite	51.10	0.07	4.84	40.64	2.30	1.68	0.02	100.66	0.107		

Table F2 continued

LAI Pair identifier	Phase	TiO_2	Al_2O_3	Fe_2O_3	FeO	MnO	MgO	Cr_2O_3	Sum	log(Mg/Mn)	T	fO_2
AX2	Magnetite	22.22	0.50	26.10	48.53	1.82	0.95	0.00	100.13	-0.037	830	-14.91
	Ilmenite	51.10	0.07	5.30	40.78	2.32	1.59	0.01	101.17	0.080		
AX3	Magnetite	22.22	0.50	26.10	48.53	1.82	0.95	0.00	100.13	-0.037	830	-14.90
	Ilmenite	51.03	0.04	5.30	40.79	2.32	1.55	0.02	101.05	0.070		
AX4	Magnetite	22.22	0.50	26.10	48.53	1.82	0.95	0.00	100.13	-0.037	858	-14.16
	Ilmenite	50.12	0.07	5.76	39.82	2.30	1.65	0.01	99.73	0.102		
AX5	Magnetite	22.22	0.50	26.10	48.53	1.82	0.95	0.00	100.13	-0.037	842	-14.59
	Ilmenite	50.44	0.07	5.46	40.18	2.28	1.62	0.00	100.05	0.098		
AX6	Magnetite	22.22	0.50	26.10	48.53	1.82	0.95	0.00	100.13	-0.037	788	-16.08
	Ilmenite	51.25	0.05	4.54	40.83	2.28	1.66	0.02	100.63	0.109		
AX7	Magnetite	22.22	0.50	26.10	48.53	1.82	0.95	0.00	100.13	-0.037	834	-14.80
	Ilmenite	51.09	0.05	5.35	40.51	2.28	1.76	0.01	101.06	0.134		
AX8	Magnetite	22.22	0.50	26.10	48.53	1.82	0.95	0.00	100.13	-0.037	827	-14.97
	Ilmenite	51.14	0.06	5.25	40.70	2.28	1.68	0.03	101.14	0.112		
AY1	Magnetite	22.52	0.54	25.89	48.93	1.80	1.01	0.02	100.71	-0.006	810	-15.48
	Ilmenite	51.10	0.07	4.84	40.64	2.30	1.68	0.02	100.66	0.107		
AY2	Magnetite	22.52	0.54	25.89	48.93	1.80	1.01	0.02	100.71	-0.006	834	-14.82
	Ilmenite	51.10	0.07	5.30	40.78	2.32	1.59	0.01	101.17	0.080		
AY3	Magnetite	22.52	0.54	25.89	48.93	1.80	1.01	0.02	100.71	-0.006	835	-14.82
	Ilmenite	51.03	0.04	5.30	40.79	2.32	1.55	0.02	101.05	0.070		
AY4	Magnetite	22.52	0.54	25.89	48.93	1.80	1.01	0.02	100.71	-0.006	863	-14.07
	Ilmenite	50.12	0.07	5.76	39.82	2.30	1.65	0.01	99.73	0.102		
AY5	Magnetite	22.52	0.54	25.89	48.93	1.80	1.01	0.02	100.71	-0.006	846	-14.50
	Ilmenite	50.44	0.07	5.46	40.18	2.28	1.62	0.00	100.05	0.098		
AY6	Magnetite	22.52	0.54	25.89	48.93	1.80	1.01	0.02	100.71	-0.006	792	-16.00
	Ilmenite	51.25	0.05	4.54	40.83	2.28	1.66	0.02	100.63	0.109		
AY7	Magnetite	22.52	0.54	25.89	48.93	1.80	1.01	0.02	100.71	-0.006	838	-14.72
	Ilmenite	51.09	0.05	5.35	40.51	2.28	1.76	0.01	101.06	0.134		
AY8	Magnetite	22.52	0.54	25.89	48.93	1.80	1.01	0.02	100.71	-0.006	832	-14.89
	Ilmenite	51.14	0.06	5.25	40.70	2.28	1.68	0.03	101.14	0.112		
AZ1	Magnetite	22.14	0.55	26.33	48.36	1.84	1.04	0.01	100.27	-0.003	804	-15.60
	Ilmenite	51.10	0.07	4.84	40.64	2.30	1.68	0.02	100.66	0.107		
AZ2	Magnetite	22.14	0.55	26.33	48.36	1.84	1.04	0.01	100.27	-0.003	827	-14.95
	Ilmenite	51.10	0.07	5.30	40.78	2.32	1.59	0.01	101.17	0.080		
AZ3	Magnetite	22.14	0.55	26.33	48.36	1.84	1.04	0.01	100.27	-0.003	828	-14.95
	Ilmenite	51.03	0.04	5.30	40.79	2.32	1.55	0.02	101.05	0.070		
AZ4	Magnetite	22.14	0.55	26.33	48.36	1.84	1.04	0.01	100.27	-0.003	856	-14.21
	Ilmenite	50.12	0.07	5.76	39.82	2.30	1.65	0.01	99.73	0.102		

Table F2 continued

LAI Pair identifier	Phase	TiO_2	Al_2O_3	Fe_2O_3	FeO	MnO	MgO	Cr_2O_3	Sum	log(Mg/Mn)	T	fO_2
AZ5	Magnetite	22.14	0.55	26.33	48.36	1.84	1.04	0.01	100.27	-0.003	839	-14.64
	Ilmenite	50.44	0.07	5.46	40.18	2.28	1.62	0.00	100.05	0.098		
AZ6	Magnetite	22.14	0.55	26.33	48.36	1.84	1.04	0.01	100.27	-0.003	786	-16.12
	Ilmenite	51.25	0.05	4.54	40.83	2.28	1.66	0.02	100.63	0.109		
AZ7	Magnetite	22.14	0.55	26.33	48.36	1.84	1.04	0.01	100.27	-0.003	831	-14.85
	Ilmenite	51.09	0.05	5.35	40.51	2.28	1.76	0.01	101.06	0.134		
AZ8	Magnetite	22.14	0.55	26.33	48.36	1.84	1.04	0.01	100.27	-0.003	825	-15.02
	Ilmenite	51.14	0.06	5.25	40.70	2.28	1.68	0.03	101.14	0.112		
BA1	Magnetite	22.39	0.51	26.13	48.74	1.84	1.01	0.01	100.63	-0.017	807	-15.54
	Ilmenite	51.10	0.07	4.84	40.64	2.30	1.68	0.02	100.66	0.107		
BA2	Magnetite	22.39	0.51	26.13	48.74	1.84	1.01	0.01	100.63	-0.017	831	-14.89
	Ilmenite	51.10	0.07	5.30	40.78	2.32	1.59	0.01	101.17	0.080		
BA3	Magnetite	22.39	0.51	26.13	48.74	1.84	1.01	0.01	100.63	-0.017	831	-14.88
	Ilmenite	51.03	0.04	5.30	40.79	2.32	1.55	0.02	101.05	0.070		
BA4	Magnetite	22.39	0.51	26.13	48.74	1.84	1.01	0.01	100.63	-0.017	859	-14.14
	Ilmenite	50.12	0.07	5.76	39.82	2.30	1.65	0.01	99.73	0.102		
BA5	Magnetite	22.39	0.51	26.13	48.74	1.84	1.01	0.01	100.63	-0.017	843	-14.57
	Ilmenite	50.44	0.07	5.46	40.18	2.28	1.62	0.00	100.05	0.098		
BA6	Magnetite	22.39	0.51	26.13	48.74	1.84	1.01	0.01	100.63	-0.017	789	-16.06
	Ilmenite	51.25	0.05	4.54	40.83	2.28	1.66	0.02	100.63	0.109		
BA7	Magnetite	22.39	0.51	26.13	48.74	1.84	1.01	0.01	100.63	-0.017	835	-14.79
	Ilmenite	51.09	0.05	5.35	40.51	2.28	1.76	0.01	101.06	0.134		
BA8	Magnetite	22.39	0.51	26.13	48.74	1.84	1.01	0.01	100.63	-0.017	828	-14.95
	Ilmenite	51.14	0.06	5.25	40.70	2.28	1.68	0.03	101.14	0.112		
BB1	Magnetite	22.52	0.57	25.86	48.91	1.80	1.02	0.01	100.69	0.000	811	-15.47
	Ilmenite	51.10	0.07	4.84	40.64	2.30	1.68	0.02	100.66	0.107		
BB2	Magnetite	22.52	0.57	25.86	48.91	1.80	1.02	0.01	100.69	0.000	835	-14.81
	Ilmenite	51.10	0.07	5.30	40.78	2.32	1.59	0.01	101.17	0.080		
BB3	Magnetite	22.52	0.57	25.86	48.91	1.80	1.02	0.01	100.69	0.000	835	-14.81
	Ilmenite	51.03	0.04	5.30	40.79	2.32	1.55	0.02	101.05	0.070		
BB4	Magnetite	22.52	0.57	25.86	48.91	1.80	1.02	0.01	100.69	0.000	863	-14.07
	Ilmenite	50.12	0.07	5.76	39.82	2.30	1.65	0.01	99.73	0.102		
BB5	Magnetite	22.52	0.57	25.86	48.91	1.80	1.02	0.01	100.69	0.000	847	-14.50
	Ilmenite	50.44	0.07	5.46	40.18	2.28	1.62	0.00	100.05	0.098		
BB6	Magnetite	22.52	0.57	25.86	48.91	1.80	1.02	0.01	100.69	0.000	792	-15.99
	Ilmenite	51.25	0.05	4.54	40.83	2.28	1.66	0.02	100.63	0.109		
BB7	Magnetite	22.52	0.57	25.86	48.91	1.80	1.02	0.01	100.69	0.000	839	-14.71
	Ilmenite	51.09	0.05	5.35	40.51	2.28	1.76	0.01	101.06	0.134		

Table F2 continued

LAI Pair identifier	Phase	TiO_2	Al_2O_3	Fe_2O_3	FeO	MnO	MgO	Cr_2O_3	Sum	log(Mg/Mn)	T	fO_2
BB8	Magnetite	22.52	0.57	25.86	48.91	1.80	1.02	0.01	100.69	0.000	832	-14.88
	Ilmenite	51.14	0.06	5.25	40.70	2.28	1.68	0.03	101.14	0.112		
BC1	Magnetite	22.62	0.52	25.72	48.98	1.82	1.02	0.02	100.70	-0.007	812	-15.44
	Ilmenite	51.10	0.07	4.84	40.64	2.30	1.68	0.02	100.66	0.107		
BC2	Magnetite	22.62	0.52	25.72	48.98	1.82	1.02	0.02	100.70	-0.007	836	-14.79
	Ilmenite	51.10	0.07	5.30	40.78	2.32	1.59	0.01	101.17	0.080		
BC3	Magnetite	22.62	0.52	25.72	48.98	1.82	1.02	0.02	100.70	-0.007	836	-14.78
	Ilmenite	51.03	0.04	5.30	40.79	2.32	1.55	0.02	101.05	0.070		
BC4	Magnetite	22.62	0.52	25.72	48.98	1.82	1.02	0.02	100.70	-0.007	865	-14.04
	Ilmenite	50.12	0.07	5.76	39.82	2.30	1.65	0.01	99.73	0.102		
BC5	Magnetite	22.62	0.52	25.72	48.98	1.82	1.02	0.02	100.70	-0.007	848	-14.47
	Ilmenite	50.44	0.07	5.46	40.18	2.28	1.62	0.00	100.05	0.098		
BC6	Magnetite	22.62	0.52	25.72	48.98	1.82	1.02	0.02	100.70	-0.007	794	-15.97
	Ilmenite	51.25	0.05	4.54	40.83	2.28	1.66	0.02	100.63	0.109		
BC7	Magnetite	22.62	0.52	25.72	48.98	1.82	1.02	0.02	100.70	-0.007	840	-14.69
	Ilmenite	51.09	0.05	5.35	40.51	2.28	1.76	0.01	101.06	0.134		
BC8	Magnetite	22.62	0.52	25.72	48.98	1.82	1.02	0.02	100.70	-0.007	834	-14.85
	Ilmenite	51.14	0.06	5.25	40.70	2.28	1.68	0.03	101.14	0.112		
BD1	Magnetite	22.36	0.55	26.21	48.65	1.83	1.07	0.01	100.68	0.013	806	-15.55
	Ilmenite	51.10	0.07	4.84	40.64	2.30	1.68	0.02	100.66	0.107		
BD2	Magnetite	22.36	0.55	26.21	48.65	1.83	1.07	0.01	100.68	0.013	830	-14.90
	Ilmenite	51.10	0.07	5.30	40.78	2.32	1.59	0.01	101.17	0.080		
BD3	Magnetite	22.36	0.55	26.21	48.65	1.83	1.07	0.01	100.68	0.013	830	-14.90
	Ilmenite	51.03	0.04	5.30	40.79	2.32	1.55	0.02	101.05	0.070		
BD4	Magnetite	22.36	0.55	26.21	48.65	1.83	1.07	0.01	100.68	0.013	858	-14.16
	Ilmenite	50.12	0.07	5.76	39.82	2.30	1.65	0.01	99.73	0.102		
BD5	Magnetite	22.36	0.55	26.21	48.65	1.83	1.07	0.01	100.68	0.013	842	-14.59
	Ilmenite	50.44	0.07	5.46	40.18	2.28	1.62	0.00	100.05	0.098		
BD6	Magnetite	22.36	0.55	26.21	48.65	1.83	1.07	0.01	100.68	0.013	788	-16.08
	Ilmenite	51.25	0.05	4.54	40.83	2.28	1.66	0.02	100.63	0.109		
BD7	Magnetite	22.36	0.55	26.21	48.65	1.83	1.07	0.01	100.68	0.013	834	-14.80
	Ilmenite	51.09	0.05	5.35	40.51	2.28	1.76	0.01	101.06	0.134		
BD8	Magnetite	22.36	0.55	26.21	48.65	1.83	1.07	0.01	100.68	0.013	828	-14.97
	Ilmenite	51.14	0.06	5.25	40.70	2.28	1.68	0.03	101.14	0.112		
BE1	Magnetite	22.65	0.49	25.66	49.10	1.84	0.95	0.04	100.73	-0.042	813	-15.43
	Ilmenite	51.10	0.07	4.84	40.64	2.30	1.68	0.02	100.66	0.107		
BE2	Magnetite	22.65	0.49	25.66	49.10	1.84	0.95	0.04	100.73	-0.042	837	-14.77
	Ilmenite	51.10	0.07	5.30	40.78	2.32	1.59	0.01	101.17	0.080		

Table F2 continued

LAI Pair identifier	Phase	TiO_2	Al_2O_3	Fe_2O_3	FeO	MnO	MgO	Cr_2O_3	Sum	log(Mg/Mn)	T	fO_2
BE3	Magnetite	22.65	0.49	25.66	49.10	1.84	0.95	0.04	100.73	-0.042	837	-14.76
	Ilmenite	51.03	0.04	5.30	40.79	2.32	1.55	0.02	101.05	0.070		
BE4	Magnetite	22.65	0.49	25.66	49.10	1.84	0.95	0.04	100.73	-0.042	866	-14.02
	Ilmenite	50.12	0.07	5.76	39.82	2.30	1.65	0.01	99.73	0.102		
BE5	Magnetite	22.65	0.49	25.66	49.10	1.84	0.95	0.04	100.73	-0.042	849	-14.45
	Ilmenite	50.44	0.07	5.46	40.18	2.28	1.62	0.00	100.05	0.098		
BE6	Magnetite	22.65	0.49	25.66	49.10	1.84	0.95	0.04	100.73	-0.042	794	-15.95
	Ilmenite	51.25	0.05	4.54	40.83	2.28	1.66	0.02	100.63	0.109		
BE7	Magnetite	22.65	0.49	25.66	49.10	1.84	0.95	0.04	100.73	-0.042	841	-14.67
	Ilmenite	51.09	0.05	5.35	40.51	2.28	1.76	0.01	101.06	0.134		
BE8	Magnetite	22.65	0.49	25.66	49.10	1.84	0.95	0.04	100.73	-0.042	835	-14.84
	Ilmenite	51.14	0.06	5.25	40.70	2.28	1.68	0.03	101.14	0.112		
BF1	Magnetite	22.75	0.50	25.55	49.20	1.83	0.97	0.01	100.81	-0.030	814	-15.40
	Ilmenite	51.10	0.07	4.84	40.64	2.30	1.68	0.02	100.66	0.107		
BF2	Magnetite	22.75	0.50	25.55	49.20	1.83	0.97	0.01	100.81	-0.030	838	-14.74
	Ilmenite	51.10	0.07	5.30	40.78	2.32	1.59	0.01	101.17	0.080		
BF3	Magnetite	22.75	0.50	25.55	49.20	1.83	0.97	0.01	100.81	-0.030	839	-14.74
	Ilmenite	51.03	0.04	5.30	40.79	2.32	1.55	0.02	101.05	0.070		
BF4	Magnetite	22.75	0.50	25.55	49.20	1.83	0.97	0.01	100.81	-0.030	868	-13.99
	Ilmenite	50.12	0.07	5.76	39.82	2.30	1.65	0.01	99.73	0.102		
BF5	Magnetite	22.75	0.50	25.55	49.20	1.83	0.97	0.01	100.81	-0.030	851	-14.42
	Ilmenite	50.44	0.07	5.46	40.18	2.28	1.62	0.00	100.05	0.098		
BF6	Magnetite	22.75	0.50	25.55	49.20	1.83	0.97	0.01	100.81	-0.030	796	-15.92
	Ilmenite	51.25	0.05	4.54	40.83	2.28	1.66	0.02	100.63	0.109		
BF7	Magnetite	22.75	0.50	25.55	49.20	1.83	0.97	0.01	100.81	-0.030	842	-14.64
	Ilmenite	51.09	0.05	5.35	40.51	2.28	1.76	0.01	101.06	0.134		
BF8	Magnetite	22.75	0.50	25.55	49.20	1.83	0.97	0.01	100.81	-0.030	836	-14.81
	Ilmenite	51.14	0.06	5.25	40.70	2.28	1.68	0.03	101.14	0.112		
BG1	Magnetite	22.58	0.54	25.84	49.05	1.81	0.98	0.00	100.80	-0.021	811	-15.46
	Ilmenite	51.10	0.07	4.84	40.64	2.30	1.68	0.02	100.66	0.107		
BG2	Magnetite	22.58	0.54	25.84	49.05	1.81	0.98	0.00	100.80	-0.021	835	-14.81
	Ilmenite	51.10	0.07	5.30	40.78	2.32	1.59	0.01	101.17	0.080		
BG3	Magnetite	22.58	0.54	25.84	49.05	1.81	0.98	0.00	100.80	-0.021	835	-14.80
	Ilmenite	51.03	0.04	5.30	40.79	2.32	1.55	0.02	101.05	0.070		
BG4	Magnetite	22.58	0.54	25.84	49.05	1.81	0.98	0.00	100.80	-0.021	864	-14.06
	Ilmenite	50.12	0.07	5.76	39.82	2.30	1.65	0.01	99.73	0.102		
BG5	Magnetite	22.58	0.54	25.84	49.05	1.81	0.98	0.00	100.80	-0.021	847	-14.49
	Ilmenite	50.44	0.07	5.46	40.18	2.28	1.62	0.00	100.05	0.098		

Table F2 continued

LAI Pair identifier	Phase	TiO_2	Al_2O_3	Fe_2O_3	FeO	MnO	MgO	Cr_2O_3	Sum	log(Mg/Mn)	T	fO_2
BG6	Magnetite	22.58	0.54	25.84	49.05	1.81	0.98	0.00	100.80	-0.021	793	-15.98
	Ilmenite	51.25	0.05	4.54	40.83	2.28	1.66	0.02	100.63	0.109		
BG7	Magnetite	22.58	0.54	25.84	49.05	1.81	0.98	0.00	100.80	-0.021	839	-14.70
	Ilmenite	51.09	0.05	5.35	40.51	2.28	1.76	0.01	101.06	0.134		
BG8	Magnetite	22.58	0.54	25.84	49.05	1.81	0.98	0.00	100.80	-0.021	833	-14.87
	Ilmenite	51.14	0.06	5.25	40.70	2.28	1.68	0.03	101.14	0.112		
BH1	Magnetite	22.41	0.46	25.67	48.63	1.84	0.96	0.02	99.99	-0.039	810	-15.48
	Ilmenite	51.10	0.07	4.84	40.64	2.30	1.68	0.02	100.66	0.107		
BH2	Magnetite	22.41	0.46	25.67	48.63	1.84	0.96	0.02	99.99	-0.039	834	-14.82
	Ilmenite	51.10	0.07	5.30	40.78	2.32	1.59	0.01	101.17	0.080		
BH3	Magnetite	22.41	0.46	25.67	48.63	1.84	0.96	0.02	99.99	-0.039	834	-14.82
	Ilmenite	51.03	0.04	5.30	40.79	2.32	1.55	0.02	101.05	0.070		
BH4	Magnetite	22.41	0.46	25.67	48.63	1.84	0.96	0.02	99.99	-0.039	863	-14.08
	Ilmenite	50.12	0.07	5.76	39.82	2.30	1.65	0.01	99.73	0.102		
BH5	Magnetite	22.41	0.46	25.67	48.63	1.84	0.96	0.02	99.99	-0.039	846	-14.51
	Ilmenite	50.44	0.07	5.46	40.18	2.28	1.62	0.00	100.05	0.098		
BH6	Magnetite	22.41	0.46	25.67	48.63	1.84	0.96	0.02	99.99	-0.039	792	-16.00
	Ilmenite	51.25	0.05	4.54	40.83	2.28	1.66	0.02	100.63	0.109		
BH7	Magnetite	22.41	0.46	25.67	48.63	1.84	0.96	0.02	99.99	-0.039	838	-14.72
	Ilmenite	51.09	0.05	5.35	40.51	2.28	1.76	0.01	101.06	0.134		
BH8	Magnetite	22.41	0.46	25.67	48.63	1.84	0.96	0.02	99.99	-0.039	832	-14.89
	Ilmenite	51.14	0.06	5.25	40.70	2.28	1.68	0.03	101.14	0.112		
BI1	Magnetite	22.75	0.55	25.28	48.87	1.84	1.10	0.01	100.40	0.023	816	-15.37
	Ilmenite	51.10	0.07	4.84	40.64	2.30	1.68	0.02	100.66	0.107		
BI2	Magnetite	22.75	0.55	25.28	48.87	1.84	1.10	0.01	100.40	0.023	840	-14.71
	Ilmenite	51.10	0.07	5.30	40.78	2.32	1.59	0.01	101.17	0.080		
BI3	Magnetite	22.75	0.55	25.28	48.87	1.84	1.10	0.01	100.40	0.023	840	-14.70
	Ilmenite	51.03	0.04	5.30	40.79	2.32	1.55	0.02	101.05	0.070		
BI4	Magnetite	22.75	0.55	25.28	48.87	1.84	1.10	0.01	100.40	0.023	869	-13.96
	Ilmenite	50.12	0.07	5.76	39.82	2.30	1.65	0.01	99.73	0.102		
BI5	Magnetite	22.75	0.55	25.28	48.87	1.84	1.10	0.01	100.40	0.023	852	-14.39
	Ilmenite	50.44	0.07	5.46	40.18	2.28	1.62	0.00	100.05	0.098		
BI6	Magnetite	22.75	0.55	25.28	48.87	1.84	1.10	0.01	100.40	0.023	797	-15.89
	Ilmenite	51.25	0.05	4.54	40.83	2.28	1.66	0.02	100.63	0.109		
BI7	Magnetite	22.75	0.55	25.28	48.87	1.84	1.10	0.01	100.40	0.023	844	-14.61
	Ilmenite	51.09	0.05	5.35	40.51	2.28	1.76	0.01	101.06	0.134		
BI8	Magnetite	22.75	0.55	25.28	48.87	1.84	1.10	0.01	100.40	0.023	838	-14.78
	Ilmenite	51.14	0.06	5.25	40.70	2.28	1.68	0.03	101.14	0.112		

Table F2 continued

LAI Pair identifier	Phase	TiO_2	Al_2O_3	Fe_2O_3	FeO	MnO	MgO	Cr_2O_3	Sum	log(Mg/Mn)	T	fO_2
BJ1	Magnetite	22.73	0.54	25.27	48.85	1.83	1.09	0.00	100.30	0.020	816	-15.37
	Ilmenite	51.10	0.07	4.84	40.64	2.30	1.68	0.02	100.66	0.107		
BJ2	Magnetite	22.73	0.54	25.27	48.85	1.83	1.09	0.00	100.30	0.020	840	-14.71
	Ilmenite	51.10	0.07	5.30	40.78	2.32	1.59	0.01	101.17	0.080		
BJ3	Magnetite	22.73	0.54	25.27	48.85	1.83	1.09	0.00	100.30	0.020	840	-14.71
	Ilmenite	51.03	0.04	5.30	40.79	2.32	1.55	0.02	101.05	0.070		
BJ4	Magnetite	22.73	0.54	25.27	48.85	1.83	1.09	0.00	100.30	0.020	869	-13.96
	Ilmenite	50.12	0.07	5.76	39.82	2.30	1.65	0.01	99.73	0.102		
BJ5	Magnetite	22.73	0.54	25.27	48.85	1.83	1.09	0.00	100.30	0.020	852	-14.39
	Ilmenite	50.44	0.07	5.46	40.18	2.28	1.62	0.00	100.05	0.098		
BJ6	Magnetite	22.73	0.54	25.27	48.85	1.83	1.09	0.00	100.30	0.020	797	-15.89
	Ilmenite	51.25	0.05	4.54	40.83	2.28	1.66	0.02	100.63	0.109		
BJ7	Magnetite	22.73	0.54	25.27	48.85	1.83	1.09	0.00	100.30	0.020	844	-14.61
	Ilmenite	51.09	0.05	5.35	40.51	2.28	1.76	0.01	101.06	0.134		
BJ8	Magnetite	22.73	0.54	25.27	48.85	1.83	1.09	0.00	100.30	0.020	838	-14.78
	Ilmenite	51.14	0.06	5.25	40.70	2.28	1.68	0.03	101.14	0.112		
BK1	Magnetite	22.80	0.49	25.48	48.91	1.83	1.16	0.01	100.68	0.046	814	-15.41
	Ilmenite	51.10	0.07	4.84	40.64	2.30	1.68	0.02	100.66	0.107		
BK2	Magnetite	22.80	0.49	25.48	48.91	1.83	1.16	0.01	100.68	0.046	838	-14.75
	Ilmenite	51.10	0.07	5.30	40.78	2.32	1.59	0.01	101.17	0.080		
BK3	Magnetite	22.80	0.49	25.48	48.91	1.83	1.16	0.01	100.68	0.046	838	-14.74
	Ilmenite	51.03	0.04	5.30	40.79	2.32	1.55	0.02	101.05	0.070		
BK4	Magnetite	22.80	0.49	25.48	48.91	1.83	1.16	0.01	100.68	0.046	867	-14.00
	Ilmenite	50.12	0.07	5.76	39.82	2.30	1.65	0.01	99.73	0.102		
BK5	Magnetite	22.80	0.49	25.48	48.91	1.83	1.16	0.01	100.68	0.046	850	-14.43
	Ilmenite	50.44	0.07	5.46	40.18	2.28	1.62	0.00	100.05	0.098		
BK6	Magnetite	22.80	0.49	25.48	48.91	1.83	1.16	0.01	100.68	0.046	795	-15.93
	Ilmenite	51.25	0.05	4.54	40.83	2.28	1.66	0.02	100.63	0.109		
BK7	Magnetite	22.80	0.49	25.48	48.91	1.83	1.16	0.01	100.68	0.046	842	-14.65
	Ilmenite	51.09	0.05	5.35	40.51	2.28	1.76	0.01	101.06	0.134		
BK8	Magnetite	22.80	0.49	25.48	48.91	1.83	1.16	0.01	100.68	0.046	836	-14.82
	Ilmenite	51.14	0.06	5.25	40.70	2.28	1.68	0.03	101.14	0.112		
BL1	Magnetite	22.16	0.57	26.04	48.24	1.83	1.07	0.02	99.93	0.014	806	-15.56
	Ilmenite	51.10	0.07	4.84	40.64	2.30	1.68	0.02	100.66	0.107		
BL2	Magnetite	22.16	0.57	26.04	48.24	1.83	1.07	0.02	99.93	0.014	830	-14.91
	Ilmenite	51.10	0.07	5.30	40.78	2.32	1.59	0.01	101.17	0.080		
BL3	Magnetite	22.16	0.57	26.04	48.24	1.83	1.07	0.02	99.93	0.014	830	-14.90
	Ilmenite	51.03	0.04	5.30	40.79	2.32	1.55	0.02	101.05	0.070		

Table F2 continued

LAI Pair identifier	Phase	TiO_2	Al_2O_3	Fe_2O_3	FeO	MnO	MgO	Cr_2O_3	Sum	log(Mg/Mn)	T	fO_2
BL4	Magnetite	22.16	0.57	26.04	48.24	1.83	1.07	0.02	99.93	0.014	858	-14.16
	Ilmenite	50.12	0.07	5.76	39.82	2.30	1.65	0.01	99.73	0.102		
BL5	Magnetite	22.16	0.57	26.04	48.24	1.83	1.07	0.02	99.93	0.014	842	-14.59
	Ilmenite	50.44	0.07	5.46	40.18	2.28	1.62	0.00	100.05	0.098		
BL6	Magnetite	22.16	0.57	26.04	48.24	1.83	1.07	0.02	99.93	0.014	788	-16.08
	Ilmenite	51.25	0.05	4.54	40.83	2.28	1.66	0.02	100.63	0.109		
BL7	Magnetite	22.16	0.57	26.04	48.24	1.83	1.07	0.02	99.93	0.014	834	-14.81
	Ilmenite	51.09	0.05	5.35	40.51	2.28	1.76	0.01	101.06	0.134		
BL8	Magnetite	22.16	0.57	26.04	48.24	1.83	1.07	0.02	99.93	0.014	827	-14.97
	Ilmenite	51.14	0.06	5.25	40.70	2.28	1.68	0.03	101.14	0.112		
BM1	Magnetite	22.23	0.62	25.92	48.31	1.82	1.09	0.01	100.00	0.022	808	-15.53
	Ilmenite	51.10	0.07	4.84	40.64	2.30	1.68	0.02	100.66	0.107		
BM2	Magnetite	22.23	0.62	25.92	48.31	1.82	1.09	0.01	100.00	0.022	832	-14.87
	Ilmenite	51.10	0.07	5.30	40.78	2.32	1.59	0.01	101.17	0.080		
BM3	Magnetite	22.23	0.62	25.92	48.31	1.82	1.09	0.01	100.00	0.022	832	-14.87
	Ilmenite	51.03	0.04	5.30	40.79	2.32	1.55	0.02	101.05	0.070		
BM4	Magnetite	22.23	0.62	25.92	48.31	1.82	1.09	0.01	100.00	0.022	860	-14.12
	Ilmenite	50.12	0.07	5.76	39.82	2.30	1.65	0.01	99.73	0.102		
BM5	Magnetite	22.23	0.62	25.92	48.31	1.82	1.09	0.01	100.00	0.022	844	-14.55
	Ilmenite	50.44	0.07	5.46	40.18	2.28	1.62	0.00	100.05	0.098		
BM6	Magnetite	22.23	0.62	25.92	48.31	1.82	1.09	0.01	100.00	0.022	790	-16.05
	Ilmenite	51.25	0.05	4.54	40.83	2.28	1.66	0.02	100.63	0.109		
BM7	Magnetite	22.23	0.62	25.92	48.31	1.82	1.09	0.01	100.00	0.022	836	-14.77
	Ilmenite	51.09	0.05	5.35	40.51	2.28	1.76	0.01	101.06	0.134		
BM8	Magnetite	22.23	0.62	25.92	48.31	1.82	1.09	0.01	100.00	0.022	829	-14.94
	Ilmenite	51.14	0.06	5.25	40.70	2.28	1.68	0.03	101.14	0.112		
BN1	Magnetite	22.44	0.55	26.00	48.75	1.84	1.04	0.02	100.63	-0.003	809	-15.51
	Ilmenite	51.10	0.07	4.84	40.64	2.30	1.68	0.02	100.66	0.107		
BN2	Magnetite	22.44	0.55	26.00	48.75	1.84	1.04	0.02	100.63	-0.003	833	-14.86
	Ilmenite	51.10	0.07	5.30	40.78	2.32	1.59	0.01	101.17	0.080		
BN3	Magnetite	22.44	0.55	26.00	48.75	1.84	1.04	0.02	100.63	-0.003	833	-14.85
	Ilmenite	51.03	0.04	5.30	40.79	2.32	1.55	0.02	101.05	0.070		
BN4	Magnetite	22.44	0.55	26.00	48.75	1.84	1.04	0.02	100.63	-0.003	861	-14.11
	Ilmenite	50.12	0.07	5.76	39.82	2.30	1.65	0.01	99.73	0.102		
BN5	Magnetite	22.44	0.55	26.00	48.75	1.84	1.04	0.02	100.63	-0.003	845	-14.54
	Ilmenite	50.44	0.07	5.46	40.18	2.28	1.62	0.00	100.05	0.098		
BN6	Magnetite	22.44	0.55	26.00	48.75	1.84	1.04	0.02	100.63	-0.003	791	-16.03
	Ilmenite	51.25	0.05	4.54	40.83	2.28	1.66	0.02	100.63	0.109		

Table F2 continued

LAI Pair identifier	Phase	TiO_2	Al_2O_3	Fe_2O_3	FeO	MnO	MgO	Cr_2O_3	Sum	log(Mg/Mn)	T	fO_2
BN7	Magnetite	22.44	0.55	26.00	48.75	1.84	1.04	0.02	100.63	-0.003	836	-14.75
	Ilmenite	51.09	0.05	5.35	40.51	2.28	1.76	0.01	101.06	0.134		
BN8	Magnetite	22.44	0.55	26.00	48.75	1.84	1.04	0.02	100.63	-0.003	830	-14.92
	Ilmenite	51.14	0.06	5.25	40.70	2.28	1.68	0.03	101.14	0.112		
BO1	Magnetite	22.50	0.56	25.93	48.77	1.83	1.08	0.02	100.70	0.014	810	-15.49
	Ilmenite	51.10	0.07	4.84	40.64	2.30	1.68	0.02	100.66	0.107		
BO2	Magnetite	22.50	0.56	25.93	48.77	1.83	1.08	0.02	100.70	0.014	833	-14.84
	Ilmenite	51.10	0.07	5.30	40.78	2.32	1.59	0.01	101.17	0.080		
BO3	Magnetite	22.50	0.56	25.93	48.77	1.83	1.08	0.02	100.70	0.014	834	-14.83
	Ilmenite	51.03	0.04	5.30	40.79	2.32	1.55	0.02	101.05	0.070		
BO4	Magnetite	22.50	0.56	25.93	48.77	1.83	1.08	0.02	100.70	0.014	862	-14.09
	Ilmenite	50.12	0.07	5.76	39.82	2.30	1.65	0.01	99.73	0.102		
BO5	Magnetite	22.50	0.56	25.93	48.77	1.83	1.08	0.02	100.70	0.014	845	-14.52
	Ilmenite	50.44	0.07	5.46	40.18	2.28	1.62	0.00	100.05	0.098		
BO6	Magnetite	22.50	0.56	25.93	48.77	1.83	1.08	0.02	100.70	0.014	791	-16.02
	Ilmenite	51.25	0.05	4.54	40.83	2.28	1.66	0.02	100.63	0.109		
BO7	Magnetite	22.50	0.56	25.93	48.77	1.83	1.08	0.02	100.70	0.014	837	-14.74
	Ilmenite	51.09	0.05	5.35	40.51	2.28	1.76	0.01	101.06	0.134		
BO8	Magnetite	22.50	0.56	25.93	48.77	1.83	1.08	0.02	100.70	0.014	831	-14.91
	Ilmenite	51.14	0.06	5.25	40.70	2.28	1.68	0.03	101.14	0.112		
BP1	Magnetite	22.71	0.49	25.83	49.00	1.84	1.10	0.00	100.97	0.024	811	-15.47
	Ilmenite	51.10	0.07	4.84	40.64	2.30	1.68	0.02	100.66	0.107		
BP2	Magnetite	22.71	0.49	25.83	49.00	1.84	1.10	0.00	100.97	0.024	835	-14.81
	Ilmenite	51.10	0.07	5.30	40.78	2.32	1.59	0.01	101.17	0.080		
BP3	Magnetite	22.71	0.49	25.83	49.00	1.84	1.10	0.00	100.97	0.024	835	-14.80
	Ilmenite	51.03	0.04	5.30	40.79	2.32	1.55	0.02	101.05	0.070		
BP4	Magnetite	22.71	0.49	25.83	49.00	1.84	1.10	0.00	100.97	0.024	864	-14.06
	Ilmenite	50.12	0.07	5.76	39.82	2.30	1.65	0.01	99.73	0.102		
BP5	Magnetite	22.71	0.49	25.83	49.00	1.84	1.10	0.00	100.97	0.024	847	-14.49
	Ilmenite	50.44	0.07	5.46	40.18	2.28	1.62	0.00	100.05	0.098		
BP6	Magnetite	22.71	0.49	25.83	49.00	1.84	1.10	0.00	100.97	0.024	793	-15.99
	Ilmenite	51.25	0.05	4.54	40.83	2.28	1.66	0.02	100.63	0.109		
BP7	Magnetite	22.71	0.49	25.83	49.00	1.84	1.10	0.00	100.97	0.024	839	-14.71
	Ilmenite	51.09	0.05	5.35	40.51	2.28	1.76	0.01	101.06	0.134		
BP8	Magnetite	22.71	0.49	25.83	49.00	1.84	1.10	0.00	100.97	0.024	832	-14.88
	Ilmenite	51.14	0.06	5.25	40.70	2.28	1.68	0.03	101.14	0.112		
BQ1	Magnetite	22.73	0.52	25.75	49.08	1.82	1.08	0.01	100.99	0.020	812	-15.44
	Ilmenite	51.10	0.07	4.84	40.64	2.30	1.68	0.02	100.66	0.107		

Table F2 continued

LAI Pair identifier	Phase	TiO_2	Al_2O_3	Fe_2O_3	FeO	MnO	MgO	Cr_2O_3	Sum	log(Mg/Mn)	T	fO_2
BQ2	Magnetite	22.73	0.52	25.75	49.08	1.82	1.08	0.01	100.99	0.020	836	-14.78
	Ilmenite	51.10	0.07	5.30	40.78	2.32	1.59	0.01	101.17	0.080		
BQ3	Magnetite	22.73	0.52	25.75	49.08	1.82	1.08	0.01	100.99	0.020	837	-14.78
	Ilmenite	51.03	0.04	5.30	40.79	2.32	1.55	0.02	101.05	0.070		
BQ4	Magnetite	22.73	0.52	25.75	49.08	1.82	1.08	0.01	100.99	0.020	865	-14.03
	Ilmenite	50.12	0.07	5.76	39.82	2.30	1.65	0.01	99.73	0.102		
BQ5	Magnetite	22.73	0.52	25.75	49.08	1.82	1.08	0.01	100.99	0.020	848	-14.47
	Ilmenite	50.44	0.07	5.46	40.18	2.28	1.62	0.00	100.05	0.098		
BQ6	Magnetite	22.73	0.52	25.75	49.08	1.82	1.08	0.01	100.99	0.020	794	-15.96
	Ilmenite	51.25	0.05	4.54	40.83	2.28	1.66	0.02	100.63	0.109		
BQ7	Magnetite	22.73	0.52	25.75	49.08	1.82	1.08	0.01	100.99	0.020	840	-14.68
	Ilmenite	51.09	0.05	5.35	40.51	2.28	1.76	0.01	101.06	0.134		
BQ8	Magnetite	22.73	0.52	25.75	49.08	1.82	1.08	0.01	100.99	0.020	834	-14.85
	Ilmenite	51.14	0.06	5.25	40.70	2.28	1.68	0.03	101.14	0.112		
BR7	Magnetite	22.05	0.77	26.41	47.94	1.80	1.31	0.01	100.29	0.110	831	-14.86
	Ilmenite	51.09	0.05	5.35	40.51	2.28	1.76	0.01	101.06	0.134		
BS7	Magnetite	22.26	0.78	26.18	48.25	1.77	1.31	0.00	100.55	0.115	834	-14.79
	Ilmenite	51.09	0.05	5.35	40.51	2.28	1.76	0.01	101.06	0.134		
BT7	Magnetite	22.19	1.42	25.96	48.54	1.77	1.27	0.00	101.15	0.101	843	-14.64
	Ilmenite	51.09	0.05	5.35	40.51	2.28	1.76	0.01	101.06	0.134		
BU7	Magnetite	22.27	0.82	26.07	48.33	1.76	1.27	0.00	100.52	0.102	836	-14.76
	Ilmenite	51.09	0.05	5.35	40.51	2.28	1.76	0.01	101.06	0.134		
BV1	Magnetite	22.19	0.59	26.33	48.39	1.79	1.12	0.04	100.45	0.042	805	-15.59
	Ilmenite	51.10	0.07	4.84	40.64	2.30	1.68	0.02	100.66	0.107		
BV2	Magnetite	22.19	0.59	26.33	48.39	1.79	1.12	0.04	100.45	0.042	828	-14.94
	Ilmenite	51.10	0.07	5.30	40.78	2.32	1.59	0.01	101.17	0.080		
BV3	Magnetite	22.19	0.59	26.33	48.39	1.79	1.12	0.04	100.45	0.042	828	-14.93
	Ilmenite	51.03	0.04	5.30	40.79	2.32	1.55	0.02	101.05	0.070		
BV4	Magnetite	22.19	0.59	26.33	48.39	1.79	1.12	0.04	100.45	0.042	856	-14.19
	Ilmenite	50.12	0.07	5.76	39.82	2.30	1.65	0.01	99.73	0.102		
BV5	Magnetite	22.19	0.59	26.33	48.39	1.79	1.12	0.04	100.45	0.042	840	-14.62
	Ilmenite	50.44	0.07	5.46	40.18	2.28	1.62	0.00	100.05	0.098		
BV6	Magnetite	22.19	0.59	26.33	48.39	1.79	1.12	0.04	100.45	0.042	787	-16.11
	Ilmenite	51.25	0.05	4.54	40.83	2.28	1.66	0.02	100.63	0.109		
BV7	Magnetite	22.19	0.59	26.33	48.39	1.79	1.12	0.04	100.45	0.042	832	-14.84
	Ilmenite	51.09	0.05	5.35	40.51	2.28	1.76	0.01	101.06	0.134		
BV8	Magnetite	22.19	0.59	26.33	48.39	1.79	1.12	0.04	100.45	0.042	826	-15.00
	Ilmenite	51.14	0.06	5.25	40.70	2.28	1.68	0.03	101.14	0.112		

Table F2 continued

LAI Pair identifier	Phase	TiO_2	Al_2O_3	Fe_2O_3	FeO	MnO	MgO	Cr_2O_3	Sum	log(Mg/Mn)	T	fO_2
BW1	Magnetite	22.17	0.61	26.30	48.37	1.80	1.10	0.01	100.37	0.032	805	-15.59
	Ilmenite	51.10	0.07	4.84	40.64	2.30	1.68	0.02	100.66	0.107		
BW2	Magnetite	22.17	0.61	26.30	48.37	1.80	1.10	0.01	100.37	0.032	828	-14.94
	Ilmenite	51.10	0.07	5.30	40.78	2.32	1.59	0.01	101.17	0.080		
BW3	Magnetite	22.17	0.61	26.30	48.37	1.80	1.10	0.01	100.37	0.032	829	-14.93
	Ilmenite	51.03	0.04	5.30	40.79	2.32	1.55	0.02	101.05	0.070		
BW4	Magnetite	22.17	0.61	26.30	48.37	1.80	1.10	0.01	100.37	0.032	857	-14.19
	Ilmenite	50.12	0.07	5.76	39.82	2.30	1.65	0.01	99.73	0.102		
BW5	Magnetite	22.17	0.61	26.30	48.37	1.80	1.10	0.01	100.37	0.032	840	-14.62
	Ilmenite	50.44	0.07	5.46	40.18	2.28	1.62	0.00	100.05	0.098		
BW6	Magnetite	22.17	0.61	26.30	48.37	1.80	1.10	0.01	100.37	0.032	787	-16.11
	Ilmenite	51.25	0.05	4.54	40.83	2.28	1.66	0.02	100.63	0.109		
BW7	Magnetite	22.17	0.61	26.30	48.37	1.80	1.10	0.01	100.37	0.032	832	-14.83
	Ilmenite	51.09	0.05	5.35	40.51	2.28	1.76	0.01	101.06	0.134		
BW8	Magnetite	22.17	0.61	26.30	48.37	1.80	1.10	0.01	100.37	0.032	826	-15.00
	Ilmenite	51.14	0.06	5.25	40.70	2.28	1.68	0.03	101.14	0.112		
BX1	Magnetite	22.64	0.51	25.76	48.92	1.82	1.08	0.01	100.73	0.021	811	-15.46
	Ilmenite	51.10	0.07	4.84	40.64	2.30	1.68	0.02	100.66	0.107		
BX2	Magnetite	22.64	0.51	25.76	48.92	1.82	1.08	0.01	100.73	0.021	835	-14.80
	Ilmenite	51.10	0.07	5.30	40.78	2.32	1.59	0.01	101.17	0.080		
BX3	Magnetite	22.64	0.51	25.76	48.92	1.82	1.08	0.01	100.73	0.021	836	-14.80
	Ilmenite	51.03	0.04	5.30	40.79	2.32	1.55	0.02	101.05	0.070		
BX4	Magnetite	22.64	0.51	25.76	48.92	1.82	1.08	0.01	100.73	0.021	864	-14.05
	Ilmenite	50.12	0.07	5.76	39.82	2.30	1.65	0.01	99.73	0.102		
BX5	Magnetite	22.64	0.51	25.76	48.92	1.82	1.08	0.01	100.73	0.021	847	-14.48
	Ilmenite	50.44	0.07	5.46	40.18	2.28	1.62	0.00	100.05	0.098		
BX6	Magnetite	22.64	0.51	25.76	48.92	1.82	1.08	0.01	100.73	0.021	793	-15.98
	Ilmenite	51.25	0.05	4.54	40.83	2.28	1.66	0.02	100.63	0.109		
BX7	Magnetite	22.64	0.51	25.76	48.92	1.82	1.08	0.01	100.73	0.021	839	-14.70
	Ilmenite	51.09	0.05	5.35	40.51	2.28	1.76	0.01	101.06	0.134		
BX8	Magnetite	22.64	0.51	25.76	48.92	1.82	1.08	0.01	100.73	0.021	833	-14.87
	Ilmenite	51.14	0.06	5.25	40.70	2.28	1.68	0.03	101.14	0.112		
BY1	Magnetite	22.52	0.51	26.04	48.84	1.84	1.06	0.01	100.82	0.008	809	-15.51
	Ilmenite	51.10	0.07	4.84	40.64	2.30	1.68	0.02	100.66	0.107		
BY2	Magnetite	22.52	0.51	26.04	48.84	1.84	1.06	0.01	100.82	0.008	832	-14.86
	Ilmenite	51.10	0.07	5.30	40.78	2.32	1.59	0.01	101.17	0.080		
BY3	Magnetite	22.52	0.51	26.04	48.84	1.84	1.06	0.01	100.82	0.008	833	-14.85
	Ilmenite	51.03	0.04	5.30	40.79	2.32	1.55	0.02	101.05	0.070		

Table F2 continued

LAI Pair identifier	Phase	TiO_2	Al_2O_3	Fe_2O_3	FeO	MnO	MgO	Cr_2O_3	Sum	log(Mg/Mn)	T	fO_2
BY4	Magnetite	22.52	0.51	26.04	48.84	1.84	1.06	0.01	100.82	0.008	861	-14.11
	Ilmenite	50.12	0.07	5.76	39.82	2.30	1.65	0.01	99.73	0.102		
BY5	Magnetite	22.52	0.51	26.04	48.84	1.84	1.06	0.01	100.82	0.008	844	-14.54
	Ilmenite	50.44	0.07	5.46	40.18	2.28	1.62	0.00	100.05	0.098		
BY6	Magnetite	22.52	0.51	26.04	48.84	1.84	1.06	0.01	100.82	0.008	790	-16.04
	Ilmenite	51.25	0.05	4.54	40.83	2.28	1.66	0.02	100.63	0.109		
BY7	Magnetite	22.52	0.51	26.04	48.84	1.84	1.06	0.01	100.82	0.008	836	-14.76
	Ilmenite	51.09	0.05	5.35	40.51	2.28	1.76	0.01	101.06	0.134		
BY8	Magnetite	22.52	0.51	26.04	48.84	1.84	1.06	0.01	100.82	0.008	830	-14.93
	Ilmenite	51.14	0.06	5.25	40.70	2.28	1.68	0.03	101.14	0.112		
BZ1	Magnetite	22.12	0.51	26.49	48.24	1.83	1.11	0.00	100.30	0.030	802	-15.65
	Ilmenite	51.10	0.07	4.84	40.64	2.30	1.68	0.02	100.66	0.107		
BZ2	Magnetite	22.12	0.51	26.49	48.24	1.83	1.11	0.00	100.30	0.030	825	-15.00
	Ilmenite	51.10	0.07	5.30	40.78	2.32	1.59	0.01	101.17	0.080		
BZ3	Magnetite	22.12	0.51	26.49	48.24	1.83	1.11	0.00	100.30	0.030	826	-14.99
	Ilmenite	51.03	0.04	5.30	40.79	2.32	1.55	0.02	101.05	0.070		
BZ4	Magnetite	22.12	0.51	26.49	48.24	1.83	1.11	0.00	100.30	0.030	853	-14.25
	Ilmenite	50.12	0.07	5.76	39.82	2.30	1.65	0.01	99.73	0.102		
BZ5	Magnetite	22.12	0.51	26.49	48.24	1.83	1.11	0.00	100.30	0.030	837	-14.68
	Ilmenite	50.44	0.07	5.46	40.18	2.28	1.62	0.00	100.05	0.098		
BZ6	Magnetite	22.12	0.51	26.49	48.24	1.83	1.11	0.00	100.30	0.030	784	-16.16
	Ilmenite	51.25	0.05	4.54	40.83	2.28	1.66	0.02	100.63	0.109		
BZ7	Magnetite	22.12	0.51	26.49	48.24	1.83	1.11	0.00	100.30	0.030	829	-14.89
	Ilmenite	51.09	0.05	5.35	40.51	2.28	1.76	0.01	101.06	0.134		
BZ8	Magnetite	22.12	0.51	26.49	48.24	1.83	1.11	0.00	100.30	0.030	823	-15.06
	Ilmenite	51.14	0.06	5.25	40.70	2.28	1.68	0.03	101.14	0.112		
CA1	Magnetite	22.11	0.46	26.40	48.21	1.81	1.09	0.01	100.08	0.027	802	-15.64
	Ilmenite	51.10	0.07	4.84	40.64	2.30	1.68	0.02	100.66	0.107		
CA2	Magnetite	22.11	0.46	26.40	48.21	1.81	1.09	0.01	100.08	0.027	826	-14.99
	Ilmenite	51.10	0.07	5.30	40.78	2.32	1.59	0.01	101.17	0.080		
CA3	Magnetite	22.11	0.46	26.40	48.21	1.81	1.09	0.01	100.08	0.027	826	-14.98
	Ilmenite	51.03	0.04	5.30	40.79	2.32	1.55	0.02	101.05	0.070		
CA4	Magnetite	22.11	0.46	26.40	48.21	1.81	1.09	0.01	100.08	0.027	854	-14.25
	Ilmenite	50.12	0.07	5.76	39.82	2.30	1.65	0.01	99.73	0.102		
CA5	Magnetite	22.11	0.46	26.40	48.21	1.81	1.09	0.01	100.08	0.027	837	-14.67
	Ilmenite	50.44	0.07	5.46	40.18	2.28	1.62	0.00	100.05	0.098		
CA6	Magnetite	22.11	0.46	26.40	48.21	1.81	1.09	0.01	100.08	0.027	784	-16.16
	Ilmenite	51.25	0.05	4.54	40.83	2.28	1.66	0.02	100.63	0.109		

Table F2 continued

LAI Pair identifier	Phase	TiO_2	Al_2O_3	Fe_2O_3	FeO	MnO	MgO	Cr_2O_3	Sum	log(Mg/Mn)	T	fO_2
CA7	Magnetite	22.11	0.46	26.40	48.21	1.81	1.09	0.01	100.08	0.027	829	-14.89
	Ilmenite	51.09	0.05	5.35	40.51	2.28	1.76	0.01	101.06	0.134		
CA8	Magnetite	22.11	0.46	26.40	48.21	1.81	1.09	0.01	100.08	0.027	823	-15.06
	Ilmenite	51.14	0.06	5.25	40.70	2.28	1.68	0.03	101.14	0.112		
CB1	Magnetite	22.16	0.53	26.35	48.35	1.80	1.08	0.01	100.28	0.023	804	-15.61
	Ilmenite	51.10	0.07	4.84	40.64	2.30	1.68	0.02	100.66	0.107		
CB2	Magnetite	22.16	0.53	26.35	48.35	1.80	1.08	0.01	100.28	0.023	827	-14.96
	Ilmenite	51.10	0.07	5.30	40.78	2.32	1.59	0.01	101.17	0.080		
CB3	Magnetite	22.16	0.53	26.35	48.35	1.80	1.08	0.01	100.28	0.023	827	-14.95
	Ilmenite	51.03	0.04	5.30	40.79	2.32	1.55	0.02	101.05	0.070		
CB4	Magnetite	22.16	0.53	26.35	48.35	1.80	1.08	0.01	100.28	0.023	855	-14.21
	Ilmenite	50.12	0.07	5.76	39.82	2.30	1.65	0.01	99.73	0.102		
CB5	Magnetite	22.16	0.53	26.35	48.35	1.80	1.08	0.01	100.28	0.023	839	-14.64
	Ilmenite	50.44	0.07	5.46	40.18	2.28	1.62	0.00	100.05	0.098		
CB6	Magnetite	22.16	0.53	26.35	48.35	1.80	1.08	0.01	100.28	0.023	786	-16.13
	Ilmenite	51.25	0.05	4.54	40.83	2.28	1.66	0.02	100.63	0.109		
CB7	Magnetite	22.16	0.53	26.35	48.35	1.80	1.08	0.01	100.28	0.023	831	-14.86
	Ilmenite	51.09	0.05	5.35	40.51	2.28	1.76	0.01	101.06	0.134		
CB8	Magnetite	22.16	0.53	26.35	48.35	1.80	1.08	0.01	100.28	0.023	825	-15.02
	Ilmenite	51.14	0.06	5.25	40.70	2.28	1.68	0.03	101.14	0.112		
CC1	Magnetite	22.40	0.56	26.14	48.63	1.83	1.11	0.02	100.69	0.030	807	-15.54
	Ilmenite	51.10	0.07	4.84	40.64	2.30	1.68	0.02	100.66	0.107		
CC2	Magnetite	22.40	0.56	26.14	48.63	1.83	1.11	0.02	100.69	0.030	831	-14.89
	Ilmenite	51.10	0.07	5.30	40.78	2.32	1.59	0.01	101.17	0.080		
CC3	Magnetite	22.40	0.56	26.14	48.63	1.83	1.11	0.02	100.69	0.030	831	-14.88
	Ilmenite	51.03	0.04	5.30	40.79	2.32	1.55	0.02	101.05	0.070		
CC4	Magnetite	22.40	0.56	26.14	48.63	1.83	1.11	0.02	100.69	0.030	859	-14.14
	Ilmenite	50.12	0.07	5.76	39.82	2.30	1.65	0.01	99.73	0.102		
CC5	Magnetite	22.40	0.56	26.14	48.63	1.83	1.11	0.02	100.69	0.030	843	-14.57
	Ilmenite	50.44	0.07	5.46	40.18	2.28	1.62	0.00	100.05	0.098		
CC6	Magnetite	22.40	0.56	26.14	48.63	1.83	1.11	0.02	100.69	0.030	789	-16.06
	Ilmenite	51.25	0.05	4.54	40.83	2.28	1.66	0.02	100.63	0.109		
CC7	Magnetite	22.40	0.56	26.14	48.63	1.83	1.11	0.02	100.69	0.030	835	-14.79
	Ilmenite	51.09	0.05	5.35	40.51	2.28	1.76	0.01	101.06	0.134		
CC8	Magnetite	22.40	0.56	26.14	48.63	1.83	1.11	0.02	100.69	0.030	828	-14.95
	Ilmenite	51.14	0.06	5.25	40.70	2.28	1.68	0.03	101.14	0.112		
CD1	Magnetite	22.49	0.52	26.07	48.78	1.83	1.08	0.01	100.78	0.019	808	-15.52
	Ilmenite	51.10	0.07	4.84	40.64	2.30	1.68	0.02	100.66	0.107		

Table F2 continued

LAI Pair identifier	Phase	TiO_2	Al_2O_3	Fe_2O_3	FeO	MnO	MgO	Cr_2O_3	Sum	log(Mg/Mn)	T	fO_2
CD2	Magnetite	22.49	0.52	26.07	48.78	1.83	1.08	0.01	100.78	0.019	832	-14.87
	Ilmenite	51.10	0.07	5.30	40.78	2.32	1.59	0.01	101.17	0.080		
CD3	Magnetite	22.49	0.52	26.07	48.78	1.83	1.08	0.01	100.78	0.019	832	-14.86
	Ilmenite	51.03	0.04	5.30	40.79	2.32	1.55	0.02	101.05	0.070		
CD4	Magnetite	22.49	0.52	26.07	48.78	1.83	1.08	0.01	100.78	0.019	860	-14.12
	Ilmenite	50.12	0.07	5.76	39.82	2.30	1.65	0.01	99.73	0.102		
CD5	Magnetite	22.49	0.52	26.07	48.78	1.83	1.08	0.01	100.78	0.019	844	-14.55
	Ilmenite	50.44	0.07	5.46	40.18	2.28	1.62	0.00	100.05	0.098		
CD6	Magnetite	22.49	0.52	26.07	48.78	1.83	1.08	0.01	100.78	0.019	790	-16.04
	Ilmenite	51.25	0.05	4.54	40.83	2.28	1.66	0.02	100.63	0.109		
CD7	Magnetite	22.49	0.52	26.07	48.78	1.83	1.08	0.01	100.78	0.019	836	-14.77
	Ilmenite	51.09	0.05	5.35	40.51	2.28	1.76	0.01	101.06	0.134		
CD8	Magnetite	22.49	0.52	26.07	48.78	1.83	1.08	0.01	100.78	0.019	829	-14.94
	Ilmenite	51.14	0.06	5.25	40.70	2.28	1.68	0.03	101.14	0.112		
CE1	Magnetite	22.49	0.58	26.12	48.83	1.82	1.10	0.02	100.96	0.027	808	-15.52
	Ilmenite	51.10	0.07	4.84	40.64	2.30	1.68	0.02	100.66	0.107		
CE2	Magnetite	22.49	0.58	26.12	48.83	1.82	1.10	0.02	100.96	0.027	832	-14.86
	Ilmenite	51.10	0.07	5.30	40.78	2.32	1.59	0.01	101.17	0.080		
CE3	Magnetite	22.49	0.58	26.12	48.83	1.82	1.10	0.02	100.96	0.027	832	-14.86
	Ilmenite	51.03	0.04	5.30	40.79	2.32	1.55	0.02	101.05	0.070		
CE4	Magnetite	22.49	0.58	26.12	48.83	1.82	1.10	0.02	100.96	0.027	861	-14.12
	Ilmenite	50.12	0.07	5.76	39.82	2.30	1.65	0.01	99.73	0.102		
CE5	Magnetite	22.49	0.58	26.12	48.83	1.82	1.10	0.02	100.96	0.027	844	-14.55
	Ilmenite	50.44	0.07	5.46	40.18	2.28	1.62	0.00	100.05	0.098		
CE6	Magnetite	22.49	0.58	26.12	48.83	1.82	1.10	0.02	100.96	0.027	790	-16.04
	Ilmenite	51.25	0.05	4.54	40.83	2.28	1.66	0.02	100.63	0.109		
CE7	Magnetite	22.49	0.58	26.12	48.83	1.82	1.10	0.02	100.96	0.027	836	-14.76
	Ilmenite	51.09	0.05	5.35	40.51	2.28	1.76	0.01	101.06	0.134		
CE8	Magnetite	22.49	0.58	26.12	48.83	1.82	1.10	0.02	100.96	0.027	830	-14.93
	Ilmenite	51.14	0.06	5.25	40.70	2.28	1.68	0.03	101.14	0.112		
CF1	Magnetite	22.14	0.57	26.38	48.37	1.79	1.08	0.01	100.33	0.027	804	-15.61
	Ilmenite	51.10	0.07	4.84	40.64	2.30	1.68	0.02	100.66	0.107		
CF2	Magnetite	22.14	0.57	26.38	48.37	1.79	1.08	0.01	100.33	0.027	827	-14.96
	Ilmenite	51.10	0.07	5.30	40.78	2.32	1.59	0.01	101.17	0.080		
CF3	Magnetite	22.14	0.57	26.38	48.37	1.79	1.08	0.01	100.33	0.027	828	-14.95
	Ilmenite	51.03	0.04	5.30	40.79	2.32	1.55	0.02	101.05	0.070		
CF4	Magnetite	22.14	0.57	26.38	48.37	1.79	1.08	0.01	100.33	0.027	855	-14.21
	Ilmenite	50.12	0.07	5.76	39.82	2.30	1.65	0.01	99.73	0.102		

Table F2 continued

LAI												
Pair identifier	**Phase**	**TiO_2**	**Al_2O_3**	**Fe_2O_3**	**FeO**	**MnO**	**MgO**	**Cr_2O_3**	**Sum**	**log(Mg/Mn)**	**T**	**fO_2**
CF5	Magnetite	22.14	0.57	26.38	48.37	1.79	1.08	0.01	100.33	0.027	839	-14.64
	Ilmenite	50.44	0.07	5.46	40.18	2.28	1.62	0.00	100.05	0.098		
CF6	Magnetite	22.14	0.57	26.38	48.37	1.79	1.08	0.01	100.33	0.027	786	-16.13
	Ilmenite	51.25	0.05	4.54	40.83	2.28	1.66	0.02	100.63	0.109		
CF7	Magnetite	22.14	0.57	26.38	48.37	1.79	1.08	0.01	100.33	0.027	831	-14.85
	Ilmenite	51.09	0.05	5.35	40.51	2.28	1.76	0.01	101.06	0.134		
CF8	Magnetite	22.14	0.57	26.38	48.37	1.79	1.08	0.01	100.33	0.027	825	-15.02
	Ilmenite	51.14	0.06	5.25	40.70	2.28	1.68	0.03	101.14	0.112		

Table F3: Results of two oxide thermometry for the CCI syenite ejecta

CCI syenite Pair identifier	Phase	TiO_2	Al_2O_3	Fe_2O_3	FeO	MnO	MgO	Cr_2O_3	Sum	log(Mg/Mn)	T	fO_2
A4	Magnetite	16.68	0.13	35.01	43.42	2.23	0.10	0.01	97.57	-1.111	662	-19.72
	Ilmenite	50.19	0.01	3.42	42.03	2.81	0.15	0.00	98.61	-1.023		
A5	Magnetite	16.68	0.13	35.01	43.42	2.23	0.10	0.01	97.57	-1.111	696	-18.38
	Ilmenite	50.32	0.00	4.09	42.17	2.86	0.11	0.00	99.55	-1.153		
B7	Magnetite	16.71	0.15	34.27	43.44	2.06	0.04	0.01	96.68	-1.487	699	-18.33
	Ilmenite	50.46	0.02	4.12	42.59	2.69	0.04	0.00	99.93	-1.557		
B8	Magnetite	16.71	0.15	34.27	43.44	2.06	0.04	0.01	96.68	-1.487	667	-19.54
	Ilmenite	50.20	0.04	3.51	42.73	2.31	0.05	0.00	98.84	-1.431		
C1	Magnetite	16.71	0.16	34.33	43.30	2.18	0.06	0.00	96.74	-1.308	626	-21.24
	Ilmenite	50.64	0.02	2.82	41.77	3.58	0.09	0.01	98.93	-1.368		
D7	Magnetite	16.81	0.13	33.51	43.21	2.11	0.04	0.00	95.80	-1.535	701	-18.28
	Ilmenite	50.46	0.02	4.12	42.59	2.69	0.04	0.00	99.93	-1.557		
E1	Magnetite	14.94	0.06	39.31	42.29	2.18	0.06	0.00	98.84	-1.324	616	-21.51
	Ilmenite	50.64	0.02	2.82	41.77	3.58	0.09	0.01	98.93	-1.368		
F7	Magnetite	14.93	0.10	39.58	42.39	2.26	0.04	0.01	99.32	-1.533	681	-18.74
	Ilmenite	50.46	0.02	4.12	42.59	2.69	0.04	0.00	99.93	-1.557		
G7	Magnetite	15.01	0.11	38.85	42.27	2.21	0.03	0.01	98.49	-1.573	682	-18.71
	Ilmenite	50.46	0.02	4.12	42.59	2.69	0.04	0.00	99.93	-1.557		
H7	Magnetite	15.00	0.09	38.49	42.00	2.26	0.04	0.01	97.90	-1.461	682	-18.70
	Ilmenite	50.46	0.02	4.12	42.59	2.69	0.04	0.00	99.93	-1.557		
H8	Magnetite	15.00	0.09	38.49	42.00	2.26	0.04	0.01	97.90	-1.461	654	-19.86
	Ilmenite	50.20	0.04	3.51	42.73	2.31	0.05	0.00	98.84	-1.431		
J7	Magnetite	15.12	0.07	39.08	42.54	2.20	0.04	0.00	99.04	-1.528	682	-18.71
	Ilmenite	50.46	0.02	4.12	42.59	2.69	0.04	0.00	99.93	-1.557		
K4	Magnetite	20.81	0.15	28.42	48.03	2.08	0.11	0.00	99.60	-1.028	697	-18.85
	Ilmenite	50.19	0.01	3.42	42.03	2.81	0.15	0.00	98.61	-1.023		
N1	Magnetite	15.93	0.03	36.95	43.58	1.62	0.05	0.00	98.15	-1.306	621	-21.37
	Ilmenite	50.64	0.02	2.82	41.77	3.58	0.09	0.01	98.93	-1.368		
O5	Magnetite	19.60	0.12	30.67	47.00	1.98	0.08	0.00	99.45	-1.160	724	-17.76
	Ilmenite	50.32	0.00	4.09	42.17	2.86	0.11	0.00	99.55	-1.153		
R7	Magnetite	21.34	0.08	27.53	48.83	1.93	0.03	0.00	99.74	-1.547	747	-17.23
	Ilmenite	50.46	0.02	4.12	42.59	2.69	0.04	0.00	99.93	-1.557		
S7	Magnetite	22.69	0.05	24.88	49.50	2.45	0.04	0.00	99.62	-1.533	769	-16.75
	Ilmenite	50.46	0.02	4.12	42.59	2.69	0.04	0.00	99.93	-1.557		
T4	Magnetite	21.29	0.14	27.33	48.29	2.17	0.12	0.00	99.34	-1.019	703	-18.69
	Ilmenite	50.19	0.01	3.42	42.03	2.81	0.15	0.00	98.61	-1.023		
U4	Magnetite	20.69	0.09	28.87	47.97	2.10	0.10	0.01	99.83	-1.080	694	-18.91
	Ilmenite	50.19	0.01	3.42	42.03	2.81	0.15	0.00	98.61	-1.023		
U5	Magnetite	20.69	0.09	28.87	47.97	2.10	0.10	0.01	99.83	-1.080	736	-17.47
	Ilmenite	50.32	0.00	4.09	42.17	2.86	0.11	0.00	99.55	-1.153		

Table F4: Results of alkali feldspar-melt thermometry and hygrometry of the UFG

Unit	Liquid composition											Feldspar composition							Equilibrium	T	H_2O
	Sample	SiO_2	TiO_2	Al_2O_3	FeO_t	MnO	MgO	CaO	Na_2O	K_2O	P_2O_5	Sample	SiO_2	Al_2O_3	FeO_t	CaO	Na_2O	K_2O	ΔKd_{Or-Ab}	(°C)	(wt. %)
Fur-J	SM7-1	63.53	0.58	17.83	3.60	0.24	0.48	0.89	6.71	6.06	0.10	Fsp1	66.06	19.13	0.24	0.31	7.01	7.24	0.09	941	4.6
Fur-J	SM7-1	63.53	0.58	17.83	3.60	0.24	0.48	0.89	6.71	6.06	0.10	Fsp2	65.85	19.37	0.22	0.46	6.94	7.14	0.05	940	4.5
Fur-J	SM7-1	63.53	0.58	17.83	3.60	0.24	0.48	0.89	6.71	6.06	0.10	Fsp3	65.91	19.26	0.24	0.41	6.90	7.28	0.06	939	4.6
Fur-J	SM7-1	63.53	0.58	17.83	3.60	0.24	0.48	0.89	6.71	6.06	0.10	Fsp4	65.75	19.52	0.25	0.43	7.26	6.79	0.09	946	4.4
Fur-J	SM7-1	63.53	0.58	17.83	3.60	0.24	0.48	0.89	6.71	6.06	0.10	Fsp5	66.06	19.52	0.27	0.50	6.84	6.81	0.05	942	4.3
Fur-J	SM7-1	63.53	0.58	17.83	3.60	0.24	0.48	0.89	6.71	6.06	0.10	Fsp6	65.40	19.80	0.21	0.87	7.53	6.19	0.01	950	3.8
Fur-J	SM7-1	63.53	0.58	17.83	3.60	0.24	0.48	0.89	6.71	6.06	0.10	Fsp7	66.17	19.29	0.23	0.43	6.81	7.07	0.06	939	4.5
Fur-J	SM7-1	63.53	0.58	17.83	3.60	0.24	0.48	0.89	6.71	6.06	0.10	Fsp8	65.80	19.69	0.28	0.85	7.26	6.11	0.00	949	3.8
Fur-J	SM7-1	63.53	0.58	17.83	3.60	0.24	0.48	0.89	6.71	6.06	0.10	Fsp9	65.72	19.84	0.35	1.03	7.39	5.67	-0.03	952	3.4
Fur-J	SM7-1	63.53	0.58	17.83	3.60	0.24	0.48	0.89	6.71	6.06	0.10	Fsp10	66.43	19.16	0.21	0.41	6.84	6.95	0.07	941	4.6
Fur-J	SM7-1	63.53	0.58	17.83	3.60	0.24	0.48	0.89	6.71	6.06	0.10	Fsp11	66.46	19.10	0.25	0.33	6.71	7.13	0.07	939	4.6
Fur-J	SM7-1	63.53	0.58	17.83	3.60	0.24	0.48	0.89	6.71	6.06	0.10	Fsp12	65.83	19.39	0.21	0.51	6.75	7.28	0.03	937	4.5
Fur-J	SM7-1	63.53	0.58	17.83	3.60	0.24	0.48	0.89	6.71	6.06	0.10	Fsp13	65.75	19.67	0.23	0.61	7.12	6.63	0.04	945	4.2
Fur-J	SM7-1	63.53	0.58	17.83	3.60	0.24	0.48	0.89	6.71	6.06	0.10	Fsp14	65.93	19.43	0.22	0.44	7.07	6.90	0.07	943	4.5
Fur-J	SM7-1	63.53	0.58	17.83	3.60	0.24	0.48	0.89	6.71	6.06	0.10	Fsp15	66.55	19.15	0.24	0.41	6.73	6.91	0.06	940	4.5
Fur-J	SM7-1	63.53	0.58	17.83	3.60	0.24	0.48	0.89	6.71	6.06	0.10	Fsp16	66.19	19.22	0.31	0.44	6.78	7.05	0.05	939	4.3
Fur-J	SM7-1	63.53	0.58	17.83	3.60	0.24	0.48	0.89	6.71	6.06	0.10	Fsp17	66.13	19.48	0.22	0.63	7.05	6.48	0.04	945	4.2
Fur-J	SM7-1	63.53	0.58	17.83	3.60	0.24	0.48	0.89	6.71	6.06	0.10	Fsp18	66.36	19.24	0.27	0.36	6.67	7.10	0.07	938	4.5
Fur-J	SM7-1	63.53	0.58	17.83	3.60	0.24	0.48	0.89	6.71	6.06	0.10	Fsp19	66.54	19.00	0.29	0.29	6.68	7.20	0.08	938	4.6
Fur-J	SM7-1	63.53	0.58	17.83	3.60	0.24	0.48	0.89	6.71	6.06	0.10	Fsp20	66.11	19.34	0.25	0.43	6.79	7.07	0.06	939	4.5
Fur-J	SM7-1	63.53	0.58	17.83	3.60	0.24	0.48	0.89	6.71	6.06	0.10	Fsp21	66.11	19.37	0.27	0.43	6.95	6.88	0.07	942	4.4
Fur-J	SM7-1	63.53	0.58	17.83	3.60	0.24	0.48	0.89	6.71	6.06	0.10	Fsp22	66.36	19.12	0.27	0.43	6.91	6.90	0.07	942	4.4
Fur-J	SM7-1	63.53	0.58	17.83	3.60	0.24	0.48	0.89	6.71	6.06	0.10	Fsp23	66.48	19.34	0.19	0.36	6.33	7.30	0.05	933	4.9
Fur-J	SM7-1	63.53	0.58	17.83	3.60	0.24	0.48	0.89	6.71	6.06	0.10	Fsp24	66.35	19.25	0.29	0.37	6.65	7.08	0.06	938	4.5
Fur-J	SM7-1	63.53	0.58	17.83	3.60	0.24	0.48	0.89	6.71	6.06	0.10	Fsp25	66.12	19.69	0.30	0.88	6.89	6.11	-0.02	945	3.8
Fur-J	SM7-1	63.53	0.58	17.83	3.60	0.24	0.48	0.89	6.71	6.06	0.10	Fsp26	66.43	19.26	0.21	0.40	6.77	6.92	0.07	941	4.6
Fur-J	SM7-1	63.53	0.58	17.83	3.60	0.24	0.48	0.89	6.71	6.06	0.10	Fsp27	66.43	19.33	0.26	0.49	6.90	6.59	0.06	944	4.3
Fur-J	SM7-1	63.53	0.58	17.83	3.60	0.24	0.48	0.89	6.71	6.06	0.10	Fsp28	66.39	19.30	0.27	0.41	6.62	7.00	0.06	938	4.5
Fur-J	SM7-1	63.53	0.58	17.83	3.60	0.24	0.48	0.89	6.71	6.06	0.10	Fsp29	66.58	19.07	0.28	0.35	6.63	7.09	0.07	938	4.5
Fur-J	SM7-1	63.53	0.58	17.83	3.60	0.24	0.48	0.89	6.71	6.06	0.10	Fsp30	66.54	19.27	0.26	0.42	6.67	6.82	0.06	940	4.5
Fur-J	SM7-1	63.53	0.58	17.83	3.60	0.24	0.48	0.89	6.71	6.06	0.10	Fsp31	66.48	19.33	0.25	0.38	6.59	6.96	0.06	939	4.6
Fur-J	SM7-1	63.53	0.58	17.83	3.60	0.24	0.48	0.89	6.71	6.06	0.10	Fsp32	66.21	19.26	0.24	0.49	7.26	6.54	0.08	948	4.3
Fur-J	SM7-1	63.53	0.58	17.83	3.60	0.24	0.48	0.89	6.71	6.06	0.10	Fsp33	66.44	19.12	0.27	0.37	6.93	6.85	0.08	943	4.4
Fur-J	SM7-1	63.53	0.58	17.83	3.60	0.24	0.48	0.89	6.71	6.06	0.10	Fsp34	66.46	19.18	0.22	0.42	6.51	7.20	0.04	936	4.7
Fur-J	SM7-1	63.53	0.58	17.83	3.60	0.24	0.48	0.89	6.71	6.06	0.10	Fsp35	66.32	19.23	0.29	0.35	6.40	7.41	0.05	933	4.6

Table F4 continued

Unit	Liquid composition											Feldspar composition							Equilibrium	T	H_2O
	Sample	SiO_2	TiO_2	Al_2O_3	FeO_t	MnO	MgO	CaO	Na_2O	K_2O	P_2O_5	Sample	SiO_2	Al_2O_3	FeO_t	CaO	Na_2O	K_2O	ΔKd_{Or-Ab}	(°C)	(wt. %)
Fur-J	SM7-1	63.53	0.58	17.83	3.60	0.24	0.48	0.89	6.71	6.06	0.10	Fsp36	66.60	19.12	0.25	0.38	6.23	7.39	0.04	931	4.7
Fur-J	SM7-1	63.53	0.58	17.83	3.60	0.24	0.48	0.89	6.71	6.06	0.10	Fsp37	66.22	19.58	0.29	0.75	6.86	6.30	0.01	944	4.0
Fur-J	SM7-1	63.53	0.58	17.83	3.60	0.24	0.48	0.89	6.71	6.06	0.10	Fsp38	66.54	19.25	0.25	0.39	6.46	7.10	0.05	936	4.6
Fur-J	SM7-1	63.53	0.58	17.83	3.60	0.24	0.48	0.89	6.71	6.06	0.10	Fsp39	66.41	19.39	0.29	0.63	6.42	6.86	0.00	936	4.3
Fur-J	SM7-1	63.53	0.58	17.83	3.60	0.24	0.48	0.89	6.71	6.06	0.10	Fsp40	66.71	19.04	0.28	0.35	6.50	7.12	0.06	937	4.5
Fur-J dome	SM7-1	63.53	0.58	17.83	3.60	0.24	0.48	0.89	6.71	6.06	0.10	Fsp03c	66.35	19.28	0.26	0.35	6.58	7.17	0.06	937	4.6
Fur-J dome	SM7-1	63.53	0.58	17.83	3.60	0.24	0.48	0.89	6.71	6.06	0.10	Fsp03r	66.10	19.27	0.59	0.59	6.78	6.67	0.03	941	3.7
Fur-J dome	SM7-1	63.53	0.58	17.83	3.60	0.24	0.48	0.89	6.71	6.06	0.10	Fsp04c	66.00	19.75	0.25	0.81	6.91	6.28	-0.01	944	4.0
Fur-J dome	SM7-1	63.53	0.58	17.83	3.60	0.24	0.48	0.89	6.71	6.06	0.10	Fsp04r	66.03	19.36	0.31	0.52	6.57	7.21	0.03	935	4.4
Fur-J dome	SM7-1	63.53	0.58	17.83	3.60	0.24	0.48	0.89	6.71	6.06	0.10	Fsp05c	65.64	19.83	0.21	0.91	6.48	6.93	-0.06	934	4.1
Fur-J dome	SM7-1	63.53	0.58	17.83	3.60	0.24	0.48	0.89	6.71	6.06	0.10	Fsp06c	66.02	19.29	0.25	0.49	6.24	7.72	0.01	928	4.7
Fur-J dome	SM7-1	63.53	0.58	17.83	3.60	0.24	0.48	0.89	6.71	6.06	0.10	Fsp06r	65.88	19.74	0.31	0.91	6.59	6.58	-0.05	938	3.9
Fur-J dome	SM7-1	63.53	0.58	17.83	3.60	0.24	0.48	0.89	6.71	6.06	0.10	Fsp07c	65.66	19.67	0.20	0.84	5.86	7.78	-0.07	920	4.5
Fur-J dome	SM7-1	63.53	0.58	17.83	3.60	0.24	0.48	0.89	6.71	6.06	0.10	Fsp07r	65.34	20.17	0.29	1.28	6.62	6.29	-0.14	938	3.6
Fur-J dome	SM7-1	63.53	0.58	17.83	3.60	0.24	0.48	0.89	6.71	6.06	0.10	Fsp08c	65.73	19.67	0.23	0.74	5.97	7.66	-0.04	923	4.5
Fur-J dome	SM7-1	63.53	0.58	17.83	3.60	0.24	0.48	0.89	6.71	6.06	0.10	Fsp08r	65.50	20.13	0.31	1.30	7.09	5.67	-0.12	948	3.4
Fur-J dome	SM7-1	63.53	0.58	17.83	3.60	0.24	0.48	0.89	6.71	6.06	0.10	Fsp09c	66.08	19.52	0.25	0.55	7.11	6.49	0.06	946	4.2
Fur-J dome	SM7-1	63.53	0.58	17.83	3.60	0.24	0.48	0.89	6.71	6.06	0.10	Fsp09r	66.29	19.34	0.25	0.44	6.99	6.69	0.07	944	4.4
Fur-J dome	SM7-1	63.53	0.58	17.83	3.60	0.24	0.48	0.89	6.71	6.06	0.10	Fsp10c	65.22	19.86	0.22	1.02	5.69	8.00	-0.10	915	4.3
Fur-J dome	SM7-1	63.53	0.58	17.83	3.60	0.24	0.48	0.89	6.71	6.06	0.10	Fsp10r	64.97	20.29	0.24	1.37	6.16	6.98	-0.17	927	3.8
Fur-J dome	SM7-1	63.53	0.58	17.83	3.60	0.24	0.48	0.89	6.71	6.06	0.10	Fsp11c	66.34	19.30	0.30	0.45	6.50	7.11	0.04	936	4.4
Fur-J dome	SM7-1	63.53	0.58	17.83	3.60	0.24	0.48	0.89	6.71	6.06	0.10	Fsp11r	65.60	19.86	0.49	1.24	6.90	5.91	-0.11	944	3.3
Fur-J dome	SM7-1	63.53	0.58	17.83	3.60	0.24	0.48	0.89	6.71	6.06	0.10	Fsp12c	65.36	20.01	0.20	1.06	5.61	7.75	-0.11	916	4.3
Fur-J dome	SM7-1	63.53	0.58	17.83	3.60	0.24	0.48	0.89	6.71	6.06	0.10	Fsp12r	65.55	19.81	0.39	1.10	6.48	6.66	-0.10	935	3.7
Fur-J dome	SM7-1	63.53	0.58	17.83	3.60	0.24	0.48	0.89	6.71	6.06	0.10	18 / 1 .	65.63	19.49	0.36	0.85	6.97	6.63	-0.02	942	3.8
Fur-J dome	SM7-1	63.53	0.58	17.83	3.60	0.24	0.48	0.89	6.71	6.06	0.10	18 / 2 .	65.50	19.59	0.70	0.99	7.26	5.65	-0.03	952	3.1
Fur-J dome	SM7-1	63.53	0.58	17.83	3.60	0.24	0.48	0.89	6.71	6.06	0.10	18 / 3 .	65.75	19.08	0.64	0.72	7.20	6.46	0.02	946	3.4
Fur-J dome	SM7-1	63.53	0.58	17.83	3.60	0.24	0.48	0.89	6.71	6.06	0.10	18 / 4 .	65.72	19.46	0.45	0.86	7.50	5.91	0.02	952	3.5
Fur-J dome	SM7-1	63.53	0.58	17.83	3.60	0.24	0.48	0.89	6.71	6.06	0.10	18 / 5 .	65.44	19.55	0.41	1.05	7.13	6.31	-0.06	944	3.5
Fur-J dome	SM7-1	63.53	0.58	17.83	3.60	0.24	0.48	0.89	6.71	6.06	0.10	18 / 6 .	65.59	19.46	0.41	1.00	6.96	6.50	-0.05	942	3.6
Fur-J dome	SM7-1	63.53	0.58	17.83	3.60	0.24	0.48	0.89	6.71	6.06	0.10	18 / 7 .	66.11	19.06	0.40	0.50	7.22	6.62	0.07	946	4.0
Fur-J dome	SM7-1	63.53	0.58	17.83	3.60	0.24	0.48	0.89	6.71	6.06	0.10	18 / 8 .	65.36	20.16	0.97	1.47	7.67	4.10	-0.26	965	2.1
Fur-J dome	SM7-1	63.53	0.58	17.83	3.60	0.24	0.48	0.89	6.71	6.06	0.10	18 / 9 .	65.40	19.49	0.47	1.02	8.01	5.52	0.00	958	3.2
Fur-J dome	SM7-1	63.53	0.58	17.83	3.60	0.24	0.48	0.89	6.71	6.06	0.10	18 / 10 .	65.82	18.96	0.43	0.46	6.61	7.61	0.03	933	4.2
Fur-J dome	SM7-1	63.53	0.58	17.83	3.60	0.24	0.48	0.89	6.71	6.06	0.10	19 / 1 .	65.77	19.27	0.43	0.84	7.05	6.54	-0.01	943	3.7

Table F4 continued

Unit		Liquid composition										Feldspar composition							Equilibrium	T	H_2O
	Sample	SiO_2	TiO_2	Al_2O_3	FeO_t	MnO	MgO	CaO	Na_2O	K_2O	P_2O_5	Sample	SiO_2	Al_2O_3	FeO_t	CaO	Na_2O	K_2O	ΔKd_{Or-Ab}	(°C)	(wt. %)
Fur-J dome	SM7-1	63.53	0.58	17.83	3.60	0.24	0.48	0.89	6.71	6.06	0.10	19 / 2 .	66.13	19.28	0.22	0.63	7.10	6.59	0.04	945	4.2
Fur-J dome	SM7-1	63.53	0.58	17.83	3.60	0.24	0.48	0.89	6.71	6.06	0.10	19 / 3 .	66.04	19.22	0.21	0.51	7.06	6.92	0.06	942	4.5
Fur-J dome	SM7-1	63.53	0.58	17.83	3.60	0.24	0.48	0.89	6.71	6.06	0.10	19 / 4 .	65.73	19.57	0.26	0.49	6.42	7.44	0.02	932	4.5
Fur-J dome	SM7-1	63.53	0.58	17.83	3.60	0.24	0.48	0.89	6.71	6.06	0.10	19 / 5 .	66.19	19.06	0.28	0.41	6.76	7.21	0.06	938	4.5
Fur-J dome	SM7-1	63.53	0.58	17.83	3.60	0.24	0.48	0.89	6.71	6.06	0.10	19 / 6 .	66.06	19.17	0.26	0.56	6.93	6.98	0.04	940	4.3
Fur-J dome	SM7-1	63.53	0.58	17.83	3.60	0.24	0.48	0.89	6.71	6.06	0.10	19 / 7 .	66.09	19.19	0.23	0.64	6.87	6.95	0.02	940	4.3
Fur-J dome	SM7-1	63.53	0.58	17.83	3.60	0.24	0.48	0.89	6.71	6.06	0.10	19 / 8 .	65.64	19.56	0.31	0.63	6.89	6.86	0.02	941	4.1
Fur-J dome	SM7-1	63.53	0.58	17.83	3.60	0.24	0.48	0.89	6.71	6.06	0.10	19 / 9 .	66.06	19.29	0.24	0.53	6.92	6.93	0.04	941	4.4
Fur-J dome	SM7-1	63.53	0.58	17.83	3.60	0.24	0.48	0.89	6.71	6.06	0.10	19 / 10 .	65.90	19.22	0.26	0.67	7.10	6.78	0.02	943	4.1
Fur-J dome	SM7-1	63.53	0.58	17.83	3.60	0.24	0.48	0.89	6.71	6.06	0.10	20 / 1 .	65.65	19.28	0.43	0.83	7.01	6.68	-0.01	942	3.8
Fur-J dome	SM7-1	63.53	0.58	17.83	3.60	0.24	0.48	0.89	6.71	6.06	0.10	20 / 2 .	65.97	19.38	0.26	0.62	6.99	6.75	0.03	942	4.2
Fur-J dome	SM7-1	63.53	0.58	17.83	3.60	0.24	0.48	0.89	6.71	6.06	0.10	20 / 3 .	66.14	19.19	0.31	0.63	7.05	6.60	0.04	944	4.1
Fur-J dome	SM7-1	63.53	0.58	17.83	3.60	0.24	0.48	0.89	6.71	6.06	0.10	20 / 4 .	65.97	19.28	0.25	0.66	7.06	6.71	0.03	943	4.2
Fur-J dome	SM7-1	63.53	0.58	17.83	3.60	0.24	0.48	0.89	6.71	6.06	0.10	20 / 5 .	66.12	19.18	0.27	0.52	7.11	6.76	0.06	944	4.3
Fur-J dome	SM7-1	63.53	0.58	17.83	3.60	0.24	0.48	0.89	6.71	6.06	0.10	20 / 7 .	65.93	19.24	0.24	0.52	6.90	7.10	0.04	939	4.4
Fur-J dome	SM7-1	63.53	0.58	17.83	3.60	0.24	0.48	0.89	6.71	6.06	0.10	20 / 8 .	66.55	19.69	0.65	0.51	6.85	5.44	0.10	954	3.3
Fur-J dome	SM7-1	63.53	0.58	17.83	3.60	0.24	0.48	0.89	6.71	6.06	0.10	20 / 10 .	65.96	19.31	0.25	0.62	7.09	6.70	0.04	944	4.2
Fur-J dome	SM7-1	63.53	0.58	17.83	3.60	0.24	0.48	0.89	6.71	6.06	0.10	21 / 1 .	65.70	19.36	0.21	0.77	6.50	7.42	-0.03	931	4.4
Fur-J dome	SM7-1	63.53	0.58	17.83	3.60	0.24	0.48	0.89	6.71	6.06	0.10	21 / 2 .	65.66	19.39	0.23	0.82	6.61	7.24	-0.04	933	4.2
Fur-J dome	SM7-1	63.53	0.58	17.83	3.60	0.24	0.48	0.89	6.71	6.06	0.10	21 / 3 .	65.50	19.43	0.21	0.78	6.43	7.59	-0.04	929	4.4
Fur-J dome	SM7-1	63.53	0.58	17.83	3.60	0.24	0.48	0.89	6.71	6.06	0.10	21 / 4 .	65.52	19.48	0.19	0.86	6.37	7.53	-0.05	928	4.3
Fur-J dome	SM7-1	63.53	0.58	17.83	3.60	0.24	0.48	0.89	6.71	6.06	0.10	21 / 5 .	65.54	19.60	0.23	0.86	6.56	7.17	-0.05	933	4.2
Fur-J dome	SM7-1	63.53	0.58	17.83	3.60	0.24	0.48	0.89	6.71	6.06	0.10	21 / 7 .	65.55	19.39	0.23	0.74	6.38	7.66	-0.03	928	4.4
Fur-J dome	SM7-1	63.53	0.58	17.83	3.60	0.24	0.48	0.89	6.71	6.06	0.10	21 / 8 .	65.77	19.30	0.19	0.75	6.31	7.63	-0.03	927	4.5
Fur-J dome	SM7-1	63.53	0.58	17.83	3.60	0.24	0.48	0.89	6.71	6.06	0.10	21 / 9 .	65.70	19.33	0.23	0.76	6.32	7.60	-0.04	928	4.4
Fur-J dome	SM7-1	63.53	0.58	17.83	3.60	0.24	0.48	0.89	6.71	6.06	0.10	21 / 10 .	65.61	19.44	0.21	0.83	6.45	7.38	-0.04	930	4.3
Fur-J dome	SM7-1	63.53	0.58	17.83	3.60	0.24	0.48	0.89	6.71	6.06	0.10	22 / 1 .	65.91	19.20	0.29	0.39	7.10	7.08	0.08	942	4.4
Fur-J dome	SM7-1	63.53	0.58	17.83	3.60	0.24	0.48	0.89	6.71	6.06	0.10	23 / 1 .	66.29	18.95	0.26	0.36	6.91	7.17	0.07	940	4.5
Fur-J dome	SM7-1	63.53	0.58	17.83	3.60	0.24	0.48	0.89	6.71	6.06	0.10	24 / 1 .	65.37	19.44	0.21	0.87	6.13	7.90	-0.06	922	4.4
Fur-J dome	SM7-1	63.53	0.58	17.83	3.60	0.24	0.48	0.89	6.71	6.06	0.10	25 / 1 .	65.48	19.48	0.20	0.84	6.04	7.90	-0.06	921	4.5
Fur-J dome	SM7-1	63.53	0.58	17.83	3.60	0.24	0.48	0.89	6.71	6.06	0.10	26 / 1 .	66.16	19.12	0.25	0.43	7.04	6.97	0.07	942	4.5
Fur-J dome	SM7-1	63.53	0.58	17.83	3.60	0.24	0.48	0.89	6.71	6.06	0.10	27 / 1 .	66.24	19.04	0.31	0.48	7.24	6.64	0.08	947	4.2
Fur-J dome	SM7-1	63.53	0.58	17.83	3.60	0.24	0.48	0.89	6.71	6.06	0.10	28 / 1 .	65.41	19.64	0.59	1.16	7.20	5.87	-0.08	948	3.2
Fur-J dome	SM7-1	63.53	0.58	17.83	3.60	0.24	0.48	0.89	6.71	6.06	0.10	29 / 1 .	65.08	19.85	0.65	1.44	7.86	4.96	-0.15	959	2.6
Fur-J dome	SM7-1	63.53	0.58	17.83	3.60	0.24	0.48	0.89	6.71	6.06	0.10	30 / 1 .	65.98	19.21	0.45	0.53	7.46	6.29	0.09	951	3.8

Table F4 continued

Unit		Liquid composition										Feldspar composition							Equilibrium	T	H_2O
	Sample	SiO_2	TiO_2	Al_2O_3	FeO_t	MnO	MgO	CaO	Na_2O	K_2O	P_2O_5	Sample	SiO_2	Al_2O_3	FeO_t	CaO	Na_2O	K_2O	ΔKd_{Or-Ab}	(°C)	(wt. %)
Fur-J dome	SM7-1	63.53	0.58	17.83	3.60	0.24	0.48	0.89	6.71	6.06	0.10	31 / 1 .	65.96	19.15	0.59	0.68	7.46	6.02	0.06	952	3.4
Fur-J dome	SM7-1	63.53	0.58	17.83	3.60	0.24	0.48	0.89	6.71	6.06	0.10	32 / 1 .	65.30	20.05	0.37	1.42	7.91	4.82	-0.16	960	2.8
Fur-I	S036GG01	64.17	0.48	17.64	3.36	0.23	0.34	0.70	7.33	5.66	0.08	Fsp01	66.07	18.99	0.25	0.56	7.15	6.99	0.14	885	5.4
Fur-I	S036GG01	64.17	0.48	17.64	3.36	0.23	0.34	0.70	7.33	5.66	0.08	Fsp02	66.13	18.99	0.30	0.43	7.17	6.99	0.18	886	5.4
Fur-I	S036GG01	64.17	0.48	17.64	3.36	0.23	0.34	0.70	7.33	5.66	0.08	Fsp04	66.18	19.01	0.27	0.37	7.07	7.09	0.18	885	5.6
Fur-I	S036GG01	64.17	0.48	17.64	3.36	0.23	0.34	0.70	7.33	5.66	0.08	Fsp05	66.18	18.92	0.23	0.38	7.23	7.05	0.19	886	5.6
Fur-I	S036GG01	64.17	0.48	17.64	3.36	0.23	0.34	0.70	7.33	5.66	0.08	Fsp06	65.87	19.07	0.27	0.41	7.66	6.72	0.22	892	5.4
Fur-I	S036GG01	64.17	0.48	17.64	3.36	0.23	0.34	0.70	7.33	5.66	0.08	Fsp07	66.08	18.79	0.34	0.32	7.56	6.92	0.23	890	5.3
Fur-I	S036GG01	64.17	0.48	17.64	3.36	0.23	0.34	0.70	7.33	5.66	0.08	Fsp08	66.06	18.94	0.31	0.31	7.31	7.07	0.21	887	5.5
Fur-I	S036GG01	64.17	0.48	17.64	3.36	0.23	0.34	0.70	7.33	5.66	0.08	Fsp09	66.40	18.93	0.25	0.27	7.05	7.09	0.20	885	5.7
Fur-I	S036GG01	64.17	0.48	17.64	3.36	0.23	0.34	0.70	7.33	5.66	0.08	Fsp10	66.08	19.26	0.29	0.57	7.19	6.61	0.16	888	5.3
Fur-I	S036GG01	64.17	0.48	17.64	3.36	0.23	0.34	0.70	7.33	5.66	0.08	Fsp11	66.30	19.13	0.27	0.36	6.88	7.06	0.17	884	5.6
Fur-I	S036GG01	64.17	0.48	17.64	3.36	0.23	0.34	0.70	7.33	5.66	0.08	Fsp12	66.19	18.99	0.28	0.42	7.25	6.88	0.19	887	5.5
Fur-I	S036GG01	64.17	0.48	17.64	3.36	0.23	0.34	0.70	7.33	5.66	0.08	Fsp13	66.04	19.21	0.22	0.56	6.96	7.02	0.13	883	5.5
Fur-I	S036GG01	64.17	0.48	17.64	3.36	0.23	0.34	0.70	7.33	5.66	0.08	Fsp14	66.27	18.97	0.31	0.38	7.01	7.06	0.17	885	5.5
Fur-I	S036GG01	64.17	0.48	17.64	3.36	0.23	0.34	0.70	7.33	5.66	0.08	Fsp15	66.28	18.94	0.25	0.38	7.41	6.75	0.21	890	5.5
Fur-I	S036GG01	64.17	0.48	17.64	3.36	0.23	0.34	0.70	7.33	5.66	0.08	Fsp16	66.36	19.02	0.25	0.38	6.62	7.37	0.14	879	5.8
Fur-I	S036GG01	64.17	0.48	17.64	3.36	0.23	0.34	0.70	7.33	5.66	0.08	Fsp17	66.32	18.94	0.27	0.32	6.59	7.57	0.14	877	5.8
Fur-I	S036GG01	64.17	0.48	17.64	3.36	0.23	0.34	0.70	7.33	5.66	0.08	Fsp18	65.58	19.41	0.22	0.80	6.24	7.75	0.03	870	5.5
Fur-I	S036GG01	64.17	0.48	17.64	3.36	0.23	0.34	0.70	7.33	5.66	0.08	Fsp19	66.38	18.96	0.28	0.39	7.00	6.98	0.18	885	5.5
Fur-I	S036GG01	64.17	0.48	17.64	3.36	0.23	0.34	0.70	7.33	5.66	0.08	Fsp21	65.53	19.68	0.19	0.91	6.28	7.40	0.02	872	5.4
Fur-I	S036GG01	64.17	0.48	17.64	3.36	0.23	0.34	0.70	7.33	5.66	0.08	Fsp22	65.06	20.26	0.21	1.48	6.45	6.55	-0.09	876	4.8
Fur-I	S036GG01	64.17	0.48	17.64	3.36	0.23	0.34	0.70	7.33	5.66	0.08	Fsp23	66.32	19.04	0.25	0.32	7.02	7.05	0.19	885	5.7
Fur-I	S036GG01	64.17	0.48	17.64	3.36	0.23	0.34	0.70	7.33	5.66	0.08	Fsp24	66.35	19.17	0.26	0.35	7.00	6.86	0.19	886	5.6
Fur-I	S036GG01	64.17	0.48	17.64	3.36	0.23	0.34	0.70	7.33	5.66	0.08	Fsp25	66.36	18.95	0.27	0.23	6.85	7.34	0.19	882	5.8
Fur-I	S036GG01	64.17	0.48	17.64	3.36	0.23	0.34	0.70	7.33	5.66	0.08	Fsp26	65.38	19.65	0.23	0.91	6.22	7.60	0.01	870	5.4
Fur-I	S036GG01	64.17	0.48	17.64	3.36	0.23	0.34	0.70	7.33	5.66	0.08	Fsp27	66.35	19.06	0.24	0.28	6.85	7.22	0.18	883	5.8
Fur-I	S036GG01	64.17	0.48	17.64	3.36	0.23	0.34	0.70	7.33	5.66	0.08	Fsp28	65.43	19.16	0.50	0.67	5.66	8.58	0.03	858	5.4
Fur-I	S036GG01	64.17	0.48	17.64	3.36	0.23	0.34	0.70	7.33	5.66	0.08	Fsp29	66.10	19.36	0.24	0.56	6.76	6.98	0.13	882	5.5
Fur-I	S036GG01	64.17	0.48	17.64	3.36	0.23	0.34	0.70	7.33	5.66	0.08	Fsp30	66.03	19.33	0.43	0.38	6.95	6.87	0.18	885	5.2
Fur-I	S036GG01	64.17	0.48	17.64	3.36	0.23	0.34	0.70	7.33	5.66	0.08	Fsp31	65.52	19.70	0.23	0.98	6.32	7.25	0.00	873	5.3
Fur-I	S036GG01	64.17	0.48	17.64	3.36	0.23	0.34	0.70	7.33	5.66	0.08	Fsp32	66.44	19.12	0.29	0.27	7.21	6.68	0.23	890	5.5
Fur-I	S036GG01	64.17	0.48	17.64	3.36	0.23	0.34	0.70	7.33	5.66	0.08	Fsp33	66.15	19.10	0.31	0.41	6.94	7.10	0.16	883	5.5
Fur-I	S036GG01	64.17	0.48	17.64	3.36	0.23	0.34	0.70	7.33	5.66	0.08	Fsp34	66.52	19.07	0.26	0.38	6.76	7.00	0.16	883	5.6
Fur-I	S036GG01	64.17	0.48	17.64	3.36	0.23	0.34	0.70	7.33	5.66	0.08	Fsp35	66.54	19.29	0.25	0.50	6.86	6.55	0.16	886	5.5

Table F4 continued

Unit		Liquid composition										Feldspar composition							Equilibrium	T	H_2O
	Sample	SiO_2	TiO_2	Al_2O_3	FeO_t	MnO	MgO	CaO	Na_2O	K_2O	P_2O_5	Sample	SiO_2	Al_2O_3	FeO_t	CaO	Na_2O	K_2O	ΔKd_{Or-Ab}	(°C)	(wt. %)
Fur-I	S036GG01	64.17	0.48	17.64	3.36	0.23	0.34	0.70	7.33	5.66	0.08	Fsp36	66.23	19.16	0.24	0.43	6.93	7.01	0.16	884	5.6
Fur-I	S036GG01	64.17	0.48	17.64	3.36	0.23	0.34	0.70	7.33	5.66	0.08	Fsp37	66.12	19.34	0.27	0.62	7.03	6.62	0.14	886	5.3
Fur-I	S036GG01	64.17	0.48	17.64	3.36	0.23	0.34	0.70	7.33	5.66	0.08	Fsp38	65.61	19.68	0.20	0.88	6.10	7.53	0.01	869	5.5
Fur-I	S036GG01	64.17	0.48	17.64	3.36	0.23	0.34	0.70	7.33	5.66	0.08	Fsp39	66.39	19.06	0.27	0.28	6.78	7.22	0.18	882	5.7
Fur-I	S036GG01	64.17	0.48	17.64	3.36	0.23	0.34	0.70	7.33	5.66	0.08	Fsp40	65.85	19.87	0.22	0.84	6.85	6.37	0.09	886	5.2
Fur-I	S036GG01	64.17	0.48	17.64	3.36	0.23	0.34	0.70	7.33	5.66	0.08	Fsp41	65.93	19.75	0.20	0.84	6.80	6.48	0.08	884	5.2
Fur-I dome	S036GG01	64.17	0.48	17.64	3.36	0.23	0.34	0.70	7.33	5.66	0.08	Fsp13c	65.85	19.72	0.26	0.59	7.17	6.41	0.17	889	5.2
Fur-I dome	S036GG01	64.17	0.48	17.64	3.36	0.23	0.34	0.70	7.33	5.66	0.08	Fsp13r	66.43	19.48	0.33	0.50	7.47	5.80	0.24	897	4.9
Fur-I dome	S036GG01	64.17	0.48	17.64	3.36	0.23	0.34	0.70	7.33	5.66	0.08	Fsp14c	66.36	19.31	0.30	0.42	7.32	6.29	0.22	893	5.2
Fur-I dome	S036GG01	64.17	0.48	17.64	3.36	0.23	0.34	0.70	7.33	5.66	0.08	Fsp14r	66.71	19.46	0.25	0.37	7.33	5.87	0.27	896	5.3
Fur-I dome	S036GG01	64.17	0.48	17.64	3.36	0.23	0.34	0.70	7.33	5.66	0.08	Fsp15c	65.91	19.77	0.20	0.64	6.97	6.51	0.14	887	5.3
Fur-I dome	S036GG01	64.17	0.48	17.64	3.36	0.23	0.34	0.70	7.33	5.66	0.08	Fsp15r	66.07	19.40	0.47	0.60	7.39	6.06	0.19	894	4.6
Fur-I dome	S036GG01	64.17	0.48	17.64	3.36	0.23	0.34	0.70	7.33	5.66	0.08	Fsp19c	66.49	19.19	0.27	0.33	6.80	6.91	0.18	884	5.5
Fur-I dome	S036GG01	64.17	0.48	17.64	3.36	0.23	0.34	0.70	7.33	5.66	0.08	Fsp19r	66.75	19.01	0.47	0.18	7.19	6.39	0.27	892	4.7
Fur-I dome	S036GG01	64.17	0.48	17.64	3.36	0.23	0.34	0.70	7.33	5.66	0.08	Fsp20c	66.26	19.28	0.26	0.35	7.05	6.80	0.20	887	5.5
Fur-I dome	S036GG01	64.17	0.48	17.64	3.36	0.23	0.34	0.70	7.33	5.66	0.08	Fsp20r	66.44	19.14	0.52	0.40	7.43	6.08	0.25	895	4.6
Fur-I dome	S036GG01	64.17	0.48	17.64	3.36	0.23	0.34	0.70	7.33	5.66	0.08	Fsp21c	65.96	19.44	0.23	0.61	6.70	7.06	0.11	880	5.4
Fur-I dome	S036GG01	64.17	0.48	17.64	3.36	0.23	0.34	0.70	7.33	5.66	0.08	Fsp21r	66.27	19.17	0.50	0.16	7.73	6.19	0.33	898	4.5
Fur-I dome	S036GG01	64.17	0.48	17.64	3.36	0.23	0.34	0.70	7.33	5.66	0.08	Fsp22c	66.24	19.46	0.29	0.44	6.83	6.73	0.16	885	5.4
Fur-I dome	S036GG01	64.17	0.48	17.64	3.36	0.23	0.34	0.70	7.33	5.66	0.08	Fsp22r	66.60	19.26	0.25	0.27	6.54	7.09	0.17	881	5.7
Fur-I dome	S036GG01	64.17	0.48	17.64	3.36	0.23	0.34	0.70	7.33	5.66	0.08	1 / 1 .	66.38	18.80	0.51	0.19	7.41	6.64	0.26	892	4.7
Fur-I dome	S036GG01	64.17	0.48	17.64	3.36	0.23	0.34	0.70	7.33	5.66	0.08	1 / 2 .	66.37	18.99	0.35	0.38	7.21	6.67	0.20	889	5.2
Fur-I dome	S036GG01	64.17	0.48	17.64	3.36	0.23	0.34	0.70	7.33	5.66	0.08	1 / 3 .	66.45	19.11	0.28	0.35	7.27	6.51	0.23	891	5.3
Fur-I dome	S036GG01	64.17	0.48	17.64	3.36	0.23	0.34	0.70	7.33	5.66	0.08	1 / 4 .	66.41	19.14	0.28	0.37	7.18	6.56	0.21	890	5.3
Fur-I dome	S036GG01	64.17	0.48	17.64	3.36	0.23	0.34	0.70	7.33	5.66	0.08	1 / 5 .	66.36	19.02	0.31	0.36	7.24	6.67	0.21	889	5.3
Fur-I dome	S036GG01	64.17	0.48	17.64	3.36	0.23	0.34	0.70	7.33	5.66	0.08	1 / 6 .	66.32	19.00	0.29	0.33	7.18	6.85	0.21	888	5.4
Fur-I dome	S036GG01	64.17	0.48	17.64	3.36	0.23	0.34	0.70	7.33	5.66	0.08	1 / 7 .	66.26	19.20	0.30	0.36	7.08	6.76	0.20	888	5.4
Fur-I dome	S036GG01	64.17	0.48	17.64	3.36	0.23	0.34	0.70	7.33	5.66	0.08	1 / 9 .	66.37	19.04	0.30	0.41	7.38	6.44	0.22	892	5.2
Fur-I dome	S036GG01	64.17	0.48	17.64	3.36	0.23	0.34	0.70	7.33	5.66	0.08	1 / 10 .	66.31	19.14	0.29	0.42	7.37	6.43	0.22	892	5.2
Fur-I dome	S036GG01	64.17	0.48	17.64	3.36	0.23	0.34	0.70	7.33	5.66	0.08	1 / 12 .	66.45	18.93	0.29	0.37	7.25	6.69	0.21	889	5.3
Fur-I dome	S036GG01	64.17	0.48	17.64	3.36	0.23	0.34	0.70	7.33	5.66	0.08	1 / 13 .	66.30	19.00	0.33	0.36	7.34	6.63	0.22	890	5.2
Fur-I dome	S036GG01	64.17	0.48	17.64	3.36	0.23	0.34	0.70	7.33	5.66	0.08	1 / 14 .	66.20	19.08	0.34	0.36	7.29	6.69	0.21	890	5.2
Fur-I dome	S036GG01	64.17	0.48	17.64	3.36	0.23	0.34	0.70	7.33	5.66	0.08	1 / 15 .	66.18	18.87	0.40	0.35	7.39	6.77	0.22	890	5.1
Fur-I dome	S036GG01	64.17	0.48	17.64	3.36	0.23	0.34	0.70	7.33	5.66	0.08	1 / 16 .	66.20	18.99	0.43	0.36	7.49	6.48	0.24	893	4.9
Fur-I dome	S036GG01	64.17	0.48	17.64	3.36	0.23	0.34	0.70	7.33	5.66	0.08	1 / 17 .	66.37	19.07	0.32	0.32	7.36	6.55	0.24	892	5.2

Table F4 continued

Unit		Liquid composition										Feldspar composition							Equilibrium	T	H_2O
	Sample	SiO_2	TiO_2	Al_2O_3	FeO_t	MnO	MgO	CaO	Na_2O	K_2O	P_2O_5	Sample	SiO_2	Al_2O_3	FeO_t	CaO	Na_2O	K_2O	ΔKd_{Or-Ab}	(°C)	(wt. %)
Fur-I dome	S036GG01	64.17	0.48	17.64	3.36	0.23	0.34	0.70	7.33	5.66	0.08	1 / 18 .	66.38	18.91	0.34	0.36	7.32	6.64	0.22	890	5.2
Fur-I dome	S036GG01	64.17	0.48	17.64	3.36	0.23	0.34	0.70	7.33	5.66	0.08	1 / 19 .	66.39	18.96	0.30	0.29	7.32	6.68	0.23	890	5.3
Fur-I dome	S036GG01	64.17	0.48	17.64	3.36	0.23	0.34	0.70	7.33	5.66	0.08	1 / 20 .	66.33	19.05	0.36	0.37	7.55	6.31	0.25	894	5.0
Fur-I dome	S036GG01	64.17	0.48	17.64	3.36	0.23	0.34	0.70	7.33	5.66	0.08	1 / 21 .	66.33	19.07	0.39	0.43	7.69	6.06	0.26	897	4.9
Fur-I dome	S036GG01	64.17	0.48	17.64	3.36	0.23	0.34	0.70	7.33	5.66	0.08	1 / 22 .	66.24	18.90	0.35	0.30	7.20	6.96	0.21	887	5.3
Fur-I dome	S036GG01	64.17	0.48	17.64	3.36	0.23	0.34	0.70	7.33	5.66	0.08	1 / 23 .	66.26	18.97	0.31	0.31	7.24	6.87	0.21	888	5.4
Fur-I dome	S036GG01	64.17	0.48	17.64	3.36	0.23	0.34	0.70	7.33	5.66	0.08	1 / 24 .	66.31	18.92	0.29	0.30	7.27	6.87	0.22	888	5.4
Fur-I dome	S036GG01	64.17	0.48	17.64	3.36	0.23	0.34	0.70	7.33	5.66	0.08	1 / 25 .	66.35	18.99	0.31	0.32	7.18	6.81	0.21	888	5.3
Fur-I dome	S036GG01	64.17	0.48	17.64	3.36	0.23	0.34	0.70	7.33	5.66	0.08	1 / 26 .	66.30	18.94	0.29	0.32	7.20	6.88	0.21	888	5.4
Fur-I dome	S036GG01	64.17	0.48	17.64	3.36	0.23	0.34	0.70	7.33	5.66	0.08	1 / 27 .	66.36	18.89	0.28	0.29	7.29	6.84	0.22	889	5.4
Fur-I dome	S036GG01	64.17	0.48	17.64	3.36	0.23	0.34	0.70	7.33	5.66	0.08	1 / 28 .	66.27	18.94	0.35	0.33	7.37	6.68	0.23	891	5.2
Fur-I dome	S036GG01	64.17	0.48	17.64	3.36	0.23	0.34	0.70	7.33	5.66	0.08	1 / 29 .	66.38	18.72	0.66	0.34	7.45	6.37	0.25	893	4.4
Fur-I dome	S036GG01	64.17	0.48	17.64	3.36	0.23	0.34	0.70	7.33	5.66	0.08	1 / 30 .	66.45	18.62	0.48	0.19	7.44	6.77	0.26	891	4.8
Fur-I dome	S036GG01	64.17	0.48	17.64	3.36	0.23	0.34	0.70	7.33	5.66	0.08	2 / 1 .	66.08	19.20	0.28	0.52	7.22	6.64	0.17	888	5.2
Fur-I dome	S036GG01	64.17	0.48	17.64	3.36	0.23	0.34	0.70	7.33	5.66	0.08	2 / 2 .	66.40	18.87	0.27	0.38	7.25	6.80	0.20	888	5.4
Fur-I dome	S036GG01	64.17	0.48	17.64	3.36	0.23	0.34	0.70	7.33	5.66	0.08	2 / 3 .	66.19	19.13	0.25	0.43	7.28	6.69	0.20	889	5.4
Fur-I dome	S036GG01	64.17	0.48	17.64	3.36	0.23	0.34	0.70	7.33	5.66	0.08	2 / 4 .	66.37	19.00	0.27	0.38	7.47	6.49	0.23	892	5.3
Fur-I dome	S036GG01	64.17	0.48	17.64	3.36	0.23	0.34	0.70	7.33	5.66	0.08	2 / 5 .	66.17	19.09	0.26	0.45	7.39	6.59	0.20	890	5.3
Fur-I dome	S036GG01	64.17	0.48	17.64	3.36	0.23	0.34	0.70	7.33	5.66	0.08	2 / 6 .	66.44	18.89	0.28	0.27	7.26	6.82	0.23	889	5.5
Fur-I dome	S036GG01	64.17	0.48	17.64	3.36	0.23	0.34	0.70	7.33	5.66	0.08	2 / 7 .	65.78	19.72	0.31	0.37	7.53	6.24	0.25	895	5.1
Fur-I dome	S036GG01	64.17	0.48	17.64	3.36	0.23	0.34	0.70	7.33	5.66	0.08	2 / 8 .	66.52	18.99	0.29	0.43	6.88	6.85	0.16	885	5.4
Fur-I dome	S036GG01	64.17	0.48	17.64	3.36	0.23	0.34	0.70	7.33	5.66	0.08	2 / 9 .	66.41	19.09	0.26	0.41	7.30	6.51	0.21	891	5.3
Fur-I dome	S036GG01	64.17	0.48	17.64	3.36	0.23	0.34	0.70	7.33	5.66	0.08	2 / 10 .	66.27	19.01	0.35	0.52	7.23	6.57	0.18	889	5.1
Fur-I dome	S036GG01	64.17	0.48	17.64	3.36	0.23	0.34	0.70	7.33	5.66	0.08	4 / 1 .	67.07	19.16	0.31	0.42	6.83	6.15	0.20	890	5.2
Fur-I dome	S036GG01	64.17	0.48	17.64	3.36	0.23	0.34	0.70	7.33	5.66	0.08	5 / 1 .	66.32	19.02	0.30	0.44	7.38	6.52	0.21	891	5.2
Fur-I dome	S036GG01	64.17	0.48	17.64	3.36	0.23	0.34	0.70	7.33	5.66	0.08	6 / 1 .	66.29	19.04	0.28	0.38	7.46	6.53	0.23	892	5.3
Fur-I dome	S036GG01	64.17	0.48	17.64	3.36	0.23	0.34	0.70	7.33	5.66	0.08	7 / 1 .	66.26	19.07	0.28	0.45	7.31	6.62	0.20	890	5.3
Fur-I dome	S036GG01	64.17	0.48	17.64	3.36	0.23	0.34	0.70	7.33	5.66	0.08	8 / 1 .	66.59	18.60	0.50	0.20	7.41	6.66	0.26	892	4.7
Fur-I dome	S036GG01	64.17	0.48	17.64	3.36	0.23	0.34	0.70	7.33	5.66	0.08	9 / 1 .	66.27	19.06	0.29	0.43	7.14	6.76	0.18	887	5.3
Fur-I dome	S036GG01	64.17	0.48	17.64	3.36	0.23	0.34	0.70	7.33	5.66	0.08	10 / 1 .	66.19	19.05	0.28	0.45	7.34	6.63	0.20	890	5.3
Fur-I dome	S036GG01	64.17	0.48	17.64	3.36	0.23	0.34	0.70	7.33	5.66	0.08	11 / 1 .	66.27	19.33	0.31	0.65	7.97	5.43	0.25	902	4.7
Fur-I dome	S036GG01	64.17	0.48	17.64	3.36	0.23	0.34	0.70	7.33	5.66	0.08	12 / 1 .	66.35	19.14	0.29	0.50	7.57	6.13	0.23	895	5.1
Fur-I dome	S036GG01	64.17	0.48	17.64	3.36	0.23	0.34	0.70	7.33	5.66	0.08	13 / 1 .	66.77	18.86	0.71	0.42	8.05	5.10	0.36	907	4.0
Fur-I dome	S036GG01	64.17	0.48	17.64	3.36	0.23	0.34	0.70	7.33	5.66	0.08	14 / 1 .	66.66	18.91	0.53	0.43	7.85	5.54	0.31	902	4.4
Fur-I dome	S036GG01	64.17	0.48	17.64	3.36	0.23	0.34	0.70	7.33	5.66	0.08	15 / 1 .	66.53	18.67	0.74	0.24	7.58	6.16	0.30	897	4.1

Table F4 continued

Unit		Liquid composition										Feldspar composition							Equilibrium	T	H_2O
	Sample	SiO_2	TiO_2	Al_2O_3	FeO_t	MnO	MgO	CaO	Na_2O	K_2O	P_2O_5	Sample	SiO_2	Al_2O_3	FeO_t	CaO	Na_2O	K_2O	ΔKd_{Or-Ab}	(°C)	(wt. %)
Fur-I dome	S036GG01	64.17	0.48	17.64	3.36	0.23	0.34	0.70	7.33	5.66	0.08	16 / 1 .	66.53	18.69	0.58	0.17	7.37	6.58	0.27	892	4.4
Fur-I dome	S036GG01	64.17	0.48	17.64	3.36	0.23	0.34	0.70	7.33	5.66	0.08	17 / 1 .	66.26	18.98	0.59	0.35	7.80	5.94	0.30	899	4.4
Fur-I dome	S036GG01	64.17	0.48	17.64	3.36	0.23	0.34	0.70	7.33	5.66	0.08	167 / 1 .	66.55	18.95	0.54	0.17	6.97	6.76	0.23	888	4.6
Fur-H	S004GG07	64.22	0.51	17.67	3.25	0.25	0.34	0.75	7.36	5.55	0.09	Fsp1	66.01	19.13	0.26	0.41	7.63	6.55	0.43	890	5.3
Fur-H	S004GG07	64.22	0.51	17.67	3.25	0.25	0.34	0.75	7.36	5.55	0.09	Fsp2	65.98	19.15	0.28	0.39	7.16	7.05	0.36	883	5.5
Fur-H	S004GG07	64.22	0.51	17.67	3.25	0.25	0.34	0.75	7.36	5.55	0.09	Fsp3	66.10	19.07	0.27	0.22	6.99	7.35	0.36	880	5.7
Fur-H	S004GG07	64.22	0.51	17.67	3.25	0.25	0.34	0.75	7.36	5.55	0.09	Fsp4	65.60	19.45	0.31	0.44	7.10	7.11	0.34	882	5.4
Fur-H	S004GG07	64.22	0.51	17.67	3.25	0.25	0.34	0.75	7.36	5.55	0.09	Fsp6	65.28	19.69	0.25	0.61	7.46	6.71	0.35	886	5.2
Fur-H	S004GG07	64.22	0.51	17.67	3.25	0.25	0.34	0.75	7.36	5.55	0.09	Fsp7	65.91	19.42	0.29	0.40	6.61	7.37	0.29	876	5.6
Fur-H	S004GG07	64.22	0.51	17.67	3.25	0.25	0.34	0.75	7.36	5.55	0.09	Fsp8	65.67	19.34	0.27	0.26	6.97	7.49	0.34	879	5.7
Fur-H	S004GG07	64.22	0.51	17.67	3.25	0.25	0.34	0.75	7.36	5.55	0.09	Fsp9	64.91	19.89	0.21	1.04	5.88	8.08	0.09	859	5.4
Fur-H	S004GG07	64.22	0.51	17.67	3.25	0.25	0.34	0.75	7.36	5.55	0.09	Fsp10	65.60	19.58	0.23	0.52	6.40	7.68	0.24	871	5.7
Fur-H	S004GG07	64.22	0.51	17.67	3.25	0.25	0.34	0.75	7.36	5.55	0.09	Fsp11	65.93	19.13	0.32	0.31	6.91	7.40	0.33	879	5.5
Fur-H	S004GG07	64.22	0.51	17.67	3.25	0.25	0.34	0.75	7.36	5.55	0.09	Fsp12	65.60	19.68	0.25	0.58	6.67	7.22	0.27	876	5.5
Fur-H	S004GG07	64.22	0.51	17.67	3.25	0.25	0.34	0.75	7.36	5.55	0.09	Fsp13	66.08	19.28	0.26	0.43	6.71	7.25	0.30	877	5.6
Fur-H	S004GG07	64.22	0.51	17.67	3.25	0.25	0.34	0.75	7.36	5.55	0.09	Fsp14	66.37	19.39	0.28	0.46	7.00	6.49	0.37	886	5.3
Fur-H	S004GG07	64.22	0.51	17.67	3.25	0.25	0.34	0.75	7.36	5.55	0.09	Fsp15	66.19	19.17	0.29	0.25	7.16	6.93	0.39	885	5.5
Fur-H	S004GG07	64.22	0.51	17.67	3.25	0.25	0.34	0.75	7.36	5.55	0.09	Fsp16	66.46	18.94	0.25	0.27	6.71	7.36	0.32	878	5.8
Fur-H	S004GG07	64.22	0.51	17.67	3.25	0.25	0.34	0.75	7.36	5.55	0.09	Fsp17	66.72	19.35	0.31	0.37	6.94	6.31	0.40	887	5.3
Fur-H	S004GG07	64.22	0.51	17.67	3.25	0.25	0.34	0.75	7.36	5.55	0.09	Fsp18	66.11	19.33	0.25	0.41	6.20	7.70	0.24	869	5.8
Fur-H	S004GG07	64.22	0.51	17.67	3.25	0.25	0.34	0.75	7.36	5.55	0.09	Fsp19	66.26	19.58	0.29	0.46	7.31	6.11	0.43	891	5.2
Fur-H	S004GG07	64.22	0.51	17.67	3.25	0.25	0.34	0.75	7.36	5.55	0.09	Fsp20	65.85	19.44	0.26	0.39	6.43	7.62	0.27	872	5.7
Fur-H	S004GG07	64.22	0.51	17.67	3.25	0.25	0.34	0.75	7.36	5.55	0.09	Fsp21	66.64	19.29	0.31	0.33	6.96	6.47	0.40	886	5.4
Fur-H	S004GG07	64.22	0.51	17.67	3.25	0.25	0.34	0.75	7.36	5.55	0.09	Fsp22	66.43	19.41	0.24	0.34	6.39	7.20	0.30	876	5.8
Fur-H	S004GG07	64.22	0.51	17.67	3.25	0.25	0.34	0.75	7.36	5.55	0.09	Fsp23	66.48	19.15	0.25	0.31	6.91	6.90	0.36	883	5.7
Fur-H	S004GG07	64.22	0.51	17.67	3.25	0.25	0.34	0.75	7.36	5.55	0.09	Fsp24	66.32	19.52	0.25	0.34	6.73	6.85	0.34	881	5.7
Fur-H	S004GG07	64.22	0.51	17.67	3.25	0.25	0.34	0.75	7.36	5.55	0.09	Fsp25	66.29	19.63	0.30	0.54	7.59	5.64	0.48	896	4.9
Fur-H	S004GG07	64.22	0.51	17.67	3.25	0.25	0.34	0.75	7.36	5.55	0.09	Fsp26	66.06	19.55	0.25	0.43	6.91	6.80	0.34	883	5.5
Fur-H	S004GG07	64.22	0.51	17.67	3.25	0.25	0.34	0.75	7.36	5.55	0.09	Fsp27	66.01	19.61	0.25	0.34	6.84	6.95	0.35	881	5.6
Fur-H	S004GG07	64.22	0.51	17.67	3.25	0.25	0.34	0.75	7.36	5.55	0.09	Fsp28	66.00	19.61	0.25	0.54	6.75	6.85	0.30	880	5.4
Fur-H	S004GG07	64.22	0.51	17.67	3.25	0.25	0.34	0.75	7.36	5.55	0.09	Fsp29	65.83	19.28	0.30	0.49	6.34	7.76	0.23	870	5.6
Fur-H	S004GG07	64.22	0.51	17.67	3.25	0.25	0.34	0.75	7.36	5.55	0.09	Fsp30	65.94	19.61	0.22	0.52	6.50	7.21	0.27	875	5.6
Fur-H	S004GG07	64.22	0.51	17.67	3.25	0.25	0.34	0.75	7.36	5.55	0.09	Fsp31	65.95	19.54	0.26	0.54	6.90	6.81	0.32	882	5.4
Fur-H	S004GG07	64.22	0.51	17.67	3.25	0.25	0.34	0.75	7.36	5.55	0.09	Fsp32	66.00	19.71	0.21	0.53	6.78	6.77	0.31	881	5.5
Fur-H	S004GG07	64.22	0.51	17.67	3.25	0.25	0.34	0.75	7.36	5.55	0.09	Fsp33	65.97	19.63	0.28	0.40	6.71	7.00	0.32	880	5.5

Table F4 continued

Unit		Liquid composition										Feldspar composition							Equilibrium	T	H_2O
	Sample	SiO_2	TiO_2	Al_2O_3	FeO_t	MnO	MgO	CaO	Na_2O	K_2O	P_2O_5	Sample	SiO_2	Al_2O_3	FeO_t	CaO	Na_2O	K_2O	ΔKd_{Or-Ab}	(°C)	(wt. %)
Fur-H	S004GG07	64.22	0.51	17.67	3.25	0.25	0.34	0.75	7.36	5.55	0.09	Fsp35	65.71	20.08	0.19	0.81	7.10	6.10	0.32	887	5.1
Fur-H	S004GG07	64.22	0.51	17.67	3.25	0.25	0.34	0.75	7.36	5.55	0.09	Fsp36	66.40	19.34	0.29	0.31	6.56	7.11	0.32	878	5.6
Fur-H	S004GG07	64.22	0.51	17.67	3.25	0.25	0.34	0.75	7.36	5.55	0.09	Fsp37	65.66	20.14	0.26	0.92	7.09	5.93	0.30	888	4.8
Fur-H	S004GG07	64.22	0.51	17.67	3.25	0.25	0.34	0.75	7.36	5.55	0.09	Fsp38	66.07	19.42	0.30	0.28	6.38	7.56	0.29	873	5.7
Fur-H	S004GG07	64.22	0.51	17.67	3.25	0.25	0.34	0.75	7.36	5.55	0.09	Fsp39	66.11	19.47	0.22	0.71	6.17	7.32	0.20	870	5.5
Fur-H	S004GG07	64.22	0.51	17.67	3.25	0.25	0.34	0.75	7.36	5.55	0.09	Fsp40	66.37	19.36	0.25	0.37	6.86	6.78	0.35	883	5.6
Fur-G	S008	63.54	0.43	17.56	3.83	0.28	0.26	0.74	7.71	5.61	0.05	MI01Fsp	66.59	19.25	0.26	0.35	6.88	6.67	0.24	893	5.6
Fur-F	SM4-1	63.56	0.51	17.69	3.68	0.25	0.39	0.83	7.09	5.91	0.07	Fsp3	66.16	18.93	0.50	0.20	7.19	7.03	0.22	929	4.1
Fur-F	SM4-1	63.56	0.51	17.69	3.68	0.25	0.39	0.83	7.09	5.91	0.07	Fsp6	65.76	19.45	0.32	0.34	7.18	6.95	0.19	929	4.7
Fur-F	SM4-1	63.56	0.51	17.69	3.68	0.25	0.39	0.83	7.09	5.91	0.07	Fsp7	65.33	19.50	0.28	0.33	7.42	7.14	0.20	929	4.8
Fur-F	SM4-1	63.56	0.51	17.69	3.68	0.25	0.39	0.83	7.09	5.91	0.07	Fsp8	65.26	19.72	0.26	0.48	7.14	7.14	0.15	926	4.7
Fur-F	SM4-1	63.56	0.51	17.69	3.68	0.25	0.39	0.83	7.09	5.91	0.07	Fsp9	66.05	19.15	0.27	0.24	6.94	7.36	0.18	924	5.0
Fur-F	SM4-1	63.56	0.51	17.69	3.68	0.25	0.39	0.83	7.09	5.91	0.07	Fsp10	66.16	19.02	0.58	0.14	7.29	6.81	0.25	932	3.7
Fur-F	SM4-1	63.56	0.51	17.69	3.68	0.25	0.39	0.83	7.09	5.91	0.07	Fsp11	66.07	19.47	0.29	0.38	6.96	6.83	0.17	927	4.7
Fur-F	SM4-1	63.56	0.51	17.69	3.68	0.25	0.39	0.83	7.09	5.91	0.07	Fsp12	66.01	19.40	0.24	0.29	7.13	6.92	0.20	929	4.9
Fur-F	SM4-1	63.56	0.51	17.69	3.68	0.25	0.39	0.83	7.09	5.91	0.07	Fsp13	66.15	19.20	0.31	0.28	6.94	7.12	0.18	926	4.8
Fur-F	SM4-1	63.56	0.51	17.69	3.68	0.25	0.39	0.83	7.09	5.91	0.07	Fsp14	66.04	19.34	0.24	0.37	6.82	7.19	0.15	923	5.0
Fur-F	SM4-1	63.56	0.51	17.69	3.68	0.25	0.39	0.83	7.09	5.91	0.07	Fsp15	65.86	19.47	0.25	0.51	6.94	6.96	0.14	925	4.7
Fur-F	SM4-1	63.56	0.51	17.69	3.68	0.25	0.39	0.83	7.09	5.91	0.07	Fsp16	65.67	19.54	0.27	0.29	7.12	7.10	0.19	927	4.8
Fur-F	SM4-1	63.56	0.51	17.69	3.68	0.25	0.39	0.83	7.09	5.91	0.07	Fsp17	66.05	19.37	0.29	0.37	7.05	6.87	0.18	928	4.7
Fur-F	SM4-1	63.56	0.51	17.69	3.68	0.25	0.39	0.83	7.09	5.91	0.07	Fsp18	65.98	19.38	0.23	0.31	7.30	6.79	0.21	931	4.9
Fur-F	SM4-1	63.56	0.51	17.69	3.68	0.25	0.39	0.83	7.09	5.91	0.07	Fsp19	65.59	19.47	0.26	0.26	7.15	7.26	0.19	926	4.9
Fur-F	SM4-1	63.56	0.51	17.69	3.68	0.25	0.39	0.83	7.09	5.91	0.07	Fsp20	65.99	19.45	0.27	0.32	7.43	6.54	0.23	934	4.7
Fur-F	SM4-1	63.56	0.51	17.69	3.68	0.25	0.39	0.83	7.09	5.91	0.07	Fsp21	65.97	19.46	0.32	0.51	7.20	6.54	0.17	931	4.5
Fur-F	SM4-1	63.56	0.51	17.69	3.68	0.25	0.39	0.83	7.09	5.91	0.07	Fsp22	65.72	19.42	0.25	0.41	6.98	7.22	0.15	924	4.9
Fur-F	SM4-1	63.56	0.51	17.69	3.68	0.25	0.39	0.83	7.09	5.91	0.07	Fsp23	65.96	19.30	0.24	0.34	6.91	7.25	0.16	924	5.0
Fur-F	SM4-1	63.56	0.51	17.69	3.68	0.25	0.39	0.83	7.09	5.91	0.07	Fsp24	66.14	19.39	0.23	0.45	6.76	7.04	0.14	923	4.9
Fur-F	SM4-1	63.56	0.51	17.69	3.68	0.25	0.39	0.83	7.09	5.91	0.07	Fsp25	66.25	19.15	0.52	0.11	7.38	6.60	0.28	935	3.7
Fur-F	SM4-1	63.56	0.51	17.69	3.68	0.25	0.39	0.83	7.09	5.91	0.07	Fsp26	66.11	19.16	0.33	0.29	7.06	7.04	0.19	927	4.7
Fur-F	SM4-1	63.56	0.51	17.69	3.68	0.25	0.39	0.83	7.09	5.91	0.07	Fsp27	66.12	19.31	0.24	0.25	6.95	7.13	0.19	926	5.0
Fur-F	SM4-1	63.56	0.51	17.69	3.68	0.25	0.39	0.83	7.09	5.91	0.07	Fsp28	66.20	19.13	0.27	0.31	6.91	7.18	0.17	925	4.9
Fur-F	SM4-1	63.56	0.51	17.69	3.68	0.25	0.39	0.83	7.09	5.91	0.07	Fsp29	66.10	19.52	0.26	0.42	7.21	6.49	0.20	932	4.7
Fur-F	SM4-1	63.56	0.51	17.69	3.68	0.25	0.39	0.83	7.09	5.91	0.07	Fsp30	66.03	19.36	0.26	0.27	6.93	7.16	0.18	925	5.0
Fur-F	SM4-1	63.56	0.51	17.69	3.68	0.25	0.39	0.83	7.09	5.91	0.07	Fsp31	66.07	19.30	0.27	0.31	7.34	6.71	0.22	932	4.7
Fur-F	SM4-1	63.56	0.51	17.69	3.68	0.25	0.39	0.83	7.09	5.91	0.07	Fsp32	66.34	19.19	0.29	0.31	6.71	7.15	0.16	923	4.9

Table F4 continued

Unit		Liquid composition										Feldspar composition							Equilibrium	T	H_2O
	Sample	SiO_2	TiO_2	Al_2O_3	FeO_t	MnO	MgO	CaO	Na_2O	K_2O	P_2O_5	Sample	SiO_2	Al_2O_3	FeO_t	CaO	Na_2O	K_2O	ΔKd_{Or-Ab}	(°C)	(wt. %)
Fur-F	SM4-1	63.56	0.51	17.69	3.68	0.25	0.39	0.83	7.09	5.91	0.07	Fsp33	66.22	19.45	0.28	0.31	6.87	6.87	0.18	927	4.8
Fur-F	SM4-1	63.56	0.51	17.69	3.68	0.25	0.39	0.83	7.09	5.91	0.07	Fsp34	66.09	19.51	0.21	0.43	6.70	7.06	0.14	923	5.0
Fur-F	SM4-1	63.56	0.51	17.69	3.68	0.25	0.39	0.83	7.09	5.91	0.07	Fsp35	66.28	19.19	0.26	0.26	6.72	7.29	0.17	922	5.0
Fur-F	SM4-1	63.56	0.51	17.69	3.68	0.25	0.39	0.83	7.09	5.91	0.07	Fsp36	66.47	19.15	0.28	0.23	6.66	7.23	0.17	922	5.0
Fur-F	SM4-1	63.56	0.51	17.69	3.68	0.25	0.39	0.83	7.09	5.91	0.07	Fsp37	66.78	19.49	0.26	0.62	6.96	5.90	0.16	934	4.4
Fur-F	SM4-1	63.56	0.51	17.69	3.68	0.25	0.39	0.83	7.09	5.91	0.07	Fsp38	66.46	19.17	0.26	0.40	6.97	6.74	0.18	928	4.8
Fur-F	SM4-1	63.56	0.51	17.69	3.68	0.25	0.39	0.83	7.09	5.91	0.07	Fsp39	66.52	19.37	0.25	0.30	6.62	6.95	0.17	924	5.0
Fur-F	SM4-1	63.56	0.51	17.69	3.68	0.25	0.39	0.83	7.09	5.91	0.07	Fsp40	66.54	19.32	0.29	0.40	7.03	6.41	0.20	932	4.6
Fur-E	S012bGG05	64.19	0.50	17.56	3.12	0.24	0.22	0.85	8.05	5.17	0.11	Fsp3	66.11	19.23	0.28	0.34	7.09	6.95	0.12	862	5.8
Fur-E	S012bGG05	64.19	0.50	17.56	3.12	0.24	0.22	0.85	8.05	5.17	0.11	Fsp4	66.63	18.95	0.26	0.38	6.87	6.92	0.10	861	5.9
Fur-E	S012bGG05	64.19	0.50	17.56	3.12	0.24	0.22	0.85	8.05	5.17	0.11	Fsp6	66.40	19.08	0.23	0.28	6.90	7.12	0.11	860	6.1
Fur-E	S012bGG05	64.19	0.50	17.56	3.12	0.24	0.22	0.85	8.05	5.17	0.11	Fsp7	66.26	19.44	0.23	0.64	6.72	6.72	0.04	859	5.7
Fur-E	S012bGG05	64.19	0.50	17.56	3.12	0.24	0.22	0.85	8.05	5.17	0.11	Fsp8	65.94	19.35	0.24	0.62	6.78	7.07	0.04	857	5.7
Fur-E	S012bGG05	64.19	0.50	17.56	3.12	0.24	0.22	0.85	8.05	5.17	0.11	Fsp9	66.07	19.33	0.23	0.67	6.87	6.84	0.03	860	5.7
Fur-E	S012bGG05	64.19	0.50	17.56	3.12	0.24	0.22	0.85	8.05	5.17	0.11	Fsp10	66.26	18.99	0.28	0.38	6.99	7.10	0.10	860	5.9
Fur-E	S012bGG05	64.19	0.50	17.56	3.12	0.24	0.22	0.85	8.05	5.17	0.11	Fsp11	66.17	19.11	0.30	0.35	7.09	6.99	0.11	862	5.8
Fur-E	S012bGG05	64.19	0.50	17.56	3.12	0.24	0.22	0.85	8.05	5.17	0.11	Fsp12	66.24	18.76	0.33	0.30	7.08	7.28	0.11	860	5.8
Fur-E	S012bGG05	64.19	0.50	17.56	3.12	0.24	0.22	0.85	8.05	5.17	0.11	Fsp13	66.37	19.15	0.26	0.24	7.22	6.76	0.15	865	5.9
Fur-E	S012bGG05	64.19	0.50	17.56	3.12	0.24	0.22	0.85	8.05	5.17	0.11	Fsp14	66.20	19.14	0.30	0.47	7.48	6.40	0.13	868	5.5
Fur-E	S012bGG05	64.19	0.50	17.56	3.12	0.24	0.22	0.85	8.05	5.17	0.11	Fsp15	66.12	19.33	0.18	0.56	7.08	6.72	0.07	863	5.8
Fur-E	S012bGG05	64.19	0.50	17.56	3.12	0.24	0.22	0.85	8.05	5.17	0.11	Fsp16	66.37	19.23	0.29	0.35	7.27	6.49	0.14	867	5.7
Fur-E	S012bGG05	64.19	0.50	17.56	3.12	0.24	0.22	0.85	8.05	5.17	0.11	Fsp17	66.19	19.12	0.25	0.35	7.28	6.81	0.13	865	5.9
Fur-E	S012bGG05	64.19	0.50	17.56	3.12	0.24	0.22	0.85	8.05	5.17	0.11	Fsp18	66.09	19.20	0.27	0.35	7.25	6.85	0.12	864	5.8
Fur-E	S012bGG05	64.19	0.50	17.56	3.12	0.24	0.22	0.85	8.05	5.17	0.11	Fsp19	66.54	19.12	0.30	0.35	6.93	6.75	0.11	863	5.8
Fur-E	S012bGG05	64.19	0.50	17.56	3.12	0.24	0.22	0.85	8.05	5.17	0.11	Fsp20	66.60	19.02	0.28	0.36	6.80	6.93	0.10	860	5.9
Fur-E	S012bGG05	64.19	0.50	17.56	3.12	0.24	0.22	0.85	8.05	5.17	0.11	Fsp21	66.42	19.09	0.29	0.34	7.07	6.79	0.12	864	5.8
Fur-E	S012bGG05	64.19	0.50	17.56	3.12	0.24	0.22	0.85	8.05	5.17	0.11	Fsp22	66.09	19.24	0.28	0.39	7.43	6.57	0.14	867	5.7
Fur-E	S012bGG05	64.19	0.50	17.56	3.12	0.24	0.22	0.85	8.05	5.17	0.11	Fsp23	66.14	19.54	0.23	0.58	7.10	6.40	0.08	865	5.6
Fur-E	S012bGG05	64.19	0.50	17.56	3.12	0.24	0.22	0.85	8.05	5.17	0.11	Fsp24	65.97	19.32	0.24	0.44	6.63	7.39	0.06	855	6.0
Fur-E	S012bGG05	64.19	0.50	17.56	3.12	0.24	0.22	0.85	8.05	5.17	0.11	Fsp25	66.47	19.21	0.29	0.34	6.77	6.92	0.10	860	5.9
Fur-E	S012bGG05	64.19	0.50	17.56	3.12	0.24	0.22	0.85	8.05	5.17	0.11	Fsp26	66.14	19.11	0.29	0.36	7.17	6.92	0.11	863	5.8
Fur-E	S012bGG05	64.19	0.50	17.56	3.12	0.24	0.22	0.85	8.05	5.17	0.11	Fsp27	66.32	19.10	0.27	0.37	6.97	6.97	0.10	861	5.9
Fur-E	S012bGG05	64.19	0.50	17.56	3.12	0.24	0.22	0.85	8.05	5.17	0.11	Fsp28	66.31	19.14	0.27	0.31	6.79	7.18	0.10	859	6.0
Fur-E	S012bGG05	64.19	0.50	17.56	3.12	0.24	0.22	0.85	8.05	5.17	0.11	Fsp29	66.02	19.15	0.32	0.27	7.06	7.19	0.12	861	5.8
Fur-E	S012bGG05	64.19	0.50	17.56	3.12	0.24	0.22	0.85	8.05	5.17	0.11	Fsp30	66.52	19.02	0.30	0.34	6.93	6.90	0.11	862	5.8

Table F4 continued

Unit	Liquid composition											Feldspar composition							Equilibrium	T	H_2O
	Sample	SiO_2	TiO_2	Al_2O_3	FeO_t	MnO	MgO	CaO	Na_2O	K_2O	P_2O_5	Sample	SiO_2	Al_2O_3	FeO_t	CaO	Na_2O	K_2O	ΔKd_{Or-Ab}	(°C)	(wt. %)
Fur-E	S012bGG05	64.19	0.50	17.56	3.12	0.24	0.22	0.85	8.05	5.17	0.11	Fsp31	66.23	19.14	0.29	0.34	7.09	6.89	0.12	863	5.8
Fur-E	S012bGG05	64.19	0.50	17.56	3.12	0.24	0.22	0.85	8.05	5.17	0.11	Fsp32	66.67	19.00	0.30	0.31	6.87	6.87	0.11	862	5.8
Fur-E	S012bGG05	64.19	0.50	17.56	3.12	0.24	0.22	0.85	8.05	5.17	0.11	Fsp33	65.97	19.31	0.30	0.44	7.15	6.82	0.10	863	5.7
Fur-E	S012bGG05	64.19	0.50	17.56	3.12	0.24	0.22	0.85	8.05	5.17	0.11	Fsp34	66.29	19.06	0.26	0.32	6.83	7.24	0.10	858	6.0
Fur-E	S012bGG05	64.19	0.50	17.56	3.12	0.24	0.22	0.85	8.05	5.17	0.11	Fsp35	66.54	19.03	0.27	0.43	7.01	6.72	0.10	863	5.8
Fur-E	S012bGG05	64.19	0.50	17.56	3.12	0.24	0.22	0.85	8.05	5.17	0.11	Fsp36	66.15	19.28	0.29	0.52	7.61	6.15	0.13	871	5.4
Fur-E	S012bGG05	64.19	0.50	17.56	3.12	0.24	0.22	0.85	8.05	5.17	0.11	Fsp37	65.97	19.31	0.29	0.38	7.16	6.88	0.11	863	5.7
Fur-E	S012bGG05	64.19	0.50	17.56	3.12	0.24	0.22	0.85	8.05	5.17	0.11	Fsp38	66.28	19.20	0.27	0.31	6.99	6.95	0.12	862	5.9
Fur-E	S012bGG05	64.19	0.50	17.56	3.12	0.24	0.22	0.85	8.05	5.17	0.11	Fsp39	66.12	19.22	0.27	0.29	7.09	7.00	0.12	862	5.9
Fur-E	S012bGG05	64.19	0.50	17.56	3.12	0.24	0.22	0.85	8.05	5.17	0.11	Fsp40	66.67	19.17	0.24	0.22	6.69	7.00	0.12	860	6.1
Fur-E	S012bGG05	64.19	0.50	17.56	3.12	0.24	0.22	0.85	8.05	5.17	0.11	Fsp38	66.28	19.20	0.27	0.31	6.99	6.95	0.12	862	5.9
Fur-E	S012bGG05	64.19	0.50	17.56	3.12	0.24	0.22	0.85	8.05	5.17	0.11	Fsp39	66.12	19.22	0.27	0.29	7.09	7.00	0.12	862	5.9
Fur-E	S012bGG05	64.19	0.50	17.56	3.12	0.24	0.22	0.85	8.05	5.17	0.11	Fsp40	66.67	19.17	0.24	0.22	6.69	7.00	0.12	860	6.1
Fur-E	S012bGG05	64.19	0.50	17.56	3.12	0.24	0.22	0.85	8.05	5.17	0.11	MI01fsp	66.29	18.96	0.31	0.28	7.18	6.98	0.13	863	5.8
Fur-E	S012bGG05	64.19	0.50	17.56	3.12	0.24	0.22	0.85	8.05	5.17	0.11	MI02fsp	66.02	19.06	0.42	0.34	7.52	6.63	0.15	868	5.3
Fur-E	S012bGG05	64.19	0.50	17.56	3.12	0.24	0.22	0.85	8.05	5.17	0.11	MI03fsp	65.44	19.32	0.30	0.43	7.84	6.66	0.14	869	5.5
Fur-E	S012bGG05	64.19	0.50	17.56	3.12	0.24	0.22	0.85	8.05	5.17	0.11	MI04fsp	66.18	19.06	0.22	0.39	7.33	6.82	0.12	865	5.9
Fur-E	S012bGG05	64.19	0.50	17.56	3.12	0.24	0.22	0.85	8.05	5.17	0.11	MI05fsp	66.19	19.18	0.30	0.45	7.37	6.51	0.12	867	5.6
Fur-E	S012bGG05	64.19	0.50	17.56	3.12	0.24	0.22	0.85	8.05	5.17	0.11	MI06fsp	66.36	19.21	0.25	0.25	6.97	6.96	0.13	862	6.0
Fur-C	SM1-1	62.90	0.45	17.96	4.06	0.28	0.35	0.78	7.70	5.46	0.07	Fsp2	66.00	19.46	0.19	0.55	7.28	6.52	0.00	890	5.38
Fur-C	SM1-1	62.90	0.45	17.96	4.06	0.28	0.35	0.78	7.70	5.46	0.07	Fsp5	66.18	19.21	0.24	0.41	7.27	6.68	0.03	889	5.47
Fur-C	SM1-1	62.90	0.45	17.96	4.06	0.28	0.35	0.78	7.70	5.46	0.07	Fsp6	66.68	19.28	0.25	0.21	7.13	6.45	0.08	891	5.59
Fur-C	SM1-1	62.90	0.45	17.96	4.06	0.28	0.35	0.78	7.70	5.46	0.07	Fsp7	66.66	19.21	0.22	0.39	6.52	7.00	0.00	881	5.73
Fur-C	SM1-1	62.90	0.45	17.96	4.06	0.28	0.35	0.78	7.70	5.46	0.07	Fsp8	65.59	19.68	0.24	0.40	6.51	7.57	-0.01	876	5.75
Fur-C	SM1-1	62.90	0.45	17.96	4.06	0.28	0.35	0.78	7.70	5.46	0.07	Fsp9	66.36	19.41	0.24	0.54	6.87	6.58	-0.01	886	5.37
Fur-C	SM1-1	62.90	0.45	17.96	4.06	0.28	0.35	0.78	7.70	5.46	0.07	Fsp10	66.23	19.59	0.26	0.40	6.79	6.72	0.01	885	5.50
Fur-C	SM1-1	62.90	0.45	17.96	4.06	0.28	0.35	0.78	7.70	5.46	0.07	Fsp11	65.16	20.32	0.24	0.88	7.54	5.86	-0.06	894	4.76
Fur-C	SM1-1	62.90	0.45	17.96	4.06	0.28	0.35	0.78	7.70	5.46	0.07	Fsp12	66.57	19.18	0.25	0.41	6.62	6.97	0.00	882	5.59
Fur-C	SM1-1	62.90	0.45	17.96	4.06	0.28	0.35	0.78	7.70	5.46	0.07	Fsp13	66.78	19.18	0.25	0.22	6.36	7.21	0.03	879	5.84
Fur-C	SM1-1	62.90	0.45	17.96	4.06	0.28	0.35	0.78	7.70	5.46	0.07	Fsp14	66.02	19.55	0.14	0.57	6.40	7.32	-0.04	876	5.76
Fur-C	SM1-1	62.90	0.45	17.96	4.06	0.28	0.35	0.78	7.70	5.46	0.07	Fsp15	66.40	19.45	0.24	0.34	6.77	6.80	0.03	885	5.63
Fur-C	SM1-1	62.90	0.45	17.96	4.06	0.28	0.35	0.78	7.70	5.46	0.07	MI01fsp	65.92	20.03	0.23	0.61	7.40	5.80	0.01	896	5.04
Fur-C	SM1-1	62.90	0.45	17.96	4.06	0.28	0.35	0.78	7.70	5.46	0.07	MI02fsp	66.43	19.59	0.24	0.61	6.75	6.38	-0.03	886	5.29
Fur-C	SM1-1	62.90	0.45	17.96	4.06	0.28	0.35	0.78	7.70	5.46	0.07	MI03fsp	66.49	19.80	0.21	0.65	6.89	5.97	-0.03	890	5.20
Fur-C	SM1-1	62.90	0.45	17.96	4.06	0.28	0.35	0.78	7.70	5.46	0.07	MI04fsp	65.86	19.82	0.23	0.41	6.73	6.94	0.01	883	5.61
Fur-C	SM1-1	62.90	0.45	17.96	4.06	0.28	0.35	0.78	7.70	5.46	0.07	MI05fsp	66.55	19.45	0.19	0.45	6.55	6.81	-0.01	882	5.70

Table F5: Results of alkali feldspar-melt thermometry and hygrometry of the Povoação Ignimbrite Formation

Unit	Liquid composition											Feldspar composition							Equilibrium	T	H_2O
	Sample	SiO_2	TiO_2	Al_2O_3	FeO_t	MnO	MgO	CaO	Na_2O	K_2O	P_2O_5	Sample	SiO_2	Al_2O_3	FeO_t	CaO	Na_2O	K_2O	ΔKd_{Or-Ab}	(°C)	(wt. %)
Povo fall	EPFGG01	65.16	0.46	18.20	2.20	0.19	0.24	0.81	6.77	5.97	0.00	Fsp01	65.01	20.00	0.24	0.95	4.92	8.89	0.00	870	5.8
Povo fall	EPFGG01	65.16	0.46	18.20	2.20	0.19	0.24	0.81	6.77	5.97	0.00	Fsp02	64.83	20.27	0.23	0.90	4.67	9.10	0.01	865	6.0
Povo fall	EPFGG01	65.16	0.46	18.20	2.20	0.19	0.24	0.81	6.77	5.97	0.00	Fsp03	65.18	19.74	0.27	0.99	5.11	8.72	0.00	874	5.7
Povo fall	EPFGG01	65.16	0.46	18.20	2.20	0.19	0.24	0.81	6.77	5.97	0.00	Fsp04	65.00	19.98	0.26	0.90	4.75	9.11	0.01	866	5.9
Povo fall	EPFGG01	65.16	0.46	18.20	2.20	0.19	0.24	0.81	6.77	5.97	0.00	Fsp05	64.72	20.44	0.27	1.01	4.87	8.69	-0.01	870	5.7
Povo fall	EPFGG01	65.16	0.46	18.20	2.20	0.19	0.24	0.81	6.77	5.97	0.00	Fsp06	65.19	19.58	0.30	0.73	4.61	9.58	0.04	861	6.0
Povo fall	EPFGG01	65.16	0.46	18.20	2.20	0.19	0.24	0.81	6.77	5.97	0.00	Fsp07	64.96	19.95	0.18	0.89	4.90	9.10	0.01	868	6.0
Povo fall	EPFGG01	65.16	0.46	18.20	2.20	0.19	0.24	0.81	6.77	5.97	0.00	Fsp08	65.45	19.34	0.27	0.63	4.78	9.53	0.05	865	6.2
Povo fall	EPFGG01	65.16	0.46	18.20	2.20	0.19	0.24	0.81	6.77	5.97	0.00	Fsp09	64.80	20.35	0.25	1.02	4.72	8.86	-0.02	866	5.8
Povo fall	EPFGG01	65.16	0.46	18.20	2.20	0.19	0.24	0.81	6.77	5.97	0.00	Fsp10	64.89	20.26	0.20	0.83	4.47	9.34	0.02	860	6.1
Povo fall	EPFGG01	65.16	0.46	18.20	2.20	0.19	0.24	0.81	6.77	5.97	0.00	MI01Fsp	65.41	19.61	0.25	0.80	4.84	9.10	0.02	868	6.0
Povo fall	EPFGG01	65.16	0.46	18.20	2.20	0.19	0.24	0.81	6.77	5.97	0.00	MI02Fsp	65.22	19.79	0.21	0.82	4.88	9.08	0.02	869	6.0
Povo fall	EPFGG01	65.16	0.46	18.20	2.20	0.19	0.24	0.81	6.77	5.97	0.00	MI03Fsp	65.25	19.59	0.26	0.72	4.85	9.34	0.04	867	6.1
Povo fall	EPFGG01	65.16	0.46	18.20	2.20	0.19	0.24	0.81	6.77	5.97	0.00	MI04Fsp	64.85	20.20	0.20	1.12	5.11	8.50	-0.03	875	5.7
Povo ign	Glass04	63.86	0.78	18.85	2.14	0.11	0.27	0.88	6.43	6.58	0.10	Fsp26c	65.58	19.79	0.27	0.83	5.73	7.80	0.08	944	4.5
Povo ign	Glass04	63.86	0.78	18.85	2.14	0.11	0.27	0.88	6.43	6.58	0.10	Fsp26r	65.30	19.83	0.24	1.04	5.91	7.68	0.05	946	4.3
Povo ign	Glass04	63.86	0.78	18.85	2.14	0.11	0.27	0.88	6.43	6.58	0.10	Fsp27c	65.16	19.66	0.25	0.94	5.23	8.76	0.03	928	4.6
Povo ign	Glass04	63.86	0.78	18.85	2.14	0.11	0.27	0.88	6.43	6.58	0.10	Fsp27r	64.90	19.85	0.27	1.07	5.28	8.64	0.01	928	4.5
Povo ign	Glass04	63.86	0.78	18.85	2.14	0.11	0.27	0.88	6.43	6.58	0.10	Fsp28c	65.37	19.60	0.22	0.83	5.16	8.81	0.05	927	4.8
Povo ign	Glass04	63.86	0.78	18.85	2.14	0.11	0.27	0.88	6.43	6.58	0.10	Fsp28r	65.14	19.48	0.68	1.07	5.74	7.89	0.03	941	3.8
Povo ign	Glass04	63.86	0.78	18.85	2.14	0.11	0.27	0.88	6.43	6.58	0.10	Fsp29c	65.36	19.83	0.25	1.05	5.40	8.10	0.02	935	4.4
Povo ign	Glass04	63.86	0.78	18.85	2.14	0.11	0.27	0.88	6.43	6.58	0.10	Fsp29r	65.16	19.80	0.25	1.08	5.56	8.15	0.02	937	4.4
Povo ign	Glass04	63.86	0.78	18.85	2.14	0.11	0.27	0.88	6.43	6.58	0.10	Fsp30c	64.90	20.00	0.26	1.23	5.45	8.17	-0.01	934	4.3
Povo ign	Glass04	63.86	0.78	18.85	2.14	0.11	0.27	0.88	6.43	6.58	0.10	Fsp30r	65.08	19.91	0.25	1.08	5.02	8.67	0.00	924	4.5
Povo ign	Glass04	63.86	0.78	18.85	2.14	0.11	0.27	0.88	6.43	6.58	0.10	Fsp31c	65.63	19.70	0.25	0.81	6.18	7.43	0.11	953	4.4
Povo ign	Glass04	63.86	0.78	18.85	2.14	0.11	0.27	0.88	6.43	6.58	0.10	Fsp31r	65.71	19.51	0.23	0.62	5.56	8.37	0.10	938	4.8
Povo ign	Glass04	63.86	0.78	18.85	2.14	0.11	0.27	0.88	6.43	6.58	0.10	Fsp32c	65.93	19.36	0.27	0.48	5.86	8.10	0.14	945	4.8
Povo ign	Glass04	63.86	0.78	18.85	2.14	0.11	0.27	0.88	6.43	6.58	0.10	Fsp32r	66.04	19.36	0.22	0.65	6.17	7.55	0.14	953	4.6
Povo ign	Glass04	63.86	0.78	18.85	2.14	0.11	0.27	0.88	6.43	6.58	0.10	Fsp33r	65.13	20.02	0.27	1.02	5.34	8.23	0.02	933	4.4
Povo ign	Glass04	63.86	0.78	18.85	2.14	0.11	0.27	0.88	6.43	6.58	0.10	Fsp34c	65.46	19.47	0.22	0.66	5.24	8.95	0.08	928	4.9
Povo ign	Glass04	63.86	0.78	18.85	2.14	0.11	0.27	0.88	6.43	6.58	0.10	Fsp34r	65.26	19.78	0.23	1.01	5.31	8.40	0.02	931	4.5
Povo ign	Glass04	63.86	0.78	18.85	2.14	0.11	0.27	0.88	6.43	6.58	0.10	Fsp35c	66.12	19.37	0.25	0.43	6.65	7.18	0.23	963	4.6
Povo ign	Glass04	63.86	0.78	18.85	2.14	0.11	0.27	0.88	6.43	6.58	0.10	Fsp35r	66.48	19.39	0.31	0.41	7.20	6.21	0.34	977	4.2
Povo ign	Glass04	63.86	0.78	18.85	2.14	0.11	0.27	0.88	6.43	6.58	0.10	Fsp36c	65.45	19.60	0.23	0.82	5.28	8.61	0.05	930	4.7
Povo ign	Glass04	63.86	0.78	18.85	2.14	0.11	0.27	0.88	6.43	6.58	0.10	Fsp36r	65.24	19.95	0.26	1.19	5.53	7.83	0.00	938	4.2

Table F5 continued

Unit	Liquid composition											Feldspar composition							Equilibrium	T	H_2O
	Sample	SiO_2	TiO_2	Al_2O_3	FeO_t	MnO	MgO	CaO	Na_2O	K_2O	P_2O_5	Sample	SiO_2	Al_2O_3	FeO_t	CaO	Na_2O	K_2O	ΔKd_{Or-Ab}	(°C)	(wt. %)
Povo ign	Glass04	63.86	0.78	18.85	2.14	0.11	0.27	0.88	6.43	6.58	0.10	Fsp37c	65.17	19.77	0.26	1.15	5.44	8.22	0.00	934	4.3
Povo ign	Glass04	63.86	0.78	18.85	2.14	0.11	0.27	0.88	6.43	6.58	0.10	Fsp37r	65.50	19.50	0.22	0.77	5.08	8.93	0.06	925	4.9
Povo ign	Glass04	63.86	0.78	18.85	2.14	0.11	0.27	0.88	6.43	6.58	0.10	40 / 1 .	65.22	19.29	0.26	0.77	5.26	9.12	0.06	926	4.8
Povo ign	Glass04	63.86	0.78	18.85	2.14	0.11	0.27	0.88	6.43	6.58	0.10	41 / 1 .	64.87	19.61	0.26	0.89	5.26	9.06	0.04	926	4.7
Povo ign	Glass04	63.86	0.78	18.85	2.14	0.11	0.27	0.88	6.43	6.58	0.10	42 / 1 .	65.29	19.24	0.29	0.72	5.34	8.99	0.07	929	4.7
Povo ign	Glass04	63.86	0.78	18.85	2.14	0.11	0.27	0.88	6.43	6.58	0.10	44 / 1 .	65.55	19.52	0.25	0.86	6.42	7.36	0.12	956	4.3
Povo ign	Glass04	63.86	0.78	18.85	2.14	0.11	0.27	0.88	6.43	6.58	0.10	45 / 1 .	64.64	19.97	0.33	1.31	5.73	7.97	-0.01	939	4.0
Povo ign	Glass04	63.86	0.78	18.85	2.14	0.11	0.27	0.88	6.43	6.58	0.10	46 / 1 .	65.15	19.30	0.25	0.77	5.25	9.20	0.06	925	4.8
Povo ign	Glass04	63.86	0.78	18.85	2.14	0.11	0.27	0.88	6.43	6.58	0.10	47 / 1 .	65.02	19.47	0.25	0.76	5.35	9.10	0.06	928	4.8
Povo ign	Glass04	63.86	0.78	18.85	2.14	0.11	0.27	0.88	6.43	6.58	0.10	48 / 1 .	64.75	19.60	0.25	0.98	5.51	8.84	0.03	931	4.5
Povo ign	Glass04	63.86	0.78	18.85	2.14	0.11	0.27	0.88	6.43	6.58	0.10	49 / 1 .	65.20	19.51	0.25	0.88	5.17	8.92	0.04	926	4.7
Povo ign	Glass04	63.86	0.78	18.85	2.14	0.11	0.27	0.88	6.43	6.58	0.10	MI02fsp	64.80	19.86	0.28	1.16	5.61	8.29	0.01	936	4.3
Povo ign	Glass04	63.86	0.78	18.85	2.14	0.11	0.27	0.88	6.43	6.58	0.10	MI03fsp	65.25	19.62	0.27	0.78	5.31	8.78	0.06	930	4.7
Povo ign	Glass04	63.86	0.78	18.85	2.14	0.11	0.27	0.88	6.43	6.58	0.10	MI05fsp	65.25	19.73	0.26	0.80	5.38	8.58	0.06	932	4.7
Povo ign	Glass04	63.86	0.78	18.85	2.14	0.11	0.27	0.88	6.43	6.58	0.10	MI06fsp	64.58	20.44	0.24	1.45	5.62	7.68	-0.05	939	4.0
Povo ign	Glass04	63.86	0.78	18.85	2.14	0.11	0.27	0.88	6.43	6.58	0.10	MI07fsp	65.36	19.87	0.24	0.91	4.99	8.64	0.03	925	4.7
Povo ign	Glass05	63.86	0.78	18.85	2.14	0.11	0.27	0.88	6.43	6.58	0.10	43 / 1 .	63.27	21.69	0.41	3.31	7.57	3.69	-0.15	981	1.2
Povo ign	Glass09	64.53	0.57	18.35	2.11	0.10	0.29	0.71	6.44	6.91	0.01	MI04fsp	63.40	21.73	0.31	2.73	6.57	5.26	0.03	963	2.7
Povo ign	Glass01	64.40	0.56	18.16	2.22	0.15	0.26	0.87	6.79	6.54	0.03	Fsp33c	64.18	21.22	0.28	2.43	6.57	5.32	0.04	966	2.7

Table F6: Results of two-oxide thermometry for Furnas J

Furnas J Pair identifier	Phase	SiO_2	TiO_2	Al_2O_3	Fe_2O_3	FeO	MnO	MgO	Cr_2O_3	ZnO	V_2O_3	NiO	Sum	log(Mg/Mn)	T	fO_2
C1	Magnetite	0.04	16.97	0.98	35.32	41.92	2.50	1.43	0.00	0.24	0.02	0.01	99.43	0.002	869	-12.95
	Ilmenite		48.97	0.03	8.99	34.17	3.93	3.31	0.00				99.40	0.171		
K1	Magnetite		19.42	0.45	31.93	42.06	3.44	2.29	0.00				99.59	0.069	897	-12.51
	Ilmenite		48.97	0.03	8.99	34.17	3.93	3.31	0.00				99.40	0.171		
L1	Magnetite		16.41	0.93	36.93	40.08	3.06	2.03	0.00				99.44	0.067	852	-13.22
	Ilmenite		48.97	0.03	8.99	34.17	3.93	3.31	0.00				99.40	0.171		
M1	Magnetite		16.92	0.87	36.00	40.38	2.97	2.17	0.00				99.31	0.109	859	-13.10
	Ilmenite		48.97	0.03	8.99	34.17	3.93	3.31	0.00				99.40	0.171		
N1	Magnetite		16.77	0.74	36.38	40.76	2.80	1.95	0.02				99.41	0.088	857	-13.13
	Ilmenite		48.97	0.03	8.99	34.17	3.93	3.31	0.00				99.40	0.171		
O1	Magnetite		17.51	1.24	33.90	40.87	2.86	2.17	0.02				98.57	0.126	877	-12.82
	Ilmenite		48.97	0.03	8.99	34.17	3.93	3.31	0.00				99.40	0.171		
P1	Magnetite		15.77	0.67	37.74	39.43	2.97	1.90	0.00				98.48	0.051	843	-13.36
	Ilmenite		48.97	0.03	8.99	34.17	3.93	3.31	0.00				99.40	0.171		
Q1	Magnetite		15.66	0.73	37.94	39.30	3.03	1.90	0.00				98.56	0.042	841	-13.39
	Ilmenite		48.97	0.03	8.99	34.17	3.93	3.31	0.00				99.40	0.171		
R1	Magnetite		15.55	0.76	37.85	39.03	2.98	1.96	0.00				98.13	0.064	840	-13.40
	Ilmenite		48.97	0.03	8.99	34.17	3.93	3.31	0.00				99.40	0.171		
S1	Magnetite		15.81	0.77	37.76	39.48	3.05	1.91	0.00				98.78	0.041	843	-13.35
	Ilmenite		48.97	0.03	8.99	34.17	3.93	3.31	0.00				99.40	0.171		
T1	Magnetite		17.72	1.21	33.38	41.49	2.61	2.03	0.00				98.43	0.137	883	-12.72
	Ilmenite		48.97	0.03	8.99	34.17	3.93	3.31	0.00				99.40	0.171		
U1	Magnetite		16.79	1.33	34.81	39.99	2.91	2.17	0.00				98.00	0.118	866	-12.99
	Ilmenite		48.97	0.03	8.99	34.17	3.93	3.31	0.00				99.40	0.171		
V1	Magnetite		16.72	1.29	35.29	39.97	2.95	2.20	0.02				98.44	0.119	863	-13.04
	Ilmenite		48.97	0.03	8.99	34.17	3.93	3.31	0.00				99.40	0.171		
W1	Magnetite		14.74	1.69	38.65	38.59	2.71	2.11	0.00				98.49	0.137	835	-13.48
	Ilmenite		48.97	0.03	8.99	34.17	3.93	3.31	0.00				99.40	0.171		
X1	Magnetite		16.68	1.41	36.49	41.02	2.78	2.01	0.00				100.39	0.106	860	-13.09
	Ilmenite		48.97	0.03	8.99	34.17	3.93	3.31	0.00				99.40	0.171		
Y1	Magnetite		15.73	1.24	35.89	38.86	2.90	1.98	0.00				96.60	0.079	852	-13.22
	Ilmenite		48.97	0.03	8.99	34.17	3.93	3.31	0.00				99.40	0.171		
Z1	Magnetite		17.00	1.31	34.65	40.24	2.90	2.20	0.00				98.30	0.126	868	-12.95
	Ilmenite		48.97	0.03	8.99	34.17	3.93	3.31	0.00				99.40	0.171		
AA1	Magnetite		13.64	0.56	41.50	37.58	2.80	1.79	0.00				97.87	0.051	814	-13.81
	Ilmenite		48.97	0.03	8.99	34.17	3.93	3.31	0.00				99.40	0.171		
AB1	Magnetite		14.77	0.65	39.46	38.56	2.89	1.85	0.00				98.17	0.053	829	-13.58
	Ilmenite		48.97	0.03	8.99	34.17	3.93	3.31	0.00				99.40	0.171		

Table F6: Results of two-oxide thermometry for Furnas J syenite ejecta

Furnas J syenite

Pair identifier	Phase	SiO_2	TiO_2	Al_2O_3	Fe_2O_3	FeO	MnO	MgO	Cr_2O_3	ZnO	V_2O_3	NiO	Sum	log(Mg/Mn)	T	fO_2
F2	Magnetite	0.06	17.56	0.31	33.97	42.88	3.93	0.04	0.00	0.35	0.01		99.11	-1.77	621	-21.47
	Ilmenite	0.01	51.93	0.00	2.42	31.88	14.39	0.12	0.00	0.07	0.00		100.81	-1.83		
B3	Magnetite	0.02	11.21	0.11	46.86	35.77	4.51	0.08	0.01	1.02	0.01		99.60	-1.51	629	-20.55
	Ilmenite	0.00	51.14	0.02	3.01	32.36	13.13	0.18	0.00	0.03	0.02	0.00	99.89	-1.61		
E3	Magnetite	0.14	16.94	0.14	33.52	43.34	2.30	0.03	0.00	0.31	0.01		96.73	-1.60	664	-19.68
	Ilmenite	0.00	51.14	0.02	3.01	32.36	13.13	0.18	0.00	0.03	0.02	0.00	99.89	-1.61		
G4	Magnetite	0.06	16.64	0.17	36.76	42.26	4.02	0.03	0.00	0.41	0.01		100.35	-1.92	780	-15.39
	Ilmenite	0.03	48.71	0.00	5.73	32.99	10.53	0.07	0.00	0.08	0.02	0.01	98.17	-1.93		